Conference Proceedings

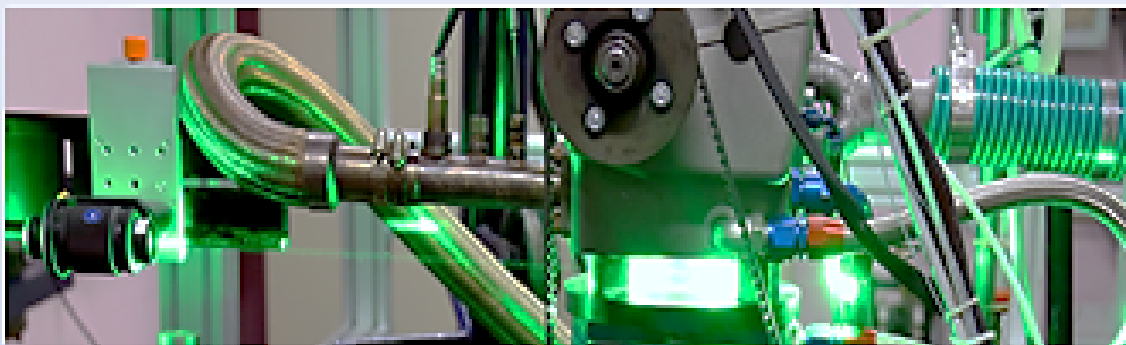## 1ˢᵗ ISEES International Conference On

Sustainable Energy and Environmental Challenges (SEEC-2017)

26th-28th February, 2017

International Society for Energy, Environment and Sustainability

Center of Innovative and Applied Bioprocessing (CIAB), Mohali, India

PIV
LDV
PDI
PLIF
TomoPIV

Advanced Flow Diagnostics

AERODYNAMICS SPRAY DIAGNOSTICS
HYDRODYNAMICS MULTIPHASE FLOWS COMBUSTION

Conference Proceedings

1st ISEES International Conference
On

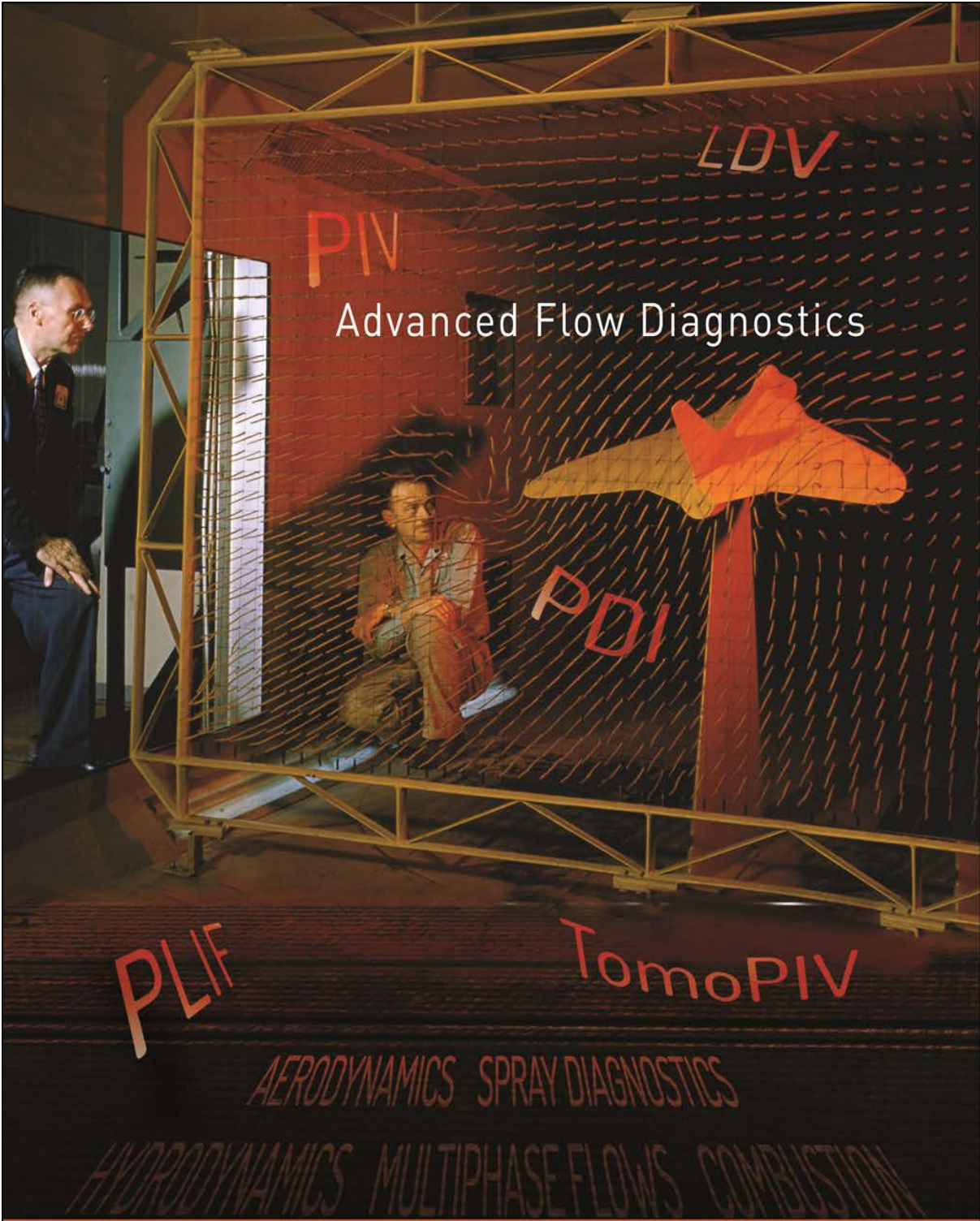# Sustainable Energy and Environmental Challenges (SEEC-2017)

26th-28th February, 2017

International Society for Energy, Environment and Sustainability

Center of Innovative and Applied Bioprocessing (CIAB), Mohali, India

© Authors

Edited by:

Dr. Akhilendra Pratap Singh

Prof. Ashok Pandey

Dr. Atul Dhar

Prof. Avinash Kumar Agarwal

Dr. Dhananjay K. Srivastava

Dr. R. S. Sangwan

Dr. Santanu De

Contents

Centre for Innovative and Applied Bioprocessing

(A National Institute under Department of Biotechnology, Ministry of Science & Technology, Govt. of India)
C-127, II Floor, Phase 8, Industrial Area, SAS Nagar
Mohali-160 071, Punjab, India

Ashok Pandey, *PhD, FBRS, FRSB, FNASc, FIOBB, FISEES, FAMI*
Eminent Scientist

Tel:+91-172-4990214
Fax:+91-172-4990204
E-mail: pandey@ciab.res.in; ashokpandey56@yahoo.co.in

13th February 2017

Welcome message

It is with great pleasure I welcome the delegates and invitees of the International Conference on Sustainable Energy and Environmental Challenges (SEEC-2017) being organized by the International Society for Energy and Environmental Sustainability (ISEES; http://isees.in) jointly with the Center of Innovative and Applied Bioprocessing (CIAB), Mohali during February 26-28, 2017 at CIAB, Mohali.

The ISEES was founded at IIT Kanpur in January 2014 with an aim to spread knowledge in the fields of Energy, Environment, Sustainability and Combustion. The Society 's goal is to contribute to the development of clean, affordable and secure energy resources and a sustainable environment for the human society and to spread knowledge in the above-mentioned areas among the people and make them more aware about the environmental challenges, which the world is facing today. The ISEES is involved in various activities such as conducting workshops, seminars, conferences, etc in the domains of its interests. The Society also recognizes the outstanding works done by the young scientists and engineers for their contributions in these fields by conferring them awards under various categories.

This is the first international conference ISEES is organizing, which is being hosted by the CIAB, Mohali. We have received an overwhelming response from the scientific fraternity from all over the country and from some other countries as well. The topic of the conference is of great relevance in present day's context and I am hopeful that the deliberations made during the conference by the experts will be highly relevant and useful.

I take the opportunity to acknowledge the support extended by various organizations to SEEC-2017, to the Organizing team comprising the members of the Executive Committee for their un-tiring efforts for the success of the conference and to CIAB, Mohali for generously agreeing to host the conference. I am quite confident that with highly enriched scientific program, each delegate will feel benefitted for the scientific and technological thrust.

On behalf of the Society and on my personal behalf, I extend warm welcome and greetings to the delegates of the SEEC-2017 and best wishes for its success. I also wish and hope that you will find some time to go around the beautiful surroundings in this tri-city, referred as Knowledge City to refresh you among your busy schedules.

Ashok Pandey
Chairman, ISEES

Formerly- Chief Scientist and Head, Biotechnology Division, CSIR-National Institute for Interdisciplinary Science and Technology, Trivandrum-695 019, India; Editor-in-chief: Bioresource Technology- Elsevier, UK; Honorary Executive Advisor: Journal of Water Sustainability, Australia; Honorary Executive Advisor: Journal of Energy and Environmental Sustainability; Subject Editor: Proceedings of National Academy of Sciences (India): Part B-Biological Sciences

INDIAN INSTITUTE OF TECHNOLOGY KANPUR
DEPARTMENT OF MECHANICAL ENGINEERING
KANPUR-208016, INDIA

Dr. Avinash Kumar Agarwal,
Professor

Tel: + 91 512 2597982 (O), + 91 512 2598682 (R)

Fax: + 91 512 259 7408

Email: akag@iitk.ac.in

http://home.iitk.ac.in/~akag

February 26th, 2017

Welcome Message

At the outset, I take the privilege to extend a warm welcome to the participants of the **First International Conference on Sustainable Energy and Environmental Challenges** (SEEC-2017) being organized under the auspices of *International Society for Energy and Environmental Sustainability (ISEES)* by the **Center of Innovative and Applied Bioprocessing (CIAB), Mohali** from February 26-28, 2017.

SEEC-2017 aims to promote research and outreach program in India and elsewhere through scientific deliberations such as keynote and invited addresses by eminent scientists, and contributed oral and poster presentations by bringing together engineers, scientists, researchers, students, science managers and professionals in order to address and discuss the emerging sustainable energy and environmental issues. The conference provides a platform for physicist, mathematicians, chemists, engineers and biologist to critically discuss key areas and trends of energy and environmental sciences. Environmental sciences research should contribute to scientific understanding of major problems in recent days arising due to extensive agriculture, industrialisation, transportation, and urbanization activities together with climate change, with special focus on developing economies.

I am glad to report to you that a very exciting scientific program of SEEC-2017 consisting of 50 keynote/ invited talks and 173 contributed papers/ poster has been put together, which will unfold in 14 oral technical sessions and two poster sessions. The contributory presentations include 52 short oral talks and 121 posters. Poster are further divided into 12 topical tracks (six engineering tracks and six biotechnology tracks). There are 200+ delegates and invitees attending this conference, which include participants and speakers from USA, South Korea, Norway, Australia and Malaysia and India.

I take this opportunity to thank our sponsors and supporters namely Department of Science and Technology, Govt. of India; CIAB, Tesscorn, TSI, Springer and Horiba. Our sincere gratitude to Director and staff of CIAB, Mohali for hosting the conference and making all necessary arrangements. I am also grateful to the Chairman, Members of the Executive Committee of the ISEES, Organising Secretaries of SEEC-2017, and Volunteers for their time and efforts for making this conference a run-away success.

I wish SEEC-2017 a great success.

Avinash Kumar Agarwal

Conference Chair, SEEC-2017 and Secretary, ISEES

Message

It is a matter of happiness that *International Society for Energy, Environment and Sustainability* (ISEES), a new scientific society founded in 2014 at Indian Institute of Technology (IIT), Kanpur, decided to hold its first international conference at Center of Innovative and Applied Bioprocessing (CIAB), Mohali during February 26-28, 2017.

I appreciate the initiative for its professional merit because when we talk about energy and environmental sustainability, only a few options remain available in the current highly and hurriedly consumptive world. These are either plenty (*which are rare now*) perennial non-earthly sources (like sunlight) or that can be produced without penalty or recycled at the same rate as consumed. It also has a dimension of time, not in years but in number of future generations. It obviously calls for sustainability in hundreds and thousands of years if we can't think beyond. Therefore, it necessarily involves biology with plant biomass as the motherly resource. Philosophically it involves solar energy harvesting through photosynthesis and technological and engineering challenges to have 'reverse photosynthesis' to recover energy from photosynthetic products. It emphasizes inter-disciplinary research and interactions for which institutional academic structures too subject-specialized to serve alone. Therefore, supplementary and catalytic expectations reside with Conferences like SEEC-2017 to serve this purpose.

I understand from the technical program of the conference that SEEC-2017 has been perfectly planned for the advantages of inter-disciplinary discussions, deliberations and interactions. I am sure this platform of colloquia would serve all stakeholders particularly young with respect to their quest for understanding new knowledge and queries thereon.

I wish to thank the ISEES for giving us the opportunity to organize this event at CIAB. I appreciate the endeavors of Prof. Ashok Pandey and Prof. K. Avinash Agarwal and their teams in planning and organizing SEEC-2017 commendably well.

I wish SEEC-2017 all the success.

(Rajender Singh Sangwan)

Organizing Committee SEEC-2017

Chief Patron
Dr. V. K. Saraswat, Member, Niti Aayog, New Delhi

Patrons
Prof. Ashutosh Sharma, DST, Govt. of India, New Delhi
Prof. N Sathyamurthy, Director, IISER Mohali
Prof. Vijay Raghavan, DBT, Govt. of India, New Delhi
Dr. M Rajeevan, Secretary, MoES, Govt. of India, New Delhi
Dr. Ajay Mathur, TERI, New Delhi
Dr. RK Malhotra, Petrofed, New Delhi
Prof. Sachin Chaturvedi, RIS, New Delhi
Dr. Rakesh Kumar, CSIR-NEERI, Nagpur
Dr. Vivek Agarwal, CDC India, Jaipur
Dr. DB Sahoo, IBSD, Imphal
Dr. Anjan Ray, CSIR-IIP, Dehradun
Dr. Sanjay Kuamr, IHBT, Palampur
Dr. B. Bhargava, ONGC EC
Dr. MR Nouni, MNRE, New Delhi
Dr TR Sharma, NABI, Mohali

General Chair
Prof Ashok Pandey, Chairman ISEES, CIAB, Mohali

Conference Chairs
Dr Rajender Singh Sangwan, Chief Executive Officer, CIAB, Mohali
Prof Avinash K. Agarwal, Secretary, ISEES, IIT Kanpur

Conveners
Dr Santanu De, IIT Kanpur
Dr Atul Dhar, IIT Mandi
Dr Dhananjay Kumar Srivastava, IIT Kharagpur

Co-Conveners
Dr. Anirudh Gautam, RITES, Lucknow
Dr. Bhola R Gurjar, IIT Roorkee

International Advisory Committee
Prof. Ramesh Agarwal, Washington Univ., St Louis, USA
Prof. Kalyan Annamalai, Texas A&M, USA
Prof.Robin Anderson, USDA, USA
Dr. Omprakash Bharadwaj, FEV, Germany
Prof Carlos Dosoretz, TECNION, Israel
Prof. Edgard Gnansounou, EPFL, Switzerland
Prof. Jega Jegatheesan, RMIT, Australia
Dr. Gautam Kalghatgi, Saudi Aramco, Saudi Arabia
Prof. Samir Khanal, University of Hawaii, USA
Prof. Christian Larroche, Univeriste Blaise Pascal, France
Prof. Chang Sik Lee, Hanyang University, South Korea
Prof. Duu Jong Lee, NTU, Taiwan
Prof. Keat Teong Lee, USM, Malaysia
Prof. A.R. Masri, Univ. Sydney, Australia

Prof. H. H. Ngo, Univ. of Technology Sydney, Australia
Dr. Deepak Pant, VITO, Belgium
Dr. Mani Sarathy, KAUST, Saudi Arabia
Dr. Pravesh C. Shukla, ECN, Nantes, France
Prof. S. J. Sim, Korea University, Korea

Prof. M. Taherzadeh, University of Boras, Sweden
Prof. R. D. Tyagi, INRS, Canada
Prof. K. Vogiatzaki, Univ. Brighton, UK
Prof. Ernst Wintner, TU Vienna, Austria
Prof. Franz Winter, TU Wien, Austria
Prof. Jonathan Wong, Baptist University, Hong Kong

National Advisory Committee

Dr. V. Arghode, IIT Kanpur
Dr. Sanjay Bajpai, DST, New Delhi
Dr. Raja Banerjee, IIT Hyderabad
Prof. U. C. Banerjee, NIPER, Mohali
Prof. Saptarshi Basu, IISc Bangalore
Dr. Thallada Bhaskar, IIP, Dehradun
Dr. Dilip Bora, Jorhat Engineering College, Jorhat
Prof. P. K. Bose, NSHM, Durgapur
Prof. B. S. Chadha, GNDU, Amritsar
Dr. S. A. Channiwala, NIT Surat
Dr. Swetopravo Choudhury, IISc Bangalore
Prof. L. M. Das, IIT Delhi
Prof. Amitava Dutta, Jadavpur University, Kolkata
Dr. Anuradda Ganesh, Cummins, Pune
Dr. Rupam Kataki, Tezpur University, Tezpur
Prof. S. K. Khare, IIT Delhi
Dr. Sunil Kumar, CSIR-NEERI, Nagpur
Dr. N. Labhsetwar, CSIR-NEERI, Nagpur
Dr. S. Maji, Delhi University, New Delhi
Prof. J. Mallikarjuna, IIT Madras
Prof. S. Mariappan, IIT Kanpur

Dr. R. K. Maurya IIT Ropar
Dr. K. Nandakumar, LPSC, ISRO, Thiruvananthapuram
Dr. S Venkat Mohan, CSIR-IICT, Hyderabad
Prof. V. S. Moholkar, IIT Guwahati
Dr. Anil Kumar Patel, DBT-Bioenergy Centre, IOCL, Faridabad
Dr. R. Praveenkumar, ARNAI, Thiruvannamalai
Dr. Pradipta Sahu, OAUT, Odisha
Dr. R. D. Mishra, NIT Silchar
Prof. A. Ramesh, IIT Madras
Prof. R. V. Ravikrishna, IISc Bangalore
Prof. Anjan Ray, IIT Delhi
Prof. M. P. Sharma, IIT Roorkee
Prof. R. P. Sharma, AIT, Jaipur
Prof. R. S. Singh, PU, Patiala
Dr. S. L. Soni, MNIT, Jaipur
Dr. K. Subramanyam, CES, IIT Delhi
Dr. R. K. Sukumaran, CSIR-NIIST, Trivandrum
Prof. I. S. Thakur, JNU, New Delhi
Dr. S. S.Thipse, ARAI, Pune
Dr. Sunita Varjani, GPCB, Gandhinagar

Local Advisory Committee

Dr. Sudesh Kumar, CIAB Mohali
Dr. S. Saravanamuragan, CIAB Mohali
Dr. Saswat Goswami, CIAB Mohali
Dr. Sasikumar Elumalai, CIAB Mohali
Dr. Bhuwan Mishra, CIAB Mohali
Dr. Sudhir Pratap Singh, CIAB Mohali
Dr. Meena Krishania, CIAB Mohali
Dr. Vinod Kumar, CIAB Mohali
Ms. Nidhi Budhalakoti, CIAB Mohali
Ms. Pankaj Preet Sandhu, CIAB Mohali
Sri. Umesh Singh, CIAB, Mohali
Sri. Virendra K. Banerjee, CIAB Mohali
Sri. Suneet K. Verma, CIAB, Mohali

Sri. Hardip Singh, CIAB Mohali
Sri. Aman Sethi, CIAB Mohali
Sri. Balwan Singh, CIAB Mohali
Sri. Sant Lal Pasi, CIAB Mohali
Sri. Sanjeev Kumar Saini, CIAB Mohali
Sri. Umesh Singh, CIAB Mohali
Sri. Jaspreet Singh, CIAB Mohali
Sri. Sukhjinder Singh, CIAB Mohali
Sri. Sabir Ali, CIAB, Mohali
Sri. Arun Kumar, CIAB, Mohali
Ms. Hema Pharswan, CIAB, Mohali
Sri. Manipal Singh, CIAB, Mohali

About International Society for Energy, Environment and Sustainability (ISEES)

International Society for Energy, Environment and Sustainability

About the Society

The International Society for Energy, Environment and Sustainability was founded at IIT Kanpur in January, 2014 with an aim to spread knowledge in the fields of Energy, Environment, Sustainability and Combustion. In this changing environmental scenario, the time has come where more emphasis has to be laid on renewable energy resources. Moreover, in this dynamic scenario of swelling competition and reducing profits, staying environmentally responsible can be extremely challenging for any organization. More efficient systems have to be developed to meet the increasing energy demands keeping in mind its environmental impact. People have to become more aware and concerned about the environmental challenges which the world is facing today to make it a better place for us and our future generations. The Society aims to spread knowledge in the above mentioned areas among people and make them more aware about the environmental challenges which the world is facing today. The Society is involved in various activities like conducting workshops, seminars, conferences, etc. in the above mentioned domains. The society also recognizes young scientists and engineers for their contributions in this field. It comprises of experts from leading research institutions working in various domains related to energy

Aims and Objectives

1. To organize Workshops/ Symposia/ Conferences/ Lectures/ Courses for wide dissemination of knowledge to its members and society at large, in the areas related to energy, combustion, sustainability, and environment related subjects.
2. To publish technical papers, monographs, books and journals in the areas mentioned above.
3. Organizing events and activities for the benefits of the underprivileged in the society as per the capability of society members.

Journal of Energy and Environmental Sustainability (JEES)

Journal of Energy and Environmental Sustainability is official publication of the International Society for Energy, Environment and Sustainability dedicated to all the areas of conventional and renewable energy that are relevant for environmental sustainability. The journal will publish two issues in a year and offer a platform for high-quality research in the interdisciplinary areas of energy and environmental science and engineering.

ISEES Membership

1. The Society shall have the grades of Student Member, Member, Fellow and Honorary Fellow. In addition, institutions and organizations will be given Institutional or Corporate membership on payment of dues and satisfying other eligibility criteria as specified by the executive body from time to time.

2. Fellow of the Society will be the highest grade of membership.

3. A graduate in engineering, technology, science, social sciences, humanities or having equivalent qualification as recognized by ISEES may apply for the membership of the Society. In case of unrecognized qualifications, ISEES executive committee (EC) will decide on the recognition of the qualifications. The same shall be updated in the membership documentation from time to time. Award of membership shall be at the sole discretion of the EC.

4. A member may withdraw permanently from the membership of the society at any time by giving a notice in writing to the secretary. In such cases, neither partial nor full refund of membership fee shall be done under any circumstances. There shall not be any exception to this provision.

5. The membership of any student member/ member/ fellow can be withdrawn by ISEES EC in case of unethical, immoral and criminal conduct of the individual concerned. Any action not in alignment with the objectives, interests and purpose of the society may also lead to suspension of the membership. The permanent withdrawal can only be done after an opportunity to present his/ her views to the EC has been given to the defaulting member. The decision of the ISEES EC in this regard shall be final and irrevocable in all such cases.

Privileges of Membership

1. A member whose subscription is paid up to date shall be entitled:

2. To be notified of all relevant activities of the Society.

3. To vote at all Annual General Body Meetings (AGBM) and special meetings of the Society and voting (online/ ballot) on various issues including elections and referendums.

4. Reduced registration fee in the events organized under the banner of the Society.

5. Receive a copy of the proceedings of the meetings (to the corporate members only).

6. To be included in a directory of experts along with the domain expertise to be published by the ISEES from time to time.

7. Corporate members will be able to send two delegates free/ subsidized rates to the events organized by the Society. They will also get partial fee waiver in the advertisement published in the society newsletters/ literature/ ISEES website.

Awards and Recognition

1. A member whose subscription is paid up to date shall be entitled:
2. To be notified of all relevant activities of the Society.
3. To vote at all Annual General Body Meetings (AGBM) and special meetings of the Society and voting (online/ ballot) on various issues including elections and referendums.
4. Reduced registration fee in the events organized under the banner of the Society.
5. Receive a copy of the proceedings of the meetings (to the corporate members only).
6. To be included in a directory of experts along with the domain expertise to be published by the ISEES from time to time.
7. Corporate members will be able to send two delegates free/ subsidized rates to the events organized by the Society. They will also get partial fee waiver in the advertisement published in the society newsletters/ literature/ ISEES website.

Membership Fees

	Type of membership	Annual Membership Fee	Five-Years Membership Fee	Life Membership Fee (10 Years)
India/ SAARC Countries	Student Members	1000 INR	--	--
	Member/ Fellow	2000 INR	5000 INR	10000 INR
	Corporate	10000 INR	--	50000 INR
	Honorary Fellow	0	0	0
USA, Europe and Developed Countries	Student Members	50 US$	--	--
	Member/ Fellow	100 US$	250 US$	500 US$
	Corporate	500 US$	--	2500 US$
	Honorary Fellow	0	0	0

ISEES Executive Committee (2016-18)

Chairman

Prof. Ashok Pandey

Vice Chairman

Dr. Anirudh Gautam

Secretary

Prof. A. K. Agarwal

Joint Secretary

Prof. B. R. Gurjar

Treasurer

Dr. Santanu De

Members

Dr. S. V. Mohan

Dr. Atul Dhar

Dr. B. Thallada

Dr. A. P. Singh

International Society for Energy, Environment & Sustainability
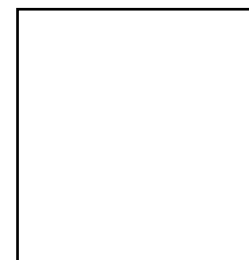
Membership Form

Photo

I would like to join ISEES and take advantage of all the membership benefits		
First Name	Middle Initial	Last Name

Membership No. (If you already have):		Designation:	
Age:	Date of birth : Date	Month	Year	Sex: M/F

Educational Record

Degree/s:	Specialisation:

Office Address		**Residence Address**	
City:	State:	City:	State:
PIN:	Telephone:	PIN:	Telephone:
Mobile:		Email ID:	

Payment Details (cheque/cash/DD payable at SBI IIT Kanpur in favour of *ISEES*)

Amount:	Cash/DD /Chq. No:	Date:
Bank:	Branch:	

Date: Signature

	Type of Membership	Annual Membership Fee	Five –Year Membership Fee	Life Membership Fee (10 Years)
India / SAARC Countries	Student Members	1000 INR	---	----
	Members / Fellow	2000 INR	5000 INR	10000 INR
	Corporate	10000 INR	---	50000 INR
USA, Europe and Developed Countries	Student Members	50 US $	---	---
	Members / Fellow	100 US$	250 US$	500 US$
	Corporate	500 US$	---	2500 US$

Mailing Address: Dr. Avinash Kumar Agarwal
Department of Mechanical Engineering, IIT Kanpur
Kanpur 208016, UP, India
08765599882 (Sujeet)
Email: akag@iitk.ac.in

Note: Attach a Demand Draft& a self-attested copy of your ID proof along with the duly filled and signed form.

ISEES
Fellows

International Society for Energy, Environment and Sustainability (ISEES)

http://www.iitk.ac.in/isees

ISEES Fellows-2014

Prof. Ashok Pandey

Dr. Ashok Pandey is Deputy Director CSIR's National Institute for Interdisciplinary Science and Technology at Trivandrum and heading the Centre for Biofuels and Biotechnology Division there. His current major research interests are on bio-based economy for the development of bio-processes and products on bio-refinery principle. He has more than 1050 publications/communications, which include 15 patents & design copyright, 40 books, 110 book chapters, 410 original and review papers, etc with h index of 71 and >21,000 citation. Dr Pandey is Editor-in-chief of Bio-resource Technology, Honorary Executive Advisors of Journal of Water Sustainability and Journal of Energy and Environmental Sustainability.

Dr. Akshai Runchal

Dr. Akshai Runchal is an acknowledged and well known expert in CFD, Combustion Modeling, and performance analysis related to combustion systems. He has performed computer modeling and numerical simulation of flow, heat and mass transport processes for diverse problems in engineering. His experience spans a range of problems including those related to design, production, operation and environmental impact of industrial and urban projects. He has consulted extensively in Computational Fluid Dynamics (CFD), Combustion, Turbulence, Environmental Pollution, and heat and mass transfer processes.

Dr. S. R. Gollahalli

Dr. S. R. Gollahalli is currently a professor in School of Mechanical and Aerospace Engineering at University of Oklahoma, USA. His research interests encompass fundamental as well as applied topics in the energy and combustion fields. The projects under his direction include combustion of liquid drops and sprays, flame characteristics of pulverized coal and synthetic fuels, combustion of bio-fuels, hybrid fuels such as emulsions and slurries, internal combustion engine and gas turbine combustors, turbulent diffusion flames in cross-flow streams, and microgravity combustion.

ISEES Honorary Fellows-2014

Dr. R. K. Malhotra

Dr. R. K. Malhotra is Director in the Board of Indian Oil Corporation (R&D).He is also the Non-Executive Chairman of Indocat Pvt. Limited, as well as the Board Member of Lubrizol India, a JV Company of Indian Oil and Lubrizol USA. He has more than 36 years of research experience in the downstream petroleum sector and is currently leading R&D Centre of Indian Oil Corporation in areas of refining technologies, lubricant technologies, alternative energy, bio-technology, nanotechnology and gasification.

International Society for Energy, Environment and Sustainability (ISEES)

http://www.iitk.ac.in/isees

ISEES Fellows-2015

Prof. L.M. Das

Prof. L. M. Das is currently Professor at the Centre for Energy Studies, IIT Delhi. He received his Bachelor's degree in Mechanical Engineering from REC Rourkela, M. Tech. from IIT Kharagpur and Ph.D. from IIT Delhi. His primary areas of research interest are development of alternative-fuelled low emission engines/ vehicles. He has published more than 80 research papers in international journals on alternative fuels such as Hydrogen, CNG, Biodiesel and Hydrogen-CNG blends. He is a member of Advisory Board for International Association of Hydrogen Energy (USA).

Prof. Suresh K. Aggarwal

Prof. Suresh K. Aggarwal is Professor of Mechanical Engineering at the University of Illinois at Chicago in USA. He did his B.S. in Aeronautical Engineering from Punjab Engineering College, Chandigarh, M.S. from IISc., Bangalore and Ph.D. from Georgia Tech. His research interests are in the areas of combustion, multiphase reacting flows, renewable fuels, and emissions. Prof. Aggarwal has made major contributions in combustion phenomena, and authored over 330 peer-viewed journal and conference papers. He received the Scholar Award and the Faculty Research Award at University of Illinois. He is an ASME Fellow, AAAS Fellow, and AIAA Associate Fellow.

Prof. Chang Sik Lee

Prof. Chang Sik Lee is a Professor of Mechanical Engineering at the College of Engineering of Hanyang University, South Korea. He received his B.S., M.S and Ph.D. in Mechanical Engineering from Hanyang University. His research interests are alternative fuel engines, alternative fuels, exhaust emission reduction, engine fuel sprays and laser measurements, and thermodynamic analysis of engine systems. Prof. Lee has authored over 250 articles in leading international journals and two books on Engineering Thermodynamics and Automobile Engineering. He was President of KSAE, ILASS-Korea, ILASS-Asia and Automotive Environment Center.

ISEES Honorary Fellows-2015

Prof. O. N. Srivastava

Prof. O. N. Srivastava is Professor Emeritus of Physics and Coordinator of Nano-science and Technology and Hydrogen Energy Centre at BHU. He received his PhD (Physics) from Banaras Hindu University (BHU) and worked as post doctoral fellow at Cornell University. Professor Srivastava has made notable research contributions in renewable energy. He has published more than 400 papers, 15 review articles and the book entitled Crystallography for Solid State Physics.

Dr. Gabriel D. Roy

Dr. Gabriel D. Roy is former Associate Director at the Office of Naval Research Global (ONRG), Singapore. He received his B.S. and M.S. in Mechanical Engineering. He graduated from University of Tennessee Space Institute (UTSI), where he received his Ph.D. degree in engineering science. He was also responsible for supporting research in his area of specialization – propulsion – which included energy storage, combustion, hypersonic, emission and noise reduction, and alternative fuels. Dr. Roy has authored over 100 research publications and 20 books.

International Society for Energy, Environment and Sustainability (ISEES)

http://www.iitk.ac.in/isees

ISEES Fellows-2016

Prof. Avinash Kumar Agarwal

Prof. Agarwal has carried out both fundamental as well as innovative, industrially relevant applied research in the areas of IC engines, alternative fuels and emission control. He has developed a low cost biodiesel pilot plant and tested biodiesel fuelled car to motivate Indian automotive industries for biodiesel applications. He has developed first prototype of the EFI system for the ALCO-DLW locomotives. He has published several books and more than 200 papers. He has been elected for Fellow of INAE, ASME and SAE International. Presently he is working as Poonam and Prabhu Goyal Endowed Chair Professor. He has been awarded for Shanti Swarup Bhatnagar (SSB)-2016, NASI-Reliance Industries Platinum Jubilee Award-2012, Dr. C. V. Raman Young Teachers Award-2011.

Dr. S. Venkata Mohan

Dr. Mohan made outstanding contributions for waste remediation and environment protection. He established a link between waste remediation and renewable biofuel generation. He has published more than 250 journal papers, 8 cover page articles, 29 chapters contributed for books and 9 review articles. He also holds 8 patents in his area. Dr. Mohan has been awarded by Shanti Swarup Bhatnagar (SSB), National Bioscience Award (2012), ProSPER.NET-Scopus Young Researcher Award in Sustainable Development (2010), NASI-Scopus Young Scientist Award (2010). Dr. Mohan has been elected as Fellow of INAE, FIEI, Andhra Pradesh/ Telengana Academy of Sciences, Alexander Von Humboldt Foundation.

Prof. Ernst Wintner

Prof. Wintner was professor for laser technology at Photonics Institute of TU Vienna and promoted honorary full professor within his university. He founded one of the first research groups in the field of laser ignition worldwide in 1999. He has submitted a number of patents with respect to a laser source for ignition, the laser window and multipoint ignition. Prof. Wintner served as editor of several journals and the European Quantum Electronics Division of the EPS. His efforts have resulted in over 250 technical papers and 4 book chapters. He received Dr. Wolfgang Houska Award (2015), Dr. Wolfgang Houska Award (2008), the largest award of the Austrian Industry AMA Price (2013), BMW Award (2007).

ISEES Honorary Fellows-2016

Dr. Satish Kumar

Dr. Kumar is a distinguished Aerospace scientist of national repute with outstanding contribution to the missiles and strategic systems. He contributed to Development of Liquid propellant rocket engines for Prithvi missile, Product ionization of highly complex LP engines at Hindustan Aeronautics Limited (HAL), Development of Propellant transfer systems and Storage facilities at various forward Army locations. Dr. Satish Kumar honored with the Technology Award by Ministry of Defence, Prime Minister's Special Award for Development of Strategic Weapons and Performance Excellence award by DRDO. He has been elected as Fellow of Aeronautical Society of India, Fellow of Society for Shock Wave Research, India, Life member of Astro-nautical Society of India and Combustion Institute of Indian Section

Prof. Ryo Amano

Prof. Amano has been very active in the development of next generation of novel advanced energy systems in both gas turbines based conventional and renewable energy production systems. Dr. Amano has contributed to enhancing energy production from wind, biomass, hydro, and propulsion energy. He has contributed to the development of turbulence theories, combustion, heat transfer, propulsion, aerodynamics and applications to gas turbine and aerospace related projects. Prof. Amano has been elected for Fellow of ASME (2001), Associate Fellow of American Institute of Aeronautics and Astronautics (2002). His efforts have resulted in over 600 technical papers, 4 books and 24 book chapters.

International Society for Energy, Environment and Sustainability (ISEES)

www.isees.in

ISEES Honorary Fellows-2017

Dr. V. K. Saraswat

Dr. V. K. Saraswat is Member of NITI Ayog, Government of India. He has led research on indigenous development of Liquid Propulsion Rocket Engines and missiles namely Prithvi, Dhanush, and Prahaar. He is the principal architect of the Ballistic Missile Defense program, which included major technology breakthroughs. Dr. Saraswat is an elected Fellow of Indian National Academy of Engineering, Institution of Engineers, India, Aeronautical Society of India, Institute of Electronics & Telecommunication Engineers, Systems Society of India, and Society for Shock Wave Research, India. Dr. Saraswat has been bestowed with several prestigious awards such as Padmabhushan, Padmashri and Vikram Sarabhai Memorial Award.

ISEES Fellows-2017

Prof. Probir Kumar Bose

Prof. Probir Kumar Bose is Director of NSHM Knowledge Campus, Durgapur, West Bengal, India. He has exceptional scientific and professional contributions in the areas of thermal engineering, internal combustion engines, alternate fuels, and automotive engineering. Prof. Bose is an elected Fellow of Institute of Engineers, India and member of Combustion Institute, Indian Institute of Welding, Indian Society of Technical Education, Indian Society of Engineers, and Indian Institute of Metals. Prof. Bose has published more than 100 peer reviewed journal papers and has several patents to his credit.

Prof. Ramesh Agarwal

Dr. Ramesh Agarwal is Professor in School of Engineering & Applied Science, Washington University, St. Louis, USA. He has received numerous prestigious awards including SAE International Medal of Honor (2015), AIAA Reed Aeronautics Award (2015), SAE Aerospace Engineering Leadership Award (2013), SAE Clarence Kelly Johnson Award (2009), AIAA Aerodynamics Award (2008), Royal Aeronautical Society Gold Award (2007), and ASME Fluids Engineering Award (2001) to name a few. He has published more than 500 peer reviewed journal/ conference papers and edited several books/ book chapters.

Prof. Bhola R. Gurjar

Dr. Bhola R. Gurjar is Professor in Department of Civil Engineering, Indian Institute of Technology Roorkee, India . He has exceptional scientific and professional contributions in the areas of Environment, Air and Water Pollution, Urban Transport, and Environmental Impact and Risk Assessment. Prof. Gurjar has received several prestigious awards including IE(I) Nawab Zain Yar Jung Bahadur Memorial Medal-1995, START Young Scientist Award-2004, IE(I) National Design Award in Environmental Engineering-2011, and IE(I) Eminent Environmental Engineer Award-2015.

Prof. Swarnendu Sen

Dr. Swarnendu Sen is professor in Department of Mechanical Engineering, Jadavpur University, Kolkata, India. He has exceptional scientific and professional contributions in the areas of heat transfer, combustion, and multiphase flows. Prof. Sen is an elected Fellow of the West Bengal Academy of Science and Technology. He has received several prestigious fellowships including DAAD Research Fellowship-2011 and 2013, Visiting Research Fellowships to University of Illinois, Chicago-2002, Virginia Polytechnic and State University, Virginia-2006. He has authored more than 90 peer reviewed journal publications.

Dr. Thallada Bhaskar

Dr. Thallada Bhaskar is Principal Scientist in CSIR-Indian Institute of Petroleum, Dehradun, India. He has received several prestigious awards including NESA Scientist of the Year Award-2016, CSIR-Raman Research Fellow- 2013, AIST-Distinguished Researcher Award-2013, and JSPS-Visiting Scientist Award-2009. Dr. Bhaskar has published more than 100 peer reviewed journal papers and edited several books.

Dr. Anirudh Gautam

Dr. Anirudh Gautam is General Manager in Rolling Stock Design Division, RITES, Ministry of Railways, India. Dr. Gautam has worked extensively on combustion, performance and emissions of locomotive engines, development of emission control systems and engine structural optimization. He has received prestigious awards such as Outstanding National Service Award by Ministry of Railways, Chief Mechanical Engineer Award, General Manager Award, Director General Award, and Railway Ministers Award.

ISEES Awardees 2017

International Society for Energy, Environment and Sustainability (ISEES)

http://www.iitk.ac.in/isees

ISEES Young Scientist Award-2017

Dr. Ankur Gupta

Dr. Ankur Gupta is Assistant Professor, School of Mechanical Sciences, Indian Institute of Technology Bhubaneswar, Odisha. Dr. Gupta has made valuable contributions in the areas of waste water treatment through nanotechnology, micro-sensor design and development, micro-fluidics, biological detection, etc. He has published over 20 peer reviewed scientific papers and two book chapters..

Dr. Sathesh Mariappan

Dr. Sathesh Mariappan, Assistant Professor, Department of Aerospace Engineering, Indian Institute of Technology Kanpur. Dr. Mariappan has made valuable theoretical and experimental contributions in the areas of combustion driven oscillations, i.e. combustion instability in gas turbine engines, and dynamic stall & laminar-to-turbulent transitions in rotorcrafts. He has published over 10 peer reviewed scientific journal/ conference papers and one book chapter.

Dr. Pallab Sinha Mahapatra

Dr. Pallab Sinha Mahapatra is Post-Doctoral Fellow, Department of Applied Mechanics, Indian Institute of Technology Madras. Dr. Mahapatra has worked on developing energy efficient strategies to enhance the heat transfer rate during natural/ mixed convection systems, jet impingement cooling, drop-wise condensation etc. He developed a computational model and a multiphase code to simulate severe accident scenario in the nuclear reactors. He has published over 50 peer reviewed scientific journal/ conference papers and one book chapter.

Dr. Sirshendu Mondal

Dr. Sirshendu Mondal, Post-Doctoral Fellow, Department of Aerospace Engineering, Indian Institute of Technology Madras. Dr. Mondal has designed and developed a laboratory-scale experimental setup for extending his work on dynamic characterization of pulse combustors. He developed tools for dynamic characterization based on observed time series data, which included using several state-of-the-art techniques. He also worked on emerging tools of non-linear dynamics like non-linear forecasting, tests of determinism like translation error and chaos. He has published over 10 peer reviewed scientific journal/ conference papers and one book chapter.

Sh. Mritunjay Kumar Shukla

Sh. Mritunjay Kumar Shukla is Scientist-C, CSIR-Indian Institute of Petroleum, Dehradun, India. Mr. Shukla has carried out engine studies using various biofuels for developing efficient and eco-friendly engines. He developed low-cost catalysts for direct decomposition of NO and fuel-borne catalysts to provide a cost effective solution for engine exhaust emission control. He has published over 25 peer reviewed scientific journal/ conference papers and two book chapters.

International Society for Energy, Environment and Sustainability (ISEES)

http://www.iitk.ac.in/isees

Best PhD Thesis Award-2017

Dr. Akhilendra Pratap Singh

Thesis Title: Mode Switching Prototype Engine Development for Low Temperature Combustion

Institute: Indian Institute of Technology Kanpur, Kanpur, India

Dr. C. Nagendranatha Reddy

Thesis Title: Advanced Bio-systems For Sustainable Remediation of Azo Dye Based Wastewater Embedded with Resource Recovery

Institute: CSIR-Indian Institute of Chemical Technology (CSIR-IICT), Hyderabad, India

Dr. Chetankumar P. Patel

Thesis Title: Spray, Engine Combustion, Performance, Emissions, Vibrations and Acoustics Studies of Biodiesel and SVO Blends

Institute: Indian Institute of Technology Kanpur, Kanpur, India

Dr. Joonsik Hwang

Thesis Title: Performance and Emission Improvement by Microwave-assisted Plasma Ignition in a Direct-injection Gasoline Engine

Institute: Korea Institute of Science and Technology (KAIST), South Korea

Dr. Souvick Chatterjee

Thesis Title: Study of Instability in a Swirling Annular Liquid Sheet

Institute: Jadavpur University, Kolkata, India

Best M.Tech. Thesis Award-2017

Ayush Jain

Thesis Title: Fuel Injection Strategy Evaluation for Ultra-Low Emission Premixed Charge Compression Ignition Engine Development

Institute: Indian Institute of Technology Kanpur, India

Krishn Chandra

Thesis Title: Combustion Visualization and Particulate Characterization of Waste Cooking Oil and Karanja Biodiesel Fuelled Engine

Institute: Indian Institute of Technology Kanpur, India

Invited Speakers

Speaker	Title
Prof. P. K. Bose	An Experimental Investigation of Performance-Emission Trade-off of a CI engine Fueled by Different Blends of Diesel-Ethanol and Diesel-Biodiesel-Ethanol
Prof. V. Ganesan	Mahua Biodiesel in a Single Cylinder Diesel Engine for Sustainable Irrigation Operation in India: An Experimental Study
Dr. Rajeev Kumar Sukumaran	Challenges in the Development of Enzymes for Biomass Hydrolysis
Dr. Thallada Bhaskar	Biomass Hybrid Conversion Pathway for Sustainable Biorefinery
Prof. Hao Huu Ngo	Performance and Evaluation of a Grid Connected Hybrid Photo-Voltaic-Wind Power System
Prof. Ramesh Agarwal	Multiphase CFD Modeling and Simulations of Fluidized Beds for Chemical Looping Combustion
Prof. Mohsen Assadi	Intermittent Renewable Energy and Security of Supply from a Technical and Economical Point of View
Prof. Vijayanand S. Moholkar	Mechanistic Study on Ultrasound-Assisted Biodiesel Production from Non-edible Mixed Oil Feedstock using Heterogeneous Catalyst
Dr. Sunil Kumar	Solid Waste Management and Climate Change in India: Existing Scenario and Strategy for Improvement
Dr. Gabrial Roy	Sustainable Alternate Transportation Fuel Development for Kerala
Prof. Swarnendu Sen	Macroscopic Spray Characteristics of Ethanol Blended Kerosene and Diesel using a Hybrid Atomizer
Prof. R. P. Sharma	Alternative Fuels for Compression Ignition Engines- Where are we going?
Prof. Sudipta De	Is Distributed Poly-Generation Utilizing Local Resources a Sustainable Energy Solution for India?
Prof. Avinash K. Agarwal	Technology Roadmap for DME Fuelled Vehicles in Indian Mega-Cities
Dr. Himanshu Tyagi	Efficient Absorption of Solar Energy Using Nanoparticle-Laden Fluids
Prof. S. L. Soni	Emerging New Alternate Fuels for IC Engines: A Review
Prof. S.Bhattacharya	Carbon Based Materials for Energy Storage Applications
Dr. Akhilendra P. Singh	Advanced Engine Combustion Technologies
Prof. Bhola R. Gurjar	Simple Modeling Tools for Air Pollution Emission Inventory and Health Risk Assessment
Prof. Sathesh Mariappan	Unsteady Motions in Vortex Shedding Combustors: A Dynamical Systems' Perspective
Prof. Nachiketa Tiwari	Diesel Locomotive Noise: Sources, Reduction Strategies, Measurement Methods and Standards
Prof. Santanu De	Modeling of Turbulent Spray Combustion Using Conditional Moment Closure Method
Dr. Anirudh Gautam	Design & Development of Common Rail Electronic Direct Fuel Injection for Diesel Locomotives of Indian Railways
Prof. P. A. Laxminarayana	MPFI and SPFI CNG Engine Design and Development
Prof. Tarun Gupta	Lab Development and Field Evaluation of a High Volume Fine Particle Inertial Impaction Based Aerosol Sampler
Prof. A. Mukhopadhyay	Characterization of Single Phase Natural Circulation Loops using Dynamical Systems Approach
Prof. Nitin Labhsetwar	Mixed Oxides as Efficient Oxygen Carriers for Chemical Looping Combustion Technologies
Prof. Dhananjay K. Srivastava	Laser Ignition of Engines

Prof. Bhupinder S. Chadha	Thermophilic Fungus *Malbranchea Cinnamomea* as Source of Catalytically Active Glycosyl Hydrolases for Bioconversion of Lignocellulosics
Prof. Amitava Datta	Combustion Characteristics of Biomass-based Fuels for Engine Applications
Dr. Reeta R. Singhania	Cellulase Production for Second Generation Bioethanol Production
Prof. Baskar Gurunathan	Nano-Composites as Modern Heterogeneous Catalyst for Biodiesel Production
Prof. Sunil Kumar Khare	Application of Ionic Liquids in Biomass Processing and Enzymatic Saccharification
Prof. Arvind Kumar Bhat	Fuel from Waste: A Scientific Solution for Waste Management and Environment Conservation
Prof. Jishnu Bhattacharya	Storing Heat from the Sun: A Critical Perspective
Prof. Wan Azlina Ahmed	Flexirubin-Type Pigment Production from *Chryseobacterium Artocarpi* CECT 8497 and Its Application as Natural Ink
Prof. Parmjit S. Panesar	Biotechnological Approaches for the Utilization of Agro-Industrial Byproducts for Lactic Acid Production
Dr. Uma Maheshwar	Powering the Future Flight -Perspectives from Environmental Challenges
Prof. P. Binod	Utilization of Biodiesel Industry Generated Crude Glycerol for the Production of 1,3-Propanediol Through Microbial Route
Prof. Ram Sarup Singh	Waste to Wealth- Utilization of Apple Industry Waste for Production of Value-added Products
Prof. Saptarshi Basu	How a Spray Interacts With Swirling Flow?
Prof. Zainul Akmar Zakria	Antioxidant Potential of Pyroligneous Acid Fraction Obtained from Pyrolysis of Palm Kernel Shell
Prof. Swetaprovo Chaudhuri	Instability Control by Actuating the Swirler in a Lean Premixed Combustor
Dr. Sarvanamurugan Shunmugavel	Inter-Conversion of Aldopentoses and Tetroses with Zeolite
Prof. R. Praveenkumar	Bioremediation of Cassava Sago Waste by *Yarrowia Lipolytica* for Production of Bio-oil
Dr. D. V. Patil	Review of Particle based Methods for Combustion Simulations
Prof. Deepak Pant	Magic of π-π Interaction for Carbon Capture
Prof. Amit Agarwal	Development of Blood-Plasma-Separation and Constant-Wall-Temperature Micro-Devices

Biography and Abstract of Invited Speakers

Prof. R P Sharma

Henry Ford Chair Professor,
Indian Institute of Technology, Madras
rpsharmaiitm@gmail.com

Biography:

Prof. R P Sharma, who retired as Henry Ford Chair Professor, Indian Institute of Technology Madras, has occupied important position in automotive industry as well as in academia during his 48 year span of service. He had served as General Manager (R& D) at Mahindra & Mahindra; Head, Engine R&D, at Ashok Leyland and General Manager, R&D at Swaraj Mazda Limited, Director , Arya College of Enquiring & Technology. He served as Chairman of several Technical Committees of Society of Automotive Industry Association over a long period. Served on assessment committees of Indian Institution of Petroleum, Dehradun and on Research Advisory Board of Indian Oil Corporation R&D center. Contributed significantly in developing industry-academia cooperation for automotive industry (CORE program of Dept. of Science and Technology) and use of hydrogen energy in engines. Currently he chairs the Projects Assessment Committee of Ministry of Non-Conventional and Renewable Energy (MNRE). He has been consultant to many prestigious companies such as Infosys, Bharat Petroleum, L& T, GE, General Motor Corporation etc. He is author of several books and published extensively. He is currently technical reviewer of more than 14 international technical journal of repute.

Title: Alternative Fuels for Compression Ignition Engines- Where Are We Going?

Abstract:

After a brief review of history of using alternative fuels, this paper discusses the current trends in use of biodiesel, ethanol and methanol and their blends including blends of these fuels with small amount of hydrogen addition. Issues related to performance, emissions and durability of compression ignition engines are discussed. Future research trends are highlighted in each of these areas.

Prof. Sudipta De

Mechanical Engineering Department
Jadavpur University, Kolkata-700032, India
de_sudipta@rediffmail.com

Biography:

Sudipta De received his Ph.D. degree from Indian Institute of Technology (IIT), Kharagpur. He was a guest researcher at the Department of Energy Sciences, Lund University, Sweden for more than one year. Currently, he is Professor at the Mechanical Engineering Department, Jadavpur University, India. Dr. De is an Indian national expert on 'Clean and Alternative Technology' of the Ministry of Environment and Forest, Government of India. He was nominated senior scientist by Indian National Science Academy (INSA), New Delhi to Germany in the field of sustainable energy under international bilateral exchange program of the Academy. He was also the selected faculty of Erasmus Mundus External Cooperation Window of the EU with specialization in sustainable energy engineering. He received his research funding from different institutes including, UGC, DST of the Government of India, European Union, German Research Foundation, Swedish Research Council etc. He is/was also member of several technical committees including that of Power and Energy Systems of The International Association of Science and Technology for Development (IASTED), Canada and international energy initiative "Explore Energy" by the Royal Institute of Technology, Sweden. He was an invited Indian expert in the round table on 'Food-water-energy nexus' of the Research Council UK-India in Delhi in November 2013. Presently he is also leading another Indo-Norwegian collaboration project of 3-year duration, funded by the UGC of India and Research Council of Norway (RCN) on low carbon energy systems of India.

Title: Is Distributed Poly-generation Utilizing Local Resources a Sustainable Energy Solution for India?

Abstract:

Providing electricity to all Indians including those at remote villages is a long term mission for the Government of India. However, most of the electricity supply in India is still from fossil fuel based large power plants and distributed through a large national grid. Unfortunately supplying electricity using this network may not be economically feasible in Indian context and has not been greatly successful till date. On the other hand, decentralized energy systems using local resources may be a long term sustainable solution for India, specifically Indian villages. Moreover, apart from electricity, drinking water, cooling, biofuels, fertilizers etc. are a few of other basic needs of these people. Efficient system integration with multiple utility outputs catering to local needs may offer a sustainable solution in Indian context. Utilizing locally available resources for these systems may be even more sustainable. Using renewable resources including biomass may also reduce environmental impact rather than using fossil fuel based energy utilities. Thus decentralized multi-generation utilizing local resources as inputs emerges to be a prospective sustainable solution. A series of studies will be reported in this work exploring the feasibility of such systems in Indian context through technological (thermodynamic), economic and environmental performance assessments.

Prof. Avinash K. Agarwal

Engine Research Laboratory,
Department of Mechanical Engineering,
Indian Institute of Technology Kanpur
Kanpur-208016, India
akag@iitk.ac.in

Biography:

Prof. Avinash Kumar Agarwal joined Department of Mechanical Engineering, IIT Kanpur in 2001 and he is currently a Professor. Prof. Agarwal worked at ERC, University of Wisconsin, Madison, USA as a Post-Doctoral Fellow (1999 – 2001). His areas of interest are IC engines, combustion, alternative fuels, hydrogen, conventional fuels, lubricating oil tribology, optical diagnostics, laser ignition, HCCI, emission and particulate control, and large bore engines.

He is associate editor of ASME Journal of Energy Resources Technology, and International Journal of Vehicle Systems Modelling and Testing and Editor-in-Chief of Journal of Energy and Environmental Sustainability. He has edited "Handbook of Combustion" (5 Volumes; 3168 pages), published by Wiley VCH, Germany. Prof. Agarwal is a Fellow of SAE (2012), Fellow of ASME (2013) and a Fellow of INAE (2015). He is recipient of several prestigious awards such as NASI-Reliance Industries Platinum Jubilee Award-2012; Dr. C. V. Raman Young Teachers Award: 2011; SAE International's Ralph R. Teetor Educational Award -2008. Prof. Agarwal is the recipient of Prestigious Shanti Swarup Bhatnagar Award-2016 in Engineering Sciences. He is the first combustion/ IC Engine researcher to get this honour in the country.

Title: Technology Roadmap for DME Fuelled Vehicles in Indian Mega-Cities

Abstract:

With ever growing concerns on environmental pollution, energy security, and future oil supplies, the global community is seeking non-petroleum based alternative fuels, along with more advanced energy technologies to increase the efficiency of energy use. Compared to other alternative fuels such as ethanol, methanol or its blends, DME is emerging as the leading alternative fuel candidates as this maintain economic, political, and environmental security for future generations. Availability, economics, acceptability, environmental and emissions, natural security, technology, versatility could be the criteria to judge the new alternative fuel. This talk will give an overview and a broader picture of implementation of DME fuel in a compression ignition diesel engine. Importance of spray, atomization, performance, and emission and combustion characteristics of a DME fuel engine will be discussed. In atmospheric condition DME exists in a gas phase. There is need to compress DME fuel to convert it to liquid state so that it can be made to pass through a fuel injection system. Therefore, there also exists a need to modify the existing fuel injection system of a diesel engine. DME can be injected into the combustion chamber by either convention mechanical injector or through modern common rail direct injection system. The fuel injection system needs to be modified to prevent low lubricity problem and to prevent corrosion of fuel injection system. Care must be taken to prevent leakage of DME through fuel injection system as DME has relatively low viscosity. DME combustion starts relatively earlier than diesel combustion due to its higher Cetane number. Due to the absence of carbon – carbon bond in DME, its emission is soot free. The low particulate matter production of DME provides adequate justification for its consideration as a candidate fuel in compression-ignition engines. Handing and transportation of DME is similar to LPG. Also, it produces lower HC and CO emission than diesel engine. DME can be produced by the conversion of various feed-stocks such as natural gas, coal, oil residues and bio-mass. Towards the end of the talk, challenges to develop a DME fuel vehicle will be addressed with respect to India. Infrastructure and storage of DME will be discussed in addition to its production.

Dr. Himanshu Tyagi

School of Mechanical, Materials & Energy Engineering
Indian Institute of Technology Ropar
Nangal Road, Rupnagar-140001 (Punjab), India
Himanshu.tyagi@iitrpr.ac.in

Biography:

Himanshu obtained his PhD from Arizona State University, USA in the field of heat transfer. Prior to his PhD he obtained his masters from University of Windsor, Canada and his bachelors from I.I.T. Delhi both in the field of Mechanical Engineering. He has been working at IIT Ropar since 2009, working to develop nanotechnology-based clean and sustainable energy sources with a team of several PhD and undergraduate students. He has previously worked in the Steam Turbine Design Division of Siemens (in Germany and India) and in the Thermal and Fluids Core Competency group of Intel Corp (in USA). His research interests include thermo-fluids engineering, bio-heat transfer, radiative and ignition properties of nanofluids, nanoscale heat transfer and its applications in energy harvesting.

Title: Efficient Absorption of Solar Energy Using Nanoparticle-Laden Fluids

Abstract:

Conventional concentrated solar collectors harness the solar energy through several steps of heat transfers. The incident solar radiations are usually directly absorbed by a solid surface (either flat such as in the case of a flat-plate type solar collector or curved as in the case of parabolic trough collectors). These surfaces in turn can transfer the thermal energy to a fluid which may then be used for various applications such as for process heating, chemical processing, electricity generation etc. One unique way in which heat transfer process within the solar collector may be improved is by employing the concept of direct absorption where a significant portion of the sunlight is directly absorbed by the fluid itself, thereby eliminating one step of heat transfer. In order to achieve direct absorption trace amounts of nanoparticles may be added to the base-fluid which is shown to have significant impact on the optical as well as thermo-physical properties of the base fluid. Once the solar energy is absorbed by the nano-fluid, it needs to be efficiently stored when later needed for a release. The addition of nanoparticles also augments the transport and storage of energy (sensible, latent and chemical). The presence of nanoparticles as well as conditions of optical optimization allows the overall system to achieve high energy storage density, energy conversion efficiency as well as good long-term durability.

Prof. S.L. Soni

Mechanical Engineering Department,
Malaviya National Institute of Technology, Jaipur
shyamlalsoni@gmail.com

Biography:

Dr Soni is Faculty Coordinator Placement and Training and is Professor in the Department of Mechanical Engineering at Malaviya National Institute of Technology Jaipur. He had been the Chairman for the Golden Jubilee Celebrations of MNIT Jaipur during the year 2012-13. Prior to this he has served as Head of the Department of Mechanical Engineering at Malaviya National Institute of Technology Jaipur for about 3.5 years. Dr. Soni passed his Bachelor of Engineering from MREC Jaipur with honours in 1979. He did his M.Tech. from IIT Delhi with CGPA of 9.6 and also obtained Ph.D. from IIT Delhi. His field of specialization is alternate fuels in I.C. engines. He has more than 36 years of teaching experience at MNIT Jaipur. He has published more than 88 research papers in National and International journals and conferences. He has guided seven research works leading to award of PhDs and eight more Doctoral research works are under progress in his supervision. He is founder Faculty Advisor of SAE student chapter at MNIT Jaipur.

Dr. Soni is Fellow of Institution of Engineers India and life member of Indian Society for Technical Education, Indian Association for Air Pollution Control, Indian Society for Combustion Engineers. He is member of advisory board in some of the leading Universities.

Title: Emerging New Alternate fuels for I.C. Engines: A Review

Abstract:

Energy demand of the world is increasing progressively. The two imperative issues world currently facing are the depletion of fossil fuels and its environmental impact. Since these fossil fuels are the major source of energy being utilized by the human race, hence the energy demand depends on availability of the fossil fuels. Therefore, increasing demand is endangering the survival and sustainability of life support system. In this regard depletion of fossil fuel reserves, energy scarcity, global warming, and increase in pollutants in atmosphere are matters of great concern today. Internal Combustion (I.C) Engines have become a major factor in transforming and organizing social life as these are the prime movers of automobiles and also used in stationary applications such as power generation. IC engines are used either in a form of Compression Ignition (C.I) or Spark Ignition (S.I) and the commonly used fuels are diesel (C.I) and gasoline (S.I) for producing power. Both diesel and gasoline are obtained from fossil reserves. So it has become necessary to look for alternate fuels for sustainable development since I.C engines will continue to dominate automotive sector and can be used in power generation in near future. Alternate fuels promise sustainable development, energy conservation, efficiency and environment preservation. Alternate fuels like biodiesels, methyl alcohol, ethyl alcohol, biogas, hydrogen and producer gas have proved themselves as successful fossil fuel substitutes for internal combustion engine. Also, various alternate fuels and polygeneration technologies can be combined, leading to sharp decrease in emission levels in most of the applications in our day today life. New fuels like Biomethane, Ammonia, Biobutanol, Liquid Nitrogen, Dimethyl Ether, Diethyl Ether, water based emulsions, P-series fuels and Acetylene have a great potential to act as future alternate fuels for IC engines and can play a vital role in mitigating the energy crises. In spite of their distinct properties, these fuels can be used in I.C engines by applying various techniques and can be utilized in the form of blends with diesel/biodiesel, in dual fuel mode and as a sole fuel. This paper briefly reviews the literature on the above mentioned new alternate fuels, their feasibility and their applications in Internal Combustion Engines.

Prof. Shantanu Bhattacharya

Microsystems Fabrication Laboratory,
Department of Mechanical Engineering,
Indian Institute of Technology Kanpur
Kanpur-208016, India
bhattacs@iitk.ac.in

Biography:

Dr. Shantanu Bhattacharya is currently working as a Professor of Mechanical Engineering Department and Head of the Design Programme at IIT Kanpur, India. He received his Ph. D. degree from University of Missouri, Columbia (2006), M. S. degree from Texas Tech University (2003) and B. E. degree from Delhi College of Engineering (1996). He has teaching/research experience of 12 years and industrial experience of 7 years. Till date he has published 50 research papers, 10 patents, 1 book, 6 general articles etc. He has received the NDRF (National Design Research Forum), IEI, Best Mechanical engineering design award-2014, ISSS (Institute of Smart Structures and Systems) Young Scientist Award- 2013, Honorary Fellow of the Institute of High Energetic Materials in Melbourne, 2011, IEI (Institute of Engineers of India), Young Engineers Award, 2010 in Mechanical Engineering. Dr. Bhattacharya has also received a fellowship from the Institution of Engineers of India in 2016 and serves as an associate editor for Journal of nanoscience and nantechnology. He is also an editorial board member in the Journal of green nanotechnology.

Title: Carbon based Materials for Energy Storage Applications

Abstract:

Carbon-based electrode materials have been widely explored for many years for energy generation, electrochemical charge storage, catalysis etc. However, environment friendly, new and advanced electrode materials are requiredin electronic and electrical devices for power storage applications.This work will be presented in two parts. In one part we have developed electrode materials with high area and high specific capacity which has been prepared by entrapping graphite nanoparticles into a sol gel network. The fabrication produces a highly porous film with a Brunauer–Emmett–Teller (BET) specific surface area of 364 m2/g. In the second part another electrode material formulated by ananocomposite developed from natural coffee waste extracted porous graphene oxide- Polyaniline and silver nanoparticles was characterized for charge storage applications. These films reveal a very high BET specific surface area of 1033 m2/g. Both the porous nano-graphite films and the nanocomposite films report a very high specific capacity for charge storage and excellent cyclic stability giving a set of materials which may find applications in super capacitors and batteries.

Dr. Akhilendra Pratap Singh

Engine Research Laboratory
Department of Mechanical Engineering,
Indian Institute of Technology Kanpur
Kanpur-208016, India
akhips@iitk.ac.in

Biography:

Dr. Akhilendra Pratap Singh: Dr. Akhilendra Pratap Singh is a CSIR Pool Scientist at Indian Institute of Technology Kanpur. He received his Masters and PhD in Mechanical Engineering from Indian Institute of Technology Kanpur, India in 2010 and 2016 respectively. His areas of research include advanced low temperature combustion; optical diagnostics with special reference to engine endoscopy and PIV; combustion diagnostics; engine emissions measurement; particulate characterization and their control; and alternative fuels. Dr. Singh has published 15 peer reviewed international journal papers and 6 peer reviewed international and national conference papers. He is a member of numerous professional societies, including SAE, ASME, and ISEES. He is a member of the editorial board of the 'Journal of Energy, Environment and Sustainability'.

Title: Advanced Engine Combustion Technologies

Abstract:

Low temperature combustion (LTC) concept has evolved over last two decades in response to demand for lowering NOx and soot emissions from direct injection (DI) diesel engines. LTC delivers improved thermal efficiency of gasoline-fuelled engines and ultra-low NOx and soot emissions of diesel-fuelled engines, which makes it a strong potential alternative technology to existing combustion technologies. Although remarkable progress has been made in LTC technology, large-scale production of LTC engines for commercial application still remains challenging and is infested with several operational difficulties. Limited operating range, lack of direct control on SoC, difficulties in obtaining homogeneous fuel-air mixture preparation and higher HC and CO emissions are the main hurdles for LTC technology adaptation in production engines and vehicles for commercial applications. Several techniques have been developed for low-load applications of LTC technology in heavy-duty engines, however full-load applications, even in light-duty engines have not been experimentally demonstrated until now. Based on engine design, operating conditions and control strategies employed, different fuels such as biodiesel, alcohols, kerosene, etc. have been demonstrated for LTC applications with partial success. Based on fuel properties, distinct fuel-air mixture preparation techniques namely, port fuel injection; early direct injection and late direct injection can be applied to LTC engines. This study was divided into three sections namely (i) partially premixed homogeneous charge compression ignition (PHCCI) combustion, (ii) premixed charge compression ignition (PCCI) combustion and (iii) mode switching between conventional CI combustion and LTC. Mode switching involves dual combustion modes, depending on operating condition, which is an effective solution for commercializing LTC technology. This study involved a journey starting with the fundamental combustion investigations of PCCI and culminating into development of commercially viable

Prof. Bhola R. Gurjar

Department of civil (Environmental) Engineering,
Indian Institute of Technology (I.I.T.) - Roorkee
Roorkee- 247 667, Uttarakhand, India
brgurjar@gmail.com

Biography:

Dr. B.R. Gurjar is a Professor in Civil Engineering Department and Head of Centre for Excellence in Transportation Systems (CTRANS) at Indian Institute of Technology (IIT) - Roorkee. He holds a PhD from IIT Delhi and conducted postdoctoral research at the Max Planck Institute for Chemistry in Mainz (Germany). He has extensive professional experience of about 25 years and several international collaborations in air pollution, emissions and climate change related areas. He has more than 140 publications to his credit. He is recipient of several international and national awards including the 2004 START Young Scientist Award conferred by the Scientific Steering Committee of the global change SysTem for Analysis, Research and Training (START), Washington, D.C., U.S.A. He is also recipient of the Nawab Zain Yar Jung Bahadur Memorial Medal (1995-96), National Design Award for Environmental Engineering (2011) and the Eminent Environmental Engineer Award (2015) given by the The Institution of Engineers (India).

Title: Simple Modeling Tools for Air Pollution Emission Inventory and Health Risk Assessment

Abstract:

There are several international models to estimate emissions from road transport sector. However, given scarcity of field studies and primary data, these models prove to be quite complex and resource intensive in Indian conditions. To fill this gap, Prof. Gurjar's research group has developed a simple spreadsheet model known as the Vehicular Air Pollution Inventory (VAPI) model to estimate emissions from exhaust, non-exhaust and evaporative emissions pertaining to on road vehicles in Indian conditions.

Dr. Sathesh Mariappan

Department of Aerospace Engineering,
Indian Institute of Technology Kanpur
Kanpur-208016, India
sathesh@iitk.ac.in

Biography:

Sathesh Mariappan is an Assistant Professor in the Department of Aerospace Engineering at Indian Institute of Technology Kanpur. He completed his Bachelors at Madras Institute of Technology, 2007 and obtained his direct Ph. D., Indian Institute of Technology Madras, 2012, both in Aerospace Engineering. Before joining IIT Kanpur, he worked in the Department of Helicopters, German Aerospace Center, Goettingen as an Alexander von Humboldt Postdoctoral fellow. His areas of interests are mechanism of dynamic stall in rotorcrafts, fundamentals of thermoacoustic interaction, application of dynamical systems' theory to thermo-fluid systems, optical flow diagnostics (TSP, PIV and high speed imaging) and acoustic measurements.

Title: Unsteady Motions in Vortex Shedding Combustors a Dynamical Systems' Perspective

Abstract:

Vortex formation and its subsequent separation occurs in the flame holders of gas turbine/ramjet combustors. Their separation and breakdown are an important source of unsteady heat release rate fluctuations in these systems. The coupling between the acoustic field and the energy released by vortex breakdown can cause combustion instability. The objective of this presentation is to perform stability analyses of this thermoacoustic interactions where vortex breakdown is the dominant cause of heat release rate fluctuations. The dynamics of the system is modelled as a kicked oscillator, where the energy released by vortex breakdown is represented as the kick. Assuming small fluctuations, periodic and low values of kick, a Poincaré map is derived analytically. The stability of the system is determined from the eigenvalues associated with the Poincaré map. The results allow us to identify the region where vortex shedding or the acoustic mode is dominant. Our experimental investigations report the transition between the two modes for variation in the flow Mach number. Similar transitions are observed in the present study.

Prof. Nachiketa Tiwari

Department of Mechanical Engineering
Indian Institute of Technology Kanpur
Kanpur, India
ntiwari@iitk.ac.in

Biography:

Prof. Nachiketa Tiwari is Currently Associate Professor in Department of Mechanical Engineering at India Institute of Technology Kapur, India.

Title: Diesel Locomotive Noise: Sources, Reduction Strategies, Measurement Methods and Standards

Abstract:

Diesel locomotives are the mainstay of modern railway systems. This is despite the fact that they are noisy and polluting. As most railway networks cut across densely populated areas, noise there is a strong need to reduce diesel locomotive noise to a minimum. Through this paper, the author analyzes different sources of locomotive noise. For this, the paper starts with a brief description of working of a typical diesel locomotive. This is followed up by a description of principal sources of locomotive noise. Such a description will aid the reader qualify the nature of each noise component from standpoints of magnitude and frequency spectrum. Next an approach to develop noise reduction strategy for diesel locomotives is offered. In this context a diverse suite of noise reduction methods have been described. These methods can be active or passive. A large number of passive methods are described in this context. This is followed up with an overview of important regulations related to locomotive noise. Finally, an exhaustive list of appropriate international standards is provided. These references will be useful to all those involved with reduction of train and locomotive noise.

Dr. Santanu De

Department of Mechanical Engineering
Indian Institute of Technology Kanpur
Kanpur, India
sde@iitk.ac.in

Biography:

Santanu De is an Assistant Professor in the Mechanical Engineering, IIT Kanpur, where he has been since December 2014. He received a Bachelor of Engineering from the North Bengal University in 2002, and an M.Tech. from IIT Kanpur in 2004, both in Mechanical Engineering. He received his Ph.D. in Aerospace Engineering from the Indian Institute of Science, Bangalore in 2012. Prior to his joining at IIT Kanpur, he ser   ved two years at the Michigan Technological University as a postdoctoral research associate, and one year at the Institute of Combustion Technology (ITV), University of Stuttgart. He also worked as a scientist at the Liquid Propulsion Systems Center, Indian Space Research Organization between years 2004 and 2005. His primary area of research is modeling of turbulent combustion, turbulent spray atomization and coal gasification. During his doctoral and postdoctoral research, he developed RANS and LES based approaches, where different state-of-the-art gas-phase combustion models were extended to turbulent reacting sprays.

Title: Modeling of turbulent spray combustion using conditional moment closure method

Abstract:

Turbulent jet diffusion flames of fuel/air mixture stabilized in a vitiated co-flow of hot combustion products has been investigated using Reynolds-averaged Navier-Stokes (RANS) based multiple mapping conditioning (MMC) method. The flame base is stabilized at a distance from the nozzle-exit, which is referred as lift-off height. The lifted flames are very sensitive to the change in the inlet conditions of the velocity/ scalars. Most of the numerical models for turbulent combustion available in the literature could not adequately capture the trend of lift-off height against the coflow temperature. Numerical results from two different lifted flames will be presented. Stochastic formulation of MMC has been used, where a mapping function is used to represent the cumulative probability distribution of the mixture fraction for non-premixed combustion. The Curl's mixing model, originally developed for the conventional PDF method has been adapted for the MMC approach. It is found that the results from the present numerical simulations give an accurate prediction of the trend observed in experiments.

Dr. Anirudh Gautam

Ministry of Railways, India
Gautam.anirudh@gmail.com

Biography:

Dr. Anirudh Gautam works with the Indian Railway Service of Mechanical Engineers. He holds degrees in Mechanical and Electrical engineering from SCRA scheme of Jamalpur, a Master's in Quality Management from BITS Pilani, and a Masters in Engineering in Engine Design from University of Wisconsin, Madison. He has served in various roles in the Indian Railways. He later worked at Diesel Locomotive Works including engine manufacturing, engine design and transfer of technology. He built India's first 4000 hp diesel locomotive indigenously under ToT with EMD, General Motors, USA, for which he was awarded a national award by the Railway Minister. He has successfully completed various R&D projects at Engine Development Directorate, RDSO. He completed his PhD from IIT Kanpur in 2013. He is presently on deputation to RITES as Group General Manager Rolling Stock Design.

Title: Design and Development of Common Rail Electronic Direct Fuel Injection for Diesel Locomotives of Indian Railways

Abstract:

Indian Railways hold a large fleet of diesel locomotives nearly 5000 in number consuming about 6 billion litres of diesel fuel per year with an annual expenditure of about Rs. 20000 Crore. These locomotives are equipped with mechanical fuel injection systems and therefore emit comparatively large amount of harmful pollutants in the atmosphere. Use of electronic fuel injection system using common rail systems and electronic fuel injectors has been used to reduce fuel consumption as well emission of harmful pollutants from diesel engines. This has resulted in Europe, a most environmentally conscisous region of the world to move to about 55% diesel road vehicles equipped with common rail fuel systems and other associate arrangements. Large bore engines such as used in marine industry also have introduced electronic common rail fuel injection systems to meet the twin goals of fuel savings and prevention of environmental degradation. On the locomotives front, companies like General Electric Transportation of USA have introduced CReDI systems on their locomotives and is one of the reasons that these locomotive engines have been able to meet US EPA Tier 4 emission standards with in-cylinder combustion optimisation without resorting to after treatment devices. Electro-Motive diesels another locomotive manufacturer in USA is working on developing CReDI systems for their 2-stroke large bore locomotive engines. Companies like Cummins and CAT who also build high speed engines for use in locomotives have completely switched over to common rail systems in their family of engines more than five years back.

It was therefore in the propriety of approach for IR to consider design and development of CReDI systems for their large fleet of diesel locomotives. Accordingly a project was put on the anvil with above objectives in mind and one locomotive was converted to work on CReDI system. This required 1-D and 3-D thermodynamic and combustion modeling, evaluation of different options, experiments with few shortlisted designs on the research engine test bed at RDSO, optimisation and calibration and fitment of one diesel locomotive with CReDI kit and field trials. Due to seizure of the dynamometer on the research engine test bed, the engine optimisation including combustion chamber redesign and multiple fuel injection could not be completed. To save the loss of time, the CReDI kit was fitted on a locomotive was performance and emissions monitoring and for reliability verification testing. A fuel saving of about 3-4% has been observed even on the non-optimised CReDI locomotive engine, significant decrease in the smoke opacity levels and enhanced transient response of the locomotive to engine notch changes. This paper discusses the efforts made, results obtained and pending works to be carried in complete optimisation of the locomotive engine. Recommendations for future actions are delineated towards the end.

Prof. P.A. Laxmi Narayana

Simpson India Pvt. Ltd, Chennai, India

Biography:

P. A. Lakshminarayanan (born 1950) studied at Indian Institute of Technology for his B. Tech, MS and PhD degrees. He served at Loughborough University of Technology and Kirloskar Oil Engines Ltd. for 5 and 20 years respectively, before moving to Ashok Leyland in 2002 to Head the Engine R&D at Hosur for nine years. He was the Chief Technical Officer at Simpson and Co., Chennai till 2016 and now he is a Technical Adviser to Simpsons.

With his teams, he has developed more than eight diesel and CNG engine platforms and 150 types highly successful commercially for the efficiency and cost effectiveness. Two engines received prizes from the Institute of Directors (India). He has authored 54 research papers in journals and conferences of international repute. Four of them received the prizes for integrity and quality of the contents from the SAE (intl.), Combustion Society (India) and AVL (Graz and Pune) in 1983, 1993, 2005 and 2010 respectively. He has co-authored a book on "Modeling Diesel Combustion" published by Springer Verlag in 2010. His next book "Critical Component wear of parts in heavy duty engines" was published in 2011 by John Wiley. He is a fellow of SAE and a fellow of the Indian National Academy of Engineering.

Title: MPFI and SPFI CNG engine design and development

Abstract:

Of many fuels alternative to diesel in high power heavy duty application, compressed natural gas, CNG is probably the most important in terms of availability, cost and ability to adapt to the reciprocating engines. Like diesel and petrol engines, emission standards drive the design and development of new CNG engines. Early engines were carbureted and held sway for a few decades. These were stoichiometric, but the severe excursion, during operation, from the exact stoichiometry resulted in emissions that are not commensurate with the new and future norms; also, the catalyst in the exhaust suffered reduced life when the hydrocarbons emitted during transient operation, released large heat of combustion damaging the catalyst. Timing of ignition was mechanical and ignition coil of relatively low ignition voltage limited the scope to run the engines at high compression ratio without knocking and efficiency suffered.

The single point fuel injection, SPFI is a scaled down version of the MPFI engine. It is more cost effective and works eminently for turbocharged and after cooled genset engines where the load and speed fluctuations are relatively milder and for naturally aspirated CNG engines. Two injectors are placed in a block instead of six in the ports of a six cylinder MPFI engine, and the gas is lead to the manifold. The injectors open simultaneously without any serious phase relationship with the engine cycle. The airflow is computed by a model based on the instantaneous temperature and pressure avoiding the expense of air mass flow meter.

The cost effective SPFI engine is attractive to the customers by virtue of its simplicity, performance and efficiency; the life of the catalyst is many times better than in case of carbureted engines it replaced, and is comparable to that of the MPFI engine.

Dr. Tarun Gupta

Department of Civil Engineering,
IIT Kanpur
tarun@iitk.ac.in; tarunelectric@gmail.com

Biography:

He is Teaching and doing research at IIT Kanpur since june, 2006. Graduated 6 PhD and 31 M.Tech. students. Has published more than 80 articles in ISI indexed journals and filed 3 applications for Indian Patent. A submicron aerosol sampler designed, developed and evaluated at IIT Kanpur has been commercialized by Envirotech (Delhi). Has developed several low flow rate as well as high flow rate impaction based samplers and a non-selective membrane based diffusion denuder.

Title: Lab Development and Field Evaluation of a High Volume Fine Particle Inertial Impaction Based Aerosol Sampler

Abstract:

Air pollution has now caught attention of everyone as it has become one of the top challenges for both urban and rural residents within our country. This study describes the retrofitting of an existing high volume PM10 device with a slit based inertial impactor to convert it into an efficient high volume PM2.5 sampler with minimum physical changes to the whole system. Lab experiments were carried out on different slit-based nozzle impactors using polydisperse test aerosol. The optimized slit nozzle-based impactor configuration selected after a set of parametric investigations had a cutoff size of 2.51 µm (aerodynamic diameter) at an operating flow rate of 215 LPM (medium flow) with a pressure drop of 0.35 kPa across the impactor stage. The length of the slit of this optimum medium flow impactor was extrapolated to a flow rate of 950 LPM to obtain the high volume multiple slit nozzle-based PM2.5 inertial impactor assembly. This novel impactor assembly was fabricated from brass and chrome-plated and then retrofitted in a high volume dust sampler downstream of the PM10 cyclone separator. High vacuum silicone grease was used as the impaction substrate. A field study was performed with co-located operation of this high volume impactor assembly and a previously well-established single stage low flow rate PM2.5 sampler. The results will be presented from this work.

Prof. Achintya Mukhopadhyay

Department of Mechanical Engineering
Jadavpur University Kolkata 700032 India
Achintya.mukho@gmail.com

Biography:

Dr. Achintya Mukhopadhyay is a Professor of Mechanical Engineering at Jadavpur University, Kolkata (Calcutta), India. He also served as Professor of Mechanical Engineering at Indian Institute of Technology Madras and held visiting positions at Technical University of Munich where he was an Alexander von Humboldt Fellow and University of Illinois at Chicago. He obtained his Bachelors, Masters and doctoral degrees from Jadavpur University, Indian Institute of Science, Bangalore and Jadavpur University, all in Mechanical Engineering. His major research interests are chemically reacting flows, multiphase flow and heat transfer and microscale flow and heat transfer. His current research activities include droplet and spray combustion, structure and dynamics of partially premixed flames, nonlinear dynamics and chaos in combustion and thermal systems, instability of liquid sheets and atomization, spray impingement heat transfer and electrokinetic and thermomagnetic microscale flows. Dr. Mukhopadhyay has over 250 research publications including 90 international journal publications and has advised a number of masters and doctoral thesis. He has also served as reviewer of a number of international journals. Dr. Mukhopadhyay is a Fellow of the West Bengal Academy of Science and Technology and life member of Indian Society of Heat and Mass Transfer, Indian section of the Combustion Institute and International Society for Energy, Environment and Sustainability.

Title: Characterization of Single Phase Natural Circulation Loops using Dynamical Systems Approach

Abstract:

Natural circulation loops find applications in a large variety of energy conversion applications spanning a wide range of scales. They include thermal and nuclear power plants, process industries, geothermal systems, gas turbine blade cooling and microscale devices like microelectronic systems. They are preferred in such applications due to their high reliability being passive in nature. In many situations, single phase loops are over preferred over phase changing loops owing to better stability. However, even for single phase systems, spontaneous dynamics of the system is crucial for the desired performance of the system. This calls for systematic characterization of the dynamics of the device for proper design and control. Due to high level of nonlinearity of the system, traditional analysis tools like FFT often prove to be inadequate for the dynamic characterization. On the other hand, dynamical systems approach provides one with tools that are suitable for such analysis. In the present work, dynamics of a square single phase natural circulation loop has been investigated using a transient model, validated with in-house experiments, that considers variations only along the flow direction. The system, which shows steady, periodic and Lorentz-like chaotic behaviour has been characterized in terms of correlation dimension and Lyapunov exponent to confirm chaotic behaviour. In addition, the dynamics of the system has been described using recurrence plots and complex networks.

Dr. Nitin Labhsetwar

Professor AcSIR and
CSIR-National Environmental Engineering Research Institute, Nehru
Marg, Nagpur-440020, India
nk_labhsetwar@neeri.res.innklneeri@gmail.com

Biography:

Dr. Nitin Labhsetwar is a Ph.D. in Chemistry with 30 years of research experience in environmental and energy related research. He has worked as STA/JSPS Fellow and Visiting Overseas Researcher at NIMS, Tsukuba, Japan and as a Visiting Professor at Kyushu University, Japan under the Global COE programme. He has also worked at other International Laboratories on development of materials including low cost and nano-materials for control of vehicular emissions, photocatalysis, GHG emissions, methane combustion water treatment, cleaner energy generation, chemical looping combustion etc. He has over 150 research publications with over 3000 citations and 22 international patents in addition to a few contributions in books. He has received 9 awards for excellence in research and also received various fellowships in India and abroad. He is a reviewer for more than ten SCI journals and supervised PhD of 15 students. He is currently involved in more than 12 R&D projects.

Title: Mixed Oxides as Efficient Oxygen Carriers for Chemical Looping Combustion Technologies

Abstract:

Increasing energy demand and availability of coal and other biomass based fuels suggest that the CO_2 emissions will remain as a challenge in near future unless carbon capture and sequestration technologies become a reality at a larger scale. While several advancements are recently reported for sequestration of CO_2, it's efficient and low-cost capture still remain a challenge to make the sequestration feasible. Relatively new but one such potential option for CO_2 capture is Chemical Looping Combustion (CLC) process. Instead of air or oxygen, a metal oxide is utilized for providing the sufficient amount of oxygen, needed for the combustion of fuel. Therefore, the off-gases will consist of only CO_2 and water from which, CO_2 can be easily separated. It was initially explored to increase the thermal efficiency of the combustion process but later it was mainly being considered to separate CO_2.

Oxygen carrier is important for the success of CLC process and therefore extensive efforts are being focused in this direction. We are among the first to report the possibility of using mixed oxides for CLC applications with certain advantages. We have synthesized pure phases of mixed metal oxides of Cu and Mn as well as Fe and Mn as low-cost, environmentally benign new generation of oxygen carriers. These show potential as alternatives to the currently available supported metal oxides based oxygen carriers for CLC application. The synthesized oxygen carriers were evaluated for CLC performance using a steady state, fixed bed evaluation assembly under different experimental conditions of temperature, feed composition and feed flow. $FeMnO_3$ showed stable multi-cycle CLC performance for methane combustion and CO_2-selectivity than that of its counter parts single metal oxides.[1] Similarly, multi-cycle methane CLC performance and the product selectivity towards CO_2 formation were obtained using $CuMn_2O_4$.[2] It was found that MnO provides the structural stability for the mixed oxides, which aids the regeneration upon oxidation in air for multi-cycle performance. These materials could be potential candidates for practical CLC applications and therefore deserve further exploration.

Prof. V. Ganesan

Former Professor (Retd.), Internal Combustion Engines Laboratory,
Department of Mechanical Engineering,
Indian Institute of Technology Madras, Chennai – 600 036, Tamil
Nadu, India
Vganeshan.iitm@gmail.com

Biography:

Dr. V Ganesan, Professor Emeritus, Department of Mechanical Engineering IIT Madras has published more than 350 research papers in national and international journals and conferences and has guided 20 M.S/ and 40 Ph.Ds. He has authored a very popular book on 'Internal Combustion Engines' and several other books on 'Gas Turbines, Computer Simulation of 4-stroke SI Engines, Computer Simulation of 4-stroke CI Engines'.

Title: Mahua Biodiesel in a Single Cylinder Diesel Engine for Sustainable Irrigation Operation in India an Experimental Study

Abstract:

This paper reports the experimental results of a single cylinder diesel engine regarding performance, combustion and emission characteristics using Madhuca Indica (Mahua) biodiesel and its blends in different proportions with petro-diesel. Compared to other seeds Madhuca Indica is largely available in India. It is the most suitable candidate for agricultural operation. The main drawback of biodiesel is that it has more NOx emissions. However, it is a blessing in disguise because of the fact that for agricultural operations we use urea. NOx emissions can be considerably controlled with ad blue (Urea) solution. Therefore, an experimental study has been carried out to evaluate the effect of SCR technique in reducing NOx. The thermo-physical properties of various blends selected for investigation have been experimentally measured for evaluation of the performance characteristics of the diesel engine. Tests have been carried out on a four stroke tangentially vertical (TV) single cylinder diesel engine at 1500 rpm using an eddy current dynamometer. This type of engine is normally used for irrigation operation in India. The nozzle opening pressure of 250 bar with constant static injection timing 20° bTDC is employed. Results with SCR are compared at full load under steady condition with conventional engine where no reduction technique is used. The comparison indicates that the SCR gives significant reduction in oxides of nitrogen as compared to without employing SCR technique. For B100 with SCR technique, the percentage reduction in NOx is found to be around 22.13% as compared to conventional engine. As already stated this research has been carried out keeping in mind the energy consumption by pumps coupled to diesel engines for irrigation purposes in developing countries.

Dr. Rajeev K. Sukumaran

Head, Biofuels and Biorefineries Section
Activity Lead, Centre for Biofuels
CSIR-National Institute for Interdisciplinary Science and Technology
Industrial Estate P.O., Pappanamcode
Thiruvananthapuram-695019, India
rajvaryaveedu@gmail.com

Biography:

Dr. Rajeev Sukumaran is a senior scientist at the CSIR-National Institute for Interdisciplinary Science and Technology (CSIR-NIIST), in Trivandrum, India. Currently he is the Head of Biofuels and Biorefineries Section, of the Microbial Processes and Technology Division of CSIR- NIIST. He did his Masters and PhD in Biotechnology from Cochin University of Science and Technology, Kochi, India (1993-2000). He had a short stint in industry where he worked as technical member of Bigtec Pvt Ltd, Bangalore, where he additionally served as consultant to the United Breweries Group R&D. He then did postdoctoral trainings in molecular immunology and Stem Cell Biology at the Mount Sinai School of Medicine, New York, USA and National University Hospital, Singapore respectively before joining CSIR in November 2004. Since then, he has been working on enzymes for biomass conversion and lignocellulosic ethanol.

He played a leading role in setting up the CBF's lignocellulosic ethanol pilot plant, and the solid state enzyme production pilot plant at NIIST. His current research interests include-Developing enzymes for biomass conversion, Glucose tolerant β-glucosidases, heterologous protein expression in fungi, and fungal genomics. He has served as consultant for the International Energy Agency, France, and for some leading Biotech companies in India. He has a total of 75 publications in International Journals, about 100 conference papers besides several book chapters and reports.

Title: Challenges in the development of enzymes for biomass hydrolysis

Abstract:
Plant Biomass is the most abundant renewable resource and probably the near term feedstock for meeting energy requirements of the world, especially for the liquid transportation fuels. Bioethanol is currently the most used renewable liquid transportation fuel by volume and technologies for its production from lignocellulosic biomass are rapidly evolving and becoming attractive commercially as well. The key to biomass conversion to ethanol is its hydrolysis to sugars, mediated by lignocellulose hydrolysing enzymes. Cellulose and hemicellulose hydrolysing enzymes have been identified as the major contributors to the cost of bioethanol and efforts are underway in different laboratories and companies across the world to bring down the cost of these enzymes, despite the fact that there is commercial biomass hydrolysing enzymes available in the market. The major reason for this is the narrow margins of profit in bioethanol industry due to the high cost of enzymes and the need to have different enzyme cocktails for different biomass types. Most of the current commercial cellulases are sourced from the filamentous fungus – Trichoderma reesei RUT C30, though the fungus is known to have lesser expression of β-glucosidase (BGL) the rate limiting enzyme in cellulose digestion cascade. Also this enzyme is inhibited by its product glucose, making it difficult to attaining high sugar concentrations and hence high ethanol yield. Most of the commercial blends therefore contain heterogeneous BGL added into them. The challenges in enzyme development for biomass hydrolysis include the attainment of cost efficiency, higher specific activity, improved yields, storage and thermal stability in addition to be able to achieve high turnovers in minimal time. These challenges are discussed in the context of biomass hydrolysis and the multiple approaches followed to reduce the production cost of cellulases and improving their efficiency are described. The efforts are CSIR-NIIST – Centre for Biofuels are elaborated and our work on cellulases and beta glucosidases are discussed in detail. Strategies for reducing production cost and developing effective enzyme cocktails are discussed and case studies on cocktail development to improve biomass hydrolytic efficiency are presented.

Prof. Amitava Datta

Department of Power Engineering,
Jadavpur University
Salt Lake Campus, Kolkata 700098, India
Amdatta_JU@yahoo.com

Biography:

Dr. Amitava Datta did his graduation from Jadavpur University and completed his PhD from IIT, Kharagpur. He received the Alexander von Humboldt Foundation Fellowship in the year 2000. His research interests are in the areas of combustion, atomization, energy, thermodynamic analysis, and application of CFD in aerodynamic and microfluidic applications. He has published more than 80 publications in International journals and guided 12 PhD theses in his area of research. Dr. Datta is attached to the Power Engineering Department of Jadavpur University for more than 26 years and is presently a Professor in the department. He has been involved in several sponsored research projects in the capacity of Principal Investigator and Co-Investigator and was a nodal person in the World Bank sponsored TEQIP (Ph I) in his University. He is presently the Head of the Department of Power Engineering and the Director of Internal Quality Assurance Cell (IQAC) of Jadavpur University.

Title: Combustion Characteristics of Biomass-based Fuels for Engine Applications

Abstract:

Internal combustion engines are widely used in different applications and petroleum based liquid fuels are used in these engines. However, petroleum is the least abundant of all fossil fuels and its combustion in large quantities adversely affects the environment and harms public health. Biomass fuels are organic materials produced in renewable manner and can replace the conventional petro-fuels in engines. Both liquid and gaseous secondary fuels can be derived from biomass through different processes for use in the engines.

The use of syngas in spark ignition engines has been studied in the literature. Even their limited use as a blend to conventional fuels can reduce the dependence on petroleum based fuels. It has been found that the blending of syngas augments the laminar burning velocity of isooctane due to increase of the thermal diffusivity of the reactant mixture and alteration in the chemistry of the flame reactions. A mixture of 30% isooctane/70% syngas is found to have the laminar burning velocity and the ignition delay time very close to those corresponding to pure isooctane. Exhaust gas recirculation is a technique employed in S.I. engines to increase the part load efficiency and for knock-minimization. It is seen that the reduction in laminar burning velocity due to the dilution by the recirculated exhaust gas can be compensated by an increase in the unburnt gas temperature. The effect of the exhaust gas dilution on the ignition delay time of 30% isooctane/70% syngas-air mixture has been found to be negligible.

Biodiesels can be used as alternative fuels in compression ignition engines. An experimental study determining the burning characteristics of diesel and biodiesel in a porous sphere experimental set up show that the burning rate of diesel exceeds that of biodiesel due to the higher evaporation rate of the former. Both the biodiesel and diesel flames show high luminosity indicating the presence of soot in them. However, presence of oxygen in biodiesel delays the formation of soot and the evidence of the particulates is only found after sufficient residence time is elapsed in the flame. The transition velocity from envelope to wake flame shows that the chemical reaction rate of biodiesel can be more than that of diesel.

Prof. B. S. Chadha

Head Department of Microbiology
Guru Nanak Dev University
Amritsar- 143005 (India)
Ph: +91-183-2258802-09 Extn. 3317 (office)
chadhabs@yahoo.com

Biography:

B S Chadha is professor at Department of Microbiology, Guru Nanak Dev University, Amritsar. His major area of research is on Industrial microbiology and fungal biotechnology. The current areas of research includes, Molecular characterization of diverse thermophilic fungi and endophytes in different ecosystems and their biotechnological potential, bioprospecting of microbial diversity for industrially important enzymes and bioactive molecules (statins, anti-cancer, anti-microbial agents, etc). Biotechnological approaches for strain improvement of thermophilic fungi for amylases, cellulases xylanases and phytase production using classical, proteome based and molecular genetic approaches. He has guided 17 PhD students and is in active research collaboration with Piramal Life Sciences, Mumbai through DBT sponsored mission mode mega project and has a joint US patent with the industry. He has handled/handling various projects sponsored by DBT, ICAR, CSIR, UGC in the area of Industrial biotechnology. He has 90publications in high impact peer reviewed international journals to his credit. His work has 1600 citations with h index of 23. He has delivered lectures at various International conferences/universities in Australia, Canada and USA.

Title: Thermophilic Fungus Malbranchea Cinnamomea as Source of Catalytically Active Glycosyl Hydrolases for Bioconversion of Lignocellulosics

Abstract:

This study reports thermophilic fungus Malbranchea cinnamomea as an important source of lignocellulolytic enzymes. The secretome analysis using LC–MS/MS orbitrap showed that fungus produced a spectrum of glycosyl hydrolases (20ellulose/20ellulose20ose), polysaccharide lyases (PL) and carbohydrate esterases (CE) in addition to cellobiose dehydrogenase (CDH) indicating the presence of functional classical and oxidative cellulolytic mechanisms. The secretome was represented by GH1, GH2, GH3, GH5, GH6, GH7, GH10, GH18, GH20, GH35, GH47, GH55, GH67, GH81, GH92 and GH125 family members of cellulases/ hemicellulases showing that culture produced a suite of enzymes for effective cellulose degradation. The presence of carbohydrate esterases (CE1, CE5, CE10, CE12 and CE15) showed the secretome was efficient in degradation of ester linked substituents in hemicelluloses. The secretome showed that cellobiose dehydrogenase (AA8), endoglucanse (GH7), beta- glucosidase (GH3) were the most represented cellulolytic proteins as indicated by high peptide spectrum match (PSM) score. The protein fractions in the secretome resolved by ion exchange chromatography were analyzed for ability to hydrolyze alkali treated carrot grass (ATCG) in the presence of Mn^{2+}/Cu^{2+}. This strategy in tandem with peptide mass fingerprinting led to identification of metal dependent protein hydrolases with no apparent hydrolytic activity, however, showed 5.7 folds higher saccharification in presence of Mn^{2+}. Furthermore, adding different protein fractions to commercial 20ellulose (Novozymes: Cellic Ctec2) resulted in enhanced hydrolysis of ATCG ranging between 1.57and 3.43 folds indicating the enzymes from M. cinnamomea as catalytically efficient. Addition of xylanase (300 U/g substrate) during saccharification (at 15 % substrate loading) of different pretreated (acid/alkali) substrates (cotton stalks, wheat straw, rice straw, carrot grass) by commercial 20ellulose (NS28066) resulted in 9–36 % increase in saccharification and subsequent fermentation to ethanol when compared to experiment with commercial enzyme only. High ethanol level 46 (g/l) was achieved with acid pretreated cotton stalk when Malbranchea crude xylanase was supplemented as compared to 39 (g/l) achived with commercial enzyme alone. Genes coding for xylanases (GH10 and GH11) from thermophilic fungus Malbranchea cinnamomea were cloned (McXGH11 and McXGH10) and expressed in Pichia pastoris as host. The observed xylanase activity of McXGH11 (571.98 U/ml) is 7.73 folds higher when compared to wild type strain Malbranchea cinnamomea (73.91 U/ml) that produces multiple xylanases. McXGH11 was purified and found to be highly thermostable at 70°C and catalytically efficient against variety of substituted (arabinoxylan) and non-substituted (beechwood and birchwood) xylans. Higher saccharification (1.8 and 2.05 folds) of alkali treated rice straw and alkali treated bagasse was observed using enzyme cocktail comprising of McXGH11 and CellicCTec2 (2:8 ratio) when compared to cellicCTec2 alone at same protein loading rate of 5.7 mg/g biomass. Thermostable xylanases from M. cinnamomea demonstrated immense potential as accessory enzymes for reducing the cost of enzymes appreciably thus useful in developing economically viable 2G ethanol technology.

Dr. Dhananjay Kumar Srivastava

Department of Mechanical Engineering
Indian Institute of Technology
Kharagpur, India
Dhananjay.srivastava@gmail.com

Biography:

Dr. Dhananjay Kumar Srivastava is currently working as Assistant Professor of Mechanical engineering at Indian Institute of Technology Kharagpur since April 2015. Dr. Srivastava has done Doctor of Philosophy from Engine Research Laboratory of IIT Kanpur in 2013. He was a Research Fellow to University of Birmingham, UK in 2014. He was also a visiting researcher to University of Vienna, Austria in 2004. His areas of expertise include laser ignition of engine, combustion visualization, emission control, engine calibration, gasoline direct injection etc. Dr. Srivastava is recipient of Gandhian Young Technological Innovation award in March 2013, Pool Scientist Fellowship by CSIR, India from 2010-2013.

Title: Laser Ignition of Engine

Abstract:

Ignition system of a spark ignition engine is responsible to initiate the combustion of fuel-air mixture inside the combustion chamber. The ignition system must generate adequately high-voltage to generate the spark between the spark plug electrodes. Over the years, spark ignition system has changed but the basic principle remains more or less same in all types of ignition systems. Development of electronic controls to trigger ignition and use of distributor-less ignition system has made them more effective and reliable. However, ignition systems pose limitations for the future development of the SI engines. Stringent exhaust emissions norms and demand for high thermal efficiency can be met by ignition of lean fuel-air mixtures. However lean combustion is associated with slower flame propagation speeds, and reduced power output. Engine power output can be improved by increasing initial in-cylinder pressure using turbo charging. An increase in the in-cylinder pressure keeping the same spark plug electrode distance would require increased secondary coil voltage, which would lead to severe erosion of electrodes over time. Flame propagation speed in lean fuel-air mixtures can be increased either by optimizing the position of ignition spot inside the combustion chamber or by multi-point ignition. However ignition spot always remains close to the top of the combustion chamber in a conventional SI engine and cannot be varied too much from this location. These limitations of conventional ignition system can be overcome by a durable high-energy, electrode-less ignition system, which also has flexibility in terms of spark location, such as laser ignition system.

Short laser pulses of few nanoseconds pulse duration, delivered by a Q-switched laser are focused by a lens system inside the combustion chamber containing combustible mixture. If the peak intensity in the focal region exceeds certain threshold intensity, breakdown of the medium occur leading to formation of a plasma spark. If the energy content of the spark is high enough, the mixture ignition take place. The objective of this talk is to give overview of research going on in the area of laser ignition worldwide.

Dr. Reeta Rani Singhania

DBT-IOC Advanced Bio-Energy Research Centre, Indian Oil Corporation;
R&D Centre, Sector-13, Faridabad-121007, India
reetasinghania@gmail.com

Biography:

Dr. Reeta Rani Singhania has been working in Bioenergy since last 13 years. She has been involved actively in research on cellulase production from filamentous fungi for bioethanol applications. She has 30 publications in peer reviewed national and international journals and 22 book chapters along with several conference communications to her credit. She is the recipient of Elsevier best paper award in 2007, AuCBT/Excellence award of BRSI in 2008 and IFIBiop Young Scientist award for the year 2013. She has more than 2900 citations and h index 20. She has been the guest editor of special issue of Renewable Energy and Bioresource Technology. She has received prestigious 'DBT- Energy Bioscience Overseas Fellowship' by DBT to work on Bioenergy in India.

She is presently working in Indian Oil Corporation Limited R&D, Faridabad, as DBT- Energy Bioscience Overseas Fellow on 'Cellulase production and its scale-up for bioethanol applications.

Title: Cellulase Production for Second Generation Bioethanol Production

Abstract:

Economic and sustainable production of bio-ethanol from biomass through enzymatic route depends on economics of cellulase availability, which is the key factor for the success of technology. It's the time to realize the dream of cellulosic ethanol in our country. Several bioethanol set-ups are coming up at pilot scale level and commercial plants are also being realized sooner but all of them are presently dependent on 'Enzyme giants' for cellulases which exerts future risks. DBT-IOC center has been actively involved in cellulosic ethanol research with commendable outputs. It has been realized that the bottleneck of the technology lies in obtaining highly efficient cellulase which could result in an economically feasible technology. In our study we have employed filamentous fungi for cellulase production at 3L bioreactor scale. In cellulase production Penicillium sp. is giving tough competition to ever winning Trichoderma sp. in lieu of the efficiency of its generated cellulase cocktail as per literature. Optimization of nutritional and physical parameters exerts positive impact on cellulase production in shake-flask level, however several challenges needs to be overcome while shifting studies to bioreactor. Some of the challenges and the future perspectives will be discussed.

Dr. Baskar Gurunthan

Department of Biotechnology,
St. Joseph's College of Engineering, Chennai – 600 119. India
basg2004@gmail.com

Biography:

Dr. Baskar Gurunthan has started his career as lecturer in chemical engineering and promoted to the level of professor of biotechnology through his 16 years of teaching and research experience. He has published more than 85 research and review articles in national and international journals, presented more than 100 research papers in national and international forum and published five chapters in books. His current research expertise in biofuels, therapeutic proteins, microbial enzymes, nanomedicine and nanocatalysis clearly indicates his thirst towards research and development in multidisciplinary areas. Besides research interests he has shaped himself as a dedicated academician. His research publications have got h-index of 13 and i10 index of 15. Currently 8 Ph.D research scholars are under his guidance in the area of biotechnology. He is an active life member of various professional bodies to keep abreast of latest trends and developments.

Title: Nano-composites as modern heterogeneous catalyst for biodiesel production

Abstract:

The use of heterogeneous catalyst is promising to reduce the present high production cost of biodiesel, making it competitive with petroleum based diesel fuels. Recently, heterogeneous catalysts derived from nanomaterials have attracted biofuel researchers for biodiesel production. Nanocatalyst characteristics, such as high catalytic activities and high specific surface area have helped overcome some limitations on heterogeneous catalysts for their applications in biodiesel production. Thus the present study discusses the latest advances in research and development related with heterogeneous nanocatalysts for produce biodiesel. The use of nanocatalysts such as ferrous doped zinc oxide nanocomposite, copper doped zinc oxide nanocomposite and manganese doped zinc oxide nanocomposite for biodiesel production were compared. Ferrous doped zinc oxide nanocatalysts produced by the co-precipitation method demonstrated an efficient catalytic activity for the transesterification of castor oil with methanol. AFM analysis of copper doped zinc oxide nanocomposite confirmed the porous and non-uniform surface of the nanocatalyst. This lead to the aggregation of copper doped zinc oxide nanocatalyst in the form of multi layered nanostructures. Stability and reusability of nanocatalyst is based on the presence of active sites. Copper doped zinc oxide nanocatalyst maintained the biodiesel yield till sixth cycles. Manganese doped zinc oxide heterogeneous nanocatalyst showed effective catalytic activity for the conversion of mahua oil into biodiesel through transesterification with methanol. Good catalytic activity of zinc Oxide was observed as a result of doping effect of manganese. Magnetic nanoparticles were functionalized by immobilizing lipase. Lipase immobilized magnetic nanocomposite was used for production of biodiesel from waste cooking oil.

Dr. Gabriel D. Roy

CPnE Consultants
9944 Great Oaks Way
Fairfax, VA 22030, USA
Phone: +1 571-418-9333
roygd@aol.com

Biography:

Gabriel D. Roy received his B.S and M.S degrees in Mechanical Engineering, and Ph.D. in Engineering Science. He served as a faculty member of the Mechanical Engineering Departments in Indian (University of Kerala) and U.S. (University of Tennessee, California State University) universities. He served as major thesis advisor for over a dozen graduate students. During his early career as Senior Research Engineer at the University of Tennessee Space Institute (UTSI), he developed the MHD diffuser and heat transfer diagnostics for hostile environments. During his industry career at TRW Inc. (presently Northrup - Grummen), he received the TRW Roll of Honor Award and patents on combustor and atomizer. During his position as Program Manager for Energy Conversion and Advanced Propulsion for the U.S. Navy at the Office of Naval Research (ONR), he introduced new areas of research including, but not limited to strained high energy hydrocarbon fuels, MHD underwater propulsion, pulsed and continuous detonation engines, combustion control, high speed noise reduction, biofuels etc. He managed the Pulse Power Program for the Ballistic Missile Defense Organization.

Title: Sustainable Alternate Transportation Fuel Development for Kerala

Abstract:

Kerala has seen substantial economic growth, increase in property value and personal and family income in the past several decades. The affluence is changing the public transport-minded community to that of a self-transport community. As the number of automobiles on the roads of Kerala increases, so is the demand for petrol and diesel oil. Availability of these fuels at affordable prices cannot be taken for granted. Already the prices are going up and economic and political scenario in oil-producing countries can cause uncertainties in the market. So instead of depending on petroleum-based fuels, the time has come to invest in research and development of alternate fuels for transportation. The logical choice is biofuel. Though there have been some work in the past to develop fuels from cashew oil and other resources, a well-funded and focused R&D for biofuels is in order.

Although biodiesel can be produced from oil and seed plants, this should not be an option if these are edible products. The fuel industry should not compete with the food industry, in particular with the food that is consumed by the poor population. Kerala is endowed with a population of abundant intellect, skill and traditional and modern education. The combination of centuries-long knowledge and modern science and technology puts Kerala in a unique position in the pursuit of developing new avenues of research that will enable energy independence and affordability. The development of biofuel needs to be a multi-faceted operation involving infrastructure, education, research, pilot plants and large scale production. Major universities and colleges should have curriculum in biofuels starting from feedstock, conversion processes involved, fuel properties analysis, enhancement of energy content etc. Kerala has a coastal length of over 580 km. and biofuel based on algae will be a good choice. Research should focus on non-edible feedstock such as sugar cane and cashew wastes, cellulosic biomass etc. and cost-effective feed stock production from other materials via technological breakthroughs. High oil content nonedible plant stock should be carefully chosen due to the limited land area available for this purpose. Focus should be on novel techniques such as genetically altering the algae to increase the oil content and growth and bacterial intervention to improve the oil conversion process. Community education is a part of the effort to get the people understand the significance of this effort and to cooperate. "C cubed" formula – Contribute Collaborate Communicate – proposed by the author several decades ago applies. In addition to individual contributions in this pursuit, collaboration within India and with other countries, dissemination and acquiring of the knowledge base by attending technical conferences and organizing special focused conferences are essential. Formation of Indo-U.S. Advanced Bioenergy Consortium (Washington University in St. Louis) and IOC-Honeywell pact are good examples. The Asian countries have come a long way in biodiesel oil production with government mandates, financial support and community involvement. Kerala should take advantage of these examples.

Prof. Swarnendu Sen

Department of Mechanical Engineering
Jadavpur University, Kolkata
Sen.swarnendu@gmail.com

Biography:

Swarnendu Sen is a Professor of Mechanical Engineering in Jadavpur University. For last 27 years he is active in teaching and research. He did his bachelor and master degree in Mechanical Engineering from Jadavpur University. In 1996, he obtained his doctoral degree in engineering from Jadavpur University. He did his post-doctoral research in University of Illinois at Chicago, Virginia Tech and Technical University of Munich. He is a DAAD fellow and fellow of West Bengal Academy of Science and Technology. His area of interest is mainly heat transfer and reacting & multiphase flow. He has authored more than 150 research papers different journals and conferences. He is associated with a number of sponsored research projects, with different agencies like BARC, DRDO, GTRE, ISRO etc. He has guided a large number of master and PhD students. He is also associated with a few administrative positions of the University.

Title: Macroscopic Spray Characteristics of Ethanol Blended Kerosene and Diesel using a Hybrid Atomizer

Abstract:

The conventional fuels are associated with problems of air pollution and their prolonged use has caused the fuel reserves to get depleted gradually. Addition of ethanol in conventional fossil fuels leads to better spray characteristics and decreases air pollution as well.

The present work deals with the spray characteristics of pure kerosene, pure diesel, pure ethanol and ethanol blended kerosene and diesel (10 and 20 percent ethanol blended diesel and 10 and 20 percent ethanol blended kerosene by volume) by using a hybrid atomizer. The novelty of the hybrid atomizer lies in the fact that the fuel stream is sandwiched between two annular air streams and tangential inlets are used for both fuel and air. Here the inner air and outer air enters the same way although from opposite directions with respect to the fuel flow direction into the atomizer and a high swirling effect occurs outside the nozzle due to the tangential inlet of the flow direction. The flow rate of inner and outer air is varied continuously. Here back-light imaging technique is used for capturing the spray images. Various stages of spray like distorted pencil, onion, tulip and fully developed spray regimes have been observed. The breakup length, cone angle and sheet width of the fuel stream are analyzed directly from the images using Image J software for different fuel and air flow rates. From the image processing, it is observed that breakup occurs at an early stage for ethanol blended kerosene and diesel due to low viscosity of ethanol. It is also observed that at higher air flow rate breakup occurs at an early stage due to turbulent nature of the fuel stream.

Prof. Sunil K. Khare

Department of Chemistry
Indian Institute of Technology
New Delhi, India
skkhare@chemistry.iitd.ac.in

Biography:

Prof. Sunil K. Khare is presently working as Professor of Biochemistry at the Department of Chemistry, Indian Institute of Technology Delhi. He received his PhD from IIT Delhi, carried out Postdoctoral Research at National Food Research Institute, Tsukuba, Japan and has been DBT visiting scientist at Northern Regional Research Laboratory, Illinois USA. He has been working in the area of solvent-tolerant and halophilic class of extremophiles and their enzymes; especially understanding structural and molecular basis of their stability. The applications of these extremozymes in various biotechnological and industrial bioprocesses have far reaching implications. His current noteworthy contributions have been in differential proteomics of solvent-tolerant and halophilic class of extremophiles and deciphering nanotoxicity mechanisms in microbial systems. The work has led to 125 publications with high impact, 2 patents, 10 book chapters to his credit, besides large number of conference publications. A large number of culture deposits in Microbial Type Culture Collection, India and GenBank submissions to National Center for Biotechnology, USA have also been made. The h-index for his work is 30 with total of 3274 citations. He has guided 14 PhD and 38 master's students. Several awards have been conferred to him and noted amongst them are United Nations Amway award, Fellow United Nations University, Fellow International Forum on Industrial Bioprocesses, France, Fellow Biotech Research Society of India and Member National Academy of Science, India. He is General Secretary of The Biotech Research Society, India, Joint Secretary of Association of Microbiologists of India, member of many National committees and professional societies including DBT committees, DST task force, Academic council member of AMU, Central University of Haryana, IP University and visiting faculty for University of Blaise Pascal, France.

Title: Application of ionic liquids in biomass processing and enzymatic saccharification

Abstract:

The use of ionic liquids (ILs) in various chemical processes has increased significantly over the years due to their nature as the "green solvents" with highly advantageous properties like thermal and chemical stability, high polarity, and very low toxicity. Owing to their unique properties, there has been a great interest in the application of ILs for biomass hydrolysis, biotransformation reactions and stabilisation of proteins/enzymes.

Utilisation of lignocellulosic biomass as the most abundant renewable source of energy seems to be a feasible approach for biofuel production considering the depleting fossil fuel reserves. In order to generate biofuels or other value added products from lignocellulosic biomass, loosening of its rigid structure is a necessary pre-requisite. The recent methods advocate biomass pre-treatment by ILs as an efficient process in making the lignocellulose more accessible to enzymatic action.

While ILs are capable in loosening lignin-cellulose bonds during biomass pre-treatment, the high sensitivity and denaturation of lignocellulosic enzymes in their presence during subsequent saccharification remains a major bottleneck. Hence, there is a good need of ILs stable enzymes for cost effective lignocellulosic biomass utilisation. There is an increasing interest to isolate, screen or engineer such enzymes. ILs stable lignocellulolytic enzymes can be put together in one pot with ILs pre-treated biomass without being inhibited by them. This allows simultaneous pre-treatment and saccharification in one pot which will improve the economical feasibility of complete biomass utilisation process.

Dr. Arvind Kumar Bhatt

Department of Biotechnology,
Himachal Pradesh University,
Summerhill, Shimla-171005, HP, India

Biography:

Dr. Arvind Kumar Bhatt is presently serving as Professor of Biotechnology, Himachal Pradesh University, Shimla with major focus on Industrial Biotechnology. He has Academic background in Biological Sciences with outstanding achievements in Academics, R&D, Industry, fellowships and University Gold Medals. He is trained at GBF, Braunschweig-Germany and has worked with Dr. YS Parmar University UHF-Solan, Beck & Co., Bremen-Germany and has advised Himachal Government on various Biotechnology policy matters while heading Industrial Biotechnology Division for a decade. His areas of interest include Industrial Microbiology, Enzyme Technology, Biofuels, healthcare, traditional foods and Indigenous Knowledge. He is member of several scientific bodies, Editorial Board of Scientific Journals, scientific advisor to various Industries, >50 research papers to his credit, presented research papers in Conferences within India and abroad.

Title: Fuel from waste: A Scientific Solution for Waste Management and Environment Conservation

Abstract:

Waste management and energy crisis are the two biggest challenges before developing countries. However, if diagnosed and managed scientifically, these major problems can provide solution to each other. Poorly managed waste is not only engulfing our valuable land, polluting rivers and rivulets, attracting wild and stray animals but also deteriorating our environment in a number of ways. This problem can be solved by conversion of solid waste into bioenergy through anaerobic digestion (AD), a widespread technology for organic waste treatment and fuel production.

Most of the world's increasing energy demands are presently met by non-renewable sources such as coal, natural gas and oil. However, depleting resources, excessive use and limited availability have resulted in sharp rise in crude oil prices besides a major contributor of environment pollution. Gradual replacement of petroleum based fuels to secure future energy supplies continues to be a major concern world over. Scientific community as a result of tremendous efforts have suggested several options i.e. the first generation biofuels derived from sources like starch, sugar, animal fats and vegetable oil, second generation biofuels like cellulosic biofuels, biohydrogen, biomethanol, bioethanol, etc besides the third generation biofuels from oleaginous organisms.

Biofuels have emerged as a centerpiece of the international public policy debate. The increasing number of oil producing nations from 70 in 2007 to > 200 in 2016 indicates a transition in global biofuel production. The Major Economies Forum (MEF) countries have called for increased global R&D and demonstration towards doubling expenditures for low-carbon technologies by 2015. In India, the energy demand is increasing at a rate of 6.5 % per annum. There have been increased R & D efforts on the bioconversion of agricultural biomass into fuel. Since in the present context, it may not be wise to use agricultural crops or land for the cultivation of petro crops, therefore viable substitutes are required to be searched. Search for new alternative fuels including biofuels such as bioethanol, biobutanol and biodiesel is the only way to overcome the upcoming energy crisis which do not require fertile land and can be obtained from varied sources including waste. Solid waste is also one of the biggest challenges of the present time to promote eco-tourism especially in the Himalayan region. Utilizing waste for alternative fuels would not only provide supply on sustainable basis but would also be environment friendly. The selection of appropriate technology for production of biofuel calls for careful selection of techniques so as to produce high quality product with reduced environmental impact. Various aspects of waste utilization for clean renewable source of energy for sustainable development of the society will be discussed in the paper.

Dr. Thallada Bhaskar

Academy of Scientific and Industrial Research (AcSIR) CSIR-Indian
Institute of Petroleum, Dehradun
India
tbhashakar@iip.res.in

Biography:

Dr. Thallada Bhaskar, FBRS, FRSC, Principal Scientist, Head, Thermo-catalytic Processes Area & Associate Professor, Academy of Scientific and Industrial Research (AcSIR) CSIR-Indian Institute of Petroleum, Dehradun. Ph.D. (Heterogeneous Catalysis) from CSIR-Indian Institute of Chemical Technology (IICT), Hyderabad SCI Journal publications 120; Total citations ca. 2875; h-index -31; Book chapters-18; Patents-13 International and National Symposia/Conf presentations-300 Editorial Board Member - 5 International Journals (Bioresource Technology, Journal of Energy Institute, Journal of Material Cycles and Waste Management etc.

Editor- 2Books (published) 1. Advances in Thermochemical Conversion of Biomass & 2. Biomass and Biofuels: Advanced Biorefineries for Sustainable Production and Distribution; 2 Books on Bioenergy are In Press. Key Awards/Honours - Chinese Academy of Sciences (CAS) Presidents International Fellowship Initiative (2016); Fellow, Royal Society of Chemistry (2016); Scientist of the Year 2016 award from National Environmental Science Academy (NESA), India; Fellow, Biotech Research Society of India (2012); CSIR- Raman Research Fellow (2013); JSPS Visiting Scientist (2009), AIST Distinguished Researcher (2013), Most Progressive Researcher Award from FSRJ, Japan (2008), Japan Science and Technology (2000).

Title: Biomass Hybrid Conversion Pathways For Sustainable Bio-refinery

Abstract:

The reliability, affordability, and environmental impact of energy supplies have become the most critical issue for the world economy. Due to world population growth, primary energy consumption has increased and will continue to increase in the future. This energy pool is mostly fossil-carbon-based and is predominantly used for transportation and energy production purposes. As a result of this, oil price has increased, and has also affected other primary energy sources Prices. This situation, along with the need for reducing foreign oil dependency and the environmental awareness of world's population has led to a search for alternative primary energy and carbon sources based upon renewable sources. Biomass, especially lignocellulosic and aquatic material, represents an abundant renewable carbon source. This is potentially convertible to energy, fuels, and speciality chemicals. The integrated production of bioenergy, biofuels, and biochemicals, through advanced technological processes of separation and conversion that minimizes carbon cycle impact, defines the biorefinery concept. The term "biorefinery" is a refinery utilizing forestry, agricultural and aquatic biomass as a feedstock to produce gaseous and liquid fuels, specialty or commodity chemicals, or other products commonly produced in petrochemical refineries, where the feedstocks are mainly fossil fuels. Process integration refers to a holistic approach that takes into account all the possible interactions between the various steps of a process and the exploitation of these interactions in order to achieve the minimization of the overall investment cost, higher product yields and an efficient process design. Process integration can be used as a tool in process design studies both for the design of new processes and plants and in retrofit designing of old processes (optimization of an existing process). Biochemically biomass converted (e.g sugar platform) into a portfolio of potential bio-products, such as: materials, chemicals, and fuels The lignin fraction (and the residues from the biochemical process) will be thermochemically converted using pyrolysis, hydropyrolysis and hydrothermal liquefaction with catalyst or without catalyst and by "syngas platform" into a syngas for the potential production of a spectrum of bio-based products, including power and/or heat, to meet the internal process power and heat requirements.

Dr. Jishnu Bhattacharya

Department of Mechanical Engineering
Indian Institute of technology Kanpur
Kanpur, India

Biography:

Jishnu Bhattacharya is currently working in the department of mechanical engineering at IIT, Kanpur as an assistant professor. He got his bachelor degree from Bengal Engineering College (Shibpur) and master degree from Indian Institute of Science. He obtained his PhD degree from University of Michigan, Ann Arbor and worked as a postdoctoral researcher in Northwestern University, Chicago. Prior to his current position, he was associated with the school of energy science and technology at IIT Kharagpur for a brief period of time. He is interested in the area of energy storage and harvesting. His specialization includes Li-ion batteries, computational material chemistry, computational fluid mechanics, solar thermal energy systems etc. He is particularly interested in cheap energy harvesting options for the future energy security of rural India.

Title: Storing Heat from the Sun: A Critical Perspective

Abstract:

Storage is often a critical bottleneck for the intermittent energy harvesting systems such as solar thermal power plants. Overall economy of performance and reliability of a solar plant depend on the efficient performance of the storage system. The major focus of the recent research in the field of solar energy is the collector technology, based on the optimization of either the geometry or the materials. Thermal energy storage systems are built based on the maximum first law efficiency, i.e, minimizing the loss in the process of energy transfer. The approach is logical only for the solar plants which are heavily backed up by fossil fuel driven conventional boilers. However, current research envisions solar thermal technology to evolve as a stand-alone and reliable power source with multiple degrees of redundancy. Towards this goal, it is essential to optimize the storage system based not only on the amount of energy recovery but also the rate of energy transfer as well as the charge-discharge cycle. In this talk, we will discuss the available technologies in solar thermal energy storage and the research efforts in both experimental and modelling fronts. The relative merits of different methods and materials will be highlighted along with the future direction in thermal storage technologies.

Dr. Parameswaran Binod

Microbial Processes and Technology Division, CSIR-National Institute for Interdisciplinary Science and Technology, Thiruvananthapuram 695019, Kerala, India

Biography:

Dr. Parameswaran Binod is currently working as a Scientist in the Microbial Processes and Technology Division of CSIR-National Institute for Interdisciplinary Science and Technology, Trivandrum, India. He obtained his PhD in Biotechnology from Kerala University, Trivandrum in 2008 and after that he did his postdoctoral studies at Korea Institute of Energy Research, Daejeon, South Korea in the area of lignocellulosic biofuels. He has nearly 85 publications including research papers, reviews and book chapters. In 2001 he received Young Scientist Award from International Forum on Industrial Bioprocesses (IFIBiop) and in 2014 he received Kerala State Young Scientist Award. His research interest includes bioprocess and bio-products including biofuels, biopolymers, biochemicals of industrial importance and Enzyme Technology.

Title: Utilization of Biodiesel Industry Generated Crude Glycerol for the Production of 1,3-Propanediol through Microbial Route

Abstract:

1,3-propanediol (1,3-PDO) is a specialty chemical monomer gained an importance from being a fine chemical to commodity bulk chemical. Though thermo-chemical production of 1,3-PDO from oleo chemicals derived from petroleum derivatives is well known, the fermentative mode of synthesis found more environmentally friendly and economical. This chemical has wide range of applications as monomer in the production of polymers like polyurethane, polyether etc. and also in cosmetic, food, pharmaceutical, textile industries. As the chemical demand increased due to various applications, it has become a challenging and important strategy to increase the titers by biological production.

The aim of the study was to evaluate a novel onsite enrichment approach to isolate a crude glycerol utilizing facultative anaerobic bacteria. An onsite enrichment in natural conditions resulted an isolate, Lactobacillus brevis N1E9.3.3, that can utilize glycerol and produce 1,3-propanediol with a yield of 0.89 g1,3-PDO/g glycerol and productivity of 0.78 g1,3-PDO/l/h at alkaline pH-8.5 under anaerobic conditions. Batch fermentation experiments with glycerol-glucose co-fermentation strategy was carried out to evaluate the production of 1,3 propanediol and other byproducts. The effect of other carbon sources as co-substrate was also evaluated. At the optimized condition, 55 g/l 1,3 propanediol was monitored from biodiesel industry generated crude glycerol.

Dr. R. S. Singh

Carbohydrate and Protein Biotechnology Laboratory,
Department of Biotechnology, Punjabi University, Patiala 147 002, India,
Tel.: +91 175 3046262; Fax: +91 175 2283073; E-mail:
rssingh11@lycos.com; rssbt@pbi.ac.in

Biography:

R.S. Singh is Professor, Department of Biotechnology, Punjabi University, Patiala, India. He obtained Ph.D (Biotechnology) from Punjabi University, Patiala. He is working in the areas of Industrial Biotechnology. His current research works include production of industrial enzymes, glycoproteins, biopolymers, organic acids, ethanol etc. The major aims of my laboratory are to develop processes for the production and purification of various metabolites and industrial enzymes/glycoproteins. He is recipient of many national and international awards which include INSA Visiting Scientist, MASHAV-UNESCO Fellowship, Israel and Fellow of Biotech Research Society, India. He was also Visiting Professor, Swiss Federal Institute of Technology, Lausanne (EPLF), Switzerland. He has published 125 research papers, books, 30 book chapters and 50 popular articles. He has two Indian Patents in his credit. He is also on the editorial board of international journals. He was Guest Editor of Biologia, Journal of Scientific and Industrial Research and Indian Journal of Experimental Biology. He is providing consultancy to many industries in Northern India.

Title: Waste to Wealth: Utilization of Apple Industry Waste for Value Added Products

Abstract:

Attempts were made to utilize the apple industry waste for the production of value added products. Solid state fermentation (SSF) of apple pomace was carried out for the production of ethanol using Saccharomyces cerevisiae, Torula utilis and Kloeckera sp. SSF of apple pomace gave higher yield for ethanol production. The production of ethanol in natural fermentation was almost half than of Saccharomyces cerevisiae. Apple pomace is a poor animal feed supplement, because of its extremely low protein content and high amount of sugars. A novel approach of bioconversion of non-protein nitrogen by fermentation into proteinaceous nitrogen has been developed. Attempts were also made to utilize the apple pomace for the production of yeast biomass i.e. Saccharomyces cerevisiae, Candida utilis and Torula utilis. It has been found to be a suitable substrate for the production of baker's yeast. Apple pomace has proved to be a good substrate for the production of inulinase by SSF from Penicillium oxalicum. A number of microorganisms such as Rhodotorula, Sarcina, Cryptococcus, Monascus purpureus, Phaffia rhodozyma, etc. are known to produce pigments. Apple pomace (10-50 g/L) has been incorporated to the basal medium for pigment production of Rhodotorula, Sarcina sp., Micrococcus and Chromobacter sp. The production of pigment in apple pomace supplemented medium employing Miccrococcus shown better yield of both biomass and carotenoids.

Prof. Ramesh K. Agarwal

William Palm Professor of Engineering
Department of Mechanical Engineering and Materials Science
Washington University in St. Louis, USA

Biography:

Professor Ramesh K. Agarwal is the William Palm Professor of Engineering and the director of Aerospace Research and Education Center at Washington University in St. Louis. From 1994 to 2001, he was the Sam Bloomfield Distinguished Professor and Executive Director of the National Institute for Aviation Research at Wichita State University in Kansas. From 1978 to 1994, he worked in various scientific and managerial positions at McDonnell Douglas Research Laboratories in St. Louis. He became the Program Director and McDonnell Douglas Fellow in 1990. Dr. Agarwal received Ph.D in Aeronautical Sciences from Stanford University in 1975, M.S. in Aeronautical Engineering from the University of Minnesota in 1969 and B.S. in Mechanical Engineering from Indian Institute of Technology, Kharagpur, India in 1968. Over a period of 35+ years, Professor Agarwal has worked in various areas of Computational Science and Engineering - Computational Fluid Dynamics (CFD), Computational Materials Science, Computational Electromagnetics (CEM), and Multidisciplinary Design and Optimization. He is the author and coauthor of over 400 publications. He has also worked in Nanotechnology and energetic materials for solar energy applications and Clean and Renewable Energy Systems. He has given many plenary, keynote and invited lectures at various national and international conferences worldwide. Professor Agarwal continues to serve on many academic, government, and industrial advisory committees.

Title: Multiphase CFD Modeling and Simulations of Fluidized Beds for Chemical Looping Combustion

Abstract:

Chemical-looping combustion (CLC) is a next generation combustion technology that has shown great promise in addressing the need for high-efficiency low-cost carbon capture from fossil fueled power plants to address rising carbon emissions. A computational fluid dynamics (CFD) simulation is developed using the Eulerian approach based on a laboratory-scale experiment with a dual fluidized bed CLC reactor. The salient features of the fluidization behavior in the air reactor and fuel reactor beds are accurately captured in the simulation. The results highlight the need for more accurate empirical reaction rate data for future CLC simulations. The spouted fluidized bed setup provides several advantages when solid coal is used as fuel for CLC. The Lagrangian approach known as Discrete Element Method (DEM) coupled with the CFD solution of the flow field provides an effective means of simulating the behavior of such a bed. The overall results using Fe-based oxygen carriers reacting with gaseous CH_4 confirm that chemical reactions have been successfully incorporated into the coupled CFD-DEM simulations. The results indicate a strong dependence of the fluidization behavior on the density of bed material and provide important insight into selecting the right oxygen carrier to improve performance. This work provides a basis for future simulations of CD-CLC systems using solid coal as fuel. Given the high computing cost of CFD-DEM, it is necessary to develop a scaling methodology based on the principles of dynamic similarity that can be applied to a CFD-DEM simulation to expand the scope of this approach to larger CLC systems up to the industrial scale. A new scaling methodology based on the terminal velocity is proposed for spouted fluidized beds. Simulations of a laboratory-scale spouted fluidized bed are used to characterize the performance of the new scaling law in comparison with existing scaling laws in the literature. It is shown that the proposed law improves the accuracy of the simulation results compared to the other scaling methodologies while also providing the largest reduction in the number of particles.

Dr. Huu Hao Ngo

Centre for Technology in Water and Wastewater, School of Civil and Environmental Engineering, University of Technology Sydney, Broadway, NSW 2007, Australia

Biography:

Dr. Huu Hao Ngo is Professor of Environmental Engineering, Deputy Director of Center for Technology in Water and Wastewater (CTWW), School of Civil and Environmental Engineering at University of Technology, Sydney. He is also a Co-Director of the joint Centre of Membrane Bioreactor founded by UTS, Tongji University and Tianjin Polytechnic University. The main research areas of his interests are membrane based water and wastewater treatment and reuse technologies, particularly membrane bioreactors, membrane hybrid system and osmosis membrane module design, biological waste treatment, water -waste-bioenergy nexus, greenhouse gas emission control and desalination. He has published more than 400 publications including four books and several book chapters/patents while receiving quite a number of highly recognized honors/awards. He has served as Editor of Bioresource Technology, Elsevier; Editor in Chief of Journal of Water Sustainability and Editorial Board member of several esteemed ISI/SCI international journals.

Title: Performance and Evaluation of a Grid Connected Hybrid Photo Voltaic-Wind Power System

Abstract:

Conventional power sources such as coal, petroleum, natural gas to produce energy are used flawlessly in this modern era. As these sources are limited, severe energy crisis will be faced in the near future. Impacts such as global warming, climate change, pollution are causing the future generation in a vulnerable situation. Solar and wind are two of the cleanest sources of energy. This study evaluates the feasibility of a grid connected combined photo voltaic-wind power system while demonstrating its usefulness and efficiency. The study shows that the combined system is more efficient than a single solar or wind energy system. Homer pro software was also used to create a prototype and from that point, the design, economic and environmental analysis was successfully discussed. There are several issues related to a system like integration problem to the main grid and the use of diesel and battery. However, the key findings of this paper will challenge the conventional system in terms of economic benefits and environmental impacts. By conducting this research, the system is well understood in respect of Western Australia and the need of its development and implementation. In conclusion, a combined photovoltaic – wind hybrid system is just a door to enter into an era of modern renewable energy technology.

Dr. Uma Maheshwar

Executive Chief Consulting Engineer
GE Aviation-India
John F Welch Technology Centre, EPIP, Whitefield Road
Bangalore-560066

Biography:

Uma Maheshwar is the Executive Chief Consulting Engineer for 750+ member GE Aviation India engineering team at Bangalore. The team is involved in design & development of next generation propulsion systems, support of engine fleet and development of customized digital and engineering tools. Uma has over 24year of experience in Advanced Design, Engineering, Manufacturing, Technology development and CAD/CAM/CAE/PLM domains.

Uma joined GE Aviation in 2001 and since then held many leadership positions in Aviation Engineering. He was instrumental in setting up & leading 200+ member world-class Advanced Technology teams at Bangalore for GE Aviation. Uma was involved in design & development of GEnx , LEAP56, LEAP-X, PASSPORT20, GE9X, ATP engine programs covering –Architectural evaluation, Cycles, Mechanical, Rotor Dynamics, Thermal systems, Combustion Aero, Turbine Aero, Acoustics design disciplines.

Prior to joining GE, Uma held positions with Larsen & Toubro (L&T) for 8years. During his association with L&T, Uma engineering of 25 mega plants for Oil& Gas, Fertilizer, Power, Petro-chemical, Defense, Nuclear sectors involving design, manufacturing and commissioning. Uma has set up and lead Advanced Design & CAE team at L&T's largest manufacturing plant, Hazira works. He was one of the Management Representative to set up Engineering Services Company for L&T. Uma holds Masters in Mechanical Engineering. Uma has presented papers/publications/key note sessions in 100+ National & International conferences and has been recognized with many awards.

Title: Powering the Future Flight -Perspectives from Environmental challenges

Abstract:

GE Aviation is a world-leading provider of commercial, military and business and general aviation jet and turboprop engines and components as well as avionics, electrical power and mechanical systems for aircraft. GE has a global service network to support these offerings. GE and its customers are also working together to unlock new opportunities to grow and deliver more productivity beyond traditional services. GE Aviation is becoming a digital industrial business with its ability to harness large streams of data that are providing incredible insights and in turn, real operational value for customers.

GE has pioneered TAPS (Twin Annual Pre Swirler) technology which dramatically reduces emissions, improves durability and efficiency. GE engineers are developing the TAPS III combustor for its new GE9X engine that will power the Boeing 777X aircraft. The TAPS III combustor will incorporate additive manufactured fuel nozzles and ceramic matrix composite inner and outer liners for high efficiency, durability and reduced NOx emissions. The research into more electric aircraft power systems, generators and electric starters along with high power conditioning and power distribution and control is ongoing. Electric aircraft research can improve fuel burn and reduce emissions. GE engineers are working on technologies to optimize cruise/descent performance as well as wind-optimized cruise efforts to improve fuel burn and reduce NOx emissions and noise. The evaluation and development of alternative fuels to achieve ASTM approval for "drop-in" fuel for aircraft engines that help reduce emissions is ongoing.

Dr. Wan Azlina Ahmad

Department of Chemistry, Faculty of Science,
Universiti Teknologi Malaysia, 81310 UTM, Johor Bahru
Malaysia

Biography:

Wan Azlina Ahmad is currently a Professor at the Department of Chemistry, Faculty of Science, Universiti Teknologi Malaysia. Her main research interests are in the areas of Industrial and Environmental Biotechnology. She has been actively researching on areas related to heavy metal toxicity and the production of natural pigments from bacteria since graduating from King's College, University of London in 1988. Her research interests focuses on developing products for the benefit of mankind.

Title: Flexirubin Type Pigment Production From Chryseobacterium Artocarpi Cect 8497 And Its Application As Natural Ink

Abstract:

Interest and demand for bacterial pigments is growing due to rising awareness of toxicity of synthetic dyes. In our previous reports, flexirubin type pigment is found to be safe and non-toxic. This study evaluates on the production of flexirubin type pigment from Chryseobacterium artocarpi CECT 8497 using liquid pineapple waste in 5 L bioreactor and its application as environmental-friendly ink. Combination of polyvinyl butyral and polyvinyl pyrrolidone was used as resin for flexirubin ink preparation and the ink was characterized using FT-IR. Results showed that liquid pineapple waste is feasible for C. artocarpi CECT 8497 growth and flexirubin production. The ink was successfully formulated with less bubble and smooth texture and the functional groups of flexirubin were indentified in the formulated ink. Flexirubin ink was stable at room temperature for 30 days. This is the first report on ink formulation of flexirubin type pigment from C. artocarpi and its potential application on plastic materials.

Dr. Parmjit S. Panesar

Food Biotechnology Research Laboratory
Department of Food Engineering and Technology,
Sant Longowal Institute of Engineering and Technology,
Longowal - 148106, Punjab, India

Biography:

Dr. Parmjit S. Panesar is working as Professor & Head, Biotechnology Research Laboratory, Department of Food Engineering & Technology, Sant Longowal Institute of Engineering and Technology (Deemed University: Established by Govt. of India), Longowal, Punjab. India. In 2005, he has been awarded BOYSCAST fellowship by Department of Science & Technology (DST), Govt. of India, to carry out advance research in Industrial Biotechnology at Chembiotech labs, University of Birmingham Research Park, UK. In 1999, Dr. Panesar was awarded Young Scientist Fellowship by Punjab State Council for Science & Technology, India.

He has successfully completed 7 research projects funded by CSIR, MHRD, AICTE, DBT New Delhi. He has published more than 100 international/national scientific papers, 50 book reviews in peer-reviewed journals, 20 chapters and has authored/edited 06 books. He is a member of the editorial advisory boards of national/international journals including 'International Journal of Biological Macromolecules'. He has also been selected as member in the international collective of experts of Foundation for Science and Technology (FCT), Portugal. His research is focused in the area of food biotechnology especially prebiotics, probiotics, application of immobilized cells/enzymes in different bioprocesses, value addition of agro-industrial wastes. Dr. Panesar has 1914 number of citations, h-index 21 (Google scholar).

Title: Biotechnological Approaches for the Utilization of Agro-industrial byproducts for Lactic Acid Production

Abstract:

The significant growth in agriculture sector and subsequently agro-industries has not only resulted in large magnitude and variety of food products but also provided employment and economic benefits. A wide range of food products of daily commodities such as fruit, vegetables, milk, beverages, cereal, pulses, oilseeds and plantation products etc. are being produced by various agro-industries. Although, quantity and variety of processed food products has increased enormously, but it has also led to the generation of significant quantity of residues and byproducts, which is a serious environmental concern. The generation of residues and byproducts, is not only an economic loss, but, would also involves additional cost for their management. The common agro-industrial wastes/residues are nutritionally rich, and dumping of these residues constitutes a significant loss of potential energy source. Thus, there is a growing need for the industries to properly recycle and utilize these byproducts. Moreover, stringent environmental legislations throughout the World have considerably added to the development of sustainable waste management techniques. During the last few decades, there has been an increasing trend to use biotechnological processes, especially the bio-processing for value-addition of agro-industrial residues. Lactic acid production is being studied with increased interest due to its wide range of applications in chemical, pharmaceutical and food processing industries. Different agro-industrial byproducts such as whey, molasses, cereal bran, potato waste liquid, corn steep liquor, apple pomace etc. have been investigated for the lactic acid production. Lactobacillus sp, Rhizopus sp., Bacillus sp., and Kluyveromyces sp. are the most commonly used microorganisms used for lactic acid production. Pretreatment of byproducts/residues in case of starchy materials is generally required and is referred as separate hydrolysis and fermentation process. However, direct fermentation using the amylolytic micro-organisms, which involves simultaneous enzymatic hydrolysis and fermentation has received increasing interest.

Prof. Mohsen Assadi

Professor, Gas Technology
University of Stavanger, Norway

Biography:
Present positions
- Professor, Gas technology, University of Stavanger, Norway
- Visiting professor, Shefield University

Previous position
- Professor in Thermal Power Engineering, Dept. of Energy Sciences, Lund University, Sweden (2006-2011).

Education
PhD in Thermal Power Engineering, Dept. of Energy Sciences, Lund University, Sweden.

Main fields of interest
Mohsen Assadi's research activities are focused on environmental friendly energy technologies, comprising energy conversion technologies, e.g. gas turbines, fuel cells and steam cycles utilising various fossil and renewable energy sources; system modelling, integration, optimization and monitoring, data driven modeling based on Artificial Neural Networks (ANN).
Mohsen Assadi has been project leader for several nationally financed project in Sweden and Norway as well as several EU-projects. Mohsen Assadi has been supervisor of 13 PhD and is currently supervising 3 PhD students. He has also been member of 17 PhD defence committees at different European Universities.

Title: Intermittent renewable energy and security of supply from a technical and economical point of view

Abstract:

The rapid growth of world's population coupled with the improved living standards have led to an increasing demand on world energy. Electricity generation represents the largest driver of energy demand by 2040 and it will account for about half of the increase in global demand for energy.
Climate change due to anthropogenic greenhouse gas (GHG) emissions is identified as the greatest threat to mankind. The major source of these GHGs is carbon dioxide emissions, and the heat and power sector is identified as the largest contributing sector to this emission. The present challenge for the power sector is to meet the ever increasing demand for electricity and simultaneously mitigate the greenhouse gas emissions, principally CO_2.
Several sustainable solutions have been developed and introduced to cover the additional demand and to mitigate CO_2 emissions in recent years. One possible option is to replace fossil fuel based power plants by renewable energy sources and the currently dominating renewable energy sources utilized are wind and solar energy. The main difficulty with these energy sources is their intermittency and the fact that the energy is produced when possible, rather than when needed. This presentation aims at addressing the challenges caused by the growth of the share of intermittent renewable energy in the existing energy system from both technical and economical point of view.

Prof. V. S. Moholkar

Department of Chemical Engineering and
Center for Energy
Indian Institute of Technology Guwahati
Guwahati – 781 039, Assam, INDIA

Biography:

Dr. V. S. Moholkar (b. 1972) is a Full Professor of Chemical Engineering at Indian Institute of Technology (IIT) Guwahati. He is also an associated faculty at Center for Energy in IIT Guwahati. He received Bachelors and Masters degree in chemical engineering from Institute of Chemical Technology (ICT) Mumbai. He received Ph.D. from University of Twente in 2002. He has held the chair of Head of the Chemical Engineering Department at IIT Guwahati between 2012-2015. His main research interests are sonochemistry, cavitation assisted physical, chemical and biological processing, and thermo- and biochemical routes to biofuels synthesis. He has published 114 papers in renowned international journals that have received more than 3300 citations (with h-index of 37). He has also filed 2 US patents on applications of hydrodynamic cavitation reactors in bioalcohol synthesis. He is a Chartered Member of Institution of Chemical Engineers UK, and a registered Chartered Engineer with Engineering Council of UK. He was elected as Fellow of Royal Society of Chemistry in July 2016. He has also been admitted as Senior Member of American Institute of Chemical Engineers in August 2016.

Title: Mechanistic Study on Ultrasound-Assisted Biodiesel Production from Non-edible Mixed oil Feedstock using Heterogeneous Catalyst

Abstract:

Biodiesel has emerged as promising sustainable alternate liquid transportation fuel. One of the major hurdles in large scale biodiesel production is abundant availability of cheap feedstock.1 In recent years, non-edible oil feedstocks such as Jatropa, Karanja, rubber seed, castor or waste cooking oil etc. have been attempted as alternate economic feedstocks for biodiesel production.2 Non-edible oils have significant content of free fatty acid (FFA) due to which conventional base (homogenous/ heterogeneous) catalyst cannot be used for the transesterification reaction. Homogenous acid catalyst such as sulfuric acid is capable to carry out simultaneous esterification and transesterification reaction but have demerits such as slow kinetics and corrosion of equipment.2 In this study we have addressed these issues related to biodiesel synthesis. The present study reports development of new heterogeneous acid catalyst from rubber seed cake for transesterification. The catalyst is synthesized through sulfonation using chlorosulfonic acid and waste rubber seed powder. As-synthesized catalyst characterized for FTIR, BET surface area analyzer, FE-SEM and XRD. The catalyst has been used for biodiesel production using mixed feedstock of non-edible oils (mixture of castor oil, palm oil, rubber seed oil and waste cooking oil). Ultrasound (or sonication) has been applied to the reaction mixture to enhance the kinetics of transesterification reaction.

In present paper, we have optimized the reaction parameters to obtain the maximum biodiesel production. Response Surface Methodology (RSM) using Central Composite Design (CCD) was employed to study the effect of the process variables like methanol to oil ratio, catalyst loading and reaction temperature. Conversion of triglyceride to biodiesel was analyzed using 1H 600 MHz Nuclear Magnetic Resonance (NMR) Spectrometer (Bruker). The biodiesel yield obtained with the application of new catalyst are comparable with the yield reported with homogenous acid catalyst.3 The application of sonication generates the intense turbulence between the reactants, results in boosting of intrinsic kinetics of esterification/ transesterification process. A distinct merit of the process discussed in present study is the feedstock flexibility in that mixture of several non-edible oils has been used without any compromise with kinetics and yield of the reaction. This novel process has potential for further study on large scale application.

Prof. Saptarshi Basu

Department of Mechanical Engineering
Indian Institute of Science, Bangalore
India
sbasu@mecheng.iisc.ernet.in

Biography:

Prof. Saptarshi Basu is currently an Associate Professor in the Department of Mechanical Engineering at Indian Institute of Science. Prof. Saptarshi basu received his M.S. and Ph. D. degrees in Mechanical Engineering from University of Connecticut in 2004 and 2007 respectively. Before that he finished his B.E in Mechanical Engineering from Jadavpur University in2000. Prof. Basu was a tenure track faculty member in the Department of Mechanical, Materials and Aerospace Engineering in University of Central Florida, USA from 2007-2010. He joined Indian Institute of Science as a faculty member in 2010. Prof. Basu is the recipient of DST Swarnajayanti Fellowship from Government of India in Engineering Sciences. He is a Fellow of the Indian National Academy of Engineering. He also received the K.N Seetharamu medal from Indian Society of Heat and Mass Transfer for his contributions in multiphase transport. Prof. Basu is a member of ASME, ISHMT and Combustion Institute.

Title: How a Spray Interacts with Swirling Flow?

Abstract:

In this work, the near field breakup and atomization of liquid sheet in a co-annular swirling gas flow field is presented. High-speed speed shadowgraphy is employed to characterize the global features and breakup dynamics of liquid sheet across a wide range of airflow rates. The parameter momentum ratio (MR) is used to illustrate the results. Breakup regimes are constructed based on the instantaneous visualization of the liquid sheet. In this study, the transition from weak to strong, spray-swirl interaction is explained based on momentum ratio (MR). Proper Orthogonal Decomposition (POD) is implemented on instantaneous PIV (and shadowgraphy images, to extract the energetic spatial eigen modes and characteristic modal frequencies. POD results suggest the dominance of KH (Kelvin-Helmholtz) instability mechanism (pure axial shear, axial + azimuthal shear) in swirl–spray interaction. For instance, the large scale coherent structures of swirl flow exhibits different sheet breakup phenomena in spatial domain. For instance, flapping breakup is induced by central toroidal recalculation zone (CTRZ) in the swirling flow field.

Dr. Zainul Akmar Zakaria

Institute of Bioproduct Development, Faculty of Chemical and Energy Engineering, Universiti Teknologi Malaysia, 81310 UTM Johor Bahru, Johor, Malaysia

Biography:

Dr. Zainul Akmar Zakaria is an Associate Professor under the Department of Bioprocess and Polymer Engineering, Faculty of Chemical and Energy Engineering, Universiti Teknologi Malaysia (UTM). He is currently a Research Fellow at the Institute of Bioproduct Development (IBD), UTM which is a National Centre of Excellence for Plant and Microbial Bioproduct. He has ISI h-index of 9 and has published 2 Research Books, 4 Edited Books and 8 Book Chapters. Dr. Zainul has served as Guest Editor for some ISI-indexed journals, Evaluator for research grants from ACS, Saudi Arabia and South Africa as well as External Examiners for doctoral candidates from South Africa and Pakistan.

Title: Antioxidant Potential of Pyroligneous Acid Fraction Obtained from Pyrolysis of Palm Kernel Shell

Abstract:

Pyroligneous acid (PA) is an aqueous liquid obtained from condensation of vapour produced during pyrolysis of plant biomass. In this study, PA was obtained by pyrolyzing the palm kernel shell (PKS) at temperature of 429°C with heating rate 1.34°C/min. The PA obtained was extracted using ethyl acetate and further fractionated using column chromatography. The total phenolic contents (TPC) of obtained fractions were evaluated and the fraction with highest TPC (673.49 ± 6.05 µg gallic acid equivalent/mg of sample) was subjected to antioxidant activity assays. The fraction showed total antioxidant activity with trolox equivalent antioxidant capacity (TEAC) value of 1101.83 ± 4.59 µg trolox equivalent/mg of sample. The IC_{50} values for free radicals scavenging were 24.53 ± 0.60 µg/ml, 283.85 ± 0.90 µg/ml, and 491.49 ± 5.99 µg/ml for DPPH, hydroxyl and superoxide anion, respectively. The reducing power with ferric reducing antioxidant power (FRAP) was 11.80 ± 0.41 mmol Fe(II)/mg of sample. These results illustrate that PA fraction from palm kernel shell exhibit very strong antioxidants activity especially the DPPH free radical scavenging, TEAC, and FRAP, which almost equal or better to that of synthetic antioxidants (BHA) and natural antioxidants (ascorbic acid).

Dr. Swetaprovo Chaudhuri

Department of Aerospace Engineering,
Indian Institute of Science, Bangalore
India
schaudhuri@aero.iisc.ernet.in

Biography:

Swetaprovo Chaudhuri is an Assistant Professor at the Department of Aerospace Engineering, Indian Institute of Science, since June 2013. Prior to this appointment he was a research staff in the Department of Mechanical and Aerospace Engineering and Combustion Energy Frontier Research Center at Princeton University. He earned his Ph.D. from the University of Connecticut in 2010 and B.E. from Jadavpur University in 2006, both in Mechanical Engineering. His research interests and outstanding contributions span over fundamental and applied aspects of turbulent combustion and functional droplets.

Title: Instability Control by Actuating the Swirler in a Lean Premixed Combustor

Abstract:

A detailed study concerning a novel, dynamic control strategy for mitigating thermo-acoustic instability in a swirl stabilized, lean premixed, lab scale combustor will be presented. The mitigation strategy is realized by rotating the otherwise static swirler, primarily meant for stabilizing the lean premixed flame. Prominent reduction of the fundamental acoustic mode amplitude: by about 25 dB is observed with this control technique. The physical mechanism responsible for the instability mitigation due to the rotating swirler is investigated by observing the distinct changes associated with the reacting flow field, using high speed Particle Image Velocimetry (PIV). An attempt has been made to probe into the self-excited flame dynamics using high speed, intensified, chemiluminescence imaging. The rotating swirler induces vortex breakdown and increased turbulence intensity, which decimates the strong flame- acoustic coupling and eventually the acoustic energy source, to render quiet, instability mitigated swirling flames.

Dr. Sarvanamurugan Shunmugavel

Scientist-E
Center of Innovative and Applied Bioprocessing (CIAB),
Mohali, India

Biography:

Dr. S. Saravanamurugan is currently Scientist-E at Center of Innovative and Applied Bioprocessing (CIAB), Mohali, India. Formerly, he was working as Senior Researcher at Centre for Catalysis and Sustainable Chemistry, Technical University of Denmark (DTU), Denmark since 2010. He moved to Korea Advanced Institute of Science and Technology (KAIST) in South Korea as Research Scientist in 2005 after obtaining his Ph.D from Anna University, Chennai in the same year. He also worked as post-doctoral fellow at Inha University, South Korea between 2006 and 2007 before moving to Denmark in January 2008. He has more than fifteen years of research experience and his main research topics include synthesis and modification of zeolite and zeotype materials, biomass transformations and ionic liquids. He has 46 publications and eight patents filed/granted with more than 1500 citations (h Index 18). He has co-authored an article in the prestigious journal Science in 2010, related to conversion of sugars to lactic acid derivatives with Lewis acid containing zeolites. He received a DST-DAAD Fellowship during his doctoral studies in 2004.

Title: Inter- Conversion of Aldopentoses and Tetroses with Zeolite

Abstract:

Isomerisation of xylose to xylulose with commercial zeolites, such as H-USY and H-Beta, with various silicon to aluminium ratio has been studied under alcohol-aqueous system in one-pot two-step reaction protocol. It has been found that the reaction proceeded through the following steps: isomerisation of xylose to xylulose in alcohol during the first step; acetalisation of xylulose to alkyl xyluloside during the first step, hydrolysis alkyl xyluloside to enhance the yield of xylulose during the second step. The highest yield of xylulose (47%) was found with H-USY-6. The reaction protocol was extrapolated to tetroses, such as erythrose, but found that interconversion took place efficiently in water rather than in alcohol, yield 45% erythrulose with H-USY-6 in one-pot one step catalytic process. This manuscript reviews based on our previously published articles.

Prof. P. K.Bose

Campus Director, NSHM Knowledge Campus Durgapur Group of
Institutions NIT Agartala, India
Pkb32@yahoo.com

Biography:

Prof. Probir Kumar Bose, Director, NSHM Knowledge Campus, Durgapur, West Bengal, India was instrumental in shaping up National Institute of Technology, Agartala, Tripura as its Director and played in crucial role in evolution of its state-of-the-art infrastructure. He also held additional charges of Director at NIT Silchar, NIT Nagaland and NIT Manipur concurrently. He initiated several post-graduate academic programs at NIT Agartala.

Prof. Bose is an elected Fellow of Institute of Engineers, India and member of Combustion Institute, Indian Institute of Welding, Indian Society of Technical Education, Indian Society of Engineers, and Indian Institute of Metals. Prof. Bose has published more than 100 peer reviewed journal papers and has several patents to his credit.

Title: Instability Control by Actuating The Swirler in a Lean Premixed Combustor

Abstract:

Ethanol due to its low latent heat of vaporization has the ability to reduce ci engine's NOx and CO2 emission. But along with that it also deteriorates the performance of the engine. On the other hand, biodiesel improves the performance of the engine but increases the emission too. The present study deals with an approach where the potentials of both ethanol and biodiesel have been combined in order to utilize the benefits of both. Initial phase of this work comprises of a miscibility study, in which the miscibility limit of ethanol in diesel has been found out and then this limit has been extended by virtue of biodiesel inclusion. The results indicate that biodiesel increases the miscibility of ethanol in diesel. The performance and emission studies indicates that low ethanol addition increase Bth and decrease the equivalent BSFC of the engine with very low emission of NOx and smoke opacity. Diesel-biodiesel-ethanol (DBE) blends show appreciable increase in bth with appreciable reduction in equivalent BSFC. DBE blends also showed commendable reduction in hydrocarbon emission.

Dr. Sunil Kumar

Solid and Hazardous Waste Management Division
CSIR-National Environmental Engineering Research Institute (NEERI),
Nehru Marg, Nagpur-440 020, India

Biography:

Dr. Sunil Kumar is a Senior Scientist in Solid and Hazardous Waste Management Division of CSIR-NEERI, Nagpur (India). He has been working in this area since 19 years. He has published 100 research papers in national and international journals. He is also Editorial Board Member of Bioresource Technology. He has edited several special issues on different aspects of waste management in many reputed international journals. A book on waste management by Taylor and Francis publication is also in his credit.

Title: Solid Waste Management and Climate Change in India: Existing Scenario and Strategy for Improvement

Abstract:

India is facing serious environmental challenges concerning solid waste management (SWM) due to rapid development, increasing population and improved standard of living in cities and urban areas leading to the generation of varied categories of wastes resulting into a trend of increase in municipal solid waste (MSW) generation. Improper MSW management leads to the degradation of MSW which produces methane and carbon dioxide which are the most important greenhouse gases (GHGs). At a global scale, the waste management sector makes a relatively minor contribution to GHG emissions, estimated at approximately 3-5% of total anthropogenic emissions in 2005. However, the waste sector is in a unique position to move from being a minor source of global emissions to becoming a major saver of emissions in India. Although minor levels of emissions are released through waste treatment and disposal, the prevention and recovery of wastes. Every waste management practice generates GHGs, both directly and indirectly. However, the overall climate impact or benefit of the waste management system will depend on net GHGs, accounting for both emissions and indirect, downstream GHG savings. In India, bridging gaps between existing activities in the context of waste and climate change catching the interest of scientific community. Scientists, Researchers, and Policy makers are more focussing on developing a strategy framework for discussion and further action. The objective of this paper is to manage the solid waste through overcome the existing problem on MSW management, which leads to the strategies for improvement of the MSW. Solid waste management component will be described in this paper. Also, proper MSW management plan will be described for Indian cities as a decentralized system with all technology available and suggested in solid waste management rules, 2016. The overall aim of the strategy is therefore to promote sustainable waste management in accordance with the waste management hierarchy reducing greenhouse gas emissions from this sector. These strategies include variety of approaches, such as Integrated Waste Management, Cleaner Production, and Sustainable Consumption and Production. There is also strong interest in Clean Development Mechanism (CDM) projects in the waste sector. CDM activity has focussed mainly on landfill gas capture (where gas is flared or used to generate energy) due to the reduction in methane emissions that can be achieved.

Prof. Amit Agrawal

Institute Chair Professor, Department of Mechanical Engineering
Indian Institute of Technology - Bombay
Powai, Mumbai 400076, India
amit.agrawal@iitb.ac.in

Biography:

Dr. Amit Agrawal joined Indian Institute of Technology (IIT) Bombay in 2004 and is currently Institute Chair Professor in the Department of Mechanical Engineering. He obtained BTech from IIT Kanpur and PhD from the University of Delaware, USA. He has worked as Engineer in Tata Motors, Pune and as a Postdoctoral Fellow at the University of Newcastle, Australia. His research interests are in micro-scale flows, turbulent flows and convective heat transfer. He has published more than 125 journal articles on these and related subjects, and filed for 10 patents. His work has appeared on the cover page of Journal of Fluid Mechanics and JM3 (SPIE Journal of Micro/ Nanolithography, MEMS, and MOEMS); and highlighted in the media. He is on the Editorial Board of Experimental Thermal and Fluid Science, Nature Scientific Reports and Sadhana, and Fellow of Indian National Academy of Engineering. He was recently awarded the DAE-SRC Outstanding Investigator Award and Prof. K.N. Seetharamu Medal by the Indian Society of Heat and Mass Transfer.

Title: Development of Blood-Plasma-Separation and Constant-Wall-Temperature Microdevices

Abstract:

In this talk, I will discuss about the development of two microfluidics based micro-devices. The first microdevice is designed to separate plasma from blood. The second micro-device can be employed for maintaining constant wall temperature.

Separating plasma from cellular elements of blood is imperative in disease diagnostics. Conventionally, blood plasma is separated in a centrifuge. However, this process of separation is difficult to replicate at the microscale, requires large sample volume, and is laborious and time-consuming. In this context, we have developed a microdevice enabling blood plasma separation. The results obtained are extremely encouraging in terms of separation efficiency. Separation efficiency of almost 100% has been achieved with whole (undiluted) blood. Our device avoids clogging of microchannels as the dimensions of the microchannels were kept comparatively large. The developed microdevice has been extensively tested with human blood. Our developed microdevice yields reliable performance for several hours at a stretch without any degradation in performance. Demonstration of very high separation efficiency at extremely low cost with extremely high reliability are the primary highlights of our developed microdevice.

The second microdevice is targeted towards the requirement of achieving isothermal condition in various lab-on-chip devices employed for chemical and biological processes. We propose the idea of employing diverging microchannel in conjunction with wall conduction for this purpose. Isothermal wall condition for a supplied constant heat flux condition is demonstrated experimentally. Subsequently, it was studied in detail using three dimensional numerical simulations to explore the idea over wider parameter range (angle, depth, length, thickness ratio, thermal conductivity thickness, mass flow rate, and heat flux). For the set of optimal parameters, diverging microchannel would yield a temperature gradient less than 0.05 °C/mm. The idea is further extended to obtain isotherm condition in series of diverging microchannels with application to thermo-cyclic processes like polymerize chain reaction (PCR).

Dr. Praveen Kumar Ramanujam

Department of Biotechnology,
Anna Bio Research Foundation,
Arunai Engineering College,
Tiruvannamalai, 606603, Tamilnadu, India.

Biography:

Prof. Praveen Kumar Ramanujam an Undergraduate in Chemical Engineering and post graduate in Industrial Biotechnology, both degrees from Annamalai University is working as Head of the Department in Department of Biotechnology, Arunai Engineering College, Tiruvannamalai, Tamilnadu, India. His area of research includes renewable energy from biomass and municipal waste. He was the chair for 1st and 2nd International Conference on Bioenergy, Environment and Sustainable Technologies (BEST2013 and BEST2015) and organized various national level symposiums and conferences. Served as International Scientific Advisory Committee member in "The 2012 Asian Biohydrogen and Bioproducts Symposium (ABBS)" conducted by Chongqing University, on November 9-12, 2012 in Chongqing, China. He has visited various countries including USA, Australia, China, Italy & Bangladesh to attend various conferences. He has chaired sessions and delivered invited talks in various International conferences which include "World Renewable Energy Congress – Australia 2013". He had done provisional registration for 4 patents. He had published more than 45 papers in peer reviewed journals. He is a life member in various professional societies which includes Biotech Research Society of India (BRSI), Indian Institute of Chemical Engineering (IICHE), International Forum on Industrial Bioprocesses (IFIBiop), Biogas Forum of India (BigFin), Indian Society for Technical Education (ISTE), Engineers Without Borders, India (EWBIndia). Currently he is serving as Management council member in Biotech Research Society of India (BRSI) and as Vice-President in the society "Engineers Without Borders – India (EWB-India)" Chennai chapter.

Title: Bioremediation of Cassava Sago Waste by Yarrowia Lipolytica for the Production of Bio-oil

Abstract:

Yarrowia lipolytica an oleaginous yeast was used for the production of single cell oil which can be easily converted to biodiesel. It was reported that this yeast can utilize various ranges of industrial wastes for the production of value added products. In this study Yarrowia lipolytica was grown on cassava sago industry effluent which is rich in starch and can yield increased biomass concentration. Raw sago industry waste and primarily treated sago industry waste were used for production of bio-oil. The yeast species produced good quantity of lipid content in the primarily treated sago industry effluent. The inorganic pollutants which were present in the raw waste water limits the growth yeast whereas the in the primarily treated waste water contains meager amount of his pollutants. 53.3% of lipid content was estimated in the preliminarily treated waste water whereas the lipid yield was found to be 5.92 g/L.

Dr. Deepak Pant

Dean and Head, Environmental Science,
Central University of Himchal Pradesh,
Dharamshala, Himachal Pradesh
India

Biography:

Dr. Deepak Pant currently working as Dean and Head, Environmental Science, Central University of Himchal Pradesh, Dharamshala, Himachal Pradesh is the recipient of Silver Jubilee Research Fellowship award for the year 2003 by Kumaun University, Nainital (India); UCOST Young Scientist Award 2009, INSA Fallow 2010, DST-SERC Visiting Fallow 2010 and DST- SERC Young Scientist Award 2011 for his research activities. He is also the chairman of Innovation club and active member for HP state innovation activities. Dr Pant has 05 patents in the area of waste management by green techniques and published 10 books, 45 research papers in various national and international journals. He has guided 02 M.Phil, 04 Ph. D. thesis and 48 M. Sc. dissertations.

He is in the editorial board of The Journal of Environmental Science and Sustainability (JESS). Dr Pant recently awarded by Visitor award 2017 by president of India for his innovation in the area of waste management.

Title: Petroleum Carcinogenecity: The Indian Challenge

Abstract:

The debate on the change in carbon pools and anthropogenic contribution has been always leading to confusion on its planning and management. Uncontrolled anthropogenic activities always create perturbation towards the projection of C in various pools. The human influence on the fluxes of carbon among the four reservoirs/ pools (atmosphere, ocean, fossil fuel and cement production and terrestrial) represents a small but significant perturbation of a huge global cycle. In the last decade (2002-2011) fossil fuel emission and cement production is responsible for 89% of the total CO_2 emission and remaining 11% is due to land use changes. The CO_2 emission rate is continuously increasing at a rate of 2.7 % per year against 1% in the year 1990. The total emission change from1960-2012 is partitioned among atmosphere (37-49%), ocean (26-27%) and terrestrial (37-24%). Weather events such as abnormally high temperature in January, 2014 (540C) in Australia, and at the same time Canada suffers from an extreme cold storms (~ -500C), breaking of 160-square-mile section of the Wilkins Ice Shelf from the coast of Antarctica (2008), droughts, bushfires, snow (almost simultaneously) in Australia in 2006, Hurricane Katrina in the United States in 2005, the European heat wave in 2003 killed more than 30,000 people making climate change as a issue of global concern. Role of π electrons are very important in terms of carbon management activities in plants, prokaryotes and bacteria. There are eight biological pathways, namely reductive pentose phosphate pathway, Hatch-Slack cycle, Crassulacean acid metabolism, reductive citric acid cycle, 3-hydoxypropionate bicycle, dicarboxylate/4-hydroxybutyrate,3-hydroxypropionate/4-hydroxybutyrate, and reductive acetyl-CoA,, known for converting inorganic carbon to organic material in cell biomass interaction. In all eight pathways carboxylation and reduction reaction are involved. Use of π-π interaction is important towards residue specific and group specific modification and can modify the cycles by synthetic-biological merger.

Dr. D. V. Patil

Indian Institute of Technology Mandi
Himanchal Pradesh, India
dhiraj@iitmandi.ac.in

Biography:

Dr. Dhiraj V. Patil* joined School of Engineering, IIT Mandi in the year 2015. He holds Ph.D. in Aerospace Engineering (2010) from the Indian Institute of Science (IISc), Bangalore and around 5 years of post-Ph.D. experience gathered from Jawaharlal Nehru Center for Advanced Scientific Research, Bangalore, India (2010 - 2011), The City College of the City University of New York, CUNY Energy Institute, USA (2011- 2013) and the University of Edinburgh, UK (2014-2015). His research so far has been in the developments and applications of the particle based lattice Boltzmann equation method in order to solve complex, multi-physics fluid flow and heat transfer problems on massively parallel computing systems. Recently, he is also involved in the numerical investigations of non-Newtonian flows, particle laden fluid flows and combustion simulations.

Title: Review of Particle based Methods for Combustion Simulations

Abstract:

Particle based methods have become increasingly attractive due to recent favorable trends in high performance computing and recent upgrades in the graphical processing units (GPUs). In this talk, we review and investigate use of particle based methods for combustion simulations. The methods reviewed are reactive molecular dynamics and lattice Boltzmann method, where later is discussed at length. One-dimensional modeling with single-step chemical kinetics is explained showing our results using a coupled finite-difference, lattice Boltzmann approach. Lastly, species mixing simulations using lattice Boltzmann for two-dimensional Y-channel are discussed.

Contributed Papers

SEEC-2017-001

HEAT TRANSFER ENHANCEMENT USING WAVY FIN ABSORBER IN SOLAR AIR HEATER

Abhishek Priyam
Department of Mechanical Engineering
N.I.T Jamshedpur,
Jharkhand, India-831014
priyamanik06@gmail.com

Prabha Chand
Department of Mechanical Engineering
N.I.T Jamshedpur,
Jharkhand, India-831014
pchand.me@nitjsr.ac.in

ABSTRACT

In the present article an experimental study has been carried out on heat transfer in a rectangular duct attached with wavy fin absorber. The performance of a wavy fin depends strongly on the fin spacing ratio ($F_p/2A$). The investigation covers a range of mass velocity from 0.0065 kg/s-m^2 to 0.033 kg/s-m^{2}and fin spacing ratio from 1.33 to 4. Use of wavy fin shows an enhancement in the performance of solar air heaters. The maximum enhancement in thermal efficiency and temperature rise is 2.21 and 2.23 times as compared to plane solar air heater.

Keywords: *wavy fin; thermal efficiency; heat transfer; temperature rise.*

NOMENCLATURE

Nomenclature	
A	amplitude(mm)
A_c	collector area(m^2)
A_o	pipe area(m^2)
C_d	coefficient of discharge
C_p	specific heat of air (J/kg-K)
F_p	fin pitch(mm)
Q_u	useful energy gain (W)
$\dot{m}$	mass flow rate(kg/s)

$F_p/2A$	fin spacing ratio
T_o	mean temperature of air at outlet (K)
T_i	mean temperature of air at inlet (K)
I	intensity of solar radiation (W/m^2)
η	thermal efficiency (%)
β	d/D
ρ	density of air (kg/m^3)
ΔP	pressure drop along orifice(N/m^2)
$\dot{m}/A_c$	mass velocity (kg/s-m^2)

INTRODUCTION

Solar energy is considered as clean and eco-friendly with an abundant source of energy. Solar collectors absorb solar radiation and transform into heat. Solar air heaters are the cheap and simple devices to collect solar energy and used to heat air for drying of medicinal plants, crop drying etc.[1] The lower efficiency of the conventional solar air heater results due to lower heat transfer coefficient of air. The efficiency of solar air heater can be enhanced by either increasing the convective heat transfer coefficient of air, heat transfer area or both. The use of turbulence promoters such as roughness and protrusions on absorber plate, packed beds, corrugated absorber, fins or fins and baffles have been used to enhance the heat transfer. [2]Investigated experimentally on the thermal performance of solar air heater having its flow channel packed with Raschig ring based on energy and exergy analysis. [3]Used protrusions arranged in angular fashion as roughness geometry. Heat transfer and friction factor has been increased as 2.89 and 2.93 times as compared to plane solar air heater.

[4]Experimentally examined the enhancement in heat transfer using protrusions as roughness and developed correlations for heat transfer and friction factor using experimental data. [5]Evaluated thermohydraulic performance of w-discrete rib in solar air heater and found a maximum enhancement of 2.79 and 1.98 in Nusselt number and friction factor. [6]Studied the heat transfer and fluid flow characteristics of rib-groove roughened solar air heater ducts. They found an enhancement of 1.5-3 times in Nusselt number and 2 to 3 folds in friction factor as compared to smooth duct. [7]Experimentally investigated on a low porosity packed bed solar air heater. They found decrease in porosity increases the volumetric heat transfer coefficient. Thermal performance of wire mesh solar air heater has been evaluated experimentally by[8].An increase in overall efficiency of 5% has been observed as compared to conventional solar air heater.[9]Studied analytically the effect of fin spacing on thermal and thermohydraulic performance of wavy finned absorber solar air heater. An enhancement of 62.53- 63.41% has been achieved in the thermal efficiency. [10]Studied the performance of finned solar air heater.

In the view of above, the present analysis is done with the objective of experimentation on wavy finned absorber solar air heater to collect the data on heat transfer and fluid flow characteristics. The effect of fin spacing ratio $\left(\dfrac{F_p}{2A} \right)$ and the mass velocities $\left(\dfrac{\dot{m}}{A_c} \right)$ on the performance of wavy finned absorber solar air heater has been done and a massive enhancement has been found in order of 2.21 times by varying fin spacing ratio.

EXPERIMENTAL SET UP

An open loop outdoor experimental set up as shown in fig. 1 has been developed that consists of inlet section, test section, convergent section, control valves, orifice plate, blower, data loggers and manometers. The dimensions of inlet section and the test section are 500 mm and 1200 mm respectively as per[11]. The inner dimensions of the both ducts were 1700 x 400 x 50 mm.

The exposed area is 0.48m^2. A packing of glass wool has been done having thickness 50mm supported by 10mm plywood as bottom. the space between absorber plate and the bottom plate was 50mm. A glass cover with 4mm thickness was placed 50mm above the absorber plate. G.I sheet has been used as an absorber plate with an attached wavy fins below it. The fins as well as plate were painted with black board paint. A total of 24 thermocouples have been used to measure the plate and air temperature of both ducts as shown in fig.2. All the thermocouples were connected to data loggers (A,B,C) to display the temperatures. The air mass flow rate flowing through duct was measured by using a calibrated orifice meter attached

with digital manometer. The outlet of the air heaters were connected to wooden convergent section coupled with G.I pipes, orifice plate, flow control valve and a 3 h.p blower.
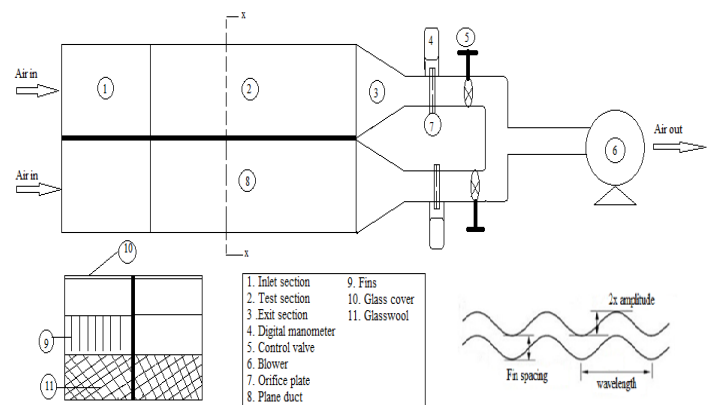
FIGURE 1. Schematic diagram of experimental set up and geometrical description of wavy fin
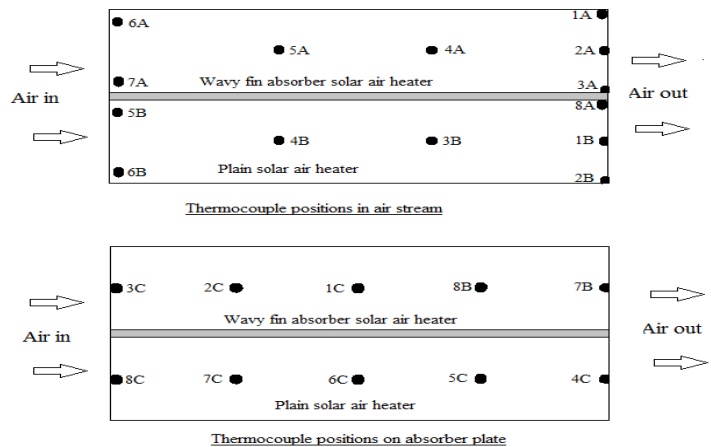
FIGURE 2. Positions of thermocouples on absorber plate and air stream

EXPERIMENTATION

The wavy fins of known physical characteristics were welded on the absorber plate. The collectors were tested in the horizontal positions as per [11] standards. Outdoor testing of both the ducts were done under identical conditions on clear sky days. Before the starting of experimentation, all the components of the set up were checked for leakage and proper operation. After that the blower is switched on and the quasi state conditions has been achieved after two hours of operation. The various thermocouple readings has been achieved and recorded in pen drive attached to data logger. The similar operations has been done by adjusting the different mass flow rates. The values of pyranometer has been recorded for the corresponding mass flow rates and fin spacing ratios. It was decided to take six values of mass flow rates (from partial opening to full opening of

control valve) to cover the usual range of mass flow rates and five sets of fin spacing ratios.

DATA REDUCTION
The data such as pressure drop across orifice plate, air and absorber plate temperature at various positions in the duct were recorded to compute the thermal efficiency and temperature rise in air along the collector. The following equations were used to calculate the air mass flow rate, energy gain by air and thermal efficiency[12].

$$\dot{m} = C_d A_0 \left[\frac{2\rho\Delta P}{1-\beta^4} \right]^{0.5} \tag{1}$$

where ΔP is the pressure drop across orifice. The calibration result gives a value of 0.65 for C_d.
The energy gain by air is

$$Q_u = \dot{m} C_p (T_0 - T_i) \tag{2}$$

For wavy fin solar air heater;

$$T_i = \frac{T_{6A} + T_{7A}}{2} \tag{3}$$

$$T_o = \frac{T_{1A} + T_{2A} + T_{3A}}{3} \tag{4}$$

also, for plane solar air heater;

$$T_i = \frac{T_{5B} + T_{6B}}{2} \tag{5}$$

$$T_o = \frac{T_{8A} + T_{1B} + T_{2B}}{3} \tag{6}$$

The thermal efficiency of flat plate collector can be given by using following equations;

$$\eta = \frac{\dot{m} C_p (T_o - T_i)}{I A_C} \tag{7}$$

Also, the error analysis has been done as per the methodology suggested by[13]. If the value of any parameter is calculated using certain measured quantities then the error in measurement of 'ϕ'(parameter) is given as;

$$\frac{\delta\phi}{\phi} = \left[\left(\frac{\delta\phi}{\partial x_1} \delta x_1 \right)^2 + \left(\frac{\delta\phi}{\partial x_2} \delta x_2 \right)^2 + \ldots\ldots + \left(\frac{\delta\phi}{\partial x_n} \delta x^n \right)^2 \right]^{0.5} \tag{8}$$

where $\delta x_1, \delta x_2, \delta x_3 \ldots\ldots \delta x_n$ are the possible errors in measurements $x_1, x_2, x_3 \ldots x_n$ and $\delta\phi$ is called as absolute uncertainty and $\delta\phi/\phi$ is known as relative uncertainty.

RESULTS AND DISCUSSION

Fig.3 shows the variation of thermal efficiency as a function of mass velocity for various fin spacing ratios.

The fin spacing ratios has been varied from 1.33 to 4. It can be seen that for a specific fin spacing ratio, the thermal efficiency increases with increase in mass velocity. This is because the increase in mass velocity decreases the collector plate temperature and thus the heat
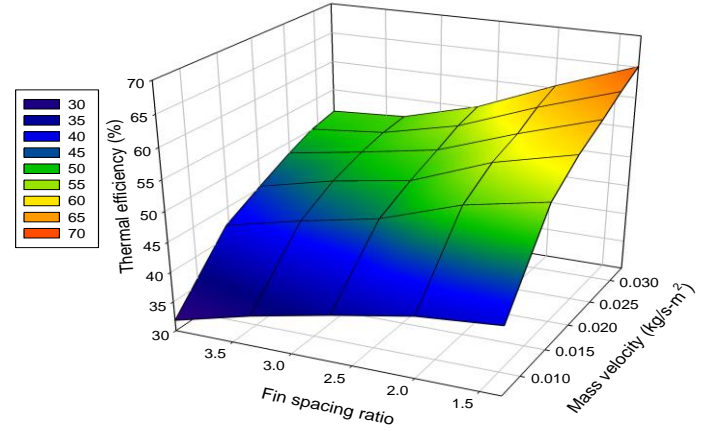
FIGURE 3. Thermal efficiency as a function of mass velocity and fin spacing ratio

losses to the surroundings. Also, the curve shows that as the fin spacing ratio decreases, the thermal efficiency of the collector increases. This is because of narrower channel widths with high flow velocities cause a larger heat transfer rate in addition to the larger surface area to the flowing air resulting in higher efficiency of the system.
Fig.4 shows the experimentally obtained temperature rise in the air as a function of mass velocity for different fin spacing ratio. A higher temperature rise is obtained for the collector having low fin spacing ratio i.e, $F_p/2A=1.33$. At higher mass flow rate there is less effect of fin spacing ratio on the air temperature rise because all curves tend to converge at higher flow velocities.
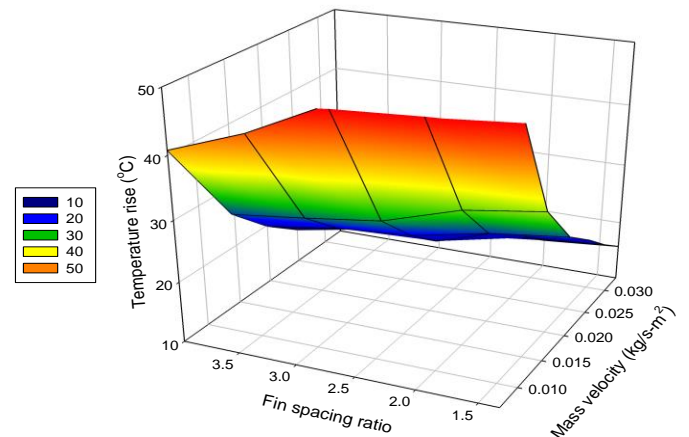
FIGURE 4. Air temperature rise as a function of mass velocity and fin spacing ratio

Thermal efficiency as a function of $\left[(T_o - T_i)/I\right]$ for various fin spacing ratio has been shown with the help of fig.5 for plane as well as wavy fin solar air heater. Results show that the performance of wavy finned absorber is a strong function of fin spacing ratio. Higher temperature rise has been obtained with the lower fin spacing ratio. Also, the maximum efficiency of 65.1% has been achieved for the lower fin spacing. It is clear from the plot that the fin spacing ratio of 1.33 shows overall best performance followed by fin spacing ratio of 2,2.67,3.33 and 4. This is due to higher value of thermal conductance of lower fin spacing ratio absorb higher energy effectively and transfer more energy to the flowing air.
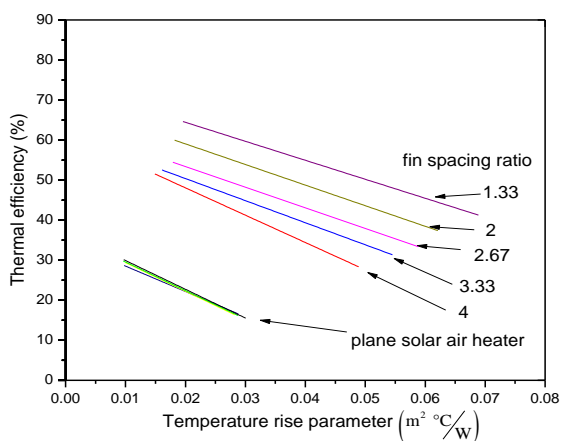
FIGURE 5. Thermal efficiency as a function of temperature rise parameter and fin spacing ratio

CONCLUSIONS

Heat transfer enhancement using wavy fin absorber in solar air heater have been studied. From the results, it can be concluded that a good augmentation in thermal efficiency and temperature rise takes place by using wavy finned absorber. Maximum augmentation has been achieved in thermal efficiency and temperature rise is 2.21 and 2.23times with least fin spacing ratio 0f 1.33 as compared to plane solar air heater. It can also be stated that fin spacing ratio and mass velocities are strong parameter for the performance enhancement of wavy fin absorber solar air heater.

REFERENCES
1. Duffie J.A and Beckman W.A. 1980 "Solar Engineering of Thermal Processes" :New York, Wiley.
2. Öztürk, H.H. Demirel.Y. 2004 "Exergy-based performance analysis of packed-bed solar air heaters". International journal of energy research; 28(5); 423-432.
3. Yadav, S. Kaushal, M. Varun, Siddhartha. 2013 "Nusselt number and friction factor correlations for solar air heater duct having protrusions as roughness elements on absorber plate". Experimental Thermal and Fluid Science, 44; 34-41.
4. Bhushan, B. Singh. R. 2011 " Nusselt number and friction factor correlations for solar air heater duct having artificially roughened absorber plate". Solar Energy: 85(5); 1109-1118.
5. Alok Kumar Rohit, Atul lanjewar. 2016 "Thermo-Hydraulic Performance Evaluation Using W-Discrete Rib in Solar Air Heater". Indian Journal of Science and Technology 9(17), DOI: 10.17485/ijst/2016/v9i17/89056.
6. Pawar CB, Aharwal KR, Choube A. 2009 " Heat transfer and fluid flow characteristics of rib-groove roughened solar air heater ducts". Indian Journal of Science and Technology. 2(11):50–4. DOI: 10.17485/ijst/2009/v2i11/29537.
7. Lalji MK, Sarviya RM, Bhagoria JL.2011 " Heat transfer enhancement in packed bed solar air heater". Indian Journal of Science and Technology; 4(7):747–9. DOI: 10.17485/ ijst/2011/v4i7/30104.
8. Velmurugan P, Ramesh P, 2011 "Evaluation of thermal performance of wire mesh solar air heater". Indian Journal of Science and Technology; 4(1):12–4. DOI: 10.17485/ ijst/2011/v4i1/29923.
9. Priyam,A. Chand, P. 2016 "Thermal and thermohydraulic performanceof wavy finned absorber solar air heater". Solar Energy;130:250-259.
10. Garg, H.P. Datta, G. Bhargava, A.K. 1989. "Performance studies on a finned air heater". Energy: 14(2), 87-92.
11. ASHRAE standard 93-77 (ANSI B 1981-1977). 1977 "Methods of testing to determine the thermal performance of solar collectors"; ASHRAE, New York.
12. Krieder J.F and Krieth. 1978 "Principles of Solar Engineering". 2nd Edition; New York: McGraw Hill Book Company.
13. Kline, S. J., and McClintock, F. A. 1953 "Describing uncertainties in single sample experiments", Mechanical Engineering, Vol. 75, pp. 3-8.

SEEC-2017-002

INVESTIGATION ON THERMAL PERFORMANCE OF DOUBLE FLOW PACKED BED SOLAR AIR HEATER

SAKET KUMAR	R. K Prasad	K. D. P Singh
Mechanical Engineering Department	**Mechanical Engineering Department**	**Mechanical Engineering Department**
NIT Jamshedpur, Jharkhand	NIT Jamshedpur, Jharkhand	NIT Jamshedpur, Jharkhand
saket.gec@gmail.com,9801884455	rkappnit@gmail.com	kdpsingh.me@nitjsr.ac.in

ABSTRACT

This paper presents an experimental investigation, carried out on thermal performance of double flow packed bed solar air heater. Blackened wire screens in the upper duct of the double flow solar air heater have been used as the packing material which work as a porous absorber of thermal energy. The investigation encompassed mass flow rate, ranges from 0.0164 to 0.0362 kg/s, packing height from 5 mm to 25 mm and the heat flux from 750 to 1050 W/m^2. The maximum enhancements in thermal efficiency and temperature rise parameter have been obtained as 1.51 and 2.03 respectively for the entire range of bed heights considered in the investigation. Also, a comparison between double flow, smooth flat plate solar air heater has been done with the investigated type of solar air heater. An enhancement in thermal performance has been obtained with the packing in upper duct of double flow packed bed solar air heater.

Keywords: packed beds; thermal performance; temperature rise; double flow

.

Nomenclature			
A_o	Orifice area (m2)	Q_U	Useful energy gain(W)
C_d	Coefficient of discharge	R	Fraction of mass flow rate (ṁ/M)
C_P	Specific heat of air(J/kg-K)	T_{f1}	Inlet fluid temperature(K)
G	Mass velocity(ṁ/A_c)	ηth	Thermal efficiency (%)
M	Total mass flow rate(kg/s)	β	diameter ratio (d/D)

1. INTRODUCTION

Solar air heaters are simple devices that utilize incident solar radiation to obtain clean energy for a wide usage. The solar air heater device intercepts solar radiation, converts this radiation to the heat in air and delivers the air for use. A packed bed solar collector for air heating is having some distinct advantages over smooth flat plate collector, because packed bed absorbs more solar radiations in depth and have high ratio of heat transfer area to volume and high heat transfer capability that results in relatively low absorber plate temperature and consequently low heat losses from the absorber to atmosphere which leads to an increase in thermal efficiency of the collector (Duffie and Beckman,1980).(Esen,2008),investigated experimentally an energy and exergy analysis for a novel flat plate solar air heater with several obstacles and without obstacles by taking different parameters viz., the inlet and outlet temperatures of air, absorber plate temperatures, ambient temperature, solar radiations and different values of mass flow rates of air.(Ozgen et.al.,2009), investigated experimentally the thermal performance of a double flow solar air heater having aluminium cans as the energy absorber and reported that by inserting aluminium cans on absorbing plate into the double pass channel in a flat plate solar air heater, the collector efficiency can be improved. (Prasad et.al.,2009), made an experimental investigation on a packed bed solar air heater using wire mesh as packing material and compared well with conventional solar air heater. They reported that the thermal efficiency of a packed bed solar air heater using wire mesh as packing material can be increased up to 76.9 to 89.5% more than the conventional one, (Sharma et.al.,1991), investigated experimentally the thermal performance of a single flow solar air heater having its duct packed with blackened wire screen matrices. They concluded that thermal performance of plane collector improves appreciably by packing its duct

with blackened wire-screen matrices and this improvement is a strong function of bed and operating parameters. (Yeh et.al.,2002), investigated experimentally the collector efficiency of double flow solar air heaters with fins attached over and under the absorber plate. (Prasad and Saini, 2002), investigated experimentally the thermal performance of wire-screen matrix bed solar air heaters of unidirectional flow and cross flow types and a plane collector. It has been reported that under similar conditions both the unidirectional flow and cross flow matrix bed collector have optimum thermal efficiency at an optical depth of bed of nearly 5. (Singh and Sharma, 2008), made theoretical parametric analysis of double flow solar air heater having expanded metal mesh as artificial roughness on both sides of the absorber plate. The effect of the friction in the upper and lower flow channels and geometrical parameters of the roughness on thermo-hydraulic efficiency of the collector has been investigated.

From review of the literature, This has motivated the present experimental study for fully developed turbulent flow under constant wall heat flux for a double flow solar air heater having wire screen matrices as porous absorber in the upper duct.

2. METHODOLOGY

2.1 EXPERIMENTAL SET-UP

The experimental set up has been designed and fabricated for the experimentation using wire screen as packing material in the upper duct of double flow solar air heater and shown in Fig.1. The total length of the rectangular duct is 3250 mm in which the flow straightener is of 1000 mm and the test section is of 2250 mm as shown in Fig1. The main components of the experimental set up are halogen lamp, wooden rectangular double duct, comprising flow straightener and test section, G.I pipes, blower, Control valve, orifice meter, U-tube manometer and thermocouple
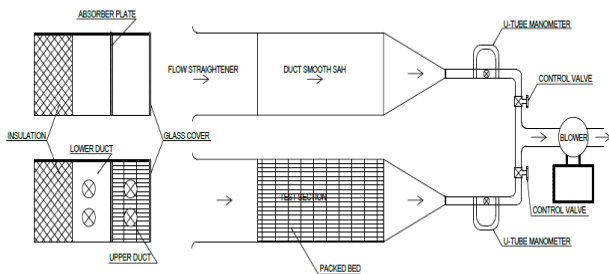
Fig.1 Schematic diagram of Experimental set up of a double flow packed bed solar air heater.
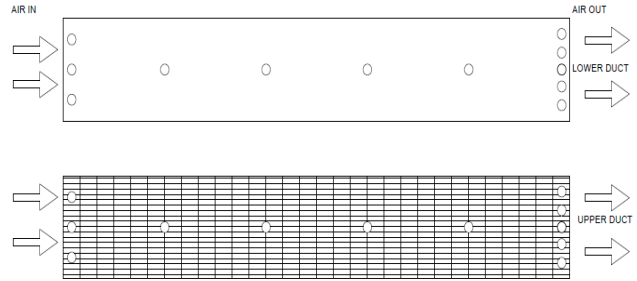
Fig.2 Positions of thermocouples to measure the air temperature in the test sections.

etc. The internal dimensions of both the lower and upper duct are 2250 mm × 400 mm ×30 mm. The indoor experiment was conducted by using a halogen lamp as the source of radiation energy. The various positions of the thermocouples to measure air temperature are shown in Fig.2.

2.2 EXPERIMENTATION

In order to collect data, experiments were conducted on the set up which have a double flow solar air heater with wire mesh packing in its upper duct and a smooth absorber plate of conventional type solar air heater. A view of wire mesh is shown in Fig.3. In this study the effect of packing height on the upper duct has been examined on the air temperature rise parameter and thermal efficiency. For a given height of wire screens, the mass flow rate has been varied and outlet temperatures have been measured by thermocouples. After the inspection of correct functioning of all the instruments and the leak proof of the joints the blower is now switched on. Five values of mass flow rates were considered for each height of wire mesh packing. The mass flow rate of air has been varied with the help of control valves. The mass flow rate in upper duct is fixed as 0.25M and the mass flow rate in lower duct is fixed as 0.75M, where M is the total mass flow rate of air. After fixing the total mass flow rate at different fractions, the various values were recorded when the system is at quasi-steady state.
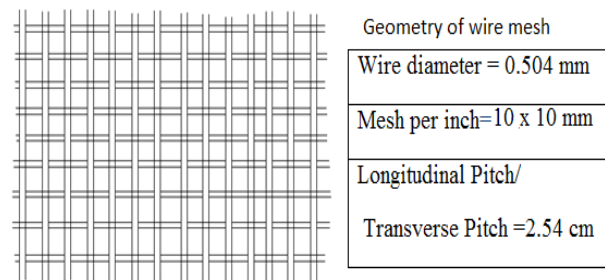
Fig.3 A view of wire mesh screen.

3. DATA REDUCTION:

The collected data was used to calculate the outlet temperature of air and thermal efficiency of double flow solar air heater with packing in upper duct. The equations used to calculate thermal efficiency are given below.

$$M = C_d A_o \sqrt{\frac{2\rho \Delta P}{1-\beta^4}} \tag{1}$$

$$\Delta P = 9.81 \rho (\Delta h_o) \tag{2}$$

$$Q_u = \dot{m} C_p (T_0 - T_i) \tag{3}$$

The useful energy gain by air at upper channel and lower channel are,

$$Q_{u_1} = \dot{m} f_1 C_P \left(T_{f_{10}} - T_{f_{1i}} \right) = GRC_P \left(T_{f_{10}} - T_{f_{1i}} \right) \tag{4}$$

and,

$$Q_{u_2} = \dot{m} f_2 C_P \left(T_{f_{20}} - T_{f_{2i}} \right) = G(1-R) C_P \left(T_{f_{20}} - T_{f_{2i}} \right) \tag{5}$$

$$\eta_{th} = \frac{M C_P (T_0 - T_i)}{I_o \times A_c} \tag{6}$$

For the calculations, air properties were used corresponding to bulk mean temperature.

4. RESULTS AND DISCUSSIONS

In the following section, results of an experimental investigation on thermal performance of a double flow packed bed solar air heater with packing in upper duct are presented. The various parameters were calculated using Equations. 1-6 by taking the following base/ range values of bed geometry and operating parameters and different graphs were plotted as given in Fig. 4-6. I= 900 W/m², W=400 mm, L= 2250 mm, H= 30 mm, ṁ=0.0164 - 0.0362 kg/s, Bed height= 5 - 25 mm.
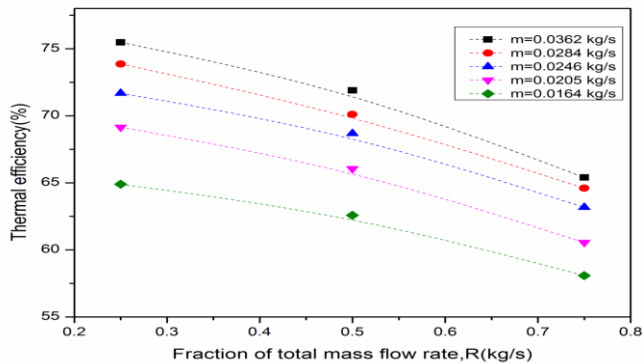
Fig.4 Thermal efficiency as a function of fraction of total mass flow rate for various mass flow.
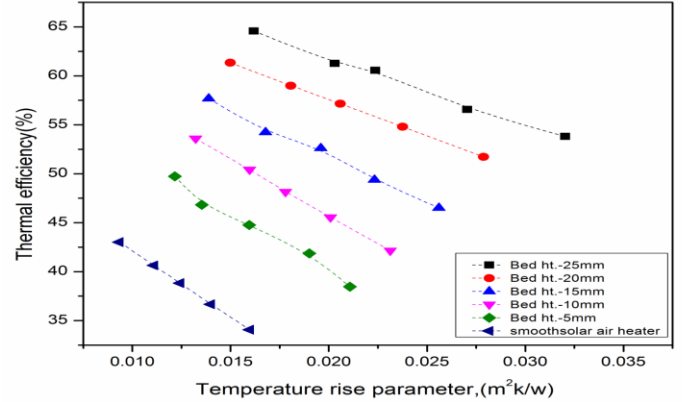
Fig.5 Variation of Thermal efficiency with temperature rise parameter for various bed height.
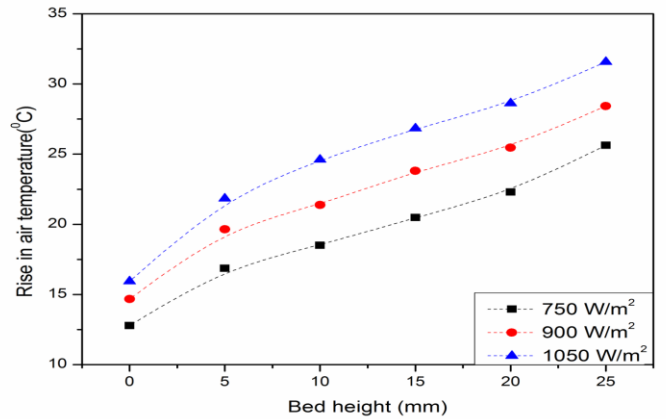
Fig.6 Variation of Rise in air temperature with bed height for different heat flux.

Fig.4 represents the variation of thermal efficiency for the fraction R of total mass flow rate and different mass flow rate. Thermal efficiency increases with the increase in total mass flow rate. For a given mass flow rate, thermal efficiency decreases with the increase in fraction of mass flow rate R..

Fig.5 for the different values of bed height are plotted against a given mass flow rate. Considerable improvement is obtained for the thermal efficiency of double flow packed bed solar air heater with packing in upper duct. Higher temperature rise parameter corresponds to lower thermal efficiency. The enhancements in air temperature rise parameter and in thermal efficiency with the use of packing in upper duct in double flow solar air heater have been achieved as 2.03 and 1.51 respectively over the double flow smooth absorber plate solar air heater increasing temperature rise parameter leads to reduced thermal efficiency because of relative lower effective conduction and radiation results higher heat transfer and lesser thermal losses.

Fig.6 shows the rise in air temperature ΔT as a function of bed height for various values of radiation intensity. The higher value of radiation intensity leads to higher value of rise in air temperature. This is because at higher value of

radiation intensity more heat is absorbed by the absorber and also transferred to the air passing through it.

5. CONCLUSIONS

1. An enhancement in the thermal efficiency and temperature rise parameter of double flow collector having its upper duct packed with wire mesh absorber can be obtained up to 1.51 and 2.03 respectively corresponding to a given height of packing and mass flow rate of air in the duct.

2. For the entire range of heat flux and maximum height of 25 mm of packed bed, the thermal efficiency and air temperature rise of such air heating system increase up to maximum of 1.24 times and 1.29 times respectively more as compared to conventional collector.

3. The rise in air temperature in the bed has been found to be a function of total bed depth. It increases with the height of packed bed depth.

6.REFERENCES

1. Duffie J.A and Beckman W.A, 1980. Solar Engineering of Thermal Processes, New York: Wiley.

2. Esen Hikmet, 2008. Experimental energy and exergy analysis of a double-flow solar air heater having different obstacles on absorber plates. Building and Environment 43, 1046–1054.

3. Ozgen Filiz, Esen Mehmet and Esen Hikmet, 2009. Experimental investigation of thermal performance of a double-flow solar air heater having aluminium cans. Renewable Energy 34, 2391–2398.

4. Prasad S.B., Saini J.S. and Singh Krishna M., 2009. Investigation of heat transfer and friction characteristics of packed bed solar air heater using wire mesh as packing material. Solar Energy 83,773–783.

5. Sharma S.P., Saini J.S. and Varma H.K, 1991. Thermal performance of packed bed solar air heaters. Solar Energy 47, 59-67.

6. Yeh H.-M. , Ho C.-D. and Hou J.-Z.,2002. Collector efficiency of double-flow solar air heaters with fins attached. Energy 27,715–727.

7. Prasad R.K. and Saini J.S., 2002. Thermal Performance study of Matrix Bed Solar Air Heaters. Proceedings of International Conference on Recent Advances in Solar Energy Conversion Systems, MANIT, Bhopal, INDIA, 55-60.

8. Singh K.D.P., Sharma S.P., 2008. Investigation on Thermo- Hydraulic Performance of Double Flow Solar Air Heater with Expanded metal mesh. Ariser 4,175-184.

SEEC-2017-003

A BREIF STUDY OF ENERGY EFFICIENCY IN ALTERNATIVE ROUTES OF EXTRACTION OF ALUMINIUM AND MAGNESIUM

Mainak Saha
Department of Metallurgical and Materials Engineering,
NIT Durgapur, India
Mainaksaha1995@gmail.com

ABSTRACT

The Hall-Héroult process for the electrolytic reduction of alumina was developed at the end of the 19th century and is still currently the only industrial process for the production of aluminium. Today this process is ranked among the most energy and CO2 intensive industrial processes, consuming about 1 % of the globally produced electric energy and producing 2.5 % of the world's anthropogenetic GHG emissions. The direct carbothermic reduction of alumina has been proposed as an alternative process which can substantially improve the sustainability of primary aluminium production Thermochemical calculations predict that by carrying out the carbothermic reduction under vacuum, not only will the required reaction temperature be considerably lowered, but also the formation of gaseous Al should occur without the accompanying formation ofAl2O, Al4C3, and of Al-oxycarbides. Alternatively, liquid Al can be produced by a combination of high temperatures and high excess of carbon thereby again avoiding carbide and sub-oxide formation. The implementation of such carbothermic reduction processes in aluminium production may lead to energy savings of up to 21 %, GHG emissions reductions of up to 52 % and exergy efficiency increase of up to 10 percentile points. Additionally, the prospect of utilizing concentrated solar energy to provide process heat can render the primary aluminium production truly sustainable. Magnesium has a number of applications, such as a light alloy in in the automotive industry an alloying element in aluminium alloys, die casting(32%) , steel desulphurisation (13%), and other applications as an industrial chemical (14%) (USGS,2009). Aluminium industry utilizes magnesium as alloying ingredients to increase the strength, ductility and corrosion resistance of aluminium alloys. Magnesium's use in both aluminium and steel production strongly links its demand to these two other metal commodities. The usage of magnesium has historically been limited by relatively high cost of production and associated energy costs. There have also been scientific issues around alloy development, in particular, increasing creep resistance for drive train applications and improving corrosion resistance.

SEEC-2017-004

PERFORMANCE CHARACTERSTICS OF DIRECT ABSORPTION SOLAR COLLECTOR FOR RESIDENTIAL PURPOSES

Vishal Bhalla
School of Mechanical, Materials and Energy Engineering
Indian Institute of Technology Ropar
vishal.bhalla@iitrpr.ac.in

Vikrant Khullar
Mechanical Engineering Department
Thapar University
vikrant.khullar@thapar.edu

Himanshu Tyagi
School of Mechanical, Materials and Energy Engineering
Indian Institute of Technology Ropar
himanshu.tyagi@iitrpr.ac.in

ABSTRACT

Solar thermal systems are one of the renewable energy systems used in the residential buildings for the heating purpose and with these systems, the usage of non renewable energy resources decreases. To improve the performance of solar collectors engineers and scientists are regularly working on it. Direct absorption based solar collectors are kind of solar collectors in which the fluid can be heated directly (without any absorption surface). The present study deals with numerical model of direct absorption based solar collector which can be used for residential purposes. The absorbed energy fraction, effect of the height, length of collector and mass flow rate on the collector efficiency has been determined. The analysis shows that collector efficiency increases with the increase of mass flow rate when the height of the fluid in the collector is same and the efficiency of the collector decreases with the increase of channel length.

Keywords: Direct absorption solar collector, Nanofluid, Volume fraction, Heat transfer

.
NOMENCLATURE

A	area
C_p	specific heat
D	diameter
f_v	volume fraction
G_T	incident solar flux on the collector, 1000 W/m^2
H	height
h	convective heat transfer coefficient
I	intensity
k	thermal conductivity
K	radiative constant
L	length
$\dot{m}$	mass flow rate
$p(\Omega'\rightarrow\Omega)$	phase function
q_r	radiative heat flux
T	temperature
T_{solar}	black body temperature
U	velocity
y	depth of penetration
η	collector efficiency
ρ	density
Ω	solid angle

SUBSCRIPTS

a	absorption
b	blackbody
e	extinction
λ	spectral
s	scattering
∞	ambient
in	inlet
out	outlet
min	minimum
max	maximum

INTRODUCTION

The demand of energy is increasing day by day due to which the usage of non renewable energy resources (coal, gas, petrol etc.) is increasing, which is influencing the environment. Solar thermal systems are one of the renewable energy systems used in the residential buildings

for the heating purpose and with these systems, the usage of non renewable energy resources is decreasing. Scientists and engineers are regularly working to improve the performance of these systems.

In the recent years, direct absorption based solar collectors have been introduced [1-3] because the radiative losses in the surface based absorption system are very high at high concentration ratio. In the direct absorption type solar collector, the solar radiation is directly absorbed by the heat transfer fluid (water, ethylene glycol, propylene glycol, Therminol VP-1 etc.). Since the absorptivity of the heat transfer fluids is very low in the visible region, so some external particles (nanoparticles) are added in the heat transfer fluid, which improve its absorptivity. Firstly, Tyagi et al. [1] found that with the use of nanoparticles the absorptivity of base fluid have increased by nine times as compare to pure fluid (water). Due to which the efficiency of direct absorption based solar collector is 10% more than the conventional flat plate solar collector. Otanicar et al. [2] found experimentally that with the usage of nanoparticles, the efficiency of the microsolar direct absorption collector was 5% more than the pure fluid. Lenert and Wang [4] prototyped a nanofluid based cylindrical receiver which had been optimized with carbon coated nanoparticles suspended in Therminol VP-1. Meijie et al. [5] experimentally found that at very low volume fraction of gold nanoparticles, photo-thermal efficiency of gold nanoparticles is more than water. In the present study, a numerical model has been studied for a flat shape direct absorption based solar collector which can be used for the water heating. In the present study, effect of various parameter like height, length and mass flow rate on the collector efficiency has been studied.

THEORETICAL MODEL

In order to evaluate the performance of direct absorption based solar collector using nanofluid (Aluminium Nanoparticles ($D = 10$ nm) and Base fluid - Water), a theoretical model for a flat shape direct absorption solar collector is established. The schematic of the flat shape solar collector is as shown in figure 1.
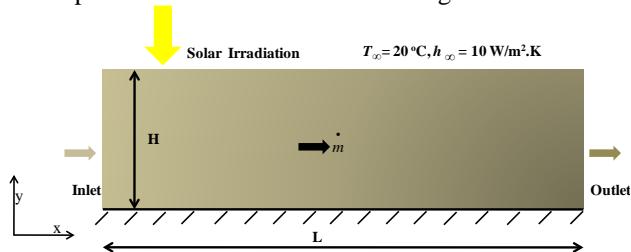
Figure 1. Theoretical model of flat shape direct absorption solar collector

The following assumption have been used for collector while solving the theoretical model:- 1)The top surface is exposed to the ambient air at $T_\infty = 20\ ^oC$ and heat transfer coefficient is 10 W/m^2.K. 2) Bottom surface is adiabatic i.e. no heat flux can pass through it. 3) Emission losses are negligible 4) No In-scattering.

In order to simulate the intensity distribution within the channel (along the height of the channel) equation (1) which is radiative transfer equation (RTE) has been used.

$$\frac{dI_\lambda(\Omega)}{dy} = -(K_{s_\lambda} + K_{a_\lambda})I_\lambda(\Omega) + K_{a_\lambda}I_{b_\lambda} + \frac{K_{s_\lambda}}{4\pi}\int_{4\pi} I_\lambda(\Omega')p(\Omega' \to \Omega)d\Omega$$

(1)

where $K_{a\lambda}$ and $K_{s\lambda}$ are the spectral absorption coefficient and spectral scattering coefficient. These coefficients have been calculated by using Ref. [6][7].

To find out the temperature gain ($\Delta T = T_{out} - T_{in}$; $T_{in} = 20\ ^oC$) in the fluid, RTE is solved simultaneously with the two dimensional energy equation. The energy equation is given in equation (2).

$$k\frac{\partial^2 T}{\partial y^2} - \frac{\partial q_r}{\partial y} = \rho C_p U \frac{\partial T}{\partial x}$$

(2)

where k is the thermal conductivity of the fluid, q_r is radiative heat flux, U is the velocity of the fluid, C_p is the specific heat of the fluid.

Finally, the collector efficiency is find out by using equation (3).

$$\eta = \frac{\dot{m}C_p \Delta T}{A G_T}$$

(3)

where $\dot{m}$ is mass flow rate, A is top cover area of the collector, G_T is the incident solar flux (1000 W/m^2).

RESULTS AND DISCUSSIONS

To understand the potential of nanofluid in the direct absorption solar collector, it is very necessary to understand the how much irradiation is getting absorbed by the fluid. To evaluate the absorbing capability of the nanofluid, we calculated the absorbed energy fraction F, which has been calculated by using equation (4). The absorbed energy fraction depends on the volume fraction (f_v) of the nanoparticles and the depth of penetration (y).

$$F = \frac{1 - \int_{\lambda_{min}}^{\lambda_{max}} I_{b\lambda}(\lambda, T_{solar})e^{-K_{e\lambda}y}d\lambda}{\int_{\lambda_{min}}^{\lambda_{max}} I_{b\lambda}d\lambda}$$

(4)

where $I_{b\lambda}$ is the black body spectral intensity, $K_{e\lambda}$ is the extinction coefficient, y is depth of penetration, T_{solar} is black body temperature (=5800K).

Figure 2 shows the absorbed energy fraction F for various volume fractions at different depth of penetration, the absorbed energy fraction for nanofluid is higher than the pure fluid ($f_v = 0\%$). Moreover, at high volume fraction the depth of penetration is low i.e. irradiation is absorbed in a very thin layer. On the other hand, at low volume fraction the irradiation can penetrate deeply in the solar

collector. This information is very useful while designing the direct absorption based solar collector.
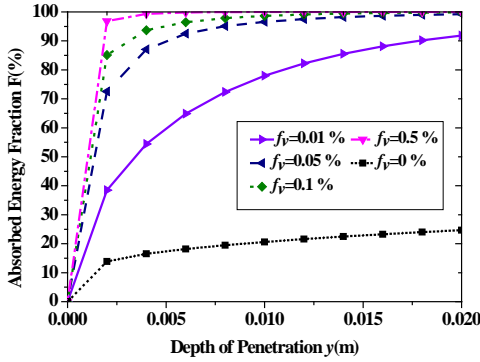
Figure 2. Absorbed energy fraction verses the depth of penetration for different volume fractions of nanofluid

The temperature rise of the fluid is an important parameter in the solar collector. Figure 3(a) and figure 4 (a) shows the temperature gain by fluid at different mass flow rates. Figure 3(b) and figure 4(b) shows the efficiency of the direct absorption solar collector using water and nanofluid at different mass flow rates and at different mass flow rates.
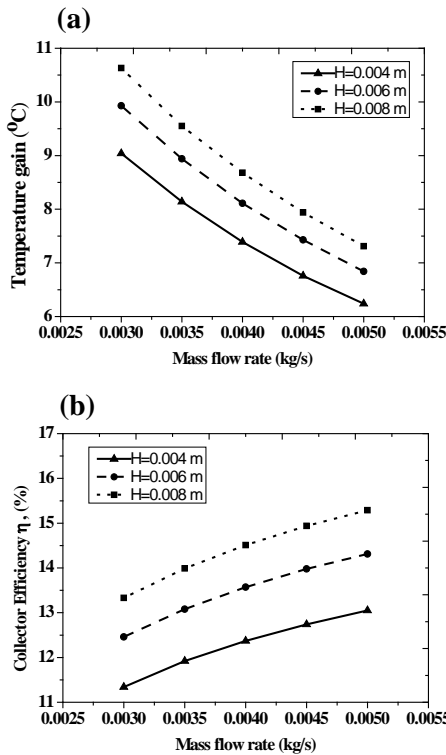
Figure 3. Performance of flat shape solar collector for pure fluid (water) at different values of mass flow rate $\dot{m}$ (a) temperature gain and (b) collector efficiency. length of the collector is 1m.

As can be seen in figure 3(a) and figure 4(a) that the trend of temperature gain decreases as the mass flow rate increases. The reason for the decreasing trend is that when the mass flow rate increases the exposure time of the sunlight is less. On the other hand, when the depth of the channel increases and the mass flow rate is constant, the amount of attenuation of sunlight increases. Due to this attenuation the nanofluid gets heated and gives high temperature gain.

In figure 3(b) and figure 4(b), the collector efficiency increases with the increase of mass flow rate $\dot{m}$ and height of the collector H. It can be understood in such a way that η is directly proportional to both $\dot{m}$ and ΔT. The rate of increase of mass flow rate is larger than the decrease in temperature gain for all values of H, thus the collector efficiency can be increased. From figure 3(b) and figure 4(b) we can conclude that the collector efficiency with nanofluid is more than the pure water.
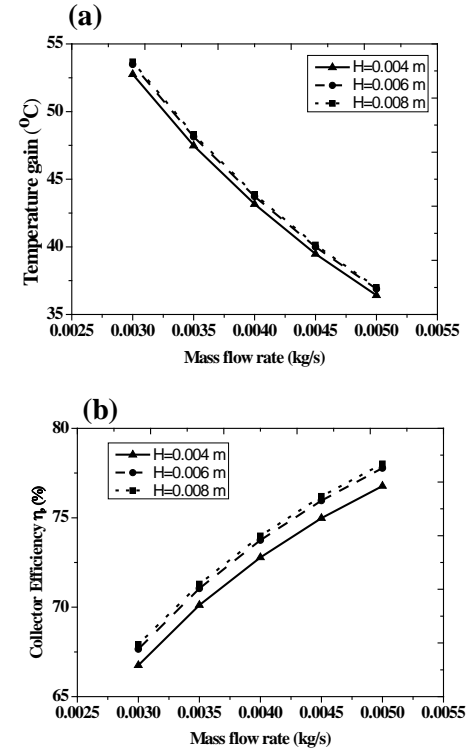
Figure 4. Performance of flat shape solar collector for nanofluid at different values of mass flow rate $\dot{m}$ (a) temperature gain; and (b) collector efficiency. length of the collector is 1m.

Another parameter that effect the performance of the solar collector is the length of the solar collector. Figure 5 shows the effect of channel length on the temperature gain and the collector efficiency.

3

From the figure 5 it can be concluded that with the increase of length of the collector the temperature gain increases because the amount of sunlight absorbed by the flowing fluid increases.
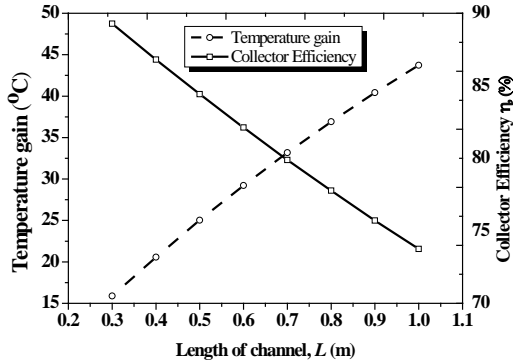
Figure 5. Effect of channel length on the temperature gain and the collector efficiency for the nanofluid based solar collector.

But similarly the collector efficiency decrease and it can be interpreted as when the length of the collector is small the temperature gain is less and correspondingly the losses to the atmosphere through convection are less due to which the collector efficiency is high. Simultaneously, on increasing the length of the collector the convective losses increases and due to which the collector efficiency decreases.

The volume fraction of the nanoparticles plays an important role in the direct absorption solar collector. Figure 6 shows the effect of the volume fraction on the temperature gain of the nanofluid. Figure 6 shows an optimum volume fraction of the nanoparticles i.e. the temperature below and above the optimum volume fraction is less. The trend of the temperature gain shows that the system is highly dependent on the volume fraction of the nanoparticles. Increasing the volume fraction increases the attenuation of the sunlight. This attenuation varies exponentially with the extinction coefficient and hence also with the volume fraction of the nanoparticles. So, there has an optimum volume fraction of the nanoparticles where the temperature gain is maximum. For this optimum volume fraction height of the collector was 0.006 m and the mass flow rate was 0.003 kg/s.
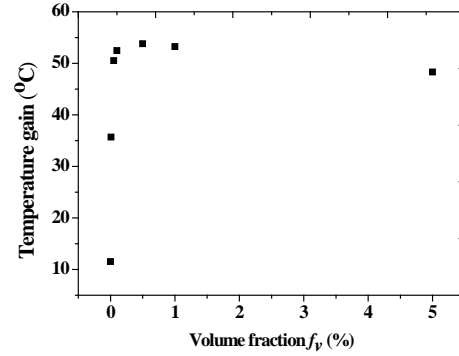
Figure 6. Effect of volume fraction on the temperature gain

CONCLUSION

The analysis shows that collector efficiency increases with the increase of mass flow rate when the height of the fluid in the collector is same and the efficiency of the collector deceases with the increase of channel length. The results shows that the with the nanofluid the temperature gain is 42 $^{\circ}$C higher than pure water.

REFERENCES

[1] Tyagi, H., Phelan, P., & Prasher, R. (2009). Predicted efficiency of a low-temperature nanofluid-based direct absorption solar collector. *Journal of solar energy engineering*, *131*(4), 041004.

[2] Otanicar, T. P., Phelan, P. E., Prasher, R. S., Rosengarten, G., & Taylor, R. A. (2010). Nanofluid-based direct absorption solar collector. *Journal of renewable and sustainable energy*, *2*(3), 033102.

[3] Taylor, R. A., Phelan, P. E., Otanicar, T. P., Walker, C. A., Nguyen, M., Trimble, S., & Prasher, R. (2011). Applicability of nanofluids in high flux solar collectors. *Journal of Renewable and Sustainable Energy*, *3*(2), 023104.

[4] Lenert, A., & Wang, E. N. (2012). Optimization of nanofluid volumetric receivers for solar thermal energy conversion. *Solar Energy*, *86*(1), 253-265.

[5] Chen, M., He, Y., Zhu, J., & Kim, D. R. (2016). Enhancement of photo-thermal conversion using gold nanofluids with different particle sizes. *Energy Conversion and Management*, *112*, 21-30.

[6] Bohren, C. F., & Huffman, D. R. (2008). *Absorption and scattering of light by small particles*. John Wiley & Sons.

[7] Brewster, M. Q. (1992). *Thermal radiative transfer and properties*. John Wiley & Sons.

NUMERICAL STUDY OF SINGLE STAGE FLASH EVAPORATION DESALINATION TECHNIQUE COUPLED WITH NANO-FLUID BASED DIRECT ABSORPTION SOLAR COLLECTOR

Kapil Garg
School of Mechanical, Materials and Energy
Engineering
Indian Institute of Technology Ropar
kapil.garg@iitrpr.ac.in

Vikrant Khullar
Mechanical Engineering Department
Thapar University
vikrant.khullar@thapar.edu

Himanshu Tyagi
School of Mechanical, Materials and Energy
Engineering
Indian Institute of Technology Ropar
himanshu.tyagi@iitrpr.ac.in skdas@iitrpr.ac.in

Sarit K. Das
School of Mechanical, Materials and Energy
Engineering
Indian Institute of Technology Ropar
himanshu.tyagi@iitrpr.ac.in skdas@iitrpr.ac.in

ABSTRACT

In the present paper a single stage flash evaporation desalination unit coupled with the nano-fluid based direct absorption solar collector is studied theoretically. The various influencing parameters which affect the fresh water production from this unit have been studied. The mathematical model is prepared for both the units such as direct absorption solar collector (DASC) and single stage flash desalination unit and is solved in MATLAB. The desired output is measured in the form of Gained Output ratio (GOR). The variation of GOR is plotted for different material of nano-particles against mean particle diameter of nano-particles, outlet temperature of brine from DASC, height of the solar collector etc.

Keywords: flash evaporation, nano-particles, solar energy, GOR

NOMENCLATURE

A	area of condenser [m^2]
C_p	specific heat [Jkg^{-1}K^{-1}]
c_o	speed of light [m/s]
D	mean particle diameter of nano-particles [nm]
$DASC$	direct absorption solar collector
E	effectiveness of the condenser
FDM	finite difference method
f_v	particle volume fraction inside base fluid
GOR	gained output ratio
h	Planck constant, $h = 6.6256 \times 10^{-34}$ J s
h_f	enthalpy of feed sea water [Jkg^{-1}]
h_{fg}	enthalpy of vaporization or condensation [Jkg^{-1}]
h_v	enthalpy of vapors of fresh water [Jkg^{-1}]
I	radiation intensity [Wm^{-3}str^{-1}]
K	radiative coefficients [m^{-1}]
k	thermal conductivity of fluid [Wm^{-1}K^{-1}]
k_B	Boltzmann constant, $k_B = 1.38 \times 10^{-23}$J/K
m	normalized refractive index, $m = n + i\kappa$
$\dot{m}$	mass flow rate of the fluid flowing [kg/s]
NTU	no. of transfer units in the condenser
N	index of refraction
P	saturation pressure [Pa]
Q	heat input [Js^{-1}]
q_r	radiative flux obtained from sun [Wm^{-3}]
T	temperature [K]
ΔT_{lm}	log mean temperature difference in the condenser
T	time [s]

| U | heat transfer coefficient of condenser [Wm^{-1}K^{-1}] |
| Y | distance from the bottom of the solar collector [m] |

Greek Symbols

κ	index of absorption
λ	wavelength of incident radiation [μm]
ρ	density [kg m^{-3}]
ϕ	solid angle [str]

Subscripts

A	absorption
b	brine
$black$	blackbody
cw	cold water
e	extinction
f	feed sea water
f_i	feed water at inlet
f_o	feed water at outlet
in	vapors of fresh water
r	radiative
v	vapor
λ	spectral

INTRODUCTION

Fresh water is the need of every human being and without fresh water the survival of human is impossible. But due to uneven distribution of fresh water on the earth, rapid growth of industrialization and increase in population demand for fresh water is increasing at a fast rate. Also many people face the fresh water shortage due to the geographical location. These are the people mainly living in arid regions such as gulf countries and etc. In order to meet the fresh water demand for every human being living on this planet, desalination is the reliable method to solve such problem which should be done using renewable energy sources instead of using conventional energy sources so that it doesn't cause any harm to environment.

There are various methods used for desalination such as multi-stage flash evaporation, multi-effect distillation and vapor compression which are actually phase change processes. The energy for phase change is provided by steam or some other source of heat. In multi-stage flash desalination sea water is heated to a saturation temperature by any heat source corresponding to saturation pressure and it then flows through a throttle valve and enters into a flash drum which is at lower pressure than initial pressure. Vapors of fresh water are obtained due to sudden reduction in pressure (flashing) which are then condensed in a condenser.

In the present model the nano-fluid based direct absorption solar collector is coupled with the single stage flash desalination unit[1]. The output of the flashing unit is measured in the form of gained output ratio (GOR) for different material of nano-particles against mean particle diameter of nano-particles, outlet temperature of brine from DASC and height of the solar collector. The mathematical model is prepared for both the units and solved in MATLAB.

THEORETICAL MODEL

In the present study a new kind of system for desalination has been proposed in which nano-particles of different materials such as Aluminum, Copper and Gold is mixed in sea water in different proportions with different mean diameter of particles and is fed to the DASC for heating of the sea water. The feed sea water having mass flow rate, $\dot{m}_f$ (kg/s) and at inlet pressure P_1 is heated to the saturation temperature T_1 in DASC as shown in Fig.1.

The saturated sea water then flows through a throttle valve and its pressure and temperature is decreased to T_2 and P_2 respectively and then it enters into the flash drum [2]. The throttling of the sea water results in the reduction of the pressure and temperature and partial vapors of fresh water are formed. The vapors draw the latent heat of evaporation through feed sea water. The vapors of fresh water (at T_3, P_3) are then fed to a condenser unit where it gets condensed giving its latent heat of condensation to the cold sea water and condensed fresh water is collected in a collection tray[3].
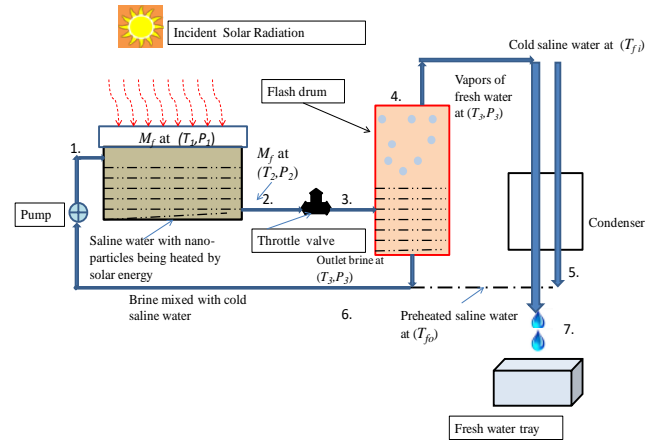
Figure 1. Schematic diagram of single stage flash evaporation unit coupled with nano-fluid based direct absorption solar collector (DASC).

NUMERICAL MODELING

This section deals with modeling of the system having two parts such as DASC and flash evaporation desalination unit. The mathematical model is developed for each part and is solved using numerical techniques with the help of MATLAB.

Modeling Of Direct Absorption Solar Collector

The incoming solar radiation is absorbed by the sea water with nano-particles of different materials such as Aluminium, Copper and Gold mixed in a fixed amount of volume fraction. This fluid inside the collector is flowing through DASC at very slow and constant velocity. The radiation is considered to be in the range of 0.3-2.5μm (wavelength band coming from sun). The intensity of incoming solar radiation can be calculated by Eqn. (1)

$$I_{black} = \frac{2hc_o{}^2}{\lambda^5 \left[\exp\left(\frac{hc_o}{k_B \lambda T_{solar}} - 1 \right) \right]} , \tag{1}$$

where h is the Planck's constant, c_o is the speed of light (in vacuum), λ is the wavelength of incident radiation, k_b is the Boltzmann constant and T_{solar} is the temperature of the sun (T_{solar} = 5800 K). The intensity of radiation which is falling on the DASC and absorbed by the fluid was assumed to vary only in the y-direction and this attenuation of intensity by the nano-particles due to absorption and scattering is given by the Eqn. (2)

$$\frac{\partial I_\lambda}{\partial y} = -(K_{a\lambda,nano\text{-}particles} + K_{s\lambda,nano\text{-}particles})I_\lambda = -K_{e\lambda,nano\text{-}particles}I_\lambda , \tag{2}$$

$$K_{a\lambda,nano-particles} = \frac{12\pi f_v}{\lambda} \text{Im}\left\{ \frac{m^2-1}{m^2+2}\left[1 + \frac{\pi^2 D^2}{15\lambda^2}\left(\frac{m^2-1}{m^2+2} \right)\right]\left(\frac{m^4+27m^2+38}{2m^2+3} \right) \right\} , \tag{2a}$$

$$K_{s\lambda,nano-particles} = \frac{8\pi^4 D^3 f_v}{\lambda^4}\left| \frac{m^2-1}{m^2+2} \right|^2 . \tag{2b}$$

The resultant extinction caused by the nano-fluid is given by the Eqn. (3).

$$\frac{\partial I_\lambda}{\partial y} = K_{e\lambda,nano\text{-}fluid}I_\lambda = -\left(K_{a\lambda,water} + K_{e\lambda,nano\text{-}particles} \right)I_\lambda , \tag{3}$$

where the $K_{e\lambda,nano\text{-}particles}$ is obtained from Eqn. (2) and $K_{a\lambda,water}$ and m is calculated as shown below

$$K_{a\lambda,water} = \frac{4\pi\kappa}{\lambda} , \tag{3a}$$

$$m = \frac{m_{particles}}{n_{fluid}} . \tag{3b}$$

The heat transfer model for nano-fluid based solar collector is steady state and one-dimensional [1] and it is solved using the finite difference implicit method [4]. The following governing Eqn. (4) is solved using finite difference technique using Matlab:-

$$k\frac{\partial^2 T}{\partial y^2} - \frac{\partial q_r}{\partial y} = \rho C_p \frac{\partial T}{\partial t} , \tag{4}$$

where k is the thermal conductivity of the nano-fluid. Properties of nano-particles and base fluid used are obtained from table 1. The temperature of the fluid varies only in the y-direction with time and q_r is the radiative flux absorbed by the nano-fluid given as Eqn. (5).

$$q_r = \iint I_\lambda d\phi d\lambda . \tag{5}$$

Table 1: Thermo-Physical properties of nano-particles and base fluid [5]

Properties (at 25ºC)	Water (H₂O)	Aluminum (Al)	Gold (Au)	Copper (Cu)
Density (kgm⁻³)	997	2700	19300	8933
Specific heat (Jkg⁻¹ K⁻¹)	4180	900	129	385
ThermalConductivity (Wm⁻¹K⁻¹)	0.49	247	317	401

Modeling Of The Single Stage Flash Evaporation Desalination Unit

In order to model this unit some assumptions were taken which are as follows. The process takes place in flashing unit and condenser are assumed to be steady state. Entire mass of the vapors is assumed to be condensed to give fresh water. There are no non-condensable gases.

To calculate the mass flow rate of the distillate produced in the flashing unit the mass flow and the energy balance is applied on the flashing and condenser unit [4].

Following are the mass flow and energy balance equations, Eqn. (6) & (7) respectively, for flashing unit which are solved in MATLAB in order to calculate the amount of fresh water obtained:-

$$\dot{m}_f = \dot{m}_b + \dot{m}_v , \tag{6}$$

$$\dot{m}_f h_f\left(T_2, P_2 \right) = \dot{m}_b h_{3b}(T_3, P_3) + \dot{m}_v h_{3v}(T_3, P_3) , \tag{7}$$

where $\dot{m}_f$, $\dot{m}_b$ and $\dot{m}_v$ are the mass flow rates of feed sea water, outlet brine and fresh water vapor (in kg/s). Also the difference between the saturation temperatures at the two stages 2 and 3 is kept only 20ºC for all cases which means during throttling the temperature of the fluid is lowered by

only 20ºC corresponding to saturation pressure at that temperature.

The energy balance equations for condenser are:-

$$\dot{m}_{cw}C_p(T_{fo} - T_{fi}) = UA\Delta T_{lm} \quad , \qquad (8)$$

$$\ln\frac{(T_{3v} - T_{fi})}{(T_{3v} - T_{fo})} = \frac{UA}{\dot{m}_{cw}C_p} = NTU \, , \qquad (9)$$

$$E = 1 - e^{-NTU} \, , \qquad (10)$$

$$(1 - E)T_{fi} + (E.T_{3v}) = T_{fo} \, . \qquad (11)$$

Solving these equations, Eqns. (8) - (11) the outlet temperature (T_{fo}) of the cold saline water from condenser can be calculated. The effectiveness of the system is measured by gained output ratio (GOR) which is shown in Eqn.(12).

$$GOR = \frac{\dot{m}_v h_{fg}}{Q_{in}} \, . \qquad (12)$$

RESULTS AND CONCLUSION

In this section the main output i.e. gained output ratio (GOR) of the nano-fluid based desalination system is plotted against various influencing parameters such as height (H) of DASC, mean particle diameter of nano-particles (D) and temperature T_2 of feed sea water at the outlet of DASC.
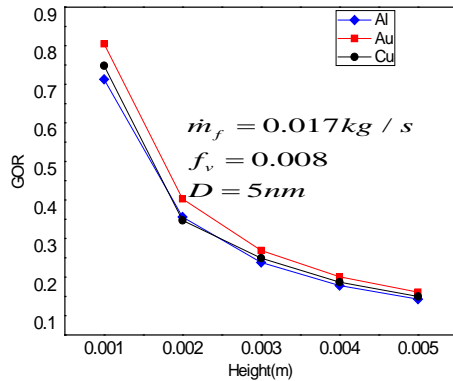
Figure2. Shows the variation of gor (GOR) versus the height (H) of the solar collector.

It can be concluded that the height of the solar collector is one of the most important parameter which influences the system productivity as can be seen from the Fig. 2. As the height (H) of the DASC increases the system productivity decreases. The mean particle diameter (D) of nano-particles have almost no effect on the system productivity as shown in Fig. 3. Also from Fig. 4 it is found that as feed sea water temperature T_2 at the outlet of

DASC increases the GOR decreases. This is due to the high energy input and limitation of the process as pressure reduction due to throttling of feed water is restricted by 20ºC in order to avoid losses. Use of DASC ensures direct absorption of solar energy by the flowing fluid inside the system.
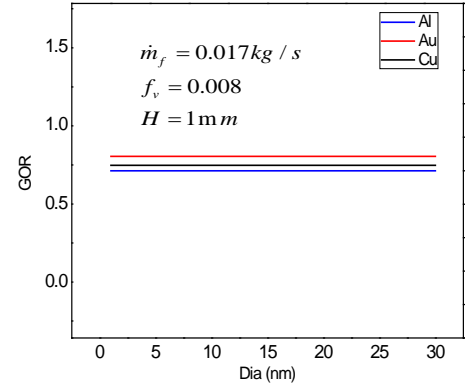
Figure 3. Plot of gained output ratio (GOR) versus mean particle diameter (D) of nano-particles
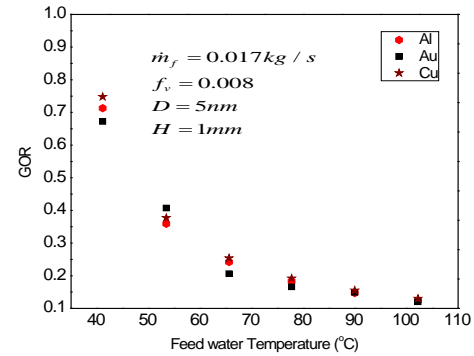
Figure 4. Shows the variation of gained output ratio versus the outlet temperature of sea water from DASC

REFERENCES

[1] Tyagi, H., Phelan, P. and Prasher, R., 2009. Predicted efficiency of a low-temperature nanofluid-based direct absorption solar collector. Journal of Solar Energy Engineering, 131(4), p.041004.

[2] Nafey, A.S., Mohamad, M.A., El-Helaby, S.O. and Sharaf, M.A., 2007. Theoretical and experimental study of a small unit for solar

desalination using flashing process. Energy Conversion and Management, 48(2), pp.528-538.

[3] El-Dessouky, H.T. and Ettouney, H.M., 2002. Fundamentals of Salt Water desalination. Elsevier.

[4] Cengel, Y.A., Heat and Mass Transfer: A Practical Approach 4th ed., Mcgraw Hill, New York, 2007.

[5] Palik, E. D. (1998). Handbook of Optical Constants of Solids (Vol. 3). Academic press.

SEEC-2017-006

PERFORMANCE AND EMISSION STUDY OF CI ENGINE FUELLED WITH DIESEL AND MICROALGAE BIODIESEL WITH EGR

Dr. SushantS. Satputaley
Department of Mechanical Engineering
Asstt. Prof., SVPCET, Nagpur
satputaley@gmail.com

ShubhamBurde
Department of Mechanical Engineering
Student, SVPCET, Nagpur
shubhamburde18@gmail.com

ShubhamTatpalliwar
Department of Mechanical Engineering
Student, SVPCET, Nagpur
shubhamtatpalliwar@gmail.com

D.B Zodpe
Department of Mechanical Engineering
Associate Prof., VNIT, Nagpur
zodpedb@rediffmail.com

Dr. N.V. Deshpande
Department of Mechanical Engineeering
Professor, VNIT, Nagpur
nishu1952@yahoo.com

ABSTRACT

An effort has been taken to study performance and emission characteristics of a diesel engine fueled with microalgae biodiesel and diesel fuel using exhaust gas recirculation (EGR). The experimental investigation was conducted on a single-cylinder, four-stroke, water cooled, direct injection CI engine (Kirloskar TV1 model, 0.661 capacity, 5.2 kW) working at a constant speed of 1500 rpm. The results obtained with microalgae biodiesel were compared with the diesel fuel. The brake thermal efficiency (BTHE) obtained using microalgae biodiesel is less as compared to the diesel fuel, which could be attributed to lower calorific value of microalgae biodiesel. Smoke and HC emissions for biodiesel were higher than that of diesel fuel. However, it was observed that a NO_X emission for microalgae biodiesel is lower than that of diesel fuel. Exhaust gas recirculation (EGR) is used to reduce NO_X emissions from a diesel engine. In this study the different rate of EGR (0%, 5%, 10%, 15% and 20%) was used to study the performance and emission characteristics of CI engine.

Keywords: Biodiesel, Microalgae and EGR

INTRODUCTION

In recent period the increase in automobile in significantly large number has increased the demand of petroleum products or we can say fossil fuels. With crude oil reserves estimated to last only for few decades, there has been an active search for alternate fuels. The extinction of crude oil in recent year would cause a major impact on the transportation and industrial sector. The various alternate fuels under consideration, biodiesel is one of the promising alternative fuel to conventional diesel fuel. [1] Various research works have proved that performance of biodiesel is nearly similar to diesel fuel with fewer emissions. Further, engine parameters such as compression ratio, injection timing and injection pressure are also found to be significant factors contributing on performance and exhaust emissions of diesel engine, fueled with biodiesel. [2] The formation of NO_X emissions in diesel engines is predominant as the temperature in the combustion chamber is high, since at

higher temperatures the tendency of nitrogen to react with oxygen causes the NO_X formation. This problem of NO_X generation can be overcome by using NO_X reduction techniques like exhaust gas recirculation, which is recirculation of some exhaust gases into intake which aids in reducing the NO_X. [3] An important property of biodiesel is its oxygen content of about 10 to 20%, which is usually not contained in diesel fuel. Biodiesel fuels have been recently stood out due to some important advantages such as requiring little or no modification for use in diesel engines. Moreover, they are non-toxic, have higher biodegradability and contain almost no sulphur. So in order to reduce NO_X emission various techniques have been developed like SCR, EGR, Humid Air Induction, Water Injection in cylinder, etc. Among this EGR is one of the most effective techniques to reduce NO_X emissions. [4]

EXHAUST GAS RECIRCULATION:

EGR works by recirculating a portion of an engine's exhaust gas back to the engine cylinders. This dilutes the O_2 in the incoming air stream and provides gases inert to combustion to act as absorbents of combustion heat to reduce peak in-cylinder temperatures. The effect of EGR on NO_X reduction can be attributed to three theories 1) increased ignition delay, 2) increased heat capacity and 3) dilution of the intake charge with inert gases. The ignition delay theory asserts that because EGR causes an increase in ignition delay, it has the same effect as retarding the injection timing. The heat capacity theory states that the addition of the inert exhaust gas into the intake increases the heat capacity (specific heat) of the non-reacting matter present during the combustion. The increased heat capacity has the effect of lowering the peak combustion temperature. According to dilution theory, the effect of EGR on NO_X is caused by increasing amounts of inert gases in the mixture, which reduces the adiabatic flame temperature [5].

% EGR= $\frac{M_{EGR}}{M_{TOTAL}} \times 100$ [5] (1)

Where, MEGR =Mass of exhaust gas which is recirculated and MTOTAL = Total mass of intake in cylinder i.e. MEGR +MAIR.

MICROALGAE OIL:

Biofuels were used and studied in three generations depending upon their availability and the yield produced from them. The 1st generation biofuels include food and oil crop like Sugar beet, rapeseed etc. The sustainability of first generation fuel has been questioned over the concerns such as reported displacement of food crop. The 2nd generation biofuels are manufactured from lignocelluloses biomass or woody crops like Jatropha seeds etc. Microalgae biodiesel is 3rd generation of biofuels and are fastest growing plants in the world. About 50% of dry algae weight is oil and per unit area yield of oil from algae is about 20,000 liter per acre which is far more than next best crop palm oil. Calorific value of algae oil is about 37.018 MJ/kg which is nearer to calorific value of diesel fuel.

PREPARATION OF BIODIESEL:

Bio-lipid microalgae oil consists of hydrocarbon compounds (triacyglycerides) that are not suitable for most diesel engines. Also, the carbon chains are too viscous for good flow and combustion. The microalgae oil can be modified for use in diesel engines by a chemical process known as "transesterification". The end product of the microalgae oil conversion using methyl alcohol is fatty acid methyl esters with the trade name of "Biodiesel". The transesterification process separates the oil into glycerol (fatty acids) and biodiesel.The biodiesel formed is further purified by washing it with water until the pH value of the biodiesel comes out to be neutral. The yield obtained for biodiesel from the microalgae oil is 85 %.

EXPERIMENTAL METHODOLOGY:

The test engine is a single cylinder four stroke direct injection water cooled diesel engine (Kirloskar TV1 model, 0.661 capacity, 5.2 kW) working at a constant speed of 1500 rpm. The EGR system, which is designed and fabricated in-house, consists of a piping system taken from the engine exhaust pipe, an orifice meter used to measure the flow rate of the exhaust gases, and a control valve to control the amount of exhaust gas recycling into the inlet manifold. Plenum chambers are installed to damp the exhaust and maintain the regular exhaust gas through pipes. The AVL 437 smoke meter is used to measure the smoke opacity and AVL Digas 4000 light, an infrared type gas analyzer was used to measure CO, CO_2, HC, NO_X and O_2. The Methodology for carrying out the experimental performance is as follows:

• The engine was fuelled with diesel and allowed to run at various loads ranging from 0 to 18kg in steps of 2 kg with 0% EGR and observations were recorded related to performance and emission parameters.
• Then, the experimentation was repeated by supplying different percentage of EGR (5%, 10%, 15% and 20%) in the engine cylinder and observations were recorded.

• Then, the engine was fuelled with microalgae biodiesel (B100) and observations were recorded with 0%, 5%, 10%, 15%, and 20% EGR.

RESULTS AND DISCUSSION:

The engine testing is done working at a constant speed of 1500 rpm fuelled with Diesel, B100 and Algae oil at different engine loads, ranging from no-load to full load with different %EGR. In each test, performance, combustion and emission parameters were measured.

Brake Thermal Efficiency:

The observations recorded at full load (5.2 kW) for BTHE using different fuel and varying EGR rates are shown in fig. 1. From the obtained results, it is observed that BTHE reduces with increase in percentage of EGR. The maximum BTHE is obtained with diesel as fuel at 0% EGR (32.81%) and minimum BTHE is observed at when engine is fuelled with B100 with 20% EGR (24.39%). The BTHE obtained for diesel is higher as compared to B100 for all EGR rates. This is because of the lower calorific value and higher viscosity of B100 as compared to diesel.
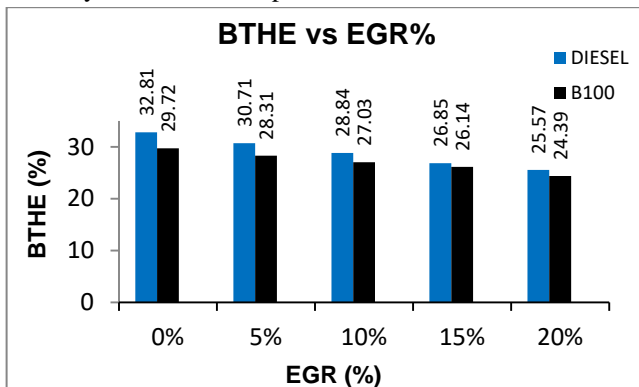
FIGURE 1. VARIATION OF BRAKE THERMAL EFFICIENCY WITH EGR %

Brake Specific Energy Consumption:

The comparison based on brake specific fuel consumption cannot be made since the fuel has different energy content. Therefore, a comparison is made based on brake specific energy consumption. BSEC is defined as the product of the BSFC and calorific value of a fuel. The observations recorded for BSEC at full load (5.2 kW) with different fuel and EGR rates is shown in fig. 2. The obtained results show that BSEC increases with increase in EGR rate. The minimum BSEC is obtained with diesel at 0% EGR (10.97 kg/kW-hr) and maximum BSEC is observed at B100 with 20% EGR (14.76 kg/kW-hr). The lower BSEC obtained for diesel as compared to B100 is due to higher calorific value of diesel.
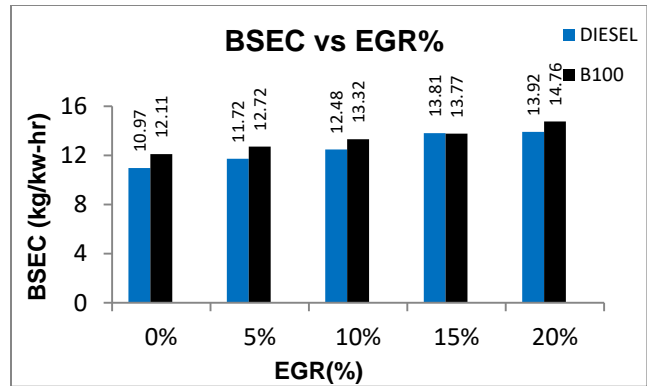
Combustion Peak Pressure:

The observations recorded at full load (5.2 kW) for combustion peak pressure using different fuel and varying EGR rates are shown in fig. 3. The combustion peak pressure is directly proportional to BTHE. From fig. 3 it is observed that the combustion peak pressure reduces with increase in EGR percentage. The pressure observed at 0% EGR for diesel and B100 is 64.4bar and 61.32 bar respectively. The lower combustion peak pressure with higher EGR rate is due to dilution of charge with the introduction of exhaust gas resulting in reduction of O_2 concentration.
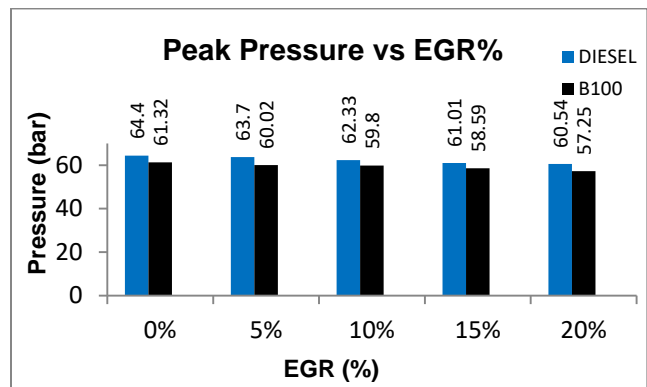
FIGURE 2. VARIATION OF PEAK PRESSURE WITH EGR%

NO_X:

The observations recorded at full load (5.2 kW) for NO_X using different fuel and varying EGR rates are shown in fig. 4. It is observed that NO_X decreases with increase in EGR%. There is significant decrease in NO_X emission with the help of EGR is observed. The highest NO_X emission was observed using diesel with 0% EGR (290 ppm) and lowest NO_X is observed using B100 with 20 % EGR (117ppm). The lower NO_X formation with higher EGR percentage was observed due to decrease in combustion temperature as there is dilution of charge with the supply of EGR. The

other reason for reduction in NO_X is reduction in O_2 concentration which otherwise promote NO_X formation.
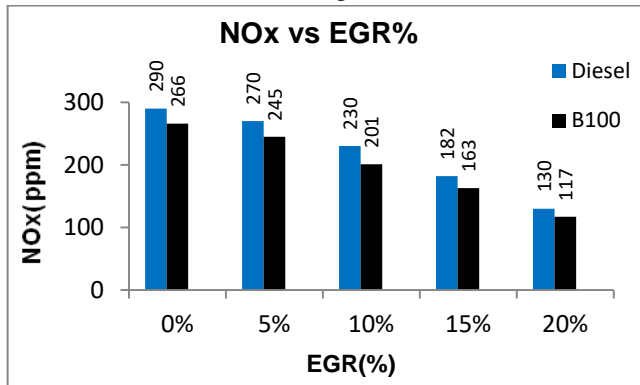
FIGURE 7. VARIATION OF NO_X WITH EGR%

UNBURNT HYDROCARBONS:

The observations recorded at full load (5.2 kW) for HC using different fuel and varying EGR rates are shown in fig. 5. Hydrocarbon shows the trend opposite to that of NO_X. It is observed that HC emission increases with EGR rate for all the fuels. The minimum HC emission is observed using diesel with 0% EGR (24 ppm) and maximum HC emission is observed using B100 with 20% EGR (30ppm). This is probably because of O_2 deficiency resulting in incomplete combustion of fuel which leads to increase HC emission in exhaust due to recirculation of exhaust gases.
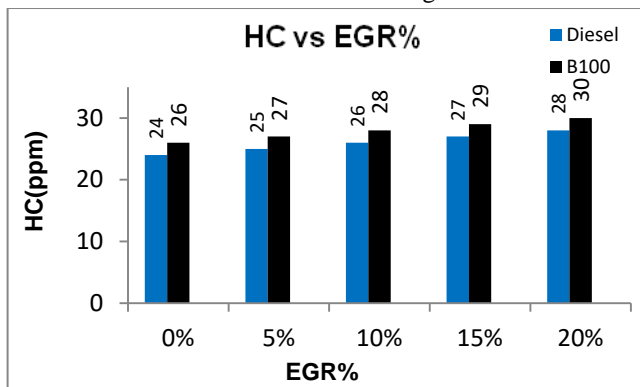
FIGURE 5. VARIATION OF HC WITH EGR%

Smoke:

The observations recorded at full load (5.2 kW) for smoke using different fuel and varying EGR rates are shown in fig.6. The minimum smoke is obtained using diesel with 0% EGR (79.32%) and maximum smoke is observed using B100 with 20 % EGR (100%). The formation of smoke is strongly dependent on engine load and type of fuel used. The air-fuel ratio increase with increase in load and decreases with increase in EGR percentage resulting in higher smoke.
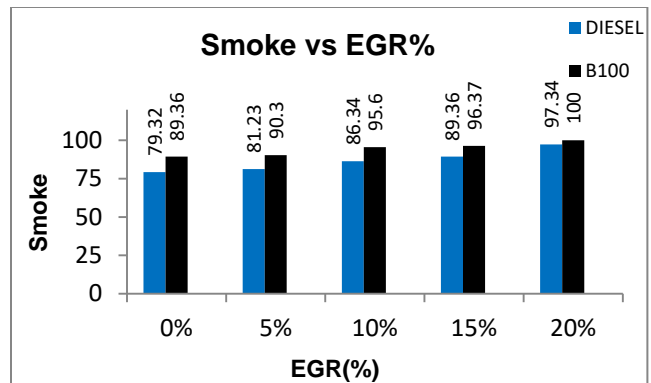
FIGURE 6. VARIATION OF SMOKE WITH EGR%

REFERENCES

[1] S. Jaichandar and K. Annamalai ,The Status of Biodiesel as an Alternative Fuel for Diesel Engine – An Overview, Journal of Sustainable Energy & Environment 2 (2011) 71-75.

[2] VishwanathShavi and AdiveppaRamapur,Study of Characteristics Performance of VCR Engine for Different Fuels, International Journal Of Engineering And Computer Science ISSN:2319-7242Volume 4 Issue 6 June 2015, Page No. 12492-12498.

[3] KavatiVenkateswarlu and BhagavathulaSree Rama Chandra Murthy, The Effect of Exhaust Gas Recirculation and Di-Tertiary Butyl Peroxide on Diesel-Biodiesel lends for Performance and Emission Studies, International Journal of Advanced Science and Technology Vol. 54. May, 2013.

[4] A. Paykani, A. Akbarzadeh and M. T. ShervaniTabar, Experimental Investigation of the Effect of Exhaust GasRecirculation on Performance and EmissionsCharacteristics of a Diesel Engine Fueled with Biodiesel, IACSIT International Journal of Engineering and Technology, Vol.3, No.3, June 2011.

[5] S, Adinarayana, YMC Sekhar, BVA Rao, M. Anil Prakash, Biodiesel as an alternate fuel in a diesel engine with the cooled exhaust gas recirculation–A measure to reduce harmful emissions, International Journal of Applied Research In Mechanical Engineering, ISSN: 2231 –5950, Volume-1, Issue-2, 2011.

[6] Achuthanunni V, Baiju B, Experimental investigation of a diesel-biodiesel fuelled compression ignition engine with exhaust gas recirculation (EGR), International Journal of Engineering and Advanced Technology ISSN: 2249 – 8958, Volume-4 Issue-1, October 2014.

SEEC-2017-007

ENHANCED ELECTRICITY GENERATION VIA MICROBIAL FUEL CELL WITH CARBON ELECTRODES AND NAFION MEMBRANE

Samantha Singh
Research Scholar, Biochemical and Bioenergy Engineering Research Laboratory, Department of Chemical Engineering, MANIT.Bhopal-462 003, Madhya Pradesh, India

S. Suresh
Assistant Professor, Biochemical and Bioenergy Engineering Research Laboratory, Department of Chemical Engineering, MANIT, Bhopal-462 003, Madhya Pradesh, India.

ABSTRACT
Fossil fuel reserves in the world are depleting at an alarming rate thus finding a renewable fuel to meet the energy requirement is necessary. Copious amounts of energy can be found in organic matter such as carbohydrates, which are found in agricultural and municipal waste. Municipal waste can constitute as much as 80 percent organic materials. Microbial fuel cells (MFC) are the latest form of clean and green energy sources. This solves two main problem currently faced on the global level i.e. need of a renewable source of energy and waste disposal However, the overall low performance of the MFC compared to other more established fuel cell technologies and the high cost of its components compared to the low value of the wastewater it treated, are the two major barriers to commercialization. The amount of energy produced depends on the material of electrodes, microorganisms used, organic matter and design of the cell.MFC designed with graphite electrodes for good conductivity and Nafion membrane for the proper proton transfer to cathode. Local polluted Khan river water was used as substrate and algae used as microorganism. Maximum Power density of 28.7mW/m2 achieved in 12 days.

SKELETAL MECHANISM FOR THE OXIDATION OF COMPONENTS IMPORTANT AS BIODIESEL SURROGATES

Aditya Dilip Lele
Department of Mechanical Engineering,
Indian Institute of Technology Madras, Chennai.
me16s084@smail.iitm.ac.in

Anand Krishnasamy
Department of Mechanical Engineering,
Indian Institute of Technology Madras, Chennai.
anand_k@iitm.ac.in

Krithika Narayanaswamy
Department of Mechanical Engineering,
Indian Institute of Technology Madras, Chennai.
krithika@iitm.ac.in

ABSTRACT

To circumvent the difficulty in integrating reaction schemes for biodiesels, which are typically of a large size, with combustion simulations, in this work, a surrogate approach to simplify the representation of its long chain methyl ester components is adopted. Firstly, a compact reaction scheme for potentially important candidates for biodiesel surrogates is derived by combining a detailed mechanism for methyl butanoate (Dooley et al., Combust. Flame, 2008) and n-dodecane (Narayanaswamy et al., Combust. Flame, 2014) and is comprehensively assessed for its component kinetic description. Thereafter, the surrogate and its kinetics are validated against available experimental data for biodiesel fuel. This work serves as the first step towards the development of a compact reaction scheme which can be used in engine combustion studies to study the effect of biodiesel and its blend with diesel.

Keywords: biodiesel surrogate, methyl butanoate, *n*-dodecane
.

NOMENCLATURE
NTC   Negative temperature co-efficient
MB   methyl butanoate
DD   *n*-dodecane
JSR   Jet Stirred Reactor
SME   Soy methyl ester

INTRODUCTION
Biodiesel has emerged as a promising candidate to partially or completely replace fossil diesel [1]. The use of biodiesel in compression ignition (CI) engines requires no major engine modifications, and therefore makes it an attractive replacement for diesel fuel [1]. To assess and quantify the use of biodiesel in practical engines, understand its combustion behavior, reactivity, and emission characteristics using computations, it is important to incorporate finite rate chemistry in these studies.

Detailed kinetic mechanisms for the real biodiesel typically runs into several thousands of species and reactions [2]. Since computations of combustion dynamics in an engine are expensive, there is a severe restriction on the size of chemical kinetic mechanism that can be coupled with the simulations. To simplify the kinetic description of biodiesel in these computations, surrogates made of simpler well studied molecules are used in place of the actual fuel, for which accurate and compact reaction mechanisms are proposed.

Several studies have investigated the use of surrogates for biodiesel [3, 4]. The presence of at least one methyl ester component such as methyl butanoate [3] or methyl decanotae [4] is typical of all these surrogates. Later studies [4] have preferred methyl decanoate, owing to its ability to reproduce the reactivity, NTC behavior, and early CO2 rise, which are characteristics of the long chain methyl esters in biodiesels [2]. Further, an *n*-alkane component such as *n*-heptane is included in the surrogate,

which helps to match the reactivity as well as the heat content of the biodiesel. A review of the existing work on surrogate fuels for biodiesels has been summarized in Ref. [5].

In developing a reaction mechanism for a surrogate fuel, it is crucial to capture the component kinetics accurately in order to make meaningful assessment about suitability of the surrogate to represent the real fuel. Thus, although methyl decanoate has been used in recent studies for the aforementioned reasons, methyl butanoate, which is the most comprehensively studied methyl ester in terms of theoretical and experimental kinetic studies [6], is a more suitable candidate to represent the ester content in biodiesel fuels. Methyl butanoate lacks the NTC behavior and reactivity characteristic of long chain molecules. This can be compensated by n-dodecane in combination with methyl butanoate.

In this work, a kinetic scheme for these two components is assembled by incorporating the reaction pathways of MB from a detailed mechanism [6] into a well-validated reaction mechanism for DD [7]. The wide experimental database available for MB and DD is leveraged to comprehensively assess the kinetics of these components in the combined reaction mechanism. Thereafter, a surrogate comprised of these components is proposed to represent soy methyl ester (SME) and validated against ignition delay of the real fuel. All numerical calculations have been performed using FlameMaster (version 3.3.9) [8].

MECHANISM DEVELOPMENT

Starting with the detailed reaction scheme for MB oxidation (275 species, 1545 reactions) proposed by Dooley et al. [6], a compact mechanism is derived using DRGEP [9] method. The database used to carry out the reduction includes homogeneous isochoric reactor configurations at low to high temperatures T = 700–1500K, pressure P = 13.5bar, and equivalence ratio φ = 1. The resulting reduced mechanism consists of 89 species and 560 reactions.
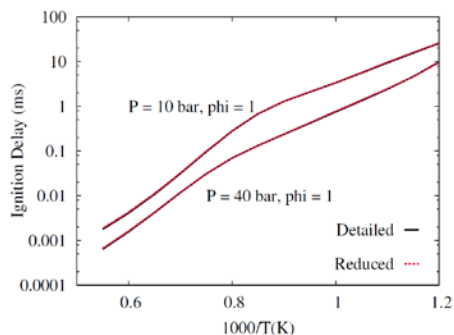
FIGURE 1: Comparison between detailed and reduced mechanism simulations for ignition delays in a constant volume reactor, continuous lines: detailed mechanism, dashed lines: reduced mechanism

Figure 1 shows the comparison between detailed and reduced mechanism for ignition delays in a constant volume reactor. The maximum error between the reduced and the reference mechanisms is < 5%. Similar level of agreement has also been observed for lean and rich fuel/air mixtures at different pressures and shock tube species profile simulations. It can be concluded that the reduced mechanism retains the predictive capabilities of the detailed mechanism very well considering the degree of reduction achieved. This kinetic scheme is used in the subsequent mechanism development to describe MB oxidation.
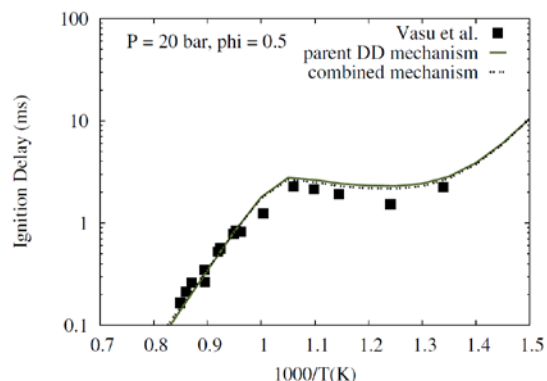
(a) Comparison of ignition delays at P = 20 bar, φ = 0.5.; symbols: experiments [10], continuous lines: reference DD mechanism, dashed lines: combined mechanism
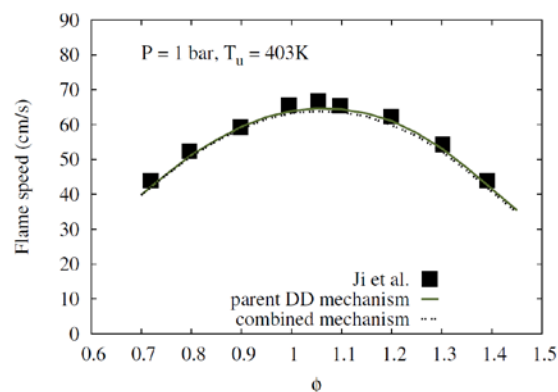
(b) Comparison of laminar flame speeds at P = 1 bar, T_u = 403K, symbols: experiments[11], continuous lines: reference DD mechanism, dashed lines: combined mechanism

FIGURE 2: Validation of n-dodecane kinetics

The kinetics of DD are taken from the reaction mechanism proposed by Narayanaswamy et al. [7]. MB and DD mechanisms are then combined using an interactive tool [12] that automatically identifies common species and reactions from the different mechanisms, and incompatibilities between the kinetic data sets. In the combined mechanism, the more recent base chemistry $(C_1, C_2, H_2\text{-}O_2)$ from the DD mechanism [7] is retained and

appropriate changes have been made to ensure consistency between the component sub-mechanisms. The ability of the combined mechanism to predict the component kinetic behavior is assessed next.

The combined mechanism is first compared against the reference DD mechanism [7] for (a) ignition delays spanning a wide range of temperatures (700–1400K), pressures (6–40bar) and equivalence ratios (0.5–1), (b) species profiles in shock tube and laminar flame speeds at atmospheric pressure. Some of these results are shown in Fig. 2. The combined mechanism shows similar predictions for the reactivity, species profiles and flame speeds of DD when compared to its reference mechanism. This is mainly because the DD sub-mechanism as well as its base chemistry is same as in the reference mechanism [7].
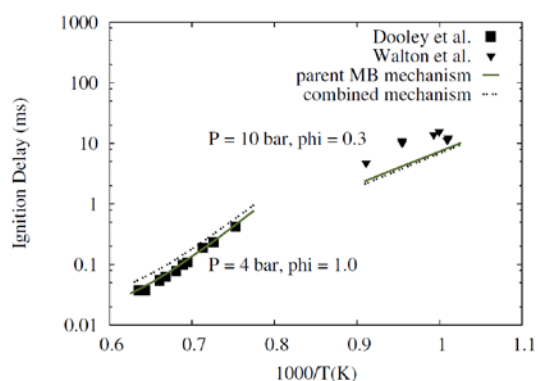
(a) Ignition delays at P = 4, 10 bar, φ = 0.3, 1, symbols: experiments [6], continuous lines: reference MB mechanism, dashed lines: combined mechanism
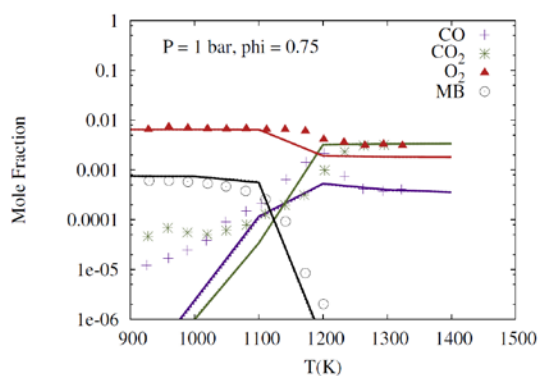
(b) Species profiles in a Jet Stirred Reactor (JSR) at P = 1 bar, φ = 0.75, symbols: experiments [13], continuous lines: reference MB mechanism, dashed lines: combined mechanism

FIGURE 3: Validation of methyl butanoate kinetics

Similarly, the combined mechanism is compared with the reference MB mechanism [6] and available experimental data sets, that includes ignition delays and species profiles in jet stirred reactors at a wide range of conditions (T=800– 1600 K, 1–20 bar, φ = 0.25–2). Figure 3 shows some representative results. The combined mechanism shows similar reactivity at temperatures T<1200K but it is less reactive compared to the reference MB mechanism at high T (>1200K). Both the kinetic schemes show shorter ignition delays compared to experiments at T < 1100K.

Considering species profiles in jet stirred reactor (JSR) at fuel lean conditions, the combined mechanism shows similar results as the reference MB mechanism. However, the species profiles at T<1100K show significant differences compared to experiments and this needs to be addressed. To investigate the differences in ignition delays predicted by the reference MB mechanism and the combined mechanism derived here, a sensitivity analysis was performed to identify reactions that influence the ignition times the most in both the reaction schemes at high temperatures. Only a small difference is found in the sensitivity factors for the important reactions. Hence it can be concluded that the differences observed in ignition delays at high temperatures for MB when using the combined mechanism is a collective effect due to the differences in base chemistry in the combined mechanism, which now comes from the DD mechanism [7].

Nonetheless, it can be observed that the ignition delays computed using the combined mechanism are within 60% of the experiments at the high temperatures. The kinetic description of MB at high and low temperatures will be further improved as part of our future work. Hence, it can be concluded that the combined mechanism is as good as the reference mechanism in its predictive capabilities, barring any differences arising due to differences in C_0–C_2 chemistry.

RESULTS AND DISCUSSION

This kinetic scheme valid for DD and MB, which are suited as components of biodiesel surrogates, consists of 280 species and 1600 reactions. In this section, its applicability is demonstrated here by considering a soy methyl ester fuel. The composition of SME used for experiments leads to an average formula of $C_{16.93}H_{32.12}O_2$. To match the C-content of the fuel a surrogate is considered to be made of a mixture of 1 mole of MB and 1 mole of DD.

Simulations performed using the surrogate shown in Figure 4 show excellent agreement with reactivity of SME experiments despite the differences (up to 60%) that were observed between the simulations and experimental ignition delays of MB at high temperatures when using the combined kinetic mechanism. This is because, between DD and MB, the former is more reactive over the entire temperature range of interest (T = 800–1600K). Reactivity

of surrogate is dominated by reactivity of DD, which is accurately represented in the combined mechanism, following the reference DD mechanism [7]. This agreement suggests that MB and DD mixture is a good representative for biodiesel fuel at T>1000K.
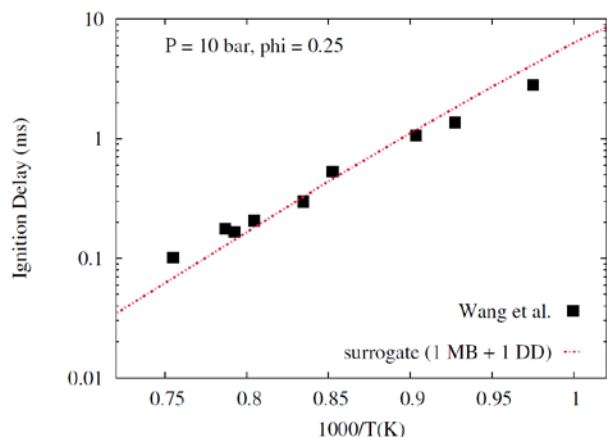
FIGURE 4: Ignition delays of SME, symbols: experiments [14], dashed lines: simulations using surrogate mechanism

CONCLUSION AND FUTURE SCOPE

A chemical kinetic mechanism has been derived for methyl butanoate and *n*-dodecane consisting of 280 species and 1600 reactions in lieu of their relevance as components of biodiesel surrogates and it has been extensively validated for these components. Good agreement has been found for both the components. Matching the C-content with SME, a surrogate comprised of DD and MB is proposed, and it is found to agree well with ignition delay measurements for the real fuel. This study suggest that a mixture of DD and MB is a promising surrogate for biodiesel.

Future studies will include refinement of combined mechanism to improve the kinetic description of methyl butanoate. A better surrogate formulation strategy based on constrained optimization approach will be used to propose an optimal surrogate for biodiesel. This refined mechanism will be reduced in size so that it can be employed in reactive flow simulations to get insights into the combustion dynamics in CI engines.

REFERENCES

[1] K Anand, R. P. Sharma, and P. S. Mehta. A comprehensive approach for estimating thermo-physical properties of biodiesel fuels. Applied thermal engineering, 31(2):235–242, 2011.

[2] C. K. Westbrook, C. V. Naik, O. Herbinet, W. Pitz, M. Mehl, S. M. Sarathy, and H. J. Curran. Detailed chemical kinetic reaction mechanisms for soy and rapeseed biodiesel fuels. Combustion and Flame, 158(4):742–755, 2011.

[3] W. Liu, R. Sivaramakrishnan, M. J. Davis, S. Som, D. E. Longman, and T. F. Lu. Development of a reduced biodiesel surrogate model for compression ignition engine modeling. Proceedings of the Combustion Institute, 34(1):401–409, 2013.

[4] Z. Luo, T. Lu, M. J. Maciaszek, S. Som, and D. E. Longman. A reduced mechanism for high-temperature oxidation of biodiesel surrogates. Energy & Fuels, 24(12):6283–6293, 2010.

[5] A. D. Lele, K. Anand, and K. Narayanaswamy. Biofuels:Technology, Challenges and Prospects, chapter Surrogates for biodiesel: review and challenges. Springer. (In press).

[6] S. Dooley, H. J. Curran, and J. M. Simmie. Autoignition measurements and a validated kinetic model for the biodiesel surrogate, methyl butanoate. Combustion and Flame, 153(1):2–32, 2008.

[7] K. Narayanaswamy, P. Pepiot, and H. Pitsch. A chemical mechanism for low to high temperature oxidation of *n*-dodecane as a component of transportation fuel surrogates. Combustion and Flame, 161(4):866–884, 2014.

[8] H. Pitsch and M. Bollig. Flamemaster, a computer code for homogeneous and one-dimensional laminar flame calculations. Institut fur Technische Mechanik, RWTH Aachen, 1993.

[9] P. Pepiot-Desjardins and H. Pitsch. An efficient error propagation-based reduction method for large chemical kinetic mechanisms. Combustion and Flame, 154(1-2):67–81, 2008.

[10] S. S. Vasu, D. F. Davidson, Z. Hong, V. Vasudevan, and R. K. Hanson. *n*-dodecane oxidation at high-pressures: Measurements of ignition delay times and OH concentration time-histories. Proceedings of the Combustion Institute, 32(1):173–180, 2009.

[11] C. Ji, E. Dames, Y. L. Wang, H. Wang, and F. N. Egolfopoulos. Propagation and extinction of premixed C5–C12 n-alkane flames. Combustion and Flame, 157(2):277–287, 2010.

[12] P. Pepiot-Desjardins. Automatic strategies for chemical mechanism reduction. PhD thesis, Stanford University, Department of Mechanical Engineering, June 2008.

[13] S. Gail, M. J. Thomson, S. M. Sarathy, S. A. Syed, P. Dagaut, P. Di´evart, A. J. Marchese, and F. L. Dryer. A wide-ranging kinetic modeling study of methyl butanoate combustion. Proceedings of the Combustion Institute, 31(1):305–311, 2007.

[14] W. Wang, S. Gowdagiri, and M. A. Oehlschlaeger. The high-temperature autoignition of biodiesels and biodiesel components. Combustion and Flame, 161(12):3014–3021, 2014.

SEEC-2017-009

THERMAL AND THERMOHYDRAULIC PERFORMANCE OF DOUBLE FLOW FLAT PLATE AND CORRUGATED ABSORBER SOLAR AIR HEATERS

Som Nath Saha
Department of Mechanical Engineering
NIT Jamshedpur
Email: somnath.rvs@gmail.com

S. P. Sharma
Department of Mechanical
Engineering
NIT Jamshedpur
Email: spsharma.me@nitjsr.ac.in

ABSTRACT

In this paper thermal and thermohydraulic performance of double flow flat plate and corrugated absorber solar air heaters are analytically investigated. Three types of collectors are considered in this study, first one has flat plate absorber (SA-1), second has corrugated absorber (SA-2) and third one has corrugated absorber and bottom plates (SA-3). The aim of the use of the corrugated absorbing plate and bottom plate is to enhance the turbulence and the heat transfer rate inside the air flow channel which help to improve the performance of collector. The performance of these three types of solar air heater are analyzed on the basis of effective parameters such as mass flow rate and insolation. The results show that the corrugated absorber solar air heaters (SA-2 and SA-3) have much higher efficiencies than the flat plate solar air heater (SA-1) although performance of SA-3 collector is superior to that of SA-2 collector. The results also show that increasing the solar intensity leads to achieve higher air temperature rise and efficiency.

Keywords: Solar air heater, double flow, corrugated absorber, thermal efficiency, thermohydraulic efficiency
.

NOMENCLATURE

A_c	area of collector (m^2)
b	half height of v-groove (m)
C_p	specific heat of air at constant pressure (J/kg K)
D_h	hydraulic diameter (m)
f	friction coefficient
h	heat transfer coefficient (W/m^2 K)
H	height of air flow channel (m)
H_{gc}	height of glass cover (m)
I	insolation (W/m^2)
k	thermal conductivity (W/m K)
L	collector length (m)
m	mass flow rate (kg/s)
Nu	Nusselt number
Q	energy gain by air (W)
R	resistance factor
Re	Reynolds number
T	temperature (K)
U	loss coefficient (W/m^2 K)
V	velocity of wind (m/s)
v	velocity of air (m/s)
W	collector width (m)

Greek symbols

|	
α	absorptivity
ε	emissivity
φ	fraction of mass flow rate
ΔP	pressure drop (N/m^2)
η	efficiency
ρ	density of air (kg/m^3)
τ	transmissivity
θ	angle of v-groove absorbing plate (˚)

Subscripts

a	ambient
ap	absorber plate
B	bottom
bp	bottom plate
c	convective
ch	channel

1

e	net
en	entrance
ex	exit
f	total flow
$f1$	flow above the absorber plate
$f2$	flow under the absorber plate
gc	glass cover
$gc1$	lower glass cover
$gc2$	upper glass cover
in	inlet
max	maximum
min	minimum
o	outlet
r	radiative
T	top
eff	thermohydraulic (effective)
u	useful

INTRODUCTION

Solar energy is one of the renewable source of energy which is sustainable, abundant and clean. Among various applications of solar energy, air heating through the solar air heaters are very simple and economic. Solar air heaters are mainly used for low to medium grade thermal energy, like space heating, cooling, crop drying etc. Even though it is simple in design, low maintenance and operating cost, its efficiency is low due to poor thermophysical properties of air. To improve the performance of solar air heaters several designs are developed by many researchers. Such design includes honeycomb collectors, extended surface absorber, use of artificial roughness on the absorber plate, packing of porous material in air flow channel. One of the effective ways to improve the convective heat transfer rate is to increase the heat transfer surface area and to increase turbulence inside the channel by using fin or corrugated surfaces [1,2].

Ho-Ming et al. [3] investigated the performance of double flow flat plate solar air heater and found more effective than conventional solar air heater. A parametric study of cross corrugated solar air collectors with different parameters such as mass flow rate, insolation and inlet temperature have been performed by Wenxian et al. [4] and Wenfeng et al. [5] and found that the cross corrugated collector have superior thermal performance than that of the flat plate. Mohammadi and Sabzpooshani [6] investigated the influence of fins and baffles attached over the absorber plate on the performance of single pass solar air heater. Vimal and Sharma [7] theoretically investigated the thermal performance of packed bed solar air heater with wire screen matrices. Paisarn [8] studied numerically about heat transfer characteristics and performance of double pass flat plate solar air heater with and without porous media. A comprehensive study of solar air heater having roughness elements on the absorber plate with different geometry, presented by Mittal et al. [9]. Karmare

and Tikekar [10] presented the analysis of fluid flow and heat transfer in a rib grit roughened surface solar air heater.

This paper present analyticaly investigations of thermal and thermohydraulic performance of double flow flat plate and corrugated absorber solar air heaters. Three types of solar ait heaters are considered, SA-1 (Fig. 1) has flat plate absorber, SA-2 (Fig. 2) has corrugated absorber plate and SA-3 (Fig. 3) has corrugated absorber and bottom plate having convergence-divergence flow channel.

THEORETICAL ANALYSIS

Figure 1 shows the schematic diagram of double flow solar air heater with two glass cover. The analysis is based on analytical solutions for energy balance equations. The energy balance equations are made under the following assumptions:

- Air temperature variation is the functions of the flow directions only.
- Temperature drop across the glass cover, absorber plate and bottom plate is negligible.
- The systems operate under quasi steady state.
- Glass covers and flowing air do not absorb radiant energy.
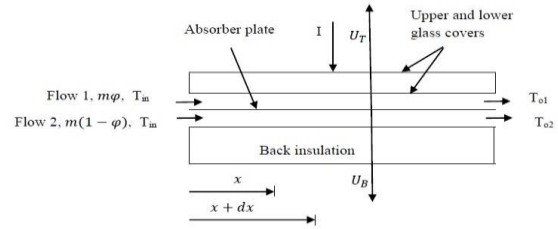
FIGURE 1. FLAT PLATE DOUBLE FLOW SOLAR AIR HEATER

Energy Balance Equations

Considered a differential element of length dx at a distance x from the inlet. The energy balance equations are written as:

Glass cover 1 (lower glass cover)
$$h_{r,ap-gc1}(T_{ap} - T_{gc1})Wdx + h_{c,f1-gc1}(T_{f1} - T_{gc1})Wdx = U_{gc1-a}(T_{gc1} - T_a)Wdx \quad (1)$$

Absorber plate
$$I\alpha_{ap}\tau_{gc}^2 Wdx = U_T(T_{ap} - T_a)Wdx + U_B(T_{ap} - T_a)Wdx + h_{c,ap-f1}(T_{ap} - T_{f1})Wdx + h_{c,ap-f2}(T_{ap} - T_{f2})Wdx \quad (2)$$

Bottom plate
$$h_{r,ap-bp}(T_{ap} - T_{bp})Wdx + h_{c,f2-bp}(T_{f2} - T_{bp})Wdx = U_{bp-a}(T_{bp} - T_a)Wdx \quad (3)$$

Air flow 1 (air flowing over the absorbing plate)

$h_{c,ap-f1}(T_{ap} - T_{f1})Wdx = m\varphi c_p dT_{f1} + h_{c,f1-gc1}(T_{f1} - T_{gc1})Wdx$ (4)

Air flow 2 (air flowing under the absorbing plate)

$h_{c,ap-f2}(T_{ap} - T_{f2})Wdx = m(1-\varphi)c_p dT_{f2} + h_{c,f2-bp}(T_{f2} - T_{bp})Wdx$ (5)

Solving Eqs. (1) – (5), the outlet temperature of flow 1 and flow 2 are respectively as [11]:

$$T_{f1,o} = \left[\frac{Y_1 - \frac{M_5}{1-\varphi}}{\frac{M_4}{(1-\varphi)}}\right]C_1 e^{\frac{Y_1}{Z}} + \left[\frac{Y_2 - \frac{M_5}{1-\varphi}}{\frac{M_4}{(1-\varphi)}}\right]C_2 e^{\frac{Y_2}{Z}} - \frac{M_5}{M_4}\left(\frac{M_3 M_4 - M_1 M_6}{M_1 M_5 - M_2 M_4}\right) - \frac{M_6}{M_4} + T_a$$ (6)

and

$$T_{f2,o} = C_1 e^{\frac{Y_1}{Z}} + C_2 e^{\frac{Y_2}{Z}} + \frac{M_3 M_4 - M_1 M_6}{M_1 M_5 - M_2 M_4} + T_a$$ (7)

Where $z = \frac{mc_p}{A_c}$

and Y's and C's are the functions of M and M's are in the terms of the convective heat transfer coefficient, loss coefficients and physical properties [11].

$$\eta = \frac{mc_p}{IA_c}(T_{f,o} - T_{f,in}) = \frac{Z}{I}\Delta T$$ (8)

Heat Transfer Coefficients

For flat plate absorber

The convective heat transfer coefficient for air.

$$h_{c,ap-f} = \frac{Nuk_f}{D_h}$$ (9)

For laminar flow, the equation presented by Heaton et al. [12].

$$Nu = 4.4 + \frac{0.00398(0.7ReD_h/L)^{1.66}}{1+0.0114(0.7ReD_h/L)^{1.12}}$$ (10)

For turbulent flow the correlation derived from Kays [13], data with the modification of McAdams [14].

$$Nu = 0.0158Re^{0.8}[1 + (D_h/L)^{0.7}]$$ (11)

For v-corrugated absorber
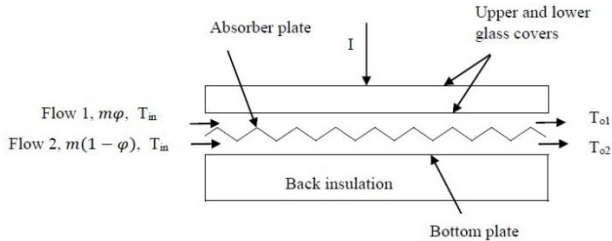
FIGURE 2. CORRUGATED ABSORBER DOUBLE FLOW SOLAR AIR HEATER

The convective heat transfer coefficient for air [16]

$$h_{c,ap-f} = \frac{Nuk_f}{D_h} \times \frac{1}{\sin\left(\frac{\theta}{2}\right)}$$ (12)

Hollands and Shewen [15] developed the correlation of Nusselts number (Nu) and modified by Karim et al. [16] as:

If $Re < 2800$

$$Nu = 2.821 + 0.126\, Re\frac{2b}{L}$$ (13)

If $2800 \leq Re \leq 10^4$

$$Nu = 1.9 \times 10^{-6}Re^{1.79} + 225\frac{2b}{L}$$ (14)

If $10^4 \leq Re \leq 10^5$

$$Nu = 0.0302Re^{0.74} + 0.242Re^{0.74}\frac{2b}{L}$$ (15)

For v-corrugated absorber and bottom plate
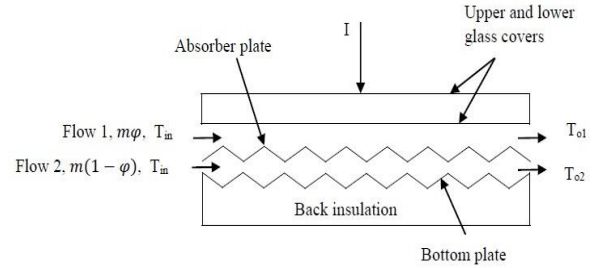
FIGURE 3. CORRUGATED ABSORBER AND BOTTOM PLATE DOUBLE FLOW SOLAR AIR HEATER

Benli [17] present the correlation of Nusselts number as:

$$Nu = 0.5999Re^{0.419}$$ (16)

Thermohydraulic Efficiency

The net energy can be written as:

$$Q_e = Q_{uf} - P_m/C_f$$ (17)

where P_m is the work energy lost in friction in the heater channel, given by:

$$P_m = m\Delta P/\rho$$ (18)

C_f is the conversion factor to transform different efficiencies (thermal to mechanical) and is taken 0.2 [18].

The pressure drop ΔP is calculated from the following expression;

$$\Delta P = \Delta P_{ch} + \Delta P_{en} + \Delta P_{ex}$$ (19)

The pressure drop through the upper and lower channel ΔP_{ch} is calculated by the relation [19-21];

$$\Delta P_{ch} = 2\rho v_{ch}^2 fL/D_h$$ (20)

The friction factor is given by [19-22];

for turbulent flow

$$f = 0.059Re^{-0.2}$$ (21)

for laminar flow

$$f = 16/Re$$ (22)

The friction factor for SA-3 is given by [17];

$$f = 1.0866Re^{-0.6635}$$ (23)

The sum of the inlet and outlet pressure drop ($\Delta P_{en} + \Delta P_{ex}$) can be determined by Hegazy [23];

$$\Delta P_{en} + \Delta P_{ex} = (R_{en} + R_{ex})\frac{\rho v_p^2}{2} \qquad (24)$$

where the sum of the entrance and exit resistance factor $(R_{en} + R_{ex})$ is taken 1.5 [24].

The thermohydraulic efficiency of the solar air heater can be expressed as;

$$\eta_{eff} = \frac{Q_e}{A_c I} = \frac{Q_{uf} - (P_m/C_f)}{A_c I} \qquad (25)$$

RESULTS AND DISCUSSION

In this section, results of thermal and thermohydraulic performance of double flow flat plate and corrugated absorber solar air heaters are presented. The following values are used for the parameters under the typical configuration and operating conditions:

L = 1.25 m, W = 0.80 m, H_{gc} = 0.025 m, H_{min} = 0.02 m, H_{max} = 0.045 m, τ_{gc} = 0.875, α_{ap} = 0.96, ε_{gc} = 0.94, ε_{ap} = 0.80, ε_{bp} = 0.94, $U_B \approx 0$, T_a = 30 ˚C = 303 K, V = 1 m/s, b = 0.00625 m, I = 200 – 1000 W/m^2, m = 0.014 – 0.083 kg/s, φ = 0.5.
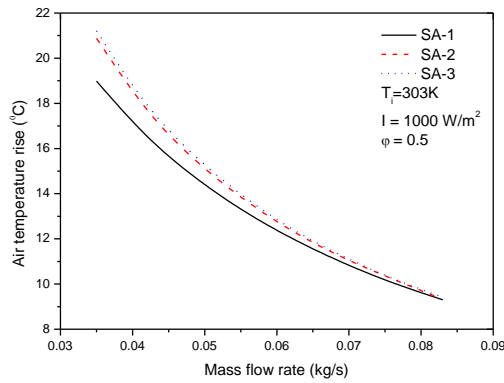
FIGURE 4. AIR TEMPERATURE RISE VS. MASS FLOW RATE

Figure 4 shows the variation of air temperature rise with mass flow rate for double flow flat and corrugated absorber solar air heaters for I = 1000 W/m^2. Air temperature rise continuously decreases with increase in mass flow rate for all solar air heaters. It is seen from the figure that the considerable amount of gain in air temperature rise at lower mass flow rate is observed due to corrugated absorber however at higher mass flow rate gain in air temperature rise drastically decreases. This type of trend is due to almost equal temperature of absorber and air at higher mass flow rate.
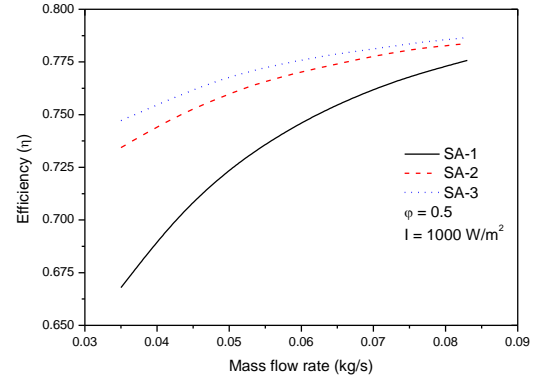
FIGURE 5. EFFICIENCY VS. MASS FLOW RATE

Figure 5 illustrate the effect of mass flow rate on efficiency. Efficiency increases with increase in mass flow rate due to increase in thermal conductance. It can be observed that at lower mass flow rate, percentage enhancement in efficiency of corrugated absorber to flat plate collector is higher. The AS-3 collector has the maximum efficiency throughout the mass flow rate investigated. The percentage enhancement in efficiency of SA-3 collector with respect to SA-1 collector is 11.86 % and 1.40 % at m = 0.035 kg/s and 0.83 kg/s respectively.
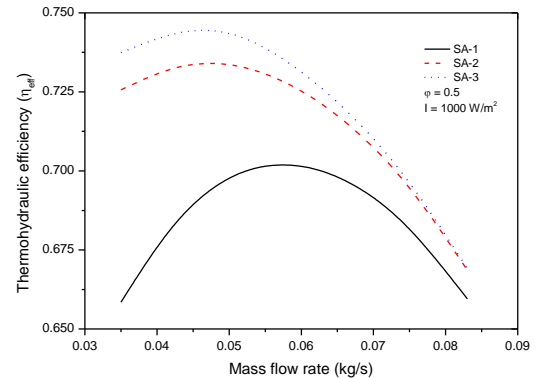
FIGURE 6. THERMOHYDRAULIC EFFICIENCY VS. MASS FLOW RATE

The effect of mass flow rate on thermohydraulic efficiency is shown in Fig. 6. Figure reveals the thermohydraulic efficiency increases with increase in mass flow rate upto a critical value of flow rate at which it attains a maximum value and there after decreases sharply. Results indicate that the thermohydraulic efficiency of double flow flat plate solar air heater (SA-1) reaches maximum value at m = 0.0575 kg/s, whereas for SA-2 and SA-3 collectors pick values of thermohydraulic efficiency shifted towards lower mass flow rates of 0.0475 kg/s and 0.046 kg/s respectively. This type of trends is observed due

to increase in pressure drop of flowing air in case of corrugated absorber / channels.
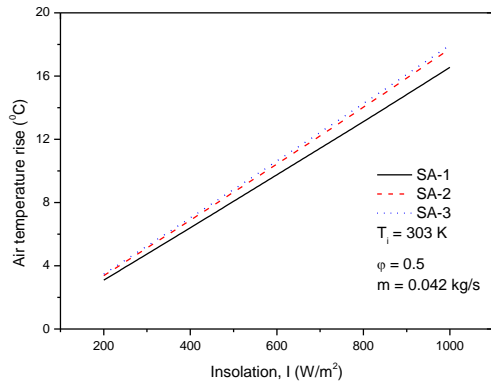
FIGURE 7. AIR TEMPERATURE RISE VS. INSOLATION

The variation of air temperature rise with insolation, for flat plate and corrugated absorber collectors at m = 0.042 kg/s, are shown in Fig. 7. It evident that air temperature rise increase linearly with increase in insolation. It is also evident from the figure that corrugated absorber collectors have higher air temperature rise to the flat plate collector. The maximum air temperature rise is 16.5 ˚C at I = 1000 W/m^2 for SA-3 collector.
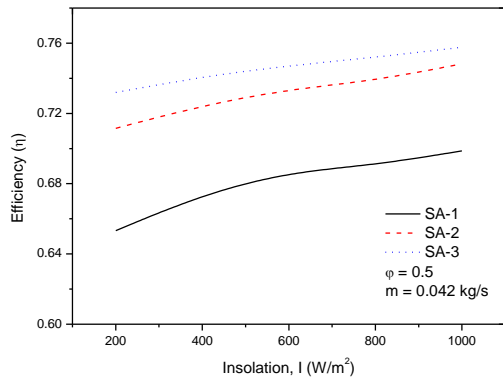
FIGURE 8. EFFICIENCY VS. INSOLATION

Figure 8 shows the variation of efficiency as a function of insolation at m= 0.042kg/s for a set of parameters. Figure reveals that the SA-2 and SA-3 collectors have much higher efficiencies than the flat plate collector (SA-1) and SA-3 collector performs superior to the SA-2 collector for all the values of insolation considered. This is because of increase in turbulence of air flow leads to increase convective heat transfer rate.
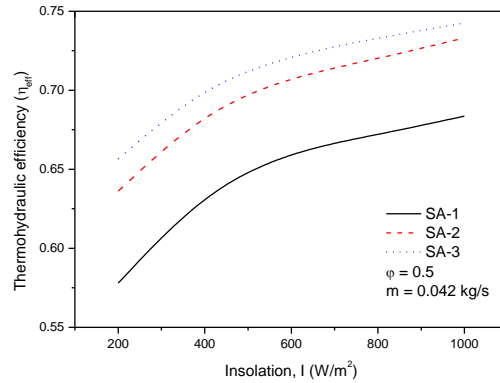
FIGURE 9. THERMOHYDRAULIC EFFICIENCY VS. INSOLATION

Figure 9 shows the effect of insolation on thermohydraulic efficiency for m = 0.042 kg/s. It can be observed that thermohydraulic efficiency monotonically increases with increase in insolation then a slight fall is observed in the rate of increase of thermohydraulic efficiency as insolation increases due to at lower insolation heat gain is low and at high insolation heat gain is high. The maximum thermohydraulic efficiency is 74.25 % at I = 1000 W/m^2 for SA-3 collector.

CONCLUSIONS

In this study, thermal and thermohydraulic analysis of double flow flat plate and corrugated absorber solar air heaters as a function of different parameters such as mass flow rate and insolation have been performed. Results indicated that the air temperature rise decreases while efficiency increases with increase in mass flow rate. It is observed that thermohydraulic efficiency increases upto a certain limit of mass flow rate and there after it decreases. The SA-3 solar air heater attains maximum value of thermohydraulic efficiency at air mass flow rate of 0.046 kg/s. There is significant enhancement in air temperature rise and efficiency of double flow corrugated absorber to that of the flat plate absorber solar air heater. For a specific mass flow rate air temperature rise, efficiency and thermohydraulic efficiencies are increses with increase in insolation.

REFERENCES

[1] Goldstein, L. and Sparrow, E.M., 1976. "Experiments on the transfer characteristics of a corrugated fin and tube heat exchanger configuration". Transaction of the ASME, Journal of Heat Transfer, 98, pp. 26-34.
[2] Goldstein, L. and Sparrow, E.M., 1977. "Heat/mass transfer characteristics for flow in a corrugated wall channel". Transaction of the ASME, Journal of Heat Transfer, 99, pp. 187-195.

[3] Ho-Ming, Yeh, Chii-Dong, Ho and Jun-Ze, Hou, 1999. "The improvement of collector efficiency in solar air heaters by simultaneously air flow over and under the absorbing plate". Energy, 24, pp. 857-871.

[4] Wenxian, Lin, Wenfeng, Gao and Tao, Liu, 2006. "A parametric study on the thermal performance of cross corrugated solar air collectors". Applied Thermal Engineering, 26, pp. 1043-53.

[5] Wenfeng, Gao, Wenxian, Lin, Tao, Liu and Chaofeng, Xia, 2007. "Analytical and experimental studies on the thermal performance of cross corrugated and flat pate solar air heaters". Applied Energy, 84, pp. 425-441.

[6] Mohammadi, K. and Sabzpooshani, M., 2013. "Comprehensive performance evaluation and parametric studies of single pass air heater with fins and baffles attached over the absorber plate". Energy, 57, pp. 741-750.

[7] Vimal, Ku., Chouksey and Sharma, S.P., 2016. "Investigations on thermal performance characteristic of wire screen packed bed solar air heater". Solar Energy, 132, pp. 591-605.

[8] Paisarn, Naphon, 2005. "Effect of porous media on the performance of the double pass flat plate solar air heater". International Communications in Heat and Mass Transfer,32, pp. 140-150.

[9] Mittal, M.K., Varun, Saini, R.P. and Singal, S.K., 2007. "Effective efficiency of solar air heaters having different types of roughness element on the absorber plate". Energy, 32, pp. 739-745.

[10] Karmare S.V. and Tikekar A.N., 2010. "Analysis of fluid and heat transfer in a rib roughened surface solar air heater using CFD". Solar Energy, 84, pp. 409-17.

[11] Som Nath Saha and Sharma S.P., 2016. "Analysis of thermohydraulic performance of double flow v-corrugated absorber solar air heater". International Energy Journal, 16, pp. 131-142.

[12] Heaton, H.S., Reynolds, Wc. and Kays, W.M., 1964. "Heat transfer in annular passages. Simultaneous development of velocity and temperature fields in laminar flow". Int J Heat Mass Transfer, 7, pp. 763-81.

[13] Kays, W.M., 1980. Convective heat and mass transfer. New York, McGraw Hill.

[14] McAdams, W.H., 1954. Heat transmission. New York, McGraw-Hill.

[15] Hollands, K.G.T. and Shewen, E.C., 1981. "Optimization of flow passage geometry for air heating plate type solar collectors". ASME J Solar Energy Eng, 103, pp. 323-30.

[16] Karim, M.A., Perez, E. and Amin, Z.M., 2014. "Mathematical modelling of counter flow v-grove solar air collector". Renewable Energy, 67, pp. 192-201.

[17] Benli H., 2013. "Experimentally derived efficiency and exergy analysis of a new solar air heater having different surface shapes". Renewable Energy, 50, pp. 58-67.

[18] Bahrehmand, D., Ameri, M. and Gholampour, M., 2015. "Energy and exergy analysis of different solar air collector systems with forced convection". Renewable Energy, 83, pp. 1119-1130.

[19] Wong, H.Y., 1977. Handbook of essential formula and data on heat transfer for engineers. London: Longman.

[20] Choudhury, C., Andersen, S.L. and Pekstad, J., 1988. "A solar air heater for low temperature applications". Solar Energy. 40, pp. 77.

[21] Tan, H.M. and Charters, W.W.S., 1969. "Effect of thermal entrance region on turbulent forced convective heat transfer for an asymmetrically heated rectangular duct with uniform heat flux". Solar Energy, 12, pp. 513.

[22] Douglas, J.F., Gasiorek, J.M. and Swaffield, J.A., 1992. "Fluid mechanics". 2nd ed. England: Longman Singapor Publishers.

[23] Hegazy, A.A., 2000. "Thermohydraulic performance of air heating solar collectors with variable width, flat absorber plates". Energy Convers Manage, 41, pp. 1361-78.

[24] Griggs, E.I. and Sharifabad, F.K., 1992. "Flow characteristics in rectangular ducts". ASHRAE Trans, 98(1), pp. 116-27.

SEEC-2017-010

An Experimental Investigation into the burning of freely falling liquid fuel droplets

Rahul Varshney
Department of Mechanical Engineering
A.M.U. Aligarh, India

Shah Shahood Alam
Department of Mechanical
Engineering A.M.U. Aligarh, India

Naeem Ahmad
Department of Mechanical
Engineering A.M.U. Aligarh, India

ABSTRACT

The combustion of single fuel droplet is a part of overall problem of combustion of a spray of fuel. The combustion of a fuel droplet can be considered as a combined problem of the physical process of diffusion, heat transfer, evaporation and the chemical reaction. From the practical point of view, it is more desirable to study freely falling droplets since the complete evaporation and burning of droplet could be studied both experimentally and theoretically while falling in a hot ambience. The study of evaporation of single droplet is necessary for characterizing and understanding spray vaporization and combustion. Vaporization of a liquid fuel droplet at high pressures and high temperature environments is also an important feature of spray combustion. In recent years a growing interest is being given to the research concerning alternative fuels such as bio-fuels.

SEEC-2017-011

COMPARATIVE EVALUATION OF β-GLUCOSIDASES FOR ENHANCING THE BIOMASS HYDROLYZING POTENTIAL OF CELLULASES

Prajeesh K.V[1, 2], Meena S[2], Rajasree KP[3], Amith Abraham[2], Rajeev Kumar Sukumaran[1,2*]

[1]Academy of Scientific and Innovative Research (AcSIR), CSIR-NIIST Campus, Thiruvananthapuram
[2]Centre for Biofuels, Microbial processes and Technology Division
CSIR-National Institute for Interdisciplinary Science and Technology,
Industrial Estate P.O., Thiruvananthapuram 695019, India
[3]Department of Biochemistry and Molecular Biology, Miller School of Medicine, University of Miami, FL, USA

* Corresponding author. Tel: +91 471 2515368, Fax: +91 471 2491712, E-mail: rajeevs@niist.res.in

ABSTRACT

β- Glucosidase (BGL) catalyses the final step of cellulose hydrolysis and converts cellobiose to glucose. The enzyme is inhibited by its own product and hence the hydrolytic reaction catalyzed by the enzyme is the rate limiting step in biomass hydrolysis. Currently available biomass hydrolyzing enzyme preparations are mostly sourced from strains of Trichoderma reesei which is naturally deficient in BGL. Also, the T. reesei enzyme is inhibited by ~50mM glucose, making it absolutely necessary to blend in heterogeneous BGLs in these enzyme cocktails. BGL produced from Aspergillus unguis NII 08123 contains a glucose tolerant BGL isoform with an inhibition constant of 800mM. This BGL preparation was evaluated as a supplement to T. reesei cellulase and to commercial biomass hydrolyzing enzymes for hydrolysis of pure celluloses as well as different pretreated lignocellulosic feedstock. Comparisons were made with BGL sourced from an A.niger previously reported to be a high producer of BGL and to commercial BGL preparations. Comparisons provided interesting insights into the performance of cellulase blends containing BGL preparations from different fungi. Results are discussed.

Keywords

Aspergillus unguis, Aspergillus niger, beta glucosidase, biomass hydrolysis, cellulase, enzyme blends, bioethanol..

NOMENCLATURE

BGL	β-glucosidase
T. reesei	*Trichoderma reesei*
A.niger	*Aspergillus niger*
CAC	*commercial acid cellulase*

INTRODUCTION

Plant biomass to bioethanol conversion by using fungal enzyme has a significant role in biofuel industry. Plant biomass is made up of lignocellulose which consists primarily of polysaccharides such as cellulose and hemicellulose. Fungal enzymes like (cellulase, hemicellulase and other accessory enzymes etc) are involved in the conversion of these polysaccharides into bioethanol by breaking down the polysaccharides into monomeric carbon molecules, which are then utilized by yeasts to produce ethanol [1]. Cellulase is composed of endoglucanase (EC 3.2.1.4), exoglucanase (EC 3.2.1.91) and beta-glucosidase (BGL) (EC 3.2.1.21) [3-4]. Among these enzymes, BGL is the rate limiting enzyme which converts the disaccharide cellobiose into glucose. *Trichoderma reesei* is the widely used fungus for production of cellulolytic enzyme, which contains very less amount of BGL [5-6]. By blending the cellulase with BGL, its hydrolytic efficiency and hence sugar yield from biomass can be improved. Glucose tolerant BGLs can produce high amount of sugar when compared with normal BGL since these are not inhibited at high glucose

concentrations. Here, blending of the *T. reesei* enzyme with common BGL from *A.niger* and glucose tolerant BGL from a rare *A. unguis* producing different BGL isoforms [7] was attempted for evaluating their efficiencies in hydrolysis of biomass.

RESULT AND DISCUSSION

Hydrolysis of pure cellulose using *T. reesei* cellulase alone showed release of 189 mg/g of reducing sugar. Blending of 100U/g *A. niger* BGL with *T. reesei* cellulase released 652 mg/g reducing sugar from cellulose. The same concentration of BGL from *A. unguis* along with *T.reesei* cellulase showed release of 633 mg/g reducing sugar.

Fig 1. Hydrolysis of alkali pretreated rice straw using cellulase blends containing different BGLs
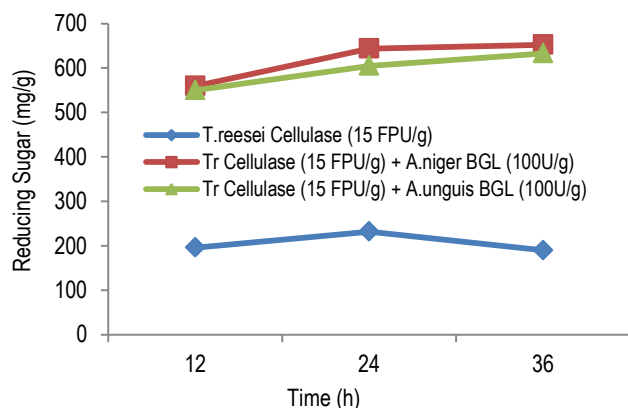
Hydrolysis of alkali pretreated rice straw (pretreatment conditions–15% Biomass loading, 2% Alkali loading, 121 °C for 1h) using CAC produced a sugar yield of 429mg/g with 50.86% efficiency. CAC blend with *A. unguis* BGL (50U/g) showed more hydrolytic potential.

Table 1. Hydrolysis of pretreated biomass using CAC cellulase blends with 50 IU/g BGL

Hydrolytic Performance (36h)	CAC Cellulase (15 FPU/g)	CAC Cellulase (15 FPU/g) + *A. unguis* BGL (50U/g)	CAC Cellulase (15 FPU/g) + *A. niger* BGL (50U/g)
Sugar Yield (mg/g)	429	575.8	511
Efficiency (%)	50.86	68.27	60.58

The combination had a hydrolytic efficiency of 68.27% which was ~18% more than CAC alone. The experiment

was also conducted with *A. niger* (50U/g) BGL blended with CAC and the hydrolytic potential was 60.58%. It was ~10% more efficient than CAC alone. Comparison of hydrolytic potential between two enzyme blends showed that CAC + *A. unguis* BGL had more hydrolytic potential (8.2%) than CAC + *A. niger* BGL.

In another trial, hydrolysis of the alkali pretreated rice straw using *T. reesei* cellulase showed 62.6% efficiency while *T. reesei* cellulase supplemented with 100U/g *A.unguis* BGL showed ~14% more efficiency than *T. reesei* alone. The blend of *T. reesei* cellulase with 100U/g *A.niger* BGL showed ~26% more efficiency than T. *reesei* cellulase alone. Blending of *T. reesei* cellulase with *A. niger* BGL was more efficient (14.45%) than *A. unguis* BGL

Table 2 Hydrolysis of pretreated biomass using *T.reesei* cellulase blends containing 100 U/G BGL

Hydrolytic Performance (36h)	*T. reesei* Cellulase (15 FPU/g)	*T. reesei* Cellulase (15 FPU/g) + *A. unguis* BGL (100U/g)	*T. reesei* Cellulase (15 FPU/g) + *A. niger* BGL (100U/g)
Sugar Yield (mg/g)	528	631	754
Efficiency (%)	62.6	74.85	89.3

CONCLUSIONS

The study proved that the utilization of BGL as a blend with both CAC (commercial acid cellulase) and *T. reesei* cellulase improves biomass hydrolyzing potential of these enzymes. Hydrolytic potential CAC blends with *A unguis* BGL was more efficient than CAC+*A .niger* BGL when rice straw was used as substrate. If *T. reesei* cellulase was used for blending, *A.niger* BGL was more efficient than *A.unguis* BGL. *A. unguis* BGL was more compatible with CAC and *A. niger* BGL was more compatible with *T. reesei* cellulase.

REFERENCES

[1] Hahn-Hagerdal, B., Galbe, M., Gorwa–Grauslund, MF.,Liden, G., Zacchi, G., 2006. Bioethanol from-the fuel of tomorrow from residues of today. Trends Biotechnol., 24,549-556.

[2] Lynd, L.R., Weimer, P.J., van Zyl,W.H., Pretorius, I.S., 2002. Microbial cellulose utilization: Fundamentals and biotechnology. *Microbiol. Mol. Biol. Rev.*, *66*, 506–577.

[3] Zhang, Y.-P., Himmel, M.E., Mielenz, J.R., 2006. Outlook for cellulase improvement: Screening and selection strategies. *Biotechnol. Adv*, *24*, 452–481.

[4] Mandels,M., Reese, E.T., 1957. Induction of cellulase in *Trichoderma viride* as influenced by carbon sources and metals. *J. Bacteriol.* 73,269–278.

[5] Gomes, I., Gomes, J., Steiner, W., Esterbauer ,H., 1992. Production of cellulase and xylanase by a wild strain of *Trichoderma viride*. *Appl. Microbiol. Biotechnol.* 36,701–707.

[6] Rajasree,K.P.,Mathew,G.M., Pandey,A., Sukumaran, R.K., 2013. Highly glucose tolerant b-glucosidase from Aspergillus unguis: NII 08123 for enhanced hydrolysis of biomass. *J Ind Microbiol Biotechnol*, 40,967–975

SEEC-2017-012

THERMAL PERFORMANCE OF GLASS BEADS MATRIX PACKED BED SOLAR AIR HEATER

Vimal Ku. Chouksey
Mechanical Engineering Department
National Institutu of Technology Jamshpur
Email: vimalkumarchouksey@gmail.com

S.P. Sharma
Mechanical Engineering
Department
National Institutu of Technology
Jamshpur
spsharma.me@nitjsr.ac.in

ABSTRACT

An analytical model for solar collector efficiency factor, F', for glass beads matrix packed bed solar air heater has been developed in order to predict the thermal performance of such collector. Effect of system parameters such as diameter of spherical glass beads, bed thickness (depth) and operating parameter viz. air flow rate, insolation, and inlet temperature on the thermal performance are presented and results are compared with flat plate (plane) collector.

Keywords Solar energy, matrix, packed-bed, insolation, solar air heater, plane collector

.
NOMENCLATURE

A_{fr}	Bed frontal/cross-section area of duct, m^2
A_c	Collector area, m^2
B	Width of collector, 1m
C_p	Specific heat of air, J/kg-^{0}C
D	Depth of bed, m
D_H	Hydraulic diameter
D_P	Diameter of glass beads, m
F'	Collector efficiency factor
F_R, F_{PR}	Heat removal factor for plane and packed bed (matrix) collector
G	Flow rate of air per unit width, kg/s-m
G_o	Air mass velocity in bed, kg/m-s^2
h_{cf} , h_{pf}	Convective heat transfer coefficient between cover and fluid and absorber plate and fluid respectively, W/m^2-^{0}C
$h_{r,1-2}$	Radiative heat-transfer coefficient between cover and absorber, W/m^2-^{0}C [4]
h_v	Volumetric heat transfer coefficient, W/m^3-^{0}C
I	Insolation = 950 W/m^2; $(\tau\alpha)_e = 0.85$
L	Length of collector, 1.5 m
m	Mass flow rate of air, kg/s
Nu	Nusselt number
Re	Reynolds number
S	Incident radiation absorbed by the matrix, W/m^2-^{0}C = $I(\tau\alpha)_e$
T_a	Ambient temperature, ^{0}C
T_b,T_f	Temperature of bed and air respectively, ^{0}C
T_c, T_p	Temperature of cover and absorber (plane) respectively, ^{0}K
$U_l^{'}$	Overall loss coefficient, W/m^2-^{0}C
v	Volume of the bed, m^3
V	Velocity of air in plane collector, m/s
μ	Absolute viscosity of air, kg/s-m
ρ	Density of air, kg/m^3
ε_c	Emissivity of cover 0.88
ε_p	Emissivity of absorber plate, 0.95
p	Porosity of bed matrix

INTRODUCTION

Solar air heaters are best alternative for low to moderate temperature applications and simple in construction and can be used for space heating and cooling, drying

agricultural products, timber seasoning, process heat and power generation.

Several variations in designs of such collectors have been developed and tested over the years. Many attempts (Chiou, El-Wakil and Duffie, 1965; Swartaman and Ogunlade, 1966; Mishra and Sharma, 1981; Parker 1981; Hastani, Itaya and Adachi, 1985) have been made to improve their performance.

Packed-beds absorb solar radiation "in depth" and have a high ratio of heat transfer surface area to volume and high heat transfer rate, resulting in lower absorber surface temperatures; this results in decrease in heat losses and consequently increases the performance of collector.

Mishra and Sharma (1981) have tested the performance of packed bed solar air-heaters using iron turnings, aluminum turnings and gravels as packing materials. A solar air heater having its flow channel packed with glass spheres, glass tubes was proposed (Hastani, Itaya and Adachi, 1985) and energy collection and thermal storage characteristics were investigated theoretically and experimentally.

Sharma, Saini and Varma (1991); Varshney and saini (1998) and Prasad, Saini and Singh (2009) investigated experimentally the solar air heater having its duct packed with wire-screen matrices. Absorbers having a bed packed with crushed glass matrices by Collier (1979) have been reported.

Varshney and Saini (1998) have experimentally investigated the heat transfer and flow friction characteristics of solar air heater having its duct packed with wire mesh screen.

Similar type of experimental investigations on wire mesh screen were reported by Thakur et al. (2003) and Prasad et al. (2009) for different porosities range i.e. 0.667 to 0.880 and 0.599 to 0.816 respectively. Mittal and Varshney (2006) experimentally investigated the thermo-hydraulic performance of packed bed solar air heaters having its duct packed with blackened wire screen matrices of different geometrical parameters. Aldabbagh et al. (2010) experimentally investigated the thermal performance of double pass steel wire screen packed bed solar air heater and reported that the efficiency of the double pass is found to be higher than the single pass. Lalji et al. (2011) experimentally investigated the heat transfer, flow friction and exergy analysis of wire screen packed bed solar air heater for high porosity range (0.9614-0.9984) and for different shapes.

Verma and Varshney (2015) developed a mathematical model to investigate the effect of system and operating parameters on the thermal and thermo-hydraulic performance of wire screen packed bed solar air heater for low porosity range (0.50 to 0.76).

In the present investigation an analytical model for collector efficiency factor, F′, has been developed to predict the thermal performance of glass beads matrix packed-bed solar air-heaters. Effect of system and operating parameters on performance has also been investigated.

We have the pleasure to invite you to participate in the first International Conference of International Society for Energy, Environment and Sustainability on "Sustainable Energy and Environmental Challenges" to be organized jointly by the Center of Innovative and Applied Bioprocessing, Mohali, India, and International Society for Energy, Environment and Sustainability. The conference will be held in the Convention Centre, Center of Innovative and Applied Bioprocessing Mohali, India, during 26th to 28thFebruary 2017.

Center of Innovative and Applied Bioprocessing (CIAB) at Mohali (Punjab, India), formerly Bioprocessing Unit, is a national institute under the Department of Biotechnology (Govt. of India). It is a member institute of the Knowledge City Cluster of Institutions comprising of CIAB, IISER, INST, ISB, PBTI, and BTP.

The International Society for Energy, Environment and Sustainability was founded at IIT Kanpur in January, 2014 with an aim to spread knowledge in the fields of Energy, Environment, Sustainability and Combustion. In this changing environmental scenario, the time has come where more emphasis has to be laid on renewable energy resources. Moreover, in this dynamic scenario of swelling competition and reducing profits, staying environmentally responsible can be extremely challenging for any organization. More efficient systems have to be developed to meet the increasing energy demands keeping in mind its environmental impact. People have to become more aware and concerned about the environmental challenges which the world is facing today to make it a better place for us and our future generations. The Society aims to spread knowledge in the above mentioned areas among people and make them more aware about the environmental challenges which the world is facing today. The Society is involved in various activities like conducting workshops, seminars, conferences, etc. in the above mentioned domains. The society also recognizes young scientists and engineers for their contributions in this field. It comprises of experts from leading research institutions working in various domains related to energy.

THEORETICAL ANALYSIS

Plane Collector

The following analytical equations are available in the literatures (Duffie and Beckmann, 1974; Parker, 1981) for collector efficiency factor, F′, for air heaters shown in Figures 1(a) and 1(b).
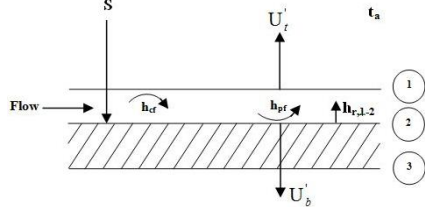
Fig. 1 (a) Plane Surface Absorber
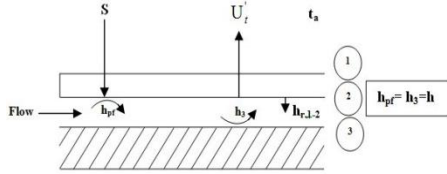
Fig. 1 (b) Plane Surface Absorber

(i)   Flow over the Absorber, Figure 1(a)

$$F' = \frac{h_{r,1\text{-}2}h_{cf} + h_{pf}U_t' + h_{r,1\text{-}2}h_{pf} + h_{cf}h_{pf}}{\left(U_t' + h_{r,1\text{-}2} + h_{cf}\right)\left(U_b' + h_{pf} + h_{r,1\text{-}2}\right) - h_{r,1\text{-}2}^2} \quad (1)$$

$$h_{r,1\text{-}2} = \frac{\sigma\left(T_c^2 + T_p^2\right)\left(T_c + T_p\right)}{\dfrac{1}{\varepsilon_c} + \dfrac{1}{\varepsilon_p} - 1} \quad (2)$$

(ii)   Flow under the absorber, Figure 1(b)

$$F' = \left(1 + \frac{U_l'}{h_e}\right)^{-1} \quad (3)$$

where, $h_e = h + \dfrac{h_{r,1\text{-}2}h}{h_{r,1\text{-}2} + h}$ \quad (4)

Here, $h_{cf} = h_{pf} = h$

and $h_{r,1\text{-}2}$ is given by Equation (2)

2.2 Packed-bed Solar Collector

Considering a packed-bed solar collector as shown in Figure 1(c), the channel with a cover glass of width B, Depth D and length L with an aspect ratio comparatively small, is uniformly heated from upper surface by radiations.

Assuming that **(a)** the particles are small or have a high thermal diffusivity such that any given lump could be considered to be at the uniform temperature at any given instant; **(b)** the resistance to transfer of heat by conduction in the fluid itself or in the solid itself is negligible; **(c)** radiation effects are negligible and **(d)** the physical properties of packed material are independent of temperature.
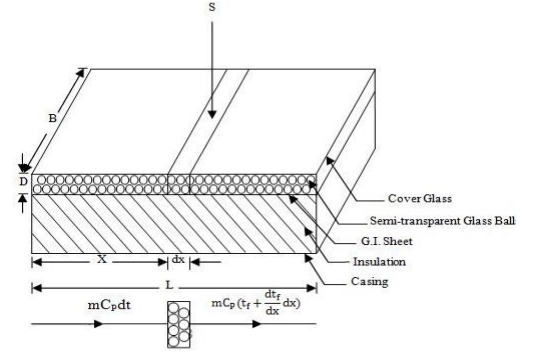
Fig. 1(c) Packed-Bed Absorber

Then the energy balance for element of length dx in the flow direction in steady state condition of the absorption matrix and fluid element are respectively given by the following equation:

For Matrix Material:
Rate of incident radiation absorbed by the matrix of width B, length dx = Rate of energy carried away by flowing air + rate of energy losses from matrix to ambient.
or,

$$S\left(Bdx\right) = h_V A_{fr} dx \left(T_b - T_f\right) + U_l'\left(Bdx\right)\left(T_b - T_a\right)$$

where, S = Incident radiation absorbed by the matrix = $I(\tau\alpha)_e$
T_b and T_f = temperatures of bed and air respectively.

or, $S = h_V D\left(T_b - T_f\right) + U_l'\left(T_b - T_a\right)$ \quad (5)

For Air Stream:
Rate of energy carried away by air due to convection = Rate of sensible energy increase of air through element of length, dx

or, $h_V A_{fr}\left(T_b - T_f\right)dx = mc_P \dfrac{dT_f}{dx}dx$

or, $h_V A_{fr}\left(T_b - T_f\right) = mc_P \dfrac{dT_f}{dx}$ \quad (6)

Combining Equations (5) and (6), rate of useful energy gain per unit collector area, q_u is given by

$$q_u = \frac{mc_P}{B}\frac{dT_f}{dx} = F'\left[S - U_l'\left(T_f - T_a\right)\right] \quad (7)$$

Here F′ is the collector efficiency factor and expressed as:

$$F' = \frac{\dfrac{1}{U_l'}}{\dfrac{1}{U_l'} + \dfrac{1}{h_V D}} \quad (8)$$

In order to predict the thermal performance of glass beads matrix solar collectors, the volumetric heat transfer co-

3

efficient, h_V must be known and it is evaluated by using the correlation

$$h_V = h \cdot \frac{A_c}{v} \qquad (9)$$

The value of convective heat transfer coefficient h, can be calculated as follow (Whitaker, 1972).

$$Nu = \left(0.5\,Re^{0.5} + 0.2\,Re^{0.66}\right)Pr^{0.33} \qquad (10)$$

where, $\quad Re = \dfrac{D_p \cdot G_o}{\mu(1-p)} \qquad (11)$

and $\quad Nu = \dfrac{hD_p}{k}\left(\dfrac{p}{1-p}\right) \qquad (12)$

Here, G_o is the mass velocity of air equal to $\rho Q / A_{fr}$.

The following correlations may be used for laminar flow and turbulent flow respectively in a plane rectangular channel duct (Yeh, 1999).

$$Nu = 4.4 + \frac{0.00398\left(0.7\,Re \cdot D_H / L^0\right)^{1.66}}{1 + 0.00114\left(0.7\,Re \cdot D_H / L^0\right)^{1.12}} \qquad (13)$$

$$Nu = 0.0158\,Re^{0.8}\left[1 + \left(\frac{D_H}{L}\right)^{0.7}\right] \qquad (14)$$

where, $\quad Re = \dfrac{\rho v D_H}{\mu}$

$U_l^{'} = 10$ W/m^2.K assumed as constant in the present investigation, as it is weak function of bed temperature (Sharma, Saini and Varma, 1991).

2.3 Temperature of Air in Flow Direction

If T_{fi} is the inlet temperature of air, then the temperature of air at any position x can be expressed as (Duffie and Beckmann, 1974)

$$\frac{T_f - T_a - \dfrac{S}{U_l^{'}}}{T_{fi} - T_a - \dfrac{S}{U_l^{'}}} = \exp\!\left[-\frac{F'U_l^{'}A_c}{\dot{m}C_p}\,x\right] \qquad (15)$$

If L is length of the collector, then the outlet temperature T_{fo} is found by replacing L for x in Equation (15).

$$\frac{T_{fo} - T_a - \dfrac{S}{U_l^{'}}}{T_{fi} - T_a - \dfrac{S}{U_a}} = \exp\!\left[-\frac{F'U_l^{'}A_c}{\dot{m}C_p}\,L\right]$$

$$(16)$$

2.4 Collector Heat Removal Factor

The collector heat removal factor can be written as (Kays and London, 1964; Duffie and Beckmann, 1974).

$$F_R = \frac{\dot{m}C_p}{A_c U_l^{'}}\left[1 - \exp\!\left(-\frac{A_c U_l^{'}F'}{\dot{m}C_p}\right)\right]$$

$$(17)$$

The quantity F_R is equivalent to a conventional heat exchanger effectiveness, which is defined as the ratio of the actual heat transfer to the maximum possible heat transfer.

2.5 Collector Efficiency

The efficiency of collector can be expressed as

$$\eta = \frac{\dot{m}C_p\left(T_{fo} - T_{fi}\right)}{A_c \cdot I}$$

RESULTS AND DISCUSSIONS

Figure 2 shows collector efficiency factor, (F′) calculated with help of Equation (1)-(2) for plane and Equation (9) for glass beads matrix solar air heater as a function of bed-depth. Results show that collector efficiency factor (F′) of matrix solar collector increases slightly as thickness of bed increases, while for plane collector it decreases drastically. It may also be noted that as diameter of spherical glass beads decreases, collector efficiency factor is found to increase. This appears due to fact that decrease in diameters of beads increase the heat transfer rate because of increase in heat transfer surface area and more turbulence.
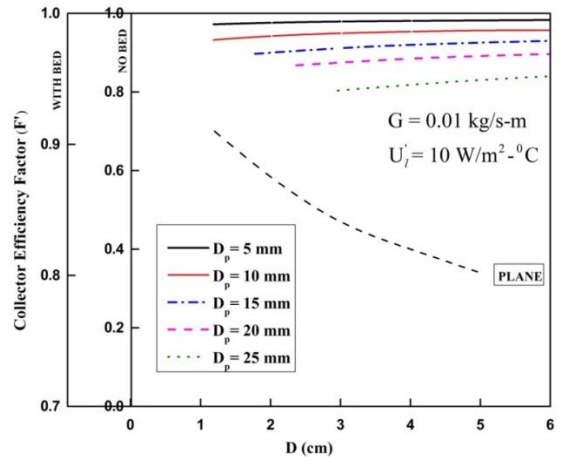
Fig. 2 Effect of bed thickness on collector efficiency factor

Figure 3 shows the effect of air mass flow rate on collector efficiency factor. Here curves show that as the air

mass flow rate increases, the collector efficiency factor increases for both plane as well as matrix solar collectors.
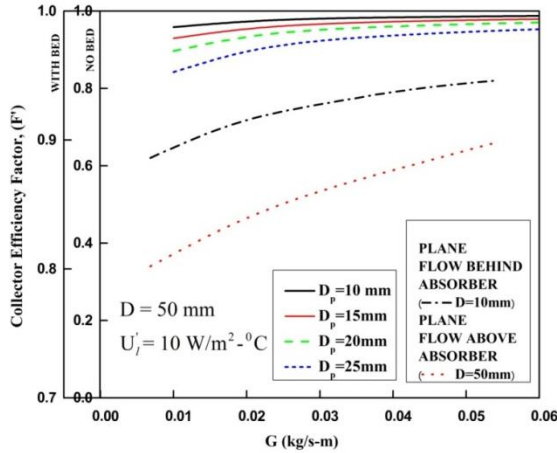
Fig. 3 Effect of mass flow rate on collector efficiency factor

It is seen that the increase in air mass flow rate beyond 0.03 kg/s-m has little effects on collector efficiency factor for matrix collector, while for plane collector effects are more pronounced.

Figure 4 shows the effect of bed thickness on collector heat removal factor (F_R) for different size of packing materials, from the figure it is seen that F_R increases as thickness of bed increases. The increase in the value of F_R attributed to the fact that any decline in the value of convective heat transfer coefficient as a result of decrease in superficial mass velocity of air is effectively compensated by corresponding increase in the heat transfer surface area of packing materials. It is also seen that as packing materials diameter decreases, collector heat removal factor increases. This results in fact is due to decrease in particle diameter, increases the total surface area of packing materials and consequently increases the convective heat transfer rate from bed matrix to air.
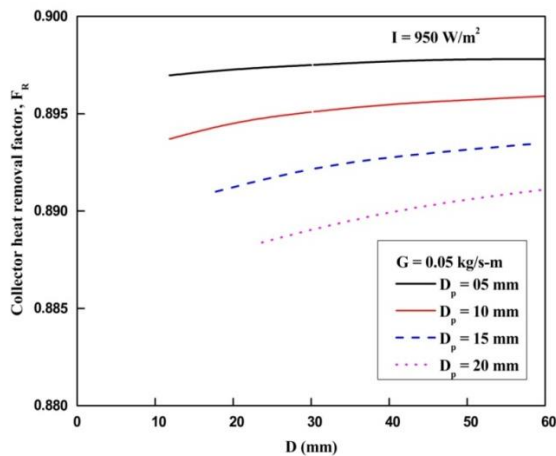
Fig. 4 Effect of bed thickness on collector heat removal rate

Figure 5 shows the collector heat removal factor as a function of specific air flow rate for different values of

glass beads diameter. From the figure it is found that F_R increases as G increases because of increase in convective heat transfer rate. A substantial enhancement of these parameters with smaller diameter of glass beads is the index of beneficial influence.
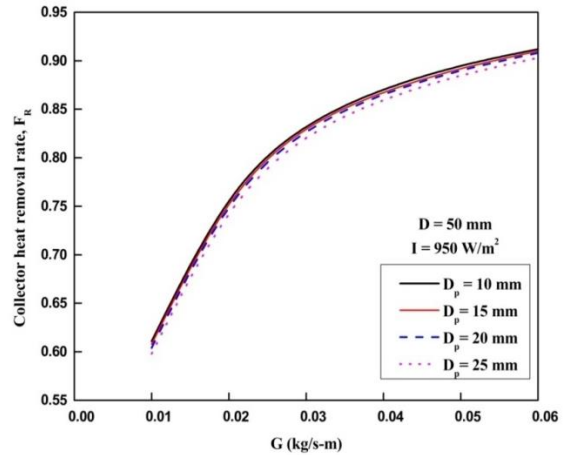
Fig. 5 Effect of mass flow rate on collector efficiency factor

Figure 6 shows the plot of the ratio of collector heat removal factor of matrix collector to that of plane collector as a function of air mass flow rate. Enhancement of performance up to 100% at low air mass flow rate (0.01 kg/s-m) to 46% at high air mass flow rate (0.05 kg/s-m) over plane collector with flow above the absorber is observed. It is 30.7% to 18.7% over plane collector with flow below the absorber plate.
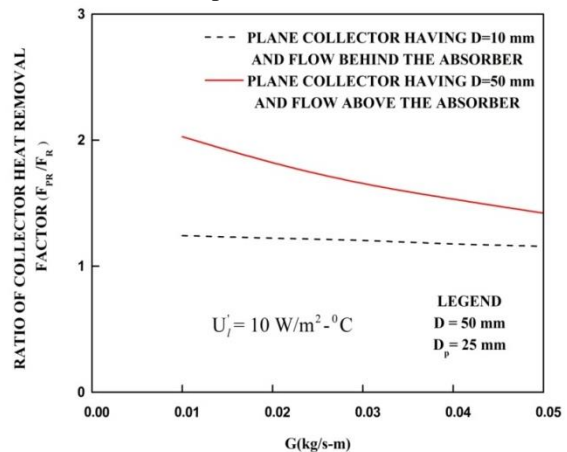
Fig. 6 comparison of performance between plane and packed-bed collectors

The effect of air mass flow rate and diameter of glass beads on collector efficiency was shown in Figure 7. It is seen from the figure that the efficiency increases for both plane as well as glass beads matrix collectors with an increase in air mass flow rate and with a decrease in diameter of glass beads. This appears due to the fact that more turbulence is created in the flow as the diameter of glass beads decreases and the flow passage becomes more tortuous and narrower.
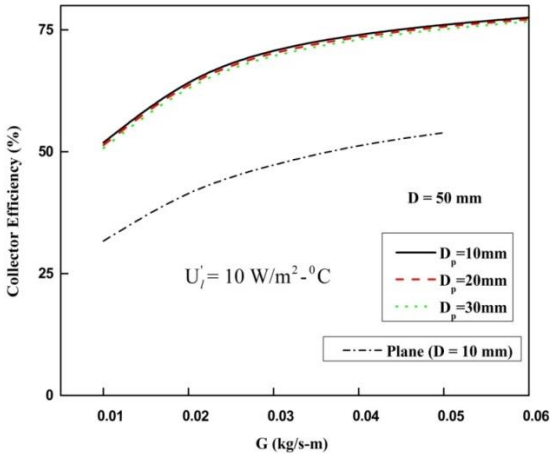
Fig. 7 Effect of mass flow rate on collector efficiency

CONCLUSIONS

(i) An analytical expression for collector efficiency factor for glass beads matrix packed-bed solar air heaters has been developed which provides a means of analytical comparison of thermal performance of such collectors with that of plane collector.

(ii) The performance of plane collector is found to improve appreciable by packing it with semi-transparent materials.

(iii) Effects of system parameters such as depth of bed and diameter of packing materials on the thermal performance have been investigated.

REFERENCES

[1]. Chiou, J.P., El-Wakil, M.M. and Duffie, J.A., 1965. "Slit and expanded aluminum foil matrix solar collector". Solar Energy, 9 (2), pp. 73-80.

[2]. Swartaman, R.K. and Ogunlade, O., 1966. "An investigation on packed-bed collectors". Solar Energy, 10, pp. 106-110.

[3]. Mishra, C.B. and Sharma, S.P., 1981. "Performance study of air-heated packed-bed solar energy collectors". Energy, 6, pp. 153-157.

[4]. Parker, B.F., 1981. "Derivation of efficiency and loss factors for solar air heaters". Solar Energy, 26(1), pp. 27-32.

[5]. Hastani, M., Itaya, Y. and Adachi, K., 1985. "Heat transfer and thermal storage characteristics of optically semi-transparent material packed-bed solar air heater". Current Research in Heat and Mass Transfer, IIT Madras pp. 61-70.

[6]. Sharma, S.P., Saini, J.S. and Varma, H.K., 1991. "Thermal performance of packed-bed solar air heaters". Solar Energy, 47(2), 59-67.

[7]. Varshney, L. and Saini, J.S., 1998. "Heat transfer and friction factor correlations for rectangular solar air heater duct packed with wire mesh screen matrices". Solar Energy, 62(4), pp. 255-262.

[8]. Prasad, S.B., Saini, J.S. and Singh, KM, 2009. "Investigation of heat transfer and friction characteristics of packed bed solar air heater using wire mesh as packing material". Solar Energy, 83, pp. 773-783.

[9]. Collier, R.K., 1979. "The characterization of crushed glass as a transpired air heating solar collector material". Proc. of Int. Solar Energy Society, Atlanta, Georgia, pp. 264-268.

[10]. Thakur, N.S,, Saini, J.S. and Solanki, S.C., 2003. "Heat transfer and friction factor correlations for packed bed solar air heater for a low porosity system". Solar Energy, 74, pp. 319-329.

[11]. Mittal, M.K. and Varshney, L., 2006. "Optimal thermo-hydraulic performance of a wire mesh packed bed solar air heater". Solar Energy 80, pp. 1112–1120.

[12]. Aldabbagh, L.B.Y., Egelioglu, F. and Ilkan, M. 2010. "Single and double pass solar air heaters with wire mesh as packing bed". Energy, 35, 3783-3787.

[13]. Lalji, M.K., Sarviya, R.M. and Bhagoria, J.L., 2011. "Experimental investigations on packed bed solar air heater". Current World Environment, 6(1), pp. 151-157.

[14]. Verma, P., and Varshney, L., 2015. "Parametric investigation on thermo-hydraulic performance of wire screen matrix packed solar air heater". Sustainable Energy Technologies and Assessments, 10, pp. 40-52.

[15]. Duffie, J.A. and Beckmann, W.A., 1974. "Solar Engineering Thermal Processes". 3rd ed. John Wiley and Sons, New York.

[16]. Whitaker, S., 1972. "Forced convection heat transfer correlations for flow in pipes, past flat plates, single cylinders, single spheres and for flow in packed beds and tube bundles". AIChE Journal, pp. 361-371.

[17]. Yeh, Ho-Ming. and Chii-Dong, HO., 1999. "The improvement of collector efficiency in solar air heaters by simultaneously air flow over and under the absorbing plate". Energy, 24, pp. 857-871.

[18]. Kays, W.M. and London, A.L., 1964. "Compact Heat Exchangers". 2nd ed. McGraw Hill, New York.

SEEC-2017-013

COMBUSTION CHARACTERISTICS OF GRAPHENE ISROSENE NANO-FLUID

Amit Kumar Yadav
Liquid propulsion system center,
ISRO,Thiruvananthapuram,Kerala,India
amitkumar@lpsc.gov.in

AtulSrivastav
Indian institute of technology Bombay, Mumbai,
Maharashtra, India
atulsr@iitb.ac.in

Arindrajit Chowdhury
Indian institute of technology Bombay, Mumbai,
Maharashtra, India
arindra@iitb.ac.in

Nandakumar K
Liquid propulsion system center,
ISRO,Thiruvananthapuram,Kerala,India
nandakumar_k@lpsc.gov.in

ABSTRACT

Isrosene is refined kerosene, a suitable fuel for rocket application with liquid oxygen as an oxidizer. Combustion characteristics of Isrosene and graphene nano-particle (GNP) added Isrosene was studied using droplet combustion. The percentagemass loading of GNP in Isrosene wasdecided based on the previous study carried out to study its heat transfer characteristics in order to improve the regenerative cooling of rocket engines. The synthesis of Nano-fluid was carriedout using the same setup with similar procedure as in previous study.

It is found that by addition of GNP in Isrosene the mass burning rate of the Isrosene was improved by a maximum of 12 %. This improvement wasseen up to themass loading of the 0.1%of GNP in Isrosene. Further increase of the GNP percentage reduced the mass burning rate. The addition of surfactant for stability of nano-fluidreduced the mass burning rate. Droplet combustion was found to obey the D^2-t law.Flame diameter and flame standoff ratio was not significantlyaffected with addition of GNP in Isrosene. Micro explosions were observed during the combustion of GNP-IsroseneNano-fluid droplets for 0.1% loading and 0.2% loading.

Keywords: Nano-fluid, Droplet combustion, GNP-Isrosene, d^2-t curve, Micro-explosion, Flame standoff ratio.

NOMENCLATURE

GNP   Graphene Nano Particles
v_e Volume of ellipsoid droplet (mm^3)
d_{max} Major diameter of ellipsoid(mm)
d_{min} Minor diameter of ellipsoid(mm)
d   Instantaneous diameter of the droplet(mm)
d_0 Initial diameter of droplet(mm)
k   Burning rate constant(mm^2/s)
$\dot{m}$ Mass burning rate (mg/s)
ρ_l Density of fuel

1. INTRODUCTION

Concept of Nano-fluid has made a fairly good impact in research community where majority of the work conducted is limited to improvement of the heat transfer characteristicsof the fuel [1-3].The application of Nano-fluid in rocket engines because of better heat transfer characteristics provoke the need to study the combustion characteristics of Nano-fluid in comparison with base fuels,since after cooling the thrust chamber the same fuel is combusted in rocket.

Yayan and Li Q [4] studied the burning characteristics of ethanol and n-decane by addition of nanometersized and micron sizedaluminium particles.Javed et al.[5] studied the ignition and combustion characteristics of kerosene and aluminium at elevatedtemperature and reported a significant enhancement in burning rate by the addition of aluminium nano-particles. Yayan et al. [6] studied the combustion characteristics of boron and iron nano-particles added in ethanol and n-decane, where they explained differences in the flame structure.Chen et al. [7] studied the evaporation characteristics of water droplet with the

addition of laponite, Fe_3O_4 and silvernano-particles separately, and concluded that there is remarkable increase in evaporation rate.

In the present study combustion characteristics of GNP-Isrosene Nano-fluid is determined using suspended dropletcombustion technique.

GNP, having a specific surface area (SSA) of 750 m^2/g, isadded in different percentages by mass i.e. 0.05%, 0.1%, 0.2%, and 0.5%to Isrosene. For making a stable colloidal solution,0.03%(by mass) ofoleylamine surfactant is added. Apart from above mentioned percentagemass loading,oleylamine and Isrosene combustion characteristics are also studied to isolate the effect of oleylamine.The methodology of droplet combustion is adopted because of its simple, one-dimensional, and fairly accurate way to gather information about the spray combustion [9-13]. The effect of GNP on mass burning rate, burning rate constant, flame radius, and flame standoff ratio isinvestigated.

2. EXPERIMENTAL METHOD

2.1 Fuel preparation:

The experimental setup and procedure to prepare Nano-fluidis explained in details elsewhere [2, 3]. Briefly, in measured quantityof Isrosene (50 grams), GNP of specific surface area750 is added in desired quantities 0.025, 0.05, 0.1, and 0.25 grams.

The present combination is decided based on previous experience and it is found that this combination is stable and has better thermal properties [3]. To avoid the agglomeration of GNP,suitable surfactant (oleylamine) is added in minimum required quantity, i.e. two drops (~0.06 grams). The prepared colloidal solution isultrasonicated thereafter.

2.2 Droplet combustion experimental setup:

The droplet combustion experimental set up as shown in Fig-1consists ofthe following.

Droplet combustion chamber: Combustion of droplets is conducted in combustion chamber to avoid the influence of surrounding disturbances. Chamber hasinner diameter of 156 mm, outer diameter of 162 mm,and length of 300 mm. Both ends of the cylinder are closed with flange joint with gasket to prevent leaks. The dimensions of the combustion chamber are taken to be greater than 50 d where d is the maximum size of droplet to avoid the depletion of ambient oxygen and thus an alteration in the boundary conditions during combustion. There are three glass windows for optical accessibility on the surface of the cylinder located ninety degree apart. Apart from the glass windows, there were ten ports, fouron the top flange, three on chamber and three on the bottom flange for mechanical accessibility and incorporating various measurement systems for controlling the various parameter such as chamber pressure, temperature, and mole fraction of oxygen in the chamber.

Droplet depositing mechanism with suspension support:A 5 cm long 0.25 mm diameter quartz rod is used for suspension of dropletsize ~1.75 mm in diameter. A micro syringe of capacity 10 µl is used to deposit the droplets on thetip of thequartz rod.

Ignition system: The droplet was ignited bya spark at ~ 3 mm vertically down from the bottom tip of the droplet using two electrodes. Spark was generated using an ignition transformer forduration of ~ 0.30 s which is just sufficient for the ignition of the droplets.

High-speed camera: To capture the droplet size variation with time, a Phantom make high-speed imager (12000 fps) with a resolution of 1280x800pixels withbacklight support is employed.Combustion phenomenon isrecorded at100 frames per second (fps).

Thermal Imaging camera: To observe the flame structure and flame diameter change with timeFLIR make thermal imaging camera X6540-X6550 SCis used. Combustion is recorded at 100 fps.

After each experiment, the suspension rod is cleaned to ensure the absence of any carbon deposits on it. Each experiment was repeated three times to ensure repeatability.
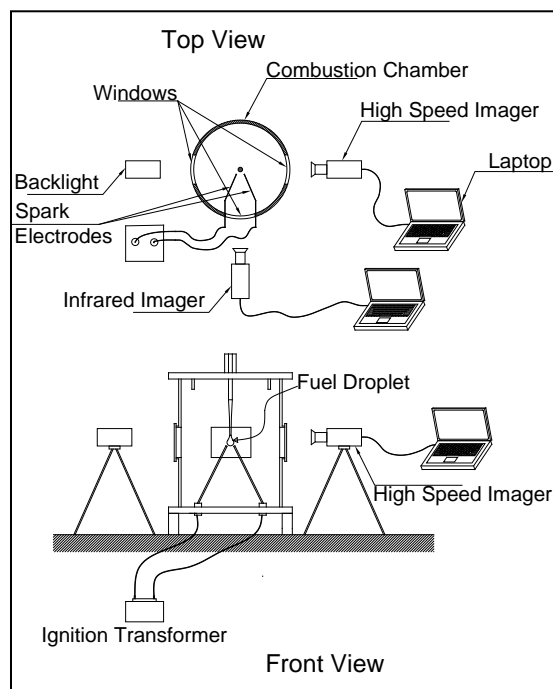
Figure-1 Schematic of droplet combustion experimental setup

2.3 Data deduction procedure: Once the set of experiments was completed, the recordedsequence of images of droplet surface history from the high-speed imager and flame surface history and flame temperature with the sequence of images from thermal imager is analysed. Analysis involvesplotting the D^2-t curve and determining the slope of the curve i.e. burning rate constant [10]. In the experimental data, the shape of the droplet

isnot exactly spherical. Instead, it is ellipsoidal in nature.For the purpose of analysis, the volume of the droplet isconverted to equal volume of the sphere, and droplet diameter was determined using equations-1 and-2 and D^2-t curve is plotted. Once the burning rate constant is computed, usingequation-4 mass burning rateis also computed [12].

$$v_e = \frac{\pi}{6} \times d_{max} \times (d_{min})^2 ....(1)$$

$$d = (\frac{6}{\pi} v_e)^{1/3} ....(2)$$

$$d^2 = d_0^2 - kt ....(3)$$

$$\dot{m} = \frac{\pi \rho_l d_0 k}{4} ....(4)$$

Flame of GNP-Isrosene droplet is sooty in nature. The method adopted for computing the flame diameter is shown in Fig-2.The ratio of instantaneous flame diameter to instantaneous droplet diameter is termed as flame standoff ratio [12].
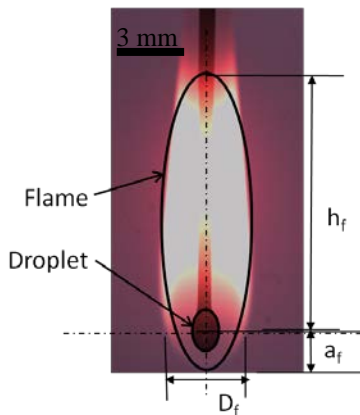
Figure-2 A typical flame around the GNP-Isrosene combusting droplet

3. RESULTS AND DISCUSSIONS:

3.1 D^2-t Law: To determine the droplet combustion characteristics of GNP-Isrosene more than 20 experiments are conducted where the droplets of GNP-Isrosene are combusted at atmospheric pressure and temperature under normal gravity by using air as an oxidizer. The variation of the square of the droplet diameter with respect to time is computed and plotted for all the experiments. A typical plot of D^2-t is shown in Fig-3. The size of the droplets is kept constant in all the experiments.It can also be inferred from the figure that droplet combustion of GNP-Isrosene combination obeys D^2-t law. The slope of the $(d/d_0)^2$–t/$(d_0)^2$ curve shows the burning rate constant (K). The maximum slope is observed for GNP (0.1%)-Isrosene combination indicating the highest burning rate constant as compared to any other combination.
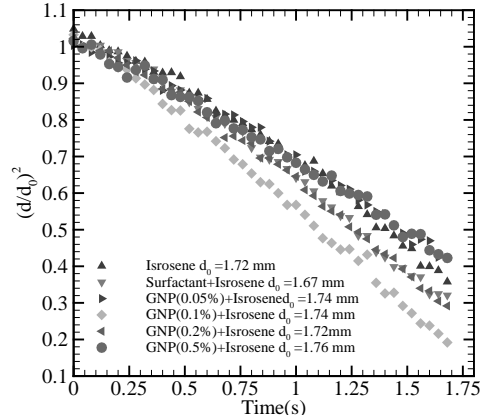
Figure-3 $(d/d_0)^2$-t curve for GNP-Isrosene combusting droplets

3.2 Burning Rate and Burning Rate Constant: From the $(d/d_0)^2$-t curve, the slope of the curve is deduced for a set of 3 experiments. Using the average slope of a set of data and equation-3 the burning rate constant isdeduced. Similar exercise is conducted for all combination of GNP-Isrosene droplets and plotted in Fig-4.
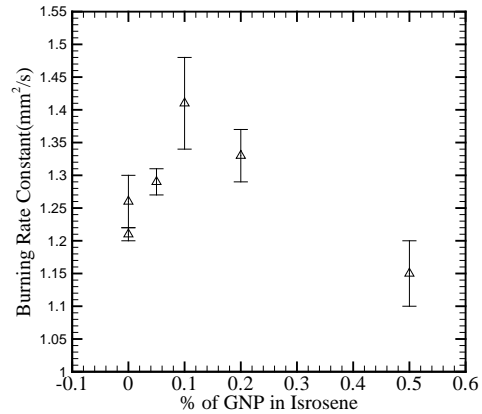
Figure-4 Burning rate constant with percentage mass loading of GNP in Isrosene

One can see in figure-4 that there are two points for the 0 % of the GNP loading.The upper point indicates the burning rate constant for the Isrosene droplets and lower one indicates the burning rate constant for the surfactant added Isrosene droplets. Thisindicates that by addition of oleylamine (surfactant) there is a small reduction in the burning rate constant. One may also notice that, initially there isincrease intheburning rate constant with increase ofpercentage loading of GNP and then it reduces.Maximum burning rate constant is observed at 0.1% loading of GNP in Isrosene and the maximum increase is found to be ~12% compared to the base value. The increase in burning rate constant may be attributed to enhancement of transport and optical properties of the fluid by addition of GNP [8].Higher thermal conductivity and higher absorption capacity of the fluid by addition of GNP, may have increased the evaporation rate and hence the

combustion rate. By addition of more GNP than the optimum value, there could be fast agglomeration of GNP, whichreduces the burning rate constant. Similar trend of burning rate constant is reported by Ghamri and Ratner for GNP-RP1 droplets [13].
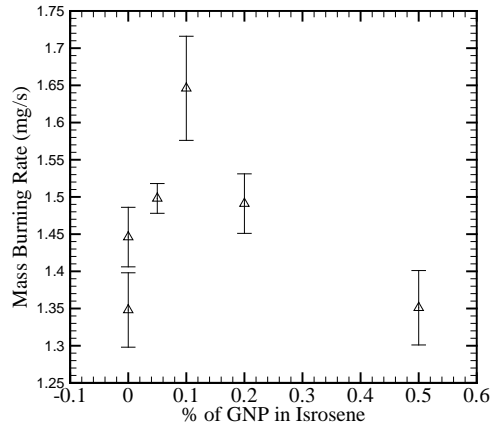
Figure-5 Mass burning rate with percentage mass loading GNP in Isrosene

Figure-5 shows the mass burning rate, which is obtained from the burning rate constant using equation -4, which is a derived quantity from burning rate constant and shows the similar trend.

3.2 Flame diameter and flame standoffratio: Using the procedure as discussed in section 2, the flame diameter (D_f) and flame standoff ratio (D_f/d) is extracted for all the experiments. In the Fig-6, flame diameters are shown whereone may observe that relative variation in flame diameter is within the experimental error.A noticeable point is the abrupt change in the flame diameter for the droplet containing the 0.1% and 0.2% of the GNP mass loading.One may also observed that in such experiments where this phenomenon is spotted, immediately after this change, there is a fast reduction in the flame diameter which indicates the consumption of more fuel and may also be the cause of increase in burning rate constant and mass burning rate as reported in section 3.1
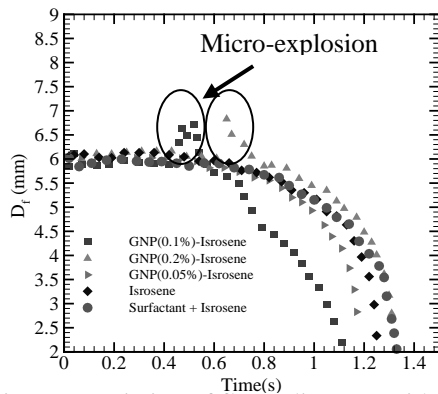
Figure-6 Variation of flame diameter with time for different mass loading of GNP in Isrosene

4. CONCLUSIONS:

Combustion characteristics of GNP-Irosene Nano-fluid are studied using droplet combustion methodology.

The major highlights of work carried out are listed below.

- Droplet combustion of GNP-Isrosene droplets follows the D^2-t law.
- The addition of surfactant (oleylamine)reduces the mass burning rate of base fuel
- Addition of GNP in Isrosene improved the mass burning rate of the fuel by 12 %. This enhancementis seen up to a particular loading of the GNP
- Further increase of the GNP mass loading reduces the mass burning rate.
- The absolute value of flame diameter and flame standoff ratio is not affected because of GNP addition in Isrosene.
- Phenomenon of micro explosion iswitnessed during the combustion of GNP-Isrosene Nano-fluid droplets for 0.1% loading and 0.2% loading.

5. ACKNOWLEDGMENTS

6. REFERENCES:

[1] S.U.S. Choi, "Enhancing thermal conductivity of fluids with nanoparticles," The Proceedings of the 1995 ASME Int. Mechanical Engineering Congress and Exposition, ASME, San Francisco, USA, 1995, pp. 99e105

[2] Agarwal D. K, Vaidyanathan A., Kumar S. S., "Synthesis and characterization of kerosene-alumina Nano-fluids"Applied Thermal Engineering 60 (2013) 275-284.

[3] Agarwal D. K, Vaidyanathan A., Kumar S. S., "Experimental Investigation on Thermal Performance of Kerosene-Graphene Nano fluid", Experimental Fluid and Thermal Science 71 (2016) 126-137

[4] Y. Gan and Li Qiao, "Combustion characteristics of fuel droplets with addition of nano and micron-sized aluminum particles" Combustion and Flame 158 (2011) 354–368

[5] Irfan Javed, SeungWookBaek, Khalid Waheed, "Auto ignition and combustion characteristics of kerosene dropletswith dilute concentrations of aluminum Nano-particles at elevatedtemperatures"Combustion and Flame 162 (2015) 774–787.

[6] YananGan, Yi Syuen Lim, Li Qiao "Combustion of Nano-fluid fuels with the addition of boron and iron particles at dilute and dense concentrations" Combustion and Flame 159 (2012) 1732–1740.

[7] Ruey-Hung Chen, Tran X. Phuoc, Donald Martello, "Effects of nanoparticles on nanofluid droplet evaporation" International Journal of Heat and Mass Transfer 53 (2010) 3677–3682.

[8] YananGan and Li Qiao, "Optical Properties and Radiation-Enhanced evaporation of Nanofluid Fuels"50th AIAA Aerospace Sciences Meeting including the New Horizons Forum and Aerospace Exposition 09 - 12 January 2012, Nashville, Tennessee.

[9] A Ambekar, AChowdhury, SChalla, D Radhakrishna, "Droplet combustion studies of hydrocarbon-monopropellant blends", Fuel 115 (2014) 697–705

[10] T. Farouk , F. L. Dryer, "Microgravity droplet combustion: effect of tethering fiber on burning ate and flame structure"Combustion Theory and Modeling Vol. 15, No. 4, 2011, 487–515

[11] Ambekar, A., A. Chowdhury. "Experimental Prediction of Intrinsic Burning Rate Constants of Liquid Fuel Droplets". ASPACC 2015 - 10th Asia-Pacific Conference on Combustion. SCOPUS. Web. 22 May 2016

[12] SR Turns. "Introduction to combustion Concepts and Applications" McGraw-Hill 2000, 2nd edition,Chapter-10,362-421

[13] Mohsen Ghamari,and Albert Ratner "Combustion characteristics of colloidal droplets of jet fuel and carbon based nanoparticles" Fuel 188 (2017) 182–189

SEEC-2017-014

INTERACTING SWIRL FLOW DYNAMICS

Rahul B.V.
National Center for Combustion Research and Development
Indian Institute of Science

P. M. Tilak
Department of Aerospace Engineering
Indian Institute of Science

Swetaprovo Chaudhuri
Department of Aerospace Engineering
National Center for Combustion Research and Development
Indian Institute of Science
Email: swetaprovo@gmail.com

ABSTRACT

Swirling flows exhibit complex characteristics due to presence of embedded rotation in the otherwise axial flow. The present work tries to explain the interesting flow features emerging from mutual interaction between adjacent swirling flows at variable degrees of swirl, issued into a semi-confined chamber, as it would happen in a three cup sector of an annular combustor of a modern gas turbine engine. A central swirling flow with a fixed swirl vane angle is allowed to interact with its neighboring swirling flows at varied swirl levels. The presence of swirling or diverging jets on either side of the central swirler significantly alters its flow patterns. It is observed that an increase in amount of swirl in neighboring swirling flows enhances the recirculation levels in central swirling flow resulting into a well-established bubble type vortex breakdown. Asymmetric flow patterns are found in the neighboring flows on their interacting sides. There is a tendency for neighboring jets to show better recirculation in comparison with their non-interacting sides. In light of these interactions, we proceed to reacting flows and discover more interesting features.

*Keywords***:** swirl, recirculation, vortex breakdown

NOMENCLATURE

S1	Left Extreme Swirler
S2	Central Swirler
S3	Right Extreme Swirler
s	Spacing between swirlers, center to center
d	Diameter of swirler
V	Axial velocity

INTRODUCTION

Swirling flows are generated by imparting tangential momentum to an otherwise straight jet issuing out of an annular outlet. The translating and rotating fluid often give rise to a special feature called vortex breakdown which has been the subject of intense research throughout the second half of twentieth century after it was first reported by Peckham & Atkinson [1] in their study of flow over delta wings. It was followed by systematic studies by Harvey [2] and Sarpkaya [3] that provided some basic properties of vortex breakdown. Faller and Leibovich [4] studied internal structure of the breakdown. Many theoretical, computational and experimental studies were done in this area. Nevertheless, the understanding of mechanism causing vortex breakdown is still not complete [5]. Vortex breakdown is a problem of great interest because of its application in combustion processes *especially in gas turbines.*
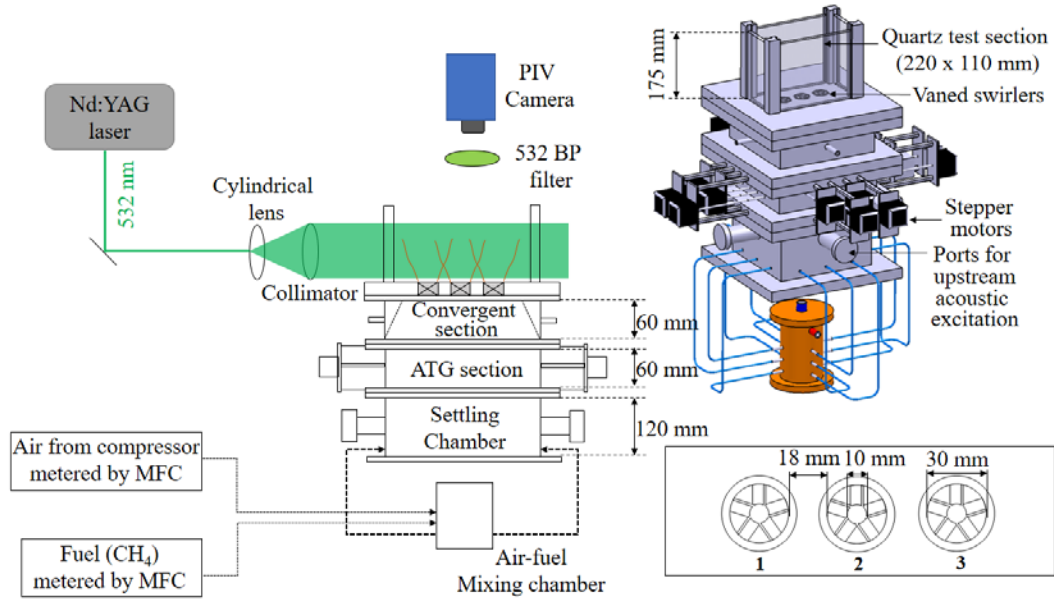
FIGURE 1. Schematic of the experimental setup. Swirlers are interchangeable from 5 vane (30º) to 8 vane (45º).

Occurrence of vortex breakdown in swirling flows depends on characteristic velocity ratio of azimuthal to axial components [2-4, 6] or in terms of swirl number. Swirl number defined as the ratio of axial flux of tangential momentum to the axial flux of axial momentum is conventionally used as an important parameter to characterize these swirl flow phenomena. Increasing swirl number beyond 0.6 causes toroidal re-circulating regions i.e. vortex breakdown in the form of axisymmetric bubble [7-8]. In this paper, we first focus on non-reacting swirl flows issued into confined space. Unlike earlier studies which were done by varying flow parameters i.e. by changing characteristic velocity ratio [2-4] or by changing swirl number [7-8], here we keep the flow parameters of central swirler fixed and vary the properties of neighbouring flows. This inline arrangement of three swirlers can be thought of as a limiting case of present day gas turbine engines which adapt to annular combustion chambers of finite radius annulus. The interactions between reacting swirl flows is ubiquitous in such arrangements and studying the flow phenomena involved serves as a guiding light to better understand combustion processes. The difference between cold and reacting flow configurations was studied for a single swirler case in [9-12] i.e. without the effects of interaction. Multiple swirler case with interactions between swirling flows was also studied [13, 14]. The comparison of velocity profiles was made [13] between single nozzle and multiple nozzle cases where in both cases are reacting and changes in recirculation velocities and jet spread angle were reported for a given non-dimensionalized spacing $(s/d) \sim 3$.

Experiments reported in this paper with three swirlers arranged inline have s/d = 1.6. Before proceeding to the reacting case, we first investigate isothermal flow for striking changes in nature of flow itself on account of interaction. One important difference between case reported in [13] and ours is that we see a stabilized flame only in the case of interacting flows, due to fluid mechanical effects arising out of mutually interacting jets which will be clear in succeeding sections.

EXPERIMENTAL APPARATUS

In the present study, a model gas turbine combustor consisting of three inline swirl burners has been utilized, the schematic of which is shown in Fig. 1. The air flow is supplied from a compressor through a series of pressure regulators and metered by a mass flow controller (ALICAT MCR, range: 0-4000 slpm) to obtain the desired mass flow rate. Fuel (Methane, 99% purity) is metered using a mass flow controller (ALICAT MCR, range: 0-500 slpm), which is then premixed with air in a mixing chamber. The mixture enters the settling chamber through 12 ports and flows through the ATG (Active turbulence grid) followed by a square convergent section and into the quartz test section where it is ignited. The winglets in the ATG are placed in horizontal position (plane of the burner) throughout this study. Three fixed vane angle swirlers having an outer diameter (D) of 30 mm and hub diameter 10 mm are arranged linearly with an edge to edge spacing of 18 mm which mimics a sector of an annular gas turbine combustor. The flow field for both cold flow and reacting flow cases was characterized using a PIV system from LaVision Inc. comprising of a 200mJ/pulse Nd:YAG laser (Litron Nano L

series), 1024 x 1280 CCD camera (Imager Intense) and DaVis 8.3 post processing software. The PIV camera was coupled with a Nikon 50mm lens and a 532nm bandpass filter to capture the scattered laser light downstream of the swirler. The final interrogation window for PIV algorithm used was 24 x 24 px giving a resolution of 1.33 mm. The laser sheet was created using an f=-20 mm cylindrical lens to an area of interest spanning 180 x 145 mm. The data acquisition rate for all the readings was 4.5 Hz.

The 45° swirler consisted of 8 vanes and 30° swirler consisted of 5 vanes with the same geometric dimensions, which were replaced for different flow conditions studied. For the case where jet was introduced into the flow along with a central swirler, the outer swirlers were removed to create an axisymmetric jet. All the flow conditions studied here correspond to a Reynolds number (Re) of 8000 based on the bulk flow at the exit of the central swirler.

RESULTS AND DISCUSSION

Experiments were conducted for different configurations by fixing swirl angle of central swirler at 45° in all cases. As a first case, we will consider flow only through the central swirler with adjacent ports (swirlers S1 and S3) being closed. As observed from the Fig.2(a), the flow doesn't exhibit the conventional vortex bubble configuration which suggests that the swirl number in this case is < 0.6 [7,8]. As a second case, we start introducing flow through neighbouring ports by removing swirlers S1 and S3 and creating an axisymmetric jet flow on both sides of the central swirler. It can be seen in Fig. 2(b) that the straight jets do not seem to interfere much with the central swirling jet. However, the difference in axial flow velocities lead to K-H type instabilities along the shear layer.

Furthermore, suction towards the hub of central swirler
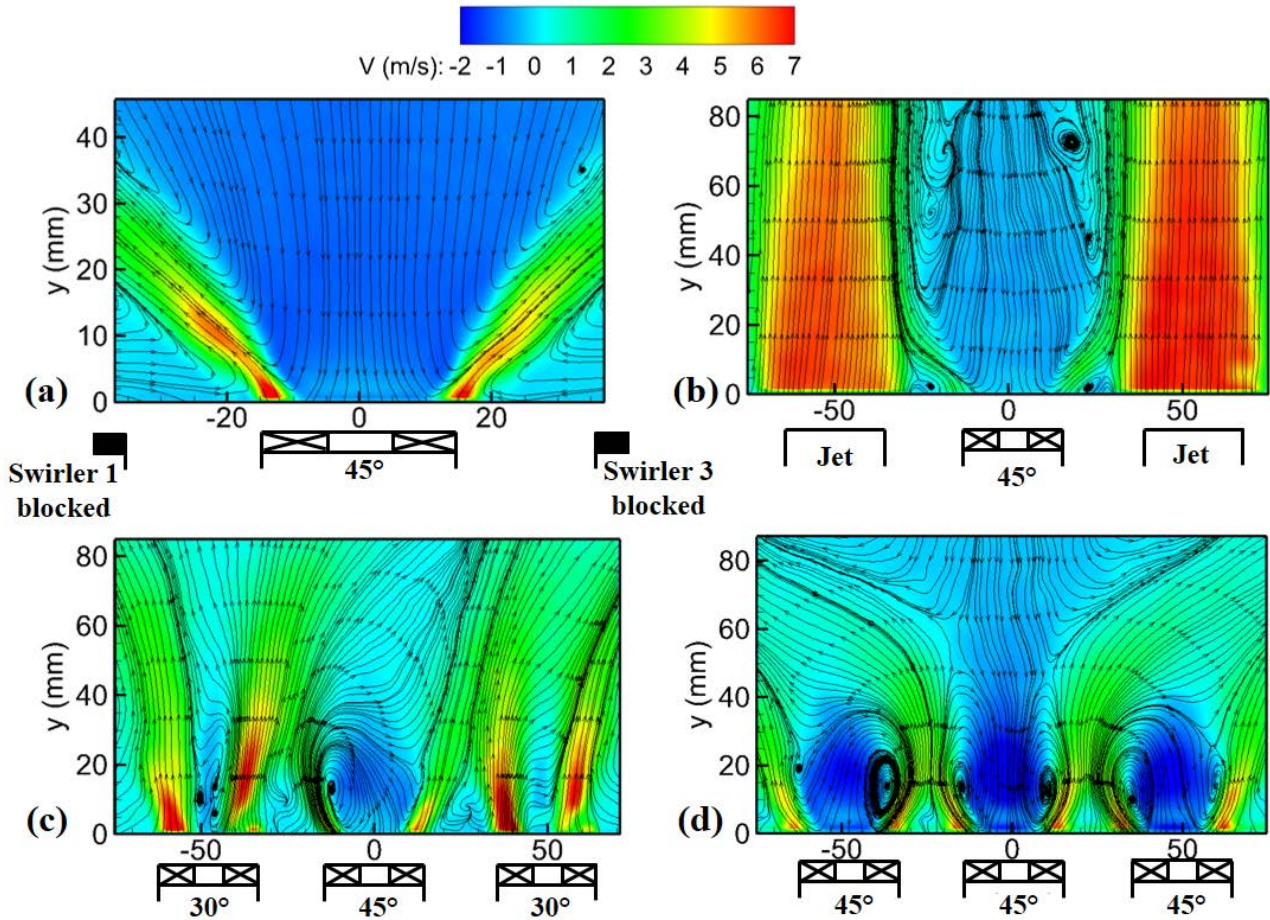
FIGURE 2. Stream lines overlaid on time-averaged axial velocity (V) in all the plots. (a) Flow from central swirler (Zoomed in view), and outer swirlers blocked. (b) Axisymmetric jet flows issued along with central swirling flow. (c) Swirlers S1 and S3 were introduced with swirl angle 30° resulting a visible vortex disruption for central swirler. (d) Swirl angle increased to 45° for swirlers S1 and S3 and thus establishing a 'Vortex Bubble' type breakdown in the central swirler.

combined with the confinement from the outer jets creates smaller recirculation zones. However, the conventional vortex breakdown bubble is still absent. In the third case, we provide small tangential momentum to the jet flows emerging from ports 1 and 3 by introducing the swirlers S1 and S3 with swirl angle of 30º. The central swirler as always has a swirl angle of 45º. In this case, visible vortex disruption takes place in the central swirling jet which can be seen in Fig. 2(c).

Due to the presence of swirl, the flow from adjacent swirlers interfere with the central swirl flow. Recirculating region starts developing for the central swirler and weak recirculating regions are found with neighbouring swirlers. Further increase in swirl angle to 45º in swirlers S1 and S3 results into what is known as the conventional vortex bubble pattern. Unlike the way conventional vortex breakdowns [2-4] are triggered, here a bubble form of breakdown in Fig.2(d) is established through interference from neighbouring swirlers, without directly controlling any of the flow parameters corresponding to the central swirler. It is observed in Fig.2(d) that the vortex breakdown in swirlers S1 and S3 is not symmetric about their axes. As the swirl angle for neighbouring flows was increased to 45º, the flows emerging out encounter each other with a more constricted passage due to increased divergence. Hence, the flow tends to curl back causing increased re-circulation associated with swirlers S1 and S3 on their interacting sides. Whereas, on their non-interacting sides, the horizontal component of the flow velocity is maintained and hence, the flow shows lesser tendency to re-circulate. This explains the asymmetry in the recirculation zones seen in Fig. 2(d).
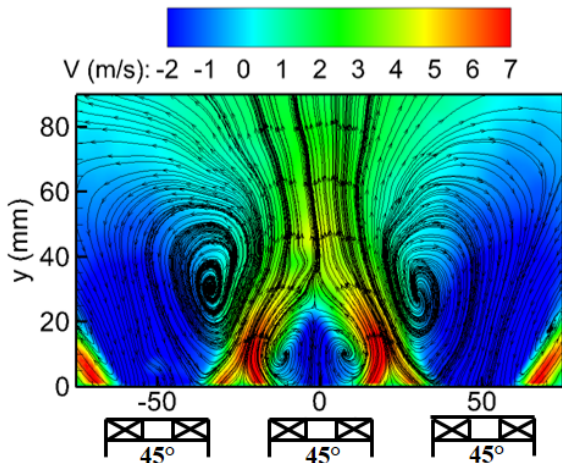
FIGURE 3. Reacting flow case: Streamlines overlaid on contours of time-averaged axial velocity (V) showing an increase in the size of recirculation zones for swirlers S1 and S3 and shift of flow symmetry towards the axis of the central swirler.

In all the four cases studied, flame could be established only for the third (Fig.2(c)) and fourth cases (Fig.2(d)). Now, we consider the fourth case and ignite the mixture. Significant changes in flow patterns are observed in comparison with its corresponding isothermal case (Fig.2(d)) as shown in Fig.3.

CONCLUSIONS

Experiments reveal that a central swirling flow is quite sensitive to swirl levels of its neighbouring flows. Vortex bubble type of breakdown could be established by raising the swirl levels of flows around the central swirling flow, while such a structure is absent in a standalone swirling jet of identical swirl angle. The interacting sides of neighbouring swirl flows show a tendency to have better recirculation compared with their non-interacting sides. Reaction causes significant changes in recirculation zone sizes associated with swirlers S1 and S3 in comparison to their isothermal state.

REFERENCES

[1] Peckham, D.H., Atkinson, S.A., 1957. "Preliminary results of low speed wind tunnel tests on Gothic Wing of aspect ratio 1.0", Aero.Res.counc.CP508.
[2] Harvey, J. K., 1962. "Some Observations of the Vortex Breakdown Phenomenon". Journal of Fluid Mechanics 14:pp.585-892.
[3] Sarpkaya, T., 1971. "On Stationary and Travelling Vortex Breakdowns". Journal of Fluid Mechanics Vol.45, part 03 pp.545-559.
[4] Faler, J. H. and S. Leibovich., 1978. "An Experimental Map of the Internal Structure of a Vortex Breakdown". Journal of Fluid Mechanics, vol. 86, part 2, pp. 313-335.
[5] Lucca-Negro O, O'Doherty T., 2001, "Vortex Breakdown: A Review", Progress in Energy and Combustion Science, Vol.27, pp.431-481.
[6] Leibovich, S., 1978. "The Structure of Vortex Breakdown", Annual Review of Fluid Mechanics, Vol.10, pp.221-246.
[7] Beer, J.M, Chigier, N.A., 1972. Combustion Aerodynamics. New York: Wiley.
[8] Gupta A, Lilley G, and Syred, N., 1984. Swirl Flows. Kent, Engl.: Abacus
[9] Chigier, N.A., Dvorak, k., 1975. "Laser Anemometer measurements in Flames with Swirl", Fifteenth Symposium (International) on Combustion, Combustion Institute, Vol.15, Issue 1, pp.573-585.
[10] Syred, N., Chigier, N.A. and Beer, J.M., 1971. "Flame Stabilization in Re-circulating zones of Jets with Swirl", Thirteenth Symposium (International) on Combustion, Combustion Institute, Vol.13, Issue 1, pp.617-624.
[11] Fujii, S., Eguchi, K. and Gomi, M., 1981. "Swirling Jets with and without Combustion", AIAA Journal, Vol.19, pp.1438-1442.

[12] Ballal, D.R., 1988, "Combustion Generated Turbulence in Practical Combustors", Journal of Propulsion and Power, Vol.4, No.5, pp.385-390.

[13] Smith, T., Emerson, B., Chterev, I., Noble,D.R. and Lieuwen, T., 2016. "Flow Dynamics in Single and Multi-Nozzle Swirl Flames", ASME Turbo Expo 2016: Turbomachinery Conference and Exposition, Vol.4B: Combustion,Fuels and Emissions.

[14] Aguilar, M., Malanoski, M., Adhitya, G., Emerson, B., Acharya, V., Noble, D. R., and Lieuwen, T., 2015. "Helical Flow Disturbances in a Multinozzle Combustor," Journal of Engineering for Gas Turbines and Power, Vol. 137.

SEEC-2017-015

HETEROGENEOUS REACTIVITY ONTO SURFACE OF FINE-FRACTION MINERAL DUST

Pradhi Rajeev
Department of Civil Engineering, Indian Institute
of Technology Kanpur.
Email: pradhi@iitk.ac.in

Prashant Rajput
Department of Civil Engineering, Indian Institute
of Technology Kanpur.

Vikram Chaudhary
Department of Civil Engineering, Indian Institute
of Technology Kanpur.

Fena Sorathia
Department of Civil Engineering, Indian Institute
of Technology Kanpur.

Tarun Gupta
Professor
Department of Civil Engineering, Indian Institute
of Technology Kanpur.
Email: tarun@iitk.ac.in

ABSTRACT

Fine-fraction ambient aerosols ($PM_{2.5}$; n= 32) have been studied during the South-west monsoon (July–September, 2015) at Kanpur (central Indo-Gangetic Plain). To assess the undergoing processes in atmosphere, water-soluble ionic species (WSIS) have been measured. $\sum WSIS$ varied from 4–32 $\mu g/m^3$ in $PM_{2.5}$. NH_4^+ and SO_4^{2-} were found to be predominant in $PM_{2.5}$ (16–120 $\mu g/m^3$). Ca^{2+} and Mg^{2+} were associated with HCO_3^-, while NO_3^- and SO_4^{2-} are neutralized predominantly by the NH_4^+ and $\sum^-/\sum^+$ ratio is ≈ 1. Furthermore, co-variability of nss-SO_4^{2-} with nss-Ca^{2+} indicates heterogeneous formation of SO_4^{2-} onto the surface of fine-fraction mineral dust.

***Keywords*:** Heterogeneous reactivity, fine-fraction mineral dust, South-west monsoon, IGP, Ionic composition.

INTRODUCTION

Complexity in fine particulate matter composition arising due to secondary aerosol formation has been a matter of concern from the view point of atmospheric chemistry, human health and other environmental issues.

Massive anthropogenic emissions and their reactivity due to photochemical reactions, high RH condition, fine-fraction mineral dust and transition metals are potential factors enhancing secondary aerosol species contribution [1-6]. Formation mechanism of secondary species through homogeneous pathway has been assessed and well documented in literature for most of the identified species in atmosphere [7-9]. However, heterogeneous phase reactivity occuring in ambient atmosphere demands to cater many studies [10-13]. Recently, many studies have observed enhanced role of heterogenous phase chemistry in influencing atmospheric budget of secondary species (SO_4^{2-}, NO_3^-) [12-17].

In year 2015, weak SW-monsoon due to El-Niño has resulted in less rainfall (~ 375 mm) [26]. Relatively high wind-speed during the study period (~ 8m/s) compared to other seasons of the year, has led to higher upliftment of mineral dust [14]. Manifestation of high abundance of fine-fraction mineral dust and low precipitation (inefficient wet-scavenging) could result into enhanced collisions of pollutants.

METHODOLOGY

Aerosol sampling was done from July−September, 2015 at Kanpur (26.30°N, 80.14 °E, 142m above mean sea level). During South-west monsoon in 2015, low precipitation events were recorded (~ 40% of the normal precipitation) which has led us to assess aerosol chemical characteristics during this period. Ambient temperature varied from 22−37 °C whereas RH from 53−97% during the sampling period. Using a high-volume air-sampler, $PM_{2.5}$ samples (n = 32) were collected onto the pre-baked quartz filters (Whatman^{TM}; 20.3 x 25.4 cm^2) (Figure 1) [18-19]. Mass concentrations of $PM_{2.5}$ have been ascertained gravimetrically after equilibrating quartz filters at 25 ± 2 ℃ temperature and 40 ± 5% RH. The cations (Na^+, NH_4^+, K^+, Ca^{2+} and Mg^{2+}) and anions (F^-, Cl^-, NO_3^-, SO_4^{2-} and PO_4^{3-}) have been measured in aerosol extracts using a dual-channel ion-chromatograph (Metrohm, Swiss) [14, 20-23]. HCO_3^- concentration has been measured in all samples by titration using a 5mM HCl solution and Methyl orange indicator (Thomas Baker).Analyses of samples in duplicate provided analytical uncertainty of the measurement (± 7%),while quality control of the data has been assured from check standards and procedural blanks.
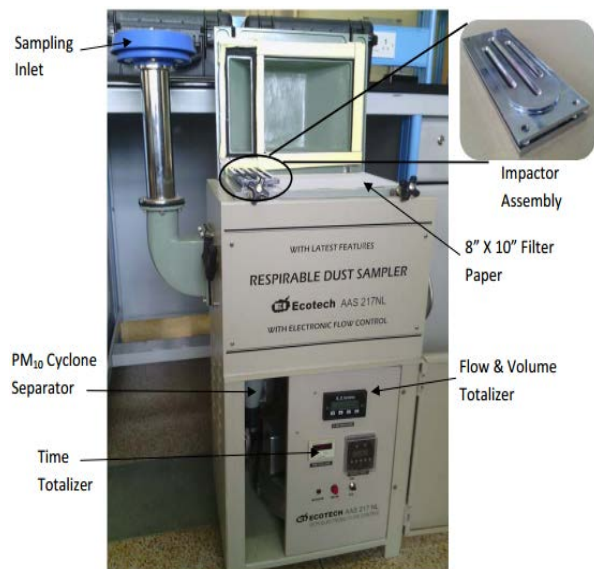
FIGURE 1. High- volume $PM_{2.5}$ sampler equipped with the novel slit impactorassembly (HVIA) [18].

RESULTS AND DISCUSSION

Mass concentration of $PM_{2.5}$ varied from 15.9−119.6 (35.8 ± 20.5) µg/m^3. Major ion chemistry in aerosols ($PM_{2.5}$) collected during the SW-monsoon (July–September, 2015) have been assessed in this study.Water-soluble inorganic species (WSIS) including Na^+, NH_4^+, K^+, Ca^{2+}, Mg^{2+}, HCO_3^-, F^-, Cl^-, NO_3^-, PO_4^{3-} and SO_4^{2-} have been analyzed, which constitute 35% of the $PM_{2.5}$. ΣWSIS concentration varied from 3.9−32.1(11.6 ± 5.6) µg/m^{3}of

which major ions (NH_4^+, K^+, Ca^{2+}, HCO_3^-, NO_3^-, PO_4^{3-} and SO_4^{2-}) accounts for 97% of the ΣWSIS and the rest was accounted by Na^+, Mg^{2+}, F^-, Cl^-. Figure 2 shows the mass concentration of $PM_{2.5}$ and the percentage ionic composition of several ions constituting $PM_{2.5}$ mass. In $PM_{2.5}$, the dominant ionic species follows the following trend : SO_4^{2-} (11%) > NH_4^+ (8%) > HCO_3^-(5.2%) > PO_4^{3-} (4.7%) > NO_3^- (3.3%) > Ca^{2+} (1.5%). Thus, high abundance of anthropogenic species was observed in this region as reported earlier [20]. HCO_3^- and Ca^{2+} concentration in $PM_{2.5}$ indicates the presence of significant fraction of mineral dust in fine fraction aerosols. The method detection limit (MDL) for ionic composition varied from 0.02−0.07 µg/m^3.
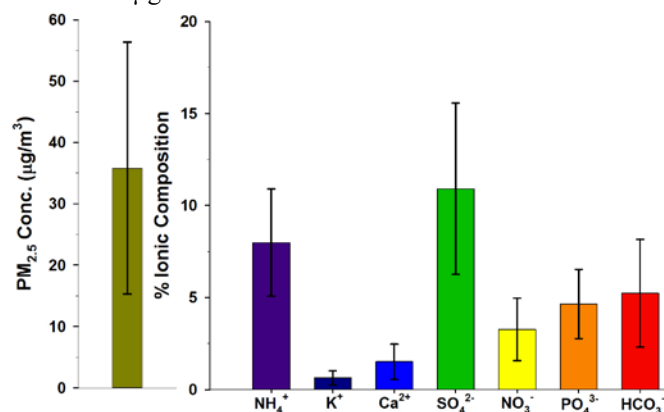
FIGURE 2. $PM_{2.5}$ concentration and percentage ionic composition.

A strong correlation of Ca^{2+} with HCO_3^- (R^2 = 0.96) represents a characteristic feature of mineral dust in fine fraction over the IGP (Figure 3). As reported earlier in previous studies, that major mineral in the mineral dust over IGP is calcite ($CaCO_3$) [14, 24].
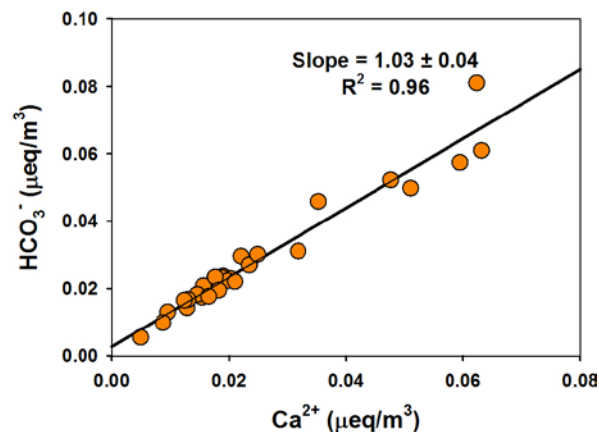
FIGURE 3. Scatter plot of Ca^{2+} with HCO_3^-.

Temporal variability plot of equivalence ratio of NH_4^+/ (NO_3^- + SO_4^{2-}) (Figure 4a) indicates complete

neutralization of acidic species by NH_4^+. It means that NH_4^+ is present in excess ($NH_4^+/(NO_3^- + SO_4^{2-} = 1.39 \pm 0.05$) during the study. The excess NH_4^+ was associated with PO_4^{3-}, indicating agricultural activities in IGP as one of the major sources of atmospheric ammonia. Apart from this, all anions and cations are also charge balanced ($\Sigma^-/\Sigma^+ = 0.96\pm0.01$) within the analytical uncertainty (Figure 4b).

We have collected fine-fraction ($PM_{2.5}$) aerosols owing to its larger surface-area as compared to coarser particles as our major interests in this study was to assess the heterogeneous formation of SO_4^{2-} aerosols. Moreover, it is widely known that SO_4^{2-} aerosol is formed predominantly during daytime and therefore we preferably collected the $PM_{2.5}$ samples during daytime only. The formation of $CaSO_4$ by heterogeneous reaction of SO_4^{2-} with $CaCO_3$ is overruled in this study as we have shown above that all SO_4^{2-} is neutralized by NH_4^+. Figure 5 shows the co-variability of nss-Ca^{2+} with nss-SO_4^{2-}.
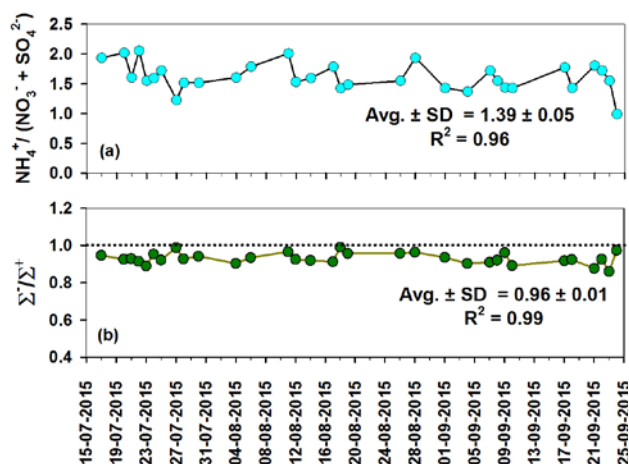
FIGURE 4. Temporal variability of equivalence ratio of: (a) $NH_4^+/(NO_3^- + SO_4^{2-})$ and (b) Σ^-/Σ^+.

The non-sea salt ionic concentration has been estimated by following formulae using the sea-water ratios well documented in literature [25, 27] :

$$nss\text{-}Ca^{2+} = (Ca^{2+})_{aerosol} - (Na^+)_{aerosol} \text{ X } (Ca^{2+}/Na^+)_{sea\text{-}water}$$
(i)

$$nss\text{-}SO_4^{2-} = (SO_4^{2-})_{aerosol} - (Na^+)_{aerosol} \text{ X } (SO_4^{2-}/Na^+)_{sea\text{-}water}$$
(ii)
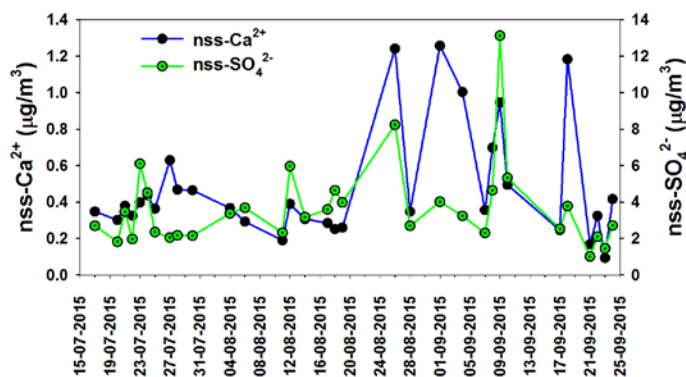
FIGURE 5. Co-variability of nss-Ca^{2+} and nss-SO_4^{2-}.

Thus, it is logical to infer the occurrence of heterogeneous formation of SO_4^{2-} onto the surface of fine mineral dust (a field-based evidence). Heterogeneous formation of SO_4^{2-} onto the surface of fine-fraction aerosols in presence of high RH condition have been reported in several studies [13]. However, further analysis has to be conducted to have a better understanding of heterogeneous reactivity occurring in the fine aerosol.

CONCLUSION

We document here the chemical characteristics of ambient $PM_{2.5}$ during the SW-monsoon (July–September 2015) in the Indo-Gangetic Plain. The SO_4^{2-} (33.6%) and NH_4^+ (23%) contributions to $\sum$WSIS are predominant. HCO_3^- is associated with Ca^{2+} and Mg^{2+}, whereas NO_3^- and SO_4^{2-} are completely neutralized by NH_4^+ in fine-aerosols. Heterogeneous formation of sulfate aerosols onto the surface of fine-fraction mineral dust has been inferred in this study.

ACKNOWLEDGMENTS

REFERENCES

[1] Kawamura, K., Imai, Y., Barrie, L.A., 2005. Photochemical production and loss of organic acids in high Arctic aerosols during long-range transport and polar sunrise ozone depletion events. Atmospheric Environment 39, 599-614.

[2] Weber, R.J. et al., 2007. A study of secondary organic aerosol formation in the anthropogenic-influenced southeastern United States. J. Geophys. Res. 112, D13302.

[3] Pathak, R.K., Wu, W.S., Wang, T., 2009. Summertime $PM_{2.5}$ ionic species in four major cities of China: nitrate formation in an ammonia-deficient atmosphere. Atmospheric Chemistry and Physics 9, 1711-1722.

[4] Kaul, D.S. et al., 2011. Secondary Organic Aerosol: A Comparison between Foggy and Nonfoggy Days. Environmental Science & Technology 45, 7307-7313.

[5] Singh, D.K. Gupta, T., 2016. Role of transition metals with water soluble organic carbon in the formation of secondary organic aerosol and metallo-organics in PM_1 sampled during post monsoon and pre-winter time. Journal of Aerosol Science 94, 56-69.

[6] Chakraborty, A., Ervens, B., Gupta, T. and Tripathi, S. N., 2016.Characterization of organic residues of size-resolved fog droplets and their atmospheric implications. J. Geophys. Res. Atmos., 121,doi:10.1002/2015JD024508.

[7] Atkinson, R. Arey, J., 1994. Atmospheric Chemistry of Gas-phase Polycyclic Aromatic Hydrocarbons: Formation of Atmospheric Mutagens. Environmental Health Perspectives 102, 117-126.

[8] Atkinson, R., 2000. Atmospheric chemistry of VOCs and NOx. Atmospheric Environment 34, 2063-2101.

[9] Seinfeld, J.H. Pandis, S.N., Atmospheric Chemistry and Physics - From Air Pollution to Climate Change (2nd Edition). John Wiley & Sons, New York (2006).

[10] Esteve, W., Budzinski, H. Villenave, E., 2004. Relative rate constants for the heterogeneous reactions of OH, NO_2 and NO radicals with polycyclic aromatic hydrocarbons adsorbed on carbonaceous particles. Part 1: PAHs adsorbed on 1-2 mm calibrated graphite particles. Atmospheric Environment 38, 6063-6072.

[11] Esteve, W., Budzinski, H. Villenave, E., 2006. Relative rate constants for the heterogeneous reactions of NO_2 and OH radicals with polycyclic aromatic hydrocarbons adsorbed on carbonaceous particles. Part 2: PAHs adsorbed on diesel particulate exhaust SRM 1650a. Atmospheric Environment 40, 201-211.

[12] Usher, C.R., Michel, A.E. Grassian, V.H., 2003. Reactions on Mineral Dust. Chemical Reviews 103, 4883-4940.

[13] Rajput, P., Gupta, T.,Kumar, A., 2016. The diurnal variability of sulfate and nitrate aerosols during wintertime in the Indo-Gangetic Plain: implications for heterogeneous phase chemistry. RSC Adv., 6, 89879-89887.

[14] Rajeev, P., Rajput, P., Gupta, T., 2016. Chemical characteristics of aerosol and rain water during an El-Niñoand PDO influenced Indian summer monsoon.Atm. Environ., 145, 192-200.

[15] Wang, G. et al.,2016. Persistent sulfate formation from London Fog to Chinese haze. PNAS, 113, 48, 13630–13635.

[16] Cheng, Y. et al., 2016. Reactive nitrogen chemistry in aerosol water as a source of sulfate during haze events in China. Sci. Adv., 2: e1601530.

[17] Perraudin, E., Budzinski, H. Villenave, E., 2007. Identification and quantification of ozonation products of anthracene and phenanthrene adsorbed on silica particles. Atmospheric Environment 41, 6005-6017.

[18] Kumar, A. Gupta, T., 2015. Development and laboratory performance evaluation of a variable configuration $PM_1/PM_{2.5}$ impaction-based sampler. Aerosol and Air Quality Research 15, 768-775.

[19] Rajput, P., Mandaria, A., Kachawa, L., Singh, D. K., Singh, A. K., Gupta,T., 2015. Wintertime source-apportionment of PM_1 from Kanpur in the Indo-Gangetic plain. Climate Change 1, 503-507.

[20] Rajput, P., Mandaria, A., Kachawa, L., Singh, D. K., Singh, A. K., Gupta,T., 2016. Chemical characterization and source-apportionment of PM_1 during massive loading at an urban location in Indo-Gangetic Plain: Impact of local sources and long-range transport. Tellus B, 68, 30659.

[21] Rajput, P., Sarin, M. M., Sharma, D., Singh, D., 2014. Characteristics andemission budget of carbonaceous species from post-harvestagricultural-waste burning in source region of the Indo-Gangetic Plain. Tellus-B doi.org/10.3402/tellusb.v66.21026.

[22]Chakraborty, A. Gupta, T., 2010. Chemical Characterization and Source Apportionment of Submicron (PM_1) Aerosol in Kanpur Region. Aerosol and Air Quality Research 10, 433-445.

[23] Gupta, T. Mandaria, A., 2013. Sources of Submicron Aerosol during Fog Dominated Wintertime at Kanpur. Environmental Science and Pollution Research DOI: 10.1007/s11356-11013-11580-11356.

[24] Pipal, A.S. et al., 2014. Study of Surface Morphology, Elemental Composition and Origin of Atmospheric Aerosols ($PM_{2.5}$ and PM_{10}) over Agra, India. Aerosol and Air Quality Research 14, 1685-1700.

[25] Keene, W.C. et al., 1986. Sea-Salt Corrections and Interpretation of Constituent Ratios in Marine Precipitation. J. Geophys. Res. 91, 6647-6658.

[26]Zhang, Y., Wallace, J.M. Battisti, D.S., 1997. ENSO-like Interdecadal Variability: 1900-93. Journal of Climate 10, 1004-1020.

[27] Rajput, P., Sarin, M. M., Sharma, D., Singh, D., 2014. Organic aerosols and inorganic species from post-harvest agricultural-waste burning emissions over northern India: impact on mass absorption efficiency of elemental carbon. Environ. Sci. Process. Impacts 16, 2371-2379.

SEEC-2017-016

STABLE CARBON ISOTOPE ANALYSIS OF WINTERTIME AEROSOLS FROM KANPUR

Gyanesh Singh
Department of Civil Engineering, Indian Institute of
Technology Kanpur
Email: gyanesh@iitk.ac.in

Debajyoti Paul
Associate Professor
Department of Earth Sciences, Indian Institute of
Technology Kanpur
Email: dpaul@iitk.ac.in

Tarun Gupta
Professor
Department of Civil Engineering, Indian Institute of
Technology Kanpur
Email: tarun@iitk.ac.in

Prashant Rajput
Department of Civil Engineering, Indian Institute of
Technology Kanpur

Amit Kumar Singh
Department of Civil Engineering, Indian Institute of
Technology Kanpur

ABSTRACT

This study assesses stable carbon isotopic composition ($\delta^{13}C$) of total carbon (TC) in ambient aerosols ($PM_{2.5}$) during wintertime (December 2014) from Kanpur (26.30 °N, 80.14 °E) in northern India. Chemical constituents viz. organic carbon (OC), elemental carbon (EC) and water-soluble ions in $PM_{2.5}$ have also been measured. Back trajectories of air-masses arriving at the sampling site (Centre for Environmental Science and Engineering, IIT Kanpur) have been utilized to infer the air-mass transport. Most of the trajectories showed their origin from North-western region during the study period. Average $PM_{2.5}$ and TC concentrations were centered around 240 μg m^{-3} and ~ 91 μg m^{-3}, respectively. The OC+EC concentrations averaged at 58 ± 15 μg m^{-3}. Significant linear correlation between OC and EC in conjunction with high OC/EC ratio (9 to 12) suggests dominance of anthropogenic combustion sources of organic aerosols. Concentration of anthropogenic ionic species (SO_4^{2-} + NO_3^- + NH_4^+) averaged at 46.74 μg m^{-3}. The average $\delta^{13}C$ values of TC in the integrated 24-hour samples was centred around -25‰. Integrated data analyses of chemical constituents and stable C isotope suggests the influence of mixed emission sources. Future studies are required to better constraint the observations.

Keywords: $PM_{2.5}$; Total Carbon; Stable isotopes; Kanpur; Indo-Gangetic Plain.

INTRODUCTION

Atmospheric aerosols originiate from a wide variety of natural as well as anthropogenic sources [1]. High concentration of fine particles can cause an adverse effect on human health [2]. Residence time of fine aerosols is quite high as compared to coarser particles. They can exert potential impacts through long-range transport and atmospheric chemistry and further influence radiation budget and climate. Organic matter (OM) and elemental carbon (EC) constitute a dominant fraction of atmospheric fine-particles. Complexity in characterizing emission sources of carbonaceous aerosols arise due to atmospheric transformation [3]. Also, the increasing anthropogenic activities in conjunction with varying ventilation coefficient leads to increased polycyclic aromatic hydrocarbons (PAHs) concentration which possess a health hazard risk particularly in an urban environment [4-5]. Biomass burning, industrial emissions and fossil-fuel

combustion are the major sources of anthropogenically derived aerosols. The abundance of organic aerosols is governed by their primary emissions and secondary transformations in ambient atmosphere. However, EC is only derived from primary emissions.

Various isotopes are useful in atmospheric research such as carbon, nitrogen, sulfur, oxygen and lead. Stable isotope ratios are important and useful tool to characterize particulate matter. Application of both the compound specific and bulk analysis of stable isotope have been reported previously, e.g. [6-7]. Assessment of aerosol ageing can also be done using stable carbon isotope ratios [8-9]. Isotope analysis in association with the chemical composition can provide a significant information to better characterize the carbonaceous aerosols. This study has been conducted to asess chemical characteristics of ambient aerosols in northen India.

STUDY AREA

Study area at Kanpur is located in central part of the Indo-Gangetic plain (IGP). It is the 5th largest city in India based on areal extension and is a prime center for industrial activities. IGP provides shelter to over 60% of the human people in India. Aerosol sampling (PM$_{2.5}$) was carried out in Indian Institute of Technology Kanpur premises at the rooftop of the Centre for Environmental Science and Engineering (CESE) building (26.30 °N; 80.14 °E; 142 m above mean sea-level) during winter (December, 2014). IIT Kanpur is a research institute located 15 kilometers upwind of Kanpur city. The atmospheric particulate matter concentration of anthropogenic origin in Kanpur is governed by activities of vehicular emissions (petrol and diesel traffic), biomass burning, solid-fuel (coal) combustion and industrial emissions. Major concern in IGP during wintertime is a thick haze cover of pollutants over the entire region and its downwind advection towards the Northern Indian Ocean causing perturbation in radiation balance over the ocean. Large-scale biomass burning emissions and fossil-fuel combustion activities [10] contribute to haze episodes over the IGP.

SAMPLE COLLECTION

Aerosol (PM$_{2.5}$) samples were collected continuously for 24 hours on pre-combusted 47 mm diameter quartz-fiber filters at the roof top of CESE building, IIT Kanpur. These samples were stored at -19 °C untill chemical and isotopic anlysis. Sampling was conducted during winter season in the month of December 2014. Sampling was performed by an air-sampler working at a flow-rate of 15 L/min (Fig.1). Air sampler designed and developed at IIT Kanpur was used for the sampling of ambient aersols (Fig. 1). The impactor in the sampler is designed to collect ≤ 2.5 µm onto filter, whereas particles greater than 2.5 µm in the air-stream are impacted onto vacuum grease [11-12].
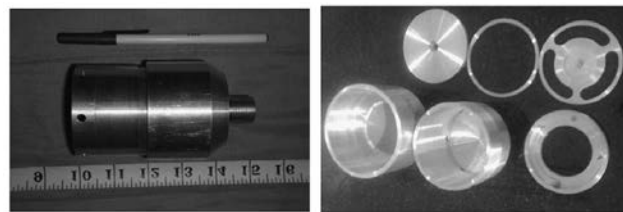
FIGURE 1. PM$_{2.5}$ air-sampler and its internal components, designed and developed at IIT Kanpur [11].

CHEMICAL ANALYSIS

Measurements of total carbon (TC), organic carbon (OC), elemental carbon (EC), water-soluble organic carbon (WSOC), stable carbon isotope of TC, and inorganic ions in the ambient aerosol samples have been performed. The ion chromatography (Metrohm compact IC 761) was carried out to quantify ions in samples and the detailed procedure is mentioned in Singh et al. 2016 [13] . For determination of stable isotopes, appropriate filter size was taken based on mass to signal ratio and placed into pre-cleaned tin cup and closed, which was then inserted into an elemental analyzer (Flash EA 2000, Thermo Scientific) using an auto sampler. Carbon isotopic ratio in the samples have been measured on a Continuous flow isotope ratio mass spectrometer (EA-IRMS).

Stable isotope ratio mass spectrometer (Thermo Scientific Delta V Plus) used for the measurement is coupled with elemental analyzer and conflo IV universal interface. It is housed in the Advanced Centre for Material Science (ACMS) lab, IIT Kanpur. High precision stable carbon (δ^{13}C), nitrogen (δ^{15}N), oxygen (δ^{18}O) and hydrogen (δ^{2}H) isotope ratio analysis in various types of organic and inorganic samples such as aerosols, plants, soil, water, carbonate sediments, atmospheric gases etc. can be performed using this assembly. Here, δ represents the isotopic composition of elements and is expressed as given in equation 1:

$$\delta = [(R_{Sample}/R_{Standard} - 1)] \times 1000 ‰ \text{ (per mil)}$$
(1)

Where, R represents the ratio of heavy to light isotope. Therefore, measure of ratio of heavy to light isotopes in a sample versus a reference standard is represented by δ . Hence, the isotopic composition of carbon can be represented by Eqn. (2):

$$\delta^{13}C_{sample} (‰, \text{V-PDB}) = [(^{13}C/^{12}C)_{sample} / (^{13}C/^{12}C)_{V-PDB} - 1] \times 10^{3}$$
(2)

The carbon isotopic data is reported relative to the Vienna Pee Dee Belemnite (PDB) standard. The calibration of EA-IRMS was done using various internal standards such as CH3 (−24.724‰) and IAEA 601 (Benzoic Acid,

─28.81‰). For the case of carbon isotope analysis, the uncertainty involved was less than 0.2‰.

RESULTS AND DISCUSSION

SOURCE REGION OF AIR MASSES

Hybrid Single Particle Lagrangian Integrated Trajectory (HYSPLIT) model was used to identify the origin of air-masses during the sampling period [14]. A 5 day back trajectory at 1000 m above mean sea level (amsl) was performed for the sampling period. Variability in $\delta^{13}C$ values of aerosol samples as a function of air-mass transport has been reported previously [3]. The trajectories revealed that North-westerly winds were prevailing during the entire campaign as seen in Fig.2. Air masses from upwind IGP (specifically through Punjab, Haryana) influences atmospheric composition and chemistry during this time period of the year in downwind region of IGP. Post-harvest paddy-residue burning emissions can have a significant impact on the aerosol composition over northern India during the wintertime [15-17]. Thus, the region is impacted by large scale biomass burning during winter. Observations on air-mass back-trajectory analysis were found to be consistent with the previous studies [18].
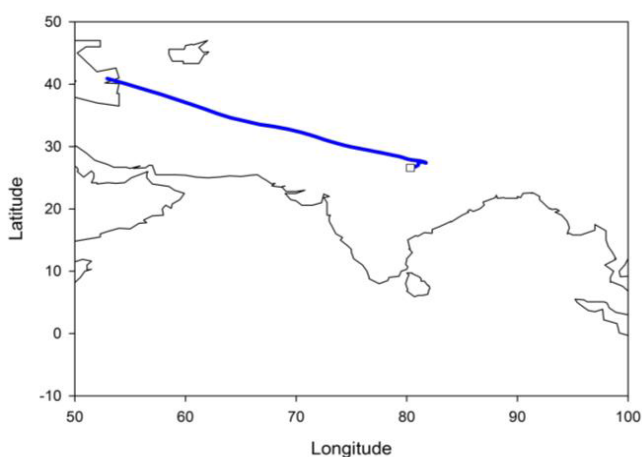
FIGURE 2. A 5-day integrated air-mass back trajectory during the campaign.

PM$_{2.5}$, TOTAL CARBON (TC), ORGANIC CARBON (OC) and ELEMENTAL CARBON (EC)

PM$_{2.5}$ mass concentration obtained is centering around 240 µg m^{-3}. TC concentrations ranged from 20.43 to 77.23 µg m^{-3}. Local emission sources and long-range transport of pollutants from upwind IGP give rise to higher TC concentrations in ambient aerosols. OC concentration ranged from 20.43 to 77.23 µg m^{-3} whereas EC concentration ranged from 2.35 to 6.56 µg m^{-3}. OC+EC concentration in the samples averaged at 58 ± 15 µg m^{-3} as shown in Fig. 3.
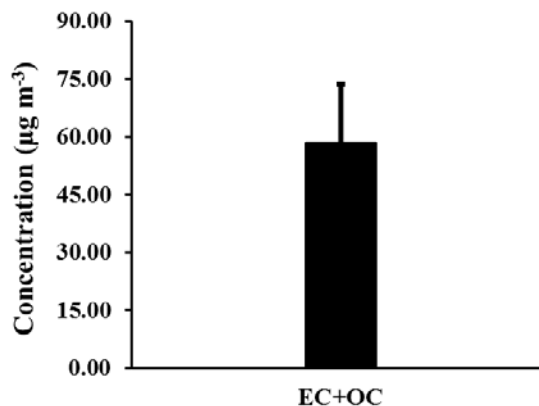
FIGURE 3. Mass concentration of OC + EC.

During October to January, OC and EC concentrations have been found to be higher in IGP as compared to other months [15]. The extent of emission source strength viz. biomass burning, fossil-fuel combustion and contributions from secondary organic aerosols (SOA) results in the variability of carbonaceous aerosols concentration [15]. Singnificant correlation between OC and EC and a fairly high OC/EC ratio (9 to 15) in these set of samples suggests the dominance of anthropogenic emissions. Biomass and bio-fuel burning emissions exhibit higher OC/EC ratios as compared to fossil-fuel combustion sources [19-21].

ANTHROPOGENIC IONIC SPECIES

For the entire duration of sampling, percentage contribution of inorganic species to total WSIS (ΣWSIS) has been shown in Fig.4. The major contributors to WSIS mass were anthropogenic ions (NH$_4^+$ + NO$_3^-$ + SO$_4^{2-}$). The contribution of these species to ΣWSIS was ~ 86%. Temporal variability record of anthropogenic ionic species is shown in Fig. 5. SO$_4^{2-}$ contribution was highest followed by NH$_4^+$ and NO$_3^-$.
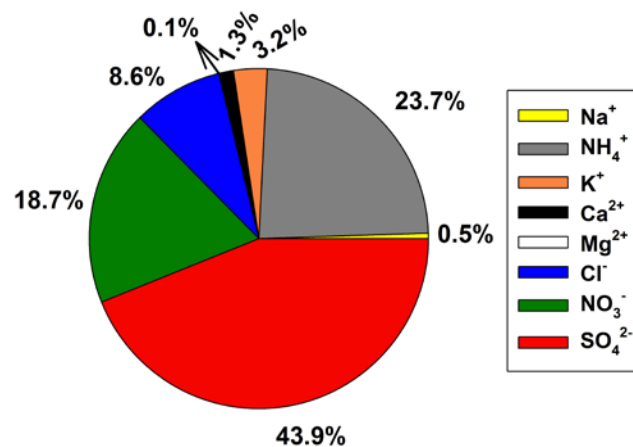
FIGURE 4. Percentage contribution of inorganic species to ΣWSIS.
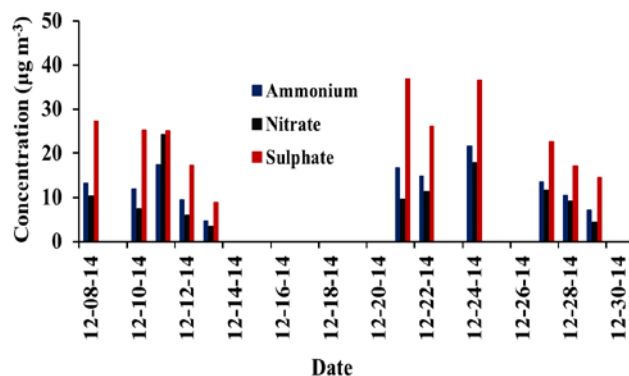
FIGURE 5. Temporal variability of anthropogenic ions (NH_4^+, NO_3^-, SO_4^{2-}) during the study period at Kanpur.

The measured average concentration of anthropogenic ions (i.e. SO_4^{2-} + NO_3^- + NH_4^+) was 46.74 μg m^{-3}. All these species are secondary and form in the atmosphere from their precursors. Secondary aerosol contribution to total PM during winter is quite significant in the IGP [22]. A complete charge-balance between anions and cations (Σ^-/Σ^+; $R^2 = 0.98$) has been observed in this study.

STABLE CARBON ISOTOPE ANALYSES

Temporal variability of $\delta^{13}C$ values in atmospheric aerosols has been shown in Fig. 6. $\delta^{13}C$ of the TC varied from ~ –26.2 to –24.5‰ in aerosol samples. Influence of mixed sources such as vehicle exhaust (–28 to –26‰) [23], coal combustion (–24.9 to –21‰) [23-24], biomass/bio-fuel combustion emissions (–29.4 to –25.9‰) [25], C3 plants (–20 to –32‰) [26] and C4 plants (–6 to –19‰) [27] can give rise to $\delta^{13}C$ values obtained in ambient aerosols. The variability in carbon isotope value obtained on different sampling events represents the dominance of different sources. Like for the days when coal combustion was dominant the values tended to be on the positive side (i.e. closer to –24‰).

The carbon isotope ratio in aerosols depends on several factors. Atmospheric processing can influence the $\delta^{13}C$ value. The fractionation due to kinetic isotope effect or equilibrium fractionation can alter $\delta^{13}C$ value. Thus, difference in the mass of isotopes gives rise to fractionation during physical processes (e.g. diffusion, evaporation etc.). Furthermore, various chemical reactions may also contribute to fractionation; for the same reaction different isotopes can have varying affinity and that causes fractionation. Fractionation is primarily controlled by temperature and pressure condition.
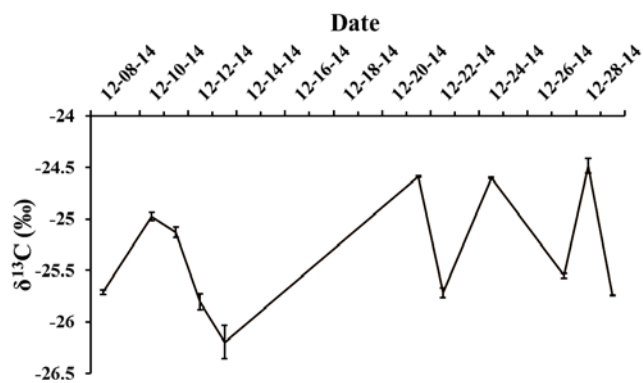
FIGURE 6. Temporal variability of $\delta^{13}C$ in atmospheric aerosol samples.

Since, Kanpur in the IGP is located far off from the ocean therefore the prominent sources of carbonaceous aerosols can be biogenic emission and/or biomass and fossil-fuel combustion. In aerosol samples (PM$_{2.5}$), we have observed the $\delta^{13}C$ of TC centering around -25‰ (Fig. 7.).

In this study, it is observed that with increase in the carbon content there is an enrichment in the ^{13}C of the TC. $\delta^{13}C$ of the black carbon (BC) do not change significantly from source on transport. However, tremendous interaction of OC with atmospheric oxidants is also recorded in variability of isotope ratio. As seen in the previous study [28], WSOC enriched in ^{13}C influences the $\delta^{13}C$ of TC. Higher fraction of WSOC can cause an increase in $\delta^{13}C$ and vice-versa but more studies would be required.
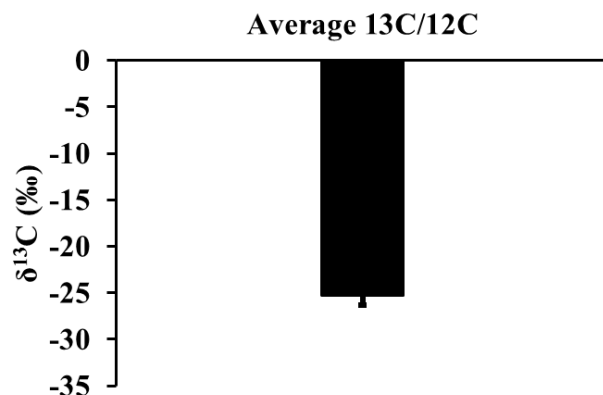
FIGURE 7. Average $\delta^{13}C$ in the aerosol samples during wintertime at Kanpur.

SUMMARY

This study presents information about $\delta^{13}C$ values in ambient aerosols (PM$_{2.5}$) collected from Kanpur. Back trajectory analysis along with the determination of TC, OC and EC concentrations and anthropogenic ionic species provided insight into the chemical characteristics of aerosols during wintertime. Integrated analysis of chemical constituents and stable isotopes provide a better constraint

on emission characteristics from anthropogenic sources. Higher TC concentrations can be attributed to impact of anthropogenic emission sources of local origin versus long-range transport from upwind IGP. Secondary aerosols contribution to PM mass is quite significant in IGP during wintertime.

ACKNOWLEDGEMENT

REFERENCES

[1] Putaud, J.-P., R. Van Dingenen, A. Alastuey, H. Bauer, W. Birmili, J. Cyrys, H. Flentje, S. Fuzzi, R. Gehrig and H.-C. Hansson (2010). "A European aerosol phenomenology–3: Physical and chemical characteristics of particulate matter from 60 rural, urban, and kerbside sites across Europe." Atmospheric Environment 44(10): 1308-1320.

[2] Dockery , D. W., C. A. Pope , X. Xu , J. D. Spengler , J. H. Ware , M. E. Fay , B. G. J. Ferris and F. E. Speizer (1993). "An Association between Air Pollution and Mortality in Six U.S. Cities." New England Journal of Medicine 329(24): 1753-1759.

[3] Garbaras, A. (2008). "Tracing of atmospheric aerosol sources using stable carbon isotopes." Lithuanian Journal of Physics and Technical Sciences 48: 259-264.

[4] Singh, D. K. and T. Gupta (2016). "Effect through inhalation on human health of PM1 bound polycyclic aromatic hydrocarbons collected from foggy days in northern part of India." Journal of Hazardous Materials 306: 257-268.

[5] Singh, D. K., S. Sharma, G. Habib and T. Gupta (2015). "Speciation of atmospheric polycyclic aromatic hydrocarbons (PAHs) present during fog time collected submicron particles." Environmental Science and Pollution Research 22(16): 12458-12468.

[6] Hoefs, J. and J. Hoefs (1997). Stable isotope geochemistry, Springer.

[7] Flanagan, L. B. (2005). 1 - Introduction: Stable Isotopes and Earth System Science. Stable Isotopes and Biosphere Atmosphere Interactions. San Diego, Academic Press: 1-5.

[8] Rudolph, J. (2007). Gas Chromatography–Isotope Ratio Mass Spectrometry. Volatile Organic Compounds in the Atmosphere, Blackwell Publishing Ltd: 388-466.

[9] Wang, H. and K. Kawamura (2006). "Stable carbon isotopic composition of low-molecular-weight dicarboxylic acids and ketoacids in remote marine aerosols." Journal of Geophysical Research: Atmospheres 111(D7).

[10] Rajput, P., A. Mandaria, L. Kachawa, D. K. Singh, A. K. Singh and T. Gupta (2015). "Wintertime source-apportionment of PM_1 from Kanpur in the Indo-Gangetic plain." Climate Change 1(4): 503-507.

[11] Gupta, T. and S. Dubey (2011). "Field performance evaluation of a newly developed PM 2.5 sampler at IIT Kanpur." Science of the Total Environment 409(18): 3500-3507.

[12] Kumar, A. and T. Gupta (2015). "Development and Field Evaluation of a Multiple Slit Nozzle-Based High Volume PM2. 5 Inertial Impactor Assembly (HVIA)." Aerosol and Air Quality Research 15(4): 1188-1200.

[13] Singh, D. K. and T. Gupta (2016). "Role of transition metals with water soluble organic carbon in the formation of secondary organic aerosol and metallo-organics in PM1 sampled during post monsoon and pre-winter time." Journal of Aerosol Science 94: 56-69.

[14] Stein, A. F., R. R. Draxler, G. D. Rolph, B. J. B. Stunder, M. D. Cohen and F. Ngan (2015). "NOAA's HYSPLIT Atmospheric Transport and Dispersion Modeling System." Bulletin of the American Meteorological Society 96(12): 2059-2077.

[15] Rajput, P., M. M. Sarin and S. S. Kundu (2013). "Atmospheric particulate matter ($PM_{2.5}$), EC, OC, WSOC and PAHs from NE–Himalaya: abundances and chemical characteristics." Atmospheric Pollution Research 4(2): 214-221.

[16] Rajput, P., M. M. Sarin, D. Sharma and D. Singh (2014). "Organic aerosols and inorganic species from post-harvest agricultural-waste burning emissions over northern India: impact on mass absorption efficiency of elemental carbon." Environmental Science: Processes & Impacts 16(10): 2371-2379.

[17] Rajput, P., A. Mandaria, L. Kachawa, D. K. Singh, A. K. Singh and T. Gupta (2016). "Chemical characterisation and source apportionment of PM_1 during massive loading at an urban location in Indo-Gangetic Plain: impact of local sources and long-range transport." Tellus B, 68, 30659.

[18] Rajput, P., T. Gupta and A. Kumar (2016). "The diurnal variability of sulfate and nitrate aerosols during wintertime in the Indo-Gangetic Plain: implications for heterogeneous phase chemistry." RSC Advances 6(92): 89879-89887.

[19] Andreae, M. O. and P. Merlet (2001). "Emission of trace gases and aerosols from biomass burning." Global biogeochemical cycles 15(4): 955-966.

[20] Saarikoski, S., H. Timonen, K. Saarnio, M. Aurela, L. Järvi, P. Keronen, V. Kerminen and R. Hillamo (2008). "Sources of organic carbon in fine particulate matter in northern European urban air." Atmos. Chem. Phys 8(20): 6281-6295.

[21] Zhu, C.-S., C.-C. Chen, J.-J. Cao, C.-J. Tsai, C. C.-K. Chou, S.-C. Liu and G.-D. Roam (2010). "Characterization of carbon fractions for atmospheric fine particles and nanoparticles in a highway tunnel." Atmospheric Environment 44(23): 2668-2673.

[22] Gupta, T. and A. Mandariya (2013). "Sources of submicron aerosol during fog-dominated wintertime at Kanpur." Environmental Science and Pollution Research 20(8): 5615-5629.

[23] Widory, D. (2006). "Combustibles, fuels and their combustion products: A view through carbon isotopes." Combustion Theory and Modelling 10(5): 831-841.

[24] Gleason, J. D. and T. K. Kyser (1984). "Stable isotope compositions of gases and vegetation near naturally burning coal."

[25] Agnihotri, R., T. K. Mandal, S. G. Karapurkar, M. Naja, R. Gadi, Y. N. Ahammmed, A. Kumar, T. Saud and M. Saxena (2011). "Stable carbon and nitrogen isotopic composition of bulk aerosols over India and northern Indian Ocean." Atmospheric Environment 45(17): 2828-2835.

[26] Smith, B. N. and S. Epstein (1971). "Two categories of 13C/12C ratios for higher plants." Plant physiology 47(3): 380-384.

[27] Deines, P. (1980). "The isotopic composition of reduced organic carbon." Handbook of environmental isotope geochemistry: 329-406.

[28] Fisseha, R., M. Saurer, M. Jaggi, R. T. W. Siegwolf, J. Dommen, S. Szidat, V. Samburova and U. Baltensperger (2009). "Determination of primary and secondary sources of organic acids and carbonaceous aerosols using stable carbon isotopes." Atmospheric Environment 43(2): 431-437.

MODE SWITCHING STRATEGY DEVELOPMENT FOR DIESOHOL FUELLED ENGINE

Akhilendra Pratap Singh
Engine Research Laboratory
Department of Mechanical Engineering
Indian Institute of Technology Kanpur
Kanpur-208016, India
Email: akhips@iitk.ac.in

Avinash Kumar Agarwal
Engine Research Laboratory
Department of Mechanical Engineering
Indian Institute of Technology Kanpur
Kanpur-208016, India
Email: akhips@iitk.ac.in

ABSTRACT

Premixed charge compression ignition (PCCI) combustion is a novel combustion technique, which has the potential to be operated by alternative fuels such as alcohols. PCCI combustion emitted significantly lower oxides of nitrogen (nox) and particulate matter (pm) and resulted thermal efficiency similar to conventional CI engines. However, PCCI combustion cannot be used in production grade engines due to its incapability to operate at high engine loads. This study focused on development of hybrid combustion engine, which can operate in both combustion modes such as CI combustion as well as PCCI combustion mode. Hybrid combustion system was controlled by an open ecu, which varied the fuel injection parameters for mode switching between CI and PCCI combustion modes. At low-to-medium engine loads, engine was operated in PCCI combustion mode and at higher engine loads ecu automatically switched the engine operation in CI combustion mode. Experiments were carried out using diesohol (10% ethanol in mineral diesel, v/v) at constant engine speed (1500 rpm) and load was varied from idling to full load (6 bar bmep). To explore the emission behavior in different combustion modes and mode transition periods, continuous sampling of exhaust gas was carried out, which included regulated emission measurement, unregulated gaseous species measurement and particulate measurement. Results showed significantly lower nox and particulate from PCCI combustion however performance of PCCI combustion was slightly inferior compared to CI combustion.

Keywords: PCCI combustion, Mode switching, Open ECU, Unregulated emissions.

INTRODUCTION

Due to concerns of fossil-fuel depletion, environmental preservation and global warming, production engines with high fuel conversion efficiency and lower exhaust emissions are being developed. Diesel engines are becoming increasingly popular in powering light- duty vehicles and are regarded most efficient as they offer superior fuel economy, reliability, durability, low carbon dioxide (CO_2) emission, high compression ratios and high specific power output. At the same time, diesel engines also cause environmental pollution because of their high nitrogen oxides (NOx) and particulate matter (PM) emissions. Considerable efforts have been made to reduce these emissions as they have inimical effects on human health and environment. Because of these, diesel engines are subjected to stringent emission control standards. In order to comply with stringent future emission standards, these emissions together with carbon monoxide (CO) and hydrocarbon (HC) emissions must be significantly minimized. Lower regulated emission limits can be obtained by employing different methods   such as alternative fuels, advanced combustion processes and after-treatment of the exhaust. Considerable progress has been made in both combustion and catalytic emission control pathways to reduce emissions. There is a provision of employing diesel particulate filters (DPF) for PM control and selective catalytic reduction (SCR) for NOx control in the after-treatment of engine exhaust. After- treatment systems have some drawbacks in terms of cost and system complexity. To alleviate these problems, in-cylinder control of emissions through application of low-temperature combustion (LTC) techniques has been the focus of intense investigations. This is an important field in research and development of modern diesel engines for

simultaneously reducing PM and NOx emissions from diesel exhaust.

In several studies, a different approach of fueling strategy was followed for mode transition between CI and HCCI combustion. To achieve better control of RoPR, Han et al. [1] used multiple injections during transition from CI to HCCI and suggested to increase the fuel injection quantity during early transitional cycles. Asad et al. [2] developed a mode-switching algorithm for transition from single injection LTC to multi-injection LTC based on in-cylinder pressure. Rohani et al. [3] conducted experiments in a single cylinder heavy duty diesel engine and studied the effects of fuel injection strategy on mode transition emission characteristics. They proposed a strategy based on gradual mode switching wherein they took few engine cycles as the transition period during which injection timing and quantity were varied. Using this technique, they observed 41% reduction in HC emissions compared to the case with simple abrupt shift in injection timing and fuel quantity.

In present study, experiments were performed on a two cylinder, medium-duty, direct-injection compression-ignition (DICI) commercial engine. The main objective of this study was to implement the PCCI combustion strategy on a production grade engine using diesohol. An open ECU was installed on this engine to achieve the mode switching between conventional CI and PCCI combustion modes.

EXPERIMENTAL SETUP

To perform the experiments, PCCI combustion was achieved in a production grade engine using an open ECU. A typical medium-duty transportation DICI engine (Mahindra and Mahindra, 0.9L 2CY CRDe NA) was used for the implementation of mode switching strategy. Test engine was a two-cylinder, four-stroke, variable-speed, transportation engine with direct-injection of fuel. The engine was a water cooled engine with wet sump lubrication system. The experiments were carried out to achieve mode switching between conventional CI combustion mode and PCCI combustion mode using mineral diesel and diesohol (10% ethanol in mineral diesel, v/v) at constant engine speed (1500 rpm) and load was varied from idling to full load (6 bar BMEP). To explore the feasibility of mode switching, the mode switching experiments were performed using diesohol and the performance and emission results of experiments were compared with baseline mineral diesel. Schematic of experimental setup is shown in Figure 1.

The engine was equipped with a common rail direct injection (CRDI) fuel injection system. This CRDI system had an inline high pressure fuel pump, capable of generating pressurized fuel upto 1200 bar. This pump received fuel from pre-supply pump and delivered high pressure fuel to the common rail. Common rail distributed

the high pressure fuel amongst the two solenoid fuel injectors. The fuel injectors had six-hole nozzles and were controlled by the ECU. To avoid high temperature of fuel (returning from injector and rail), a fuel conditioning unit was installed in between fuel tank and high pressure components of the fuel injection system.
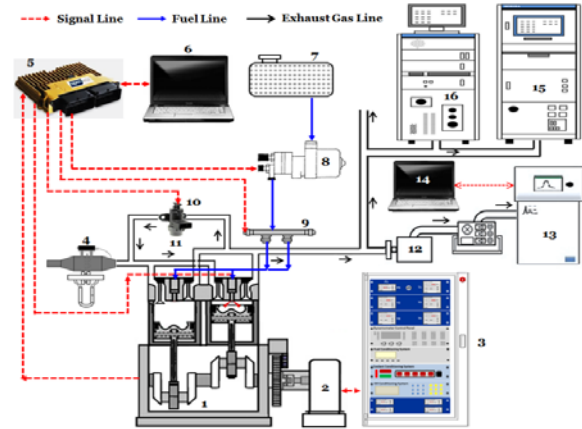
1- Test Engine, 2- Eddy Current Dynamometer, 3- Dynamometer Controller, 4- Laminar Flow Element, 5- Open ECU, 6- ECU Interface System, 7- Fuel Tank, 8- Fuel Pump, 9- Fuel Rail, 10- EGR Valve, 11- EGR Loop, 12- Thermo-diluter, 13- Engine Exhaust Particle Sizer, 14- EEPS Data Logger, 15- FTIR Analyzer, 16- Exhaust Gas Emission Analyzer

FIGURE 1: Schematic of the experimental setup for mode switching

For PCCI combustion mode, provision for EGR was also made. A fraction of exhaust gas from the surge tank was supplied to the intake manifold through a PID controlled EGR valve. The EGR valve was controlled by an open ECU through pulse width modulated (PWM) signals. The engine was coupled to an eddy-current dynamometer for controlling the engine speed and load. To control various operating parameters such as FIP, SoPI, SoMI, fuel injection quantity and EGR, the OEM's ECU (Bosch) was removed and an open ECU was connected to the engine sensors and actuators. Open ECU system was significantly different from that of the OEM ECU. OEM ECU was a closed loop system which performed action based on predetermined logic (map) stored in its microprocessor chip and did not offer any flexibility in terms of changing the logic during the experiments. Such flexibility is offered by open ECU. The open ECU system can be divided into four sections namely ECU, wiring harness, interface box and control software.

RESULTS AND DISCUSSION

Experiments were performed on a production grade two-cylinder engine to achieve mode switching between PCCI combustion mode and conventional CI combustion mode. Mode switching strategy was based on two main control parameters namely fuel injection and EGR rate. To achieve

a dynamic control of these parameters, OEM ECU of the engine was replaced with an open ECU. This open ECU had the flexibility to control fuel injection parameters such as number of injections (pilot and main), fuel injection quantities (pilot and main), start of injection (SoI) timings, fuel injection pressure (FIP) and EGR. Open ECU controlled the fuel injection parameters based on throttle position; therefore fuel injection quantities were decided at different throttle positions. In mode switching experiment, maximum fuel injection quantity (at 100% throttle) was fixed for both test fuels, which resulted in ~ 5.5 bar BMEP in CI combustion mode. Difference in fuel injection quantities of mineral diesel and diesohol was due to difference in their calorific values. Diesohol had relatively lower calorific value compared to mineral diesel therefore slightly higher fuel injection quantity was required to provide equal energy input. Entire mode switching experiment was performed at constant engine speed (1500 rpm). Engine was started in conventional CI combustion mode and minimum fuel quantity was supplied to each cylinder. After warm up, engine was loaded up to 55% throttle position (BMEP ~ 2.95 bar) in PCCI combustion mode. For mode transition between CI and PCCI combustion modes, fuel injection parameters were changed gradually. For achieving smooth transition from CI to PCCI, engine was loaded gradually with a fixed ramp time (5 sec.). During PCCI combustion, pilot injection was activated at 30 to 35° bTDC and pilot injection quantity was varied from 10 to 20% of main injection quantity (depending upon engine load). FIP was varied from 550 bar to 700 bar. Variation in FIP was decided based on start of main injection (SoMI), which was varied from 15 to 20° bTDC. At the starting of PCCI combustion, EGR was 0% and after complete mode transition from CI to PCCI combustion, EGR was kept constant at 15% during the entire duration of PCCI combustion. At 55% throttle position, engine showed significantly higher combustion noise due to excessive RoPR. Presence of relatively higher fuel in the combustion chamber at higher engine loads resulted in faster fuel-air chemical kinetics, which led to severe knocking. Early SoMI timing also resulted in slightly inferior fuel-air mixing due to less intense in-cylinder conditions. This resulted in higher HC and CO emissions compared to lower engine loads. After 60% throttle, engine was again switched back to conventional CI combustion mode by suitably adjusting fuel injection parameters and EGR. CI combustion, pilot injection and EGR were deactivated and SoMI was retarded to 6° bTDC. At higher engine loads, FIP was decreased to 400-500 bar to avoid fuel spray impingement on the cylinder walls. Due to optimization of all injection parameters, engine reached up to ~ 5.5 bar BMEP in conventional CI combustion mode.

Mineral diesel fueled engine exhibited slightly higher BTE compared to diesohol (Figure 2). At lower engine loads

(idle), BTE was much lower and it increased with increasing engine load. During PCCI combustion mode, BTE increased up to ~ 33% and then became constant. Further increase in BTE occurred during mode transition from PCCI to CI combustion mode. During mode transition and CI combustion, EGR was turned off, which resulted in slightly higher peak in-cylinder temperature, which improved the combustion. At 80% throttle position, BTE slightly reduced. Diesohol combustion showed slightly lower BTE compared to mineral diesel. This was mainly due to lower calorific value of ethanol, which resulted in inferior combustion. EGT variation w.r.t. engine load showed significantly lower EGT in PCCI combustion region compared to CI combustion region. During mode transition from PCCI to CI combustion mode, EGT increased by ~100°C, which was the main reason of higher NOx emissions in CI combustion mode. EGT of mineral diesel was relatively lower compared to diesohol. This difference was dominant in CI combustion region. Higher EGT of diesohol fueled combustion was mainly due to lower calorific value of ethanol.
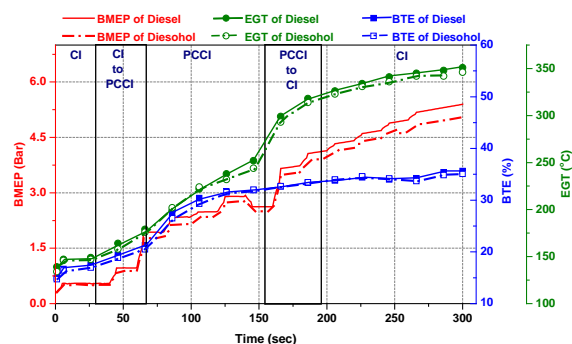
FIGURE 2: Variations in BTE and EGT with BMEP during different combustion modes and mode transitions

Figure 3 shows the variations of CO, HC and BMEP w.r.t. time. Higher CO and HC emissions from PCCI combustion showed the degree of incomplete combustion, which was mainly due to lower bulk in-cylinder gas temperature.
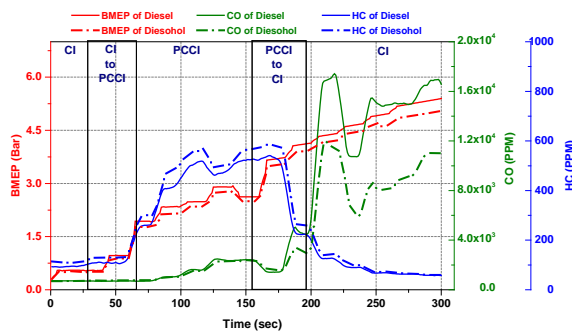
FIGURE 3: Variations in CO and HC emissions with BMEP during different combustion modes and mode transitions

HC emissions increased with increasing engine load during PCCI combustion and reached up to 600 ppm. During mode transition from PCCI to CI combustion mode, HC emissions decreased suddenly. This happened mainly due to increase in bulk in-cylinder temperature, which promoted fuel oxidation. During CI combustion mode, HC emission further decreased with increasing engine load. This was another reason of higher EGT during CI combustion mode. diesohol showed slightly higher HC emissions compared to mineral diesel. This difference was slightly higher in PCCI combustion regions and reduced to ~ 0 in CI combustion region. Inferior fuel-air mixing due to poor atomization characteristics and lower fuel volatility were the main reasons of this behavior. CO emissions showed significantly different trend during CI and PCCI combustion modes. Literature shows that CO emissions were higher in case of PCCI combustion. However, mode switching from conventional PCCI to CI combustion mode resulted in higher CO emission in CI combustion mode. This was an important observation. This trend was similar for both test fuels. This may be due to presence of relatively richer fuel-air mixture, where lack of oxygen prevented the oxidation of CO into CO_2. Slightly lower CO emissions from diesohol also supported this. Presence of oxygen in ethanol promoted CO oxidation and led to lower CO emission compared to mineral diesel.

Figure 4 shows that variation of total particulate number (TPN), NOx and BMEP w.r.t. time. Particulate characteristics were measured using EEPS. EEPS was continuously operated for 300 seconds, which helped in measurement of particulate data during mode transitions between conventional CI and PCCI combustion modes. In this figure, different background colors represented the operating combustion mode. Mode switching experiments were carried out using mineral diesel and diesohol separately and combined results are shown here.
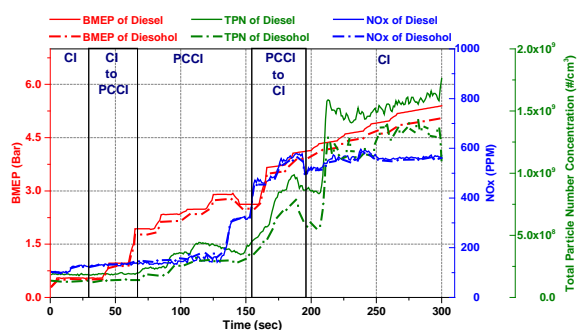
FIGURE 4: Variations in NOx and TPN emissions with BMEP during different combustion modes and mode transitions

Figure 4 shows the variation of TPN and NOx w.r.t. time. Significantly lower TPN and NOx in PCCI region clearly indicated the advantages of PCCI combustion compared to conventional CI combustion mode. With increasing engine load, increase in TPN and NOx increased in both regions (CI and PCCI). Relative magnitude of TPN in CI combustion region was an order of magnitude higher compared to PCCI combustion region. In PCCI region, mineral diesel fueled PCCI combustion resulted in ~ $4x10^8$ particles/ cm^3 of exhaust however mineral diesel fueled CI combustion resulted in ~ $1.75x10^9$ particles/ cm^3 of exhaust. Maximum variation in TPN was observed during mode transition from PCCI to CI combustion mode and start of CI combustion region. This was mainly due to effectiveness of variation in fuel injection parameters, which resulted in heterogeneous fuel-air mixture. Presence of fuel-rich localized zones promoted soot formation and resulted in higher TPN compared to PCCI combustion. TPN results showed slightly lower TPN of diesohol fueled PCCI and CI combustion. This was due to presence of oxygen in diesohol, which increased fuel oxidation and led to relatively lower TPN. In PCCI region, diesohol fueled PCCI combustion resulted in ~ $3x10^8$ particles/ cm^3 of exhaust and mineral diesel fueled CI combustion resulted in ~ $1.25x10^9$ particles/ cm^3 of exhaust.

Relative magnitude of NOx in PCCI combustion region was significantly lower compared to CI combustion region. Maximum NOx concentration was ~150 ppm in mineral diesel fueled PCCI combustion region however it reached ~ 575 ppm in mineral diesel fueled CI combustion region. Maximum NOx increase was observed during mode transition from PCCI to CI combustion mode. Increase in in-cylinder combustion temperature was the main reason for this trend, which was due to advanced SoMI timing and deactivation of EGR. At the end of PCCI combustion region, trend of sudden rise in NOx also supported PCCI to CI mode transition limit. NOx reduced slightly at the end of mode transition from PCCI to CI combustion mode. This may be due to thermal stabilization after sudden increase in combustion temperature. Diesohol fueled engine showed slightly higher NOx emission compared to mineral diesel. Relative increase in NOx from biodiesel CI combustion was slightly higher compared to biodiesel PCCI combustion. This was due to more dominant effect of biodiesel on CI combustion compared to PCCI combustion. Maximum NOx concentration was ~ 200 ppm in diesohol fueled PCCI combustion however it reached ~ 650 ppm in diesohol fueled CI combustion.

Figure 5 shows the variation of sulfur dioxide (SO_2), isocyanic acid (HNCO) and BMEP w.r.t. time. Previous studies indicate that HNCO is formed in higher quantities when NO, CO, and H_2/ NH_3 react over precious metal catalysts. Literature shows that carbamylation of proteins by cyanateanions (NCO^-) is responsible for several negative health effects ranging from cardiovascular and ocular impairments, to chronic diseases such as rheumatoid arthritis [4].
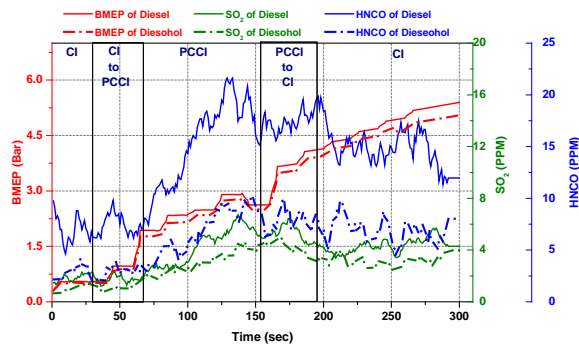
FIGURE 5: Variations in SO_2 and HNCO emissions with BMEP during different combustion modes and mode transitions

SO_2 emissions were less than 6 ppm for both test fuels in all engine combustion modes. Presence of sulfur in mineral diesel led to formation of SO_2 during combustion. In CI combustion region, SO_2 concentration reduced compared to PCCI combustion region. This was mainly due to formation of sulfur trioxide (SO_3), which resulted in formation of sulfuric acid (H_2SO_4) in presence of moisture. The presence of sulfuric acid vapors in the exhaust acts as a site for condensation of volatile materials, which promotes particulate formation with higher adsorbed organic content. Therefore conversion of SO_2 into particulate resulted in higher particulate concentration in CI combustion region (Figure 4) and subsequently lower SO_2 emission in gas phase. SO_2 emission was slightly lower from diesohol compared to mineral diesel. This was mainly due to 20% reduction in sulfur containing mineral diesel in the test fuel. In PCCI combustion region, HNCO emission increased with increasing load, however it slightly reduced in CI combustion region. This trend was common for both test fuels however diesohol showed slightly lower concentration of HNCO. Maximum HNCO concentration for mineral diesel reached up to ~ 23 ppm and it was ~ 11 ppm in case of diesohol.

CONCLUSIONS

The experiments were performed on a two-cylinder, medium-duty, direct-injection compression-ignition (DICI) production grade engine. Main objective of the experiments was to implement PCCI combustion strategy on a production grade commercial engine. An open ECU was installed on this engine to achieve mode switching between conventional compression ignition (CI) and PCCI combustion modes, depending on engine load. Mode switching strategy was based on three operating parameters namely SoI timings, FIP and EGR rate for smooth transition between CI and PCCI combustion modes. Results of mode switching showed significant differences in performance and emission characteristics during transition from CI to PCCI mode. A transient study was

also carried out during transition from CI to PCCI combustion mode using mineral diesel and diesohol. Diesohol exhibited slightly inferior performance however transition from CI to PCCI combustion mode was relatively smoother compared to baseline mineral diesel. During mode transition from CI and PCCI combustion, both test fuels showed slightly different patterns. Diesohol fueled engine exhibited relatively lower particulate number and NOx emissions compared to baseline mineral diesel. In CI combustion mode, diesohol exhibited relatively lower unregulated emissions (HNCO, SO_2, etc.) compared to baseline mineral diesel.

Finally, it can be concluded that mode switching technique has significant potential for commercial application of HCCI/ PCCI combustion in production grade engines. This technique can be easily employed in any production grade engine and give cost effective solution of challenges offered by HCCI combustion technique, with enhancement in engine performance and emission characteristics.

REFERENCES

[1] Han S, Kim H, Bae C, 2013. "Strategy for mode transition between low temperature combustion and conventional combustion in a diesel engine", SAE International Journal of Engines; 6:1706-15.

[2] Asad U, Zheng M, Ting DS-K, Tjong J, 2015 "Implementation challenges and solutions for homogeneous charge compression ignition combustion in diesel engines", Journal of Engineering for Gas Turbines and Power;137:101505.

[3] Rohani B, Park SS, Bae C, 2016. "Effect of injection strategy on smoothness, emissions and soot characteristics of PCCI-conventional diesel mode transition", Applied Thermal Engineering; 93:1033-42.

[4] Brady JM, Crisp TA, Collier S et al., 2014. "Real-Time Emission Factor Measurements of Isocyanic Acid from Light Duty Gasoline Vehicles", Environ. Sci. Technol.; 48: 11405−11412.

SEEC-2017-019

EFFECT OF ENGINE SPEED ON IN-CYLINDER AIR FLOW CHARACTERISTICS

Akhilendra Pratap Singh
Engine Research Laboratory
Department of Mechanical Engineering
Indian Institute of Technology Kanpur
Kanpur-208016, India
Email: akhips@iitk.ac.in

Avinash Kumar Agarwal
Engine Research Laboratory
Department of Mechanical Engineering
Indian Institute of Technology Kanpur
Kanpur-208016, India
Email: akhips@iitk.ac.in

ABSTRACT

Better understanding of flow phenomena inside the combustion chamber of a diesel engine and accurate measurement of flow parameters is necessary for engine optimization. Airflow structures developed inside the engine combustion chamber significantly influences the air-fuel mixing. In this study, in-cylinder air flow characteristics of a motored, four-valve diesel engine were investigated using time-resolved high-speed tomographic Particle Imaging Velocimetry (PIV). Single cylinder optical engine provides full optical access of combustion chamber through a transparent cylinder and flat transparent piston top. Experiments were performed in different vertical planes at different engine speeds during the intake, compression and exhaust stroke under motoring condition. For visualization of air flow pattern, graphite particles were used for flow seeding. In the experiments, highly swirling air flow pattern was found, which was dominant in the vicinity of valves. Swirling patterns significantly affected by engine speed and increased at higher engine speed. The average structure of the flow field was analyzed, which showed a clear orientation of the average velocity, which changed during different phases of the cycle. Vorticity analysis shows higher vorticity beneath the intake valve that affects turbulence in air flow. Different components of velocity as Vx, Vy and Vz shows that engine speed and z-location affects all velocity component in which maximum variation takes place in Z-direction.

Keywords: Air flow characteristics, Vorticity, Tomographic PIV, Velocity component, Turbulent kinetic energy.

INTRODUCTION

In-cylinder flows in an IC engine are mainly governed by the intake manifold and piston geometry. Air induced in the intake stroke of an engine cycle interacts with the piston and cylinder walls to form complex 3D flow structures. It is believed that the large flow structures formed in the intake stroke distort and break into smaller structures in later stages of compression stroke, which enhance turbulence at the time of fuel injection. Swirl and tumble are commonly known flow structures generated inside the cylinder. These flow structures are vortices with axis of rotation being parallel and perpendicular to the cylinder axis. Combination of these flow patterns produces complex and highly turbulent flow structures. These flow structures lead to more uniform fuel distribution, resulting in leaner PCCI combustion. Therefore, it becomes important to quantify the in-cylinder flows. Hot wire anemometry (HWA), laser Doppler anemometry (LDA) and particle imaging velocimetry (PIV) are widely known techniques for flow measurements and characterization.

PIV is a non-intrusive, optical, indirect flow visualization and measurement technique in which illuminated tracer particles are captured on a photographic film or by digital camera and images are further processed to obtain instantaneous velocity field. In this volumetric visualization method, flow field is seeded with small tracer particles, which are believed to faithfully follow the flow of air. The area of interest in the flow field is illuminated by double pulsed, high intensity laser sheet at two instances with a small time lag between them. Light scattered by the tracer particles is captured by cameras usually placed at 90° to the illumination plane. Acquired images are processed by dividing each image into small interrogation regions, which are auto-correlated or cross-

correlated to obtain average displacement vectors of tracer particles in the photographic coordinates. These camera scale displacements are converted into global coordinates using a calibration process. Further, with known time separation between consecutive laser illuminations, velocity vectors for the area of interest are calculated. Typical basic PIV setup for flow acquisition and analysis is shown in Figure 1.
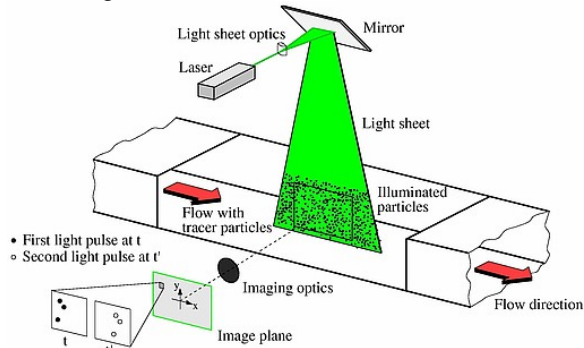
FIGURE 1: Typical PIV setup for flow field acquisition and measurement [1]

EXPERIMENTAL SETUP

Schematic of single cylinder optical research engine equipped with PIV system is shown in figure 1.

1	Laser controller
2	Nd-YAG Laser
3	Beam Deflector
4	Collimator
5	High Speed Camera
6	Inclined Mirror
7	Seeder
8	Image Acquisition Computer
9	High speed controller

Single Cylinder Optical research Engine
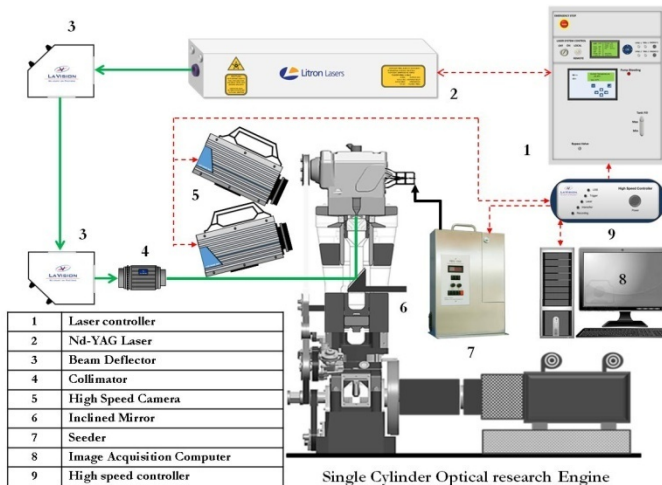
FIGURE 2: Schematic of SCRE with PIV

Experiments were conducted on a single cylinder optical research engine (AVL 5402) coupled with an AC dynamometer. Test engine is equipped with fuel conditioning, lubricating oil conditioning and coolant condition systems for conducting investigations at various engine operating conditions. For the current investigations, lubricating oil temperature and coolant temperature were kept constant (80^0C and 60^0C respectively) for the entire duration of experiments. Engine load and speed were controlled by AC dynamometer (Wittur Electric Drives, 2SB 3). This dynamometer can motor the engine upto 3000 rpm. State–of-the-art intake air measurement system (ABB Automation, Sensy-flow P), gravimetric fuel flow meter (AVL, 733S.18) were used for performing engine tests. In-cylinder pressure was measured using a piezoelectric pressure transducer (AVL, QC34C) and charge amplifier along with a high speed combustion data acquisition and analysis system (AVL,Indismart)on a crank angle basis using a high precision shaft encoder (AVL,365CC/ 365X). Maximum motoring pressure for optical head assembly is 34 bar.

For PIV experiments, optical head assembly of test engine was used. In this system, engine has a full length quartz liner and a sapphire window in the piston crown to provide full optical access of the combustion chamber. A high pressure air jet was supplied below extended piston for piston cooling. Constant 60ºC coolant temperature was used to avoid thermal concentration in quartz window. PIV setup consisted of a double pulse Nd:YLF laser (Litron, LDY series Laser) with maximum output 150W was used as the light source for illumination for seeding particles. Two beam deflectors were used to direct the laser beam in the desired direction to a collimator. The collimator converts the laser beam into a light sheet which was deflected by a 45° inclined mirror which is fixed inside the extended piston. This piston has a sapphire window in the piston crown from where laser sheet enters inside the optical combustion chamber of engine. The quartz optical window provided optical access to the combustion chamber. The laser sheet was aligned with the central axis of the cylinder in line with the fuel injector. Two high speed CCD cameras (LaVision, 1024x1024 pixels, 12 bits) having schiempflug adapters were used in double frame mode to capture the images. For the visualization of flow pattern, intake air was seeded with graphite particles at 2.5 bar pressure using solid particle disperser (Palas, RBG 1000). For the experiments, calibration was performed in the centre plane along the central axis of combustion chamber where the laser sheet was aligned just beneath the injector. A rectangular level 3-D calibration plate and polynomial calibration model was used to perform the calibration.

Davis 8.2 software (LaVision) was used to perform the tomographic processing of the images. As a part of pre-processing of the images, 5x5 sliding minimum was subtracted from the images to get a constant background across the images. For smoothening of vector field, Gaussian smoothing of 3x3 pixels was applied during analysis. Geometric mask was used to select the desired area in the captured images. The volume reconstruction of the images was done using Fast MART (Multiplicative Algebraic Reconstruction Technique). Direct correlation was done for volume correlation with four window sizes, first being 128 voxel with 75% overlap and other 3 being 64 voxels with 75% overlap with decreasing volume binning for each step. This was followed by vector post-processing in which universal outlier detection was done to

remove spurious vectors. A Gaussian smoothing of 3x3x3 and a second order polynomial filter was applied during post processing to the vector fields.

RESULTS AND DISCUSSION

Results are divided into four sub-sections namely absolute velocity analysis, vorticity analysis, velocity component analysis, average velocity and turbulent kinetic energy analysis.

Effect of Engine Speed on Absolute Air Velocity

Figure 3 shows the air-flow pattern at mid-compression stroke (at 90º CAD) at different engine speeds. At this position, piston attained maximum velocity in upward direction. In compression stroke, air velocity was significantly lower compared to intake stroke [2]. Continuous dissipation of flow kinetic energy due to interaction with piston and cylinder walls was the main reason for this behavior. Intake air jet characteristics played an important role in flow pattern during compression stroke and a large number of studies have been carried out for improving air-flow characteristics during the intake stroke [2].
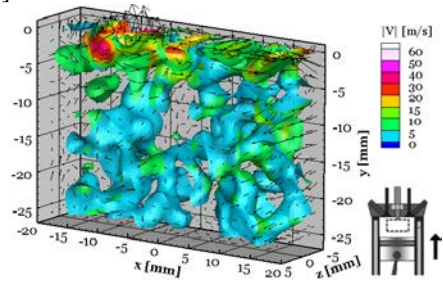
(a) Absolute air velocity (V) at 1000 rpm
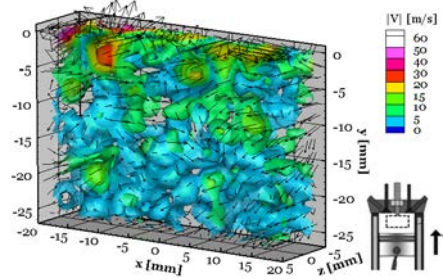
(b) Absolute air velocity (V) at 1500 rpm
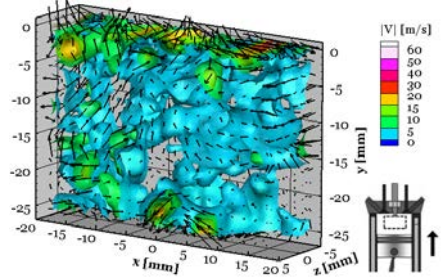
(c) Absolute air velocity (V) at 2000 rpm

FIGURE 3: Absolute air velocity (V) at different engine speeds at mid-compression stroke

At 1000 rpm (Figure 3 (a)), most velocity vectors were in horizontal direction, however, at 2000 rpm (Figure 3 (b)), most velocity vectors were vertical. Higher piston speed pushed the air in upward direction and after striking the cylinder head, this air jet changed its direction towards the piston. This showed that air-flow pattern during compression stroke was influenced by both factors namely flow pattern of intake air jet and piston movement. At 1000 rpm, effect of piston movement dominated over effect of intake air jet characteristics, however, at 2000 rpm, effect of intake air jet characteristics dominated over the effect of piston movement. At 1500 rpm, these two factors were in trade-off and resulted in a mixed velocity pattern containing both horizontal and vertical velocity vectors. Increasing engine speed from 1000 rpm to 1500 rpm (Figure 3 (a) and (b)) resulted in relatively higher air velocity, which was instrumental in improving fuel-air mixing. However, further increasing engine speed did not result in any further increase in air velocity. This happened due to high intake velocity during intake stroke, which resulted in reverse flow of air towards the piston. These two opposite motions of air prevented further increase in air velocity at 2000 rpm (Figure 3 (c)). Comparison of air-flow pattern at three different engine speeds showed that the main difference in absolute velocity occurred in the central region of the AoI (y = -10 mm to y = 10 mm). At 1000 rpm, velocity vectors were not present in this region, however, at 2000 rpm, small magnitude velocity vectors were observed. At 2000 rpm, air velocity was higher at the bottom and top regions of AoI, however their distribution was not uniform. At 1500 rpm, air velocity was distributed throughout the AoI, which showed superior fuel-air mixing tendency compared to 2000 rpm. This was the main reason for selecting 1500 rpm engine speed for the PCCI experiments in this study.

Effect of Engine Speed on Vorticity

Figure 4 shows the vorticity distribution in the AoI at different engine speeds. Vorticity is a measure of strength of rotation of in-cylinder flows hence higher vorticity directly influences the heat transfer and fuel-air mixing. Figure 4 shows that during the compression stroke, maximum vorticity occurred near the cylinder head i.e. at the TDC zone.
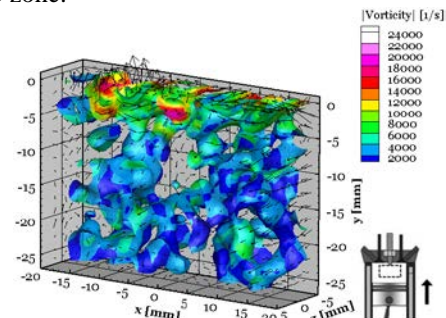
(a) Vorticity at 1000 rpm
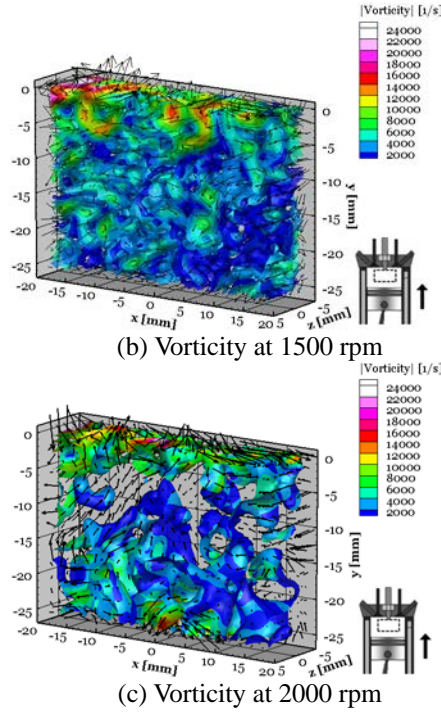
(b) Vorticity at 1500 rpm

(c) Vorticity at 2000 rpm

FIGURE 4: Vorticity at different engine speeds at the mid-compression stroke

Dominance of piston movement over localized air-flow structures inside the combustion chamber was the main reason for this behavior. Upward movement of piston pushed the air towards the cylinder head and these air streams struck the cylinder head. This collision led to downward movement of air, which followed a vertical path and resulted in higher vorticity near cylinder head. In general, vorticity increased with increasing engine speed. However, this study showed slightly different vorticity behavior at higher engine speeds. Increasing engine speed from 1000 rpm to 1500 rpm resulted in slightly higher vorticity and vorticity pattern was more uniformly distributed at 1500 rpm compared to 1000 rpm (Figure 4 (a) and (b)). Further increasing the engine speed from 1500 rpm to 2000 rpm resulted in relatively lower vorticity and vorticity pattern became relatively narrower at 2000 rpm (Figure 4 (c)). At 1500 rpm localized vortical structures throughout the volume of interest were observed. These localized vortical structures improved fuel-air mixing by the turbulent transport of fuel spray, which reduced pollutant formation. Similar to velocity results, vorticity results also supported 1500 rpm as suitable engine speed for PCCI experiments.

Effect of Engine Speed on Velocity Components

Figure 5 shows the variations of velocity components namely u, v and w in volume of interest. In each figure, vectors show absolute velocity (V) and background color shows different velocity components. u shows the velocity parallel to cylinder bore, v shows the velocity parallel to cylinder axis and w shows the velocity from intake valves

to the exhaust valves. In IC engines, understanding of these velocity components is very important because variations in each velocity component can be different having different effects. Previous research showed that z component of absolute velocity (w) affects flow pattern significantly [3]. Therefore, all three components of velocity were investigated at three different engine speeds.
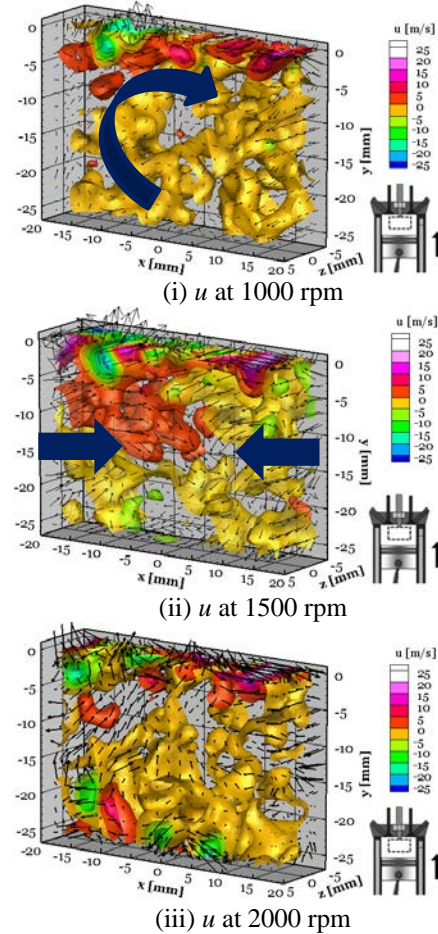
(i) u at 1000 rpm

(ii) u at 1500 rpm

(iii) u at 2000 rpm

FIGURE 5: Variation of u at different engine speeds

Figure 5 shows the variation of u at different engine speeds. Comparison of flow patterns showed that increasing engine speed did not affect u significantly. Increasing engine speed from 1000 rpm to 1500 rpm resulted in slightly higher u. At 1500 rpm, stagnation zone was observed at x = 0 mm. This stagnation zone formed due to opposite air streams as shown (by arrows) in Figure 5 (ii). Further increment in engine speed did not affect u. u showed a common variation at all engine speeds as u was positive near the cylinder head, however in remaining volume of interest, u was negative. This showed a circulating pattern from bottom to the top of the volume of interest (Figure 5 i).

(i) *v* at 1000 rpm

(ii) *v* at 1500 rpm

(iii) *v* at 2000 rpm
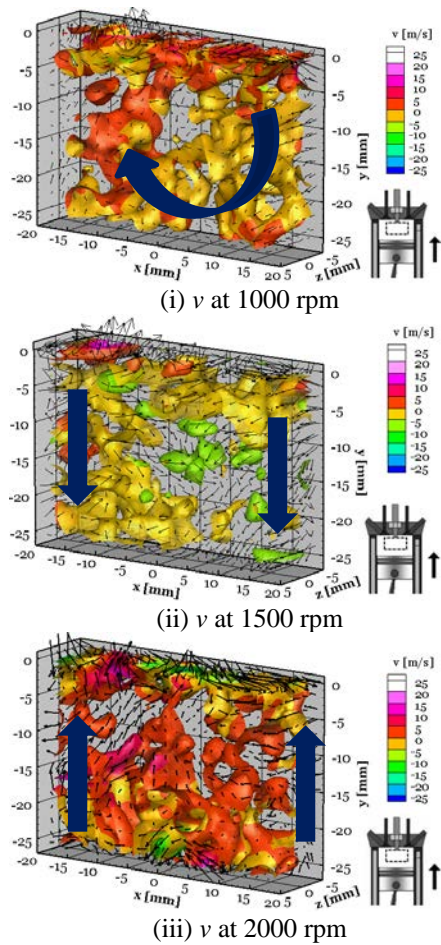
FIGURE 6: Variation of v at different engine speeds

Figure 6 shows the variation of v at different engine speeds. Comparison of velocity pattern clearly indicates dominating effect of piston movement and intake air jet. At 1000 rpm (Figure 6 i)), v was negative in the region x = 0 to x = 20 mm, and in remaining volume v was positive, which shows the circulation pattern of v. At 1500 rpm, v was negative in entire volume of interest. This shows that after striking the cylinder head, air was moving towards the piston. At 2000 rpm, v was positive in most of volume of interest. This showed the influence of high speed intake air during the intake stroke. At all three engine speeds, v showed different behavior near the cylinder head because at 1000 rpm, v was positive near the cylinder head, however at 1500 and 2000 rpm, v was negative.
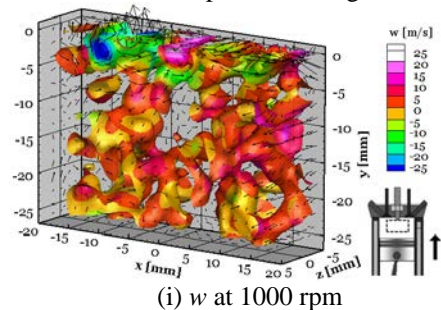
(i) *w* at 1000 rpm
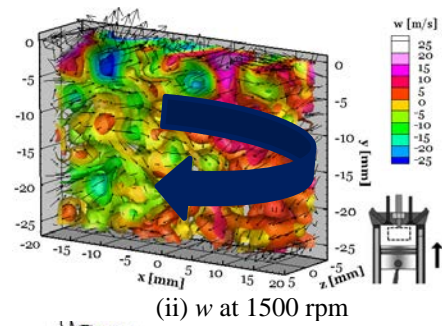
(ii) *w* at 1500 rpm
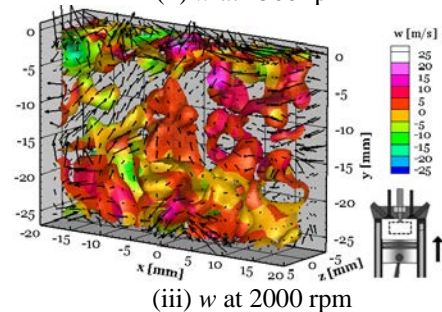
(iii) *w* at 2000 rpm

FIGURE 7: Variation of w at different engine speeds

Figure 7 shows the variation of w at different engine speeds. Comparison of velocity pattern showed that w was significantly affected by the engine speed. At 1500 rpm, w showed maximum variations in entire volume of interest. w was negative in x = 0 mm to x = 20 mm and it was positive in x = 0 mm to x = - 20 mm. This showed a circulating pattern around the cylinder axis (Figure 7 (ii)). This kind of circulating pattern was not present at 1000 rpm and 2000 rpm, therefore fuel-air mixing is expected to be superior at 1500 rpm. From Figure 5 to 7, it can be concluded that variation of different velocity components behaved in different manner. Amongst three tested engine speeds, 1500 rpm showed maximum variation in all three velocity components.

Effect of Engine Speed on Average Air Velocity and Turbulent Kinetic Energy (TKE)
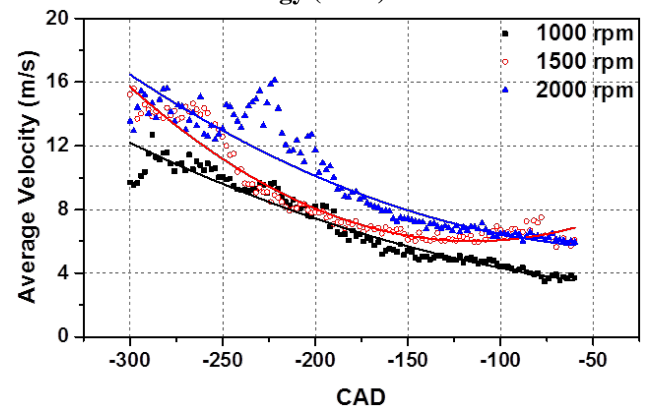
FIGURE 8: Average velocity at different engine speeds during intake and compression strokes

Figure 8 shows the variation in average air velocity during the intake and the compression strokes in crank

angles ranging from -300º to -60° CAD. Absolute air velocity at each crank angle position was calculated by averaging the velocity field present at z = 0 mm (vertical plane below the injector). Averaging the velocity vectors present in any plane were significantly affected by turbulence characteristics, which resulted in random behavior during the intake stroke.

During compression stroke, highly turbulent air-flow inside the combustion chamber resulted in slightly higher average velocity from -160º to -100° CAD. Effect of engine speed on rate of energy dissipation was another important observation. Figure 8 also shows that the rate of energy dissipation was higher during later stages of the intake stroke (from -250 to -180 CAD) compared to the compression stroke. Average air velocity fluctuations were very high in the intake stroke, however these fluctuations reduced significantly in the compression stroke. Average velocity trends showed significantly lower air velocity during the compression stroke (-180 to -60 CAD) compared to the intake stroke (-300 to -180 CAD). This happened mainly due to dissipation of flow energy by interaction with the cylinder walls and the piston surface. Average velocities during the intake stroke varied from 8 to 17 m/s, however they reduced from 4 to 10 m/s during the compression stroke.

Figure 9 shows the variations of average turbulent kinetic energy (TKE) at different engine speeds during the intake and compression strokes. Average TKE was calculated using mathematical expression given as;

$$KE = \frac{1}{2}\rho V_{rms}^2 = \frac{1}{2}\rho u_{rms}^2 + \frac{1}{2}\rho v_{rms}^2 + \frac{1}{2}\rho w_{rms}^2$$

Where, u, v and w are average velocity components in x, y and z directions respectively (at z = 0 mm). Here, density 'ρ' is assumed to be 1 kg/m3 for air. Average TKE shows the strength of flow in turbulent flows.
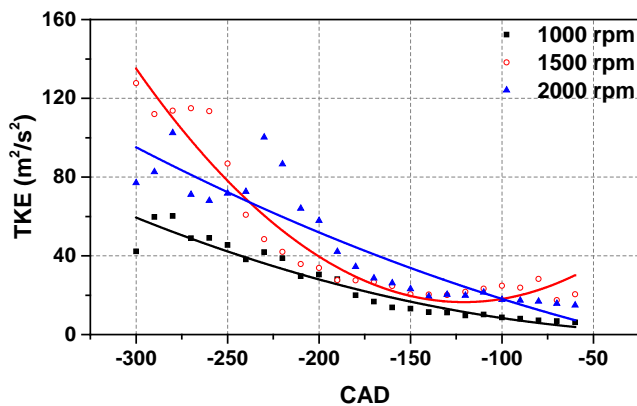
FIGURE 9: Turbulent kinetic energy at different engine speeds during the intake and compression strokes

Figure 9 shows that average TKE first increased slightly during the intake stroke and then decreased with further movement of piston in downward direction. During early intake stroke, intake valves were opening and piston was accelerating downwards, which increased the air

velocity hence enhanced TKE. After 270° CAD, intake valve further opened, however piston speed decreased, which resulted in relatively lower TKE. During the compression stroke, a major fraction of TKE dissipated due to internal collision of air streams and its interaction with cylinder walls.

At 2000 rpm, TKE was also higher, which reduced relatively faster compared to lower engine speeds (1000 and 1500 rpm). During early compression stroke, 2000 rpm exhibited relatively higher TKE due to faster piston speed, which promoted turbulent characteristics in the in-cylinder flows. However in later compression stroke, 1500 rpm exhibited higher TKE compared to 2000 rpm due to relatively lower effect of intake stroke. TKE results were also in agreement with velocity and vorticity results as 1500 rpm was suitable for PCCI experiments.

CONCLUSIONS

Results show engine speed significantly affected in-cylinder flow patterns inside the engine combustion chamber. This air flow measurement showed that increasing engine speed improved in-cylinder flow characteristics, however at very high engine speeds airflow pattern deteriorated and resulted in slightly inferior conditions for in-cylinder fuel-air mixing. Therefore, an intermediate speed (1500 rpm) was found relatively better compared to 1000 and 2000 rpm.

REFERENCES

[1]   http://aim2.dlr.de/measurement-techniques/particle-image-velocimetry-piv/index.html; Accessed on 23rd March 2016.

[2] Gadekar S, Singh AP, Agarwal AK, 2016. "Tomographic PIV Evaluation of In-Cylinder Flow Evolution and Effect of Engine Speed", SAE Technical Paper 2016-01-0638.

[3] Singh AP, Gadekar S, Agarwal AK, 2016. "In-Cylinder Air-Flow Characteristics Using Tomographic PIV at Different Engine Speeds, Intake Air Temperatures and Intake Valve Deactivation in a Single Cylinder Optical Research Engine", SAE Technical Paper 2016-28-0001.

SEEC-2017-020

EFFECT OF FUEL INJECTION PRESSURE AND EGR ON DIESOHOL FUELLED PCCI ENGINE

Akhilendra Pratap Singh
Engine Research Laboratory
Department of Mechanical Engineering
Indian Institute of Technology Kanpur
Kanpur-208016, India
Email: akhips@iitk.ac.in

Avinash Kumar Agarwal
Engine Research Laboratory
Department of Mechanical Engineering
Indian Institute of Technology Kanpur
Kanpur-208016, India
Email: akhips@iitk.ac.in

ABSTRACT

Use of alternative fuels such as alcohol blending seems to be a feasible approach towards achieving cleaner combustion modes. The main advantage in using biomass derived fuels in diesel engines is the improvement in power generation with significant reduction in CO_2 coming out in engine exhaust. This study explores premixed charge compression ignition (PCCI) combustion in a single cylinder research engine (SCRE) fuelled with diesel-butanol blend (diesohol). In diesel PCCI, issues such as low volatility and auto ignition of mineral diesel, mixture preparation and control of combustion phasing are major challenges for the researchers. The test engine was equipped with highly advanced and flexible fuel injection system, which is capable of controlling injection parameters such as fuel injection pressure, number of injections, injection duration and injection timings. PCCI combustion was achieved by using early in-cylinder fuel injection and high EGR, which simultaneously reduced NOX and PM emissions. Experiments were conducted with single injection strategy at different fuel injection pressures (350, 600 and 850 bar) and fuel injection timings. The results depicted that PCCI combustion using diesohol was indeed an effective method to control emissions without compromising the thermal efficiency. Diesohol exhibited superior combustion and emission characteristics, however slightly inferior engine performance, compared to diesel.

Keywords: PCCI combustion, Fuel injection pressure, Diesohol, Exhaust gas recirculation.

INTRODUCTION

In the past few decades, the extensive exploitation of conventional resources of energy has led to a serious energy crisis. Eventually, this will result in depletion of fossil fuels including petrol, diesel etc. Therefore, there is a need to develop alternative fuels to tackle this problem. Biofuels in the form of biodiesel, bioethanol etc., seem to be attractive options towards this end. These biofuels are mainly produced from biomass that can be obtained from various sources like industrial waste, agricultural waste, domestic waste etc.

The main advantage of using these biofuels in diesel engine is to effectively control exhaust emissions including CO_2, NOx and particulates (PM) either by using after treatment devices or by developing an alternate combustion strategy. However, the high investment in after-treatment devices puts a serious limitation to their usage. This led to the development of a new combustion concept of PCCI combustion which proved to be very effective in controlling NOx and PM emissions simultaneously. Araki et al. [1] and Laguitton et al. [2] had investigated the effect of variation in compression ratio on exhaust emissions in PCCI engine. They reported a significant NOx reduction and a slight increase in HC and CO emissions under low temperature combustion (LTC). Some researchers including Horibe et al. [3] have worked on optimization of PCCI combustion using split injection. They used advanced single injection strategy and observed that NOx and PM can be controlled simultaneously with improved thermal efficiency. Further, to tackle the problems of combustion phasing and mixture preparedness in PCCI combustion, which occurs mainly due to low volatility and low auto-ignition temperature of mineral diesel, researchers have explored various alternative fuels

like biodiesel, Di-methyl ether (DME) etc. in PCCI combustion engine. Zhao et al. [4] and Mohammadi et al. [5] had investigated combustion and emission characteristics using DME and bio-ethanol diesel blend respectively. Yoon et al. [6] determined the effect of spray cone angle on DME combustion. They observed an improvement in thermal efficiency with lower regulated emissions at early injection timings. The effect of advance injection strategies using biodiesel have been studied by Fang et al. [7-8]. They observed low soot luminosity and lower NOx emissions compared to diesel for all the injection timings. Kitano et al. [9] determined the effect of fuel cetane number on PCCI combustion. They reported that low cetane number is used to suppress ignitability in high load conditions and reduce NOx emissions.

EXPERIMENTAL SETUP

This study deals with the optimization of PCCI combustion strategy using diesohol as the test fuel. All the experiments have been performed on single cylinder research engine (SCRE) (AVL, 5402). AC transient dynamometer (Wittur Electric Drives, 2SB 3) was coupled with the engine. The test engine specifications are given in Table 1 and the engine schematic is shown in Figure 1.
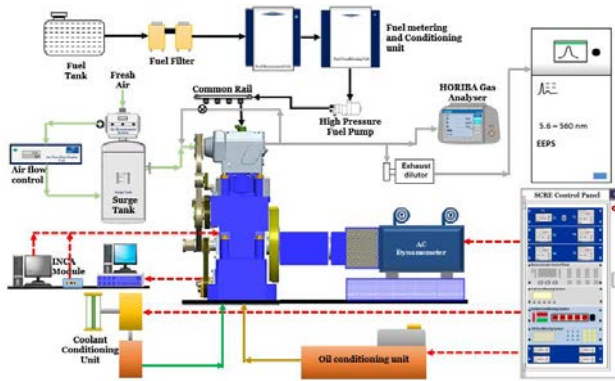
Figure 1: Schematic of engine setup

Table 1: Technical Specifications of the engine

Engine Parameters	Specifications
Engine model	AVL 5402
Number of cylinders	1
Cylinder bore/ stroke	85/ 90 mm
Swept volume	510.7 cc
Compression ratio	17.5
Maximum power	6.25 kW
Fuel injection system	Direct injection
Engine management system	AVL-RPEMS + ETK7 BOSCH
Valves per cylinder	4 (2 inlet, 2 exhaust)

Fuel conditioning and metering units were used to maintain a constant fuel temperature at 25^0C and for measuring the fuel flow rate respectively. Coolant and Lubricating oil

conditioning units have been installed to maintain coolant at 60^0C and oil temperature at 90^0C. Horiba analyser was used to measure the regulated exhaust emissions such as CO, CO_2, NO_X and unburnt HC. The engine was equipped with common rail direct injection system, with advanced features for controlling the fuel injection pressure (FIP) and start of injection (SoI) timings. This system was capable of multiple injections (2 pilot injections and 1 post injection in addition to the main injection). In-cylinder pressure was measured using a piezoelectric pressure transducer (AVL; 6013) mounted flush onto the cylinder head. Crank position was measured by an angle encoder (AVL; 365) with resolution of 0.1 crank angle degree (CAD). For data acquisition and analysis, a high speed combustion data acquisition system (AVL; Indi-micro) was installed with the engine.

RESULTS AND DISCUSSION

The experiments have been performed at four different SoI timings for three different (350,600 and 850 bar) fuel injection pressures. The injection timings have been selected in such a way so that mode switching from conventional CI to PCCI combustion can be achieved. Finally, the effect of exhaust gas recirculation (EGR) has also been investigated by reiterating the above mentioned conditions at two different (15% and 30%) EGR rates. In order to understand the effect of injection parameters on PCCI combustion, the results have been represented in three sections: combustion, performance and emission characteristics.

Combustion Characteristics

The parameters such as in-cylinder pressure history, heat release rate (HRR) etc. are very effective tools for analysing the engine combustion behaviour. In this study, pressure-crank angle data was acquired using a high speed data acquisition system in which an average data of 250 cycles was taken to eliminate cycle-to-cycle combustion variability.
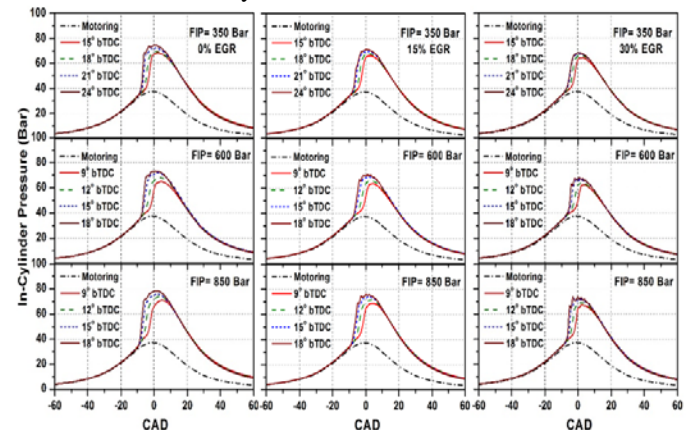
FIGURE 2: In-cylinder pressure variation w.r.t. crank angle position at diffferent FIP, SoI timings and EGR

Figure 2 represents the variation of in-cylinder pressure data w.r.t. crank angle position for 3 different fuel injection pressures (350,600 and 850 bar) at 4 different SoI timings (9^0 bTDC to 24^0 bTDC) and EGR rates(0%, 15%, 30%). In all the curves, the separation of pressure curve form the motoring curve represents the start of combustion (SoC). Moreover, it can be observed that SoC advances with early SoI timings i.e. the tendency of PCCI combustion increases with advanced SoI timings. At retarded SoI timing, due to lesser time availability for fuel-air mixing, mainly diffusion combustion takes place. An increase in FIP from 350 bar to 850 bar resulted in superior atomization of fuel droplets which in turn leads to a more homogeneous air-fuel mixture, thereby, reducing the ignition delay. Due to lower ignition delay, for the same injection timing, combustion started earlier at higher FIP. The peak in-cylinder pressure also increases with an increase in FIP due to improved combustion. For a fixed FIP, the peak in-cylinder pressure decreases with an increase in EGR rate. This occurs mainly due to the reduction in fuel quantity with an increase in EGR (relative air fuel ratio (λ) is kept constant = 2.0). In the exhaust gas, presence of high heat capacity gases absorbs combustion energy and lowers in-cylinder pressure peak. These non-reactive exhaust gas species also reduces the rate of fuel-air kinetics and thus, shifts the in-cylinder pressure curve away from top dead centre (TDC).

Figure 3 represents the HRR w.r.t. crank angle position at different injection strategy and EGR. The mode switching from conventional CI combustion to PCCI combustion is clearly evident from these HRR curves. It can be observed that majority of heat release took place in the premixed phase for PCCI combustion while for CI combustion it was in the diffusion phase. For a constant FIP and EGR rate, the tendency of PCCI combustion increases with advance SoI timings. Moreover, the duration of diffusion combustion increases with retarded SoI timings and thus, it is termed as conventional CI (diffusion) combustion. The peak HRR in premixed phase was approximately 250 kJ/bar/m^3 which was much higher as compared to the heat release in diffusion combustion. For a fixed SoI timing, HRR peak showed a significant increment with an increase in FIP from 350 bar to 850 bar. This occurs mainly due to improved fuel atomization resulting in faster fuel evaporation, and thus, better combustion. For a fixed FIP, HRR peaks showed a compelling decrement with an increase in EGR rate, mainly due to reduction in fuel quatity. This decrement signifies that EGR affects PCCI combustion to a much greater extent than it affects CI combustion (no major changes in HRR). Also, the combustion duration of premixed phase increases with EGR due to slower chemical kinetics of fuel-air mixture.
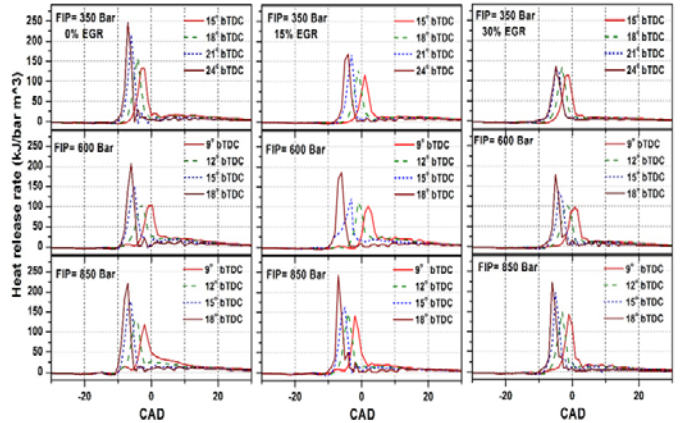
FIGURE 3: Heat release rate (HRR) variation w.r.t. crank angle position at diffferent FIP, SoI timings and EGR

Variation of start of combustion (SoC), combustion phasing (CP) and combustion duration (CD) w.r.t. SoI timing, FIP and EGR rates have been depicted in figure 4.
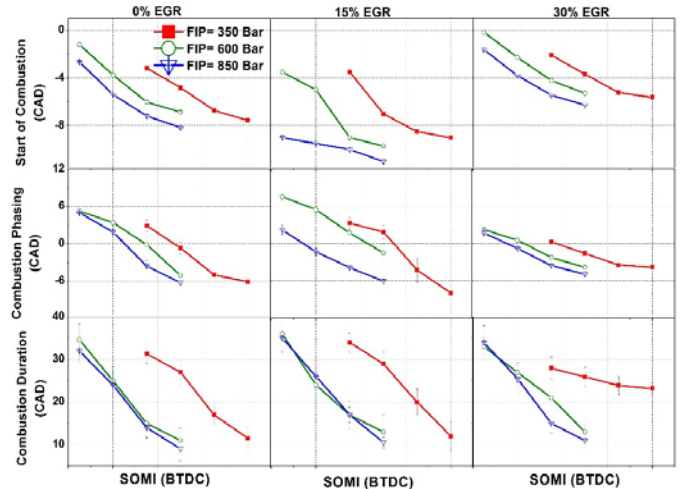
FIGURE 4: SoC, combustion phasing and combustion duration w.r.t. SoI timings at different FIP's and EGR

It is clearly seen that SoC is strongly dependent on SoI timing and thus, decreases with early injection. Moreover, for a constant SoI timing, SoC decreases with an increase in FIP. This is mainly due to better fuel atomization resulting in early SoC. Further, with an increase in EGR, for a fixed SoI timing, SoC increases significantly due to slower chemical kinetics of fuel-air mixture because of unreactive species in exhaust gas. CP represents crank angle position corresponding to 50% cummulative heat release (CHR) and is a measure of overall combustion in an engine cycle. Too advanced and too retarded CP decreases the efficiency of PCCI combustion. CP decreases with advanced SoI timings, irrespective of FIP and EGR rate. For the same SoI timing, it shows a noticable reduction with an increase in FIP due to the reasons stated above. PCCI combustion is greatly affected by higher EGR

3

rates. CP is a strong function of EGR for higher FIP as compared to lower FIPs due to increasing tendency of PCCI combustion at higher FIP. Thus, it shows a monotonous decrement with increasing EGR. The crank angle position difference between 10% and 90% mass fraction burned is defined as combustion duration. CD decreases significantly for PCCI combustion, mainly because of early SoI timings and formation of homogeneous air-fuel mixture which facilitates faster and better combustion.

Performance Characteristics

Figure 5 represents the variation of engine performance parameters with FIP, EGR and SoI timings.
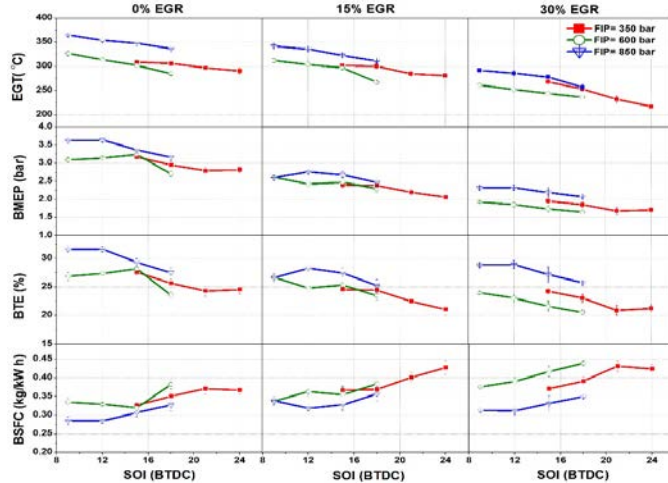
FIGURE 5: EGT, BMEP, BTE and BSFC variation w.r.t. SoI timings at different FIP's and EGR rates

Exhaust Gas Temperature (EGT) decreases with advancing SoI timings mainly due to absence of diffusion combustion at early injection. Due to the absence of diffusion phase, there is a local temperature hike but overall temperature will be lower. EGT decreases further with increasing EGR rates due to absorbtion of combustion energy by non-reactive, high heat capacity exhaust gas species. Brake Mean Effective Pressure (BMEP) shows a continuous reduction with the advancement of SoI timings irrespective of EGR and FIP. This is due to premixed combustion, which increases with advanced SoI timing leading to more negative work done on the piston as compared to conventional (retarded) injection timings. Further, increasing FIP led to better fuel atomization which improves fuel-air mixing. All these serve as an ideal condition for homogeneous combustion and higher BMEP. Further, Brake Thermal Efficiency (BTE) reduces slightly for advanced SoI timings but increases with increasing FIP. Thus, it can be concluded that for a specific EGR rate, since BTE was almost constant, BMEP and brake specific fuel consumption (BSFC) must be having an inverse proportionality which is also evident from the above figure.

BMEP, in general, shows a monotonous decrement whereas BSFC increases continuously.

Emission Characteristics

The variation of engine exhaust emissions w.r.t. SoI timings, FIP and EGR have been indicated in Figure 6. As evident from the figure, HC and CO emissions increases with increasing EGR, mainly due to low in-cylinder temperature which results in incomplete or poor combustion. Moreover, increasing EGR quantity facilitates low temperature combustion which serves as an unfavorable condition for the conversion of CO to CO_2. HC and CO emissions decreases with increasing FIP because of improvement in fuel atomization which results in homogeneous fuel-air mixture, thus complete combustion. For any EGR rate, NO_X emissions have shown a significant reduction with advanced SoI timings. This can be attributed to low temperature combustion (PCCI combustion) resulting mainly from early fuel injection timings. Moreover, an addition of EGR further reduces the in-cylinder temperature, thereby, lowering the NO_X significantly.
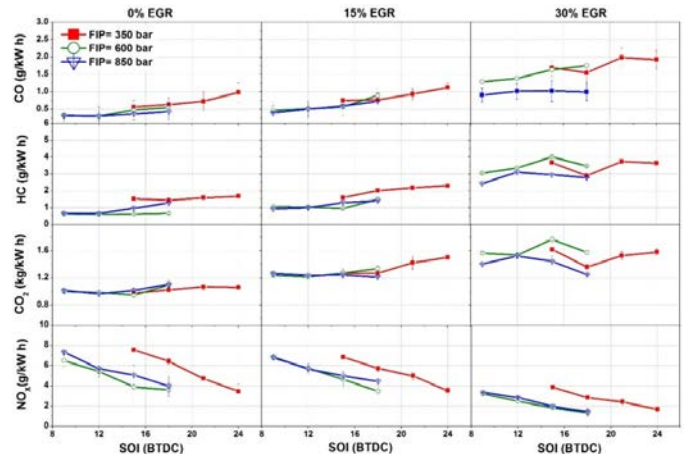
FIGURE 6: CO, HC, CO_2 and NO_x emissions variation w.r.t. SoI timings at different FIP's and EGR rates

CONCLUSION

In the present study, diesohol fuelled PCCI experiments were carried out in a single cylinder research engine equipped with flexible injection system. In these experiments, effect SoI timing, FIP and EGR were investigated. Results showed that the peak in-cylinder pressure increased with advancement of SoI timings at constant injected fuel quantity. Increasing FIP also increased peak in-cylinder pressure due to inproved fuel air-mixing. In PCCI combustion, premixed phase of HRR was found dominating over diffusion phase. Relatively higher peaks of premixed phase HRR at advanced fuel injection timings is another important finding of this study. EGT during PCCI combustion was found slightly lower as compared to conventional CI combustion. BTE and BMEP

4

were reduced with advancing SoI timing, however, increasing FIP resulted in higher BTE and BMEP. Emission results showed significant reduction in NO_X, however, HC and CO were slightly higher for PCCI combustion. Therefore, it can be concluded that combustion, performance and emission characteristics in PCCI combustion are strongly dependent on fuel injection parameters.

REFERENCES
[1] Araki M., Umino T., Obokata T., Ishima T., Shiga S., Nakamura H., 2005, Effects of compression ratio on characteristics of PCCI diesel combustion with a hollow cone spray, SAE International, 2005-01-2130.
[2] Laguitton O., Crua C., Cowell T., Heikal M.R., Gold M.R., 2007, The effect of compression ratio on exhaust emissions from a PCCI diesel engine, Energy Conversion and Management, 48 (2007) 2918–2924.
[3] Horibe N., Harada S., Ishiyama T., Shioji M., 2009, Improvement of premixed charge compression ignition based combustion by two-stage injection, International Journal of Engine Research, 10.1243/14680874JER02709.
[4] Zhao Y., Wang Y., Li D., Lei X., Liu S., 2014, Combustion and emission characteristics of a DME (dimethyl ether)- diesel dual fuel premixed charge compression ignition engine with EGR (exhaust gas recirculation), Energy, 72 (2014) 608-617.
[5] Mohammadi A., Kee S., Ishiyama T., Kakuta T. and Matsumoto T., 2005, Implementation of ethanol diesel blend fuels in PCCI combustion, SAE International, 2005-01-3712.
[6] Yoon S., Cha J., Lee C., 2010, An investigation of the effects of spray angle and injection strategy on dimethyl ether (DME) combustion and exhaust emission characteristics in a common-rail diesel engine, Fuel Processing Technology, 91 (2010) 1364–1372.
[7] Fang T., Lee F., 2009, Biodiesel effects on combustion processes in an HSDI diesel engine using advanced injection strategies, Proceedings of Combustion Institute, 32 (2009) 2785–2792.
[8] Fang T., Lin Y., Foong T., Lee C., 2009, Biodiesel combustion in an optical HSDI diesel engine under low load premixed combustion conditions, Fuel, 88 (2009) 2154–2162.
[9] Kitano K., Nishiumi R., Tsukasaki Y., Tanaka T., 2003, Effect of fuel properties on premixed charge compression ignition combustion in a direct injection diesel engine, SAE International, 2003-01-1815.

SEEC-2017-021

BIODIESEL SPRAY CHARACTERISTICS AT DIFFERENT FUEL INJECTION PRESSURES IN AMBIENT CONDITIONS

Akhilendra Pratap Singh
Engine Research Laboratory
Department of Mechanical Engineering
Indian Institute of Technology Kanpur
Kanpur-208016, India
Email: akhips@iitk.ac.in

Avinash Kumar Agarwal
Engine Research Laboratory
Department of Mechanical Engineering
Indian Institute of Technology Kanpur
Kanpur-208016, India
Email: akhips@iitk.ac.in

ABSTRACT

Spray pattern is the shape of spray leaving the injector nozzle. Spray pattern was obtained by capturing the spray images using a high speed camera. Spray patterns were obtained for biodiesel blends and mineral diesel at different fuel injection pressures (FIPs) and atmospheric pressures (APs) in a constant volume spray chamber (CVSC). Spray pattern analysis was used to characterize the spray shape and spray evolution, which affects in-cylinder combustion and particulate formation. Results show that increasing FIP resulted in longer fuel spray penetration length and reduced spray cone angle. Increasing AP resulted in shorter fuel spray penetration length and increased spray cone angle. Increasing biodiesel content in test fuels first improved spray characteristics however higher biodiesel blends resulted in slightly inferior spray characteristics.

Keywords: Spray characteristics, Fuel atomization, Biodiesel, Spray evolution.

INTRODUCTION

The homogeneity in fuel-air mixture inside the engine cylinder directly affects PCCI combustion, performance and emission characteristics; therefore, it becomes necessary to study the spray formation, spray breakup and atomization similar to in-cylinder conditions. Physical and thermal properties of test fuels such as kinematic viscosity, ambient gas density, bulk modulus of compressibility, volatility, surface tension, rate of vaporization, boiling temperature, etc., play a prominent role in spray formation and fuel-air mixture formation. Study of spray parameters in a real engine combustion chamber makes the task

extremely challenging. Therefore, most reported research has been conducted in constant volume spray chambers. The constant volume spray chamber can generate actual engine combustion chamber conditions, except temperature and turbulence. Fuel is introduced through an injector nozzle by creating a pressure difference between the ambient air and injector into the spray chamber. Quality of combustion in a PCCI engine is highly dependent on quality of spray formation and atomization during fuel injection. A good spray should ensure that the injected fuel jet enters the chamber at sufficiently high velocity and atomizes the fuel into small droplets to enable rapid vaporization and mixing with ambient air to form a combustible mixture. When mineral diesel is replaced by biodiesel, it is essential to optimize the fuel injection system for the new fuel. Relatively higher viscosity, surface tension and density of biodiesel and blends exhibit inferior spray characteristics, which results in poor fuel-air mixing. Liquid fuel distribution visualization in an engine cylinder or in a constant volume spray chamber provides useful information on the evolution of mineral diesel spray, spray penetration, spray cone angle, spray-wall interaction and spray area. A typical top view and front view of a six-hole injector is shown in Figure 1.
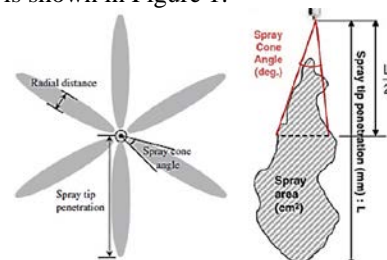
FIGURE 1: Macroscopic spray characterization [1]

Images are taken with help of a high speed CCD camera and using segmentation processing method, the macroscopic spray parameters can be determined from the same. Spray penetration length is spray length from the tip of the injector nozzle to the farthest point, where the spray diminishes. Spray cone angle is the angle created by the tip of injector nozzle and tangents drawn to the spray boundary. This spray boundary is defined with the help of radial distance shown in Figure 1. Spray area is the area covered by droplets within the spray regime. It can also be defined as the sum total of the image pixels captured by the camera (Figure 1).

EXPERIMENTAL SETUP

An experimental setup was designed to understand spray behavior in a cold, non-reacting environment. This setup provided the same (pressure) conditions as that of engine combustion chamber, however, without turbulence and heat release. The schematic experimental setup is shown in Figure 2.
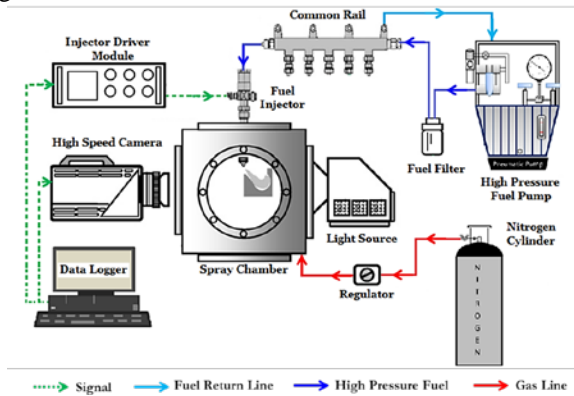
FIGURE 2: Schematic of spray analysis setup

To investigate the spray characteristics, a square constant volume spray visualization chamber was designed at the Engine Research Laboratory, IIT Kanpur [2]. The square chamber had four side flanges (for illuminating the chamber using an intense white light source and for capturing images by a high speed camera), one flange at the top (for mounting the solenoid fuel injector) and one bottom flange (for N_2 inlet, N_2 outlet and mounting a pressure gauge). Fuel spray was injected into the chamber by a solenoid common rail injector (Bosch, CP3 VCO), similar to the injector used in PCCI experiments of this study. A high speed camera was used to capture the spray images. The chamber was pressurized by nitrogen gas and chamber pressure controlled by a pressure regulator fitted on the nitrogen bottle, which was connected to the spray chamber. Triggering of fuel injector was synchronized with the camera in order to eliminate delay between fuel injection and images captured. Captured images were processed using a MATLAB code and various spray parameters were calculated.

RESULTS AND DISCUSSION

The results are divided in three sub-sections namely: effect of FIP on spray development; effect of AP on spray development; and effect of fuel composition on spray development.

Effect of Fuel Injection Pressure (FIP)

Figure 3 shows the spray images of mineral diesel captured by high speed camera (frame rate = 10000 fps) at different FIPs. During this experiment, AP was kept constant at 20 bar. All experiments were carried out at fixed fuel injection quantity (10 mg/ cycle).
Figure 3 shows that higher FIP resulted in more evolved spray structure in shorter duration. Shortly after the fuel spray was fully developed, slight fluctuation in spray profile can be observed (at t= 1.2 sec). These fluctuations were due to breaking of fuel droplet clusters around the periphery of the fuel spray, with the maximum effect on the leading edge of the spray tip (Figure 3). Higher FIP improved the fuel droplet vaporization due to larger surface area of the relatively smaller fuel droplets of liquid. Ejim et al. [3] also reported that increasing FIP improved the evaporation of the spray droplets due to smaller Sauter mean diameter (SMD).

FIGURE 3. Effect of FIP on spray evolution at constant ambient pressure using mineral diesel in a CVSC

Higher FIP increased the mass flow rate which increased the diameter of fuel spray core. This caused deposition of smaller droplets within the upper canopy near the nozzle orifice. A considerable influence of higher FIP can be observed in Figure 3. Increasing FIP resulted in relatively longer spray penetration due to collapsing cavitation bubbles present inside the orifice. Spray penetration depends on the momentum of fuel droplets, droplet evaporation and fuel-air mixing.

Higher FIPs resulted in higher velocity of liquid fuel in the injector orifice, leading to effective fuel atomization. However, higher velocity of fuel resulted in higher momentum of fuel droplets, therefore longer spray penetration. The cavitation phenomenon was another important mechanism of fuel flow in the orifice, which resulted in longer penetration length at higher FIPs. Cavitation mechanism happened due to fluid acceleration, fluid directional changes and the pressure difference between FIP and the discharge pressure. Tendency of cavitation phenomenon diminished with decreasing FIP and consequently spray penetration length decreased. At lower FIPs, cavitation phenomenon inside the injector nozzle occurred in very small region and its effect on the penetration length was not significant. This was due to lower pressure difference between FIP and the discharge pressure. However, at very high FIPs, intensity of the cavitation inside the injector orifice increased drastically, which resulted in longer spray tip penetration length. At higher FIPs, spray cone angle reduced, which resulted in narrower sprays compared to lower FIP. Reduction in spray cone angle was mainly due to longer spray tip penetration length. In engines, higher FIP resulted in better fuel atomization, which improved fuel-air mixing. However, too high FIP led to spray impingement at piston bowl lip and cylinder liner. This spray impingement leads to relatively inferior engine performance and higher HC emissions. Therefore selection of suitable FIP for PCCI experiments is essential for satisfactory engine performance and emissions characteristics.

Effect of Ambient Pressure (AP)

Figure 4 shows the spray images of mineral diesel captured by high speed camera (frame rate = 10000 fps) at different APs (10, 20 and 30 bar). APs were selected on the basis of in-cylinder pressures at different SoI timings (pilot and main) in motoring condition. During this experiment, FIP was kept constant at 700 bar. All experiments were carried out for fixed fuel injection quantity (10 mg/ cycle).

Fast movement of air surrounding the dispersion of spray causes movement of spray penetration and prevents to reach its maximum tip penetration. Similar situation occurred in CVSC at higher AP conditions. Higher surrounding pressure caused the spray leaving the nozzle to disperse in a shorter spray tip penetration. Therefore, increasing AP inside the spray chamber increased the

density of air and affected the spray tip penetration as well. Spray images showed that increasing AP resulted in relatively shorter spray penetration length. Increasing spray cone angle with increasing AP was another important observation. Resistance offered by dense air was the main reason for this behavior. Overall, it can conclude that spray evolution was much superior at higher AP, which promoted the dispersion of fuel droplets. This ultimately resulted in improved fuel-air mixing in engines operated at high compression ratios.

FIGURE 4: Effect of ambient pressure on spray evolution at constant FIP using mineral diesel in CVSC

Effect of Fuel Composition

Figure 5 shows the spray images of mineral diesel, B20 and B40 captured by high speed camera (frame rate = 10000 fps) at constant AP (20 bar) and FIP (700 bar). All experiments were carried out for fixed fuel injection quantity (10 mg/ cycle).

Figure 5 showed the fuel properties played an important role in spray atomization, which included kinematic viscosity, density and surface tension. Due to higher kinematic viscosity and surface tension of biodiesel compared to mineral diesel, poor atomization was exhibited by biodiesel blends. This issue can be resolved by increasing FIP for biodiesel blends which resulted in higher breakup rate. Comparison of spray images of mineral diesel, B20 and B40 showed that the spray cone

angle of mineral diesel was the highest among all test fuels at 700 bar FIP and 20 bar ambient pressure. Spray cone angle decreased slightly when ratio of biodiesel was increased in test fuels.

Time (ms)	AP= 20 bar, FIP= 700 bar, Q_{fuel}= 10 mg/ cycle		
	Diesel	B20	B40
0.1			
0.2			
0.4			
0.8			
1.2			
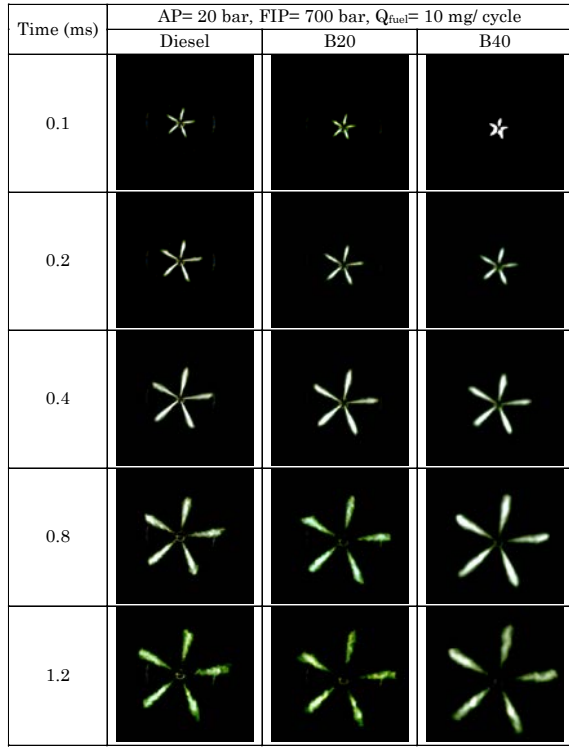
FIGURE 5: Comparison of spray evolution of mineral diesel, B20 and B40 at constant AP and FIP in CVSC

Large concentration of biodiesel in test fuels (high viscosity and density) resulted in relatively larger droplet size, which caused poor atomization. This resulted in longer spray penetration, therefore B20 and B40 showed narrower spray cone. Fuel with higher blending ratio of biodiesel (B40) showed a longer, denser potential core and quality spray pattern. This can be visualized in spray development as spray images of B40 showed relatively more whitish color compared to mineral diesel and B20. This was due to relatively high viscosity of fuel which resulted in larger SMD compare to lower biodiesel blended fuel (B20). The vortex shape spray of B20 and B40 with high viscosity was clearer than mineral diesel because the breakup frequency of viscous fuels were low. Lower break up rate of B20 and B40 produced larger droplet size and caused the spray pattern to become clearer compared to mineral diesel fuel. Comparison of spray images also revealed that for the same instant after the start of injection, B20 and B40 showed slightly retarded spray development compared to mineral diesel. This happened mainly due to delayed response of injector for viscous fuels like B20 and B40.

Effect of FIP and AP on Spray Parameters

In this investigation, three FIPs (400 bar, 700 bar and 1000 bar) were chosen to investigate the fuel spray macroscopic characteristics of mineral diesel, B20 and B40 at four APs (1 bar, 10 bar, 20 bar and 30 bar). All experiments were performed three times and average of the image post-processing results was presented. Figure 6 shows the comparison of three important fuel spray parameters namely spray penetration length, spray cone angle and spray area. Spray penetration length was calculated by joining a line from the tip of the injector orifice to the farthest point, where spray diminished. Results showed that spray penetration length increased with increasing FIP and this trend was followed by all test fuels. AP showed relatively weaker effect on spray tip penetration compared to FIP. Increasing AP decreased the spray length due to higher air resistance and led to wider spray cone angle. Since amount of fuel used for atomization process was considered constant, it was obvious that larger area of spray dispersion resulted in shorter spray length.
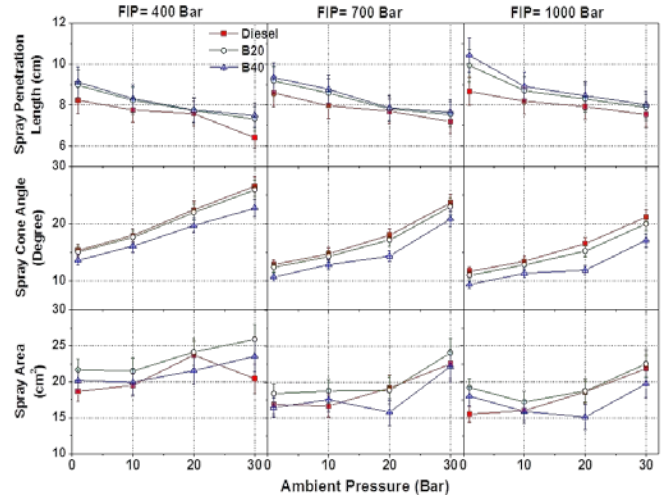
FIGURE 6: Spray penetration, spray cone angle and spray area at different FIPs and APs for mineral diesel, B20 and B40

Figure 6 shows that spray penetration of mineral diesel was the lowest at all APs. This was because of the lowest density and viscosity of mineral diesel amongst all test fuels, which resulted in rapid atomization of mineral diesel compared to other test fuels. Atomization was an important phenomenon in IC engines because it resulted in breakup of bulk liquid jets into small droplets. Adequate atomization of mineral diesel enhances fuel-air mixing and results in complete combustion in a DI diesel engine and therefore it significantly affects engine emission and performance characteristics. Viscosity also affected spray characteristics because it controlled both the formation of the continuous film immediately after exit from the injector nozzle and of the subsequent ligament disruption into individual droplets. In case of B20 and B40, viscous forces

decreased the rate of distortions in the liquid and reduced the rate of disruption of the droplets formed initially and finally increased the spray penetration length and final droplet size. Fuel density (specific gravity) and surface tension may be other factors behind the variation in fuel spray characteristics. Fuel density affected the spray compactness and penetration, however, its effect was not significant. Spray parameters showed a direct relationship with surface tension. Longer penetration length of B20 and B40 compared to mineral diesel was controlled by relatively higher surface tension of B20 and B40. Surface tension forces opposed the formation of distortion or irregularity on the surface of the continuous jet and delayed the formation of ligaments and the disintegration of the jet. From Figure 6, it can be observed that B20 and B40 showed narrower spray cone angle compared to mineral diesel and the spray cone angle decreased with increasing ratio of the biodiesel blend in test fuel. These factors in case of B20 and B40 spray resulted in slightly inferior fuel atomization compared to mineral diesel. Smaller spray cone angle for biodiesel blends during atomization process and higher FIP in IC engines led to higher NOx emission. It happened mainly due to spray impingement into high temperature region where abundance of oxygen readily oxidizes fuel and resulted in higher NOx. Spray area showed an irregular behavior at different FIPs and APs. This irregular behavior was attributed due to relative dominance of spray penetration length and spray cone angle. At most of the conditions, B20 showed maximum spray area however, B40 exhibited minimum spray area. With increasing FIP spray area of all test fuels decreased, which shows the dominance of spray penetration length over spray cone angle. Increasing AP resulted in higher spray area of mineral diesel and B20, however, spray area of B40 increased at 400 bar and decreased at higher FIPs. This happened mainly due to higher resistance offered at higher APs, which became more effective at higher FIPs. Higher AP applied in fuel atomization promoted the breakup of fuel particles into smaller size, which subsequently produced larger spray cone angle and spray width but shorter spray length with denser spray pattern.

CONCLUSIONS

Experimental results showed that B20 was the most ideal test fuel to substitute mineral diesel for engines. B20 has the fuel chemical properties very close to mineral diesel especially viscosity which directly influenced spray characteristic such as spray cone angle, spray width, spray penetration length and spray pattern. Relatively smaller droplets size of B20 compared to B40 provided larger surface area for fuel-air interaction and resulted in homogeneous fuel-air mixture. Narrow spray cone angle of B20 compared to mineral diesel during atomization increased spray impingement in the piston bowl, however, relatively longer spray penetration length of B40 may

result spray impingement outside of piston bowl and lead to relatively higher HC emissions.

REFERENCES

[1] Kim, HJ, Park, SH, Lee, CS, 2010, "A study on the macroscopic spray behavior and atomization characteristics of biodiesel and dimethyl ether sprays under increased ambient pressure" Fuel Processing Technology; 91:354-63.

[2] Goel H. Microscopic and Macroscopic Spray Characterization of Biodiesel in a Constant Volume Spray Chamber.Master's Thesis, IIT Kanpur, India, 2014.

[3] Ejim, C, Fleck, B, Amirfazli, A, 2007 "Analytical study for atomization of biodiesels and their blends in a typical injector: surface tension and viscosity effects. Fuel;86:1534-44.

SEEC-2017-23

A CHEMICAL KINETIC MODELING STUDY OF THE EFFECTS OF OXYGENATED SPECIES ON SOOT EMISSIONS FROM DIESEL ENGINES

Rohit Khare
Department of Mechanical Engineering
Indian Institute of Technology Madras
me15s089@smail.iitm.ac.in

V. Raghavan
Department of Mechanical Engineering
Indian Institute of Technology Madras
raghavan@iitm.ac.in

Krithika Narayanaswamy
Department of Mechanical Engineering
Indian Institute of Technology Madras
krithika@iitm.ac.in

ABSTRACT

The role of oxygenated hydrocarbons in reducing soot precursors from diesel engines is studied using a detailed chemical kinetic model. Since diesel is a complex mixture of several hundreds of hydrocarbons, it is represented by a surrogate made of n-dodecane and m-xylene, whose compo- sition is defined to match the threshold sooting index of the real fuel. Two oxygenates, namely methanol and dimethyl ether are considered, owing to their revelance as alterna- tive fuels. Our analysis reveals that oxygenates decrease the overall equivalence ratio of the mixture thus produc- ing higher ignition temperatures and more radical species to consume more soot precursor species, leading to lower soot production. These observations, which are in line with cur- rent understanding of the action of oxygenates on reduction of soot, are exemplified by a fundamental path flux analy- sis of the production and consumption routes of acetylene, which is the dominant soot precursor in this case.

Keywords: soot, oxygenates, diesel

NOMENCLATURE

  DME Dimethyl ether

INTRODUCTION

Emissions from automobiles, especially diesel engines, continue to be a serious environmental concern. Although a lot of work has been done on reducing emissions from diesel engines in the recent past, the emission norms have also been steadily tightened. To meet these strict regulations, fundamental knowledge about soot production is absolutely necessary. Different hydrocarbon fuels can produce differ- ent amounts of soot and altering the fuel composition can help in reducing soot production [1]. Methanol and DME are being increasingly investigated as additives to diesel fu- els for this purpose (for instance, Refs. [2]).

Methanol is a promising alternative fuel due to its advan- tages of low price and high oxygen fraction. It is consid- ered CO_2-neutral with regard to the greenhouse effect be- cause the same amounts of carbon dioxide (CO_2) and water (H_2O) that result from complete combustion are needed for the photosynthesis of plants from which they are produced. The global demand for methanol has increased steadily in re- cent decades because of its direct use as liquid fuel to power passenger cars and its role as feedstock for the production of DME, which is of interest as a potentially clean alternative to diesel fuel.

DME is a liquefied gas that can be produced from a vari- ety of feed stock, is non-toxic and environmentally benign. DME's main feature as an efficient alternative fuel for use in compression-ignition engines is its high cetane number (>55). It is as easy to handle as LPG since it is condensed by pressurizing above 0.5 MPa. The fast evaporation of DME can lead to better mixing with air in the engine cylinder and its high oxygen content can achieve smokeless combustion through low formation and high oxidation rates of particu- lates.

Many previous studies have shown that addition of oxy- genates to diesel fuel reduces the amount of soot pro- duced [1, 3, 4]. Miyamoto et al. [4] performed experi-

ments and found that soot emissions from diesel engines were reduced when oxygenated hydrocarbons were blended with diesel fuel. Litzinger et al. [5] combined experimental and kinetic modeling analysis of the soot-reducing effects of oxygenated species (i.e., ethanol and DME) on sooting laminar premixed and diffusion ethane-air and ethylene-air flames, and while these flames and fuel are quite distinct from diesel combustion, they provide valuable chemical insights into soot reduction chemistry.

The present work is a continuation of the previous work of Westbrook et al. [3]. In that study, detailed chemical kinetic modeling was used to study soot reduction in diesel engines by addition of oxygenates using n-heptane as a surrogate for diesel. In the present study, a similar analysis to that of Westbrook et al. [3] is performed, nonetheless, with a surrogate that is more representative of the sooting behaviour of the real diesel fuel. The objective of this study is to investigate (a) the importance of the fuel representation itself on the effectiveness of methanol and DME as additives to diesel fuel and (b) delineate the pathways producing and consuming soot precursors in the presence of these oxygenates quantitatively using a reaction path flux analysis.

MODELING APPROACH

The conceptual model for diesel combustion developed by Dec [6], describes the major chemical and physical steps that occur during diesel combustion. The important process which produces the soot precursor species is the fuel-rich premixed ignition, whose products cannot be oxidized completely, due to the absence of any more oxygen. These incompletely oxidized species such as CO, H_2 and small intermediate hydrocarbon species including acetylene, ethene, propene and others then react to produce soot. These small unsaturated hydrocarbon species have been identified as major contributors to soot production in diesel engines.

In this study, the rich, premixed diesel ignition is computed using a detailed chemical mechanism for the diesel fuel and the oxygenated species. The ignition calculation is carried out under conditions of pressure, temperature and fuel/air ratios that are characteristic of a diesel engine at the top of the piston stroke, as identified by Westbrook et al. [3].

To carry out these calculations, a surrogate approach is taken to represent the real diesel fuel. In the present study two different surrogates are considered for diesel fuel: (a) a mixture of 45% n-dodecane and 55% m-xylene (Surrogate A) and (b) a mixture of 73% n-dodecane and 27% α-methylnaphthalene (Surrogate B). The surrogates have been obtained by a constrained optimization approach [7] so as to match their sooting index with that of diesel fuel, since we are interested in the sooting characteristics of diesel fuel

combustion. Table 1 shows a comparison of the properties of the surrogates and that of the target diesel fuel.

TABLE 1: Properties of diesel fuel and surrogates.

Property Name	Diesel Fuel	Surrogate A	Surrogate B
Threshold Sooting Index	29	28.15	29
Cetane Number	45–50 [8]	54	69
H/C	1.93 [8]	1.75	1.85
Liquid density (kg/l)	0.840 [8]	0.791	0.795

The simulations are performed in a constant pressure, spatially homogeneous environment, effectively decoupling the ignition process from the rest of the combustion chamber. The initial temperature is 767 K, φ = 3.0 and the combustion chamber pressure is assumed to be 10 MPa, following the same conditions as that of Westbrook et al. [3].

Reaction Kinetics

A single reaction mechanism is obtained for both the surrogates using a component library framework [7]. The kinetic scheme consists of around 250 species and about 1400 reactions. The kinetics of methanol and dimethyl ether are derived from the San Diego mechanism [9]. The mechanisms for the surrogates and the oxygenates are combined using an interactive tool [10]. The combined mechanism is tested for the kinetic description of n-dodecane, m-xylene, α-methylnaphthalene (which constitutes the surrogates), as well as methanol and DME and verified to result in similar performance as the reference mechanisms [9, 11].

COMPUTATIONAL RESULTS DISCUSSION

Relevance Of Threshold Sooting Index As A Target For Surrogate Definition

To investigate the importance of TSI as a target in surrogate definition, the rich premixed ignition of surrogate/air mixtures are simulated at φ = 3, T = 767K, and P = 10MPa using both surrogates in the absence of any oxygenates. Concentrations of the important soot precursor species are plotted for both the surrogates in Fig. 1. As can be observed, the concentration of all the soot precursor species are similar between the two surrogates. This in turn suggests that the surrogates and the real fuel, having nearly the same value of TSI, are likely to have similar amounts of soot precursors in the reactive pool from the rich premixed ignition. In the remainder of the study, surrogate A (Table 1), comprised of n-dodecane and m-xylene is used to represent the diesel fuel.

Effect Of Addition Of Oxygenates

The above calculations are repeated for cases in which the surrogate fuel is replaced gradually with increasing amounts
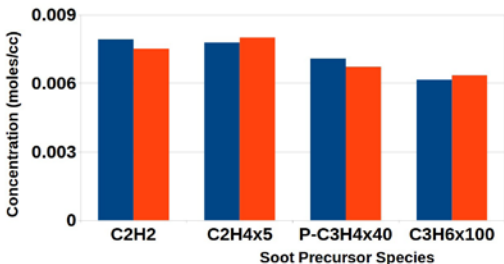
FIGURE 1: Concentrations of soot precursor species obtained with surrogate A (blue bar) and surrogate B (red bar), calculated at an initial temperature of 767K, $\varphi = 3$ and P = 10MPa.

of methanol and DME separately. As shown in Fig. 2, just as the surrogate is increasingly replaced by oxygenate, the soot precursor level continues to decrease and becomes insignificant when the oxygen content has reached about 30% of the total mass of the fuel mixture, containing *n*-dodecane and *m*-xylene and the oxygenate (methanol or DME). This no soot condition corresponds to a fuel mixture containing 14% surrogate A + 86% methanol and 12% surrogate A + 88% DME, respectively.

It is interesting to note that the oxygen content in the fuel mixture needed to achieve negligible soot precursor in this work is similar to the finding reported by the previous study of Westbrook et al. [3] (30% by mass), who neglected the aromatic fraction in diesels, by using *n*-heptane as a surrogate. Further analysis is warranted to make conclusive remarks here, since the reaction mechanisms used in these two studies are significantly different in terms of their soot precursor chemistry descriptions.
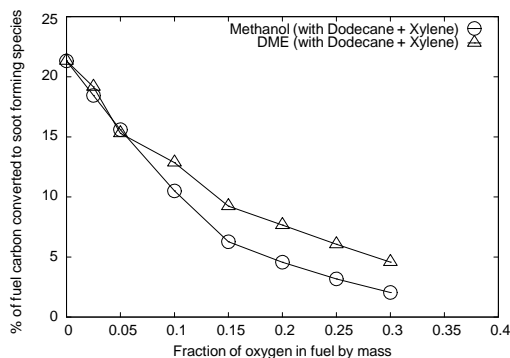
FIGURE 2: Effect of addition of oxygenated species on soot forming species (acetylene, ethene, propene, allene, propyne, cyclopentadiene, propargyl, allyl, cyclopentadienyl, benzene, naphthalene, pyrene)

Reaction Flux Analysis

To understand the change in reaction dynamics concerning soot precursor formation and consumption due to the addition of oxygenates, a path flux analysis is performed here for the case of methanol addition. Since acetylene is the major soot precursor, a flux analysis is performed for this species with two different fuel compostions (a) surrogate A, i.e. containing *n*-dodecane + *m*-xylene (baseline case) and (b) 14% surrogate A + 86% methanol by moles (no soot case). The contribution of different pathways to the production and consumption of acetylene is summarized in Fig. 3 for the two cases. Figure 3 clearly depicts that at the no soot condition, more than 85% of acetylene is consumed by reactions with O and OH whereas for the baseline case, most of the acetylene forms vinyl radical (C_2H_3), cyclopentadiene (C_5H_6), and phenyl acetylene ($A_1C_2H_2$), which in turn leads to formation of additional soot precursors and polycyclic aromatic hydrocarbons. Figure 4 further shows that with the addition of oxygenates to the fuel and the corresponding leaner fuel/air mixture ratios, there is a raise in peak temperatures as well as the amounts of radicals (O, OH, H etc.). This increased amounts of radicals now contribute to consuming soot precursor species, such as acetylene, as indicated in the flux analysis presented in Fig. 3.

CONCLUSION

Present study indicates that when significant fractions of diesel fuel are replaced by oxygenated hydrocarbons, the soot precursor levels are reduced to insignificant amounts. But since the fractions of oxygenates required to completely eliminate soot precursor formation are so large, approaching 75–80%, it is practically impossible to attempt this degree of fuel modification in actual diesel engine, nevertheless, this gives valuable insights into the processes leading to soot mitigation.

Our study with the surrogate defined to match the sooting index of the real fuel shows similar results as compared to the work of Westbrook et al. [3], who neglected the aromatic fraction in diesels. However further analysis is needed to make conclusive remarks, since the reaction mechanisms used in these two studies are significantly different in terms of their description of soot precursor kinetics.

Surrogate A

(a) Baseline case

14% surrogate A + 86% methanol

(b) No soot case
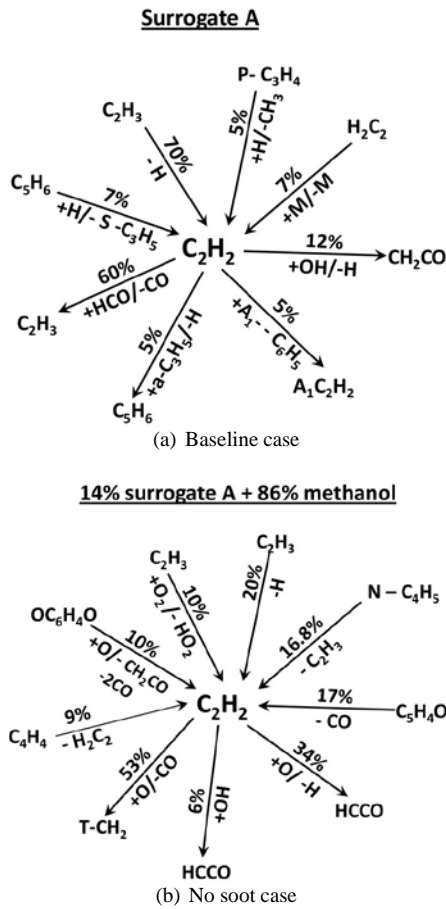
FIGURE 3: Reaction flux analysis for acetylene showing the most significant pathways of production and consumption.
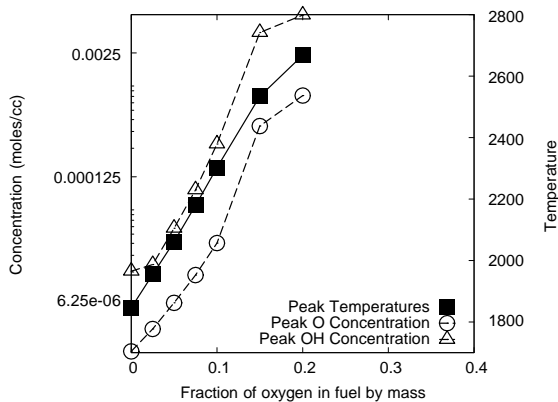
FIGURE 4: Effect of addition of oxygenated species on maximum temperature, peak values of radicals (O, OH).

REFERENCES

[1] K. Nakakita, K. Akihama, W. Weissman, and J. T. Farrell. Effect of the hydrocarbon molecular structure in diesel fuel on the *in*-cylinder soot formation and exhaust emissions. International Journal of Engine Research, 6(3):187–205, 2005.

[2] C. Yao, C. S. Cheung, C. Cheng, Y. Wang, T. L. Chan, and S. C. Lee. Effect of diesel/methanol compound combustion on diesel engine combustion and emissions. Energy conversion and management, 49(6):1696–1704, 2008.

[3] C. K. Westbrook, W. J. Pitz, and H. J. Curran. Chemical kinetic modeling study of the effects of oxygenated hydrocarbons on soot emissions from diesel engines. Journal of Physical Chemistry A, 110(21):6912–6922, 2006.

[4] N. Miyamoto, H. Ogawa, N. Nurun, K. Obata, and T. Arima. Smokeless, low NO_x, high thermal efficiency, and low noise diesel combustion with oxygenated agents as main fuel. Technical report, SAE technical paper, 1998.

[5] K. Song, P. Nag, T. A. Litzinger, and D. C. Haworth. Effects of oxygenated additives on aromatic species in fuel-rich, premixed ethane combustion: a modeling study. Combustion and Flame, 135(3):341–349, 2003.

[6] J. E. Dec. A conceptual model of DI diesel combustion based on laser-sheet imaging. SAE, (412):970873, 1997.

[7] K. Narayanaswamy, H. Pitsch, and P. Pepiot. A co*m*ponent library framework for deriving kinetic mechanisms for multi-component fuel surrogates: Application for jet fuel surrogates. Combustion and Flame, 165:288–309, 2016.

[8] C. Arcoumanis, C. Bae, R. Crookes, and E. Kinoshita. The potential of di-methyl ether (dme) as an alternative fuel for compressio*n*-ignition engines: A review. Fuel, 87(7):1014–1030, 2008.

[9] San Diego Mechanism web page. Chemical-kinetic mechanisms for combustion applications, version 2014-10-04. Mechanical and Aerospace Engineering (Combustion Research), University of California at San Diego. Available at http://web.eng.ucsd.edu/mae/groups/combustion/mechanism.html.

[10] P. Pepiot. Automatic strategies to model transportation fuel surrogates. PhD thesis, Stanford University, 2008.

[11] K. Narayanaswamy, P. Pepiot, and H. Pitsch. A che*m*ical mechanism for low to high temperature oxidation of *n*-dodecane as a component of transportation fuel surrogates. Combustion and Flame, 161(4):866–884, 2014.

COMBUSTION AND NOISE CHARACTERISTICS OF ETHNAOL/ DIESEL BLENDS IN A DIESEL GENSET ENGINE

Dev Prakash Satsangi
Department of Mechanical Engineering
Indian Institute of Technology Kanpur
Email: satsangi@iitk.ac.in

Nachiketa Tiwari
Department of Mechanical Engineering
Indian Institute of Technology Kanpur
Email: ntiwari@iitk.ac.in

Avinash kumar Agarwal
Department of Mechanical Engineering
Indian Institute of Technology Kanpur
Email: akag@iitk.ac.in

ABSTRACT

Currently, over 30% of India's electricity needs are met by diesel based genset engines. These engines are noisy and vibrate excessively. Fuel composition has a direct effect on combustion phenomena of diesel engines. Combustion process is the source of mechanical impacts and cylinder pressure fluctuations which in turn are responsible for engine's noise and vibration. The alternative fuels have to be evaluated for noise and vibration in addition to their engine performance and emissions. Towards this goal, a comprehensive study of different diesohol (ethanol-diesel) fuels has been conducted. Comprehensive experimental investigations have been conducted on a direct injection diesel genset-engine to analyze noise, vibrations and combustion, characteristics when fuelled on ethanol-diesel blends. The genset was operated at fixed engine speed of 1500 RPM, and tests were conducted at six different loads. Results show correlation between specific combustion parameters like heat release rate, rate of pressure rise with noise and vibration characteristics. The technological viability of using such blended fuels for genset applications has also been explained.

Keywords: A-Weighting noise (dBA), 1/3rd octave band, Compression ignition engine, Engine vibrations, Fast Fourier Transform (FFT).

INTRODUCTION

Diesel engines are widely used in areas of agriculture, transportation, and industries. The contribution of diesel vehicles to environmental pollution is increasing due to their increasing demand. Stationary diesel engines conventionally use diesel as a fuel. Alcohols can also be used as a fuel in unmodified engines or engines with minimal modifications [1-3]. Uludamar et al. [4] have experimentally investigated noise and vibrations in an unmodified diesel engine using different biodiesel blends. They conducted regression analysis of linear and non-linear models to predict the relationship between fuel properties with noise and vibration characteristics of the diesel engine. They found a reduction in vibrations of engine block using biodiesel in CI engine due to role of inherent oxygen in the fuel. Patel et al. [5] investigated combustion noise and vibrations in a direct injected CI engine using karanja-biodiesel blends and diesel fuel. They observed similarity between heat release rate, combustion noise and vibration. They reported the effect of calorific value, oxygen content and viscosity of blends on engine noise. Taghizadeh-Alisaraei et al. [6] conducted experiments on diesel engine using canola and soybean biodiesel blends and observed lower vibration for diesel fuel compare to biodiesel.

Air and noise pollution, both are responsible for serious health issues related to cardiovascular, respiratory

and hearing loss. Increasing global concerns over these hazardous pollution issues and rapid depletion of petroleum reserves forces search of clean and sustainable alternative form of energy sources. Fuels such as alcohols, biodiesels and ethers are being increasingly investigated due to their potential capability to reduce environmental pollution. A significant amount of research work has been conducted on the combustion, but not many researchers reported on noise and vibration characteristics of internal combustion engines. Present research involves preparation of diesel-ethanol blends their utilization in genset engines, and studies on noise and vibrations for such fuels.

EXPERIMENTAL SETUP AND METHODOLOGY

Current research involves a vertical, single cylinder, water-cooled, 4-stroke, direct injection diesel genset. It has a capacity of 7.4 KVA, with rated 1500 RPM. The schematic of the complete experimental setup is shown in Figure 1.
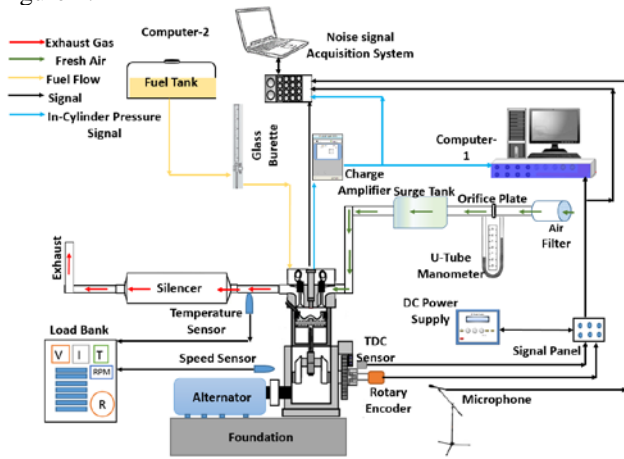
Figure 1. Schematic of experimental set-up

In-cylinder pressure signal was acquired using a piezoelectric pressure transducer along with information of crank angle rotation. This in-cylinder pressure together with crank rotation information was used to calculate rate of pressure rise and combustion noise. Total engine noise was measured as per ISO 9614-2 using a microphone. Experiments were conducted at 1500 RPM, injection pressure of 20 MPa and at six engine loads, i.e., from 0% to 100% in steps of 20%. In-cylinder pressure signal was acquired for 250 cycles to minimize cyclic variations.

Test Fuel Preparation and their Characterization

Blends of alcohol and diesel are referred as "Diesohol". Co-solvent, 1-Dodecanol was used to avoid phase separation between ethanol and diesel blends. Fuel blends were prepared on the basis of their oxygen content represented by numerical digit. Test fuel's properties are shown in Table 1.

TABLE 1: Test Fuel Characterization

Test fuel	Density (kg/m^3@30°C)	Kinematic Viscosity (m^2/s@40°C)	Calorific value (MJ/kg)
Diesel	828	2.89e-6	43.86
DEDOD1	826	2.61e-6	43.56
DEDOD2	824	2.67e-6	42.81
DEDOD3	823	2.81e-6	42.71

RESULTS AND DISCUSSION

Combustion

Rate of pressure rise (ROPR) is derivative of in-cylinder pressure w.r.t. crank angle rotation. The amount of combustible fuel accumulated during ignition delay period when burns during pre-mixed combustion phase leads to ROPR [7]. Figure 2 shows variation of ROPR for test fuels w.r.t. engine load.
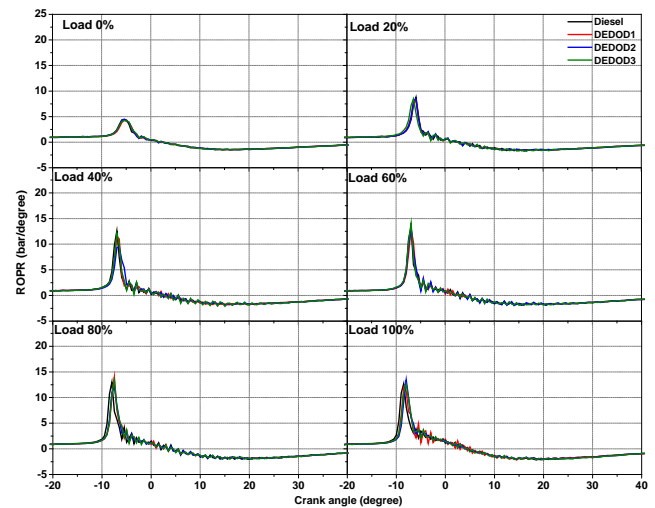
Figure 2. ROPR w.r.t. CAD at different engine loads

ROPR varies between -10 to 0 CAD with its amplitude between ~3.6 to 13.5 bar/degree. ROPR$_{max}$ for all test fuels observed in pre-mixed combustion region.

Noise

Figure 3 shows generated combustion noise due to ignition of fuel and which leads to ROPR. Post processing of in-cylinder signal was filtered for 1/3rd octave band with Lucas structural attenuation decay filter [8]. The combustion noise level was observed in the range of 77 to 90 dBA for all test fuels. Diesohol shows reduction of ~ 0.1 to 3.5 dBA in combustion noise up to 60% engine load and thereafter these diesohol shows higher combustion

noise compared to diesel fuel. It was due to the dominant role of oxygen at higher loads.
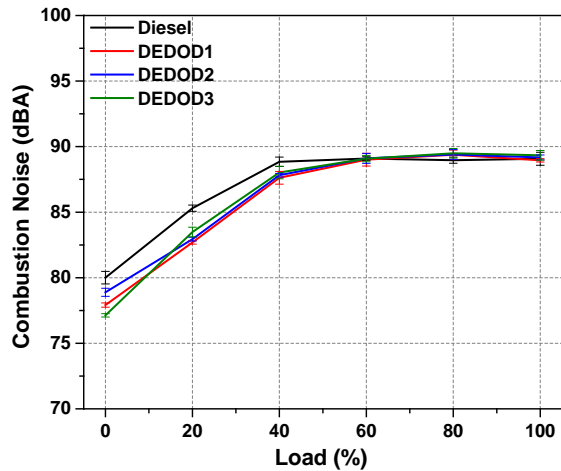
Figure 3. Combuastion noise variation at different engine loads

Total engine noise is shown in Figure 4. It comprises of combustion, mechanical and ambient noises. Total engine noise was observed higher compare to combustion noise. Test fuel DEDOD3 generates the least amount of total engine noise among diesohol while DEDOD1 produces highest.
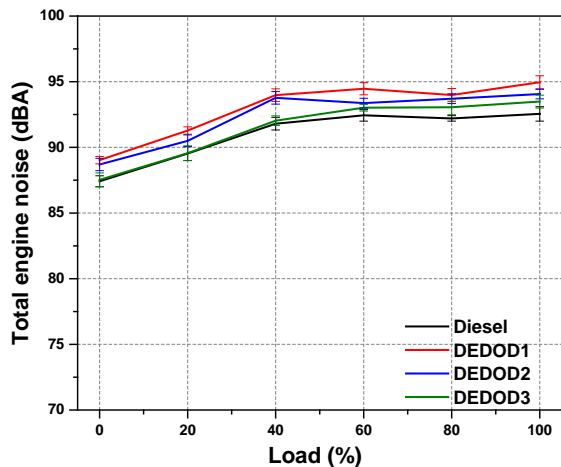
Figure 4. Total engine noise variation at different engine loads

CONCULSIONS

Combustion phenomena and emitted noise analysis of three diesohol were compared to diesel fuel in a diesel genset. DEDOD3 blend shows a maximum reduction of combustion noise (~ 3.0 dBA) at no load condition. All diesohol blend shows reduction of combustion noise up to 60% engine load. However, after 60% engine load, combustion noise was observed slightly more for diesohol compared to diesel fuel. This was due to the effect of inherent oxygen of diesohol which play an important role at higher in-cylinder temperature.

Frequency spectrum analysis of total noise shows its peak value at central frequency of 2000 Hz in 1/3rd octave bands. This was due to high stiffness of engine components. Frequency of resonance in total noise, suggest dominant behaviour of 12.5 (combustion cyclicity) and 25 Hz (engine speed) with their harmonics. Combustion noise and $ROPR_{max}$ correlated well with each other.

REFERENCES

[1] Agarwal, AK. "Biofuels (alcohols and biodiesel) applications as fuels for internal combustion engines." Progress in energy and combustion science, 2007; 33(3) ;233-271.

[2] Sharma A, Murugan S. "Combustion, performance and emission characteristics of a DI diesel engine fuelled with non-petroleum fuel: a study on the role of fuel injection timing". J Energy Inst 2014;88:364-75.

[3] Muthukumaran N, Saravanan CG, Prasanna Raj Yadav S, Vallinayagam R, Vedharaj S, Roberts WL. "Synthesis of cracked Calophyllum inophyllum oil using fly ash catalyst for diesel engine application". Fuel 2015;155:68-76.

[4] Erinç, U., Tosun, E., and Aydın, K. "Experimental and regression analysis of noise and vibration of a compression ignition engine fuelled with various biodiesels." Fuel, 2016 ;177: 326-333.

[5] Patel, C., Agarwal AK., Tiwari, N., Lee, S., Lee, CS., Park, S. "Combustion, Noise, Vibrations and Spray Characterization for Karanja Biodiesel Fuelled Engine." Applied Thermal Engineering ,2016;106:506-517.

[6] Taghizadeh-Alisaraei, A. and Rezaei-Asl, A., "The effect of added ethanol to diesel fuel on performance, vibration, combustion and knocking of a CI engine". Fuel,2016 185, 718-733.

[7] Taghizadeh-Alisaraei, A, Ghobadian, B., Tavakoli-Hashjin, T., Mohtasebi, SS. "Vibration analysis of a diesel engine using biodiesel and petrodiesel fuel blends" Fuel,2012 ;102 : 414-422.

[8] Söderberg, A. "Definition of structural attenuation from engine block using loudspeaker tests and acoustic camera." 2013.

SEEC-2017-27

DROPLET SIZE AND VELOCITY MEASUREMENT OF KARANJA BIODIESEL SPRAYS

Chetankumar Patel
Department of Mechanical Engineering
Indian Institute of Technology, Kanpur
Email: chetanp@iitk.ac.in

Nikhil Sharma
Department of Mechanical Engineering
Indian Institute of Technology, Kanpur
Email: snikhil@iitk.ac.in

Nachiketa Tiwari
Department of Mechanical Engineering
Indian Institute of Technology, Kanpur
Email: ntiwari@iitk.ac.in

Avinash Kumar Agarwal
Department of Mechanical Engineering
Indian Institute of Technology, Kanpur
Email: akag@iitk.ac.in

ABSTRACT
Diesel engines are widely employed over small to large size ranges of vehicles. These are mostly used in fields of agriculture, construction, and power generation. Biodiesel from non-edible oils such as Karanja can be used as an alternative fuel without major modifications to the engine hardware. Fuel atomization is largely influences by higher viscosity of biodiesel. In the present work droplet size and velocity investigations were conducted to understand spray behavior of the biodiesel. The investigation was conducted to measure spray droplet's sauter mean diameter (SMD), droplet velocity and its variation with respect to time at lower injection pressure of 200 bar at atmospheric condition for Karanja biodiesel (KB100) and mineral diesel. Higher SMD and slightly lower velocity were observed for KB100 vis-à-vis baseline mineral diesel.

Keywords: Sauter Mean Diameter (SMD), Karanja biodiesel (KB100), Fuel Sprays.

INTRODUCTION
Biodiesel from non-edible vegetable oils has emerged as a strong alternative which could replace diesel in near future. Biodiesel possess higher viscosity, and density which largely affects fuel injection characteristics and ultimately affects fuel spray atomization. Engine emissions are largely depend on the fuel atomization. Microscopic and Macroscopic spray investigations have drawn large attention of researchers in last few decades, which have helped to understand the behavior of fuels in the combustion chamber.

Agarwal et al. [1] reported that cavitation, turbulence and velocity of the fuel at the nozzle exit are critical parameters for spray atomization. These parameters influence fuel atomization characteristics. Som et al. [2] investigate biodiesel and diesel flow in the injector and observed that biodiesel cavitate less compared to mineral diesel because of its low vapour pressure. They also found that higher viscosity of biodiesel results in reduction of the injection velocity. Faria et al. [3] observed that increasing biodiesel content in the biodiesel/diesel blend results into reduction of spray atomization quality. They also observed that higher average sauter mean diameter (SMD) results into reduction of mass transfer during combustion process. Chong and Hochgreb [4] reported reduction of spray droplet sizes of Jet A-1 fuel compared to Rapeseed Methyl Ester (RME) by 23%. This was reported due to lower viscosity and higher volatility of JET A-1 fuel, which promote spray vaporization. Gao et al. [5] reported higher SMD of non-edible oil based biodiesel blends due to higher viscosity and surface tension compared to conventional diesel. Kim et al. [6] investigated the effects of DME blending with biodiesel on the SMD. They reported that droplet size of DME blended biodiesel was similar to that of diesel, regardless of fuel injection pressure.

The investigations were carried out to measure spray droplet size and velocity distributions of mineral diesel and Karanja biodiesel at atmospheric conditions and 40 mm downstream to the fuel injector.

EXPERIMENTAL SETUP AND METHODOLOGY

Droplet size and velocity distributions were measured by Phase Doppler Interferometry (PDI) instrument (Figure 1a). Spray measurement direction are shown in Figure 1b.

Table 1: Properties of test fuels

Test fuel	Calorific value (MJ/kg)	Density (g/cm^3)	Kinematic Viscosity @ 40°C (cSt)
Mineral Diesel	43.22	0.820	2.67
KB100	40.34	0.886	5.74
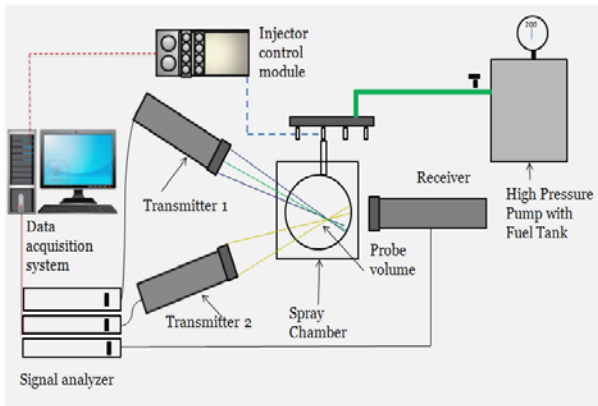
Figure 1a. Schematic of experimental setup for microscopic spray characterization using PDI
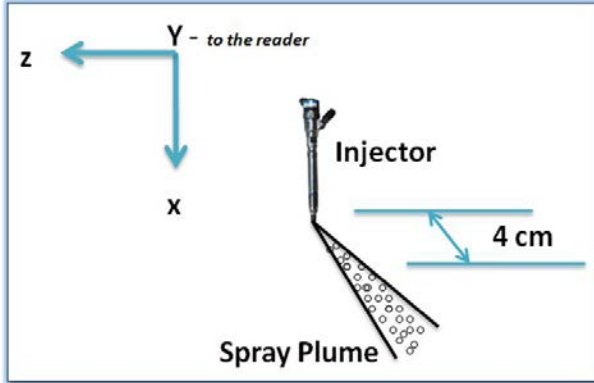
Figure 1b: Spray measurement direction for test fuel

Spray droplet velocity directions are indiated as X, Y and Z (Figure 1b). Table 1 shows properties of the test fuels. PDI experimental set up consists of two transmitters (1 and 2), a receiver, three advanced signal analyzers and the processing software. Three diode pump solid state (DPSS) lasers are used in the PDI experiment. Transmitter 1 emits two lasers, green (532 nm) and blue (491 nm); while transmitter 2 emits yellow laser (561 nm). A beam splitter splits each of the laser beams into two beams of nearly equal intensity and a grating is used for creating a slight phase shift in these two beams of the same wavelength. These six laser beams were then carefully aligned to meet at a single point, which is called 'Probe volume'. Alternate dark and bright fringes develop in the probe volume, where two laser beams of same wavelength with same phase shift intersect. When a spray droplet passes through the probe volume, changes in phase difference and frequency variations are observed. The changes in frequency are directly proportional to droplet velocity components, while the phase difference is directly proportional to the droplet diameter. A solenoid injector injected the fuel spray in a constant volume spray chamber (CVSC) and the injector was controlled by an injector driver module (NI; 9411). Fuel was pressurized by a pneumatic high pressure fuel pump (Maximator) and then supplied to the injector via high pressure pipe lines. Investigations were carried out 40 mm downstream of the injector nozzle under atmospheric conditions. This investigation was carried out at lower fuel injection pressure of 200 bar (typical of mechanical fuel injection systems) with varying fuel injection quantities (12 to 32 mg/ injection). Only one of the holes of the injector was used for generating spray plume. Other nozzle holes were covered by a customized cap.

RESULTS AND DISCUSSION:

Microscopic spray investigations were carried out for diesel and Karanja biodiesel by varying fuel injection quantities (i.e., 12, 16, 20, 24, 28, 32 mg). The results of SMD, droplet size distribution, velocity distributions in different directions were experimentally determined.

Sauter Mean Diameter (SMD)

Droplet size and droplet velocity distribution plays an important role in fuel spray atomization, mixing of fuel- air and resulting into combustion and emissions characteristics of an internal combustion engine.
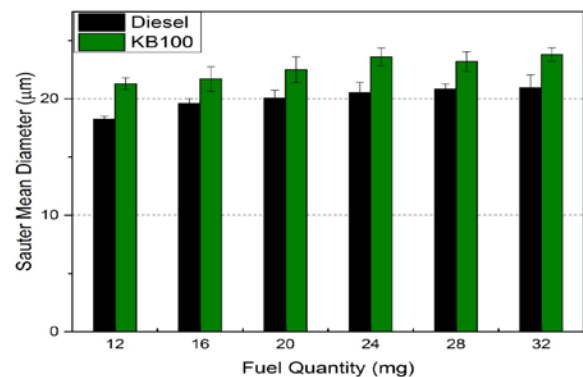
Figure 2: Variation of droplet SMD's of test fuels at different injection quantities

Figure 2 shows SMD of Karanja biodiesel and baseline mineral diesel. Figure 3 shows SMD variations w.r.t. time at different fuel injection quantities. It was observed that SMD of biodiesel was relatively higher than

baseline mineral diesel for all fuel injection quantities. Karanja Biodiesel also showed higher SMD after energizing of solenoid injector w.r.t. time. Higher SMD of the biodiesel was observed primarily due to relatively higher fuel viscosity and surface tension in case of biodiesel, which affected spray breakup and spray evolution after the fuel injection. Higher viscosity also resulted in higher van-der-wall forces among the biodiesel fuel molecules, which led to larger droplet size distributions.
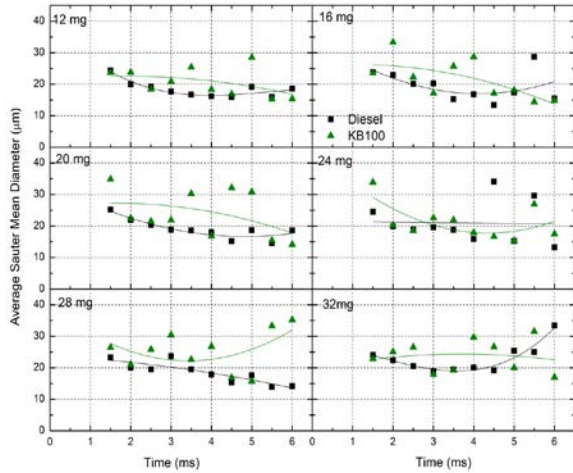
Figure 3: Average SMD variations w.r.t. time for varying fuel quantities

Droplet Velocity Distribution

Figure 4 shows the average droplet velocity variations in X-direction for varying fuel quantity per injection. Maximum average velocity was observed to be ~60 m/s for both test fuels.
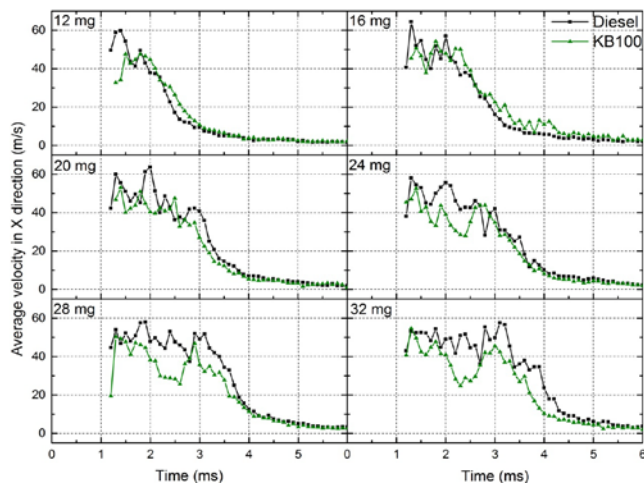
Figure 4: Average spray droplet velocity variations in X-direction for 12 to 32 mg fuel per injection

There were no significant difference observed in average velocity of the Karanja biodiesel and diesel droplets at lower fuel injection quantities (i.e., 12 and 16 mg/injection). Slightly lower average droplet velocity was observed for Karanja biodiesel for higher fuel quantities of 20, 24, 28 and 32 mg per injection. This may be due to the reduction of injection velocity at the exit of the nozzle for biodiesel fuel due to higher aerodynamic drag, which is observed due to larger droplet sizes [2].

Figure 5 shows the average droplet velocity variations in Y-direction. Average velocity in Y-direction showed trends similar to X-direction but with reduction of maximum velocity. Diesel droplets exhibits maximum velocity in the range of ~30-40 m/s however, it was ~25-30 m/s for KB100.
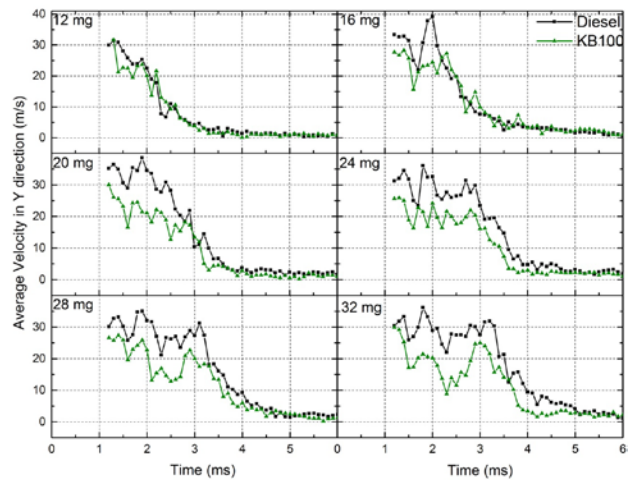
Figure 5: Average spray droplet velocity variations in Y-direction for 12 to 32 mg fuel per injection
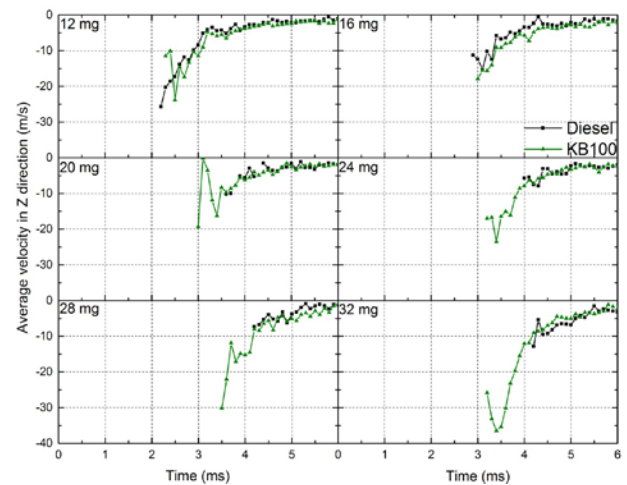
Figure 6: Average spray droplet velocity variations in Z-direction for 12 to 32 mg fuel per injection

Figure 6 shows maximum average droplet velocity which ranges from ~20 to 30 m/s irrespective of test fuels or fuel injection qunaity. These spray investigations were followed by performance and emission characteristics of biodiesel w.r.t. baseline mineral diesel.

CONCULSIONS

In current study microscopic spray investigations were carried out to measure droplet size distribution and droplet velocity distribution in different directions when varying fuel injection quantities of Karanja biodiesel w.r.t. diesel. Conclusions from these experiments are as follows:

1. SMD and SMD distributions were relatively higher for biodiesel compared to baseline mineral diesel, due to the effect of higher viscosity and surface tension of KB100.
2. Average spray droplet velocities were similar for both test fuels at lower fuel injection quantities of 12 and 16 mg in X and Y-directions. It slightly decreased for KB100 for higher fuel injection quantities of 20, 24, 28 and 32 mg.
3. Droplet velocity variations in Z direction were lower because majority of the spray zone was in X and Y direction.

REFERENCES

[1] Agarwal, A.K., Som, S., Shukla, P.C., Goyal, H. and Longman, D., In-nozzle flow and spray characteristics for mineral diesel, Karanja, and Jatropha biodiesels. *Applied Energy*, 156:138-148(2015).
[2] Som, S., Longman, D.E., Ramírez, A.I. and Aggarwal, S.K., A comparison of injector flow and spray characteristics of biodiesel with petrodiesel. *Fuel*, 89(12):4014-4024(2010).
[3] Faria, M.D.C., Valle, M.L.M. and Pinto, R.R.D.C. "The influence of physico-chemical properties of diesel/biodiesel mixtures on atomization quality in diesel direct injection engines" .SAE technical paper 2005-01-4154
[4] Chong, C.T. and Hochgreb, S., Spray flame structure of rapeseed biodiesel and Jet-A1 fuel. *Fuel*, 115:551-558(2014).
[5] Gao, Y., Deng, J., Li, C., Dang, F., Liao, Z., Wu, Z. and Li, L., Experimental study of the spray characteristics of biodiesel based on inedible oil *Biotechnology Advances,* 27(5):616-624(2009).
[6] Kim, I., Hyun, G., Goto, S. and Ehara, R., Spray Characteristics of DMEBlended Biodiesel Oil. SAE Technical Paper 2001-01-3636.

SEEC-2017-28

EFFECTS OF COMBUSTION ON NOISE AND VIBRATIONS IN BIOFUELLED ENGINE

Chetankumar Patel
Department of Mechanical Engineering
IIT Kanpur
Email: chetanp@iitk.ac.in

Nachiketa Tiwari
Department of Mechanical Engineering
IIT Kanpur
Email: ntiwari@iitk.ac.in

Avinash kumar Agarwal
Department of Mechanical Engineering
IIT Kanpur
Email: akag@iitk.ac.in

ABSTRACT

Noise and vibration characteristics of engines are largely affected by combustion.In this study, experiments were carried out to investigate the effects of Soybean biofuel and its blends with diesel on engine combustion and its subsequent effects on noise, vibrations in a single cylinder genset engine. It was observed that combustion characteristics like HRR_{max} of the test fuels correlated well with combustion noise, exhaust noise and vibrations in vertical direction.

*Keywords***:** Soybean biofuels, combustion investigations, noise investigations, vibration investigations

NOMENCLATURE

dB(A)	A-weighting noise
HRR_{max}	Maxiumu heat rease rate
SB100	Soybean biodiesel
SB20	20% blends of soybean biodiesel with diesel
g	Acceleration

INTRODUCTION

Compression ignition engines are mainly depends on mineral diesel as a fuel.However, many researchers investigated various liquid alternative fuels and its blends to assessed the performance, combustion and emission characteristics. However, few researchers investigated its effects on noise and vibration.Vegetable oils are easily available alternative liquid fuels which can be utilized for CI engines. However, high viscosity of vegetable oil makes it difficult to use it directly in the internal combustion engines. There are four ways to use the vegetable oil directly in the engine. These are direct use and blending, micro-emulsion, pyrolysis and trasnesterification [1]. Noise investigation carried lot of attention of researchers in past decade as it has severe health effects. Taghizadeh-Alisarai et al.[2] investigated six fuel blends B20, B40, B60, B80, pure biodiesel (B100) and pure petrodiesel (D100) on two different four stroke diesel engines (a single cylinder engine and a six- cylinder engine). They observed higher vibrations with B40 and B20 while lower vibrations observed with D100 and B80 fuel blends. Patel et al. [3,4] conducted investigations on single cylinder gen-set engine by using Karanja and Jatropha biodiesel as a fuel. They observed that heat release rate variations were directly proportional to the combustion noise and vibration. Uldumar et al. [5] investigated vibration and noise characteristics on unmodified four stroke four cylinder compression ignition engine fuelled by 20% and 40% v/v ratio of sunflower canola and corn biodiesel. They observed decrease in engine block vibration with biodiesel blends. They also observed slight decrease in sound pressure level dB (A) by using biodiesel blends. Tagahizadeh-Alisaraei and Rezaei-Asl [6] observed 4.79% increase in engine body vibration with 6% addition of bioethanol in diesel fuel. They argued that these variations were due to the cylinder pressure variations and inertia of components. Giakoumis et al. [7] stated that higher combustion noise was the result of higher peak in the premixed combustion phase. Agarwal and Dhar [8] observed lower peak heat release rate in premixed

combustion phase for Karanja oil and its blends with diesel. In this study, experiments were performed to understand the effect of biofuels combustion on noise and vibration characteristics. Biofuels for this investigation were Soybean biodiesel(SB100), 20% blends of soybean and Rapseed biodiesel with diesel(SB20) and 20% blends of soybean and Rapseed vegetable oil with diesel(S20). Experimental results for these biofuels compared with mineral diesel.

EXPERIMENTAL SETUP AND METHODOLOGY
This engine investigation was carried out on a single cylinder compression ignition (CI) genset engine and it was controlled by generator control panel which consists of load bank, voltmeter, and ammeter. Table 1 shows the important properties of test fuels and Figure 1 shows the engine experimental set up used for this investigation.

Table 1: Important properties of test fuels

Test Fuel	Calorific value (MJ/kg)	Density (g/cm³)	Kinematic Viscosity @ 40°C(cSt)
Mineral Diesel	43.07	0.82	2.71
S20	42.73077	0.83687	4.17333
SB20	42.7089	0.82333	3.14333
SB100	41.34693	0.87333	4.55333
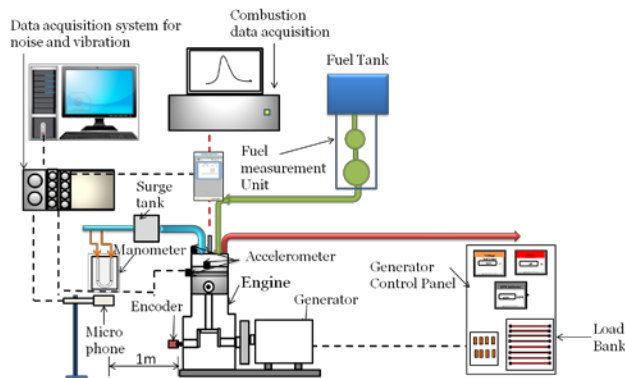
FIGURE 1. SCHEMATIC FOR ENGINE COMBUSTION, NOISE & VIBRATIONS CHARACTERIZATION

Piezoelectric pressure transducer (Kistler; 6613CQ09-01) was used to measure the combustion pressure inside the engine cylinder. Charge amplifier (Kistler; 5015) was utilized to amplify the signals acquired by pressure transducer. Shaft encoder (Encoders India; ENC 58/6-720ABZ) was used to receive the signal at 0.5 crank angle degrees. High speed combustion data acquisition system (Me-DAQ) was utilized to acquire pressure and shaft

encoder signals which were further analyzed for other combustion parameters. This combustion data further utilized by another data acquisition system (NI driven) which calculate the combustion noise from this pressure traces and encoder signals. Engine external noise investigation was carried out with the NI Labview signal express software, high speed NI cDAQ 9178 data acquisition chassis and a NI 9232 module by keeping sampling rate 102.4 kS/s. Engine external noise was measured by microphone (B & K 4192) which is placed 1 m away from the engine. Vibration was measured in vertical, longitudinal and lateral direction by using a miniature tear drop CCLD accelerometer (B& K: 4517).

RESULTS AND DISCUSSION:
Combustion Characteristics:
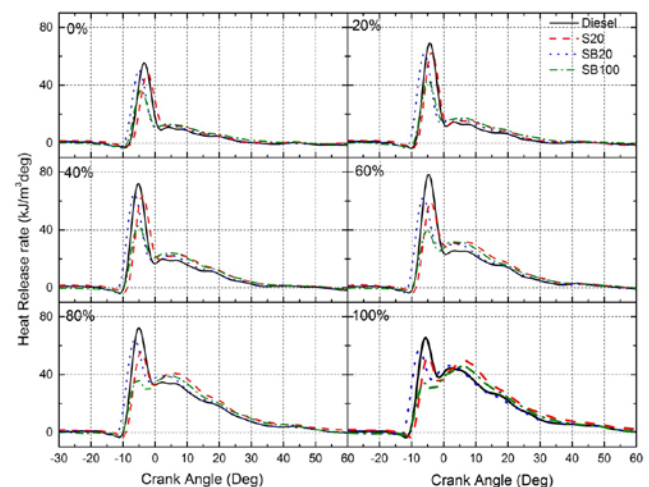
FIGURE 2. HEAT RELEASE RATE AS A FUNCTION OF CAD AT DIFFERENT ENGINE LOADS

Figure 2 shows the heat release rate for the selected test fuels for no load to full load condition. Heat release rate comprises of three important stages: Ignition delay, premixed combustion and mixing controlled combustion. Majority of the combustion were taking place in the premixed combustion phase which is followed by mixing controlled combustion phase for test fuels. Peak Heat release rate (HRRmax) observed higher for diesel followed by S20, SB20 and SB100.Most test fuels generated lower HRRmax at most loads. In particular, SB100 generates least HRRmax which ranges from -35.12 to -48.82%. S20, SB20 also observed lower HRR_{max}.

Combustion noise and External Noise

Figure 3 shows combustion noise for the selected test fuels. Combustion noise initially increases with increasing engine load, peaks when load is 40%, and then keeps on decreasing till load becomes 100%. Since sound level can be directly correlated to change in pressure (a parameter strongly coupled to HRR), it makes sense to examine the correlation between combustion noise and HRR. From

figure 2, it can be noted that HRRmax as well initially increases with increasing load and peak at load levels between 60% in premixed combustion phase. Beyond this load, it drops off to the load of 100%. Another important observation with SB100 fuel is that it has lower HRRmax and that was reflected in lowest combustion noise.
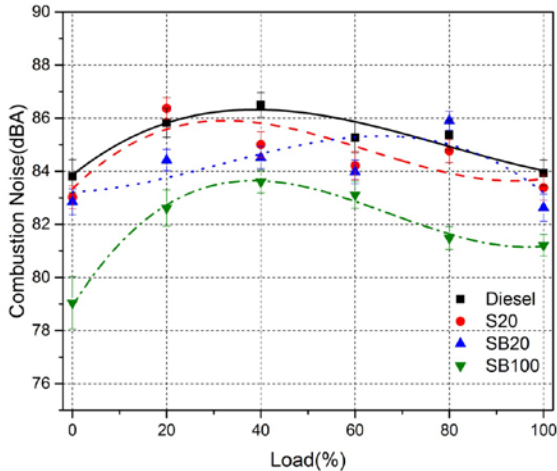
FIGURE 3. COMBUSTION NOISE FOR TEST FUELS AT VARYING ENGINE LOADS
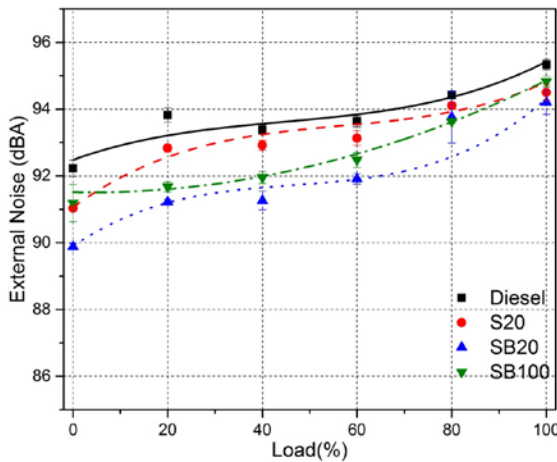
FIGURE 4. EXTERNAL NOISE FOR TEST FUELS AT VARYING ENGINE LOADS

There is a strong correlation between HRRmax and combustion noise. The higher the value of HRRmax the higher is level of combustion noise. These observations are true for all test fuels. Further, it is observed that most test fuels produce lower noise compared to mineral diesel at all loads. Combustion noise for majority of the test cases was ~0.25 to 7 dB(A) lower than that produced by mineral diesel.

Finally, it is also noted that an increase in biodiesel content tends to reduce combustion noise. This observation can also be explained in reference to HRRmax.

Figure 4 shows the engine noise for the selected test fuels. It is observed that external noise for the diesel run lies in the range of 92.22 to 95.33 dB(A) and its value is higher than that for combustion noise at all load levels. It was also observed that all the tested biofuels have ~1-3 dBA lower external noise compared to mineral diesel. It was also noted that in general, external noise increased with increasing load.

To understand phenomenon of external noise, it must be considered that external noise from an engine has many sources, including combustion and friction inside the engine, piston slap, and rotating as well as reciprocating engine components such as flywheel, piston, connecting rod, crank shaft, radiator fan, pump, etc. All these sources contribute to the overall engine noise. Given the complexity of various phenomena leading to external noise, a direct one-to-one correlation between combustion parameters and HRR with external noise may not be possible. Majority of the test fuels shows reduction in engine noise. The difference in noise for all test fuels and loads, relative to diesel lies within ± 2.0 dB(A) range. Such variation in noise level from an acoustic standpoint can be barely perceived. Despite of multiple sources of external noise and variability of test environment which was beyond control, this study have good correlation between combustion noise, external noise, and engine combustion parameters such as HRR and HRR_{max}.

Vibration Characteristics:

Figure 5 shows the vibration in all three directions for test fuels. It was observed that diesel have higher vibration in vertical and lateral direction compared to soybean biofuels. While S20 and SB20 shows higher vibration compared to diesel in longitudinal direction. It was observed that for most biodiesel and SVO blends, vibrations in vertical direction shows reduction of 8 to 30% lower at all loads compare to biodiesel. This is consistent with earlier observations for combustion noise, HRR, and HRRmax This trend is also consistent with combustion noise, external noise and HRR trends for these test fuels. Thus, in general, vertical vibrations, combustion noise, and HRR are positively correlated. If HRR in the premix combustion zone decreases, so does the combustion noise, and vertical vibration.
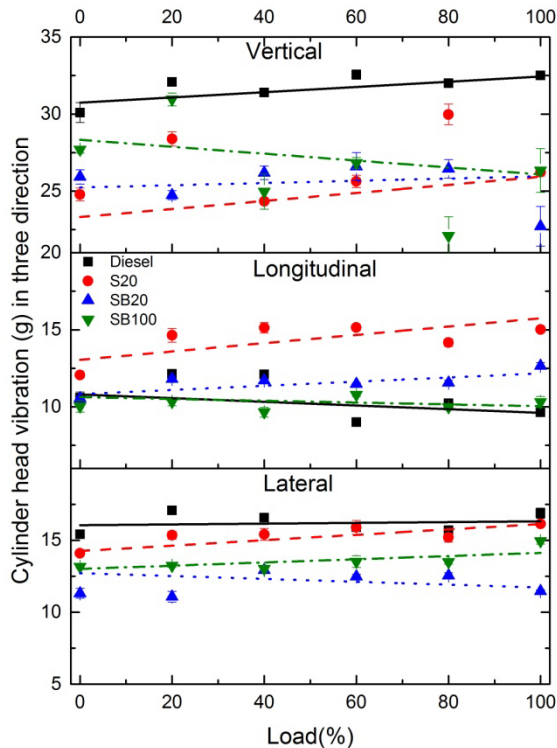
FIGURE 5. CYLINDER HEAD VIBRATION FOR TEST FUELS AT VARYING ENGINE LOADS

CONCULSIONS

Experimental investigation carried out to assess the combustion, noise and vibration, performance, emission investigation for Soybean biofuels.

Following are the conclusions from this study.

1. HRRmax was observed to be lower for all biofuels compared to diesel.
2. Lower combustion noise (~0.25 to 8 dB(A)) emanated from biofuels compared to baseline mineral diesel. A lower value of HRRmax corresponds to lesser level of combustion noise and vice versa.
3. External measured noise was relatively higher compared to combustion noise. Difference in external noise relative to baseline diesel was up to 2 dB(A) from biofuels compared to baseline mineral diesel, which was very low. External noise also correlates well with HRRmax.
4. Noise and vibration signatures were closely coupled in the context of CI engines. Similar correlations for vibrational amplitudes were observed as well. Vibrations in vertical direction were higher regardless of test fuel. Lower vertical vibrations (up to 30%) were observed from biofuels compared to baseline mineral diesel,.

This correlated well with lower HRRmax. Majority of biofuels exhibited reduction in lateral vibrations (up to 35%) at 40% load compared to baseline mineral diesel. This also correlates well with HRRmax.

5. Higher longitudinal vibrations were observed for most biofuels at higher engine loads compared to baseline mineral diesel.

REFERENCES

[1] Agarwal, A.K., 2007. "Biofuels (alcohols and biodiesel) applications as fuels for internal combustion engines". Progress in energy and combustion science, 33(3), pp.233-271.

[2] Taghizadeh-Alisaraei, A., Ghobadian, B., Tavakoli-Hashjin, T., Mohtasebi, S.S., Rezaei-asl, A. and Azadbakht, M., 2016. "Characterization of engine's combustion-vibration using diesel and biodiesel fuel blends by time-frequency methods: A case study". Renewable Energy, 95, pp.422-432.

[3] Patel, C., Agarwal, A.K., Tiwari, N., Lee, S., Lee, C.S. and Park, S., 2016. "Combustion, Noise, Vibrations and Spray Characterization for Karanja Biodiesel Fuelled Engine. Applied Thermal Engineering".

[4] Patel, C., Lee, S., Tiwari, N., Agarwal, A.K., Lee, C.S. and Park, S., 2016. "Spray characterization, combustion, noise and vibrations investigations of Jatropha biodiesel fuelled genset engine". Fuel, 185, pp.410-420.

[5] Uludamar, E., Yıldızhan, Ş., Aydın, K. and Özcanlı, M., 2016. "Vibration, noise and exhaust emissions analyses of an unmodified compression ignition engine fuelled with low sulphur diesel and biodiesel blends with hydrogen addition. International Journal of Hydrogen Energy".

[6] Taghizadeh-Alisaraei, A. and Rezaei-Asl, A., 2016. "The effect of added ethanol to diesel fuel on performance, vibration, combustion and knocking of a CI engine". Fuel, 185, pp.718-733.

[7] Giakoumis, E.G., Rakopoulos, D.C. and Rakopoulos, C.D., 2016. "Combustion noise radiation during dynamic diesel engine operation including effects of various biofuel blends: A review". Renewable and Sustainable Energy Reviews, 54, pp.1099-1113.

[8] Agarwal, A.K. and Dhar, A., 2013. "Experimental investigations of performance, emission and combustion characteristics of Karanja oil blends fuelled DICI engine". Renewable energy, 52, pp.283-291.

SEEC-2017-29

SPRAY CHARACTERISTICS OF GDI INJECTOR AT VARYING FUEL INJECTION PRESSURES

Nikhil Sharma
Engine Research Laboratory,
Department of Mechanical Engineering,
Indian Institute of Technology Kanpur, Kanpur-
208016, India
Email: snikhil@iitk.ac.in

Avinash Kumar Agarwal
Engine Research Laboratory,
Department of Mechanical Engineering,
Indian Institute of Technology Kanpur, Kanpur-
208016, India
Email: akag@iitk.ac.in

ABSTRACT

In order to meet stringent emission norms, it becomes necessary to understand the behavior of atomized fuel spray droplets of a GDI engine. An experimental study was carried out to find droplet size and velocity distributions using phase droplet interferometry (PDI). Experiments were performed in ambient condition using a gasoline direct injection (GDI) injector at two fuel injection pressure (FIP) of 40 and 200 bar and fixed fuel injection quantity of 24 mg. Experiments were performed 50 mm downstream of the GDI injector nozzle for gasoline as a test fuel. Droplet size and droplet velocity results were plotted for gasoline fuel at two different FIP. In the end D_{10}, D_{20}, D_{32} and D_{43} were plotted which gave the better understanding of the behavior of fuel injection pressures responsible for an improved fuel-air mixture. It was found that higher FIP results in significantly higher droplet velocity and lower droplet diameter. SMD was ~27μm for 40 bar FIP and ~17μm for 200 bar FIP. Arithmetic mean diameter was observed to be ~7.5 μm for 40 bar FIP and ~5 μm for 200 bar FIP.

Keywords: Atomization, droplet size distribution, droplet velocity distribution.

.
NOMENCLATURE
GDI   Gasoline Direct Injection
PDI   Phase Doppler Interferometry
G100   Pure Gasoline
D10   Arithmetic Mean Diameters
D20   Area Mean Particle Diameters
D32   SauterMeanParticle Diameters
D43   De Brouckere or Herdan
Ch   Channel
FIP   Fuel Injection Pressure

INTRODUCTION

Gasoline direct injection is not a new concept. Foundation of today's GDI technology was put long back during the World War II. Researchers around the world are trying to benchmark GDI technology with diesel engine such that it should have higher fuel economy and higher power with lesser engine noise. Today's modern GDI engines work on both, homogenous and stratified mode, with the help of advanced electronic control unit Injector specifications plays vital role in achieving the right amount of fuel injection at right time and correct pressure. It becomes necessary to understand the fundamental of GDI spray at various engines operating condition. A novel spray concept needs to be developed at various operating conditions. Moreover, fuel injection plays an important role for example at high engine load where fuel has to be injected at an early stage. Again, stringent emission norms also need to be studied. Figure 1 shows the schematic of primary and secondary break-up from a GDI injector
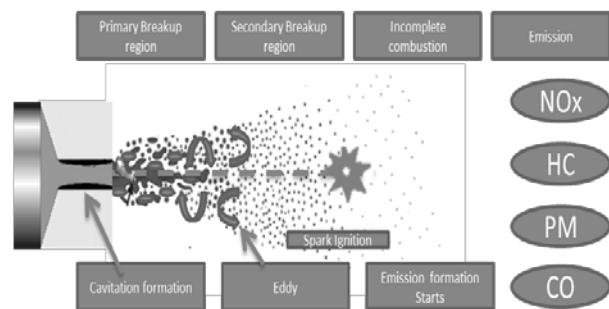
FIGURE 1: SCHEMATIC OF PRIMARY AND SECONDARY BREAK-UP FROM A GDI INJECTOR [1].

Lee and Park [2] investigated influence of FIP (5, 10, 20 and 30 MPa) on atomization of a 6-hole GDI injector

using gasoline as a test fuel. Nd:YAG laser (wavelength of 532 nm, a power of 25 mJ) was used to find velocity distribution patterns using phase Doppler particle analyzer (PDPA) experiments. Authors found that at 5 MPa FIP, axial velocity decreased because larger droplet lost their momentum quickly. At the initial stage, the droplets in the front collapse because they experience drag force. This results in rapid reduction in initial velocity. At the centre of plume, velocity tends to rise to a maximum level which further decreases to zero at the end which marks the finishing of atomization processes. Axial velocity was found to increase with an increase in FIP.

Four different GDI injectors with either different hole arrangement or hole number were investigated by Kim et al. [3]. As the fuel injection pressure was increased, the droplet size distribution decreased. In another study, Romunde et al. [4] used a multi-hole injector to investigate spray evolution process in a spark ignition direct injection engine under different ambient conditions. They reported that spray tip penetration increased as the ambient pressure decreased. Spray tip penetration was also found to decrease as the ambient temperature decreased. Pielecha et al.[5] studied the influence of different FIPs (5 and 20 MPa) and fuel temperature (20 and 120 °C) using E85 and pure gasoline as fuels in a high-pressure CVSC maintained at 1.5 MPa. These experiments were conducted to find linear and radial spray penetration at different FIP. The physical properties of the fuels had a significant influence on the width and spray penetration length. Whereas, the temperature of the fuel had little influence. For E85, droplet size was found to be lower compared to gasoline at all operating conditions. Many researchers have studied GDI spray characteristics during the past few years with significant contributions in this field. The formation of fuel–air mixtures depends on various factors such as the internal structure of the liquid jet, the atomization process and fuel evaporation characteristics [6]. Many other studies in open literature have investigated gasoline-ethanol blends in SI engines [7,8,9]. Nauwerck et al. [10] were able to measure high velocity of smaller size droplets at higher injection pressure and ambient conditions. These smaller droplets shorten the time of evaporation. The initial spray momentum decreases when the difference between ambient pressure in the chamber and fuel pressure in the injector is reduced. Consequently, drag forces are significantly lower, because they are proportional to the square of velocity.

In this study, effect of two FIP (40 and 200 bar) on mixture preparation was investigated in a GDI engine using gasoline as a test fuel. The difference between two FIP was intentionally kept large. In a GDI engine, maximum FIP is of the range 120-140 bar. It is possible that in near future significantly higher FIP may be required to enhance fuel-air mixture quality. Therefore, this study gave an insight of positive and negative aspect of using significantly higher FIP. Parameters such as Droplet size and droplet velocity were investigated and compared with 40 and 200 bar FIP.

EXPERIMENTAL SETUP

PDI is a tool used to extract information related to droplet size and droplet velocity of any liquid spray such as water, diesel, gasoline and biodiesel. In this paper real-time, non-intrusive characteristics of gasoline are investigated to understand the fundamental of the fuel-air mixture. Detailed experimental set-up is shown in Figure 2. Experimental setup consists of two transmitters and one receiver. Through transmitter one, two laser beam comes out. One laser beam of green color (532 nm) and other is blue color (491 nm). Through transmitter number two, only one laser beam of yellow color with wave length of 561 nm comes out. The point where all the three laser beam intersects is called probe volume. A signal processing software was part of the experimental setup. Gasoline direct injection injector is placed in such a way that the spray is orthogonal to the probe volume. Moreover, a cap is placed on the injector tip such that only one plume comes out of the injector. A fuel surge tank is placed in the fuel line in order to damp the pressure oscillation. NI injector module is used to drive peak and hold injector. Also, PDI setup was synchronized with injector driver module such that readings are captured only when spray plume passes through the probe volume. The primary and secondary breakup of sprays emitted from the GDI injector were captured with a high speed camera.
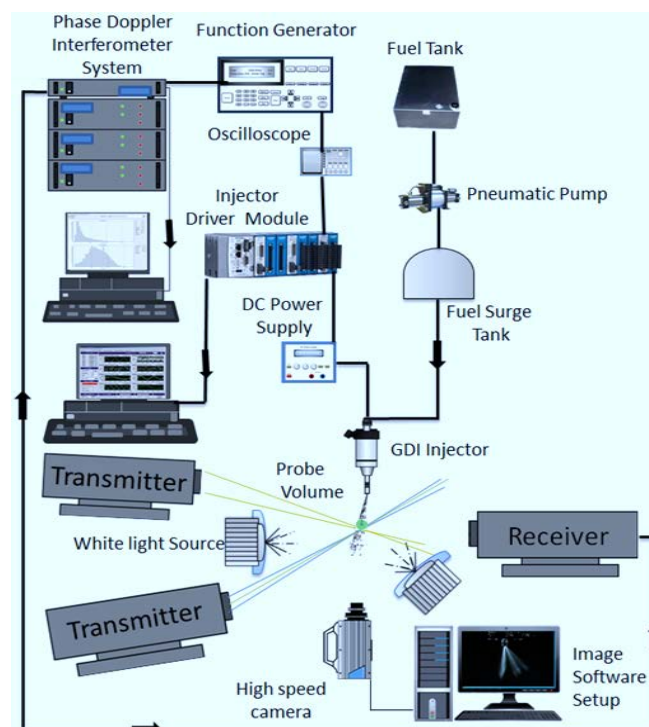
FIGURE 2. EXPERIMENTAL SET FOR PHASE

DOPPLER INTERFEROMETRY USING HIGH SPEED CAMERA

Figure 3 shows the point of measurement for downstream of the plume. It was found that 50 mm downstream of the injector is the optimum position to find the droplet size and droplet velocity. Also, data was taken at various downstream positions but only the optimum data is reported in this paper. The injector was calibrated for 24 mg fuel quantity per injection. Oscilloscope and function generator had their specific assigned role.
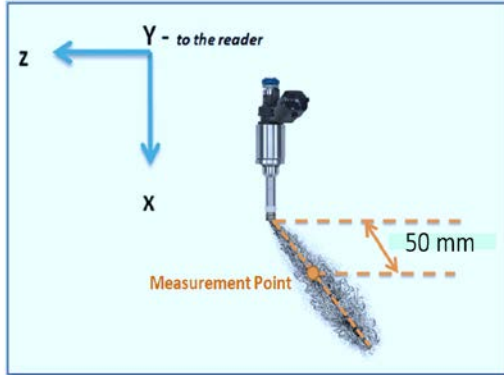
FIGURE 3: DOWNSTREAM POINT, 50 MM, WHERE MEASUREMENT WAS TAKEN FOR PDI

The high power, diode pump solid state laser systems used in the PDI experiment was class 3B lasers. The function of the three channels shown in the experimental setup was to collect the raw data signal and to perform the necessary mathematical calculation to find out the accurate droplet size and droplet velocity of the atomized drop. In this experiment 500 mm focal length for transmitters and 350 mm focal length of receiver were used. Sauter mean diameters, arithmetic mean diameter used in the results are given below.

$$\textbf{Sauter Mean Diameter } (D_{32}) = \frac{\sum i^{n_{c(i)} d_i^3}}{\sum i^{n_{c(i)} d_i^2}}$$

$$\textbf{Arithmetic Mean Diameter } (D_{10}) = \frac{\sum i^{n_{c(i)} d_i}}{\sum i^{n_{c(i)}}}$$

The velocity and diameter of the droplet are given by:-

$$v = f_d \times \delta \quad \text{..} \quad (1)$$
$$f_d = f_r - f_s \text{...} \quad (2)$$
$$d = \frac{f \times \delta}{s \times \Lambda} \text{...} \quad (3)$$

Where,
v = velocity of fuel droplet,
f_r = raw signal is a combination of Doppler signal and frequency shift
f_s = frequency shift generated by Bragg cell which is used for the resolution of direction ambiguity of droplet whether in positive and negative direction. Table 1 gives the specifications of PDI system.

Table 1: PDI Specifications

Instrument Specifications	
Droplet size range	0.5 to 2000 μm
Estimated accuracy	± 0.5 μm
Estimated resolution	± 0.5 μm
Velocity measurement range	-100 to 300 m/s
Velocity accuracy	± 1%
Volume flux accuracy	± 15%
Receiver focal length	350, 500, 750, 1000 mm
Transmitter focal length	350, 500, 750, 1000 mm
Laser Type	Diode Pumped Solid State (DPSS)
Wavelength of Lasers	Blue-492 nm, Green- 532 nm and Yellow- 660 nm

Results and Discussions

The experiments were performed on pure gasoline at two different injection pressures. Droplet size and droplet velocity were the main findings from this study in addition to the mean droplet diameters. Spray droplet velocity distribution variation can be divided into several sub-sections. These are: injection delay, detection time, head and tail sections. Injection delay is the time difference between the starting of en-ergizing the injector solenoid and the start of actual injection. Detection time is the time interval between the start of injection and initial velocity signal of the spray droplets detected by the system. Head section is the zone after the signal detection where fuel droplets are ensemble in a particular region. This region has droplets with significant velocity. Tail section is the zone where velocity is relatively less and remains nearly constant with time.
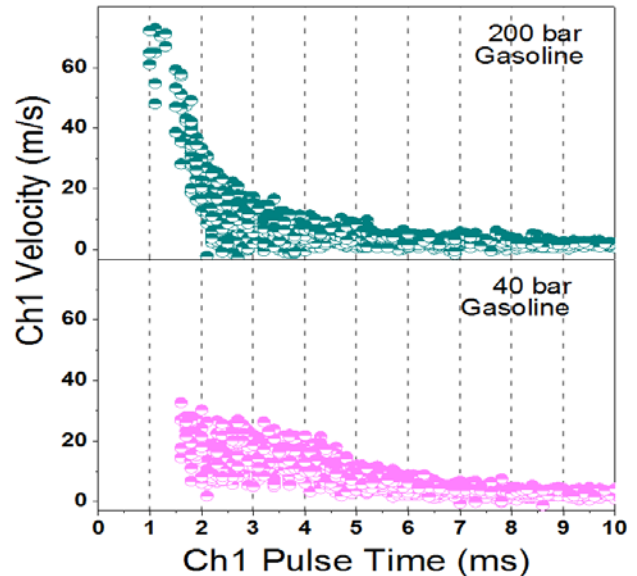
FIGURE 4. VARIATION OF DROPLET VELOCITY WITH PULSE TIME FOR CHANNEL CH-1 AT 24 MG FUEL INJECTION QUANTITY.

Figure 4 shows the variation of channel 1 spray droplet velocity distribution with pulse time for 40 and 200 bar FIP for 24 mg fuel injection quantity. For 40 bar FIP head section was observed from 1.5 to 4 ms and after 4 ms, the tail section started. As the FIP was increased to 200 bar, velocity of the droplet increased upto ~75 m/s and no clear head section was observed. That is, no clear constant velocity region of head section was defined.

All velocity components of channel 1 were in positive direction. The lower head section indicated that the fuel droplets evaporated earlier, which was desirable. Lower head section was achieved at lesser FIP. In another study, it was reported that as the FIP increased, head section width also increased [1]. With increasing FIP, the head section tends to be thinner because of increased velocity of individual droplets. The lower head section in the results indicates that atomization of the test fuel takes place relatively earlier. This results in superior velocity distribution and larger scattering of atomized fuel. Therefore, narrower head section is desirable throughout the results. The reason for this is that smaller droplets have higher surface area/ volume ratio, therefore, they interact with ambient air and evaporate at higher FIP before they reach the probe volume.
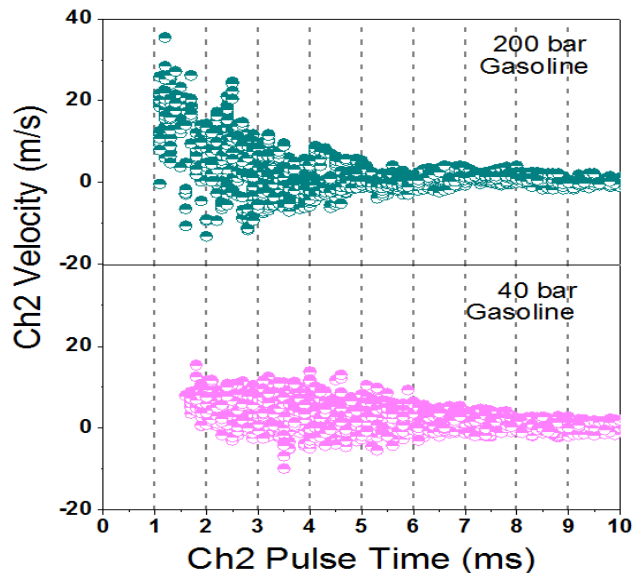
FIGURE 5. VARIATION OF DROPLET VELOCITY WITH PULSE TIME FOR CHANNEL CH-2 AT 24 MG FUEL INJECTION QUANTITY.

Figure 5 shows the variations in channel 2 velocity distribution of spay droplets with pulse time for FIP of 40 and 200 bar for 24 mg fuel injection quantity. No clear distinguish head section at 40 bar FIP was observed in Ch2 velocity. That is the velocity is nearly same at lower FIP with time. However, at higher FIP of 200 bar Ch2 velocity was highest at 1ms, which decreased upto 4ms

pulse time and then remain constant upto 10 ms. Negative velocities were visible in Ch2 velocity component.

However, Ch3 velocity with pulse time showed opposite trend (Appendix A, figure 8). Velocity was nearly same for all time duration at 200 bar FIP. However, significant negative velocity was noticed at 40 bar FIP. Negative velocities signify the opposite direction of the velocity which may be due to eddies generated in the fuel injection. Also, negative velocity indicates the re-circulation zone created by the swirl flow.

Recirculation zone is dependent on the injection pressure, ambient condition and drag experienced by the fuel droplet. The significance of these eddies lies in the fact that they are responsible for improved mixing in the immediate vicinity of the recirculation zone created by the injector.
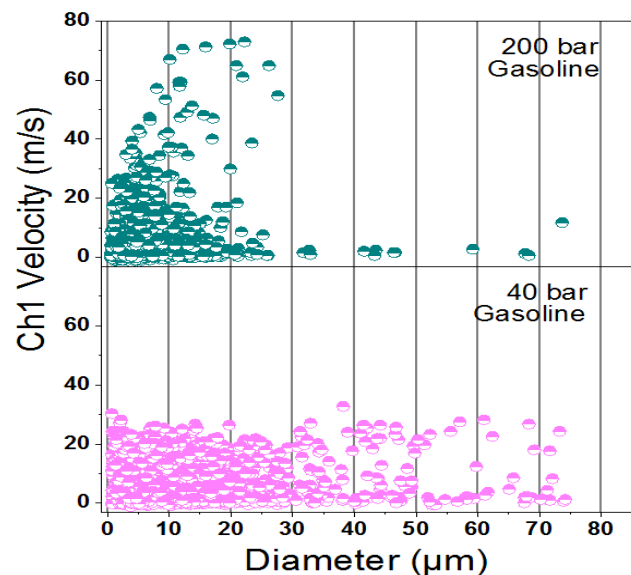
FIGURE 6. VARIATIONS IN SPRAY DROPLET DIAMETER DISTRIBUTIONS WITH DROPLET VELOCITY AT 24 FUEL INJECTION QUANTITY.

Figure 6 shows the ensemble average distribution of Ch1 spray droplet velocity with spray droplet diameter for multiple injections for 40 and 200 bar FIP at 24 mg fuel injection quantity. Maximum droplet velocity for 40 bar FIP was found to be ~37 m/s whereas for FIP of 200 bar maximum droplet velocity was found to be ~75 m/s. At lower FIP all the droplets were distributed throughout the entire range from 0 to 75 μm diameter. While for 200 bar FIP bulk of the droplets were smaller and were found to be concentrated near the origin. The droplets with lesser injection pressure are less scattered and as the fuel injection pressure increases, the droplets tend to scatter in all the directions. This is because, with an increase in pressure, the velocity of the droplet increases and mass of the particles decreases. In another way, smaller particles

have lesser surface area and may they get evaporated at higher injection pressure.
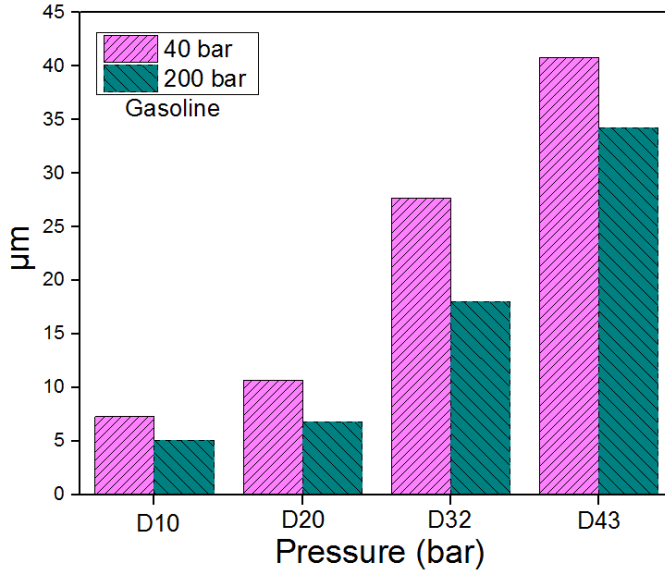
FIGURE 7. DIFFERENT MEAN DIAMETERS AT 24 MG FUEL INJECTION QUANTITY.

Figure 7 shows different mean diameters for the gasoline sprays for 24 mg fuel injection quantity at two FIP. All the mean diameters for 200 bar FIP were relatively lesser than 40 bar FIP. SMD was ~27μm for 40 bar FIP and ~17μm for 200 bar FIP. The arithmetic mean diameter was observed to be ~7.5 μm for 40 bar FIP and ~5 μm for 200 bar FIP. Table 2 shows the physical significance of mean diameters.

TABLE 2: PHYSICAL SIGNIFICANCE OF MEAN DIAMETERS

Symbol	Common Name	Definition	Application
D_{10}	Arithmetic Mean (Length)	$\dfrac{\sum N_i D_i}{\sum N_i}$	Comparison
D_{20}	Surface Mean (Surface Area)	$\left[\dfrac{\sum N_i D_i^2}{\sum N_i}\right]^{1/2}$	Surface Area Controlling
D_{32}	Sauter Mean (Volume-surface)	$\dfrac{\sum N_i D_i^3}{\sum N_i D_i^2}$	Mass Transfer Reaction
D_{43}	Herdan Mean (De Brouckere or Herdan) (Weight)	$\dfrac{\sum N_i D_i^4}{\sum N_i D_i^3}$	Combustion Equilibrium

CONCLUSIONS

Phase Doppler interferometry was found to be a challenging experiment for obtaining GDI spray droplet size distribution and velocity distribution. However, this system was sensitive to alignment of laser beams. These results were useful in predicting in-cylinder behavior of GDI injector for fuel-air mixture preparation at various fuel injection pressures. As the FIP was increased to 200 bar, velocity of the droplet increased upto ~75 m/s and no clear head section was observed at this FIP. Shorter head section in the spray results indicated that atomization of the test fuels takes place relatively earlier. This results in larger scattering of atomized fuel. The velocity component Ch2 was less scattered compared to Ch1 for all the test fuel. Ch3 was the least scattered plot. Negative velocity indicated the droplets moving in opposite direction, primarily due to eddies created by recirculation zone. These recirculation zones play a vital role in mixing the fuel with ambient air. As the FIP decreased, scattering of the droplet shifted from y-axis to the x-axis. Smaller droplets had higher surface area/ volume ratio therefore they evaporated first at higher fuel injection pressure. SMD was ~27μm for 40 bar FIP and ~17μm for 200 bar FIP. Arithmetic mean diameter was observed to be ~7.5 μm for 40 bar FIP and ~5 μm for 200 bar FIP.

REFERENCES

[1] Sharma, N. and Agarwal, A.K., 2016. "Microscopic and Macroscopic Spray Characteristics of GDI Injector Using Gasohol Fuels at Various Injection Pressures" (No. 2016-01-0868). SAE Technical Paper.
[2] Lee, S. and Park, S., 2014. "Experimental study on spray break-up and atomization processes from GDI injector using high injection pressure up to 30MPa". International Journal of Heat and Fluid Flow, 45, pp.14-22.
[3] Kim, H.J., Park, S.H. and Lee, C.S., 2014. "Light intensity and image visualization of GDI injector sprays according to nozzle hole arrangements. Optik-International Journal for Light and Electron Optics", 125(12), pp.2763-2767.
[4] Van Romunde, Z., Aleiferis, P.G., Cracknell, R.F. and Walmsley, H.L., 2007. "Effect of fuel properties on spray development from a multi-hole DISI engine injector" (No. 2007-01-4032). SAE Technical Paper.
[5] Sankar, S.V., Maher, K.E., Robart, D.M. and Bachalo, W.D., 1999. "Rapid characterization of fuel atomizers using an optical patternator". Journal of engineering for gas turbines and power, 121(3), pp.409-414.
[6] Yamakawa, M., Isshiki, S., Lee, J. and Nishida, K., 2001. "3-D PIV analysis of structural behavior of DI gasoline spray" (No. 2001-01-3669). SAE Technical Paper.
[7] Sharma, N. and Agarwal, A.K., 2016. "An Experimental Study of Microscopic Spray Characteristics

of a GDI Injector Using Phase Doppler Interferometry (No. 2016-28-0006)". SAE Technical Paper.

[8] Bayraktar, H., 2005. "Experimental and theoretical investigation of using gasoline–ethanol blends in spark-ignition engines". Renewable Energy, 30(11), pp.1733-1747.

[9] Yüksel, F. and Yüksel, B., 2004. "The use of ethanol–gasoline blend as a fuel in an SI engine". Renewable energy, 29(7), pp.1181-1191.

[10] Nauwerck, A., Pfeil, J., Velji, A., Spicher, U. and Richter, B., 2005. "A basic experimental study of gasoline direct injection at significantly high injection pressures" (No. 2005-01-0098). SAE Technical Paper.

APPENDIX A: Ch3 VELOCITY V/S PULSETIME
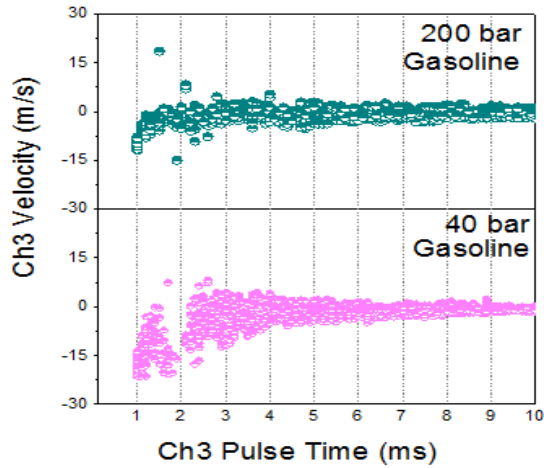
FIGURE 8. VARIATION OF DROPLET VELOCITY WITH PULSE TIME FOR CHANNEL Ch-3 AT 24 MG FUEL INJECTION QUANTITY.

APPENDIX B: DROPLETCOUNT V/S DROPLET VELOCITY
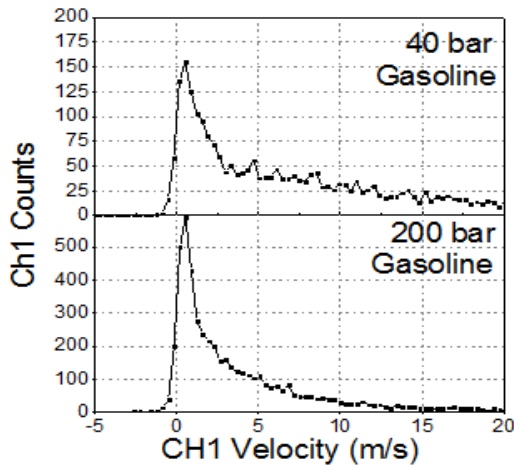
FIGURE 9. DROPLET COUNTS OF Ch1 VELOCITY
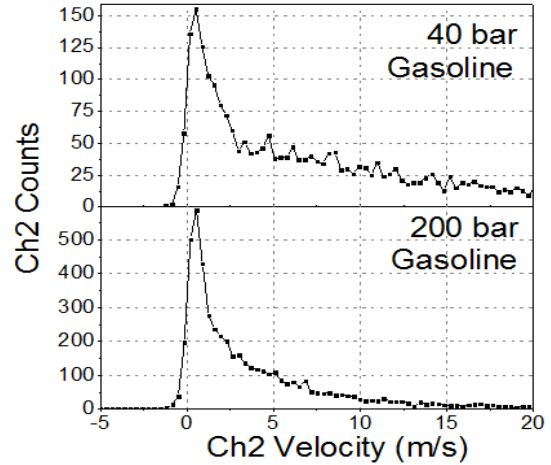
FIGURE 10. DROPLET COUNTS OF Ch2 VELOCITY
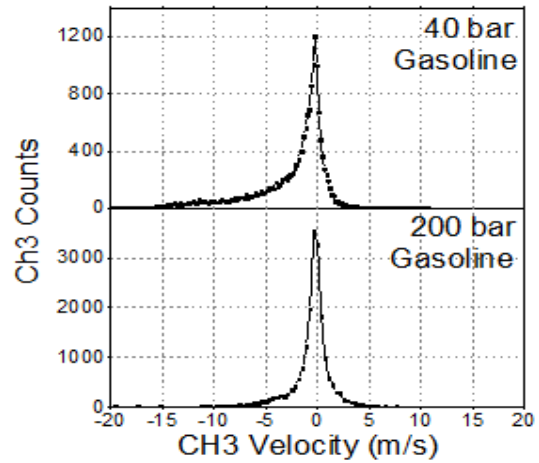
FIGURE 11. DROPLET COUNTS OF Ch3 VELOCITY

6

SEEC-2017-30

EFFECT OF OXYGEN CONTENT OF DIESOHOL ON ENGINE NOISE AND VIBRATIONS

Dev Prakash Satsangi
Department of Mechanical Engineering
Indian Institute of Technology Kanpur
Email: satsangi@iitk.ac.in

Nachiketa Tiwari
Department of Mechanical Engineering
Indian Institute of Technology Kanpur
Email: ntiwari@iitk.ac.in

Avinash kumar Agarwal
Department of Mechanical Engineering
Indian Institute of Technology Kanpur
Email: akag@iitk.ac.in

ABSTRACT

The interest in use of renewable alternative fuels compared to conventional diesel fuel in compression ignition engine has increased due to environmental concerns. Oxygen enriched fuels are preferred for improving in-cylinder combustion and to curb environmental pollution. Therefore, worldwide acceptendace of alcohol blended diesel fuels has increased significantly. A large-scale switch over to such fuels require their comprehensive assessment. In the present work a comparative evaluation of noise and vibration, were performed on a genset engine when fuelled on alcohol blends with 2% oxygen content by weight. Fuel blends were prepared using methanol/diesel, ethanol/diesel, and n-butanol/diesel. Experiments were conducted on a diesel genset engine at 1500 RPM, for six different loads. Noise and vibration characteristics were compared against diesel. This work helps to explore correlation between noise and vibration phenomena of the engine. This provides phenomenological explanations of different correlations, and also the technological viability of using such blended fuels for genset applications.

*Keywords***:** A-Weighting noise (dBA), 1/3rd octave band, Compression ignition engine, Engine vibrations, Fast Fourier Transform (FFT), central frequency.

INTRODUCTION

Diesel engines are most commonly used internal combustion engines. These engines possess excellent drivability and fuel economy. Increasing global concerns over hazardous air and noise pollution issues forcing researchers to work out promising alternative solutions. For, the last few years, researchers have tried a number of techniques to improve the fuel combustion and reduce the emissions with considerable success rates. The presence of oxygen at the time of combustion plays a significant role and affects the engine characteristics. Chin [1] has investigated the role of oxygen during the combustion process and found that on increasing oxygen in the combustion cylinder leads to reduce the energy required to burn the combustible mixture. Uludamar et al. [2] have experimentally investigated noise and vibrations in an unmodified diesel engine using different biodiesel blends. They found reduction in vibrations of engine block using biodiesel in CI engine due to role of inherent oxygen. Fattah et al. [3] investigated effect of biodiesel fuel on noise generation through diesel engine and observed that the chemical and physical properties also plays a significant role in production of combustion noise. They reported reduction of noise while using biodiesel fuels through reduction of in-cylinder peak pressure compared to diesel fuel. Redel-Macias et al. [4] tested diesel fuel, straight and blended with olive pomace oil methyl ester in a CI engine. They observed reduction of noise from diesel engine while using biodiesel fuel due to their high cetane

number. Torregrosa et al. [5] observed reduction of combustion noise with increase in percentage of biodiesel due to difference in combustion phasing and injection rate of fuel and thus oxygen content. Taghizadeh-Alisaraei et al. [6] conducted experiments on diesel engine using canola and soybean biodiesel blends and observed lower vibrations for diesel fuel compare to biodiesel.

A significant amount of research work has been conducted on performance, emissions and combustion but not many researchers have reported on noise, vibrations of internal combustion engines. Current research involves preparation of diesohols by keeping a fixed oxygen content and the effect of these blends on generation of noise and vibrations of a genset engine.

EXPERIMENTAL SETUP AND METHODOLOGY

Current experimental work utilized a vertical, single cylinder, water-cooled, 4-stroke, direct injection diesel genset with a capacity of 7.4 KVA. The schematic of complete experimental setup is shown in Figure 1.
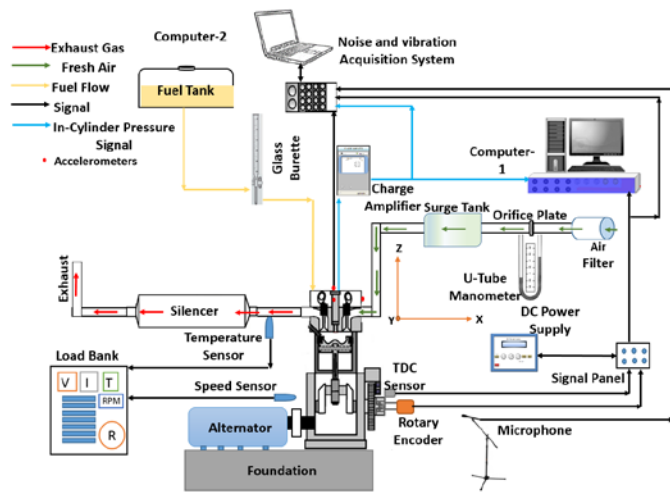
Figure 1. Schematic of experimental set-up

In-cylinder pressure signal was acquired using a piezoelectric pressure transducer. The information of crank angle rotation was obtained by rotary encoder which was attached to crank shaft. In-cylinder pressure with crank angle rotation information was used to calculate the combustion noise. Total engine noise was measured by a microphone positioned according to ISO 9614-2. Three single-axis accelerometers were used to measure engine vibrations in three different directions (X, Y and Z). Experiments were conducted at 1500 RPM, FIP of 20 MPa for six engine loads (i.e., from 0 to 7.4 kW in steps of 1.48 kW). The pressure signal was acquired for 250 cycles to minimize cyclic variations.

Test Fuel Preparation and their Characterization

Co-solvent, 1-Dodecanol was used to avoid the phase separation problem when methanol/ethanol blended with diesel. There is no need of stabilizer when n-butanol blended with diesel. Oxygen content was fixed at 2% (%w/w) for all test blends. Test fuel's properties are shown in Table 1.

TABLE 1: Test Fuel Characterization

Test fuel	Density (kg/m^3@15°C)	Kinematic Viscosity (m^2/s@40°C)	Calorific value (MJ/kg)
Diesel	830	2.89e-6	43.86
DB2	826	2.42e-6	42.45
DEDOD2	828	2.67e-6	42.81
DMDOD2	829	2.87e-6	43.12

RESULTS AND DISCUSSION
Combustion noise

Combustion noise generates due to ignition of fuel, in engine cylinder. As shown in Figure 2, combustion noise level varies in the range of 77 to 93 dBA for all test fuels. It was observed that combustion noise increases with increase of engine load for all test fuels up to 60% load and becomes almost constant thereafter. It was due to quantity of fuel injected and the oxygen content.

Among all test fuels, DEDOD2 shows lowest combustion noise up to 60% engine load. However, DB2 blend shows highest combustion after 20% engine load. This attributable to role of cetane number and oxygen concentration at high in-cylinder temperatures.

Figure 2. Combuastion noise variation at different engine loads

Total engine noise

Figure 3 shows total engine noise for all test fuels. Total engine noise includes combustion, mechanical and ambient noises. Total engine noise was observed higher for diesohols compared to diesel. Fuel DEDOD2 and diesel generates the highest and least total engine noise respectively among all test fuels.
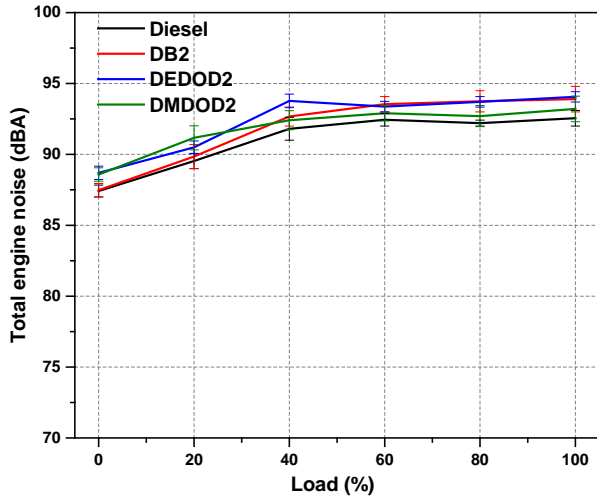
Figure 3. Total engine noise variation at different engine loads

Vibrations

Figure 4 shows root mean square (rms) value of vibration
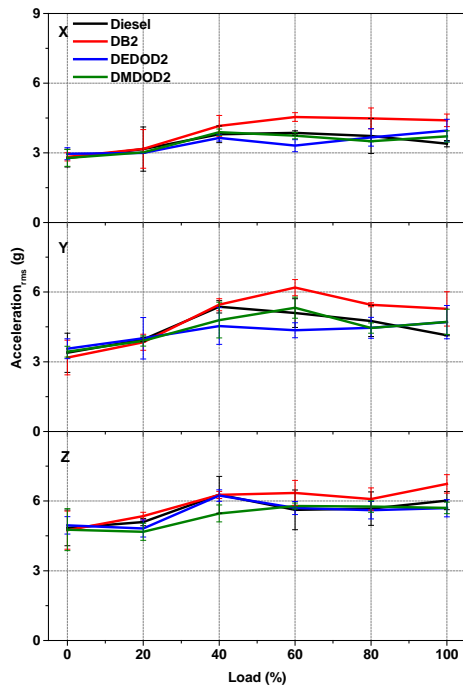
Figure 4. Acceleration rms variation at different engine loads

signals in X, Y and Z directions as indicated in Figure 1. Slightly higher vibrations were observed in Z- direction w.r.t. to X and Y directions. It was due to the movement piston along Z direction during the combustion process.

CONCULSIONS

In current research effect of diesohol's inherent oxygen in generation of noise and vibration characteristics is explored by experiments. All test fuels shows a sharp increase of combustion noise and total engine noise up to 60% engine load, however, after 60%, both noises shows slight variation. Combustion noise was observed higher for diesohols at higher engine loads relative to diesel. Total engine noise of diesel was least among all test fuels at all engine loads. Diesohol shows less vibration in all measured directions at lower engine loads compare to diesel. Combustion noise and accelerations were correlated with each other. Fast Fourier analysis of total noise, accelerations suggest 12.5 (combustion cyclicity) and 25 Hz (engine speed) with their harmonics.

REFERENCES

[1] Chin, J. "Analysis of the effect of oxygen addition on minimum ignition energy." Journal of energy, 1983, 7(6): 710-715.

[2] Erinç, U., Tosun, E., and Aydın, K. "Experimental and regression analysis of noise and vibration of a compression ignition engine fuelled with various biodiesels." Fuel, 2016 ;177: 326-333.

[3] Fattah, IMR., Masjuki, HH., Liaquat, AM., Ramil, R., Kalam, MA., Riazuddin, VN. "Impact of various biodiesel fuels obtained from edible and non-edible oils on engine exhaust gas and noise emissions." Renewable and Sustainable Energy Reviews,2013; 18: 552-567.

[4] Redel-Macías, M. D., Pinzi, S., Leiva, D., Cubero-Atienza, AJ., Dorado, MP. "Air and noise pollution of a diesel engine fueled with olive pomace oil methyl ester and petrodiesel blends." Fuel,2012; 95: 615-621.

[5] Torregrosa, AJ., Pla, B., Monico, LF. "Impact of Fischer–Tropsch and biodiesel fuels on trade-offs between pollutant emissions and combustion noise in diesel engines" Biomass and Bioenergy, 2013; 52: 22-33.

[6] Taghizadeh-Alisaraei, A. and Rezaei-Asl, A., "The effect of added ethanol to diesel fuel on performance, vibration, combustion and knocking of a CI engine" Fuel, 2016; 185; 718-733.

SEEC-2017-031

SYSTEMS STRESS FACTOR INFLUENCE ON FATTY ACID PRODUCTIVITY AND PROFILE DURING CULTIVATION OF CHLORELLA SP.

M V Rohit
CSIR-IICT
Email: rohit761@gmail.com

S Venkata Mohan
CSIR-IICT
Email: vmohan_s@yahoo.com

ABSTRACT

Photosynthetic machinery is gaining grounds to transform solar energy and CO2 into high value bio-based products. In this direction, microalgae cultivation has several attributes of not only producing energy rich lipids but also accumulation of primary and secondary metabolites of high commercial values. Mixotrophic and heterotrophic cultivations are key technologies for achieving high biomass, lipid productivities and scaling up of algal bioprocess. Optimization of stress conditions for lipid induction and fatty acids is specific to microalgal species. The isolated strain Chlorella sp. SVMBIOEN2 was evaluated with design of experiments (DOE) methodology using Taguchi orthogonal array (OA) towards high lipid producing conditions. Various triggering factors for fatty acid synthesis were studied to understand multi-parametric stress mediated stimulation of lipids and gain knowledge on underlying fatty acid (FA) synthesis mechanism. Enhanced lipid productivities with diverse fatty acid profiles will pave new avenues for capturing spectrum of bioproducts and empowers bio-based economy.

Keywords: Biodiesel, Nutraceuticals, Fatty acids, Microalgae, Mixotrophic, Heterotrophic
.

SEEC-2017-32

EMISSIONS FROM A GASOHOL FUELLED HOMOGENEOUS CHARGE GDI ENGINE

Nikhil Sharma
Department of Mechanical Engineering,
Indian Institute of Technology Kanpur
Email: snikhil@iitk.ac.in

Avinash Kumar Agarwal
Department of Mechanical Engineering,
Indian Institute of Technology Kanpur
Email: akag@iitk.ac.in

ABSTRACT

Researchers are working across the globe to meet stringent emission norms for GDI engines. PM and gaseous emissions from GDI engine pose serious concerns associated health issues. Ethanol obtained from biomass and non-edible crops have been considered as feasible alternative to gasoline fuel, which is green, clean, and renewable in nature. In this study, a single-cylinder, wall-guided GDI engine was investigated for its emission characteristics using a stoichiometric mixture of gasohol at 2000 rpm. Ethanol 15% (v/v) blended with 85% gasoline (v/v) and gasoline were the test fuels investigated for gaseous and particle mass/ particle number (PM/PN) emission characteristics in a homogenous charge mode of GDI engine. The particle size-number distributions were determined using an Engine Exhaust Particle Size Analyzer^{TM} (EEPS) at fuel injection pressures (FIP) of 80 bar. The experiments demonstrated that there is a need to control PM/ PN emissions from a GDI engine in order to meet stringent emission norms applicable in near future. CO was in the range of 22.3 to 2.9 g/kWh for both the test fuels. NO_x emission increased with increasing engine load, irrespective of the test fuel used. PM/PN emission was greatly influenced by oxygen content of the fuel.

Keywords: GDI, ethanol, gaseous emission, particulate number; particulate surface area, CMD.

NOMENCLATURE

GDI   Gasoline Direct Injection
E15   15% Ethanol blended with 85% Gasoline by volume
EEPS   Engine Exhaust Particle Size
EGT   Exhaust Gas Temperature
FIP   Fuel Injection Pressure
G100   Unleaded gasoline
PM   Particle Mass
PN   Particle Number
CMD   Count Mean Diameter

INTRODUCTION

Goals of the automotive industry for high power, low specific fuel consumption, and low emissions can be fulfilled by gasoline direct injection (GDI) engine. GDI engines uses CRDI system which have the capability of split injection such as pilot injection, main injection and post injection in one complete cycle. Incorrect fuel-air mixture and its injection timing leads to higher gaseous and particulate emissions. Emissions level can be reduced by optimizing fuel-air mixtures and their spray characteristics. Amongst alcohols, ethanol is the most suitable candidate and is being used by most of the countries. Oxygen in a fuel can result in complete combustion of fuel-air mixture inside the combustion chamber.
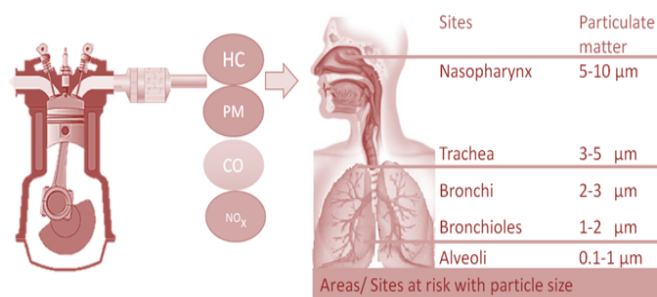
FIGURE 1: Engine exhaust particulate's effect on human respiratory system

Particle matter (PM) emissions from GDI engines pose serious concerns due to various health issues associated with them [1-4]. PM emissions are the most important negative aspect of internal combustion engines, especially GDI and compression-ignition (CI) engines. Figure 1 shows different zones of the human respiratory system affected by various sizes of PM. These PM emissions affect human health adversely [5] because they penetrate deep into the human respiratory system (Nasopharynx, Trachea, Bronchi, Bronchioles, Alveoli) [6,7] by process of inhalation and therefore, contaminate the respiratory system with toxic substances, adsorbed onto its surface.

Chen et al. [8] reported an increase in ethanol to gasohol led to increase in both PM/ PN in a cold engine. Lue et al. [9] investigated the effect of ethanol-gasoline blends on PM/ PN from a GDI engine and reported that ethanol-gasoline blends (gasohols) increased the PN concentration at lower loads and vice-versa at higher loads.

Topguil et al. [10] reported a decrease in HC emissions by using various ethanol-gasoline blends in SI engine. Oxygenated fuel allowed to further increase compression ratio without engine knock. The Higher compression ratio can further increase in cylinder temperature [11]. The higher in-cylinder combustion temperature resulted in complete combustion of the remaining fuel which may not have burned completely. Inner geometry of combustion chamber dictates the HC emission. Parameters such as engine speed and nose shape geometry of piston increases turbulence inside the combustion chamber. This results in complete combustion of charge leading to a reduction in HC emissions. The higher compression ratio and higher surface to volume ratio lead to relatively lower HC emissions [11-13]. Due to uniform distribution of fuel-air inside the combustion chamber, there is no over mixed region and there is lesser flame quenching which resulted in reduced HC emissions. Hsieh et al. [14] reported that HC production decreased as ST was retarded from maximum brake torque (MBT) location. This was reported due to increase in the time available to form a homogeneous mixture.

Daniel et al. [15] found large NO_x benefits while using bio-fuels such as ethanol, methanol, and butanol with little degradation in engine performance. NO_x emission increased with increase in engine load. This was because of in-cylinder temperature increased with load. Oxygenated fuel showed lesser NO_x emission than gasoline. The reason for lower NO_x emission was lower flame temperature and presence of oxygen in ethanol fuel which decreases in-cylinder temperature.

In this study, comparative evaluation of E15 (15% ethanol blended with 85% gasoline by volume) was investigated for PM and PN emissions in addition to gaseous emission under steady-state engine operating conditions in homogeneous charge mode in a GDI engine. This study provides valuable insights of particulate number–size, particle mass-size, and particle surface area-

size distributions for the engine. Engine performance characteristics and gaseous regulated emissions such as total hydrocarbons (THC), carbon monoxide (CO), and oxides of nitrogen (NOx) emission were also measured for all test fuels.

EXPERIMENTAL SETUP

The experimental setup consisted of a 500 cc single cylinder GDI research engine (Mobiltech; HMC Seta 0.5L), which delivered rated torque of 30 Nm @ 2000 rpm. Specifications of the test engine are given in Table 2. The test engine was coupled with a 36 kW transient AC dynamometer (Dynomerk Controls; 6-2013). Figure 2 shows the schematic of the experimental setup. An optical angle encoder (AVL; 365C) was attached to the engine crank shaft, which delivered 720 pulses in single a revolution of the crankshaft. This encoder was attached to a 4-channel high-speed combustion data acquisition and analysis system (AVL; Indi-micro) through a signal conditioning unit (AVL; 365-C). An indicating spark plug (AVL; ZI31_Y5S) was mounted on the engine cylinder head and its output of in-cylinder pressure signals was provided to the combustion analyzer, via an in-built charge amplifier. GDI injector peak and hold driver (Zenobalti; ZB-5100G) was attached to the engine through the open ECU, which received the trigger signal from the optical encoder.
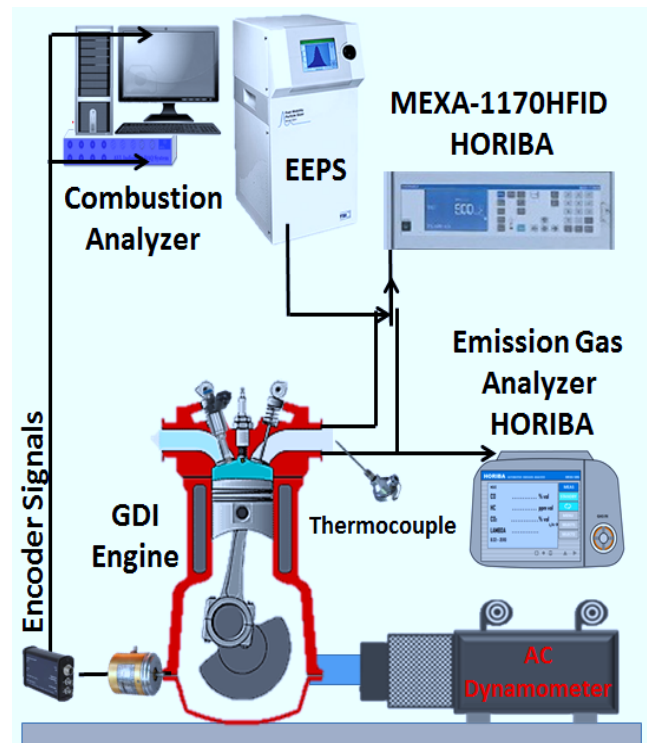
FIGURE 2. Schematic of the engine experimental setup

An Engine Exhaust Particle Sizer^{TM} (EEPS) (TSI Inc., EEPS-3090) was used for particulate number-size,

mass-size, and surface area-size distributions of the soot particles emitted from the test engine. In addition, engine oil, coolant, and fuel conditioning units (AVL; Fuel System Compact™) were connected to the engine experimental setup. Regulated gaseous emissions namely CO and NO_x were measured using non-dispersive infrared (NDIR) (Horiba, MEXA-584L) method. THC was measured using flame ionization detection (Horiba, MEXA-1170HFID) principle. The entire measurements were done according to Indian Standard IS/ISO 8178-4 (2007) [16].

TABLE 1: Engine specifications

Engine type	Single Cylinder GDI engine
Bore/ Stroke	86 mm/ 86 mm
Displacement volume	500 cc
Connecting rod length	196 mm
Compression ratio	10.5
Maximum power	10 KW @ 3000 rpm
Maximum torque	32 Nm @ 3000 rpm
No. of Injector holes	6

TABLE 2: Specifications of EEPS 3090

Particle size range	5.6-560 nm
Particle size resolution	16 channels per decade (32 in total)
Electrometer channels	22
Mode of operation	Unipolar diffusion charger
Cyclone 50% cut-point (μm)	1
Maximum data rate (Hz)	10

Results and Discussion

This experimental investigation provides detailed insights of particle size-number, particle mass-size and particle surface-size distribution emitted from GDI engine, fuelled with E15 and baseline gasoline.

Figure 3 shows the variation of EGT with IMEP. it can be observed that as IMEP increases, EGT also increases. EGT was relatively higher for E15 fuel. Possible reason for this could be inherent oxygen content, which leads to complete combustion of E15.
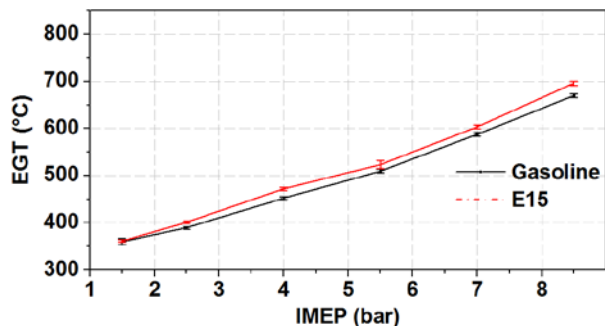
FIGURE 3. EGT variation with IMEP

PFI results in strongly premixed and almost homogeneous mixture in the combustion chamber. In other words, there is no fuel-air rich region in the combustion chamber. Homogeneity of the fuel-air mixture in GDI engine is relatively lower. This is because of less time available for fuel evaporation and mixing with air. This inevitably results in high-temperature regions, however, there is relatively lower oxygen present in such locations. This may lead to significant endothermic pyrolysis reactions, which contribute to soot formation. Another aspect, which results in relatively higher PM emissions from GDI engine, is fuel spray impingement on the piston.
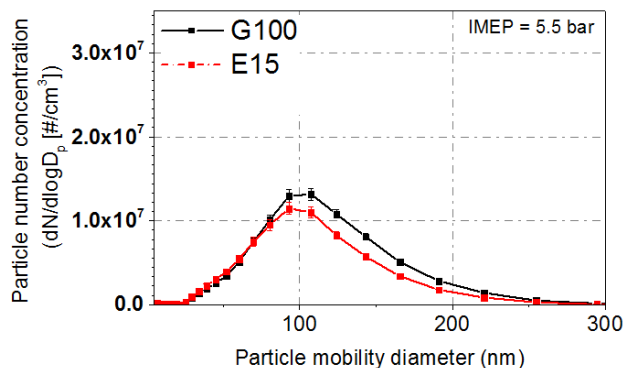
FIGURE 4(a). Particulate number vs particulate mobility diameter

Figure 4(a) shows the particle number-size distributions for E15 and baseline gasoline at 5.5 bar IMEP at 2000 rpm with 80 bar FIP. Particulate emissions were relatively lower for E15 at lower IMEP in comparison to baseline gasoline. E15 emitted relatively lower PN because of the higher oxygen content, lower boiling point, lower carbon/ hydrogen ratio and higher octane number compared to baseline gasoline. The oxygen content of E15 promotes the combustion efficiency of charge. Oxygen present in ethanol improved the combustion by locally altering the fuel-air ratios. When ethanol blended with gasoline, soot precursor concentration gets reduced. This is because of the absence of aromatic components in ethanol which are responsible for soot formation. Fuel-borne oxygen assists in attaining a higher degree of oxidation of unburnt and pyrolysed hydrocarbons.
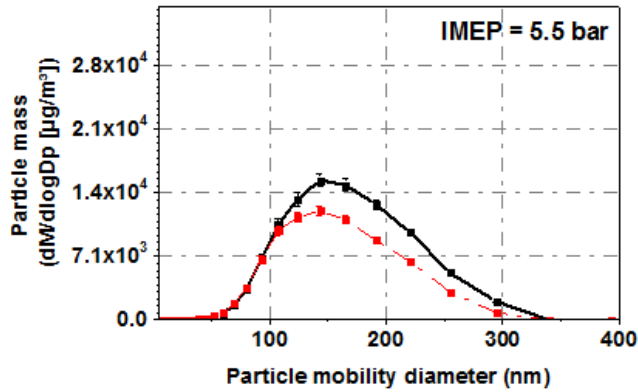
FIGURE 4(b). Particle mass-size vs. particulate mobility diameter

Figures 4(b) illustrate the particle mass-size distributions for E15 and gasoline at 5.5 bar IMEP at 2000 rpm at FIP of 80. Larger diameter particles contribute more towards mass. Particle mass-size distributions showed that E15 generated relatively lower PM emissions at 5.5 bar IMEP. This was because of relatively lower. number-size distribution of particulates at 5.5 bar IMEP Particulate with higher mass will have lower atmospheric retention time and will settle in relatively lesser time compared to lighter particulate.
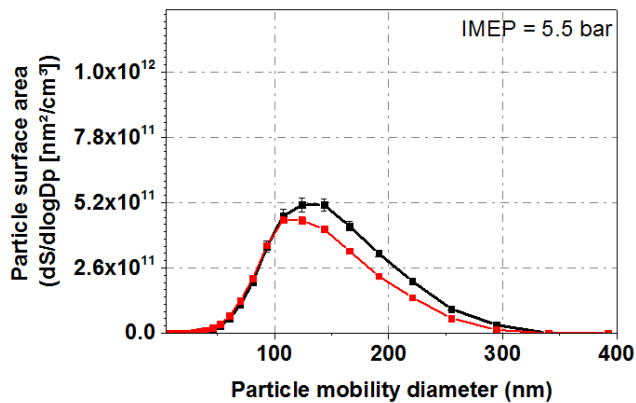
FIGURE 4(c). Particulate surface area-size vs. particulate mobility diameter

Figure 4(c) shows the particle surface area-size distributions for E15 and gasoline at 5.5 bar IMEP, 2000 rpm. Surface area-size distributions for E15 was relatively lower at 5.5 bar IMEP compared to baseline gasoline. Organic compounds adsorbed on agglomerate surfaces may penetrate deeper into the blood stream and can be carcinogenic. Larger the surface area-size distribution of particulate, higher will be the probability of this combustion generated PAH's to get adsorbed onto the agglomerate surface and cause greater health hazard
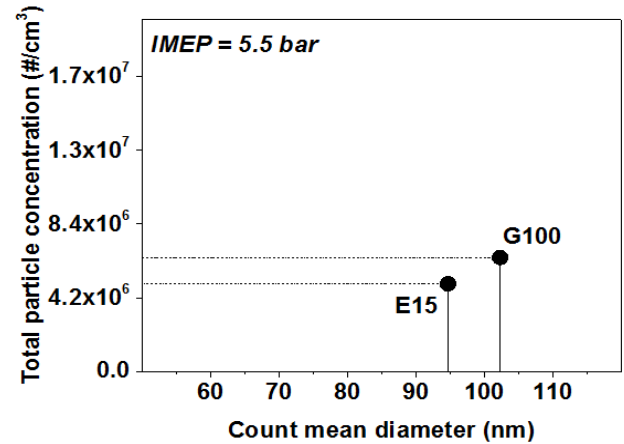
FIGURE 4(d). : Variation of CMD with total particulate number

For comparison of average particle size at a particular operating load, CMD was calculated and plotted against total particulate number. CMD gives a better estimate of the adverse health effects of engine's particulate emissions compared to total PN emission. It is not desirable to have higher number of particles with smaller sizes, which can easily penetrate deeper into the human respiratory system via inhalation and malfunction the respiratory system with toxic components adsorbed onto the agglomerate surfaces.

Figure 4(d) shows CMD and total particle concentration was relatively higher for gasoline than E15. It is desirable to have lower total PN concentration however if the CMD is smaller, then it indicates higher availability of surface area per unit mass of PM for adsorption of toxic compounds, which makes it highly toxic and undesirable.
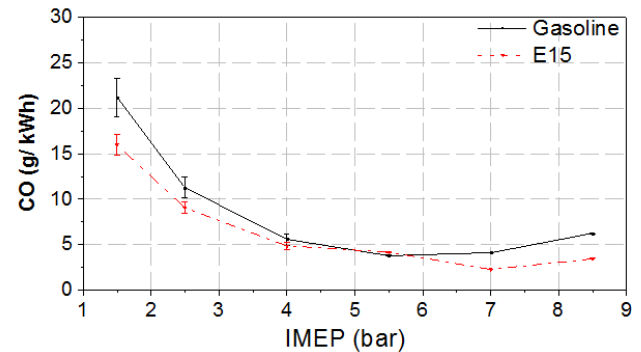
FIGURE 5(a). CO variation with IMEP
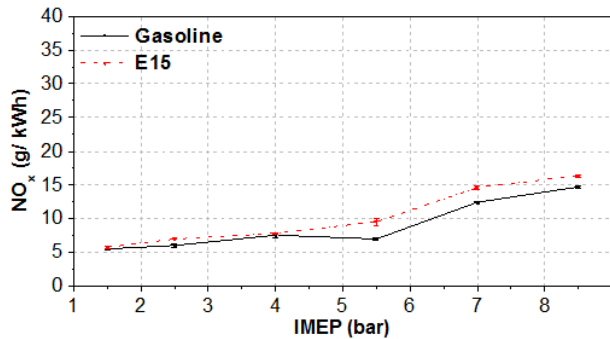
FIGURE 5(b). NO$_X$ variation with IMEP
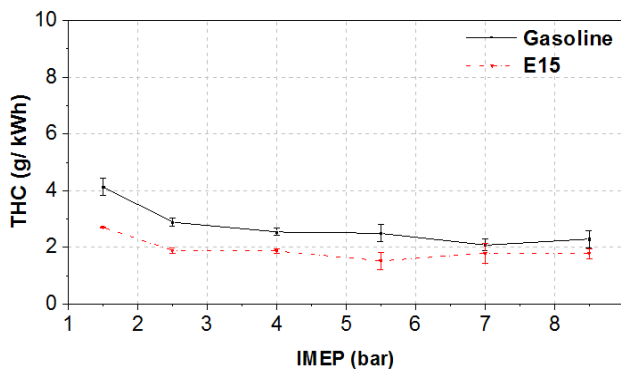
FIGURE 5(c). THC variation with IMEP

Figure 5a-c shows the variations of regulated gaseous emissions (g/kWh) at FIP of 80, and 2000 rpm for increasing IMEP. CO is a product of incomplete combustion in the combustion chamber. CO emission decreased with increasing IMEP because fuel-to-air ratio was maintained constant throughout the experiments, which lead to a complete combustion in the entire range of engine load (IMEP). CO was observed in the range of 22.3 to 2.9 g/kWh for both the test fuels. NO$_x$ emissions increases with increasing engine load, irrespective of the test fuel. The oxygen content of E15 leads to a complete combustion, which increases the peak in-cylinder temperature. NO$_x$ formation in an engine cylinder is a highly temperature dependent phenomena. NO$_x$ formation increases with increase in peak in-cylinder temperature, therefore, NO$_x$ emissions were higher from the oxygenated fuel. THC emissions decreased with increasing engine load. THC formation takes place due to flame quenching near the combustion chamber walls, which results in partial burning of fuel molecules.

CONCLUSIONS

This experimental investigation provides detailed insights of particle size-number, particle mass-size and particle surface-size distribution emitted from GDI engine, fuelled on E15 and baseline gasoline. It was found that E15 emitted relatively lower PN emissions, particle surface area and particle mass than baseline gasoline in a GDI engine in homogeneous charge mode at part load condition. CMD of

E15 was lower than gasoline at part load condition. CO was in the range of 22.3 to 2.9 g/kWh for both test fuels. NOx emissions increased with increasing engine load, irrespective of the test fuel used. THC emissions decreased with increasing engine load. It was because oxygen in a fuel can result in complete combustion of fuel-air mixture inside the combustion chamber.

REFERENCES
[1] Zhan, R., Eakle, S.T. and Weber, P., 2010. "Simultaneous reduction of PM, HC, CO and NOx emissions from a GDI engine" (No. 2010-01-0365). SAE Technical Paper.
[2] Samuel, S., Hassaneen, A. and Morrey, D., 2010. "Particulate matter emissions and the role of catalytic converter during cold start of GDI engine" (No. 2010-01-2122). SAE Technical Paper.
[3] Qin, J., Li, X. and Pei, Y., 2014. "Effects of Combustion Parameters and Lubricating Oil on Particulate Matter Emissions from a Turbo-Charged GDI Engine Fueled with Methanol/Gasoline Blends" (No. 2014-01-2841). SAE Technical Paper.
[4] Whelan, I., Samuel, S. and Hassaneen, A., 2010. "Investigation into the role of catalytic converters on tailpipe-out nano-scale particulate matter from gasoline direct injection engine" (No. 2010-01-1572). SAE Technical Paper.
[5] Stuart, B.O., 1984. "Deposition and clearance of inhaled particles.Environmental health perspectives", 55, p.369.
[6] Chakraborty, A. and Gupta, T., 2010. "Chemical characterization and source apportionment of submicron (PM1) aerosol in Kanpur region", India. Aerosol Air Qual. Res, 10(5), pp.433-445.
[7] Gupta, T. and Mandariya, A., 2013. "Sources of submicron aerosol during fog-dominated wintertime at Kanpur". Environmental Science and Pollution Research, 20(8), pp.5615-5629.
[8] Chen, L., Stone, R. and Richardson, D., 2012. "A study of mixture preparation and PM emissions using a direct injection engine fuelled with stoichiometric gasoline/ethanol blends". Fuel, 96, pp.120-130.
[9] Luo, Y., Zhu, L., Fang, J., Zhuang, Z., Guan, C., Xia, C., Xie, X. and Huang, Z., 2015. "Size distribution, chemical composition and oxidation reactivity of particulate matter from gasoline direct injection (GDI)

engine fueled with ethanol-gasoline fuel". Applied Thermal Engineering, 89, pp.647-655.

[10] Topgül, T., Yücesu, H.S., Cinar, C. and Koca, A., 2006. "The effects of ethanol–unleaded gasoline blends and ignition timing on engine performance and exhaust emissions". Renewable energy, 31(15), pp.2534-2542.

[11] Huang, J. and Crookes, R.J., 1998. "Assessment of simulated biogas as a fuel for the spark ignition engine". Fuel, 77(15), pp.1793-1801.

[12] Adams, W.H., Hinrichs, H.G., Pischinger, F.F., Adamis, P., Schumacher, V. and Walzer, P., 1987. "Analysis of the combustion process of a spark ignition engine with a variable compression ratio" (No. 870610). SAE Technical Paper.

[13] Pulkrabek, W.W., 1997. "Engineering fundamentals of the internal combustion engine" (No. 621.43 P8).

[14] Hsieh, W.D., Chen, R.H., Wu, T.L. and Lin, T.H., 2002. "Engine performance and pollutant emission of an SI engine using ethanol–gasoline blended fuels". Atmospheric Environment, 36(3), pp.403-410.

[15] Daniel, R., Tian, G., Xu, H. and Shuai, S., 2012. "Ignition timing sensitivities of oxygenated biofuels compared to gasoline in a direct-injection SI engine". Fuel, 99, pp.72-82.

[16] IS/ISO 8178-4., 2007: Reciprocating Internal Combustion Engines – Exhaust Emission Measurement [TED 2: Automotive Prime movers]

SEEC-2017-33

VALORIZATION OF CRUDE GLYCEROL FOR THE PRODUCTION OF POLYHYDROXYALKANOATES (PHA) IN SUSTAINABLE MANNER

Geeta Gahlawat*
Postdoctoral fellow
Department of Microbiology
Panjab University,Chandigarh
India-160014
Email: geeta.gahlawat@gmail.com

Sanjeev Kumar Soni
Professor
Department of Microbiology
Panjab University, Chandigarh
India-160014
Email:sonisk@pu.ac.in

ABSTRACT

Glycerol is a major by-product of biodiesel industry and huge amounts of it are generated in the form of waste, thereby raising serious concerns for its disposal. An interesting solution is the valorization of this waste glycerol into value added product - polyhydroxyalkanoates (PHAs). The feasibility of producing PHAs by Cupriavidus necator was evaluated using waste glycerol (WG). Batch cultivation on WG showed a total biomass of 5.7 g/L and PHB concentration of 3.42 g/ with PHA content of 59.8% of cell dry weight. Thereafter, various cultivation strategies for the production of poly(3-hydroxybutyrate-co-3-hydroxyvalerate) were attempted by adding various precursors (valeric acid, propionic acid etc.) at different concentrations. A high poly(3HB-co-3HV) content of 64% along with high 3HV content of 30.8 mol% was obtained with valeric acid (4g/L). Further detailed batch kinetics study of poly(3HB-co-3HV) copolymer production resulted in accumulation of 6.76 g/L biomass containing 4.84 g/L poly(3HB-co-3HV) on WG.

Keywords: *Polyhydroxyalkanoates, Cupriavidus necator, Waste glycerol, Sustainability, Microbial cultivation*.

NOMENCLATURE
PHB-Polyhydroxybutyrate
PHA-Polyhydroxyalkanoate
P(3HB-co-3HV)- poly(3-hydroxybutyrate-co-3-hydroxyvalerate)
WG- waste glycerol
CG- commercial glycerol

INTRODUCTION

An indiscriminate utilization of fossil fuels and toxic petroleum-based plastics have turned research efforts towards the production of biodegradable plastics-Polyhydroxyalkanoates (PHAs). The biotechnological production of PHAs biopolymers from renewable resources provides a sustainable alternative to petroleum derived-plastics and also reduces the dependency on rapidly disappearing fossils fuels [1]. PHAs are biodegradable and biocompatible polymers with their material properties quite similar to petrochemical derived plastics. They have various potential applications particularly in newly emerging areas such as tissue engineering, targeted drug delivery and agricultural fields [2].

Polyhydroxybutyrate or PHB is the first member of PHAs group which has been studied in detail. However, the industrial application of PHB is restricted by its poor mechanical and physical properties such as brittleness and stiffness. Incorporation of other monomeric units such as 3-hydroxyvalerate (3HV) into PHB yields copolymer with improved physico-mechanical properties such as flexibility and toughness [1]. Therefore, the production of copolyester of 3HB and 3HV, poly(3-hydroxybutyrate-co-3-hydroxyvalerate) can solve issues of brittleness and thermal unstability.

The high cost of PHAs production process further prevents its market penetration and commercialization [3]. This major obstacle have shifted focus towards cost reduction by use of renewable resources which account for 40-50% of the total production cost. Industrial by-products such as glycerol (from the biodiesel industry), rice bran, molasses and cheese whey can be used as inexpensive

renewable carbon sources for PHAs production. Glycerol is a by-product of many industrial processes and huge amounts of waste glycerol are generated (1 gallon of waste glycerol is obtained for every 10 gallon of biodiesel produced) against a meager demand resulting in a severe loss to the industry thereby necessitating a search for the method of its disposal [4]. An interesting solution is the conversion of this waste glycerol into value added product such as PHAs. Therefore, the present study was dedicated to evaluating the possibility of PHB and P(3HB-co-3HV) copolymer production from waste glycerol using *Cupriavidus necator*

MATERIAL AND METHODS

MICROORGANISM AND MAINTENANCE

Cupriavidus necator DSM 545 was procured from German Collection of Microorganisms and Cell Cultures (DSMZ), Germany. The strain was maintained on nutrient agar slants at 4°C and subcultured monthly. *C. necator* culture was stored in the form of glycerol stocks at -70°C.

MEDIA AND CULTURE CONDITIONS

A mineral salt medium consisting of 10 g/L glucose, 3.59 g/L Na_2HPO_4, 2 g/L $(NH_4)_2SO_4$, 1.5 g/L KH_2PO_4, 0.2 g/L $MgSO_4.7H_2O$, 0.02 g/L$CaCl_2.2H_2O$, 0.05 g/L NH4Fe(III)citrate, 1mL trace element solution (SL6) was used as the basal medium for the initial cultivation studies [4]. The trace element solution SL6 was composed of (per liter): $ZnSO_4.7H_2O$, 100 mg; H_3BO_3, 300 mg; $CoCl_2.6H_2O$, 200 mg; $CuSO_4$, 6 mg; $NiCl_2.6H_2O$, 20 mg; $Na_2MoO_4.2H_2O$, 30 mg; $MnCl_2.2H_2O$, 25 mg. In case of *C. necator*, glucose was replaced by commercial glycerol (CG) and waste glycerol (WG). Waste glycerol (containing around 40% glycerol) was collected as a by-product from Jatropha based biodiesel production plant in Centre for Rural Development Technology, Indian Institute of Technology Delhi. The pH of the media was adjusted aseptically to 6.8 using 2N NaOH/HCl.

EFFECT OF DIFFERENT GLYCEROL CONCENTRATION

Preliminary studies were carried out in 250 mL shake flasks containing 50 mL medium (pH 6.8) to study the effect of different concentration (10 g/L to 60 g/L) of CG and WG on specific growth rate of *C. necator*. Other constituents of the media and fermentation conditions were kept unchanged. Shake flasks were inoculated with 5% (v/v) exponentially growing culture from the inoculum flasks. Shake flasks were then kept in incubator shaker maintained at 30°C and 200 rpm. Samples were collected at regular intervals for analysis. All the experiments were performed in duplicates and average values are reported.

PHB PRODUCTION

For PHB production, inoculum was grown in 250 mL shake flasks containing 50 mL medium (pH 6.8). The exponentially growing culture (5% v/v) was further inoculated into 1 L flasks containing 200 mL basal media for batch kinetic study. The culture flasks were incubated at 30°C and 200 rpm and allowed to grow for 48 h. Samples were withdrawn at regular intervals. Batch kinetic study was performed to determine the initiation time of PHA production phase which would be helpful in copolymer production studies.

PRODUCTION OF POLY (3-HYDROXYBUTYRATE-CO-3-HYDROXYVALERATE) OR POLY (3HB-CO-3HV)

It has been reported in literature that the PHB is very brittle, stiff and therefore thermally unstable during processing which limits its use for various applications as opposed to polypropylene. Therefore, there is a need to produce PHB copolymers such as Poly (3HB-co-3HV) which features better thermal processability and elasticity primarily equivalent to petroleum derived polymers. Attempt was therefore made to produce the copolymers in the present investigation by addition of organic acid (or copolymer precursors).

EFFECT OF ADDITION OF DIFFERENT ORGANIC ACIDS ON THE POLY (3HB-CO-3HV) COPOLYMER PRODUCTION

Various shake flask experimental studies were conducted to find out the appropriate acid concentrations levels required for copolymer production. Effect of addition of different organic acids: valeric acid, propionic acid, butyric acid, acetic acid and sodium propionate on copolymer production by *C. necator* was studied in 250 mL flasks containing 50 mL basal medium. All the organic acids were tested at different concentrations: 2 g/L, 4 g/L and 6 g/L to investigate their effects on copolymer production. The acids were added in four equal pulse installments (for example 0.5 g/L each for 2 g/L or 1g/L each for 4g/L or 1.5 g/L each for 6 g/L) at an interval of 8 h i.e. 12 h, 20 h, 28 h, and 36 h. In all the cases the pH of the medium was adjusted to 6.8 using 2N NaOH/2N HCl after addition of acids. The flasks were thereafter incubated in an incubator shaker at 30°C and 200 rpm. The flasks were harvested after 40 h for analysis.

ANALYTICAL METHODS

Optical density of suitably diluted culture broth was measured at 600 nm against a medium blank using spectrophotometer. Biomass was measured from a plot of OD600nm vs. dry cell mass (g/L). Samples were collected at time intervals of 6 h and then centrifuged at 10,000 rpm for 15 min at 4°C. Cell pellet was dried at 80°C till constant weight was obtained to establish biomass

concentration; it was then used for PHAs analysis. PHAs content in dried cells was analyzed by gravimetric method [3] and gas chromatography [5]. Residual glycerol concentrations in supernatant were measured by high performance liquid chromatography (HPLC) using refractive index detector. Separation was performed on Waters Sugar-Pak I column (300×6.5 mm) using 0.0001 M Calcium EDTA as mobile phase at a flow rate of 0.5 ml/min at 90°C temperature. For PHAs extraction, 250 mg dried cells were re-suspended in 30 mL chloroform in 250 mL screw capped borosil bottles and incubated at 28°C for 36 h with vigorous agitation [1]. The contents of the bottle were then filtered and precipitated using chilled ethanol. The extracted PHA was characterized by Fourier Transform Infrared Spectroscopy (FTIR) analysis.

RESULTS AND DISCUSSION

EFFECT OF DIFFERENT GLYCEROL CONCENTRATIONS

C. necator was cultivated in shake flask using basal medium to test whether the growth rate and polymer yield of culture was affected with increasing initial concentrations of CG or WG. Fig. 1 shows that initial concentrations of CG within the studied range do not significantly affect the growth rate. On the other hand, results on WG indicate that the specific growth rate is maximum (approximately 0.26 h^{-1}) in the range 20–30 g/L. Above this range, a decrease in the growth rate is observed which may be due to the accumulation of sodium in the culture medium (assuming that WG contains 3% (w/w) of Na$^+$). Therefore 20 g/L was selected as the optimized value for further experiments. Biomass and polymer yield were then studied by *C. necator* using 20 g/L concentration of CG and WG (Table 1). At the end of cultivation, a total biomass of 6.69 g/L and PHB concentration of 4.33 g/L were obtained on CG with an overall PHA content of 64.72% of CDW. On the other hand, maximum biomass and PHB concentration on WG were 5.7 g/L and 3.42 g/L respectively, with PHAs content of 59.8% of CDW.

PHB PRODUCTION KINETIC STUDY

Fig. 2 shows the batch kinetics of *C. necator* in 1 L shake flask containing 20 g/L WG as carbon source and all other components were same as reported in literature [4]. The culture metabolism exhibited an initial lag phase of around 3 h after which it started to grow exponentially. The PHAs production phase started at 12 h and PHB concentration reached to 5.26 g/L in 36 h of cultivation period. The yield of PHB from waste glycerol was 0.328 g/g and PHB productivity was 0.15 g/L.h. The pH value measured at the end of the cultivation was found to be 5.12 as against an initial value of 6.8. It was presumed that decrease in pH resulted in unfavorable growth conditions that led to reduced growth and thus the consumption of nutrients eventually stopped.

Figure 1 The effect of initial glycerol concentration on the specific growth rate of *C. necator*.

Table 1. Comparison of biomass, product yields and content during *C. necator* cultivation on CG and WG

Carbon source (2%)		Biomass (g/L)	PHB (g/L)	PHB content (%)	PHB productivity (g/L.h)
(CG)*	Day 1	3.75	1.84	49.12	0.08
	Day 2	6.69	4.33	64.72	0.09
(WG)*	Day 1	2.8	1.25	44.64	0.052
	Day 2	5.7	3.42	59.80	0.07

Note: CG-Commercial glycerol; WG: waste glycerol

Figure 2 Time course of batch PHB fermentation kinetics of *C. necator*

EFFECT OF ADDITION OF DIFFERENT ORGANIC ACIDS ON THE POLY (3HB-CO-3HV) PRODUCTION

The shake flask cultivations for the production of poly (3HB-co-3HV) were attempted by adding various organic acids at different concentrations levels i.e. 2 g/L, 4 g/L and 6 g/L. Acids were added in the form of multiple pulses to prevent growth inhibition that might be caused

due to acidic nature of these acids if entire amount was added in single pulse. These acids were added in four equal pulse installments at an interval of 8 h (i.e. four pulses of 1 g/L each for 4 g/L and 0.5 g/L each for 2 g/L). Addition of organic acids was initiated during PHAs production phase i.e. at 12 h when active polymer accumulation phase has been started. Of all the organic acids examined, poly (3HB-co-3HV) copolymer production was achieved only with the valeric acid and propionic acid (Table 2).

Table 2 Effect of addition of different organic acids on biomass and copolymer accumulation

Organic acids	Biomass (g/L)	3HB(g/L)	3HV (g/L)	Total PHA (g/L)	PHA content (%)
Valeric acid (2 g/L)	3.24	1.18	0.55	1.73	53.30
VA (4 g/L)	**5.32**	**2.36**	**1.05**	**3.41**	**64.10**
VA (6 g/L)	4.16	1.37	0.74	2.11	50.72
Propionic acid (2 g/L)	3.42	1.05	0.36	1.41	41.22
PA (4 g/L)	4.51	1.92	0.65	2.57	57.00
PA (6 g/L)	3.36	1.21	0.55	1.76	52.38
Sodium propionate (2 g/L)	2.47	1.25	-	1.25	50.61
SP (4 g/L)	2.06	0.74	-	0.74	35.92
SP (6 g/L)	1.87	0.58	-	0.58	31.02

None of the other organic acids supported the addition of 3 HV monomers in the polymeric chain. Feeding of sodium propionate, acetic acid and butyric acid resulted in production of 3-hydroxybutyric acid monomer units. However, of all the above mentioned valerate copolymers precursors, the maximum concentration of 3-hydroxybutyrate (3HB) and 3-hydroxyvalerate (3HV) units was obtained only with valeric acid (4 g/L) addition. Shake flask cultivation with valeric acid (4g/L) featured an overall accumulation of 5.32 g/L biomass and 3.41 g/L poly (3HB-co-3HV) concentration with an overall PHAs content of 64 % of CDW. Addition of valeric acid led to an incorporation of high percentage of 3HV units in polymeric chains as compared to propionic acid. Based on the above results, a high poly (3HB-co-3HV) concentration of 3.41 g/L along with high 3HV content of 30.8 mol% was obtained with valeric acid, 4g/L. Therefore valeric acid was selected as the most suitable organic acid for poly (3HB-co-3HV) production by *C. necator.*

CONCLUSION

The present study demonstrated that crude glycerol from biodiesel industry can be used an alternative renewable carbon source for sustainable production of PHAs. *C. necator* was capable of accumulating an appreciable amounts of PHB of 60% of CDW from crude glycerol. Evaluation of different cultivation strategies for copolymer production showed that this strain is also capable of accumulating high poly (3HB-co-3HV) content of 64% of CDW using valeric acid (4g/L) as precursor. The proposed process will help in the valorization of waste glycerol as well as reduction of production cost of valuable biodegradable polymers.

REFERENCES
1. J. M. B. T. Cavalheiro, R. S. Raposo, M. C. M. D. de Almeida, M. Teresa Cesário, C. Sevrin, C. Grandfils, M. M. R. da Fonseca, Effect of cultivation parameters on the production of poly(3-hydroxybutyrate-co-4-hydroxybutyrate) and poly(3-hydroxybutyrate-4-hydroxybutyrate-3-hydroxyvalerate) by *Cupriavidus necator* using waste glycerol, Bioresource Technology 111 (2012) 391-397.
2. S. Chanprateep, Current trends in biodegradable polyhydroxyalkanoates, Journal of Bioscience and Bioengineering 110 (2010) 621-632.
3. E. Grothe, M. Moo-Young, Y. Chisti, Fermentation optimization for the production of poly (β-hydroxybutyric acid) microbial thermoplastic, Enzyme Microbial Technology 25 (1999) 132–41.
4. I.V. Špoljarić, M. Lopar, M. Koller, A. Muhr, A. Salerno, A. Reiterer, K. Malli, H. Angerer, K. Strohmeier, S. Schober, M. Mittelbach, Mathematical modeling of poly [(R)-3-hydroxyalkanoate] synthesis by *Cupriavidus necator* DSM 545 on substrates stemming from biodiesel production, Bioresource technology 133 (2013) 482-494.
5. V. Riis, W. Mai, Gas chromatographic determination of poly-β-hydroxybutyric acid in microbial biomass after hydrochloric acid propanolysis, Journal of Chromatography A 445 (1988) 285-289.

SEEC-2017-034

GROUND WATER DESALINATION THROUGH MICROBIAL DESALINATION CELL

Manupati Hemalatha
Bioengineering and Environmental Sciences Lab,
EEFF Department, CSIR-Indian Institute of
Chemical Technology (CSIR-IICT),
Hyderabad- 500007, India.
E-mail: hemalathamanupati@yahoo.com

Sai Kishore Butti
Bioengineering and Environmental Sciences Lab,
EEFF Department, CSIR-Indian Institute of
Chemical Technology (CSIR-IICT),
Hyderabad- 500007, India.
E-mail: kishore288@gmail.com

G.Velvizhi
Bioengineering and Environmental Sciences Lab,
EEFF Department, CSIR-Indian Institute of
Chemical Technology (CSIR-IICT),
Hyderabad- 500007, India.
E-mail: gvels@yahoo.com

S. Venkata Mohan*
Bioengineering and Environmental Sciences Lab,
EEFF Department, CSIR-Indian Institute of
Chemical Technology (CSIR-IICT),
Hyderabad- 500007, India.
E-mail: vmohan_s@yahoo.com

ABSTRACT
The present study evaluates the desalination efficiency of synthetic ground water (SGW) in three chambered MDC reactor with biotic anode (organic substrate-3 g/l), abiotic cathode (distilled water) and middle chamber (SGW-2.5 g TDS/l). The microbial metabolism oxidizes organic matter in anode chamber and generates bioelectricity. The negatively charged species move from middle chamber towards anode chamber through anion exchange membrane and positively charged species towards cathode chamber through cation exchange membrane. Thus movement of ion species desalts saline water without supply of external energy. Salinity and organic carbon removal efficiency were observed to be 49% and 62% in anode and middle chamber with maximum OCV (482 mV). Bioelectrogenic and bioelectrochemical characterization were performed to understand ionic movements for desalination processes.

Keywords:
Substrate utilization, Product recovery, Bioelectricity, Ionic movement, Wastewater Treatment

INTRODUCTION
Availability of clean and safe drinking water is becoming scarce due to rise in pollution. To alleviate this problem, conventional technologies such as reverse osmosis and electrodialysis are currently in use. These processes are energy intensive and associated with high operating expenses. Microbial desalination cell (MDC) is a sustainable technology used for treating saline water with relatively little energy consumption along with wastewater treatment and resource recovery. The objective of the study is to evaluate the microbial desalination process for salts removal from ground water.

Groundwater may vary in composition from place to place. Seasonal variations in the composition of groundwater from a single well generally results in a change in chemical state of groundwater, i.e., temperature, pH and redox potential. These parameters influence the amount and character of the dissolved constituents and therefore produce changes in the taste, odor, appearance etc., possible causes of changes in the chemical state include different water levels and annual recharge events. The variations described are the result of natural causes. It is important to recognize this, so as not to attribute these changes in water potability to anthropogenic causes.

MATERIALS AND METHODS

Design of MDC
Three chambered bioreactor for desalination was fabricated manually in the laboratory using Teflon. The reactor consists of the bioanode (BA), abiotic cathode (AC)

and middle desalination chamber (DC) separated by anion exchange membrane and cation exchange membrane. The chambers are clamped together with gaskets (a silica sheet) and O-rings are inserted between the membrane and chamber to prevent water leakage. Non-catalyzed carbon cloth with geometrical surface area of $28.2cm^2$ is used as anode and cathode, prior to use carbon cloth was treated using 0.5% NH_4Cl solution to increase the conductivity.

MDC Operation

Synthetic ground water (SGW) [2] was prepared by dissolving $CaCO_3$-200mg/l, $CaSO_4$-272mg/l, $4MgCO_3.Mg(OH_2).5H_2O$-194mg/l, $NaHCO_3$-252mg/l, KCl -75mg/l in distilled water and fed to the desalination chamber. The anode chamber was inoculated with anaerobic sludge with feed solution composed of design synthetic wastewater with organic substrate (glucose) of 3g/l where as cathode chamber was fed with milliQ. Prior to start up pH of anolyte and SGW was adjusted to 6 (0.1NHCl) and 7 (0.1M H_2SO4) respectively. MDC was operated in batch mode (open circuit (OC); closed circuit (CC)) at room temperature. Samples were collected at an interval of 12h and the feed of the individual chambers were replaced for every 48h.

Desalination Calculations

The electrical conductivity (EC) and TDS of electrolytes of BA, AC and DC were measured using a bench top meter (HANNA HI 76312 and HANNA HI 1131). The desalination efficiency was calculated by the following equation [3]:

$$DE\ (\%) = \frac{Eci - Ece}{ECi} \times 100 \qquad (1)$$

Where E_{ci} and E_{ce} is the influent and effluent electrical conductivity (mS/cm).

Bioparametric analysis

Parameters like pH, chemical oxygen demand (COD) (closed refluxing method) and volatile fatty acids (VFA) were analysed according to the standard methods (APHA 1998).

Bio-electrochemical Analysis

Bioelectrochemical behavior in terms of cyclic voltametry (CV), linear sweep voltametry (LSV) and open circuit voltage of MDC reactor was measured against Ag/AgCl (3.5 M KCl) reference electrode using controlled potentiostat/galvinostat system (Bio-Logic-VMP₃, France). After stabilized OCV is achieved polarization analysis were performed by applying variable resistor to estimate the maximum power point (MPP). The same is applied on MDC reactor as an external load and influence of system performance was evaluated in closed circuit (CC).
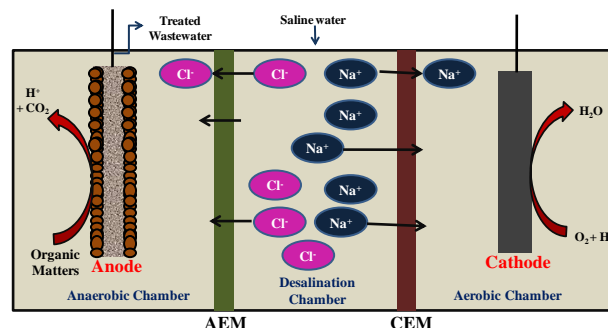
SCHEMATIC REPRESENTATION OF MICROBIAL DESALINATION CELL

RESULTS AND DISCUSSION

Desalination

Desalination efficiency (DE) of MDC during the experimental operation showed 51.5% and 34.3% in open and closed circuit system. Ionic gradient drives mobility of ions from DC to BA and AC based on charge, where the DC gets desalinated and resource recovery is observed at BA and AC. The conductivity in DC chamber decreased from 3900mS/cm to 1890mS/cm in CC; 2560mS/cm in OC while BA (open circuit-0.429mS/cm to 0.722mS/cm; closed circuit-0.429mS/cm to 0.858mS/cm) and AC (open circuit-0.022mS/cm to 0.304mS/cm; closed circuit-0.022mS/cm to 0.515mS/cm) showed slight increment at 48h.

Substrate utilization and Resource recovery

In anode chamber anaerobic bacteria metabolizes organic matter and releases electrons (e⁻) and protons (H⁺) into the solution resulting in COD removal of 69% and 53% for OC and CC operation. The affinity of H⁺ ions towards Cl⁻ ion migrated from desalination chamber through AEM results in formation of acid signifying the drop in pH. Migration of positive ions from DC to AC through CEM results in alkali formation thus increment in pH is observed. The loss of ions from DC infers the desalination process.

Bioelectrogenesis

The maximum OCV produced during open circuit was 482 mV. The gradual rise in OCV is an indication of biofilm formation and microbial enrichment. The polarization behavior of the reactor was analyzed and the MPP at applied external resistance was determined. Therefore the reactor is left for long term implication by applying the external resistance of 1kΩ. The voltage generation followed a sigmoidal increase, attributed to the lag phase required for biofilm formation in the anode. The anolyte solution was frequently replaced (every 48h) to avoid substrate limitations or pH changes for bacteria on the anode.

CONCLUSION

The study concludes that MDC could be the cost effective and greener technologies for reducing salt concentration with simultaneous product recovery and wastewater treatment. Effective desalination was observed in the middle chamber for both circuit operations, with a maximum TDS removal and treatment efficiency in external circuit operation. A gradual rise in OCV is a characteristic feature of microbial enrichment and biofilm formation, the OCV is proportional to higher substrate degradation. Cathodic product recovery makes sense for future application in secondary wastewater treatment or as pretreatment to reverse osmosis.

ACKNOWLEDGMENTS

REFERENCES

[1] Nikhil, G.N., Dileep Kumar Yeruva, Venkata Mohan, S., Swamy, Y.V., 2016 "Assessing potential cathodes for resource recovery through wastewater treatment and salinity removal using non-buffered microbial electrochemical systems". Bioresour Technol. 215, September, 247-253.

[2] Stewart, D.I., Csõvári, M., Barton, C.S., Morris, K. and Bryant, D.E., 2006. Performance of a Functionalised Polymer-Coated Silica at Treating Uranium Contaminated Groundwater from a Hungarian Mine Site. Engineering Geology, 85 (1-2). pp. 174-183.

[3] Zuo, K., Cai, J., Liang, S., Wu, S., Zhang, C., Liang, P., Huang, X., 2014. A ten liter stacked microbial desalination cell packed with mixed ion-exchange resins for secondary effluent desalination. Environ. Sci. Technol. 48 (16), 9917–9924.

SEEC-2017-35

Sustainable Valorisation of Biogenic Municipal Solid Waste to Biobased Products

A. Naresh Kumar
Bioengineering and Environmental Sciences (BEES)
CSIR-Indian Institute of Chemical Technology (CSIR-IICT), Hyderabad- 500 007, India.

S. Venkata Mohan
Bioengineering and Environmental Sciences (BEES)
CSIR-Indian Institute of Chemical Technology (CSIR-IICT), Hyderabad- 500 007, India.

ABSTRACT
Minimizing the dependency on fossil-based resources and reducing the generation of solid wastes represent the main challenges for the modern society. Biogenic municipal solid waste (BMSW) a potential feedstock to harness the energy and biobased products. Currently, open dumping is the common practice of BMSW disposal followed by biomethanation and incineration. In the present study, re-engineering of anaerobic fermentation process for the high rate production of biobased products (reducing sugars, short chain carboxylic acids and biohydrogen) using biogenic municipal solid waste as a feedstock. Initially, to convert the polysaccharides into monomers novel bio-electro hydrolysis (BEH) system is designed as a pretreatment unit to carry the hydrolysis of BMSW with simultaneous bioelectricity generation. Resulting sugar rich effluents were used as a substrate in acidogenic fermentation process (stage-I) to produce short chain carboxylic acids (SCCA) along with biohydrogen (H2) as co-product. Further, the resulting effluent from stage-I rich in SCCA was used as feedstock for polyhydroxy alkanoates (PHA) production (stage-II), which was carried out in two steps viz., PHA culture enrichment followed by PHA production. Bacteria capable of accumulating PHA were enriched in a sequencing batch reactor operated at two different cycle lengths (CL-24h; CL-12h). Higher PHA production as well as SCCA removal was achieved in CL-12 operation followed by CL-24. The results enumerate the advantages of integrated multistage process for the production of biobased products by simultaneously addressing the solid waste remediation in the framework of biorefinery.

SEEC-2017-036

EFFECT OF TRACE METALS ON THE SPECIFIC ACID PRODUCTION USING WASTEWATER AS SUBSTRATE

Shikha Dahiya
Bioengineering and Environmental Science
(BEES) Lab,
EE&FF Department
CSIR-Indian Institute of Chemical Technology
Hyderabad 500 007, India
Email: shikhabiotech17@gmail.com

S Venkata Mohan*
Bioengineering and Environmental Science
(BEES) Lab,
EE&FF Department
CSIR-Indian Institute of Chemical Technology
Hyderabad 500 007, India
Email: vmohan_s@yahoo.com

ABSTRACT
Dark-fermentative acidogenic process produces biohydrogen (H_2) co-generating short chain carboxylic acid [volatile fatty acid (VFA)] from waste and harvesting these valuable chemicals, makes the process more economical and sustainable. Optimising the parameters to enhance specific volatile fatty acid and H_2 from different wastes makes it more economical feasible. Main objective of the proposed work is to enhance production of specific VFA with different Co^{2+} and Zn^{2+} concentration in mixed fermentation using designed synthetic wastewater. The composition of fatty acids showed a marked variation with both fermentation time and metals concentration used where acetic acid, propionic acid, butyric acid and ethanol accumulation found with different concentration of metals. H_2 production and DH activity was well correlated with the specific acid production. VFA production at optimum metal concentration with simultaneous H_2 will give a new facet to waste management and production of high monetary valued products.

Keywords: Waste valorization, Volatile fatty Acids, Acidogenesis, Biohydrogen, Propionic acid

INTRODUCTION
Waste is being considered as potential and renewable feedstock for the production of a gamut of bio-based products ranging from fuel to platform chemicals [1]. The development of environmental innovative strategies to utilize such waste into useful products is now became an area of importance and relevance. Among the biological routes, acidogenic fermentation process for H_2 production and VFA showed a promising and practical viability due to its feasibility of utilizing different types of wastes as feedstock [2] H_2 and VFA are two important value added products of acidogenic fermentation and if harvested properly in an integrated approach will make the whole process environmentally sustainable and economically viable [3]. Acidogenic H_2 production was well studied and documented with various feedstock and at present it is at upscaling stage. VFA contain a functional group whose reactivity allows the formation of other compounds, such as esters and amides. Additional, innovative applications for VFA includes, thermal conversion to ketones and subsequent hydrogenation to alcohol fuels, electron donors in microbial fuel cells and feedstock for microalgae based biodiesel production [4]. VFA are important bulk chemicals that are used as building blocks for the production of polymers, as acidulants, preservatives and favouring agents or as precursors for the synthesis of chemicals [4]. Thus, this study was conducted to investigate the influence of Co^{2+} and Zn^{2+} on the specific VFA and H_2 production.

MATERIALS AND METHODS

Anaerobic Consortia
Anaerobic consortium sampled from full scale anaerobic pilot plant reactor treating composite wastewater was used as parent inoculum.

1

Experimental Details

11 identical bench scale anaerobic reactors were fabricated using borosilicate-glass bottles with total/working volume of 250/200 ml. All the reactors were operated at an ambient temperature with organic load of 5 g COD/lit with DSW. Each reactor was supplemented with increasing concentration of Co^{2+} and Zn^{2+} (1:2 ratio) respectively (C_1, C_2, R_1, to R_7, R_{Co} and R_{Zn}). Control were kept without metals. Pure nitrogen gas was sparged to the reactor for 5 min after every feeding and sampling event to maintain anaerobic conditions. Prior to feed, the inlet feed pH was adjusted to pH 7 using 1 N HCl or 1 N NaOH.

Analyses

VFA composition was analyzed using high performance liquid chromatography (HPLC; Shimadzu LC10A) employing UV–Vis detector (210 nm) with C18 reverse phase column and mobile phase of milli-Q water. Sample injection of 20 µl volume was used. Biogas composition was monitored using gas chromatography (GC; NUCON 5765) using thermal conductivity detector (TCD) with 1/ 800 X 2 m Heysep Q column employing Argon as carrier gas. Chemical oxygen demand (COD-closed refluxing titrimetric method), VFA and pH were estimated by the standard methods.

RESULTS AND DISCUSSION

pH profile

The pH was observed with a time interval of 12 h. In the two controls, C_1 and C_2, a sharp pH decrease has been observed while in the reactors with different concentrations of metals (R_1, R_2, R_3, R_4, and R_5); a gradual decrease was observed. However, a very low decrease has been observed in R_6 and R_7. The decrease in pH was well corelated with the VFA produced in the respective systems .

Volatile Fatty acid

VFA production was analyzed at a time interval of 12 h of the operating cycles. In all the conditions studied, it was observed that VFA production started without much lag and there was a noticeable increase from the 12th h of cycle operation. In control reactors, C_2 showed comparatively higher VFA production than C_1 . Reactor 1 had the highest VFA production compared to other systems, followed by R_2 and R_3. It is observed that reactor systems 4 and 5 have almost equal amount of VFA production. Reactors 6 and 7 have a very low VFA production. Reactors R_{Co} and R_{Zn} illustrated optimum VFA production in varied concentrations due to individual effect of metal ions.

Degree of acidification

The degree of acidification varied within different reactors. Total degree of acidification was highest in C_2 followed by R_1 and R_2. Acetic acid contributed highest degree of acidification in reactor R_{Co} and R_{Zn} while acetic acid and butyric acid in C_1 and C_2. Propionic acid was found to be major contributor of degree of acidification in reactor R_2.

Cumulative Hydrogen Production Profile

The CHP profile was studied using H_2 sensor readings. In C_1, i.e., the reactor without any metals, we observe very low amount of H_2 production. However, in C_2, i.e, reactor without Co^{2+} and Zn^{2+}, we observe a moderate production of H_2. R_2 has been observed with having the highest amount of H_2. However R_1 and R_3 have comparatively lower production than R_2. Reactors 4, 5, 6 and 7 follow the trend of decreasing productivity and R_7 has the lowest production of H_2. Individual reactors Co^{2+} and Zn^{2+} have approx. similar H_2 productivity values owing to individual metal ion effect.

COD Removal Efficiency

Experimental results revealed steady increment in the substrate degradation efficiency for all the reactors. Compared to controls, C_1 and C_2, all the other reactors have lower substrate degradation rates possibly implying that the presence of metals is responsible for lower degradation of substrates. However, R_2 has high rate of COD removal owing to high dehydrogenase activity. Reactors 1, 3, 4 and 5 have a moderate degradation rate signifying that with increase in metal concentrations, there is a reduced removal efficiency. R_7 has the lowest degradation rate whereas R_{Co} and R_{Zn} have the highest substrate degradation.

Dehydrogenase activity

Interestingly, experimental results presented a pattern of overall increase in DH activity in all the reactors. In C_1, a sharp increase of DH activity has been observed in the 12th hour which gradually decreases with time. However, C_2 shows the highest DH activity at the mid-cycle. In R_1, there is a gradual increase in the activity in the initial hours and a corresponding decrease in the later hours of the cycle. R_2 and R_3 had high DH activity even in the 48th hour of the cycle indicating that the bacterial activity is still being maintained. However, in R_4 and R_5, almost equal activity has been observed. For R_6 and R_7, it was observed that these reactors have the lowest DH activity. In R_{Co}, the DH activity in the 6th hour itself in higher compared to R_{Zn}.

CONCLUSION

Metal ion concentration played a vital role in the production of specific volatile fatty acid production and also in the biohydrogen production. Degree of acidification varied significantly based on the metal ion concentration. Using wastewater for the production of platform chemicals documents a new dimension for

production of value added chemical from waste in the framework of biorefinery

REFERENCES

[1] Venkata Mohan, S., Nikhil, G. N., Chiranjeevi, P., Nagendranatha Reddy, C., Rohit, M. V., Naresh Kumar, A., and Sarkar, O., 2016. "Waste biorefinery models towards sustainable circular bioeconomy: Critical review and future perspectives". Bioresource technology, 215, pp. 2-12.

[2] Mohanakrishna, G. and Venkata Mohan, S., 2013. "Multiple process integrations for broad perspective analysis of fermentative H 2 production from wastewater treatment: technical and environmental considerations."Appl. Energy. 107, pp. 244–254.

[3] Dahiya, S., Sarkar, O., Swamy, Y.V., Venkata Mohan, S., 2015. "Acidogenic fermentation of food waste for volatile fatty acid production along with co-generation of biohydrogen." Bioresource Technology. 182, pp. 103-113.

[4] Sarkar, O., Kumar, A. N., Dahiya, S., Vamshi Krishna, K., Yeruva, D. K. and Venkata Mohan, S., 2016. "Regulation of acidogenic metabolism towards enhanced short chain fatty acid biosynthesis from waste: metagenomic profiling." RSC Adv. 6, pp. 18641-18653.

SEEC-2017-037

Biodiesel Production through Waste Derived Fatty Acid Fermentation using *Cryptococcus curvatus*

Sulogna Chatterjee
Bioengineering and Environmental Sciences Lab,
EE&FF Department, CSIR-Indian Institute of
Chemical Technology (CSIR-IICT),
Hyderabad- 500007, India.

E-mail: sulogna16@gmail.com

S. Venkata Mohan*
Bioengineering and Environmental Sciences Lab,
EE&FF Department, CSIR-Indian Institute of
Chemical Technology (CSIR-IICT),
Hyderabad- 500007, India.

E-mail: vmohan_s@yahoo.com

ABSTRACT

The use of Volatile Fatty Acid (VFA) as substrate for fermentation processes yielding valuable products is very attractive. In this study, the utilization of VFA as a growth substrate for the cultivation of oleaginous yeast Cryptococcus curvatus was studied with the aim to produce intracellular lipids. Therefore two stage fed-batch strategies were designed: the yeast was initially grown on designed synthetic waste water containing glucose then sequentially VFA's viz., acetic acid, butyric acid, propionic acid and mixture of all three were added in respective reactors under nitrogen limiting condition. The final lipid content was observed highest in media containing only glucose as substrate followed by media containing glucose plus mixture of VFA's. The results depicted the ability of Cryptococcus curvatus to transform organic acids. Therefore, it can be concluded that the waste derived fatty acids could become a potential feedstock for biodiesel production in the framework of biorefinery.

Keyword: Cryptococcus curvatus, Volatile Fatty Acid, Biodiesel, Biorefinery, Lipids

INTRODUCTION

The limited availability of global fossil fuel prompted notable interest in the investigation and development of Eco-friendly & renewable energy alternatives to fulfil the growing energy demands. Biodiesel is one of the most promising alternatives to fossil fuels as its production is non-toxic, sustainable, and energy efficient. Waste is being considered as potential and renewable feedstock for the production of bio-based products ranging from biofuels to platform chemicals [1]. Different types of biogenic wastes can be used for biohydrogen (H_2) and volatile fatty acids (VFA) production through acidogenic fermentation [2]. Waste derived VFA can be considered as a potential feedstock for biodiesel production by oleaginous yeast. Oleaginous yeast are of special interest among microorganisms for the production of lipid feedstock as they can be cultured on a variety of substrates and few fungal strains are reported to accumulate inherently higher neutral lipid than bacteria or microalgae. Their production does not compete with the food supply, since it can utilize agro-industrial wastes and by-products such as lignocellulosic biomass as well as Municipal waste.

MATERIAL AND METHODS

Inoculum Preparation

C.curvatus strain was obtained from MTCC, Chandigarh, India. The *C.curvatus* was grown in 500ml Erlenmeyer flask containing 250 ml of Yeast extract 10g/l, Peptone 20g/l and Dextrose 20g/l at 25°C with initial pH of 7 on a rotary shaker at 180 rpm for 2 days.

Main Culture

Designed synthetic waste water was prepared. Glucose was used as carbon source in the concentration of 30g/l, Nitrogen source (NH_4Cl 0.5g/l), KH_2PO_4 0.25g/l, K_2HPO_4 0.25g/l, $MgCl_2 \cdot 6H_2O$ 0.3g/l, $NiSO_4$ 16mg/l, $CoCl_2$ 25mg/l, $ZnCl_2$ 11.5mg/l, $CuCl_2$ 10.5mg/l, $CaCl_2$ 5 mg/l, $MnCl_2$ 15mg/l, $FeCl_2$ 100mg/l. 5g/l VFAs viz., acetic acid, butyric acid, propionic acid and mixture of all three in the ratio of 1:1:1 were added after the exhaustion of glucose.

Two-stage Fed-Batch Bioreactor Fermentation

5 reactors were operated with working volume of 100 ml. The culture in the bioreactor was composed of different phases. Initially the carbon source was glucose in order to obtain high cell density. In a second phase, after the exhaustion of glucose, 5g/l VFA (acetic acid, butyric acid, propionic acid and mixture of all three) were added to the respective bioreactor.

Determination of Biomass

Biomass was assessed by absorbance and dry biomass. For the dry cell weight, 10 ml of broth was taken in a pre-weighed vial and centrifuged at 5000 rpm for 5 minutes. The pellet obtained was dried overnight. Cell dry weight was determined by drying the cells to constant weight at 60°C. For absorbance readings, aliquots of 5 ml were taken during fermentation at 24-hour intervals, properly diluted in water and measured at 600 nm.

Lipid extraction

Lipid extraction was performed using the chloroform- methanol method [3].

RESULT AND DISCUSSION

Biomass Assessment

Biomass was assessed by both absorbance and dry biomass. In all cases, biomass concentration reached atleast 15-20 g/l after 4 days of incubation. The highest biomass productivity was observed with media containing only glucose as carbon source followed by media containing glucose plus mixture of all three VFA's.

Lipid Productivity

The highest final lipid productivity was obtained with media containing glucose followed by media containing glucose plus acetic acid.

Effects of Various Carbon Sources

Glucose is the most commonly used carbon source for microbial oil production. Therefore, it is important to use a low cost carbon source or alternative carbon source instead of glucose in order to reduce the cost of microbial oil production. Thus, different carbon substrates were used for lipid production by *C. curvatus*. After cultivation with glucose medium was supplemented with VFA's viz, acetic acid, butyric acid and propionic acid as a carbon substrates with pH 6.0 at 25°C for 4 days, *C. curvatus* grew well on media containing VFA as a carbon source. Mixture of all three VFA's supported the maximum biomass productivity and acetic acid containing media supported highest lipid productivity.

CONCLUSION

The results of this study revealed that the oleaginous yeast *C. curvatus* has potential to be a lipid producer for biodiesel production. Two stages fed batch strategy is an efficient way of producing lipids from VFAs. Therefore, it can be concluded that the waste derived fatty acids could become a potential feedstock for biodiesel production in the framework of biorefinery.

REFERENCES

[1] S. Venkata Mohan, G. N. Nikhil, P. Chiranjeevi, C.Nagendranatha Reddy, M. V. Rohit, A. Naresh Kumar, and O. Sarkar. Bioresource technology 215 (2016): 2-12.

[2] G. Mohanakrishna and S. Venkata Mohan, Appl. Energy. 107 (2013), 244–254.

[3] Bligh,E.G. and Dyer,W.J. 1959. A rapid method for total lipid extraction and purification. *Can.J.Biochem.Physiol.* 37:911-917.

MICROBIAL ELECTROSYNTHESIS OF CARBOXYLIC ACIDS FROM CO_2: COMMUNITY STRUCTURE ANALYSIS

J. Annie Modestra
Bioengineering and Environmental Sciences Lab,
EE&FF Department, CSIR-Indian Institute of
Chemical Technology (CSIR-IICT),
Hyderabad- 500007, India.

E-mail: anniemodestraj@gmail.com

S. Venkata Mohan*
Bioengineering and Environmental Sciences Lab,
EE&FF Department, CSIR-Indian Institute of
Chemical Technology (CSIR-IICT),
Hyderabad- 500007, India.

E-mail: vmohan_s@yahoo.com

ABSTRACT

Microbial electrosynthesis is an attractive and promising strategy of transforming CO_2 into valuable chemicals by exploiting the capabilities of bacteria. As biocatalyst is considered as prime factor in CO_2 reduction, we used an enrichment technique comprising of heat pretreatment (suppress methanogens) of parent inoculum followed by enrichment under gas mixture of H_2 and CO_2. Here, we use a double chambered BES wherein cathode chamber was inoculated with enriched acetogenic (homoacetogenic) bacteria, subsequently polarized with a voltage of -0.8 V vs Ag/AgCl (s). BES operation resulted in the synthesis of carboxylic acids, with the major proportion confined to production of acetic acid (12.57 mM) with a maximum current density of 650 ± 50 mA/m^2 generated in response to applied voltage. Phylogenetic analysis was comparatively made between untreated and heat treated enriched bacteria which revealed the members belonging to Clostridiaceae, dominant in heat treated inoculum.

***Keywords*:** *Homoacetogenic bacteria, pretreatment, bioelectrochemical system, phylogenetic analysis.*

INTRODUCTION

People perception was limited in seeing CO_2 as a green house and toxic gas. However, with rapid discoveries about the potential benefits offered by CO_2, it is being considered as a valuable resource [1]. Although many conventional and electrochemical reduction methods exist, they encounter limitations pertaining to cost and storage issues [2]. Recently, there has been a paradigm shift from using traditional methods of CO_2 storage to utilization of biological processes/biocatalysts for synthesis of valuable chemicals from CO_2[3]. Major advancements in CO_2 utilization were made using bio-electrochemical (BES) or microbial electrosynthesis systems which uses biologically driven electrode potential as a source of reducing equivalents replacing the external supply of hydrogen. BES comprises of various components viz., biocatalyst, electrode materials, reactor configuration, membrane etc. which play a key role in determining BES performance [4]. Among all these components, microbial community can be considered as corner stone in BES, as they promote biochemical reactions for utilizing CO_2 to synthesize multi-carbon organic chemicals. Keeping in view about the microbial community and BES system, a double chambered BES was designed and enriched biocatalyst was used at cathode chamber along with the polarized potential of -0.8 V for bioelectrochemical reduction of CO_2 towards synthesis of multi-carbon organic chemicals. Bacterial community structure is identified and comparatively analyzed by considering prior to and post enrichment.

Materials and Methods

Biocatalyst

Indigenous mixed anaerobic bacteria obtained from full scale anaerobic reactor treating wastewater is used as the parent inoculum. Bacteria used as biocatalyst is different at anode and cathode chambers. Anode chamber of BES was inoculated with anaerobic and untreated parent inoculum enriched in synthetic wastewater containing glucose (1.5 g/l) as carbon source [5]. While in the case of cathode chamber, parent inoculum was subjected to heat pretreatment at 80-90°C for 2-3 h to enrich acidogenic bacteria and to eliminate non-spore forming hydrogen consuming methanogenic bacteria [6]. The culture resulted

after heat pretreatment was subjected to a headspace gas mixture of H_2 and CO_2 (80:20) to selectively enrich homoacetogenic bacteria [7, 5]. This homoacetogenic bacteria is ultimately used as biocatalyst at cathode chamber.

Reactor Configuration

A double chambered BES was designed and fabricated using Schott-Duran glass bottles with a total/working volume of 2.5/2.0 l. BES consisted of an anode and a cathode chamber separated by a proton exchange membrane. Non-catalyzed graphite plates were used as electrodes at both anode and cathode chambers to aid in microbial electron transfer reactions. Copper wires were used to establish contact with electrodes. Proper leak proof sealing was done to ensure anaerobic environment at both the chambers.

Experimental Operation

A two stage experimental methodology was employed for the bioelectrochemical reduction of CO_2 to carboxylic acids. During stage-I, enrichment of homoacetogenic bacteria was carried out followed by utilizing the resultant culture as biocatalyst at cathode chamber in stage-II. BES was operated with a polarized potential of -0.8 V vs Ag/AgCl (S) chronoamperometrically using a potentiostat-galvanostat system (EC-Lab). Drop in carboxylic acids concentration (acetic acid) and reductive catalytic currents were used an indicator for feed change. Experiment was carried out in fed batch mode with each cycle operated for a retention time of 72 hrs.

Results and Discussion
Pretreatment and enrichment of homoacetogenic biocatalyst

Selective enrichment of homoacetogenic bacteria was carried out in two phases. During phase-I, parent inoculum was subjected to heat pretreatment to suppress methanogenic bacteria. During phase-II, enrichment of homoacetogens was conducted by growing the bacteria resulted from phase-I by subjecting to a head space gas mixture of $CO_2:H_2$ (20:80) [5]. Confirmation of homoacetogens growth was determined by gas consumption profiles with respect to time analyzed through gas chromatography. Decrement in headspace gas composition was presumed to be the enrichment of homoacetogens. A maximum of 57% and 62 % of CO_2 and H_2 reduction was observed during enrichment which depicts the consumption of headspace gas for its growth and metabolism towards acetogenesis (homoacetogenesis). This enriched culture was subsequently used for microbial electro synthesis reaction.

Acetic acid production

The enriched homoacetogenic bacteria was during stage-II. Experiments were conducted by applying a potential of -0.8 V vs Ag/AgCl (S) on bio-cathode considering it as working electrode against anode as counter electrode and Ag/AgCl (s) as reference electrode through a potentiostat-galvanostat system. CO_2 as sole carbon source was supplemented in the form of sodium bicarbonate (20 mM) with a pH of 8.5 (alkaline). While in the case of anode chamber, untreated culture was used as biocatalyst and glucose as carbon source. The reducing equivalents generated through the metabolic activity of anodic bacteria will be driven towards cathode with the aid of applied potential for the reduction of CO_2 into carboxylic acids. A maximum of 14 mM (3.01 g/l) of acetic acid was produced during microbial electrosynthesis reaction catalyzed by enriched biocatalyst.

Total Carboxylic acids production

Although biocatalyst used at cathode is enriched homoacetogenic bacteria, study depicted the bio-electrochemical synthesis of a mixture of carboxylic acids upon CO_2/bicarbonate reduction. A total of 3.72 g/l of carboxylic acids were bioelectrochemically synthesized by utilizing bicarbonate as sole carbon source along with an applied potential as driving force for directing the reducing equivalents. Among the mixture of carboxylic acids synthesized, acetic acid concentration was high followed by butyric and propionic acids. This is in congruence with the enrichment adopted during the study, wherein the major population of bacteria was homoacetogens which would specifically direct the metabolism towards acetic acid synthesis by utilizing CO_2/bicarbonate as carbon source. Total carboxylic acids production was also monitored at regular time intervals. A gradual increment in concentration of carboxylic acids was noticed till 60 h followed by a decrement at 72 h. The decrement in carboxylic acids concentration might be due to the utilization of C2-C4 compounds as carbon source by other bacteria co-existing in mixed population or utilization for the synthesis of other compounds viz., alcohols or other carboxylic acids (not analyzed during study).

Bicarbonate reduction

Initially 20 mM of bicarbonate was supplemented and the concentration was observed to decrease with the increase in time for each cycle operation. Samples were collected at regular time intervals for each cycle operation to monitor the changes in bicarbonate concentration. High reduction in bicarbonate reduction was depicted during BESH operation which depicts the utilization of bicarbonate as inorganic carbon substrate by biocatalyst. Prevalence of alkaline range of pH also favored dissolution of bicarbonate in catholyte which in turn aided in the utilization of bicarbonate for carboxylic acids synthesis.

Phylogenetic analysis

Phylogenetic analysis was performed for parent inoculum which is untreated and mixed anaerobic bacteria (UN C), untreated and enriched under head space gas atmosphere of

H_2 and CO_2 (UN C_{En}), untreated, enriched and operated at cathode in BES (UN C_{BES}), heat treated and enriched under gas atmosphere of H_2 and CO_2 (H_{En}) and heat treated, enriched and operated at cathode in BES (H_{BES}). Microbial community analysis was performed by isolating DNA from the samples according to Qiagen kit protocol and processed for 16S rDNA amplification by PCR. Purified PCR product was subjected to denaturing gradient electrophoresis (DGGE) and sequenced the different 16S rDNA bands which were resolved based on the thermal melting temperatures. The band sequences were analysed for phyologenetic distribution based on neighbor-joining method using MEGA software.

Parent inoculum which is untreated and anaerobic acquired from wastewater treatment plant was characterized for microbial population and showed the members belonging to Phyla *Proteobacteria, Bacteroides, Firmicutes* and other uncultured bacteria. Also, members of *Bacilleacea*, methylotrophs and *Clostridieacea* are noticed. This population was further enriched under the headspace gas mixture of H_2 and CO_2 which demonstrated the presence of bacteria belonging to *Methylobacterium* sp., uncultured type-II methylotrophs, uncultured bacteria and a few *Firmicutes* in UN C_{En}. In the case of UN C_{BES}, a few shifts in population were identified showing the presence of members belonging to *Proteobacteria* and *Clostridiaecea*.

phylogenetic analysis performed for heat pretreated culture (H_{En} and H_{BES}) demonstrated shifts in microbial community. H_{En}, which depicts the heat treated and enriched bacteria under gas mixture of H_2 and CO_2 revealed the presence of members belonging to *Clostridiaecea, proteobacteria*, uncultured bacteria and few bacterial population comprising of *Bacillus sp.* and methylotrphs. Interestingly, members of *Rhodospirillum* and *Rhodocycleacea* were enriched during H_{BES} operation. *Rhodospirillum sp.* is known to grow at diverse conditions viz., aerobic and anaerobic with CO_2 as carbon source.

Conclusions

This study demonstrates the potential of CO_2 as a valuable resource by using bioelectrochemical systems by enriching efficient microbial community. Heat pretreatment used as a strategy for enriching acetogenic bacteria is proved to be efficient in the development of a microbial community dominantly comprising of members belonging to Clostridiaecea. BES_H operated with enriched microbial population resulted in the synthesis of mixture of carboxylic acids, with acetic acid being the major fraction. Voltammetric analysis of BES_H depicted the involvement of NAD/NADH, membrane bound proteins, Fe-S proteins, flavins etc. as electron carriers during bio-electrochemical reduction reactions. Study unraveled the potential of BES in not only synthesizing the multi-carbon organic chemicals but also can generate high energy simultaneously minimizing the gaseous waste.

REFERENCES

[1] S. Venkata Mohan, J. Annie Modestra, K. Amulya, Sai Kishore Butti, G. Velvizhi. Trends in Biotechnology 34 (2016) 506-519.

[2] R.C. Franca, A. Azapagic, J. CO2 Util. 9 (2015), 82-102.

[3] S. Venkata Mohan, Sai Kishore Butti, K. Amulya, Shikha Dahiya, J. Annie Modestra. Trends in Biotechnology 34 (2016) 852-855.

[4] S. Venkata Mohan, G. Velvizhi, J.A. Modestra, S. Srikanth, Renew. Sustain. EnergyRev. 40 (2014) 779–797.

[5] J. Annie Modestra, B. Navaneeth, S. Venkata Mohan, Journal of CO_2 Utilization 10 (2015) 78–87.

[6] S Venkata Mohan. Int. J. of Hyd. Energy. 34 (2009) 7460-7474.

[7] K.P. Nevin, Appl. Environ. Microbiol. 77 (2011) 2882–2886.

SEEC-2017-039

BIOGENIC PRODUCTION OF PBSE QUANTUM DOTS THROUGH *BACILLUS SUBTILIS*

Dileep Kumar Yeruva
Bioengineering and Environmental Sciences Lab,
EE&FF Department, CSIR-Indian Institute of
Chemical Technology (CSIR-IICT),
Hyderabad- 500007, India.

E-mail: yeruvadileep@gmail.com

J. Shanthi Sravan
Bioengineering and Environmental Sciences Lab,
EE&FF Department, CSIR-Indian Institute of
Chemical Technology (CSIR-IICT),
Hyderabad- 500007, India.

E-mail: shanthisravankumar@gmail.com

Sai Kishore Butti
Bioengineering and Environmental Sciences Lab,
EE&FF Department, CSIR-Indian Institute of
Chemical Technology (CSIR-IICT),
Hyderabad- 500007, India.

E-mail: kishore288@gmail.com

S. Venkata Mohan*
Bioengineering and Environmental Sciences Lab,
EE&FF Department, CSIR-Indian Institute of
Chemical Technology (CSIR-IICT),
Hyderabad- 500007, India.

E-mail: vmohan_s@yahoo.com

ABSTRACT

Chalcogenide semiconductor quantum dots are emerging as promising nano materials due to their size tunable optoelectronic properties. The present chemical synthesis protocols and their subsequent integration for practical uses have contorted largely due to the toxicity and cost issues. Accordingly, there is an immediate need to develop alternative environment friendly synthesis procedures. Microbial factories hold immense potential to achieve this objective. Biological production of QDs follow green chemistry principles, there is either minimized or completely avoided to use of hazardous chemicals, high temperature and high pressure. While a large number of microbial sources have recently emerged as potent sources for biosynthesis of chalcogenide quantum dots (QDs), studies regarding their biomimetic strategies that initiate QD biosynthesis are inadequate. The present study describes several mechanistic aspects of PbSe QD biosynthesis using Bacillus subtilis. High resolution transmission electron microscopy, X-ray diffraction, UV-Vis spectroscopy, luminescence spectroscopy, and energy dispersive X-ray spectroscopy were applied to characterize the PbSe QDs. The effects of reactant concentrations, bacteria incubation times, and reaction times on QD growth were systematically investigated. Structural characterization by x-ray diffraction shows that the dots might have mean diameters between 2 and 2.5 nm. Moreover, this study demonstrated an economical and environmentally friendly approach to fabricating for the biosynthesis of semiconductor quantum dot.

Keywords: *Semiconductor, nano crystal, Biosynthesis, Bacillus Subtilis, Metal chalcogenide.*

INTRODUCTION

Semiconductor nanocrystals known as quantum dots (QDs) possess unique electronic and optical properties due to quantum confinement effects. Over the past two decades QDs of different sizes, shapes and compositions have been extensively studied for practical applications, such as fluorescent biological labels, optoelectronic transistor components and solar cells [1]. Conventional chemical synthesis based on high-temperature organometallic processes is extremely toxic and expensive, and involves unstable species. For practical purposes, an alternative "green chemistry" scheme that is safe, simple, inexpensive, and suitable for industrial upscaling is extremely attractive [2]. Nature's miniature microbial factories were utilized for the shape controlled biosynthesis of biocompatible chalcogenide quantum dots, rods and wires [3], to capacitate their use in medical and biological imaging

applications [4]. Out of all the chalcogenide quantum crystallites, PbSe nanoparticles rank higher with regard to the quantum confinement effects due to excellent band-gap tailoring amenability. The proposed Study for PbSe biosynthesis can be testified as a significant approach that can open prospects for harnessing the excellent quantum efficiency of these nanomaterials in capsitor sector via their large scale, eco-friendly and cost effective synthesis.

MATERIALS AND METHODS

Biocatalyst
Bacillus Subtilis was grown in freshly prepared Luria Britani (LB) broth contains the Tryptone-10g/l, NaCl-10g/l, Yeast extract-5g/l with initial pH of 7 on a rotary shaker at 110 rpm for 12hours.

Tolerance study
Busillus Subtilis was subjected to tolerance studies in LB Broth amended with Sodium selenite and Lead nitrite in a concentration range of 0.5–3 mM and mediawithout metal solution is considered as control. The culture broth containing respective concentrations of the metals were inoculated with1 ml of freshly prepared bacterial suspension and put on shaker at 115 rpm at 37°C for 48 hours. Bacterial growth was measured at each 2h intravel with spectrophotometrically at 600nm..

Experimental Operation
Biosynthesis of lead selenide (PbSe) nanoparticles was initiated in Pb and Se tolerant *Bacillus subtilis* by a low cost green methodology as under conditions akin to optimum temperature. Initially The extracellularly biosynthesized nanosized PbSe was subjected to further characterization studies using scanning and transmission electron microscopy (SEM, TEM), X-ray diffraction (XRD), UV–vis and Fourier transfer infra-red (FTIR) spectroscopic analysis. XRD and absorption characteristics were used to apprehend the crystallite size, band gap energy and the quantum confinement of the biosynthesized PbSe quantum rods.

RESULTS AND DISCUSSION

Tolerance potential
Results on the analysis of the Bacterial culture growth in the presence and absence of metal solution showed non inhibitory growth at maximum concetration i.e 5mM.

Extracellular synthesis and characterization of Lead Selinde quantum dots
The size and surface morphology of the biosynthesized PbSe quantum rods are in par with their chemically synthesized counterparts reported in literature [5]. The inter-planar spacing was calculated from the XRD peak

values and our results were found to be in concordance with the standardized data.

UV–vis spectra recorded from the biosynthesized PbSe nanoparticles dissolved in tetrachloroethylene exhibit the appearance of aweak absorption edge after 275nm. The flouroscent emission was reveld the colour of Qds is lighit bule colour. This is indictes the size of particals were laid between to 2-5nm.

Conclusions
Fluorescent, semiconductor lead selenide quantum rods were synthesized in a cost effective and eco-friendly biosynthesis procedure employing lead and selenium tolerant *B.Subtilis*. The morphological and optical characterization by XRD, UV–vis spectroscopy reveal properties in par with the chemically synthesized counter parts. Further, to be analyse the structure by (TEM and SEM) and electrical properties were conformed to the systenthasised nano quntom dots A wider energy gap in the nanofabrication and the presence of weak quantum confinement were analyzed theoretically using the Tauc plot and the mass approximation method respectively.

REFERENCES
[1] H. Bao, Z. Lu, X. Cui, Y. Qiao, J. Guo , J. M. Anderson, C. M. Li, Acta Biomaterialia 6 (2010) 3534–3541
[2] S. H. Kang, K. N. Bozhilov, N. V. Myung, A. Mulchandani, W. ChenAngew, Chem. Int. Ed. 47(2008) 5186 –5189
[3] V. Bansal, A. Bharde, R. Ramanathan, SK. Bhargava, Adv Colloid Interface Sci. 179 (2012)150–68
[4] J. M. Jacob , B. R. Mohan, K. U. Bhat, Mate Let. 124(2014) 279-281.
[5] K. Li, X. Meng, X. Liang, H. Wang, H. Yan, J Solid State Electrochem , 109 (2008) 48–53

SEEC-2017-040

ROLE OF NADH DEHYDROGENASE II IN EXO-CELLULAR ELECTRON TRANSPORT IN MICROBIAL ELECTROCHEMICAL SYSTEMS

Vamshi Krishna K
CSIR- INDIAN INSTITUTE OF CHEMICAL TECHNOLOGY
Email: VAMSIKRISHNAIND@GMAIL.COM

Venkata Mohan S
CSIR- INDIAN INSTITUTE OF CHEMICAL TECHNOLOGY
Email: vmohan_s@yahoo.com

ABSTRACT

Microbial electrochemical systems (MES) can function as renewable and sustainable option for converting organic waste to bio-energy and various bio-based products. However, to make the process more commercially viable and more efficient, understanding of the mechanism underlying the process is required. In MES, transport of electrons from bacteria to an external electrode is the key to its working, but the mechanism by which bacteria exocellularly transport electrons is not well understood. So in this study, a single chambered MES (anaerobic conditions) using fluorine coated tin oxide (FTO) plates as anode and stainless steel 316 as cathode was used to understand the role of NADH dehydrogenase II (ndh2) (from Bacillus subtilis) in exoelectron transport. To understand this, ndh2 gene coding electron transport protein NADH dehydrogenase II was over-expressed in E. coli and its electrogenic profile was studied. Expression construct was created in pET23a vector and cloned into E. coli BL21 strain. Exo-electrogenic ability of the modified strain was estimated using various electrochemical techniques like chrono-amperometry and cyclic voltammetry. In addition to these analyses, various assays like iron oxide reduction assay, protein film voltammetry and plate based assay were performed to quantify the exo-electrogenesis. Cell free culture filtrate was analyzed using HPLC to know the metabolic flux of NADH+H+. qRT-PCR was performed to understand the influence of NADH Dehydrogenase on other electron transport proteins. The final outcome of the study will give the details about the role of NADH dehydrogenase in MES and its effect on other metabolic pathways.

SEEC-2017-041

INFLUENCE OF PHASIC OXYGEN AVAILABILITY IN BIOFUEL CELL OPERATION

J.Shanthi Sravan
Bioengineering and Environmental Sciences Lab,
EEFF Department, CSIR-Indian Institute of
Chemical Technology (CSIR-IICT),
Hyderabad- 500007, India.
E-mail: shanthisravankumar@gmail.com

Sai Kishore Butti
Bioengineering and Environmental Sciences Lab,
EEFF Department, CSIR-Indian Institute of
Chemical Technology (CSIR-IICT),
Hyderabad- 500007, India.
E-mail: kishore288@gmail.com

S. Venkata Mohan*
Bioengineering and Environmental Sciences Lab
EEFF Department, CSIR-Indian Institute of Chemical Technology (CSIR-IICT)
Hyderabad- 500007, India.
E-mail: vmohan_s@yahoo.com

ABSTRACT

The optimization of efficient, economic and self-sustainable MFCs towards maximum power output is a priority in fossil dependent world. Cathode interventions for enhancing power productions in MFCs are much needed. Two MFCs with cathode as the only variation were operated in continuous mode (open and closed circuit), one MFC with dissolved oxygen (DO) cathode (MFC-DC) and the other MFC with air cathode (MFC-SC), towards studying the influence O_2 as TEA. Cell potentials were continuously monitored for analyzing performance of MFCs. A maximum power density was observed in MFC-DC ($769\ mWm^{-2}$) when compared to MFC-SC ($684\ mWm^{-2}$). Electrochemical characterization showed variations in electron transfer rates (Kapp). Cyclic voltammograms, redox Tafel's slopes ($\beta a/\beta c$) and electron transfer co-efficient ($\alpha a/\alpha c$) explained higher performance of MFC-DC over MFC-SC. Results prove the influence of phase availability of TEA on ORR of MFCs towards enhanced power production.

Keywords
Bioelectrochemical systems (BES); Biofuel cell; Bio-electro catalyzed reduction; Oxidation reduction reaction (ORR); Power systems; Bioremediation.

INTRODUCTION

Voluminous consumption of fossils in the current scenario has led to their fast depletion and has led to climate changes and disposal of unprocessed wastes into the natural habitats. At this pace, the challenges posed by these huge waste quantities generation and climate changes cannot be neglected. Interest for the production of non-fossil based electricity from different biological sources (biomass) is gaining importance. Microbial fuel cell (MFC) is capable of harnessing electrons from microbial Electrometabolic activities to generate bioelectric currents. The microorganisms in the anodic chamber oxidize the organic substrate, releasing electrons (e^-) and protons (H^+) to the anode. Low power generation in MFC is a major concern to be addressed. Hence, there has to be a controlled e^- and H^+ flow through the circuit for recovering maximum amount of power densities. To overcome the limitation, a Terminal electron acceptor (TEA) is required in the cathode chamber that acts as an effective driving force for drawing the electrons towards higher reduction. TEA's such as Oxygen (O_2), nitrate, sulfate, Iron, metals. etc., could act as effective neutralizing agents when present in the cathode chamber. In this study, MFC-Double chamber (MFC-DC) and MFC-Single chamber (MFC-SC) were operated in continuous mode for monitoring the role of O_2 as TEA for enhancing the power production. MFC's have numerous activities with the potential to lower the carbon foot print on the environment along with harnessing

bioelectricity and wastewater treatment and garner significance towards a Biobased circular bioeconomy.

Material and Methods

MFC Setup

Two dual-chambered Microbial fuel cells (MFC) (Double chamber – MFC-DC; Single chamber – MFC-SC) were constructed. PEM of appropriate dimensions was used as separator between the two blocks, which individually act as anode and cathode. Carbon cloth was used as electrodes in both anode and cathode chambers. Copper wires were used to maintain contact with the electrodes for external electrical contact. Each chamber was specifically designed for continuous mode of operation having inlet and outlet ports. This design and operation of the MFC's purely differentiates based on only the cathodic performance of the MFC.

Biocatalyst

Pre-treated anaerobic consortium acquired from reactor treating industrial wastewater was used as Inoculum in anode chambers of both MFC-DC and MFC-SC reactors.

Operation of MFC

MFC-DC and MFC-SC reactors were operated in continuous mode. The TEA influence in MFC-DC (oxygenated water cathode) and MFC-SC (air cathode) for enhancing electrogenic activity was evaluated. The oxygenated water was continuously supplied to cathode of MFC-DC. But MFC-SC was maintained as air-cathode by sparging air. The anode chambers of MFC-DC and MFC-SC were inoculated with mixed pre-treated Inoculum in phosphate saline buffer (PBS) with acetate (6g/l). The operation of both MFCs lasted for 30 days. The comparative influence of O_2 as TEA to enumerate cathode performance comprehensively was studied.

Bioprocess monitoring

Physicochemical parameters like pH, EC and COD were analyzed to follow influence of O_2 on system performance.

Bio-electrochemical analysis

Bioelectrochemical behaviour in terms of open circuit voltage (OCV), current, Cyclic Voltammetry (CV), electron discharge rates (Kapp) and Tafel's slopes were studied. All electrochemical assays were performed with anode as working electrode and cathode as counter electrode against Ag/AgCl (3.5M KCl) reference electrode.

RESULTS AND DISCUSSION
Stabilization of MFCs in open circuit conditions

MFC-DC and MFC-SC were started up in continuous mode and on attaining stable performances in open circuit, MFC's were operated in closed circuit (1KΩ) and monitored for O_2 influence of TEA on power production.

Cell Potentials

The OCV of MFC-DC was stabilized at 970-990 mV and MFC-SC at 770-800 mV. The potential difference is critical parameter in studing influence of O_2 as TEA. The anode potentials of MFC-DC (-462 mV), MFC-DC 1 KΩ (-0.0391 mV), MFC-SC (364 mV) and MFC-SC 1 KΩ (-0.0331 mV) were observed vs. Ag/AgCl (3.5M KCl). Cathode potential is major determining factor in determining power output of MFC's. The cathode potentials of MFC-DC (525 mV), MFC-DC 1 KΩ (0.0452 mV), MFC-SC (433 mV) and MFC-SC 1 KΩ (0.0401 mV) were observed vs. Ag/AgCl (3.5M KCl).

Dissolved Oxygen (DO)

The catholyte DO concentration of MFC-DC showed saturation limit and varied between 4.2 mg/l to 4.3 mg/l during operation.

Polarization profile

Polarization was done for MFC-DC and MFC-SC at stabilization The change in PD and V with respect to external load was plotted against CD for both the reactors. MFC-DC showed a maximal PD of 0.355 mWm^{-2} whereas MFC-SC with 0.288 mWm^{-2} at 1 KΩ.

Bioelectrogenic activity

CV's were taken in both open and closed circuit mode of operation at multi scan rates (100-0.05 mVS^{-1}). Profiles showed proportional increase in oxidation and reduction currents (mA) with respect to scan rates.

First order derivative

The first order derivative for CV's of 30 mV.S^{-1} derives rate of change of biocatalytic current (i) with respect to electrode potential E (di/dE) and correspond to specific redox shuttlers during electrochemical interactions.

Tafel analysis

The tafel analysis drawn from CV provide direct evidence to quantitatively compare the Electrometabolic activity in terms of electron discharge rates on enhanced power density in presence of a TEA.

Electrochemical behavior (Kapp Calculations)

The Kapp value was derived from Laviron equations provides direct evidence of electron discharge rates under varied microenvironments.

$$E_{pc} = E^{0'} + RT/\alpha nF \ln RTK_s/\alpha nF - RT/\alpha nF \ln v \quad (1)$$

$$E_{pa} = E^{0'} + RT/(1-\alpha)nF \ln RTK_s/(1-\alpha)nF + RT/(1-\alpha)nF \ln v \quad (2)$$

The Kapp for MFC-DC 1KΩ (525.64 S^{-1}) was significantly higher followed by MFC-SC 1KΩ (296.39 S^{-1}), MFC-DC (202.32 S^{-1}) and MFC-SC (108.31 S^{-1}).

Power Density (PD)

The power densities of MFC-DC and MFC-SC were calculated from closed circuit operation with CDP (1 KΩ). A maximum PD of 769 mW m^{-2} was observed in MFC-DC operation whereas for MFC-SC operation it was 684 mW m^{-2}.

CONCLUSIONS

The O_2 influence as TEA in cathode chamber of both MFCs showed marked influence on bioelectrogenic activity and electron discharge rates (Kapp) for enhanced power production. CV and its derivatives i.e., tafel slopes, electron discharge rates (Kapp) also supported influence of O_2 as TEA on enhanced power production.

ACKNOWLEDGEMENTS

REFERENCES

[1] S. Venkata Mohan, R. Saravanan, S. V. Raghavulu, G. Mohanakrishna, P.N. Sarma, Bioelectricity production from wastewater treatment in dual chambered microbial fuel cell (MFC) using selectively enriched mixed microflora: effect of catholyte, Bioresoure Technol. 99 (2008) 596-603.

[2] S. Oh, B. Min, B.E. Logan, Cathode performance as a factor in electricity generation in microbial fuel cells, Environ. Sci. Technol. 38 (2004) 4900–4904.

[3] J. C. Biffinger, J. N. Byrd, B. L. Dudley, B. R. Ringeisen, Oxygen exposure promotes fuel diversity for Shewanella oneidensis microbial fuel cells, Biosens. Bioelectron. 23 (2008b) 820–26.

[4] S.B. Pasupuleti, S. Srikanth, X. Dominguez-Benetton, S.V. Mohan, D. Pant, Dual gas diffusion cathode design for microbial fuel cell (MFC): Optimizing the suitable mode of operation in terms of bioelectrochemical and bioelectro-kinetic evaluation, Journal of chemical technology and biotechnology. 91 (3) (2014) 624-639.

[5] B.Ozkaya, A.Y.Cetinkaya, M.Cakmakci, D.Karadag, E.Sahinkaya, Electricity generation from young landfill leachate in a microbial fuel cell with a new electrode material, Bioprocess Biosyst Eng. 18 (2013) 399-405.

SEEC-2017-42

Comparative study of CO$_2$ Conversion to Methane with Biological and Bioelectrochemical Processes

G.Velvizhi*
Bioengineering and Environmental Sciences
EEFF Division
CSIR-Indian Institute of Chemical Technology (CSIR - IICT),
Hyderabad - 500 007, India
Email: gvels@yahoo.com

Sai Kishore Butti
Bioengineering and Environmental Sciences
EEFF Division
CSIR-Indian Institute of Chemical Technology (CSIR - IICT),
Hyderabad - 500 007, India
Email: kishore288@gmail.com

S.Venkata Mohan
Bioengineering and Environmental Sciences
EEFF Division
CSIR-Indian Institute of Chemical Technology (CSIR - IICT),
Hyderabad - 500 007, India
Email: vmohan_s@yahoo.com

ABSTRACT

Comparative evaluation of CO$_2$ sequestration to methane was performed with different biological and bioelectrochemical systems (BES). Control (Anaerobic reactors without electrode assembly), BES$_{OC}$ (Electrode assembly with open circuit), BES$_{CC}$ (Electrode assembly with closed circuit) and BES$_{Ap}$ (Electrode assembly with applied potential) were operated. A single chamber reactor was designed and fabricated using Schott-duran glass bottles using carbon cloth/stainless steel mesh hybrid electrodes with dimension of 5×3×1cm were used as anode and cathode electrodes. The reactors were supplied with 3.63 g/l of CO$_2$ in the form of bicarbonate with sparging of hydrogen. The methanogenic microbial catalyst reduces the CO$_2$ into methane by the electron derived biological reductive reaction. The study hypothesis that CO$_2$ to methane conversion will be higher in BES$_{AP}$ followed by BES$_{CC}$, BES$_{OC}$ and Control reactors. The study infers that the introduction of electrodes in the fermentation processes regulates the methanogenic community at biocathode surfaces which directly accept the electrons from the electrode and intracellularly transfer them for reduction of carbon dioxide to methane.

Keywords: *Electrofermentation; Microbial electrochemical systems; Redox mediators; Electron transfer mechanism; CO$_2$ reduction.*

NOMENCLATURE

CO$_2$ Carbon dioxide
CH$_4$ Methane
BES *Bioelectrochemical systems.*
CCU Carbon capture and utilization
AD Anerobic deigestion
NaHCO$_3$ Biocarbonate
ORP Oxidation reduction potential
VFA Voltaile fatty acids
CV Cyclic voltammeter

INTRODUCTION

Global emissions of carbon dioxide (CO$_2$) have been increasing over the past decade and by contrast, it is estimated that the CO$_2$ emissions should be reduced to limit the rise of the global average temperature to 2 °C by 2050 [1]. CO$_2$ is the ultimate source of the fossil fuel used in our daily life style hence the emission might not be immediately reduced but methods to capture and store CO$_2$ through geological formations, in the ocean, in mineral carbonates, or for use in industrial processes are in practice. However these methods are considered to be energy intensive and have high operational costs. Research on biological CO$_2$ sequestration methods using microorganisms as catalysts could come out with

outstanding breakthroughs in CO_2 sequestration which are less energy intensive and render an added advantage in the production of value added products [2].

Pathways for CO_2 fixation through biological means use diverse mechanisms and enzymes for processing CO_2 by making C−H and C−C bonds and cleaving C−O bonds reactions involved in the production of synthetic fuels and biobased products [3]. The conversion of, organic products to methane by enriched methanogenic bacteria is closely related to hydrolysis and fermentation in anerobic deigestion (AD) has been developed long way. Microbial electrosynthesis is novel processes where inorganic carbon is reduced via electrons derived through electroactive biofilm of anode for oxidation and cathode for reduction to value added products [4,5]. The exoelectrogens in the bio-anode oxidize organic matter anaerobically and discharge electrons, transferred through electron transport chain to the cathode. The product formation from CO_2 is largely influenced by the bacteria and its metabolic functions and electrical potential that drives the process. The potential applied in BES system drives the redox equivalents for substrate reduction for the synthesis of carboxylic acids [6,7].

Bacteria which use electrodes as electron acceptors are used to oxidize organics and correct the redox balance in fermentation processes leads to bioenergy generation [8] Similarly, micro-organisms using electrodes as electron donors to reduce inorganics into useful products and redirect the fermentation pathways [9]. Using CO_2 as a substrate has multiples advantages such as unlimited availability, land-independence and limited toxicity to the micro-organisms. There are three main classes of substrate that methanogens can use for methane production; CO2-type substrates, methyl substrates and acetotrophic substrates (CH3COO-) the reaction depends on the type of substrate in the cell and methanogens (hydrogenotrophic and acetoclastic) [4]. Methanogenesis and acetogenic bacteria usually share the same condition to simultaneously produce CH_4 and CH_3COOH from CO_2 with microbial biocathode [10].

The present study comparatively evaluates CO_2 sequestration to methane with different biological and bioelectrochemical systems (BES). Four different bioreactor configurations viz., Control (Anaerobic reactors without electrode assembly), BES_{OC} (Electrode assembly with open circuit), BES_{CC} (Electrode assembly with closed circuit) and BES_{Ap} (Electrode assembly with applied potential) were operated and intake of CO_2 thorough biological and bioelectrocehmical systems were evaluated.

METHODOLOGY

OPERATION DETAILS

A single chambered bioelectrochemical systems (BES) reactor with three electrode setup was designed and fabricated using schott-duran glass bottles with a working/total volume of 200/250ml. The reactors were designed with a provision for CO_2 sparging ports, provision for electrode placement and sampling ports. Leak proof sealing was employed to maintain anaerobic micro environment. Carbon cloth/ Stainless steel mesh hybrid electrodes with the dimension of 5×3×1 cm were used as anode and cathode electrodes for all the reactors. The electrodes were arranged such that Ag/AgCl as reference electrode, anode as counter electrode and cathode as working electrode. The electrodes were intertwined with stainless steel wire as current collector. The reactor was supplied with CO_2 in the form of sodium bicarbonate, 3 g/l of $NaHCO_3$ which is equivalent to 2.178 g/l bicarbonate along with synthetic composition of NH_4Cl: 0.5 g/l, KH_2PO_4: 0.25 g/l, K_2HPO_4: 0.25 g/ l, $MgCl_2$: 0.3 g/l, $CoCl_2$: 25 mg/l, $ZnCl_2$: 11.5 mg/l, $CuCl_2$: 10.5 mg/l, $CaCl_2$: 5 mg/l, $MnCl_2$: 15 mg/l, $NiSO_4$: 0.16 g/l, $FeCl_3$: 0.03 g/l. The reactor was fed with 10 % of mixed consortium as inoculums which was collected from a full scale anaerobic bioreactor. Prior to feeding, pH of the anolyte was adjusted to 7. The reactor was operated with a retention time of 72 hrs based on the reduction in inorganic carbon source for duration of 90 days. The reactors were continuously sparged with N_2 gas to maintain the anaerobic environment. Four different bioreactors are designed as Control (Anaerobic reactors without electrode assembly), BES_{OC} (Electrode assembly with open circuit), BES_{CC} (Electrode assembly with closed circuit of 100 Ω) and BES_{Ap} (Electrode assembly with applied potential of 0.4 V) were operated and intake of CO_2 thorough biological and bioelectrocehmical systems were evaluated.

ANALYSIS

Methane gas in the headspace were measured using a gas chromatograph equipped with a mol-sieve column running continuously at an oven temperature of 70 °C (GC; NUCON 5765) using thermal conductivity detector with 1/8 m Heysep Q column employing (argon as carrier gas). The injector and detector were maintained at 60 °C each and the oven was operated at 40 °C isothermally. Quantitative estimation of VFA was analyzed using high performance liquid chromatography (Shimadzu LC10A) employing UV–Vis detector (210 nm) and C18 reverse phase column (250 mm, 4.6 mm diameter; 5 mm particle size, flow rate: 0.6 ml/h; wave length: 210 nm). Mobile phase of (40% acetonitrile in 1 mN H_2SO_4; pH, 2.5–3.0) and 20 ml sample injection was used. Biochemical parameters viz., pH, ORP, VFA and bicarbonate reduction were estimated according to the standard methods (APHA,

1998). Open circuit voltage (V) was recorded using a data acquisition system (Keithley Instruments, Inc. OH). Cyclic voltammeter (CV) was used to study the electrochemical behaviour of biocatalyst during stabilized phase of operation using potentiostat system to get mechanistic insights into the electrochemical reactions (Autolab-PGSTAT12, Ecochemie). Voltammograms were recorded by applying a potential ramp vmohan_s@yahoo.com at a scan rate of 5 mV/s. Linear sweep voltammetry was performed by applying a potential ramp (+ 0.50 to - 0.50 V) using (Ag-AgCl(S)) as reference electrode, anode as counter electrode and cathode as working electrode.

RESULTS AND DISCUSSIONS

Carbon dioxide, with electrons and protons, are oxidized by methanogens and electrochemical active bacteria to methane in BES by direct and indirect transfer of electrons. In direct electron transfer, electrons are directly used by methanogens to reduce CO_2 to methane and *indirect extracellular electron transfer,* the hydrogen and acetate is produced initially as an intermediate and then are utilized for methane prodution. Studies reported that it is possible for cells to accept electrons directly from electrode to reduce CO_2 to CH_4. CO_2 was reduced to CH4 at potentials of -700 mV vs. Ag/ACl using methanogens as biocatalyst [5].

The study comparatively evaluates CO_2 sequestration to methane with different biological and bioelectrochemical systems (BES). Four different bioreactors viz., Control (Anaerobic reactors without electrode assembly), BES_{OC} (Electrode assembly with open circuit), BES_{CC} (Electrode assembly with closed circuit) and BES_{Ap} (Electrode assembly with applied potential). The anaerobic mixed culture was enriched using methanogenesis enriched medium for using designed synthetic feed for three weeks and randomly reduing the glucose as feed to CO_2 in terms of biocarbonate as feed. The enriched incoculum was feed to four the reactors using biocarbonate as the only source of carbon. Utilization of bicarbonate in the bioreactor at different time intervals was evaluated to understand the growth of chemoautotrophs and correlate it to the gas productivity. The initial feed concentration given was 3 gm/l as the bacterial cultures start to grow the utilization of bicarbonates, from the 6 hour of operation the utilization was observed to be steep as the uptake during the growth phase of the biocatalyst is higher. After 48 h of operation the utilization of feed showed stabilization showing the fact that the bacteria has started reaching their stationary phase. The study hypothesizes that CO_2 to methane conversion will be higher in BES_{AP} followed by BES_{CC}, BES_{OC} and Control reactors. The study infers that the introduction of electrodes in the fermentation processes regulates the methanogenic community at biocathode surfaces which directly accept the electrons from the electrode and intracellularly transfer them for reduction of carbon dioxide to methane.

REFERENCES
1. IPCC, Climate Change 2014 Synthesis report Summary for policymakers.
2. Venkata Mohan, S., Annie, J., Amulya, K., Butti, S.K., Velvizhi,G.,2016. A circular bioeconomy with biobased products from CO_2 Sequestration Trends in Biotechnology. 34, 506- 519.
3. Appel,A, M., John E. Bercaw,J.E., Andrew B. Bocarsly, A.B. Holger Dobbek, DuBois,D.L. et al., 2013. Frontiers, Opportunities, and Challenges in Biochemical and Chemical Catalysis of CO_2 Fixation. Chem.Rev 113, 6621-6658.
4. Madigan, M.T., Martinko, J.M., Stahl, D. et al. 2009 Brock biology of Microorganisms (13th edition) Pearson Prentice Hall
5. Cheng, K., Xing, D. 2009 Direct biological conversion of electrical current into methane by electromethanogenesis. Env. Sci. tech. No. 45 796-802.
6. Modestra,J.A.,Navaneeth,B.,.VenkataMohan,S. 2015. Bioelectrocatalytic reduction of CO_2: Enrichment of homoacetogens and pH optimization towards enhancement of carboxylic acids biosynthesis. J. CO_2 Utilization, 10, 78-87.
7. Cao, X. Huang,X., P. Liang, N. Boon, M. Fan, L. Zhang, X. Zhang, 2009. Energy Environ. Sci. 2 498–501.
8. Flynn, J.M., Ross, D.E., Hunt, K.A., Bond, D.R. and Gralnick, J.A. 2010. Enabling unbalanced fermentations by using engineered electrode-interfaced bacteria. MBio 1, e00190–10
9. Clauwaert, P., Rabaey, K., Aelterman, P., De Schamphelaire, L., Ham, T.H., Boeckx, P., Boon, N. and Verstraete, W. 2007. Biological den Biological denitrification in microbial fuel cells. Environmental Science & Technology 41:3354-60.
10. Moss,A.R., Jouany, J.P, Newbold, J. 2000. Methane production by ruminants: its contribution to global warming. Annales de Zootechnie,49:231-53.

SEEC- 2017-043

DIRECT NUMERICAL SIMULATION OF IGNITION KERNEL GROWTH IN A TURBULENT PREMIXED ENVIRONMENT

Kedar G. Bhide
IC Engines and Combustion Laboratory
IIT Bombay, Mumbai, India
Email: kedarbhide@iitb.ac.in

S. Sreedhara
IC Engines and Combustion Laboratory
IIT Bombay, Mumbai, India
Email: sreedhara.s@iitb.ac.in

ABSTRACT

Flame-surface density transport equation is used to close terms in the premixed combustion models. Surface density function(SDF) and displacement speed (S_d) are important parameters in this equation. 3D as well as 2D Direct Numerical Simulation (DNS) of ignition kernel growth have been carried out to study the correlation of SDF with mean curvature and tangential strain rate. Three-step irreversible chemistry of lean CH_4-air combustion has been used in the present study. The results reveal that SDF is negatively correlated with mean curvature and positively correlated with tangential strain rate. 3D as well as 2D simulations show a similar trend of these correlations. However 2D slice of 3D simulation is not able to show negative correlation between SDF and mean curvature.

Keywords: DNS, Ignition, Surface Density Function

NOMENCLATURE

a_T	Tangential strain rate
a_N	Normal strain rate
c	Reaction progress variable
$|\nabla c|$	Surface density function
l_t	Integral scale (cm)
S_L	Laminar flame speed (cm/s)
T_0	Unburned gas temperature (K)
T_{ad}	Adiabatic flame temperature (K)
δ_L	Laminar flame thickness (cm)
κ_m	Mean curvature (cm^{-1})
φ	Equivalence ratio
τ_c	Chemical time-scale (ms)
$\dot{w}$	Rate of consumption of species (g/cm^3-s)

INTRODUCTION

Study of ignition kernel growth is relevant to the combustion in SI engine and relighting of aero-gas turbine. Direct Numerical Simulation (DNS) can provide fundamental insights into the process of kernel growth in turbulent premixed environment. Extensive experimental study of effect of turbulence parameters on ignition was done by Ballal and Lefebvre [1]. Pera *et al.*[2] recently studied the effect of turbulence intensity, integral scale, and equivalence ratio on cycle-to-cycle variations (CCVs) using 2D DNS study. Different realizations of turbulence with same statistics were shown to have more impact than turbulence intensity and integral scale on CCVs. Also lean mixture was more susceptible to such variation than stoichiometric mixture. However using lean air-fuel mixture has benifits like reduced No_x emissions [3]. Reddy and Abraham [4] have assessed the accuracy of flame surface density (FSD) modeling used in the large eddy simulation (LES) using 2D DNS study with multi-step chemistry. Displacement speed and magnitude of gradient of progress variable ($|\nabla c|$) are important factors in many such premixed combustion models. Effect of strain rate and curvature on $|\nabla c|$, known as Surface density function has been studied in this paper.

2D as well as 3D DNS have been carried out using simplified chemistry of 3-step CH_4-air combustion [5]. Statistics obtained from 2D and 3D simulations have been compared. In addition, statistics was also obtained from a 2D slice of 3D simulation. Extraction of statistics from a 2D slice of 3D simulation has relevance for interpreting data obtained from measurement techniques like OH-PLIF technique [6]. Thevenin *et al.*[7] compared 2D and 3D DNS of ignition kernel. It was observed that kernel in 3D

simulation grew slower than kernel in 2D simulation when effective radius was considered. However comparison between important statistics of 2D and 3D simulations for ignition kernel has not been discussed in the literature.

NUMERICAL SCHEMES AND INITIAL CONDITIONS

DNS was performed using the PENCIL code. PENCIL code is an open-source DNS code capable of handling multi-step chemistry. It has been parallelized using MPI libraries [8]. The code uses sixth-order finite difference scheme for spatial discretization proposed by Lele [9] with low storage third-order Runge-Kutta scheme proposed by Williamson [10] for time-stepping. Three step irreversible chemistry of Methane-air combustion was used [5]. Initial velocity field was created based on Passot-Pouquet spectrum [11] for given turbulence intensity and integral scale. Diffusion coefficients were calculated using power-law based temperature dependence [12]. Initial ignition kernel was created in the form of sphere of diameter 0.25 cm at temperature of 1660 K, which is the adiabatic flame temperature obtained from CHEMKIN calculations using three-step chemistry. Ignition kernel contained products of complete combustion of methane–air mixture. Periodic boundary conditions were applied on all the boundaries. Equivalance ratio,φ, was 0.6 and temperature was 300 K in rest of the domain. Initial pressure was 1 atm. Laminar flame speed S_L of unstrained flame at 1 atm, $\varphi = 0.6$, and unburned gas temperature of 300 K is 13.8 cm/s. Flame thickness δ_L based on maximum temperature gradient is 0.083 cm. Chemical time-scale ($\tau_c = \delta_L/S_L$) based on laminar flame is 6.01 ms. Initial temperature was assigned using the profile given by Eqns. (1) and (2) to prevent sharp temperature gradients at kernel boundary. Here r is the distance of point from centre of domain and R=0.15 cm. It created high temperature zone of radius 0.125 cm. Domain size is 4 cm in every direction which has been discretized using 256 grid points for 2D as well as for 3D DNS. Karlovitz number of this flame is 7.2 and flame belongs to thin-reaction zone regime. Reaction progress variable is defined by Eqn. (3).

$$T = T_0 + (T_{ad} - T_0)\left[H(r) - H(r - R)\right] \tag{1}$$

H is Heaviside step function defined as Eqn. (2). Here k is taken as 80.

$$H(x) = \frac{1}{1 + e^{-2kx}} \tag{2}$$

$$c = \frac{T - T_0}{T_{ad} - T_0} \tag{3}$$

Other parameters used in the study such as turbulence intensity (u_{rms}), integral scale (l_t), eddy-turnover time (τ_f), and Damkohler number (Da) are given in Tab. 1. Displacement speed of an iso-contour is a speed at which it moves relative to the flow in the direction of flame normal. It is given by Eqn. (4).

$$S_d = \frac{(-\dot{w} - \nabla.(\rho D \nabla Y))/\rho}{|\nabla Y|} \tag{4}$$

TABLE 1: PARAMETERS USED FOR THE STUDY

u_{rms}	l_t	$\tau_f = l_t/u_{rms}$	$Da=\tau_f/\tau_c$
69 cm/s	0.2 cm	2.89 ms	0.48

RESULTS AND DISCUSSION

Figure 1 shows temperature contours for 2D DNS. Considerable wrinkling has occurred by the time statistics was extracted from the flame. Scatter plots of SDF with mean curvature and tangential strain rate have been presented in Figs. 2-4. Values were extracted at time 6.0 ms, which is close to chemical time-scale based on laminar flame. This is comparable with the value typically considered in other studies [For eg. 13]. Also, these values were obtained at an iso-contour of $c = 0.7\pm0.02$. All the quantities, except RHS of Eqn.(4), have been non-dimensionalized using appropriate reference quantities based on properties of flat laminar flame.

Based on scatter plots in Fig.2 and Fig.3, it can be observed that SDF is negatively correlated with curvature and positively correlated with tangential strain rate in 2D as well as in 3D simulations. Respective conditional average is also shown with a thick line in each figure. This is in agreement with previous study by Klein *et al.*[13]. Positively curved regions of flame, which are convex towards unburned air-fuel mixture, loose heat to these surrounding cold reactants. This loss of heat slows down the reaction rate in the flame front resulting in the thickening of the flame. As flame becomes locally thick, the magnitude of gradient of progress variable ($|\nabla c|$) falls. With increasing tangential strain rate, normal strain rate falls. Dilation is related to tangential strain rate as given by Eqn. (5) [13]. a_T and a_N are tangential and normal strain rates respectively. As magnitude of tangential strain increases, magnitude of normal strain rate falls consequently and even may become negative. In such a case flame front is compressed so that iso-contours of progress variable come closer to each other. This result in the rise of SDF reflected in the positive correlation between SDF and tangential strain rate.

$$\nabla \cdot \bar{u} = a_T + a_N \tag{5}$$
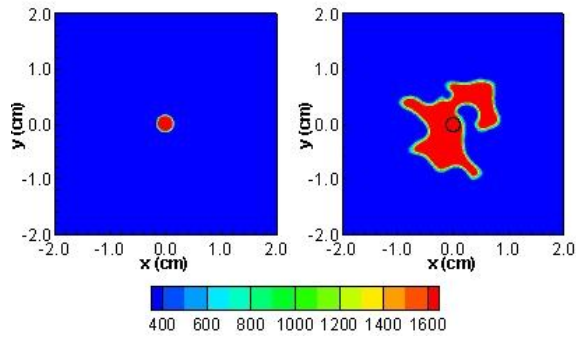
FIGURE 1 TEMPERATURE CONTOURS AT TIME 0 *ms* AND 6 *ms* IN 2D DNS
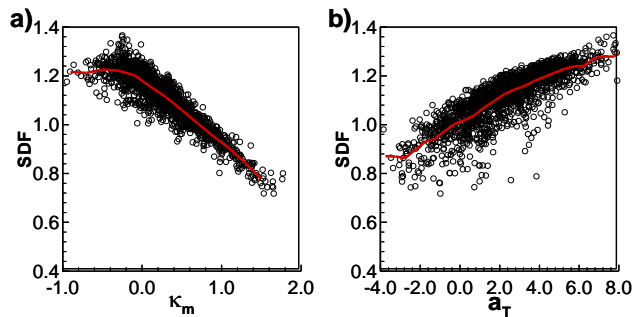
FIGURE 2. SCATTER PLOT OF SDF WITH a) CURVATURE b) TANGENTIAL STRAIN RATE IN 3D DNS
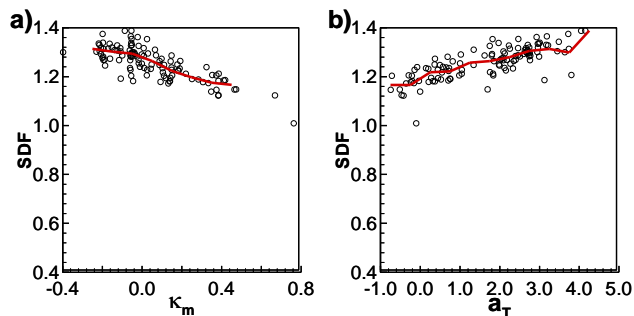
FIGURE 3. SCATTER PLOT OF SDF WITH a) CURVATURE b) TANGENTIAL STRAIN RATE IN 2D DNS

2D simulation is also effectively capturing both correlations of SDF. Magnitudes of SDF captured by 2D and 3D simulations are also comparable. Strain rate and mean curvature predicted by 2D simulation have smaller range compared to 3D simulation, as observed from the range on X axis. However, 2D slice of a 3D simulation is not able to capture mean curvature values effectively and

SDF values are crowded about a single mean curvature value. Similar trends were obtained for X plane.
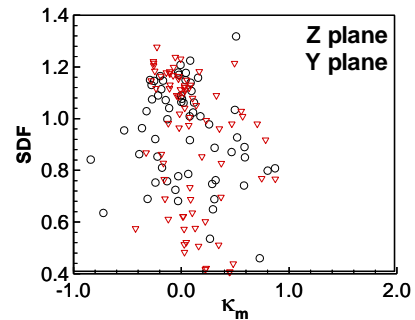
FIGURE 4. SCATTER PLOT OF SDF WITH CURVATURE IN A 2D SLICE OF 3D SIMULATION
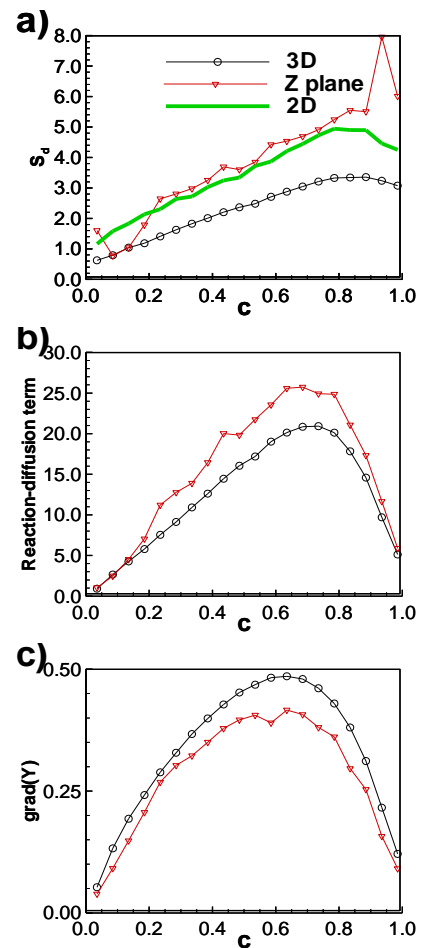
FIGURE 5. CONDITIONAL AVERAGE OF a) DISPLACEMENT SPEED b) REACTION-DIFFUSION TERM c) $|\nabla Y|$ WITH PROGRESS VARIABLE

Displacement speed is a result of the interaction between reaction and diffusion in the flame. CH_4 was chosen as species to evaluate reaction-diffusion term,

3

which is in the numerator of Eqn. (4). As shown in Fig. 5(a) 2D slice over-predicts S_d across the entire flame. Values of displacement speed obtained from this slice are closer to the ones obtained by actual 2D simulation. 2D slice predicts higher values of reaction-diffusion term as shown in Fig. 5(b). 2D slice predicts smaller values of SDF than a 3D simulation as shown in Fig.4. Similar effect causes 2D slice to predict smaller values of $|\nabla Y|$ as shown in Fig. 5(c). These two effects together contribute to the higher prediction of S_d in a 2D slice. It shows that care should be taken while interpreting data obtained from a plane of an essentially 3D phenomenon.

Both simulations were carried out on 16 Intel 2.0 GHz Xeon processors using time-step of 0.125 μs. 2D simulation took 5 hours while 3D simulation took 15 days of wall-clock time.

CONCLUSIONS

2D as well 3D simulations were carried out to study the effect of number of dimensions on interaction between ignition kernel and turbulence. Correlations of SDF with curvature and tangential strain rate were studied for this purpose. SDF is negatively correlated with curvature and positively correlated with tangential strain rate. Even 2D simulation is able to capture these correlations. There are differences in the range of values of SDF, mean curvature, and tangential strain rate predicted by 2D and 3D simulations. 2D simulation predicts smaller range of SDF, mean curvature, and tangential strain rate. Based on this, it can be said that 2D simulation can also capture the interaction between ignition kernel and turbulence. More simulations at higher Karlovitz number close to broken reaction zone regime should be carried out to check the agreement between 2D and 3D simulations at higher Karlovitz number. Results obtained from a 2D slice of 3D simulation were not satisfactory. Negative SDF-curvature was not predicted in 2D slice and displacement speed was over-predicted compared to 3D simulation.

REFERENCES

[1]   Ballal, D. R., and Lefebvre, A. H., 1975, "The influence of flow parameters on minimum ignition energy and quenching distance," Symp. Combust., **15**(1), pp. 1473–1481.

[2]   Pera, C., Knop, V., and Reveillon, J., 2015, "Influence of flow and ignition fluctuations on cycle-to-cycle variations in early flame kernel growth," Proc. Combust. Inst., **35**(3), pp. 2897–2905.

[3]   Reddy, H., and Abraham, J., 2010, "Ignition kernel development studies relevant to lean-burn natural-gas engines," Fuel, **89**(11), pp. 3262–3271.

[4]   Reddy, H., and Abraham, J., 2012, "Two-dimensional direct numerical simulation evaluation of the flame-surface density model for flames developing from an ignition kernel in lean methane/air mixtures under engine conditions," Phys. Fluids, **24**(10).

[5]   Bibrzycki, J., and Poinsot, T., 2010, "Reduced chemical kinetic mechanisms for methane combustion in O2/N2 and O2 /CO 2 atmosphere," Work. note ECCOMET WN/CFD/10/17, CERFACS.

[6]   Gashi, S., Hult, J., Jenkins, K. W., Chakraborty, N., Cant, S., and Kaminski, C. F., 2005, "Curvature and wrinkling of premixed flame kernels-comparisons of OH PLIF and DNS data," Proc. Combust. Inst., **30**(1), pp. 809–816.

[7]   Thévenin, D., Gicquel, O., De Charentenay, J., Hilbert, R., and Veynante, D., 2002, "Two- versus three-dimensional direct simulations of turbulent methane flame kernels using realistic chemistry," Proc. Combust. Inst., **29**(2), pp. 2031–2039.

[8]   Babkovskaia, N., Haugen, N. E. L., and Brandenburg, A., 2011, "A high-order public domain code for direct numerical simulations of turbulent combustion," J. Comput. Phys., **230**(1), pp. 1–12.

[9]   Lele, S. K., 1992, "Compact finite difference schemes with spectral-like resolution," J. Comput. Phys., **103**(1), pp. 16–42.

[10]   Williamson, J. H., 1980, "Low-storage Runge-Kutta schemes," J. Comput. Phys., **35**(1), pp. 48–56.

[11]   Bansal, G., and Im, H. G., 2011, "Autoignition and front propagation in low temperature combustion engine environments," Combust. Flame, **158**(11), pp. 2105–2112.

[12]   Savre, J., Carlsson, H., and Bai, X. S., 2013, "Tubulent methane/air premixed flame structure at high karlovitz numbers," Flow, Turbul. Combust., **90**(2), pp. 325–341.

[13]   Klein, M., Chakraborty, N., Jenkins, K. W., and Cant, R. S., 2006, "Effects of initial radius on the propagation of premixed flame kernels in a turbulent environment," Phys. Fluids, **18**(5).

PYROLYSIS OF COIR PITH: ANALYSIS OF BIO-OIL YIELD AND THERMOKINETIC PARAMETERS

Vaibhav Dhyani [1], Jitendra Kumar [1], Bijoy Biswas [1], Thallada Bhaskar [1, 2,*]
[1] Thermo-catalytic processes area (TPA), Bio-Fuels Division (BFD), CSIR-Indian Institute of Petroleum (IIP),
Dehradun 248005, India
[2] Academy of Scientific and Innovative Research (AcSIR)
Email ID: tbhaskar@iip.res.in, Telephone number: 0135-2525820

ABSTRACT

Coir pith which is an agricultural waste and also an environmental hazard can be used for the production of valuable hydrocarbons by pyrolysis. In work presented in this paper, slow pyrolysis of coir pith was conducted at different temperatures for quantitative and qualitative analysis of the yield of bio-oil and bio-char. An independent kinetic analysis of the apparent pyrolysis reaction was executed using thermogravimetry and isoconversional methodology. The thermodynamic parameters (ΔH, ΔS, and ΔG) were subsequently evaluated at different points of conversion using the values of activation energy obtained from the kinetic analysis.

The bio-oil produced from pyrolysis was observed to be rich in phenolic hydrocarbons. Although the bio-oil yield didn't show sizable quantitative variation with reaction temperature, significant variation in the composition of bio-oil was observed in the qualitative analysis.

The activation energy showed a variation from 28.41 to 200.09 kJ/mol, with the mean value being 140 kJ/mol.
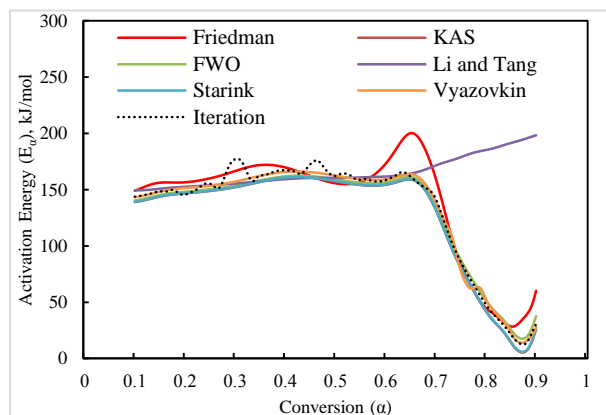
Keywords: Coir pith, Pyrolysis, Bio-Oil, Kinetics

NOMENCLATURE

α Conversion, −
A_α Pre-exponential factor, s^{-1}
E_α Activation energy, kJ/mol

INTRODUCTION

Coir is the term given to the fibers constituting the husk/mesocarp of the coconut (*Cocos nucifera*), which are used for the manufacture of ropes, matting, and other hard-fiber based products. Coir pith is a spongy material that binds the coconut fiber in the husk and constitutes up to 70% of the husk. It is an agricultural waste produced during the processing of coconut fiber. Dumping of coir pith is not only a management problem but also an environmental issue, because of contamination of ground water by percolation of phenolic compounds from these dumps. India is a leading producer of coir pith, marking an annual production of around 7.5 million tons per year [1].

Much of the research done with coir pith, has been fixed around its use as an adsorbent in waste water treatment, by chemical/physical treatment. Various researchers have studied the removal of contaminants such as dyes [1–3], phosphate [4], transition metal ions [5–7], etc. Studies have also been done in analyzing coir pith as a substitute of sphagnum or sedge peat in soilless cultivation [8]. However little work has been done in the field of energy production or extraction of important phenolic compounds from coir pith.

MATERIALS AND METHODS
Feedstock

Coir pith fibers were obtained from Coir Board, Kerala. The fibers were ground before conducting experiments. 10 g ground Coir pith was used for slow pyrolysis, while in the Thermogravimetric analysis (TGA), approximate 5 mg sample was used in each run.

Pyrolysis Experiment

Pyrolysis of coir pith was conducted at 300, 350, 400 and 450 °C, in a laboratory scale pyrolysis unit, the schematic diagram of which has been illustrated in Figure 1. Each pyrolysis experiment was initiated with a non-isothermal regime, in which feed was heated at 10 °C/min

until the aimed temperature was reached, where the temperature was held constant for an hour. The reactor temperature was controlled using a PID temperature controller. Nitrogen was used to create an inert atmosphere in the reactor and also to carry the products of pyrolysis from reactor to an external condenser, where bio-oil was condensed and separated from the non-condensable gasses.
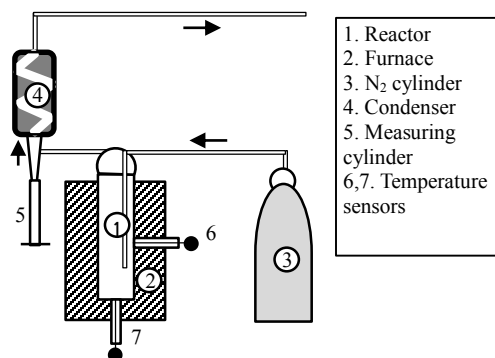
FIGURE 1. Schematic representation of pyrolysis reactor

The aqueous fraction of the bio-oil produced was separated and removed using a separating funnel, leaving an organic fraction rich bio-oil, which was further analyzed using GC-MS, FT-IR, and NMR. The bio-char was collected as the post-reaction residue in the pyrolysis reactor, and analyzed by CHNS, FT-IR, and XRD.

Thermogravimetric and Kinetic Analysis

Kinetic analysis was performed using TGA, which was carried out in a DTG-60 unit (Shimadzu, Japan). The ground coir pith samples were heated from room temperature to 900 °C at six different heating rates (5, 10, 15, 20, 30 and 40 °C/min). Nitrogen gas at a flow rate of 100 ml/min, was used as an inert purge gas to displace air in the pyrolysis zone, thus avoiding unwanted oxidation of the samples.

Kinetic analysis was performed using the weightloss data from thermogravimetry. Both differential (Friedman) and integral (KAS, FWO, Vyazovkin, Starink, Li and Tang and Iterative) isoconversional methods were used for computation of activation energy [9]. Pre-exponential factor
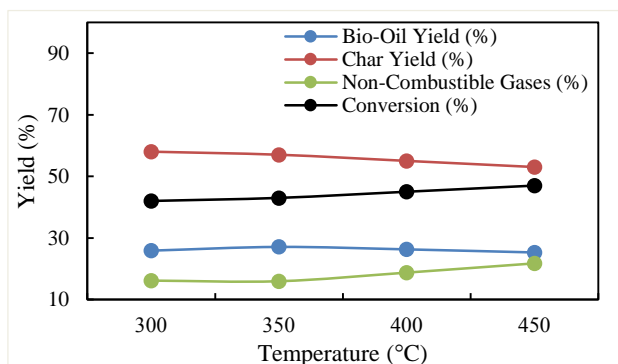
FIGURE 2. Yield of liquid, solid and non-condensable gases from coir pith pyrolysis

was calculated using Kissinger's equation, and reaction model was predicted using z-master plot.

RESULTS AND DISCUSSION
Yield from Pyrolysis

The yield of bio-oil, bio-char and non-condensable gases, calculated on weight basis are graphically illustrated in Figure 2. It can be observed that although total conversion (yield of liquid + gases) increases with temperature, the yield of bio-oil decreases after 350 °C. Also the bio-oil yield which varies from 25.3 to 27.1 %, showed a maxima at 350 °C. The yield of bio-char was above 33 % in all the experiments, while the yield of non-condensable gases varied from 15.9 to 21.7 %.

Analysis of Bio-Oil
Results from GC-MS. The analysis report from GC-MS is shown in Table 1. Phenolic compounds constituted the major part of the bio-oil obtained from pyrolysis (as much as 88.14 %). Maximum phenolic compounds were obtained at 350 °C, which is also the temperature of maximum bio-oil yield. In the phenolic compounds, pure phenol showed the maximum constitution, followed by p-Cresol, catechol, alky phenols and phenolic ethers. The abundance of pure phenol, which was 56.13 % in bio-oil obtained from pyrolysis at 300 °C, decreased with increasing temperature, while the alkyl-phenols showed simultaneous increase in abundance.
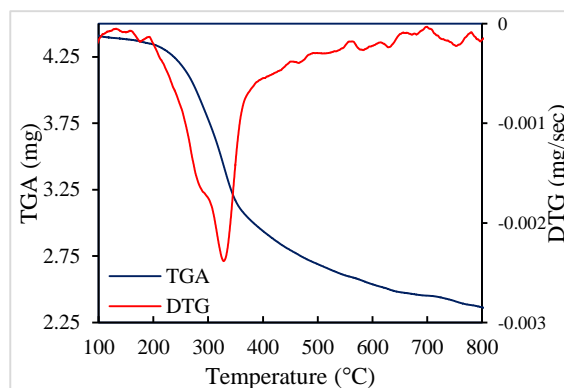
FIGURE 3: TGA/DTG curve at 10 °C/min
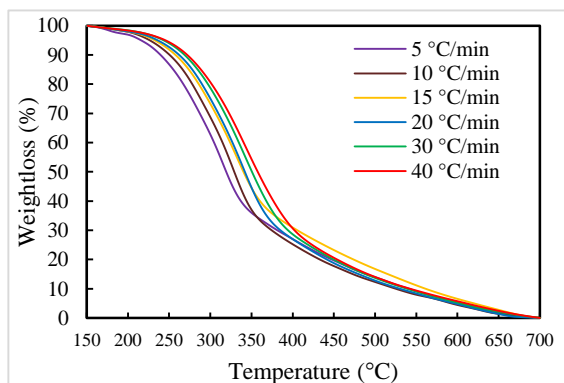
FIGURE 4: Weightloss curves at different heating rates
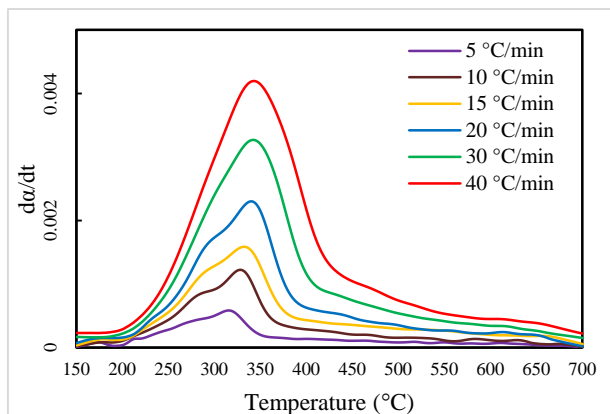
FIGURE 5: Rate of conversion at different heating rates
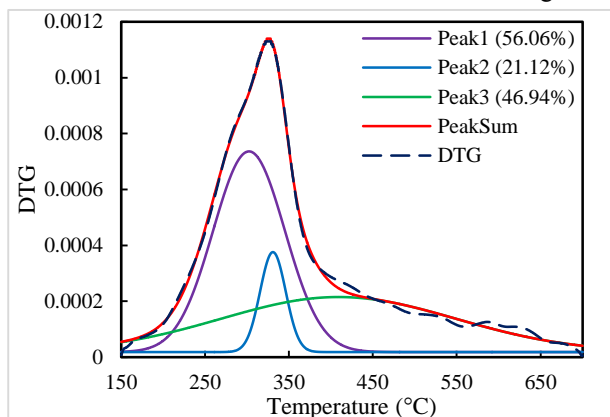
FIGURE 6: De-convoluted DTG curve vs. Conversion

FIGURE 7: Activation energy versus conversion
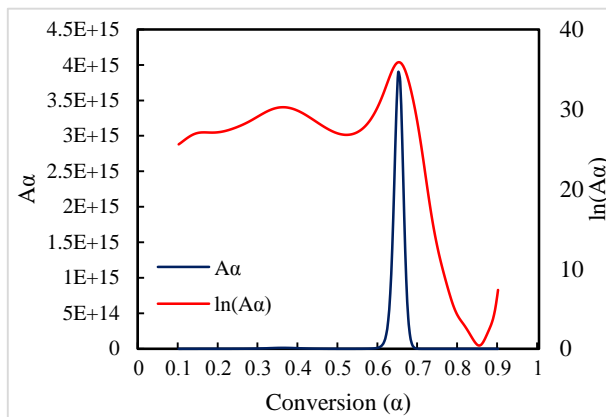
FIGURE 8: Pre-exponential factor versus conversion

Thermogravimetric Analysis

The results of thermogravimetric analysis (Figure 3 to 6) showed that the thermal decomposition of coir-pith took place in a wide range of temperature. The average weightloss of 47.8 % was observed from 25 to 900 °C, with the maximum weightloss occulting in the range of 200 to 500 °C (~ 30 % of initial weight).

Kinetic Analysis

Values of activation energy (E_α) and pre-exponential factor (A_α) calculated using different isoconversional methods has been illustrated in Figures 7 and 8, respectively. The activation energy showed an increase until a conversion value of 0.7, followed by a steady decline. The activation energy showed a variation from 28.41 to 200.09 kJ/mol, with the mean value being 140 kJ/mol.

The experimental data was fitted to n-th order reaction model, and it was observed that the order of reaction increased as the reaction proceeded (from 0 to 0.35).

The thermodynamic parameters (ΔH, ΔS, and ΔG) were subsequently evaluated at different points of conversion using the values of activation energy obtained from kinetic analysis, to explicate the reaction progression from an energy viewpoint.

CONCLUSIONS

Coir-pith can be converted to bio-oil using pyrolysis, a thermal depolymerization reaction. Although the overall conversion was observed to increase with temperature, the maximum liquid yield was obtained at 350 °C. At higher temperatures, the yield shifted towards non-condensable gasses. Phenolic compounds constituted the major part of the bio-oil obtained from pyrolysis (as much as 88.14 %).

The decomposition pattern studied using TGA showed maximum decomposition taking place in the temperature zone of 200 to 500 °C. TGA data was successfully used for calculation of kinetic parameters, which showed an average kinetic energy of 140 kJ/mol, for the reactions taking place.

REFERENCES

[1] Namasivayam, C., Kavitha, D., 2002, "Removal of Congo Red from water by adsorption onto activated carbon prepared from coir pith, an agricultural solid waste", Dye and Pigment, 54, pp. 47–58

[2] Kavitha, D., Namasivayam, C., 2007,"Experimental and kinetic studies on methylene blue adsorption by coir pith carbon", Bioresoure Technology, 98, pp. 14–21

[3] Namasivayam, C., Kumar, M. D., Selvi, K., Begum, R. A., Vanathi, T., Yamuna, R.T., 2001, "Waste coir pith - a potential biomass for the treatment of dyeing wastewaters" Biomass and Bioenergy, 21, pp. 477–483

[4] Krishnan, K.A., Haridas, A., 2008, "Removal of phosphate from aqueous solutions and sewage using natural and surface modified coir pith", J. Hazard. Mater., 152, pp. 527–535

[5] Namasivayam, C., Sureshkumar, M. V., 2008, "Removal of chromium (VI) from water and wastewater using surfactant modified coconut coir pith as a biosorbent", Bioresour. Technol., 99, pp. 2218–2225

[6] Suksabye, P., Nakajima, A., Thiravetyan, P., Baba, Y., Nakbanpote, W., 2009, "Mechanism of Cr (VI) adsorption by coir pith studied by ESR and adsorption kinetic", J. Hazard. Mater., 161, pp. 1103–1108

[7] Parab, H., Joshi, S., Shenoy, N., Lali, A., 2006, "Determination of kinetic and equilibrium parameters of the batch adsorption of Co(II), Cr(III) and Ni (II) onto coir pith", Process Biochem., 41, pp. 609–615

[8] Meerow, A. W., 1994, "Growth of Two Subtropical Ornamentals Using Coir (Coconut Mesocarp Pith) as a Peat Substitute", HortScience, 29, pp. 1484–1486

[9] Vyazovkin, S., Burnham, A. K., Criado, J. M., Pérez-maqueda, L. A., Popescu, C., Sbirrazzuoli, N., 2011, "Thermochimica Acta ICTAC Kinetics Committee recommendations for performing kinetic computations on thermal analysis data", Thermochim. Acta, 520, 1–19

SEEC-2017-045

EFFECT OF PROCESS PARAMETERS ON HYDROTHERMAL LIQUEFACTION OF CORN COB BIOMASS RESIDUE FOR BIO-OIL PRODUCTION

Yashasvi Bisht[1], Bijoy Biswas[1], Jitendra Kumar[1], Thallada Bhaskar[1, 2*]
[1] Thermo-catalytic processes area (TPA), Bio-Fuels Division (BFD), CSIR-Indian Institute of Petroleum (IIP), Dehradun 248005, India
[2] Academy of Scientific and Innovative Research (AcSIR)
Email ID: tbhaskar@iip.res.in, Telephone number: 0135-2525820

ABSTRACT

The aim of the study is to examine the effect of process variables such as the effect of temperature, role of solvent (water, methanol, and ethanol) and influence of alkali catalysts(KOH and K_2CO_3) on hydrothermal liquefaction of Corn Cob using an autoclave reactor. Hydrothermal liquefaction has been carried out at 260,280 and 300 °C temperatures, with a residence time of 15 min. The yield of bio-oil was high in the presence of water and increased to ca. 38 wt% at 280 °C. The alkali catalysts could not improve the yield of the bio-oil but improved the selectivity of the phenolic compounds. The bio-oil products were comprehensively characterized using GC–MS, FT-IR, and ^1H NMR. From the GC-MS analysis of bio-oil, the phenolic compounds were observed higher (60 wt%) in the case of water solvent than methanol, and ethanol (57 wt% and 46 wt% respectively). FTIR, CHNS, and TOC of bio-chars indicated the organic carbon in the corn cob converted into products.

Keywords: Hydrothermal Liquefaction, Corn Cob, Biomass, Solvents, Catalysts, Bio-oil.

INTRODUCTION

The declining fossil fuel reserves and increasing concerns over greenhouse gas emissions and climate change have led to a worldwide interest in seeking alternatives to fossil resources for energy and chemicals/fuels production. Biomass is a sustainable and renewable alternative to fossil fuels for energy and chemicals/fuels due to its high abundance and renewability [1]–[3].Hydrothermal conversion is a thermochemical process, in which biomass is depolymerized to gaseous, aqueous, bio-oil (or bio-crude), and solid byproducts in a heated, pressurized and oxygen-free reactor in the presence of water or other solvents. Compared with other thermochemical conversion processes, such as gasification and fast pyrolysis, HTL is conducted at lower temperatures and does not require feedstock drying. Residues from food crops in many agricultural countries are abundant and often simply discarded as waste or underutilized. Some of the corncobs are used as boiler fuel in power plants, but the unused corncobs have a high potential to be converted into liquid fuel or chemical feedstock [4]. In this section, the primary compounds and structure in these feedstock's will be summarized and the potential functions in hydrothermal have been explored. The effect of operating conditions including reaction temperature, retention time, a biomass solid content, and catalyst loading on gaseous, aqueous, and solid products production from the HTL of Corn Cob have been studied [5]-[7].

The aim of this work is to understand the role of various solvents and catalysts and compare their effects on products distribution, yields, and oil compositions. The liquid products were analyzed for different physical and chemical properties by using different chromatographic and spectroscopic technique such as FT-IR, ^1H NMR, and GC/MS. The co-product of pyrolysis i.e. bio-char obtained at different temperatures were also analyzed for different physical and chemical properties.

MATERIALS AND METHODS
Feedstock
Agriculture corn cob biomass residue was used in this study has been obtained from Uttarakhand, Dehradun district (India). The sample was dried in sun and then crushed and sieved to obtain particle size between 0.5 and 2 mm.

Characterization methods
TG-DTG of corn cob was carried out on Shimadzu DTG-60 under N_2 flow and the gross calorific value was found using Parr 6300 Bomb Calorimeter. The elemental analysis has been carried out in Elementar vario micro cube unit. Moisture content has been obtained using HR- 83 Mettler Toledo Halogen Moisture Analyzer. The ^{1}H NMR spectra have been recorded in the Bruker Avance 500 Plus instrument using $CDCl_3$ as a solvent. Powder X-ray diffraction patterns were collected on Bruker D8 advance X-ray diffractometer fitted with a Lynx eye high-speed strip detector and a Cu Kα radiation source. Diffraction patterns in the $2°-80°$ region has been recorded with a 0.04 step size (step time= 4s). The FT-IR spectra were recorded on Nicolet 8700 FTIR spectrometer with the sample powder diluted in KBr. SEM images have been collected on FEI Quanta 200 F, using tungsten filament doped with lanthanum hexaboride (LaB_6) as an X-ray source, fitted with an ETD (Everhart-Thornley Detector), which preferentially work as a secondary electron detector. The sample for SEM has been subjected to disperse on a carbon paper coated adhesive followed by gold coating. The organic fraction of the bio-oil was analyzed using gas chromatography–mass spectrometry (GC/MS, Agilent 7890 B). The carrier gas was He and column flow rate was 1 ml min^{-1}. HP-1 column (25 m × 0.32 mm × 0.17 µm) was used for the separation. An oven isothermal program was set at 50 °C for 2 min, followed by a heating rate of 5 °C min^{-1} till 280 °C where it was held for 5 min. The injected volume was 0.4 µL in a splitless mode. TOC analysis of feed and bio-char was performed using Shimadzu TOC-L unit with solid sample module SSM-5000A. The volatile matter has been calculated by measuring the weight loss in the sample after placing it in a muffle furnace at 950 °C for 2 minutes similar to ASTM D3175. Volatile matter and ash analysis of the feed was carried out using oven dried feedstock.

REACTION PROCEDURE

Hydrothermal liquefaction experiments were conducted in a 100 ml high-pressure autoclave (Parr reactor) made of Hastelloy at different reaction conditions of temperature. In a typical hydrothermal liquefaction experiment, the reactor was loaded with corn cob and solvent (water, methanol, and ethanol) (1:6 by weight) and KOH and K_2CO_3 catalyst with water (0.5N and 1N). Then the reactor was purged five times with nitrogen to remove the inside air. Reactants were agitated using stirrer (~200 rpm). The temperature was then raised up to desired value and kept for 15 minutes at that reaction temperature. The pressure during the process was autogenous and maximum pressure was in the range of (43–156 bar) under different reaction conditions. After the reaction, the procedure of separation of bio-oil1, bio-residue and bio-oil2 was given in our earlier communication [8]. The experiments were repeated several times and the deviation of the liquid yields are within ± 1%. Various equations to calculate the yield of various fractions

$$Conversion\ (\%) = \frac{W1-W2}{W1}\ x\ 100$$

$$Bio\ oil\ yield\ (wt.\%) = \frac{W\ ether\ soluble}{W1}\ x\ 100$$

$$Bio\ oil\ 2\ yield\ (wt.\%) = \frac{W\ acetone\ soluble}{W1}\ x\ 100$$

$$Solid\ residue\ yield\ (wt.\%) = \frac{W\ solid}{W1}\ x\ 100$$

$$Gas\ yield\ (wt.\%) = (W\ (vessel + feed + water\ )before\ HTL$$
$$- W\ (vessel + feed$$
$$+ water)after\ HTL)$$
$$/(Amount\ of\ feed\ taken\ (g)$$
$$+ amount\ of\ water\ added\ (g))\ x\ 100$$

$$Other\ yield\ (wt.\%)$$
$$= 100$$
$$- (bio - oil\ 1 + bio\ oil\ 2$$
$$+ solid\ residue + gas)$$

W1, is the weight of corn cob feed; *W2*, is the weight of bio-residue; *W ether soluble*, is the weight of ether soluble bio-oil (bio-oil1); W *acetone soluble*, is the weight of acetone soluble bio-oil (bio-oil2). All yields were calculated on a dry basis of material. Others correspond to the water soluble oxygenated hydrocarbons and some loses.

RESULTS AND DISCUSSION
Feed characterization
The results of the proximate and ultimate analysis of the corn cob sample have been presented in Table1. Total volatiles collected at 950 °C represent 91.16 wt% of the total product. The moisture, ash and fixed carbon content of the feedstock were found to be 12.77%, 2.30%, and 6.54% respectively. Ultimate analysis showed the composition of the key element as 42.10% C, 5.90% H, 0.49% N, 0.48% S and 51.03% O (Calculated by difference

Table 1. Ultimate and proximate analysis of corn cob

Ultimate analysis, wt.%		Proximate analysis	
C	42.10	Moisture	12.77
H	5.90	Volatiles	91.16
N	0.49	Fixed Carbon	6.54
O	51.03	Ash	2.30
S	0.48		

The pyrolytic characteristics of the corn cob at a temperature between 25-900 °C was determined by TGA/DTG. The percentage of the existing weight as a function of temperature (TG curve) showed that there were three stages occurring during the pyrolysis process. The first stage (up to about 200 °C) was dehydration; the weight loss was due to moisture removal from the sample. The next stage (200-460 °C) was devolatilisation; the weight loss in this stage was high due to the loss of volatile components. The last stage (460-900 °C) was solid decomposition; at this stage, the weight loss was slower.

Product yields

Hydrothermal liquefaction of Corn Cob has been carried out at 260,280 and 300 °C with a residence time of 15 min. The water medium showed the best performance considering the bio-oil yield. The bio-oil yield with water solvent was increased to ca. 38 wt % at 280 °C more than the yield using methanol, ethanol, and alkali catalyst.

Analysis of bio-oil

GC-MS analysis of bio-oil
The GC-MS results are shown in Fig.1. It has been observed that carbonyl, ester, phenol derivatives and aromatic compounds present in the bio-oils. In all bio-oils, the phenolic compounds were observed higher (60 wt%) in the case of water solvent at 280 ºC temperature which is also the temperature of maximum bio-oil yield than methanol and ethanol (57 wt% and 46 wt% respectively).

FT-IR analysis of bio-oil
The FT-IR spectra of corn cob have been shown in Fig.2. According to FT-IR results, the functional groups in all oils produced in the presence or absence of methanol and ethanol and catalyst are similar. The absorption peaks between 1650 and 1750 cm^{-1} were attributed to the C=O stretching from carboxylic acids and ester groups in the crude bio-oil. The bands from 1350 cm^{-1}-1470 cm^{-1} were attributed to C-H bending, which indicated alkyl groups in the obtained oil. However, the type of solvents and catalysts strongly affected the chemical composition of bio-oils. With a water solvent of HTL phenol derivatives, some of the major compounds identified in the bio-oil are Phenol, 2,6-dimethoxy-, Phenol, 2-methoxy-.

^{1}H NMR analysis of bio-oil
According to ^{1}H NMR results, the integral region from 1.5 to 3.0 ppm represents protons on aliphatic carbon atoms that may be bonded to a C=C double bond. All the bio-oils have a higher percentage of protons in the spectral region from 0.5 to 3.0 ppm. The region of the spectrum between 6.0 and 8.5 ppm corresponds to the aromatic region. The maximum proton content of bio-oil was obtained in the case of methanol solvent around 11.31 % in this region.
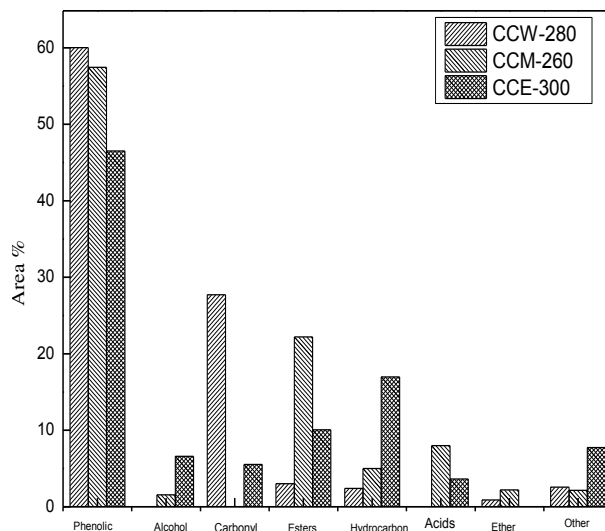
FIGURE 1: GC-MS of bio-oil
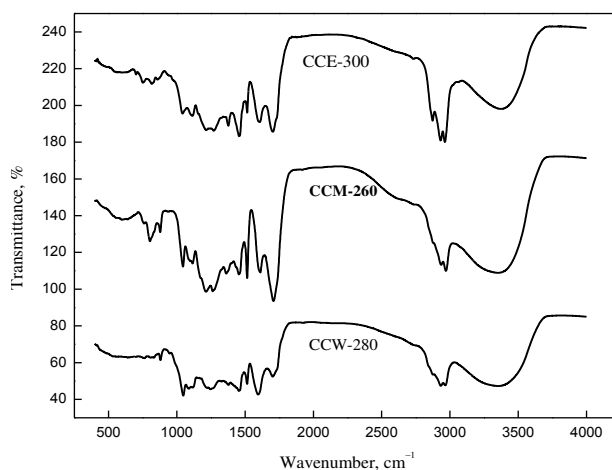
FIGURE 2: FT-IR of bio-oil

Aromatic/heteroaromatic functionality was also observed in all bio-oils (6.0–8.5 ppm) in agreement with findings from FT-IR. All bio-oil1 samples displayed a low percentage of methoxy/carbohydrate functionality (4.5–6.0 ppm). Negligible proton resonated in this region using water as a reaction medium for liquefaction. Aldehyde functionality (8.5–10.0 ppm) was absent from all samples.

CONCLUSIONS

Hydrothermal liquefaction was identified to be a promising option for the crude bio-oil production from waste biomass residue. The preferable liquefaction conditions were determined as the reaction temperature of 280 °C with water as solvents (38wt. %) than methanol, ethanol, KOH and K$_2$CO$_3$ catalysts. From the GC/MS analysis, it has been shown that all the bio-oils contain phenolic compounds. The phenolic compounds observed, were the

predominantly higher in the case of HTL with water than methanol, ethanol, KOH and K_2CO_3 catalysts, and it is evidently compared with the FT-IR and NMR. From the bio-char analysis by TOC, CHNS and FT-IR it has been seen that the bio-char is a carbon rich and corn cob feed was decomposed to products.

REFERENCES

[1] Li, H., Hurley, S., Xu, C., 2011. "Liquefactions of peat in supercritical water with a novel iron catalyst". Fuel, 90(1), 412–420.

[2] Xu, C., Etcheverry, T., 2008. "Hydro-liquefaction of woody biomass in sub- and supercritical ethanol with iron-based catalysts". Fuel, 87(3), 335–345.

[3] Yang, C., Jia, L., Chen. C., Liu, G., 2011. "Fang W. Bio-crude oil from hydro-liquefaction of Dunaliella salina over Ni/REHY catalyst". Bioresour Technol, 102 (6)4580–4584.

[4]Khampuang, K., Boreriboon, N., Prasassarakich, P., 2015. "Alkali catalyzed liquefaction of corncob in supercritical ethanol water". Biomass and Bioenergy, 83,460-466.

[5] Gan, J., Yuan, W., Nelson, NO., Agudelo, SC., 2010. "Hydrothermal conversion of corn cobs and crude glycerol". Biol Eng, 2(4), 197–210.

[6] Yu, F., Ruan, R., Chen, P., Deng, S., Liu, Y., Lin, X., 2007. "Liquefaction of corn cobs with supercritical water treatment". Trans ASABE, 50(1), 175–80.

[7] Zhang, B., Keitz, MV., Kenneth, V., 2008. "Maximizing the liquid fuel yield in a bio refining process". Biotech Bioeng, 101(5), 903–12.

[8] Singh, R., Balagurumurthy, B., Bhaskar, T., 2015. "Hydrothermal liquefaction of macro algae: Effect of feedstock Composition". Fuel, 146, 69–74.

SEEC-2017-46

EPOXY COMPOSITE COATINGS FOR EXTREME CONDITION APPLICATION

Vikram Kumar
Dept. of Mechanical Engg.
Indian Institute of Technology Kanpur
Email: vikramk@iitk.ac.in

Sujeet K. Sinha
Dept. of Mechanical Engg.
Indian Institute of Technology Delhi
Email:sks@mech.iitd.ac.in

Avinash K. Agarwal
Dept. of Mechanical Engg.
Indian Institute of Technology Kanpur
Email:akag@iitk.ac.in

ABSTRACT

Tribological performances of machine components have been enhanced by using lubricant additives (sulphates and phosphates) which are very harmful to the environment. Epoxy-based composites coatings on steel surfaces are promising tribological coatings to reduce the use of these additives. Epoxy and its composite (with 10 wt. % of graphene nano-filler) films have been coated onto cylindrical steel substrates and friction and wear tests have been performed on a ball-on-cylinder tribometer under dry and base oil lubricated conditions. The steel ball has been used as counter face for the experiments. The wear life of epoxy has been increased by 5 times keeping the coefficient of friction nearly same (0.18) by reinforcement of graphene nano-particle. Epoxy/graphene coating showed negligible wear rate under base oil lubrication tests.

Keywords: Epoxy, Graphene, Graphite, Lubrication.

INTRODUCTION

Government has made regulations in various countries over environment concerns, and there are active efforts made to reduce the use of harmful additives which has been achieved by using coatings [1]. Epoxies are thermoset polymers having one or more active epoxide group. Epoxy polymers have excellent chemical resistance, adhesion, durability at high and low temperatures, good electrical resistance, mechanical properties (high strength and toughness), and low shrinkage [2-4]. Epoxy coating can provide good protective layer against wear if the epoxy is suitably modified for low friction and wear resistance.

Epoxies with reinforcement of carbon nano tube (CNT) have excellent mechanical properties with enhanced tribological properties [5]. In addition of wax with CNT in epoxy has reduced hardness and Young modulus and very low coefficient of friction causing low wear rate [6]. Thermal properties like thermal decomposition temperature have been also enhanced by addition of graphene oxide including mechanical properties improvement [7]. Mechanical and tribological properties were further improved by adding filler material like graphene and graphite [8]. The wear life and load bearing capacity of polymer coatings have been also improved by in-situ lubrication [9, 10]. The lubrication of polymers coating have been studies by various researchers under different lubrication regimes [11]. Base oil lubrication without any additives is good option for the polymer lubrication.

By literature survey as above, it can be concluded that environment friendly lubrication can be achieve by replacing conventional lubrication with polymer coatings lubricated with base oil.

2. EXPERIMENTAL PROCEDURE
2.1 MATERIALS

Cylindrical shaft (diameter = 40 mm width ~12 mm and roughness ~ 0.40 micron) of D2 steel was used to coat epoxy (Araldite AY 103, hardener HY 951 supplied by Huntsman Advanced Material Pvt. Ltd.) and its composites of thickness 40-50 micrometer. The nanoparticle graphene (supplied by Reinste nano ventures Pvt Ltd, Noida, India) has been used to make the epoxy composite coatings. The counterface for all tribological tests is stainless steel (SAE 52100) ball of 4 mm diameter. For base oil lubricated tests, SN 150 (provided by Indian oil corporation Limited) of Group-I having viscosity index 95 was used under boundary lubrication condition.

2.2 SAMPLE PREPARATION

The specimens have been thoroughly cleaned with acetone and dried at room temperature then treated with oxygen plasma for 2 minutes using plasma cleaner to remove the organic contaminants and to generate hydroxyl groups on the surface which enhance adhesion between the substrate and coating. The cleaned steel shafts were coated with epoxy and epoxy/graphene (10%wt) by a lab-fabricated dip-rotating-coating machine. The coatings were cured initially at room temperature for 16 hours followed by thermal curing at 80 ^{0}C for 4 hours. The air bubbles were removed by using a vacuum pump.

2.3 MECHANICAL AND THERMAL PROPERTIES OF EPOXY COMPOSITES

The ASTM D638 standard samples have been prepared for the tensile test of epoxy and epoxy/graphene composites and test results are shown in table 1. Hardness of epoxy and its composites coated on steel substrates were measured by Vickers fully automatic hardness tester (Barreiss, Germany) at 0.2 N normal load and measured values are shown in Table 1. Thermal stability of epoxy and its composite have been analyzed by Thermo Gravimetric Analysis (PerkinElmer Thermal Analysis) and thermal decomposition temperatures have been mentioned in table 1.

TABLE 1. Mechanical and thermal properties

Material	Epoxy	Epoxy/graphene
Tensile strength (MPa)	40±3	34±3
Young modulus (GPa)	0.815±0.23	0.852±0.31
Hardness (MPa)	216±27	235±18
Thermal decomposition temperature (°C)	305	348

2.4 TRIBOLOGICAL CHARACTERIZATION

Dry and lubricated (in base oil SN 150) friction and wear tests have been carried out using lab-fabricated ball-on-cylinder tribometer setup (Figure 1). The tests have been conducted at different normal loads (1.5, 2.5, 3, 4 and 5 N) and at various speeds (100 rpm, 200 rpm and 300 rpm equivalent to linear speeds of 0.21 m/s, 0.42 m/s and 0.63 m/s, respectively) for maximum number of cycles till the coefficient of friction (CoF) reached 0.3 at room temperature (25^{0}C) and relative humidity of 45 %.
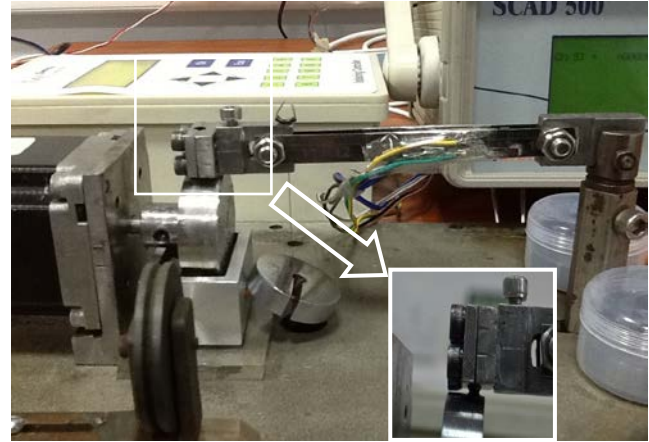
FIGURE 1. Ball-on-cylinder type tribometer and inset picture shows larger image of the ball on the shaft.

3. RESULTS AND DISCUSSION

Coatings of epoxy and its composites with film thickness ~30 µm have been formed on d2 steel shaft. Dry and lubricated wear tests have been carried out by using ball-on-cylinder type tribometer at various conditions such as by varying the speed and normal load in normal environmental conditions. The following results have been obtained.

3.1 FRICTION ANALYSIS

Coefficient of friction of epoxy and its composites coatings are nearly same (0.17) at 0.63 m/s speed and 1.5 N load and only epoxy/graphene bear higher load (3 N) Figure 2 (a). Epoxy coating has not survived at higher speed at 3 N load but epoxy/graphene coating sustain up to 0.63 m/s speed with marginal change of coefficient of friction (from 0.15 to 0.18) Figure 2 (b). Epoxy and epoxy/graphene coatings under base oil lubricated condition test have shown nearly constant coefficient of friction (~0.08) at various loads (1.5, 3, 4 and 5 N) and different speeds (0.21, 4.2, and 0.63 m/s) as shown in Figure 2 (a), (b).

epoxy is much higher than epoxy graphene and increases with load.

(a)

(b)
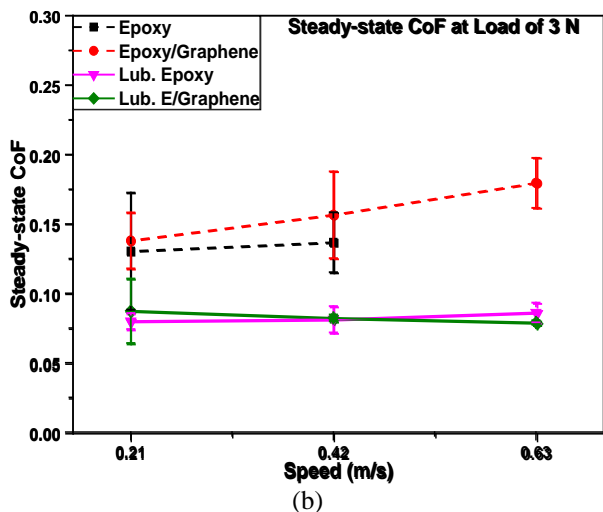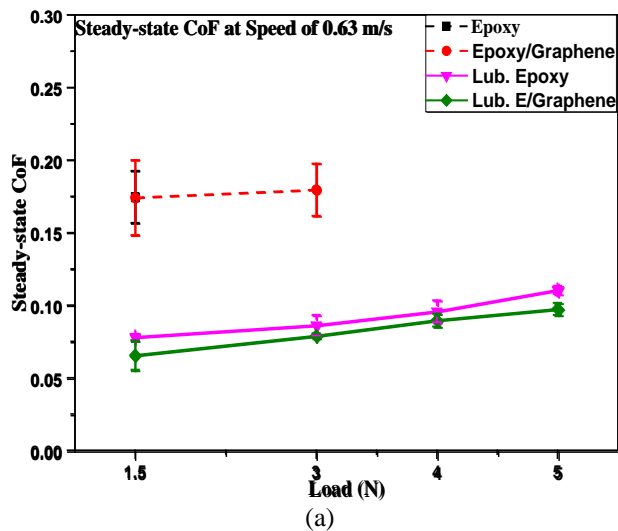
FIGURE 2. Variation of coefficient of friction with (a) normal load (at 0.63 m/s speed) and (b) speed (at 3 N load) for epoxy and epoxy/graphene in dry and base oil lubricated conditions.
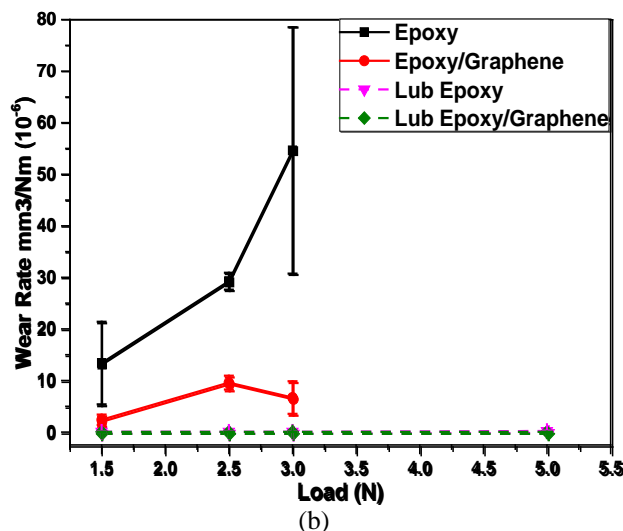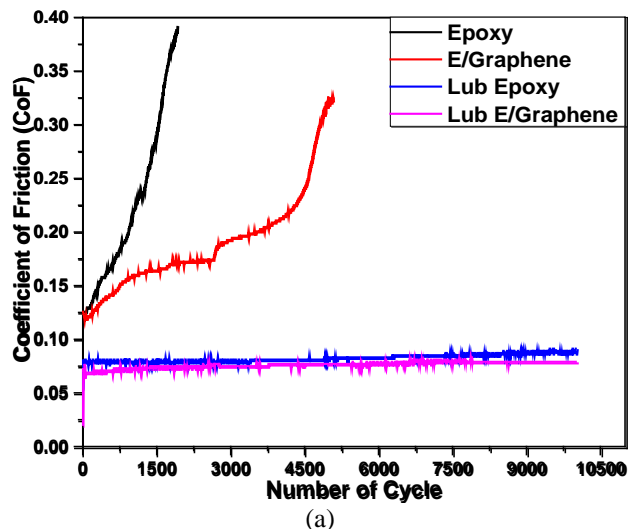
FIGURE 3. (a) Coefficient of friction variation with number of cycle at 3 N load and (b) wear rate variation with load, at 0.63 m/s (300 rpm), for epoxy and epoxy/graphene in dry and lubricated conditions.

3.2 WEAR ANALYSIS

Wear lives (in terms of number of cycles) of epoxy and its composites have been estimated from the CoF versus number of cycles graph as shown in figure 3 (a). It has been observed from these data that pure epoxy coating is much poorer in wear life compared with the epoxy/graphene in dry condition tests. Epoxy and its composites coatings have been sustained more than 200,000 number of cycle in base oil lubricated condition at 3 N load and 0.63 m/s (300 rpm) speed. The wear life has been mention on the basis of coefficient of friction.

Therefore, in order to further understand the wear behavior of the coatings, we conducted wear volume measurements, and wear rate is calculated. Wear rate of

4. CONCLUSION

Filler particle of graphene in epoxy coating improves the mechanical properties such as Young's modulus increase by 14% and hardness by 13% for epoxy/graphene. The coefficients of friction in dry sliding for epoxy and epoxy/graphene are nearly same but wear life enhanced by 5 times and wear rate by 8 times as compare to epoxy coating at 0.18 at 3N normal load and 0.63 m/s (300 rpm) sliding speed. Under lubricated tests

coefficient of friction varied between 0.07-0.09 and very low wear rate 2.5×10^{-8} mm^3/N-m.

Finally, we conclude that epoxy/graphene is a potential coating for steel surfaces which can give low friction and long wear life under base oil lubricated condition.

REFERENCES

[1] Ng, E., Satyanarayana, N., Sinha, SK., Lim, C., Zheng, Z.,2014. "Tribological performances of ZDDP and ashless triphenyl phosphorothionate (TPPT) as lubricant additives on Ti-N and Ti-Al-n coated steel surfaces". Tribology - Materials, Surfaces & Interfaces, 8, 209-221.

[2] Bilyeu, B., Brostow, W., Menard, KP., "Epoxy thermosets and their applications I: chemical structures and applications". J Mater 21, 281–286.

[3] Bilyeu, B., Brostow, W., Menard, KP., 2001. "Determination of volume changes during cure via void elimination and shrinkage of an epoxy prepreg using a quartz dilatometry cell". Polimery, 46, 799–802.

[4] Bilyeu, B., Brostow, W., Menard, KP., 200. "Epoxy thermosets and their applications II. Thermal analysis". J Mater, 22, 107–130.

[5] Dong, B., Yang, Z., Huang, Y., Li, HL., 2005. "Study on tribological properties of multi-walled carbon nanotubes/epoxy resin nano composites". Tribology Letters, 20, 251-254.

[6] Qi, B., Lu, SR., Xiao, XE., Pan, LL., Tan, FZ., Yu, JH., 2014. "Enhanced thermal and mechanical properties of epoxy composites by mixing thermotropic liquid crystalline epoxy grafted graphene oxide". Express Polymer Letters, 8, 467–479.

[7] Khun, NW., Zhang, H., Yang, J., Liu, E., 2013. "Mechanical and tribological properties of epoxy matrix composites modified with microencapsulated mixture of wax lubricant and multi-walled carbon nanotubes". Friction, 4, 341–349.

[8] Kumar, V., Sinha, SK., Agarwal, AK., 2015. "Tribological studies of epoxy and its composite coatings on steel in dry and lubricated sliding". Tribology-Material surface & Interface, 9, 144-153.

[9] Saravanan, P., Sinha, SK., Jayaraman, S., Duong, HM., "A comprehensive study on the self-lubrication mechanism of SU-8 composites". Tribology International, 95, 391-405

[10] Kumar, V., Sinha, SK., Agarwal, AK., 2017. "Tribological studies of epoxy composites with solid and liquid fillers". Tribology international, 105, 27-36.

[11] McCooka, NL., Burrisa, DL., Bournea, GR., Steffensa, J., Hanrahanb, JR., Sawyer, WG., 2005. "Wear resistant solid lubricant coating made from PTFE and epoxy". Tribology Letters, 18, 119-124.

SEEC-2017-47

SELF LUBRICATION OF EPOXY COMPOSITE COATINGS ON D2 STEEL

Vikram Kumar
Dept. of Mechanical Engg.
Indian Institute of Technology Kanpur
Email: vikramk@iitk.ac.in

Sujeet K. Sinha
Dept. of Mechanical Engg.
Indian Institute of Technology Delhi
Email:sks@mech.iitd.ac.in

Avinash K. Agarwal
Dept. of Mechanical Engg.
Indian Institute of Technology Kanpur
Email:akag@iitk.ac.in

ABSTRACT

Epoxy and its composite coatings have been used to protect and enhance the tribological properties of the machine element such as bearing and piston rings without using any harmful additives. Epoxy filled with graphene and graphite and liquid lubricant (SN150 and PFPE) have been coated on D2 steel. It has been observed that epoxy filled with graphene and SN150 provide very low coefficient of friction and wear rate.

Keywords: *Epoxy, Graphene, Graphite, Lubrication*.

INTRODUCTION

Modern days lubrication of contacting surfaces are achieved by protective coating on interfacing surfaces or by lubrication with oil with taking care of environmentally harmful additives [1]. Polymer coatings are also applied for protecting the machine parts to protect and reduce the friction and wear of rubbing surfaces. Polymers have very good adhesion properties with mechanical components and low wear and friction [2, 3]. It is a softer material which adhere any type of surfaces. The mechanical and wear properties of polymers can be further improved by adding some filler materials like graphite, graphene, carbon-nanotubes etc. Amongst these polymer epoxy is a thermos-set polymer which are used in various application such as protective coating and tribological application. Its mechanical and tribological properties have been further improved by adding filler material like graphene and graphite [4]. The wear life and load bearing capacity of polymer coatings can be improved by in-situ lubrication [5, 6, 7, 8].

2. EXPERIMENTAL PROCEDURE
2.1 MATERIALS

Cylindrical shaft of D2 steel have been used to coat epoxy filled graphene and liquid lubricant (SN150 and PFPE) of thickness 40-50 micrometer [4]. The counterface for all tribological tests is stainless steel (SAE 52100) ball of 4 mm diameter

2.2 SAMPLE PREPARATION

D2 steel cylindrical shaft have been cleaned and then plasma treated to enhance the bonding by generating hydroxyl group and remove organic contaminant. After that, cleaned samples have been coated with epoxy composites. Curing of epoxy composite coating have been performed 16 hours at room temperature then thermally cured at 80 °C for four hours. The specimens have been thoroughly cleaned with acetone and dried at room temperature [4].The various coated samples are as given below:

 (i) Epoxy/graphene(10 wt%)/SN150 (10 wt%) (named as E/Gn/SN150),

(ii) Epoxy/SN150 (10 wt%) (named as E/SN150),

(iii) Epoxy/graphene (10 wt%)/PFPE (10 wt%) (named as E/Gn/PFPE),

(iv) Epoxy/PFPE (10 wt%) (named as E/PFPE).

2.4 TRIBOLOGICAL CHARACTERIZATION

Friction and wear tests of epoxy composites have been carried out using lab-fabricated ball-on-cylinder tribometer setup (Figure 1) at load (3, 6 and10 N) 0.63 m/s speed in environment condition room temperature (25^0C) and

relative humidity of 45 %. Coefficient of friction and specific wear rate has been calculated by measuring the wear track profiles using an optical surface profiler.
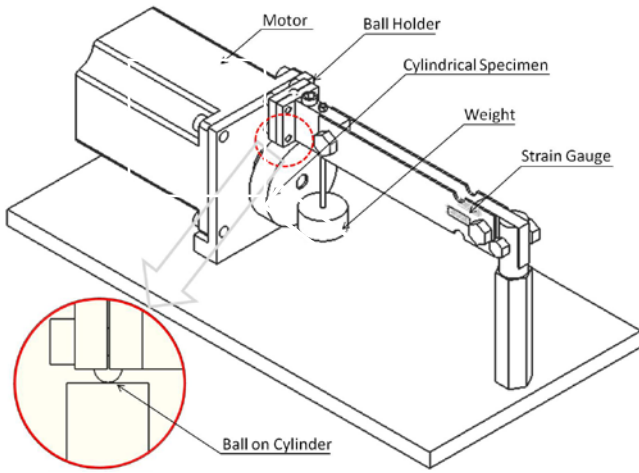
FIGURE 1. Schematic of ball-on-cylinder type tribometer

3. RESULTS AND DISCUSSION

Coatings of epoxy composites with film thickness ~40 µm have been formed on D2 steel shaft. Wear tests have been carried out by using ball-on-cylinder type tribometer at various conditions such as by varying the speed and normal load in normal environmental conditions. The following results have been obtained.

3.1 FRICTION ANALYSIS

The variation of coefficient of friction with load of epoxy composites coatings are shown in figure 2 (a) and it has been observed that epoxy/graphene/SN150 coating provide low coefficient of friction (~0.09) at all load whereas epoxy coating filled with PFPE not survived above 6 N load. Epoxy composite coatings filled with PFPE offer higher coefficient of friction due to higher viscosity as compare to SN150. Figure 2 (b) represents the coefficient of friction variation with sliding speed at different loads (3, 6 and 10 N). As speed increases the coefficient of friction increases and after 0.42 m/s became nearly constant.

(a)

(b)
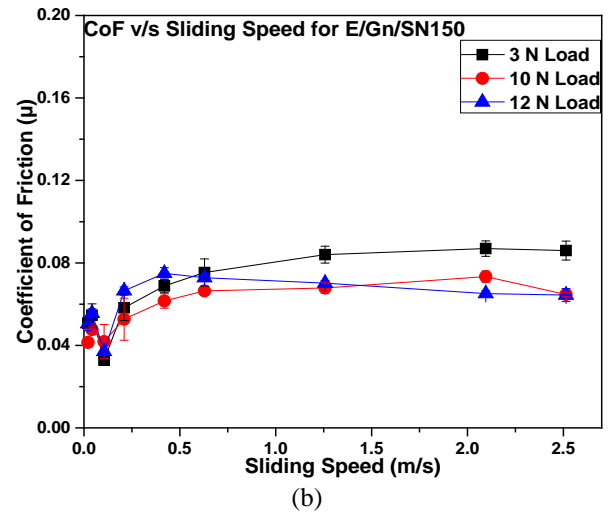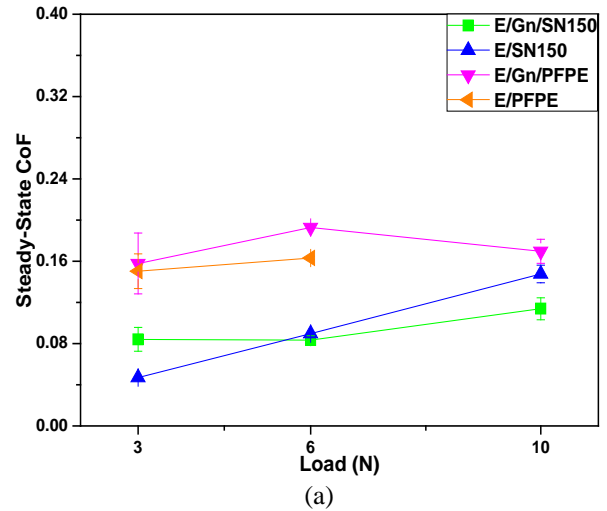
FIGURE 2 Variation of coefficient of friction (a) with normal load (at 0.63 m/s speed) and (b) with speed (at 3, 6 and 10 N load) for epoxy composite coatings.

3.2 WEAR ANALYSIS

Wear lives (in terms of number of cycles) of epoxy composite coatings have been estimated from the CoF versus number of cycles graph as shown in figure 3 (a). It has been observed from these data that epoxy/PFPE coating is much poorer in wear life compared with other coatings (wear life >200,000 number of cycle) at 10 N load and 0.63 m/s (300 rpm) speed. Wear properties have been further understood by wear rate calculation and observed that epoxy/graphene/SN150 coating have least wear rate as compare to other coatings at all loads.
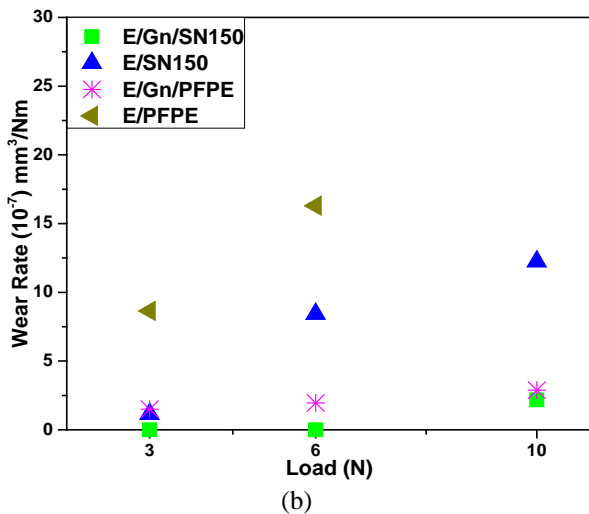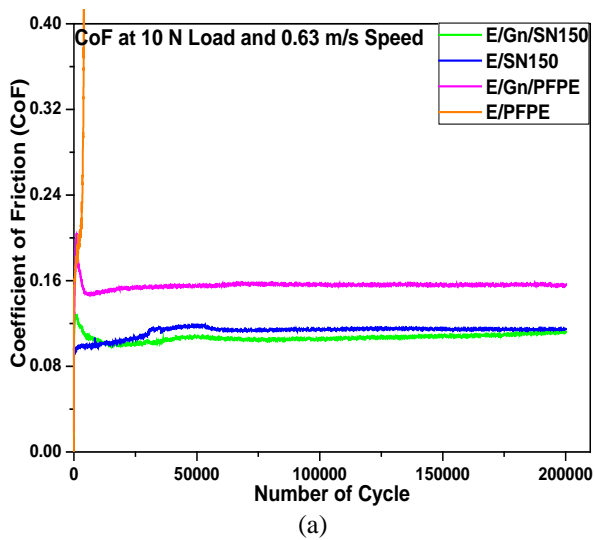
(a)

(b)

FIGURE 3 (a) coefficient of friction variation with number of cycle at 10 N load and 0.63 m/s speed and (b) wear rate variation with load, at 0.63 m/s (300 rpm), for epoxy composites.

4. CONCLUSION

Epoxy composites (with 10 wt% graphene nano-particles and liquid lubricant SN150 or PFPE) have been coated on steel shaft surfaces and tested for tribological properties in dry conditions. The coefficients of friction has been reduced to half in dry sliding for epoxy/graphene/SN150 (CoF~0.09) and wear life has been enhance by more than 200 times. The wear rate of epoxy/graphene/SN150 has lower value (2.5×10^{-7} mm^3/N-m) at 10 N load and 0.63 m/s speed.

Finally, we conclude that epoxy/graphene/SN150 is a potential coating for steel surfaces which can give low friction and long wear life under dry condition.

REFERENCES

[1] Vizintin, J., Kalin, M., Dohda, K., Jahanmir, S., 2004 Tribology of Mechanical Systems: A Guide to Present and Future Technologies. American Society of Mechanical Engineers, USA.

[2] Tribophysics, 1986. Suh, NP., Prentice-Hall, Englewood Cliffs, NJ.

[3] Abdul, SM., Satyanarayana, N., Sinha, SK., 2010. "Tribology of UHMWPE film on air-plasma treated tool steel and effect of PFPE overcoat". Surf. Coat. Technol, 204, 1330–1338.

[4] Kumar, V., Sinha, SK., Agarwal, AK., 2015. "Tribological studies of epoxy and its composite coatings on steel in dry and lubricated sliding". Tribology-Material surface & Interface, 9, 144-153.

[5] Saravanan, P., Sinha, SK., Jayaraman, S., Duong, HM., "A comprehensive study on the self-lubrication mechanism of SU-8 composites". Tribology International, 95, 391-405

[6] Kumar, V., Sinha, SK., Agarwal, AK., 2017. "Tribological studies of epoxy composites with solid and liquid fillers". Tribology international, 105, 27-36.

[7] Khun, NW., Zhang, H., Yang, J., Liu, E., 2013. "Mechanical and tribological properties of epoxy matrix composites modified with microencapsulated mixture of wax lubricant and multi-walled carbon nanotubes". Friction, 4, 341–349.

[8] McCooka, NL., Burrisa, DL., Bournea, GR., Steffensa, J., Hanrahanb, JR., Sawyer, WG., 2005. "Wear resistant solid lubricant coating made from PTFE and epoxy". Tribology Letters, 18, 119-124.

[9] Proceedings of the Royal Society of London, Series A, Mathematical and Physical Sciences, 1952. 212, Tabor D., (Discussion Meeting) Part III, Boundary and Extreme Pressure Lubrication Mechanism of Boundary Lubrication, 498-505.

[10] Ng, E., Satyanarayana, N., Sinha, SK., Lim, C., Zheng, Z.,2014. "Tribological performances of ZDDP and ashless triphenyl phosphorothionate (TPPT) as lubricant additives on Ti-N and Ti-Al-n coated steel surfaces". Tribology - Materials, Surfaces & Interfaces, 8, 209-221.

SEEC–2017–048

EXPERIMENTAL INVESTIGATION OF TEMPERATURE VARIATION IN AUTOMOTIVE EXHAUST THERMOELECTRIC GENERATOR WITH EXHAUST PIPE LENGTH

Sarthak Nag
School of Engineering
IIT Mandi, India
iamsarthaknag@gmail.com

Surya Bharathi Thangavelu
Department of Mechanical Engineering
SSN College of Engineering, India
suryabharathi35@gmail.com

Atul Dhar
School of Engineering
IIT Mandi, India
add@iitmandi.ac.in

Gaurav Tripathi
School of Engineering
IIT Mandi, India
grvtri@gmail.com

Arpan Gupta
School of Engieerning
IIT Mandi, India
agupta@iitmandi.ac.in

ABSTRACT

The technology of thermoelectrics has good potential for its application as automotive exhaust based thermoelectric generator (TEG). In this work, the temperature variation on the surface of the automotive exhaust thermoelectric generator (AETEG) has been studied. Experiments have been carried out by varying the distance of the AETEG from the engine exhaust side by increasing pipe's length. In addition to it, the load on the engine was also varied to study its effects. These experimental results have been validated by simulating the same cases in CFD solver Star CCM. The experimental results show good agreement with the computed results. Simulation and experiments, both reveal that the variation in length of the pipe has very little effect on the temperature distribution on AETEG, however increasing the load increases the temperature on AETEG due to the increase in exhaust temperature.

Keywords: thermoelectric generator (TEG), internal combustion engines, automotive exhaust, CFD modelling, waste heat recovery.

INTRODUCTION

Internal combustion engine uses petrol or diesel as fuels, which causes pollution. Morever, there has been a global energy crisis due to depleting reserves of fuels [1, 2]. This has pushed the engine waste heat recovery a lot, as nearly 30% of the engine's heat goes out of the engine unused in the form of exhaust [3-5]. Using thermoelectric (TE) modules is one solution to recover the waste heat from the exhaust. TE module converts the waste heat energy into useful electrical energy. It works on the principle of Seebeck effect [6], which states that if the temperature gradient is applied between two dissimilar electrical conductors or semiconductors, voltage difference is produced between them. Exhaust gives the high temperature to the TEG from one side. On the other side, coolant/ cooling water has to be flown to maintain it at low temperature and hence to give TE module a temperature gradient [7].

The major advantage of using TEG is low failure rate due to no moving components [2], but the low efficiency of TE modules is its drawback. Hence we need an efficient

heat exchanger which passes the exhaust heat effectively to the surface of AETEG, so that maximum heat can be utilized. Positioning of heat exchanger or AETEG with respect to engine is also important parameter, which the author has tried to explore in this work

EXPERIMENTAL SETUP AND PROCEDURE

SETUP PREPARATION

Figure 1 shows the heat exchanger unit of AETEG which is made of aluminium sheet of thickness 3 mm. The exterior dimensions of the channel are 210 x 81 x 34 mm. Figure 2 shows the points where the temperature was measured. The temperature was measured using thermocouple wires and was displayed using a temperature displayer. The thermocouples were attached on the heat exchanger using thermal paste. This unit was installed on the exhaust side of the engine. Figure 3 shows the temperature measurement arrangement. A thermocouple is installed in the inlet side of the heat exchanger unit to measure the exhaust temperature to the inlet of heat exchanger unit (figure 4).
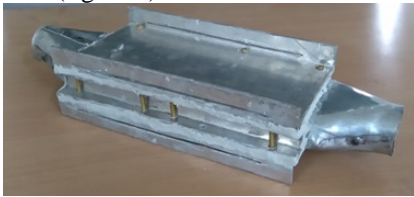
FIGURE 1. HEAT EXCHANGER OF AETEG UNIT

The length of the pipe from the thermocouple point to the inlet of heat exchanger is varied in the experiments.
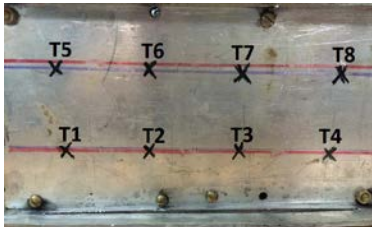
FIGURE 2. TEMPERATURE MEASUREMENT POINTS.

FIGURE 3. TEMPERATURE MEASUREMENT SETUP

FIGURE 4. INLET TEMPERATURE MEASUREMENT THERMOCOUPLE

ENGINE OPERATION POINTS AND PROCEDURE

Figure 5 shows the schematic diagram of the experimental setup. The heat exchanger was mounted on Kirloskar TV 1 diesel engine. The specifications of the engine are shown in table 1.

TABLE 1: Specifications of the test engine.

Cycle	4 Stroke
Cylinders	1
Swept Volume	661 cc
Stroke length	0.11 m
Bore diameter	0.0875 m
Speed	1500 rpm
Compression Ratio	17.5:1
Power	5.2 kW
Loading Device	AC transient dynamometer

The engine is operated at 4 load points, ie no load (0%), 0.52 kW (10%), 1.04 kW (20%) and 1.56 kW (30%). The upper limit is choosen to be 30% because the exhaust temperature beyond 30% load exceeds the maximum allowable temperature on the TE modules. For each load the distance of the heat exchanger unit is varied by changing the pipe length i.e. 140 mm, 210 mm and 280 mm.

EXPERIMENTAL RESULTS

The variation of exhaust temperature is shown in figure 6. The trends are general and the temperature of the exhaust increases as the load is increasing.

Figure 7, 8 and 9, when compared with each other clearly shows that there is no substantial effect of varying the length of the exhaust pipe between the heat exchanger and the engine exhaust from 140 mm to 280 mm, keeping the load constant. However, the temperature on the surface of the heat exchanger increases as the load on the engine increases. This finding implies that the application of TE modules on the AETEG will produce same amount of power, no matter where the AETEG is in the exhaust line.
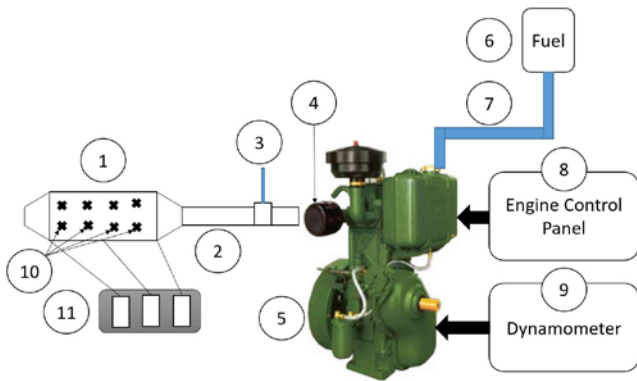
1. AETEG; 2. Variable exhaust length region; 3. Exhaust thermocouple; 4. Engine exhaust; 5. Test engine; 6. Fuel tank; 7. Fuel line; 8. Control panel; 9. Dynamometer; 10. Temperature measuring points; 11. Temperature displayer.

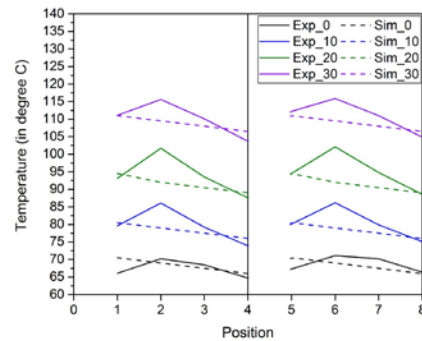**FIGURE 5.** SCHEMATIC DIAGRAM OF EXPERIMENTAL SETUP.
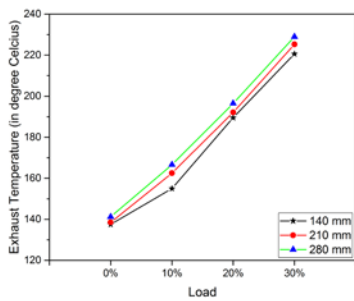
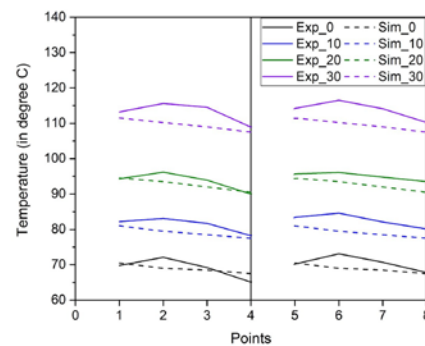**FIGURE 6.** VARIATION OF EXHAUST TEMPERATURE WITH LOAD
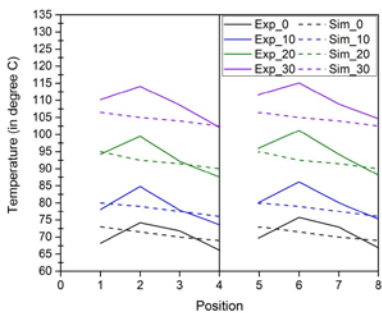
FIGURE 7. VARIATION OF EXHAUST TEMPERATURE WITH LOAD AT PIPE LENGTH 140 MM.

These experimental findings when compared with the CFD and heat transfer simulations done on Star CCM software showed similar trends. Figure 10 shows the temperature contours on heat exchangers for cases of 140 mm, 210 mm and 280 mm at 30% load. The value of heat transfer co-efficient when optimised with experimental findings comes out to be 17 W/m^2.K.

FIGURE 8. VARIATION OF EXHAUST TEMPERATURE WITH LOAD AT PIPE LENGTH 210 MM.

FIGURE 9. VARIATION OF EXHAUST TEMPERATURE WITH LOAD AT PIPE LENGTH 280 MM.
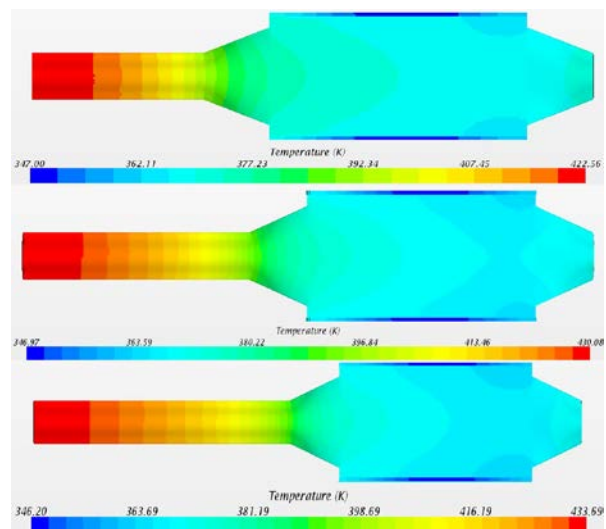
FIGURE 10: TEMPERATURE CONTOURS FOR VARIOUS LENGTH AT 30 % LOAD (TOP TO BOTTOM: 140 MM, 210 MM AND 280 MM)

CONCLUSIONS

The main objective of this study was to experimentally investigate the affect of length of exhaust pipe on the performance of AETEG heat exchanger unit. The heat exchange channel was rectangular in cross-section and was manufactured using aluminium sheet. Thermocouples were used to measure temperature on the sheet where TE modules are proposed to be installed in future work. The length of the exhaust was varied usind fittings on different sizes. The AETEG heat exchanger was then tested on Kirloskar TV-1 diesel engine at a fixed 1500 rpm and load of 0%, 10%, 20% and 30%. The results showed that the variation in length has negligible effect on the temperature of the heat exchanger. Hence, same voltage can be expected from the AETEG irrespective of its location. This also leads us to the conclusion that only factor that may come while setting the location of AETEG in any automobile may be the space requirements in the exhaust line.

REFERENCES

[1] Kim, Tae Young, Seokhwan Lee, and Kernyong Kang. "Performance and emission characteristics of a high-compression-ratio diesel engine fueled with wood pyrolysis oil-butanol blended fuels." Energy, 93, 2015, pp. 2241-2250.

[2] Kim, T.Y., Negash, A.A. and Cho, G. "Waste heat recovery of a diesel engine using a thermoelectric generator equipped with customized thermoelectric modules". Energy Conversion and Management, 124, 2016, pp. 280-286.

[3] Yang, Jihui, and Francis R. Stabler. "Automotive applications of thermoelectric materials." Journal of Electronic Materials, 38(7), 2009, pp. 1245-1251.

[4] Baglione, M.L., 2007. Development of system analysis methodologies and tools for modeling and optimizing vehicle system efficiency (Doctoral dissertation, University of Michigan).

[5] Lu, H., Wu, T., Bai, S., Xu, K., Huang, Y., Gao, W., Yin, X. and Chen, L. "Experiment on thermal uniformity and pressure drop of exhaust heat exchanger for automotive thermoelectric generator". Energy, 54, 2013, pp. 372-377.

[6] Martínez, A., J. G. Vian, D. Astrain, A. Rodríguez, and I. Berrio. "Optimization of the heat exchangers of a thermoelectric generation system." Journal of electronic materials, 39, No. 9, 2010, pp. 1463-1468.

[7] Deng, Y.D., Liu, X., Chen, S., Xing, H.B. and Su, C.Q. "Research on the compatibility of the cooling unit in an automotive exhaust-based thermoelectric generator and engine cooling system" Journal of Electronic Materials, *43*(6), 2014, pp.1815-1823.

SEEC-2017-049

ROLE OF TEMPERATURE AND ENVIRONMENT ON PYROLYSIS OF SORGHUM BIOMASS RESIDUE FOR BIO-OIL PRODUCTION

Ganesh Kumar Gupta[1], Jitendra Kumar[1], Bijoy Biswas[1], Thallada Bhaskar[1,2*]

[1]Thermo-catalytic Processes Area (TPA), Bio-Fuels Division (BFD),
CSIR-Indian Institute of Petroleum (IIP), Dehradun 248005, India
[2]Academy of Scientific and Innovative Research (AcSIR),
New Delhi, India
*corresponding author: Ph No: +91 135 2525820, Fax No: +91 135 2660202;
e-mail: tbhaskar@iip.res.in; thalladab@yahoo.com

ABSTRACT

Pyrolysis of Sorghum biomass has been performed at 300 °C to 450 °C and at 0.1, 1 and 2 MPa pressure under H_2, CO_2 & N_2 atmosphere in high pressure fixed bed reactor. The maximum bio-oil yield were observed (31.1 wt.%, 33.3 wt.% and 30.3 wt.% respectively) under H_2 (0.1 MPa), CO_2(0.1 MPa) and N_2(2 MPa) environments at 450 °C, 400 °C and 350 °C. The yield of bio-char was higher under the N_2 atmosphere pyrolysis than CO_2 and H_2 atmosphere pyrolysis. The details bio-oil characterization has been carried out by using of GC-MS, ^1H NMR and FT-IR. It has been observed that in the bio-oils the phenolic compounds percentage were higher under N_2 atmosphere pyrolysis bio-oils than CO_2 and H_2 atmospheres. The aromatic hydrocarbons were obtained higher percentage in the case of H_2 atmosphere pyrolysis bio-oils than N_2 and CO_2 atmosphere.

Keywords: Pyrolysis, Sorghum, Different Atmosphere, Bio-Oil, Bio-Char.

INTRODUCTION

Biomass is the term used to describe all biologically produced matter. Biomass is composed of mainly cellulose, hemicelluloses and lignin, the relative concentrations of which can vary enormously between plant species. [1] Lignocellulosic biomass is the most abundant, and inexpensive sustainable source of carbon that can be used to produce renewable fuels and chemicals. The developments of energy-efficient processes for biomass conversion are of utmost interest to avoid environmental issues and utilization of biomass resources. Biomass fast pyrolysis is a novel and most effective method to convert biomass into energy-dense liquid fuels denoted as bio-oils with yields as high as 80% based on dry feed [2].

Pyrolysis of biomass can be described as the direct thermal decomposition of the organic matrix in the absence of oxygen to obtain an array of solid, liquid and gas products. The liquids obtained from pyrolysis contain many chemical compounds that can be used as feedstock for synthesis of chemical, adhesives, fertilizers etc. For instance, the Bio-char obtained from pyrolysis usually has a porous structure and a surface area that is appropriate to use as active carbon. [3] Burning the biomass residue is increasing the environmental pollution and global warming. Due to this we need to choose alternative application of biomass residue for value addition application. Thermo-chemical conversion has potential to use the entire biomass residue without separation. Most of their pyrolysis experiments were conducted using inert atmosphere (mainly N_2 and He). Up to now, there are no literature reports focusing on the effects of pyrolysis gas pressure atmospheres (H_2, CO_2 and N_2) on product distribution and liquid composition. CO_2 and H_2 are totally different compared to inert gas especially CO_2 (mild oxidative atmosphere), H_2 (strong reductive atmosphere). [4] Such reactive atmospheres may significantly influence yields and quality of products. [5] In this work, the pyrolysis of sorghum was

conducted in a pyrolysis fixed bed reactor under N_2, CO_2 and H_2 atmospheres with pressure and without pressure, respectively. The effect of the pyrolysis atmosphere on the liquid, non-condensable gas, char and coke yields were studied. The chemical compositions of the non-condensable gas and the liquids were obtained by GC and GC/MS analysis. Their contents under different atmospheres were compared and discussed.

MATERIAL AND METHODS

Sorghum residue has been taken from Dehradun, Uttarakhand, India and has been sieved using standard mesh to obtain particle size between 0.5 and 2 mm. The thermogravimetric analysis was carried out in Shimadzu DTG-60 instrument under nitrogen atmosphere with a heating rate of 10 °C min^{-1}. The trace metal analysis of Sorghum was carried out using DRE, PS-3000 UV, Leeman Labs Inc., Inductively Coupled Plasma- Atomic Emission Spectroscopy. The gross calorific value of the feed has been obtained using the Parr 6300 Bomb Calorimeter. The ultimate analysis has been carried out using Elementar vario micro cube unit. The FT-IR spectra were recorded on a Nicolet 8700 FTIR spectrometer with the sample powder diluted in KBr. SEM images have been collected on a FEI Quanta 200 F, using tungsten filament doped with lanthanum hex boride (LaB6) as an X-ray source, fitted with an ETD (Everhart-Thornley Detector), which preferentially work as a secondary electron detector. The sample for SEM analysis has been dispersed on a carbon coated adhesive followed by gold coating. ^{1}H NMR of the bio-oils was carried out in Bruker Ultra shield 500 Plus instrument using $CDCl_3$ as solvent. The organic fraction of the bio-oil was analyzed using gas chromatography–mass spectrometry (GC/MS, Agilent 7890 B). The carrier gas was He and column flow rate was 1 ml min^{-1}. A HP-1 column (25 m × 0.32 mm × 0.17 μm) was used for the separation. An oven isothermal program was set at 50 °C for 2 min, followed by a heating rate of 5 °C min^{-1} till 300 °C where it was held for 5 min. The injected volume was 1.0 μl in a split mode.

Experimental procedure

The schematic diagram of the Hydropyrolysis unit has been provided in an earlier communication [6]. In brief, sorghum is weighed (10 g) and loaded into the reactor. The reactor is purged with hydrogen, carbon dioxide and nitrogen to remove the inside air and then pressurized using till the desired pressure (0.1 Mpa, 1 Mpa and 2 Mpa) is reached. It is heated in an electrical furnace which is controlled by a temperature programmed controller. The thermocouples are placed in the skin and in the heart of the reactor inside the thermo well provided. The gas from the cylinder is passed into the reactor. The required final temperature (300, 350, 400 and 450 °C) and heating rate (20 °C min^{-1}) are set and the final temperature is maintained for 1 h. The pressure is maintained constant by the means of a needle valve. The product stream from the reactor is passed through a shell and tube heat exchanger with water in the shell side at 5 °C.

Water in the bio-oil was removed by the addition of anhydrous sodium sulphate and diethyl ether was used to recover the organic fraction. The remaining solid after the reaction left in the reactor is termed as bio-char. The equations for calculation of bio-oil, bio-char and gas have been provided in our earlier paper [7].

RESULTS AND DISCUSSION
Product yield

Pyrolysis of sorghum under H_2, CO_2 and N_2 atmosphere has been carried out at 300, 350, 400 and 450 °C. The maximum bio-oil yield were observed (31.1 wt.%, 33.3 wt.% and 30.3 wt.% respectively) under H_2(0.1 MPa), CO_2(0.1 MPa) and N_2(2 MPa) environments at 450 °C, 400 °C and 350 °C. The yield of bio-char was higher under the N_2 atmosphere pyrolysis than CO_2 and H_2 atmosphere pyrolysis. As bio-oil is the desired product, 400 °C at 0.1 Mpa has been considered as the most favorable temperature for pyrolysis of sorghum under carbon dioxide atmosphere. The most suitable conditions for obtaining the high yields of oils from pyrolysis of sorghum under hydrogen, carbon dioxide and nitrogen environments have been established and the characterization of the pyrolysis products such as bio-oil and bio-char has been performed for the better understanding of the effect of reaction atmosphere.

Characterizations of bio-oil
GC/MS analysis of bio-oil

The identified compounds have been classified into various groups such as phenolic derivatives and aromatic hydrocarbon which are majorly derived from the lignin component of lignocellulosic biomass, furans, acids/esters, hydrocarbons, carbonyl compounds, alcohols and other non-classified compounds. Furans, acids/esters, hydrocarbons, carbonyl compounds, alcohols are produced

generally from the holocellulose fraction and the aromatic ethers, phenolic compounds are produced generally from the lignin fraction. It has been observed that in the bio-oils the phenolic compounds percentage were higher under CO_2 atmosphere pyrolysis bio-oils than N_2 and H_2 atmospheres. The aromatic hydrocarbons were obtained higher percentage (9.14%) in the case of H_2 atmosphere pyrolysis bio-oils than N_2 and CO_2 atmosphere.

FT-IR analysis of bio-oil

All the bio-oil has been seen same FT-IR bands provided in fig.1. From the spectra, it can be observed that the O-H stretching vibrations from 3200 to 3500 cm^{-1} are present in all the bio-oils. Conjugated carbonyl or carboxyl structures are present in both the bio-oils as the the peak is observed at 1713 cm^{-1} and higher intensity was observed in the case of carbon dioxide atmosphere bio-oil. The peak at around 1600-1640 cm^{-1} corresponding to C=C stretching vibration is observed in feed and both the bio-oils. The stretching aromatic ring vibration is found at around 1511 cm^{-1} in all the bio-oil. Several functionalities that are present in the feed are not present in the bio-oil which shows breakdown of the macromolecular structure. When compared to bio-oil obtained under different atmosphere which indicates differences in the cleavage pattern under different atmospheres.
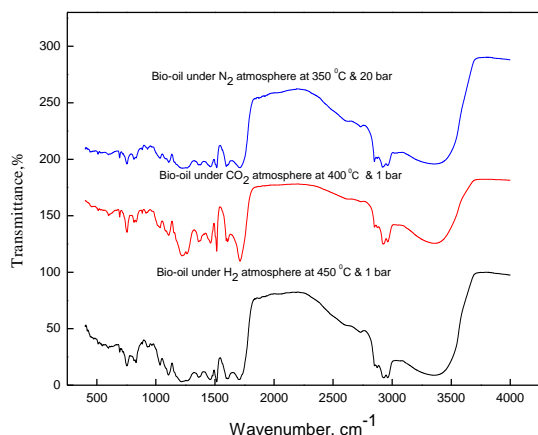
FIGURE NO.1: FT-IR of bio-oil

^{1}H-NMR analysis of bio-oil

NMR spectra are used to get information regarding the various types of protons present in the bio-oil. The most downfield region 0.5-1.5 ppm corresponds to the protons present in short chain aliphatic attached to carbon atoms which are at least

2 bonds away from C=C or heteroatom. The next region from 1.5 to 3 ppm corresponds to protons on aliphatic carbon atoms which are bonded to C=C either aromatic or olefinic or are two bonds away from a heteroatom. The next region 3-4.5 ppm corresponds to protons that are attached to carbon atoms next to an aliphatic alcohol or ether or a methylene group which bonds two aromatic rings. The region from 4.4 to 6.0 ppm represents aromatic ether protons. The range 6-8.5 ppm represents the aromatic region of the spectrum. It encompasses the protons in benzenoid molecules and heteroaromatics. The high number of protons in the aromatic region indicates the presence of valuable phenolic compounds in the bio-oil as well as hydrocarbon. It also contains around less than 1% protons on aldehydes or carboxylic acids.

CONCLUSIONS

Sorghum could be a potential biomass among the agricultural residue to produce the renewable phenolic compounds. Pyrolysis of Biomass under nitrogen atmosphere gives the higher percentage of phenolic compounds (83.48%) than carbon dioxide (76.72%) and hydrogen (72.12%) atmosphere. While the highest bio-oil yield has been observed in the case of carbon dioxide environment ca. 33.3 % at pyrolysis temperature of 400 $°C$ with 0.1MPa pressure.

References

[1] Demirbas, A., 2007. "The influence of temperature on the yields of compounds existing in bio-oils obtained from biomass samples via pyrolysis". Fuel, (88), pp. 591–597

[2] Bridgwater, A.V., Peacocke, G.V.C., 2000. "Fast pyrolysis processes for biomass" Renew. Sustain. Energy, (4), pp. 1–73.

[3] Yaman, S., 2004. "Pyrolysis of biomass to produce fuels and chemical feedstocks". Energy Conversion and Management, (45), pp. 651–671

[4] Jindarom, C., Meeyoo, V., Rirksomboon, T., Rangsunvigit, P., 2007. "Thermochemical decomposition of sewage sludge CO2 and N2 atmosphere". Chemosphere, (67), pp. 1477–1484.

[5] Minkova, V., Marinov, S.P., Zanzi, R., Bjornbom, E., Budinova, T., Stefanova, M., Lakov, L., 2000. "Thermochemical treatment of biomass in a flow of steam or in a mixture of steam and carbon dioxide". Fuel Process Technol, (62), pp.45–52.

[6] Balagurumurthy, B., Bhaskar, T., Kumar, K.L.N.S., Goyal, H.B., Adhikari D.K., 2013. "Effect of pressure on the hydropyrolysis of Jatropha seed deoiled cake". J Mater Cycles Waste Manage, (15) pp. 328-334.

[7] Krishna, B., Biswas, B., Ohri P., Kumar, J., Singh, R.., Bhaskar T., 2016. "Pyrolysis of Cedrus deodars saw mill shavings in hydrogen and nitrogen atmosphere for the production of bio-oil". Renewable Energy, pp. 1-7.

SEEC-2017-50

EXPERIMENTAL STUDIES ON ENHANCED PRODUCTION OF HYDROGEN IN THE CONTEXT OF WATER INFLUX DURING IN-SITU COAL GASIFICATION

Surya Kanta De
Department of Chemical Engineering
Indian Institute of Technology Guwahati, Assam-781039, INDIA
Email: surya.de@iitg.ernet.in

V.Prabu
Department of Chemical Engineering
Indian Institute of Technology Guwahati, Assam-781039, INDIA
Email: v.prabu@iitg.ernet.in

ABSTRACT

Underground water present in aquifer has the tendency to encroach while underground coal gasification (UCG) operation because of pressure reduction in reservoir. The ground water can act as a source of H_2 production following the water gas reaction. The enhanced production of H_2 raises the production of hydrocarbons in product gas composition. These high calorific value gases are beneficial for electricity generation in thermal power plants. In the present study, two experiments were conducted on two different coal blocks having similar properties to simulate the water influx condition. A comparative study of the two experiments shows how ground water can be utilized for enhanced production of H_2. Results show 34% of H_2 in product gas composition at water saturated condition of coal.

*Keywords***:** underground coal gasification (UCG), water influx, enhanced production of H_2.
.

INTRODUCTION

Underground coal gasification is a promising technology to produce synthetic gas and also eliminates the need of mining [1, 2]. During UCG process, in-situ coal seam reacts with gasifying mediums like oxygen, air or steam and produces combustible gaseous products such as hydrogen, carbon monoxide, methane having high calorific value [2].In the first step of UCG process, Injection and production wells are drilled vertically from surface to underground coal seam and a permeable channel is created between them [3]. Theoretical and experimental studies have been made on UCG techniques in early 1900s in the former Soviet Union, United States, Poland, Belgium, France and in the United Kingdom [4]. Linc Energy Chinchilla project in Australia produced syngas for 3 years and converted 35,000 ton of underground coal [5].

Hydrogen is considered as a clean, reliable and affordable energy source which is produced from a variety of energy sources. Comparitive study of production of hydrogen from gasification of coal and from natural gas shows a high cost effectiveness [6]. H_2 generation in UCG reactor is due to the reaction between H_2O and coal. Porada et al. [7] investigated the kinetics of steam gasification and found out the main reactions which in three separate zones. In combustion zone the oxidation of carbon takes place.

$$C + O_2 \leftrightarrow CO_2 \qquad \Delta H = -393.51 \text{ kJ/mol} \qquad (1)$$

$$C + 0.5O_2 \rightarrow CO \qquad \Delta H = -110.53 \text{ kJ/mol} \qquad (2)$$

$$CO + 0.5O_2 \rightarrow CO_2 \qquad \Delta H = -282.98 \text{ kJ/mol} \qquad (3)$$

In the gasification zone reactions occur between carbon present in coal seam and supplied steam.

$$C + H_2O \leftrightarrow H_2 + CO \qquad \Delta H = +131.28 \text{ kJ/mol} \qquad (4)$$

$$C + CO_2 \rightarrow 2CO \qquad \Delta H = +172.45 \text{ kJ/mol} \quad (5)$$

$$C + 2H_2 \rightarrow CH_4 \qquad \Delta H = -74.81 \text{ kJ/mol} \quad (6)$$
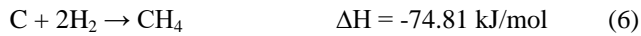
In pyrolysis zone, water gas shift reaction takes place between CO and H_2O to produce CO_2 and H_2.

$$CO + H_2O \leftrightarrow CO_2 + H_2 \qquad \Delta H = -41.2 \text{ kJ/mol} \quad (7)$$

Temperature and pressure are critical parameters of the above reactions [1]. The Boudouard reaction (Eqn.(5)) is favored by high temperature (at least 700°C) and low pressure as well as the water gas reaction (Eqn.(4)). Low temperature and high pressure promotes the methanation (Eqn.(6)) reaction. Steam injection is one of the reliable and feasible approach for hydrogen enriched syn gas production while UCG operation but it shows considerable drawbacks. Injection of low temperature steam (150°C) causes difficulty in sustaining the fire front [8]. Alternative approach of introducing H_2O should be undertaken for higher production of hydrogen and hydrocarbons. One way is to utilize the water source already available in the underground. Almost all hydrocarbon reservoirs contain water bearing rock layer above them. These are called "aquifers" [9]. When reservoir fluids are produced reservoir pressure declines and water from the above strata enters into the reservoir. This is known as "water influx". Similar phenomenon can be visualized in UCG operation also. As gasification proceeds, water from the surrounding layers enter the cavity formed due to gasification and participates in reaction [10]. Boyd et al. [11] investigated on the occurrence and effects of groundwater on *in-situ* coal gasification. It was observed that 0.1 to 0.3 pounds of water are consumed per pound of coal gasified under optimum conditions. Thorsness et al. [12] did water influx calculations with phreatic surface for a UCG system and compared with the solutions obtained for simplified equation sets resulting from the Dupuit approximation. According to their study, water can enter a UCG cavity as a result of thermal decomposition of coal and rock or because of reflux action when gas losses are present. Verma et al. [13] reviewed that the water influx occuring into cavity participates in the water gas reaction (Eqn.(4)). But when water enters the downstream carbonized link zone it participates in the water gas shift reaction (Eqn. (7)). Water decreases the temperature of the product gases and production well as well as surface piping system reducing the potential for surface heat exchange to recover the sensible heat of the product gases. McKee et al. [14] determined the time required for critical saturation of coal seam is determined by developing numerical expression. Shu-qin et al. [15] simulated ground water influx in laboratory scale in the UCG central laboratory of China University of Mining and Technology in Beijing by conducting experiment on lignite coal seam with water spray on the injection borehole. Around 45% of

concentration of hydrogen was achieved at the water influx ratio of water to coal of 0.4.

EXPERIMENTAL DETAILS

In the present study, the effect of water influx on underground coal gasification was simulated on laboratory scale by taking two different coal blocks having similar properties. The study was made on Indian coals of sub-bituminous type supplied from the mines of Bapung, Nagaland, India. Proximate analysis, Ultimate analysis and Calorimetry (Using Bomb Calorimeter) of samples taken from these four coal blocks are carried out first. First experiment was conducted on a coal of length in the range of 41-44 cm, width in the range of 40-42 cm and height in the range of 22-26 cm. It was first kept it in a large bucket of water. The water volume inserted into the bucket was nearly 20 litres. After keeping it dipped for 13 hours, sample was taken from one side of the coal. Moisture content of the sample was analyzed after keeping it in hot air oven at temperature of 108°C for 3 hours and it was seen that moisture content was increased only by 2%. Borehole Combustion technique [16] was implemented in this case. The coal block was prepared for experiment by making a channel of diameter of 2.5 cm. Surface of the coal was also smoothen with the help of cutter saw and chainsaw. The length of the coal was divided to four equal zones and marked with chalk. To fill the gaps between the refractory bricks, plaster of Paris was used. When the plaster of Paris was totally dried, the coal block was placed in the platform. M-seal was used to fill the gaps between the block and platform to prevent gas leakage. Then again plaster of Paris was poured at the sides of the coal block and kept it for one day sothat it got dried. Next day, a layer of mud was put over it to make the system totally leak proof and sustain the system for at least 5-6 hours. Highly temperature sensitive K-type thermocouple were used to determine the temperature of all four zones. Thermocouples were connected to Agilent 34970A Data Logger and checked if the connections are right. Small pieces of camphor were placed inside the borehole. They are put on fire with the help of joss stick. Then oxygen was supplied from the cylinder at the injection point sothat the coal catches fire and combustion takes place properly. The pressure of flow of oxygen was kept constant at the value of 1 kg/cm^2 and flow rate was controlled with the help of rotameter. Four thermocouples were inserted into four zones according to the length of each zone. A pipe made of stainless steel was inserted at the other end of bore hole. A rubber pipe was joined with the stainless steel pipe to make the collection point of product gases. Both ends of the passage created on the coal are then closed with mud after inserting the injection pipe of oxygen into the borehole in such a way that it remains in the first zone. A small pot was placed below the collection pipe to collect the tar condensed in pipe. Gas samples from the collection point were taken every 15 minuates later with the help of

medical syringe and stored in vacutainer. The sample was analyzed in Thermo Fisher Scientific TRACE 1310 Gas Chromatograph (GC) to know the compositions present in

TABLE 1. Average properties of coals

Properties of coal	Values
Proximate analysis (weight %, dry basis)	
Moisture	4
Volatile matter	41
Fixed Carbon	51.75
Ash	3.25
Ultimate analysis (weight %)	
Carbon	74.86
Hydrogen	5.58
Nitrogen	1.67
Sulphur	3.41
Oxygen	11.23
Calorific value (kJ/kg)	32144.2

product gas.Time to time, mud was put at the sides of the block to prevent gas leakage. After 5 hours 45 minuates the experiment was terminated due to heavy leakage.

The second experiment was conducted on a coal block having almost a rectangular dimension of length in the range of 42-45 cm, width in the range of 17-22 cm and height in the range of 20-24 cm. A channel of 2 cm depth was made in this case. But this time the block was not kept in water. The experiment was conducted for 6 hours 45 minuates. The flow rate of oxygen was changed from 0.2 to 1 in a regular interval. The experimental setup for the above two experiments are shown in Fig.1.

RESULTS AND DISCUSSION

The proximate analysis of the coal block are shown in Table 1.Coal has low moisture and ash and therefore, it has high fixed carbon and volatile matter.The ultimate analysis of coal has shown a high carbon of 75% and less hydrogen of 5-6%. Also, a significant amount of sulfur of about 3-4% and fuel nitrogen of 1-2%, which may produce SO_x and NO_xduring UCG operation. Calorific value data also shows a high calorific value of coal.

Experiment 1: Experiment On Water saturated Coal Block

Water saturated coal block contains 8% moisture. A 13 hour immersion of coal block in water has raised the moisture level with increase of 2% only. This shows the coal has low permeability and void volume. Initially the flow rate of $O_2$was kept at 0.3 lpm and was increased to

0.5 lpm after 2.5 hours. Zone#1 (5 cm from inlet) near the ignition point shows a high temperature of 746°C and further increase of oxygen flow leads to 900°C in the first two zones and the temperature was sustained for the entire
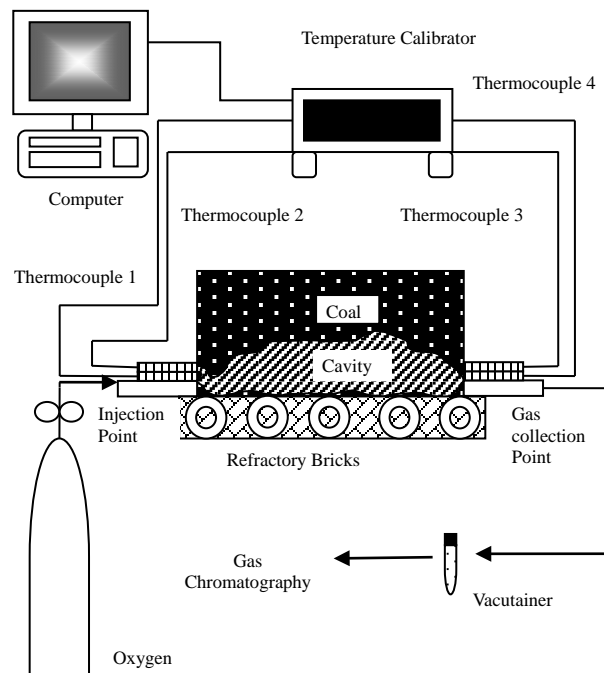
FIGURE 1. Schematic diagram of laboratory scale UCG experiment

duration of the experiment. Zone#3 (Thermocouple #3) and zone#4 (Thermocouple #4) did not gain a high value as these zones are only pyrolysed with the generated hot product gas. A significant level of syngas was generated with H_2 concentration of about 17-30 % and CO in the range of 10-27%because of the water gasification (Eq. (4)). Fig.2 illustrates the profile of hydrogen, hydrocarbons and feed gas flow rate. As coal block was water saturated and it leads to the addition of 2% of excess moisture and this water was acting as a source for hydrogen generation. It was also observed that the CO concentration was lesser than the hydrogen concentration due to the water gas shift reaction (Eq. (7)). A higher percentage of CO_2 of about 30-60% was found due to combustion (Eqn.(1)) and water gas shift reaction. Higher percentage of methane may be due to methanation reaction (Eqn. (6)) and Sabatier reaction (Eqn. (8)).

Sabatier reaction:$CO_2 + 4H_2 \leftrightarrow CH_4 + 2H_2O + Heat$ (8)

As the feed gas flow rate was increased to 0.5 lpm, high

3

amount of CO_2 generation (about 90%) occurred due to complete combustion. C_2H_6 (in the range of 1-2%) were obtained in a less quantity. The average calorific value of product gases was found out to be 233.7 kJ/mol.
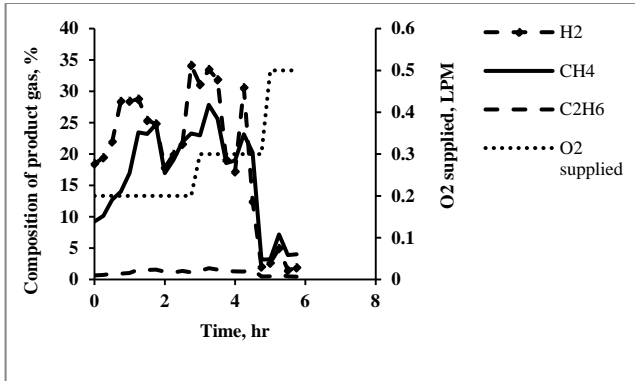
FIGURE 2. Composition of product gas during O_2 gasification of wet coal block

Experiment 2: Experiment On Unsaturated Coal Block

Experiment using an unsaturated coal block was carried out in order to compare the gas composition under water influx conditions. Fig.3 shows the profile of H_2 and hydrocarbons of the product gas and O_2 feed gas flow rate. The first two zones reached a higher temperature of nearly 1000°C with first two hours and this temperature was sustained till the end of the combustion experiment.
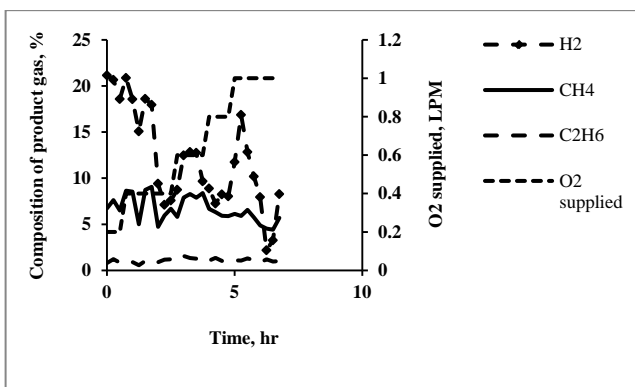
FIGURE 3. Composition of product gas during O_2 gasification of unsaturated coal block

Zone#3 (thermocouple#3) and zone#4 (thermocouple#4) shows a less temperature in the range of 50-350°C, which shows the outlet temperature of the product gas. This shows the combustion front had prevailed only at the first two zones. It was observed that the product gas contains a significant H_2 content of about 15-22% and CO in the range of 25-36% for the first two hours. Steam gasification was predominant due to the inherent moisture of the coal. A higher concentration of CO may be due to partial combustion of coal (Eqn.(2)). However, after 2 hours of the experimental run, H_2 concentration suddenly decreased to 7-16% and CO was present in the range of 2-9%, which is less than H_2 content. Therefore, water gas shift reaction may get progressed and converted CO into H_2. As the inherent moisture get deficient on the coal char, a complete combustion of carbon resulted in enhanced CO_2 production. CH_4 gas had present in the product gas of about 9% at the beginning of UCG experiment and reduced to 6% at the moisture deficient conditions. Methanation reaction and volatile matter liberation were the sources for methane generation. C_2H_6 were obtained at a concentration of 1-2%. The average calorific value of the product gases during pure O_2 gasification was estimated to be 135.44 kJ/mol.

Comparative Study of the Results

Figure 4 shows H_2 concentration profile in the product gas in the above mentioned two conditions. In unsaturated coal gasification, H_2 gas declines whereas it raises in wet coal conditions. However, H_2 concentration is not sustained at those conditions as the coal char deficits with moisture content. The comparison of calorific values of product gas for the above two cases also shows a higher value of 98.26 kJ/mol in case of water saturated coal gasification.
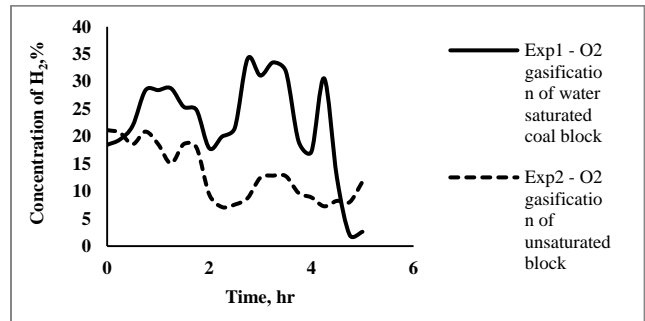
FIGURE 4. Comparison of concentration of H_2 in the above two experiments

CONCLUSION

Water influx condition gasification were simulated using borehole gasification UCG experimental set-up in order to determine the effect of moisture on product gas composition. Water influx into the cavity may enhance declines the calorific value of the product gas and depends

upon the quantity of water encroachment into the cavity for the gasification reaction.

REFERENCES

[1] Wiatowski M, Kapusta K, Ludwik-Pardała M, Stan´czyk K. Ex-situ experimental simulation of hard coal underground gasification at elevated pressure. Fuel 2016:184:401-408.

[2] Kapusta K, Stan´czyk K. Pollution of water during underground coal gasification of hard coal and lignite. Fuel 2011:90:1927-1934.

[3] Gregg D, Edgar TF. Underground coal gasification. AIChE J 1978;24:753.

[4] Stan´czyk K, Howaniec N, Ski A S, Drowski J S´, Kapusta K, Wiatowski M, Grabowski J, Rogut J. Gasification of lignite and hard coal with air and oxygen enriched air in a pilot scale ex situ reactor for underground gasification. Fuel 2011:90:1953-1962.

[5] Duan T, Lu C, Xiong S, Fu Z, Chen Y. Pyrolysis and gasification modeling of underground coal gasification and the optimisation of CO_2 as a gasification agent. Fuel 2016:183:557-567.

[6] Stiegel GJ, Ramezan M. Hydrogen from coal gasification: An economical pathway to a sustainable energy future. International Journal of Coal Geology 2006:65:173-190.

[7] Porada S, Czerski G, Dziok T, Grzywacz P, Makowska D. Kinetics of steam gasification of bituminous coals in terms of their use for underground coal gasification. Fuel Processing Technology 2015;130:282–291.

[8] Daggupati S, Ramesh N, Mahajani SM, Ganesh A, Chapru RK, Sharma RK, et al. Laboratory studies on cavity growth and product gas composition in the context of underground coal Gasification. Energy 2011;36:1776-1784.

[9] Ahmed T. (2006) Reservoir Engineering Handbook. Linacre House, Jordan Hill, Oxford OX2 8DP, UK: Gulf Professional Publishing.

[10] Bhutto AW, Bazmi AA, Zahedi G. Underground coal gasification: From fundamentals to applications. Progress in Energy and Combustion Science 2013;39:189-214.

[11] Boyd RM, Fischer DD, Humphrey AE, King SB, Whitman DL. Method for In Situ Coal Gasification Operation. Report No. 152,716, U.S.PATENT, 1981.

[12] Thorsness CB, Grens EA. Unconfined Flow as a Mechanism of Water Influx to a UCG System. Report No. UCRL-97203, U.S.DOE. Livermore, CA: Lawrence Livermore National Laboratory; 1987.

[13] Verma RP, Mandal R, Chaulya SK, Singh PK, Singh AK, Prasad GM. Contamination of groundwater due to underground coal gasification. International Journal of Water Resources and Environmental Engineering 2014:6(12):303-311.

[14] Mckee CR, Santoro RD. Gas leakage and Water influx from in situ coal gasofication. Report No. DE-AP-20-80-LC00193 , Laramie, Department of Energy Laramie Energy Technology Center; 1980.

[15] Shu-qin L, Yuan-yuan W, Ke Z, Ning Y. Enhanced-hydrogen gas production through underground gasification of lignite. Mining Science and Technology 2009:19:0389-0394.

[16] Prabu V, Jayanti S. Simulation of cavity formation in underground coal gasification using bore hole combustion experiments. Energy 2011;36:5854-5864.

SEEC-2017-51

EMERGING ROLE OF GIS IN AGRO-RESIDUE BIOMASS ENERGY PLANNING

Moonmoon Hiloidhari
School of Environmental Sciences
Jawaharlal Nehru University, New Delhi-110067, India
Email: hiloidhari@gmail.com

Kristina Medhi
School of Environmental Sciences
Jawaharlal Nehru University, New Delhi-110067, India
Email:kristi0310@gmail.com

IS Thakur
School of Environmental Sciences
Jawaharlal Nehru University, New Delhi-110067, India
Email: isthakur@hotmail.com

ABSTRACT

Agro-residues are promising feedstock for biomass energy generation for both household and industrial applications. However, agro-residues are geographically distributed with spatio-temporal variation in its availability. Resource distribution mapping, supply chain logistics planning and power plant design-- are spatially inter-linked and thus necessitate geo-spatial intervention for successful planning of biomass power projects. Spatial tools such as Geographical Information System (GIS) have been found very handy in agro-residue biomass energy planning. The present paper discusses the various applications of GIS in agro-residue biomass energy planning by highlighting the role of GIS in resource assessment, supply chain logistics planning and power plant site selection and design.

Keywords: *Geographical Information System, Agro-residue, Biomass energy, Energy planning*

INTRODUCTION

Agro-residues covers range of biomass produced as the by-products (e.g. straw, stalk, pulp, peel, bagasse, stubble, stover, husk, cobs and leaves) of agricultural production system. Global agro-residue production is estimated at 3.8 billion Mg, of which 74% is contributed by cereals [1].

Renewable energy generation from biomass *via* modern biomass energy conversion technologies have been getting popularity all over the world. Estimates on global scale suggest gross biomass energy production on agricultural land varies from 64 to 161 EJ yr^{-1} in 2050 [2]. The advantages of agro-residues are: (i) suitability for generation of renewable heat and power, biofuel, (ii) wide range of by-products are generated in the energy generation process, which can be used as precursors for industrial product development through biorefinery process, (iii) bioenergy emits less carbon di-oxide than fossil fuels during its life cycle, thus helps to combat climate change, (iv) scope for biomass energy based rural entrepreneurial activities, (v) feasibility of generating energy at decentralized level to empower remote areas.

Agro-residues are geographically distributed with variation in spatio-temporal availability. Prior and precise information regarding residue availability, seasonal and regional fluctuation (peak and lean period of availability) is important for viable commissioning of biomass power projects. Logistics such as residue harvest, collection, storage, transport also require meticulous planning. Adequacy, precision, reliability of data collected through traditional methods (survey or secondary data collection) for biomass project planning remain insufficient. In this context, use of GIS (Geographical Information System) has been found to be very handy in biomass energy planning. GIS is a software based computation tool designed to store, analyze, manipulate and retrieve spatial data both in map and tabular formats. The generated information can be retrieved and updated at user will.

Here we present an overview of various applications of GIS in agro-residue biomass energy planning.

THE NEED OF GIS IN BIOMASS ENERGY PLANNING

Environmental assessment including renewable energy planning needs specific Decision Support System (DSS) for effective planning because of the complexity of interaction among ecological, economic and political variables and lack of data availability which often lead to difficulty in bringing together large scale analysis and local planning systems [3]. Spatial tool like GIS is an important decision making tool which aids in evaluation of renewable energy resources for integrated and accurate decision making for policymakers and investors [4]. Knowledge of geospatial distribution of biomass resources can guide the industries more effectively and efficiently for effective collection of raw material, allocation of primary production factories and projects and cost-benefits analysis [5]. Furthermore, precise spatial database of biomass energy potential at global, regional, national scale, and even smaller spatial scales, could play a great role in success of the biomass energy sector.

GIS IN AGRO-RESIDUE BIOMASS AVAILABILITY ASSESSMENT

Accurate estimation of agricultural residue availability is very important for biomass energy planning, particularly in agriculturally dominant countries like India [6]. However, despite increasing interest among the developers, in several instances, biomass projects appear to be non-viable due to techno-economic-environmental factors. For technical, economical and environmental viability of biomass projects, a comprehensive planning is required which could provide precise and detail information on biomass resource availability, optimization of biomass management (collecting and transport), costs and emissions [7]. Such planning could be done with the help of GIS. Another challenge in biomass energy project is to ensure sustainable feedstock supply. Seasonal variation in feedstock availability could risk viability of biomass power plants. Therefore, prior knowledge of lean period of feedstock supply would allow user to make necessary arrangements for alternative feedstock supply, which can be indicated through GIS assessment [8]. Even though agro-residue biomass is available in large quantities, it is not feasible to utilize all the residue for energy purpose due to geographical, logistics, technical and economical constrains. The estimation of actual or net amount of residue available for biomass energy utilization can be effectively done through GIS [9]. The GIS assisted Spatial Decision Support Systems (SDSS) such as Biomass Energy Potential Assessment (BEPA) for decentralized renewable energy planning can be designed to gather data from a wide range of data sources, and then to analyze and present in a way that can be interpreted by the decision maker to deliver the precise information needed to make timely decisions [10]. Shi et al.[11] used remote sensing data (MODIS/Terra satellite data) in GIS environment to map available biomass in order to assess the feasibility of setting up new biomass power plants and optimizing the locations of plants in Guangdong, China. GIS is also found to be useful in mapping village level biomass resource potential for decentralized energy planning [12, 13]. Melico et al. [14] used GIS with CORINE land cover data to assess availability, techno-economic feasibility and environmental aspects of using forestry and agricultural residue for heat generation in southwestern Europe.

GIS IN AGRO-RESIDUE LOGISTICS PLANNING

Uneven geographical distribution of agro-residues demands proper logistics planning for collection and transfer of residues from fields to power plants in a timely and cost efficient manner. Biomass supply chain plays a crucial role in the sustainable management of biomass energy production process [15]. Many factors involved in biomass supply chain including the supplier of biomass, transportation and distribution entities, energy production facility developers and operators, the government and utility firms who provide the incentives and the end users

[15]. The chain of residue harvest, collection, storage, processing and transport requires human/animal or mechanical power and thus demands substantial economic input. These logistic parameters add to overall biomass procurement cost and hence biomass energy cost. Among the logistics parameters, transportation could be cost intensive depending upon the distance of transport, medium and mode of transport (railway, roadway, waterway), amount and nature of feedstock to be transported (loose or dense) and transport route condition. Another important parameter needing attention is the selection of optimal site for power plant installation, where multiple factors come into play. The site should be easily accessible by transport route, near to utility points, feasible for optimum planning of power transmission lines. It is also required to install the plant in reasonable distance from residential areas, nature reserves in order to minimize potential negative impacts to human and ecosystem health that may arise due to operation of power plant and disposal of waste [11]. All these issues can be efficiently handled and planned with GIS. Logistics cost arising from biomass harvesting, collection and transportation could be minimized with GIS based planning [11, 16]. Implementing a network of regional facilities might help private agents to act in a common efficient framework by sharing costs, logistics, and personnel. Beccali et al. [46] developed a GIS method to assess techno-economic potential of biomass for energy generation in Sicily through identification of efficient transportation network and optimal biomass collection areas [16]. For effective bio-based products manufacturing using agro residue, construction of collection site near existing road or railway network helps in easy and bulk transportation of biomass, as demonstrated by Haddad and Anderson [17] in a GIS study in USA. The rising competition for production areas, raw materials and infrastructure demand comprehensive spatially explicit logistics planning [18]. Optimal site slection is crucial for viabale biomass power plant planning. The GIS based site selection is done *via* two approaches: (i) suitability analysis (ii) optimally analysis [11]. Suitability analysis mainly uses geo-processing procedures (such as buffer and overlay) to locate *suitable* sites based on a number of constraining and favouring factors (e.g., land use, distance to road, distance to transmission line etc.). On the other hand, optimally analysis considers the relationship between biomass and power plants in order to find the optimal power plant locations at minimum transportation cost. Using optimally analysis approach, Shi et al. [11] identified suitable sites for biomass power plants in Guangdong Province, China, considering transportation cost to be the prime factor in developing bioenergy plant. The optimization of biomass power plant location could be done either through location-allocation modeling or supply-area modelling in GIS. The location-allocation modeling optimizes plant locations based on all usable biomass in the area, even if some of the biomass locations

are beyond the reasonable transportation distance to the plant locations. On the other hand, supply-area modeling puts power plants at those locations, surrounded by high local biomass densities indicating non usefulness of biomass too distant from a power plant while choosing location for a plant. Supply-area modeling is appropriate when there is a threshold for transportation cost, which is usually the case in power plant planning. Logistic planning for collection of biomass may be further influenced by type of land holding [19]. For example, in China, collecting agro residue biomass from farmland may appear to be complicated compared to West, due to small agricultural landholding by the farmer. For the same collection radius, the collectors have to deal with larger number of farmers, with organized logistics of contracting, collection and transportation. In a long supply chain, distributed biomass receiving stations (satellite storage) must be optimized for least cost delivery of biomass. However, as reported by Gomez et al. [9], size of a collection area produces two counteracting effects on the final cost of energy generated. A large biomass collection area results in higher power plant capacity, making the power plant economically reliable, but, it increases the transportation costs of the biomass to the plant. To address this issue, it was suggested that in a large scale study with large geographical biomass supply area (e.g. country, province), it is impractical to optimize the size and location of every possible plant. Better option to deal with this is to use the same collection area for the whole of the territory and size of this area is to be determined in a way to fulfil individual plant' a minimum installed capacity [9]. Egbendewe-Mondzozo et al., [20] proposed a *spatial bioeconomic model*, an integration of biophysical - GIS - economic regional mathematical optimization model to estimate biomass supply from cellulosic crop residues. The GIS part of the model supplies transportation distance and time parameters to the bioeconomic model. This GIS integrated model can predict how biomass supply and environmental consequences respond to changes in genetic and biological management as well as market prices and government policy. Network Analyst extension of ArcGIS can be used to model road network for delivering biomass feedstock from source to user location as shown in a case study of Valencian Community, Spain [7, 21]. Network Analyst allows one to perform multiple network-based spatial functions of optimal route, travel directions, closest facility, service area, shortest path, drive-time and origin-destination analysis. This tool also allows users to dynamically model realistic network conditions, including turn restrictions, speed limits, connectivity, and traffic conditions. Use of IBSAL-MC model (an internet based GIS tool), which is integration of BIMAT (Biomass Inventory Mapping and Analysis Tool) and IBSAL (Integrated Biomass Supply Analysis & Logistic) was found to be effective for the Canadian scenario [22]. Singh et al. [23] developed a GIS method combined with mathematical models to assess agro-

residue potential for bioenergy and also to select suitable location for power plant installation at development block level for a district of Punjab, India. Existing road network and information on spatially varied biomass sources may be required for GIS based bioenergy logistics for selection of optimal locations, sizes and numbers of biogas plants [24]. The optimal location in a rural area consisting of cluster of villages could be determined by matching the required installed capacity with demand for power, minimizing biomass transportation cost and cost of distribution of power from generation centre to the user locations [25]. Such model was successfully validated through a case study in Tumkur district of Karnataka state, India.

CONCLUSIONS

The paper highlighted the need and significance of pre-planned spatial assessment of agro-residue using GIS. Main conclusions of this paper are:

(i) The complex interactions among different environmental variables demand spatial decision support system for renewable energy planning. GIS assisted resource analysis helps policy makers in informed decision making.

(ii) The limitations of traditional methods of resource assessment could be overcome with GIS based analysis.

(iii) The physical, geographical, technical and environmental limits of biomass resource avialbility could be identified with GIS.

(iv) Sustained supply of feedstock is crucial for biomass power plant viability. Variation in residue availability could be assessed using GIS and accordingly alternative feedstock supply to power plant could be managed for lean supply period.

(v) Logistics such as cost-effective transport network modelling, identification of optimal biomass collection radius, optimal site selection for biomass power plant could be effectively handled *via* GIS tool.

REFERENCES

[1]   Lal, R., 2005. World crop residues production and implications of its use as a biofuel. Environment International, 31, 575–584.

[2]   Haberl, H., Erb, K., Krausmann, F., Bondeau, A., Lauk, C., Müller, C. et al., 2011. Global bioenergy potentials from agricultural land in 2050: Sensitivity to climate change, diets and yields. Biomass Bioenerg, 35, 4753–4769.

[3]   Sacchelli, S., Meob, I. D., Palett, A., 2013. Bioenergy production and forest multifunctionality: A trade-off analysis using multiscale GIS model in a case study in Italy. Appl Energ, 104, 10–20.

[4]   Yue, C., Wang, S., 2006. GIS-based evaluation of multifarious local renewable energy sources: a case

study of the Chigu area of southwestern Taiwan. Energy Policy, 34, 730–742.

[5] Long, H., Li, X., Wang, H., Jia, J., 2013. Biomass resources and their bioenergy potential estimation: A review. Renew Sust Energ Rev, 26, 344–352.

[6] Jiang, D., Zhuang, D., Fu, J., Huang, Y., Wen, K. 2012. Bioenergy potential from crop residues in China: Availability and distribution. Renew Sust Energ Rev, 16, 1377–1382.

[7] Alfonso, D., Perpin, C., Pérez-Navarro, A., Peňalvo, E., Vargas, C., Cardenas, R., 2009. Methodology for optimization of distributed biomass resources evaluation, management and final energy use. Biomass Bioenerg, 33, 1070–1079.

[8] Stephen, J. D., Sokhansanj, S., Bi, X., Sowlati, T., Kloeck, T., Townley-Smith, L., et al., 2010. Analysis of biomass feedstock availability and variability for the Peace River region of Alberta, Canada. Biosystem Engineering,105,103–111.

[9] Gomez, A., Rodrigues, M., Montanes, C., Dopazo, C., Fueyo, N., 2010. The potential for electricity generation from crop and forestry residues in Spain. Biomass Bioenerg, 34, 703–719.

[10] Ramachandra, T.V., Krishna, S.V., Shruthi, B.V., 2005. Decision support system to assess regional biomass energy potential. Int J Green Energy, 1, 407–428.

[11] Shi, X., Elmore, A., Li, X., Gorence, N.J., Jin, H., Zhang, X., et al., 2008. Using spatial information technologies to select sites for biomass power plants: A case study in Guangdong Province, China. Biomass Bioenerg, 32, 35–43.

[12] Hiloidhari, M., Baruah, D.C., 2011. Crop residue biomass for decentralized electrical power generation in rural areas (part 1): Investigation of spatial availability. Renew Sust Energ Rev, 15, 1885–92.

[13] Hiloidhari, M., Baruah, D.C., 2011. Rice straw residue biomass potential for decentralized electricity generation: a GIS based study in Lakhimpur district of Assam, India. Energ Sustain Dev,15: 214–222.

[14] Malico, I., Carrajola, J., Gomes, C.P., Lima, J.C., 2015. Biomass residues for energy production and habitat preservation. Case study in a montado area in Southwestern Europe. J Cleaner Production, 1–8.

[15] Mafakheri, F., Nasiri, F., 2014. Modeling of biomass-to-energy supply chain operations: Applications, Challenges and research directions. Energy Policy, 67, 116–126.

[16] Beccali, M., Columba, P., D'Alberti, V., Franzitta, V., 2009. Assessment of bioenergy potential in Sici-

ly: A GIS-based support methodology. Biomass Bioenerg, 33, 79–87.

[17] Haddad, M.A., Anderson, P.F., 2008. A GIS methodology to identify potential corn stover collection locations. Biomass Bioenerg, 32, 1097–1108.

[18] Fiedler, P., Lange, M., Schultze, M., 2007. Supply logistics for the industrialized use of biomass – principles and planning approach, LINDI 2007, In: International Symposium on Logistics and Industrial Informatics, 13–15 September, 2007, Wildau, Germany.

[19] Yu, H., Wang, Q., Ileleji, K.E., Yu, C., Luo, Z., Cen, K., et al., 2012. Design and analysis of geographic distribution of biomass power plant and satellite storages in China. Part 1: Straight-line delivery. Biomass Bioenerg, 46, 773–784.

[20] Egbendewe-Mondzozo, A., Swinton, S.M., Izaurralde, C.R., Manowitz, D.H., Zhang, X., 2011. Biomass supply from alternative cellulosic crops and crop residues: A spatially explicit bioeconomic modeling approach. Biomass Bioenerg, 35, 4636–4647.

[21] Perpina, C., Alfonso, D., Pe´rez-Navarro, A., Penalvo, E., Vargas, C., Cardenas, R., 2009. Methodology based on Geographic Information Systems for biomass logistics and transport optimization. Renewable Energy, 34, 555–565.

[22] Ebadian, M., Sowlati, T., Sokhansanj, S., Stumborg, M., Townley-Smith, L., 2011. A new simulation model for multi-agricultural biomass logistics system in bioenergy production. Biosystem Engineering, 110, 280–290.

[23] Singh, J., Panesar, B.S., Sharma, S.K., 2011. Geographical distribution of agricultural residues and optimum sites of biomass based power plant in Bathinda, Punjab. Biomass Bioenerg, 35, 4455–4460.

[24] Höhn, J., Lehtonen, E., Rasi, S., Rintala, J., 2014. A Geographical Information System (GIS) based methodology for determination of potential biomasses and sites for biogas plants in southern Finland. Appl Energy, 113, 1–10.

[25] Kaundinya, D.P., Balachandra, P., Ravindranath, N.H., Ashok, V., 2013. A GIS (geographical information system)-based spatial data mining approach for optimal location and capacity planning of distributed biomass power generation facilities: A case study of Tumkur district, India. Energy, 52, 77–88.

THERMOPHILIC FUNGUS *MALBRANCHEA CINNAMOMEA AS* SOURCE OF CATALYTICALLY ACTIVE GLYCOSYL HYDROLASES FOR BIOCONVERSION OF LIGNOCELLULOSICS.

B.S Chadha
Department of Microbiology
Guru Nanak Dev University, Amritsar

ABSTRACT

This study reports thermophilic fungus Malbranchea cinnamomea as an important source of lignocellulolytic enzymes. The secretome analysis using LC–MS/MS orbitrap showed that fungus produced a spectrum of glycosyl hydrolases (cellulase/hemicellulase), polysaccharide lyases (PL) and carbohydrate esterases (CE) in addition to cellobiose dehydrogenase (CDH) indicating the presence of functional classical and oxidative cellulolytic mechanisms. The secretome was represented by GH1, GH2, GH3, GH5, GH6, GH7, GH10, GH18, GH20, GH35, GH47, GH55, GH67, GH81, GH92 and GH125 family members of cellulases/ hemicellulases showing that culture produced a suite of enzymes for effective cellulose degradation. The presence of carbohydrate esterases (CE1, CE5, CE10, CE12 and CE15) showed the secretome was efficient in degradation of ester linked substituents in hemicelluloses. The secretome showed that cellobiose dehydrogenase (AA8), endoglucanse (GH7), beta- glucosidase (GH3) were the most represented cellulolytic proteins as indicated by high peptide spectrum match (PSM) score. The protein fractions in the secretome resolved by ion exchange chromatography were analyzed for ability to hydrolyze alkali treated carrot grass (ATCG) in the presence of Mn2+/Cu2+. This strategy in tandem with peptide mass fingerprinting led to identification of metal dependent protein hydrolases with no apparent hydrolytic activity, however, showed 5.7 folds higher saccharification in presence of Mn2+. Furthermore, adding different protein fractions to commercial cellulase (Novozymes: Cellic CTec2) resulted in enhanced hydrolysis of ATCG ranging between 1.57and 3.43 folds indicating the enzymes from M. cinnamomea as catalytically efficient. Addition of xylanase (300 U/g substrate) during saccharification (at 15 % substrate loading) of different pretreated (acid/alkali) substrates (cotton stalks, wheat straw, rice straw, carrot grass) by commercial cellulase (NS28066) resulted in 9–36 % increase in saccharification and subsequent fermentation to ethanol when compared to experiment with commercial enzyme only. High ethanol level 46 (g/l) was achieved with acid pretreated cotton stalk when Malbranchea crude xylanase was supplemented as compared to 39 (g/l) achived with commercial enzyme alone. Genes coding for xylanases (GH10 and GH11) from thermophilic fungus Malbranchea cinnamomea were cloned (McXGH11 and McXGH10) and expressed in Pichia pastoris as host. The observed xylanase activity of McXGH11 (571.98 U/ml) is 7.73 folds higher when compared to wild type strain Malbranchea cinnamomea (73.91 U/ml) that produces multiple xylanases. McXGH11 was purified and found to be highly thermostable at 70˚C and catalytically efficient against variety of substituted (arabinoxylan) and non-substituted (beechwood and birchwood) xylans. Higher saccharification (1.8 and 2.05 folds) of alkali treated rice straw and alkali treated bagasse was observed using enzyme cocktail comprising of McXGH11 and CellicCTec2 (2:8 ratio) when compared to cellicCTec2 alone at same protein loading rate of 5.7 mg/g biomass. Thermostable xylanases from M. cinnamomea demonstrated immense potential as accessory enzymes for reducing the cost of

enzymes appreciably thus useful in developing economically viable 2G ethanol technology.

Malbranchea cinnamomea (CM-10T) isolated from composting soil samples was identified on the basis of morphological, microscopic as well as amplified sequence analysis of ITS1-5.8S-ITS2 region (KJ563258). The culture was grown on YpSs agar at 45°C and maintained at 4 oC. For production of cellulases and hemicellulases the culture was grown on solidified medium containing sorghum straw as carbon source, employing SSF approach. The extracts were used for assay of endoglucanase, cellobiohydrolase, xylanase, β- glucosidase, Fpase, α-arabinofuranosidase, β-xylosidase, β-D-cellobiosidase, acetyl xylan esterase, XAE and feruloyl esterase. The experiment was carried out in triplicates. Secretome analysis was carried out using protein sample (3mg/ml) reconstituted in ammonium bicarbonate buffer (40mM) followed by reduction and alkylation using 5mM DTT (60°C for 45 min) and 20mM iodoacetamide, respectively. The sample was degassed using trypsin (1:20 enzyme: protein sample) at 37°C for 12-16 h (Harsha et al., 2012). Briefly, Tandem mass spectrometric analysis was carried out using LT Q Orbitrap Velos mass spectrometer (Thermoscientific, Bremen, Germany) interfaced with Easy nanoLC II chromatography system. The raw mass spectroscopy was searched using Proteome Discoverer software suite (Version 1.4, Thermoscientific, Bremen, Germany).

The proteins in the secretome were fractionated by liquid chromatography using ion exchange column each fraction was studied for its ability to saccharify alkali pre-treated carrot grass in presence of metal ions. To identify catalytically efficient Q-sepharose eluted protein fractions capable of enhancing hydrolysis an experiment was set up using combinations of commercial enzyme (Novozyme: Cellic CTec2) and different fractions. For the identification of proteins in active fractions the proteins were identified using MALDI TOF/ TOF.

SEEC-2017-053

BIOHYDROGEN PRODUCTION FROM WASTE: SCALE-UP OPERATION

Omprakash Sarkar
CSIR-Indian Institute of Chemical Technology
Email: ommsarkar@gmail.com

P Chiranjeevi
CSIR-Indian Institute of Chemical Technology
Email: chiru.p7@gmail.com

S Venkata Mohan
CSIR-Indian Institute of Chemical Technology
Email: vmohan_s@yahoo.com

ABSTRACT

Biohydrogen (Bio-H2) is a renewable clean energy resource with the potential to solve the current energy crisis leading to a sustainable future. Waste derived Bio-H2 production is evaluated for the first time with 10m3 pilot scale capacity at CSIR-IICT in a specifically designed acidogenic bioreactor. Composite food waste collected from the canteen is used as the organic substrate for Bio-H2 production with the design specifications enabling maximum acidification and gas generation. The specific hybrid design of the acidogenic bioreactor includes fixed dynamic biofilm system with L/D ratio of 2 continuously controlling redox conditions. An initial organic load of COD 30g/l will be used in a batch mode with an up-flow velocity of 0.50 m/day at mesophilic conditions. Post the optimization, enhancement strategies for Bio-H2 production will be evaluated at varying operational parameters. The hybrid acidogenic bioreactor is a holistic waste remediation technology with efficient resource recovery and concurrent value addition. The continuous Bio-H2 production data will be recorded with the function of varying operational parameters with simultaneous waste valorization will be discussed.

Keywords: Biohydrogen, Pilot scale, Mixed microflora, waste valorization
.

SEEC-2017-54

High temperature stress: Protective mechanisms of heat tolerance in crop plants

Kumari Sita
Department of botany
Panjab university, Chandigarh
Research Scholar
Email: sitas191@gmail.com

Harsh Nayyar
Department of botany
Panjab university, Chandigarh
Professor
Email:harshnayyar@hotmail.com

ABSTRACT

Ambient temperatures have increased since the beginning of the century and are predicted to continue rising under climate change. Such increases in temperature can cause heat stress-a severe threats to crop production in most the countries. Constantly high temperatures cause an array of morpho-anatomical, physiological and biochemical changes in crop plants, which affect plant growth and development and may lead to a drastic reduction in economic yield. Heat stress affects plant growth throughout its ontogeny, though heat-threshold level varies considerably at different developmental stages. The susceptibility to high temperatures in plants varies with the stage of plant development, heat stress affecting to a certain extent all vegetative and reproductive stages. The observed effects depend on species and genotype, with abundant inter- and intraspecific variations. For instance, during seed germination, high temperature may slow down or totally inhibit germination, depending on plant species and the intensity of the stress. Various physiological injuries have been observed under elevated temperatures, such as scorching of leaves and stems, leaf abscission and senescence, shoot and root growth inhibition or fruit damage, which consequently lead to decreased plant productivity. At later stages, high temperature may adversely affect photosynthesis, respiration, water relations and membrane stability, and also modulate levels of hormones and primary and secondary metabolites. Heat stress induces changes in respiration and photosynthesis and thus leads to a shortened life cycle and diminished plant productivity. In addition, by causing injuries to the cell membrane, organization of micro- tubules and ultimately to the cytoskeleton, heat stress changes membrane permeability and alters cell differentiation, elongation, and expansion. The maintenance of cellular membrane function under high temperature stress is thus essential for a sustained photosynthetic and respiratory performance. The responses of plants to heat stress vary with extent of temperature increase, its duration and the type of plant. A direct result of stress-induced cellular changes is overproduction of reactive oxygen species (ROS) in plants which are produced in such a way that they are confined to a small area and also in specific pattern in biological responses. ROS (superoxide; O^{-2}, hydroxyl radicals; OH^-, alkoxyl radicals and non-radicals like hydrogen peroxide; $H2O2$ and singlet oxygen; $1O2$) are highly reactive and toxic and cause damage to proteins, lipids, carbohydrates which ultimately results in oxidative stress. ROS may also serve as signaling molecules in mediating important signal transduction pathways that coordinate an astonishing range of diverse plant processes under temperature stress. The detrimental effects of heat on chlorophyll and the photosynthetic apparatus are also associated with the production of injurious reactive oxygen species. High temperature modifies the activities of carbon metabolism enzymes, starch accumulation, and sucrose synthesis, by down-regulating specific genes in carbohydratemetabolism. Plants combat heat stress using various defense mechanisms for their survival within a physiological

tolerance limit. Plants show varying responses to heat stress depending on the intensity, duration, and rate of temperature change. The various mechanisms include changes at the molecular, cellular, biochemical, physiological, and whole-plant levels. It is well established that plants can respond defensively to heat stress. A preliminary treatment with a moderately elevated, non-lethal temperature can temporarily render plants more resistant to a subsequent potentially lethal heat shock and this phenomenon is known as heat acclimation. Tolerance and acclimation to heat stress are important for crops. Acquisition of thermo-tolerance is particularly important for plants that experience daily temperature fluctuations and are unable to escape to more favourable environments. Short-term avoidance or acclimation mechanisms include changing leaf orientation, transcriptional cooling, altering membrane lipid composition, reflecting solar radiation, leaf shading of tissues that are sensitive to sunburn, and extensive rooting. Under heat stress, early maturation is closely related to smaller yield losses in many crops, which may be attributed to the engagement of an escape mechanism. Increased formation of ROS is a general feature of abiotic stresses, such as extreme temperature, high light, and drought. In order to limit oxidative damage under stress conditions, plants have developed a series of detoxification systems which include enzymes such as POX, APX, CAT, and SOD. Furthermore, throughout plant ontogeny, enhanced expression of a variety of heat shock proteins, other stress-related proteins, and production of reactive oxygen species (ROS) constitute major plant responses to heat stress. In order to cope with heat stress, plants implement various mechanisms, including maintenance of membrane stability, scavenging of ROS, production of antioxidants, accumulation and adjustment of compatible solutes, induction of mitogen-activated protein kinase (MAPK) and calcium-dependent protein kinase (CDPK) cascades, and, most importantly, chaperone signaling and transcriptional activation. Osmolyte production under heat stress is thought to increase protein stability and stabilize the structure of the membrane bilayer. Secondary metabolites such as phenolics including flavonoids, anthocyanins, and plant steroids are also significantly involved in plant responses under heat stress and generally play roles in abiotic stress responses generally associated with tolerance to heat. Other major tolerance mechanisms including ion transporters, osmoprotectants, free-radical scavengers, late embryogenesis (LEA) abundant proteins and factors, ubiquitin, dehydrins involved in signaling cascades and transcriptional control are essentially significant to counteract stress effects. LEA proteins can prevent protein aggregation and protect cit- rate synthesis under heat and drought stress. Heat stress alters the stability, compartmentalization, content, and homeostasis of many molecules, especially hormones. In response to stresses, plants accumulate various thermo-protectants such as proline (Pro), glycine betaine (GB), and trehalose (Tre). Heat tolerance is induced by many other phyto-hormones such as salicylic acid (SA), abscisic acid (ABA), polyamines (PA), brassinosteroids (BRs), and ethylene (Eth) and putative signaling components such as nitric oxide (NO). The level of ABA rises under heat stress, which helps in thermo-tolerance through upor down-regulation of various genes. HSPs act as molecular chaperones and serve to attain a proper folding of misfolded or aggregated proteins and to prevent misfolding of proteins depending on the level and duration of heat stress. HSPs may be induced or enhanced when plants are exposed to elevated temperatures. The expression of HSPs positively correlates with the acquisition of thermo-tolerance, and the over-expression of HSPs often results in enhanced thermo- tolerance and ultimately improves physiological parameters such as photosynthesis, assimilate partitioning, along with water and nutrient efficiency of the plants . The production of ethylene (Eth) also varies in different plant species in response to heat stress, Eth levels decreased at 40°C. Plants accumulate various compounds of low molecular mass, known collectively as compatible solutes such as Pro, GB, and Tre, as an adaptive mechanism against stress conditions. These solutes have several protective roles in heat-stressed cells, which have been related to acquisition of thermo-tolerance . Besides these molecules, some phyto-hormones like SA, ABA, BRs, and PAs play an important role in thermo-tolerance. NO has emerged as a putative signaling molecule in response to heat stress. All these mechanisms, which are regulated at the molecular level, enable plants to thrive under heat stress. Based on a complete understanding of such mechanisms, potential genetic strategies to improve plant heat-stress tolerance include traditional and contemporary molecular breeding protocols and transgenic approaches. While there are a few

examples of plants with improved heat tolerance through the use of traditional breeding protocols, the success of genetic transformation approach has been thus far limited. The latter is due to limited knowledge and availability of genes with known effects on plant heat-stress tolerance, though these may not be insurmountable in future. In addition to genetic approaches, crop heat tolerance can be enhanced by preconditioning of plants under different environmental stresses or exogenous application of osmoprotectants such as glycinebetaine and proline. Acquiring thermotolerance is an active process by which considerable amounts of plant resources are diverted to structural and functional maintenance to escape damages caused by heat stress. In summary, high temperatures negatively affect various physiological processes including photosynthesis, primary and secondary metabolism, or lipid and hormonal signaling. Heat stress has negative effects on plant growth and development by disrupting the stability of various proteins, membranes, and cytoskeleton structures. The most affected stage is the reproductive growth and the affected process is pollen grain development. Heat induces accumulation of HSPs which prevent protein degradation and it also causes a state of metabolic imbalance and the build-up of toxic by-products, such as ROS, which ultimately affect plant vegetative and reproductive development, with negative consequences on fruit set and yield quality. Plants may accumulate various thermo-protectants phytohormones and signaling molecules under heat stress which contribute to impart thermo-tolerance through up- and down-regulation of various genes. The metabolic pathways and their genes need to be identified especially in reproductive components to address heat tolerance in the future. The poster presentation would cover the high temperature stress in plant and protective mechanism to cope up with heat stress.

SEEC-2017-55

NITRIC OXIDE (NO): A NOVEL SENSOR AND PROTECTOR IN STRESSED PLANTS

Lomeshwar Sharma & Anju Rani
Department of Botany
Punjab University, Chandigarh, India
Email: lomeshsharma12@gmail.com

Harsh Nayyar
Department of Botany
Punjab University, Chandigarh, India
harshnayyar@hotmail.com

ABSTRACT

Nitric oxide (NO) is an inorganic free radical in living organism, considered to a phytohormone and a key signaling molecule functioning in various physiological processes including stress physiology of plants. There are various routes of nitric oxide (NO) production in plants cells. NO can be synthesized enzymatically from nitrite (NO_2-) by nitrate reductase (NR). There is also considerable evidence for l-arginine-dependent NO synthase (NOS) activity in plant cells. Evidence also exists for the activity of a nitrite: NO reductase in roots and for the ability of both chloroplasts and mitochondria to convert NO_2- to NO. NO plays important role in physiological processes like seed germination, growth, senescence and photosynthesis as well as responds to specific environment stress. Depending on its concentration and location in plant cell or tissue, NO might function as an antioxidant and scavenge some other reactive intermediates. Many studies has shown direct and indirect involvement of NO in plant defence mechanisms under water stress, drought, metal stress, salinity, temperature stress and ultraviolet radiation stress. Abiotic stress is major cause of worldwide crop production losses. Some studies showed application of exogenous NO provide certain level resistant against various stress condition by activating different biochemical pathways. NO may help plant to survive stressful condition as its role as an important signalling molecule in the activation of

some antioxidant enzymes or its direct reaction with reactive oxygen species (ROS), lipid, and nitrogen free radicals. Important signalling molecules include reactive oxygen species (ROS), salicylic acid (SA), abscisic acid (ABA), jasmonate (JA) and ethylene dependent on the stage of development or type of environmental stimuli. Since several years we know that nitric oxide (NO) is also a key player in stress response signalling, but also an important signalling molecule during plant development. Different mode of action mechanisms of NO signalling has also been reported in plants. The most studied is protein S-nitrosylation, the covalent attachment of an NO group to the thiol side of protein cysteine (Cys). Protein S-nitrosylation, as a reversible posttranslational modification (PTM), can affect protein activity (activation or inhibition), translocation and protein function. In addition, other major types of modifications of NO have been also reported, such as metal nitrosylation or tyrosine (Tyr) nitration, the later one is an irreversible reaction of a nitrating agent with a Tyr residue of a target protein. NO is able to influence gene expression at multiple levels. Since NO is a diffusible gas, it can be present in all extraand intracellular spaces, where it easily interacts with the surrounding environment. In this way, NO can initiate signalling cascades and modify proteins involved in signal transduction pathways, which results in altered gene expression. The other possibility of NO to affect gene expression is through

a direct regulation of transcription factors or other regulatory elements on gene promoters. NO is likely involved in the response to low temperature since, among other stresses, cold stress is one of the most effective in inducing nitric oxide synthase (NOS)-like andSnitrosoglutathione reductase (GSNOR) activities, as well as NO production. This may reflect an important role of NO in this stress condition. One of the most important responses to NO production might be the activation of C-repeat binding factors (CBF) genes. There were remarkable reductions in the levels of CBF in A. thaliana defective in NR under chilled environment. CBF genes appear to be important regulators in cold response as a constitutive expression of CBF2was capable of inducing 85 of the 302 surveyed genes that were up-regulated under cold stress. Apparently, the activation of CBF genes leads to the accumulation of DELLA proteins by up-regulating GA-2-oxidase, an enzyme responsible for the inactivation of gibberellins. These results indicate a possible link between NO and GA in response to cold, with NO acting through expression of CBF proteins to activate GA-2-oxidase and, consequently, inhibit GA response.GA inhibition resulted in an accumulation of DELLA proteins. Apparently, DELLAs confer a degree of stress tolerance associated with a decrease in growth, resulting in enhanced survivability. One of the most important responses to drought is stomatal closure, which diminishes water loss to the environment. The signalling pathways for stomatal control are well studied, and a number of interesting reviews are currently available. Available evidence shows an involvement of NO in stomatal closure and ABA. Application of NO donors significantly reduced the transpiration and, therefore, increased water retention of detached wheat leaves. ABA and NO donors or scavengers substantiated the claim that NO might be indispensable to the ABA-mediated stomatal closure. Another key component of stomatal closure seems to be H2O2. The production of this ROS is enhanced by ABA and controls the influx of Ca2+ into the cytosol, causing the closure of stomata. Salt stress leads to many responses in plants treated with the NO donor sodium nitroprusside (SNP) fared better than those left untreated and showed lower levels of H2O2, suggesting that NO may act in resistance to salinity. DELLAs play an important role in restricting growth and regulating development during salt stress but seem to be less effective in metabolic responses, such as expression of proteins with chaperone function. Based on the study of mutants lacking DELLAs which were insensitive to ethylene or ABA, they concluded that DELLA is a convergence point between these two pathways. Salt stress results in DELLA accumulation due to a drop in GA content by enhanced GA-2-oxidase activity. Therefore, in response to salt stress, DELLAs could regulate the inhibition of growth in response to ABA, GA, and ethylene. To date, no interaction between DELLAs and NO has been shown during salt stress, but since it is likely to occur in other stresses, this may also happen during salt stress. Salicylic acid (SA) also appears to be involved in salt stress response. Application of high concentrations of SA increased H2O2 and NO amounts but decreased viability of root. The mechanisms underlying these responses, however, are still undefined. SA application, however, improved the growth under NaCl stress. A schematic representation of possible pathways leading to salt stress.NO functions as a signalling molecule and triggers the cascade of events leading to expression of numerous genes. NO has been emerging to be a key signalling molecule in plant signal transduction pathways, where cyclic guanosine 3,5-monophosphate (cGMP) may be its downstream mediator. NO may directly or indirectly interact with other signaling molecules. It was shown that the expression of tobacco genes responsible for the synthesis of protective metabolites is induced by NO, cGMP, and cyclic adenosine diphosphate ribose (cADPR). Established that in plants, as well as in animals, cGMP and cADPR participate as signalling mediators between NO and the genome NO can regulate the activity of cytosolic and mitochondrial aconitase, catalase, ascorbate peroxidase, cytochrome c oxidase inactivating them by nitrosylation. Besides, NO can transducer a signal by tyrosine nitrosylation. It was found that nitration of tyrosine residues in proteins occurred in olive leaves under salt stress and in tobacco mutants overproducing NO. Existence of S-nitrosylation as physiologically significant transduction mechanisms in plants involves the reversibility of the process. De-S-nitrosylation could be mediated by GSH to form Snitrosoglutathione (GSNO), an endogenous donor of NO pool in cells. It is shown that GSNO-reductase plays an important role in triggering S-nitrosothiols-mediated effects (in particular, the development of systemic acquired resistance) in plants infected by pathogens. Physical and chemical properties (small molecule, fast metabolism, the lack of electric charge,

and high diffusion coefficient) allow NO to react with a variety of intracellular targets. One of the fastest reactions of NO in biological systems is its interaction with ROS. Furthermore, NO can break down chain reactions of oxidation and, thus, minimize oxidative damage to cells. NO can also bind superoxide radicals generated in the electron transport chains of chloroplasts and mitochondria, preventing the formation of highly toxic hydroxyl radicals. It has been found that NO interferes with plant photooxidative stress induced by bipyridinium herbicide Diquat. It has been demonstrated that two NO donors, sodium nitroprusside (SNP) and S-nitroso-N-acetylpenicillamine (SNAP), strongly reduced lipid peroxidation and the protein loss caused by the application to potato leaf pieces or isolated chloroplasts of high doses of Diquat. NO donors also protected the RNA against oxidative damage. Their results have provided the evidence that NO is a potent antioxidant in plants and that its action may, at least in part, be explained by its ability to directly scavenge ROS. NO was demonstrated to confer a water-deficit tolerance to both detached wheat leaves and wheat seedlings under drought stress condition, as NO availability to induces stomatal closure. NO was postulated to act as an antioxidant and protect membranes and lipoproteins from oxidation either directly by inactivating ROS such as lipid hydroxyl radical or indirectly by inhibiting lipoxygenase activity. Lipid peroxidation is the consequence of oxidative damage of the cell. NO rapidly reacts with lipid alcoxyl or lipid peroxyl radicals and breaks the self perpetuating chain reaction during lipid peroxidation. NO applied at low nanomolar concentrations diminished the impacts of H2O2-induced oxidative stress in tobacco leaves. NO acts as an antioxidant in plants by preventing the formation of MDA, a lipid peroxidation product. NO performs protective role during oxidative stress induced in potato plants treated with Diquat and in rice plants treated with Paraquat. High concentrations of ROS can activate the programmed cell death (PCD), which is characterized by a fragmentation of chromatin and the release of low molecular DNA fragments. It has been found that H2O2-induced fragmentation of total DNA was entirely suppressed by NO applied in the form of SNP. It was supposed that H2O2 induced the synthesis of new soluble proteins, which was manifested in the increase in total protein content in the cytosol. This increase in protein content in

tobacco leaves was fully prevented by the addition of 100lM SNP, even though SNP applied alone had no effect on protein content. Experiments with SNP in the presence of an NO antagonist, 2-(4-carboxyphenyl)-4,5-dihydro-4,4,5,5- tetramethyl-1H-imidazole-1-oxyl-3-oxide potassium salt (cPTIO) confirm that the protective effect is caused directly by NO and not by the source substance (SNP itself). NO can trigger the expression of certain genes and promote the protective oxidative stress-induced responses of plants due to its signaling nature. Besides defense genes (PR-1, PAL), NO activates the expression of antioxidant genes such as glutathione-S-transferase (GST), chalcone synthase (CHS), glutathione peroxidase (GPX), and alternative oxidase (AOX1a) genes and inhibits gene expression of thylakoid ascorbate peroxidase (tAPX) modulating oxidative status of plant cell. NO plays a crucial role in plant immune response. For example, in soybean cell suspensions inoculated with avirulent Pseudomonas syringaepv.glycinea, NO participates in cooperation with other ROS and activated hypersensitive response and PCD. At the same time,NO functioned independently of other ROS to induce defence genes for the synthesis of protective natural products. Moreover, various studies have shown that the inhibitors of NO synthesis potentiated the hypersensitive diseaseresistance response of Arabidopsis leaves to avirulent Pseudomonas syringaepv.maculicola, promoting disease and bacterial growth. To understand the details of NO metabolism and functions in plant, genetic, proteomic and various studies are required. The presentation would focus on source of NO plants, its physiological roles, role as a stress protectant under stress environment would be discussed.

SEEC-2017-56

STRESS PROTEINS: THE VITAL PLAYERS IN ABIOTIC STRESS TOLERANCE IN PLANTS

Manu Priya
Department of Botany
Panjab University, Chandigarh
Priya.manu1989@gmail.com

Harsh Nayyar
Department of Botany
Panjab University, Chandigarh
harshnayyar@hotmail.com

ABSTRACT

Plant growth and productivity are affected by various environmental stress factors to which plants are exposed during their life period. As plants are sessile, they cannot avoid these stresses and must have strong defense mechanisms to cope with them. Abiotic stress poses major threat to agriculture and increasing efforts are being made to understand plant stress response and tolerance mechanisms to develop new tools that lead to sustainable agriculture. Stresses such as drought, salt, cold, heat, and others, frequently act together and trigger various adaptive and protective mechanisms in plants. Basic mechanism of plant water uptake from soil is also passive as they are governed by differences between soil and plant cell water potential. However, plants actively exchange energy, water, and thousands of chemical compounds between themselves and their environment. Therefore, plants can sense changes in their environment and respond to them in order to prevent damage. Proteins play a critical role in plant stress response since they are directly involved in maintaining homeostasis and shaping the final phenotype. They constitute plant cell structure and actively participate on metabolism of all cellular components. The up regulation of stress proteins, which occurs against stressful environmental conditions, relative to normal environmental conditions, is one of the main components of the adaptive response. Subcellular proteins such as ion and water transporters, reactive oxygen species (ROS) scavengers, and the proteins related to signaling and transcriptional regulation (LEA), osmotins, antifreeze proteins and NAC transcription factors are frequently reported as being involved in stress tolerance. Most receptor proteins are located in the plasma membrane such as aqua-porins and thus the plasma membrane is directly involved in stress sensing. As an integral regulator of plantwater relations, they are presumed to play an important role in plant defense responses against various abiotic stresses. Plants have evolved special mechanisms to cope with intracellular water loss i.e. dehydration. The enhanced accumulation of LEA proteins was described as most common mechanism developed against abiotic stress tolerance. LEA proteins are part of a more widespread group of proteins called as hydrophillins that protect other proteins from aggregation, desiccation or osmotic stress. They got accumulated in maturing seeds, or are induced in vegetative tissues during salinity, drought, cold and freezing stress. There are five major LEA proteins subclasses such as LEA I, II, III, IV, V, VI (a typical LEA proteins) proteins. Dehydrins (DHNs) constitute a distinct biochemical group of LEA proteins, which is known as group 2 LEA (or LEA II) proteins or LEA-D11 proteins.

SEEC-2017-57

PLANTS' RESPONSES TO ABIOTIC STRESS IN COMBINATION

Akanksha Sehgal
Department of Botany,
PU Chandigarh, India
Godeous.red@gmail.com

Harsh Nayyar
Department of Botany,
PU Chandigarh, India
harshnayyar@hotmail.com

ABSTRACT

At present, global agriculture is facing a serious threat from climate change, which is predicted to result in reduced productivity. Increasing food prices and greater global food insecurity are the outcomes of decreased productivity. Crop plants are affected worldwide by a variety of abiotic stresses like drought, extreme temperature, salinity, oxidative stress, etc. and it has been estimated that approximately 70% of yield reduction is the direct result of abiotic stresses. These environmental challenges that adversely affect plant growth and productivity, lead to a wide range of responses in plants, including morphological, physiological, biochemical and molecular changes. Abiotic stress conditions could potentially cause the accumulation of reactive oxygen species (ROS), including H2O2 that function as signal transduction molecules, but can also cause extensive cellular damage and inhibition of photosynthesis. To prevent damage, ROS are normally removed by antioxidant machinery, which can be, in turn, impaired by the effect of stresses themselves. Importantly, all transcriptomic and proteomic analyses, performed in several plant species subjected to different stress combinations, have highlighted the importance of the antioxidant defense machinery. Plants with higher antioxidant capacity or lower ROS accumulation have generally showed increased tolerance to stress combination. In addition to ROS, plant responses to abiotic stress are mediated by phytohormones, which coordinate complex stressadaptive signaling cascades. Although ABA is the most studied stress-responsive hormone, the role of cytokinins, brassinosteroids, and auxins during environmental stress is emerging. Salicylic acid is an important endogenous signal molecule under abiotic stress. It acts as a thermoprotectant and controls nodulation in leguminous plants under stress conditions. It controls stomatal movements as well. Another important molecule nitric oxide (NO) possesses antioxidant properties and might act as a signal in activating ROSscavenging enzyme activities under abiotic stress. NO plays an important role in resistance to salt, drought, temperature (high and low), UV-B, and heavy metal stress. Plant cells perceive stress stimuli via various sensors that in turn activate signaling pathways involving secondary messengers, plant hormones, signal transducers and transcriptional regulators. Multiple signals, therefore, converge to regulate stress-inducible genes that encode proteins and enzymes directly involved in stress metabolism, contributing to the specificity of the acclimation response to a given stress stimuli. Based on the recent models for climate change, the probability that plants will encounter new or more severe combinations of abiotic stresses in the near future is likely to be higher than previously anticipated.

SEEC-2017-58

BIOTREATMENT OF INDUSTRIAL WASTE WATER USING ALGAE— A VIABLE GREEN SOLUTION

TCSM Gupta*
R&D Centre
Apar Industries ltd.
Rabale, Navi Mumbai-400701
Email: tcsm.gupta@apar.com

Kavita Mahadik
Apar Industries ltd.
Rabale, Navi Mumbai-400701
Email:kavita.mahadik@apar.com

Saie Phoujdar
Apar Industries ltd.
Rabale, Navi Mumbai-400701
Email:saie.phoujdar@apar.com

ABSTRACT

 Dumping of untreated industrial waste water into natural water bodies causes heavy pollution and may lead to eutrophication due to addition of chemicals and nutrients. Conventional waste water treatment reduces chemical load of the water, but these are expensive and require large area, infrastructure, heavy power consumption and leads to development of high volumes of sludge. Waste water treatment using algae base processes reduce most of the above issues. Algae efficiently reduces the chemical load without much addition of cost and minimizes sludge formation. On the contrary, algae treatments generates valuable biomass which can be used as biofertiliser, for power generation or can be used as raw material in biofuel synthesis. The treated water can be directly mixed with natural bodies or used for gardening and floor washing purpose. The study confirms that utilization of algae is an efficient, cost effective and sustainable process.

SEEC-2017-59

Optimization of process parameters: Biodiesel production from carbon dioxide sequestering bacterium

Manish Kumar & Khushboo Khosla
School of Environmental Sciences,
JNU, New Delhi, India
Manishkumar.bt@gmail.com

Indu Shekhar Thakur
School of Environmental
Sciences,
JNU, New Delhi, India.
isthakur@hotmail.com

ABSTRACT

A carbon dioxide (CO2) sequestering chemolithotrophic bacterium Serratia sp. ISTD04, isolated from marble mine rocks was investigated for production and optimization of biodiesel .The bacterium was cultured in MSM with sodium bicarbonate as sole source of carbon. The bacterial biomass harvested after 48hrs was transesterified by in situ transesterification using H_2SO_4 as a catalyst. This method combines the extraction and transesterification into a single step and thus reduced the production cost and enhanced the production efficiency by minimizing the use of solvent and processing time. Box–Behnken design and Response surface methodology were used to optimize the in-situ transesterification and increase the yield of biodiesel. Three variables (Temperature, Duration, Catalyst concentration) were optimized. Optimized conditions (Temperature 40.52°C, Duration 22.93hrs and catalyst concentration 2.04% v/v of methanol) and fatty acid methyl ester yield was 41.47% of dry bacterial biomass. The characterization of biodiesel was done by GC–MS, FT-IR and NMR ($_1$H and $_{13}$C).

SEEC-2017-60

INVESTIGATION OF CYCLIC VARIABILITY IN A NON ROAD DIESEL ENGINE FUELED WITH DIESEL/BUTANOL BLENDS

Mohit Raj Saxena
Department of Mechanical Engineering
Indian Institute of Technology Ropar, Rupnagar-
140001, India
Email: mohitraj@iitrpr.ac.in

Rakesh Kumar Maurya
Department of Mechanical Engineering
Indian Institute of Technology Ropar, Rupnagar-
140001, India
Email: rakesh.maurya@iitrpr.ac.in

ABSTRACT

This study presents the experimental investigation of cyclic variations in a non-road single cylinder compression ignition engine using diesel and butanol blends. The experiments were conducted using neat diesel, 10%, 20% and 30% butanol/diesel (B10, B20, B30) blends as fuel for low, medium and high engine load conditions. Experimental in-cylinder pressure data were recorded for 2000 consecutive engine combustion cycles and combustion parameters were estimated for each cycle. Cyclic variations were investigated for indicated mean effective pressure (IMEP) using statistical and wavelet techniques. Results indicated that cyclic variations in IMEP were higher at lower load condition and decreases with engine operating load. The results also revealed that the addition of butanol in diesel fuel can increase the cyclic variations after certain specific blend ratio for same injection parameters as diesel fuel.

*Keywords***: Cyclic Variation; IMEP; Butanol; Diesel Engine; wavelets;**
.

INTRODUCTION

The World is facing the crisis of depletion of fossil fuels and degradation of the environmental conditions. Diesel engines (compression ignition engines) are generally used in the power generation, heavy-duty vehicles and irrigation purpose engines (such as gensets) because of their higher thermal efficiencies and the engine power output. In addition to their higher thermal efficiency, industries must meet the emission legislation limits. However, the development of renewable and clean combustion fuel is essential to fulfill the energy demand across the world. Several alternative fuels (like various biodiesel and alcoholic fuels) were suggested in several studies [1-5] for the compression ignition (CI) engine. Because of their limitations (such as the higher viscosity of biodiesel, miscibility etc.), these fuels were not prominently used in vehicles. Currently the researchers are more focused towards the butanol as an alternative fuel for the diesel engine due to its unique properties. Butanol is easily miscible with diesel fuel and has a higher cetane number as compared to other alcoholic fuels. Combustion process in the CI engines is quite complicated and is dependent on the several parameters (such as in-cylinder temperature, fuel injection pressure and injection timing etc.). It is a well-known fact that combustion cycles of an internal combustion engines are not similar. Engine cycles seem similar to the fingerprints. That means, two cycles are not the same which affects the combustion and emission characteristics of the engine. Excess variations in engine cycles may cause damage to engine or reduce the engine life. To run an engine with stable combustion, these cyclic variations must be minimized. However, it is necessary to analyze and minimize the cycle-to-cycle variations in the CI engine fueled with any fuel. Several researchers investigated the cyclic variations in previous studies [6-11] in the internal combustion (IC) engines with different fuel blends using different techniques. Rakopoulos et al. [6] experimentally investigated the effect of different biofuel blends with fossil diesel on cyclic variations in the diesel engine using statistical techniques. They recorded in-cylinder pressure history data for 400 consecutive engine cycles to diagnose the cyclic variations in peak pressure,

peak pressure rise rate, indicated mean effective pressure (IMEP) and ignition delay. Several researchers [9, 12-16] prominently used wavelet transform to diagnose the cyclic variations in an IC engine cycle because non-stationary signal could be easily diagnosed in frequency and time domain simultaneously using wavelets. In the previous study, Maurya et al. [9] experimentally investigated the effect of engine operating load and the compression ratio on the cyclic variability in the combustion parameters of a stationary diesel engine. Their results demonstrated that cyclic variations in the total heat release rate are higher at lower load condition and decreases with an increase in the engine operating load. Highest cyclic variability was observed at idle load condition with lower compression ratio. Cyclic variations were also reduced with an increase in the compression ratio.

However, it is essential to perceive the cyclic variations in the diesel engine to operate the engine efficiently with any fuel. Several studies were found to characterize the cyclic variations in the diesel engine but few studies are available for stationary diesel engine. This study focuses on the cyclic variations in indicated mean effective pressure (IMEP) of stationary diesel engine at different engine operating load condition using statistical and wavelet techniques. Cyclic variations in stationary diesel engine are investigated for neat diesel and diesel/butanol fuel blends i.e. B10, B20 and B30.

EXPERIMENTAL SETUP

Experiments were performed on a non-road stationary diesel engine equipped with eddy current dynamometer. A schematic diagram of experimental test rig is shown in figure 1.
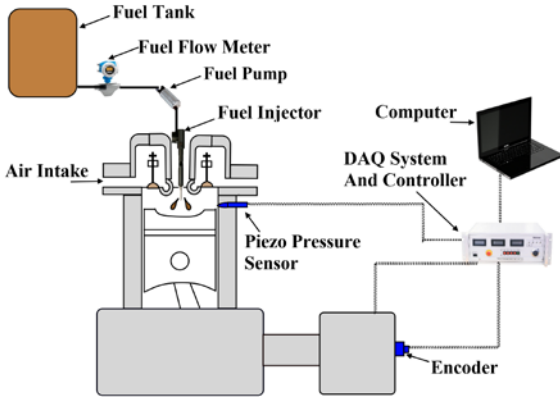
FIGURE 1. SCHEMATIC DIAGRAM OF EXPERIMENTAL TEST RIG

Neat diesel and diesel/butanol blends were directly injected into the cylinder using mechanical fuel injector at 23° bTDC. In-cylinder combustion pressure was measured with flush mounted piezoelectric pressure transducer in the cylinder head. The crank angle position was measured by

using an encoder of 1CAD resolution. Cylinder pressure data is recorded for 2000 consecutive engine combustion cycles. Equations used to calculate the IMEP and coefficient of variation (COV) of IMEP in this study are given below.

$$IMEP = \frac{W_{ind}}{V_d} \qquad (1)$$

Where, W_{ind} is an indicated work and V_d is a displacement volume.

$$COV_{IMEP} = \frac{Std. \; deviation \; in \; IMEP}{mean \; of \; IMEP} x \; 100 \qquad (2)$$

RESULTS AND DISCUSSION

This section presents the investigation of cyclic variation in the IMEP of stationary diesel engine for different fuel blends. Firstly, statistical technique was applied to analyse the cyclic variations in IMEP for 2000 consecutive engine combustion cycles. Secondly, for detail characteristics of cyclic variation, continuous wavelet transform (CWT) was used. Figure 2 indicates the COV in IMEP of 2000 consecutive combustion engine cycles at different load conditions for neat diesel and butanol/diesel fuel blends. Figure 2 reveals that the higher cyclic variations were obtained at lower load condition. At lower engine operating load, amount of fuel injected is lower which results in lower combustion temperature. Lower combustion temperature leads to increase the cyclic variations. Figure 2 also indicates that at lower load condition, up to 20% addition of butanol in the diesel fuel, COV in IMEP is close to COV in IMEP with neat diesel fuel. However, higher COV was observed above 25% butanol fraction in the blended fuel.
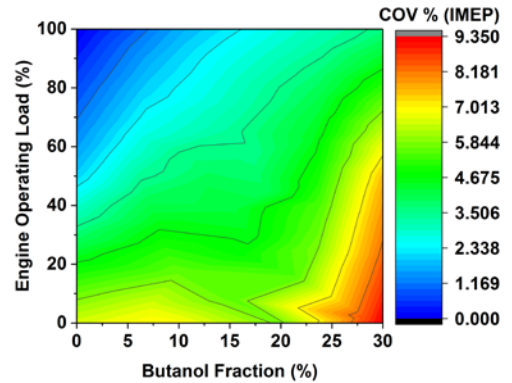
FIGURE 2. EFFECT OF ENGINE OPERATING LOAD ON THE CYCLIC VARIATION OF IMEP FOR DIFFERENT DIESEL/BUTANOL BLENDS

To analyse the frequency of cyclic variation with time in 2000 consecutive engine combustion cycles, wavelet transform was used. It provides the time and frequency info simultaneously [17, 18]. With the help of CWT, wavelet power spectrum (WPS) and global wavelet

spectrum (GWS) are created from the time series of IMEP of 2000 consecutive cycle. WPS represents the energy of the signal and it is the square modulus of CWT [19]. The time average of WPS is called GWS. Figure 3 and 4 shows the WPS and GWS for neat diesel and butanol/diesel blends at different engine operating conditions. Horizontal axis in WPS represents the number of engine combustion cycles, while the vertical axis indicates the periodicity of IMEP time series. Horizontal axis in GWS represent the power while the vertical axis indicates the period. Peaks in the GWS plot reveals the prevalent periodicities in the time series of IMEP. Colours in the WPS represent the frequency of the signal. Red and blue colour indicate the maximum and minimum energy of the signal respectively. U-shape curve in the bottom of WPS is known as the cone of influence (COI). It is the area where edge effect is important [17]. The area above the COI is only considered.

Figure 3(a) indicates that periodic band of moderated intensity 16-32 occurs during cycle's 126-185. The presence of strong periodicity represents the higher cyclic variability. In addition to this, periodic band of moderated or low intensity 4-16 occurs intermittently till 1000 cycles. Figure 3(b) represents the WPS and GWS of IMEP at 50% engine operating load. Figure 3(b) reveals that strong intensity of periodic bands 32-64, 128-256 and 32-64 occurs during the cycles 942-1197, 332-651 and 1530-1934 respectively. Moreover, figures 3 also indicate peak power of GWS reduces with an increase in the engine operating load. It represents the reduction in variation of IMEP with an increase in the engine load. Similar results were also obtained with statistical method (COV of IMEP). The cyclic variations are lowest at higher load condition that's why WPS and GWS at full load condition is not presented in this extended abstract.
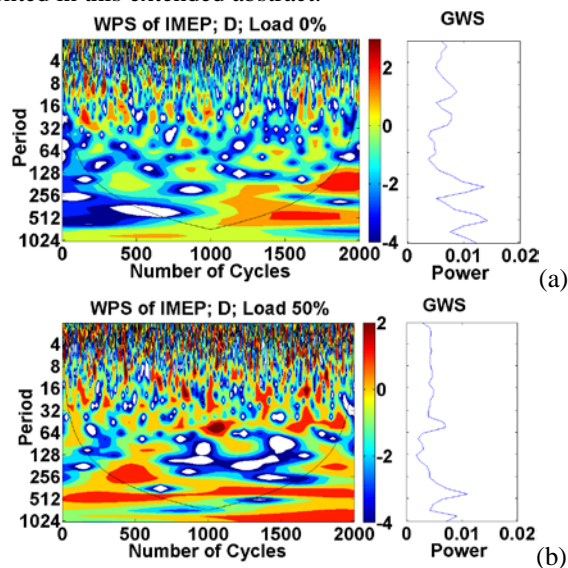
FIGURE 3. WPS AND GWS OF IMEP FOR NEAT DIESEL AT (A) 0% LOAD; (B) 50% LOAD CONDITIONS

Since the cyclic variations were higher at lower load condition (as shown in figure 2 and 3), wavelet analysis is only presented for 10%, 20% and 30% butanol/ diesel blends at lower load conditions. Figure 4 shows the WPS and GWS of IMEP for 10%, 20% and 30% butanol/ diesel blends at lower load condition. Figure 3 (a) shows strong periodicity bands 32-128, 64-128, 256-512 occurs during the 304-479, 1168-1500 and 746-1622 cycles respectively. Moderated frequency periodic bands also observed alternatingly during the cycles.
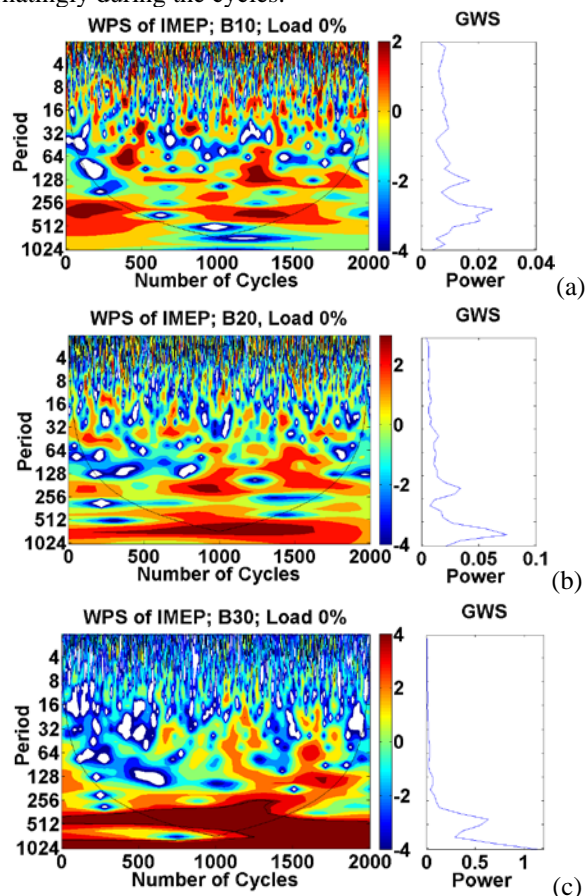
FIGURE 4. WPS AND GWS OF IMEP FOR (a) 10%; (b) 20%; (c) 30% BUTANOL/DIESEL BLEND AT 0% LOAD CONDITIONS

Similarly, in figure 4(b) a strong periodic bands of 128-256, 64-256 and 512-1024 observed during 672-1159, 1280-1752 and 845-1200 cycles respectively. A strong periodic band of 256-512 observed during 494-1426 consecutive cycles (as shown in figure 4(c)). GWS also reveals that peak power by 10% and 20% butanol/diesel blends are comparable to the GWS peak power of neat diesel at lower load condition. It represents that there were not too much cyclic variation with 10% and 20% butanol blends. However, intense cyclic variations were observed with 30% butanol/diesel blended fuel. It might be because of the combined effect of lower cetane number and higher oxygen contents which results into unstable combustion.

Addition of butanol in diesel fuel has a better combustion and emission characteristics for the stationary diesel engine is already presented in another study by the authors [20], however, addition of butanol in certain specific ratio in diesel fuel has ability to reduce the cyclic variations.

CONCLUSIONS

This study investigated the cyclic variations in a non-road diesel engine using statistical and wavelet techniques. The experiments were performed for neat diesel, 10%, 20% and 30% butanol/diesel blended fuels at 0% load, 50% load and 100% load conditions. Results revealed that GWS power is higher at lower load condition and reduces with an increases with increase in engine operating load. It indicated that cyclic variations was higher at lower load condition. Statistical technique also indicated the similar results. Wavelet analysis shows that at lower load condition (in case of neat diesel), periodic band of moderated or low intensity 4-16 occurs intermittently till 1000 cycles. Moreover, at medium load condition, strong intensity of periodic bands 32-64, 128-256 and 32-64 occurs during the cycles 942-1197, 332-651 and 1530-1934 respectively. Results also indicated that up to 20% addition of butanol in the diesel fuel, cyclic variations were close to the variation in neat diesel fuel. On further increasing the butanol fraction in the blended fuel, intense variations was observed.

REFERENCES

[1] Ibrahim, A. (2016). Performance and combustion characteristics of a diesel engine fuelled by butanol–biodiesel–diesel blends. Applied Thermal Engineering, 103, 651-659.

[2] Imdadul, H. K., Masjuki, H. H., Kalam, M. A., Zulkifli, N. W. M., Alabdulkarem, A., Rashed, M. M., ... & How, H. G. (2016). Higher alcohol–biodiesel–diesel blends: an approach for improving the performance, emission, and combustion of a light-duty diesel engine. Energy Conversion and Management, 111, 174-185.

[3] Agarwal, A. K., Singh, A. P., Agarwal, A., Jeon, J., Lee, C. S., & Park, S. (2016). Spatial combustion analysis of biodiesel fueled engine using combustion chamber endoscopy and modeling. Renewable Energy.

[4] Giakoumis, E. G., Rakopoulos, D. C., & Rakopoulos, C. D. (2016). Combustion noise radiation during dynamic diesel engine operation including effects of various biofuel blends: A review. Renewable and Sustainable Energy Reviews, 54, 1099-1113.

[5] Li, N., Tang, D., Xu, Y., & Zhao, W. (2015). Combustion and emission characteristics of an off-road diesel engine fuelled with biodiesel–diesel blends. International Journal of Sustainable Energy, 34(7), 417-430.

[6] Rakopoulos, D. C., Rakopoulos, C. D., Giakoumis, E. G., Komninos, N. P., Kosmadakis, G. M., & Papagiannakis, R. G. (2016). Comparative Evaluation of Ethanol, n-Butanol, and Diethyl Ether Effects as Biofuel Supplements on Combustion Characteristics, Cyclic Variations, and Emissions Balance in Light-Duty Diesel Engine. Journal of Energy Engineering, 04016044.

[7] Labarrere, L., Poinsot, T., Dauptain, A., Duchaine, F., Bellenoue, M., & Boust, B. (2016). Experimental and numerical study of cyclic variations in a Constant Volume Combustion chamber. Combustion and Flame, 172, 49-61.

[8] Rakopoulos, D. C., Rakopoulos, C. D., Giakoumis, E. G., & Dimaratos, A. M. (2013). Studying combustion and cyclic irregularity of diethyl ether as supplement fuel in diesel engine. Fuel, 109, 325-335.

[9] Maurya, R. K., Saxena, M. R., & Akhil, N. (2016). Experimental Investigation of Cyclic Variation in a Diesel Engine Using Wavelets. In Intelligent Systems Technologies and Applications (pp. 247-257). Springer International Publishing.

[10] Foakes, A. P., & Pollard, D. G. (1993). Investigation of a chaotic mechanism for cycle-to-cycle variations. Combustion science and technology, 90(1-4), 281-287.

[11] Maurya, R. K., & Agarwal, A. K. (2012). Statistical analysis of the cyclic variations of heat release parameters in HCCI combustion of methanol and gasoline. Applied Energy, 89(1), 228-236.

[12] Ali, O. M., Mamat, R., Masjuki, H. H., & Abdullah, A. A. (2016). Analysis of blended fuel properties and cycle-to-cycle variation in a diesel engine with a diethyl ether additive. Energy Conversion and Management, 108, 511-519.

[13] Sen, A. K., Litak, G., Finney, C. E., Daw, C. S., & Wagner, R. M. (2010). Analysis of heat release dynamics in an internal combustion engine using multifractals and wavelets. Applied Energy, 87(5), 1736-1743.

[14] Sen, A. K., Litak, G., Edwards, K. D., Finney, C. E., Daw, C. S., & Wagner, R. M. (2011). Characteristics of cyclic heat release variability in the transition from spark ignition to HCCI in a gasoline engine. Applied energy, 88(5), 1649-1655.

[15] Sen, A. K., Zheng, J., & Huang, Z. (2011). Dynamics of cycle-to-cycle variations in a natural gas direct-injection spark-ignition engine. Applied Energy, 88(7), 2324-2334.

[16] Efe, Ş., & Ceviz, M. A. (2016). Investigation of the Effect of Canola Methyl Ester on Cyclic Variation Using Wavelet Analysis Method. In Sustainable Aviation (pp. 17-25). Springer International Publishing.

[17] Torrence, C., & Compo, G. P. (1998). A practical guide to wavelet analysis. Bulletin of the American Meteorological society, 79(1), 61-78.

[18] Wu, J. D., & Chen, J. C. (2006). Continuous wavelet transform technique for fault signal diagnosis of internal combustion engines. Ndt & E International, 39(4), 304-311.

[19] Sen, A. K., Ash, S. K., Huang, B., & Huang, Z. (2011). Effect of exhaust gas recirculation on the cycle-to-cycle variations in a natural gas spark ignition engine. Applied Thermal Engineering, 31(14), 2247-2253.

[20] Saxena, M. R., & Maurya, R. K. (2016). Effect of Butanol Blends on Nano Particle Emissions from a Stationary Conventional Diesel Engine. Aerosol and Air Quality Research, 16(9), 2255-2266.

SEEC-2017- 61

ABUNDANCE AND GEOCHEMISTRY OF TRACE ELEMENTS IN COAL: UTILISATION AND ENVIRONMENTAL ASPECTS

Debasree Saha
Name of Department: Chemistry
Affiliation: University of Kalyani

Email: debasrees123@gmail.com

Debashis Chatterjee
Name of Department: Chemistry
Affiliation: University of Kalyani

Email: dbchat2001@rediffmail.com

ABSTRACT

The abundance of several environmental concern trace elements (Co, Sb, Zn, Cd, Ni, Be, Cu As, Mn, Se) has been noticed in the coal collected from a borehole of Samaleswari open cast coal block (S-OCB). Among the analysed elements Co, Mn, Cd, Pb, As, Ni, Cu, Zn exhibit principally an inorganic affinity whereas Be, Se and Sb show an organic affinity. Quartz, kaolinite, illite siderite, apatite and rutile are the notable mineral symphony of the samples. SiO_2, Al_2O_3 and Fe_2O_3, accounts over 85% of the total ash composition in the S-OCB coal. Proximate parameters reflect that rank of the coal varies from lignite and high-volatile bituminous in the borehole. This chemical data set is a guideline for suitable use of this coal along with a better understanding of the trace element composition, which is often of concern from the environmental as well as economic and technological point of view.

Keywords*: *Coal, Trace elements, Rank, Utilisation

NOMENCLATURE
A, ash
VM, volatile matter
M, moisture
FC, fixed carbon
ad, air dried basis
daf, dry ash free basis
r, correlation coefficient

INTRODUCTION
Coal plays a crucial role in power generation (~40%), throughout the globe [1]. India has a significant coal reserves (~117.4 billion tons) and remarkable role in global coal production (~540 Mt, 2011-2012) [1-2].

Generally high-ash (up to 45 wt. %) bituminous coal is used in the thermal power plants throughout the country [1-2].

The abundance and affinity of trace elements reflects the knowledge of technological performance, environmental impact and coal genesis [3-4]. Thermal power plants are the important source for environmental pollution because a significant amount of environmental concern trace elements (Hg, As, Pb, cd etc) are emitted into the different compartment of the environment such as air, water and soil due to combustion [1, 3, 5]. This may affect various living organism of the environment [1, 6]. Additionally, concentration and distribution of trace elements can also provide information of geological history of coal bed formation and depositional environment [5].

The study deals with the abundance, distribution and affinity of trace elements in coal collected from Samaleswari open cast coal block (S-OCB) including proximate parameters, sulphur content, major elements oxide concentration and mineralogical analysis to understand the quality of coal as well as proper utilisation and environmental impact of S-OCB coal.

STUDY AREA

The study area of the present work, Samaleswari open cast coal block (S-OCB) is situated in the Sundargarh district of Orissa. It is one of the identified production sectors of the Ib River valley coal field of India.

METHODS AND MATERIALS

The samples have been collected from different seams in the vertical stratigraphic sequence of a borehole as a full seam composite sample. Proximate analysis (ash, volatile matter, moisture) was done as per Indian standard (IS: 1350, Part, 1984) and total sulfur was analyzed by CHNS Elementar analyzer. The coal samples, and also the ashes (as per ASTM D 3174-11), were acid digested with HNO_3 and HF (HNO_3: HF= 2:1, Suprapur, Merck) using microwave digester (Milestone) for chemical analysis. Determination of trace elements was performed by Inductively Coupled Plasma Mass Spectrometry (ICP-MS, model-ELAN, DRC) from the digested coal samples and the major element oxides were determined from the digested ash samples by Inductively Coupled Plasma Optical Emission Spectroscopy (ICP-OES, model-VISTA MPX). Mineralogical analysis was performed with the low temperature ash (LTA, at 370°C) residues of the coal samples by X-ray diffraction (Bruker model D-8 Discover), using Ni-filtered Cu Kα radiation and a scanning range of 10-70° 2θ at a scan rate of 2°/min and JCPDS library (ICDD, PDF 2 version 2009). SPSS software was used for statistical analysis.

RESULT AND DISCUSSION

COAL QUALITY

The overall ash yield of S-OCB coal samples in the studied borehole is high (A_{ad}%, 33%, on average). The mean value of volatile matter (VM_{daf},%) and fixed carbon (FC_{daf},%) is 35.45% and 64.55% respectively. Whereas, the moisture (M_{ad}%, 3.62%, on average) and sulphur content (0.56%, on average) of the coal samples is low. These proximate parameters (A_{ad}, VM_{daf}, M_{daf}) of S-OCB coal samples are nearly similar to the coal used in the thermal power plants of India [1, 2]. The stratigraphic vertical variation of VM_{daf} and FC_{daf} shows a rank variation from lignite (~50% VM_{daf} %) to high volatile bituminous (~25% VM_{daf} %) in the borehole [5]. The vertical variations of rank indicators (VM_{daf}, VM_{daf}) in the borehole reflect a progress of metamorphism from older to younger coal seams of the studied borehole [5].

MINERALS

XRD analysis shows that the major minerals in S-OCB samples are quartz (25.35%, on average), kaolinite (50.42%, on average) and illite (15.58%, on average). The other minor constituents are siderite, apatite and rutile. The positive correlation (r > + 0.8) of quartz and apatite with ash indicates their detrital origin [4, 5]. Whereas, kaolinite and rutile have negative correlation with ash (r > - 0.75) which suggests they are mostly authigenic in nature [4, 5]. Notably, illite and siderite have weak correlation with ash (r < + 0.5). This shows their mixed detrital-authigenic origin [4, 5].

MAJOR ELEMENTS

The major elements Si, Al and Fe contribute over 85% of the total ash composition. Whereas, Na, Ca, K, Mg, Ti, P shows their little contribution to total ash composition. The SiO_2/ Al_2O_3 ratio varies (1.4-2.8) in the borehole which reflects presence of substantial clay and some quartz in the S-OCB coal samples [3, 4, 6].

TRACE ELEMENTS

 The abundance of several environmental concern trace elements Se (Mean, 0.5µg/g), Be (Mean, 1.5µg/g), Sb (Mean, 3.2µg/g), Co (Mean, 40.54µg/g), Mn (Mean, 75.54µg/g), As (Mean, 3.25µg/g), Pb (Mean, 9.62µg/g), Cd (Mean, 0.65µg/g), Cu (Mean, 5.15µg/g), Ni (Mean, 4.45µg/g) and Zn (Mean, 6.75µg/g)) are also observed in the stratigraphic column of the studied S-OCB borehole. The concentration of few trace elements Se, Be and Sb systematically increase with depth in the stratigraphic column. These elements have no paralytic in trend to ash or sulfur but have strong alliance with fixed carbon (dry, ash-free). However, two other trace elements, Co and Mn, more or less decrease in concentration in the older coal horizons, and have a significant relationship with ash. Nevertheless, another group of trace elements (As, Pb, Cd, Cu, Ni and Zn) show a sudden increase in concentration at the middle portion of depth of the borehole. These trace elements also show a similar vertical trend as well as strong association to sulfur (r > + 0.8). The statistical tools, correlation coefficient, hierarchical cluster and linear multiple regression are further used to understand several possible affinities or mode of occurrence of the trace elements such as inorganic, organic and multiple. Among the analyzed trace elements Co, Mn, Cd, Pb, As, Ni, Cu, Zn exhibit principally an inorganic affinity, whereas Be, Se and Sb show an organic affinity. The linear multiple regression study reveals that an appreciable part of Sb, Be, Se may be associated with organic fraction. It has also been found that fixed carbon values (FC_{daf} %) are also increasing in nearly a similar pattern and have a positive correlation (r > + 0.9) with these elements. The present study also provides an example of a major

variation of rank indicators (FC$_{daf}$ and VM$_{daf}$,) along with an increase in concentration of some trace elements (Sb, Be, Se) with depth. This variation pattern of organically associated trace elements (Sb, Be, Se) may be related in some way to the consequence of coal rank or degree of metamorphism [4-6].

The S-OCB coal samples are slightly enriched in Co, Sb, Zn, Cd, Ni, Be, Cu whereas As, Mn, Se are relatively depleted, when compared with world average abundances of trace elements in coal [7]. The work based on trace elements concentrations and their mode of occurrence also reflects an understanding of possible utilization of S-OCB coal in various sectors (power generation, metallurgical industry, house-hold, commercial) from clean coal technology aspects [1-6]. Samaleswari is a new production project and the data set will provide a guideline for suitable use of this coal of rank between lignite and high-volatile bituminous, along with a better understanding of the trace element composition (Fig.1), which is often of concern in developing counties from the environmental as well as economic and clean coal utilization point of view.
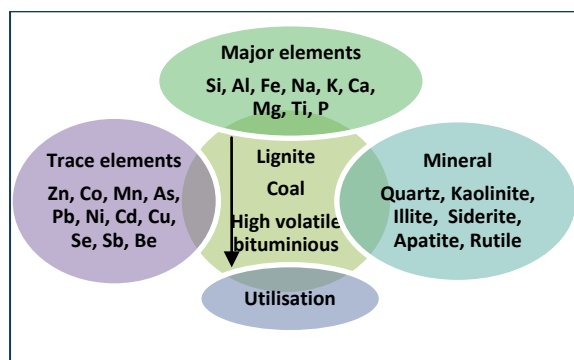
Fig. 1. GEOCHEMICAL QUALITY OF S-OCB COAL.

CONCLUSION

The study highlights a geochemical quality (proximate parameters, sulfur contents, mineral composition, trace elements and major element concentrations) of S-OCB coal samples collected from different seams of a borehole. The coals are high ash in quality and have low moisture as well as low sulfur content. The vertical variations in rank indicators (fixed carbon, volatile matter) reflect that the rank of the coal increases from lignite to high-volatile bituminous with increasing depth in the borehole. S-OCB coals have detrital (quartz, apatite), authigenic (kaolinite and rutile) and mixed detrital-authigenic (illite and siderite) minerals input. The major oxides of element Si, Al, Fe have a dominant influence in the total ash composition of the coals in the borehole because

their concentrations reflect mineralogical delineation. The several environmental trace elements Se, Be, Sb, Co, Mn, As, Pb, Cd, Cu, Ni and Zn are present in S-OCB coal. The trace elements Co, Mn, Cd, Pb, As, Ni, Cu, Zn has principally an inorganic affinity, whereas Be, Se and Sb show an organic affinity. Additionally, the concentration variation and mode of occurrence of few trace elements (Se, Be, Sb) focus some light towards the progress of coal maturation in the stratigraphic column. These geochemical data sets will provide the information of proper utilisation of S-OCB coals from technological and environmental point of view.

ACKNOWLEDGEMENT

REFERENCES

[1] Vejahati F, Zhenghe X, Gupta R. Trace elements in coal: Associations with coal minerals and their behavior during coal utilization- A review. Fuel 2010; 89: 904-911.

[2] Energy statistics. Ministry of statistics and programme implementation, Government of India; 2013.

[3] Tang Q, Liu G, Zhou C, Sun R. Distribution of trace elements in feed coal and combustion residues from two coal fired power plants at Huainan, Anhui, China. Fuel 2013; 107: 315-322.

[4] Dai S, Ren D, Chou CL, Finkelman RB, Seredin VV, Zhou Y. Geochemistry of trace elements in Chinese coal: A review of abundances, genetic types, impact of human health, and industrial utilization. International Journal of Coal Geology 2012; 94: 3-21.

[5] Taylor GH, Teichmuller M, Davis A, Diessel CFK, Littke R, Robert P. Organic petrology: a new handbook incorporating some revised parts of Stach's textbook of coal petrology. ISBN 978-3-443-010396-2; 1998.

[6] Finkelman RB. Modes of occurrence of potentially hazardous elements in coal: levels of confidence. Fuel Processing Technology 1994; 39: 21-34.

[7] Ketris MP, Yudovich Ya E. Estimation of clarkes for carbonaceous biolithes: world average for trace element contents in black shale and coals. International Journal of Coal Geology 2009; 78: 135-148.

SEEC–2017–062

EXERGY ANALYSIS OF A BIOMASS BASED POLYGENERATION

Kuntal Jana
Department of Mechanical Engineering, Jadavpur
University, Kolkata 700 032, India
Email: kuntaljana@gmail.com

Avishek Ray
Department of Mechanical Engineering, Jadavpur
University, Kolkata 700 032, India
Email: avi_rkm@yahoo.co.in

Sudipta De
Department of Mechanical Engineering, Jadavpur
University, Kolkata 700 032, India
Email: de_sudipta@rediffmail.com

Mohsen Assadi
Faculty of Science and Technology, University of
Stavanger, Stavanger, Norway
Email: mohsen.assadi@uis.no

Subha Mondal
Department of Mechanical Engineering,
Aliah University, Kolkata-156, India
Email: subhamondal53@gmail.com

ABSTRACT

Energy is a basic need for civilization and improving the standard of living. This living standard has strong correlation with per capita energy consumption. However, the use of fossil fuels for secondary energy generation is critical. Apart from climate change, energy security is also important for developing countries. In this context, biomass based energy system play an important role as developing countries like India is rich in biomass. This biomass can be utilized in decentralized way for multiple utility generation i.e., through polygeneration. However, for the maximum utilization of biomass, proper design of energy system is necessary. For this purpose, exergy analysis gives better insight about the scope of the possible improvement. Higher the destruction of exergy lower is the thermodynamic performance of an energy conversion system. Results indicate the critical components and processes of the polygeneration from the viewpoint of exergy. Most of the exergy losses and destructions occur in gasification, ethanol production and combustion processes.

*Keywords***:** *polygeneration, exergy, biomass, ethanol*

NOMENCLATURE

Ex	Exergy (kJ)
$\dot{Ex}$	Exergy rate (kW)
ex	Specific exergy (kJ/kg)
h	Enthalpy (kJ/kg)
$\dot{m}$	Mass flow rate (kg/s)
η	Efficiency
p	pressure (bar)
$\dot{Q}$	Heating/cooling (kW)
R	Gas constant (kJ/kg-K)
s	Entropy (kJ/kg-K)
T	Temperature (K)
$\dot{W}$	Power (kW)
x	Mass fraction

Subscript

0	reference state
b	boiler
c	cooling
ch	chemical
D	destruction
f	fuel
h	heating
ph	physical
Q	heat
ref	reference

INTRODUCTION

Biomass can be a good source of secondary energy if it is used properly. For proper utilization of biomass, suitable conversion technology is required. This technology should be energy efficient for the betterment of the economic performance of the plant. However, possible improvement in energy efficiency can be measured through the exergy analysis.

Rice straw is a good source of ligno-cellulosic biomass with reasonable calorific value [1]. Plenty of rice straw is available in developing countries like India, China etc [2]. This straw can be used to cater to the needs of local people through polygeneration. Polygeneration is a plant for generating multiple utility in a single unit through heat, mass and process integration [3]. Proper integration improves the performance of polygeneration compared to a stand-alone unit. Exergy analysis of this polygeneration helps to find the loss of energy potential in various processes within the polygeneration.

In this paper, exergy analysis of a polygeneration fuelled by rice straw is done. This polygeneration is designed for delivering power and bio-ethanol along with utility heat and cooling.

MATERIALS AND METHOD

Rice straw is abundantly available in India and most of the straw are under-utilized or unutilized. Though this straw can be utilized as energy resource for the production of secondary energy as it has significant calorific value. The properties of rice straw are HHV 14.56 MJ/kg, LHV 13.76 MJ/kg, FC 13.33%, VCM 62.31%, Ash 24.36%, C 34.6%, H 3.93%, O 35.38%, N 0.93%, S 0.16%, Residue 25%.

In this paper, an energy system is modeled to deliver power, ethanol, heating and cooling. The schematic of the system is shown in Fig.1. The conversion of biomass is thermo-chemical i.e., through gasification. After gasification, syngas is cooled and cleaned. During the cooling, heat of the syngas is utilized for superheating of steam and generating process heat for subsequent use. Then 60% of the produced syngas is used in combined cycle (CCGT) power generation and rest is used for ethaol production. However, this can be varied according to demand of the utilities. Power required in the ethanol production unit is supplied from the power generating unit of CCGT. In downstream process, latent heat of the process steam is used for vapor absorption refrigeration for cooling utility. Utiliy heat is obtained both from the gas cooling process and from the ethanol synthesis process. Ethanol synthesis is done by the reaction between CO and H_2 as given below in presence of catalyst (MoS_2).

$$2CO+4H_2 \leftrightarrow C_2H_5OH+H_2O \qquad \Delta H_{298}=-255.7 \text{ kJ/mol}$$
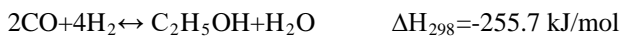
To obtain the desired H_2 and CO ratio (2:1), WGS reaction is done before ethanol synthesis as given below.

$$CO+H_2O \leftrightarrow CO_2+H_2 \qquad \Delta H_{298}= -41.0 \text{kJ/mol}$$

Both rections are exothermic, hence, heat can be obtained from this reaction. Operating parameters of the polygeneration is given in Table 1.

EXERGY ANALYSIS

Exergy analysis was done for both overall system performance and individual equipment within the system. Exergy balance for each component was done by following equations,

$$\sum_{in} \dot{Ex}_k + \dot{Ex}_Q = \sum_{out} \dot{Ex}_k + \dot{Ex}_D + \dot{Ex}_w \quad (1a)$$

$$\sum_{in} \dot{Ex}_k + \dot{Ex}_Q = \sum_{useful} \dot{Ex}_k + \sum_{loss} \dot{Ex}_k + \dot{Ex}_D + \dot{Ex}_w \qquad (1b)$$

Equation (1b) was used when a part of output exergy from a component was lost to environment (e.g. in the form of ash from gasifier or flue gas through stack).

$$\dot{Ex}_Q = \left(1 - \frac{T_o}{T_h}\right) \dot{Q}_h \qquad (2)$$

$$\dot{Ex}_w = \dot{W} \qquad (3)$$

Total exergy input to a component was in the form of physical and chemical exergies (neglecting kinetic and potential exergies). Total exergy through a stream is,

$$\dot{Ex} = \dot{Ex}_{ph} + \dot{Ex}_{ch} . \qquad (4)$$

If a stream consists of multi component, then exergy flow rates of individual species were calculated by the following equation,

$$\dot{Ex}_i = \dot{m}_i ex_i . \qquad (5)$$

Exergy of a stream consists of physical and chemical exergy. Physical and chemical exergies were calculated by equations (6) and (7) respectively.

$$ex_{ph} = (h - h_0) - T_0(s - s_0) \qquad (6)$$

$$ex_{ch} = \sum_{i=1}^{n} x_i ex_{ch,i} + RT_0 \sum_{i=1}^{n} x_i \ln x_i \qquad (7)$$

Enthalpy and entropy values were obtained from Aspen Plus® simulation. Enthalpy and entropy at the reference state were obtained by using temperature and pressure of the dead state of respective streams [4]. Chemical exergies of individual species were obtained from literature [5]. Exergy of cooling is calculated by the equation (8).

$$\dot{Ex}_c = \dot{Q}_c \left|\left(1 - \frac{T_0}{T_{evp}}\right)\right| \qquad (8)$$

Exergy of biomass was calculated using following equation (Kotas, 1985)

$$Ex_f = \beta \cdot LHV_f$$

where, $\beta = \dfrac{1.0438+0.1882\left(\frac{H}{C}\right)-0.2509\left(1+0.7256\left(\frac{H}{C}\right)\right)+0.0383\left(\frac{N}{C}\right)}{1-0.3035\left(\frac{O}{C}\right)}$,

for 2.67> (O/C)> 0.667. $\qquad (9)$

Fig.1. Schematic of the polygeneration process with associated state point [3]

Table 1: OPERATING PARAMETERS OF THE POLYGENERATION PLANT [3]

Configurations	Parameters	Value
Biomass feed	Mass flow rate	1 t/h
Reaction in gasification	Pressure	1 atm
	Equivalence ratio	35 % of stoichiometric air
Air compression,	Pressure ratio	10
Syngas compression	Isentropic efficiency	0.9
Gas cleaning	Separation efficiency of solids particles	85 %
Gas turbine combustor	Pressure	10 atm
	Heat duty	0
Gas turbine	Discharge pressure	1atm
	Isentropic efficiency	0.9
Heat recovery steam generator (HRSG)	HP stage temperature	480 ^{o}C
	HP stage pressure	7 MPa
	LP stage temperature	500 ^{0}C
	LP stage pressure	3.2 MPa
HP and LP Steam turbine	Isentropic efficiency	0.92
	LP-ST discharge pressure	0.07 MPa
NH_3-H_2O mixture feed to refrigerant pump	Total mass flow rate	2000 kg/h
	NH_3 mass fraction	0.5
Evaporator	Temperature	-5 ^{0}C
Water gas shift reactor	Pressure	4 MPa
	Temperature	215 ^{o}C

Ethanol synthesis reactor	Pressure	9.6 MPa
	Temperature	220 $^{\circ}$C
Two phase separator of liquid (water-ethanol) and gas mixtures	Temperature	40 $^{\circ}$C
CO_2 capture	Efficiency	90 %

RESULTS AND DISCUSSION

Table 2: OUTPUTS OF THE POLYGENERATION FOR FEED RATE OF 1TPH

Outputs	Value
Net GT power	560 kW
HPST power	52 kW
LPST power	263 kW
Power input for ethanol	160 kW
Ethanol production rate	734 t/y
Refrigeration	235 kW
Utility heat	105 kW

Outputs of the polygeneration is given in Table 2. From the Table 2, it is noted that power is generated in GT, HPST and LPST. However, significant power is required in ethanol production process. Significant amount of ethanol is produced from this polygeneration. Cooling and utility heat are the other two outputs of this polygeneration.
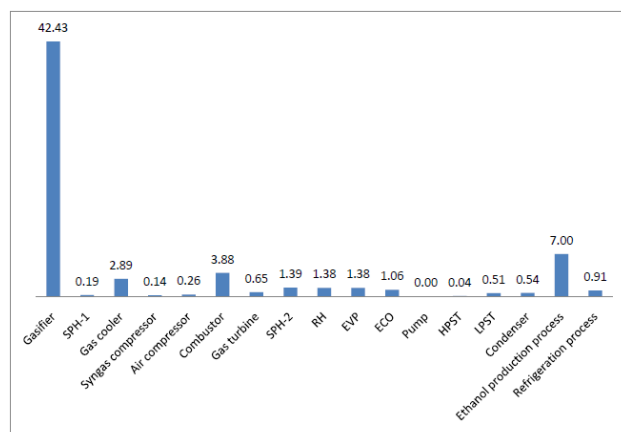
Fig.2. Percentage of exergy losses and/or destructions in different components of the polygeneration

In Fig.2, percentage of exergy losses and/or destructions in different components are shown. It is noted that the maximum of exergy input is lost and destructs in gasifier, combustor and ethanol production processes due to chemical and thermal irreversibility.

CONCLUSION

Significant amount of power, ethanol, heating and cooling can be obtained through this polygeneration. Results indicate that the critical components and processes of the polygeneration for exergy losses and destructions are gasification, ethanol production and combustion. This is due to irreversibility in chemical reactions and losses through ash.

ACKNOWLEDGEMENTS

REFERENCES

[1] Bentsen, N.S., Felby, C., Thorsen, B.J., 2014. "Agricultural residue production and potentials for energy and materials services". Progress in Energy and Combustion Science, 40, pp. 59-73.

[2] Gadde, B., Menke, C., Wassmann, R., 2009. "Rice straw as a renewable energy source in India, Thailand, and the Philippines: Overall potential and limitations for energy contribution and greenhouse gas mitigation". Biomass and Bioenergy, 33, pp. 1532–1546.

[3] Jana, K., De, S., 2015. "Polygeneration using agricultural waste: Thermodynamic and economic feasibility study". Renewable Energy, 74, pp. 648-660.

[4] Jana, K., De, S., 2015. "Sustainable polygeneration design and assessment through combined thermodynamic, economic and environmental analysis". Energy, 91, pp. 540-555.

[5] Kotas, T.J., 1985. "The exergy method of thermal plant analysis". Butterworths, London, UK.

OPTIMIZATION OF MIXED REFRIGERANTS FOR SUSTAINABLE REFRIGERATION.

Sumit Rajeshkumar Suthar
Department of Mechanical Engineering
Faculty of Technology and Engineering,
The Maharaja Sayajirao University of
Baroda, Vadodara
Email: plusitapp@gmail.com

Milind Naineshkumar Modi
Coromandel International Ltd.,
Murugappa Group
Email: milindmodi94@gmail.com

Rohitkumar N Mehta
Department of Mechanical Engineering
Government Engineering College,
Surat
Email: rnm7228@yahoo.com

ABSTRACT

Since the 1987 Montreal protocol on Substances that Deplete the Ozone Layer, commercial refrigeration industry has been facing a major challenge to retrofit the cooling devices with refrigerants that are free from Chlorofluorocarbons (CFCs) and thus Ozone friendly. In search of viable replacements, the industry has now switched over to the use of a mixture of non-reacting refrigerants instead of a single refrigerant. However, the challenge lies in finding the composition of the mixture that can produce same (or perhaps even better) cooling. Conventionally the industry has relied on experimentations to obtain the composition but, in recent years with the advent of better computing infrastructure, it is very convincing to opt for numerical methods. In this paper we consider a typical Mixed Refrigerant Joule-Thomson (MRJT) cooling device and propose a method to obtain an optimal composition of the mixture using genetic algorithm and compare the results with some other method.

Keywords: Sustainable refrigeration, Mixed Refrigerant Joule-Thomson (MRJT) Cycle, optimization.

NOMENCLATURE

h	Enthalpy, kJ/kg.
T	Temperature, K.
p	Pressure, kPa.
T_{freeze}	Freezing temperature of the mixture, K.
T_{rej}	Temperature at which the after-cooler rejects heat to the ambiance, K.
T_{load}	Steady state temperature of the refrigeration room at which the heat is extracted from the room, K.
p_{low}	Lower pressure in a typical MRJT cycle - pressure in the tube after expansion valve but before the compressor, kPa.
p_{high}	Higher pressure in a typical MRJT cycle - pressure in the tube after compressor but before expansion valve, kPa.
x_i	Mole fraction of the 'i^th' refrigerant.
$\bar{x}$	Vector representing mole fraction of each refrigerant.
RE	Refrigeration effect, kJ/kg.
$\dot{Q}_{load}$	Refrigeration load, kW.

INTRODUCTION

A typical Mixed Refrigerant Joule-Thomson (MRJT) cooling device consists of a compressor, an after cooler, an expansion valve, a refrigeration room and a recuperative heat exchanger (also called 'recuperator') (see Fig.1). On using a combination of mutually non-reacting refrigerants, which have very different boiling points, isobaric evaporation or condensation no longer occur at constant temperature. In case of mixed refrigerant the two-phase region (also referred to as 'vapor dome') is spanned over a large range of temperatures. The temperature glide implies that in such a system the Joule-Thomson effect can result in a larger change in temperature compared to that in a system with a pure refrigerant. Such a temperature glide can be further increased by using a specific composition of the mixture. However, this specific composition is something that needs to be computed using rigorous optimization techniques. Hence, systems running on optimized mixed refrigerant will have comparatively lower

power consumption. Furthermore, as presented in [1], properties of mixed refrigerants can also be exploited to make effective use of sorption compressors.

The advantages of using mixed refrigerants have long been known to the commercial refrigeration industry. However, lack of sufficient literature that presents a strong mathematical technique to obtain the optimal composition, makes exhaustive experimentations inevitable. In a patent published in 1997, W. A. Little [2] proposed a method to optimize the composition of mixture by maximizing the heat transfer capacity of the counter-flow heat exchanger. However, not much was discussed regarding the optimization technique. Alexeev et. al. [3] explained a simple method of optimization, wherein only low and high volatile components of the mixture are optimized, to reduce the computational complexity. Based on some observations, certain mathematical approximations were employed in the optimization technique to maximize the second law efficiency. Another attempt was made by Gong et. al. [4], in which second law efficiency was maximized by using "complex optimization algorithm". Keppler et. al. [5] did a comparison of the results obtained by optimization of the COP, refrigeration effect, and refrigeration per unit of heat exchanger conductance. The recuperator was divided into many finite parts to find the temperature difference between the streams at the hot end of the recuperator. This was accomplished by an iterative process to converge the pinch point temperature difference to a proposed input value. However, discretizing the heat exchanger unavoidably adds to computation cost. In this paper, we propose a method to eliminate the need to discretize the heat exchanger.
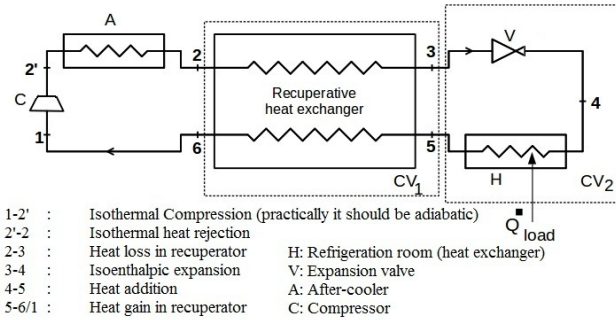
FIGURE 1. A TYPICAL MRJT CYCLE SHOWING TWO CONTROL VOLUMES.

FORMULATION OF OPTIMIZATION PROBLEM

Consider control volume 1 (CV_1) from Fig.1 and applying law of conversation of energy we get,

$$h_2 - h_3 = h_6 - h_5. \tag{1}$$

Similarly applying law of conservation of energy to CV_2 we get,

$$\frac{\dot{Q}_{load}}{\dot{m}} = h_5 - h_3 = \text{Refrigeration Effect (RE)}. \tag{2}$$

Combination of Eqn. (1) and Eqn. (2) yields,

$$RE = h_6 - h_2. \tag{3}$$

To calculate enthalpy of a mixture at a given state point, we need to know the temperature, total pressure, and mole-fraction of all the refrigerants at that state point. Since mutually non-reacting refrigerants are used, the mole-fraction of the refrigerants remain constant throughout the cycle. For mathematical simplicity, it is assumed that there is no pressure variation in the cycle except for the compression and expansion process. The values of p_{low} and p_{high} are made available for a given system and parasitic heat losses are neglected. Since our goal is to maximize the refrigeration effect, the objective function becomes,

$$Max: RE(\bar{x}) = h(T_6, p_6, \bar{x}) - h(T_2, p_2, \bar{x}). \tag{4}$$

However, the value of T_6 is unknown and therefore we cannot find the enthalpy at point 6. In [5], Keppler et. al. implemented an iterative method to find T_6 so that the resulting pinch point temperature difference of the recuperative heat exchanger converges to a specified input value. As already mentioned before, though this method is precise, it comes at a cost of larger computation time (we call this approach as *Method-I*).

If we consider Eqn. (1), Eqn. (4) and a p-h diagram, it is clear that the state points 2, 3, 5 and 6 form a parallelogram (refer to Fig.2). Therefore, maximization of the refrigeration effect is equivalent to minimization of the diagonal 2-5 (we call this approach as *Method-II*). Hence, the objective function is modified to,

$$Min: F(\bar{x}) = h_2 - h_5 \tag{5}$$

or,

$$Min: F(\bar{x}) = h(T_{rej}, p_{high}, \bar{x}) - h(T_{load}, p_{low}, \bar{x}). \tag{6}$$

It can be noted that as state point 6 is not required for minimization, there is no need to discretize the recuperator.

Since the mole fraction of the refrigerants is positive but less than one and its sum is equal to unity, the following constraints are implemented in both the approaches.

$$\sum_{i=1}^{N} x_i = 1 \text{ and } 0 \le x_i \le 1. \qquad (5)$$

In *Method-I*, an additional freezing point constraint is also implemented.

PROPERTY CORRELATION

To obtain the thermodynamic properties at the required state points, NIST Database 23 (also known as REFPROP) was used. REFPROP libraries were directly called using a function obtained from NIST website. As revealed in [5], since REFPROP uses computationally complex Benedict Web Rubin Equation of State (EOS), it does not converge effectively for temperatures lower than 150 K. Therefore, to reduce the computational complexity, the MATLAB function was configured to instruct REFPROP to use Peng-Robinson EOS. However, REFPROP still failed to converge at dew points and bubble points. To resolve this issue, the thermodynamic properties at bubble points and dew points were approximated by considering some of the neighboring points for cubic spline interpolation.
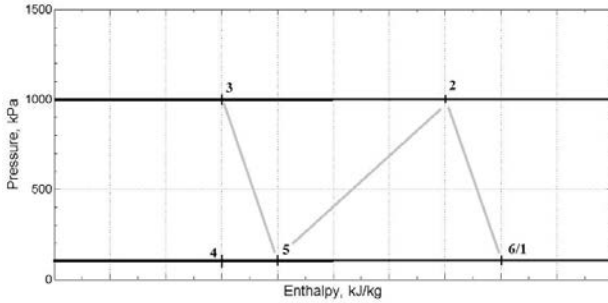
FIGURE 2. PRESSURE VS ENTHALPY DIAGRAM SHOWING THE PARALLELOGRAM FORMED BY POINTS 2, 3, 5, 6.

OPTIMIZATION METHOD

As evident in [6], Sequential Quadratic Programming (SQP) is commonly used for multi-variable optimization. However, in the present case where one of the objective functions has discontinuities, SQP is avoided. As discussed in [5], Genetic Algorithm (GA) is a robust optimization algorithm that is designed to locate global optimum even in presence of false optima, discontinuities, and constraints. In the current work, we have used GA for optimization.

SAMPLE CASE

As a sample case, we consider a mixture of Methane, Ethane, and Nitrogen. The mixture is optimized for rejection temperature of 230 K and load temperature of 180 K. The MRJT cycle operates between p_{low}=100kPa and p_{high}=1000kPa. The results obtained on optimization with *Method-I* and *Method-II*, under these parameters, are tabulated in Tab.1. Figure 3 shows the Enthalpy difference v/s temperature diagram for the results.

DISCUSSION

In Fig.3 it can be seen that the mixture obtained by *Method-II* produce similar result as that of *Method-I*. However, if the value of objective function of *Method-I* is computed with both the results then, the result of *Method-I* outperforms. But, on computing the value of objective function of *Method-II*, the result of *Method-II* produces lower value than that of the result of *Method-I*.

Unlike *Method-I*, in *Method-II* the freezing point constraint is not implemented. Implementation of freezing point constraint requires the knowledge of temperature at state point 4 and hence, in order to find the temperature at point 4, discretization of the recuperator becomes inevitable.
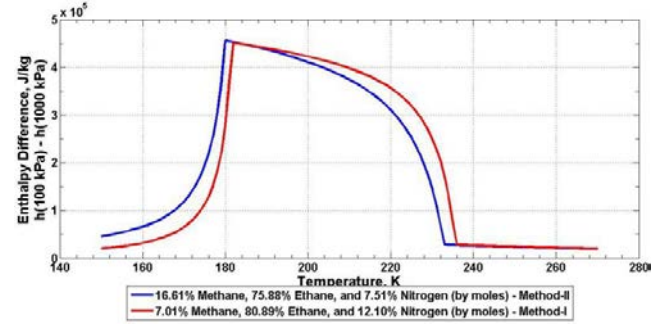
FIGURE 3. ENTHALPY DIFFERENCE V/S TEMPERATURE DIAGRAM

TABLE 1: RESULT OBTAINED ON OPTIMIZATION WITH *METHOD-I* AND *METHOD-II* (T_{rej}=230K, T_{load}=180K, p_{low}=100kPa and p_{high}=1000kPa)

Method	Mole fraction of Methane	Mole fraction of Ethane	Mole fraction of Nitrogen
Method-I	0.0701	0.8089	0.1210
Method-II	0.1661	0.7588	0.0751

CONCLUSION

In preliminary test, the proposed method seems to produce results comparable to that of *Method-I*. However, the lack of freezing point constraint may result in mixture that can choke the pipe after expansion in the valve. Nevertheless, since *Method-II* completely eliminates the need to perform computation on discretized recuperator, the convergence rate is extremely higher than that of *Method-I*.

The lack of freezing point constraint warrants further investigation. Therefore, it is highly recommended that the proposed method be tested with other combinations of refrigerants before adopting it for large scale computations.

REFERENCES

[1] R. N. Mehta, S. L. Bapat & M. D. Atrey. 2012. Characterization of sorption compressor for mixed refrigerant J-T cryocooler, Advances in Cryogenic Engineering, AIP Conf. Proc. 1434, pp. 1797-1804.

[2] Little, W.A. 1997. Method for efficient counter-current heat exchange using optimized mixtures. U.S. Patent No. 5644502.

[3] Alexeev, A., Ch. Haberstroh, and H. Quack. 1997. Further development of a mixed gas Joule Thomson refrigerator. Advances in Cryogenic Engineering, Vol. 43, pp. 1667-1674.

[4] Gong, M.Q., E.C. Luo, Y. Zhou, J.T. Liang, and L. Zhang. 2000. Optimum composition calculation for multicomponent cryogenic mixture used in Joule-Thomson refrigerators. Advances in Cryogenic Engineering, Vol. 45, pp. 283-290.

[5] Florian Keppler, Gregory Nellis & Sanford A. Klein. 2004. Optimization of the Composition of a Gas Mixture in a Joule-Thomson Cycle, HVAC&R Research, 10:2, 213-230.

[6] Venkatarathnam, G., 2008. Cryogenic Mixed Refrigerant Processes. Springer, NewYork, Chap. 5. pp. 117-136.

SEEC-2017-64

AN EVOLUTIONARY ADAPTATION OF *KLUYVEROMYCES MARXIANUS* NIRE-K3 FOR ENHANCED XYLOSE UTILIZATION

NILESH KUMAR SHARMA
Biochemical Conversion Division, Sardar Swaran Singh National Institute of Bio-Energy, Kapurthala, Punjab-144601
nilesh.sbt@gmail.com

SHUVASHISH BEHERA
Biochemical Conversion Division, Sardar Swaran Singh National Institute of Bio-Energy, Kapurthala, Punjab-144601

RICHA ARORA
Biochemical Conversion Division, Sardar Swaran Singh National Institute of Bio-Energy, Kapurthala, Punjab-144601

SACHIN KUMAR
Department of Chemical & Biological Engineering, South Dakota School of Mines & Technology, Rapid City, USA
sachin.biotech@gmail.com

ABSTRACT

The evolutionary adaptation was approached on the thermotolerant yeast Kluyveromyces marxianus NIRE-K3 at 45 ^{o}C on xylose as carbon source up to 60 batches for enhancement of xylose uptake. Evolved strain K. marxianus NIRE-K3.1 showed comparatively higher specific growth rate and xylose uptake rate than that of native strain i.e. 3.75 and 3-fold, respectively during aerobic growth. Moreover, short lag phase was also observed for adapted strain.Furthermore, during batch fermentation, K. marxianus NIRE-K3.1 utilized 96 % of xylose in 72 h and produced 4.67 and 15.7 g l^{-1} of ethanol and xylitol, respectively, which were 9.72 and 4.63-fold higher than that of native culture. Likewise, specific sugar consumption rate obtained by the K. marxianus NIRE-K3.1 cells were found to be 5.07-fold higher than that of native culture. Similarly,xylitol and ethanol yield of K. marxianus NIRE-K3.1 was 1.15 and 2.44-fold higher as compared to native strain, respectively.

*Keywords***:** Evolutionary adaptation; xylose; *K. marxianus* NIRE-K3; ethanol; xylitol.

INTRODUCTION

Several environmental issues including global warming and climate change are major concern for the researchers, which primarily caused by conventional transportation fuels and burning the crop residues [1]. Therefore, utilization of crop residues for production of alternative transportation fules such as bio-ethanol could be a better solution to resolve these issues. Moreover, bio-ethanol has already been proved as better alternative of conventional fuels as a blend in gasoline [1, 2]. Lignocellulosic biomass (LCB) contains glucose, galactose, mannose, xylose and arabinose, in which glucose and xylose covers about 90% of total sugar present [2, 3]. Hence, LCB could be better source for economic bio-ethanol production due to its abundance and low cost and utilization of both these sugars. Conventional yeast *Saccharomyces cerevisiae* can only ferment glucose but unable to ferment xylose [2-4]. However, numerous yeast are there which have the ability to ferment xylose [4]. Some of them including *Scheffersomyces stipitis, Candida shehatae, C. intermedia* and *Debaryomyces hansenii* have showed better fermentation ability on xylose [4, 5]. However, there are various hurdles including low productivity of ethanol, less sugar, ethanol tolerance and low xylose uptake [4, 5]. Since a decade several researchers have mademany efforts to resolve these issues. Moreover, various attempts have also been made to establish xylose metabolic pathway into *S. cerevisiae*through genetic engineering, but co-fermentation of xylose and glucose was not a success [6]. Moreover, mesophiles also have limitation like simultaneous saccharification and fermentation at low temperature,energy requirements for mixing and productrecovery, which increases the process cost [2, 7]. Besides, *K. marxianus*, thermotolarant yeast showed various advantages including higher rate of saccharificationand fermentation, broad range of substrate and less energy requirement formixing and product recovery and lower cost of pumping and steering [2, 3, 7]. On the other hand, evolutionary engineering together with genetic engineering maybe a better approach to develop a robust culture for the sustainable and economic process [3, 6]. This strategy has already been tried along with various conventional techniques including metabolic engineering

and proved as useful approach for the development of sustainable technology [3, 6-8]. In the current study, comparative assessment of native and adapted strains was performed on the basis of growth, sugar uptake rate and product yield and productivity on xylose as acarbon source.

METERIAL AND METHODS
MICROORGANISM AND GROWTH CONDITIONS

Thermotolarant yeast *Kluyveromyces marxianus* NIRE-K3 (MTCC 5934) was used for evolutionary adaptation study. The yeast culture was grown at 45 °C and maintained on yeast extract-peptone (YEP) medium [(g l^{-1}): yeast extract, 10; peptone, 20; glucose/xylose, 20; pH, 5.5]. Growth was performed for 24h at 45 °C and 150 rpm on an orbital shaker incubator for the cells of native and adapted, respectively. The samples were collected at an interval of 2h and analyzed for dry cell weight (DCW), xylose, glucose and extracellular metabolites concentrations. Yeast culture was maintained at -80°C in stock with 30% glycerol. Moreover, evolved strain *K. marxianus* NIRE-K3.1 was also grown and maintained as the same as native strain.

EVOLUTIONARY ADAPTATION

Evolutionary adaptation was executed in 100 ml of cotton plugged erlenmeyer flask containing 20 ml YEP medium with 2% xylose as carbon source through sequential transfer of culture. The initial batch was performed by culturing loopful cells from phytagel plate in erlenmeyer flask and incubated for 24h at 45 °C in an orbital shaker incubator (New Brunswick Innova 43/43R Shaker, Germany) at 150 rpm. Furthermore, 1% inoculum was used for continual batch for subsequent growth.

FERMENTATION CONDITIONS

Fermentation profile was performed to check out the improvements in xylose utilization and fermentation capability of *K. marxianus* NIRE-K3.1 as compared to native. Inoculum for fermentation by *K. marxianus* NIRE-K3 and NIRE-K3.1 were prepared using YEPX medium with similar composition as that of growth medium except 30 g l^{-1} xylose. Fermentation was performedin 1 L screw-caped erlenmeyer flask with working volume of 200 ml YEPX medium at a temperature of 45 °C and pH 5.5 with agitation of 150 rpm in an orbital shaker incubator. The initial cell mass concentration was kept at 2 g l^{-1}.

ANALYTICAL METHODS

Samples collected during growth and fermentation were centrifuged at 5,000 g for 10 min, followed by DCW and analysis of various sugars and metabolites including glucose, xylose, ethanol, xylitol, glycerol and acetic acid. Sugars and metabolites were analyzed using HPLC (Agilent Technologies) with HiPlex H column. All the experiments were carried out in triplicate, and the given values are the mean values.

KINETICS

Fermentation kinetic parameters were calculated according to Sharma et al. [3].

RESULT AND DISCUSSIONS

Potential of adapted strain *K. marxianus* NIRE-K3.1 for xylose uptake during growth and fermentation was compared with native strain.

ADAPTATION OF *K. MARXIANUS* NIRE-K3

An evolutionary adaptation was approached on *K. marxianus* NIRE-K3 through sequential culturing in YEP medium containing 20 g l^{-1} xylose. The reliability of strategy was evaluated by monitoring improvement in growth and sugar assimilation after each batch. Up to first 10 batches exponential xylose utilization was observed i.e. *K. marxianus* NIRE-K3 reached 29.1% from 17.43%, which was 1.66-fold higher than that of native culture (FIGURE 1). After 50 batches, *K. marxianus* NIRE-K3 utilized 82.28% of initial sugar i.e. 16.45 g l^{-1} out of20 g l^{-1}. Simultaneously, 5.8 g l^{-1} cell mass was produced. Furthermore, reculturing was continued up to 60 batches and 86.28% of xylose utilization was observed with the formation of 5.9 g l^{-1} cell mass (FIGURE 1).
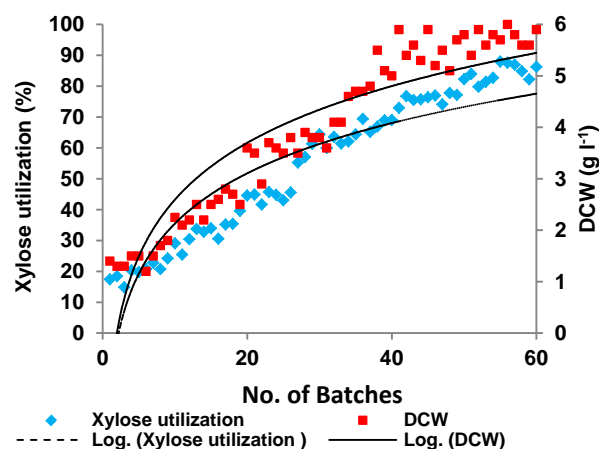
FIGURE 1. ADAPTATION OF *K. MARXIANUS* NIRE-K3 IN YEPX MEDIA

COMPARATIVE GROWTH ANALYSIS OF *K. MARXIANUS* NIRE-K3 and NIRE-K3.1

Improvement in adapted culture was observed by analysing growth parameters. Both native and adapted strains were cultivated as described above. In xylose containing medium, *K. marxianus* NIRE-K3.1 utilized 16.93 ± 0.36 g l^{-1} xylose along with shorter lag phase, whereas NIRE-K3 utilized only 5.35 ± 0.23 g l^{-1} xylose (FIGURE 2). There was significant improvement in specific growth rate of NIRE-K3.1 (0.075 ± 0.01 h^{-1}) as compared to NIRE-K3 (0.02 ± 0.003 h^{-1}), which was 3.75-fold higher in NIRE-K3.1 (Table 1). Further, xylose uptake rate in NIRE-K3.1 was 0.38 ± 0.02 g g^{-1} h^{-1},whereas, NIRE-K3 showed only 0.13 ± 0.01 g g^{-1} h^{-1} (Table 1). Similarly, ethanol and xylitol yields of NIRE-K3.1 were

6.67 and 2.42-fold higher than that of NIRE-K3, respectively. However, cell yield ($Y_{x/s}$, g g^{-1}) of NIRE-K3.1 was 0.22 ± 0.01 g g^{-1} whereas, NIRE-K3 showed 0.43 ± 0.06 g g^{-1} cell yield on xylose (Table 1). On the other hand, growth of NIRE-K3 and NIRE-K3.1 was also compared in glucose containing medium (FIGURE 3). Both the strains showed smilar specific growth rate (μ_{max}, h^{-1}) and cell yield ($Y_{x/s}$, g g^{-1}) (Table 1). However, ethanol yield of NIRE-K3.1 was 1.17-fold higher than NIRE-K3 on glucose (Table 1). In present study, evolutionary adaptation on *K. marxianus* NIRE-K3 resulted an improved aerobic growth on xylose as carbon source.

FERMENTATION PROFILE OF *K. MARXIANUS* NIRE-K3 AND NIRE-K3.1

A comparative fermentation analysis of *K. marxianus* NIRE-K3 and NIRE-K3.1 was carried out as discribed. During fermenatation, *K. marxianus* NIRE-K3.1 utilized 28.92 ± 0.2 g l^{-1} xylose whereas NIRE-K3 utilized only 7.26 ± 0.22 g l^{-1} xylose in 72h, respectively (FIGURE 4). Similarly, in the same duration of fermentation *K. marxianus* NIRE-K3.1 produced 4.67 ± 0.33 and 15.7 ± 0.4 g l^{-1} ethanol and xylitol, whereas, *K. marxianus* NIRE-K3 produced only 0.48 ± 0.02 and 3.39 ± 0.15 g l^{-1} ethanol and xylitol, respectively (FIGURE 4). Moreover, volumetric substrate uptake (Q_S) in *K. marxianus* NIRE-K3.1 was 0.40 ± 0.002 g l^{-1}h^{-1} while NIRE-K3 showed 0.1 ± 0.003 g l^{-1}h^{-1} (Table 2). Xylitol yield ($Y_{p/s(xylitol)}$ = 0.54 ± 0.015 g g^{-1}), ethanol yield ($Y_{p/s(ethanol)}$ = 0.16 ± 0.01 g g^{-1}) andvolumetric product productivity ($Q_{p(xyitol)}$= 0.22 ± 0.005 g l^{-1}h^{-1}); ($Q_{p(ethanol)}$ = 0.065 ± 0.004 g l^{-1}h^{-1}) of *K. marxianus* NIRE-K3.1 were more than that of NIRE-K3 cells as $Y_{p/s (xyitol)}$ (0.46 ± 0.035 g g^{-1}), $Y_{p/s (ethanol)}$ (0.066 ± 0.0042 g g^{-1}) and $Q_{p (xylitol)}$ (0.047 ± 0.002 g l^{-1}h^{-1}), $Q_{p (ethanol)}$ (0.007 ± 0.0003 g l^{-1}h^{-1}) (Table 2).

FIGURE 3. COMPARISON OF GROWTH PATTERN BETWEEN NATIVE (----) AND ADAPTED YEAST (——); USING GLUCOSE AS A CARBON SOURCE, (Δ) RESIDUAL GLUCOSE; (■) DCW; (●) ETHANOL.

Table 1: Growth kinetics of *K. marxianus* NIRE-K3 and NIRE-K3.1

Kinetic parameters	*K. marxianus* NIRE-K3		*K. marxianus* NIRE-K3.1	
Growth	Glucose	Xylose	Glucose	Xylose
Specific growth rate (μ_{max}, h^{-1})	0.29±0.01	0.02±0.003	0.31±0.01	0.075±0.01
Ethanol yield ($Y_{p/s}$, g g^{-1})	0.35±0.007	0.009±0.001	0.41±0.002	0.06±0.001
Xylitol yield ($Y_{p/s}$, g g^{-1})	-	0.07±0.009	-	0.17±0.01
Cell yield ($Y_{x/s}$, g g^{-1})	0.26±0.005	0.43±0.06	0.27±0.002	0.22±0.01
Specific sugar consumption rate (Xylose) (q_s, g g^{-1} h^{-1})	-	0.13±0.01	-	0.38±0.02

FIGURE 2. COMPARISON OF GROWTH PATTERN BETWEEN NATIVE (----) AND ADAPTED YEAST(UP TO 60 BATCHES) (——) USING XYLOSE AS A CARBON SOURCE; (♦) RESIDUAL XYLOSE; (■) DCW.
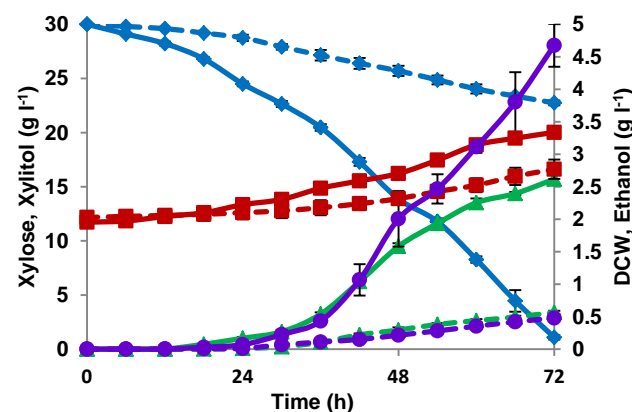
FIGURE 4. FERMENTATION PROFILE OF NATIVE (----) AND ADAPTED CULTURES (——)USING XYLOSE AS A CARBON SOURCE; (♦) XYLOSE; (■) DCW; (●) ETHANOL; (▲) XYLITOL.

Table 2: Fermentation kinetics of native and adapted culture

Kinetic parameters	*K. marxianus* NIRE-K3	*K. Marxianus* NIRE-K3.1
Ethanol ($P_{ethanol}$, g l^{-1})	0.42±0.02	4.67±0.33
Xylitol ($P_{xylitol}$, g l^{-1})	3.39±0.15	15.7±0.4
Cell yield ($Y_{x/s}$, g g^{-1})	0.10±0.015	0.047±0.0019
Ethanol yield ($Y_{p/s}$, g g^{-1})	0.066±0.0042	0.16±0.01

Xylitol yield ($Y_{p/s}$, g g^{-1})	0.46±0.035	0.54±0.015
Volumetric substrate uptake (Q_s, g l^{-1}h^{-1})	0.10±0.003	0.40±0.002
Volumetric product productivity (Ethanol) (Q_p, g l^{-1}h^{-1})	0.007±0.0003	0.065±0.004
Volumetric product productivity (Xylitol) (Q_p, g l^{-1}h^{-1})	0.047±0.002	0.22±0.005
Specific sugar consumption rate (Xylose) (q_s, g g^{-1} h^{-1})	0.012±0.001	0.061±0.0014
Specific product formation rate (Ethanol) (q_p, g g^{-1} h^{-1})	0.0016±0.0003	0.025±0.001
Specific product formation rate (Xylitol) (q_p, g g^{-1} h^{-1})	0.011±0.001	0.08±0.0016
Conversion rate (%) into ethanol	13.23±0.83	32.35±2.47
Conversion rate (%) into xylitol	46.40±3.49	53.75±1.51

DISCUSSION

The results obtained after evolutionary adaptation of *K. marxianus* NIRE-K3 has been proven the significance of strategy for the development of strain. Moreover, the evolved strain *K. marxianus* NIRE-K3.1 has been showed noteworthy improvement in the xylose uptake during growth and fermentation. During growth,*K. marxianus* NIRE-K3.1 showed 2.92-fold higher specific xylose uptake rate than that of NIRE-K3 (Table 1). Similarly, NIRE-K3.1 showed comparatively higher xylitol and ethanol yield during growth (Table 1). The possible reason behind may be decrease in cell yield of NIRE-K3.1, which was 1.95-fold lower as compared to NIRE-K3 (Table 1). Liu et al. [9]; developed a xylose utilizing *S. cerevisiae* through combination of genetic engineering and adaptation, which showed improved xylose utilization with higher specific growth rate (0.225 h^{-1}) than native recombinant strain (0.055 h^{-1}) by using xylose as carbon source under aerobic environment. It was also recommended that the adapted strain has much shorter lag phase than that of unadapted strain [10, 11]. By understanding the aforesaid results, significance of evolutionary adaptation has been rationalized, since the adapted culture could be more stable and could ferment sugar in comparatively less time. Further, *K. marxianus* NIRE-K3.1 showed 3.98-fold higher xylose utilization with 1.16 and 2.44-fold higher ethanol and xylitol yields, respectively than NIRE-K3 in anaerobic environment (Table 2). Similarly, volumetric xylose uptake in *K. marxianus* NIRE-K3.1 was also 4-fold higher than that of NIRE-K3 (Table 2). In the same environment, xylitol and ethanol yields of *K. marxianus* NIRE-K3.1 were 1.17 and 2.42-fold higher than that of NIRE-K3, respectively (Table 2). However, cell yield of *K. marxianus* NIRE-K3.1 was 2.12-fold lower than that of NIRE-K3 under anaerobic environment as similar as aerobic environment (Table 2). Several researchers acquired adaptation strategy on ethanologens to enhance xylitol and ethanol yield from lignocellulosic biomass [9]. Further, adaptation strategy also stabilizes heterologous gene expression in mutant strains [12, 13]. The aforesaid illustrations signify the success of adaption, also its importance to develop a process for production of ethanol and other value added products from lignocellulosic biomass.

CONCLUSION

Growth and fermentation study of adapted strain *K. marxianus* NIRE-K3.1 showed significant decrease in lag phase and improved xylitol and ethanol yield. Moreover, *K. marxianus* NIRE-K3 showed higher productivity of ethanol and xylitol. Higher xylose utilization rate was observed through adaptation. However, xylitol production could be enhanced by blocking the pathway or ethanol production could be enhanced through prevention of xylitol efflux.

ACKNOWLEDGMENTS

REFERENCES

[1] Kumar, S., Singh, S. P., Mishra, I. M., Adhikari, D. K., 2009. "Recent advances in production of bioethanol from lignocellulosic biomass". Chem Eng Technol, 32, pp. 517-526.

[2] Kumar, S., Singh, S. P., Mishra, I. M., Adhikari, D. K., 2010. "Feasibility of ethanol production with enhanced sugar concentration in bagasse hydrolysate at high temperature using *Kluyveromyces* sp. IIPE453". Biofuels, 1, pp. 697-704.

[3] Sharma, N. K., Behera, S., Arora, R., Kumar, S., 2016. "Enhancement in xylose utilization using *Kluyveromyces marxianus* NIRE-K1 through evolutionary adaptation approach". Bioprocess Biosyst Eng, 39, pp. 835-843.

[4] Kuhad, R. C., Gupta, R., Khasa, Y. P., Singh, A., Zhang, Y. H. P., 2011. "Bioethanol production from pentose sugars: current status and future prospects". Ren Sus Energy Rev, 15, pp. 4950-4962.

[5] Sharma, N. K., Behera, S., Arora, R., Kumar, S., 2014. "Genetic modification in yeast for simultaneous utilization of glucose and xylose". Kumar, S., Sarma, A. K., Tyagim, S. K., Yadav, Y. K., Eds., Recent advances in bioenergy research, Vol III. SSS-NIRE, Kapurthala, pp 194–207.

[6] Liu, E., Hu, Y., 2010. "Construction of a xylose-fermenting *Saccharomyces cerevisiae* strain by combined approaches of genetic engineering, chemical mutagenesis and evolutionary adaptation". Biochem Eng J, 48, pp. 204-210.

[7] Zhang, B., Li, L., Zhang, J., Gao, X., Wang, D., Hong, J., 2013. "Improving ethanol and xylitol fermentation at elevated temperature through substitution of xylose reductase in *Kluyveromyces marxianus*". J Ind Microbiol Biotechnol, 40, pp. 305-316.

[8] Pereira, S. R., Sanchez, I., Nogue, V., Frazao, C. J., Serafim, L. S., Gorwa-Grauslund, M. F., Xavier, A. M., 2015. "Adaptation of *Scheffersomyces stipitis* to hardwood spent sulfite liquor by evolutionary engineering". Biotechnol Biofuels, 8, pp. 50.

[9] Liu, E., Hu, Y., 2010. "Construction of a xylose-fermenting Saccharomyces cerevisiae strain by combined approaches of genetic engineering, chemical mutagnesis and evolutionary adaptation". Biochem Eng J, 48, pp. 204-210.

[10] Mihoub, F., Mistou, M. Y., Guillot, A., Leveau, J.Y., Boubetra, A., Billaux, F., 2003. "Cold adaptation of Escherichia coli: microbiological and proteomic approaches". Int J Food Microbiol, 89,171-184.

[11] Landaeta, R., Aroca, G., Acevedo, F., Teixeira, J. A., Mussatto, S. I., 2013. "Adaptation of a flocculent *Saccharomyces cerevisiae* strain to lignocellulosic inhibitors by cell recycle batch fermentation". Appl Energy, 102, pp. 124-130.

[12] Diao, L., Liu, Y., Qian, F., Yang, J., Jiang, Y., Yang, S., 2013. "Construction of fast xylose-fermenting yeast based on industrial ethanol-producing diploid *Saccharomyces cerevisiae* by rational design and adaptive evolution". BMC Biotechnol. 13, pp. 110.

[13] Lee, S. M., Jellison, T., Alper, H. S., 2014. "Systematic and evolutionary engineering of a xylose isomerase-based pathway in Saccharomyces cerevisiae for efficient conversion yields". Biotechnol Biofuels, 7, pp. 122.

A NOVEL PROCESS FOR PRODUCTION OF PREBIOTIC AND FUNCTIONAL BIOMOLECULES FROM BY-PRODUCTS OF CANE SUGAR AND DAIRY INDUSTRIES

Kusum Lata
CIAB Mohali
Email: kusum.nigam@gmail.com

Manisha Sharma
CIAB Mohali
Email: manishasharma@ciab.res.in

Satyanarayan Patel
CIAB Mohali
Email: satyanarayan@ciab.res.in

Rajender Singh Sangwan
CIAB Mohali
Email: sangwan@ciab.res.in

Sudhir Pratap Singh
CIAB Mohali
Email: sudhirsingh@ciab.res.in

ABSTRACT

Molasses is a dark viscous fluid generated as by-product in a huge volume, in a proportional to the production of sugar, during the processing of sugarcane juices into table sugar in cane industry. At present, molasses is largely used for ethanol production. However, efforts have been made to use this by-product for the synthesis of value added molecules such as succinic acid, citric acid, biosurfactants, trehalose, astaxanthin, poly L-diaminopropionic acid, L-ornithine, erythritol, lactic acid, etc. Whey is a processing waste liquid generated during the preparation of milk derived products such as cheese and paneer from milk. Liquid whey has been attempted to process in several products ranging from whey powder to fractionated biomolecules such as lactose, lactoglobilins, lactalbumin, bioactive peptides etc. However, disposal of these large volume agro-industrial wastes, cane molasses and dairy wastes, into the environment poses a serious hazardous impact on environment due to high BOD and COD value of these wastes, and, thus, their disposal is highly contaminating. Therefore, it is desirable to develop novel approached for the transformation of agro-industrial wastes into high value biomolecules. We have developed an integrated bioprocessing approach for simultaneous utilization transformation of cane molasses and whey for production of prebiotic and functional ingredients. The integrated bioprocessing approach employed microbial cells expressing proteins with catalytic activities of glucosyltransferase and sugar isomerization/epimerization or cell free enzyme preparation therefrom. The enzymatic bioprocessing of the feedstock derived from molasses and whey resulted the production of prebiotic trisaccharide molecules, 2-α-D-glucopyranosyl-lactose. Quantitative analysis estimated production of about 166 trisaccharide (2-α-D-glucopyranosyl-lactose) per kg of fresh cane molasses. During the glucosyltransferase acceptor dependent reaction free D-fructose is generated as byproduct. We have developed a chimeric protein, Smt3-d-psicose 3-epimerase, with improved operational stability and better catalytic efficiency. The enzymatic treatment of the glucosyltransferase treated feedstock led to D-allulose production to the extent of 25–30% conversion (w/w) of D-fructose present in the reaction. Further, the feedstock treated by glucosyltransferase was sequentially contacted with the biocatalysts, β-galactosidase and L- arabinise isomerase. The catalytic action of β- D- glactosidase on trisaccharides generated kojibiose and galactose. The catalytic action of L- arabinise isomerase resulted bioconversion of 15-20% D-galactose into D-tagatose. Thus, we developed an integrated bioprocessing of cane molasses and whey for the production of prebiotic and functional ingredients employing multi-biocatalysts approach. The aforementioned process is IPR protected.

Keywords: glucosyltransferase, β-galactosidase, L-arabinise isomerise, prebiotics, 2-α-D-glucopyranosyl-lactose
.

SEEC-2017-66

OPTIMUM DESIGN OF PV-WIND-BIOMASS-FUEL CELL BASED POLYGENERATION SYSTEM BY USING META HEURISTIC ALGORITHM

Avishek Ray
Department of Mechanical Engineering
Jadavpur University
Email: avi_rkm@yahoo.co.in

Kuntal Jana
Department of Mechanical Engineering
Jadavpur University
Email: kuntaljana@gmail.com

Sudipta De
Department of Mechanical Engineering
Jadavpur University
Email: de_sudipta@rediffmail.com

Mohsen Assadi
Faculty of Science and Technology
University of Stavanger, Norway
Email: mohsen.assadi@uis.no

ABSTRACT

In some remote villages grid connectivity is almost impossible due to terrain conditions. Decentralised generation may be a suitable option for the electrifiucation of these villages. The decentralised generation may be achived by diesel generator sets or renewable sources of energy. Renewable sources of energy are clean sources of energy but these are intermittently available. Moreover the initial investment for the renewable sourcs of energy are high. So to supply uninterrupted power renewable energy systems needs either storage facility or one or more renewable energy systems need to be hybridised together. In this paper a renewable energy system is modelled using solar photovoltaic, wind turbine, biogas systems, biomass gasifier, electrolyser and a fuel cell to supply electricity in a hamlet. In this paper the size of the individual components are calculated using Cuckoo Search algorithm.The economic value of other utility outputs reduces the Levelized Cost of Electricity.

Keywords :Polygeneration, *Cuckoo Search*, *Hydrogen*
.

NOMENCLATURE

BG	Biomass Gas
CPV_{total}	Cost of PV module, INR
CFC_{total}	Cost of fuel cell, INR
CW_t	Total cost of wind turbine, INR
CE_{total}	Total cost of electrolyser, INR
CH_{2store}	Total cost of hydrogen storage, INR
D	Cost of cattle dung, INR/kg
EL	Electrolyser
I_t	Total radiation on a tilted surface, Watt/m^2
I_b	Beam radiation on a tilted surface, Watt/m^2
I_d	Diffuse radiation on a tilted surface, Watt/m^2
θ	Angle of incidence of solar radiation, radians
θ_z	Zenith angle, radians
δ	Declination angle, radians
φ	Latitude of the place, radians
ω	Hour angle, radians
ρ	Albedo
β	Collector slope, radians
$V_{mp}(t)$	Instantaneous output voltage
$I_{mp}(t)$	Instantaneous output current
I_{sc}	Short circuit current
T_a	Ambient temperature
T_r	Reference temperature
TU	Total units of electricity generated, kWh
V	Wind velocity.m/s
C_p	Betz limit
U	Annualised total selling price of all utltities except electricity, INR
PEM	Proton Exchange Membrane
P_{biogas}	Instantaneous power output of biomass gasifier, kW
PV	Photovoltaic
P_{wind}	Power generated by wind turbine, kW
LCOE	Levelized Cost of Electricity
$L_{solarkw}$	Land requirement per kW of solar PV,m^2
$L_{biogaskw}$	Land requirement per kW of solar, m^2
MH	Metal Hydride Storage
GHG	Green House Gas
CS	Cuckoo Search
GE	Gas Engine
PEMFC	Proton Exchange Membrane Fuel Cell
WT	Wind Turbine
WHRS	Waste Heat Recovery System

1.INTRODUCTION

Resource management is an effective way to provide clean energy to the people at a reasonable cost. Hence generating power and other utilities from the locally available resources may lead tothe solution for sustainable energy supply. The primary energy consumption has increased steadily over time. Moreover energy has to be supplied when it is required. So storing of energy is a significant issue for reliable power supply. The fossil fuel reserves are also diminishing. The renewable sources are clean sources of energy but these sources are generally intermittent in nature. Jana and De [1] designed a suitable polygeneration system using biomass as the local resource. They have shown that 20% of the primary energy savings is achieved by the process integration. This also leads to reduction of 25kt carbon –dioxide emission per annum. Saeed Belgana et al [2] designed a hybrid renewable energy system with photovoltaic (PV) panel, wind turbine , diesel generator set and a battery bank using the Multi Objective Optimization technique to optimise the annualised system cost and the reliability of power supply of the system.

In this paper, a polygeneration system has been designed using solar photovoltaic module, wind turbine, PEM electrolyser, a PEM fuel cell, a biogas digester coupled with a gas engine , a biomass gasifier-gas engine and a metal hydride storage facility to supply electricity, potable water, hydrogen and process heat as the four utility outputs. The levelized cost of electricity (LCOE), land requirement and green house gas (GHG) emission are the three objective functions. All these components are to be minimized. The objective function is formulated using the weighted sum method. The optimization is carried out using the Cuckoo Search (CS) algorithm .

2. SYSTEM DESCRIPTION

The proposed renewable energy based polygeneration system as shown in Fig 1.

FIG 1: SCHEMATIC OF POLYGENERATION SYSTEM
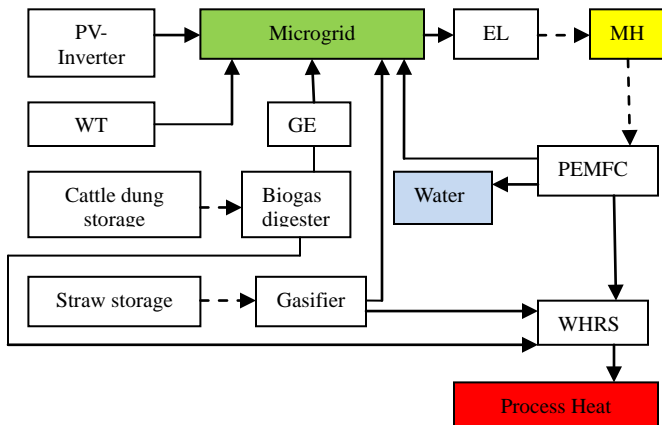
During daytime the solar module generates electricity. Electricity is also generated by the wind turbine in different magnitudes depending on the instantaneous velocity of the wind. The excess electricity which is not used to cater the instantaneous load is fed to the PEM electrolyser to generate hydrogen. The hydrogen is stored in a metal hydride tank.The hydrogen is fed to a PEM fuel cell during night to generate electricity. The hydrogen which remains in excess after meeting the electrical load is sold as fuel.. There is excess hydrogen at many instances because of the variation of the magnitude of the electrical load , solar radiation and wind speed throughout the day in different seasons. The PEMFC generates waste heat and potable water which are two other utility outputs. During night the electrical demand is met by biomass gasifier-gas engine, biogas engine and the fuel cell.

2.1 Modelling of PV system

The solar insolation is incident on the solar panels which generates electricity by the following equation. The module is placed south. The total solar radiation on a tilted surface is given by the following equation [3].

$$I_T = I_b r_b + I_d r_d + (I_b + I_d) r_r \qquad (1)$$

The tilt factor for the beam radiation r_b for a south facing surface is given by the following equation [4].

$$r_b = (\cos θ)/(\cos θz) \qquad (2)$$

The angle of incidence θ is given for a south facing surface is given by [4]

$$\cos θ = \sinδ\sin(φ-β)+\cosδ\cos(φ-β)\cosω \qquad (3)$$

The Zenith angle θz for a collector facing due south is given by [4]

$$\cos θz = \sinδ\sinφ + \cosφ\cosδ\cosω \qquad (4)$$

The tilt factor for diffuse radiation r_d is given by [4]

$$r_d = \frac{1+\cosβ}{2}$$

The tilt factor for the reflected radiation is given by

$$r_r = = \frac{(1-\cosβ)ρ}{2} \qquad (5)$$

The instantaneous output voltage $V_{mp}(t)$ and instantaneous output current $I_{mp}(t)$ of a PV module is given by the following equations [5]

$$V_{mp}(t) = V_{max} [1+0.0539 \log (\frac{I_{incident}}{I_{standard}})] + αTa(t) + 0.02 I_{incident} \qquad (6)$$

$$I_{mp}(t) = [I_{sc} + sTa(t) – Tr] \times (\frac{I_{incident}}{I_{standard}}) \qquad (7)$$

The instantaneous power output of the solar module is given by

$$P_{solar}(t) = I_{mp}(t) \times V_{mp}(t) \qquad (8)$$

2. 2 Modelling of the biogas system

The biogas is produced in an anaerobic biogas digester from the cattle dung available in the village. Almost 70% is used in the cooking purpose. The rest is used in

the gas engine to produce electricity at night by the following equation [5].

$$P_{biogas}(t) = \frac{BGavail \times CVbio \times \eta}{365 \times Operating\ hours\ per\ day} \quad (9)$$

2.3 Modelling of the PEM electrolyser

The instantaneous amount of hydrogen $H_{elec}(t)$ produced by the PEM electrolyser is

$$H_{elec}(t) = (E_{elec}(t) \times \frac{\eta_{elec}}{CV_{hydro}}) \quad (10)$$

2.4 Modelling of PEM fuel cell

The hydrogen generated by the electrolyser is stored in the metal hydride storage. Then the hydrogen is fed to the fuel cell to generate electricity. The electricity generated by the fuel cell E_{fc} is given by

$$E_{fc} = H_{fc} \times CV_{hydro} \times \eta_{fc} \quad (11)$$

The waste heat generated by the fuel cell W_{fc} is given by

$$W_{fc} = H_{fc} \times CV_{hydro} \times (100-\eta_{fc}) \quad (12)$$

2.5 Modelling of Metal hydride tank

The metal hydride tank is designed to store the hydrogen for one day even when the solar radiation is least.

2.6 Modelling of Wind turbine

The instantaneous power output P_{wind} of a wind turbine is given by

$$P_{wind} = 0.5 \times A \times \sigma \times v^3 \times C_p \quad (13)$$

3. Calculation of Land requirement

The land requirement L for the entire polygeneration is given by

$$L = L_{solarkw} \times PV_{installed} + L_{biogaskw} \times BG_{installed} \quad (14)$$

The land requirement of the other components are much less and hence not included here.The land requirement for solar PV and biogas systems are 30 m^2/kWand 144m^2/kW respectively.

4. Calculation of GHG emission

The GHG emission is given by

$$G = G_{S \times} PV_{installed} + F_g \times F_{installed} + BG_g \times BG_{installed} + G_g \times G_{installed} \quad (15)$$

The GHG emission for PV, FC, WT and biogas system in g-CO$_2$/kWh is 98,70,100,102 [6] respectively.
in various domains related to energy.

5. ECONOMIC MODELLING

The economic model is essential to make the polygeneration socially acceptable to the villagers. The various input data for economic modelling is shown in Table 1.

Serial No	Name of component	Value
1	1 USD	60 INR
2	1 CHF	70.18
3	Cost of fuel cell per kW	30 USD
4	Solar Module cost per watt peak	1.02 USD
5	Electrolyser capital cost per kW	1090 CHF
6	Cost of hydrogen storage per kg for metal hydride storage	100 INR
7	Cost of hydrogen transportation per kg for metal hydride transport via roadways	170 INR
8	Cost of hydrogen per kg	3.70 USD
9	Cost of distil water per litre	20 INR
10	Utility heating price	0.8 INR/kWh
11	Cost of cattle dung	0.2 INR/kg
12	Cost of waste heat recovery systems for heating utility per kW	100 INR
13	Plant life	25 years
14	Efficiency of PEM fuel cell	65%^{m}
15	Efficiency of gas engine	27%
16	Efficiency of PEM electrolyser	80%^{o}
17	Efficiency of PV	14%

5.1 Cost Of Solar PV

The total cost of PV installation, CPV_{total} is given by

$$CPVtotal = P_{solarkw} \times PV_{installed} \quad (16)$$

5.2 Cost of Fuel cell

The total cost of fuel cell installation, CFC_{total} is given by

$$CFC_{total} = P_{fckw} \times FC_{installed} \quad (17)$$

Where Pfckw is the cost of fuel cell per watt and FCinstalled is the total installed capacity of the fuel cell system.

5.3 Cost Of Biogas System

The cost of biogas systems do not increase linearly with scale. The cost of biogas system is given by the following equation [7].

$$C_{eqb} = Ceqa \left(\frac{Capacity_b}{Capacity_a}\right)^S \quad (18)$$

5.4 Cost Of Electrolyser

The initial cost of electrolyser, E_{total} is given by

$$CE_{total} = P_{elec} \times EL_{installed} \quad (19)$$

5.5 Cost Of Hydrogen Storage

The cost of hydrogen storage H2store is given by

$$CH_{2store} = H_{2storeperkg} \times H_{2reqperday} \quad (20)$$

5.6 Cost Of WT

The total cost of wind turbine installation

$$CWT = WT_{ins} \times WT_{cap} \quad (21)$$

5.7 Calculation of LCOE

The LCOE is a convenient tool to assess the competitiveness of different generating technologies. The LCOE is calculated taking into consideration the capital cost, fuel cost, fixed and variable operation and maintenance cost and an assumed utilization rate for each type of plant.

LCOE=

$$\frac{CPVtotal + CFCtotal + C_{eqb} + CElectrototal + CH2store + +D+WH-U}{TU} \quad (22)$$

6 Optimization Scheme

Cuckoo Search is a nature inspired metaheuristic algorithm that has been broadly used for solving hard-hitting optimization problems. The detail operation of the algorithm in this optimization problem is shown in. CS is based on the brood parasitism of the cuckoo species. It also uses a balanced composition of a local random walk and global explorative random walks, controlled by a switching parameter p_a. The local random walk can be defined by the following equation [8]:

$$x_i^{t+1} = x_i^t + \alpha s \otimes H(p_a - \epsilon) \otimes \theta(x_j^t - x_k^t) \quad (23)$$

x_j^t and x_k^t are two different candidate solutions selected randomly by random permutation, H is a Heaviside function, ϵ is a random number drawn from a uniform distribution and s is the step size. Here, $\otimes \theta$ stands for the entry-wise of two vectors.

7 RESULTS AND DISCUSSIONS

In this paper, the size of the various components of the polygeneration system is shown in Table 2 which is determined by the CS algorithm by developing a programme in MATLAB 2013.

Table 2: Optimized size of the components

Serial No	Name of component	Size
1	PV	117.623kW
2	Wind turbine	2.745
3	Fuel Cell	60.213 kW
4	Gas Engine	1 kW
5	Land required	3654 m^2

8 Conclusion

Thus it can be seen that by the process integration the electricity can be produced at a comparable rate. Thus the electricity with other three utilities can be produced in a environment friendly manner. The process integration increases the efficiency of the entire system. Thus it is a means of proper resource management.

ACKNOWLEDGEMENTS

REFERENCES

[1] Jana, K., De, S., 2015. Sustainable polygeneration design and assessment through combined thermodynamic, economic and environmental analysis. Energy, 91, pp. 540-555

[2] Belgana,S., Alba D, Hasnae B, Mohammed M, 2013. IEEE Int. Conf. Renew. Energy Res. Appl., Madrid

[3] Ghribi, D.,Khelifa,A., Diaf,S.,Belhamel,M., 2013.Study of hydrogen production by using PV solar energy and PEM electrolyser in Algeris. International Journal o Hydrogen nergy;38; 3480-3490.

[4] Solanki, C., ed 2009. Solar Photovoltaics, Fundamentals, technologies and Applications, PHI Learning Private Limited

[5] Chauhan A., Saini, R., 2016. Discrete harmony search based size optimisation of Integrated Renewable Energy System for remote rural areas of Uttarakhand state in India. Renewable Energy, 94, pp. 587-604

[6] Akella A.K, Saini RP., SharmaMP., Social, economic and environmental impacts of renewable energy systems, 2009 Renewable Energy. 390–396.

[7] Jana, K., De, S., 2015. Polygeneration using agricultural waste: Thermodynamic and economic feasibility study. Renewable Energy, 91, pp. 540-555

[8] Yang X., ed 2014. Nature Inspired Optimization Algorithm. Elsevier

SEEC-2017-067

EFFICIENT AND COST EFFECTIVE RECOVERY OF XYLITOL PRODUCED BY FERMENTATION OF CORN COB ACID HYDROLYSATE

Vinod Kumar
CIAB Mohali
Email: vinodudsc@gmail.com
Rajender S. Sangwan
CIAB Mohali
Email: sangwan.lab@gmail.com

Meena Krishania
CIAB Mohali
Email: meena@ciab.res.in

ABSTRACT

Xylitol, a five-carbon sugar alcohol, is a valuable sugar substitute and is widely used in the pharmaceutical, odonatological and food industry due to its low-calorie sugar properties. In the past decades, the xylitol industry has grown rapidly and more attention has been focused on xylitol purification. In this report, a useful process purification and crystallisation of xylitol from the fermentation broth of using corncob hydrolysates as the substance was developed. The hydrolysate obtained by acid hydrolysis of corncobs was detoxified with charcoal, concentrated and fermented using Candida tropicalis. After biomass removal, the fermentation medium that contained xylitol (0.6249 kg/kg) along with minor amounts of inorganic components, proteins, non-fermented sugars (xylose and arabinose). This medium was containing xylitol subjected to sequential through steps by process charcoal treatment and ion exchange process to obtain food-grade xylitol. Charcoal treatment experiments were carried out at various solid-to-liquor ratios. Under optimal conditions (20 g of charcoal/1 kg of liquors), almost total decoloration was achieved. The resulting liquor was concentrated by evaporation to increase xylitol concentration, and further desalted with a combination of two ion-exchange resins (H+ and OH-), refined liquors (containing 0.7303 kg of xylitol/kg) were concentrated again. Under selected conditions, 43.7% of xylitol contained in the initial fermentation broth was recovered xylitol accounted for 75-80% of the total oven-dry weight. Material balances are presented for the whole processing scheme considered in this work.

Keywords: Hydrolysis, detoxification, Fermentation

SEEC-2017-68

A NOVEL SURFACTANT ASSITED TRANSITION METAL PRETREATMENT OF CHILI POST HARVEST RESIDUE FOR THE PRODUCTION OF BIOETHANOL

Raveendran Sindhu
Centre for Biofuels, National Institute for Interdisciplinary Science and Technology, CSIR, Trivandrum - 695 019, India
Email: sindhurgcb@gmail.com

Parameswaran Binod
Centre for Biofuels, National Institute for Interdisciplinary Science and Technology, CSIR, Trivandrum - 695 019, India

Amith Abraham
Centre for Biofuels, National Institute for Interdisciplinary Science and Technology, CSIR, Trivandrum - 695 019, India

Ashok Pandey
Centre for Biofuels, National Institute for Interdisciplinary Science and Technology, CSIR, Trivandrum - 695 019, India
Center of Innovative and Applied Bioprocessing, Mohali 160 071, Punjab, India

Kamal Jerina
Centre for Biofuels, National Institute for Interdisciplinary Science and Technology, CSIR, Trivandrum - 695 019, India

Anil Kuruvilla Mathew
Centre for Biofuels, National Institute for Interdisciplinary Science and Technology, CSIR, Trivandrum - 695 019, India

Edgard Gnansounou
Ecole Polytechnique Federale de Lausanne, Institute of Urban and Regional Sciences, GC A3, Station 18, CH-1015, Lausanne, Switzerland

ABSTRACT

Increase in consumption as well as depletion of fossil fuels and environmental concerns about the consequences of burning fossil fuels leads to search for alternative renewable fuels. Lignocellulosic biomasses are plenteous in nature and are rich in celluloses which can be converted to fermentable sugars for the production of bioethanol. Lignocellulosic biomass is composed of cellulose, hemicelluloses and lignin. Many physio-chemical, structural and compositional factors hinder the enzymatic digestibility of cellulose present in the lignocellulosic biomass. Pretreatment is to be carried out to make cellulose accessible for enzymatic saccharification by the removal of hemicelluloses and lignin. A common pretreatment strategy cannot be used for all feed stock since there is large variation in composition even between samples of same biomass from different sources.

Chili post harvest residue is an underexploited lignocellulosic biomass and India has over a surplus availability of 0.5 million tons of this residue. Conversion of this feedstock to ethanol requires pretreatment to make it more accessible for the enzymes used in saccharification. Though several pretreatment regimens have been developed for addressing biomass recalcitrance, only very few seem to be promising as an industrial process. The aim of the study was to develop a novel surfactant- assisted transition metal pretreatment strategy to exploit the surplus available biomass in India- the chili post harvest residue for the production of bioethanol as well as to optimize various process parameters affecting pretreatment and hydrolysis.

NOMENCLATURE

CPHR   Chili post harvest residue

SATMP   Surfactant assisted transition metal pretreatment

INTRODUCTION

Environmental, economic and national security concerns leads to research and developmental activities on renewable fuels and chemicals (Mosier et al., 2005). Burning fossil fuels release large amount of CO_2 which is a major cause of global warming.

Lignocellulosic biomass serves as a renewable source for the production of biofuels. It is composed of cellulose, hemicelluloses and lignin. Pretreatment is one of the major unit operations in lignocelluloses based biorefinery. Pretreatment alter the structure of lignocellulosic biomass and make cellulose accessible for enzymatic saccharification and it is one of the most expensive steps in the conversion of lignocellulosic biomass to fermentable sugars (Lynd et al., 1996). The most common pretreatments currently in practice includes acid, alkali, organosolvents, organic acids or other chemicals. Most of the currently available pretreatment strategies are energy intensive and economically nonviable. An ideal pretreatment strategy should produce maximum reducing sugar and minimum degradation products.

The objective of the present study was to select the best transition metal for surfactant assisted transition metal pretreatment of chili post harvest residue (CPHR) and to optimize various process parameters affecting surfactant assisted transition metal pretreatment of CPHR (SATMP CPHR) and utilization of the hydrolyzate obtained after enzymatic saccharification for the production of bioethanol.

MATERIALS AND METHODS

Feed stock

Chili post-harvest residue (CPHR) received from Virudhanagar, Tamil Nadu, India was used in this study. The samples were dried and milled using a knife mill. Compositional analysis of native and pretreated samples was carried out by adopting NREL protocol (Sluiter et al., 2008).

Screening of various transition metals for surfactant assisted transition metal pretreatment of chili post-harvest residue (SATMP CPHR)

Initial screening experiments were carried out with four different transition metals ($FeSO_4$, $CuSO_4$, $ZnSO_4$ and $MnSO_4$) at an initial concentration of 1% w/w, biomass (solid) loading of 10% w/w and surfactant concentration of 3% w/w. Pretreatment carried out in a laboratory autoclave at 121°C for 60 min. After pretreatment the samples were used for hydrolysis after washing and drying.

Optimization of various process parameters affecting surfactant assisted transition metal pretreatment of chili post-harvest residue

Optimization of various process parameters affecting surfactant assisted transition metal pretreatment of CPHR was carried out by adopting a Taguchi design. The experiment consists of a total of 16 runs. The parameters selected were biomass (solid) loading, surfactant concentration, $FeSO_4$ concentration and pretreatment time. Parameters like biomass loading, surfactant concentration, $FeSO_4$ concentration and pretreatment time were selected at four levels.

Inhibitor analysis of the hydrolyzate

The hydrolyzate obtained after enzymatic saccharification of SATMP CPHR was centrifuged to remove the unhydrolyzed biomass and filtered through 0.2µm PES membrane filters (Pall, USA) and the filtrate was evaluated for inhibitors such as furfural, 5-hydroxymethylfurfural, citric acid, succinic acid, propionic acid, acetic acid and formic acid by HPLC. The inhibitors were analyzed using a photodiode array detector kept at 55°C. Rezex ROA columns (Phenomenex) were used with an injection volume of 10µl and flow rate was maintained at 0.6 ml/min. The concentrations of inhibitors were analyzed using the standard curve.

RESULTS AND DISCUSSION

Compositional analysis of native and pretreated chili post-harvest residue

Compositional analysis of the biomass revealed that the native biomass contains 39.95% cellulose, 17.85% hemicelluloses and 25.32% lignin. Control 1 (water alone) contains 41.05% of cellulose, 16.79% of hemicelluloses and 24.11% of lignin. SATMP CPHR contains 42.11% of cellulose, 11.23% of hemicelluloses and 12.13% of lignin. Mass balance analysis revealed a 31% loss of biomass during the pretreatment process. SATMP was found to be effective in removing hemicelluloses and lignin.

Screening profile of various transition metals for surfactant assisted transition metal pretreatment of chili post-harvest residue

Four different transition metals – $FeSO_4$, $CuSO_4$, $MnSO_4$ and $ZnSO_4$ at 1% w/w were used for initial screening to select the best transition metal for SATMP of CPHR. Control experiments were carried out with water alone Initial screening were carried out with 10% w/w of biomass (solid) loading, surfactant concentration of 3% w/w and pretreatment time of 60 min in a laboratory autoclave at 121°C. Control samples were the pretreatment carried with water alone gave a reducing sugar yield of 0.05 g/g. Surfactant assisted $MnSO_4$, $ZnSO_4$, $FeSO_4$ and $CuSO_4$ gave a reducing sugar yield of 0.076, 0.090, 0.160 and 0.122 g/g respectively. SATMP CPHR gave a better reducing sugar yield when compared to transition metal pretreated alone or surfactant pretreated alone samples. Since surfactant assisted $FeSO_4$ gave higher reducing sugar yield it was selected for further optimization of different process parameters affecting SATMP of CPHR by adopting a Taguchi design.

Effect of different process parameters on SATMP of chili post-harvest residue

Maximum reducing sugar yield (0.245 g/g) was observed in Run No: 2 where the conditions of pretreatment were surfactant concentration of 2% w/w, $FeSO_4$ concentration of 2% w/w, biomass loading of 5% w/w and pretreatment time for 20 min.
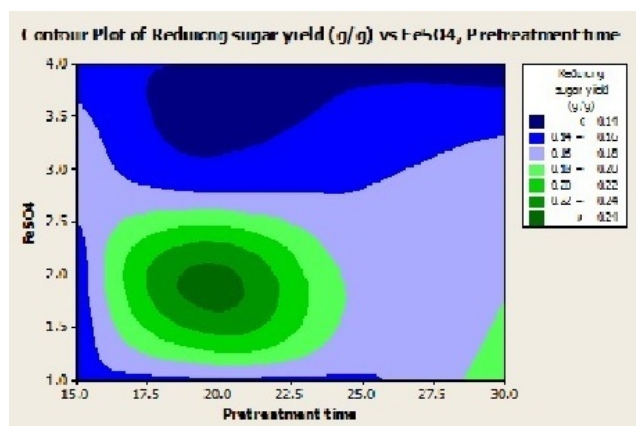
Fig.1. Contour plots showing interaction between pretreatment time and $FeSO_4$ concentration on reducing sugar yield

Fig. 1 shows an interaction between pretreatment time and $FeSO_4$ concentration. At low levels of pretreatment time (15 – 18 min) the reducing sugar yield is low (0.22 g/g). It increases with increase of pretreatment time (20 min). At low levels of $FeSO_4$ concentration (1.0 – 1.5% w/w) the reducing sugar yield is low (0.22 g/g); it increases with increase of $FeSO_4$ concentration. Maximum reducing sugar yield (0.24 g/g) was observed with middle levels of $FeSO_4$ concentration (1.5 – 2.0% w/w) and middle levels of pretreatment time (20-22 min).

Inhibitor profile of the hydrolyzate obtained after SATMP CPHR

Major fermentation inhibitors like furfural, 5-hydroxymethylfurfural and organic acids like formic acid, citric acid, succinic acid and propionic acid were absent in control and pretreated samples. Acetic acid was present in control and SATMP CPHR hydrolyzate.

CONCLUSION

Compositional analysis data revealed that hemicelluloses and lignin were removed during SATMP of CPHR. The major fermentation inhibitors like furfural, 5-hydroxymethyfurfural and organic acids like citric acid, succinic acid, formic acid and propionic acid were absent. Absence of inhibitors will eliminate the detoxification step. To the best of our knowledge, this is the first report on SATMP of CPHR. Fine tuning of various process parameters will make the process economically viable.

References

[1] Mosier, N., Wyman, C., Dale, B., Elander, R., Lee, Y. Y., Holtzapple, M., Ladisch, M., 2005. Features of promising technologies for pretreatment of lignocellulosic biomass. Bioresour. Technol. 93: 673-686.

[2] Lynd, L. R., Elander, R. T., Wyman, C. E., 1996. Likely features and costs of mature biomass ethanol technology. Appl. Biochem. Biotechnol. 57: 741-761.

[3] Sluiter A., B. Hames, R. Ruiz R, C Scarlata, J Sluiter, D. Templeton, and D. Crocker (2008) NREL Technical Report, NREL/TP-510-42618.

SEEC-2017-69

UTILIZATION OF CARROT POMACE FOR THE PRODUCTION OF INULINASE FROM *PENICILLIUM OXALICUM* BGPUP4

Ram Sarup Singh
Carbohydrate and Protein Biotechnology
Laboratory, Department of Biotechnology, Punjabi
University, Patiala, 147 002, Punjab, India

Kanika Chauhan & Jagroop Singh
Carbohydrate and Protein Biotechnology
Laboratory, Department of Biotechnology, Punjabi
University, Patiala, 147 002, Punjab, India

ABSTRACT

Inulinases are an important class of industrial enzymes which produces high fructose syrup (HFS) and fructooligosaccharides (FOSs) by degrading β, 2-1 linkages of inulin. Considering the importance of inulinases at industrial scale, it is the need of the day to develop easy and economical methods for inulinase production. In present study, response surface methodology has been implemented for the utilization of carrot pomace for inulinase production from Penicillium oxalicum BGPUP-4. A central composite rotatable design (CCRD) with 15 runs was practiced to optimize the range of three independent variables: moisture (70-90%), incubation time (4-6 days) and pH (5-7), where inulin (2%), $NH_4H_2PO_4$ (0.2%), $NaNO_3$ (0.2%), KH_2PO_4 (0.2%), $MgSO_4.7H_2O$ (0.05%) and $FeSO_4.7H_2O$ (0.001%) were kept constant. Solid state fermentations were carried out at 30°C in flask cultures. A substantial increase in inulinase production (322.1 IU/gds) was obtained under optimized conditions: moisture (90%), incubation time (4.0) and pH (7.0). The corresponding inulinase/invertase (I/S) ratio (3.38) was also high. Multiple correlation coefficients 'R' for inulinase production and I/S ratio was 0.9995 and 0.9947, respectively. The good agreement between experimental results and predicted values and 'R' value close to one validates the model.

1

SEEC-2017-070

Global Biodiesel Production and Consumption

Sulekha Saini
Department of Mechanical Engineering,
Govt. Women Engineering College, Ajmer,
Rajasthan, India
Email: sulekhasaini.ajm@gmail.com

Jai Gopal Gupta
Department of Mechanical Engineering,
Govt. Women Engineering College, Ajmer,
Rajasthan, India
Email: jaigopalg@gmail.com

ABSTRACT

Petroleum based fuels have huge demand in today world. But the fossil fuel presence in the world is less for the future demand. It also emitted toxic gases like carbon mono oxide, oxides of nitrogen, sulphur di oxide etc. These emissions are harmful for human being as well as for nature. Some alternative methods have been evolved to reduce these emission such as after treatment devices. Also alternative fuel can replace fully or partially carbon base fuels. Biodiesel is a bio fuel that can be used as alternative fuel in blended (B20, B40, B60 etc,) as well as pure form (B100). Edible or non-edible oil, animal fat, algae etc. may be used as raw material for biodiesel production. Biodiesel has huge demand on global level. United States of America is the largest biodiesel consumer and producer in the world. They produced 280 million litre biodiesel in 2016 and consumed 238 million litre. The major biodiesel consumption is for army vehicles in USA. Soya bean oil is the major resource for biodiesel production in USA. Brazil (castor bean), Germany (rapeseed), France (rapeseed), Argentina (soya bean oil), Netherland, Indonesia (palm oil), Thailand (palm oil), Malaysia, Belgium also are top 10 countries of the world that are producing the biodiesel. World bio fuels production increased by 1.49% in 2015 and in 2016 it increased by 1.59%. The data for major biodiesel producer and supplier countries and their capacity of production will be presented in the poster. Major source and major field of utilization of biodiesel for the country will be included with the help of pictorial views, graphs etc. to present the most recent data.

Keywords:Biodiesel, raw material, production comsumption.

NOMENCLATURE

ASTM International (American Society for Testing and Materials)
Quarter(Q)- A three month period on a financial calendar that acts as a basis for the reporting of earning and the paying of dividends.
1Q- January, Febrary, March
2Q- April, May, June
3Q- July, August, September
4Q- October, November, December

INTRODUCTION

Most of countries are based on petroleum fuels for transportation and industrial processes. Raw material used for petroleum fuel is crude oil. But it is a fossil fuel that is not abundantly available. Refineries are producing thousands of barrels crude oil per day because of huge demand.
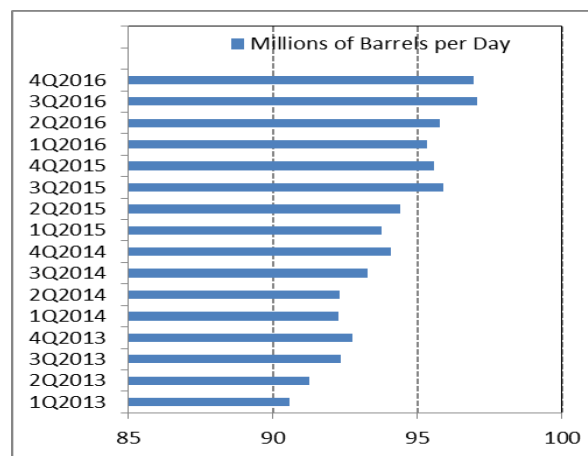
FIGURE 1. WORLD OIL DEMAND [1]

Due to the heavy demand of fossil fuel and also harmful emissions from these fuel causes need of some alternative fuels to overcome dependace on petroleum based fuels. Bio fules may be used as a alternative fuel. In a book titled 'Diesel Engines for Land and Marine Work', Rudolf Diesel state, " In 1900 a small Diesel engine was exhibited by the Otto company was run on arachide oil, and operate so well very few people aware of the fact. The motor was built for ordinary oil, and witout any modification was run on vegetable oil" [2]. It is true now because biodiesel is being used as a fuel in compression ignition engines. Biodiesel define as a mixture of monoalkyl ester of long chain fatty acids derived from vegetable oil or animal fat [3,4].

Advantages of the Use of Biodiesel [5]:

- ✓ Low toxicity, in comparison with diesel fuel.
- ✓ No sulfur dioxide emission.
- ✓ High flah point(minimum 373.15K).
- ✓ Lubricant property is good.
- ✓ It is only alternative fuel use directly in engine without modification.
- ✓ Lower health risk.

Disadvantages of the Use of Biodiese [5]:

- ✓ Higher fuel consumption lower calorific value.
- ✓ Oxides of nitrogen emission is high.
- ✓ Higher freezing point then diesel.
- ✓ Impact on engine performance.

Disadvantages of biodiesel may overcome by blending biodiesel with diesel. Methods used for producing biodiesel are transesterification and esterification. The transesterification process is the reaction of a triglyceride (fat/oil) with an alcohol to form esters and glycerol. In esterification process, the triglyceride is reacted with alcohol in the presence of a catalyst, usually a strong alkaline like sodium hydroxide [6].

Methodology:

Figure 2 shows outline of production process for biodiesel from transesterification.
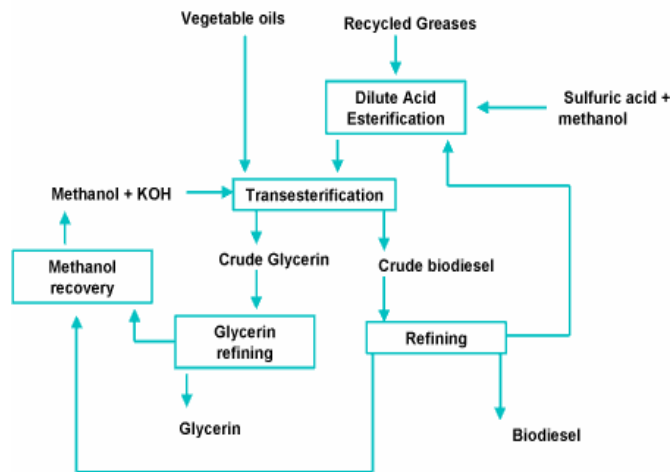
FIGURE 2. BASIC TECHNOLOGY OF TRANSESETERIFICATION PROCESS [7]

TABLE 1. PROPERTIES OF BIODIESEL [3]

Common name	Biodiesel
Chemical formula range	Fatty acides
Kinematic viscosity range (mm^2/s, at 313K)	3.3-5.2
Density range (Kg/m^3, at 288K)	860-894
Boiling point range (K)	>475
Flash point range (K)	420-450
Distillation range (K)	470-600
Vapor pressure (mm Hg, at 288K)	470-600
Solubility in water	Insoluble
Physical appearance	Light to dark yellow, clear liquid
Odor	Light soapy odor
Reactivity	Stable, but avoid strong oxidizing agents

RAW MATERIALS FOR BIODIESEL PRODUCTION

2

The raw material use for biodiesel is vegetable oil and animal fat. The most oils used for biodiesel production worldwide are rapeseed, soybean, palm and sunflower, although other oils are also used, including peanut, linseed, used vegetable oils, and also animal fats [5]. The major crops used for biodiesel production in different countries are shown in table 2.

TABLE 2. MAJOR SOURCES OF BIODIESEL IN DIFFERENT COUNTRIES

S. NO.	COUNTRIES	MAJOR SOURCE OF BIODIESEL
1.	United state of America	Soybean oil [8]
2.	Thailand	Palm oil [9]
3.	Argentina	Soybean oil [10]
4.	Indonesia	Palm oil [11]
5.	Canada	Cooking oil [12]
6.	China	Waste cooking oil [13]
7.	India	jatropha curcas [14]
8.	Brazil	Palm Oil, Castor Oil [15]
9.	European Union	used cooking oil , palm oil [16].

BIODIESEL BLENDS

Biodiesel can be blended and used in many different concentration. The most common blend is B5.

Low level blends

ASTM international develops specifications for conventional diesel fuel (ASTMD9750) this specification allow for biodiesel concentration upto 5% (B5) to be called diesel fuel, with no sepration labeling required at the pump. Low-level biodiesel blends, such as B5 are ASTM approved for safe opration in any compression ignition engine desgined to be oprated on petroleum diesel. This can be included in light duty and heavy duty diesel cars and trucks, tractors, boats, electric generator.

B100 and high level blends

Higher blends of biodiesel provide lower fuel energy due to their lower calorific value. High level biodiesel blend can also impact engine warranties, wax formation in cold temperature, and also increase nitrogen oxides emission, although it greatly reduces other toxic emission [13].

The Government of India (GoI) approved the National Biodiesel Mission (NBM) on December 24, 2009. The policy encourages use of renewable energy resources as alternate fuel to supplement transport fuels and had proposed an indicative target to replace 20% of petroleum fuel consumption with biofuels (bioethanol and biodiesel) by end of 12th Five-Year Plan (2017) [14].

BIODIESEL PRODUCTION AND CONSUMPTION

Global biodiesel production and consumption is for cast to rise by 14% from 2016 to 2020 driven by the fulfilment of current biofuel poilices in the US, Argentina, Brazil, Indonesia and the European Union. The production amount is predicted to increase upto 37.9 billion liters in 2020 from 33.2 bllion liters in 2016 and an increase in consumption to 38.1 billion liters in 2020 from 33.5 billion liters in 2016 [17].
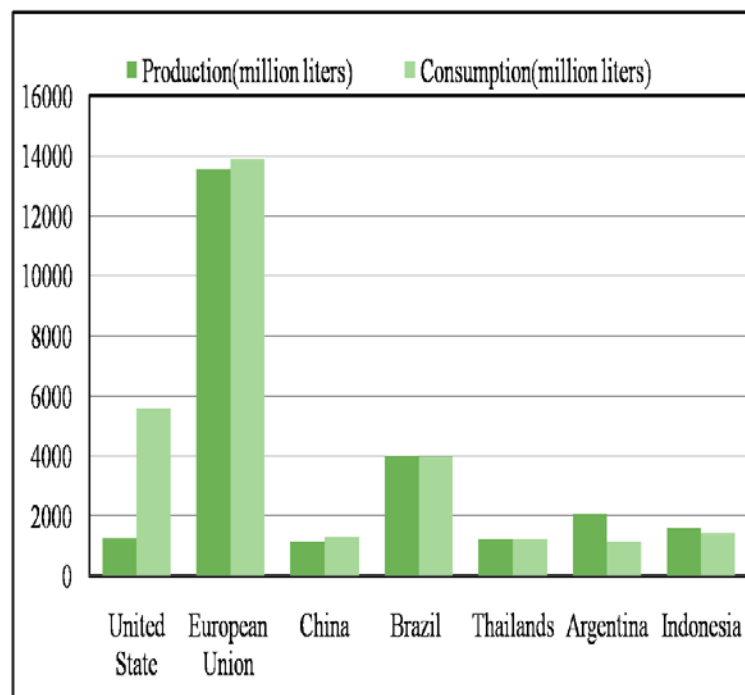
FIGURE 3. MAJOR BIODIESEL PRODUCING AND CONSUMING COUNTRIES IN THE WORLD IN 2015 [8-11,13,15,16].

Around the world, militaries—including the navies of Australia, Chile, Italy, and the United States—continued to pursue biofuels development [20]. The US military announced the first successful supersonic flight fuelled by renewable isobutanol in December 2014 [20].

The GoI had launched the NBM identifying jatropha (jatropha curcas) as the most suitable inedible oilseed for

biodiesel production. The Planning Commission of India had set an of target of planting 11.2 to 13.4 million hectares to jatropha by the end of 11th Five Year Plan (2011/12) [4]. India biodiesel production and consumption for 2010-17 is shown in figure 4.
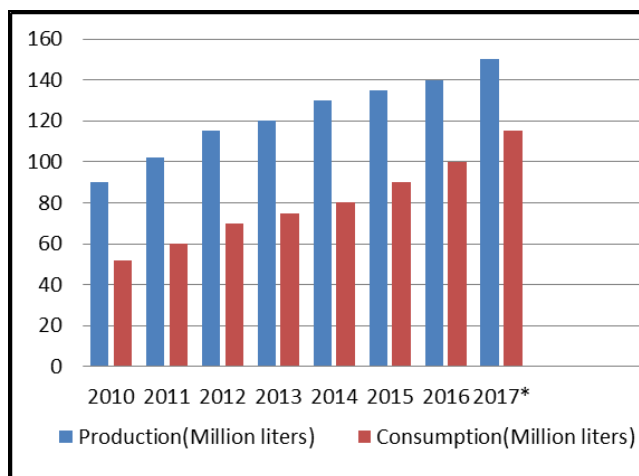
FIGURE 4. Biodiesel production and consumption in India[21].

*2017 is projected

Conclusion

Biodiesel have a huge demand in the world. This alternative fuel is now being used in industries and transportation. Countries are apply many polices to incress production of biodiesel.

REFERENCES
[1] Oil market report, www.iea.org
[2] Chalkley, A.P., 1917. Diesel engines for land and marine work. D. Van Nostrand.
[3] Mujeeb, M.A., Vedamurthy, A.B. and Shivasharana, C.T., Current strategies and prospects of biodiesel production: A review.
[4] Demirbas, A., Biodiesel: a realistic fuel alternative for diesel engines, 2008. Springer-Verlag London Limited, 10, pp.978-1.
[5] Romano, S.D. and Sorichetti, P.A., 2010. Dielectric spectroscopy in biodiesel production and characterization. Springer Science & Business Media.
[6] http://www.esru.strath.ac.uk/EandE/Web_sites/02-03/biofuels/what_biodiesel.htm.
[7] www.cogeneration.net/ transesterification.htm
[8] Monthly Biodiesel Production Report 2016; U.S. energy information administration.
[9] Sakchai Preechajarn, A., Ponnarong Prasertsri , B., Thailand Bio fuels Annual 2016; Global Agricultural

Information Network (GAIN) Report number: TH607.
[10] Ken Joseph, A., Argentina Bio fuels Annual 2016; Global Agricultural Information Network (GAIN).
[11] Thom Wright, A., Arif Rahmanulloh, B., Indonesia Thailand Bio fuels Annual 2015; Global Agricultural Information Network (GAIN) Report number: ID1525.
[12] Darlene Dessureault, A., Canada Bio fuels Annual 2016; Global Agricultural Information Network (GAIN) Report number: CA16038.
[13] Andrew Anderson Sprecher, A., James Ji, B., China Bio fuels Annual 2015; Global Agricultural Information Network (GAIN) Report number:CH15030.
[14] Aradhey, A., India Bio fuels Annual 2016; Global Agricultural Information Network (GAIN) Report number: IN6088.
[15] Sergio Barros, A., Brazil Bio fuels Annual 2016; Global Agricultural Information Network (GAIN) Report number: BR16009.
[16] Bob Flach, A., Sabine Lieberz, B., Marcela Rondon, C.,Barry Williams, D., and Candice Wilson, E., EU Bio fuels Annual 2016; Global Agricultural Information Network (GAIN) Report number: NL6021.
[17] www.platts.com
[18] Aradhey, A. India Biofuels Annual 2013; Global Agricultural Information Network (GAIN) Report number: IN3073.
[19] www.statista.com
[20] Adib, R., 2015. Renewables 2015 Global Status Report.
[21] Aradhey, A. India Biofuels Annual 2016; Global Agricultural Information Network (GAIN) Report number: IN6088.

SEEC – 2017 – 71

DEVELOPMENT OF PHOTOSENSITIZER NANOCONJUGATES THROUGH A BIOINSPIRED PATHWAY[§]

Jayeeta Bhaumik
Center of Innovative and Applied Bioprocessing (CIAB),
Mohali, Punjab, India
Email: jbhaumi@gmail.com

Seema Kirar, Neeraj S. Thakur, Uttam C. Banerjee, Joydev K. Laha
National Institute of Pharmaceutical Education
and Research (NIPER), Mohali, Punjab, India
Email: jklaha@gmail.com

ABSTRACT

An approach to improve biological delivery of photosensitizers by including them into nanomaterials has been established. In order to prepare photosensitizer nanoconjugates as biocompatible and selective probes, initially, bioconjugatable porphyrinic photosensitizers were developed via rational methods. The porphyrins with carboxyl groups (as conjugatable handles) were successfully attached on the surface of the bioinspired nanoparticles (through a stable ester bond formation) affording hydrophilic and biocompatible nanophotosensitizers. The loading efficiency of the photosensitizer into nanomaterials was found to be 12–16%. Given their biocompatibility and efficient loading on nanoparticles, the photosensitizers prepared in this study could find use in photodynamic therapy and dual photodynamic–photothermal therapy.

Keywords porphyrins, photosensitizers, nanconjugates, nanosensitizers, photodynamic therapy

INTRODUCTION

Photodynamic therapy (PDT) has become an important therapeutic tool for the treatment of many diseases including cancer, microbial infection and cardiovascular diseases.[1–3] Photosensitizers (PSs) are essential components of PDT, which upon absorption of light are activated, and generate singlet oxygen that causes tumor cell destruction.[4,5] Among other photosensitizers, tetrapyrrolic macrocycles have found an extensive use as photosensitizers due to their unique absorption properties in the visible and/or near infrared region of the electromagnetic spectrum.[6,7] Porphyrins or their hydrogenated derivatives such as chlorins are effective tetrapyrrolic photosensitizers due to their high stability and ease of synthesis.[8] For example, commercially available Photofrin, a porphyrin, or Foscan, a chlorin has found large applications for the treatment of certain cancer.[9] However, limitations of tetrapyrrolic macrocycles as photosensitizers may include their hydrophobicity, biocompatibility, and non-selective delivery to biological systems.[8]

Herein the development of porphyrin-nanoconjugates as biocompatible photosensitizers for potential applications in PDT and/or dual PDT–PTT is reported. Initially, several conjugatable heterocycles containing compact trans-AB porphyrinic photosensitizers (PSs) were synthesized via rational routes. Those compact porphyrins with a carboxyl tether were then successfully attached to the surface of the bioinspired metal nanoparticles (rich in –OH group) via covalent (ester) bond formation. These nanophotosensitizer conjugates were further characterized (by absorption spectroscopy, FTIR spectroscopy and HPLC) and the photosensitizer loading efficiency on nanoscaffolds was also determined. Overall, these bioinspired photosensitizer nanoconjugates with enhanced biocompatibility are promising candidates for photomedical applications.

RESULTS AND DISCUSSION
Rational synthesis of conjugatable porphyrins
The preparation of synthetic precursors to porphyrins is shown in Scheme 1. The synthesis of dipyrromethanes was carried out using one of the following approaches

developed earlier by us: (a) TFA-catalyzed reaction at room temperature, (b) InCl$_3$-catalyzed reaction at room temperature or an elevated temperature in the presence of a large excess pyrrole,[11] or (c) heating a neatmixture at an elevated temperature. Thus, aldehyde **1** was treated with excess pyrrole in the presence of TFA (10 mol%), which upon chromatographic purification produced dipyrromethane **5** in 66% yield (Scheme 2).[12] Reaction of a mixture of benzaldehyde **2** and excess. pyrrole at room temperature (25 °C) in the presence of a catalytic amount of InCl3 (20 mol%) followed by chromatography gave dipyrromethane **6** in 73% yield. A neat mixture of 4-pyridine carboxaldehyde and excess pyrrole was heated at 80 °C for 16 h, which upon chromatographic separation gave the desired 5-pyridyldipyrromethane (**7**) in 75% yield.[13] Likewise, compounds **3a** and **4a** afforded 5-[1-butyl-imidazol-2-yl]dipyrromethane (**8**) and 5-[1-butylindol-3-yl]dipyrromethane (**9**) in 58 and 40% yields, respectively. Diformylation of dipyrromethanes **5, 6** or **7** at 1,9-positions, following a protocol previously demonstrated by us,[14] yielded 1,9-diformyldipyrromethanes (**10–12**) in 20–40% yield. Using a protocol developed by us earlier,[15] the synthesis of trans-AB porphyrins was achieved by the condensation of 1,9-diformyldipyrromethanes and dipyrromethanes in the presence of excess n-propylamine in THF and subsequent metalation with Zn(OAc)$_2$. Thus, reaction of 1,9-diformyldipyrromethane **12** and dipyrromethane **5** delivered porphyrin **13** as a purple solid (Scheme 3, 20% yield). However, acquisition of spectroscopic data for the characterization of porphyrin **13** was largely impeded probably because of self-aggregation, encountered due to the co-ordination between pyridyl nitrogen and zinc metal. The central zinc atom from the porphyrin macrocycle was therefore needed to be removed. Demetalation of trans-AB porphyrin **13** was achieved by treating a solution of **13** in CH$_2$Cl$_2$ with excess TFA at room

temperature (25 °C) for 2 h, which upon subsequent purification afforded porphyrin **14**. The free-base porphyrin **14** provided satisfactory characterization data. Next, the ester group in porphyrin **14** was subjected to base mediated hydrolysis to engender carboxylic acid tether required for conjugation to nanoparticles. Thus, treating a solution of **14** in THF with LiOH·H$_2$O at room temperature and subsequent acidification with 10% HCl afforded porphyrin **15** containing a carboxylic acid handle. The pyridyl nitrogen in porphyrin **15** was methylated with excess methyl iodide to obtain **16** (80% yield in two steps).

FIGURE 1. Synthetic design towards the development of nanophotosensitizer conjugates. [Reproduced from reference no. 10 with permission from the Centre National de la Recherche Scientifique (CNRS) and The Royal Society of Chemistry.]

SCHEME 1. Synthetic precursors to dipyrromethanes: (a) synthesis of aldehydes containing masked conjugatable groups; (b) synthesis of butylated heterocyclic aldehydes. [Reproduced from reference no. 10 with permission from the Centre National de la Recherche Scientifique (CNRS) and The Royal Society of Chemistry.]

SCHEME 2. Synthesis of conjugatable and heterocyclic dipyrromethanes, and 1,9-diformyldipyrromethanes as porphyrin precursors. [Reproduced from reference no. 10 with permission from the Centre National de la Recherche Scientifique (CNRS) and The Royal Society of Chemistry.]

SCHEME 3. Preparation of a trans-AB porphyrin with a cationic and a conjugatable hand. [Reproduced from reference no. 10 with permission from the Centre National de la Recherche Scientifique (CNRS) and The Royal Society of Chemistry.]

Nanophotosensitizer preparation
Central to this study was to demonstrate the conjugation of

porphyrin **16** with metal NPs, prepared by us previously.[15] Silver and gold nanoparticles (AgNPs and AuNPs) were prepared from Camellia sinensis (CS, green tea) and Potentilla fulgens (PF, vajradanti) in high yields. Three types of bioinspired nanoparticles (CS-AgNPs, CS-AuNPs and PF-AuNPs) were developed where plant materials acted as reducing, stabilizing and capping agents. The biomaterials present (from plant extracts) on the surface of the metal nanoparticles are a class of flavonoids that are rich in hydroxyl functionalities.[15] The carboxylic acid moiety in the porphyrin **16** could be easily coupled with the hydroxyl groups present in metal NPs via an ester linkage (Scheme 2, top panel). The conjugation of porphyrin **16** and metal NPs was carried out via EDC mediated coupling reaction. The analytical data (FTIR, UV-vis, and HPLC) obtained for the samples prepared from these reactions strongly support the formation of conjugated nanophotosensitizers from porphyrin **16**. For example, FTIR data showed a peak at 1732 nm as a characteristic of ester functionality present in porphyrin-nanoconjugates. UV-visible spectra of porphyrin-nanoconjugates are distinct from those of their unconjugated metal NPs or porphyrin 16 (Fig. 2a–g). For example, the UV-visible spectrum of porphyrin **16** shows a strong intense band at 410 nm, while UV-visible spectra of silver nanoparticles in our study showed a peak at 450 nm, and UV-visible spectra of gold nanoparticles appeared at 535 nm. For example, the porphyrin-nanoconjugates of silver nanoparticles (CS-AgNPs) showed broad absorption peaks at 411 and 450 nm (Fig. 2a). Similarly, porphyrin conjugated gold nanoparticles (both CS-AuNPs and PF-AuNPs) also showed two peaks at 411 and 535 nm (Fig. 2b and c). Further confirmation of porphyrin-nanoconjugates is apparent from the fact that treatment with NaOH resulted in the hydrolysis of the ester bond formed between porphyrin and metal nanoparticles. Centrifugation of the supernatant revealed the appearance of only one peak at 411 nm upon absorption spectroscopy indicating release of the porphyrin from the nanomaterial surface. As photosensitizers show therapeutic efficacy at lower concentration,2 photosensitizers loaded with nanoparticles at the 12–16% level have successfully been delivered. The ability of porphyrin 16 loaded on CS-AgNPs, CS-AuNPs, and PF-AuNPs was estimated to be 16, 12, and 16%, respectively (by the HPLC method). The observed loading efficiency of 16 is proportional to the number of hydroxyl functionalities present on metal nanoparticles. Notably, the loading efficiency of porphyrin **16** is found to be significant for drug delivery and also leaves room to develop phototheranostic nanoagents by the incorporation of diagnostic and targeting agents on the nanoparticles. Overall these bioinspired photosensitizers are substantial precursors for phototheranostic nanoagents for finding better treatment using PDT or dual PDT–PTT.

FIGURE 2. (top panel) Development of nanophotosensitizer conjugates via the condensation of a conjugatable porphyrin on the surface of biosynthesized metal nanoparticles. (bottom panel) Conjugation of porphyrin with metallic NPs: (a) conjugation with CS-AgNPs; (b) conjugation with CS-AuNPs, and (c) conjugation with PF-AuNPs. Red line: UV-vis spectra before NaOH treatment; blue line: UV-vis spectra after NaOH treatment; absorption spectra of (d) CS-AgNPs, (e) CS-AuNPs (f) PF-AuNPs and (g) free pyridyl porphyrin **16**. [Reproduced from reference no. 10 with permission from the Centre National de la Recherche Scientifique (CNRS) and The Royal Society of Chemistry.]

CONCLUSIONS

Photosensitizer metal nanoconjugates were developed as better alternatives to conventional photosensitizers for PDT or combined PDT–PTT applications. First, various building blocks (aldehydes, dipyrromethanes and diformyldipyrromethanes) containing heterocyclic (pyridyl, imidazole, and indole) and conjugatable moieties as precursors to porphyrins were synthesized. Later, rational syntheses of versatile cationic (positively charged) and conjugatable tetrapyrrolic macrocycles were accomplished. Unlike the statistical route, which generates a mixture of porphyrinic derivatives, the rational route resulted in single porphyrinic species in highly pure form. Afterwards, newly constructed conjugatable tetrapyrrolic photosensitizers were characterized by different analytical techniques including absorption spectroscopy, NMR and mass spectrometry. Taking the advantage of hydroxyl functionalities present on the periphery of bioinspired noble metal nanoparticles (silver and gold), porphyrins containing carboxyl tethers were attached on their surface via ester bond formation (through EDC mediated coupling). The loading efficiency of the photosensitizers on nanoscaffolds was determined by both absorption spectroscopy and HPLC methods. These nanophotosensitizers were designed in order to possess enhanced biocompatibility as observed by their stability under physiological conditions. These photosensitizer nanoconjugates can serve as PDT or dual PDT–PTT agents with improved efficacy compared to native PSs or NPs.

These bioengineered nanophotosensitizer probes are potential candidates for photomedicines.

ACKNOWLEDGMENTS

REFERENCES

[1] J. Bhaumik, A. K. Mittal, A. Banerjee, Y. Chisti and U. C. Banerjee, 2015, "Biosynthesis of silver nanoparticles: elucidation of prospective mechanism and therapeutic potential", Nano Res., 8, 1373–1394.

[2] P. Mroz, J. Bhaumik, D. K. Dogutan, Z. Aly, Z. Kamal, Khalid, H. L. Kee, D. F. Bocian, D. Holten, J. S. Lindsey and M. R. Hamblin, 2009, "Imidazole metalloporphyrins as photosensitizers for photodynamic therapy: role of molecular charge, central metal and hydroxyl radical production", Cancer Lett., 282, 63–76.

[3] J. R. McCarthy, E. Korngold, R. Weissleder and F. A. Jaffer, 2010, "A light-activated theranostic nanoagent for targeted macrophage ablation in inflammatory atherosclerosis", Small, 6, 2041–2049.

[4] D. E. Dolmans, D. Fukumura and R. K. Jain, 2003, "Photodynamic therapy for cancer", Nat. Rev. Cancer, 3, 380–387.

[5] J. Bhaumik, J. R. McCarthy and R. Weissleder, 2009, "Synthesis and photophysical properties of sulfonamidophenyl porphyrins as models for activatable photosensitizers", J. Org. Chem., 74, 5894–5901.

[6] H. L. Kee, J. Bhaumik, J. R. Diers, P. Mroz, M. R. Hamblin, D. F. Bocian, J. S. Lindsey and D. Holten, 2008, "Photophysical characterization of imidazolium-substituted Pd (II), In (III), and Zn (II) porphyrins as photosensitizers for photodynamic therapy", J. Photochem. Photobiol., A, 200, 346–355.

[7] C. Muthiah, J. Bhaumik and J. S. Lindsey, 2007, "Rational routes to formyl-substituted chlorins", J. Org. Chem., 72, 5839–5842.

[8] M. Ethirajan, Y. Chen, P. Joshi and R. K. Pandey, 2011, "The role of porphyrin chemistry in tumor imaging and photodynamic therapy", Chem. Soc. Rev., 40, 340–362.

[9] L.B. Josefsen and R.W. Boyle, 2012, "Unique Diagnostic and Therapeutic Roles of Porphyrins and Phthalocyanines in Photodynamic Therapy, Imaging and Theranostics", Theranostics, 2, 916–966.

[10] Bhaumik, J., Gogia, G., Kirar, S., Vijay, L., Thakur, N. S., Banerjee, U. C., Laha, J. K., 2016, "Bioinspired nanophotosensitizers: synthesis and characterization of porphyrin–noble metal nanoparticle conjugates", New J. Chem. 40, 724-731.

[11] J. K. Laha, S. Dhanalekshmi, M. Taniguchi, A. Ambroise and J. S. Lindsey, 2003, "A Scalable Synthesis of Meso-Substituted Dipyrromethanes", Org. Process Res. Dev., 7, 799–812.

[12] Z. Yao, J. Bhaumik, S. Dhanalekshmi, M. Ptaszek, P. R. Rodriguez and J. S. Lindsey, 2007, "Synthesis of porphyrins bearing 1–4 hydroxymethyl groups and other one-carbon oxygenic substituents in distinct patterns", Tetrahedron, 63, 10657–10670.

[13] D. Gryko and J. S. Lindsey, 2000, "Rational Synthesis of meso-Substituted Porphyrins Bearing One Nitrogen Heterocyclic Group", J. Org. Chem., 65, 2249–2252.

[14] J. Bhaumik, Z. Yao, E. K. Borbas, M. Taniguchi and J. S. Lindsey, 2006, "Masked imidazolyl-dipyrromethanes in the synthesis of imidazole-substituted porphyrins", J. Org. Chem., 71, 8807–8817.

[15] J. Bhaumik, N. S. Thakur, P. K. Aili, A. Ghanghoriya, K. Mittal and U. C. Banerjee, 2015, "Bioinspired Nanotheranostic Agents: Synthesis, Surface Functionalization and Antioxidant Potential", ACS Biomater. Sci. Eng., 6, 382–392.

EFFECT OF ACCELERATED AGING ON THE CHEMICAL COMPOSITION OF PYROLYTIC OIL OBTAINED FROM THE PYROLYSIS OF SACCHARUM RAVENNAE

Philip Bernstein Saynik
Indian Institute of Technology Guwahati
Email: p.saynik@iitg.ernet.in

Vijayanand Moholkar
Indian Institute of Technology Guwahati
Email: vmoholkar@iitg.ernet.in

ABSTRACT

Pyrolysis, being one of the promising techniques for waste management along with bio-oil production is being studied for its applicability in India by experimenting with various lignocellulosic biomass. Storage stability in terms of the chemical composition is crucial for further processing of the bio-oil into transportation fuel. Accelerated aging technique of bio-oil involves heating it to temperatures of 80-90°C for a duration of 24 hr. The technique revealed the varying chemical compositions thereby indicting the various possible reactions occurring during the aging of bio-oils with a maximum variation in the furans, phenols and acids concentration from 8.74 to 0.66%, 66.56 to 52.00% and 2.56 to 0%. A study on the use of various additives could be done to reduce the chemical and physical reactions thereby improving the storage stability.

Keywords: Saccharum Ravennae, Storage stability, Accelerated aging, Bio-oil

EFFECT OF DILUTE ACID AND ALKALI PRETREATMENTS ON THE HOLOCELLULOSE AND LIGNIN CONTENTS OF SORGHUM STALK FOR BIOETHANOL PRODUCTION

Sumitha Banu J
Indian Institute of Technology Guwahati
Email: sumitha@iitg.ernet.in

Vijayanand Moholkar
Indian Institute of Technology Guwahati
Email: vmoholkar@iitg.ernet.in

Arun Goyal
Indian Institute of Technology Guwahati
Email: arungoyl@iitg.ernet.in

ABSTRACT

Various lignocellulosic feedstock including agricultural wastes around the world are being characterized aiming for their use as a potential resource for bioethanol production. Pretreatment plays a major role in rendering the cellulose and hemicellulose part exposed to the hydrolytic enzymes for further saccharification. This study compares the various methods of pretreatment involving either dilute acid (1% H2SO4) or dilute alkali (1% NaOH) combined with oven heating at 120°C, autoclaving, microwave or ultrasonication on powdered sorghum stalk for its application as a potential feedstock for bioethanol production. Among those pretreatments, dilute alkali (1% NaOH) treatment combined with autoclaving at 121°C and 15 psi for 20 minutes was found to be the effective one with respect to the gravimetric analysis of holocellulose and acid insoluble lignin (ADL) contents and Crystallinity index (CrI) of the untreated and the pretreated biomass samples. Secondary optimization of the treatment at different time durations will give deep understanding of the role of time factor on the process.

Keywords: Sorghum stalk, Pretreatment, Holocellulose, saccharification, Crystallinity index

SEEC-2017-074

INTERCONVERSION OF ALDOPENTOSES AND TETROSES WITH ZEOLITES*

S.Saravanamurugan
Center of innovative and Applied
Bioprocessing, Mohali, Inida and
Centre for Catalysis and Sustainable Chemistry
Department of Chemistry, Technical University
of Denmark
Email: saravana@ciab.res.in

Marta Paniagua, Juan A. Melero
Chemical and Environmental Engineering Group,
ESCET
Universidad Rey Juan Carlos, C/Tulip.n s/n, E-
28933
Mûstoles, Madrid (Spain)

**Mayra Melian-Rodriguez and Anders
Riisager**
Centre for Catalysis and Sustainable Chemistry
Department of Chemistry, Technical University
of Denmark
2800 Kgs. Lyngby (Denmark)

Compiled based on previously published articles [1,2]

ABSTRACT

Isomerisation of xylose to xylulose with commercial zeolites, such as H-USY and H-Beta, with various silicon to aluminium ratio has been studied under alcohol-aqueous system in one-pot two-step reaction protocol. It has been found that the reaction proceeded through the following steps: isomerisation of xylose to xylulose in alcohol during the first step; acetalisation of xylulose to alkyl xyluloside during the first step, hydrolysis alkyl xyluloside to enhance the yield of xylulose during the second step. The highest yield of xylulose (47%) was found with H-USY-6. The reaction protocol was extrapolated to tetroses, such as erythrose, but found that interconversion took place efficiently in water rather than in alcohol, yield 45% erythrulose with H-USY-6 in one-pot one step catalytic process. This manuscript reviews based on our previously published articles[1,2].

Keywords: *xylose, erythrose, zeolite, alcohol, water*

INTRODUCTION

It has projected that limited fossil resources will be dwindling in the coming decades and reflects that alternative, sustainable resources, such as biomass, wind and solar energy, would play a major role to substitute fossil based chemicals and fuels to keep the value chain [3]. In this context, industries/academia have been striving towards to find out potential substitutes derived from biomass which can be economically viable to replace the existing technology[4-6]. For example, it has been realized that 2,5 furan dicarboxylic acid (FDCA) can be a sustainable substitute to terephthalic acid which is one of the precursors for making PET plastics [7]. In the past decades, ample number of reports have been published in connection with valorisation of cellulosic sugars and lignin/lignin model compounds to, for example, high-value chemicals lactic acid and aromatic chemicals, respectively.

Isomerisation of aldoses to ketoses is an important interconversion in the biomass transformations, for example, isomerization of glucose to fructose in one of the significant industrial processes for producing high fructose corn syrup (HFCS). In this regard, isomerisation of aldopentoses and tetroses are thus important as dehydration of xylose lead to form furfural (platform chemical) via xylulose and vinyl glycolic acid via erythrulose from erythrose, respectively. This manuscript summarise/review the results obtained from our previously published articles related to isomerization of

xylose and erythrose with commercially available Beta and Y zeolites [1,2]

The isomerization xylose to xylulose were performed in one-pot two-step catalytic process with
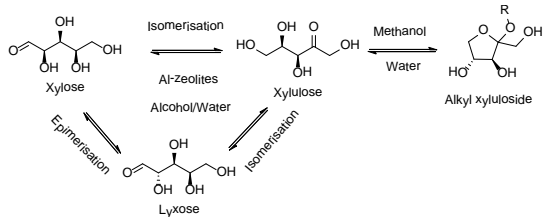
zeolites in alcohol and aqueous medium as the Al-zeolites functioned in alcohol during the first step to form isomerized and acetalised products fructose and alkyl fructoside, respectively. During the second step, water was added in order to hydrolyse formed alkyl fructoside to form additional fructose to enhance the yield. The similar reaction protocol has been extended to erythrose isomerization in one-pot approach. Interestingly, it was found that isomerization took place to a large extent in water rather than in alcohol to yield erythrulose. The isomerization reaction pathways are shown in Scheme 1 and 2.

Scheme 1. The plausible reaction pathway for xylose isomerisation [1].
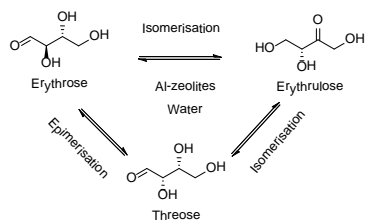
Scheme 1. The plausible reaction pathway for erythrose isomerisation in water [2].

RESULTS AND DISCUSSION

Initial experiments were performed with zeolites to optimise the ratio between methanol and water during the first and second step to get the highest yield of xylulose. Y and USY zeolites with various silicon to aluminium ratio were employed as catalyst for the isomerization xylose under optimized amount of methanol and water. A moderate yield of xylulose (23%) was obtained with H-Y-2.6 with trace amount of methyl xyluloside at a conversion of 34% xylose in methanol. The yield of xylulose (25%) slightly improved after adding water during the second step (Table 1). However, a significant enhancement in the yield of xylulose was observed when changing the catalyst to H-USY-6. After the first step of the reaction in methanol, 39% of xylulose along with 13% of methyl xyluloside was obtained at 68% conversion of xylose. The yield of xylulose increased to

47% after hydrolysing in water during the second step, suggesting that formed methyl xyluloside (13%) was able to be hydrolysed with the same zeolite H-USY-6. As the silicon to aluminium ratio increased from 6 to 30 in H-USY zeolite, a very poor yield of xylulose was obtained, demonstrating that acid sites distribution might have varied in each zeolite and thus perturbed the product distribution. In line with this, the catalysts were subject to pyridine adsorption studies and found that H-USY-6 possessed slightly more Brønsted to Lewis acid sites ratio could have influenced on the yield of xylulose.

When other zeolites H-beta employed as catalysts, a comparable yield of xylulose (31%) after the first step in methanol and increased to 39% during second step after adding water with H-beta-12.5. However, a trace amount of isomerized product xylulose was obtained. A significant yield of xylulose (20%) was obtained with H-beta-12.5

Table 1. Conversion xylose to xylulose in one-pot two-step process [1]

Zeolite	Step	Product distribution (mol %)			B/L ratio[c]
		Xylose	Xylu-lose	Methyl xyluloside	
H-Y-2.6	1	66	23	<1	0.49
	2	65	25	<1	
H-USY-6	1	31	39	13	1.07
	2	31	47	4	
H-USY-30	1	92	4	5	0.95
	2	87	4	4	
H-Beta-12.5	1	46	31	11	0.76
	2	45	39	5	
H-Beta-19	1	71	16	8	0.33
	2	71	20	5	
H-Beta-150	1	>99	trace	-	
	2	>99	trace	-	
H-USY[b]	1	25[b]	29	8	
	2	26[b]	37	2	

[a] Reaction conditions: catalyst (75 mg), xylose (125 mg), methanol (4 g), 100 °C. [b] Substrate was lyxose

after the second the step. This indicate that the yield of xylulose decreased as the silicon to aluminium ratio increased as can be seen with H-USY-6 and -30. The another C5 sugar lyxose was subjected to isomerization with H-USY- and found to be yielding 37% of xylulose after the second step. In all cases where xylose as substrate yielded a trace amount of lyxose, implying that employed Al-zeolites did not facilitate epimerization of xylose to lyxose. Likewise, negligible amount of xylose was formed when using lyxose as substrate with H-USY-6 as catalyst.

Table 2. Influence of H-USY (6) catalyst loading on product distribution obtained for xylose conversion after the first and second reaction step[a] [1]

m_{cat} (mg)	$m_{xylose}:m_{cat}$	Step	Reaction time (h)	Product distribution (%)	
				Xylose	Xylulose
5	25	1	24	46	27
		2	1	42	36
20	6.3	1	5	43	29
		2	1	39	37
30	4.2	1	3	43	31
		2	2	39	41
50	2.5	1	1	38	31

Catalyst	Conv. ERO(%)	Product distribution (%)		
		ERO	ERU	THO
H-Y-2.6	70	30	37	3
H-USY-6	52	48	39	2
H-USY-30	10	90	4	trace
H-beta-12.5	29	71	19	1
H-beta-19	14	86	4	trace
H-ZSM-5-11.5	17	83	6	1

		2	2	37	44
75	1.7	1	1	31	39
		2	1	31	47

[a] Reaction conditions: Step 1: xylose (125 mg), methanol (4 g), 100 °C; Step 2: water (4 g), 100 °C.

The influence of catalyst loading was studied on the yield of xylulose. Table 3 evidently showed that even at low catalyst amount of H-USY-6 (5mg) yielded 36%, however, the reaction time during the first step needed to be prolonged to 24h to achieve the higher yield. As the catalyst amount increased, the reaction time decreased during the first step to get the comparable yield of xyluose after the second step.

Table 3. Isomerization of ERO over various zeolites in water[a][2]

[a] Reaction conditions: 5.58 g of aqueous solution of 0.093 M ERO, 0.0375 g of catalyst, 120 °C, 3 h.

This similar approach was extended to erythrose isomerization with the same zeolites in water as the interconversion did not proceed well in methanol, and the results are presented in Table 3. H-usy-6 yielded a highest conversion to erythrulose (ERU) (39%) under aqueous medium. HY-2.6 also gave next highest ERU yield (37%). However, the yields were drastically decreased when changing the catalyst to beta and ZSM-5 catalysts.

CONCLUSION

It was demonstrated that zeolites, especially H-USY-6, can efficiently catalyse the the isomerization of xylose and xylulose in two steps in alcohol and water media and erythrose to erythrulose in water. The obtained results clearly displayed that H-USY-6 was not able to epimerise neither xylose to lyxose nor erythrose to threose and vice versa to a large extent.

REFERENCES
[1] Paniagua, M., Saravanamurugan, S., Melian-Rodriguez, M., Melero, J. A., Riisager, A., 2015. "Xylose Isomerization with Zeolites in a Two-Step Alcohol–Water Process". ChemSusChem, 8, 1088 – 1094.
[2] Saravanamurugan, S., Riisager, A., 2014. "Zeolite-catalyzed isomerization of tetroses in aqueous medium". Catal. Sci. Technol., 4, 3186–3190.
[3] Corma, A., Iborra, S., Velty, A., 2007, "Chemical routes for the transformation of biomass into chemicals". Chem. Rev., 107, 2411−2502.
[4] Himmel, G. W., Ding, S.-Y., Johnson, D. K., Adney, W. S., Nimlos, M. R., Brady, J. W., Foust, T. D., 2007. "Biomass recalcitrance:Engineering plants and enzymes for biofuels production". Science, 315, 804−807.
[5] Saravanamurugan, S., Paniagua, M., Melero, J. A., Riisager, A., 2015. "Efficient isomerization of glucose to fructose over zeolites in consecutive reactions in alcohol and aqueous media". J. Am. Chem.Soc. 135, 5246−5249.
[6] Wettstein, S. G., Alonso, D. M., Chong, Y., Dumesic, J. A., 2012. "Production of levulinic acid and gamma-valerolactone (GVL) from cellulose using GVL as a solvent in biphasic systems". Energy Environ.Sci. 5, 8199−8203.
[7] Zhang, Z., Deng, K., 2015. "Recent Advances in the Catalytic Synthesis of 2,5-Furandicarboxylic Acid and Its Derivatives" ACS Catal. 5, 6529−6544

SEEC-2017-75

UTILIZATION OF APPLE POMACE FOR PULLULAN PRODUCTION BY *AUREOBASIDIUM PULLULANS* BGPUP-6

R.S. Singh
Carbohydrate and Protein Biotechnology
Laboratory, Department of Biotechnology,
Punjabi University, Patiala 147 002, Punjab, India

G. Singh & H. Kaur
Carbohydrate and Protein Biotechnology
Laboratory, Department of Biotechnology,
Punjabi University, Patiala 147 002, Punjab, India

ABSTRACT

In the present investigation, pullulan production was carried out from apple pomace using a new isolate of Aureobasidium pullulans BGPUP-6. Six pullulan producing fungal strains were isolated and screened for pullulan production in a sucrose based fermentation medium. All the fungal isolates were identified on the basis of colonial and morphological characteristics. Fungal isolate Aureobasidium pullulans BGPUP-6 has shown maximum (1.68%, w/v) pullulan production. Apple pomace was selected as substrate for pullulan production in shake-flasks to make the process more cost effective. Apple pomace extracts in water were prepared by boiling and under pressure at 10, 15 and 20 psi. Maximum total sugars (2.37%, w/v) and reducing sugars (0.37%, w/v) were found in the aqueous extract prepared from 10% (w/v) of apple pomace at 20 psi. This extract was used for pullulan production by Aureobasidium pullulans BGPUP-6 and a yield of 2.04 (%, w/v) was obtained. Pullulan production was more in apple pomace based medium as compared to sucrose based medium. TLC analysis of crude pullulan hydrolysate has shown the presence of maltosyl units which confirms the produced metabolite is pullulan. FTIR spectra and DSC thermograms for pullulan produced from fungal isolate BGPUP-6 as well as those for commercial pullulan (Sigma, USA) exhibited similar results, confirming the identical chemical structure and degradation pattern.

SEEC-2017-76

Experimental Study of Compression Glass-Metal Joint for Parabolic Trough Receiver Tube application

Rakesh Joshi
Department of Mechanical Engineering,
Indian Institute of Technology
Jodhpur, Rajasthan, India

Rahul Chhibber
Department of Mechanical Engineering,
Indian Institute of Technology
Jodhpur, Rajasthan, India

ABSTRACT

The concentrated solar power plant technology has proven to be a latest source of renewable energy. The performance of concentrated solar power plant depends upon the efficiency of the parabolic trough receiver tube or heat collecting element (HTC).In this paper, experimental study on the fabrication of glass metal joint was carried out for parabolic trough receiver tube .Borosilicate glass tube joined with austenitic stainless steel using compression glass-metal type geometry with the help of induction heating system. The experimentation parameters for joining were selected on the basis of wettablity, pre-oxidation and microstructure studies. Modeling of stress generation at glass metal interface was using theory of thin shell. From the modeling it has been observed that maximum tensile stresses were developed near glass-metal at the interface which causes the cracking of glass tube at interface.

SEEC-2017-77

Qualitative and proteomic characterization of the strain ISTP10 for bioremediation and plant growth promoting ability

Moni Kumara & Rashmi Rathour
School of Environmental Sciences
JNU, New Delhi, India

Indu Shekhar Thakur
School of Environmental Sciences
JNU, New Delhi, India

ABSTRACT

The present study deals with the previously isolated Paenibacillus sp. ISTP10 screened for the degradation of wide range of persistent organic contaminants. The alternation in the morphology of the strain was studied. The remediation potential of the strain was further confirmed by proteomic characterization. The presence of cytochrome P450, FAD linked oxidase domain protein, prolyl-oligopeptidase, acetyltransferase, GNAT family, Beta-ketoadipate enol-lactone hydrolase, glutaryl Co-A dehydrogenase, putative alcohol dehydrogenase that provide evidence of the bioremediation and detoxification potential of ISTP10. Later the strain is also characterized for its plant growth promoting ability by various biochemical, proteomic and in vivo studies

SEEC-2017-78

DIVERSITY OF TREE PHENOLOGICAL PATTERNS IN DRY TROPICS

C.P. Kushwaha
Axis Institute of Technology and Management,
Kanpur, India

ABSTRACT

Climate change will affect many aspects of the biology of tropical trees, and its effect on tree phenology would be of immense significance. Quantification of tree phenological patterns provides a potential tool to address critical questions related to climate change modeling and monitoring. In recent years, therefore, the focus of phenological studies has shifted to questions of how phenology will be affected by global climate change and what consequences any climatic change may have for species distribution and ecosystem function. With respect to phenological patterns in tropical deciduous forest trees, huge diversity in phenological events in association with variable often confusing terminology makes difficulties with respect to transfer of species data into useful information at the biome level, and generalization of results to broader geographical area. Thus, an quantitative approach to phenological studies, at species or functional types level that reveal great deal of diversity, is urgently required in tropical deciduous forests. Phenology-as-usual (e.g. community level phenology) may not be appropriate for climatic change issues because it hide more and reveal less diversity in phenological events. Recent species level quantitative phenological studies of tropical trees involving precise documentation of timing and duration of different phenological events at level of species or functional types, their interrelations and possible causal links between environmental variables and phenology advances our understanding with respect to vegetative and reproductive phonologies and revealed the great deal of diversity for both these events. Widely distributed tropical deciduous forests may be broadly defined as tree dominated communities growing in climates with a pronounced seasonality in rainfall, and a drought period lasting 4-8 months during each annual cycle, during which the ratio of potential evaporation to rainfall is greater than one. These forests play significant role in global carbon and regional water cycles, sustain large human populations, acts as sites of 2 biological and cultural conservation, and have large economic values. In view of the prolonged drought in these forests, the predominant tree species should be deciduous showing early dry season leaf fall and growth resumption after the on set of rainy season. The tropical deciduous forests, however, constitute a mosaic composed of several phenological functional types adapted to seasonal drought in different ways resulting in maintenance of high leaf cover well beyond the rainy season and least synchronization between periodic growth period of trees and duration of dry season. Thus, at a time when world wide emphasis is on increasing growing season length of temperate deciduous forest trees because total area of tropical deciduous forests is significantly greater than that of temperate deciduous forests.

EXTRACTION OF LIGNIN AND ITS CHARACTERIZATION FROM VARIOUS INVASIVE WEEDS FOR BIOREFINERY PROSPECT

Arup Jyoti Borah
Indian Institute of Technology Guwahati
Email: arup.jyoti@iitg.ernet.in

Mriganka Saha
Indian Institute of Technology Guwahati
Email: mriganka.saha@iitg.ernet.in

Prachi Arya
Indian Institute of Technology Guwahati
Email: aryaprachi15@gmail.com

Shivangi Jha
Indian Institute of Technology Guwahati
Email: jhashivangi2014@gmail.com

Vijayanand Moholkar
Indian Institute of Technology Guwahati
Email: vmoholkar@iitg.ernet.in

Arun Goyal
Indian Institute of Technology Guwahati
Email: arungoyl@iitg.ernet.in

ABSTRACT

Fast adaptation and commercialization of biofuels has been hindered due to plethora of generic and non-sustainable constriction. Invasive weeds on the other hand, cause a negative impact in the current economy around the globe. Sustainable utilization of this waste biomass as a feedstock for biorefinery prospect would nullify the cost required for managing and manipulating the ecosystem and also its dependency of feedstock availability, which plays a critical role in biofuel Industry. Up to the present time no such measures of success has been achieved to use weeds for the extraction of the lignin in native form. The aim of this experiment is to extract the lignin and also to obtain all the byproducts obtained during the extraction for an eco-friendly process. In this study, lignin was extracted from seven different invasive weeds by Soxhlet extraction method. Lignin obtained from this method is in native form and also to obtain the other products present in the biomass. The lignin was extracted by treating biomass with the solvent in a soxhlet extractor. Lignin was dissolved in the solvent which was then recovered by distillation, using the vacuum rotary evaporator until a concentrated solution is obtained. The recovered solvent was reused. The concentrated lignin solution was precipitated using warm water and small amount of ammonium chloride dissolving sugars and carbohydrates. Sugar were released in the water when the concentrate was washed with warm water and was estimated which can be used for fermentation and other process. The precipitated lignin was dried and was then washed with diethyl ether dissolving all the fatty acids, resins and waxes. Isolated lignin were purified to remove impurities and characterized by Fourier transform infrared spectroscopy (FTIR), Thermogravimetric analysis (TGA) and Differential scanning calorimetry (DSC) analysis to compare thermal properties and chemical composition.

Keywords: Lignin, Invasive weeds, Soxhlet apparatus, Thermogravimetric Analysis, Fourier Transform Infra Red Spectroscopy

SEEC–2017–80

NUMERICAL STUDY OF EFFECT OF DIESEL INJECTION STRATEGY ON HYDROGEN DIESEL DUEL FUEL COMPRESSION IGNITION COMBUSTION

Gaurav Tripathi
School of Engineering
IIT Mandi
Email: g_tripathi@ students.iitmandi.ac.in

Priybrat Sharma
School of Engineering
IIT Mandi
Email:priybrat_s@students.iitmandi.ac.in

Atul Dhar
School of Engineering
IIT Mandi
Email: add@iitmandi.ac.in

ABSTRACT

Hydrogen has many desirable combustion properties, suitable for compression ignition engines. Hydrogen enriched diesel combustion results in lower soot and unburned hc. But hydrogen enrichment generally increases the nox production as the average in-cylinder temperature increases with the addition of hydrogen. In this numerical study, the dual-injection technique is used to attain premixed charge compression ignition (pcci) in hydrogen-diesel dual fuel compression ignition engine. Dual injection allows better mixing of the fuel and reduces the peak temperature inside the cylinder. Numerical model created for this study is validated against published data. Hydrogen is injected through intake manifold and diesel is injected directly into cylinder with varied injection strategies. Several parameters are studied including the premixed hydrogen amount, timing and mass of diesel injected according to various injection strategies. From studies, it is inferred that pcci dual fuel combustion mode improves imep and reduces nox emissions due to lower combustion temperature and also is effective in reducing soot emissions.

Keywords：dual fuel, premixed charge, emission reduction.

NOMENCLATURE

ATDC   After Top Dead Center
BTDC   Before Top Dead Center
CA   Crank Angle

INTRODUCTION

Particulate Matter (PM) and nitrogen oxides (NOx) are primal emissions which need to be reduced in a diesel engine to make them more eco-friendly. Low-temperature combustion (LTC) techniques tend to result in reduced particulate matter and nitrogen oxides emissions [1-3]. Low-temperature combustion can be achieved by premixing of fuel, causing the advanced start of combustion (SOC) and resulting in longer combustion duration. The amount of premixing is categorized further, predominantly as homogeneous charge combustion ignition (HCCI) technique and premixed charge combustion ignition (PCCI) technique [4]. HCCI technique present a problem of controlling the start of combustion and combustion phasing [5-6]. This issue can be resolved in PCCI technique as combustion phasing can be controlled by controlling injection timing of the primary fuel [4].Merging dual fuel combustion with PCCI improves the overall air-fuel ratio of and reduces PM and NOx emission in compression ignition engines (CI) [7]. In a study by Saravanan et. al. they showed that 20% premixing of ethanol and gasohol (90% gasoline and 10% ethanol) followed by direct injection of diesel fuel in four-stroke naturally aspirated air cooled constant speed CI engine results in 67% and 70% reduction in smoke in case of ethanol and gasohol premixing. They also reported 24% and 30% reduction in NOx in ethanol and gasohol premixed case and 20% increase in brake thermal efficiency (BTE) in ethanol and gasohol premixing in dual

fuel mode [8].In last few decades used of hydrogen in internal combustion engine as primary and secondary fuel is extensively researched. Hydrogen provides good control over emission because of various benefits associated, such as wide flammability range and better mixing with air owing to high diffusivity [9-11]. The present work explores the possibility of PCCI in hydrogen-diesel dual fuel in compression ignition engine. The integration of PCCI and dual fuel is done and its effect on reduction in emission and enhancement in the efficiency of CI engine is studied.

MODEL DESCRIPTION AND VALIDATION

A duel fuel CI engine model has been developed with the help of CONVERGE CFD numerical tool. Modelled engines specification are described in table 1. Hydrogen is naturally aspirated with intake air and diesel is injected directly. Hybrid KH-RT model is used for model atomization and the break-up of spray along with NTC collision model [7, 12-14]. RNG k-Ɛ model is used for turbulent flow along with wall function model i.e. O'Rourke and Amsden wall heat transfer model, which numerically predicts the heat transfer through the boundary [15]. CONVERGE CFD uses SAGE detailed combustion chemistry solver, also known as integrated LLNL chemistry solver code. Developed model uses N-Heptane as fuel surrogate because of its Cetane number being close to that of diesel. Hiroyasu soot model and extended Zeldovich model are used to determine the amount of soot and NOx produced [16-17]. For simulation 50,000 diesel sprays parcels are used along with 1.4 mm grid size. Adaptive mesh refinement and fixed embedding are used in boundary and spray, respectively. To study multi-injection strategy in hydrogen- diesel dual fuel engine, case iterations are run after varying injection timing and mass in the split injection.

TABLE 1: ENGINE SPECIFICATION IN MODEL

S. No.	Parameter	Specification
1	Engine type	CI engine
2	Bore (mm)	102
3	Stroke (mm)	116
4	Displacement volume (CC)	947.3
6	Compression ratio	19.5:1
7	Rated speed (rpm)	1500
8	IVO and IVC (Degree crank angle)	43° bTDC and -113° bTDC
9	EVO and EVC (Degree crank angle)	-93°aTDC and 39°aTDC

In order to validate the developed model, in-cylinder pressure data is compared with V. Chintala et. al. experimental data [18]. The Pressure trace of simulation shows a close match with experimental data within an acceptable deviation of 2.4 % (Fig. 1).
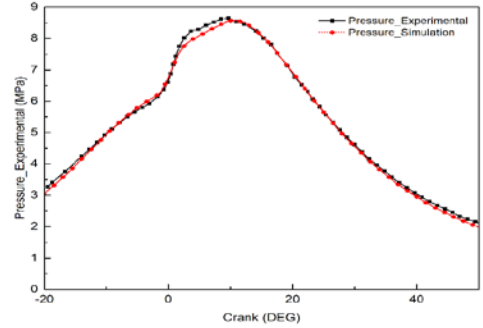
FIGURE 1. PRESSURE TRACE OBTAINED FROM EXPERIMENT AND SIMULATION

RESULT AND DISCUSSION

EFFECT OF START OF INJECTION (SOI) VARIATION FOR SINGLE INJECTION

EMISSION CHARACTERISTICS

Figure 2 (a) shows HC and CO variation with SOI timing. In this figure, when SOI timing varied from -2° ATDC to -23° ATDC, HC and CO emissions decreases. Maximum CO and HC emissions formed when SOI is timed at -2° ATDC. As the SOI timing is changed from -2° ATDC to -23° ATDC, soot value decreases while NO_x value increases (Figure 2 (b)). Soot value is minimum at -23° ATDC while NO_x value is minimum at -2° ATDC.
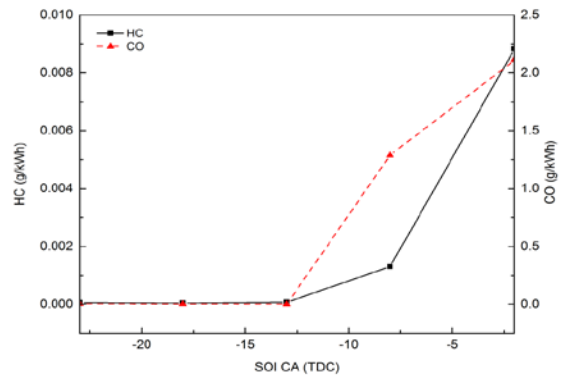
(a)
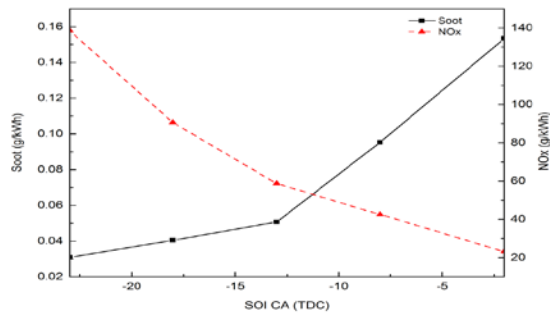
(b)

FIGURE 2. (a) HC, CO AND (b) SOOT, NO$_X$ VARIATION FOR DIFFERENT SOI TIMING WITH SINGLE INJECTION

COMBUSTION AND PERFORMANCE CHARACTERISTICS

Advancing the injection timing from 2°BTDC to 23°BTDC increases the peak in-cylinder pressure and peak heat release rate (figure 3(a)). On changing SOI timing from -2°ATDC to -23°ATDC, gIMEP first increases and then starts to decreases. The maximum value of gIMEP is registered at -8°ATDC. As injection timing is advanced, there is a continuous increase in RPR (figure 3(b)).
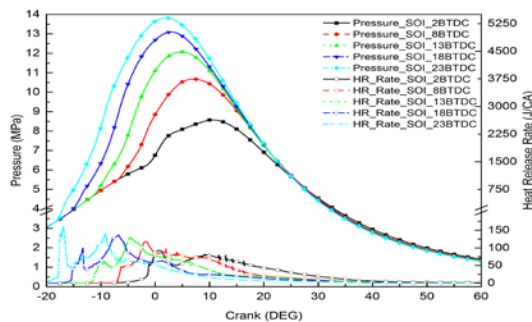
(a)
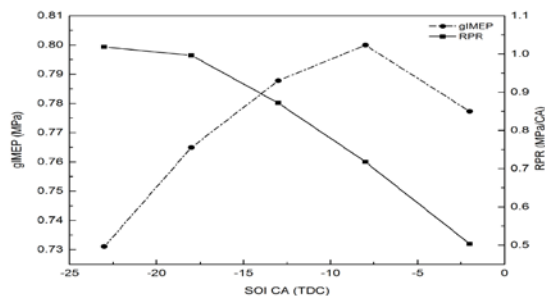
(b)

FIGURE 3. (a) IN-CYLINDER PRESSURE AND HEAT RELEASE RATE AND (b) GIMEP, RPR VARIATION FOR DIFFERENT SOI TIMING WITH SINGLE INJECTION

EFFECT OF MASS VARIATION

EMISSION CHARACTERISTIC

Figure 4 (a) shows HC and CO variation with SOI timing for a different amount of pilot mass injection. Minimum CO and HC is formed at -16° ATDC for all cases from 30% to 10% pilot mass injection. Soot and NO$_x$ value trade-off can be seen in Figure 4 (b) as the SOI1 timing and mass is varied. When SOI1 timing is changed from -24° ATDC to -12° ATDC, for 30% pilot injection NO$_x$ value first increases then decreases while soot value first decreases and then increases (figure 4(b)).
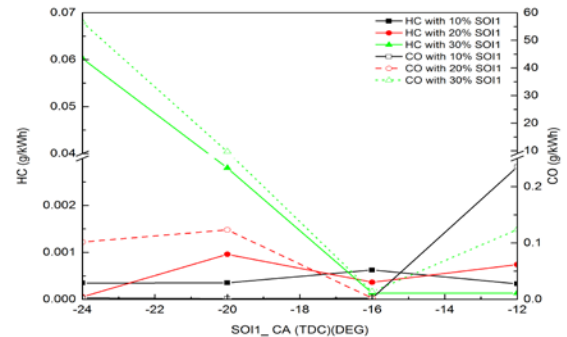
(a)
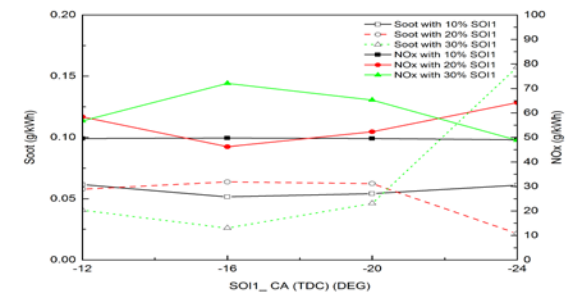
(b)

FIGURE 4. (a) HC, CO AND (b) SOOT, NO$_X$ VARIATION WITH DIFFERENT PILOT INJECTION TIMING FOR DIFFERENT PILOT MASS INJECTION

CONCLUSIONS

Following conclusions are drawn from the investigations.

1. When SOI timing for single injection is varied from 2°BTDC to 23°BTDC. CO and HC emissions are decreases. The gIMEP value maximum at 8°BTDC. Considering the trade-off between soot and NO$_x$ value, 8°BTDC to 13°BTDC obtained as an optimum range. Peak in-cylinder pressure and HRR maximum at 23°BTDC.
2. When first injection timing varies from 12°BTDC to 24°BTDC. HC and CO emissions are first

3

decreases and then increases. Minimum HC and CO emissions are obtained at 16°BTDC for 30%, 20% and 10% pilot mass injection. Peak in-cylinder pressure and HRR maximum at 23°BTDC for 30%, 20% and 10% pilot mass injection. Highest in-cylinder pressure and HRR is obtained for 30% pilot mass injection in comparison to 20% and 10% pilot mass injection.

3. When first injection timing varies from 12°BTDC to 24°BTDC. NO$_x$ value first increases then decreases and minimum NO$_x$ value occur at 24°BTDC for 30% pilot mass injection. NO$_x$ value first decreases then increases and minimum NO$_x$ value occur at 16°BTDC for 20% pilot mass injection. And soot value first decreases then increases and minimum soot value occur at 16°BTDC for 30% pilot mass injection. And soot value first increases then decreases and minimum soot value occur at 24°BTDC for 20% pilot mass injection. For 10% pilot mass injection, soot and NO$_x$ value approximately remain constant with varying first injection timing.

REFERENCES

[1] Uyumaz, A., 2015, "An Experimental Investigation Into Combustion and Performance Characteristics of an HCCI Gasoline Engine Fueled With n-Heptane, Isopropanol and n-Butanol Fuel Blends at Different Inlet Air Temperatures," Energy Convers. Manage., 98, pp. 199–207.

[2] Canakci, M., 2012, "Combustion Characteristics of a DI-HCCI Gasoline Engine Running at Different Boost Pressures," Fuel, 96, pp. 546–555.

[3] Benajes, J., Novella, R., Garcia, A., Domenech, V., and Durrett, R., 2011, "An Investigation on Mixing and Auto-Ignition Using Diesel and Gasoline in a Direct-Injection Compression-Ignition Engine Operating in PCCI Combustion Conditions," SAE Paper No. 2011-37-0008.

[4] Musculus, P. B., Miles, C., and Pickett, L. M., 2013, "Conceptual Models for Partially Premixed Low-Temperature Diesel Combustion," Prog. Energy Combust. Sci., 39(2–3), pp. 246–283. Operation—An Experimental Investigation," Energy, 35(9), pp. 3614–3622.

[5] He, B. Q., Liu, M. B., and Zhao, H., 2015, "Comparison of Combustion Characteristics of n-Butanol/Ethanol–Gasoline Blends in a HCCI Engine," Energy Convers. Manage., 95, pp. 101–109.

[6] Yao, M., Zheng, Z., and Qin, J., 2006, "Experimental Study on Homogeneous Charge Compression Ignition Combustion With Fuel of Dimethyl Ether and Natural Gas," ASME J. Eng. Gas Turbines Power, 128(2), pp. 414–420.

[7] Saxena, S., Bedoya, I.D., 2013, "Fundamental phenomena affecting low temperature combustion and HCCI engines, high load limits and strategies for extending these limits," Prog. Energy Combust. Sci. **39**, 457–488

[8] Saravanan, S., Pitchandi, K., Suresh, G., 2015, "An experimental study on premixed charge compression ignition-direct ignition engine fueled with ethanol and gasohol," Alexandria Engineering Journal, 54, 897–904.

[9] Verhelst, S., Wallner, T., 2009, "Hydrogen-fueled internal combustion engines," Prog Energy Combust Sci;35:490–527. doi:10.1016/j.pecs.2009.08.001.

[10] White, C.M.M., Steeper, R.R.R., Lutz, A.E.E., 2006, "The hydrogen-fueled internal combustion engine: a technical review," Int J Hydrogen Energy;31:1292–305. doi:10.1016/j.ijhydene.2005.12.001.

[11] Verhelst, S., 2014, "Recent progress in the use of hydrogen as a fuel for internal combustion engines," Int J Hydrogen Energy 2014;39:1071–85. doi:10.1016/j.ijhydene.2013.10.102.

[12] Dukowicz, J.K., 1980, "A particle-fluid numerical model for liquid sprays," J Comput Phys;35:229–53. doi:10.1016/0021-9991(80)90087-X.

[13] Reitz, R.D., Beale, J.C., 1999, "Modeling spray atomization with the kelvin-elmholtz/rayleigh-taylor hybrid model," At Sprays;9:623–50. doi:10.1615/AtomizSpr.v9.i6.40.

[14] Schmidt, D.P., Rutland, C.J., 2000, "A New Droplet Collision Algorithm," J Comput Phys;164:62–80. doi:10.1006/jcph.2000.6568.

[15] Han, Z., Reitz, R.D., 1995, "Turbulence Modeling of Internal Combustion Engines Using RNG κ-ε Models," Combust Sci Technol;106:267–95. doi:10.1080/00102209508907782.

[16] Hiroyasu, H., Kadota, T., 1976, "Models for Combustion and Formation of Nitric Oxide and Soot in Direct Injection Diesel Engines," SAE Int:513–26. doi:10.4271/760129.

[17] Heywood, J.B., 1988, "Internal Combustion Engine Fundamentals". vol. 21.

[18] Chintala, V., Subramanian, K.A., 2016, "Experimental investigation of hydrogen energy share improvement in a compression ignition engine using water injection and compression ratio reduction," Energy Convers Manag;108:106–19. doi:10.1016/j.enconman.2015.10.069.

SEEC-2017-081

Bioelectrochemical system for harnessing sustainable energy from Pharmaceutical wastewaters

R. Kannaiah Goud*
Department of Microbiology,
Palamuru University,
Mahabubnagar,
Telangana State -509001, India.
E-mail: rk_goud10 @yahoo.co.in

Pavan Kumar Pindi
Department of Microbiology,
Palamuru University,
Mahabubnagar,
Telangana State -509001, India.
E-mail: pavankumarpindi@gmail.com

S. Venkata Mohan
Bioengineering and Environmental Sciences Lab,
EEFF Department, CSIR-Indian Institute of Chemical Technology (CSIR-IICT),
Hyderabad- 500007, India.
E-mail: vmohan_s@yahoo.com

ABSTRACT

The potential impacts of pharmaceutical residues in the environment have been an emerging research area during recent years. In order to develop a system for synergistic removal of organics and salts from these wastewaters while enabling energy and nutrient recovery is proposed, studying the effect of salt on organic removal was necessary. The microbial electrolysis cell capable of hydrogen production was developed using A microbial fuel cell (MFC) anode evolved for salt tolerance. Conversion of organic contaminants in pharmaceutical wastewater to hydrogen was investigated. This was attained during the first few days of the optimization process using different salt concentrations. The MFC performance was measured by current density and power density to quantify the bioenergy production from the organic contaminants. The results indicated tolerance of up to 30 g/L salt and optimal anode performance at 20 g/L salt concentration. Improved current density was observed with medium salt concentrations.

Keywords
*Bioelectrochemical systems (BES); Biofuel cell; .
Pharmaceutical wastewater; Microbial diversity analysis.*

INTRODUCTION

Energy security is a major challenge that needs innovative solutions. The potential impacts of pharmaceutical residues in the environment have been an emerging research area during recent years. Recent investigations of Chinese and Indian production units have shown that certain production sites are contributing to environmental pollution levels far above those previously reported. Hyderabad is one of the world's largest hubs for the bulk drug industry, supplying Europe, the United States, and other regions with many of the most widely used generic active substances. These pollutants are the special concern owing to their recalcitrance and persistence in the environment which require effective treatment prior to disposal. Toxic pollutant present in pharmaceutical wastewater needs a specific treatment process viz., physical, physico-chemical and biological which are cost effective and retreatment is needed. Hence finding an alternative technology with low-cost and ecofriendly means of treating these wastewaters is necessary and important. Microbial fuel cell (MFC) as bioelectrochemical treatment presents an exciting and sustainable alternative technology for simultaneous energy generation and wastewater treatment. Bio-electrochemical systems (BES) facilitate direct transformation of chemical energy stored in bio-convertible material/wastewater to electrical energy via a series of bio-electrochemical reactions in defined fuel cell. A new approach to remove organics and salts from these wastewaters while enabling

energy and nutrient recovery is proposed. The goal of this research is to evaluate the potential of complex chemical wastewater to bioelectrosynthesis of biofuels through microbial electrolysis systems and salt removal. It consists of a coupled microbial electrolysis-fuel cell system to generate electricity from organic waste. The approach has potential to improve efficiency because the unit operations used are intrinsically energy-efficient.

Material and Methods

Pharmaceutical wastewater

Real-field PW acquired from a bulk drug manufacturing unit in Polepally, Jadcherla, Mahabubnagar, Telangana, India was used to evaluate the performance of Dual-chambered Microbial fuel cell. The sample collected from the manufacturing unit was stored at 4˚C. Prior to usage, the wastewater was adjusted to ambient temperature and further diluted to the required COD level with tap water. Characteristically, the wastewater was complex and recalcitrant in nature due to its low biodegradability (BOD/COD, 0.31) and high salts concentration.

Biocatalyst

Anaerobic consortium collected from a full scale anaerobic reactor treating chemical wastewater was used as inoculum for startup of anodic chamber. Prior to inoculation, the parent inoculum was washed twice with saline buffer (5000 rpm, 20° C) and enriched in DSW under anaerobic microenvironment at pH 7.0 at a temperature of 25˚C for duration of 24 h.

MFC Setup

The bioelectrochemical system used in this study consisted of a two-chamber cell that was convertible between MFC and MEC. Dual-chambered Microbial fuel cell with open air-cathode was fabricated using perspex material with a total/working volume of 0.5/0.44 l. Non-catalyzed graphite plates (7 cm X 3.5 cm; 0.6 cm thick) with a surface area of 61.6 cm^2 of surface area were used as electrodes. Nafion-117 (Sigma-Aldrich) was used as the proton exchange membrane (PEM). The anode was completely submerged in the anolyte (wastewater). The cathode was partially in contact with the anolyte and the top portion was exposed to air where oxygen acts as terminal electron acceptor. After adapting the system initially with DSW, the feed was shifted to pharmaceutical wastewater. Feeding and recirculation operations were performed by peristaltic pumps. Proper care was taken in the design to maintain anaerobic condition throughout the operation.

Analytical procedures

The performance of systems with respect to treatment efficiency was evaluated by monitoring chemical oxygen demand (COD) (closed-reflux (titrimetric) method 5220-C), TDS (2540-C), color (2120-B), sulfates (4500-E), nitrates (4500-B), phosphates (4500-D), chlorides (4500-B), pH (4500-H+B) and turbidity (2130-B) according to standard methods (APHA, 1998). Voltage and current were measured using a digital multi-meter. Cyclic voltammetry (CV) was used to study the bioelectrochemical behavior of biocatalyst in both systems during stabilized phase of operation using potentiostat-galvanostat system (Autolab-PGSTAT12, Ecochemie).

Chronoamperometry

The air–cathode was converted to an oxygen-free cathode by sparging with N2 to enable operation of the system as MEC. Additionally, the cathode chamber was filled with 10 ml of 100 mM phosphate buffer. A viton tube was attached to the cathode outlet for graduated cylinder containing distilled water for gas collection. Chronoamperometric measurements were conducted by poising the anode electrode at a potential of -0.2 V relative to a Ag/AgCl reference electrode. The cell potential was also recorded to determine the total energy applied to the cell. Salt concentrations up to 30 g/L were tested in batch studies to assess hydrogen production. The current and hydrogen production was studied in an MEC for 25 g/L salt concentration was compared with no added salt in a duplicated experiment conducted over two consecutive days for a period of 18 hours. At the end of each run, the volume displaced by hydrogen production was measured, gas samples for GC analysis were taken from the cathode outlet to confirm hydrogen production.

Molecular studies

Microbial composition was investigated to determine the microbial community changes by using 16s rRNA analysis.

RESULTS AND DISCUSSION

Bioanode development and current production

A chemical-tolerant microbial consortium was developed by exposing the anode to gradually increasing different salt (NaCl 5 g/L to 35 g/L) concentrations over a period of two months. The system was operated as a MFC during this enrichment period. Effect of organic loading on MFC performance was examined and current trends were observed. A current density of 4.88 A/m^2 was observed at an organic loading of 0.2 g/L-day. Effect of poised potential on MEC performance indicated that current production did not increase above an anode poised potential of -0.2V vs. Ag/AgCl. All subsequent MEC experiments were conducted at an anode poised potential of -0.2V vs. Ag/AgCl electrode.

MEC performance under batch conditions

Performance of the bioanode was examined under batch conditions at an Glucose concentration of 0.3 g/L. The PW concentration was varied from 0 to 0.5 g/L, and the current density, efficiency and rate of hydrogen production were measured. Current and hydrogen production began immediately addition of substrate and lasted for a period of 14 to 18 hours. The current production and corresponding hydrogen evolution was highest at the beginning of the run and diminished steadily with time. The decay in current was potentially to be due to a gradual decrease in substrate concentration. This was examined further by operating the MEC under different substrate concentrations. The PW concentration showed an interesting effect on the MEC performance. Typically, an increase in current is observed with increasing PW concentration up to a certain concentration, after which the high PW concentration inhibits the microbial activity. It was observed that the rate of decay of the current with substrate concentration decreased with increasing organic loading concentration.

Substrate loading effect on current production

The batch experiments demonstrated current production with time to determine efficiency of bio anode increasing substrate loading. The effect of substrate on current production was examined at different loading rates in batch MECs. The experiments were conducted for a 3-18 hour period at each substrate loading condition. The current increased linearly with substrate loading. Steady production of current for several hours shows stability of MEC operation and confirms the effect due to the change in substrate loading.

CONCLUSIONS

The Experimental data successfully documented an efficient waste-to-energy powered, synergistic technology for simultaneous salt and organic removal, which can be applied to treatment of pharmaceutical waste water. Salt adapted bio anode enriched catalytic microenvironment promoted multi-pollutant removal from wastewater with simultaneous power production from a low biodegradable pharmaceutical waste water.

ACKNOWLEDGEMENTS

REFERENCES

[1]. K. Wang, S. Liu, Q. Zhang, Y. He, Pharmaceutical wastewater treatment by internal micro-electrolysis–coagulation, biological treatment and activated carbon adsorption, Environmental Technol. 30 (2009)1469–1474.

[2]. G. Velvizhi, S. Venkata Mohan, Biocatalyst behavior under self-induced electrogenic microenvironment in comparison with anaerobic treatment: Evaluation with pharmaceutical wastewater for multi-pollutant removal, Bioresource Technol. 102 (2011) 10784–10793.

[3]. C. Tyler Pannell, R. Kannaiah Goud, J. Daniel, J. Schell, AP. Borole, Effect of fed-batch vs. continuous mode of operation on microbial fuelcell performance treating biorefinery wastewater, Biochemical Engineering Journal. 116 (2016) 85–94.

[4]. S. Venkata Mohan, S. Veer Raghavulu, P. Dinakar, P.N. Sarma, Integrated function of microbial fuel cell (MFC) as bio-electrochemical treatment system associated with bioelectricity generation under higher substrate load. Biosens. Bioelectron, 24 (2009) 2021–2027.

[5]. T. Sleutels, S. Molenaar, A. ter Heijne, C.J. Buisman, Low substrate loadinglimits methanogenesis and leads to high coulombic efficiency inbioelectrochemical systems, Microorganisms. 4 (2016) 1–11.

CO₂ BASED COMBINED POWER AND REFRIGERATION CYCLE – A SCHEME FOR LOW GRADE WASTE HEAT RECOVERY

Subha Mondal
Department of Mechanical Engineering
Aliah University, Kolkata-700156
subhamondal53@gmail.com

Sudipta De
Department of Mechanical Engineering
Jadavpur University, Kolkata-700037
de_sudipta@rediffmail.com

Mohsen Assadi
Faculty of Science and Technology
University of Stavanger, Stavanger, Norway
assadi@uis.no

ABSTRACT

CO_2 at supercritical state is a preferable working fluid for low grade waste heat recovery due to a low critical temperature of CO_2. In the present study a CO_2 based combined power and refrigeration cycle is proposed in which CO_2 coming out from the evaporator of the refrigeration system is pressurized to heat recovery unit pressure. The cycle is driven by the low grade waste heat of industrial flue gas containing small amount of SO_2. It is observed that improved refrigeration effect achieved by allowing a larger mass fraction of CO_2 flow into the evaporator leads to a reduction in net cycle power output. However, overall cycle performance (represented by 1st law efficiency) improves as larger mass fraction of CO_2 enters the evaporator. Exponential growth of the physical size (i.e. NTU) of the regenerator limits the maximum practical value of CO_2 mass flow into the evaporator.

*Keywords***:**
Combined power and refrigeration, CO_2, NTU
.

NOMENCLATURE

h	Enthalpy in kJ/kg
c_{Pg}	Specific heat of flue gas in kJ/kgK
C_{min}	Minimum heat capacity in kJ/K
m_{CO2}	CO_2 flow rate in kg/s
m_g	Flue gas flow rate in kg/s
NTU_{REGEN}	Number of transfer unit for the regenerator
P_{COOLER}	Cooler pressure in MPa
Q_{RE}	Refrigeration effect in kW
r	Fraction of CO_2 mass entering the evaporator
T_{gi}	Flue gas inlet temperature in K
T_{go}	Flue gas outlet temperature in K
W_{NET}	Cycle power output in kW
W_{REF}	Requisite power for producing Q_{RE} refrigeration effect by a vapor compression cycle in kW
η_I	1st law efficiency
1-10	state points

INTRODUCTION

As a substantial part of industrial energy input through combustion of fuel is finally rejected as low grade waste heat waste heat recovery would appear as one of the sustainable options in the energy sector. Secondary energy can be generated using industrial waste heat through transcritical and subcritical organic Rankine cycles [1-5]. CO_2 at supercritical state is preferred for low grade heat recover due to better matching of temperature of its temperature profile with that of heat source [6]. Also CO_2 is having zero ODP and one GWP. Substantial studies are conducted to explore the capability of CO_2 based power

cycle for generating power [7-9]. Also CO_2 is utilized as the working fluid in refrigeration and heat pump cycle [10-11].

In the present study a transcritical CO_2 cycle is proposed that can produce simultaneous power output and refrigeration effect using low grade heat of industrial flue gas with smaller amount of SO_2 content. Thus flue gas is not allowed to cool below 120^0C to avoid sulphuric acid condensation. In the proposed cycle the CO_2 stream coming out from the refrigerator evaporator is pressurized to gas heater pressure and allowed to mix with the main CO_2 steam coming out from the regenerator. Thus, CO_2 enters the heat recovery unit at some higher temperature and using same waste heat larger mass of CO_2 can be heated.

SYSTEM DESCRIPTION

P-h diagram of the proposed cycle is presented in the FIG.1. The CO_2 stream coming out from the turbine (i.e. state-2) after being cooled in the regenerator (i.e. process 2-3) and cooler (i.e. process 3-4) is split into two streams. One stream after undergoing a throttling process (i.e. process 4-5) enters the refrigerator evaporator. Another stream is pressurized to heat recovery unit pressure (i.e. state5).
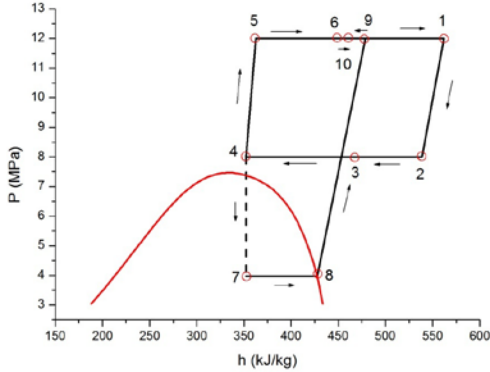
FIGURE 1. P-h diagram of the proposed cycle

The CO_2 stream coming out from the evaporator at state-8 is pressurized to heat recovery unit pressure (i.e. state-9) and allowed to mix with the CO_2 stream coming out from the regenerator at state-6. After mixing the total CO_2 mass enters the heat recovery unit at state-10 and is heated to turbine inlet condition (i.e. state-1).

MATHEMATICAL MODELLING

During the mathematical modelling it is assumed that 20 kg/s of flue gas is available at 170^0C as the heat source. The flue gas exit temperature for gas heater is restricted to 120^0C to avoid sulphuric acid condensation. Turbine and compressor isentropic efficiencies are 85% and 80% respectively. In the regenerator, CO_2 stream coming out from the turbine is

cooled to lowest possible temperature assuming a 10^0 C pinch point temperature difference.

From the energy balance of the heat recovery unit

$$m_{CO_2} = \frac{m_g c_{Pg}(T_{gi} - T_{go})}{h_1 - h_{10}} \quad (1)$$

Now cycle power output will be

$$W_{NET} = m_{CO_2}(h_1 - h_2) - m_{CO_2}(1 - r)(h_5 - h_4) \\ - m_{CO_2} r(h_9 - h_8) \quad (2)$$

Refrigeration effect can be calculated by equation-(3) as follows:

$$Q_{RE} = m_{CO_2} r(h_8 - h_7) \quad (3)$$

Now 1st law efficiency will be

$$\eta_I = \frac{W_{NET} + W_{REF}}{m_g c_{Pg}(T_{gi} - T_{go})} \quad (4)$$

In equation (4), W_{REF} is the power input would have been required to run a vapour compression refrigerator between the evaporator and cooler pressure for obtaining Q_{RE} refrigeration effect.

The physical size of the refrigerator is denoted by NTU and this can be determined as follows:

$$NTU_{REGEN} = \sum_{i=1}^{20} NTU_i \quad (5)$$

For determining NTU of regenerator entire regenerator is divided in 20 elements. In the above equation NTU_i is the NTU of ith element.

$$NTU_i = \frac{\Delta Q_i}{LMTD_i \, C_{min}} \quad (6)$$

RESULTS AND DISCUSSION

In the present study a CO_2 based combined power and refrigeration cycle is proposed. Assuming 150^0C turbine inlet temperature and 12MPa turbine inlet pressure, effects varying cooler pressure and CO_2 mass fraction flow to evaporator on cycle performance are evaluated. During the analysis evaporator temperature is assumed to be fixed at 5^0C and corresponding CO_2 exit temperature form cooler be 35^0C.

Effect of varying cooler pressure on net cycle power output is shown in FIG.2. It is observed that there exists an optimum cooler pressure for a maximum cycle power output. Both turbine power output and power input to the compressor operating between cooler and regenerator decrease with an increase in cooler pressure. Initially compressor power input drops sharply due to larger shift of compression line in towards the left of P-h diagram along

the 35^0C isotherm. However, for higher cooler pressure this shifting is negligible. Thus above the optimum cooler pressure net cycle power output decreases due to dominating effect of decreasing turbine power output.
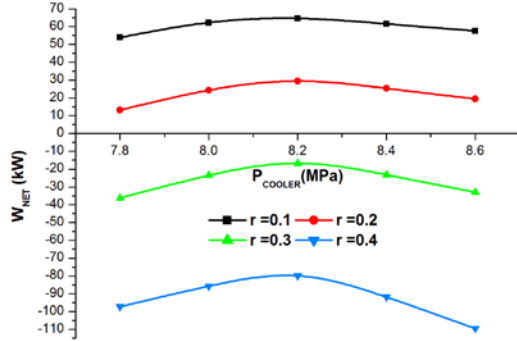
FIGURE 2. W_{NET} vs. P_{COOLER}

From FIG.2 it is also clear that cycle power output sharply decreases as larger fraction of CO_2 mass enters into the evaporator due to larger power consumption of the compressor operating between evaporator and gas heater pressures. Above certain value of CO_2 mass fraction entering the evaporator cycle power output even becomes negative or cycle becomes merely a refrigeration cycle.
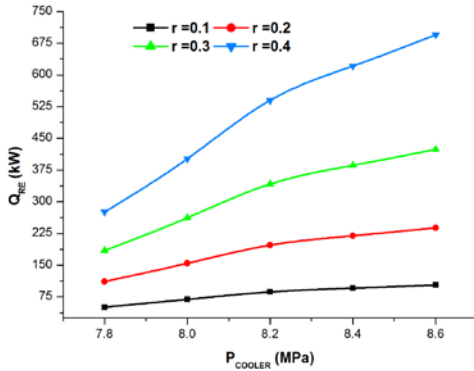
FIGURE 3. Q_{RE} vs. P_{COOLER}

It is observed in FIG.3 that refrigeration effect increases with an increase in cooler pressure as enthalpy of CO_2 stream at evaporator inlet or cooler exit decreases. It is clear from FIG.3 that refrigeration effect increases as larger mass fraction of CO_2 enters the evaporator.

It is observed in FIG.4 that there exists an optimum cooler pressure for the maximum 1st law efficiency for a specified flow rate of CO2 entering into the evaporator. Initially 1st law efficiency increases with an increase in cooler pressure as both cycle power output and refrigeration effect increase.
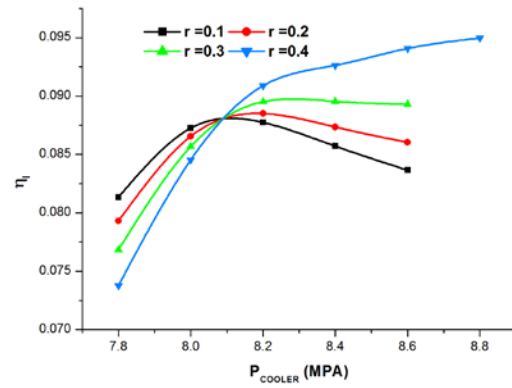
FIGURE 4. η_I vs. P_{COOLER}

However, cycle power output starts to decrease beyond a certain value of cooler pressure. Beyond the optimum value of cooler pressure decreasing trend of cycle power output becomes the dominating factor. Also it is observed that optimum value of 1st law efficiency improves as larger fraction of CO_2 mass enters the evaporator. With larger mass fraction of CO_2 entering into the evaporator, not only refrigeration effect improves but also larger mass of CO_2 can be heated by using same heat input in the heat recovery unit as CO_2 enters the heat recovery unit at some higher temperature. The optimum cooler pressure corresponding to maximum 1st law efficiency also increases as larger mass of CO_2 enters the evaporator. This is due to corresponding improvement of refrigeration effect associated with the larger mass flow of CO_2 in to the evaporator.
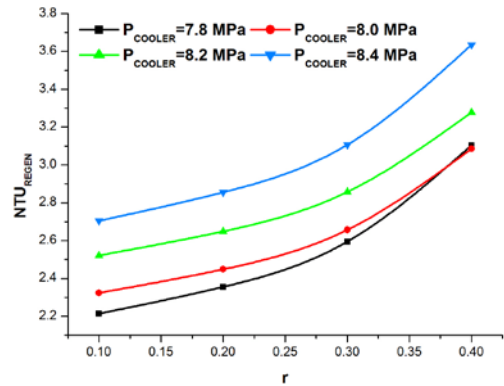
FIGURE 5. NTU_{REGEN} vs. R

It is observed in FIG.5 that an increment in mass flow rate of CO_2 into the evaporator leads to a larger size of regenerator (specified by NTU). For specified cooler pressure above certain value of CO_2 mass fraction flow this increment in NTU of the rgenerator is very rapid. Thus CO_2 mass fraction flowing into the evaporator should not be increased above certain value for maintaining an economically feasible size of the regenerator. It is evident from FIG.5 that NTU of the rgenerator increases with an increment in cooler pressure due to larger heat duty of the

regenerator (As turbine exit temperature increases with an increase in cooler pressure). Obviously effective temperature difference increases between hot and cold fluids with an elevated cooler pressure. However this effect is becomes less effective with larger cooler pressure as inlet temperature of cold fluid into the regenerator becomes almost constant for larger cooler pressures. Thus regenerator size increases at a slower rate with an initial increment in cooler pressure. However, this increment becomes faster as cooler pressure increases.

CONCLUSIONS

In the present study a CO_2 based combined power and refrigeration cycle driven by low grade heat of flue gas is proposed. It is observed that cycle power output decreases as larger fraction of CO_2 mass enters the evaporator. However, this results in larger refrigeration effect. Cycle performance is represented by the 1st law efficiency to consider combined effect of the cycle power output and the refrigeration effect. It is observed that there exists an optimum cooler pressure for maximum 1st law efficiency for specified mass fraction of CO_2 entering to the evaporator. The optimum value of 1st efficiency increases with larger mass fraction of CO_2 entering to the evaporator.

However, the mass fraction of CO_2 entering to the evaporator should not be increased above a certain value to maintain a practically feasible size of the regenerator.

REFERENCES

[1] Wang E.H, Zhang H.G, Fan B.Y, Ouyang M.G, Y. Zhao , Mu Q.H., 2011. "Study of working fluid selection of organic Rankine cycle (ORC) for engine waste heat recovery". Energy, 36, pp. 3406-3418.

[2] Wang Jiangfeng, Wang Zhequan, Wang Man, Ma Shaolin, DaiYiping, 2013. "Thermodynamic analysis and optimization of an (organic Rankine cycle) ORC using low grade heat source". Energy, 49. pp.356-365.

[3] Hung T.C, Shai T.Y, Wang S.K, 1997. "A review of organic Rankine cycles (ORCs) for the recovery of the low-grade waste heat". Energy, 22. pp.661-667.

[4] Yang Min-Hsiung, 2016. "Optimizations of the waste heat recovery system for a large marine diesel engine based on transcritical Rankine cycle". Energy, 113. pp. 1109-1124

[5] Tian Ran, An Qingsong, Zhai Huixing, Shi Lin, 2016. "Performance analyses of transcritical organic Rankine cycles with large variations of the thermophysical properties in the pseudocritical region". Applied thermal engineering, 101. pp. 183-190.

[6] Chen Y, and Lundqvist P , 2011. "The CO_2 power cycle for low grade heat recovery: Discussion on temperature profiles in system heat exchangers". ASME Power Conference 1. pp. 385-392.

[7] Mondal S, De S, 2015. "Transcritical CO_2 power cycle – effects of regenerative heating using turbine bleed gas at intermediate pressure". Energy, 87, July, pp.95-103.

[8] Mondal S, De S, 2015. "CO_2 based Power cycle with multi-stage compression and intercooling for low temperature waste heat recovery". Energy, 90, October, Pp. 1132-1143.

[9] Mondal S, De S, 2017. "Power by waste heat recovery from low temperature industrial flue gas by Organic Flash Cycle (OFC) and Transcritical-CO2 power cycle: a comparative study through combined thermodynamic and economic analysis". Energy, January, http://dx.doi.org/10.1016/j.energy.2016.12.126

[10] Sarkar J, Bhattacharyya Souvik, Ram Gopal M, 2005. "Transcritical CO_2 heat pump systems:exergy analysis including heattransfer and fluid flow effects". Energy conversion and management, August, pp. 2053-2067.

[11] Robinson Douglas M., Groll Eckhard A., 1998. "Efficiencies of transcritical CO_2 cycles with and without an expansion turbine: Rendement de cycles transcritiques au CO_2 avec et sans turbine d'expansion". International Journal of Refrigeration, Volume 21(7), November , pp. 577-589.

MAGIC OF Π-Π INTERACTION FOR CARBON CAPTURE

Deepak Pant
Himachal Pradesh Central University, Dharamshala
Email: dpant2003@gmail.com

ABSTRACT

The debate on the change in carbon pools and anthropogenic contribution has been always leading to confusion on its planning and management. Uncontrolled anthropogenic activities always create perturbation towards the projection of C in various pools. The human influence on the fluxes of carbon among the four reservoirs/ pools (atmosphere, ocean, fossil fuel and cement production and terrestrial) represents a small but significant perturbation of a huge global cycle. In the last decade (2002-2011) fossil fuel emission and cement production is responsible for 89% of the total CO2 emission and remaining 11% is due to land use changes. The CO2 emission rate is continuously increasing at a rate of 2.7 % per year against 1% in the year 1990. The total emission change from1960-2012 is partitioned among atmosphere (37-49%), ocean (26-27%) and terrestrial (37-24%). Weather events such as abnormally high temperature in January, 2014 (540C) in Australia, and at the same time Canada suffers from an extreme cold storms (~ -500C), breaking of 160-square-mile section of the Wilkins Ice Shelf from the coast of Antarctica (2008), droughts, bushfires, snow (almost simultaneously) in Australia in 2006, Hurricane Katrina in the United States in 2005, the European heat wave in 2003 killed more than 30,000 people making climate change as a issue of global concern.

Role of π electrons are very important in terms of carbon management activities in plants, prokaryotes and bacteria. There are eight biological pathways, namely reductive pentose phosphate pathway, Hatch-Slack cycle, Crassulacean acid metabolism, reductive citric acid cycle, 3-hydoxypropionate bicycle, dicarboxylate/4-hydroxybutyrate, 3-hydroxypropionate/4-hydroxybutyrate, and reductive acetyl-CoA,, known for converting inorganic carbon to organic material in cell biomass interaction. In all eight pathways carboxylation and reduction reaction are involved. Use of π-π interaction is important towards residue specific and group specific modification and can modify the cycles by synthetic-biological merger.

Keywords: Pi-Pi, carbon management, climate change, anthropogenic contribution, carbon pools

SEEC-2017-084

MECHANISTIC INVESTIGATION ON ULTRASONIC ENHANCEMENT OF DIHYDROXYACETONE PRODUCTION FROM GLYCEROL BY IMMOBILIZED GLUCONOBACTER OXYDANS MTCC 904

Pritam Kumar Dikshit
Indian Institute of Technology, Guwahati
Email: biotech.pritam@gmail.com

Vijayanand Moholkar
Indian Institute of Technology, Guwahati
Email: vmoholkar@iitg.ernet.in

ABSTRACT

With rapid increase in biodiesel sector in recent years, the production of crude glycerol from biodiesel industry surges rapidly. So to reduce the biodiesel cost and maintain the biodiesel production, it is necessary to find out a new applications of the side products produced from biodiesel industry. Glycerol, one of the by-product from biodiesel industry can be used as a potential carbon source for the production of various fine chemicals. Dihydroxyacetone (DHA) is one of the viable chemical widely used in food, cosmetic and pharmaceutical industries. Microbial fermentation route is one of the widely used process for the production of pharmaceutical products, as it is more efficient, economical and eco-friendly from chemical synthesis route. One of the principal demerit of fermentation process is its slow kinetics, so enhancement of the kinetics is one of the most effect practice to scale–up biochemical processes. In this study we have discussed this important issue using ultrasound irradiation for enhancement of DHA production. The cells were immobilized over polyurethane support as the carrier material which provides larger surface area for binding of cells over the surface. The fermentation experiments were carried out with previously optimized media components with three different glycerol concentration (viz. 20, 30, 50 g/L).Sonication experiments were carried out in an ultrasound bath (Make: Elma, Frequency: 35 kHz, Power: 35W) with optimized duty cycle of 20% (2 min ON and 8 min shaking). Results of ultrasound experiments were compared with control which were carried out in an incubator shaker (31 °C, 150 rpm). The percentage enhancement in DHA production was observed to be 76.56% with 20 g/L of initial crude glycerol concentration. Experiments were also conducted using pure glycerol as substrate and results are compared with crude glycerol.

Keywords: Immobilized cells, Gluconobacter oxydans, Glycerol, Dihydroxyacetone, Ultrasonication

SEEC-2017-85

COMBINATION OF CLASSICAL, MOLECULAR AND PROTEOMIC APPROACHES FOR ENHANCED CELLULASE PRODUCTION BY DEREGULATED MUTANTS DERIVED FROM RECOMBINANT *ASPERGILLUS* STRAIN

Bajjit Kaur
Department of Microbiology
Guru Nanak Dev University, Amritsar
India

HS Oberoi
Department of Microbiology
Guru Nanak Dev University, Amritsar
India

BS Chadha
Department of Microbiology
Guru Nanak Dev University, Amritsar
India

ABSTRACT

A heterokaryon 28, derived through protoplast fusion carried out between Aspergillus nidulans and Aspergillus tubingensis, was subjected to four cycles of mutagenesis followed by selection on increasing levels of (2 deoxy glucose) 2-DG as selectable marker. The derived deregulated cellulase hyper producing mutant '64', when compared to the wild type strain, produced 15.85, 27.07, 14.30, 9.36 and 23.65 folds higher endoglucanase, β-glucosidase, cellobiohydrolase, FPase and xylanase respectively, in shake flask cultures. The molecular analysis of amplified βG gene from wild and mutant showed nucleotide deletion/substitution. The developed mutant also showed highly catalytic efficient βG as indicated by observed low Km & high Vmax values. The expression profile as observed through zymogram analysis also indicated towards overexpression of βG and EG/xylanase. The mutant strains also showed distinct protein profiles and presence/absence of expressed proteins that were identified by peptide mass finger printing using LC/MS-MS. Furthermore the produced cellulases/hemicellulase from mutants showed efficient hydrolysis of alkali treated rice straw releasing higher levels of glucose and xylose as indicated by HPLC analysis. The developed cellulase was also employed in devising sequential two step process for efficient utilization of alkali treated rice straw.

SEEC- 2017-086

PRODUCTION, ULTRASONIC EXTRACTION, AND CHARACTERIZATION OF POLYHYDROXYBUTYRATE (PHB) USING BACILLUS MEGATERIUM AND RALSTONIA EUTROPHA AS POTENTIAL MICRO-ORGANISM

Sushobhan Pradhan
Indian Institute of Technology, Guwahati
Email: pradhan.sushobhan27@gmail.com

Maneesh Kumar Poddar
Indian Institute of Technology, Guwahati
Email: p.maneesh@iitg.ernet.in

Vijayanand Moholkar
Indian Institute of Technology, Guwahati
Email: vmoholkar@iitg.ernet.in

ABSTRACT

Being used in different industrial and domestic applications, petroleum –derived plastics such as polyethylene and polypropylene has become an essential part of our contemporary life. These petroleum-derived plastic are extremely persistent in nature, causing several complications to aquatic and terrestrial habitat. So it is necessary to develop a sustainable and permanent solution to resolve waste disposal problem in terms of developing biodegradable polymers. Polyhydroxyalkanoates (PHAs) are one of the attractive substitutes among various biodegradable polymer because of their similar material properties to various thermoplastics and elastomers, and complete degradability upon disposal under various environments. Polyhydroxybutyrate (PHB) and its copolymers are best characterized polymer among these with material properties similar to polypropylene and have been one of the industrial interest because of its biodegradable and/or biocompatible nature. The use of PHB in various industries such as packaging, medicine and agriculture has been increased recent days. PHB is synthesized by various micro-organisms as a carbon and energy reserve material when the microbes under go to environmental stresses such as nitrogen, phosphate or oxygen limitations. In this study, two different PHB producing strains such as Bacillus megaterium and Ralstonia eutropha were used using glucose and fructose as the carbon source in the fermentation medium. The fermentation experiment was carried out at 30°C, 150 rpm for 50 h. The cells were harvested and subjected to free drying followed by extraction of PHB granules using ultrasonic irradiation technique. Characterization of PHB was carried out using FTIR, NMR spectroscopy, XRD, DSC, and TGA analysis.

Keywords: Polyhydroxybutyrate, Bacillus megaterium, Ralstonia eutropha, Fermentation.

SEEC-2017-87

STRAIN IMPROVEMENT THROUGH INTER-SPECIFIC PROTOPLAST FUSION BETWEEN *ASPERGILLUS NIDULANS* AND *ASPERGILLUS TUBINGENSIS* FOR ENHANCED CELLULASE PRODUCTION

Jyoti Bhagat
Department of Microbiology
Guru Nanak Dev University, Amritsar
India

Baljit Kaur & BS Chadha
Department of Microbiology
Guru Nanak Dev University, Amritsar
India

ABSTRACT

The inter-specific protoplast fusion was carried out between two cellulolytic strains of Aspergillus nidulans and Aspergillus tubingensis. Thirty heterokaryons growing on selective medium containing 2- deoxyglucose (0.2% w/v) and showing intermediate spore color were picked for cellulase production under shake flask culture and solid substrate culturing at $40{_o}C$. Fusant 51 and 28 exhibited appreciably higher levels of endoglucanase, cellobiohydrolase, β- glucosidase and FPase activities when compared to parental strains. Employing proteomic based approaches the differential expression of proteins in secretome of fusants and parental strains were analyzed using two dimensional electrophoresis. The expression of some of the proteins in the fusants was found to be upregulated/down-regulated. The upregulated proteins in the fusant 51 were identified by liquid chromatography mass spectroscopy (LC/MS) as endoxylanase, endochitinase, β- glucosidase as well as hypothetical proteins. The cellulases produced by fusants 28 and 51 showed improved saccharification of alkali treated rice straw when compared to the parental strains.

SEEC-2017: 88

RICE HUSK AND STRAW VALORISATION VIA CHEMICAL PROCESSING FOR BIOENERGY APPLICATION AND ENVIRONMENT PROTECTION: A CRITICAL REVIEW

Shubham Kochhar
Chemical Conversion Division
Sardar Swaran Singh National Institute of Bio-Energy (MNRE) Kapurthala
Email : 42.shubham@gmail.com

Anil Kumar Sarma
Chemical Conversion Division
Sardar Swaran Singh National Institute of Bio-Energy (MNRE) Kapurthala
Email : draksarma@gmail.com

ABSTRACT

Sustainable development demands the conversion of agricultural wastes into useful form. Cellulose extraction from biomass, can be a way to produce bio fuels, taking us another step forward towards green energy. Traditional methods are difficult, costly and require solvents which are non reusable, thus posing an environment threat. Here in this paper, the most recent sustainable method of extracting cellulose from Rice husk and Rice straw, using Ionic Liquids is reviewed. Cellulose can be extracted using various hydrophilic Ionic Liquids which can be efficiently regenerated, making it a green process. The extracted cellulose is amorphous and can be more easily fermented and converted into biofuels. Also, the left biomass is free of soluble metals, which hinder in the extraction of silica from Rice husk and Straw. With the involved benefits and focus on green energy, further research could be carried out in order to make this process economical.

Keywords : Ionic liquids, Cellulose, Dissolution, Extraction. Hydrogen bonding, sustainable, Green method, biofuel

INTRODUCTION

Plumes of smoke arising from the fields is a common sight during rice harvesting season.In Asia, around 730 Metric tonnes of biomass are burned every year by both human and natural influences.Out of which, 250 Metric tonnes of biomass is burnt on the field after harvesting the crop[1].Rice straw is one of the main residues, and its management varies widely. Burning of rice husk and straw emits trace gases like carbon dioxide, methane, carbon monoxide, nitrogen oxide, sulphur oxide and large amount of particulate matters, which adversely affect human health as well as the environment[2]. Last year, the magnitude of stubble burning was so high that it received international attention. The National Aeronautics and Space Administration (NASA) released a satellite image showing large number of fires across millions of hectares of agriculture fields in India.Every year about 12 million tonnes of rice straw is burned in Punjab alone[3].Farmers consider burning of rice husk and straw as a quick and easy way to get rid of their agricultural wastes. The composition ofligno cellulose (LC)material in rice husk and ricestraw is around 72 to 85 %[4,5]. In recent studies conducted on the green sources of energy, a convincing scope of conversion of LCbio mass into bio-fuelshas been put forward [5]. Thus, extraction of LC material from rice waste, can bring a revolution to convert this agricultural waste into an energy source.

Traditional methods of extracting LC involves the use of cupro- ammoniumcompounds, xanthates and other solvents that are difficult, costly and cannot be reused.

As these solvents cannot be recovered after the dissolution process[6], they pose a threat to the environment, and their continued use questions the sustainable development that we aim for.
In past few years, after the discovery of Ionic

Liquids,(IL) there has been an increasing interest towards green methods of LC extraction using IL, which are also known as "Green Solvents", or "The solvents of future"[7].

ILs are ionic, salt-like materials that are liquid below 373 K. They can be put to use as process chemicals (e.g., solvents, separation media) and performance chemicals (Like electrolytes). IL tend to have appealing solvent properties and are miscible with water or organic solvents[7,5].Here in this paper, the dissolution of LC found in rice husk and rice straw, using IL has been reviewed, and also important future prospects in this field have been mentioned.

IONIC LIQUID AND LIGNOCELLULOSE – A RECENT APPROACH

The roots of this concept involving the use of IL to dissolve cellulose go back to 1934 when C. Graenacher dissolved cellulose using molten N-ethyl pyridinium chloride. Becausehe used a molten compound, the convenience of this process was very limited. Also, he wasn't able to regenerate the compound efficiently because of high temperature conditions[8].Another breakthrough in this field was achieved in year 2002, and then in 2011 when Rogers and his co-workers, studied the extraction of LC using different ionic liquids, and their recovery, thus presenting a clearer picture for further research[9,12].

RICE HUSK AND STRAW TREATMENT

LC from rice husk and rice straw dissolves without pretreatment, in various hydrophilic ILs like (1-alkyl-3-methlimidazolium Chloride)[$C_n$mim]Cl (n=2-8), (1-butyl-2,3dimethylimidazolium Chloride)[C_4mmim]Cl, (N-Butyl-3-methylpyridinium Chloride)[C_4mPy]Cl, (1-Ethyl-3-methylimidazolium acetate)[C_2mim][OAc], (1-Butyl-3-methylimidazolium acetate)[C4mim][OAc] and many others.
Solubility of various LC components in rice waste varies with the IL chosen, temperature at which extraction is carried out and also the time given for the process to complete[9,11]. In some cases, it is found that microwave heating and ultrasound treatment also increases the efficiency of extraction. Solutions with upto28.5% cellulose can be prepared in [C_4mim][OAc] at 343 K [9].

The process of dissolution ofLC occurs via hydrogen bond formation between the anion of IL and hydrogen present in LC, overcoming the H-bonds that already exist in cellulose and forming more stronger H-bonds with the anion.[10] This method provides amorphous cellulose with higher structural disruption which undergoes chemical conversion into other compounds, more easily and efficiently.[11,13] Thus, the choice of anion depends of their tendency to form better and stronger H bonds with oxygen atoms of LC, as compared to intra-lignocellulose H-bonding. The dissolved LC mass, is then easily precipitated using simple common solvents

like Ethanol, Acetone or water.[9,11] On adding these solvents to the sample containing IL and dissolved LC, the solvent molecules engulf the ions of Ionic liquids, forming H-bonds themselves and letting free the dissolved LC components, which precipitate[11].Ionic liquids containing anions that are non- coordinating in nature, including [BF4]- and [PF6]- do not show much dissolution [12].

The quantitative precipitation of a particular LC component among lignin, cellulose and hemicellulose depends on the IL used, solvent added for precipitation and the temperature conditions.
Water is found to preferentially precipitate cellulose, while ethanol precipitates out lignin and hemi cellulose preferentially. Amount of cellulose, hemicelluloses and lignin in the precipitate can be roughly analysed using Fibre analysis and precipitate analysis using filter bag technique [11].

In order to extract LC from rice waste, weight ratio of IL to Rice husk should be taken at least 15:1 for best results [5]. Pre-treatment of rice waste and IL, before dissolution process involves drying them, so as to eliminate all possible water component present, as water molecules hinder in the extraction process.After precipitation of LC material, filtration was carried out in a muffle furnace, maintained at a desired temperature, to decrease the viscosity and prevent crystallization of IL used [11]. The precipitated material is filtered off, and the residual IL in the filtrate can be reused by a simple evaporation process, thus giving clean regenerated sample [14].

Different ILs showed variable preference for dissolution of LC component. When considered three ILs, namely EMIM Ac, HMIM Cl, and AMIM Cl, it was found that EMIM Ac dissolved 100% lignin, 60% Hemicellulose and 5-10% cellulose, HMIM was not found to dissolve lignin or cellulose, but was very efficient in dissolving hemicelluloses (70%).AMIM Cl also efficiently dissolved hemicelluloses to 75%, Cellulose 30% but no dissolution of lignin was observed [11].

Study done by Rogers and group, showed that solubility of lignin was highest when [CH_3SO_4]$^-$ anion was used (at 323 K) followed by Cl$^-$ and Br$^-$ with imidazolium cations, whereas for cellulose extraction, the highest efficiency was found with [C_4mPy]Cl (at 378 K) followed by [C_4mim][OAc] (at 343 K) and [Amim]Cl [9].Since the temperature condition required for [C_4mPy]Cl is far above the normal room temperature, there remains a doubt as to which is the most efficient solvent for cellulose between [C_4mPy]Cl and [C_4mim][OAc].
Imidazolium ions, owing to their hydrophilic nature, and presence of a ring that allows greater flexibility in substituting any functional group by modifying the cation, and has a close contact with sugar structure through van der waals forces [10].

As already specified, not only the type of anion influences the dissolution abilities, but cation also plays an important role. It has been proven with the help of simulation results, especially RDF and decomposed interaction energies that the anions and cellulose form strong hydrogen bonds with strong electrostatic interactions, while the cations have a strong interactions with cellulose by van der waals interaction. It is also proposed that cations are involved in the dissolution process and small cations show coordination with oxygen atoms of hydroxyl groups present in cellulose structure[10]. Previous studies in this field have mostly been done on imidazolium ILs. Further research needs to be carried out considering a more broader range of imidazolium cations, and also othernon-aromatic cations to have a better picture.

Studies on converting rice waste (husk and straw) into useful compounds concentrated on extraction of Silica from Rice waste ash, which could be further used in different industrial needs[15]. The residue that is left after ILdissolution process, canalso be used to extract Silica, thus increasing the usability of rice waste and helping us in another way to convert this waste into useful products. The presence of water soluble metal ions in rice waste like potassium ions hinder in the extraction process of silica, but after IL treatment, this problem is also overcome as the soluble metal ions are removed. This provides us two way benefits, of extraction of both cellulose and silica in amorphous form, thus making this process more vital [5]. Although IL treatment of rice waste provides multiple benefits along with environment sustainability, further research needs to be done in order to make this process economical for commercial use.

APPLICATIONS

The applications of this evolving green method of turning agricultural waste into useful products involve fractionation of cellulose, hemicellulose and Lignin differently. Using this method, we can achieve flexibility in the extent of extraction achievable with respect to different components of LC material.

[11]. Cellulose films and composites can also be formed using this novel method.The cellulose derivatives are also recommended for different biomedical applications such as drug delivery and tissue engineering [17]. Another useful application can be the homogeneous acetylation of cellulose without the involvement of catalyst and in less acute conditions, unlike those involved in present methods[16]. New studies indication the conversion of LC material into bio-fuels can also be an important application [18].

FUTURE PROSPECTS

Majority of the available studies on cellulose extraction using ILs have been done using Imidazolium cations. There is a direct relation between LC extracted, and H-bonding abilities of anionic group, but the effect of cation still remains a matter of doubt. Thus, there is a need for further research which could establish the effect of changein cation, on the LC dissolution. Different ILs can be chosen keeping the anionic entity same, so as to demonstrate the extent to which thecation can effect the extraction capability. Further study can be done taking ILs other than those of Imidazolium and new methods for the synthesis of Ionic liquids need to be searched for, or the existing methods need to be made more feasible. Cations containing active elements for H bond formation can also be chosen, to see whether the presence of highy electronegative entities in the cation form H bond, and to what extent. In case we are able to find an IL that results in better LC dissolution, it can make this process more economical.

ACKNOWLEDGMENT

REFERENCES

[1] Streets, D.G., and Yarber, K.F., 2003. "Biomass burning in Asia: Annual and seasonal estimates and atmospheric emissions". Global Biogeochemical cycles, 17(4), October, pp 1-20

[2] Arai, H., Hosen, Y., and HongVan N., 2015. "Greenhouse gas emissions from rice straw burning and straw-mushroom cultivation in a triple rice cropping system in the Mekong Delta". Soil Science and Plant Nutrition, pp 1-17

[3] Sood, J., 2013. Not a waste until wasted, http://www.downtoearth.org.in/coverage/not-a-waste-until-wasted-40051, June

[4] Jin, S., and Chen, H., 2007. " Near-infrared analysis of the chemical composition of Rice Straw". Industrial Crops and Products, 26, March, pp. 207-211

[5] Chen, H., Wang, W., and Martin, J., 2013. "Extraction of Lignocellulose and Synthesis of Porous Silica Nanoparticles from Rice Husks : A Comprehensive Utilization of Rice Husk Biomass". ACS Sustainable Chem. Eng., 1, December, pp. 254-259

[6] Zhu, S., Wu, Y., and Chen, Q., 2006. "Dissolution of cellulose with ionic liquids and its application: a mini-review". The Royal Society of Chemistry, 8, pp. 325-327

[7] Seddon, K., 1997. "Ionic Liquids for Clean Technology". J. Chem. Tech .Biotechnol, 68, pp. 351-356

[8] Graenacher, C. Cellulose Solution. U.S. Patent 1,943,176, 1934

[9] Sun, N., Rodriguez, H., and Rahman, M., 2011. "Where are ionic liquid strategies most suited in the pursuit of chemicals and energy from lignocellulosic biomass?". The Royal Society of Chemistry, 47, pp. 1405-1421

[10] Liu, H., Sale, K. L., and Holmes, B. M., 2010. "Understanding the Interactions of Cellulose with

Ionic Liquids: A Molecular Dynamics Study". J. Phys. Chem, 114(12), February, pp. 4293-4301

[11] Lynam, J. G., Reza, M.T., and Vasquez, V.R., 2012. " Pretreatment of Rice hulls by ionic liquid dissolution". Bioresource Technology, 114, March, pp. 629-636

[12] Swatloski, R., Spear, S. and Holbrey, J., 2002. "Dissolution of cellulose with Ionic Liquids". J. AM. CHEM. SOC. , 124(18), April, pp. 4974-4975

[13] Ang, T.M., Ngoh, G.C., and Chua, A., 2012. "Elucidation of the effect of ionic liquid pre-treatment on rice husk via structural analysis". Biotechnology for Biofuels, 5(67), September, pp. 1-10

[14] Cao, Y., Wu, J., and Meng, T., 2007. "Acetone soluble cellulose acetates prepared by one-step homogeneous acetylation of cornhusk cellulose in an ionic liquid 1-allyl-3-methylimidazolium chloride". Carbohydrate Polymers, 69, February, pp. 665-672

[15] Kalapathy, U., Proctor, A., and Shultz, J., 2000. "A simple method for production of pure silica from rice hull ash". Bioresource Technology, 73, September, pp. 257-262

[16] Turner, M.B., Spear, S.K., and Holbrey, J.D., 2004. " Production of bioactive cellulose films reconstituted from ionic liquids". Biomacromolecules, 5, 1379–1384.

[17] Shukla, S.K., Sudha, N., and Namrata, P., 2013. "Preparation and characterization of cellulose derived from rice husk for drug delivery". Advanced Materials Letters, 4 (9), pp. 714-719

[18] Wi., S. G., Cho, E. J. and Lee, D. S., 2015. "Lignocellulose conversion for biofuel: a new pretreatment greatly improves downstream biocatalytic hydrolysis of various lignocellulosic materials". Biotechnol Biofuels, 8(228), pp. 1-11

SEEC-2017-089

Extraction of Fuel from Plastic for its Application in CI Engine

Yuvraj Jadhav

Automotive Technology

College of Engineering, Pune

Email: yuvraajadhav@gmail.com

Y B Sonawane

Applied Science Department

College of Engineering, Pune

Email: yogitabs@gmail.com

Aatmesh Jain

ARAI Academy

ARAI, Pune

Email: aatmeshjain@gmail.com

M P Khond

Department of Mechanical
Engineering   College of
Engineering, Pune

Email: mpk.mech@coep.ac.in

M Y Khaladkar

Department of Applied Science

College of Engineering, Pune

Email: myk.appsci@coep.ac.in

ABSTRACT

The present rate of economic growth is unsustainable without saving of natural energy. Thus, mankind will soon have to rely on alternate renewable energy sources. Also, suitable waste management strategy is another important aspect of sustainable development. Plastics have been one of the materials with the fastest growth because of their wide range of applications due to versatility and relatively low cost. The present work involves the synthesis of a petroleum-based fuel by the pyrolysis of plastics. Thermal conversion process was applied with three types of waste plastic mixture namely HDPE, LDPE, and PP in the ratio 2:2:1 per the waste found in college campus. without adding any kind of catalyst. The reaction temperature ranges between 400∘C and 450∘C. Finally, performance analysis of the selected oil sample has to be carried out on a CI engine for different blends. The results are to be compared with the performance and emissions of same engine operated on diesel fuel.

Keywords: Pyrolysis, Distillation, GC-MS

INTRODUCTION

Plastic products are everywhere we look, society is dependent on convenience and therefore single use plastics. Almost all aspects of daily life involve plastics. Plastics are inexpensive, lightweight, strong, durable, corrosion-resistant materials, with high thermal and electrical insulation properties. The diversity of polymers and the versatility of their properties are used to make a vast array of products that bring medical and technological advances, energy savings and numerous other societal benefits. Therefore, the production of plastics has increased substantially.

While society benefits from the sheer convenience of plastics, the oceans are tragically suffering the consequences. Majority of plastics that are used today are non-biodegradable in nature, they remain in environment for long period which affects environmental quality. In India, plastic waste accounts to be about ten thousand tons per day of generated municipal solid waste. As there is no effective segregation and recycling system for these plastic

wastes generated, it increases load on landfill sites because of their non-biodegradable nature and ultimately causes environmental problems like air, soil, and ground water pollution as well as loss of marine biodiversity. Every year millions of single use plastics end up in landfills, rivers, streambeds, and eventually the oceans. The plastics, used once and disposed of, last much longer in the ocean than they did at the hands of their user. Their short life ends in the giant ocean currents called gyres, where plastics slowly degrade into smaller pieces.

Plastics are made up of long chain molecules called polymers. They are light weight polymers of carbon along with hydrogen, nitrogen, Sulphur, and other organic and inorganic elements. There are mainly two types of plastics: Thermoplastics and Thermosetting plastics. In general, these plastics are indicated with recycling numbers to determine the type of plastic. These are namely as Polyethylene Terephthalate, High Density Polyethylene, Polyvinyl Chloride, Low Density Polyethylene, Polypropylene, Polystyrene and others respectively having recycling number from one to seven.

MATERIALS AND METHOD

Waste plastic is converted into plastic fuel by pyrolysis process. It is one of the best methods to reduce load of plastic waste on available landfills. It converts plastic waste into different petroleum fractions which can be used in many industries as an alternative fuel for running boilers. By using suitable catalyst, process yield can be enhanced and reaction time can be minimized which ultimately achieves efficiency in the process. Two major steps in making of plastic fuels are mechanical recycling and pyrolysis. Here the fuel obtained is to use for CI engine, hence here distillation of the pyrolysis fuel is done to remove heavy oil fractions. Here as the setup for the pyrolysis is laboratory setup it is very difficult to put plastic waste inside the round bottom flask. So, here we have used plastic granules as a raw material for the oil production. Plastic granules are the small pieces of the plastics available per their type of plastic. These plastic granules are available in different colors such as white, black, blue, green etc.

HDPE and LDPE are the major components in a plastic waste stream and generally used for making carry bags, plastic bottles and milk and food containers etc. Here the plastic is taken as per their proportion found in the waste. Hence the types of plastic HDPE, LDPE and PP are taken as 40%, 40% and 20% respectively.

Pyrolysis

Pyrolysis technology is thermal degradation process in the absence of oxygen. Plastic waste is treated in a cylindrical reactor at temperature of 400ºC–450ºC. The plastic waste is gently cracked by adding catalyst and the gases are condensed in a series of condensers to give a low Sulphur content distillate. All this happens continuously to convert the waste plastics into fuel. The catalyst used in this system will prevent formation of all the dioxins and Furans.

Here the experiments are conducted without use of any catalyst. Also, the nitrogen has not been used. In pyrolysis nitrogen is used to create an inert atmosphere to stop the formation of water vapor inside the flask. Though use of nitrogen improves the performance of setup it also increases the manufacturing cost of the fuel.
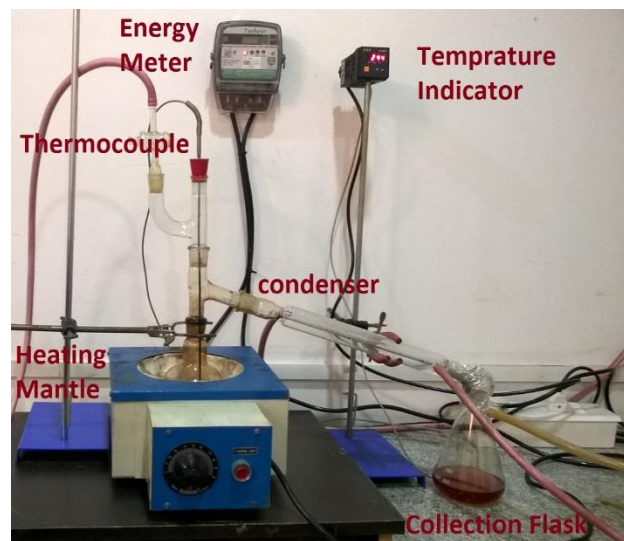
FIGURE 1: LABORATORY SETUP OF PYROLYSIS

Distillation

Distillation is a process of separating the component or substances from a liquid mixture by selective evaporation and condensation. This process applied for petrol and diesel grade fuel production process. Waste plastic to fuel was use for further distillation process and making petrol and diesel grade fuel. The distillation of the oil obtained from the pyrolysis is done up to the temperature 350ºC. Distillation is done in the same setup used for the pyrolysis.

A pycnometer or specific gravity bottle, is used to determine the density of a liquid. Ostwald's viscometer is used to measure the viscosity of a fluid. Pensky-Marten Closed Tester (ASTM D93-79) is used to determine the flash point of the plastic fuel. A bomb calorimeter is used in measuring the heat of combustion of a reaction. CHNS analysis of organic matter is done to determine the Carbon, Hydrogen, Nitrogen, and Sulphur content.

EXPERIMENTAL RESULTS

Quantity of Oil Obtained

The quantity of oil obtained, time required, and energy consumption for pyrolysis of one kilograms of plastic has

been tabulated below, these values are taken as average after producing nearly ten liters of distilled plastic fuel from mixed plastic.

TABLE 1: QUANTITY OF OIL OBTAINED AFTER PYROLYSIS

Quantity (gm)	Oil obtained (ml)	Reaction Time (hr)	Energy Consumption (KWh)
1000	1075	3.5	2

Also, the oil obtained, time required and energy consumption for one litre of pyrolysis oil has been tabulated below,

TABLE 2: QUANTITY OF OIL OBTAINED AFTER DISTILLATION

Quantity of oil taken (ml)	Quantity of oil obtained(ml)	Time required (hr)	Energy Required (KWh)
1000	670	1.5	0.9

In other terms one kilograms of plastic waste will give 1050-1100 ml of plastic fuel after pyrolysis and will give 720-750 ml of plastic fuel after distillation.

Density

The density of plastic fuel after pyrolysis comes in the range 780-785 Kg/m^3. And that after comes in the range of 690-700 Kg/m^3.

Percentage Yield

It is ratio of mass of oil obtained to mass of plastic used. Hence, percentage yield oil after distillation comes to 50 to 55 percent.

Kinematic Viscosity

Here the kinematic viscosity of the mixed plastic fuel is in the range of 1.42 to 1.40 cSt after the pyrolysis. The viscosity of the plastic fuel reduces to the range of 0.985-1.00 cSt after the distillation.

Flash Point

The flash point of plastic fuel comes to 23°C.

Calorific Value

The calorific value of plastic fuel comes in the range of 44-46 KJ/ Kg.

CNHS Analysis

TABLE 3: PERCENTAGE COMPOSITION OF CHNS IN PLASTIC FUEL

Component	Percentage composition
C	82.15
H	12.44
N	0.83
S	Not Detected

Cetane Index

Cetane index is a calculated value, which is derived from relatively easily measured fuel properties. Thus, cetane index can provide a measure of fuel ignition quality without the need to run the costly cetane number test. The cetane index is calculated based on the fuel's density and distillation range. The Cetane Index of the plastic fuel produced is 63.

COST ESTIMATION

The main component in running the setup are plastic waste and continuous electricity supply. As in this case the setup is laboratory setup, the fixed cost or initial cost of setup has not been considered. Hence, the running cost per liter can be calculated as below [4],

Considering the maximum cost of electricity as Rs. 6/unit.

From Table 1 and Table 2, it can be calculated that for one litre of distilled plastic fuel it requires nearly 1.5Kg of plastic and 3.5 units of electric energy. Here, plastic granules have been used instead of plastic waste their combined cost comes to Rs. 83/ Kg (HDPE, LDPE cost Rs. 85/Kg and PP costs Rs. 75/Kg). Hence, in this case the cost of distilled fuel per litre comes to be around Rs. 150.

Considering cost of plastic waste Rs. 10/Kg. Then, the final cost of the plastic fuel comes in the range of Rs. 36-40 per litre.

COMPARISON WITH FUEL STANDARDS

As the fuel is to be used for the automotive applications it need to be compared with the fuel standards which are in the current use. Here we are comparing the plastic fuel with the diesel fuel specifications given by the Indian standards IS1460[5].

TABLE 4: COMPARISON OF PLASTIC FUEL WITH DIESEL FUEL STANDARDS

Characteristics	Diesel Standard	Plastic Fuel	Method of Test
Density (Kg/m^3)	820 - 845	780-790	ISO 3675 or ISO 12185
Kinematic Viscosity (cSt)	2 – 4.5	0.98-1	ISO 3104

3

Flash Point (˚C) Pensky Martens	66	23	IS 1448 [P: 20]
Calorific Value, (MJ)	44-45	44-46	-
Carbon	84	82.15	-
Hydrogen	12	12.44	-
Nitrogen	-	0.83	-
Oxygen (% by mass)	0.6	-	Annex B of IS 1460
Sulphur	50	ND	ASTM D 4294
Cetane Number	51	-	ISO 5156
Cetane Index	46	63	ISO 4264

FUTURE WORK

The main part is to perform tests on CI engine per the standards and to evaluate performance and emission parameters such as Brake power, friction power, specific fuel consumption, Mechanical efficiency, Thermal efficiency, Volumetric efficiency etc. and CO, HC, NOx, PM etc. respectively.

The tests are to be performed by blending the plastic fuel in different proportions with the diesel fuel to get the optimum blend. The blends to be tested are,

i.   P5 (5% plastic fuel and 95% Diesel fuel),

ii.   P10 (10% Plastic fuel and 90% Diesel fuel),

iii.   P15 (15% Plastic fuel and 85% Diesel fuel),

iv.   P20 (20% plastic fuel and 80% Diesel fuel)

The next step after testing is to compare the test results with the performance of same engine operated on standard diesel fuel.

REFERENCES

1. Y B Sonawane, S R Shindikar, M Y Khaladkar, "Onsite Conversion of Thermoplastic Waste into Fuel by Catalytic Pyrolysis", IJIRSET Technical paper ISSN: 2319-8753, September 2014 (Vol. 3, Issue 9)

2. Y B Sonawane, S R Shindikar, M Y Khaladkar, "Use of Catalyst in Pyrolysis of Polypropylene Waste into Liquid Fuel", International Research Journal of Environment Sciences, ISSN 2319–1414, July 2015 (Vol. 4, Issue 7)

3. Y B Sonawane, S R Shindikar, M Y Khaladkar, "High density polyethylene waste treatment by using catalytic pyrolysis to recover liquid fuel", International Journal of Science, Environment and Technology, ISSN 2278-3687(O), 2277-663X (P), (Vol. 5)

4. S S Thipse, "Ecofriendly plastic fuel", Alternative Fuels Concepts, Technologies and Developments, Jaico Publishing House

5. Indian Standards, Automotive Diesel Fuel Specifications, Fifth Revision IS 1460:2005

SEEC-2017-90

THERMAL DECOMPOSITION STUDY ON ETHYLENE DIAMINE BISBORANE FOR HYDROGEN ENERGY USING IONIC LIQUIDS

Basudhrity Banerjee
Department of Chemical Engineering
Indian Institute of Technology,Guwahati
Email: basudhrity@iitg.ernet.in

Tamal Banerjee
Department of Chemical Engineering
Indian Institute of Technology,Guwahati
Email: tamalb@iitg.ernet.in

G.Pugazhenthi
Department of Chemical Engineering
Indian Institute of Technology,Guwahati
Email: pugal@iitg.ernet.in

ABSTRACT

Hydrogen Fuel is considered globally as the new face of energy sector and Ethylenediamine Bis-borane (EDAB) is known to releases 10 wt% of Hydrogen. COSMO-SAC (COnductor like Screening MOdel Segment Activity Coefficient) model was used to select the Ionic liquids (IL) for dehydrogenation experiment. ILs with the lowest Infinite dilution activity coefficient (IDAC) were selected, as the lower the IDAC higher the solubility of EDAB in IL. The following ILs are 1-Ethyl-3-methyl imidazolium acetate ([EMIM][OAc]) ,1-Butyl-3-methyl imidazolium acetate ([BMIM][OAc]), 1-Butyl-1-methyl pyrrolidinium methyl carbonate ([Bmypr][CH_3CO_3]), Tributylmethylammonium methyl carbonate [N_{1444}][CH_3CO_3], Trihexyl (tetradecyl) phosphphonium bis (2,4,4-trimethylpentyl) phosphinate ([TDTHP][Phosph]) and Trihexyl (tetradecyl) phosphphonium dicyanamide ([TDTHP][DCA]). The experiments were carried out at a vacuum and at temperature of 95°C and 105°C .The highest Equivalent of Hydrogen (3.96) was released from [BMIM][OAc]. Further analysis of the residue was done for better understanding about the role of IL as catalyst and EDAB as consummate for hydrogen production.

Keywords: Hydrogen Energy, Ethylene diamine Bis-borane, Ionic Liquids.
.

NOMENCLATURE
AB   Ammonia Borane
EDAB   Ethylenediamine Bis borane
IL   Ionic Liquids
COSMO-SAC COnductor like Screening MOdel Segment Activity Coefficient
IDAC   Infinite Dilution Activity Coefficient
[EMIM][OAc] 1-ethyl-3-methyl imidazolium acetate
[BMIM][OAc] 1-butyl-3-methyl imidazolium acetate
[Bmypr][CH_3CO_3] 1-butyl-1-methylpyrrolidinium methyl carbonate
[N_{1444}][CH_3CO_3] Tributylmethylammonium methyl carbonate
[TDTHP][Phosph] Trihexyl(tetradecyl)phosphphonium bis (2,4,4-trimethylpentyl) phosphinate
[TDTHP][DCA] Trihexyl(tetradecyl)phosphphonium dicyanamide

INTRODUCTION
Hydrogen Fuel is considered globally as the new face of energy sector because of its environment friendly nature, it leaves no pollutant after burning. But storage of hydrogen is a major concern that is when chemical hydrides comes into the picture [1]. Amine borane complexes are the most promising candidate in chemical hydride family when

1

dehydrogenation reactions are considered. These complexes are known to release a decent amount of hydrogen with very less pollutants. Ammonia borane (AB) and Ethylenediamine Bis borane (EDAB) are the most promising candidates in chemical hydride family and are considered best for dehydrogenation process. AB and EDAB are known to releases 14 wt% and 10 wt% of Hydrogen respectively [2]. Few disadvantages of AB are formation of Borazine and Ammonia during thermolysis [3-5]. EDAB on the other hand produces less wt% of H_2 but is less pollutant and also shows absence of an induction period as well as the rate of dehydrogenation is faster than AB .Ionic Liquids (IL) plays an important role as solvents. IL suppresses the induction period and helps in the faster release of hydrogen [6]. ILs also acts as a catalytic agent and reduces the activation energy in the formation of the intermediate namely Diammine Diborane (DADB) from AB.

EXPERIMENTAL/THEORETICAL STUDY

Quantum chemical based COSMO-SAC (COnductor like Screening MOdel Segment Activity Coefficient) model was used for selection of ILs. Infinite dilution activity coefficient (IDAC) EDAB in 32 RTILs from 5 different families i.e. phosphonium, sulfonium, pyrrolidinium, basionics and Imidazolium were considered for this work. IL's with lower IDAC were selected for dehydrogenation of EDAB. EDAB were separately dissolved in the following ILs : [EMIM][OAc] , [BMIM][OAc], [Bmypr][CH$_3$CO$_3$], [N$_{1444}$][CH$_3$CO$_3$],[TDTHP][Phosph] and [TDTHP][DCA] separately . The experiments were carried out at a vacuum of 4 x 10-2 mbar (gauge pressure) and at temperature of 95°C and 105°C.The run time for total exhaustion of EDAB differed for every different IL systems. The residue was further used for ^{1}H NMR and TGA analysis to have a better idea about the reaction mechanism of both the EBAB as well as the IL.

RESULTS AND DISCUSSION
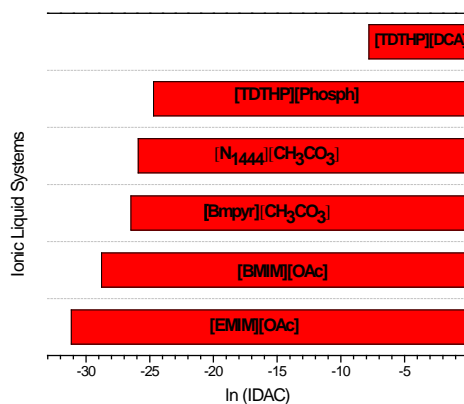
FIGURE 1. Logarithmic value of infinite dilution activity coefficient [*ln (IDAC)*] EDAB dissolved in 9 ILs.

The most challenging and difficult part are in removing the last traces of EDAB species from Ionic Liquid. The infinite dilution activity coefficient (IDAC) is an important indicator which quantifies this very phenomenon. Lesser the IDAC values from unity, greater are the tendency for the IL to remove EDAB species. Imidazolium, phosphonium, pyrrolidinium, pyridinium, sulfonium, ammonium and basionics ILs available through Sigma-Aldrich are considered and solubility of EDAB were tested in 205 pairs of cation-anion combinations of ILs. Highly soluble ILs are selected as best candidate for IL facilitated hydrogen generation from EDAB. We quantify the solubility of EDAB in ILs by capacity, which is expressed as

$$C^\infty = \left(\frac{1}{\gamma_{EDAB}^\infty} \right) \tag{1}$$

Where, γ_{EDAB}^∞ is IDAC of EDAB in ILs. Higher the value better will be solubility and higher will be the release of hydrogen.

The screening of the IL plays a very important role so as to select the IL best suited for dehydrogenation experiments. COnductor like Screening MOdel-Segment Activity Coefficient model (COSMO–SAC) was employed for the selection of Ionic Liquids based on their IDAC value [8].
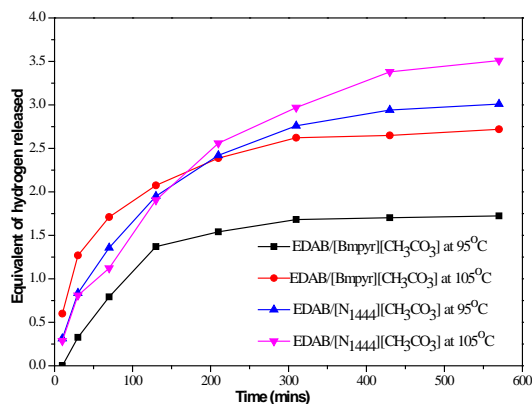
FIGURE 2. Dehydrogenation of EDAB along with Methyl carbonate anion based IL.
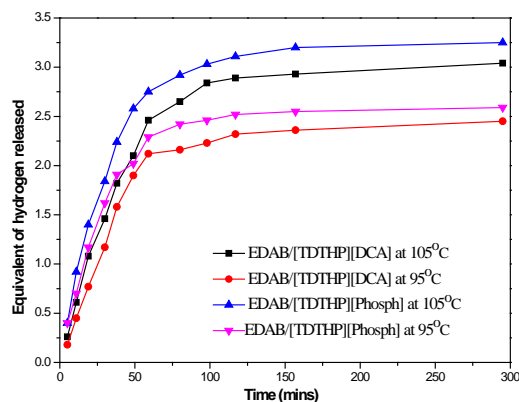
FIGURE 3. Dehydrogenation of EDAB along with Phosphonium based IL
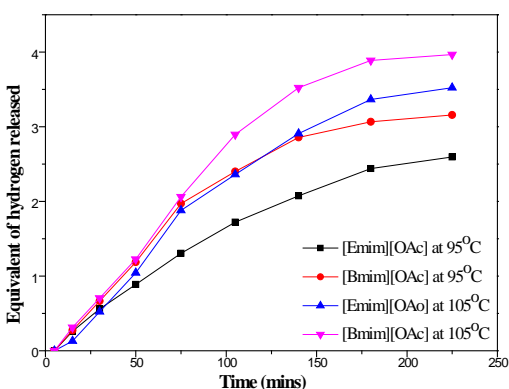
FIGURE 4. Dehydrogenation of EDAB along with acetate anion based IL.

The dehydrogenation experiment with different anion based groups were conducted and as seen The highest Equivalent of Hydrogen (3.96) was released from

EDAB/[BMIM][OAc] at 105°C. Detailed study from Figure 2 shows that EDAB/[BMIM][OAc] and EDAB/[EMIM][OAc] released 3.15 ,3.96 and 2.59,3.52 Equivalent of Hydrogen at 95°C and 105°C respectively.

Figure 3 shows the 1.72 and 2.72 equivalent of H_2 being released from [Bmypr][CH_3CO_3] and 3.01 and 3.50 equivalent of H_2 was released from [N_{1444}][CH_3CO_3]. Similar release of equivalent of hydrogen 2.45, 3.25 and 2.59, 3.04 respectively was also recorded for the last system of [TDTHP][Phosph] and [TDTHP][DCA] ionic liquids. The operating Temperature for the dehydrogenation experiment were 95°C and 105°C. The residues obtained after every experiment were collected and further analysis like ^{1}H NMR, TGA and FTIR were done. The confirmation of hydrogen was done by Gas Chromatography technique.

CONCLUSIONS

From the COSMO-SAC model by IDAC values the following IL were selected for EDAB dehydrogenation

The highest Equivalent of Hydrogen (3.96) was released from [BMIM][OAc] at 105°C. IL completely suppressed the induction period for all EDAB dehydrogenation experiment.

The presence of IL had catalytic effects on the thermal dehydrogenation of EDAB in inert medium. When studying the reaction at two different temperatures, we found that though the cumulative production of hydrogen released after the reaction at 95°C produced slightly lesser equivalents than 105°C.

ACKNOWLEDGMENTS

REFERENCES

[1] Satyapal S., Petrovic J., Read C, Thomas G., and Ordaza G., 2007.The US. Department of energy's national hydrogen storage project: progress towards meeting hydrogen-powered vehicle requirements. *Catal Today*.120, 246.

[2] http://www.sigmaaldrich.com/content/dam/sigma-aldrich/ articles/material-matters/pdf/ metal-borohydrides.pdf (accessed 10.06.14)

[3] Staubitz A., Robertson A.P.M., and Manners I. 2010. "Ammonia-borane and related compounds as dihydrogen sources". *Chem Rev.* 110, 4079-124.

[4] Jaska C. A., Temple K, Lough C. A. And Manners I., 2003. "Transition Metal-Catalyzed Formation of Boron-Nitrogen Bonds: Catalytic Dehydrocoupling of Amine-Borane Adducts to Form Aminoboranes and Borazines." *J. Am. Chem. Soc.*, 125, 9424.

[5] Mal S. S., Stephens F. H. and Baker R. T., 2011."Transition metal catalysed dehydrogenation of amine-borane fuel blends." *Chem. Commun.*, 1, 47, 2922.

[6] Neiner D., Karkamkar A, Bowden M.,Joon Choi Luedtke A,. Holladay J, Fisher A., Szymczak N. and Autrey T, 2011." Kinetic and thermodynamic investigation of hydrogen release from ethane 1,2-di-amineborane". *Energy Environ. Sci.*, 4, 4187.

[7] Banerjee B., Kundu D., Pugazhenthi G., and Banerjee T.,2015. "Quantum chemical and experimental insights for the ionic liquid facilitated thermal dehydrogenation of ethylene diamine bisborane," RSC Adv. 5 85280.

SEEC-2017-92

DEVELOPMENT OF ADVANCED MICROBIAL FUEL CELL BY APPLICATION OF ELECTROGENIC BACTERIA IN A SUSTAINABLE WASTE WATER TREATMENT PROCESS

Kulwinder Singh
Department of Biotechnology
Thapar Institute of Engineering and Technology University
Email: samaysran@gmail.com

Moushumi Ghosh
Department of Biotechnology
Thapar Institute of Engineering and Technology University
Email: mghosh@thapar.edu

ABSTRACT

Microbial fuel cells (MFCs) have received intense importance as a promising technology to achieve sustainable energy.The working capacity and utility of MFCs rely substantuially on the intrinsic capabiloities of bacterial strains employed. In the present study we exploited the electrogenic property of anaerobic bacterial culture from domestic wastes for construction of Salt bridge based Microbial fuel cells (MFC). Five strains were isolated from waste water and screened on the basis of their Electrogenic ability. Of these one microbial culture(K3) isolated from sewage waste water sample had ability for being simultaneously exoelectrogenic and organics degradation. A dual chambered ''H'' shaped salt bridge microbial fuel cell was operated with a pure culture of K3 growing in the anode compartment in a defined medium containing glucose. Salt bridge based MFC was operated in a batch mode under a constant external resistance of 1000Ω and current density measured from the plankton bacterial cells 0.338mA/cm².The highest recorded voltage of 711 mV was obtained on eighth day and highest recorded current was 7 mA.The results of our study demonstrated the potential of the MFC and tested microbial culture in water treatment and energy production.

Keywords: Microbial fuel cell,Voltage, Exoelectogenic, Conductivity,saltbridege

NOMENCLATURE

Ω ohm
mV   milli volt

mA   milli amp

INTRODUCTION

Microbial fuel cell technology represents a multi-disciplinary approach to the quest for alternate sources of energy "[1]". The energy conversion can be achieved with the help of microbial fuel cells in which microbial catabolic activity to directly generate electricity from degradation of organic matter provides access to cheap and environmental friendly energy sources "[2]". Variety of substrates are utilized by bacteria for their respiration and electrons are produced that can be transferred onto the surface of an anode with the help of some redox mediators. These electrons are then allowed to pass through an external circuit to a cathode where they are taken up by electron acceptors. Oxygen is used as terminate electron acceptor in cathode chamber. When electrons reach cathode they are combined with protons and oxygen to give water as product "[3]". Unfortunately, at the present stage wastewater treatment processes are generally energy intensive and require high investment and operating costs. During the treatment a considerable amount of greenhouse gases (GHGs), such as carbon dioxide (CO_2) and nitrous oxide (N_2O), and other volatile substances are released into

the atmosphere. Electricity generation using domestic wastewater, landfill leachate, swine wastewater and corn stove hydrolysates as fuel were reported using several different MFC models . In fact, technology using microbial fuel cells (MFCs) that converts the energy stored in chemical bonds of organic compounds into electrical energy achieved through the catalytic reactions by microorgan-isms has generated considerable interests among academic researchers in recent years "[4-7]" Bacteria can be used in MFCs togenerate electricity while accomplishing the biodegra-dation of organic matters or wastes "[8]".In the present study we report the application of a microbial fuel cell developed using anaerobic bacterial strain from domestic waste water capale of organic degradation and simultaneous production of electricity .

MATERIALS AND METHODS

Isolation and Identification of the Electrogenic Strain

Domestic waste water was collected from ten different sites and transported to laboratory under ice in sterile containers, samples were isolated using standard produres "[9]". Five selected bacterial isolates were spread on LB plates and placed in anaerobic jar. Using optimized growth and MFC parameters, the isolates were studied for their electrogenicity with 500ml anolyte which constitute KH_2PO_4 (12g/L), K_2HPO_4 (7g/L), $(NH_4)_2SO_4$ (2g/L), $MgSO_4$ (120mg/L), Casamino Acids (5gm/L) against catholyte. Sterilized Glucose (2gm/L) at experiment-specific concentrations was used as the carbon source. The pH was maintained in the range of 6.9 to 7.1 using 1M KOH. The cathode compartment consists of 50mM phosphate buffer. Fast growing strain with optimal electrogenic ability was selected and named as K3.

MFC Fabrication and Operation

Two salt bridge based MFCs were operated separately to assess and compare the relative efficiencies of microbial fuel cell in bioelectricity generation. Dual chambered ''H'' shaped MFCs were constructed using plexiglass material. Both MFCS were run in batch mode with a chemically defined medium such as glucose solution to generate electricity. A side opening of 1.3 cm radius was made at a height of 5 cm from the bottom of the container on each container and the connection between these two chambers with the help of PVC pipe "[10]". The chambers are connected in the middle with PVC pipe (Salt Bridge). The PVC pipe containing the salt-agarose mixture was fixed between the two containers using epoxy material and behaved like the salt-bridge assisting in the proton transfer mechanism during the MFC operation "[11]".

Components of MFC

Electroplating was carried out on copper sheet with silver. Copper wires (2mm diameter, cleaned with sandpaper) were cut to 10-cm lengths and bent at one end into a J-shape and passed through electrode hole. Then, silver coated electrode installed in microbial fuel (anaerobic Chamber) cell as an anode. Graphite rods (2×7cm) purchased online (www.fuelcellstore.com) with porosity of 16% were used as cathodes. The electrodes were installed into respective chambers while circuit connections were set with copper wire fixed into the drilled holes of the electrodes.
A sebo SB-108 sparger was connected through flanges to the glass bottle and used for injecting air into catholyte to make it aerobic.

Electrochemical Measurement

Anode and cathode were connected with a 1000Ω resistor. Microbial Fuel cells were monitored using a multimeter (RISH Max-12) and a potentiostat. A constant external resistance of 1000Ω was applied to the MFC. The current produced was calculated by measuring the voltage across a resistor after every 4 hours using a multimeter. During data acquisition both chambers were mixed using a magnetic stirrer. The coressponding value(s) of current (amperes) and power (watt) was determined from the cell potential using Ohm's law (V=IR) for each voltage reading.

RESULTS & DISCUSIONS

Growth Kinetics of the Selected Strain K3

The selected strain was cultured under anaerobic condition (anaerobic jar) by sparging nitrogen gas and growth pattern was studied upto six days. The lag phase persisted till 16 hours followed by late log/stationary phase that continued till 96 hours shown in Fig. 1. The specific growth rate of K3 was calculated to be 0.43 h^{-1}.
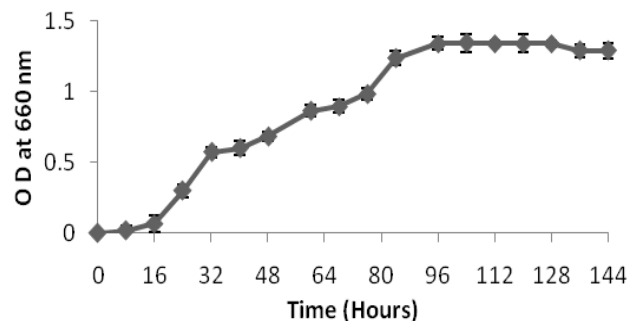
FIGURE 1. Growth kinetics of the K3 strain

TABLE 1. Electrical Conductance Parameters of K3 Isolate (Salt bridge MFCs)

Time (Days)	Mean Voltage (mV) ±S.D	Current (mA)	Power (mW)	Current Density mA/cm^2	Power Density mW/cm^2
0	168±1	1.68	282.24	0.08	13.44
1	323±3	3.23	1046.29	0.153	49.82
2	501±1	5.01			
3	539±5	5.39	2560.36	0.240	121.92
4	625±3	6.25	3906.25	0.297	186.01
5	679±4	6.79	4610.41	0.323	219.54
6	708±4	7.08	5012.64	0.337	238.69
7	713.5±1.5	7.13	5087.255	0.339	242.50
8	711.5±1.5	7.11	5058.765	0.338	240.89
9	711±1	7.11	5055.21	0.338	240.72
10	712±1	7.12	5069.44	0.339	241.40

Under anaerobic conditions, microorganisms produce electrons by metabolising glucose as a substrate utilized for their respiration and electrons produced and transferred to the surface of anode with the help of some redox mediators. These electrons then allowed passing through an external circuit to a cathode where they are taken up by some electron acceptors. Oxygen is used as terminated electron acceptor in cathode chamber. When electrons reach cathode they are combined with protons and oxygen to give water as product.
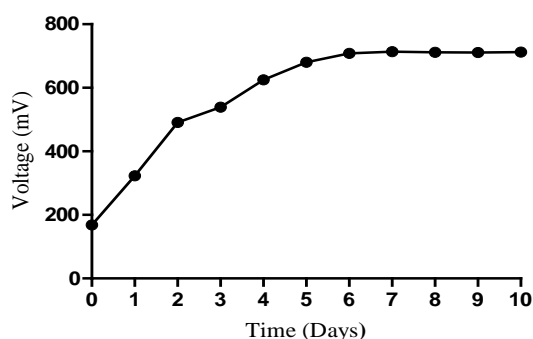
Figure 2. Voltage Generation by Strain K3 From Salt Bridge Based MFC

The voltage and power generated for each individual batch was steady as shown in Tab. 1. Using multimeter the voltage readings were recorded for the MFCs in two replicates for ten days. The optimum recorded voltage obtained was 625mV. Maximum voltage readings were obtained between fifth and seventh day. Voltage generation by strain K3 from salt bridge based MFC is shown in Fig. 2. The voltage profiles demonstrate the presence of

relatively stable voltage after sixth day "[13-14]". Highest recorded current was 7.13mA, while highest recorded power was 5087.25 mW. The highest power density generation calculated was 242.50mW/cm^2 at 7th day "[12]". Current density values were calculated and highest current density value was 242.50mA/cm^2. The values obtained were significantly($p<0.05$) higher when compared with previous report where voltage obtained was 700mV "[11]". This signifies the efficiency of our strain to high generate electricity.

FIGURE 3. Setup of Salt Bridge Based MFC

CONCLUSION

Microbial fuel cells are evolving to become a simple, robust and sustainable energy technology. The present study confirms the usage of domestic waste water bacteria as biocatalyst for the production of bioelectricity. The study also reveal the better usage of the waste towards the commercial utilization for the generation of alternate energy to sustain the demand of future. The results obtained suggest the presence of electrogenic bacteria present in the domestic water could exploited for theier metabolism for bioelectricity production.We are currently investigating the metabolic processes of these strains for engineering changes to advance the electricity productioncoupled with organic degradation.

REFRENCES

[1] Logan, B.E., Hamelers, B., and Rozendal, R., 2006. " Microbial fuel cells: methodology and technology". Environmental science & technology. 40(1), September, 5181-519

[2] Rahimnejad, M., Ghoreyshi, A.A., Najafpour, G., and Jafary, T., 2011. "Power generation from organic substrate in batch and continuous flow microbial fuel cell operations". Applied Energy, 88(11) November, 3999-4004

[3] Allen, R.M., Bennetto, H.P., 1993. "Microbial fuel-cells" Applied biochemistry and biotechnology, 39:27-40.

[4] Allen RM., and Bennetto HP., 1993. "Microbial fuel-cells: electricity produc-tion from carbohydrates". Appl Biochem Biotechnol 1993;39/40:27–40.

[5] Masih, S.A., and Devasahayam, M., 2013. "Developments in Microbial Fuel Cell System for Electricity Generation". Trends in Biosciences. 6: 701-704.

[6] Devasahayam, M., and Masih, S.A., 2012. "Microbial fuel cells demonstrate high coulombic efficiency applicable for water remediation". Indian Journal of Experimental Biology. 50: 430-438

[7] Choi Y., Jung E., and Kim S., 2003. "Membrane fluidity sensoringmicrobial fuel cell". Bioelectrochemistry 2003;59:121–7

[8] Oh SE., and Logan BE., 2005. "Hydrogen and electricity production from a food processing waste water using fermentation and microbial fuel cell technologies". Water Res 2005;39:4673–82.

[9] Du, Z., Li, H., and Gu, T., 2007. "A state of the art review on microbial fuel cells a promising technology for wastewater treatment and bioenergy". Biotechnology advances, 25: 464-482

[10] Gil GC., Chang IS., and Kim BH., 2003. "Operational parameters affecting the performance of a mediator-less microbial fuel cel"l. Biosens Bioelectron 2003;18:327–34

[11] Nair, R., Renganathan, K., Barathi, S., and Venkatraman,K., 2013. "Performance of salt-bridge microbial fuel cell at various agarose Concentrations using hostel sewage waste as substrate". International Journal of Advancements in Research & Technology. 2: 326-330.

[12] Oh, S.E., and Logan, B.E., 2006. "Proton exchange membrane and electrode surface areas as factors that affect power generation in microbial fuel cells". Applied microbiology and biotechnology, 70: 162-169

[13] Shantaram, A., Beyenal, H., and Veluchamy, R.R.A., 2005. "Wireless sensors powered by microbial fuel cells". Environmental science & technology. 39: 5037-5042

[14] Stams, A.J., De Bok., and Plugge, C.M; 2006. "Exocellular electron transfer in anaerobic microbial communities". Environmental Microbiology. 8: 371-382

SEEC-2017-093

LOW TEMPERATURE COMBUSTION WITH TWO-SHOT INJECTION STRATEGIES FOR SIMULTANEOUS REDUCTION OF NO$_X$ AND PM IN COMPRESSION IGNITION ENGINES

Nikhil Khedkar
Student
College of Engineering, Pune
Email: ndk.khedkar@gmail.com

Vehzan Rustomji
Student
Manipal Insitute of Technology, Manipal
Email:
vehzan.rustomji@gmail.com

P. Brijesh
Deputy Manager
Automotive Research Association of India, Pune
Email:
patel.pga@araiindia.com

S. Sreedhara
Professor
Mechanical Engg. Dept., IIT Bombay, Mumbai
Email:
sreedhara.s@iitb.ac.in

ABSTRACT

Compression ignition (CI) engines are generally preferred over spark ignition engines due to their benefit of higher brake thermal efficiency (BTE). But, the issue of simultaneous control of oxides of nitrogen (NO$_x$) and particulate matter (PM) becomes more difficult in CI engines. In this work, optimization of various parameters like injection timing, injection pressure and cooled exhaust gas recirculation (EGR) has been carried out using Taguchi statistical tool. Results showed that combination of –5 CAD aTDC injection timing, 270 bar injection pressure and 30% cooled EGR to be the optimum set of operating parameters for the diesel engine which resulted in a low temperature combustion (LTC). A simultaneous reduction in NO$_x$ (~98%) and PM (~61%) with ~13% reduction in BTE was achieved with LTC mode of operation. The improvement in BTE was achieved with a two-shot injection strategy: 10(–24):18:90(–5), with an acceptable increase in NO$_x$ and PM.

Keywords: Low temperature combustion, Taguchi statistical tool, cooled EGR, two-shot injection strategy

NOMENCLATURE

Φ	Equivalence ratio
T	Temperature, K
CAD	Crank angle in degrees
aTDC	After top dead center
10(–24):18:90(–5)	Pilot fuel % (inj. tim., CAD aTDC):dwell between inj.:main fuel % (inj. tim., CAD aTDC)

INTRODUCTION

NO$_x$ and PM are two main emissions coming out from compression ignition (CI) engines which are falling under stringent emission limits. In-cylinder solutions are efficient ways to reduce these emissions. Formation of NO$_x$ is a function of three parameters: temperature, presence of oxygen and sufficient time for reactions [1]. PM formation occurs due to inefficient droplet evaporation and improper mixing of air-fuel which leads to a formation of fuel-rich pockets. Raeie et al. [2] found that NO$_x$ was decreased with retarded injections but at the same time PM was increased due to incomplete combustion of diesel.

A typical trend of NO$_x$ and soot production during combustion process in CI engines was explained by Potter and Durrett [3] using the Φ-T plane. It showed that NO$_x$ and soot can be reduced simultaneously when combustion occurs in low temperature combustion (LTC) regime.

An exhaust gas recirculation (EGR) is generally used for achieving LTC. EGR increases the heat capacity of an in-cylinder mixture and reduces the amount of air going into the engine, effectively reduces the oxygen content in the cylinder which limits the peak combustion temperature [4]. A study by Zheng et al. [5] showed that NO$_x$ and PM can be reduced simultaneously with EGR above 55%. An increase in ignition delay was a reason for the reduction in PM at higher EGR, which improved the mixing of air-fuel, resulted in lower local equivalence ratio. Brijesh et al. [6] and Yin et al. [7] observed that with cooled EGR (below 75° C) and late injection, there was a simultaneous reduction in NO$_x$ and

PM emissions with an expense of brake thermal efficiency (BTE).

Recent developments in high-pressure electronically controlled common-rail injection systems give freedom to optimize the fuel injection schedule to reduce NO_x and PM levels as much as possible. Multiple injection strategies offer a better solution for reducing emissions with lower effect on engine performance [7, 8]. Zheng and Kumar [9] also found similar results which were further improved by optimizing dwell between two injections in split injection strategies. To have advantages of both LTC and multiple injections, the combination of multiple injections with EGR was used by Sarangi et al. [10] which resulted in near zero NO_x emissions and a significant reduction in PM. Similar experiments were conducted by Yin et al. [7] which showed that BTE with LTC was improved with multiple injection strategies.

In this work, LTC strategy has been demonstrated with a simultaneous reduction in NO_x and PM. Two-shot injection strategies have also been proposed with LTC to reduce the loss in BTE due to LTC.

EXPERIMENTAL SETUP AND TESTING METHODOLOGY

EXPERIMENTAL SETUP

The work has been carried out on a naturally aspirated, 661 cubic centimetre (cc), variable compression ratio (VCR) diesel engine having provision for cooled EGR and multiple injection strategy. The detailed configuration of the engine and test rig may be found in Ref. [6].

TAGUCHI DESIGN OF EXPERIMENT (DOE)

In the current study, Taguchi method of design of experiment was used to get an essence of a large number of tests with a smaller number of experiments [11]. Based on a literature study, retarded injection timing, injection pressure and cooled EGR were selected as parameters to be varied to achieve low temperature combustion. Three levels of each parameter were used to conduct the experiments which are tabulated in Table 1.

TABLE 1: SELECTION OF LEVELS

Parameters	Level 1	Level 2	Level 3
Cooled EGR, %	10	20	30
Injection timing, CAD aTDC	−15	−10	−5
Injection pressure, bar	240	270	300

Having 3 levels of each parameter, 3^3=27 experiments needed to be conducted to understand the effect of each parameter on combustion and emissions. Therefore, Taguchi orthogonal array technique was used to reduce the number of experiments [11]. Taguchi L9 array (i.e. 9 experiments) was used to get the experiment matrix. Table 2 shows L9 array which was used for experimentation. Each run is a combination of one of the 3 levels of each parameter. For example, Run 8 corresponds to 30% cooled EGR, −10 CAD aTDC injection timing and 240 bar injection pressure.

TABLE 2: TAGUCHI L9 ARRAY

	Cooled EGR, %	Injection timing, CAD aTDC	Injection Pressure, bar
Run 1	L1(10)	L1(−15)	L1(240)
Run 2	L1(10)	L2(−10)	L2(270)
Run 3	L1(10)	L3(−5)	L3(300)
Run 4	L2(20)	L1(−15)	L2(270)
Run 5	L2(20)	L2(−10)	L3(300)
Run 6	L2(20)	L3(−5)	L1(240)
Run 7	L3(30)	L1(−15)	L3(300)
Run 8	L3(30)	L2(−10)	L1(240)
Run 9	L3(30)	L3(−5)	L2(270)

All experiments were conducted at the rated speed of 1500 RPM. EGR temperature was maintained in the range of 313 K to 321 K. As per engine manufacturer, ideal injection starts at −27 CAD aTDC and injection pressure is 240 bar; this condition was taken as the configuration for base reading. All experiments were performed at moderate load i.e. 50% of engine's maximum capacity.

MULTI RESPONSE SIGNAL TO NOISE RATIO (MRSN) ANALYSIS

MRSN analysis has been done to find the optimum combination of parameters. The main objective of this work is to achieve lower NO_x and PM without affecting BTE. Hence, 0.4, 0.3 and 0.3 weighting factors (w_i) were assigned to NO_x, PM and BTE respectively. NO_x was given more weightage, as future emission norms mainly focus on reduction of NO_x [12].

MRSN ratio was calculated by using Eqn. 1

$$MRSN = -10\,log_{10}\left(\Sigma\left(w_i\frac{L_{ij}}{L_{avg}}\right)\right)$$
(1)

$$SN = -10\,log_{10}\left(L_{ij}\right) \tag{2}$$

$$L_{ij} = \frac{1}{n}\sum_{k=1}^{n}\frac{1}{y_{ijk}} \text{ (For BTE, where Larger is Better)} \tag{3}$$

$$L_{ij} = \frac{1}{n}\sum_{k=1}^{n}y_{ijk}\text{(For }NO_x\text{ and PM, where Smaller is Better)} \tag{4}$$

where, L_{ij} is the loss function, L_{avg} is the average loss function, 'n' indicates the number of times the particular experiment is repeated and y_{ijk} is the experimental value of the ith response variable in the jth experiment for the kth test.

A higher value of MRSN ratio signifies a desirable outcome. From MRSN analysis (see Table 3), it is found that Run 9 (30% cooled EGR, −5 CAD aTDC, 270 bar)

shows the most desirable result with highest MRSN ratio of 2.75. Runs 7 and 3 also show encouraging results.

TABLE 3: MRSN ANALYSIS OF EXPERIMENTS

Run No.	Cooled EGR	Injection timing	Injection Pressure	MRSN
Run 1	10	−15	240	−2.5883
Run 2	10	−10	270	−1.092
Run 3	**10**	**−5**	**300**	**0.83347**
Run 4	20	−15	270	−0.7867
Run 5	20	−10	300	0.81871
Run 6	20	−5	240	0.5787
Run 7	**30**	**−15**	**300**	**1.70286**
Run 8	30	−10	240	0.15418
Run 9	**30**	**−5**	**270**	**2.74809**

SIGNAL TO NOISE (SN) RATIO ANALYSIS

SN ratio study was done to understand the effect of selected parameters on NO_x, PM and BTE. A higher value of SN ratio (calculated from Eqn. 2) is better for that particular parameter. Figure 1b shows a simultaneous reduction in NO_x and PM with retarded injection (near to TDC). Figure 1a shows an exponential drop in NO_x and a marginal increase in PM with an increase in cooled EGR. Effect of injection pressure, in the range of study, was found insignificant on the outputs, hence not shown here.
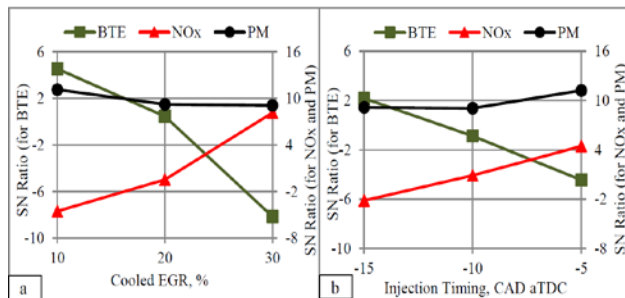
FIGURE 1. SN RATIO ANALYSIS OF A) COOLED EGR AND B) INJECTION TIMING ON BTE, NO_x AND PM

HEAT RELEASE ANALYSIS

Figure 2 shows heat release traces for Runs 3, 7, 9, base run and optimum two-shot injection strategy (explained later). Cooled EGR led to dilution and increase in heat capacity of the air-fuel mixture. In addition to that, the cooling effect of expanding gases in expansion stroke slowed down the chemical reaction rate during combustion. These effects can be clearly seen on the HRR traces of Runs 3, 7 and 9 with their reduced slopes and lower heat release peaks than that of the HRR of the base run (see Fig. 2). Consequently, lower NO_x emissions were observed for the cases with cooled EGR compared to the base run. The exhaust gas temperatures with Runs 3, 7, 9

and the base run were measured and found to be 572 K, 534 K, 612 K and 509 K respectively. As injection timings were retarded, a majority of the combustion took place in the expansion stroke with Runs 3, 7 and 9, due to which the exhaust gas temperatures were much higher than the exhaust temperature in the base run.
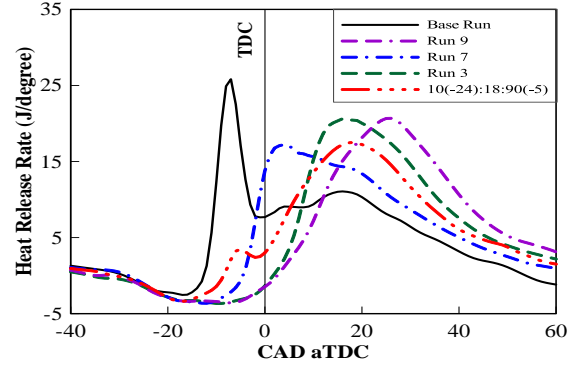
FIGURE 2. HEAT RELEASE RATE TRACES

This higher exhaust temperature improved the soot oxidation process at later part of expansion and exhaust strokes, which might be responsible for the reduction in PM with Runs 3, 7 and 9 as compared to the base run. The higher exhaust gas temperatures with Runs 3, 7 and 9 were also responsible for the increase in heat energy loss (associated with exhaust gases which were coming out of engine) as compared to the base run, due to which lower BTE was observed with Runs 3, 7 and 9 as compared to that of base run. The effective expansion ratios for Runs 3, 7, 9 and base run were calculated and found to be 2.35, 2.55, 1.81 and 3.57 respectively. The effective expansion ratios for Runs 3, 7 and 9 were lesser than that of the base run, effectively reduced the BTE.

IMPROVED LTC USING TWO-SHOT INJECTION STRATEGIES

Two-shot injection strategy was implemented on optimized LTC run i.e. Run 9 (30% EGR, −5 CAD aTDC, 270 bar). Effect of various parameters such as dwell between injections (10 CAD, 14 CAD and 18 CAD) and amount of fuel in the pilot injection (10%, 30% and 50%) have been studied to find an optimum two-shot injection strategy. Main injection timing was fixed at −5 CAD aTDC.

The analysis of result showed that 10(−24):18:90(−5) two-shot injection strategy seemed to be the optimum which offered improvement in BTE by around 8% with a minor increase in NO_x and PM as compared to optimized LTC run (see Table 4). The effective expansion ratios for the optimized LTC run (i.e. Run 9) and two-shot optimum injection strategy (i.e. 10(−24):18:90(−5)) were calculated and found to be 1.81 and 2.22 respectively. As effective expansion ratio was increased in the latter case, BTE with optimum two-shot injection strategy was observed to be higher than that with optimized LTC run. The exhaust gas temperature

for optimum two-shot injection strategy was measured and found to be 557 K which was lower than that for optimized LTC run (612 K). The soot oxidation process might be deteriorated with a reduction in exhaust gas temperature, resulting in higher PM emissions. This reduction in exhaust gas temperature reduced the heat loss (associated with exhaust gases which were coming out of the engine) which was also responsible for the improvement in BTE. As can be seen in Fig. 2, combustion phasing was advanced with optimum two-shot injection strategy (10(−24):18:90(−5)) compare to optimized LTC run (Run 9). Heat release during compression stroke might have led to increase in local peak temperature which was responsible for the marginal increase in NO_x with optimum two-shot injection strategy as compared to that of optimized LTC run.

RESULTS

As an advantage of LTC, NO_x and PM were reduced simultaneously by ~98% and ~61% respectively (see Table 4). Optimum two-shot injection strategies with LTC offered improvement in BTE by around 8% (as compared to optimized LTC) with a minor increase in NO_x and PM.

TABLE 4: RESULTS

Runs	NO_x (g/kWhr)	PM (g/kWhr)	BTE (%)
Base run (−27, 240 bar, 0%)	14.61	0.66	21.42
Optimized LTC run (−5, 270 bar, 30%)	0.25 (98.2↓)	0.25 (61.4↓)	18.65 (12.94↓)
Optimum two-shot injection strategy (10(−24):18:90(−5))	0.45 (96.9↓)	0.44 (33.8↓)	20.06 (6.34%↓)

CONCLUSION

Effect of cooled EGR, injection timing, injection pressure on emission and performance was investigated by using SN ratio and MRSN ratio analysis. Effect of two-shot injection strategy was studied too.
1. Retarded injections showed more potential for simultaneous reduction in NO_x and PM.
2. Cooled EGR had more effect on NO_x and BTE than it had on PM.
3. The combination of late injection, cooled EGR and higher injection pressure resulted in LTC which showed a sharp reduction in NO_x and PM with a slight reduction in BTE.
4. Slopes and peaks of HRR traces were reduced with LTC runs which reduced NO_x and PM emissions.
5. The loss in BTE with LTC was reduced by adopting a two-shot injection strategy with LTC.

ACKNOWLEDGMENTS

REFERENCES

[1] Heywood, J.B., 1988. "Internal combustion engine fundamentals". McGraw-Hill, New York.
[2] Raeie, N., Emami, S. and Sadaghiyani, O.K., 2014. "Effects of injection timing, before and after top dead center on the propulsion and power in a diesel engine". Propulsion and Power Research, 3(2), pp.59-67.
[3] Potter, M. and Durrett, R., 2006. "High-efficiency clean combustion design for compression ignition engines". 12th Annual Diesel Engine Emissions Reduction (DEER) Conference, Detroit, USA.
[4] Lachaux, T., Musculus, M.P., Singh, S. and Reitz, R.D., 2008. "Optical diagnostics of late-injection low-temperature combustion in a heavy-duty diesel engine". Journal of Engineering for Gas Turbines and Power, 130(3), pp.032808.
[5] Zheng, M., Han, X. and Reader, G.T., 2010. "Empirical studies of EGR enabled diesel low temperature combustion". Journal of Automotive Safety Energy, 1(3), pp.219-228.
[6] Brijesh, P., Chowdhury, A. and Sreedhara, S., 2013. "Effect of ultra-cooled EGR and retarded injection timing on low temperature combustion in CI engines". SAE Technical Paper, 2013-01-0321.
[7] Yin, B., Wang, J., Yang, K. and Jia, H., 2014. "Optimization of EGR and split injection strategy for light vehicle diesel low temperature combustion". International Journal of Automotive Technology, 15(7), pp.1043-1051.
[8] Brijesh, P. and Sreedhara, S., 2016. "Experimental and numerical investigations of effect of split injection strategies and dwell between injections on combustion and emissions characteristics of a diesel engine". Clean Technologies and Environmental Policy, 18(7), pp.2325-2334.
[9] Zheng, M. and Kumar, R., 2009. "Implementation of multiple-pulse injection strategies to enhance the homogeneity for simultaneous low-NO_x and-soot diesel combustion". International Journal of Thermal Sciences, 48(9), pp.1829-1841.
[10] Sarangi, A.K., Garner, C.P., McTaggart-Cowan, G.P., Davy, M.H., Wahab, E. and Peckham, M., 2013. "The effects of split injections on high exhaust gas recirculation low-temperature diesel engine combustion". International Journal of Engine Research, 14(1), pp.68-79.
[11] Ross, P.J., 1996. "Taguchi techniques for quality engineering: loss function, orthogonal experiments,

parameter and tolerance design". 2nd ed., McGraw-Hill, New York.

[12] EURO VI, 2009. http://eur-lex.europa.eu/legal-content /EN/ALL/?uri=CELEX%3A32009R0595

SEEC-2017-094

BIOELECTRICITY GENERATION FROM OIL SEED CAKES IN MICROBIAL FUEL CELLS

Bhim Sen Thapa
Bhupat and Jyoti Mehta School of Bioscience,
Department of Biotechnology
Indian Institute of Technology Madras
E mail: bhim.thapa19@gmail.com

T. S Chandra
Bhupat and Jyoti Mehta School of Bioscience,
Department of Biotechnology
Indian Institute of Technology Madras
E Mail: chandra@iitm.ac.in

ABSTRACT

 Microbial fuel cell (MFC) is an advanced technology for generating fuels like Hydrogen, Electricity etc. by the action of microorganisms. In MFC under strict anaerobic conditions, microorganisms metabolize carbon compound for their energy purpose. In this study, we are using complex substrate like oil seed cake as a carbon source for bioelectricity generation in MFC. Different seed cakes like cotton seed, groundnut seed and sesame seed cake were tried for bioelectricity generation. Among them, sesame seed cake was found to give better voltage and sustainability. Current density measured was higher using sesame seed cake ($9.8mA/m_2$) in comparison to groundnut and cotton seed cake, which gave $4.6mA/m_2$ and $6.3mA/m_2$ respectively. Maximum power density of 420 mW/m_2 and Open Circuit Voltage (OCV) of 650 mV was achieved within 24hrs of operation with sesame seed cake.

SEEC-2017-095

MOF DERIVED FE-XEROGEL FOR HIGH PERFORMANCE SUPERCAPACITORS

Bandhana Devi
Indian Institute of Technology, Mandi
Email: bandana.gupta000@gmail.com

Lalita Sharma
Indian Institute of Technology, Mandi
Email: lalita9257@gmail.com

Rik Rani Koner
Indian Institute of Technology, Mandi
Email: rik@iitmandi.ac.in

Aditi Halder
Indian Institute of Technology, Mandi
Email: aditi@iitmandi.ac.in

ABSTRACT

Supercapacitors are the promising energy storage devices with their high power density, long cyclic life, low maintenance cost and environmental affable nature. These desirable properties make them quite useful for portable electronic devices, backup power supplies and storage device for electronic hybrid vehicles. The increasing attention towards supercapacitors is due to their higher capacitance than conventional capacitors and better power density than batteries. However, there is need of efficient materials to improve energy density of supercapacitors for practical applications.

Supercapacitors are generally classified into two types – electrical double layer capacitors(EDLCs) which store charge non-Faradically at electrode-electrolyte interface and mostly use carbon as electrode material and second pseudocapacitors which involve Faradic reaction for charge storage and use transition metal oxides like RuO_2, NiO, MnO_2, Co_3O_4 but these two types of conventional electrode materials cannot fulfil all requirements for high performance of supercapacitors due to their high cost, low capacitance and poor stability. Low surface area and high aggregation of nanoparticles upon cycling mostly limits their practical applications. This problem can be solved by incorporating these metal nanoparticles over some high surface area conductive material like porous carbon. For this, we need some cost effective method to make such kind of structure for their application in supercapacitor

Metal organic frameworks (MOFs) also known as coordination polymers or organic- inorganic hybrid materials have number of exciting properties like high surface area, tuneable pore size, open metal sites and ordered crystalline structure which accounts for their place of pride in various applications like catalysis, magnetism, fluorescence, gas storage and gas separation. MOFs are electrochemically active materials and have applications in fuel cells, lithium-ion rechargeable batteries, solar cells and supercapacitors. MOFs can give rise to metal oxides with more voids and spaces along with graphitised conductive support on annealing, thus combining the properties of redox active metal oxides and porous carbon for supercapacitor application.

In this study, we synthesise a MOF based new xerogel known as metal organic xerogel (MOX) by using a solvothermal method.The metal selected for gel formation is Fe because of its encouraging properties like wide abundance, higher conductivity and redox active nature. We anneal our sample at a particular temperature i.e. 700°C to generate $Fe_3O_4/Fe/carbon$ composite and further used as an electrode material for application in supercapacitors. The $Fe_3O_4/Fe/Carbon$ composite exhibits specific capacitance of 265 F g -1 at a current density of 1 A g -1. The corresponding energy density is 40Wh/Kg and power density is 1600W/kg. Thus we are proposing a simple and cost effective method to fabricate xerogel based electrode materials with high capacitance for application in supercapacitors.

Keywords: MOF, Xerogel, Supercapacitors, Capacitance, Energy density, Power density.

ENHANCED ELECTROCATALYTIC PERFORMANCE OF CaCu$_3$Ti$_4$O$_{12}$ SUPPORTED Fe$_2$O$_3$ NANOCUBES FOR ALKALINE FUEL CELLS

Ankita Mathur
School of Engineering, Indian Institute of Technology Mandi, Mandi, HP
Email: ankita_mathur@students.iitmandi.ac.in

Himmat Singh Kushwaha
School of Engineering, Indian Institute of Technology Mandi, Mandi, HP
Email: himmat_46@yahoo.co.in

Rahul Vaish
School of Engineering, Indian Institute of Technology Mandi, Mandi, HP
Email: rahul@iitmandi.ac.in

Aditi Halder
School of Basic Sciences, Indian Institute of Technology Mandi, Mandi, HP
Email: aditi@iitmandi.ac.in

ABSTRACT

Sluggish kinetics, poor durability and high cost of platinum has led to the search of alternative catalysts for ORR, which occurs at cathodic side of polymer electrolyte membrane fuel cell (PEMFC). Low cost metal oxides have gained considerable attention as alternatives of platinum. In this article, we have utilized the properties of composite of iron oxide (α-Fe$_2$O$_3$) and double perovskite calcium copper titanate CaCu$_3$Ti$_4$O$_{12}$ (CCTO) as electrocatalyst for ORR. Physical characterization by X-Ray Diffractometer and Field Emission Scanning Electron Microscope (FESEM) revealed presence of cubic shaped Fe$_2$O$_3$ nanoparticles over CCTO particles. Electrochemical studies with rotating disc electrode and rotating ring disc electrode have shown that the composite display excellent electrocatalytic activity with the increase in the amount of CCTO. This work demonstrates efficiency of composite Fe$_2$O$_3$- CCTO as efficient electrocatalyst for ORR.

Keywords : *Oxygen Reduction Reaction, CCTO, Fe$_2$O$_3$*

INTRODUCTION

Depletion of fossil fuels and petroleum products have become a global concern, hence there is an urgent need to find their suitable alternative. Fuel cells are seen as promising alternatives with capability of energy production [1]. Oxygen reduction reaction (ORR) is the heart of any fuel cell, which involves reduction of oxygen to produce water molecules [2]. Platinum is the best electrocatalyst for ORR but sluggish kinetics, poor durability and high cost of platinum has led to the search of alternative catalysts for ORR, which occurs at cathodic side of polymer electrolyte membrane fuel cell (PEMFC) [3]. Low cost metal oxides have gained considerable attention as alternatives of platinum. In this article, we have utilized the properties of composite of iron oxide (α-Fe$_2$O$_3$) and double perovskite calcium copper titanate CaCu$_3$Ti$_4$O$_{12}$ (CCTO) as electrocatalyst for ORR. Perovskites suffer from conductivity and stability issues, but it's composite with iron oxide show excellent activity towards catalysing ORR [4]–[6]. CCTO is a cubic double perovskite material in which A site is occupied by Ca^{2+} and Cu^{2+} and B site by Ti^{4+}. The mixed valence state due to the presence of two transition metal ions influence the ORR activity. Iron oxide on the other hand is known for its catalytic activity, low cost, abundance and better durability [7]–[9]. ORR occurs in two steps- first step involves adsorption of oxygen on carbon sites and subsequent breakdown to peroxide ions; the second step involves further breakdown of peroxide ion to water at neighbouring oxygen sites of electrocatalyst [10].

Herein, the composite of CCTO with Fe$_2$O$_3$ has been prepared by lost cost hydrothermal method in three different compositions by varying the proportion of CCTO.

Physical characterization of the samples has been done by X-Ray Diffractometer to study the crystal structure and composition. Field Emission Scanning Electron Microscope (FESEM) revealed cubic shaped Fe_2O_3 nanoparticles over CCTO particles. Cyclic voltammetry and linear sweep voltammetry studies has been done by rotating disc electrode and kinetic studies has been done by rotating ring disc electrode to gain information bout the intermediate formed and the path of reaction. This work demonstrates efficiency of composite Fe_2O_3- CCTO as efficient electrocatalyst for ORR.

EXPERIMENTAL
Material Synthesis

All chemical reagents are of analytical grade purchased from Sigma Aldrich. For the synthesis of 1 : 1 molar ratio of Fe_2O_3– $CaCu_3Ti_4O_{12}$ composite, referred as Fe_2O_3–CCTO 1 : 1, 0.86 M (10 mL) ferric chloride hexahydrate $(FeCl_3.6H_2O)$ solution was mixed with 10 mL triethylamine. The mixture was vigorously stirred for 20 minutes. Later, 0.86 M (10 mL) solution of CCTO was added to the reaction mixture and was stirred continuously till a homogeneous solution was prepared. The solution was transferred into a Teflon-lined stainless steel autoclave at 180°C for 18 hours. After the autoclave was cooled naturally to room temperature, the solution was centrifuged with distilled water, washed with absolute ethanol thrice and kept for air drying at room temperature. The same procedure was followed for preparing 1 : 0.5 and 1 : 0.33 molar ratio of Fe_2O_3– CCTO composite (referred as CCTO 1 : 0.5 and CCTO 1 : 0.33, respectively). Bare Fe_2O_3 and CCTO were also synthesized for comparing its activity with the composite, following modified procedures reported earlier [11], [12].

Electrochemical Measurement

Electrochemical measurements for ORR were carried out on an Autolab electrochemical workstation (Metrohm) at room temperature in a three-electrode system using 0.1 M KOH as electrolyte. Rotating glassy carbon disk electrode (RDE) with diameter of 5 mm was used as working electrode, Ag/AgCl as reference electrode and platinum wire as counter electrode. To prepare the ink for

working electrode, 5 mg CCTO– Fe_2O_3 and 10 mg Vulcan XC-72 were dispersed in 2.5 mL distilled water and 2.5 mL isopropyl alcohol. 300 mL Nafion solution (5 wt%) was also added. The entire solution was ultra-sonicated for an hour and 20 µL of the suspension was drop-casted over the glassy carbon substrate. Rotating ring disk electrode (RRDE) measurements were also done at room temperature on Pine Instruments setup connected to Autolab bi-potentiostat.
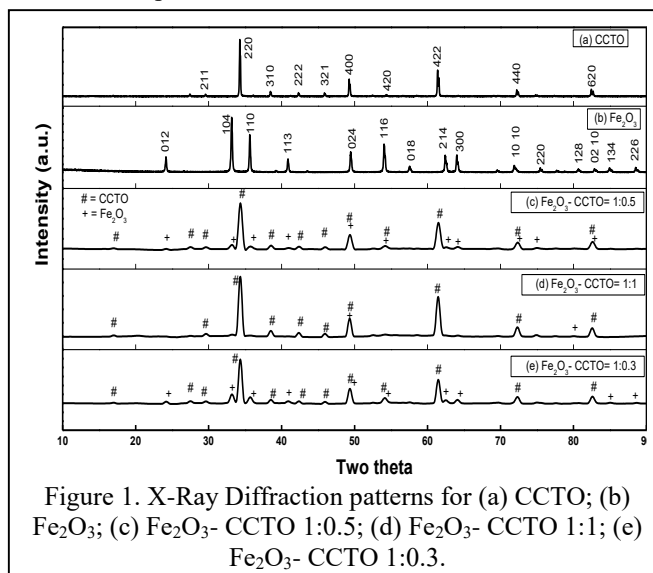
Figure 1. X-Ray Diffraction patterns for (a) CCTO; (b) Fe_2O_3; (c) Fe_2O_3- CCTO 1:0.5; (d) Fe_2O_3- CCTO 1:1; (e) Fe_2O_3- CCTO 1:0.3.

RESULTS AND DISCUSSION

The synthesis of iron oxide nanoparticles were done using wet chemical route, where triethylamine acted as reducing agent as well as capping agent. The proposed mechanism for this reaction is given below [11]:

$FeCl_3 + 3H_2O + 3(CH_3\text{-}CH_2)_3 –N \rightarrow Fe(OH)_3 + 3[(CH_3\text{-}CH_2)_3 \text{-}NH^+] Cl^-$ (1)

Ferric hydroxide $(Fe(OH)_3)$ generated in the intermediate step got transformed first into α-FeOOH in hydrothermal environment and then into α- Fe_2O_3 through thermal decomposition.

$2Fe(OH)_3 \rightarrow 2\, α\text{-} FeOOH \rightarrow α\text{-} Fe_2O_3$ (2)

Figure 1 show the XRD data of bare CCTO, iron oxide and three different iron oxide-CCTO composites. Figure 1(a) shows the XRD pattern of bare CCTO confirming pure phase of CCTO. From the XRD pattern shown in Figure 1(b), the product can be identified as hematite Fe_2O_3 (JCPDS No. 033-0664, rhombohedral crystal system). No other peak of impurity was observed. Figure 1(c), 1(d) and 1(e) shows the XRD pattern of Fe_2O_3-CCTO composites with different molar ratio (1:1, 1:0.5 and 1:0.33 respectively). The peaks matches with the peaks of both bare CCTO (Figure 1(a)) and bare Fe_2O_3 (Figure 1(b)). From the XRD data it is clearly observed that with the increase of amount of CCTO in the composites how the intensity of iron oxide and CCTO peaks varied. In figure 1(d), Fe_2O_3-CCTO 1:1 where highest amount CCTO is present, some of the iron oxide peaks were very small intensity.
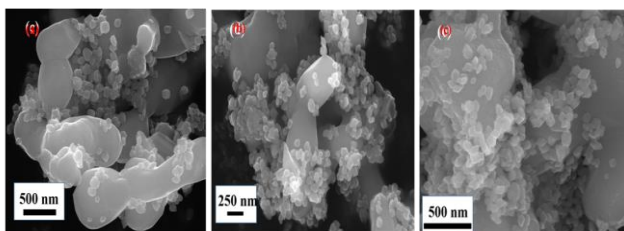
Figure 2. The SEM micrograph of the nanocomposites shows the morphology of (a) Fe_2O_3- CCTO 1:1; (b) Fe_2O_3-CCTO 1:0.5; (c) Fe_2O_3- CCTO 1:0.3.

Figure 2 shows the FESEM images of all the samples. Figure 2 (c), (d) and (e) shows CCTO- Fe_2O_3 composite. It can be observed that the larger CCTO particles are fully decorated with smaller cubic shaped Fe_2O_3 particles. Moreover, the increase in amount of Fe_2O_3 is also clearly evident in the images. It was also observed that increasing ratio of CCTO did not affect the particle shape and size of Fe_2O_3.

Electrochemical Studies

Figure 3 is the polarization curve which shows that with increased amount of CCTO, the ORR activity of the composite increases. ORR was studies using rotating disc electrode from 0.2 to -1.5V at scan rate of 50mV/sec and giving rotation rate of disk electrode of 100 to 1600rpm in 0.1M KOH. There is a gradual shift of onset potential of ORR towards more positive potential with the increment of CCTO in the composites. The onset potential of ORR activity for Fe_2O_3 nanoparticles has been shifted towards more positive potential in the nanocomposites following the order (Figure 3)-
Fe_2O_3 < Fe_2O_3-CCTO 1:0.33 < Fe_2O_3-CCTO 1:0.5 < Fe_2O_3- CCTO 1:1.

Figure 3 clearly indicates that with the increase in concentration of CCTO in the catalysts how the over potential decreases. This clearly indicates that CCTO has a
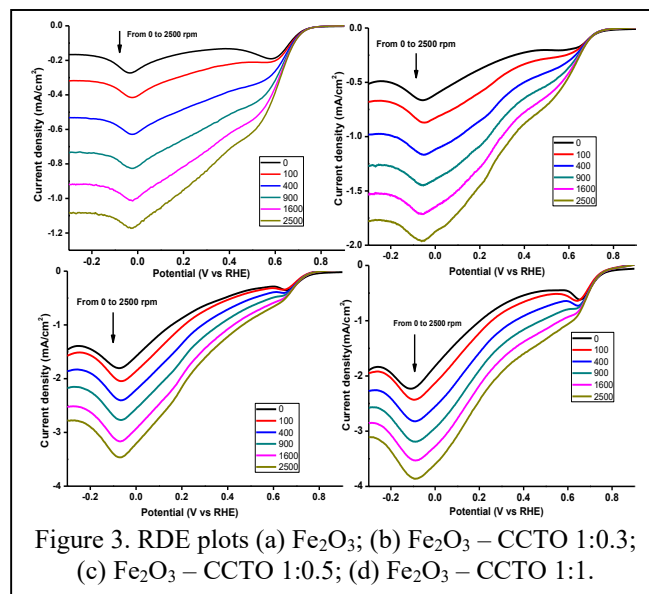
Figure 3. RDE plots (a) Fe_2O_3; (b) Fe_2O_3 – CCTO 1:0.3; (c) Fe_2O_3 – CCTO 1:0.5; (d) Fe_2O_3 – CCTO 1:1.

positive impact on the ORR activity of iron oxide in the composites.

To study the mechanistic pathways of iron oxide-CCTO nanocomposites, RRDE experiments are performed (Figure 4). RDDE technique is very useful to identify the nature of the various intermediate formed in the different steps of ORR reaction and study the kinetic of ORR by a given catalyst. For performing RRDE, glassy carbon disc electrode and gold ring electrode was used (collection efficiency 37.5%). We have used the following formula for calculating the number of electron transfer in this process

$$n = 4I_D/ [I_D + I_R/N] \qquad (3)$$
$$\%H_2O_2 = 2 \times [I_R/N]/ [I_D + I_R/N] \times 100\% \qquad (4)$$

where I_D is Faradaic current at the disk; I_R is Faradaic current at the ring; N is the collection efficiency (0.37 in this case). The ring current follow the order: Fe_2O_3 < Fe_2O_3- CCTO 1:0.33 < Fe_2O_3- CCTO 1:0.5 < Fe_2O_3-CCTO 1:1. From eq. (3) and (4), it is found that n remains close to 4 in all cases (Figure 4) and percentage of peroxide evolution increases with increase in rotation per minute. Table (1) shows the performance of Fe_2O_3-CCTO towards hydrogen peroxide generation. The amount of hydrogen peroxide generation actually increases linearly with the increment of CCTO in the composites.

CCTO provides plenty of active sites in the composites. In CCTO, Cu 3d9 act as major charge carrier and display a direct movement of charge from Cu 3d- O 2p to Ti 3d band. Cu3d and O 2p form the valence band of CCTO and the conduction band is comprised of Ti 3d band. Thus CCTO shows good photo-electrocatalytic behavior under the illumination of visible light as Cu^{2+} and

Ti^{4+} gets excited to Cu^{3+} and Ti^{3+} reported earlier by us [12] showing a very photo-electrocatalytic behavior.

The presence of more oxide sites on the surface of composites in comparison to that on bare iron oxide is mainly responsible for more hydrogen peroxide generation in composites [13]. The oxygen vacancy in perovskite also leads to better electron transfer, ultimately more hydrogen peroxide formation.

Table 1 Performance of different catalysts

Name of Material	Onset Potential (V vs RHE)	% H$_2$O$_2$ (V vs RHE)			
		0V	0.2V	0.4V	0.6V
Fe$_2$O$_3$	0.73	0.263	0.468	1.28	4.80
Fe$_2$O$_3$ -CCTO-1:0.3	0.75	1.52	1.509	3.58	5.72
Fe$_2$O$_3$ -CCTO-1:0.5	0.76	1.84	1.38	4.58	5.56
Fe$_2$O$_3$ -CCTO-1:1	0.77	1.37	1.76	4.31	7.08
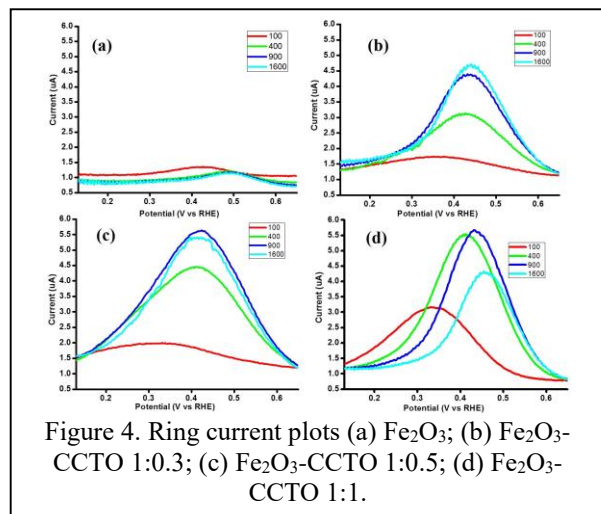
Figure 4. Ring current plots (a) Fe$_2$O$_3$; (b) Fe$_2$O$_3$-CCTO 1:0.3; (c) Fe$_2$O$_3$-CCTO 1:0.5; (d) Fe$_2$O$_3$-CCTO 1:1.

CONCLUSIONS

In summary, a new type of composite of metal oxide-perovskite (Fe$_2$O$_3$-CCTO) was synthesized in different molar ratios (1:0.3; 1:0.5 and 1:1 respectively) via hydrothermal method. The microstructural characterization techniques reveal the composite contains phases of both CCTO and α- Fe$_2$O$_3$, and that ~60nm cubic shaped α-Fe$_2$O$_3$ are decorated over CCTO particles. Electrochemical analysis shows that the composites have better electrocatalytic activity towards ORR process in comparison to bare Fe$_2$O$_3$. RRDE study indicates that with increment of CCTO in the composites more hydrogen peroxide generation happens due to the presence more

active oxide sites contributed by CCTO and the ORR activity increased in the order: α- Fe$_2$O$_3$ < Fe$_2$O$_3$ –CCTO 1:0.3 < Fe$_2$O$_3$ –CCTO 1:0.5 < Fe$_2$O$_3$ –CCTO 1:1. The RRDE analysis also shows that the electron transfer number in ORR is close to 4, indicating that the composites exhibit four electron transfer pathway method. Thus, this new type of Fe$_2$O$_3$-CCTO nanocomposite has the potential to be an effective non precious non noble metal electrocatalyst for fuel cells and batteries.

REFERENCES

[1] H. B. Gray, "Powering the planet with solar fuel," *Nat. Chem.*, vol. 1, p. 7, 2009.

[2] N. M. Markovic, T. J. Schmidt, V. Stamenkovic, and P. N. Ross, "Oxygen Reduction Reaction on Pt and Pt Bimetallic Surfaces : A Selective Review," *Fuel Cells*, vol. 1, no. 2, pp. 105–116, 2001.

[3] H. A. Gasteiger, S. S. Kocha, B. Sompalli, and F. T. Wagner, "Activity Benchmarks for Pt , Pt-alloy and non- Pt oxygen reduction catalysts for PEMFCs . Appl Catal B reduction catalysts for PEMFCs," *Appl. Catal. B Environ.*, vol. 56, pp. 9–35, 2005.

[4] Y. Miyahara, K. Miyazaki, T. Fukutsuka, and T. Abe, "Catalytic Roles of Perovskite Oxides in Electrochemical Oxygen Reactions in Alkaline Media," *J. Electrochem. Soc.*, vol. 161, no. 6, pp. F694–F697, 2014.

[5] S. Yagi, I. Yamada, H. Tsukasaki, A. Seno, M. Murakami, H. Fujii, H. Chen, N. Umezawa, H. Abe, N. Nishiyama, and S. Mori, "Covalency-reinforced oxygen evolution reaction catalyst.," *Nat. Commun.*, vol. 6, no. May, p. 8249, 2015.

[6] S. Gupta, W. Kellogg, H. Xu, X. Liu, J. Cho, and G. Wu, "Bifunctional Perovskite Oxide Catalysts for Oxygen Reduction and Evolution in Alkaline Media," *Chem. Asian J.*, vol. 11, pp. 10–21, 2016.

[7] H. Zhu, S. Zhang, Y. Huang, L. Wu, and S. Sun, "Monodisperse MxFe3-xO4 (M=Fe, Cu, Co, Mn) Nanoparticles and Their Electrocatalysis for Oxygen Reducation Reaction," *Nano Lett.*, vol. 13, pp. 2947–2951, 2013.

[8] Y. Liang, Y. Li, H. Wang, J. Zhou, and J. Wang, "Co 3 O 4 Nanocrystals on Graphene as a Synergistic Catalyst for Oxygen Reduction Reaction," *Nat. Mater.*, vol. 10, pp. 1–44, 2011.

[9] Z.-S. Wu, S. Yang, Y. Sun, K. Parvez, X. Feng, and K. Mullen, "3D Nitrogen-Doped Graphene Aerogel-Supported Fe3O4 Nanoparticles as

Efficient Electrocatalysts for the Oxygen Reduction Reaction," *J. Am. Chem. Soc.*, vol. 134, pp. 9082–9085, 2012.

[10] J. Sunarso, A. A. J. Torriero, W. Zhou, P. C. Howlett, and M. Forsyth, "Oxygen reduction reaction activity of La-based perovskite oxides in alkaline medium: A thin-film rotating ring-disk electrode study," *J. Phys. Chem. C*, vol. 116, no. 9, pp. 5827–5834, 2012.

[11] Z. Li, X. Lai, H. Wang, D. Mao, C. Xing, and D. Wang, "Direct hydrothermal synthesis of single-crystalline hematite nanorods assisted by 1,2-propanediamine.," *Nanotechnology*, vol. 20, p. 245603, 2009.

[12] H. S. Kushwaha, N. A. Madhar, B. Ilahi, P. Thomas, A. Halder, and R. Vaish, "Efficient Solar Energy Conversion Using CaCu3Ti4O12 Photoanode for Photocatalysis and Photoelectrocatalysis," *Nat. Scienfic Reports*, vol. 6, p. 18557, 2016.

[13] E. Yeager, M. Razaq, D. Gervasio, A. Razaq, and D. Tryk, "The Electrolyte Factor in O2 Reduction Electrocatalysis," in *Proceedings of The Electrochemical Society*, 1993, pp. 440–473.

SEEC-2017-098

ROLE OF BIOCHAR IN AGRICULTURE- (A STUDY ON *TRIFOLIUM ALEXANDRINUM*)

Varinder Kaur
Department of Environmental Science and
Engineering, Guru Jambheshwar University, Hisar
India

Praveen Sharma
Department of Environmental Science and
Engineering, Guru Jambheshwar University, Hisar
India

ABSTRACT

Soil properties can be significantly influenced by addition of biochar and is a subject matter to enhance plant productivity and soil quality. In pot experiment, we investigated the effect of different concentrations of biochar (1%BC, 5%BC and 10%BC) with PAH content (50mg Naphthalene and 100mg Phenanthrene) and studied various plant parameters. It was observed that plant height, biomass and percentage dry weight arising from biochar application lead to decreased mobilization of PAH content. Growth characteristics of Trifolium alexandrinum also varied at regular intervals. The maximum plant height and plant biomass were shown at 5% biochar and at 10% biochar and control showed little change in plant growth rate. Different doses of Naphthalene and Phenanthrene were added in soil to checkout biochar high sorption capability with the help of Trifolium alexandrinum. It is noticed that biochar adsorption capability increases with increase of biochar concentration in soil and crop productivity also enhances.

SEEC-2017-099

COMBUSTION CHARACTERISTICS OF MUNICIPAL SEWAGE SLUDGE WITH COTTON STALK IN A BUBBLING FLUIDIZED BED UNDER AIR AND OXYGEN-ENRICHED CONDITIONS

Rajesh Kumar
Department of Mechanical Engineering, Birla Institute of Technology & Science, Pilani, Pilani Campus, Rajasthan, India.
Email: rajesh.narota@gmail.com

Ravi Inder Singh
Department of Mechanical Engineering, Birla Institute of Technology & Science, Pilani, Pilani Campus, Rajasthan, India.
Email: dr.rjassar@gmail.com

ABSTRACT

In this study, municipal sewage sludge (MSS) is co-fired with cotton stalk (CS) in a 20kW bubbling fluidized bed (BFB) combustor under both air and oxygen-enriched (O-E) conditions. The ratio of 25%MSS/75%CS is selected and examine for combustor zone temperature, emission, combustion efficiency and composition of ash. The combustion characteristic of fuel is distinctive under both air and oxygen-enriched condition. Oxygen introduce to the combustor in the range 8-10% under O-E condition. Thermogravimetric analysis (TGA) is performed to investigate combustion behavior of the fuel. DTG profile of the fuel shows two peaks in combustion region. The experimental investigation of BFB combustor demonstrates that the considered ratio of MSS/CS burns efficiently and the combustion efficiency improves under O-E condition. The flue gasses are found within permissible limit and maximum conceivable combustion efficiency of BFB combustor is 94.1% under O-E condition. The fly ash produced is analyzed by using SEM/EDX.
.

Keywords: *Municipal sewage sludge (MSS),Bubbling fluidized bed, Oxygen-enriched (O-E), Combustion, Emission.*

NOMENCLATURE

S_L Flue losses
T_{fg} Flue gas temperature (^{o}C)
T_a Ambient air temperature (^{o}C)

INTRODUCTION

In the recent year, India takes two major initiative "Make in India" and "Clean India Mission". "Make in India" is an initiative to encourage companies to manufacture their products in India whereas "Clean India Mission" aims to provide a healthy environment to human being. On one side, these initiative will help to gear up the industrial and social growth on other hand any mismanagement can cause adverse environmental impacts, public health risk and other socio-economic problem. To successfully accomplish these goals, India requires to implement or test new advance technologies for energy security, clean environment, and waste management. The industrial revolution and growing urbanization will increased the production of municipal sewage sludge (MSS). Disposal of MSS is one of the most complex environmental problem[1]: as land filling takes up a lots of land and contaminates, dumping into sea is harmful and some of MSS products are not suitable for the agriculture. Incinerations is one of the promising method among all disposal methods which gives the advantage of burning low calorific and high moistures MSS. It also reduced the big amount of MSS into a small amount of ash, which is easy to handle in comparison to untreated waste. Werther et al. [2] discussed the three groups of thermal processing of sewage sludge like; mono combustion incineration, co-combustion and alternative process. Co-combustion is helpful to burn low calorific fuel by mixing with some base fuel having high calorific value [3]. Fluidized beds are used extensively for MSS incarnation worldwide. The advance combustion technologies like

1

oxy-fired or oxygen-enriched fluidized bed combustor are under developing stage and it can take years to utilize the benefits of this technology[4]. it proves that the co-combustion of municipal sewage sludge with biomass under oxygen-enriched or oxy-fired condition gives some advantages over conventional technologies [5].

The main objective of this work is to burn the MSS as a co-fuel with biomass inside the oxygen-enriched (O-E) bubbling fluidized bed. Cotton Stalk (CS) one of major crop residues is selected as a base fuel which is available in surplus quantity in Rajasthan, India [6]. The satisfactory combustion of selected blend will increase the share of renewable energy resource, reduce the problem of MSS disposal and provide some clean energy. A ratio of 25%MSS/75%CS is examined in BFB and observations are made of the temperature profile, flue gas emission, and combustion efficiency. The fly ash produced is analyzed by using SEM/EDX.

METHODOLOGY

Fuel property:

In this study MSS is used as a co-fuel and cotton stalk (CS) is used as base fuel (shown in FIGURE 1.). MSS used is collected from the sewage treatment plant Bits-pilani, pilani campus in dry form and CS is collected from the pilani village. The unprepared CS is first chopped into small particle size less then 2cm and then dried into direct sun light. A ratio of 25% MSS/ 75% CS is consider for the test. The proximate and ultimate analyses of MSS are shown in the Table 1. The MSS/CS have the 10.69 MJ/kg gross calorific value. Sulphur concentration in MSS was not found.

TABLE 1: PROPERTIES OF FUEL BLEND

	MSS/CS
Proximate Analysis (Wt.%)	
Moisture	4.03
Volatile matters	33.79
Ash	46.9
Fixed carbon	15.2
Ultimate Analysis (Wt.%)	
Carbon	26.6
Hydrogen	3.6
Nitrogen	1
Sulphur	--
Oxygen	20
GCV (MJ/kg)	10.69

FIGURE 1. FUEL USED (CS AS A BASE FUEL & MSS AS A CO-FUEL)

TGA analysis of fuel:

TGA test is performed for MSS/CS on a Perkin-Elmer TGA-4000 installed in chemical engineering department Bits-Pilani, India to find out the combustion characteristic parameters. The fuels is heated from 30 °C to 800 °C at a rate of 40 °C/min under air-fired condition and hold for 1 min at 800 °C. Air optimized at the constant flow rate of 20 ml/min. FIGURE 2(B) shows two peaks in combustion region, one is at 350 °C and other is at 448 °C.
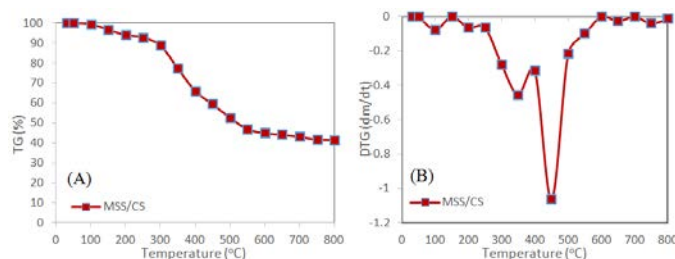
FIGURE 2. TG/DTG CURVES FOR COMBUSTION OF MSS/CS UNDER THE AIR-FIRED CONDITIONAT A RATE OF 40 °C/min: (A) TG; (B) DTG.

The combustion characteristics of MSS/CS used were determined and reported in TABLE 2.

TABLE 2 TGA CHARACTERISTICS OF MSS/CS USED AT A HEATING RATE 40 °C/MIN

Temperature (°C)				DTG_{ma} (%/min)	DTG_{mean} (%/min)
T_i	P_1	P_2	T_b		
282	350	448	562	1.1	0.15
Time (min)				Ignition index (D_i)	Burnout index (D_b)
t_c	t_i	t_b	$\Delta t_{1/2}$		
11.15	7.25	13.9	4.8	0.0136	0.00149

Ti -ignition temperature; P_1-peak 1; P_2-peak 2; T_b-burnout temperature; t_c-time corresponding to DTG max; t_i- ignition time; $\Delta t_{1/2}$-time zone of DTG/DTG$_{max}$ = 1/2.

Experimental setup and procedure:

The work described in this paper is performed in a 1.8 m long square bubbling fluidized bed combustor is shown in FIGURE 3 a schematic view& in FIGURE 4

actual view of test rig. The test rig consist two cyclone, one heat exchanger, hopper, ID fan, two blower, data logger, and chimney. Premixed fuel is entered into the splash zone of combustor through hopper and screw feeder arrangement. The screw feeder is driven by a stepper motor which further control the supply of fuel. Ash is used as a bed material and primary air for fluidization is entered into the bed from bottom of combustor through distributer nozzle. The secondary air for the combustion is entered into the combustor freeboard though side. Temperature is measured by placing 9-thermocouple on combustor at suitable height. The excess amount of oxygen for O-E condition is supplied from bottom as well from side of combustor by using an oxygen cylinder. LPG is used to initiate the combustion process. The port "S" in the freeboard is used for measurement of gas concentration. The net thermal capacity of this system is below 20 kW. The combustor is made of stainless steel (SS310) to resist with higher temperature.
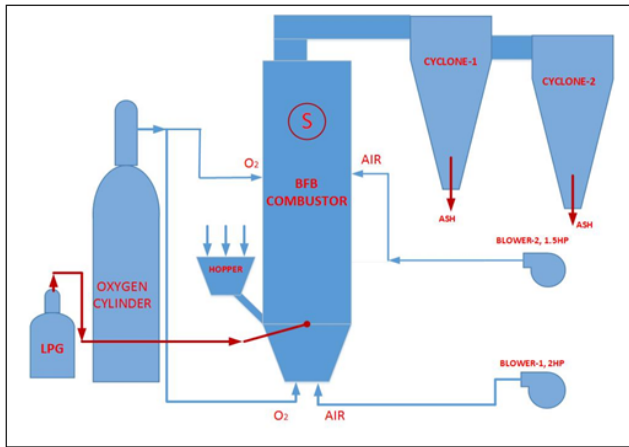
FIGURE 3. EXPERIMENTAL SETUP SCHEMATIC

FIGURE 4. EXPERIMENTAL SETUP ACTUAL VIEW

Performance measure:

Combustion efficiency measure of how efficiently energy from the fuel is converted into useful energy. Here the combustion efficiency is calculated by the following equation

$$Combustion\ efficiency,\quad \eta_C = 100 - S_L \qquad (1)$$

Flue gas passing out of the stack is calculated by "Siegert" formula as follows;

$$S_L = k_S \times \left[\left(T_{fg} - T_a \right) / CO_2 \right] \qquad (2)$$

The Siegert constant value is 0.62 for MSS/CS.

RESULTS AND DISCUSSIONS

Tests are performed for 25%MSS/75%CS in a 20kW bubbling fluidized bed combustor when steady state is reached to investigate the effect of MSS (under both air-fired and oxygen-enriched condition) on the performance of a fluidized combustor and gas emission. The oxygen enhanced up to 8-10% for O-E conditions and a constant fuel feed rate of approximately 6 kg/hr was maintained throughout the experiments.

Temperature profile & flue gas emission:

Temperature is measured along the height of combustor for bed, splash zone and freeboard by employing thermocouple at different location. FIGURE 5 shows the temperature variation along the height of combustor for MSS/CS under both air-fired and oxy-fired conditions. It observed that temperature in combustor bed above distributor (at 0.2, 0.4, 0.6 m height) is low as compare to splash zone and free board. This is because the density of fuel is low and fuel burn above the bed in splash zone and freeboard. The maximum temperature in combustor is observed at 1m height from the distributor in the splash zone because most of the fuel burnt above the bed in splash zone and freeboard. Remaining fuel is burned in the freeboard. Combustion is improved inside the combustor under O-E condition when extra amount of primary oxygen introduced to bed through distributor and secondary oxygen to splash zone. Under O-E condition combustion is smooth and burning is improved in the freeboard.

The species concentration of gases is measured in the freeboard when steady state is reached by using testo 350 professional portable gas analyzer. FIGURE 6. (A) shows the CO concentration for MSS/CS under both A-E and O-E condition. Under O-E condition combustion is improved and became more stable as the oxygen content is higher. It observed that the amount of carbon

monoxide decreases with increase in oxygen concentration.
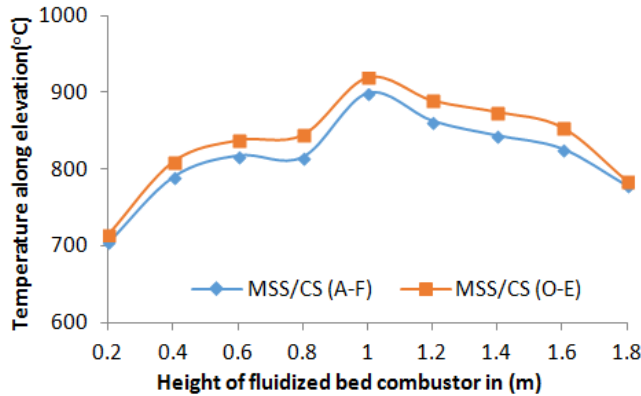
FIGURE 5. TEMPERATURE PROFILE ALONG THE HEIGHT OF COMBUSTOR FOR AIR-FIRED (A-F) AND O-E CONDITION.

FIGURE 6 (B) shows the CO_2 concentration by mass %age for both A-E and O-E condition. CO_2 concentration in emitted gases is increased with oxygen enhancement in the combustor, which is responsible for increase in combustion rate.
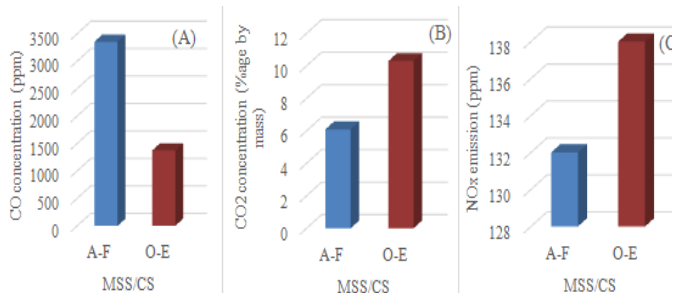
FIGURE 6. GASEAS EMISSION UNDER A-F AND O-E CONDITION (A) CO CONCENTRATION (B) CO_2 CONCENTRATION (C) NO_X EMISSION

NOx concentration for MSS/CS under steady-state A-E and O-E condition is shown in FIGURE 6 (C). Generally, NO x production depends on nitrogen contents in fuels and it increases with increase in temperature. From TABLE 1 be observed that MSS/CS contains very little nitrogen content and hence NOx emission here much depend on temperature increase. With increase in oxygen concentration inside combustor, the combustion rate is increased which further increases the temperature and hence NOx increases.

Combustion efficiency:

FIGURE 7 shows the combustion efficiency for both A-E and O-E condition and it observed that the combustion efficiency increases as the oxygen concentration is increased inside the combustor because the rate of the fuel oxidation is proportional to power of oxygen concentration. A maximum possible combustion efficiency of 94.1 % is achieved for 25%MSS/75%CS under O-E condition.
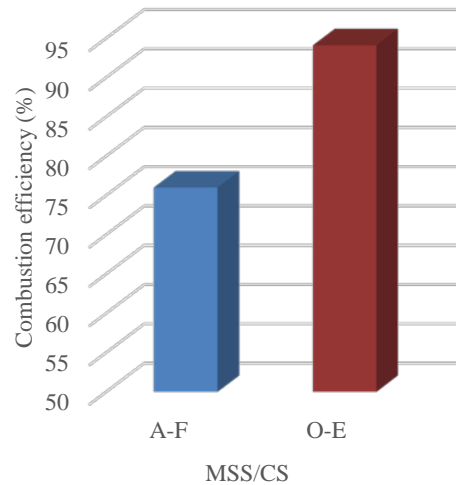
FIGURE 7. COMBUSTION EFFICIENCY

Ash analysis:

The ash produced during the test was collected at three places in bed (bed ash), cyclone 1 (Fly ash) and cyclone 2 (fly ash). Bed ash produce is very low as maximum fuel burn in splash zone & in freeboard. The produced ash elutriates out of the combustor with air. Fly ash collected in cyclone 2 is again very low compare to cyclone 1. Scanning Electron Microscopy (SEM) in combination with Energy Dispersive X-ray spectroscopy (EDX) was performed on the fly ash collected from the cyclone 1 to analyze the elemental composition. FIGURE 8 shows the microstructure and composition profile for fly ash. It was observed from the figure that the element like B and carbon is dominated in fly ash whereas; Ca and Si are presented in less amount.
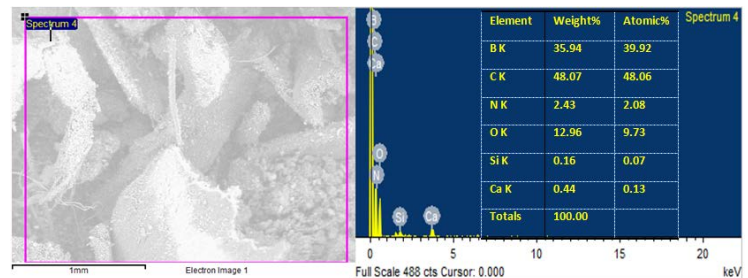
FIGURE 8. SEM/EDX OF MSS/CS

CONCLUSION

An experimental study of an oxygen-enriched (O-E) bubbling fluidized bed combustor has been carried out for co-firing MSS with CS to examine the combustor zone temperature, emission, combustor performance and composition of ash under air-fired and oxy-fired condition. The following points are concluded from the above study.

1. From TGA analysis it observe that the fuel mixture combusted effectively under controlled environment.

2. 25%MSS as a co-fuel combusted successfully with 75 % base fuel under bubbling fluidized bed combustor and the burnout of the blend is improved under O-E condition.

3. When steady state is reached the amount of the fuel supplied is stable and the oxygen concentration is increased inside the combustor. With the increase in combustion rate the concentration of CO reduces gradually and NOx concentration increases. CO2 concentration in emitted gases is increased with oxygen enhancement in the combustor.

4. A maximum possible combustion efficiency of 94.1 % could be achieved under O-E conditions.

5. The bonding agent like sodium presents in less amount in fly ash where's, toxic element B present in considerable amount in fly ash.

ACKNOWLEDGMENTS

REFERENCES

[1] Gupta N, Yadav KK, Kumar V. A review on current status of municipal solid waste management in India. Journal of Environmental Sciences 2015;37:206–17.

[2] Werther J, Ogada T. Sewage sludge combustion. Progress in Energy and Combustion Science 1999;25:55–116. doi:10.1016/S0360-1285(98)00020-3.

[3] Kumar R, Singh RI. An investigation in 20 kWth oxygen-enriched bubbling fluidized bed combustor using coal and biomass. Fuel Processing Technology 2016;148:256–68. doi:10.1016/j.fuproc.2016.02.037.

[4] Singh RI, Kumar R. Current status and experimental investigation of oxy-fired fluidized bed. Renewable and Sustainable Energy Reviews 2016;61:398–420. doi:10.1016/j.rser.2016.04.021.

[5] Jang H, Kim J, Back S, Sung J, Yoo H, Seok H, et al. Combustion characteristics of waste sludge at air and oxy-fuel combustion conditions in a circulating fluidized bed reactor. Fuel 2016;170:92–9.

[6] BIOMASS FUEL SUPPLY STUDY (Rajasthan) for Rajasthan Renewable Energy Corporation Limited Prepared by ABI ENERGY CONSULTANCY SERVICES PRIVATE LIMITED. 2015.

SEEC-2017-100

DIFFERENTIAL PRETREATMENT OF SUGARCANE BAGASSE AND DEVELOPING ENZYME COCKTAIL FOR EFFICIENT HYDROLYSIS OF PRETREATED BIOMASS

Meena Sankar[#], Pallavi Varghese[#], Rajeev K Sukumaran*,

Centre for Biofuels, Microbial Processes and Technology Division
CSIR-National Institute for Interdisciplinary Science and Technology,
Thiruvananthapuram 695019, Kerala, India
* Tel: +91 471 2515368, fax: 0471 2491712. Email: rajeevs@niist.res.in
[#] These authors contributed equally to this work.

ABSTRACT

Bioethanol production from lignocellulose faces major challenges in the form of high crystalline nature of cellulose, non specific enzyme binding to lignin, enzyme dosage and composition etc. Pretreatment helps in changing the biomass structure, so that cellulose and hemicelluloses are exposed for the enzymatic attack.

In this study, sugarcane bagasse was pretreated by different methods like dilute acid, alkali, acid pre-soaked alkali pretreatment and alkali pre-soaked acid pretreatment. Hydrolysis of differentially pretreated bagasse showed that acid pre-soaked alkali pretreatment was better with 400mg/g of total reducing sugars yield after36h. Structural characterization of differentially pretreated bagasse was done. SEM images revealed that acid pre-soaked alkali pretreatment resulted in greater disruption as well as increased porosity and FTIR of the sample also showed increased disturbances in the lignin bonds as well as increased contents of cellulose and hemicellulose. Hydrolysis of the pretreated SCB with different combinations of cellulase, beta-glucosidase and xylanase were done to achieve maximum conversion efficiency. Maximum sugar yield and conversion efficiency (81%) was obtained when higher loadings of beta glucosidase and xylanase were used.

Keywords

bioethanol, pretreatment, sugarcane bagasse, enzyme cocktail, enzymatic hydrolysis, biomass hydrolysis

NOMENCLATURE

SCB	Sugarcane bagasse
BGL	β-glucosidase
TRS	Total reducing sugar
FTIR	Fourier transform infrared spectroscopy
AFEX	Ammonia Fiber Expansion

INTRODUCTION

Lignocellulosic biomass is the most potent renewable and sustainable resource for production of biofuels, limited only by the lack of cost effective technologies for overcoming its recalcitrance to hydrolysis. Plant biomass like sugarcane bagasse or cereal straws have 50-60% of polysaccharides (Wang et al, 2012), which on pretreatment becomes accessible to enzymes. Different pretreatment strategies results in changes in the biomass composition, structure and surface properties leading to differences in enzyme binding, which in turn leads to different hydrolytic efficiencies. Multiple factors like de-ligninification, hemicelluloses solubilization, porosity, enzyme accessibility, cellulose crystallinity etc interact with each other and affect the biomass hydrolysis. So, pretreatment is the first crucial step that dictates how the enzyme will act. The most commonly used pretreatment methods include dilute acid, alkali, AFEX, liquid hot water, ionic liquids etc. Acid pretreatment results in removal of hemicelluloses and partial hydrolysis of cellulose but cellulose accessibility to enzymes are hindered due to redeposition of lignin (Hongiia et al, 2014). Alkali pretreatment results in removal of lignin, changes in inter and intra molecular

bonding pattern of cellulose and hemicellulose, increase in porosity, reduced degree of polymerization with separation of structural linkages between lignin and carbohydrates etc. This helps in specific binding of enzymes to cellulose and hemicelluloses and thus, a better efficiency is achieved.

Enzymatic saccharification follows pretreatment, another crucial step in the bioethanol production. Hydrolysis of biomass requires synergistic action of cellobiohydrolases, endo- and exo-glucanases, xylanases, β-glucosidases, β-xylosidases etc. (Hui-Ting et al., 2016). In addition to these, there are other accessory enzymes and proteins like arabinofuranosidase, α-glucosidases, swollenins etc that aid in hydrolysis. The combined and synergistic action of all these enzymes and proteins results in efficient conversion of pretreated biomass to sugars. Design of efficient enzyme cocktails for biomass hydrolysis requires the blending of multiple different activities, often heterogenous enzymes and is a challenge in itself; as the requirement of component enzymes is different for the different biomass types.

RESULTS AND DISCUSSION

Differential chemical pre-treatment of sugarcane bagasse was carried out to improve the hydrolysis process. A two stage pre-treatment (Kim et al., 2011) can be more effective in degrading lignocellulosic material ie, acid followed by alkali and vice versa. In this study, four different types of pre-treatment viz., acid (0.5% w/v H_2SO_4) pre-soak followed by alkali pre-treatment (1% w/v NaOH), alkali pre-soak (0.5% w/v NaOH) followed by acid pre-treatment (1% w/v H_2SO_4) and acid (1% w/v H_2SO_4) or alkali pre-treatment alone (1% w/v NaOH) was carried out. The efficacy of different pretreatment strategies was assessed by hydrolysis with commercial cellulase. It was found that with 20 FPU/g of commercial cellulase, acid followed by alkali pretreatment gave the maximum sugar yield of 400mg/g (Fig. 1).

Fig1: Hydrolysis of differentially pretreated SCB
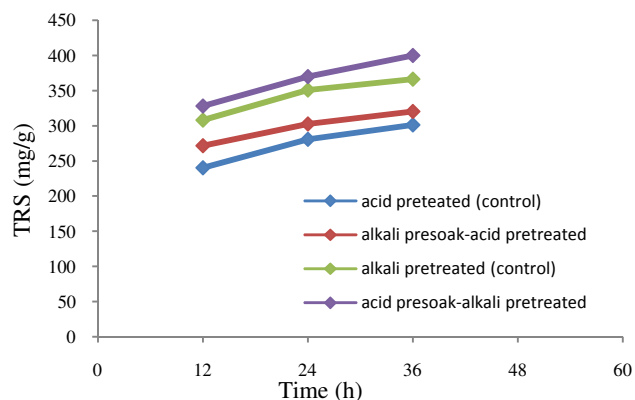
STRUCTURAL CHARACTERIZATION OF SCB

The differentially pretreated SCB resulted in biomass with different structures. This was analyzed using composition analysis, SEM, FTIR etc. Table 1 shows that cellulose content increases on alkaline pretreatment while lignin is reducing. This combined delignification along with deacetylation makes it highly efficient compared to other pretreatment methods (Wu et al., 2011).

Table 1. Composition analysis of differentially Pretreated SCB

Type of pretreatment	Cellulose (%)	Hemi-cellulose (%)	Lignin (%)	Ash (%)
Native	48.4	20.5	20.3	2.0
Acid pretreated	55.4	9.0	25.9	2.0
Alkali pretreated	51.7	21.4	15.7	1.4
Acid pre-soaked & Alkali pretreated	56.5	21.2	15.1	1.6

SEM and FTIR results show that acid pretreatment resulted in the re-deposition of lignin onto biomass which prevented the enzymes from binding to cellulose. This is one of the main reasons behind lesser efficiency in case of acid pretreatment.

ENZYME BLENDING STUDIES

Cellulase was blended with BGL and xylanase in different proportions and it was found that with higher loadings of BGL and xylanase, an efficiency of 80% was achieved (Fig.2).

Figure 2. Enzyme blending with BGL and xylanase
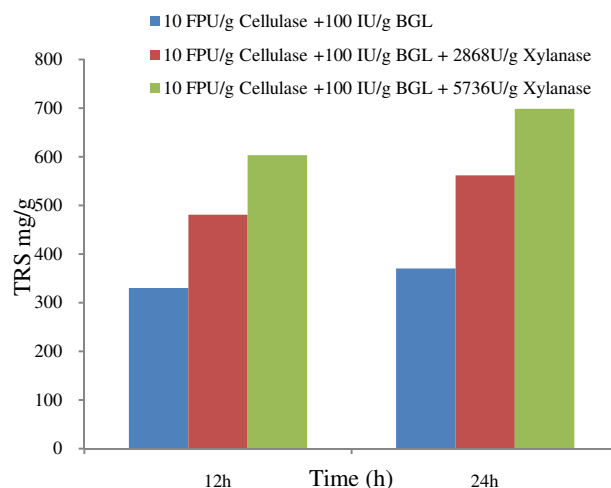
These results are in accordance with studies by Qing *et al.*, 2010, which suggest that hemicelluloses, especially in the form of xylans can act as an important physical barrier in blocking the access of cellulase enzymes to cellulose. It has been suggested that xylan can form a sheath on cellulose microfibril or can be found zipped into cellulose fibrils during their formation (Scheller and Ulvskov., 2010).

CONCLUSION

Acid presoaked alkali pretreatment is one of the best conditions of pretreatment, which change the biomass structure in such a way that enzymes can bind to celluloses. Enzyme blend containing higher loadings of BGL and xylanases convert nearly 80% of available cellulose and hemicelluloses into fermentable sugars, which can then be converted into bioethanol.

Acknowledgments

References

[1]   Wang, W., Zhuang, X., Yuan, Z., Yu, Q., Qi, W., Wang, Q., Tan, X., 2012. "Effect of structural changes on enzymatic hydrolysis of eucalyptus, sweet sorghum bagasse, and sugarcane bagasse after liquid hot water pretreatment". Bioresources 7 (2), pp. 2469-2482.

[2]   Hongjia, L., Yunqiao, P., Rajeev, K., Arthur, J, R., Charles, E, W., 2014. "Investigation of Lignin Deposition on Cellulose During Hydrothermal Pretreatment, Its Effect on Cellulose Hydrolysis, and Underlying Mechanisms". Biotechnol. Bioeng. 111(3), March, pp.485-492.

[3]   Hui-Ting, S., Yuan, G., Yi-Min, Y., Wen-Jing, X., Shi-Hui, L., Wu-Cheng, X., Zi-Lu, L., Li, Y., Zheng-Beng, J., 2016. "Synergistic effect of cellulase and xylanase during hydrolysis of natural lignocellulosic substrates". Bioresor technol. 219, pp. 710-715.

[4]   Kim, J,W., Kim, K,S., Lee, J,S., Park, S,M., Cho, H,Y., Park, J,C., Kim, J,S., 2011. "Two-stage pretreatment of rice straw using aqueous ammonia and dilute acid. Bioresour Technol., 102(19), Oct, pp.8992-8999.

[5]   Wu, L., Arakane, M., Ike, M., Wada, M., Takai, T., Gau, M., Tokuyasu, K., 2011, "Low temperature alkali pretreatment for improving enzymatic digestibility of sweet sorghum bagasse for ethanol production". Bioresour. Technol. 102 (7), pp.4793–4799.

[6]   Qing, Q., Yang, B., Wyman, C,E., 2010, "Xylooligomers are strong inhibitors of cellulose hydrolysis by enzymes." Bioresour Technol 101(24), pp. 9624-9630.

[7]   Scheller, H., Ulvskov, P., 2010, "Hemicelluloses". Annual Review of Plant Biology, 61, pp. 263-289.

3

SEEC-2017-101

CO_2 enhanced oxy-coal gasificationintegrated with steam turbine power plant

Geeta Kumari
Department of Chemical Engineering
Indian Institute of Technology Guwahati
Email: k.geeta@iitg.ernet.in

Dr. Prabu Vairakannu
Department of Chemical Engineering
Indian Institute of Technology Guwahati
Email: v.prabu@iitg.ernet.in

ABSTRACT

Underground coal gasification (UCG) technology is an efficient and an economic in-situ clean coal technology, which converts the unmineable coal into calorific gases. The steam gasification process leads to operational difficulties and is not economical. So by the use ofIn-situ CO_2-oxy coal gasification, the operational difficulty of the steam gasification process may eliminate and we can utilize CO_2 which is also a greenhouse gas. The conversion of clean gasified energy from underground coal gasification to clean combustion energy is obligatory. So to attainthe efficient clean power production, the present work explores the thermodynamic suitability of integration of CO_2/O_2 based UCG with steam turbine which is one of conventional power generation system.The detailed energy analysis of CO_2 enhanced IUGST shows net themalefficiencyof 27.59% with CCS.

Keywords:

(UCG)Underground coal gasification,CO_2 gasification,(IUGST) Integrated underground coal gasification steam turbine cycle,CCS (carbon capture and sequestration)

.
NOMENCLATURE

<Times New Roman, 10 pt, left aligned.>.
A   Put your nomenclature here
ἀ   There are two arguments for each entry of the nomenclature environment, the symbol and the definition.

1. INTRODUCTION

Underground coal gasification is a clean coal technology which utilize the coal which cannot be mined easily.In India more than 70% of electricity production depends upon coal.coal on combustion produces greenhouse and pollutant gases such as CO_2, SO_x, NO_x, and H_2S etc. These gases affect the environment and human beings. Therefore, the development of clean technologies on coal combustion is essential to convert the dirty fuel into a clean fuel. Therefore Underground Coal Gasification (UCG) suggested as clean source of energy by converting in-situ coal into syngas that can be used either as a fuel or as a chemical feedstock.In India about 37% of coal are more than 300 meter depth, which is not economical for mining, so for utilization of these coal resources UCG is the best technique.
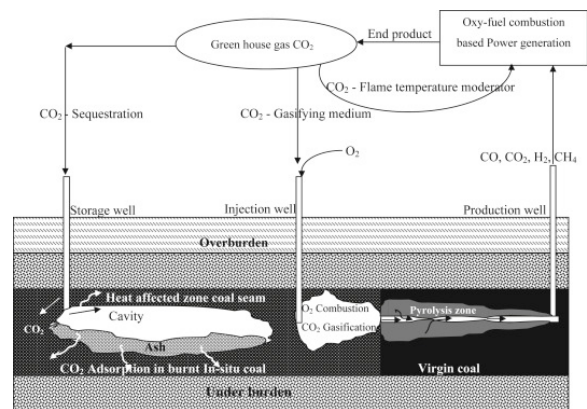
FIGURE 1.SCHEMATIC REPRESENTATION OF CO_2 GASIFICATION OF UCG [3].

Low temperature steam as a gasifying medium to the combustion cavity may exterminate the fire font in the cavity and introduction of superheated steam in the combustion cavity to more than 300 m depth is problematic and leads to the losses of huge amount of energy"[1-2]". So to overcome these we introduce CO_2 as a gasifying medium, which is easily available supplementfor gasification. CO_2 gasification enhances Boudouard reactionshown in Eqn.(1),which leads to the production of more CO.

$$C + CO_2 \rightarrow 2CO \qquad\qquad (1)$$

Several literatures have been reported the kinetics of CO_2 gasification with coal and concluded that it increases the CO/H_2 ratio, which will increase the calorific value of the gas. "[4-5]" .

The outflow of CO_2 from thermal power plant is the main factor for environmental pollution leads to global warming. So capturing CO_2 and further convert it into useful product gases or capture it into unused coal seam. Figure1 shows the schematic diagram of CO_2 basedoxyenUCG arrangement. In the given arrangement the final product CO_2 from the thermal power plant is further recycle and use some part of it to the UCG coal seam as a gasifying medium and rest for sequestration in the coal seam.

2. Energy analysis of the CO_2 blown UCG integrated steam turbine power generation system.
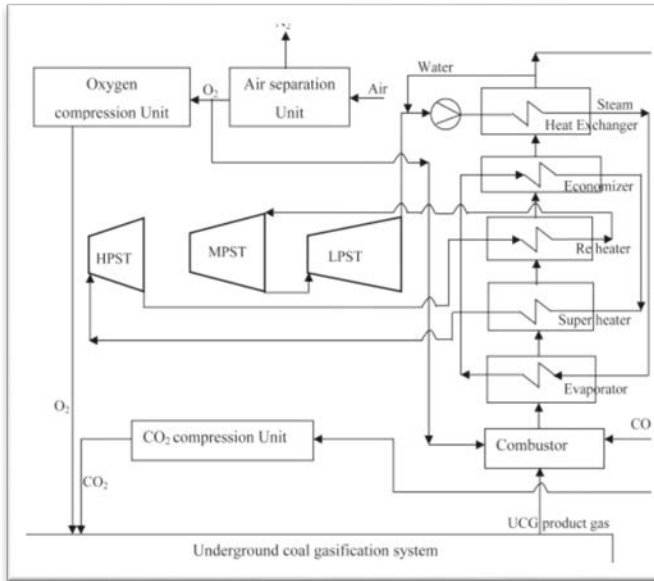
FIGURE 2. Schematic representation of CO_2 gasification of UCG integrated with steam turbine cycle power plant [3].

2.1 Methology for power plant simulation.

The power plant calculation has been done by using excel sheet and Matlab programing by calculating energy and mass balance of each component for 500 MW power plant. The Underground coal seam has been operated on the pressure 3.6 bar.The schematic flow sheeting of UCG integrated steam turbine cycle power plant shown in Fig.2.

In the present paper the gas composition taken from our own experimental data from CO_2 gasification of coal. The Tab.1 shows the proximate and ultimate analysis of the coal. Tab.2 Shows the gas composition of the coal at CO_2/O_2 mole ratio 0.4.

The detailed flowsheeting of UCG integrated power plantis given in Fig.3 CO_2 and O_2 given to combuster at temperature 68 °C. CO_2 flowrate to the combustor is being adjusted so that the adiabatic flame temperature of the combuster should not increase more than 1750 °C. 10% excess oxygen was given for complete combustion. Heat capacity equations has been used to calculate the enthalpy of the streams [5].

Flue Gas Desulphurization (FGD) is used for Sulphur free fuel. Lime is used in FGD unit for the recovery of SO_2 by Sulphation process.

Sulphation reaction

$$CaCO_3 + SO_2 + \frac{1}{2}O_2 \rightarrow CaSO_4 + CO_2 \qquad (2)$$
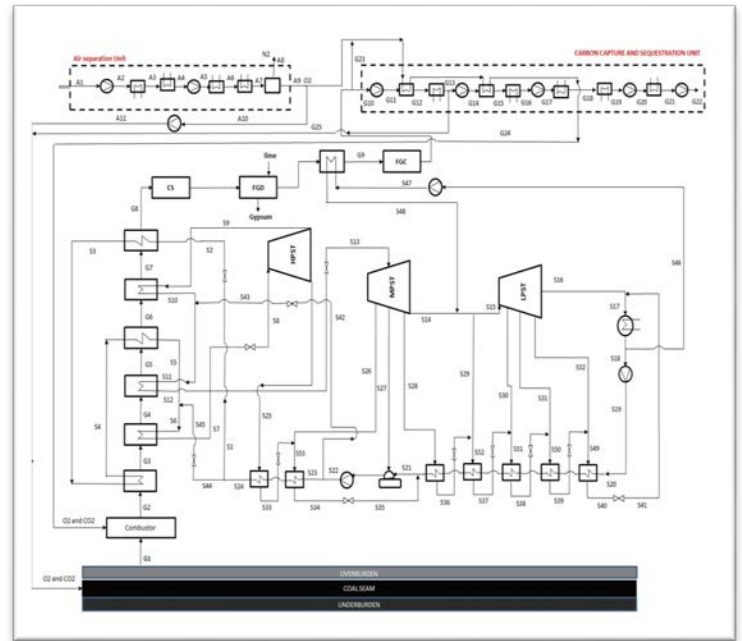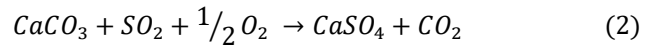
FIGURE 3. Layout of CO_2 enhanced UCG power plant integrated with Steam turbine power plant

2.2 These are the following equations which has been used to calculate the thermal efficiency of the IUGST system

- Power required for compression is given as

$$P_{COM} = \frac{0.371 T_a \gamma Q_0}{(\gamma - 1)\eta_{com}}\left[PR^{\left(\frac{\gamma-1}{\gamma}\right)} - 1\right] \qquad (3)$$

P_{COM} is power required for compression in kW ,P_a and P_b inlet and outlet pressure in bar, η_{com} (85%) is efficiency for compressor,Q_o is volumetric flow rate of the gases [3].

- Feed water pump unit power is calculated as

$$P_{FWP} = {}^{mW_p}/_{\eta_{pump}} \qquad (4)$$

Where m is mass flow rate of water (Kg/s) , W_p is work done by the pump per unit mass flow of water and η_{pupm} is efficiency of pump.

- The gross power ($P_{gross(IUGST)}$) of the IUGST system is calculated by the equation below

$$P_{gross(IUGST)} = P_{HP} + P_{MP} + P_{LP} \qquad (5)$$

Where P_{HP}, P_{MP} and P_{LP} denoted the power generated for high ,medium and low pressure turbine.

- The net power generated with CCS is calculated as equation below

$$P_{net\ with\ CCS} = P_{gross(IUGST)} - P_{UCG(Compression)} - P_{CCS(compression)} - P_{ASU} - P_{FWP} \qquad (6)$$

Where $P_{UCG(compression)}$, $P_{ccs(compression)}$ are the power required for gas compression in UCG and CCS units respectively. P_{ASU} and P_{FWP} are the consumed power for ASU and for feed water pumping unit respectively.

- Gross efficiency of the IUGST system is given by the equation below

$$\eta_{gross} = {}^{P_{gross}}/_{E_{coal}} \qquad (7)$$

Where E_{coal} is thermal energy of coal.

TABLE 1. **Properties of coal**

Properties of coal	Values
Proximate analysis (weight %,dry basis)	
Volatile matter	38.1
Fixed carbon	52.9
Ash	9.0
Ultimate analysis (weight %)	
Carbon	74.65
Hydrogen	5.716
Nitrogen	1.316
Sulphur	3.746
Oxygen	14.572
Higher heating value (MJ/kg)	31.14
Lower heating value (MJ/kg)	30.21

3. Results and discussions

TABLE 2. **Gas composition of the product gases from UCG to combustor.**

Component	CO_2/O_2 Molar Ratio (0.4)			
	UCG		Steam Turbine	
	Inflow (Kg/s)	Out Flow (Kg/s)	Inflow (Kg/s)	Out Flow (Kg/s)
CO_2	23.21	26.5	148.69	194.72
H_2O	0	0	0	14.78
O_2	42.2	3.08	35.2	2.9
N_2	0	0	0	0
H_2	0	1.04	1.04	0
CO	0	25.07	25.07	0
CH_4	0	2.4	2.4	0
Total	65.41	58.11	212.4	212.4

TABLE 3. **Detailed thermodynamic analysis of CO_2 blown UCG integrated steam turbine cycle power plant**

Power generating system	IUGST
Operating pressure (bar)	3.6
CO_2/O_2 ratio	0.4
Power production Unit (MW)	
High pressure turbine	62.57
Medium pressure turbine	85.59
Low pressure turbine	105.11
Gross electric power production (MW)	253.27
Power consumption in Auxiliary units (MW)	
ASU Load for UCG	36.48
ASU Load for CMOC combustor	27.77
Oxygen compression to UCG	4.63
CO_2 compression to UCG	2.22
CCU load for sequestration	24.39
Water pumping	6.37
Total power consumption in auxiliary units (MW)	101.87
Total useful output (MW)	151.40
Thermal energy of the coal (MW)	548.60
Gross efficiency	46.17
Net efficiency (with CCS)	27.59

The detailed power plant layout is given in Fig. 3. Gas composition of the product gases and detailed analysis of the CO_2 blown UCG system is given in Tab.2 and Tab.3 respectively. The total useful power observed with CCS for CO_2 blown IUGST is 151.4 MW whereas the gross electric power production is calculated to be 254 MW. Approximetly 100 MW of power is consumed by the auxiliary unit, out of this 25 % is consumed by CCS unit.

REFERENCES

[1] Mandapati RN, Daggupati S, Mahajani SM, Aghalayam P, Sapru RK, Sharma RK, et al. Experiments and Kinetic Modeling for CO_2 Gasification of Indian Coal Chars in the Context of

Underground Coal Gasification. Ind Eng Chem Res 2012;51:15041–52.

[2] Stanczyk K, Howaniec N, Smoliskia.Wiadrowski J, Kapusta K, Wiatowski M et.al. gasification of lignite and hard coal with air and oxygen enriched air in a pilot scale ex situ reactor for underground gasification. Fuel 2011;90:1953–62.

[3] Mandapati RN, Daggupati S, Mahajani SM, Aghalayam P, Sapru RK, Sharma RK. Experiments and kinetic modeling for CO2 gasification of indian coalchars in the context of underground coal gasification. IndEng Chem Res. 2012;51:15041-52.

[4] Chen F, Pan X, Liu HT, Yao K. O2/CO2 underground coal gasification model test. J China Coal Soc2013;88:495-500.

[5] Bhatt BI, Vora SM. Stoichiometry. 4th ed. New Delhi: Tata McGraw Hill Publication;2004.

SEEC-2017-102

EFFECT OF BIOMASS FEEDSTOCK ON ENERGY TRANSFER IN BIO-HYDROGEN GENERATION THROUGH GASIFICATION AND PRESSURE SWING ADSORPTION

Mayurakshi Mondal
Power Engineering Department
Jadavpur University
Kolkata, India
mayurakshimondal@gmail.com

Atmadeep Bhattacharya
Power Engineering Department
Jadavpur University
Kolkata, India
and
Mechanical Engineering Department
National Institute of Technology
Jamshedpur, India
atma1987@gmail.com

Amitava Datta
Power Engineering Department
Jadavpur University
Kolkata, India
amdatta_ju@yahoo.com

ABSTRACT

A thermodynamic analysis of a gasification-based bio-hydrogen generation system consisting of a cryogenic air separation unit (ASU), a gasifier followed by a water gas shift reactor (WGSR) and pressure swing adsorption (PSA) unit has been done for comparing the performance with different biomass feed stocks, viz. wheat straw, rice straw, coconut shell and bamboo. Thermodynamic equilibrium model is assumed for both gasifier and the water gas shift reactor. A variation in hydrogen yield has been found with the biomass feed stocks. The specific hydrogen yield for coconut shell and bamboo are found to be much more compared to wheat straw and rice straw. Pressure swing adsorption unit is assumed to be in quasi equilibrium. The changes in column volume and power input in PSA unit have been evaluated for different biomass, within a fixed pressure range of 2000 kPa – 4000 kPa.

Keywords: *biomass, gasification, water gas shift reaction, pressure swing adsorption, hydrogen, energy transfer*

NOMENCLATURE

ASU	Air separation unit
FFR	Feed flow rate
$LHV_{biomass}$	Lower heating value of biomass
LHV_{H_2}	Lower heating value of hydrogen
$\dot{m}_{biomass}$	mass flow rate of biomass
$\dot{m}_{H_2}$	mass flow rate of hydrogen
PSA	Pressure swing adsorption
SMR	Steam methane reforming
Ws	Water to syngas ratio
φ	Equivalence ratio

INTRODUCTION

Hydrogen is a clean energy carrier and can be the future fuel to support the scarcity of non-renewable fuels. Furthermore, it will not provide any environmental hazards and therefore sustainable. At present, globally 80 – 85% hydrogen is produced through SMR [1], which requires fossil fuel. Therefore, hydrogen produced through SMR is neither considered to be ecofriendly nor it is sustainable, due to the rapid depletion of fossil fuels. Oxygen-blown biomass gasification is one of the effective processes for bio-hydrogen generation. In this process, biomass is first gasified under the influence of an oxygen-rich stream, which results in the production of syngas consisting of hydrogen, carbon monoxide, carbon dioxide and a negligible amount of nitrogen and methane along with water vapour. The gas mixture is further passed through a water gas shift reactor, where the CO is shifted to CO_2 by injecting water/steam, thereby increasing the amount of hydrogen in the mixture. The syngas is then dried up and the CO_2 is separated from the gas mixture to generate hydrogen. Among the different separation processes available, PSA is an efficient one to separate CO_2 from the mixture of CO_2 and H_2 [2-3].

Several researchers have established that the purity of hydrogen is more than 99.99% through PSA separation process [2-3]. Mondal and Datta [4] have worked on the energy consumption of a PSA system within a certain pressure range considering the gasification of a particular biomass. As the availability of a particular biomass always remains uncertain, it is also interesting to determine the effect of change of biomass on the energy transfer and change in process time in the PSA system.

In the present work, the effects of four different biomass, viz. wheat straw, rice straw, coconut shell and bamboo, on the operation of the PSA system has been studied. Correspondingly, the PSA column volume has been calculated for a fixed adsorption cycle time. Furthermore the effect of cycle timing has been calculated for the different biomass feed stock considering a particular column design. The energy consumption and the heat rejection of the system has also been calculated with different biomass gasification.

THEORETICAL FORMULATION

Description of the Process Scheme
A process scheme of hydrogen generation from biomass gasification is presented in this paper. The general schematic of the process flow path is shown in Fig. 1.

The following assumptions have been taken for the analysis of the process:

1. Air from atmosphere enters the ASU at 100 kPa pressure and 300 K temperature as a binary mixture of 79% N_2 and 21% O_2 by volume.
2. The oxygen rich stream after air separation consists of 95% pure oxygen and leaves the air separation unit at 100 kPa pressure and 300 K temperature .
3. The biomass used for gasification is completely dry.
4. There is negligible amount of tar present in the syngas after gasification.
5. Chemical equilibrium prevails among the constituent gas species in the syngas at both gasifier and water gas shift reactor exit.
6. Nitrogen being an inert gas does not take part in any chemical reaction.
7. Water at 100 kPa pressure and 300 K temperature is injected in the water gas shift reactor at a constant W_s of 3.
8. The water gas shift reactor operates under adiabatic condition.
9. The product gas species are in equilibrium among themselves in gasifier and water gas shift reactor.
10. PSA is considered to be in quasi-equilibrium.
11. Four adsorption columns are utilized in the PSA system for continuous hydrogen production.
12. PSA column temperature is maintained at 320 K.
13. The adsorption cycle timing is considered as 10 mins for the base case.
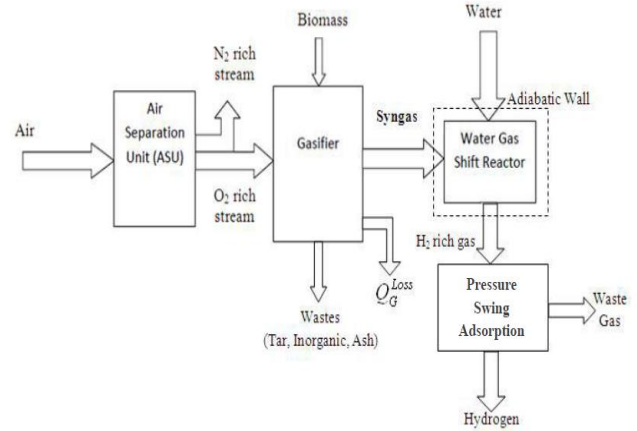
Figure 1. Process flow path

Energy Balance of the Plant

ASU: The detailed modeling of ASU is done following Bhattacharya et al. [5] for oxygen separation from air.

Gasifier: Dry biomass is fed to the gasifier under sub-stoichiometric condition, which is governed by the equivalence ratio (φ = actual fuel-air ratio/stoichiometric fuel-air ratio). The gasifier efficiency is considered to be 95% considering heat loss from the gasifier. The species balance equations, energy balance equation and the relations for equilibrium constants are taken from Bhattacharya et al. [5] and the ultimate analysis data are taken from Roy et al. [6] to calculate the species concentrations and the gasifier temperature.

WGSR: In the water gas shift reactor, water is additionally injected into the syngas from the gasifier exhaust in order to shift the composition of the gas mixture towards higher concentration of hydrogen and lower the concentration of carbon monoxide. The shift reactor is assumed to be at adiabatic condition. The detailed energy based modelling of WGSR is considered following Bhattacharya et al. [5].

PSA: In pressure swing adsorption carbon dioxide has been adsorbed by Maxsorb III activated carbon powder considering Toth isotherm [4]. The detail design of PSA unit is described in the work of Mondal and Datta [4].
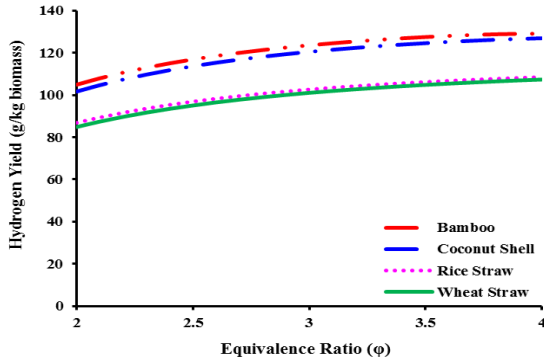
Efficiency of the System
Efficiency of the entire system is calculated as,

$$\eta = \{\dot{m}_{H_2} LHV_{H_2}/(\dot{m}_{biomass} LHV_{biomass} + power\ consumption\ in\ ASU + power\ consumption\ in\ PSA)\} \times 100\%$$

RESULTS AND DISCUSSION

Figure 2 shows the variation of hydrogen yield on mass basis for the four types of biomass used in the study. It may be seen from the figure that the bamboo and coconut shell

FIGURE 2. Variation in hydrogen yield after WGSR with equivalence ratio (φ) for different biomass
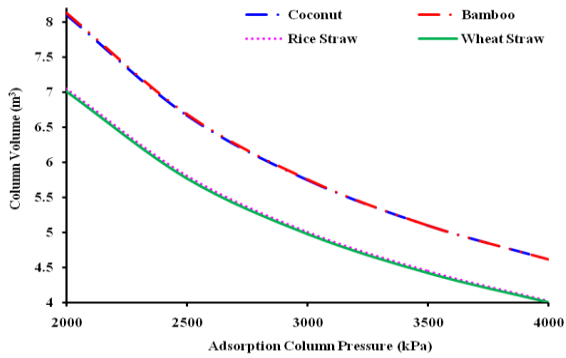
FIGURE 3. Variation of PSA column volume with adsorption column pressure for different biomass
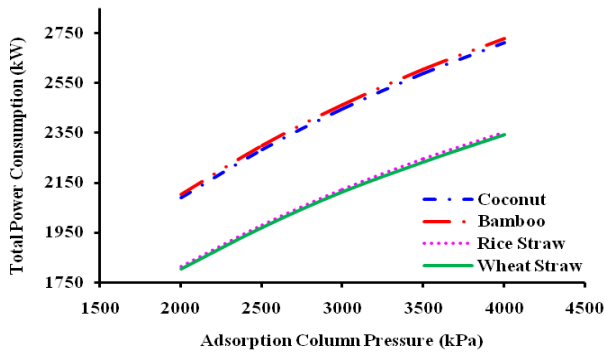
FIGURE 4. Variation of PSA power consumption with adsorption column pressure for different biomass

produce considerably higher hydrogen yield than wheat straw and rice straw. In this regard, it is worth mentioning that the H_2 yield per unit mass of feed stock depends upon the ash content of the fuel. As ash is non-combustible, higher ash content leads to lower yield. Therefore, the fuels with lower ash content like bamboo and coconut shell produce higher hydrogen yield compared to wheat straw and rice straw (Fig. 2).

The feed flow rate (FFR) of syngas, as listed in Table 1, is fed to the PSA from the gasification of 100 kg of the respective biomass. The composition and temperature of the syngas at the outlet of the WGSR are listed in Table 2. The

feed flow rate and the syngas composition has been considered at gasifier equivalence ratio of 4.

Figure 3 shows the decrease in column size with the increase in column pressure for all the biomass due to the proportional relation between the CO_2 adsorption capacity of the adsorbent with the pressure. The column size of the coconut shell – bamboo and the wheat straw – rice straw almost coincided due to the close values of CO_2 mole fraction between the pair.

Table 1. Data of different biomass feedstock taken in the present analysis at gasifier equivalence ratio of 4

Serial No.	Biomass Feedstock	Representative Formula	Heating Value [6] (kJ/kg)	FFR to PSA (Nm³/s)
1.	Coconut Shell	$CH_{1.36}O_{0.647}$	20498	4.18
2.	Rice Straw	$CH_{1.55}O_{0.82}$	14850	3.63
3.	Wheat Straw	$CH_{1.49}O_{0.82}$	17988	3.61
4.	Bamboo	$CH_{1.55}O_{0.65}$	20547	4.21

Table 2. Mole fractions of H_2 and CO_2 and temperature for syngas after WGSR at gasifier equivalence ratio of 4

Serial No.	Biomass Feedstock	Mole fraction of H_2	Mole fraction of CO_2	WGSR temperature (K)
1.	Coconut Shell	0.597	0.394	501
2.	Rice Straw	0.589	0.403	544
3.	Wheat Straw	0.585	0.404	596
4.	Bamboo	0.604	0.386	485

Figure 4 depicts the increase in total power consumption of the PSA unit with pressure due to the increase in compressor work input. As the feed flow rate of coconut shell and bamboo or rice straw and wheat straw are very close, the power consumption results seem to coincide for them,.

The total rate of heat rejection increases with adsorption column pressure for all types of biomass, due to the increase in heat rejection by the intercoolers and aftercoolers of the multi-stage compressor (Figure 5). The PSA unit heat generation is dependent upon the exothermic adsorption process, compressor work and the cooling of syngas coming from WGSR. Although the flowrate of coconut shell is lower than bamboo, the mole fraction of CO_2 is higher in coconut shell syngas, which gives a higher number of moles of CO_2 to be adsorbed (i.e. higher exothermic heat generation). The heat rejection at the cooler after WGSR is

3
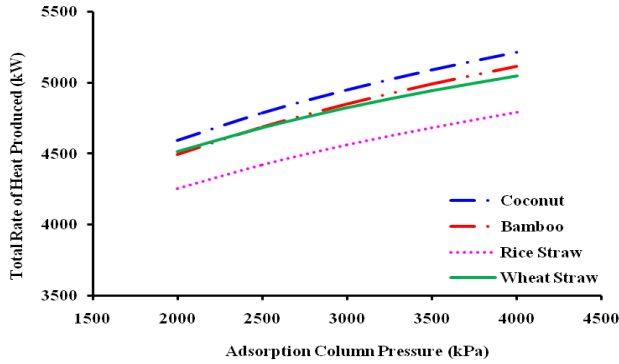
FIGURE 5. Variation of total rate of heat rejection in PSA with adsorption column pressure for different biomass

FIGURE 6. Variation in adsorption cycle time for different biomass considering a fixed column design at 4000 kPa pressure for rice straw

FIGURE 7. Cold gas efficiency (CGE) and overall system efficiency (eff) for different types of biomass at 4000 kPa adsorption pressure and $\varphi = 4$

also higher for the WGSR outlet temperature. The WGSR temperature of the wheat straw fed system is the highest; whereas the temperature for bamboo is the lowest among the four biomass considered. This temperature disparity brings the heat generation curve very close, almost discarding the effect of FFR and syngas composition for the two.

The study has been further extended to observe the effect on adsorption cycle time for different biomass at a fixed column design (Figure 6). The column at 4000 kPa pressure with feed as rice straw produced syngas is considered as the base case. The cycle time is inversely proportional to the flow rate of carbon dioxide. So, rice straw and wheat straw with lower CO_2 flow rates are having higher adsorption cycle time than the other two biomass.

Figure 7 shows the variation in cold gas efficiency and the overall system efficieny for different types of biomass. The efficiencies have been calculated considering the gasifier equivalence ratio and adsorption pressure as 4 and 4000 kPa respectively.

CONCLUSION

Thermodynamic modeling of a bio-hydrogen generating system has been done. The analysis is based on the production of hydrogen using different types of biomass as the gasification feedstock. By gasifying different types of biomass followed by a WGSR, a variation in the composition of syngas has been found, along with the changes in feed flow rate. From the results we can have the following conclusions –

- Among the four biomass considered, use of rice straw as feedstock is providing the highest efficiency of around 80% along with a lower energy consumption rate. However, bamboo holds the highest position in terms of specific hydrogen yield.
- In addition, the use of rice straw as feedstock can be beneficial both in terms of the low capital cost, owing to low adsorption column volume, and low operating cost, owing to the low power consumption.
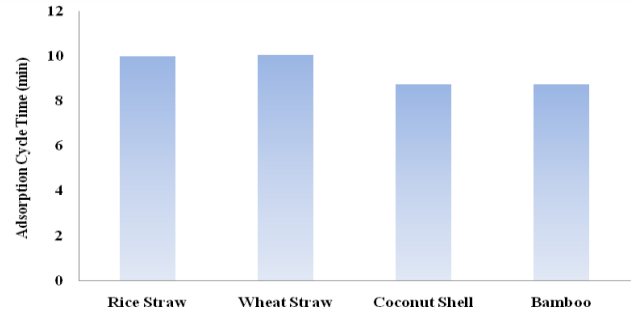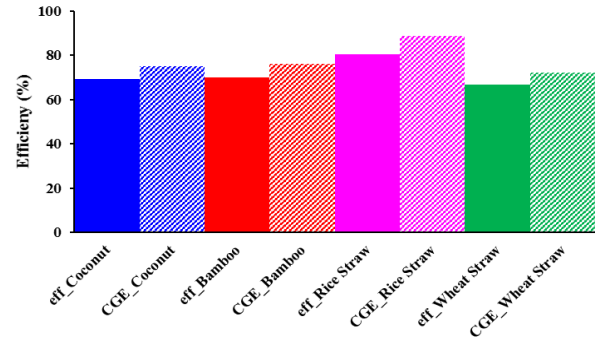
REFERENCES

[1] Simpson AP, Lutz AE., 2007. "Exergy analysis of hydrogen production via steam methane reforming". International Journal of Hydrogen Energy, 32(18):4811–4820.

[2] Yang S, Choi DY, Jang SC, Kim SH, Choi DK., 2008. "Hydrogen separation by multi-bed pressure swing adsorption of synthesis gas". Adsorption, 14(4–5):583–590.

[3] Ribeiro AM, Grande CA, Lopes FV, Loureiro JM, Rodrigues AE, 2008. "A parametric study of layered Bed PSA for hydrogen purification. Chemical Engineering Science". 63(21):5258–5273.

[4] Mondal, M. and Datta, A., 2016. "Energy transfer in hydrogen separation from syngas using pressure swing adsorption (PSA) process: a thermodynamic model". International Journal of Energy Research.

[5] Bhattacharya, A., Das, A. and Datta, A., 2014, "Exergy based performance analysis of hydrogen production from rice straw using oxygen blown gasification", Energy, 69:525-533.

[6] Roy, P.C., Datta, A. and Chakraborty, N., 2013. "An assessment of different biomass feedstocks in a downdraft gasifier for engine application", Fuel,106 : 864 – 868.

SEEC-2017-103

Extraction, Preparation and Characterization of nanocellulose from Wheat Straw an agricultural waste material

Mandeep Kaur & Praveen Sharma
Deptt of Environmental Science & Engineering
Guru Jambheshwar University of Science &
Technology, Hisar-125001,Haryana,India

Santosh Kumari
Deptt of Bio & Nano Technology
Guru Jambheshwar University of Science &
Technology, Hisar-125001,Haryana,India

ABSTRACT

Nanocellulose is a modern day material derived from cellulosic biomass and has large specific surface area, high modulus and highly hydrophilic in nature. It comprises of two structural forms viz., nanofibrillated cellulose and nanocrystalline cellulose. Cellulose is the most abundant biomass available on earth. Cellulose is an organic compound with the formula $(C_6H_{10}O_5)_n$, a polysaccharide consisting of a linear chain of several hundred to many thousands of $\beta(1 \rightarrow 4)$ linked D- glucose units. Present study intended to characterize nanocellulose extracted from wheat(Triticum aestivum) straw an agricultural waste by chemical treatment. Fibres were obtained by succumbing wheat straw to alkai (NaOH) and bleaching $(NaClO_2)$ treatments. Nanocellulose was isolated from these fibres by acid (H_2SO_4) hydrolysis. Morphological investigation was performed using Transmission electron microscopy (TEM). Fourier transform infrared (FTIR) spectroscopy showed the progressive removal of non-cellulosic components. X-ray diffraction (XRD) analysis revealed that the crystalinity increased in successive treatments. The result showed that nanocellulose was 50-100nm in diameter. The developed nanocellulose would be a resourceful and renewable material.

APPLICATION OF LOW-COST SILICA-LIPASE NANO BIO-CONJUGATES FOR EFFICIENT AND ECOFRIENDLY BIODIESEL SYNTHESIS

Bharathiraja B
Department of Chemical Engineering,
Vel Tech High Tech Dr. RR Dr. SR Engineering
College, Chennai – 62
btrbio@gmail.com

Chakravarthy M
Centre for Biotechnology
Anna University, Chennai - 25.
Chakra27031994@gmail.com

ABSTRACT

A successive method has been used to prepare monodisperse and uniform-sized Silica Nano Particles (SiNP) using ultrasonication by sol–gel process. The hydrolysis of tetraethyl orthosilicate (TEOS) in ethanol medium was adopted for the synthesis of silica particles of size 15 ± 5 nm and tested for the immobilization of lipase from rPichia pastoris. The SiNPs synthesized were examined under SEM and DLS for confirmation of size and shape. In addition to the above observations, the effect of temperature on particle size was also studied to ensure the homogeneous dispersion of silica-lipase bio-conjugates in ultrasound assisted biodiesel synthesis. The immobilization time and initial enzyme concentration was optimized and successful conjugation of silica with lipase was confirmed with Fourier transform infrared spectroscopy and thermogravimetric analysis. The binding efficiency was determined from the MALDI technique. The lipase activity of free enzyme and SiNP-LP bio-conjugates were determined using p-NPA assay. The employability of enzyme and bio-conjugates were studied from real time bio-diesel synthesis. The process was optimized for temperature, catalyst loading, reaction time and investigations on compatibility of catalyst to various biodiesel synthesis strategies are being made. A promising conversion of 95% biodiesel yield was obtained and the catalyst retained 50% of its activity after 10 successive cycles.

Keywords: Biodiesel, Lipase, Oil, Transesterification, nano-bio-conjugates, methanolysis
.

NOMENCLATURE

SiNP   Silica nanoparticles
SiNP-LP Silica-Lipase nano-particles
BDF   Biodiesel Fuel
SEM   Scanning Electron Microscopy
DLS   Dynamic Light Scattering
p-NPA   para – Nitro Phenyl Acetate

INTRODUCTION

The production of biodiesel from vegetable oil has been in demand in the last decade in Asian countries, since many of them have diverse and high yield crops of oleaginous plants [1, 2]. This is relevant to the world's rapid industrialization and increasing population [3]. It was reported that the biodiesel consumption increased by 35% in the year 2012[4]. The worldwide biochemical mechanism adopted to produce biodiesel was transesterification of vegetable oils by short chain alcohols (methanol or ethanol) catalyzed by lipase (EC 3.1.1.3) [5] It was reported that to yield biodiesel from soybean oil up to 80 and 90%, free lipases from *Candida rugosa*and *Pseudomonas cepacia*can be used [6]. As the free lipase based technology is costly and the reaction rate is low [7, 8]. Immobilized lipase methods have been introduced to improve lipase stability and reusability. Herein immobilized enzymes are defined as "enzyme physically confined or localized in a certain defined region of space with retention of their catalytic activities, which can be used repeatedly and continuously" [9]. Immobilization methods are also various, for example, adsorption on acrylic resin, celite, and anion resin, covalent bonding

using silica-PVA and styrene-divinylbenzene, entrapment using hydrophobic sol-gel support, and cross-linking using glutaraldehyde [10, 11]. Since biodiesel production technology is competitive in terms of low cost and reusability of materials, Asian countries are increasingly producing biofuels. To this end, we carried out the synthesis of a novel biocatalyst consisting of lipase tagged with silica nanoparticles. Silica nanoparticles occupy a noticeable position in scientific research, because of their easy preparation and their wide uses in various industrial applications, such as catalysis, pigments, pharmacy, electronic and thin film substrates, electronic and thermal insulators, and humidity sensors. Here we describe its apparent biochemical and morphological properties and its application in biodiesel production from non-edible oil.

MATERIALS AND METHODS

Chemicals and enzyme

Tetraethyl orthosilicate (TEOS) (Aldrich), ethanol (Aldrich), and ammonium hydroxide (28%, Sigma Aldrich) were used without any further purification. Milli-Q water was used throughout the experiment. Lipase produced by *rPichia pastoris* expressing *Candida Antarctica* lipase was obtained and used for conjugation with silica nanoparticles.

Synthesis of silica-lipase nano-bioconjugate (SiNP-LP)

Ethanol was taken and kept in a sonication bath. After 10 min, a known volume of TEOS was added while sonicating, and after 20 min, 28% ammonium hydroxide was added as a catalyst to promote the condensation reaction. Sonication was continued for a further 60 min to get a white turbid suspension. All the above experiments were conducted at room temperature. Silica nanoparticle of size 15 ± 5 nm were synthesized. 20mL of Si NP solution was mixed well with 20mL of Tris-HCl buffer 20mM (pH8.5). Afterwards, 40mL of mixture solution was added dropwise (100 μL/15 s) to a 40mL lipase solution for 1 hours, 180rpm at 4° C. The formation of an amorphous immobilized lipase complex was observed immediately after addition of lipase solution. The complex was collected after centrifugation at 12000 rpm for 20 min and stored at 4∘C prior to further experiment. For the immobilization yield, supernatant was taken for lipase activitymeasurement as described below and protein concentration was determined as described by Bradford.

Characterization of silica-lipase nano-bioconjugate (SiNP-LP)

The morphologies and dimensions of samples were characterized by Scanning and Transmission Electron Microscopy (SEM and TEM)(Technai 16410 and JEM 1010 JOEL Ltd., Japan) with accelerating voltage of10 kV and 70 kV, respectively. Dynamic light scattering (DLS,

Horiba) was employed for measuring the size of the particle and zeta potential was measured using Zetaseister. MALDI-TOF was used to analyze the binding efficiency of SiNP with Lipase.

Biochemical characterization of SiNP-LP's

The temperature dependence of immobilized lipase activity was investigated in temperature range from 30 to 80 C in comparison to soluble lipase and activities of both forms were determined. The thermal stability of immobilized lipases was investigated by determining its activity at optimal operating temperature after incubation at different temperatures for 1h. pH stability was also checked by using three different buffer systems for varied pH. Enzyme loading was optimized for optimal conversion by assaying the biodiesel productivity at different enzyme loads.

Lipase activity assay

Lipase activity was quantitated by using p-NPA as substrate. 0.9ml of 1:4:95 ratio of acetonitrile-p-NPA:ethanol:phosphate buffer was added to 0.3ml of lipase solution. Acetonitrile-p-NPA was made by adding 0.2mg p-NPA in 1ml of methanol and 60ml of 50mM phosphate buffer. The reaction was carried out at 40ºC and stopped after 15min incubation. The contents were read for absorbance at 405nm against blank. One unit of enzyme activity is defined as the amount of enzyme required to liberate 1µg of pNPA per minute.

Biodiesel Production

Reaction was performed in a 100mL Duran bottle containing 5 g oil. For the conversion of rubber seed oil was with oil to methanol ratio of 1 : 3 (w/w) was implemented because this strategy has been widely proposed for biodiesel production studies. An appropriate amount of SiNP and lyophilized lipase was applied. The reaction mixture was continuously stirred at 120 rpm for 6 hours at 40∘C (optimal conditions). For reusability tests, the reaction mixture was centrifuged at 10,000 rpm for 30min at 4∘C to collect the immobilized lipase pellet and the pellet was then reused with fresh substrates for further batch of biodiesel production.

RESULTS AND DISCUSSION

Synthesis of SiNPs

with fresh The SiNPs, were synthesized by solgel method, for the following reasons: (1) they can be used as a supporting core for the lipase immobilization to enhance the stability of lipase and to build morphologically controllable particles; (2) their size could be controlled, from 10 to 20nm in diameters, so the smaller size particles will enlarge the total acting surface of reacting silver particles in reaction mixture. Obviously, this would lead to

higher binding amount of lipase molecules massively; (3) colloidal SiNPs are not precipitated and agglomerated.

Scanning Electron Microscopy and Transmission Electron Microscopy

The electron beam is generally scanned in a raster scan pattern, and the beam's position is combined with the detected signal to produce an image. From the Figure 1 it was observed that the size range of the particle was about 20 nm. The size measurements were done using Image J software.In order to ascertain the size pattern of SiNPs obtained by SEM, TEM analysis was also done. SiNPs samples prepared with TEOS were chosen. TEM images were captured for each of the samples. Particle sizes were measured for each of the 5 samples, averaged and the mean particle size was measured using Image J software and was found to be in the range of 10-20 nm. (Figure 2) and a comparative study was performed with the measurements observed by DLS. The sizes measured by TEM were time and again found to be smaller than the hydrodynamic diameter measured by DLS (in solution) which was quite expected. Nevertheless, the pattern of sizes observed by TEM analysis was in concordance with the sizes obtained by DLS.
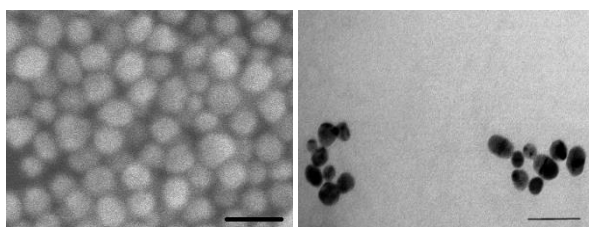
FIGURE 1. SEM image of SiNP and TEM image of SiNP-LP. Scale bar - 50nm.

Dynamic Light Scattering
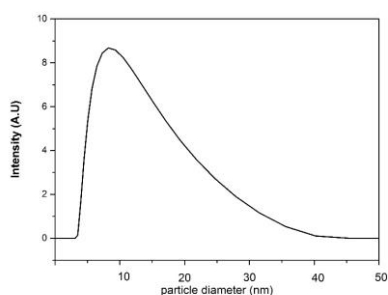
FIGURE 2. SiNP size detection using DLS.

In the scope of DLS, temporal fluctuations are usually analyzed by means of the intensity or photon auto-correlation function (also known as photon correlation spectroscopy or quasi-elastic light scattering). The DLS data also interprets that the size range of the nanoparticle varied in the range from 10-30 nm (figure 2). Thus, from the TEM, SEM and DLS results it was characterized that the particle size was about 10-20 nm. No significance increase in the particle size was absorbed after loading with the Lipase.

Matrix Assisted Laser Desorption and Ionization

By irradiating the sample (SiNPs conjugated with lipase in DHB matrix)with laser, the molecules are ionized and form characteristic peaks based on their mass-to-charge ratio (m/z), from which the analytes were detected. For instance, the figure 3. illustrates a predominant peak corresponding to the (m/z = 300-350) in the positive ion mode, taken as control. No other strong ion signals were observed. The mass spectra were collected in both the negative and positive ion modes and were averaged for 100 laser shots. The figure also shows sharp peaks corresponding to the major anionic species of lipase (m/z = 150) in negative ion mode, which coincides with the previous reports. Thus, the results confirmed the strong binding efficiency of lipase to silica nanoparticles.
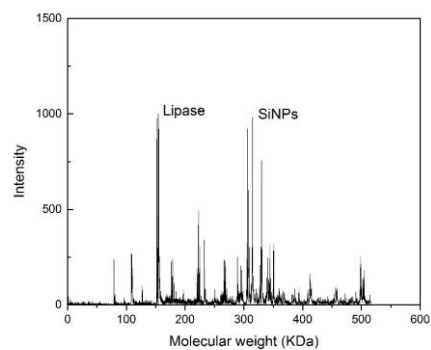
**FIGURE 3.** MALDI spectrum of SiNPand TEM image of SiNP-LP

Biodiesel production and reusability of SiNP-LP's

Fatty acid methy esters were produced from the non-edible waste oil mixture using pure lipase and SiNP-LP.
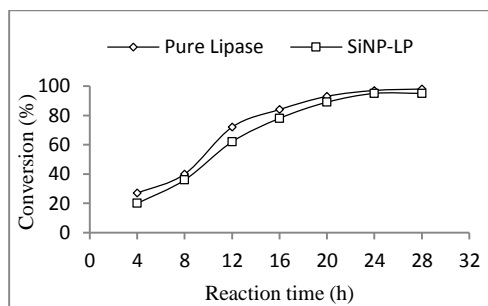
FIGURE 4. Production of biodiesel using pure lipase and SiNP-LP conjugates. 1:3 oil to methanol, 40°C, 3% SiNP-LP, 28hr.

3

The ability to convert oil was investigated with respect to time. Both catalysts promoted almost 90% conversion in 20h reaction time signifying higher conversion rate than most heterogenous nanocatalysts (Figure 4). SiNP-LP catalysed 95% conversion in a minimal time of 24h. Pure lipase catalyzed 98% conversion in 30h reaction time. The rate of reaction of pure lipase continues productively after 24h on one side whereas the SiNP-LP conjugates reached maximal conversion (95%) in 24h reaction time and no further significant increase in the conversion was noted.
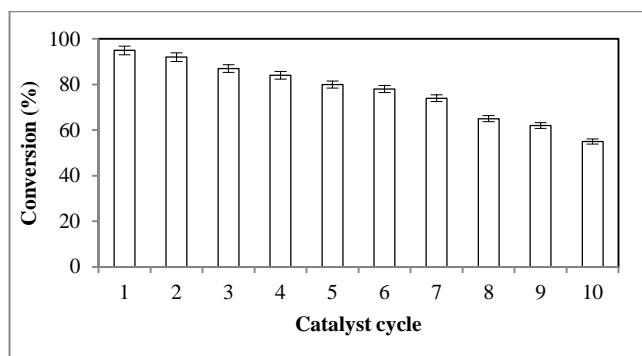
FIGURE 5. Production of biodiesel and reusability analysis of SiNP-LP conjugates. 1:3 oil to methanol, 40ºC, 3% SiNP-LP, 28hr.

The conversion ratio of biodiesel to oil was high as 95% in the first batch of reaction (figure 4&5). The SiNP-LPs when recovered and reused for further conversion gave good conversion. The results were much significan as the first 4 reaction cycles showed more than 80% conversion and the catalyst activity retained was more than 70% of the initial catalyst activity.

CONCLUSION

Succesive immobilization of lipase on silica nanoparticles has been done and the synthesized SiNP-LP showed remarkable conversion of 95% on 1:3 molar rato of oil to methanol at 3% catalyst load. However, the lipase immobilization on SiNP did not showed any added advantage of thermal stability and pH stability but contrastingly, SiNP-LP catalyst produced significant conclusions on the usability of lipase in a matrix mediated-packed bed reactor for continuous biodiesel production as the catalyst retains more than 50% of the initial enzyme activity after 7 succesive cycles and the conversion after 9 succesive cycles reached 52% which is notably higher for any nano carrier-lipase conjugate for biodiesel conversion proposed till date.

REFERENCES

[1] Mukta, N., and Y. Sreevalli, 2010. "Propagation techniques, evaluation and improvement of the biodiesel plant, Pongamia pinnata (L.) Pierre - a review". Industrial Crops and Products, 5(3), pp. 1–12.

[2] Murphy, H.T., O'Connell, D, A., Seaton, G., et al., 2012. "A common view of the opportunities, challenges, and research actions for pongamia in Australia". Bioenergy Research, 5(3), pp. 778–800.

[3] Hoffmann, U., 2011. "Some reflections on climate change, green growth illusions and development space". United Nations Conference on Trade and Development Discussion Papers.

[4] Preechajarn, S., and Prasertsri, P., 2012. "Biofuels Annual Bangkok Thailand 2012". GAIN Report, TH2064.

[5] Fan, X., Niehus, X., and G. Sandoval, G., 2012. "Lipases as biocatalyst for biodiesel production". Methods in Molecular Biology, 861, pp.471–483.

[6] Kaieda M., Samukawa, T., Kondo, A., and Fukuda, H., 2001. "Effect of methanol and water contents on production of biodiesel fuel from plant oil catalyzed by various lipases in a solvent-free system". Journal of Bioscience and Bioengineering, 91, pp.12-15.

[7] Zhang, Y., Dub´e, M.A., McLean, D.D., and Kates, M., 2003. "Biodiesel production from waste cooking oil: 1. Process design andtechnological assessment". *Bioresource Technology*, 89(1), pp. 1–16.

[8] Fjerbaek, L., Christensen, K.V., and Norddahl, B., 2009. "A review of the current state of biodiesel production using enzymatic transesterification". *Biotechnology and Bioengineering*, 102(5), pp. 1298–1315.

[9] Jegannathan, K.R., Abang, S., Poncelet, D., Chan, E.S., and Ravindra, P., 2008. "Production of biodiesel using immobilized lipase a critical review". *Critical Reviews in Biotechnology*, 28(4), pp. 253–264.

[10] Tan T.,, Lu J.,, Nie K., Deng, L., and Wang, F., 2010. "Biodiesel production with immobilized lipase: a review". *Biotechnology Advances*, 28(5), pp. 628–634.

[11] Salis, A., Pinna, A., Monduzzi, M., and Solinas, V., 2008."Comparison among immobilised lipases on macroporous polypropylene toward biodiesel synthesis". *Journal of Molecular Catalysis B:Enzymatic*, 54(1), pp. 19–26.

SEEC-2017-105

PHYTOREMEDIATION OF CHROMIUM FROM SYNTHETIC WASTE WATER BY *LEMNA MINOR*

Ekta Chaudhary
Dept. of Environmental Sciences
Engineering,GJUS&T, Hisar

Praveen Sharma
Dept. of Environmental Sciences
Engineering,GJUS&T, Hisar

ABSTRACT

The Biosphere is getting polluted by the release of various natural and synthetic pollutants which proves to be very harmful for living organisms. Several industries release heavy metals (cadmium, copper, chromium, nickel, lead etc.) in the wastewater. Phytoremediation is a noval technology for wastewater treatment as well as for heavy metal removal. The objective of this study was to evaluate the removal efficiency of Chromium (Cr) by Lemna minor in contaminated water. Plants were treated to different Cr concentrations ranged from 1-9 mg/L. The results show that after 14 days of treatment, percentage Cr removal rates varies from 97% to 58% for 1mg/l to 9mg/l, respectively, and the Bioconcentration factor (BCF) and plant growth rate of Cr in Lemna minor were highest at initial Cr concentration and decreased as the Cr concentration increased. Cr removal by Lemna minor therefore is a suitable option for the treatment of Cr contaminated water.

REMOVAL OF MALACHITE GREEN FROM AQUEOUS SOLUTION BY *ASPERGILLUS VERSICOLOR(MTCC280)*

Surajit Bag, Debabrata Bera
Deptt of Food Technology & BioChemical
Engineering, Jadavpur University, Kolkata, India

Atanu Mitra, Ananya Bardhanh & Dipankar Halder
Sree Chaitany College, Habra, W.B., India

ABSTRACT

Dyes are extensively used in textile, tannery, food, paper and pulp, printing industries to color their products. About 10–15% of the annual global production (2,80,000 tons) of dyes are discharged as effluent mainly by textile and paint industries. The majority of the dyes are toxic and cause damage to aquatic life. In this study biosorption of Malachite Green (MG) onto the dried Aspergillus versicolor biomass (AVB) was investigated with variation in pH, temperature, contact time, biosorbent dose and dye concentration. Characterization of the dye-biosorbent interaction was studied by scanning electron microscopy. It was observed from the present study that the bio-sorption of Malachite green was maximum at pH 5, temperature of 30ºC, and adsorbent dose of 2g/l. The rate of adsorption was found to be very fast at the initial phase and the equilibrium reached at 270min following the pseudo-second order rate kinetics. The adsorption process followed Freundlich Isotherm model. The results show that the present study may help designing a promising route in bioremediation of the hazardous chemical malachite green.

SEEC-2017-107

COMPARATIVE ANALYSIS FOR BIODIESEL PRODUCTION FROM MARINE ALGAE *Nannochloropsis occulata* AND POND ALGAE *Chlorella vulgaris* BY TRANSESTIRIFICATION METHOD USING LIPASE CATALYST

B. Bharathiraja, J. Vinoth Arulraj, R. Praveen kumar, A. Williamjohnson, K. Mukilan
Vel Tech High Dr Rangarajan Dr. Sakunthala EC, Chennai.

S. Surendar
Arunai Engineering college,
Tiruvannamalai, India

ABSTRACT

The needs of world petroleum are increased; in contrast, the fuel productions are getting decreased. Therefore, it has lead to the search for bio-fuel as an alternative energy. Biodiesel is typically made by chemically reacting lipids from a vegetable oil or animal fat with an alcohol producing fatty acid esters, such as methyl or ethyl ester. The present study aims to produce biodiesel from microalgae by the transesterification process using homogeneous catalyst. The initial part of this project was to separate biomass from the algal culture and extract the oil from biomass. The homogeneous alkali catalyst (NaOH) was used in the production of biodiesel (transesterification process). Marine algae Nannochloropsis occulata and pond algae chlorella vulgaris was used as feed stocks. Algae fatty acid methyl esters (algae FAME) has been obtain from the following reaction conditions; reaction temperature of 50◦C, reaction period of 180 minutes and ratio of oil to methanol at 1:1 with a lipase catalyst at different concentration. .The conformation of biodiesel was done by the Ferric chloride test and Hydroxamic acid. The characterization of biodiesel was carried out using GC-MS study.

SEEC-2017-108

FLEXIRUBIN TYPE PIGMENT PRODUCTION FROM *Chryseobacterium artocarpi* CECT 8497 AND ITS APPLICATION AS NATURAL INK

Mohamad Ainuddin Wahidin, Claira Arul Aruldass, Mohd. Amir Asyraf Mohd Hamzah, Siti Aminah Setu amd Wan Azlina Ahmad
Department of Chemistry, Faculty of Science,
Universiti Teknologi Malaysia, 81310 UTM, Johor Bahru, Malaysia
e-mail: azlina@kimia.fs.utm.my

ABSTRACT

Interest and demand for bacterial pigments is growing due to rising awareness of toxicity of synthetic dyes. In our previous reports, flexirubin type pigment is found to be safe and non-toxic. This study evaluates on the production of flexirubin type pigment from Chryseobacterium artocarpi CECT 8497 using liquid pineapple waste in 5 L bioreactor and its application as environmental-friendly ink. Combination of polyvinyl butyral and polyvinyl pyrrolidone was used as resin for flexirubin ink preparation and the ink was characterized using FT-IR. Results showed that liquid pineapple waste is feasible for C. artocarpi CECT 8497 growth and flexirubin production. The ink was successfully formulated with less bubble and smooth texture and the functional groups of flexirubin were indentified in the formulated ink. Flexirubin ink was stable at room temperature for 30 days. This is the first report on ink formulation of flexirubin type pigment from C. artocarpi and its potential application on plastic materials.

SEEC-2017-110

THEORETICAL ROUTE TO PREDICT THE HEATING VALUE OF BIODIESEL

S. Debbarma	**R.D. Misra**	**B. Das**
Department of Mechanical Engineering	Department of Mechanical Engineering	Department of Mechanical Engineering
NIT Silchar, Assam-788010	NIT Silchar, Assam-788010	NIT Silchar, Assam-788010
Email: sumita.mech09@gmail.com	Email: rdmisra@gmail.com	Email: biplab.2kmech@gmail.com

ABSTRACT

Biodiesel consists of alkyl esters of fatty acids from vegetable oils or animal fats. It is an environmental friendly, biodegradable, renewable, energy efficient that can be used as an alternative of highly depleting petroleum fuel. The properties of biodiesel depend on the type of vegetable oil used for the transesterification process. The objective of the present work is to theoretically develop a relation between calorific value of different biodiesels with their density and viscosity values. The values of different properties are taken from the available published results. A theoretical model is developed to predict the calorific value of any biodiesel from the corresponding density and viscosity value. The predicted results show that the correlation coefficient of the equation is 0.998 with anaverage relative deviation of 0.44%.

Keywords: *Biodiesel; calorific value; density; viscosity; correlation*

INTRODUCTION

The world is facing twin crisis: fossil fuel depletion and environmental degradation,which are continuously intensified due to increase in energy consumption. These factors coupled with rapid increase in price of petroleum fuelsdrive the researchers to find some immediate renewable alternative of the petroleum fuels for energy sector in general and automotive sector in particular. Though some renewable alternatives like solar, wind and biomass is explored, tested, but their adoption is still very slow because of economic constraints, technical know-how of the users and required modification of the present engine [1-2]. On the contrary, sustainable and economic production of biodiesel has gained popularity, as it can be used directly in the presently available IC engine without or with little engine modification [1-5].

Calorific value (CV) or heating value is the measure of energy level of any fuel, obtained by the complete combustion of a unit quantity of fuel.Measure of CV will give the amount of heat evolved after complete combustion of one unit weight of a compound.Thus, higher the value of CV indicates higher the number of carbon and hydrogen molecules. For diesel engine, viscosity and density are the other two key fuel properties, and alternative fuels have to maintain standard at per diesel fuel. In a diesel engine, at the end of compression process atomization of sprayed liquid fuel occurs nearer to the nozzle exit. Quality of atomization and size of fuel droplet is highly affected by the viscosity of fuel[6]. As highly viscous fuel tends to form larger fuel droplets resulting poor atomization during spray to the compressed air. This further, leads to increase in engine deposits, wears injectors and fuel pump elements, and requires more power to pump the fuel. Thus, high viscosity results in poor combustion as well as raise exhaust smoke and emissions [7]. Density directly affects the engine performance characteristics, such as cetane number and heating value [8]. Change in density of fuel affects the neat mass of injected fuel, and thus the air-fuel ratio. Since volume of fuel is measured by the fuel injection pump instead of mass, thus denser fuel will results in greater mass of injected fuel. Thus, the variation in the fuel density will results in variation of engine power output [6].Thus, the effect of density and viscosity on engine performance are inter linked.

Estimation of heating values of biomass-derived fuels have been performed using their proximate and ultimate analysis data [9-10]. Prediction of combustion properties of liquid fuels like vegetable oils, alcohols, diesel fuels, and alkanes are highlighted by Demirbas [11]. Later estimation of the heating values of vegetable oils is performed

usingsaponification value and iodine value[12].Mathematical relationships between higher heating value (HHV) and viscosity, density or flash point of various vegetable oilsand biodiesel are presented by Demirbas[13].Mathematical prediction of iodine value and saponification value from the fatty acid esters content is attempted by Gopinath et al. [14]. Verification of the proposed model is done by predicting the calorific value form the corresponding predicted iodine value and saponification value by using the established correlation of Demirbas[12].Comparison of different models for predicting viscosity of different biodiesel is recently made by Chavarria and Catalan [15]. Prediction of viscosity of neat biodiesel and blended biodiesel are highlighted in literature Geacai et al. [16]. Correlation to predict the biodiesel density for extended ranges of temperature and pressure is highlighted recently by Prieto et al. [17].

From the pertinent literature it can be identified that many researchers have attempted to establish correlation between the physical properties of biodiesel, to find the interrelation among them. Here in this article an attempt is made to develop a mathematical relation to predict the calorific value of biodiesel from the combined value of density and viscosity, so that some experimentation can be avoided for determining this property.

METHOD

PROPERTIES OF DIFFERENT METHYL EASTER:
Various physical properties of biodiesel are obtained fromDemirbas[13], Gopinath et al. [14], Sahoo and Das [18], and Debbarma et al. [19], tabulated in Table 1.

REGRESSION: It is well known that interpolation and extrapolation of data from past experiments at new conditions is preferable, as time and costs always preclude new experimentation. One of the criterions of any good correlation is the magnitude of correlation coefficient, which varies between 1 (best) and 0 (worst). The correlation coefficient is evaluated as [1-(mean square error/total sum of square of variable)]$^{0.5}$. After regression the best correlation with greater correlation coefficient is presented. Comparison of different proposed correlations is discussed in the following section.

RESULTS AND DISCUSSIONS

The relation between calorific value, density, and viscosity is investigated through a regression analysis in order to find out a suitable correlation so that the calorific value of any biodiesel can be predicted from the known value of its density and viscosity. During regression, to obtain the best possible correlation, criterion of correlation coefficient is considered as one of the measure. Total 10 nos. of oil methyl easter are chosen to make the correlation. To obtain the correlation of calorific value

(CV) of biodiesel with its density (ρ), viscosity (μ) and a guidance from Das and Giri[20] has been considered.

TABLE 1. PROPERTIES OF BIODIESEL.

Methyleaster	Viscosity (cSt)	Density (kg/m^3)	CV (MJ/kg)
Cotton oil	3.75	871	41.18
Mustard oil	4.1	866	41.3
Palm oil	3.94	867	41.24
Soyabean oil	4.08	865	41.28
Sun flower oil	4.16	863	41.33
Jatropha oil	4.23	873	42.67
Mahua seed oil	4	872	41
Rapseed oil	4.6	857	41.55
Crambe oil	5.12	848	41.98
Polanga oil	3.99	869	41.4

CORRELATION OF CALORIFIC VALUE (*CV*) WITH DENSITY (*P*) AND VISCOSITY (*µ*)

Variation of calorific value with density and viscosity are exemplified in Fig. 1 and Fig. 2 respectively. Results indicate that calorific value of the biodiesel,in general, shows a decreasingtrend with density, while the same increases with viscosity. This may be because of chain length (number of carbon atoms) of fatty acid components. At higher chain length density decreases while viscosity increases. Further, magnitude of energy content of the higher length acid per unit weight is less, but for lower length acid magnitude of energy content is balanced by higher density. Thus, the final value of energy content for any methyleaster is a combined effect of both lower and higher length acids, and the same can also be replicated in their density and viscosity.

Using the experimental value available in literature to predict the value of *CV*, the following correlation between *CV*of biodiesel with$\rho$is proposed:

$$CV = -0.032\rho + 69. \qquad (1)$$

Correlation coefficient of the above equation is found out to be 0.99.
Further to predict the value of *CV* from the value of $\mu$of biodiesel, following correlation is proposed:

$$CV = 0.56\mu + 39. \qquad (2)$$
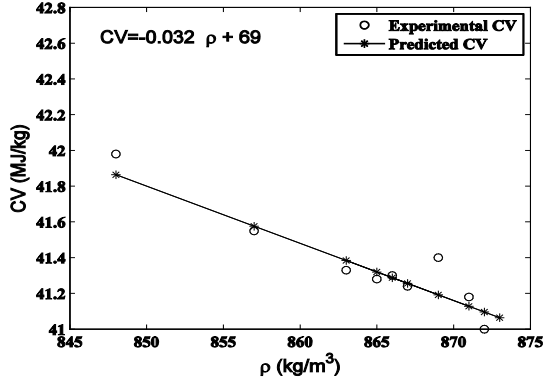
Correlation coefficient for the same is 0.99.

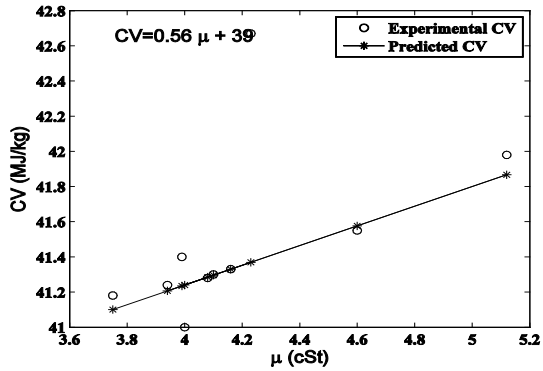**FIGURE 1.** PLOT OF CORRELATED AND EXPERIMENTAL CALORIFIC VALUE WITH DENSITY.

FIGURE 2. PLOT OF CORRELATED AND EXPERIMENTAL CALORIFIC VALUE WITH VISCOSITY.

As mentioned above, fatty acid content of the biodiesel affects the physical properties density, viscosity, and calorific value very significantly. So an attempt has been made in the present work to predict the calorific value of biodiesel from the known value of both density and viscosity. The behaviour of the variationof CV with respect to combined effect of density and viscosity is exemplified in Fig. 3.Based on the behaviour following best suited correlation is proposed (Eq. (3)). Overall correlation coefficient found out to be 0.999.

$$CV^{0.8}/\mu^{0.168} = 1.92\rho^{0.477} - 32.85 \qquad (3)$$

RELATIVE DEVIATION OF PREDICTION CALORIFIC VALUE (CV)

Following Meng et al. [21], to compare the predictive accuracy of the correlations (Eqs. (1)-(3)), relative deviation value for all biodiesel are presented in Fig. 4. The relative deviation (*RD*) is calculated using Eq. (4). Magnitude of *RD* values represents the deviation of predicted value from the corresponding experimental value for each biodiesel. For the sake of comparison, relative deviation of predicted *CV* of biodiesel from the corresponding value of *μ* using the correlation proposed by

Demirbas [13] for the same is also presented in Fig. 4. This graphical presentation clearly depicts that Eq. (3) predicts the value of *CV* better, for the considered biodiesel.

$$RD = (CV_{\exp} - CV_{\mathrm{pre}})/CV_{\exp} \times 100 \qquad (4)$$
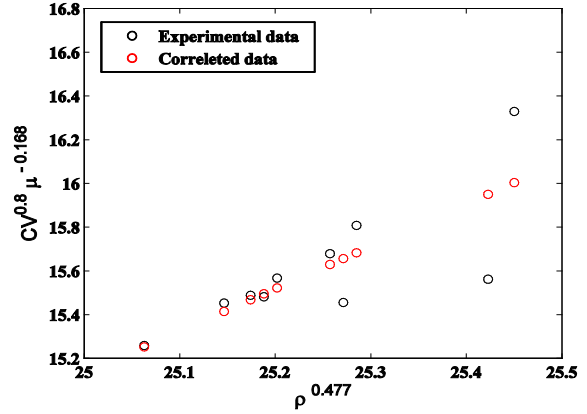
FIGURE 3. PLOT OF CORRELATED AND EXPERIMENTAL CALORIFIC VALUE WITH BOTH DENSITY AND VISCOSITY.

Further, overall average relative deviations ($ARD = \sum |RD|/n$) of prediction of *CV* of biodiesel with different correlations are presented in Table 2. From the table it can be observed that Eq. (3), i.e., the correlation made considering both the value density and viscosity predicts the value of *CV* with better accuracy. Moreover, as combined effect of both the easily measurable key properties,i.e., density and viscosity, are considered, the proposed correlation will be of much useful for practitioners.

TABLE 2. AVERAGE PERCENTAGE OF RELATIVE DEVIATION FOR EACH CORRELATIONS.

Methods	ARD (%)
Eq. (1)	0.53
Eq. (2)	0.47
Eq. (3)	0.44
Dembris (2008)	0.48

CONCLUSIONS

Biodiesel properties depend on the type of vegetable oil being used. Three key properties of fuel (i.e., density, viscosity, and calorific value) are considered in the present investigation, to find the best possible combination of relation among them. Correlation coefficient and relative deviation are taken as the measure of accuracy of prediction. Crux of the present work is to make a

correlation to predict the heating value of biodiesel using two easily measurable properties like density and viscosity. Three different correlations are proposed – two being considering density and viscosity separately, and theother is made considering both the effect of density and viscosity. The predicted results show that the correlation coefficientsfor all the equations are 0.99.Further, published correlation to predict CV, along with the present three correlations are compared with respect to their relative deviation (RD). Results indicate that, the average value of RD for the correlation made considering both the effect of density and viscosity predicts with better accuracy.
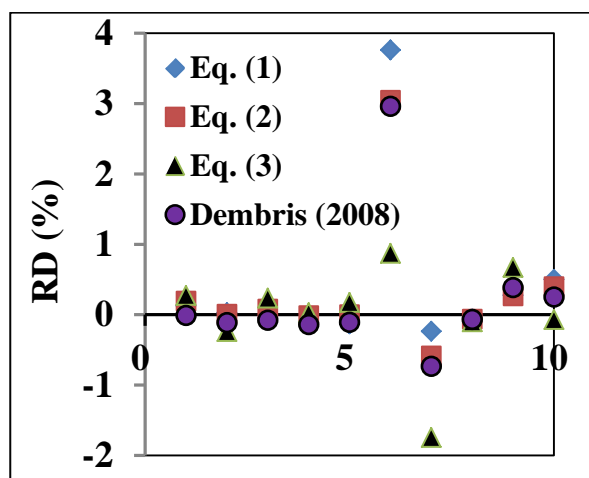
FIGURE 4. PERCENTAGE OF RELATIVE DEVIATION FOR EACH CORRELATION.

REFERENCES

[1] Misra, R.D., Murthy, M,S., 2010. Straight vegetable oils usage in a compression ignition engine—A review. Renewable and Sustainable Energy Reviews ; 14:3005-13.

[2] Jena, J., Misra, R.D., 2014. Effect of fuel oxygen on the energetic and exergetic efficiency of a compression ignition engine fuelled separately with palm and karanja biodiesels. Energy; 68:411-19.

[3] Qi, D.H., Chen, H., Geng, L.M., Bian, Y.Z., 2010. Experimental studies on the combustion characteristics and performance of a direct injection engine fueled with biodiesel/diesel blends. Energy Convers Manage; 51:2985–92.

[4] Rahman SMA, Masjuki HH, Kalam MA, Abedin MJ, Sanjid A, Sajjad H. Impact of idling on fuel consumption and exhaust emissions and available idle-reduction technologies for diesel vehicles – a review. Energy Convers Manage 2013; 74:171–82.

[5] Ong, H.C., Silitonga, A.S., Masjuki, H.H., Mahlia TMI, Chong, W.T., Boosroh, M.H., 2013. Production and comparative fuel properties of biodiesel from non-edible oils: Jatropha curcas, Sterculiafoetida and Ceibapentandra. Energy Convers Manage; 73:245–55.

[6] Alptekin, E., Canakci, M., 2008. Determination of the density and the viscosities of biodiesel–diesel fuel blends. Renew. Energ., 33 (12), 2623-2630.

[7] Knothe, G., Steidley, K.R., 2005. Kinematic viscosity of biodiesel fuel components and related compounds. Influence of compound structure and comparison to petrodiesel fuel components. Fuel, 84 (9), 1059-1065.

[8] Tat, M.E., Gerpen, J.H., 2000. The specific gravity of biodiesel and its blends with diesel fuel. J. Am. Oil Chem. Soc., 77 (2), 115-119.

[9] Demirbas, A., Gullu, D., Caglar, A., Akdeniz, F., 1997. Estimation of calorificvalues of fuels from lignocellulosic. Energy Source;19:765–70.

[10] Demirbas, A., 1997. Calculation of higher heating values of biomass fuels.Fuel; 76: 431–34.

[11] Demirbas, A., 2000. A direct route to the calculation of heating values of liquid fuels by using their density and viscosity measurements. Energy Convers Manage;41:1609–1614.

[12] Demirbas, A., 1998. Fuel properties and calculation of higher heating valuesof vegetable oils. Fuel; 77: 1117–20.

[13] Demirbas, A., 2008. Relationships derived from physical properties of vegetable oil and biodiesel fuels. Fuel; 87:1743–48.

[14] Gopinath, A., Puhan, S., Nagarajan., G., 2009. Theoretical modeling of iodine value and saponification value of biodiesel fuels from their fatty acid composition. Renewable Energy; 34: 1806–11.

[15] Chavarria-Hernandez, J.C., D.E. Pacheco-Catalan, (2014). Predicting the kinematic viscosity of fames and biodiesel: empirical models. Fuel, 124, 212-220.

[16] Gecai, S., Lulian, O., Nita, I., 2015. Measurements, correlation and prediction of biodiesel blends viscosity. Fuel, 143, 268-274.

[17] Prieto, N.M.C.T., Ferreira, A.G.M., Portugal, A.T.G., Moreira, R.J., Santos, J.B., 2015. Correlation and prediction of biodiesel density for extended ranges of temperature and pressure. Fuel, 141, 23-38.

[18] Sahoo, P.K., Das, L.M., 2009. Process optimization for biodiesel production from Jatropha, Karanja and Polanga oils. Fuel; 88:1588–94.

[19] Debbarma, S., Das, B., Giri, A., Majumder, S., Bose, P., 2011. Back propagation artificial neural network (BPANN) based performance analysis of diesel engine using biodiesel. Journal of Renewable and Sustainable Energy; **3:**013101-11.

[20] Das, B, Giri, A., 2014. Conjugate conduction and convection underneath a downward facing non-isothermal extended surface: A numerical study. Energy Convers Manage; 88: 15–26.

[21] Meng, X., Jia, M., Wang, T., 2013. Predicting biodiesel densities over a wide temperature range up to 523 K. Fuel, 111, 216-222.

SEEC-2017-111

OPTIMIZATION OF CULTURE CONDITIONS FOR LIPID PRODUCTION BY MICROALGA *DESMODESMUS SUBSPICATUS* AND EVALUATION OF LIPIDS FOR BIODIESEL PRODUCTION

Rajni Chaudhary[1] J.I.S Khattar[2], and D.P Singh[3]

Department of Agriculture, Baba Farid College, Deon (Bathinda), India

[2]Departmet of Botany, Punjabi University, Patiala, India

Email: rajnichaudhary36@yahoo.com

ABSTRACT

Culture conditions were optimized for lipid production in *Desmodesmus subspicatus,* an isolate from Lahul Spiti, India. Under N limitation, biomass production decreased and the amount of lipids increased by 11% over control cultures (29% lipid content). Under continuous illumination and at pH 6.4 of the medium the biomass of the organism increased by 10% and 9%, respectively, while lipid content increased by 9% and 8%, respectively. The fatty acid profile of lipids of the organism under optimized conditions also changed. Under nitrogen limitation saturated fatty acid (SFA) content was 47%, monosaturated fatty (MUFA) were 30% and polyunsaturated fatty acids (PUFA) were 23%; under continuous illumination SFA were 47%, MUFA were 27% and PUFA were 13% compared to control cultures with 32% SFA , 27% MUFA and 46% PUFA. This indicated that fatty acid profile of lipids under optimized conditions was better from biodiesel production point of view.

INTRODUCTION

Microalgae are a vast and diverse group of unicellular or multicellular aquatic organisms with significant potential to produce valuable natural products [1]. Pigments of microalgae, especially carotenoids and phycobiliproteins, have been proposed to have applications that range from food colorants to effective agents in disease prevention in humans [2]. In recent years, focus has turned to the production of cellular storage lipids from microalgae (namely triglycerides or TAGs) for the production of biodiesel [3]. Algal cells have the capacity to rapidly accumulate lipids that contain fatty acids important for high value biodiesel. The lipid accumulation has been reported in several microalgae [4]. Algal fuels are considered to be good alternative to fossil fuels because algal feedstocks are much more reliable and using them for biofuel production may decrease the dependence on fossil fuels. Screening and selection of microalgae producing high amounts of neutral lipids is very crucial for the commercial success of algae-based biofuel production. Although some of naturally occurring algal strains have been screened but the criteria for the selection of algal strains as a feedstock for biofuel production have not been well defined. Studies on algal biofuels have shown that the quantity and quality of lipids within the algal cell biomass can vary as a result of changes in growth conditions [5]. The present study was focused on optimization of culture conditions not only to increase biomass and lipid productivity but also to get better fatty acids composition from green microalga *Desmodesmus subspicatus*. Also an attempt was made to optimize 10 parameters; dry cell weight, net lipid productivity, lipid content (% of DCW), number of fatty acids in lipids, content of C16-C18 fatty acids of total lipid (TLC), content of fatty acids with C=C $\geq$ 4, content of linolenic acid, content of saturated, monounsaturated and polyunsaturated fatty acids in lipids of the test strain.

MATERIAL AND METHODS

Desmodesmus subspicatus CLS50 is an isolate from fresh water source of Koksar village of Lahul Spiti (32º 24' 16.59" N; 77º 15' 49.25" E) of cold desert area of Himachal Pradesh, India. The isolate was purified following serial dilution and purification method of Stanier [6]. *D. subspicatus* is a subgenus of *S. quadricauda*. Cells of *D. subspicatus* are cylindrical and linearly arranged in 4- celled flat coenobium, cell wall is with spines which originate from outer cell wall of lateral sides of the coenobium. Cells have single parietal chloroplast with pyrenoid. Cells are 2-9 μm long and 6-12 μm broad with 6.5-8 μm long spines (Fig. 1). The cultures of test organism were propagated in BG11 medium [7] incubated in a culture room at 28 °C ±2 °C under 44.5 μmol photon flux density m^{-2} s^{-1} at the surface of culture vessels for 14 h a day. The isolate was identified on morphological basis as well as with partial 18S rRNA gene sequencing. Total lipids were extracted from the biomass by slightly modifying the method of Bligh and Dyer [8] and determined gravimetrically. Fatty acid composition of lipids was analyzed through HPLC. The viscosity and density of lipids was measured through viscometer and pycnometer at room temperature.

The influence of nutritional and physical factors on lipid production as well as on fatty acid composition of lipids of test strain was studied by growing the cultures in varied nutritional and physical conditions. Altered nutrient conditions included N limitation while altered physical factors included change in pH of medium and incubation of cultures under continuous light. Basal medium contained 17.6 mM NaNO3. Nitrogen limitation in the basal medium was induced by decreasing NaNO$_3$ concentration from 17.6 mM to 2 mM through 8 mM and 4 mM. To study the effect of pH on the growth and lipid production of test organism, pH of the medium ranged from 5.4 to 9.4 through 6.4, 7.4 and 8.4. To study the effect of continuous light on lipid production the experimental cultures were incubated under continuous light

RESULTS AND DISCUSSION

The relationship between lipid content and day growth rate in microalgae was found to be inversely related in nitrogen deficient condition [9]. When nitrate concentration in medium was decreased to 4 mM, biomass production decreased but the amount of lipids increased by 11 % over control cultures (29% lipid content). Under continuous light, biomass and lipid content of the organism increased by 10%. When pH of the medium was decreased by one unit from 7.4 to 6.4, biomass as well as lipid content increased by 9% and 10% respectively, over control cultures. These conditions not only affected the biomass production and lipid content but fatty acid profile of lipids also changed. It was observed that amount of saturated fatty acids (SFA) increased in all optimized conditions while amount of polyunsaturated fatty acids decreased. The algal lipids rich in saturated as well as monosaturated fatty acids and with low amount of polyunsaturated fatty acids are desirable for biofuel production [10]. The lipids with high amounts of saturated fatty acids give an excellent cetane number and oxidative stability to biofuel [11]. Under nitrogen limitation the fatty acid composition of lipids changed to 47% saturated fatty acids (SFA), 30% monounsaturated fatty acid (MUFA) and 23%polyunsaturated fatty acid (PUFA), in acidic condition SFA were 50%, MUFA were 21 % and PUFA were 29% and under continuous light SFA were 47%, MUFA were 27% and PUFA were 13%, respectively, over control cultures where saturated fatty acids were 32%, monounsatured fatty acids were 22.3% and polyunsaturated fatty acids were 46% of total lipid content (Table 1). Fatty acids with C16-C18 also increased under optimized conditions, which are highly evaluated for biodiesel production. Most of algal oils possess high amounts of polyunsaturated fatty acids with four or five double bonds which are not desirable from biodiesel point of view [12]. In present study, the content of fatty acids with C=C ≥ 4 were less. Density and viscosity of lipids of test organism obtained under optimized conditions were within the range prescribed by EN1214 standard for biodiesel. So the best condition for the good quality and high quantity of *D. subspicatus* was continuous light. In the earlier studies, only total lipid content in a particular microalgal species has been considered as an important parameter for the selection of algal strain for biodiesel production, but results obtained from the present study suggested that to determine the suitability of algal biomass as feedstock for lipid based algal biofuel; biomass yield, lipid content, its fatty acid composition and appropriate life cycle phase to harvest biomass should be criteria for selection of a particular microalgal strain. There is need to extend this work for mass cultivation of these microalgae on low cost substrates so that cost of biomass production can be reduced.

REFERENCES
[1]. Plaza, M., Amigo, M., Ibañez, E., Del Castillo, M. D. and Herrero, M. (2010). Neoformation of antioxidants in glycation model systems treated under

subcritical water extraction conditions. *Food Res. Int.*, 43:1123-1129.

[2]. Vílchez, C., Forján, E., Cuaresma, M., Bédmar, F., Garbayo, I. and Vega, (2011). Marine carotenoids: biological functions and commercial applications. *J. Mar. Drugs*, **9**: 319-333.

[3]. Christenson, L. and Sims, R. (2011). Production and harvesting of microalgae for wastewater treatment, biofuels, and bioproducts. *Biotechnol. Adv.*, **29**: 686-702.

[4]. Selvakumar, P. and Umadevi K. (2014). Mass cultivation of marine micro alga *Nannochloropsis gaditana* KF410818 isolated from Visakhapatnam offshore and fatty acid profile analysis for biodiesel production. *J. Algal Biomass Utli.,* **5**: 28-37.

[5]. López -Alonso, D., Belarbi, E. H., Fernández-Sevilla, J. M., Rodríguez-Ruiz, J. and Molina, G. E. (2000). Acyl lipid composition variation related to culture age and nitrogen concentration in continuous culture of the microalga *Phaeodactylum tricornutum*. *Phytochem.*, 54: 461-471.

[6]. Stanier, R. Y. and Cohen-Bazire, G. (1977). Phototrophic Prokaryotes: The Cyanobacteria. In: Annual Review of Microbiology. (Eds.), M. P. Starr, J. L. Ingraham, and A. Balows Palo Alto, CA: Annual Reviews Inc. p. 225-274.

[7]. Rippka, R., Deruelles, J., Waterbury, J. B., Herdman, M. and stanier, R. Y. (1979). Generic assignment, strain histories and properties of pure cultures of Cyanobacteria. *J. Gen. Microbiol.*, **111**: 1-61.

[8]. Bligh E.G and Dyer, W. J. (1959). "A rapid method of total lipid extraction and purification". *Canad. J. Biochem. Physiol.*, **37**: 911-17.

[9]. Abomohra, A., Wagner, M., El-Sheekh, M. and Hanelt, D. (2013). Lipid and total fatty acid productivity in photoautotrophic fresh water microalgae: screening studies towards biodiesel production. *J. Appl. Phycol.*, **25**: 931-936.

[10]. Ramos, M. J., Fernández, C. M., Casas, A., Rodríguez, L. and Pérez, A. (2009). Influence of fatty acid composition of raw materials on biodiesel properties. *Bioresour. Technol.*, **100**: 261-268.

[11]. Li, Y., Horsman, M., Wu, N., Lan, C. Q. and Dubois-Calero, N. (2008). Biofuels from microalgae. *Biotechnol. Progress*, **24**: 815-820.

[12]. Damiani, M. C., Popovich, C. A., Constenla, D. and Leonardi, P. I. (2010). Lipid analysis in *Haematococcus pluvialis* to assess its potential use as biodiesel feedstock. *Bioresour. Technol.*, **101**: 3801-3807.

FIG. 1. A COENOBIUM OF *DESMODESMUS SUBSPICATUS*

TABLE 1. FATTY ACID COMPOSITION OF *D. SUBSPICATUS* KT151950 UNDER OPTIMIZED CONDITIONS

Optimized Condition	No. of fatty acid	SFA (% of TLC)	MUFA (% of TLC)	PUFA (% of TLC)	% of fatty acids with C16-C18	Fatty acids with $\geq$ =4 C=C bond s (% of TLC)
Control	9	38.9±1.9	22.6±1.1	38.5±1.9	63±3.1	0
4 mM NO$_3$	9	47±2.3	23±1.5	23±1.1	67±3.3	1±0.09
pH 6.4	9	50±2.3	21±1	29±1.3	67±3.3	1±0.09
Continuous light	9	57±2.3	20±1.4	23±1.3	72±3.4	1±0.09

SFA= saturated fatty acid, MUFA= monounsaturated fatty acids PUFA= Polyunsaturated fatty, TLC=total lipid content

SEEC-2017-112

NOVEL METHOD OF UTILIZATION OF DISTILLER'S INDUSTRY WASTE – IT'S MODIFICATION FOR HUMAN CONSUMPTION

Puja Mukherjee
Dept. of Food Technology & Biochemal
Engineering,
Jadavpur University
Pmpujamukherjee068@gmail.com

Debabrata Bera
Dept. of Food Technology & Biochemal
Engineering, Jadavpur University
beradebabrata@yahoo.co.in

Lakshmishri Roy
Dept. of food technology,
Techno India, Salt Lake
Lakshmi1371@gmail.com

ABSTRACT

In the recent years there has been a rapid growth of the ethanol production. After production of ethanol from rice or whole grain, Distilleries Dried Grain Soluble, Condensed Distillers Syrup and Carbon dioxide are produced. During alcohol fermentation process starch is converted to alcohol and other fermented products, whereas nutrients remains in Distillers dried grains making it an important nutritional source. Generally DDGS are sold as animal feed. In this present study an attempt has been made to evaluate and modify the rice DDGS for novel human application. Using few laboratory methods for nutritional analysis and determined few physical properties including moisture content, water activity, bulk density, angle of repose. Nutritional analysis of present DDGS samples includes; high protein approx. 40%, moderate amount fibre and low fat (<6%). Moisture content is approx. 10%. And the samples are free flowing and non-cohesive. Also the product is free from Naturally Occurring Toxins.

*Keywords***:** DDGS, Novel, Waste, Utilization

INTRODUCTION

In the recent years there has been a rapid growth of the many ethanol manufacturing plants. In the USA, bioethanol production increased from about 6.5 billion litres in 1999 to over 52 billion litres in 2011. A major process for making ethanol from grain is the dry grind method, since the capital cost of building a dry-grind plant is comparatively lower than a wet-milling plant. The ethanol industry is rapidly producing their co-products based on a mixture of several grains used during the fermentation process. Ethanol industry is flourishing economically and is producing phenomenal waste materials, i.e. 100 kg grains produces 32 kg distiller dried grains with soluble (DDGS) and Condensed Distillers Syrup (CDS) and 32 kg Carbon dioxide and 40 litre ethanol. DDGS are mainly obtained from corn, followed by wheat. DDGS also come from other grains like barley, sorghum and rice as well as grain blends "[7]". During alcohol fermentation process starch is converted to alcohol and other fermented products, whereas nutrients remain in the distiller's dried grains making it an important nutritional source. Generally DDGS is used for animal and poultry feed. To overcome environmental issues and the food security and the food crisis issues, it is important to utilization of waste materials (DDGS).

Hence authentic mode of utilization of DDGS is essential. i.e. for human consumption. The objectives of this study are evaluation of rice DDGS for human consumption, modification of rice DDGS for human consumption and application of modified DDGS. This particular study is focussing only the part of evaluation of DDGS.

MATERIAL AND METHODS

Material

The samples of rice DDGS in this study were collected from IFB. The samples were stored at room temperature in

seal plastic packets. All physical properties were done at room temperature.
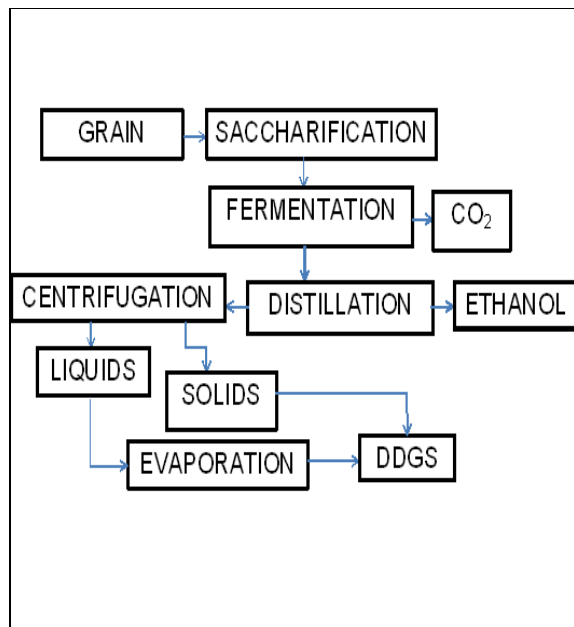
FIGURE 1. FLOW DIAGRAM OF PRODUCTION OF ETHANOL AND IT'S BY PRODUCTS

Experimental Procedures

Physical Analysis

Colour and odour of the sample have been identified by viewing and smelling it respectively.

Flowability Properties

Particle Size Distribution it plays a significant role in flowability property. And it also affect the volume and acceptability of baked products incorporated with DDGS. Particle size distribution was measured with a series of eight test sieves (Nos. 8, 18, 30, 44, 60, 100, 200, and 270) and a pan, fitted into a sieve shaker. Basically 100 g of DDGS sample, without any additional processing, was sieved with shaking for 10 minutes "[4]".

Angle of Repose it is defined as the angle between the horizontal where a sample to flow onto a flat surface and the slope of a heap of granular material dropped from some designated elevation "[3]". It is very common method to assess the flow properties of the sample. Lower angle of repose indicate free flowing where as higher angle of repose indicate poor flowing. Carr as mentioned by Riley et al. (1978), classified powders according to their flowability using the angle of repose "[6]". Measurement of Static Angle of Repose: In this study glass conical funnel was used to assess the angle of repose, fixed on a metal stand. Then 200g sample was poured into the funnel.

Then open the pre closed funnel outlet and the powder material flowed out to form a cone on the base.

TABLE 1. CARR CLASSIFICATION OF POWDER FLOWABILITY BASED ON ANGLE OF REPOSE "[6]"

Description	Angle of Repose
Very free flowing	25 – 30°
Free flowing	30 - 38°
Fair to passable flow	38 – 45°
Cohesive	45 - 55°
Very cohesive	>55°

Density Measurement bulk density is important for powder materials for transport and storage purpose. Bulk density is the mass of particles that occupies a unit volume of a container or measuring cylinder. Bulk density of the powder is decreased when the particle size of the powder is increased "[3]". Tapped density was measured by tapping the measuring cylinder in hand until a maximum packing condition was achieved. The level of powder in the measuring cylinder was checked after every 10 taps till there was no further reduction in level. This is called tapped volume which is used for calculating the tapped density "[1]". Hausner Ratio is the ratio between tapped & bulk density. It is used as internal friction index in cohesive powders.

Proximate Analysis

Sample was analysed for contents of moisture, ash, total solid, and water absorbance capacity. The pH was measured with a laboratory pH meter. The moisture and ash analysis were done according to the AOAC methods. Moisture content was done by hot air oven at 105°C "[9]". Ash content was done by muffle furnace at 600°C "[9]".

Biochemical Analysis

Sample was analysed for contents of protein, fat and fibre. The following analyses were done according to the AOAC methods. Carbohydrate content was done with the help of anthrone, the estimation of nitrogen done by Kjeldhal method. Fat content was determined by soxhlet extraction method [920.39 (AOAC 2003)] "[8]". Crude fibre content was also determined by AOAC method with the help of H_2SO_4 solution and NaOH solution (0.313 ± 0.0005 N). "[8]".

2

Analysis for Presence of Naturally Occurring Toxins

Presence of natural toxins in food can causes harmful effect in body. This toxicity test was performed in efrac (Edward Food Research & Analysis Centre Limited) laboratory (Research and Analysis Centre).

RESULTS AND DISCUSSIONS

The DDGS sample was analysed for physical, proximate and biochemical composition. And also analysed the presence of naturally occurring toxins.

Physical Analysis

The colour of the sample DDGS is golden yellow and odour of the sample is sweet, fermented and smoky smell. The pH of the sample was 3.94.

Flowability Related Properties in this study the largest proportion of rice DDGS was retained on No. 18 and 60 mesh. The result is quite similar with previous research (2008) where the largest proportion of corn DDGS was retained on No.60 mesh but passed through No. 35 mesh. Study reported that particle size of wheat flour is < 350 microns and greater than 250 microns. Hence if we modify the particle size then we can get DDGS flour like wheat flour and we can use this flour in bakery industry and others fields also.
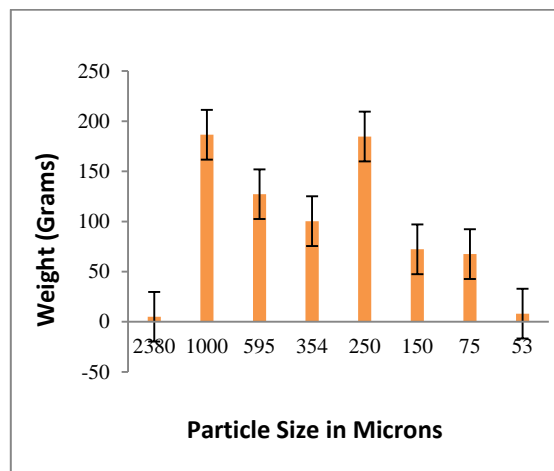
FIGURE 2. PARTICLE SIZE DISTRIBUTON OF RICE DDGS

The standard value of angle of repose for free flowing is 30° - 38°. The angle of repose value for the rice DDGS is 31.61°. It indicates that the DDGS have free flowing property. The bulk density of the rice DDGS is 0.68gm/cc & tapped density is 0.79gm/cc. A study indicated that the angle of repose of corn DDGS ranges from 41° to 46° and bulk density was 0.507g/cm3 to 0.601g/cm3 "[3]". The

standard value of carr indices for free flowing is < 25%. The value of carr indices of rice DDGS is 13.92%. The standard HR ratio of non-cohesive material is <1.4.The HR ratio of the rice DDGS is 1.16. So its indicate the sample is non-cohesive.

Proximate Analysis

The moisture content of rice DDGS was 9.39%. Moisture is important because it influences microbial growth and thus affects shelf life during storage. The ash content of rice DDGS was 5.53%. the pH of the sample is 3.94. The soluble solid present in rice DDGS was 20%. And water absorption capacity was 290 ml.

Biochemical Analysis

The fat and crude fibre of the rice DDGS on average was 5.3% & 5.65 % respectively. The carbohydrate content of the sample was 9.17%. The protein content of the DDGS was approximately 40%.

The results of physical and chemical property are shown in table 2.

TABLE 2. PHYSICAL AND BIOCHEMICAL ANALYSIS OF DDGS SAMPLE

DDGS	Unit (%)
Moisture	9.39
Ash	5.53
Carbohydrate	9.17
Crude protein	42
Crude fat	5.3
Crude fibre	5.65

The previous work (2008) showed that the protein, crude fat, and ash content of corn DDGS were 26.5% to 42.3%, 11.3% to 13.1%, and 2.1% to 4.9% respectively "[2]". In 2005 scientist were investigated that DDGS content ash 3.9%, crude protein 30%, crude fat 9.8%, crude fibre 5.34% "[5]".

Analysis for Presence of Naturally Occurring Toxins

The sample is free from NOTS. All the results showed less than the upper limit.
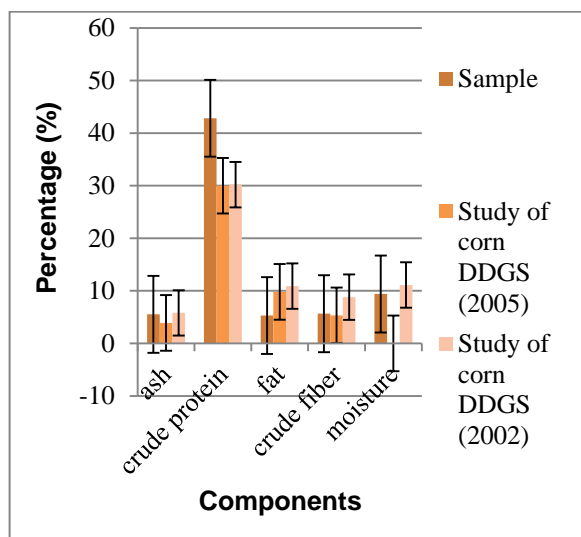
FIGURE 3. COMPARISON OF BIOCHEMICAL COMPOSITION OF RICE DDGS AND OTHER DDGS

TABLE 3. ANALYSIS FOR PRESENCE OF NATURALLY OCCURRING TOXINS

Test Parameter	Unit of Measurement	Results
Hydrocysnic Acid	mg/kg	<0.1
Agaric Acid	mg/kg	<5.0
Hypericine	mg/kg	<1.0
Safrole	mg/kg	<2.5

Instrument Used: UV-Visible Spectrophotometer, HPLC

CONCLUSION

The goal of this research work was to evaluation of rice DDGS for human consumption. The colour and smell of the rice DDGS sample is accepted. From particle size distribution and flowability properties of the sample it may be concluded that the rice DDGS is free flowing and non-cohesive. Shelf life of rice DDGS may be good because moisture content is low. DDGS rich in nutrients i.e. it specially has high amount of protein. It is free from toxins and hence safe for consumption. Thus it possesses immense scope for further utilization.

Thus for global utilization of DDGS, it's evaluation, modification and application in food industry since an enticing option.

ACKNOWLEDGEMENT

REFERENCES
REFERENCES

1. Abdullah, E. C., and Geldart, D., 1999, "The use of bulk density measurements as flowability indicators". Powder Technol, 102, pp. 151-165
2. Ganesan, V., Rosentrater, K. A., and Muthukumarappan, K., 2008. "Effect of Moisture Content & Soluble Level On The Physical, Chemical, And Flow Properties of Distillers Dried Grains With SolubleS (DDGS)". Cereal Chemistry, 85(4), pp. 464 – 470.
3. Ganesan, V., Rosentrater, K. A., and Muthukumarappan, K., 2008. "Flowability and Handling characteristics of bulk solids and powders – a review with implication for DDGS". Biosystems Engineering, pp. 425 – 435.
4. Liu, K., 2008. "Particle Size Distribution of Distillers Dried Grains With Solubles (DDGS) And Relationships to Compositional And Color Properties". Bioresource Technology, 99, pp. 8421 – 8428.
5. Lumpkins, B. S., Batal, A. B., 2005, "The bioavailability and phosphorus in distillers dried grains with solubles", Poultry Science, 84, pp. 581 – 586.
6. Riley, G. S., Mann, S. and Jesse, R. O., 1978, "Angle of repose of cohesive powders", J.Powder & Bulk Sol. Technol. 2 (4), pp. 15-18.
7. Tres, A., Heenan, S. P., and Ruth, S., 2014. "Authentication of Dried Distilled Grain With Solubles (DDGS) by Fatty Acid And Volatile Profiling". Lebenson Wiss Technol, 59(1), pp. 215 – 221.
8. AOAC International (AOAC). 2003. Official Methods of Analysis of the Association of Analytical Chemists, 17th edn., The Association, Gaithhersburg.
9. AOAC International: Arlington, VA, 2002. AOAC (Association of Official Analysis Chemists). AOAC Official Methods of Analysis.

SEEC-2017-113

THERMO-CHEMICAL CONVERSION OF *SESAME STALK*: CANDIDACY FOR ALTERNATE RENEWABLE FUEL

Samar Gogoi, Ruprekha Saikia, Neonjyoti Bordoloi, Lina Gogoi, Rumi Narzari, Debashis Sut, Rupam Kataki
Deptt of Energy, Tezpur University
Tezpur, India

Moonmoon Hiloidhari
JNU, New Delhi
India

ABSTRACT

The necessity to move towards a feasible sustainable and economical alternative renewable source of energy is increasing day by day due to deminuting availability of the conventional fossil based resources, regular hike in prices of fossil based fuels and increased emissions of anthropogenic greenhouse gases to the atmosphere [1]. In this regard, Sesame stalk an agro-processing waste was investigated in this study for its suitability as a prospective bioenergy feedstock for thermo-chemical conversion. Present study aims at utilization of this agro-processing waste through the process of pyrolysis at different temperatures (350ºC-650ºC), at heating rate 40ºCmin-1 to study the product distribution and their characterization and to identify the optimum condition for bio-oil yield.

SEEC-2017-114

VALORIZATION OF PINEAPPLE POST HARVEST AND FRUIT PROCESSING WASTES BY EXTRACTION OF HIGH VALUE BROMELAIN AND USE OF RESIDUES FOR ETHANOL PRODUCTION

Anil Kuruvilla Mathew[1*], Meera Christopher[1], Emrin George[1], Amith Abraham[1], Raveendran Sindhu[1], Ashok Pandey[2] and Rajeev K Sukumaran[1]

[1]*Centre for Biofuels, National Institute for Interdisciplinary Science and Technology, CSIR, Trivandrum - 695 019, India*
[2] *Center of Innovative and Applied Bioprocessing, Mohali 160 071, Punjab, India*
* Tel: +91 471 2515426, fax: 0471 2491712. Email: rajeevs@niist.res.in

ABSTRACT

Translation of lignocellulosic bioethanol technologies from lab to commercial scale production has taken longer than expected and continuous to be a major challenge. Economics is the major obstacle towards commercialization of lignocellulosic bioethanol process. Process economics could be improved by extracting high value compound along with bioethanol production. Bromelain, a high value compound as well as monomeric sugars for the production of bioethanol can be extracted from pineapple (Ananas comosus) waste generated during harvest and processing. In the present study, bromelain was extracted from pineapple waste and the specific activity of bromelain present in the pineapple fruit processing waste (PFPW) was estimated to be 336 GDU/mg protein. After extracting the bromelain from PFPW, more than 95% of the solids remained as residue. The residue was further processed for sugar extraction through pretreatment and enzymatic hydrolysis. A maximum sugar yield of 415 mg glucose/g biomass was obtained. Fermentation of hydrolysate obtained was carried out for 48 h and an ethanol yield of 78% was achieved.

Keywords

bromelain, bioethanol, pretreatment, enzymatic hydrolysis,

NOMENCLATURE

PPHR   Pineapple post harvest residue

PFPW   Pineapple fruit processing waste

GDU   Gelatin digestion unit

INTRODUCTION

Biofuels produced from bio-based materials are good alternative to conventional fossil based fuels. Pineapple (*Ananas comosus*) is one of the commercially important fruit crops in India. India is the sixth largest producer of pineapple in the world with an annual output of about 1.7 million tons. In India, the pineapple cultivation has increased from 57 thousand ha in 1991-92 to 91 thousand ha in 2011-12 whereas its production doubled from 0.8 million tons to 1.6 million tons during this period. According to the estimates, waste leaf generation from pineapple cultivation in Kerala is 193 kilo tones and approximately 157 kilo tons of pineapple process waste including peel, crown etc are generated annually (Doraiswami and Chellamani, 1993). Together, the state generates approximately 350 thousand tons of pineapple waste including waste leaf and fruit processing wastes, which are currently not used for any commercial applications. Fruit residues may cause serious environmental problems since it accumulates in agro-industrial yards and rots attracting insect and pests.

In addition, the cost of production of pineapple has increased tremendously to about Rs. 14-15 per kg due to the increase in fertilizer, pesticide and labor cost as compared to Rs 10-11 per kg few years before. Prices of first-grade pineapple fruit have dropped to Rs 10-13 per kg at the farm-gate, compared to Rs 20 per kg levels in mid-2014. To improve the current economics of pineapple cultivation and to manage the disposal issues, value addition to the waste streams is a potential option, and if the entire waste can be utilized, that serves the dual purpose of disposal along with revenue generation, which are much needed boost to this industry. Bromelain - a cysteine protease is naturally present in the stem and fruits of pineapple, has been extracted and exploited commercially in various applications including food, meat tenderization, cosmetic, pharmaceutical and textile industries (Arshad et al., 2014). The residue left after bromelain extraction, has significant amount of carbohydrates and thus an ideal source for bioethanol production.

The present study focuses on the valorization of waste generated from harvesting and processing of pineapple by extracting bromelain from it and recovery of the residue for producing sugars that can be converted through fermentation to fuel grade ethanol.

MATERIALS AND METHODS

Feed stock

Pineapple post-harvest residues (PPHR: mainly leaves) were collected from Vazakulam, Kerala, India was used in the present study. Pineapple fruit processing waste (PFPW: mainly crown) was collected from PIO food products, Vazakulam, Kerala.

Protein extraction

Pineapple waste was chopped, blended with 0.01M sodium phosphate buffer at 1:1 ratio. The solid-liquid mixture was separated and a clear extract was obtained by centrifugation. The extract was further concentrated using ice cold acetone.

Pretreatment and enzymatic hydrolysis of residue

Residue left after protein extraction was sun dried and milled to particle size < 3mm. The residue was pretreated using 2% (w/w) NaOH, 10% (w/w) biomass loading for a pretreatment time of 20 min at 120ºC. After pretreatment the solid fraction was collected and was further processed for enzymatic hydrolysis. It was carried out at 10% (w/w) using commercial cellulase at an enzyme loading 20 FPU/g biomass.

Fermentation of the hydrolysate

Fermentation of the hydrolysate were carried out screw cap glass vials and yeast strains (RPP-03N) was used at a concentration of 4% wet (w/v) (7×10^7 cells/ml), at a temperature of 30ºC. Fermentation was carried out for a period of 48h.

Analysis

Protein content in extract was determined using Bradford method using BSA as standard. The proteolytic activity of bromelain was determined using gelatin digestion unit (GDU) assay. Compositional analysis of native and pretreated samples was carried out according to Sluiter et al., 2008. The sugar and ethanol concentration was measured by HPLC using Rezex RPM and ROA columns using RID and PDA detector, respectively.

RESULTS AND DISCUSSION

Extraction of bromelain from pineapple waste

Bromelain was extracted from the PPHR and PFPW. The total protein content and specific activity of bromelain is presented in Table 1. Extracts obtained from pineapple processing wastes had a higher protein content and bromelain activity when compared with post-harvest residues.

Table 1: Protein content and proteolytic activity of extracts

Pineapple Parts studied	Volume of crude extract (ml)	Protein (mg/ml)	Total protein (mg)	Specific activity (GDU/mg)
PFPW	110	0.73	80.3	336
PPHR	150	0.36	54.0	158

Pretreatment and enzymatic hydrolysis of residue

Alkaline pretreatment of the residue was carried out after extracting bromelain from the pineapple waste. Difference in composition is shown Figure 1 and the structural changes shown in Figure 2. In both cases, lignin has significantly reduced after alkaline pretreatment and a corresponding increase in cellulose and hemicelluloses was observed. A maximum sugar yield of approximately 415 and 370 mg glucose/ g was obtained from the PPHR and PFPW subjected to enzymatic hydrolysis, respectively. This corresponds to a maximum cellulose conversion efficiency of 64% when the pretreated material was subjected for enzymatic hydrolysis using commercial cellulase.
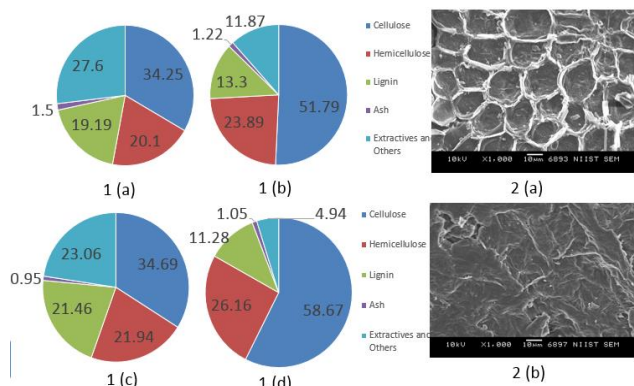
Figure 1: Compositional changes before and after pretreatment of crown (Fig 1a and 1b) and leaves (Fig 1c and 1d)
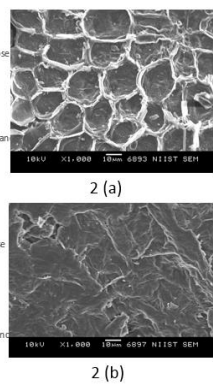

Figure 2: SEM of pineapple crown before 2 (a) and after 2 (b) pretreatment of pineapple crown

Ethanol fermentation

The hydrolysate obtained after enzymatic hydrolysis was tested for ethanol production without any further unit operations such as detoxification. Glucose was completely utilized by 48h and an ethanol yield of 78% was achieved.
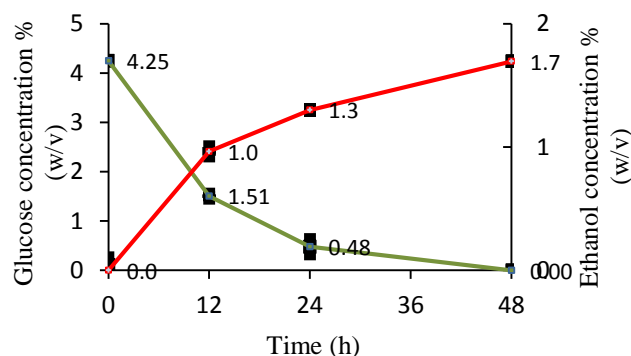

Figure 3: Fermentation of hydrolysate into ethanol

CONCLUSION

From the present study it can be concluded that the PPHR and PFPW could be used as a potential source for bromelain. Fermentable sugars such as glucose can be extracted from the leftover residue after bromelain extraction, which can further used for the production of ethanol or value added compounds (e.g. organic acids). Valorization concept proposed in the present study enables the extraction of bromelain and ethanol from the pineapple waste generated. If successfully integrated into the processing industries, this approach can generate additional income and to help the disposal problem of the waste generated from industries.

References

[1] Arshad, Z.I., Amid, A., Yusof, F., Jaswir, I., Ahmad, K., Loke, S.P., 2014. Bromelain: an overview of industrial application and purification stratergies. Appl. Biochem. Biotechnol. 98: 7283-7297.
[2] Doraiswamy, I. and Chellamani, P. 1993. Pineapple leaf fibre. The Textile Institute, Manchester, UK, 24, 1-37.
[3] Sluiter A., B. Hames, R. Ruiz R, C Scarlata, J Sluiter, D. Templeton, and D. Crocker (2008) NREL Technical Report, NREL/TP-510-42618.

SEEC – 2017 – 115

IN-SILICO CHARACTERIZATION OF NOVEL BETA-GLUCOSIDASE ISOFORMS FROM *ASPERGILLUS UNGUIS* FOR IDENTIFYING POTENTIAL ENZYMES FOR BIOMASS HYDROLYSIS

Amith Abraham
Centre for Biofuels, Microbial Processes and Technology Division
CSIR-National Institute for Interdisciplinary Science and Technology, Thiruvananthapuram 695019, Kerala, India.

Prajeesh KV
Centre for Biofuels, Microbial Processes and Technology Division
CSIR-National Institute for Interdisciplinary Science and Technology, Thiruvananthapuram 695019, Kerala, India.
Academy of Scientific and Innovative Research (AcSIR), CSIR-NIIST Campus, Thiruvananthapuram

Athira Raj SR
Centre for Biofuels, Microbial Processes and Technology Division
CSIR-National Institute for Interdisciplinary Science and Technology, Thiruvananthapuram 695019, Kerala, India
[2]Academy of Scientific and Innovative Research (AcSIR), CSIR-NIIST Campus, Thiruvananthapuram

Raveendran Sindhu
Centre for Biofuels, Microbial Processes and Technology Division
CSIR-National Institute for Interdisciplinary Science and Technology, Thiruvananthapuram 695019, Kerala, India

Anil Kuruvilla Mathew
Centre for Biofuels, Microbial Processes and Technology Division
CSIR-National Institute for Interdisciplinary Science and Technology, Thiruvananthapuram 695019, Kerala, India

Rajeev K Sukumaran
Centre for Biofuels, Microbial Processes and Technology Division
CSIR-National Institute for Interdisciplinary Science and Technology, Thiruvananthapuram 695019, Kerala, India.
Academy of Scientific and Innovative Research (AcSIR), CSIR-NIIST Campus, Thiruvananthapuram
Email: rajeevs@niist.res.in

ABSTRACT

The whole genome sequencing of a novel Aspergillus unguis strain NII 08123 isolated at CSIR-NIIST and found to produce glucose tolerant beta glucosidase was performed by Next Generation Sequencing (Illumina platform). Genomic data mining was carried out which revealed a total of seventeen β-glucosidase (BGL) genes in the filamentous fungus. Three of them belonged to glycoside hydrolase family 1 (GH1) while the rest (14) belonged to family 3 of glycosyl hydrolases (GH3). The cluster analysis of β-glucosidase (GH3) protein sequences showed two major clusters and revealed the evolutionary closeness among sequences. Secretary nature of these proteins were analysed and six of them showed extracellular nature. The properties of these secretary β- glucosidases were predicted using various bioinformatics tools showing the various physicochemical properties and secondary structure elemental pattern. This study showed that the genome of Aspergillus unguis contains various isoforms of β- glucosidase with diverse properties for different applications. This also opens the way for cloning of the glucose tolerant BGL from this fungus for biofuel applications and also in elucidating the mechanisms for glucose tolerance in the enzyme.

Keywords

β-glucosidase, *Aspergillus unguis*, cellulase, biofuel biomass hydrolysis, glycoside hydrolase

NOMENCLATURE

BGL	β-glucosidase
A. unguis	*Aspergillus unguis*
UPGMA	Unweighted Pair Group Method with Arithmetic Mean
BLASTP	Basic Local Alignment Search Tool Protein
CFSSP	Chou & Fasman Secondary Structure Prediction

INTRODUCTION

The utilization of cellulosic biomass to produce fuels and chemicals presents significant technical and economic challenges, and its success depends largely on the development of highly efficient and cost-effective biocatalysts for conversion of pretreated biomass to fermentable sugars. Therefore, interest in β--glucosidases has been revitalized in last few years as it has an important role in cellulose saccharification reaction. β-glucosidases (β-D-glucoside glucanohydrolase) are grouped in EC 3.2.1.21, as enzymes that hydrolyze O- and S-glycosyl compounds or catalyzing the hydrolysis of terminal, non-reducing β-D-glucosyl residues. In other words, it is capable of producing simple sugars from disaccharides and oligosaccharides. It is also one of three key enzymes in the cellulose system [1]. This integral part of cellulase enzyme system works synergistically with endoglucanase and cellobiohydrolase to achieve superior cellulose hydrolysis [2]. β-glucosidase is involved in the terminal step of cellulose saccharification by degrading cellobiose into glucose and releasing the former two enzymes from cellobiose inhibition [3].

A few of the fungal strains are known to be efficient producers of β-glucosidase [2]. Fungal β-glucosidases are primarily placed in the family 3 of glycosyl hydrolases with the active site signature pattern defined below, where the aspartate (D) is the active site residue involved in catalysis.

[LIVM](2)-[KR]-x-[EQKRD]-x(4)-G-[LIVMFTC]-[LIVT]-[LIVMF]-[ST]-**D**-x(2)-[SGADNIT]

The multiplicity of β-glucosidase is common among fungi. The production of multiple β-glucosidases, four by *Aspergillus tubingensis*, seven by *Trichoderma reesei* and six by thermophilic fungus, *Humicola grisea*, has been reported [4, 5,6].
This paper reports the characterization of novel isoforms of β-glucosidases from the genome of *A. unguis*. These β-glucosidases were characterized on the basis of their sequence similarities and physico-chemical parameters.

MATERIALS AND METHODS

Genomic data mining

The identification of *A. unguis* β-glucosidases were carried out by genomic data mining of *A. unguis* genome. Sequence obtained was then aligned using BLASTP to ensure the sequence identities.

Conserved motif and family identification

Motifs were identified in sequences using the expectation maximization approach implemented in Multiple EM for Motif Elicitation (MEME) server. Motif families were identified by sequence searching in Pfam database. Subsequently, the glycoside hydrolase family were predicted and the proteins of GH3 families were selected for further study.

Cluster analysis

The UPGMA approach implemented in the MEGA program was employed for constructing phylogenetic relationships among sequences. Evolutionary distances were computed using the Maximum Composite Likelihood method and are in the units of the number of base substitutions per site. All positions containing gaps and missing data were eliminated from the dataset. The resulted tree was analyzed by bootstrap test using 1000 replicates. They were then grouped into clades if the bootstrap values are over 50%.

Properties of *A. unguis* β-glucosidases

Sub cellular localization and signal peptides cleavage sites of β-glucosidase were analysed using TargetP and SignalP. Physicochemical properties like Molecular weight, Theoretical pI, Aliphatic Index and Grand Average of Hydropathicity (GRAVY) of proteins were calculated using ExpasyProtPARAM server. Secondary structure of protein sequence was predicted using CFSSP server.

RESULTS AND DISCUSSION

Motifs were predicted using Multiple EM for Motif Elicitation server and motif family were identified among selected β-glucosidases from *A. unguis* genome. Out of 17 β-glucosidases, 14 showed similarity to GH3 family and others showed similarity to GH1 family. Cluster analysis of GH3 family β-glucosidases from *A. unguis* showed two major clusters as shown in Figure 1. Cluster A consisted of eight sequence which was further divided into two sub-clusters. Custer B contains six sequences. The evolutionary closeness among sequences was clear from cluster data.
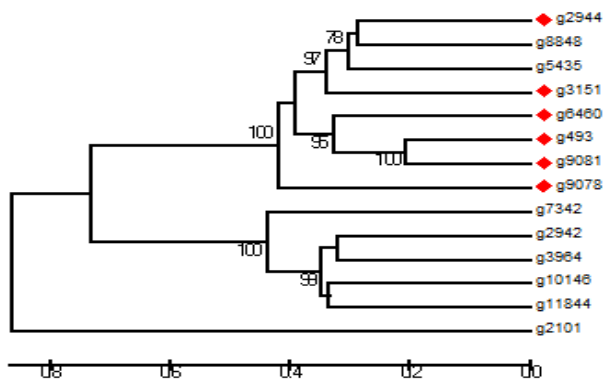
FIGURE.1. Phylogenetic tree of β-glucosidases proteins from *A. unguis* using UPGMA method

Sub cellular location of proteases was identified by TargetP and it has been found that out of 14, six proteins showed extracellular nature (protein Id No. g493, g2944, g3151, g6460, g9078, g9081) and are present in secretary pathways (Table 1). In phylogenetic tree all these secretary proteins were clustered together with high bootstrap support.

Protein Id. No.	Extracellular nature of protein	Signal peptide cleavage site position in protein
g493	Secretary	17,18 AFS-VP
g2101	-	-
g2942	-	-
g2944	Secretary	19,20 SLA-LP
g3151	Secretary	19,20, ASA-QD
g3964	-	-
g5435	-	-
g6460	Secretary	23,24 VRA-QE
g7342	-	-
g8848	-	-
g9078	Secretary	17,18 ALA-AN
g9081	Secretary	17,18 SGA-QD
g10146	-	-
g11844	-	-

TABLE.1. Evaluation of extracellular nature and signal peptide cleavage site of the β-glucosidases proteins from *A. unguis*

Present study focuses on comparison of amino acid sequences of different isoforms of secretary GH3 β-glucosidases. Number of amino acids in a protein gives rough idea about the complication of the tertiary structure it achieves. It is well known that more the amino acids number of protein, more beta turns and coiled-coiled conformation it achieves during protein folding. The number of amino acids was found in range of 768 to 1244. Present investigation shows molecular weight within a range of 82 KDa to 135 KDa (Table 2). Determination of the molecular weight of protein gives a clear view about the method one should adopt for the purification of the protein.

The values of iso-electric point (pI) of the β-glucosidases from *A. unguis* were in the range 4.89 to 5.47 indicating that all are acidic in nature (Table 2). These predictions will be helpful in developing buffer system when these enzymes are to be purified in solution by isoelectric focusing method

Protein Id. No	No. of amino acids (aa)	Molecular Weight (Kd)	pI
g493	773	84.7	5.43
g2944	1244	135.18	5.47
g3151	850	92.09	4.94
g6460	823	89.57	4.89
g9078	801	84.87	4.92
g9081	768	82.81	5.11

TABLE.2. Physico-chemical properties (MW and pI) of the β-glucosidases proteins from *A. unguis*

The aliphatic index (AI), defined as the relative volume of a protein occupied by aliphatic side chains, is regarded as a positive factor for the increase of thermal stability of globular proteins. Lower aliphatic index determine the fact that particular protein would not be involved in electrophilic substitution reaction, which is characteristic of aromatic reactions. More aliphatic index corresponds to increased stablilty of the protein. Aliphatic index for the β-glucosidases from *A. unguis* ranged from 72.36 – 82.46 (Table 3). The very high aliphatic index of these sequences indicated that the *A. unguis* β-glucosidases will be stable over a wide temperature range

GRAVY index of the protein predicts the hydrophobic character of the protein. The Grand Average hydropathy (GRAVY) value for a peptide or protease is calculated as the sum of hydropathy values of all the amino acids, divided by the total number of residues present in the β-glucosidases sequence. GRAVY indices for the sequences ranged from -0.346 to -0.190(Table 3). This low range of value indicated better interaction with water.

Protein Id. No	Aliphatic Index	Grand average of hydropathicity (GRAVY)
g493	78.31	-0.190
g2944	72.85	-0.463
g3151	75.08	-0.344
g6460	74.31	-0.346
g9078	72.36	-0.256

g9081	82.46	-0.228

TABLE.3. Physico-chemical properties (Alipatic Index, GRAVY) of the β-glucosidases proteins from *A. unguis*

Secondary structural features were predicted by CFSSP (Table. 4). The results revealed that random coils dominated among secondary structure elements. The conformational entropy associated with random coils significantly contributes to stabilization and protein folding.

Protein Id. No	Alpha Helix	Beta Sheets	Turns	Coil
g493	22.90	28.20	11.25	37.65
g2944	28.78	18.25	7.80	45.18
g3151	28.59	18.59	8.47	44.35
g6460	25.64	21.26	9.23	43.86
g9078	26.84	24.47	9.61	39.08
g9081	26.43	22.66	10.81	40.10

TABLE.4. Predicted secondary structure elements of the β-glucosidase proteins from *A. unguis*

CONCLUSION

In the present study, we have characterized amino acid sequences of β-glucosidases (GH3) isoforms from *A. unguis* genome. 14 β-glucosidases (GH3) sequences were used or cluster analysis. Six secretary sequences have been analyzed to acquire an understanding about their functional properties, physico-chemical properties and protein secondary structure levels using *in silico* techniques. Primary structure analyses revealed that the β-glucosidases (GH3) were hydrophilic and are expected to be stable over wide range of temperature. Secondary structure analysis established that in most of the sequences, random coils were the dominating secondary structure elements followed by alpha helix, and beta turns. This study will provide understanding about the physicochemical properties and function of β-glucosidases (GH3) in *A. unguis* which will further aid in formulating their uses in academics and industries.

ACKNOWLEDGMENTS

REFERENCES

[1] Sukumaran, R.K., Abraham, A., and Mathew, A., 2017. Enzymes for Bioenergy. In: Abdulhameeed A, Sugathan S, Pradeep NS (eds) Bio-resources and Bioprocess in Biotechnology.V1., Springer, Singapore. In Press.

[2] Lynd, L. R., Weimer, P. J., van Zyl, W.H., and Pretorius, I.S., 2002. Microbial cellulose utilization: fundamentals and biotechnology. Microbiology and Molecular Biology Reviews. 66(3), pp.506-577

[3] Enari, T.M. and Niku-Paavola, M.L.,1987. Enzymatic hydrolysis of cellulose: Is the current theory of the mechanism of hydrolysis valid?. *Critical Reviews in Biotechnology*, 5, pp. 67-87

[4] Decker, C.H., Visser, J., and Schreier, P., 2001. β-glucosidase multiplicity from *Aspergillus tubingensis* CBS 643.92: purification and characterization of four β-glucosidases and their differentiation with respect to substrate specificity, glucose inhibition and acid tolerance. Applied Microbiology and Biotechnology, 55(2),pp.157-163

[5] Foreman, P.K., Brown, D., Dankmeyer, L., Dean, R., Diener, S., Dunn Coleman, N.S., Goedegebuur, F., Houfek, T.D., England, G.J., Kelley, A.S., Meerman, H.J., Mitchell, T., Mitchinson, C., Olivares, H.A., Teunissen, P.J., Yao, J., and Ward, M.,2003. Transcriptional regulation of biomass-degrading enzymes in the filamentous fungus *Trichoderma reesei* J. Biol. Chem., 278 , pp. 31988–31997

[6] Takashima, A., Nakamura, M., Hidaka, H., Masaki, T., and Uozumi., 1999. Molecular cloning and expression of the novel fungal β-glucosidase genes from *Humicola grisea* and *Trichoderma reesei.* J. Biochem., 125, pp. 728–736

SEEC-2017-117

Scale up of hydrogen production in 150 liter pilot scale through dark fermentation route by a purified anaerobe

Sanjukta Subudhi, N Ram Kumar, Tanmaya Nayak, PD Anupama, Banwari Lal
Environmental and Industrial Biotechnology Division, The Energy and Resources Institute, Habitat Place, Darbari Seth Block, Lodhi Road, New Delhi, India;

ABSTRACT

Present study explored on scale up of hydrogen production process through dark fermentation route in 100 liter pilot scale from sugar industry waste (molasses) by employing a purified anaerobe, Clostridium butyricum-TM9A. This anaerobe was selected based on its hydrogen yield efficiency (3.1 mol of H2 per mole of glucose). Further this anaerobe has significant potential to utilize a range of pentose and hexose sugars including di-, tri and poly-saccharides like; xylose, ribose, glucose, rhamnose, galactose, fructose, mannose, sucrose, arabinose, raffinose, cellulose, cellobiose and starch. Considering these properties, TM9A strain was employed for hydrogen production form molasses (containing around 50% of sucrose) and process parameters were optimized. 45 mmol/L of hydrogen production was obtained at laboratory scale at 37 oC temperature, pH 8, 2.5% substrate concentration (molasses) C/N ratio of 8. This strain followed mixed acid fermentation pathway and produced acetic acid and butyric acid as major soluble metabolites. This process was then scaled up in 10 liter scale and then in 150 liter pilot scale bioreactor (100 liter working volume) in batch mode. Scale up of this process enhanced hydrogen production to 65 mmoL/L and 96mmol/L in 10 L scale and in 150 L scale, respectively. Biogas was composed of H2 (55-60%) and CO2 (40-45%). Hydrogen yield efficiency was 10 mol H2 per Kg of COD reduced.

SEEC-2017-118

Reduction of emission of a 110 cc 4-stroke IC engine using petrol-HHO hybrid Fuel

Sanjib Das, Diptanu Dey, Dr. Priyanath Das, Dr. Rahul Banerjee
NIT Agartala
India

ABSTRACT

The main objective of this work is to replace the conventional air-fuel mixture with a combination of air-petrol-HHO gas mixture as a fuel and study the emission of a 4-stroke, 110 cc IC engine. In this work, we were trying to use the full advantage of HHO gas by employing an internal mixing method in IC engine. First of all fuel-air mixture were injected into the combustion chamber then the produced HHO gas by electrolysis(KOH solution) in a chamber of copper electrode was fed into the same combustion chamber through a high pressure nozzle by giving a low spark ignition then these air-fuel-HHO gas mixed up and combusted fully and gives wide flame. We tested both the produced gas sample which were fed into the combustion chamber and the emitted gas sample which comes out from that IC engine. The sample HHO gas was tested through a nozzle which gives a high speed bluish flame and the emitted gas gives lesser amount of NOx, CO, and HC in amount of 9%, 4%, and 19% respectively, which is lesser in amount compared to emission of that IC engine while using only fuel-air mixture the emission was NOx of 11%, CO of 9% and HC of 31%. From these tests we can say that the HHO gas is an environment friendly gas which is very useful for the future generation because it has another good quality that, while mixing with the fuel its helps to reduce the amount of fuel consumption in the IC engine. This HHO gas can be use any type of combustion chamber for reducing the amount of fuel consumption and good performance. There is some improvement also needed for the electrodes which were used to produce HHO gas.

SEEC-2017-120

DRAFT:INVESTIGATION OF COMBUSTION INSIDE A RAMJET ENGINE

Mahboob Ahmed
Department of Mechanical Engg
B.Tech.
Email: maddymak9956@gmail.com

Sameer Hasan
Department of Mechanical Engg
B.Tech.
Email: sameerhad12@gmail.com

Mohd Danish Ansari
Department of Mechanical Engg
B.Tech.
Email: danish.ansari1995@gmail.com

Dr Mirza S. Faisal Baig
Department of Mechanical Engg
Professor
Email: drmfbaig@yahoo.co.uk

ABSTRACT

The present work focuses on the CFD analysis of a 2-dimensional lab scale model of a ramjet engine. ANSYS Fluent is used to perform the computations. The prime focus of this work is to investigate the non-premixed mixing of fuel(hydrogen H_2) and oxidizer(air) and the combustion phenomenon using steady laminar flamelet model(SLFM). The models associated with the detailed 9 species and 21 reversible chemical reaction mechanism to predict the combustion process inside the engine. The steady laminar flamelet model uses two additional equation for mixture fraction and variance to determine the reaction flow field. The results obtained are compared with the data of the experiment performed by M Torrez [1] and are in close agreement. The simulation is done for subsonic combustion, simulation for will also be performed for supersonic combustion.

Keywords:
Non-premixed combustion
Turbulence
Steady laminar flamelet model
Ramjet

NOMENCLATURE

u_i	velocity component
ρ	density
P	pressure
τ_i	stress tensor
h	enthalpy of the mixture
q	heat flux vector
k	turbulence kinetic enrgy
ε	kinetic energy dissipation rate
χ	scalar dissipation rate
Z	mixture fraction

INTRODUCTION

In this fast-moving world, the speed of transportation is achieving new heights. The use of ramjet and scramjet engine can push up the speed limits, and can become a reliable and fastest mode of transportation in near future.

1

Researchers are being done in this field all over the globe. Latest one is NASA's X-43 A which has attained a speed of 7200km/hr. Still there are a lot of problems to be solved regarding the ramjet and scramjet engines. One of these is that these engines need assisted take-off. They cannot move the aircraft from standstill. The second problem is of combustion of fuel inside the combustion chamber. As these engines moves at a very high speed, the combustion phenomenon becomes even more complex. High speed creating high turbulence makes it very difficult to simulate the combustion phenomenon. This work emphasizes on the analysis of 2D non-premixed combustion model using commercial CFD software ANSYS Fluent. The combustion model considers finite rate chemistry within the steady laminar flamelet model. To account for the turbulence/chemistry interaction the steady laminar flamelet model employs a presumed probability distribution function closure model. The steady laminar flamelet model includes the effect of strain rates, species and momentum diffusion with changing duct velocity and fuel jet velocity.

Experimental setup

A non-premixed experimental combustion was carried out on a lab scale model of a ramjet/scramjet engine in University of Michigan by M. Torrez [1]. The experimental setup is divided into three parts

(i) Mach 2.2 converging diverging nozzle.
(ii) Constant area isolator.
(iii) Combustor part which has 4degree divergence.
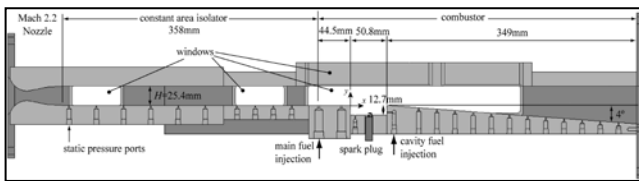
Figure 1 experimental setup

CFD Modeling

Flow modeling

ICEM CFD is used to make the geometry of the model shown in fig 1 to perform computations. Fluid flow is modeled by a steady state CFD simulation using pressure based solver. Reynolds Averaged Naviers-Stokes equation been solved for continuity and momentum using ANSYS Fluent. Density is calculated using compressible ideal gas law. For modeling turbulence, realizable k-ε model with standard wall functions is used.

EQUATIONS

Continuity
$$\frac{\partial \rho u_i}{\partial x_i} = 0 \ (1)$$

Momentum
$$\frac{\partial(\rho u u_i)}{\partial x_i} = -\frac{\partial(p)}{\partial x_i} + \frac{\partial(\tau_i)}{\partial x_i}(2)$$

Energy
$$\frac{\partial}{\partial x}[\rho u(h + 0.5u_i u_i)] = \frac{\partial}{\partial x}(u\tau_i) - \frac{\partial}{\partial x}q \ (3)$$

Turbulence kinetic energy
$$U\frac{\partial k}{\partial x} = \tau_i \frac{\partial U_i}{\partial x} - \varepsilon + \frac{\partial}{\partial x}[(\nu + \frac{\nu_T}{\sigma})\frac{\partial k}{\partial x}] \qquad (4)$$

Specific dissipation rate
$$U\frac{\partial \varepsilon}{\partial x} = \frac{C^1\varepsilon}{k\tau_i U \frac{\partial U_i}{\partial x}} - C^{2}\varepsilon^2 + \frac{\partial}{\partial x}[(\nu + \frac{\nu_T}{\sigma})\frac{\partial k}{\partial x}](5)$$

BOUNDARY CONDITIONS

Table 1 boundary conditions

	T_o	P_o	T	P	U
Air	1370K	333kPa	1280K	261kPa	458m/s
Fuel	298K	829kPa	248K	438kPa	1200m/s

COMPUTATIONAL GRID

The meshed region has excluded the nozzle part as shown in figure 2. The mesh is more densely clustered near the fuel injector to capture the physics of the fuel –air mixing accurately. The mesh is also denser near the leading and trailing edges of the stabilization cavity to capture their influence on the down-stream thermal choke point. The total length of the engine is 802 mm and the isolator has cross- section of 25.4x38.1mm.
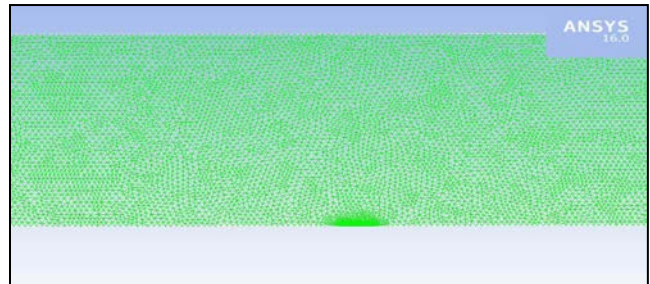

Figure 2 meshing at injector

2

Table 2

Mesh details	
Relevance centre	Fine
Element size	1mm
Element size near inlet outlet and injector	0.1mm
Total number of faces	76363
Total number of elements	50099
Total number of nodes	26265

COMBUSTION MODEL

The flamelet concept considers the turbulent flame as an aggregate of thin, laminar, locally one-dimensional flamelet structures present within the turbulent flow field. In steady laminar flamelet model we have given nine species detailed reaction mechanism of hydrogen and air with its thermodynamic database as input. The composition of air is given in terms of mass fraction, 0.611 nitrogen, 0.251 oxygen, 0.138 water vapor. For calculating flamelet the input is given as described in table 4. Maximum number of flamelets is taken 20 which specifies the maximum number of flamelet profiles to be calculated. Maximum number of grid points is 32 which specifies the variation of oxidizer and fuel in a flamelet. Initial scalar dissipation rate is given as 0.01 per second and scalar dissipation step of 5. The data obtained can be post processed for visualizing the variation of species fraction or temperature with mean mixture fraction or scalar dissipation rate. The pdf table is also calculated which requires additional input given in table 3 along with falmelet data.

Flamelet conservation equations

$$\frac{\partial Y_к}{\partial t} = \frac{\chi}{2}\frac{1}{Le}\left(\frac{\partial^2 Y_к}{\partial Z^2}\right) + \frac{\omega}{\rho} \quad (6)$$

$$Cp\frac{\partial T}{\partial t} = \frac{\chi}{2}\left(\frac{\partial^2 h}{\partial Z^2}\right) - \sum_{k=1}^{n} h_к\{\frac{\chi}{2}\left(\frac{\partial^2 Y_к}{\partial Z^2}\right) + \frac{\omega}{\rho}\} \quad (7)$$

The mixture fraction and scalar dissipation rate are assumed to be statistically independent in the FLUENT implementation. The PDF of the mixture fraction is assumed to be a beta function. Fluctuations in the scalar dissipation rate are ignored, so the PDF of scalar dissipation rate becomes a delta function.

Table 3

| PDF table setting	
Maximum number of mean mixture fraction points	40
Number of mean mixture variance points	40
Minimum temperature	248K
Number of mean enthalpy points	41

Table 4

| Settings for flamelet calculation	
Maximum number of flamelets	20
Number of grid points in flamelet	32
Initial scalar dissipation rate	0.01/s
Scalar dissipation step	5

RESULTS AND DISCUSSIONS

Contours of temperature, pressure, and velocity obtained are shown in figure 4, figure 5, and figure 6. In temperature contour the static temperature is varying from 248K to 1165K. And all the variations are taking place near injector portion and the diffuser part. The high temperature region shows the combustion region and it shows the mixing of fuel with air. And in the lower part of diffuser where no mixing of fuel took place the temperature is decreasing due to simple expansion of air. In pressure contour the static pressure is increasing in the diffuser section. In the velocity contour the velocity is increasing in the diffuser portion.
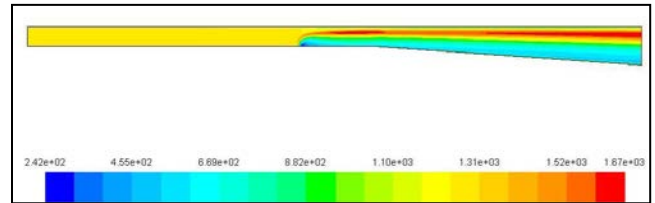
Figure 3 static temperature contour
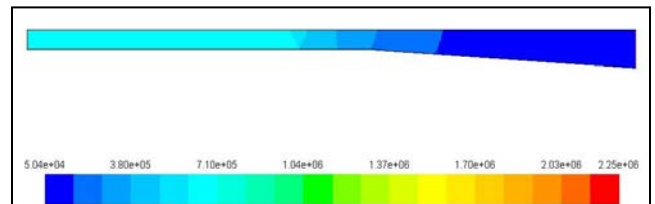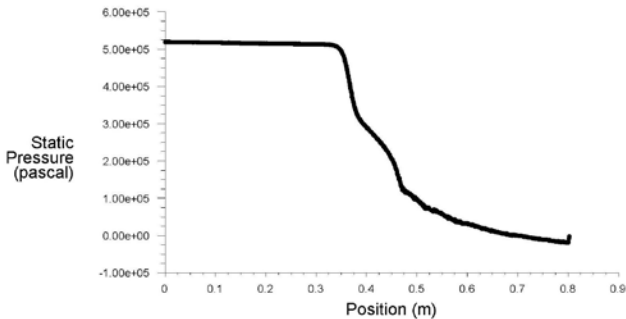

Figure 4 pressure contour

3
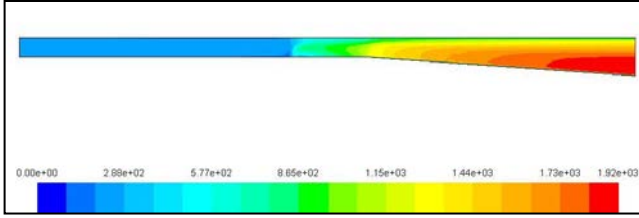
Figure 5 velocity contour

Variation of static temperature with distance along the mean line is shown in figure 7. The trend obtained is as expected as it is constant in the isolator and after combustion starts the values increases and reaches a maximum value of 1670K.
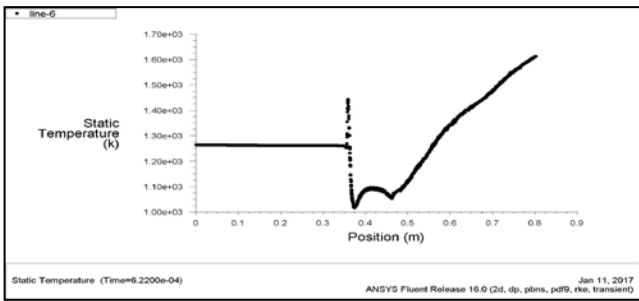

Figure 6 temperature plot

Figure 7 static pressure

Figure 7 shows the plot of static pressure along the length about the mean line. The pressure is constant along the isolator and it decreases as the fuel is injected the velocity increases and the slightly increases in the ignition region then further decreases in the diverging section as flow is in supersonic region.

Figure 8 shows the variation of Mach number with distance along the mean line parallel to x-axis. The flow change to supersonic regime from subsonic regime due to heat addition.
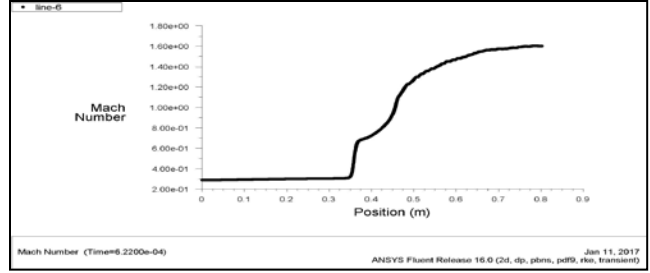
Figure 8 Mach number plot

CONCLUSION

The results obtained so far are quite satisfactory and are in close agreement with the results of the experiment and computations performed by M. Torrez [1]. The present work is in its initial stage and in near future the simulations will also be performed on 3D computational domain and combustion will be modeled for supersonic flow.

AKNOLEDGEMENT

REFERENCES

[1] Sean M. Torrez,James F. Driscoll,Matthias Ihme, and Matthew L. Fotia., 2011. "Reduced-Order Modeling of Turbulent Reacting Flowswith Application to Ramjets and Scramjets". JOURNAL OF PROPULSION AND POWER Vol. 27, No. 2, March–April 2011.
[2]Rene Prieler , Martin Demuth , Davor Spoljaric , Christoph Hochenauer, "Evaluation of a steady flamelet approach for use in oxy-fuelcombustion" Fuel, Elsevier,Volume 118, 15 February 2014, Pages 55–68.
[3] Chavez, F. R., and Schmidt, D. K., "Analytical Aeropropulsive/ Aeroelastic Hypersonic-Vehicle Model with Dynamic Analysis," Journal of Guidance, Control, and Dynamics, Vol. 17, No. 6, 1994, pp. 1308–1319.
[4] Tarpley, C., and Lewis, M. J., "Stability Derivatives for a Hypersonic Caret-Wing Waverider," Journal of Aircraft, Vol. 32, No. 4, 1995, pp. 795–803.
[5] Heiser, W. H., and Pratt, D. T., Hypersonic Airbreathing Propulsion, AIAA, Washington, D.C., 1994.
[6] Dalle, D. J., Fotia, M. L., and Driscoll, J. F., "Reduced-Order Modeling of Two-Dimensional Supersonic Flows with Applications to Scramjet Inlets," Journal of Propulsion and Power, Vol. 26, No. 3, 2010, pp. 545–555

SEEC-2017-121

FEASIBILITY OF USING PHASE CHANGE MATERIAL FOR THERMAL STORAGE AT HIGH TEMPERATURE FOR CONCENTRATED SOLAR COOKERS: A NUMERICAL APPROACH

Kumar Venkateshwar
Department of Mechanical Engineering,
IIT Jodhpur
Email: venkateshwar.1@iitj.ac.in

Vanditi Mathur
Department of Mechanical Engineering,
IIT Jodhpur
Email: mathur.1@iitj.ac.in

Prodyut R Chakraborty
Department of Mechanical Engineering,
IIT Jodhpur
Email: pchakraborty@iitj.ac.in

ABSTRACT:

Concentrated solar cooker is an extremely promising technology to utilize solar energy for cooking at high temperature range 250-350°C However, timing of obtaining maximum heat flux does not match the household cooking schedule which is either early morning or the evening. This mismatch can be addressed by storing thermal energy during noon (timing of maximum obtainable heat flux) which can be utilized after sundown for cooking. In order to store the thermal energy, phase change materials (PCM) can be used to store thermal energy in the form of latent heat. Feasibility of using $NaNO_3$ as PCM with melting temperature of 307°C has been numerically investigated for latent heat storage in a concentrated solar cooker unit with a paraboloid reflector having a projected area of 1.8 m^2. Enthalpy updating method is used to predict the charging dynamics of the heat storage unit.

Keyword:
Concentrated solar cooker, Latent heat storage, Phase change Material, High temperature applications

NOMENCLATURE
C_p Specific Heat Capacity
H_{sl} Latent Heat of solid-liquid transition
T   Temperature
T_m Melting Temperature
T_∞ Ambient Temperature
k   Thermal Conductivity
ρ Density
q"   Incident Flux
h   Enthalpy
h_{con} Convective Heat Transfer Coefficients
      Subscripts
s   Solid
l   Liquid

INDTRODUCTION
Solar energy is one of the most abundantly available green renewable energy-resources. Concentrated solar cooker is a highly promising technology to utilize solar energy for cooking at high temperature range of 250-350°C. The major obstacle of solar energy is the intermittency of its availability. According to NREL data [1] the average annual Direct Normal Irradiance (DNI) at Jodhpur is approximately 700 W/ m^2 and is available only for 6-7 hours in a day. However, the cooking schedule of Indian household is either in the early part of the day or during evening. The gap between the availability and the demand of thermal energy for cooking requirements needs to be resolved for the widespread use of such solar cookers. One of the ways to address this mismatch is thermal energy storage in the form of latent heat [2]. Thermal energy can be stored either in the form of sensible heat or latent heat. However, high energy density of latent heat storage unit makes it an attractive thermal energy storage solution and needs systematic research initiatives.

Phase change processes involving solid to liquid transformation are of particular importance since the volume change during the phase change process is negligible. Thermal energy can be stored during the melting process which defines the charging of the storage unit, while this energy can be utilized during the discharging process involving solidification of the PCM. Although, melting and solidification processes have been widely studied in connection with manufacturing techniques such as casting and welding, electronic cooling, and latent heat storage type heat exchangers etc.; application of phase change material for storing thermal energy in concentrated solar cookers are rarely studies[3].

Kenisarin [4] reported the basic property of several PCM for high temperature applications. One of the major problems of this PCM is low thermal conductivity in the order of 0.2-0.5 W/m-K. The enhancement of thermal conductivity of PCM can be addressed in different ways such as adding metal fins, tubes and particles like graphite powder etc. Utilization of Compressed Expanded graphite (CEG) is one of the newly developed methods, which is very efficient in enhancing the thermal conductivity of PCM [5]. Pincemin et. al. [6] has studied composites of PCMs with melting temperature in the range of 200-300°C and graphite flakes. They used natural graphite flakes and expanded graphite powder and enhanced the conductivity 14 times.

In present work, the feasibility of using NaNO$_3$-CEG composite for thermal energy storage has been studied by capturing the melting or charging process of the storage unit. The storage unit consists of a hollow cylindrical stainless steel container filled with NaNO3-CEG composite. Enthalpy updating technique described by Chakraborty [7], Bennon and Incropera [8, 9] and Voller et. al. [10] has been used to capture the melting or charging (melting) dynamics of the storage unit. Since PCM-CEG composite is considered to be a porous structure during the melting process omission of convective terms has been considered to be a fair assumption, and a diffusion based energy equation is considered to depict the energy transportation.

METHODOLOGY
MODEL:
Fig. 1 shows schematic of the storage vessel having outer radius of 12.6 cm and height of 12.8 cm made up of Stainless Steel (SS) of thickness 2mm which encloses the PCM or PCM-CEG. The volume of the PCM is calculated using the average energy requirement for cooking food for a family of 6 people [11] and properties of the PCM. Considering the effects of shadow of the heat storage container on the reflector dish

and dust deposition on the reflector, a conservative DNI value of 400 W/m^2 has been estimated. Based on the estimated DNI value, the incident heat flux on the container has been found out to be 70,000 W/m^2 on a circular focal area of radius 5 cm at the bottom surface of the vessel. The schematic of the storage container is shown in figure 1, where, the shaded area at the bottom surface represents the focal area on which concentrated radiation is incident. Figure 2 depicts the solar-cooker integrated with the storage vessel. The thermo-physical properties of SS container and PCM-CEG composite is provided in table 1. For the numerical simulation, the entire outer surface of the container excluding the shaded focal area at the bottom of the container in figure 1 is considered to be insulated. Since the boundary conditions are favourable to axi-symmetric situation. 2-D simulation for the energy conservation is obtained in r-z direction.
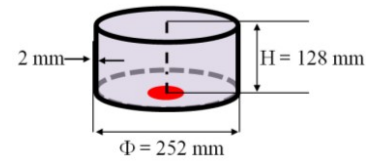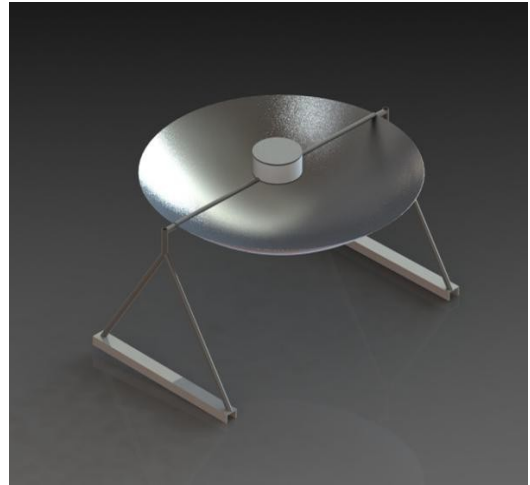

Figure 1 Schematics of the Storage Vessel

Figure 2 Schematic of Parabolic Solar Cooker with Heat Storage Unit

MATHEMATICAL AND NUMERICAL MODEL
The numerical model is based on volume averaged formulation described by Bennon and Incropera [8, 9] and energy equation reported by Chakra borty [7]. The energy equation is defined as follows

$$\frac{\partial}{\partial t}\left((\rho C_{ps}T)\right) = \nabla.(k\nabla T) - \frac{\partial}{\partial t}(f_l \rho h_{sl}) -$$
$$\frac{\partial}{\partial t}[f_l \rho (C_{pl} - C_{ps})(T - T_m)] \quad (1)$$

In eq. (1), solid and liquid enthalpies are defined in the following manner:

For solid phase:
$$h_s = C_{ps}T \qquad (2)$$

For Liquid Phase:
$$h_l = C_{ps}T_m + h_{sl} + C_{pl}(T - T_m) \qquad (3)$$

The volume averaged thermo-physical properties such as specific heat and thermal conductivities as defined as follows:

$$C_p = f_l C_{pl} + f_s C_{ps} = g_l C_{pl} + g_s C_{ps} \qquad (4)$$
$$k = f_l k_l + f_s k_s = g_l k_l + g_s k_s \qquad (5)$$

Where f_s and f_l represents solid and liquid fractions respectively.

The numerical scheme is developed in such a way that equation (1) is valid for both PCM domain as well as solid wall of the container. The only difference between the container wall and the PCM domain is the omission of second and third terms (source terms) on the right hand side of equation (1) for the container wall portion. The enthalpy updating scheme described Chakraborty [7] has been used in order to obtain the liquid and solid fractions f_l and f_s.

The boundary condition at the bottom centre for a radius of 5cm is given by equation (6) that represents the incident heat flux (q") and convective heat loss from this domain to the ambiance. For the rest of the surfaces, adiabatic boundary condition is applied.

$$-k \frac{\partial T}{\partial x} = q'' - h(T_s - T_\infty) \qquad (6)$$

The convective heat transfer coefficient is assigned a value 10 W/m^2 K. The container wall thickness is considered to be of 2 mm thickness and 8 grid points are considered for each wall, while for the PCM domain 126X126 grids are considered. A time-step of 1 s is implemented for the calculation.

Table 1 Properties of materials used

Materials Properties	SS	PCM (NaNO$_3$)	CEG
Heat Capacity	490	1820	1820
Thermal Conductivity	16.0	0.5	3.5
Density	8050	2260	2260
Melting Temperature	1850	580.16	580.16
Latent Heat of Melting		172000	172000

RESULTS AND DISCUSSION

The initial condition is considered to be ambient temperature of 25°C . The extent of melting and isotherms are shown in figure 3 to 5 after 2, 4 and 6 hrs which depicts the charging dynamics. Figure 6 shows the variation of PCM bulk mean temperature (T_b) with time.
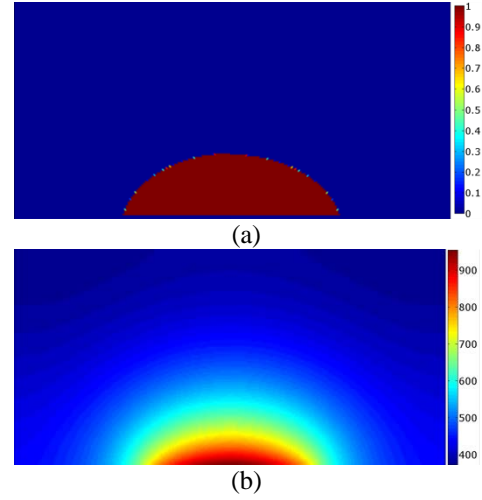

(a)

(b)

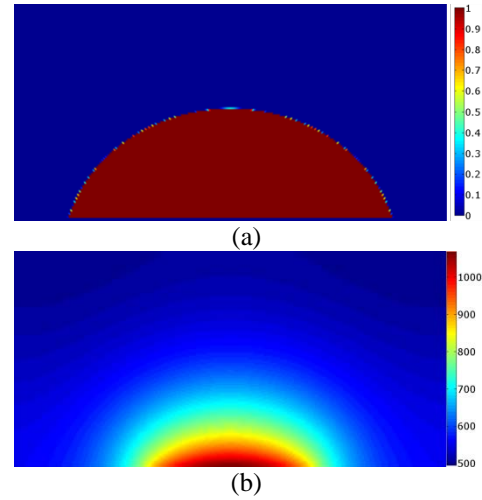Figure 3 (a) Extent of Melting and (b) Temperature profile at time t = 2hr

(a)

(b)

Figure 4 (a) Extent of Melting and (b) Temperature profile at time t = 4hr

The rate of melting process from these three figures suggests that the total time to melt the entire PCM will definitely exceed 6 hrs. However, the incident DNI is expected to be much larger, as we have considered extremely conservative DNI value of 400 W/ m^2 K. Also, a better design with a larger paraboloid might reduce the charging time to a large extent. The convective losses can also be reduced by means of protective glass sealing. Since the hot-spot shown in figure 1 by the shaded area at the bottom surface is prone to have a very high temperature the heat loss to the ambient due to convection and radiation is bound to be very large. So, the design must address this issue in order to have minimum heat loss. Also, the container material with a lager thermal conductivity as compared to SS might help in mitigating this problem. A conservative value of thermal conductivity for the PCM-

CEG composite has been considered for the present study, and convection in the porous medium has been completely ignored. The combined effect of these two factors might result in a more suitable outcome. Addition of metal fins inside the PCM domain will also help to mitigate the problem.
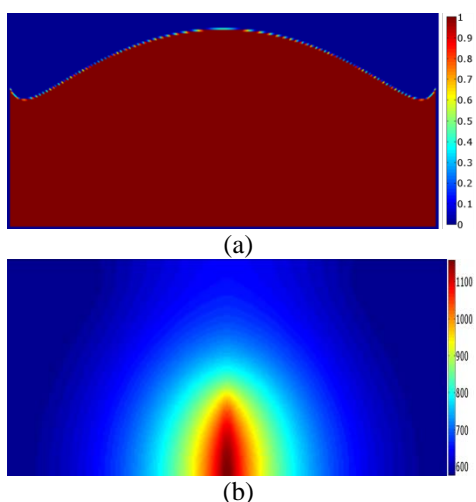

(a)

(b)

Figure 5 (a) Extent of Melting, (b) Temperature profile at time t = 6 hr

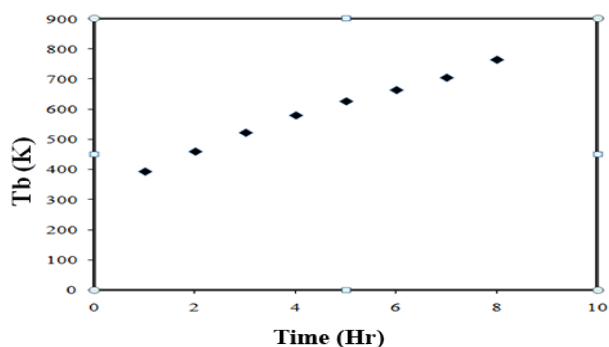Figure 6 Variation of PCM bulk mean temperature with time

CONCLUSIONS

The feasibility of NaNO$_3$-CEG composite as latent heat storage medium is studied for the charging cycle. The results suggest that the container, PCM-CEG thermal conductivity and convection in porous matrix play very crucial roles. The considered paraboloid reflector needs to be of larger size in order to obtain a more suitable charging dynamics. Since the hot-spot temperature attains a very large value (above 1000 K), container material with high thermal conductivity as well as high melting temperature is of prime requirement.

ACKNOWLEDGEMENTS

REFERENCES

[1] www.nrel.gov/gis/data_solar.html

[2] Gil,Antoni, et al. "State of the art on high temperature thermal energy storage for power generation. Part 1- Concepts, materials and modellization."Renewable and Sustainable Energy Reviews 14.1 (2010): 31-55.

[3] Buddhi, D., S. D. Sharma, and Atul Sharma. "Thermal performance evaluation of a latent heat storage unit for late evening cooking in a solar cooker having three reflectors." *Energy Conversion and Management* 44.6 (2003): 809-817.

[4] Kenisarin, Murat M."High-temperature phase change materials for thermal energy storage." *Renewable and Sustainable Energy Reviews* 14.3 (2010): 955-970.

[5] Sari, Ahmet, and Ali Karaipekli. "Thermal conductivity and latent heat thermal energy storage characteristics of paraffin/expanded graphite composite as phase change material." *Applied Thermal Engineering* 27.8 (2007): 1271-1277.

[6] Pincemin,S., et. al. "Highly conductive composites made of phase change materials and graphite for thermal storage." *Solar Energy Materials and Solar Cells* 92.6 (2008): 603-613.

[7] Prodyut R. Chakraborty. "Enthalpy porosity model for melting and solidification of pure substances with large difference in phase specific heats" Int. Com. Heat Mass Transf., 81(2017), pp. 183-189.

[8] W.D. Bennon, F.P. Incropera "A continuum model for momentum, heat and species transport in binary solid- liquid phase change system-I. Model formulation" *Int. J. Heat Mass Transf.*, 30 (1987), pp. 2161–2170.

[9] W.D. Bennon, F.P. Incropera "A continuum model for momentum heat and species transport in binary solid- liquid phase change system-II. Application to solidification in a rectangular cavity "*Int. J. Heat Mass Transf.,* 30 (1987), pp. 2171–2187

[10] A.D. Brent, V.R. Voller, K.J. Reid "The enthalpy porosity technique for modelling convection-diffusion phase change: application to the melting of a pure metal."*Numerical Heat Transf.,*13 (1988): pp.297-318.

[11] www.cliquesolar.com/Cooking.aspx

SEEC-2017-122

HIGH SPEED VISUALIZATION OF VORTEX –DROPLET INTERACTIONS IN SWIRLING GAS FLOW FIELD

Kuppuraj Rajamanickam
Mechanical Engineering
Doctoral Student
Email: kuppuraj@mecheng.iisc.ernet.in

Saptarshi Basu
Mechanical Engineering
Associate Professor
sbasu@mecheng.iisc.ernet.in

ABSTRACT

In this paper, the near field breakup and atomization of liquid sheet in a co-annular swirling gas flow field is presented. High-speed speed shadowgraphy is employed to characterize the global features and breakup dynamics of liquid sheet across a wide range of airflow rates. The parameter momentum ratio (MR) is used to illustrate the results. Breakup regimes are constructed based on the instantaneous visualization of the liquid sheet. At high airflow rates, the breakup process is shown to be a function of gas phase dominant. Theoretical expressions have been proposed for breakup length scales, the results show good agreement with experimental values

Keywords: coaxial atomization, swirl flows, high-speed imaging, near field breakup.

INTRODUCTION

The basic understanding of breakup mechanism and atomization of liquid jet/sheet in co-annular gas flow field is fundamental to liquid phase combustion systems [1]. The gas phase turbulence and complex instability modes associated with fast moving air leads to poor understanding of the problem. In particular, the swirl introduced into the co-flowing atomizing air in gas turbine engines, further complicates the problem [2]. Swirling jets are widely employed in gas turbine combustor system to stabilize the flame [3]. The unique feature of swirling jet is the formation of central toroidal recirculation zone (CTRZ) at high swirl levels ($S_G \geq 0.6$; S_G is geometric swirl number). The formation of CTRZ exhibits large-scale effects, when the secondary flow is introduced (here liquid sheet). Particularly, the recirculated flow imposes radial force on the liquid sheet. In coaxial atomization using normal jets (i.e. without swirl), the KH (Kelvin-Helmholtz) waves are mostly propagate in axial direction. Whereas, in swirling jets, the combination of axial and swirling velocity components result in formation of axial and azimuthal KH waves [4]. Lasheras, 1996 [5, 6] reported the two way coupling effect in coaxial swirl assist atomizer, i.e. weak gas phase interaction at low swirl levels and strong coupling effect with high airflow rates. In context of coaxial atomization, the breakup process in primary region (region close to nozzle exit) is essentially shown to be air dominated. For instance the experiments carried out by [7], showed that breakup process is correlated with the gas /vorticity layer thickness (δ_g) arising from primary instability of the gas-liquid interface. In addition, δ_g gives rise to oscillations of the liquid sheet at particular rates. Studies showed that shedding frequencies are well correlated with primary waves formed at liquid-gas interface. Breakup/intact, length is an important parameter in any atomization process. Classical studies have been established that, liquid sheet breaks up, if the waves at interface reach a certain critical value [8]. Hence, the breakup length scale can be approximately scaled with the wavelength formed at primary region. Further, the magnitude of wavelength depends on various parameters like flow geometry, relative velocity between liquid and air, surface tension. However at very high airflow rates, the destabilizing effect of surface tension is found to be negligible [9].

In this study, the configuration similar to lean direct injection (LDI) is considered, i.e. annular swirling gas jet with central swirling hollow cone liquid sheet [10].The main

idea of this paper is to recognize the physical mechanism underlying the breakup process. Efforts have been made to understand the temporal oscillations of the breakup length scale using high-speed diagnostics. More details of the analyses along with detailed data can be found in Ref. 16.

EXPERIMENTAL DETAILS

The experimental setup utilized in this study is schematically shown in Figure 1 a. All the experiments are conducted at atmospheric pressure; air and water are used as working fluids [16]. Throughout the experiments, liquid flow rate is kept constant ($U_l = 3$ m/s), while, airflow rate across the swirler is progressively varied from 0 to 3000 lpm ($U_a = 9.01$ to 60 m/s) using high precision computer controlled MFC. In addition, pulsation dampeners and flow straighteners (honeycombs) are placed in flow lines. The swirler which used in this study is of flat vane type with a vane angle $\Phi = 45^0$ (swirl number $S_G = 0.81$) and vane thickness $t_v = 2$mm (other geometry details are shown in Figure 1 b). The simplex nozzle (orifice diameter $D_N = 0.5$ mm) is mounted in hub of the swirler to perfectly align its centerline axis with swirler jet axis.

The spatio-temporal evolution of the liquid sheet in swirling gas field across various airflow rates are captured with high-speed shadowgraphy system. Here, the spray is illuminated with diffused light from LED strobe lamp (pulse rate-100 KHz). The instantaneous images are acquired with CMOS high-speed camera (Make- Photron, SA5). The flash duration of the strobe lamp is synchronized with the camera shutter speed to obtain time-frozen snapshots of the spray image (see Figure 1 b). The images are acquired at a rate of 20,000 fps with an acquisition time of 0.5 s for each test case (i.e. 1000 images are acquired per test case). Based on the 100 mm macro lens (Make-Tokino), the spatial field is chosen as 45x35 mm with a resolution of 704 x 520 pixels (magnification factor ~15 pixels/mm). This arrangement helped to visualize the global structure of the liquid sheet.

Further, the near-field breakup and ligament formation is visualized with the help of long distance microscope (LDM).
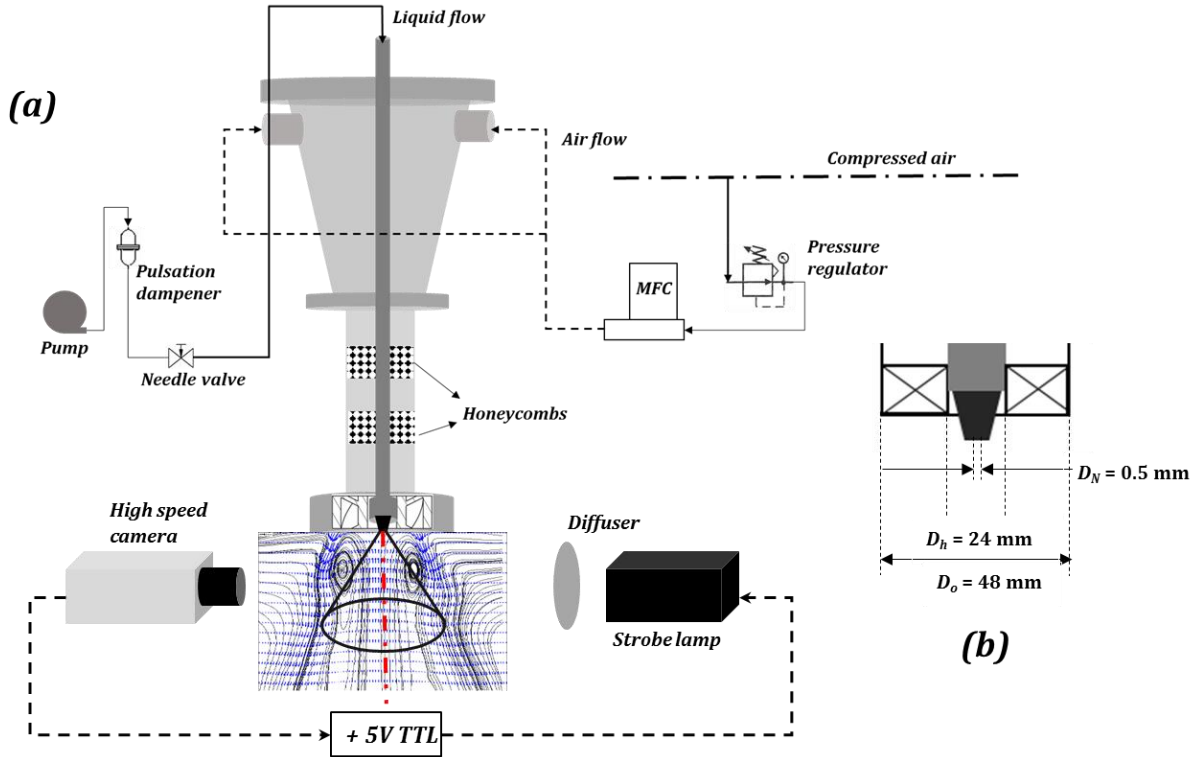
Figure 1. a. Schematic of experimental setup with high-speed shadowgraphy arrangement; **b**. Swirler and simplex nozzle geometry details

RESULT AND DISCUSSIONS

All the test cases are characterized by a non-dimensional number called momentum ratio (MR)

$$MR = \frac{\rho_a U_a^2 A_{a,eff}}{\rho_l U_l^2 A_{l,eff}} \qquad (1)$$

$$A_{a,eff} = \pi/4 \, (D_o - D_h)^2 - 0.5 n_v t_v (D_o - D_h) \quad (2)$$

$$We_\Gamma = \frac{\rho_a \left(\frac{\Gamma}{2\pi r}\right)^2 t_f}{\sigma} \quad (3)$$

Here D_o and D_h is swirler outer and inner hub diameter (m); n_v is number of swirl vanes; t_v is vane thickness (m).In addition, liquid sheet breakup phenomena is characterized by two Weber numbers, one is based on time averaged velocity at nozzle exit and second, is based on vortex strength to characterize the flapping breakup of liquid sheet.
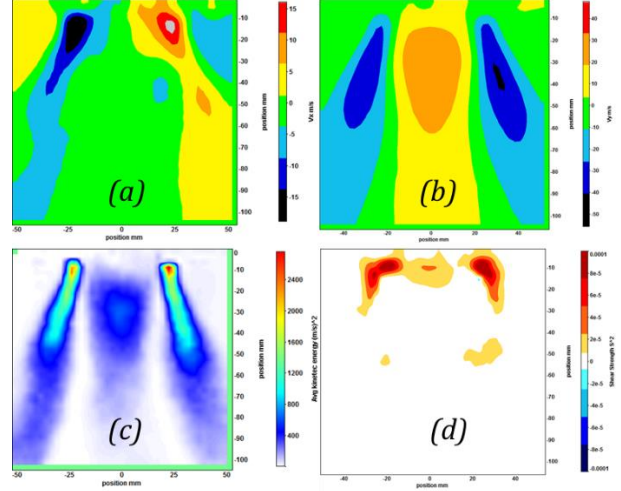
Where ρ_a, ρ_l is air and liquid density (kg/m³);U_a, U_l is gas and liquid velocity (m/s), $A_{a,eff}, A_{l,eff}$ is effective air and liquid flow area (m²)

$$We_\delta = \frac{\rho_a (U_g - U_l)^2 \delta_g}{\sigma} \quad (4)$$

Where, δ_g is vorticity/gas layer thickness, σ is surface tension, Γ circulation strength (m²/s), r is vortex core radius, t_f is film thickness. Here, $\delta_g = \frac{8.5 \, D_{eff}}{Re_g}$; D_{eff} is effective airflow path diameter across the swirler. Please see ref 16 for more details.

Global observations

The spray global structure across various levels of MR is shown in **Error! Reference source not found.** and the time averaged gas phase flow field contours are shown in Figure 2 . Here, L_s and L_b are two global length scales, which represent the breakup length and lateral expansion of the liquid sheet. For $MR \leq 338$ (**Error! Reference source not found.** a-c), it is perceived that the weak momentum coupling between the air and liquid phase (under this condition surface tension may dominate the breakup process, i.e. $We_\delta < 1$;) However, a significant change in sheet structure is observed for $MR \geq 338$ (**Error! Reference source not found.** d-h) which subsequently results in reduction of L_s and L_b values (this shows strong two-phase momentum coupling effect $We_\delta > 1$). It is interesting to note that, at higher MR values, the edges of the liquid sheet starts to flap and eventually breaks down to cluster of In swirling jets, the strong '$\boldsymbol{\theta}$' component of velocity leads to create low-pressure zone at jet centerline axis. This effect results in flow reversal at the jet axis. Further, the reversed flow induces radial force at the surface of the liquid sheet. As a result, the liquid sheet expands in radial direction (i.e. increase of spray spread scale (see **Error! Reference source not found.** c-e). Further, increase in air velocity leads to catastrophic breakup of liquid sheet and leads to a decrease of spread scale (X_s).At MR=338, considerable variation is observed in spray global structure. Hence, the flow

droplets. This is due to the circulation induced by counter rotating eddies in co-annular swirling jet. (i.e. CTRZ-central toroidal recirculation zone).

Figure 2 : Time averaged contours a. Radial velocity; b. Axial Velocity; c. Turbulent kinetic energy (TKE); d. Shear strength
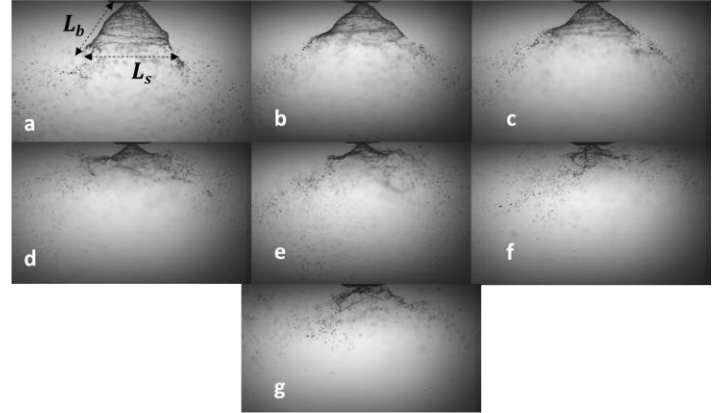

Figure 3: Instantaneous snapshots of liquid sheet global structure a. MR = 0; b. MR =138; c. MR=338; d. MR =1080; e. MR =2785; f. MR =4400; g. MR =6100

conditions corresponding to MR =338 are considered as critical values ($MR_c, We_{\delta c}, We_{\Gamma c}$).

BREAKUP REGIMES

Based on the evolution of spray global structure and length scale variation, breakup regime map is constructed in MR-We_δ paradigm (Figure 4). When a liquid sheet of thickness (t_f) injected into co-annular swirling jet, first the air tries to

3

destabilize the interface against restoring surface tension force.
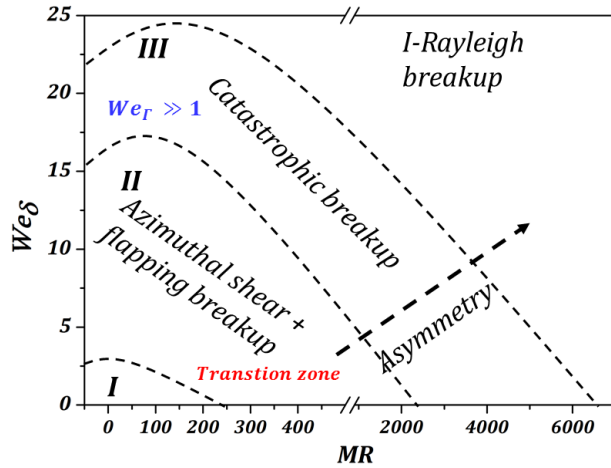
Figure 4. Breakup regimes of hollow cone liquid sheet injected in swirling gas flow field adapted from [6]

At low MR values the disturbances imposed by gas phase coherent structures are engulfed by liquid flow (see region I and II in Figure 4). In this regime, interfacial waves mostly dominate in the streamwise direction; the liquid sheet breaks up in axisymmetric manner. Hence, similarity is observed in left (Lbl) and right side (Lbr) breakup length scales [16]. However, the increase in momentum ratio leads to strong coupling effect and vortices formed at gas-liquid interface results in striping of ligaments from the liquid sheet. Beyond critical momentum ratio ($MR \geq MR_c$), increase in swirl velocity component induce waves in azimuthal (span wise) direction in addition to stream wise direction [6]. The combined span wise and stream wise waves (regime III) and the increased circulation strength of counter rotating eddies leads to oscillations of liquid sheet at the edge. At this point, liquid sheet starts to breakup in asymmetric manner and degree of asymmetry increase with MR values. At very high MR values ($338 \leq MR \leq 6100$), the higher shear strength destabilize the interface and results in catastrophic breakup of liquid sheet (regime IV). Here, the sheet breaks up very close to nozzle and ejects cluster of droplets.

CONCLUSIONS

The breakup dynamics of liquid sheet in co-annular swirling gas flow field is explained. The high-speed shadowgraphy results reveal different forms of breakup and the same has been shown in regime maps. At high airflow rates, the breakup process is shown to be a function of waves arising from primary instability of liquid-gas interface. The weak gas-liquid phase momentum coupling is also presented for low airflow rates. In addition, the temporal fluctuation of breakup length scales is shown across wide range of airflow rates.

6 References

[1] A. H. Lefebvre, *Gas turbine combustion*. CRC Press, 1998.

[2] D. J. Kang and S. P. Lin, "Breakup of a swirling liquid jet," *Int. J. Eng. Fluid Mech.*, vol. 2, no. 1, pp. 47–62, 1989.

[3] J. M. Beér and N. A. Chigier, "Combustion aerodynamics," *N. Y.*, 1972.

[4] N. A. Chigier and A. Chervinsky, "Experimental investigation of swirling vortex motion in jets," *J. Appl. Mech.*, vol. 34, no. 2, pp. 443–451, 1967.

[5] E. J. Hopfinger and J. C. Lasheras, "Explosive breakup of a liquid jet by a swirling coaxial gas jet," *Phys. Fluids 1994-Present*, vol. 8, no. 7, pp. 1696–1698, 1996.

[6] K. Rajamanickam and S. Basu, "Insights into the dynamics of spray–swirl interactions," *J. Fluid Mech.*, vol. 810, pp. 82–126, 001 2017.

[7] J.-P. Matas, S. Marty, and A. Cartellier, "Experimental and analytical study of the shear instability of a gas-liquid mixing layer," *Phys. Fluids 1994-Present*, vol. 23, no. 9, p. 94112, 2011.

[8] N. Dombrowski and W. R. Johns, "The aerodynamic instability and disintegration of viscous liquid sheets," *Chem. Eng. Sci.*, vol. 18, no. 3, pp. 203–214, 1963.

[9] P. Marmottant and E. Villermaux, "On spray formation," *J. Fluid Mech.*, vol. 498, pp. 73–111, 2004.

[10] R. Tacina, C. Wey, P. Laing, and A. Mansour, "A Low NO (x) Lean-Direct Injection, Multipoint Integrated Module Combuster Concept for Advanced Aircraft Gas Turbines," 2002.

COMPARITIVE ANALYSIS ON SIMULATION ABILITY OF SEVERAL SYNGAS REACTION MECHANISMS IN HCCI ENGINE

Rakesh Kumar Maurya, Mohit Raj Saxena
Department of Mechanical Engineering
Indian Institute of Technology Ropar, Rupnagar-
140001, India
Email: rakesh.maurya@iitrpr.ac.in

Rahul Yadav, Akshay Rathore
Department of Mechanical Engineering
Indian Institute of Technology Ropar, Rupnagar-
140001, India
Email: 2015meb1103@iitrpr.ac.in

ABSTRACT

Energy safety concern and depletion of fossil fuel resources leads towards the investigation of an efficient and clean alternative combustion strategy as well as renewable biofuels. Homogeneous charge compression ignition (HCCI) engine has demonstrated the potential to attain higher thermal efficiency along with simultaneous reduction of NOx and PM emissions to ultra-low level. Syngas is also a potential alternative fuel. Syngas HCCI engine combines the advantages of combustion strategy and biofuels. This study presents the comparative numerical analysis of performance of various syngas reaction mechanisms in the HCCI engine using at different inlet temperature and equivalence ratio using stochastic reactor model. For validating the reaction mechanisms, in-experimental in-cylinder pressure data is compared with the numerically simulated data. Results indicate that a CRECK-2014 reaction mechanism (consisting of 32-species and 172-reactions) is predicting experimental in-cylinder pressure data accurately. To compare the performance of syngas rreaction mechanisms for HCCI engine, error in peak pressure (P_{max}), SOC (CA_{10}), combustion phasing (CA_{50}), end of combustion (CA_{90}) and combustion duration (CA_{90-10}) are calculated and analysed.

***Keywords:** **HCCI, Combustion, Reaction Mechanism, Syngas, Engine**.*

INTRODUCTION

The advancement in modern society massively depends on the hydrocarbon fossil fuels. Combustion of these fossil fuels creates the energy for human requirement like electricity generation, transportation, etc. However, combustion of these fuels emits detrimental emissions in higher concentration. Diesel engines are mostly preferred in transportation or for heavy-duty vehicle and in electricity generation due to its higher thermal efficiency and power output. Simultaneously, diesel engine emits nitrogen oxides (NO_x) and soot emission in higher concentration. To meet the energy demand and to overcome the challenges of diesel engine, researchers have suggested two strategies; either to replace the fossil fuel with renewable fuel or to replace conventional combustion technology with premixed low temperature strategies (LTC). Premixed LTC strategies have a higher thermal efficiency (or similar to conventional strategies) and lower NO_x and soot emission. Among all the premixed LTC strategies, homogeneous charge compression ignition (HCCI) is the most investigated combustion mode by the researchers because of its higher thermal efficiency and ultra-low NO_x and soot emission [1, 2]. HCCI engine has a higher fuel conversion efficiency as compared to conventional engines of same size [3]. In addition to this HCCI combustion strategy has no direct control on the combustion phasing (as in conventional engines) and has higher hydrocarbon (HC) and carbon monoxide (CO) emission because of lower combustion temperature.

To meet the energy demand and decline in the supply of fossil fuels, renewable fuels (such as biofuels) is one of the options for internal combustion engines. The HCCI

combustion strategy has a potential to utilize such fuels which can be auto ignite in the combustion chamber. Several studies [4-6] have been found that HCCI engine can be operated with various fuels such as methanol, butanol, ethanol, hydrogen etc.

In the past few years, researchers were paying more attention towards the application of syngas for internal combustion engines [7-8]. Syngas is produced by the gasification process of biomass or coal. Composition of syngas (mainly consist of CO, N_2, H_2 and CO_2) depends on the type of biomass used, process of gasification etc. Use of syngas in internal combustion engine, possibly reduces the emissions (as compared to conventional fuels) and could be a good replacement of conventional fuels. Several studies [9-15] have been published with a numerous combustion reaction mechanism for syngas in the past few years. These studies mainly compared the experimental data with simulated data for conventional combustion strategies.

This work presents the comprehensive study of different syngas combustion reaction mechanism in HCCI engine. The study is carried on the stochastic reactor model (SRM) for numerical simulation in HCCI engine. Firstly, the simulation results were validated with experimental results. Later on, to determine the optimal syngas reaction mechanism the combustion characteristics (such as peak pressure rise rate (P_{max}), SOC (CA_{10}), combustion phasing (CA_{50}), end of combustion (CA_{90}) and combustion duration (CA_{90-10})) were compared to experimental results and simulated results of various syngas combustion reaction mechanisms.

METHODOLOGY

The syngas HCCI engine was numerically investigated using kinetic SRM software. Numerical investigation were conducted during closed valve condition. Various syngas reaction mechanisms were validated by comparing the in-cylinder pressure data with previously published study [22]. All the simulations were conducted using zero-dimensional SRM model. This model replaced the homogeneity inside the cylinder and real fluid particles with statistical homogeneity and virtual stochastic particles respectively. All these virtual stochastic particles has its own chemical composition, mass and temperature. In this study SRM suite software is used which is an in-cylinder engine combustion simulator.

RESULTS AND DISCUSSION

This section presents the comparison of predicted in-cylinder pressure with experimental results using various syngas combustion reaction mechanisms. In addition to this, combustion characteristics with different reaction mechanism in the HCCI engine at different operating conditions are also discussed.

To validate the different syngas reaction mechanisms, experimental results of the syngas HCCI engine from a

published study [22] is validated by comparing the in-cylinder pressure history data with numerically simulated in-cylinder pressure. Experimental results of the syngas HCCI engine are validated by comparing numerically simulated data using various syngas combustion reaction mechanisms at different operating conditions (such as different inlet valve closing temperature (T_{ivc}) and equivalence ratio (ϕ)). A combustion reaction mechanism [14] consisting of 32-species and 172- reactions is matched with experimental results of a study [22]. Figure 1 shows the comparison of predicted in cylinder pressure with experimental data using different reaction mechanisms at different T_{ivc} and ϕ. Figure 1 indicates that for both the equivalence ratio, with an increase in the T_{ivc} start of combustion (SOC) slightly advanced. That means during compression stroke combustion chamber temperature increases and priory reaches to an auto-ignition temperature, which results in the earlier SOC with higher inlet valve closing temperature. A study reported that SOC mainly depends on the T_{ivc} and have less dependency on ϕ [23]. However, with some of the syngas reaction mechanisms combustion process does not observe for HCCI engine.
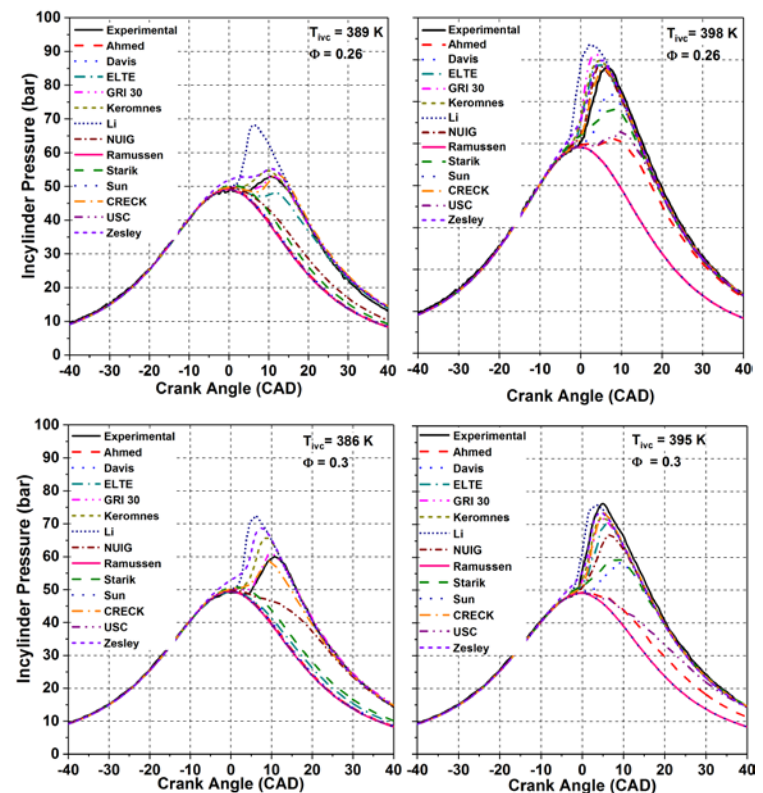
FIGURE 1. COMPARISON OF PREDICTED IN CYLINDER PRESSURE WITH EXPERIMENTAL DATA USING DIFFERENT REACTION MECHANISMS

To determine the optimal syngas reaction mechanism for HCCI engine, error in P_{max}, SOC (CA_{10}), CA_{50}, CA_{90} and CA_{90-10} are calculated for different T_{ivc} and ϕ. The error is calculated with respect to experimental data or syngas reaction mechanism CRECK-2012 [14] (because this reaction mechanism is validated with experimental data). Figure 2 indicates the variations in the error percentage of P_{max} for various syngas reaction mechanisms relative to experimental results [22] at different T_{ivc} and ϕ. Figure 2 reveals that some of the tested syngas reaction mechanisms such as GRI 3.0 -1999 [16], Keromnes-2013 [10] and Zseley-2005 [20] has small variations at lower equivalence ratio ($\phi = 0.26$) for both T_{ivc}. In addition to this, the variation of P_{max} is higher for higher equivalence ratio ($\phi = 0.3$) for all the tested mechanism. Combustion of rich mixture (higher ϕ) leads to increase the P_{max} probably that's why variations in P_{max} is higher for higher ϕ.
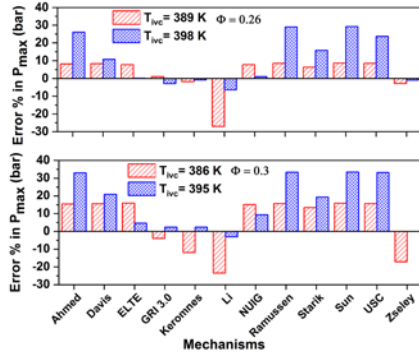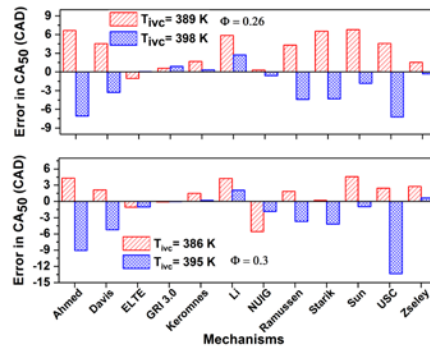

FIGURE 2. ERROR IN P_{MAX} FOR DIFFERENT REACTION MECHANISMS

In HCCI combustion strategy, SOC mainly depends on the chemical kinetics, pressure and temperature of the combustion chamber. However, SOC is an essential parameter for performance of HCCI engine perspective. With an increase in the air intake temperature (for any equivalence ratio (ϕ)), SOC advances because the higher air intake temperature leads to prior auto-ignition. Figure 3 shows the variations in SOC for various syngas reaction mechanisms relative to experimental results [22] at different T_{ivc} and ϕ. It can be depicted from the figure 3 that reaction mechanisms ELTE-2016 [21], GRI 3.0-1999 [16] and Keromnes-2013 [10] has lower variations at both the equivalence ratio and T_{ivc}. However, Starik-2009 [15] reaction mechanism has higher variations in CA_{10} for both the T_{ivc} and ϕ.
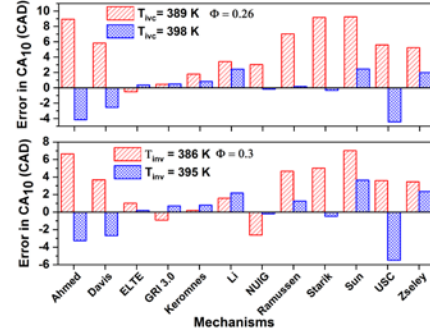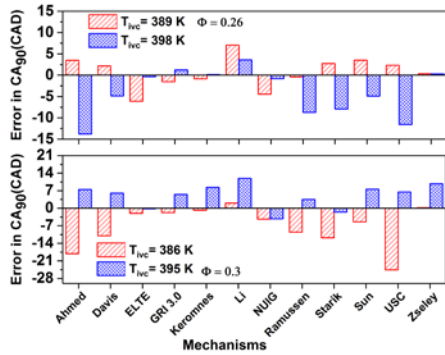

FIGURE 3. ERROR IN CA_{10} FOR DIFFERENT REACTION MECHANISMS

The overall combustion phasing during an engine combustion cycle is characterized by CA_{50}. A study reported that earlier or late combustion phasing directly affects the efficiency of HCCI engine [5]. With the variation in the air intake temperature, ignition timing strongly affects the combustion phasing (CA_{50}). In HCCI combustion strategy, with an increase in the air intake temperature, combustion phasing advances. It is because of the prior ignition of charge (due to the high temperature combustion chamber). However, combustion phasing is very sensitive to air intake temperature. Therefore, prediction of CA_{50} by syngas reaction mechanism is essential. It has been observed that with the reaction mechanisms ELTE-2016 [21], GRI 3.0-1999 [16], Zseley-2005 [20] and Keromnes-2013 [10] has small variations at both the equivalence ratio and T_{ivc} (as shown in figure 4). Results also reveals that variations in end of combustion (CA_{90}) are also lower for same mechanisms as for CA_{50} (as shown in figure 5).
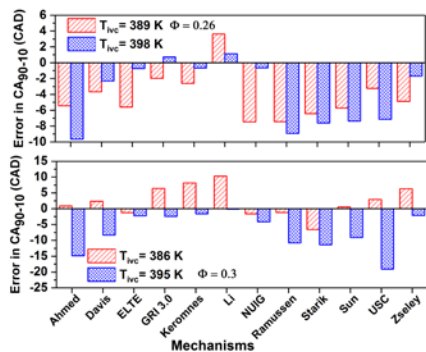

FIGURE 4. ERROR IN CA_{50} FOR DIFFERENT REACTION MECHANISMS

FIGURE 5. ERROR IN CA_{90} FOR DIFFERENT REACTION MECHANISMS

Combustion duration is defined in terms of crank angle degree (CAD) between the 90% and 10% rate of heat release during combustion i.e. CA_{90}-CA_{10}. In an HCCI engine, with the retard start of combustion timing, combustion duration increases rapidly. Therefore, it means that with an increase in air intake temperature, combustion duration decreases for both the equivalence ratio. Figure 6 represents the variation in combustion duration for various syngas reaction mechanisms at different T_{ivc} and ϕ. Figure 4 reveals that for both the equivalence ratio, the reaction mechanisms ELTE-2016 [21], GRI 3.0-1999 [16] and Keromnes-2013 [10] has lower variations for higher T_{ivc} as compared to lower T_{ivc}. However, with some of the reaction mechanism higher reductions in combustion duration observed.

FIGURE 6. ERROR IN $CA_{90\text{-}10}$ FOR DIFFERENT REACTION MECHANISMS

CONCLUSIONS

This study presents the numerical investigation on simulation ability of several syngas reaction mechanisms in HCCI engine using the stochastic reactor model. Reaction mechanisms were validated by comparing the experimental in-cylinder pressure data with numerically simulated in-cylinder pressure at different T_{ivc} and equivalence ratio (ϕ). To identify the syngas reaction mechanism which can correctly predict the combustion characteristics of HCCI engine, error in peak pressure rise rate (P_{max}), SOC (CA_{10}), combustion phasing (CA_{50}), end of combustion (CA_{90}) and

combustion duration ($CA_{90\text{-}10}$) are calculated and analysed for different T_{ivc} and ϕ. Results revealed that a CRECK-2014 reaction mechanism (consisting of 32-species and 173- reactions) is perfectly matched with experimental in-cylinder pressure data. The results also revealed ELTE-2016, GRI 3.0-1999 and Keromnes-2013 syngas reaction mechanisms has lower variations and could be used for the syngas HCCI engine in certain operating conditions. However, other syngas reaction mechanisms have higher error, which indicates these mechanisms are not suitable for syngas HCCI.

REFERENCES

[1] Maurya, R. K., & Agarwal, A. K. (2015). Experimental investigations of particulate size and number distribution in an ethanol and methanol fueled HCCI engine. Journal of Energy Resources Technology, 137(1), 012201.

[2] Maurya, R. K., & Agarwal, A. K. (2014). Particulate morphology and toxicity of an alcohol fuelled HCCI engine. SAE International Journal of Fuels and Lubricants, 7(2014-01-9076), 323-336.

[3] Yao, M., Zheng, Z., & Liu, H. (2009). Progress and recent trends in homogeneous charge compression ignition (HCCI) engines. Progress in Energy and Combustion Science, 35(5), 398-437.

[4] Komninos, N. P., & Rakopoulos, C. D. (2012). Modeling HCCI combustion of biofuels: A review. Renewable and Sustainable Energy Reviews, 16(3), 1588-1610.

[5] Maurya, R. K., & Akhil, N. (2016). Numerical investigation of ethanol fuelled HCCI engine using stochastic reactor model. Part 1: Development of a new reduced ethanol oxidation mechanism. Energy Conversion and Management, 118, 44-54.

[6] Maurya, R. K., & Akhil, N. (2017). Development of a new reduced hydrogen combustion mechanism with NO x and parametric study of hydrogen HCCI combustion using stochastic reactor model. Energy Conversion and Management, 132, 65-81.

[7] Veetil, J. E., Rajith, C. V., & Velamati, R. K. (2016). Numerical simulations of steady perforated-plate stabilized Syngas air pre-mixed flames. International Journal of Hydrogen Energy, 41(31), 13747-13757.

[8] Bhaduri, S., Berger, B., Pochet, M., Jeanmart, H., & Contino, F. (2017). HCCI engine operated with unscrubbed biomass syngas. Fuel Processing Technology, 157, 52-58.

[9] D. Healy, D.M. Kalitan, C.J. Aul, E.L. Petersen, G. Bourque, H.J. Curran, Energy Fuel 24 (2010) 1521–1528.

[10] A. Kéromnès, W.K. Metcalfe, K.A. Heufer, N. Donohoe, A.K. Das, C.-J. Sung, J. Herzler, C. Naumann, P. Griebel, O. Mathieu, M.C. Krejci, E.L. Petersen, W.J. Pitz, H.J. Curran, Combust. Flame 160 (2013) 995–1011.

[11] S.G. Davis, A.V. Joshi, H. Wang, F. Egolfopoulos, Proc. Combust. Inst. 30 (2005)1283–1292

[12] X. Li, X. You, F. Wu, C.K. Law, Proc. Combust. Inst. 35 (2015), http://dx.doi.org/10.1016/j.proci.2014.07.047

[13] H. Wang, X. You, A.V. Joshi, S.G. Davis, A. Laskin, F. Egolfopoulos, C.K. Law, USC Mech Version II. High-Temperature Combustion Reaction Model of H2/CO/C1-C4 Compounds. <http://ignis.usc.edu/USC_Mech_II.htm/>.

[14] CRECK modeling Group Hydrogen/CO mechanism version 2014. <http://creckmodeling.chem.polimi.it/kinetic.html/>.

[15] A.M. Starik, N.S. Titova, A.S. Sharipov, V.E. Kozlov, Combust. Explos. Shock Waves 46 (2010) 491–506.

[16] G.P. Smith, D.M. Golden, M. Frenklach, N.W. Moriary, B. Eiteneer, M.Goldenberg, C.T. Bowman, R.K. Hanson, S. Song, W.C. Gardiner, V.V.Lissianski, Z. Qin GRI-Mech 3.0. <http://www.me.berkeley.edu/gri_mech/>.

[17] C.L. Rasmussen, J. Hansen, P. Marshall, P. Glarborg, Int. J. Chem. Kinet. 40(2008) 454–480.

[18] H. Sun, S.I. Yang, G. Jomaas, C.K. Law, Proc. Combust. Inst. 31 (2007) 439–446.

[19] S.S. Ahmed, F. Mauß, G. Moréac, T. Zeuch, Phys. Chem. Chem. Phys. 9 (2007) 1107–1126.

[20] I.G. Zsély, J. Zádor, T. Turányi, Proc. Combust. Inst. 30 (2005) 1273–1281.

[21] T. Varga, C. Olm, T. Nagy, I.Gy. Zsély, É. Valkó, R. Pálvölgyi, H.J. Curran, T. Turányi. Development of a Joint Hydrogen and Syngas Combustion Mechanism Based on an Optimization Approach. Int. J. Chem. Kinet., 48 (8) 407–422, (2016), DOI: 10.1002/kin.21006.

[22] A.S. Bika, Synthesis Gas Use in Internal Combustion Engines, PhD Thesis, University Of Minnesota, USA, December 2010.

[23] Maurya, R. K., & Akhil, N. (2016). Numerical investigation of ethanol fuelled HCCI engine using stochastic reactor model. Part 2: Parametric study of performance and emissions characteristics using new reduced ethanol oxidation mechanism. Energy Conversion and Management, 121, 55-70.

SEEC – 2017 – 124

NUMERICAL INVESTIGATION ON EFFECTS OF INCREASING COMPRESSION RATIO ON MAXIMUM HYDROGEN ENERGY SHARE IN DUEL FUEL COMPRESSION IGNITION ENGINE

Priybrat Sharma
School of Engineering
Indian Institute of Technology Mandi
Email: priybrat_s@students.iitmandi.ac.in

Atul Dhar
School of Engineering
Indian Institute of Technology Mandi
Email: add@iitmandi.ac.in

ABSTRACT

The effect of different compression ratios on maximum possible hydrogen energy's share in a dual fuel engine is studied by creating a numerical model for engine combustion and emission characteristics. Hydrogen is inducted through the intake port into the engine. Compression ratio is varied in steps of 14.5, 16.5 and 19.5 in all the investigations. Hydrogen energy share is varied from 0 % to 55 %. The results show a clear trade-off between maximum hydrogen energy's share and compression ratio. Knock limited maximum hydrogen energy's share decreases from 45 % to 20 % as compression (CR) is increased from 14.5 to 19.5. The emissions other than NOx show a clear decrease at all compression ratios as the hydrogen energy share is increased.

Keywords: Hydrogen; Dual-fuel mode; Knock; Combustion; Emissions.

INTRODUCTION

There is an increasing stress on conventional fuel sources due to growing demand for energy. This has thrust the research towards renewable and alternative fuel sources. Hydrogen is one such alternative fuel with extremely clean combustion and possibility of production through renewable energy route.[1]

Hydrogen can be adapted as both primary or secondary fuel for internal combustion engines. In dual fuel compression ignition engines, hydrogen is preferred as a secondary fuel. It is known to improve the combustion efficiency of the engines due to its higher flame velocity, high diffusivity in the air and extremely wide flammability limits. Additionally, high autoignition temperature of 858 K makes it ideal for application in compression ignition engines. But, it offers low energy density, restricting its application as the primary fuel.[2]

The improved combustion efficiency reflects as reduced emissions and increased overall efficiency of the engine. But, the amount of diesel energy replacement with hydrogen is greatly restricted by the possibility of preignition due to localized hot spots and detonation due to extended delay period. [3–5]

The compression ratio of the CI engine dictates the temperature and pressure of the engine at any given crank angle. The temperature and pressure conditions are primordial in deciding the ignition delay period of fuel. In this study, an effort has been made to investigate the effect of compression ratio on maximum hydrogen energy share enhancement in duel fuel CI engines.

MODEL AND VALIDATION

CONVERGE CFD, a commercial I.C. engine simulation package is used as a computational framework for developing a model for hydrogen supplemented duel fuel C.I. engine. Hydrogen is port injected and considered to homogeneously distributed in the combustion chamber at the start of the simulation (at IVC). The liquid diesel injection process is simulated using standard DDM (Droplet Discrete model) and Hybrid KH-RT model is used to model atomization and break-up of spray along with

NTC collision model. RNG k-e is used to model turbulent flow along with wall function (O'Rourke and Amsden wall heat transfer model), which accounts for the heat transfer through the boundary. CONVERGE CFD uses integrated LLNL chemistry solver code (SAGE) to model the combustion with detailed chemistry.

**TABLE 1**: The details of the engine used in this model.

Description	Parameter Values
Engine type	CI Engine
Displacement Volume (CC)	947.3
Rated output (kW)	7.4
Rated Speed (rpm)	1500
Bore, Stroke (mm)	102, 116
Compression ratio	19.5:1
Connecting rod length (mm)	232.6
IVO and IVC (Degree CA)	43° bTDC and -113° bTDC
EVO and EVC (Degree CA)	-93° aTDC and 39° aTDC
Liquid injector opening pressure (bar)	250 - 260
In-cylinder peak pressure (bar)	90

The model is validated against experimental data published by V. Cintala et al.[6]. For validation cases, the compression ratio is fixed at 19.5 and start of injection timing is kept fixed at 2° bTDC. The model simulates the closed part of the engine cycle starting from IVC at 113° bTDC till EVO at 93° aTDC. Sector geometry grid of 72° with periodic boundaries, as shown in Fig. 1 is considered as the engine modeled has 5-hole injector.
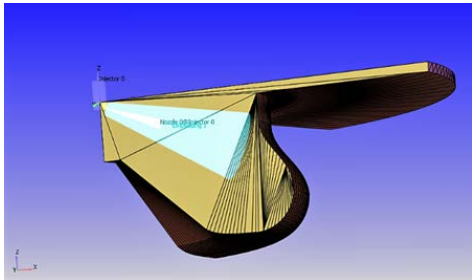
FIGURE 1. Piston bowl geometry of the Kirloskar EA 10 Engine

GRI-Mech 3.0 with Hashemi et al. hydrogen sub-mechanism is used as the basis for chemical kinetics analysis in this model. Fig. 2 shows Pressure trace obtained from the model alongside the published experimental trace. The results predicted by the model are within an acceptable deviation of 2.4%.
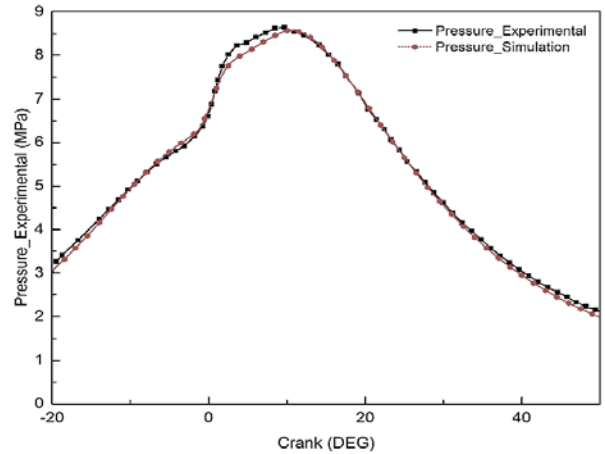
FIGURE 2. Validation case pressure vs. CA trace with HES of 18.5 % at CR 19.5.

The investigation considers Compression ratios of 14.5, 16.5 and 19.5. At each compression ratio, hydrogen energy share is varied as to 0, 10, 20, 30, 45 and 55 % and other parameters are kept constant. Total energy supplied to the engine per cycle is held constant at 1.87 KJ, which corresponds to about 80% of full load operating point of the used diesel engine.

RESULTS AND DISCUSSION

Knocking restricts the amount of hydrogen enhancement in dual fuel CI engines and is characterized by a high instantaneous rate of pressure rise (RPR). In this study RPR, value 0.15 MPa/CA is chosen as a cut-off, beyond which combustion is classified as knocking [7].

Combustion Characteristics

Fig. 3 (a), (b) and (c), shows the pressure and heat release rate against crank angle under influence of increasing the hydrogen energy share (HES) with compression ratios of 14.5,16.5 and 19.5. As can be seen, the ignition timing advances and the HRR increase in most cases when hydrogen energy share is increased. This can be attributed to the burning velocity of hydrogen, which is almost 10 times that of diesel. The shorter ignition delay can also be accounted due to premixed naturally aspirated hydrogen, the high diffusivity of hydrogen in air is responsible for more homogenous mixture in the cylinder. As the HES is increased, higher flame speed results in sudden combustion of premixed hydrogen in the fuel.

(a)

(b)

(c)
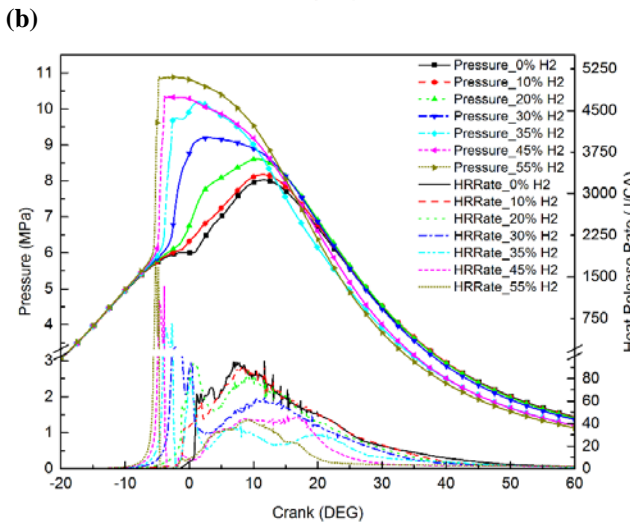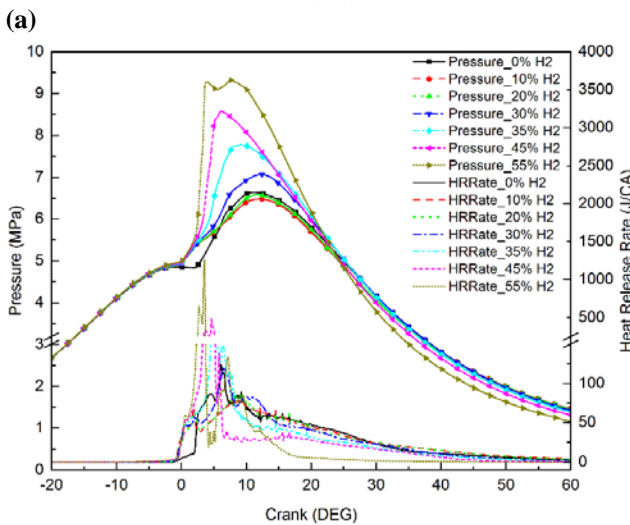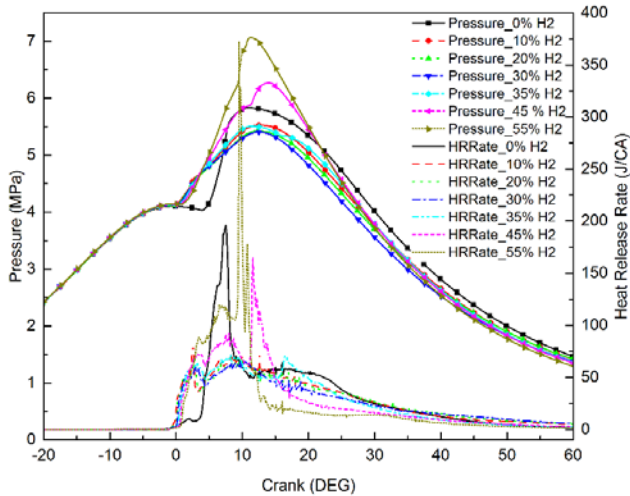
FIGURE 3 (a), (b) and (c). Pressure vs. CA trace with HES variation at CR 14.5, 16.5 and 19.5, respectively.

Performace Characteristics

Fig. 4, shows the trends observed in gIMEP and RPR as hydrogen share is increased. At CR of 16.5 and 19.5, a common trend in terms of gIMEP is observed. Till certain levels of hydrogen shares, the gIMEP increases marginally and then it increases considerably beyond which drastic drop is observed. The generalized inference from these trends is that for different CR values controlled, steady co-combustion of both fuels is observed at different levels of hydrogen share. Also, the trend clearly shows that at lower compression ratios controlled steady co-combustion of higher energy share of hydrogen with diesel is achievable. But at low CR of 14.5, no such clear trend is observed and the initial drop in gIMEP is greater than later increases at a higher share of hydrogen energy. In terms of RPR, at high CR a rapid rise is observed as the hydrogen energy share is increased due to fast flame burn velocity of hydrogen. This can also be attributed to the presence of more homogenous charge in the cylinder, resulting in faster and uniform combustion. But, at CR of 14.5 the RPR drops till 35 % hydrogen energy share and after that, it starts to increase. This is due to lower in-cylinder temperature and pressure conditions, which results in longer ignition delay period.
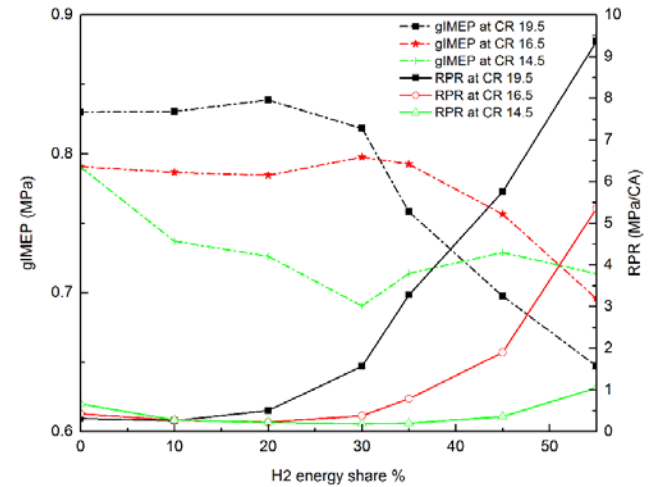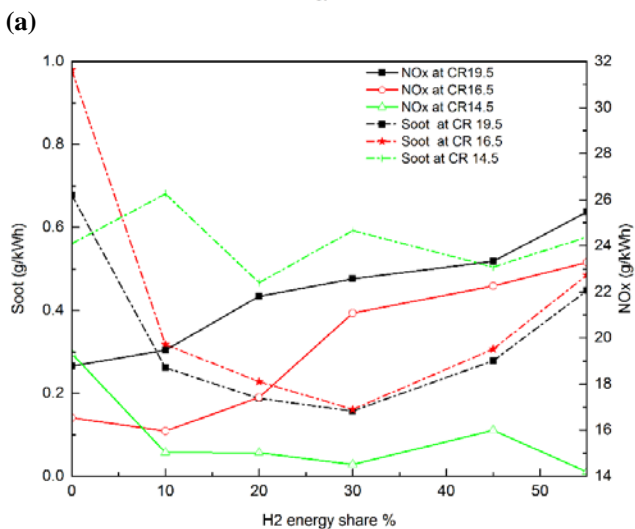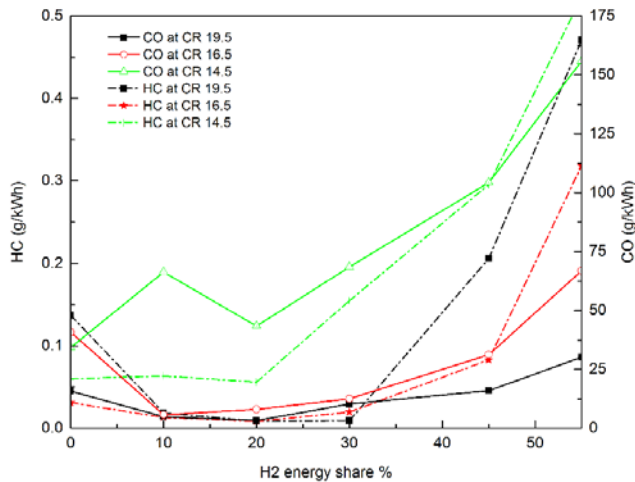

FIGURE 4. gIMEP, RPR vs. HES trace for CR 14.5, 16.5 and 19.5.

Emission Characteristics

At CR of 16.5 and 19.5 till HES of 30%, both HC and CO both decrease due to homogenous combustion after addition of hydrogen after hydrogen supplementation as seen in the Fig. 5 (a). But, as the HES is further increased the levels of HC and CO start to increase due to precess of excess hydrogen. On the other hand at CR 14.5, the HC and CO emissions increase due to low CR, resulting in improper diesel combustion.

In the case of NOx and soot, as the hydrogen share is increased till 30%, the NOx value increases, and soot amount decreases for CR 16.5 and 19.5. whereas at CR of 14.5 no clear trend is observed (Fig. 5 (b)).

(a)

FIGURE 5 (a) and (b). HC, CO, and Soot, NOx vs. HES trace for CR 14.5, 16.5 and 19.5.

CONCLUSIONS

The conclusions are drawn from the investigations follows:

1. The results from an investigation of HES increment at different compression ratios suggest that possible maximum HES strongly depends on CR of the engine and at lower CR values higher HES is possible but at CR lower than 14.5 the diesel combustion becomes inefficient due to lower temperature and pressure conditions.
2. Knocking is a key parameter restricting the HES increment. At higher CR the knocking tendency increases with HES increase.
3. Within the knock limit HC, CO and soot emissions show a considerable decrease, but NOx levels increase.
4. Higher HES allows for more homogenous combustion of charge, resulting in better combustion characteristics within knocking limit. During the

investigation, HES levels of 45%, 30%, and 20 % are found as optimum for CR 14.5, 16.5 and 19.5, respectively.
5. At CR 14.5 with HES 45 % soot gets reduced by 37 %, but NOx increase by 11 %. Similarly, at CR 16.5 with 30% HES, soot drops by 83 % and NOx increases by 27 %, while at CR 19.5 with 20 % HES soot reduces by 61 % with only 3.5 % NOx increase.
6. In terms of HC and CO, a reduction of 36 % and 69 % at CR 16.5; 93 % and 80 % at CR 19.5 is observed. But for CR 14.5 both HC and CO increases.

REFERENCES

[1] T. V Johnson, "Diesel Emissions in Review," *SAE Int. J. Engines*, vol. 4, no. 1, pp. 143–157, 2011.

[2] B. Prasath, E. Leelakrishnan, and N. Lokesh, "Hydrogen Operated Internal Combustion Engines–A New Generation Fuel," *Ijetae.Com*, vol. 2, no. 4, pp. 52–57, 2012.

[3] S. Verhelst and T. Wallner, "Hydrogen-fueled internal combustion engines," *Prog. Energy Combust. Sci.*, vol. 35, no. 6, pp. 490–527, 2009.

[4] S. Szwaja and K. Grab-Rogalinski, "Hydrogen combustion in a compression ignition diesel engine," *Int. J. Hydrogen Energy*, vol. 34, no. 10, pp. 4413–4421, 2009.

[5] R. Morgan, P. Atkins, A. Atkins, C. Lenartowicz, and M. Heikal, "Effect of Hydrogen Fumigation in a Dual Fueled Heavy Duty Engine," 2015.

[6] V. Chintala and K. a. A. Subramanian, "Experimental investigations on effect of different compression ratios on enhancement of maximum hydrogen energy share in a compression ignition engine under dual-fuel mode," *Energy*, vol. 87, pp. 448–462, 2015.

[7] A. K. Agarwal *et al.*, "Effect of fuel injection pressure and injection timing of Karanja biodiesel blends on fuel spray, engine performance, emissions and combustion characteristics," *Energy Convers. Manag.*, vol. 91, pp. 302–314, 2015.

SEEC-2017-125

A NOBLE APPROACH FOR THE CLEAN ENERGY GENERATION: SOLAR UPDRAFT TOWER

Pradeep Kumar
School of Engineering
Indian Institute of Technology Mandi
Mandi, Himachal Pradesh-175005, India
pradeepkumar@iitmandi.ac.in

Ankit Agrawal
School of Engineering
Indian Institute of Technology Mandi
Mandi, Himachal Pradesh-175005, India

ABSTRACT

The solar updraft power plant presents a novel approach to generate the clean energy. It works on three simple phenomena (1) greenhouse effect (2) chimney effect, and (3) wind turbine to generate the power. A prototype had been built in Manzanares, Spain in 1981 for the demonstration of the concept. A transition analysis of full-scale Manzanares's solar updraft power plant has been performed. The temperature variations at the collector, ground, and velocity at the turbine plane have been reported. The vorticity contours can give details of the fluid flow in the collector. The vorticity contour plots reveal that flow in the collector is radial and small swirling of the flow is happening in the shadow zone of the chimney.

INTRODUCTION

We are living in a transition phase of energy production where there is an effort to shift energy production from the conventional to renewable resources. The demand for the energy is increasing exponentially with the condition that energy should be produced in a way so that it leaves minimum impact on the environment, i.e., we are expected to provide the clean energy. There are several renewable energy resources available around us. At the first instance, they appear very low in potential; but if many such resources/potentials/phenomena/concept are strategically combined, they may generate a tremendous potential that can be harnessed for the betterment of the humankind. One of such strategic combination of multiple potentials is solar updraft tower, which combines three well-known concepts i.e. greenhouse effect, chimney effect, and wind turbine. These concepts are well known to researchers since centuries, but the first plant had been successfully constructed using these potentials in 1981 at Manzanares, Spain; purely for proof of concept and had been operated between 1981 to 1989. The capacity of the plant was 50 kW. This plant can provide a sustainable alternative to carbon-based power production technologies. It uses solar energy to generates the electricity. The working principle and construction are very simple. A big area is covered either by the glass or a plastic sheet; at the middle of this covered area, a chimney of significant height is erected, and a wind turbine is also attached to the chimney.The schematic diagram and isometric view of the plant are shown in figures 1 and 2, respectively.
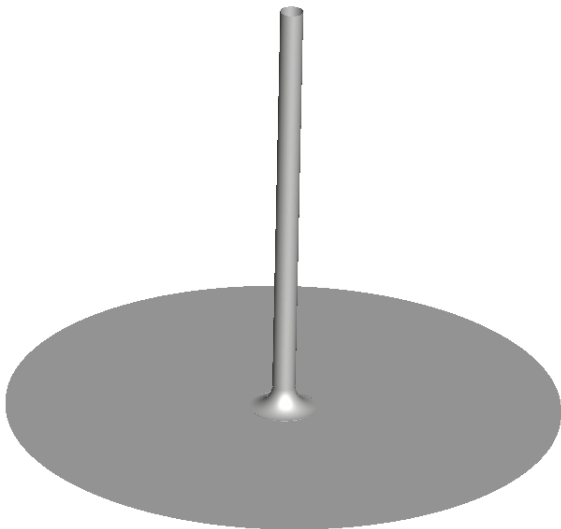
The solar radiation falls on the glass which is nearly 100% transparent to this radiation; some part of this solar energy gets absorbed by the air and the ground, this causes an increase in temperature of ground, and air, which start emiting long wavelength radiation. The glass is nearly opaque (transmissivity 0.01) to this long wavelength radiation. This long wavelength radiation remains trapped inside this enclosure, which creates a temperature difference that generates convection current through buoyancy. The chimney creates a pressure difference, which can direct the convection current generated inside the glass enclosure in the chimney. If the glass enclosure area is big enough and chimney size is also large (the pressure difference in

1
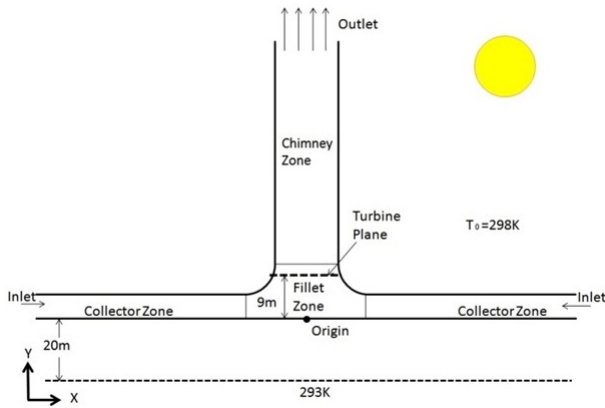
FIGURE 1. Schematic view of solar updraft plant.

FIGURE 2. Isometric view of solar updraft plant.

TABLE 1.   Plant's specifications and main dimensions

Tower Height	194.6 m
Tower Radius	5.08 m
Mean Collector radius	122 m
Mean roof height	1.85 m
Number of turbine blades	4
Turbine blade profile	FX W-151-A
Blade tip speed to air transport velocity ratio	1:10
Operating modes	stand-alone or grid connected mode
Typical collector air temperature increase	$\Delta T = 20$ K
Nominal Output	50 kW
Collector covered with plastic membrane	40,000 m^2
Collector covered with glass	6,000 m^2
Upwind Velocity on release	15 m/s

TABLE 2.   Variation in plant components size with output

Power output (MW)	Collector diameter (m)	Chimney diameter (m)	Chimney height (m)
0.05	244	10.16	194.6
5	1250	45	550
30	2900	70	750
100	4300	110	1000
200	7000	120	1000

the chimney is proportional to chimney height, and the velocity is proportional to pressure difference in the chimney), a tremendous amount of kinetic energy will be available for converting into any useful work. This kinetic energy can be extracted in one way by deploying a wind turbine. This simple principle has been used to develop a prototype in Manzanares, Spain. The plant's specifications and dimensions are summarized in table 1. The efforts have also been put to optimize the plant size for power output, but it has been found that the plant output increases with the increase of components size; only the cost of the plant construction can be a factor for the certain power output. Table 2 gives a brief overview of components size with the power output.

Due to its geometrical simplicity but structural difficulties, many researchers of different areas have performed good amount of research work on the plant.
Haaf et al. [1] have reported the principle construction of the Manzanares pilot plant and published the detailed result [2].

Apart from the publications from plant, the thermodynamic modeling [3, 4], scale down model [5]and fluid dynamics modeling [6, 7] have been used by researchers.

Schlaich et al. [8] have prepared the detailed results theory,
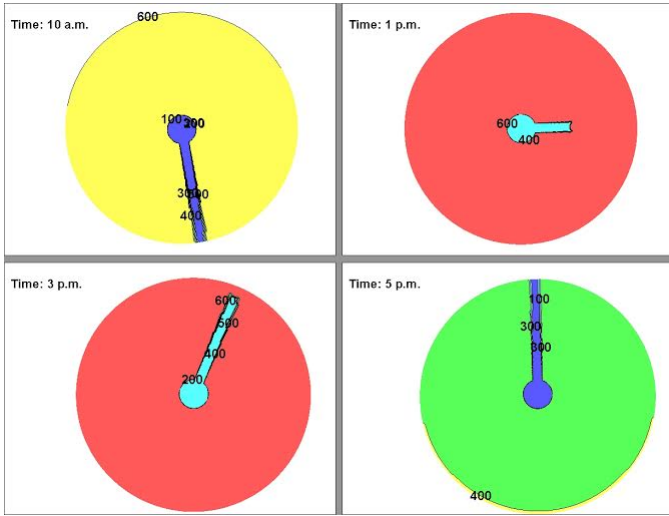
FIGURE 3.   Solar heat flux (W/m^2) at various time instances.

FIGURE 4.   Temperature (K) at the collector at various time instances.

practical experience and economy of the solar updraft tower in Manzanares, Spain. The plant uses plastic or glass material for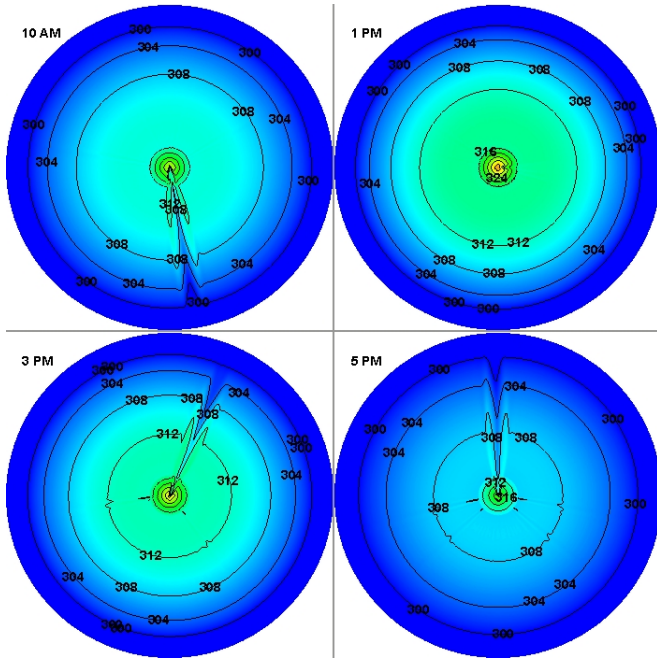 the collector to trap the long wavelength radiation. The generated power is dependent on the solar irradiance falling on the ground. The overall efficiency of the plant is the product of individual efficiency of the collector, chimney, and turbines. The kinetic energy of air inside chimney had been extracted using wind turbine. The maximum possible extracted energy depends on the pressure difference available in the chimney. Fasel et al. [5] studied the power plant using commercially available CFD tool Ansys Fluent and also with in-house developed CFD code. The two-dimensional axisymmetric model of the Manzanares plant and three-dimensional analysis for the geometrical scale of 1:30 of the plant have been taken into consideration. Since there are acceleration and mixing of fluid involved, the fluid mechanics and heat transfer can provide very good insight of fluid phenomena. They reported Reyleigh-Benerad-Poisoulli instability in the fluid flow.

From the above-reviewed articles, it has been noticed that experimental, thermodynamic, and computational analysis either by geometrical reduction techniques or by mathematical modeling of some of the components of the plants have been used to study the solar plant. The major phenomenon in the plant is natural convection. The heat transfer by radiation is equally important in the natural convection problems [7]. It has been noticed that in all above articles, the radiation model have not been used in the study except by Guo et al. [5]; they have used discrete ordinate (DO) radiation model which is the computationally expensive model. The DO radiation model assumes medium as participating, so the calculation of radiation transfer equation happens to each and every cell whereas in the present scenario surface to surface radiation model, where radiation calculation only happens at the boundaries is suitable and able to give a result similar to DO radiation model with the less computational resource.

A computational method is the powerful tool, which could be primarily deployed for the detailed analysis of a system in a quick and less expensive way. This tool helps in avoiding to create multiple prototypes for performing the experiments. However, this tool should be first validated for the models suitable for the particular scenario by existing available data and then study can be extended for analysis for optimization and large scale plants.

In the present work, we have numerically performed transient analysis for the three-dimensional, full-scale geometry of Manzanares, Spain solar updraft plant. This work is an extension of our previous work [9] where analysis has been executed for steady-state validation for the three-dimensional full-scale geometry of Manzanares, solar updraft plant using the commercial CFD software Fluent.

RESULTS AND DISCUSSIONS

The solar heat flux has been applied using the solar load model of the Fluent. The solar load model takes the date, time and location of the site in terms of latitude and longitude data and provides the solar heat flux available. For transient analysis, the start time of the simulation has been provided and software provides currently available solar flux with the advance of the simulation. Figure 3 shows the solar heat flux reaching the ground at 10 AM, 1 PM, 3 PM, and 5 PM. The chimney is considered as opaque; therefore the shadow of chimney appears on the ground. With the progress of the day, the position and size of the chimney's shadow are changing. The solar heat flux reaches a maximum around 1 PM and remains almost same till 3 PM among at the considered time. The maximum value of solar heat flux falling on ground is 900 W/m^2
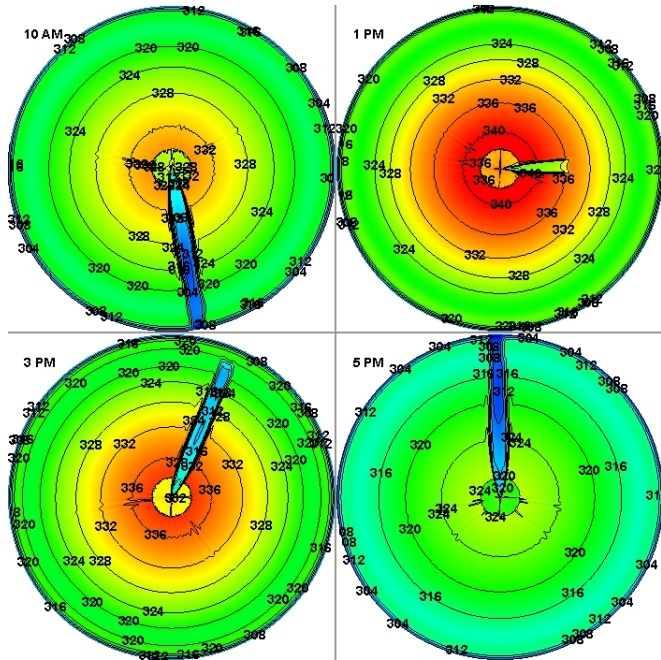
FIGURE 5. Temperature (K) at the ground at various time instances.

Figure 4 shows the temperature at the collector at various times corresponding to reported time of solar heat flux. The temperature at the collector is varying between 298-310 K, 298-324 K, 298-320 K, and 298-316 K at 10 AM, 1 PM, 3 PM and 5 PM respectively. Similarly, the temperature at the ground is also reported in figure 5 at various times. The temperature is varying between 304-328 K, 316-338 K, 316-336 K, and 304-324 K at 10 AM, 1 PM, 3 PM and 5 PM, respectively. There is an average
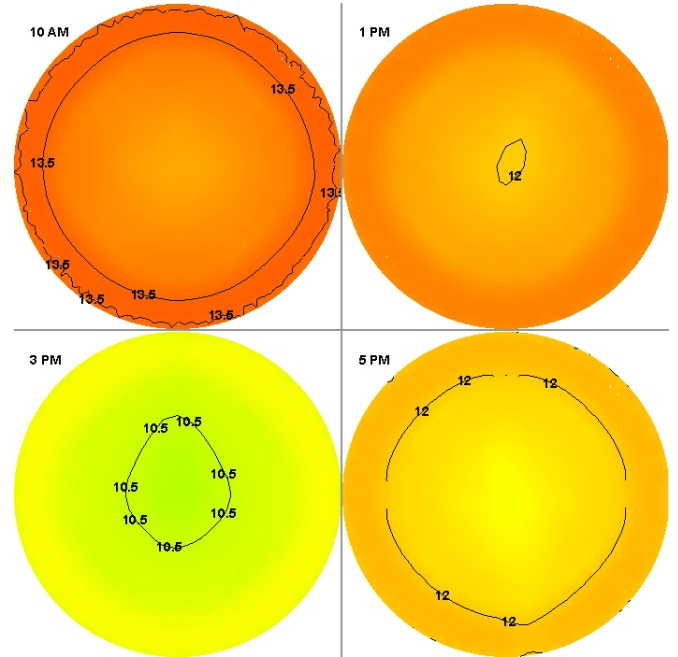
FIGURE 6. Velocity magnitude (m/s) at the turbine plane at various time instances.

temperature difference of 15 K between ground and collector, which is sufficient to generate the buoyancy flow and finally a mass flow rate at turbine which is placed 9 m from the ground as shown in fig 1.

The velocity magnitude at the turbine plane at the various time are shown in figure 6. The velocity magnitude does not vary appreciably in the considered time. The velocity is not fully developed at the turbine plane as we see that velocity is higher around the periphery and less at the centre. The place for the installation of a wind turbine is appropriately chosen as blades of the wind turbine experience high velocity.

The fluid is flowing in the collector through the inlet to the chimney. The mass flow rate is the key parameter at the turbine plane. This mass flow rate will be affected by local swirling of the fluid. It is desired that there should be no swirling for the highest mass flow rate at turbine plane. The vorticity contours at the mid plane of the collector are shown in figure 7 at the considered times. It is evident that vorticity is zero almost everywhere in the collector except in the shadow zone of the chimney. This magnitude of vorticity is very small. The shadow area does not induce vorticity at 1 PM. There is only radial velocity in the collector.

CONCLUSIONS

The transient analysis of full-scale Manzanares' solar updraft power plant has been performed using the commercial CFD

4
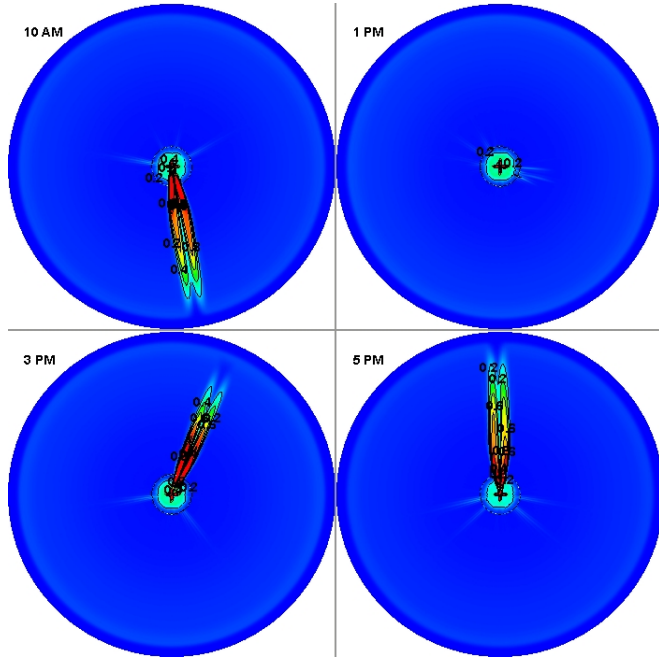
FIGURE 7. Vorticity at the collector mid plane at various time.

software Fluent. The solar flux has been applied by the solar load model of the Fluent. The following conclusions have been drawn from the study.

1) The temperature of the ground is higher than the collector's temperature. The average temperature difference of 15 K between ground and collector, is sufficient to generate buoyancy flow.

2) The average velocity magnitude at the turbine plane is around 12 m/s and this velocity remains almost constant during the day.

3) The flow in the collector is radial. There is small swirl in the shadow zone, which is not affecting the flow at the turbine plane.

REFERENCES

[1] Haaf, W., Friedrich, K., Mayr, G., and Schlaigh, J., 1983. "Solar chimneys part I: Principle and construction of the pilot plant in manzanares". *International Journal of Solar Energy,* **2**(1), pp. 3–20.

[2] Gannon, A. J., and Backström, T. W., 2000. "Solar chimney cycle analysis with system loss and solar collector performance". *International Journal of Solar Energy,* **122**(3), pp. 133–137.

[3] Fasel, H. F., Meng, F., Shams, E., and Gross, A., 2013. "CFD analysis for solar chimney power plants". *Solar Energy,* **98**, pp. 12–22.

[4] Hafizh, H., and Shirato, H., 2015. "Aerothermal simulation and power potential of a solar updraft power plant". *Journal of Structural Engineering,* **61**, pp. 388–399.

[5] Guo, P., Li, J., and Wang, Y., 2014. "Numerical simulations of solar chimney power plant with radiation model". *Renewable Energy,* **62**, pp. 24–30.

[6] Schlaich, J., Bergermann, R., Schiel, W., and Weinrebe, G., 2005. "Design of commercial solar updraft tower systems utilization of solar induced convective flows for power generation". *Journal of Solar Energy Engineering,* **127**, pp. 117–124.

[7] Audunson, T., and Gebhart, B., 1972. "An experimental and analytical study of natural convection with appreciable thermal radiation effects". *Journal of Fluid Mechanics,* **52**, pp. 57–95.

[8] Haaf, W., 1984. "Solar chimneys part II: Preliminary test results from the manzanares pilot plant". *International Journal of Solar Energy,* **2**(2), pp. 141–161.

[9] Agrawal, A., and Kumar, P. "Full-scale three-dimensional computational analysis of solar updraft tower in manzanares, spain for power generation". *ASME, Journal of Solar Engineering (submitted).*

SEEC-2017-126

SUSTAINABLE ENERGY ASSESSMENT CRITERIA OF INTERMEDIATE PYROLYSIS OF WHEAT STRAW AS A RENEWABLE ENERGY ALTERNATE

Amit Patel
School of Mechanical, Materials and Energy Engineering
Indian Institute of Technology Ropar
amitrp@iitrpr.ac.in

Himanshu Tyagi
School of Mechanical, Materials and Energy Engineering
Indian Institute of Technology Ropar
himanshu.tyagi@iitrpr.ac.in

Prabir Sarkar
School of Mechanical, Materials and Energy Engineering
Indian Institute of Technology Ropar
prabir@iitrpr.ac.in

Harpreet Singh
School of Mechanical, Materials and Energy Engineering
Indian Institute of Technology Ropar
harpreetsingh@iitrpr.ac.in

ABSTRACT

It is largely agreed that emission generation during operation stage of renewable energy is either nil or negligible. Therefore renewable energy is currently assessed purely based on the energy performance and energy produced is considered as green. However growing awareness on the emission released into the environment stresses the need of complete accounting of the energy and emission interaction for other stages of life cycle as well. Therefore, in case of a renewable energy one also needs to consider embedded energy and embedded emission liability during manufacturing, material, transport stage, as well as energy and emission recovery during disposal stage due to recycle or reuse possibility. Intermediate Pyrolysis is a renewable energy alternate it uses wheat straw residue in the form of pellets. The pellets in turn will generate biooil at pyrolyser. This biooil can be used to generate electricity at engine and can replace the use of diesel in the rural area. Present paper demonstrates a method, which considers energy and emission interaction during different scenarios of an Intermediate Pyrolysis technology for its entire life cycle, to select a better alternative.

Keywords: Intermediate Pyrolysis, Embedded Energy, Embedded emission, Energy production time, Emission production time.

1. INTRODUCTION

The use of diesel for off grid electricity generation is very common in the rural India, primarily due to poor reliability of electric supply and contribute to significant emission generation. Emission is also a cause of concern, the way agro residues are currently burned in the open fields. To remove the straw and prepare the field ready for the next harvest farmers follow widespread burning of the agro residue. Emission due to open field burning of agricultural residue is a significant component of emission, comprise of approximately 61% for Asia, and 39% for the rest of the world [1]. A sustainable power generation alternative using straw against the existing widespread open field burning will not only give positive environmental benefit but also would offset the emission resulted due to the use of diesel and other fossil fuels.

In order to address the problem of emission into the environment a technology that uses agro waste and generate electricity can certainly a best alternate. Pyrolysis is a process in which feedstock is heated in the absence of oxygen to obtain vapour and char [2]. Vapour fractions are condensed in a condenser [3], while char can be used as a fuel at boiler and for other thermal applications or as a fertiliser in the field [4] [5].

Energy generation using Intermediate Pyrolysis begins from the field where straw residue is left after harvest. Straw is fed to the chopper. Chopped pieces are supplied to pelletiser. The pellets are then fed to a pyrolyser unit. Pyrolyser will heat the pellets to generate vapours, which will be condensed to produce bio-oil. Bio-oil blend (mixture of bio-oil and biodiesel in 30:70 vol.%) is supplied to a lister diesel engine. Bio-char obtained from the pyrolysis can also be used as a fertiliser in the field, and get added advantage of carbon sequestration [6]. Figure 1

shows flow diagram showing different stages of the Intermediate Pyrolysis process.

Figure 1 Intermediate Pyrolysis process using wheat straw

The objective of the present study is to recommend a method to choose a better renewable energy alternate. For this different scenarios of the pyrolysis process are obtained. This is achieved by considering different system boundaries for the study. System boundary 'A', deals with the scenario in which the biological absorption of carbon by photosynthesis is considered within the system boundary. This will make release of biological emission ($CO_{2,\ biological}$) due to the combustion as carbon neutral to the environment. System boundary 'B', deals with the scenario in which absorption of carbon through photosynthesis considered outside the system boundary. This implies that the biological emission resulted due to the combustion of biomass is no more a carbon neutral. System boundary 'C', deals with the biological absorption of carbon within the system boundary along with the permanent absorption of the carbon within the system boundary. This type of system boundary is relevant when carbon trapped in the char is absorbed permanently inside the system by means of carbon sequestration, while the emission from bio-oil and non-condensed pyrolysis gases is considered as environment neutral. All the three system boundaries are presented in Figure 2.
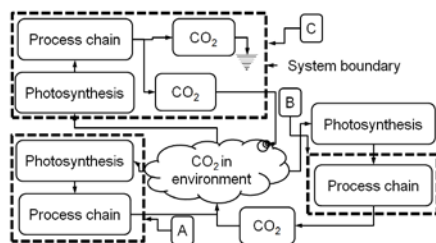
Figure 2 System boundary for case A, B and C

2. Embedded energy and emission

Determination of embedded energy and emission during material, manufacturing, transport and disposal stage will give estimate of the net energy and emission that had already incurred in the process or facility. Calculation of embedded energy and emission is carried out as per the methodology suggested in the literature [7]. Embedded energy (kJ) is converted in to the high grade energy (kWh) using conversion factors as suggested in [8]. In the present case, embedded energy and emission for scaled-up units are assumed to vary in proportion to that of the laboratory scaled unit. A comparative values for the embedded energy and emission for the power generation using diesel, laboratory scale bio-oil process chain (LIP) and scaled-up bio-oil process chain (SIP). Table 2 and 3 summarizes the embedded energy and emission data for the Intermediate Pyrolysis process.

2.1 Diesel and Intermediate Pyrolysis assisted power generation process

Quantity of diesel equivalent to 1 t of straw is considered for the analysis purpose. For 814 kg of diesel considered in the process the refining emission of the diesel is considered as 0.22 kg of CO_2/kg of diesel [9]. The diesel is assumed to be transported to the processing unit. For this transportation emission for light goods vehicle is considered as 0.097 kg of CO_2/t-km [7]. Distance between local petrol pump and nearest refinery is considered as 200 km, and distance of petrol pump from the unit is considered as 10 km. EF of grid is considered as 0.84 kg of CO_2/kWh, this is to consider indirect emission generated due to the use of electricity [10]. Table 1, summarises the inventory data for the Diesel process.

Table 1 Energy and emission during diesel assisted power generation process

	Mass kg	Operation h	Energy kWh	Emission kg of CO_2
Refining	207	--	--	45.6
Transp.	207	--	--	4.22
Engine	--	786	584	660.6
Net under diesel option			631	710.4

Table 2 Embedded energy and emission*

#	Equipment	Energy [MJ]	Energy [kWh]	Emission [kg of CO_2]
I	Chopping	1227	136	86
IIa	Pelletiser	1843	205	128
IIb	Pelletiser	2949	328	205
III	Pyrolyser	8121	902	574
Iva	Engine	3888	432	267
IVb	Engine	6221	691	427
Diesel (IVa)		3888	432	267
LIP (I+IIa+III+IVa)		15079	1675	1055
SIP (I+IIb+III+IVb)		18518	2058	1292

* As per the methodology suggested in literature [7]

Table 3 Flow of energy and emission during Intermediate Pyrolysis process

	Mass kg	Oper h	Energy kWh	Emission kg of CO_2/tonnes
1. Transp.	1000	--	--	4.9
2. Pelletiser	970	97.0	-253	213
3. Pyrolyser	970	48.5	-334	281
4. Engine (lab)	--	790	531	469
5. Gas to flare	330	--	0	503
6. Char	320	--	0	751
7. Transportation	320	--	--	1.6
8.Pelletiser (SIP)	970	1	-15.2	13
9. Engine (SIP)	--	38	733	469
Scenario LIP[A] (1 + 2 + 3 + 4)			-56	500
Scenario SIP[A] (1 + 3 + 8 + 9)			384	300
Scenario LIP[B] (1 + 2 + 3 + 4 + 5 + 6)			-56	2223
Scenario SIP[B] (1 + 3 + 5 + 6 + 8 + 9)			384	2023
Scenario LIP[C] (1 + 2 + 3 + 4 – 6)			-56	-251
Scenario SIP[C] (1 + 3 – 6 + 8 + 9)			384	-451

* lab and ind stands for laboratory and scaled-up capacity unit

3. Emission factor of different systems

Conventionally choosing of a better renewable alternate is decided based by knowing emission factor for a given renewable energy generation process. It is essential to quantify emission intensity and emission reduction potential with respect to a chosen reference system. Two possible reference scenarios considered for the study are, power generation using diesel (Diesel), wherein power generation as well as emission both considered as prime objective. Another is open field burning (OFB) of the straw, wherein objective is to determine emission only. Energy and emission from 1 tonnes of wheat straw for different scenario is presented in Table 4.

Table 4 Emission and EF

Scenario	Emission kg of CO_2 /tonnes	Reduction w.r.t.		Energy kWh/tonnes	EF kg of CO_2/kWh
		Diesel %	OFB %		
OFB*	1723	--	--	--	--
Die	710	--	--	584	1.22
LIP[A]	500	-30	-71	-56	-8.90
SIP[A]	300	-58	-83	384	0.78
LIP[B]	2223	213	29	-56	-39.58
SIP[B]	2023	185	17	384	5.27
LIP[C]	-251	-135	-115	-56	4.48
SIP[C]	-451	-164	-126	384	-1.18

* C in straw (as 47%) x mass (1tonnes of straw) x 44/12

Referring Table 4 it is inferred that scenario SIP can reduce emission by 58% and 83% when switched over from Diesel and OFB option respectively and at the same time it offers 384 kWh of electricity. Scenario LIP[B] and SIP[B] is also relevant if biomass do not satisfy sustainability criteria, e.g. land use change, or crop from peat land, etc. Such scenario actually increases the emission liability and ends up process by adding even more emission compared to the reference systems. Scenario SIP when followed biochar route (SIP[C]), provides emission reduction potential of 164% and 126% when compared with Diesel and OFB option respectively and still giving 384 kWh of electricity. It is worth noting that biochar route can give emission reduction potential greater than 100% due to carbon sequestration effect of biochar. It can be easily established that emission reduction potential or EF for Diesel and SIP[C] are 1.22 and -1.81, i.e. switching from Diesel to SIP[C] scenario may leads to emission reduction of more than 200%.

4. Relative assessment using EPT and EmPT

Limitation of considering emission factor for choosing better renewable energy alternate is that it do not take in to account the embedded energy and emission values and hence do not truly reflect the actual emission. For example, while considering emission from solar photovoltaic (PV), the emission generated to prepare cells is not considered to its fullest extent. Emission from lead oxide that is used in solar cells as a catalyst for contact formation [11] and emission embedded towards battery containing lead is not considered [12].

Embedded energy is the energy invested or sunk into developing the facility or process prior to its operation. Higher these numbers are, larger and more complex the facility required establishing plants and machinery. If a quantity of time is obtained for which the net energy produced by the system equals embedded energy in the process, such quantity will determine the time required to break-even the invested energy in installing plant and machinery. Such energy payback time can certainly be a more realistic and relevant yardstick for the technology comparison. Similarly a break-even emission production time can also be determined. The quantity of time thus obtained in case of embedded energy is referred herein as the energy payback time (EPT). Similar quantity of time in case of embedded emission is referred as emission production time (EmPT).

Quantitative determination of EPT and EmPT is obtained for the present study and presented in Table 5. It is preferred for any technology to have EPT as low as possible (EPT→0), i.e. for any technology, it is preferable to have lower embedded energy and higher Energy Generation Rate (EGR). In case of EmPT, a positive value indicates a time require for the emission while a negative value indicates the emission recovery time. It is preferable

for a given technology to have a higher positive EmPT number, i.e. it should have as lower emission generation rate as possible for a given fixed embedded emission values (EmPT→∞). However, in case of negative EmPT values, i.e. emission recovery instead of emission generation is observed in that case it is preferable to have as faster recovery rate as possible, or lower EmPT number (-EmPT→0). Figure 3, shows the behaviour of EPT and EmPT for different numeric values. It is important to note that point (0, ∞) could be an ideal choice of positives values of EPT and EmPT. However for the cases when EPT has positive values and EmPT is negative, (0, 0) could be the ideal choice. While selecting between two relative options of technology the preference should be given to the technology having lower values over the plot of EmPT v/s EPT.
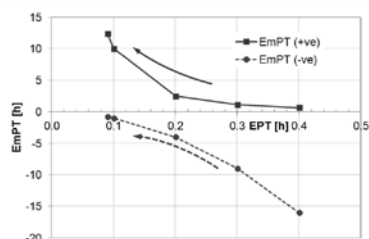
Figure 3 Behaviour of EPT and EmPT

Table 5 EPT and EmPT

Scenario	EGR kWh/h	EmGR kg of CO_2/h	EPT H	EmPT h	Switch from Diesel?
Dies	3.30	4.02	131	66	--
LIP[A]	-0.33	2.95	-5065	357	Never
SIP[A]	11.78	9.20	175	139	May be
LIP[B]	-0.33	13.13	-5065	80	Never
SIP[B]	11.78	35.22	175	36	No
LIP[C]	-0.33	-1.48	-5065	-712	Never
SIP[C]	11.78	-13.84	175	-92	Must be

Table 5, shows values of Energy Generation Rate (EGR), Emission Generation Rate (EmGR), Energy Payback Time (EPT) and Emission Production Time (EmPT). Switching from Diesel to LIP[A] or LIP[B] or LIP[C], would increase EPT. This adds limit to the feasibility of such a switch over, irrespective of increase in EmPT or decrease of EmPT. Such switch over may be environmentally attractive, but from an energy point of view it is not rewarding. Switching from Diesel to SIP[A], it is observed that there is a slight increase in EPT, but four times increase in EmPT, so in the overall such switch over is preferred, even if it is little less attractive from an energy point of view. Switching from

Diesel to SIP[B] it is observed that there is neither gain in terms of energy or emission front and no point in going for switchover. Switching from Diesel to SIP[C] it is observed that there is a slight increase in EPT. However the negative sign of EmPT suggests that there is actually emission recovery, therefore such option is more favourable and must be preferred.

REFERENCES
[1] S. Garg, "Trace gases emission from field burning of crop residues." Indian Journal of Air Pollution Control Vol. 1 pp 76-86, 2008.
[2] R. J. Evans and T. A. Milne, "Molecular characterization of the pyrolysis of biomass. 2. Applications," *Energy & fuels*, vol. 1, no. 4, pp. 311–319, 1987.
[3] A. V. Bridgwater, D. Meier, and D. Radlein, "An overview of fast pyrolysis of biomass," *Organic Geochemistry*, vol. 30, no. 12, pp. 1479–1493, 1999.
[4] D. Woolf, J. E. Amonette, F. A. Street-Perrott, J. Lehmann, and S. Joseph, "Sustainable biochar to mitigate global climate change," *Nature Communications*, vol. 1, no. 5, pp. 1–9, Aug. 2010.
[5] J. Major, "A guide to conducting biochar trials," *International Biochar Initiative*, 2009.
[6] M. Ouadi, J. G. Brammer, A. Hornung, and M. Kay, "Waste to power," *TAPPI Jr. of Bioenergy*, vol. Vol. 11 No. 2, pp. 55–64, Feb. 2012.
[7] M. F. Ashby, *Materials and the environment: eco-informed material choice*. Butterworth-Heinemann, 2012.
[8] S. Chr H. and N. Stefan, "Life Cycle Assessment of the Wave Energy Converter: Wave Dragon," 2005.
[9] UNIDO, "Global Technology Roadmap for CCS in Industry Sectoral Assessment: Refineries, for United Nations Industrial Development Organisations, Report No./DNV Reg No.:/12P5TPP-9, Draft Rev 3, 2010-08-25." 2010.
[10] M. of P. GoI, "CO2 Baseline Database for the Indian Power Sector, User Guide, Version 6.0 Government of India, Ministry of Power, New Delhi," Mar. 2011.
[11] T. Ellison and J. Szabo, "RoHS Implementation Challenges," 2006.
[12] A. Patel, P. Sarkar, H. Tyagi, and H. Singh, "Time value of emission and technology discounting rate for off-grid electricity generation in India using intermediate pyrolysis," *Environmental Impact Assessment Review*, vol. 59, pp. 10–26, Jul. 2016.

SEEC-2017-127

Synthesis of Task specific Brønsted acid Ionic liquids (BAILs) from Citrus waste as Renewable feed stock for Production of 5-hydroxylmethylfurfural (HMF) therefrom

Pratibha Dwivedi, Rajender S. Sangwan, Bhuwan B. Mishra
Center of Innovative and Applied Bioprocessing (CIAB), Knowledge City, Sector 81, Mohali,
Punjab, India

ABSTRACT

The d-limonene occurs naturally in fresh peel of citrus fruits. A substantial amount of citrus waste is generated world-wide at fruit juice industries. Global production of d-limonene in 2014- 2015 was ~80000 tons with an installed capacity of ~300 orange oil distillation plants worldwide for supply of technical grade (95% in d-limonene) or food grade (96% in d-limonene) orange oil. Despite d-limonene and its oxygenated derivatives (menthol, carveol, and carvone) have great market potentials such as insecticide, solvents, fine chemicals, flavors, fragrances, fuels etc., there is hardly any report so far as on high-value applications and products. In recent years, biobased ILs are being proposed as preferred solvents for recovery of resources from biomass and/or serving as a bioprocessing agent. Therefore, realizing a closed-loop biorefinery that sustains its own need for process solvents in addition to the production of bioderived chemicals, we investigated the citrus processing waste for extraction of d-limonene, its conversion to p-cymenesulphonic acid (p-CSA), and finally the preparation of a library of p- CSA based task specific Brønsted acid ionic liquids (BAILs) by coupling with diverse range of onium ions. The developed BAILs were further screened as a catalyst/solvent in processing of citrus waste for production of 5-hydroxyl methyl furfural (HMF), a biobased platform chemical that can be valorized into a spectrum of fuels and chemicals.

SEEC-2017-128

An Experimental Investigation of Performance-Emission Trade off of a CI engine Fueled by different blends of Diesel-Ethanol and Diesel-Biodiesel-Ethanol.

Probir Kumar Bose[1], Abhishek Paul[2] , Rahul Banerjee[2],

[1] Campus Director, NSHM Knowledge Campus Durgapur Group of Institutions
[2] Assistant Professor, NIT Agartala

Abstract

Ethanol due to its low latent heat of vaporization has the ability to reduce ci engine's NO_x and CO_2 emission. But along with that it also deteriorates the performance of the engine. On the other hand, biodiesel improves the performance of the engine but increases the emission too. The present study deals with an approach where the potentials of both ethanol and biodiesel has been combined in order to utilize the benefits of both. Initial phase of this work comprises of a miscibility study, in which the miscibility limit of ethanol in diesel has been found out and then this limit has been extended by virtue of biodiesel inclusion. The results indicates that biodiesel increases the miscibility of ethanol in diesel. The performance and emission studies indicates that low ethanol addition increase B_{th} and decrease the equivalent BSFC of the engine with very low emission of NO_x and smoke opacity. Diesel-biodiesel-ethanol (DBE) blends shows appreciable increase in b_{th} with appreciable reduction in equivalent BSFC. DBE blends also showed commendable reduction in hydrocarbon emission.

Keywords

Diesel, Ethanol, pongamia piñata methyl ester, NO_x reduction, NOx-smoke-BSFC tradeoff.

1 Introduction

Energy is one of the key factors that dictates the socio-economic development and quality of life in any modern country today. Major portion of this energy demand is met with conventional energy sources, mainly fossil fuel. Majority of the countries around the world import crude oil to meet their energy demands. As a result of which bulk of their national income is spent for purchasing petroleum and its derivatives. India also being a developing country with insignificant petroleum reserves has to spend almost 80% of its export earnings for this purpose [1].

Much of the research in the field of non-conventional fuel sources today are concentrated on biofuels. Now there are a whole bunch of sources that have the potential to become an important energy provider in near future. One such bio fuel is ethanol. Although ethanol is already used as a SI engine fuel, but the concept of its usage in CI engine is still in experimental stage. Ethanol cannot be used as CI engine fuel unless it is blended with any other heavier oils such as diesel.

The works of Lapuerta et al. [2], Huang et al. [3], Kwanchareon et al. [4] establishes the fact that ethanol has limited miscibility in diesel. As per the works of Irshad Ahmed [5] ,Ali Mohammadi et al. [6], Bang-Quan He et al.[7], Hardenberg and Schaefer [8], Li et al [9] ,Özer Can et al [10], Yan et al.[11], Lebedevas et al.[12] , Kumar et al.[13] , etc, the NO_x reduction potential of ethanol was found to be quite appreciable. These studies also pointed out an inherent penalty of reduced brake thermal efficiency, considerably high fuel consumption and high emission of unburned hydrocarbon, smoke and CO in exhaust. Again the works of kumara,et al.[14], Yamane et al. [15], Agarwal et al. [16], Banapurmath et al. [17], Nabi et al. [18], Dwivedi et al [19], Sahoo et al.[20], Basha et al. [21] explores the potential of biodiesel to improve brake thermal efficiency and reduce fuel consumption. It is also found that biodiesel and its blends increase NO_x and CO_2 emission but reduces hydrocarbon emission.

The present work aims to combine the performance and emission advantages of biodiesel and ethanol in improving the performance of a single cylinder CI engine and reducing its emission subsequently.

2 Experimental details and methodology

2.1 Fuel selection and bland preparation

Generally, ethanol can be blended with diesel with no engine modifications required [22]. One of the major research activities in the field of e-diesel is the formulation of emulsifiers as ethanol is not miscible in diesel over a wide range. Different studies have proved that water-free ethanol has good miscibility with diesel fuel at room temperature in warm countries as separation begins to occur either when the mixture is doped with water or when temperature drops below 10°C [23]. In course of the present work, the miscibility of ethanol in diesel was extensively studied. From the study it was concluded that ethanol is miscible in Diesel upto 10% V/V. So, 2 blends were seleced, on with 5% V/V ethanol in 95% diesel and the other with 10% ethanol and 90% Diesel. Further increase of ethanolshowed a delayed phase

separation. So in order to reduce this phase separation phenomenon of ethanol in diesel, *Pongamia piñata* methyl ester has been used as a co solvent. Ethanol percentage was incremented to 15 and 20% with inclusion of PPME and the blends were produced as D40E15B4 and D30E20B50. The blends are shown in Fig 1 and their properties are shown in Table-1.
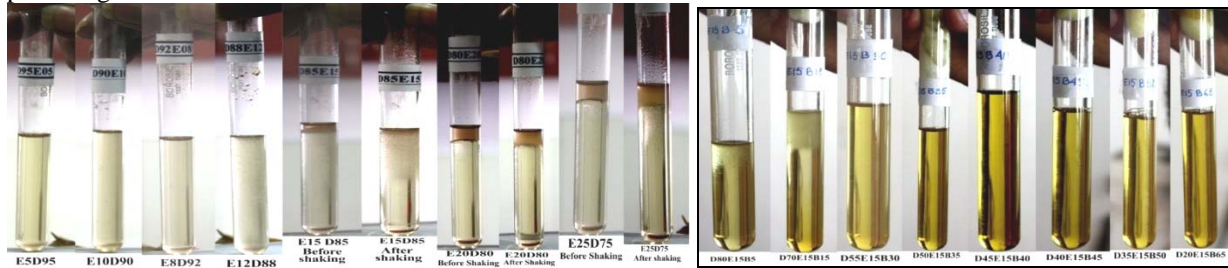
Figure:-1: Ethanol-Diesel and Diesel-ethanol-biodiesel blends

Property	Diesel	Biodiesel	Ethanol	E5D95	E10D90	D40E15B45	D30E20B50
Density (kg/m^3)	820	886	789	818.45	816.9	845.05	846.8
Kinematic Viscosity(cSt)	2.51	8.68	1.09	2.44	2.37	5.22	5.4732
Calorific Value (KJ/Kg)	42650	35866	26950	41893.24	41133.62	37250.46	36175.3
Flash Point (°C)	52	217	12.77	50.04	48.07	120.36	126.65
Fire Point (°C)	64	220	13.5	61.475	58.95	126.625	131.9
Cetane Number	46	35	7	44.05	42.1	35.2	32.7

Table -1: Properties of Fuel Blends

2.2 Experimental setup

A schematic diagram of the experimental setup is shown in Figure-2. The engine used for this study was a 3.56Kw 4 stoke single cylinder water cooled CI engine. The specifications of the engine is given in Table- 2. The engine was equipped with an eddy current dynamometer. The engine RPM was measured by a crank angle. A piezoelectric pressure transducer (Make: KISTLER) was used to measure in cylinder pressure. The analog pick up voltages of the transducers were fed to a NI-DAQ card through a signal conditioner to filter the out noise. The presence of CO_2, NO_x and UBHC in exhaust emission was detected by means of an AVL 5 gas analyzer (AVL Digas 444) and the smoke opacity was measured by an AVL smoke meter (AVL Digas 437).

Figure:-2: Complete Experimental Setup Diagram.

Engine Type	Kirloskar, Model TV-1, 4 stoke Water cooled,VCR Engine.
Bore and Stoke	87.5 mm and 110mm
Max. Power	3.6 Kw
CR Range	12-18
Swept Volume	661 cc
Combustion System	Direct Injection.
Fuel Injection Pressure	205 BAR

Table-2: Specifications of Test Engine.

3 Results and discussion

The effect of ethanol concentration in diesel and biodiesel was performed at room temperature condition and the results are represented as performance and emission parameters.

3.1 Performance parameters

In this present study brake thermal efficiency (B_{th}), and BSFC diesel equivalent has been analyzed as the indices of performance characteristics of different duel fuel operation.

3.1.1 Brake thermal efficiency.
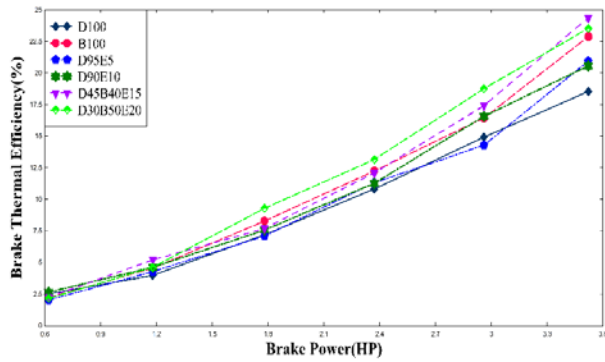
Figure: 3:- Variation of brake thermal efficiency with brake power.

Fighter: 4:- Variation of BSFC Diesel Equivalent with brake power

The variation of B_{th} of the engine for different fuel samples is shown in figure no-3. It is quite apparent from the figure that ethanol caused a small improvement in B_{th} of the engine, especially 5% ethanol (V/V) in D95E5 blend at lower load conditions. As the load increased blends with higher ethanol percentage showed better Bth. Again inclusion of PPME in the blend showed further improvement in Bth with D30E20B50 showing the highest improvement in Bth. These improvements may be attributed to the completeness in combustion due to release of fuel bound oxygen by ethanol and PPME.

3.1.2 BSFC diesel equivalent

BSFC diesel equivalent defines the fuel sample's equivalent amount of diesel that would produce a unit of power. For the present study, the fuel consumption of the engine is shown in figure-4 in terms of BSFC diesel equivalent. It can be seen in the figure increase in ethanol content in diesel increases the fuel consumption of the engine. The combination of biodiesel and ethanol in diesel also produced almost the same fuel consumption as that of diesel, with occasional reduction at low load conditions. At at 0.62Hp brake power D45B40E15 blend reduces the fuel consumption by 24.86% whereas D30B50E20

reduces it by 25.20%. At all other load conditions diesel –biodiesel-ethanol blends showed minor increase in fuel consumption, but significant improvement in brake thermal efficiency as discussed in section 3.1.1.

3.2 Emission parameters

In this present study, NO_x and Unburned hydrocarbon has been analyzed as these are of major concern in terms of pollution reduction.

3.2.1 NO_x and HC emission

Nitric oxide and Nitrogen di oxide, collectively known as NO_x is one of the most alarming emission from an engine. Figure-6 shows the variation of NO_x emission from the engine for different fuel samples. It can be seen from Fig 5 that although ethanol inclusion reduced the overall NOx emission at high load conditions, but it increased with inclusion of PPME in the blend. The HC emission shown in Fig-6 also supports this trend. The increase in NOx emission and decrease in HC emission with D-E blends may be due to cooling effect caused by ethanol. For D-E-B blends the improvement in combustion due to PPME may be the more prominent to overcome this cooling effect.

Fighter: 5:- Variation of NO_x emission with brake power.

Fighter: 6:- Variation of UBHC with brake power.

3.3 Trade off study

Figure-7 shows a comparative study of different blends on the basis of a NO_x-Smoke opacity-

BSFC diesel equivalent tradeoff analysis. The operation with plain diesel is shown by zone A. as it can be seen from the figure that biodiesel

pushes the tradeoff zone towards the higher side of the ordinate which depicts high NO_x emission. Although Zone B corresponds to very low Smoke opacity and low equivalent BSFC, but the high amount of NO_x certainly reduces it practical applicability. Zone C is the operational zone of diesel-biodiesel-ethanol blends. As it can be seen D-B-E blends not only pushes the tradeoff zone toward relatively higher NO_x emission but also towards higher smoke opacity. Only positive aspect in this region is occasional low equivalent BSFC especially with D30B50E20 blend for higher load conditions. Except at 0.6HP brake power the blend showed reasonable low equivalent BSFC at all operating conditions. The blend also shows reasonably low NO_x emission and smoke opacity compared to D30B50E20 blend, but then also it is higher than those of diesel.
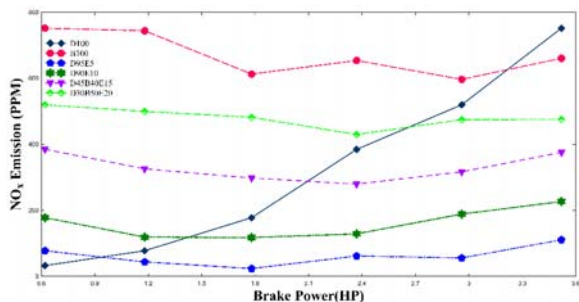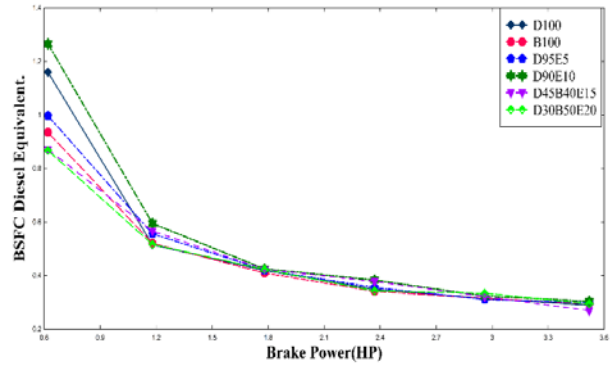

Fighter: 7:- Variation of NO_x and Smoke Opacity with BSFC Diesel Equivalent.

The blend D90E10 operates in between zone A and zone C with relatively low equivalent BSFC but higher NO_x and smoke opacity then diesel. Zone D defines the operating zone of diesel-ethanol blend D95E5. It is quite clear upon observation that of all the fuel samples tested in this study, D95E5 has the best performance-emission characteristics. Except at 3.6HP brake power all operating conditions shows lower smoke opacity then diesel. All operating conditions shows very low equivalent BSFC, which is significantly lower than diesel operation. So other than very low and very high loading conditions, D95E5 performed with significantly low equivalent BSFC, commendably low NO_x and lowest smoke opacity.

5 Conclusion

The miscibility of ethanol is by and large limited to 10% v/v in diesel. One of the method of increasing its miscibility is introduction of biodiesel that acts as amphiphilic agent and creates a bond between diesel and ethanol.

During performance test of the engine, highest brake thermal efficiency was observed with D30B50E20, followed by D45B40E15 blends Diesel-ethanol blends also showed increase in brake thermal efficiency as compared to diesel. But increase in ethanol percentage showed reduction in Bth. However, diesel-ethanol blends showed increase in equivalent BSFC and the fuel consumption increased with increasing ethanol percentage.

Upon analysis of emission parameters, it was observed that biodiesel showed highest amount of NO_x emission, followed by D30B50E20 and D45B40E15 blends respectably. It was also observed that biodiesel showed lowest unburned hydrocarbon. D30B50E20 and D45B40E15 blends also showed lower hydrocarbon emission, but noteworthy decline in NO_x emission. The tradeoff study of NO_x-smoke opacity and BSFC diesel equivalent gave a comparative assessment for all the fuel samples combining their performance-emission potentials, on the basis of which it can be clearly seen that diesel-ethanol blends even with a reduced performance index shows good potential to reduce diesel dependency in heavy duty transportation sector.

Reference

1. Sahoo PK, Naik SN, Das LM. Studies on biodiesel production technology from Jatropha curcas and its performance in a CI engine. J Agri Eng, Indian Soc Agri Eng (ISAE) 2005;42(2):18–24.

2. Lapuerta M , Armas O, Herreros JM; Emissions from a diesel–bioethanol blend in an automotive diesel engine; Fuel 87 (2008) 25–31.

3. Huang JC , Wanga YD, Li SD , Roskilly AP , Yu HD , Li HF; Experimental investigation on the performance and emissions of a diesel engine fuelled with ethanol–diesel blends; Applied Thermal Engineering 29 (2009) 2484–2490.

4. Kwanchareon P, Luengnaruemitchai A, Jai-In S; Solubility of a diesel–biodiesel–ethanol blend, its fuel properties, and its emission characteristics from diesel engine; Fuel.2006.09.034.

5. Ahmed I: Oxygenated Diesel: Emissions and Performance Characteristics of Ethanol-Diesel Blends in CI Engines; presented at Future

SEEC-2017-129

OPTIMIZATION OF ASTAXANTHIN PRODUCTION FROM YEAST MALT MEDIA BY PHAFFIA RHODOZYMA MTCC-7536

Amit H. Batghare
Indian Institute of Technology, Guwahati
Email: amit.batghare@iitg.ernet.in

Neha Singh
Indian Institute of Technology, Guwahati
Email: neha.singh@iitg.ernet.in

V S Moholkar
Indian Institute of Technology, Guwahati
Email: vmoholkar@iitg.ernet.in

ABSTRACT

Astaxanthin is a naturally occurring carotenoid found in marine organisms, including microalgae, crustaceans, salmon, and trout. This is a potent and safe anti-oxidant/anti-inflammatory that can improve the health and vitality of both humans and animals. It may also reduce oxidative stress in the nervous system, reducing the risk of neurodegenerative diseases. On commercial scale, astaxanthin is currently produced through chemical synthesis which may cause hazardous effects on human health and hence it is necessary to produce it in a greener way i.e. through the fermentation using microorganism such as Phaffia rhodozyma yeast.

The aim of this paper is to investigate the effect of medium components (YM media) and environmental factors (Initial pH and temperature) on astaxanthin production in Phaffia rhodozyma. The environmental factors were optimized using Central Composite Design and the optimum initial pH and temperature for astaxanthin production were 4.94 and 19.84 Centigrade respectively with total astaxanthin yield of 147.293 µg/g of yeast. Subsequently the optimum medium components (glucose 8.93 g/L, peptone 3.45 g/L, yeast extract 3.07 g/L and malt extract 2.31 g/L) were determined with Box-Behnken Design method. After 120 hr fermentation under the optimal incubation conditions, the maximum astaxanthin yield was 158.146 µg/g of yeast. A statistical method of RSM for evaluating process optimization was proposed for astaxanthin production from Phaffia rhodozyma.

Keywords: Phaffia rhodozyma, Astaxanthin, Medium components, Environmental factor, Optimization

SEEC-2017-130

INFLUENCE OF BIO-LUBRICANT ON THE COMBUSTION CHARACTERISTICS IN BIODIESEL OPERATED CI ENGINE

Arup Ratan Dey
Department of Mechanical Engineering
Research Scholar
Email: arupratanmech09@gmail.com

Rahul Dev Misra
Department of Mechanical
Engineering
Professor
rdmisra@gmail.com

ABSTRACT

Global warming and rapid depletion of the fossil fuel content forced the civilization to shift their paradigm of interest towards alternative sources of energy. In this regard, biodiesel, gain popularity as alternative fuel in CI engine applications. Lubrication is one of the most important part of CI engines and mineral lubricants are used in this purpose generally. Straight vegetable oils seem to be a promising alternative to the mineral lubricants due to the biodegradability. While using mineral lubricant with biodiesel blends there are certain effects of fuel in lubricant properties. Therefore, the study of the effect of infiltration of lubricant into the fuel side on the combustion characteristics have been considered in the present work. For that, the combustion characteristics of the palm biodiesel blend–palm SVO pairs are compared with Diesel–mineral lubricant pair for 60 hrs operation and it is concluded that the same PB30–palm SVO pair may be considered as the most suitable combination.

Keywords *Bio-lubricant, Biodiesel, Heat Release Rate*

INTRODUCTION

Rapid depletion of limited fossil fuel due to over exploitation along with the deterioration of environmental condition has forced the researchers to look forward towards alternative sources of energy. The major global source of Green House Gas GHG emiss ions are due to the burning of fossil fuels. Deteriorating environmental conditions have become a major issue of public concern across the globe. Due to lack of efficient and economic production technology, storage and supply, and commercial and social barriers these options are still in their preliminary stages. Clean and renewable biofuels have been touted as the answer to the issue of diminishing fossil fuels [1-3]. Although, use of fossil fuels can be reduced through the introduction of biodiesels, still mineral oils are vastly used in the engine lubrication systems. These mineral lubricants, being petroleum derived products, are very harmful for the ecosystem. Moreover, the disposal of the mineral lubricant is also dangerous for the ecosystem. Vegetable oils have been investigated as prime replacement for the mineral lubricant due to their inherent qualities like biodegradability, renewability. The use of vegetable oils as lubricants is not a new. Vegetable oils are widely used as lubricants in different applications since the Egyptian age [4]. In this context, straight vegetable oils seem to be a promising option. Many researchers work on this aspect to establish the vegetable oil as a good alternative for the mineral lubricant and found that vegetable oils have better wear property and anti-friction quality with some poor thermal and oxidation stability [5-7]. Maximum researchers explained the performance and emission characteristics of biodiesels are using mineral lubricant in CI engine and found that 20% biodiesel blends are considered as best. Some of the researchers found out better lubricating property while using biodiesel as fuel on the contrary some researchers found adverse lubrication property while using biodiesel as fuel compared to diesel as fuel. So there is a certain possibility of infiltration of lubricating oil into the combustion space [8-9]. The

combustion characteristics of the biodiesel blends such as peak pressure and the heat release rates also plays vital role in the engine operations. Therefore, the study of the effect of infiltration of lubricant into the fuel side on the combustion characteristics hasbeen considered in the present work for long term engine operation. On the basis of availability, cost and the reduction of importance as a food source palm oil and their various blends along with selected as fuel. Palm SVO and mineral lubricant SERVO 40, as specified by manufacturer is used as lubricant for the present work. The combustion characteristics of the palm biodiesel blends with palm oil parent SVO as lubricant are compared with conventional diesel fuel with mineral oil as lubricant for 60 hrs operation in order to achieve the desired goal.

MATERIALS AND METHODS

Fuel and Lubricant Samples

On the basis of the objective of the present work, any bio-oil may be selected. The palm oil is one of the leading vegetable oils produced globally, and most consumed oil around the world. The palm oils have mainly been cultivated in tropical climatic conditions like Indonesia, Malaysia and Thailand in Southeast Asia, and other African countries. Indian tropical forests and climate especially in the south Indian climate is suitable for the production of the palm oil. The refined palm oil is easily available and due to the reduction in their food value palm oil is available at reasonable cost. Therefore, the refined palm oil is selected to be used as lubricant and its transesterified derivative, i.e. palm biodiesel, as fuel in the present work. The conventional mineral lubricant considered for the present work is SERVO 40, which is most commonly used lubricant for the considered engine. This mineral lubricant is used when the engine is fuelled with diesel. Fuel samples are prepared by blending 20%, 30%, 40%, and 50% by volume of palm biodiesel with diesel oil. These 4 blends are denoted by PB20, PB30, PB40 and PB50. Diesel is also considered as one of the fuel samples. The physio-chemical properties of various biodiesel blends and the lubricant samples are presented in Table 1.

TABLE 1: PHYSIO-CHEMICAL PROPERTIES OF FUELS AND LUBRICANTS

Properties	PB20	PB30	PB40	PB50	PB100	Diesel	Palm SVO
Density, kg/m^3	842.3	848.7	854	859.4	865	835	916
Kinematic Viscosity @ 40° C, cst	3.17	3.63	3.96	4.22	4.66	2.85	36.2
Calorific value, MJ/kg	42.58	41.94	41.55	41.12	38.61	44.62	36.8
Flash point, °C	94	107	119	127	160	70	-
Cloud point, °C	9.3	10.7	11.9	12.8	14	6.40	16.0
Pour point, °C	5.5	6.1	7.7	8.1	8.50	3	11.0
Cetane index	50.21	50.65	50.83	51.11	55.8	48	-

Experimental set up

As India as an agricultural country The use of the small diesel engines in the agricultural sector is very common, In the present work a single-cylinder four-stroke water cooled diesel engine is used for evaluation of the combustion characteristics of all the palm biodiesel blends along with diesel. The test engine is coupled with an eddy current dynamometer and the loading was controlled by a load console. Two separate fuel tanks are used along with a two-way fuel supply line for supplying palm biodiesel blends and diesel separately to the engine. The entire engine test is operated by Enginesoft LV software installed on a computer.

Experimental Procedure

The fuel blends prepared for experimentation are first characterized for their properties. The experimental setup is then made ready for diesel fuel with mineral oil SERVO 40, as specified by manufacturer as lubricant. The experimentations are then carried out for 60 hours of operation as long term engine operation. The engine combustion characteristics are recorded for every 10 hrs of engine operation. After that the mineral lubricant oil is replaced with palm oil for the PB20, PB30, PB40 and PB50 fuel blends. The experimentations for each of these fuel blends are then carried out for 60 hours of operation. The engine combustion characteristics for each of these fuel blends are recorded for every 10 hrs of engine operation. The engine loading conditions for the engine performance tests are carried out following the IS: 10000, Part IX 1980. The test is conducted for a total of 60 hours for each blend consists of 6 running cycles of 10 hrs each. The combustion characteristics data are considered for the 7 different loading conditions i.e. 0%, 25%, 50%, 75%, 85%, 90% and 100%. These data are then used for comparative assessment of the considered pairs of fuel blends and lubricant. To simplify the combustion analysis the combustion data for all the biodiesel–lubricant pairs only 90% loading condition combustion data are presented in the result and discussion portion.

RESULT AND DISCUSSIONS

Various blends of palm biodiesel with diesel PB20, PB30, PB40 and PB50 are tested in the engine set up, after carrying out the fuel characterization tests for each blend. Firstly the engine is run with conventional lubricant SERVO 40 fuelled with diesel for 60 hours and then the engine is run with the parent SVO as lubricant for each of the biodiesel blend for 60 hours. In this work, results of the combustion characteristics of all the considered fuel blends with palm SVO and diesel with mineral lubricant different loading conditions on the engine, i.e., 0%, 25%, 50%, 75%, 85%, 90% and 100% for 60 hrs with 10 hrs interval are evaluated. The engine combustion parameters considered in this work are Peak pressure and Heat release rate.

In-Cylinder Peak Pressure
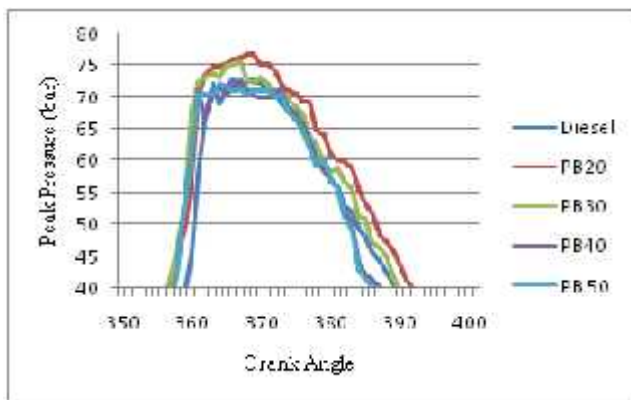
**FIGURE 1.** IN-CYLINDER PEAK PRESSURE FOR PALM BIODIESEL BLEND–PALM SVO PAIRS AFTER 60 HOURS OF ENGINE OPERATION

The variations of in-cylinder peak pressure of palm biodiesel fuel blends–palm SVO lubricant pairs along with diesel fuel–mineral lubricant pair 60 hours of engine operation at 90% load condition are presented in Fig. 1. Peak pressure of the biodiesel blends are generally increased with increase in biodiesel contents in the blends. This is mainly due to the higher cetane number of the biodiesel blends which reduces the ignition delay of biodiesel blends. Moreover, the oxygen content of these biodiesel blends, results in better combustion of these blends, may also result in higher peak pressure compared to diesel. When palm SVO is used as lubricant they reduce the frictional losses resulting in higher peak pressure. But when the less cetane number palm SVO lubricant infiltrates into the combustion space they reduce the cetane number of the biodiesels resulting in reduction of peak pressure. But the more oxygen content present in the SVO lubricants results in better combustion, may also result in

higher peak pressure compared to diesel. When PB20 and PB30 blends with palm SVO lubricant used due to the infiltration of less viscous fuels into the lubrication sump they reduce the frictional effect more, results in higher peak pressure. But in case of the PB40 and PB50 blends the viscosity of these blends are higher which results in improper combustion. Due to the improper combustion the peak pressure of the PB40 and PB50 blends gets reduced.

Heat Release Rate
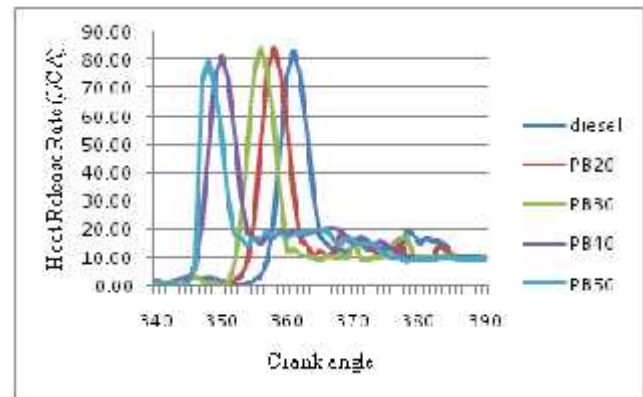
FIGURE 2. HEAT RELEASE RATE FOR PALM BIODIESEL BLEND–PALM SVO PAIRS
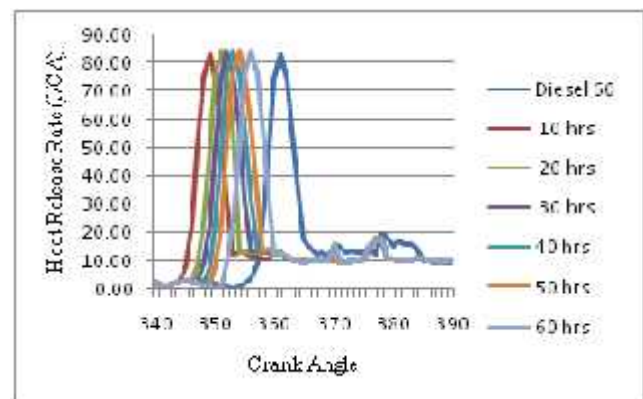
FIGURE 3. HEAT RELEASE RATE OF PB30 FOR EVERY 10 HRS OF OPERATION WITH DIESEL WITH MINERAL LUBRICANT AFTER 60 HOURS OF ENGINE OPERATIONS

The variations of heat release rate of palm biodiesel fuel blends–palm SVO lubricant pairs along with diesel fuel–mineral lubricant pair 60 hours of engine operation at 90% load condition are presented in Fig. 2 and the variations of heat release rate of PB30–palm SVO lubricant along with diesel fuel–mineral lubricant pair for every 10 hours of engine operation at 90% load condition are presented in Fig. 3. Combustion in CI engine, takes place primarily in two phases: premixed combustion and diffusion

combustion. The factors that govern the relative amounts of these two phases of combustion are engine load, injection timing, and viscosity, CN of the fuel and the oxygen contents of the fuel.

The combustion in CI engine with biodiesel blends is greatly influenced by the CN of the blends. Increased CN reduces the ignition delay resulting in lesser intense premixed combustion phase. However, the higher heat release rate of diesel is due to the increased accumulation of the fuel during relatively longer delay period. Because of shorter ignition delay, the maximum heat release rate occurs early for biodiesels than when compared with diesel. As a result of improved combustion during the main combustion phase due to the higher oxygen content of the fuel, the heat release rate for biodiesel blends is less during the late combustion phase.

When the palm biodiesel–palm SVO lubricant pairs are used the presence of palm SVO lubricant due to the infiltration of lower CN palm SVO blends into the combustion space they increase the delay period resulting in lesser heat release rate. But due to the infiltration of more oxygenated SVO increase the combustion also the palm SVO as lubricant reduce the frictional losses results in higher heat release rate. But in case of the PB40 and PB50 blends, due to the expected effects of higher viscosity on fuel spray, reduction of air entrainment and fuel/air mixing rates. At the time of ignition, less fuel/air mixture is available for combustion and as a result more burning occurs in the diffusion combustion phase rather than in the premixed phase results in reducing heat release rate

CONCLUSIONS

The work presented in this paper clearly demonstrated the effect of infiltration of bio-lubricant into the combustion space on combustion characteristics for long term engine operation. Infiltration of palm SVO lubricant into the fuel side acts as an additive to the palm biodiesel fuel blends. It is concluded that this infiltration is beneficial up to certain level and as a result PB30 palm biodiesel fuel blend with palm SVO as lubricant emerged out to be most suitable blend compared to other fuel–lubricant pairs considering combustion characteristics.

REFERENCES

[1] Chakraborty, R., Das, S., and Bhattacharjee, S.K., 2015. "Optimization of biodiesel production from Indian mustard oil by biological tri-calcium phosphate catalyst derived from turkey bone ash". Clean Technol Environ Policy, 17, pp. 455-463.

[2] Mahipal, D., Krishnanunni, P., Mohammed, R.P., and Jayadas, N.H., 2014. "Analysis of lubrication properties of zinc-dialkyl-dithio-phosphate ZDDP additive on Karanja oil *Pongamiapinnatta* as a green lubricant". Int J Eng Research, 3, pp.494-496.

[3] Aalam, S.C., Saravanan C.G., and PremAnand, B., 2015. "Reduction of Emissions from CRDI Diesel Engine Using Metal Oxide Nanoparticles Blended Diesel Fuel". Int J Appl Eng Res. 10, pp.3865-3869.

[4] Gawrilow, J., 2009. "Interfacing with the global oils and fats business, palm oil usage in lubricants". http://www.americanpalmoil.com..

[5] Najman, M.N., Kasrai, M., and Bancroft, G.M., 2004. "Chemistry of Antiwear Films from Ashless Thiophosphate Oil Additives", Tribology Letters, 17, pp. 217-229.

[6] Shah, F.U., Glavatskih, S., and Antzutkin, O.N., 2012. "Novel Alkylborate–Dithio-carbamate Lubricant Additives: Synthesis and Tribophysical Characterization" Tribology Letters, 45, pp. 67-78.

[7] Luna, F.M.T., Cavalcante, J.B., Silva, F.O.N., and Cavalcante Jr, C.L., 2015. "Studies on biodegradability of bio-based lubricants", Tribology International, 92, 301-306.

[8] Sinha, S., and Agarwal, A.K., 2008. "Experimental investigations of the tribological properties of lubricating oil from biodiesel fuelled medium duty transportation CIDI engine", SAE Technical Paper no 2008-01-1385.

[9] Gopal, K.N., and Raj, R.T.K., 2016, "Effect of pongamia oil methyl ester- diesel blend on lubricating oil degradation of DI compression ignition engine", Fuel, 165, pp.105-114.

.

SEEC-2017-131

ETHANOL PRODUCTION FROM WHEY USING A NOVEL YEAST ISOLATE

Gisha Singla
Center of Innovative and applied Bioprocessing
(CIAB), Mohali
Email: singla.gisha@gmail.com

P. S. Panesar
Sant Longowal Institute of Engineering & Technology
Longowal
Email: pspbt@yahoo.com

R. S. Sangwan
Center of Innovative and applied Bioprocessing
(CIAB), Mohali
Email: sangwan.lab@gmail.com

M. B. Bera
Sant Longowal Institute of Engineering & Technology
Longowal
Email: pspbt@yahoo.co.in

ABSTRACT
Whey is a liquid byproduct of dairy industry, which is obtained by coagulating and separating the casein proteins from whole or skim milk. During cheese making process, whey is produced as a byproduct and represents 90% of the volume and 50% of the solids of milk. The composition of whey varies according to its origin and to the cheese-making process employed. The disposal of whey by most of milk plants which do not have proper pre-treatment system is the major problem and there occurs significant loss of potential food and energy source, since whey contains lactose, soluble proteins, lipids and mineral salts. Fermentation of whey to value added products has received wide attention. In the present investigation, a new yeast isolate has been tested for the ethanol production from whey and a comparison was made with existing yeast cultures procured from different culture collection centers. Among the yeast cultures tested, maximum ethanol production was obtained with new yeast isolate identified as Kluyveromyces marxianus WIG 2. Further, the medium and process optimization was also carried by the supplementation of various nitrogen sources, salts and varying other parameters (pH, temperature and incubation period) to maximize ethanol production from whey. Maximum ethanol production (1.79%) and lactose utilization (90.25%) was observed with supplementation of corn steep liquor and sodium chloride at an optimal pH of 5, temperature 35ºC, after incubation period of 40 hrs.

Keywords: Yeast, Fermentation, Ethanol production.

SEEC-2017-132

A STUDY OF GEOGRAPHIC DIVERSITY OF ACTIVE CONSTITUENTS CONTENTS OF ANDROGRAPHIS PANICULATA AND RAUWOLFIA SERPENTINA

Surendra Jatav
Center of Innovative and applied Bioprocessing (CIAB), Mohali
Email: surendrajatav08@gmail.com

Umesh Singh
Center of Innovative and applied Bioprocessing (CIAB), Mohali
Email: umesh@ciab.res.in

Bhuwan Bhushan Mishra
Center of Innovative and applied Bioprocessing (CIAB), Mohali
Email: bbmchem@gmail.com

Rejender Singh Sangwan
Center of Innovative and applied Bioprocessing (CIAB), Mohali
Email: sangwan.lab@gmail.com

Pratibha Dwivedi
Center of Innovative and applied Bioprocessing (CIAB), Mohali
Email: dwivedipratibha15@gmail.com

ABSTRACT

Andrographis paniculata is an annual herbaceous plant belonging to Acanthaceae and Rauwolfia serpentina, or Indian snakeroot is a species of flower in the family Apocynaceae. Rauwolfia serpentina is known to produce more than 50 different alkaloids which belong to the monoterpenoid indole alkaloid family. The present study deals with the analysis of the geographic diversity of major active constituent contents i.e., indole alkaloids of Rauwolfia Serpentina and diterpenoid lactone of Andrographis Paniculata plant using high performance liquid chromatography (HPLC) followed by the mass spectrometry (MS) for identification. Multiple indole alkaloids like ajmalicine, ajmaline, yohimbine serpentine/alstonine, serpentinine, vomilenine and reserpine of Rauwolfia Serpentina and andrographolide, neoandrographolide and 14-deoxy andrographolide of Andrographis Paniculata were identified. After the identification, alkaloids and diterpenoid lactone were quantified and observed the total alkaloid content varied from 0.3% to 1.0% of dry weight of Rauwolfia serpentina roots and the diterpenoid lactone contents in Andrographis paniculata leaves varied from 3.0% to 6.0% of dry weight, depending on geographic origin. Some of the geographic origin accessions were recognized for maximum contents of indole and diterpenoid lactones as well as maximum contents of specific constituent. The phytochemical diversity data revealed recognition of geographic locations related content of specific phytochemical in the medicinal plants. Such accessions form for good candidates for variety and chemotype development.

Keywords: Rauwolfia serpentina, Andrographis Paniculata, Active constituents.

SEEC-2017-133

EFFECT OF SOLAR DEHYDRATION ON NUTRITIONAL CONTENT OF CAPSICUM

Deepak Mehta
Center of Innovative and applied Bioprocessing
(CIAB), Mohali
Email: deepakmht664@gmail.com

Alka Sharma
GJUS&T, HISAR
Email: alkabhardwaj@rediffmail.com

ABSTRACT

The use of solar energy in recent years had reached a remarkable edge and occupies growing need for society for several reasons. The continuous research for an alternative power source due to the scarcity of fossil fuels is the main driving force. Solar energy is the cleanest form of energy which can be exploited for preservation of food. From environmental protection point of view, it is expected that utilizing it will leave minimum amount of pollution. Due to seasonal availability and regional abundance of certain perishable food items it becomes essential that they are preserved safely for use in lean season and remote areas. The existing demand of high-quality foods in the market requires dried products with high nutritional and organoleptic properties with similar levels as found in the initial fresh product.

We have dried vegetables by different methods like solar drying, open sun drying and hot air drying in order to increase the shelf-life of vegetables. In this study, capsicum samples were taken for drying after giving water and steam blanching and its physical and chemical parameters were evaluated. It was found that there was an increase in chlorophyll content (2.70±0.10 mg/lt), flavonoid content (1.83±0.02 mg/lt), polyphenol content (1.29±0.01 GAE mg/100g) and vitamin A content (3.95±0.01 I.U.) in all of the solar dried samples as they become concentrated source of nutrients. There was a decrease in vitamin C content (16.6±0.1 mg/100g) in all of the samples. The aroma of capsicum slices was maintained in solar dried samples but was somewhat lost in hot air dryer and open sun drying.

Keywords: Solar drying, Preservation, Blanching.

SEEC-2017-134

EFFECT OF COST EFFECTIVE ATMOSPHERIC COLD PLASMA PROCESSING TECHNIQUE ON AMINO ACIDS LIBERATION IN WHEY

Vasudha Bansal, Priyanka Prasad, Rajender Singh Sangwan
Centre of Innovative and Applied Bioprocessing, Mohali-160071, Panjab (India)

ABSTRACT

Whey is a nutritional by-product from milk, cheese, and paneer which contain numerous nutrients in the form of 70% of lactose, 70-90% of milk minerals, vitamins originally present in milk. It is also the source of high quality proteins possessing sulphur containing amino acids. Cost effective non-thermal cold plasma technique was employed as pre-treatment method in order to study its effect on liberation of amino acids. It was found that cold plasma has imparted negligible ($p < 0.05$) effect on the separation of amino acids owing the usage of less voltage during processing. However, the pre-treatment cold plasma method needs to be optimized at higher voltage for increased time period.

SEEC – 2017 – 135

DEVELOPMENT AND VALIDATION OF A CFD MODEL FOR SIMULATING DRYOUT PHENOMENA IN CORIUM DEBRIS BEDS

Aranyak Chakravarty
Mechanical Engineering Department and School of Nuclear Studies and Application
Jadavpur University, Kolkata, India
Email: aranyakchakravarty@gmail.com

Priyankan Datta
Mechanical Engineering Department
Jadavpur University, Kolkata, India
Email: priyankan.datta43@gmail.com

Koushik Ghosh
Mechanical Engineering Department
Jadavpur University, Kolkata, India
Email: kghoshjdvu@gmail.com

Swarnendu Sen
Mechanical Engineering Department,
Jadavpur University, Kolkata, India
Email: sen.swarnendu@gmail.com

Achintya Mukhopadhyay
Mechanical Engineering Department,
Jadavpur University, Kolkata, India
Email: achintya.mukho@gmail.com

ABSTRACT

Molten fuel coolant interaction subsequent to a hypothetical core meltdown accident in a nuclear reactor may lead to the formation of a particulate corium debris bed. Significant studies carried out over the years have established that the most important criteria governing heat transfer and hence, the coolability of such a debris bed is the Dryout Heat Flux (DHF). In the present work, a numerical model has been developed which is capable of modelling the dryout phenomena. The developed model has been implemented in ANSYS FLUENT using user-defined functions (UDF) and user-defined scalar (UDS) equation utility. The developed numerical model has been validated with available experimental data from the literature.

*Keywords***:** Nuclear reactor safety, Multiphase flow, Computational fluid dynamics

INTRODUCTION

The core of a nuclear reactor is likely to undergo tremendous heating in absence of adequate heat removal mechanism and form a molten state (typically termed as corium), subsequent to a severe accident. A possible outcome of the hydrodynamic and thermal interaction between the molten corium jet and the liquid coolant is the fragmentation of the jet into very fine particles. The fragmented particles settle down in the lower head of the reactor vessel or the containment floor (depending on the accident progression sequence) as a decay heat-generating debris bed. It is essential to ensure adequate removal of heat from the debris bed since a failure may result in temperature rise within the bed and cause remelting of the bed.

The maximum limit up to which heat generated can be safely removed from the debris bed is typically given by the Dryout Heat Flux (DHF) and the associated phenomena termed as dryout. Occurrence of dryout causes minimal heat removal from the bed and rapid temperature rise. As such, knowledge of the dryout limit is essential in ensuring safety of nuclear reactors [1].

The present work attempts to numerically model the dryout phenomena using the commercial computational fluid dynamics tool ANSYS FLUENT. The governing equations, closure of the equations and validation with experimental data is presented in this paper.

MODEL DEVELOPMENT

The porous structure of a corium debris bed allows the application of porous media models in modelling of debris bed dryout phenomena. Realistic modelling of the dryout behaviour involves solving the two-phase conservation equations viz. mass, momentum and energy conservation

equations for liquid as well as the vapour phase. In addition, the solid phase of porous media also needs to be considered to account for heat transfer from the heat generating particles.

Governing Equations

$$\frac{\partial}{\partial t}(\alpha_i \rho_i) + \nabla.(\alpha_i \rho_i \boldsymbol{v}_i) = \Gamma \quad (1)$$

$$\frac{\partial}{\partial t}(\alpha_i \rho_i \boldsymbol{v}_i) + \nabla.(\alpha_i \rho_i \boldsymbol{v}_i \boldsymbol{v}_i)$$
$$= -\alpha_i \nabla P + \nabla.(\alpha_i \tau) + \boldsymbol{F}_{s,i} + \boldsymbol{F}_i + K_\Gamma + \varepsilon \alpha_i \rho_i \boldsymbol{g} \quad (2)$$

$$\frac{\partial}{\partial t}(\alpha_i \rho_i h_i) + \nabla.(\alpha_i \rho_i \boldsymbol{v}_i h_i)$$
$$= -\nabla.\boldsymbol{q}_i'' + Q_{s,i} + Q_{j,i} + Q_{sat,i} \quad (3)$$

$$\frac{\partial}{\partial t}\big((1-\varepsilon)\rho_s h_s\big) = -\nabla.\boldsymbol{q}_s'' + Q_{s,decay} - Q_{s,g}$$
$$-Q_{s,l} - Q_{sat,s} \quad (4)$$

Eqns. (1-3) represents the mass, momentum and energy conservation equations, respectively, for the fluid phases i.e. water and steam. The suffix i refers to the liquid or vapour phase as the case may be. In Eqn. (1), Γ denotes the volumetric mass transfer rate between the fluid phases. In Eqn. (2), $\boldsymbol{F}_i$ is the interfacial drag force between the fluid phases while $\boldsymbol{F}_{s,i}$ represents the drag force between the solid particles comprising the porous medium and the corresponding fluid phase. K_Γ accounts for the momentum exchange due to mass transfer between the fluid phases. In Eqn. (3), $Q_{s,i}$ accounts for heat transfer between the heat-generating solid particles and the fluid phase while $Q_{j,i}$ is the interfacial heat transfer between the fluid phases. $Q_{sat,i}$ represents the heat transfer contributing to mass transfer between the phases. In Eqn. (4), $Q_{s,l}$ and $Q_{s,v}$ represents heat transfer between the heat-generating solid particles and the liquid and vapour phases, respectively. $Q_{sat,s}$ represents boiling heat transfer from the solid particles and $Q_{decay,s}$ is the volumetric decay heat generation rate.

Closure of the Governing Equations

In order to achieve closure of Eqns. (1-4), the above listed terms need to be properly modelled. The models adopted in the present study are detailed as follows –

Drag models: Drag force models in two phase flow through porous media are usually extensions of the single phase friction model i.e. Ergun's Law. The general form can be stated as –

$$F_{s,i} = \varepsilon \alpha_i \left(\frac{\mu_i}{K.K_{r,i}}j_i + \frac{\rho_i}{\eta.\eta_{r,i}}j_i|j_i|\right) \quad (5)$$

Here, K and η represents permeability and passability of the porous medium, respectively. These are expressed as

$$K = \frac{D_p{}^2 \varepsilon^3}{150(1-\varepsilon)^2}; \eta = \frac{D_p \varepsilon^3}{1.75(1-\varepsilon)} \quad (6)$$

$K_{r,i}$ and $\eta_{r,i}$ refers to relative permeability and relative passability for the corresponding fluid phases, respectively, which takes into account the two phase flow situation.. The correlations in $K_{r,i}$ and $\eta_{r,i}$ can broadly be subdivided into the following two categories –

(a) **Models without consideration of interfacial drag**: Correlations proposed by Lipinski, Reed and Hu and Theofanous come under this category. These correlations do not account for interfacial drag between the fluid phases i.e. $\boldsymbol{F}_i = 0$. The general form of these correlations can be expressed as

$$K_{r,i} = \alpha_i{}^n; \eta_{r,i} = \alpha_i{}^m \quad (7)$$

Table 1 lists the indices for the above mentioned correlations.

TABLE 1. VALUES OF INDICES IN DRAG MODELS

Correlation	Liquid		Vapour	
	m	n	m	n
Lipinski	3	3	3	3
Reed	3	5	3	5
Hu and Theofanous	3	6	3	6

(b) **Models considering interfacial drag**: The correlations proposed by Schullenberg and Müller, Tung and Dhir and several modifications thereof come under this category. These correlations explicitly consider the interfacial drag between the fluid phases. However, detailed descriptions of each model is beyond the scope of the present paper. As such, only the Schulleneberg and Müller model, which is used in this study, is decribed below. The expressions for relative permeability and relative passability for the vapour phase are as follows –

$$K_{r,v} = \alpha_v{}^3$$
$$\eta_{r,v} = 0.09\alpha_v{}^4 \; if \; \alpha_v < 0.3$$
$$= \alpha_v{}^6 \; if \; \alpha_v \ge 0.3 \quad (8)$$

Similarly, for the liquid phase these are expressed as –
$$K_{r,l} = \alpha_l{}^3; \eta_{r,l} = \alpha_v{}^5 \quad (9)$$

The interfacial drag term (F_i) is expressed as –
$$F_i = 350\alpha_l{}^7 \alpha_v \rho_l (\rho_l - \rho_v)\frac{Kg}{\eta\sigma}(v_v - v_l)^2 \quad (10)$$

Heat transfer models: The various modes of heat transfer considered is detailed below –

(a) **Boiling heat transfer**: Heat transfer takes place from solid particles to the liquid/vapour interface

2

contributing to evaporation (or boiling). This mode is only taken into account when $T_s > T_{sat}$ and is expressed as –

$$Q_{sat,s} = a_{sat} h_{sat} (T_s - T_{sat}) \qquad (11)$$

The corresponding mass transfer is expressed as –

$$\Gamma = \frac{Q_{sat,s}}{h_{g,sat} - h_{f,sat}} \qquad (12)$$

The interfacial are density (a_{sat}) is given by

$$a_{sat} = \frac{6(1-\varepsilon)}{D_p} F(\alpha_l) \qquad (13)$$

where, $\quad F(\alpha_l) = 1 \; if \; \alpha_l \geq 0.3$
$$= \frac{\alpha_l}{0.3} \; if \; \alpha_l < 0.3$$

Boiling at the surface of solid particles is calculated using different correlations depending on boiling regime identification. This is done with respect to temperature of the solid particles by defining a minimum film boiling temperature ($T_{min}{}^{FB}$) and a maximum nucleate boiling temperature ($T_{max}{}^{NB}$). These are defined as –

$$T_{min}{}^{FB} = T_{sat} + 17 \qquad (14)$$
$$T_{max}{}^{NB} = T_{min}{}^{FB} + \Delta T_{trans} \qquad (15)$$
where, $\quad \Delta T_{trans} = 100 \; K$

If $T_s \leq T_{min}{}^{FB}$, pure nucleate boiling is assumed to occur and the heat transfer coefficient for nucleate boiling is determined using the Rhosenow correlation. It is expressed as –

$$h_{sat}{}^{NB}$$
$$= \frac{c_{p,l}{}^3 \mu_l (T_s - T_{sat})^2}{\left(h_{g,sat} - h_{f,sat}\right)^2 (0.012 Pr_l)^3 \sqrt{\frac{\sigma}{g(\rho_l - \rho_g)}}} \qquad (16)$$

If $T_s > T_{max}{}^{NB}$, pure film boiling is assumed to occur. In this case, heat transfer coefficient is determined using the Bromley correlation and is expressed as -

$$h_{sat}{}^{FB} = 0.62 \left[\frac{k_g{}^3 g \rho_g (\rho_l - \rho_g)}{D_p \mu_g (T_s - T_{sat})} \Delta h_{sat}{}^* \right]^{1/4} \qquad (17)$$

where,

$$\Delta h_{sat}{}^* = \left(h_{g,sat} - h_{f,sat}\right) \left(1 + \left(0.968 - \frac{0.163}{Pr_g} \right) Ja \right)$$

$$Ja = \frac{c_{p,g}(T_s - T_{sat})}{\left(h_{g,sat} - h_{f,sat}\right)}$$

In a transition region between $T_{min}{}^{FB}$ and $T_{max}{}^{NB}$, heat transfer coefficient is calculated by linear interpolation between pure nucleate boiling and pure film boiling regimes i.e.

$$h_{sat}{}^{trans} = [1 - W(T_s)] h_{sat}{}^{NB} \left(T_{min}{}^{FB}\right)$$
$$+ W(T_s) h_{sat}{}^{FB} \left(T_{max}{}^{NB}\right) \qquad (18)$$

$$W(T_s) = \frac{\left(T_s - T_{min}{}^{FB}\right)}{\left(T_{max}{}^{NB} - T_{min}{}^{FB}\right)} \qquad (19)$$

(b) **Solid to liquid heat transfer**: This is taken into account if the liquid temperature is below the saturation temperature (i.e. $T_l < T_{sat}$) and liquid is the continuous phase (i.e. $\alpha_l \geq 0.7$).

(c) **Solid to vapour heat transfer**: This is taken into account if the solid temperature is above the saturation temperature (i.e. $T_s > T_{sat}$) and vapour is the continuous phase (i.e. $\alpha_v \geq 0.7$).

(d) **Interfacial heat transfer between liquid and vapour phases**: This mode of heat transfer is accounted for only in case of subcooled liquid and superheated vapour with $0 < \alpha_v < 1$.

Heat transfer modes (b), (c) and (d) is modelled using the Ranz and Marshall correlation subject to the specific constraints as mentioned. This is expressed in the general form as -

$$Q = ah\Delta T \qquad (20)$$

Here,

$$h = \left(2 + 0.6 Re_i{}^{0.5} Pr_i{}^{0.33}\right) \frac{k_i}{D} \qquad (21)$$

The interfacial area density is calculated For modes (b) and (c) as –

$$a = \frac{6(1-\varepsilon)}{D_p} F(\alpha_i) \qquad (22)$$

where, $\quad F(s\alpha_i) = 0 \; if \; \alpha_i < 0.7$
$$= \frac{\alpha_i - 0.7}{0.3} \; if \; \alpha_i \geq 0.7$$

In case of mode (d), this is modified as –

$$a = \frac{6\alpha_i}{D_b} \qquad (23)$$

Implementation in ANSYS FLUENT

The governing equations, along with the aforementioned correlations of drag force and heat transfer, are solved in ANSYS FLUENT using the Eulerian two-fluid model with liquid water and water vapour as the two fluid phases. The solid energy equation is solved as a separate scalar equation using the user-defined scalar (UDS) equation utility. Transient term in the UDS equation is defined in the UDF using UDS_TRANSIENT module, while the diffusive term is defined using DEFINE_DIFFUSIVITY module. Source terms in the UDS equation as well as in liquid and vapour energy equations (i.e. the heat transfer terms) are added as DEFINE_SOURCE modules. Mass transfer is modelled using DEFINE_MASS_TRANSFER module and the interfacial drag is implemented as DEFINE_EXCHANGE_PROPERTY module. Relative

permeability and relative passability functions are defined using DEFINE_PROFILE module of UDF.

VALIDATION STUDY

Validation of the developed numerical model is carried out separately for the drag models and the heat transfer correlations as follows –

Drag models in porous media

In the present study, two drag force models – the Reed model and the Schullenberg and Müller model – are tested against experimental data provided by Li et al. [2] for two-phase air-water experiments carried out in DEBECO test facility. Simulations have been carried out for a specific composition of the porous bed with $\varepsilon = 0.4$ and $D_p = 1.44$ mm (Bed 3 in Li et al.[2]). Figure 2 represents the comparison of numerically obtained pressure gradient with the drag models against experimental data.
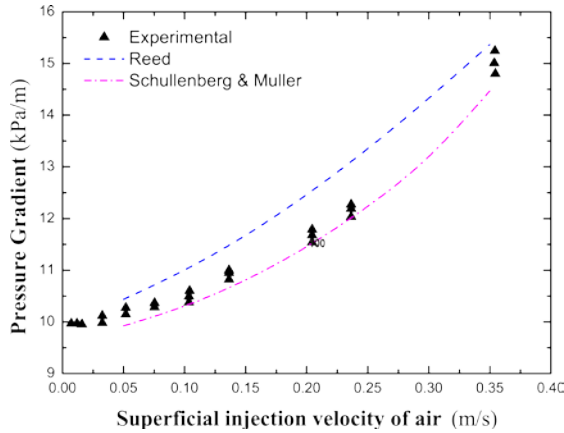
FIGURE 1. VALIDATION OF DRAG MODELS

Heat transfer in terms of dryout

Validation of the heat transfer correlations is carried out in terms of prediction of dryout in a heat-generating truncated conical-shaped corium debris bed with experimental data obtained by Takasuo et al. [1]. The Reed model as well as Schullenberg and Müller model have been used for comparison purpose. Table 2 compares the minimum dryout power as obtained from simulation with the experimental data.

TABLE 2. COMPARISON IN TERMS OF DRYOUT POWER

Experiment (Takasuo et al. []) (KW)	Reed Model (KW)	Schullenberg and Müller model (KW)
39.2	40	39

Figure 2 shows the transient variation in minimum liquid saturation and maximum solid temperature within the domain. It can be seen that the minimum liquid

saturation becomes equal to zero only in case of 40 KW (Reed model) and 39 KW (Schullenberg and Müller model) indicating dryout in these cases. The corresponding maximum solid temperature is also much higher in these cases.

It is to be noted here that the predicted zone of dryout is similar to the region identified in the experiments by Takasuo et al. [1]. However, the contour plots are not being produced here for paucity of space.

(a)

(b)
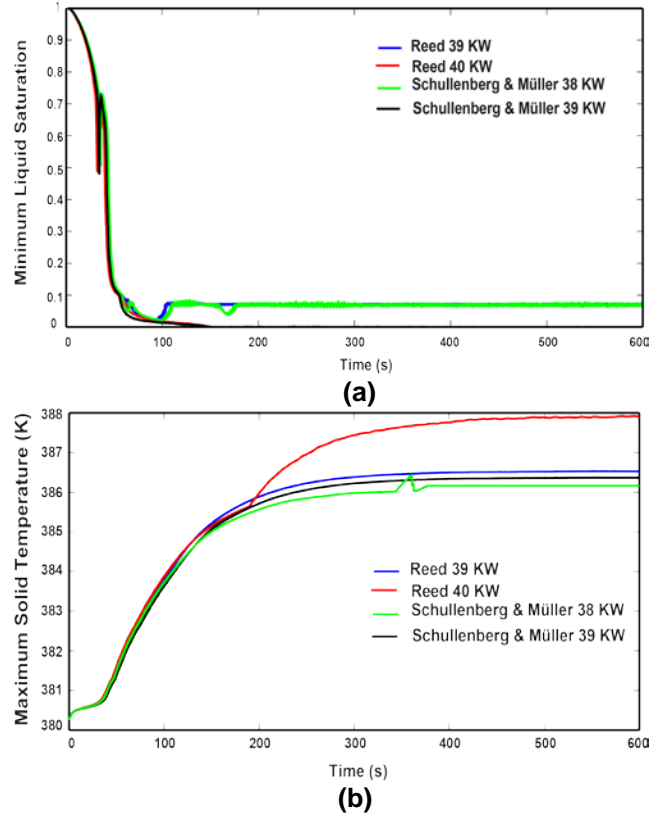
FIGURE 2. TRANSIENT HISTORY OF MINIMUM LIQUID SATURATION AND MAXIMUM SOLID TEMPERATURE

REFERENCES

[1] Takasuo, E., 2016. "An experimental study of the coolability of debris beds with geometry variations". Annals of Nuclear Energy, 92, pp. 251-261

[2] Li, L., Zuo, X., Lou, J., Li, H., and Lei, X., 2015. "Pressure drops of single/two-phase flows through porous beds with multi-sizes spheres and sands particles". Annals of Nuclear Energy, 85, pp. 290-295

SEEC – 2017 – 136

NUMERICAL INVESTIGATION OF JET BREAKUP PHENOMENON USING VOF APPROACH

Priyankan Datta
Mechanical Engineering Department
Jadavpur University, Kolkata, India
Email priyankan.datta43@gmail.com

Aranyak Chakravarty
Mechanical Engineering Department
and School of Nuclear Studies and
Application
Jadavpur University, Kolkata, India
Email aranyakchakravarty@gmail.com

Tuhin Maitra
School of Nuclear Studies and
Application
Jadavpur University, Kolkata, India
Email tuhinmaitra1920@gmail.com

Koushik Ghosh
Mechanical Engineering Department
Jadavpur University, Kolkata, India
Email kghoshjdvu@gmail.com

Achintya Mukhopadhyay
Mechanical Engineering Department
Jadavpur University, Kolkata, India
Email achintya.mukho@gmail.com

Swarnendu Sen
Mechanical Engineering Department
Jadavpur University, Kolkata, India
Email sen.swarnendu@gmail.com

ABSTRACT

The hydrodynamic fragmentation of the wood metal jet into a pool of water in presence of single acalandria tube is studied numerically using ANSYS FLUENT 14.5. To capture the two-phase interface behavior during the fragmentation phenomenon, Volume of Fluid (VOF) method is used. The analysis of the effect of the tube diameter, inlet jet velocity on the fragmentation behaviour are the salient objective of the present work.

Keywords: *VOF, Jet fragmentation, Calandria tube, ANSYS FLUENT 14.5*

INTRODUCTION

The interaction between molten corium jet with the calandria tube during a hypothetical severe accident scenario in Indian Pressurised Water Reactor (IPHWR) is a very important thermo-hydraulic phenomenon in the context of nuclear safety research. This phenomenon has gained attaention among the researchers due to its immense potential to cause serious damage to the reactor structure (e.g. pressure tube, calandria vessel etc.) followed by the further accident progression and release of radioactive products into the environment.

Literature survey [1-7] reaveals that though a significant research is carried out on hydrodynamic fragmentation of corium jet due to melt-water interaction in the context of PWRs, the numerical investigation of the corium jet and calandria tube interaction along with the jet breakup phenomenon in the context of IPHWR is quite limited. Therefore, a detailed systematic numerical investigation is needed to understand the underlying physics of jet breakup phenomenon in case of pressurised heavy water reactor systems of all designs.

The present work aims on the exploration of the hydrodynamic fragmentation of wood metal jet inside a pool of liquid water in presence of a single calandria tube using computational fluid dynamics software ANSYS FLUENT 14.5. The effect of calandria tube diameter variation, inlet jet velocity on the fragmentation behaviour are studied using the volume of fluid (VOF) approach.

PROBLEM DEFINITION

The schematic diagram of the considered problem geometry, its dimensions and the associated boundary conditions are shown in Fig. 1. The chosen flow geometry is a 2D rectangular enclosure with left, right and bottom boundary are considered as adiabatic wall. Melt jet injection takes place from an inlet located at the centre of the top boundary. The location of the calandria tube (front view) is also shown in Fig. 1.

In the present work, an interaction between wood metal and the calandria tube immersed inside a water pool is considered for the simulation purpose. The jet fragmentation phenomenon is assumed to be purely hydrodynamic in nature. The calandria tube is assumed adiabatic and a non-slip velocity boundary condition is applied at the tube and water interface. The thermo-physical properties for both the phases are given in Table 1.

TABLE 1. THEROM-PHYSICAL PROPERTIES

Material	Density (kg/m^3)	Surface tension coefficient σ (N/m)	Viscosity (Pa.s)
Wood metal	9700	1	0.00194
Water	1000	-	0.001003
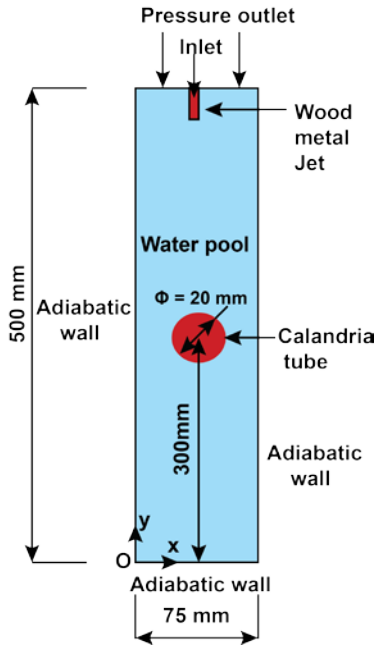
FIGURE 1. FLOW GEOMETRY AND BOUNDARY CONDITIONS

GOVERNING EQUATIONS

In the present work, the VOF multiphase flow method in ANSYS FLUENT 14.5 [8] is used. The governing equations corresponding to the volume fraction and momentum equation are presented as follows-

Volume Fraction Equation:

$$\frac{1}{\rho_q}\left[\frac{\partial}{\partial t}\left(\alpha_q \rho_q\right) + \nabla.\left(\alpha_q \rho_q V_q\right)\right] = 0 \qquad (1)$$

Here, α_q and V_q represents the volume fraction and velocity of the q-th phase.

Momentum Equation:

A single momentum equation is solved throughout the domain resulting in a shared velocity field among the phases. The dependency of the momentum equation on phasic volume fractions is ensured through the mixture density ρ and mixture viscosity μ.

$$\frac{\partial}{\partial t}\left(\rho V\right) + \nabla.\left(\rho V V\right) = -\nabla p + \nabla.\left[\mu\left(\nabla V + \nabla V^T\right)\right]$$
$$+ \rho g + F \qquad (2)$$

The mixture properties are determined as follows-

$$\rho = \sum \alpha_q \rho_q \qquad (3)$$
$$\mu = \sum \mu_q \rho_q \qquad (4)$$

subject to the constraint

$$\sum \alpha_q = 1 \qquad (5)$$

In Eq. (2), F represents the surface tension force which is modelled in the present analysis using the Continuum Surface Force (CSF) model (whcich is similar as proposed by [9]) in FLUENT. The importance of the surface tension effects is judged with the help of the Weber number (*We*) which is defined as the ratio between the inertial forces and the surface tension force, and is expressed as -

$$We = \frac{\rho V D^2}{\sigma} \qquad (6)$$

where, D and σ represent the inlet jet diameter and surface tension coefficient (as mentioned in Table 1), respectively.

The relevant parameter used in the present analysis is the breakup time which is defined as the time of detachment of the first ligament from the continuous jet. The corresponding length of the continuous jet is termed as the breakup length.

3. NUMERICAL PROCEDURE

Numerical solution of the governing Eqs. (1-2) is obtained using the volume of fluid (VOF) approach with ANSYS FLUENT 14.5. PRESTO (PREssure Staggering Option) is used as the numerical scheme for solving the pressure equation, while momentum equation is solved using second order upwind scheme. The volume fraction equation is solved using the Geo-reconstruct scheme. Pressure velocity coupling is achieved using the well-known PISO algorithm. The Scaled-Adaptive Simulation (SAS) model is used to account for the turbulence at high velocity scenario.

4. RESULTS AND DISCUSSIONS

4.1 Effect of Calandria Diameter Variation

The effect of calandria tube diameter variation on jet breakup phenomenon is shown in Fig. 2. Three different diameter (20, 25 and 30 mm) of tube is considered in the present study. In each case, inlet jet velocity is considered to be the same (5 m/s).
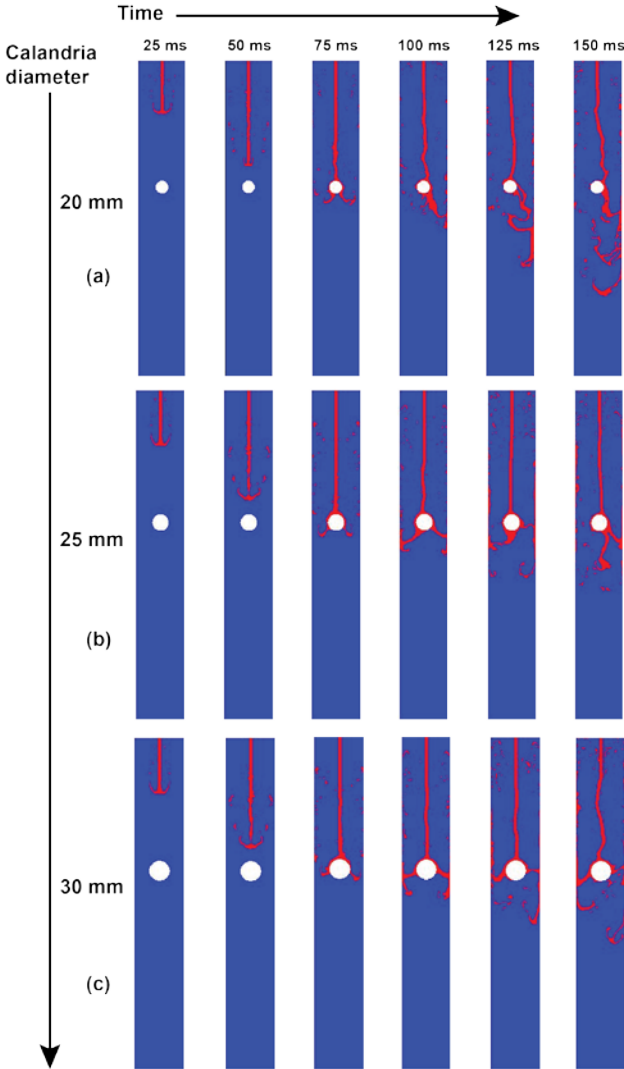
**FIGURE 2.** EFFECT OF CALADRIA TUBE DIAMETER VARIATION ON JET BREAK UP BEHAVIOUR

Fig. 2a shows upto 50 ms the only side stripping occurs from the continuous jet. However, at about 73 ms, jet interacts with the caldaria tube that results in the detachment of the first ligament from the continuous jet. The snaphot of the bifurcated jet after the interaction with calandria is shown at 75 ms. As time progresses, the continuous jet shifts towards the right and thereon, fragmentation occurs.

Results reveal that as the tube diameter increases from 20 mm, the mode of jet fragmentation phenomenon also changes. The breakup time for the 25 mm and 30 mm diameter tube is observed at about 114 ms and 107 ms respectively.

4.2 Effect of Inlet Jet Velocity

In the present section, the simulations are carried out to study the effect of inlet jet velocity variation on the fragmentation characteristics. For each case, the calandria diameter is kept fixed at 20 mm.
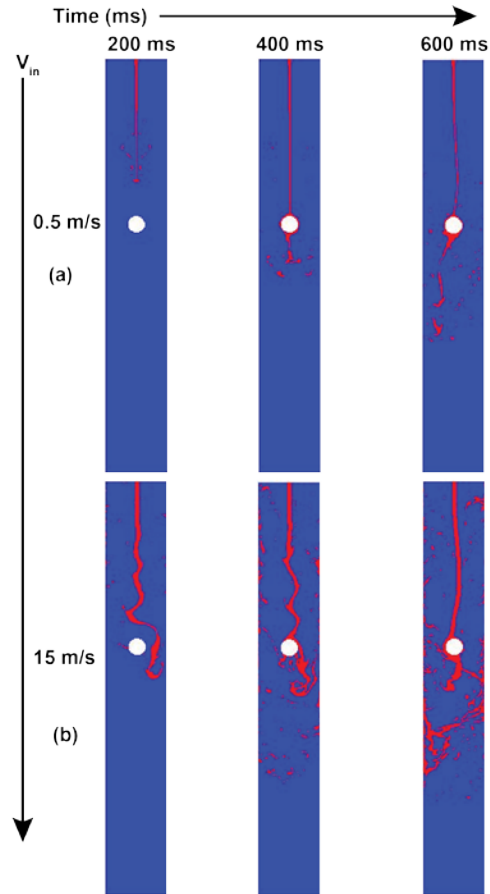
FIGURE 3. EFFECT OF INLET JET VELOCITY VARIATION ON JET BREAK UP PHENOMENON

Observation reveals jet breakup time decreases with the increase in jet velocity. For the highest jet velocity (V_{in} = 15 m/s), breakup time is found to be 27 ms. However, for the lowest inlet jet velocity (V_{in} = 0.5 m/s), jet breakup is observed at about 250 ms. In addition, the wall effect is found to be more prominent in case of large jet velocity.

5. CONCLUSIONS

In the present analysis wood-metal jet fragmentation phenomenon is studied in presence of a calandria tube. The effect of tube diameter, inlet jet velocity on the fragmentation behaviour are studied using VOF approach in ANSYS FLUENT 14.5. The salient observations are-

(i) Breakup time increases with the increase in calandria diameter. In addition, tube diameter has a strong influence on the mode of fragmentation.

(ii) Breakup time is found to be the loweset (about 27 ms) for the highest inlet jet velocity (15 m/s).

ACKNOWLEDGMENTS

REFERENCES

1. Namiech, J., Berthoud, G., Coutris, N., 2004 ."Fragmentation of a molten corium jet falling into water". Nuclear Engineering and Design, 229, pp. 265-287.
2. Burger, M., Cho, S.H., Berg, E.v., Schartz, A., 1995."Breakup of melt jets as pre-condition for premixing: modeling and experimental verification". Nuclear Engineering and Design, **155**, pp. 215-251.
3. Berg, E.v., Burger, M., Cho, S.H., Schartz, A., 1994. " Modeling of the breakup of melt jets in liquids for LWR safety analysis". Nuclear Engineering and Design, 149, pp. 419-429.
4. Thakre, S., Manickam, L., Ma, W., 2015. "A numerical simulation of jet breakup in melt coolant interactions". Annals of Nuclear Energy, 80, pp. 467-475.
5. Bang, K., Kumar, R., Kim, H., 2014. "Modeling corium jet breakup in water pool and application to ex-vessel fuel–coolant interaction analyses". Nuclear Engineering and Design, 276, pp. 153-161.
6. Koshizuka, S., Ikeda, H., Oka, Y., 1999." Numerical analysis of fragmentation mechanisms in vapor explosions". Nuclear Engineering and Design, 189, pp. 423-433.
7. Ikeda, H., Koshizuka, S., Oka, Y., Park, H.S., Sugimoto, J., 2001. "Numerical analysis of jet injection behavior for fuel-coolant interaction using particle method". Journal of Nuclear Science and Technology, 38, pp. 174-182.
8. *ANSYS FLUENT Theory guide 14.5.* 2012.
9. Brackbill, J.U., Kothe, D.B., Zemach, C., 1992. "A Continuum method for modeling surface tension". Journal of Computational Physica, 100, pp. 335-354.

SEEC – 2017 – 137

FLAME KERNAL GROWTH STUDY OF SPARK IGNITED HYDROGEN AIR PREMIXED COMBUSTION

Punit Kumar
School of Engineering
MS Scholar, IIT Mandi
Email: punit_kumar@students.iitmandi.com

P. Anil Kishan
School of Engineering
Assistant Professor, IIT Mandi
Email: kishan@iitmandi.ac.in

Atul Dhar
School of Engineering
Assistant Professor, IIT Mandi
Email: add@iitmandi.ac.in

ABSTRACT

The spark ignition of H_2-air mixture was investigated in a constant volume combustion chamber at initial pressure and temperature of 2 bars and 303 K respectively. The equivalence ratio was varied from 0.6 to 1.4. The flame propagation and pressure was recorded. The flame kernel images were processed to get the flame velocity of the mixture. It was found that the flame velocity and pressure are dependent negatively on the equivalence ratio (λ). As the equivalence ratio is increased the flame velocity, peak pressure and pressure rise rate decrease. Though peak value for all three parameters were found at $\lambda = 0.8$. A dependency of flame velocity on pressure rise was also mentioned.

Keywords: Hydrogen-air flame, Premixed combustion, Kernel Growth.
.

INTRODUCTION

At present pollution, climate change and global warming are the major threat which exist in front of the humankind. The governments are taking necessary steps to tackle the situation following the work done by researchers throughout the globe. Recent Paris climate deal is one of those steps. According to the World Energy Outlook 2016, our energy needs are going to rise continuously with 30 % increase till 2040. So accordingly, consumption of all fuel are also going to rise. In that scenario and keeping the pollution in mind, the economies around the world are shifting to renewable energy and gaseous fuels.

Hydrogen is a green fuel which gives water after combustion. The only pollutant emitted is NO_x. Hydrogen has considerably higher flammability limits which helps in burning this fuel toward very lean side. Hydrogen has higher diffusivity which helps in mixing and lower ignition energy requiremnts. Due to these qualities, the hydrogen is considered to be the fuel of the future.

K. Dharamshi et. al. [1] studied the flame kernel development and measured the flame velocity of hydrogen-air mixture in a constant volume combustion chamber. They used the laser ignition to ignite the lean mixture of $\lambda=2$-5. They noted that the peak pressure and pressure rise rate were decreased while λ was increased. D. Srivastava et. al. [2] compared the flame kernel for both laser and spark ignition and also concluded that the pressure rise rate was higher for laser ignition. T. A. Spiglanin et. al. [3] experimented to get the flame kernel growth rate, evolution of flame shape and OH distribution with the PLIF technique, in $H_2/O_2/Ar$ mixture ignited by laser spark.

Many researchers also studied the effect of hydrogen addition to the methane-air mixture on flame velocity [4]–[9]. They all concluded that the with increasing hydrogen, flame velocity incrases. Thus hydrogen is also considered to be a additive to methane air combustion.

In the current paper, hydrogen – air mixture is studied in a constant volume combustion chamber. The mixture is premixed and ignited with spark ignition. The equivalence

ratio is varied from lean to rich, to see the effect on flame velocity and pressure rise rate.

EXPERIMENTAL SETUP

All the reported results are obtained in a constant volume combustion chamber designed and developed in the lab at IIT Mandi. The chamber has an inside volume of 700 ml and can withstand 150 Bars pressure. The chamber is heated to desired temperature with 6 cartridge heaters and the temperature is measured by a k-type thermocouple. Dalton's law of partial pressure is used to make the mixture directly inside the chamber. Hydrogen is supplied from the cylinder whereas dehumidified air is obtained from the compressor-dehumidifier unit. The air fuel mixture is then left for 10 minutes to ensure proper mixing. The initial chamber pressure is measured using a static pressure sensor whereas the combustion chamber pressure is measured by Kistler make dynamic pressure sensor. The mixture is ignited by the spark plug. Simultaneously, the high speed camera is also triggered to capture the combustion phenomenon at 54000 fps. A white light source was used to illuminate the chamber to do the Shadowgraphy. Later on the images are processed in MATLAB and flame velocity was calculated.
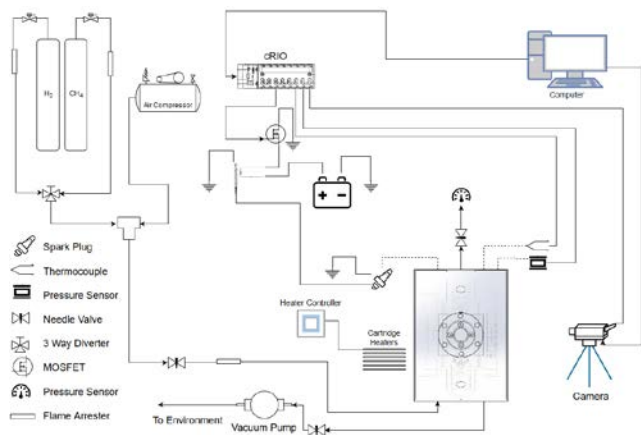
FIGURE 1. SCHEMATIC DIAGRAM OF EXPERIMENTAL SETUP

RESULTS AND DISCUSSION

Experiments were performed on hydrogen – air mixture in the CVCC at 303 K and 2 bars initial temperature and pressure respectively. The equivalence ratio (λ) was varied from 0.6 to 1.4.

Effect Of Equivalence Ratio On Pressure

Figure 2 provides pressure time history of hydrogen – air combustion. As can be seen in the graph, peak pressure

is maximum for λ = 0.8 and then it decreases when λ is either increased or decreased. For λ = 0.8, peak pressure is 12 bars whereas, for 0.6, 1.0, 1.2 and 1.4, it was 10, 11, 9.7 and 9.5 respectively. This follows the fact that a little rich mixture gives the peak heat release in a mixture. Due to this heat release temperature of the mixture increases which enhances the flame velocity.

In addition to the peak pressure, pressure rise rate can also be deduced from the fig. 2 by noticing the slope of the curves. The pressure rise rate is also maximum for λ = 0.8 and decreases on both sides. This can also be explained by the peak heat release at λ = 0.8.
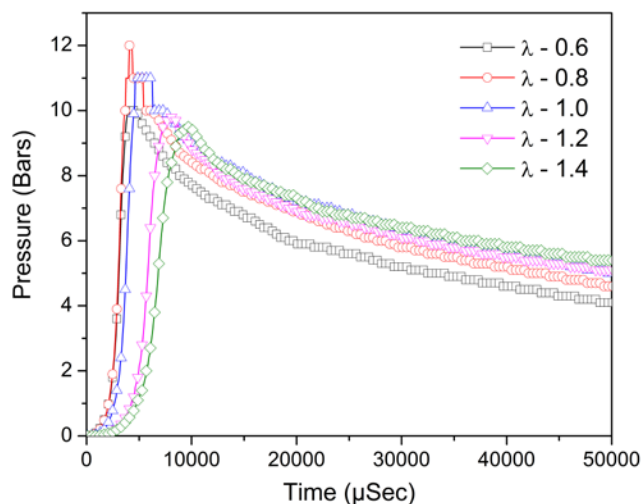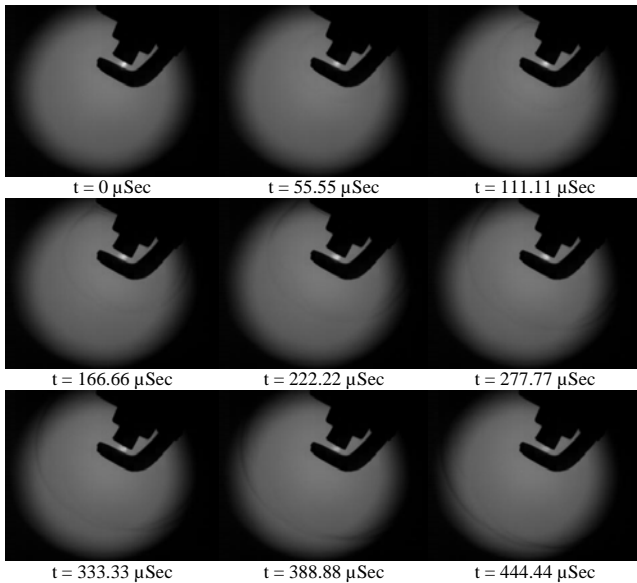

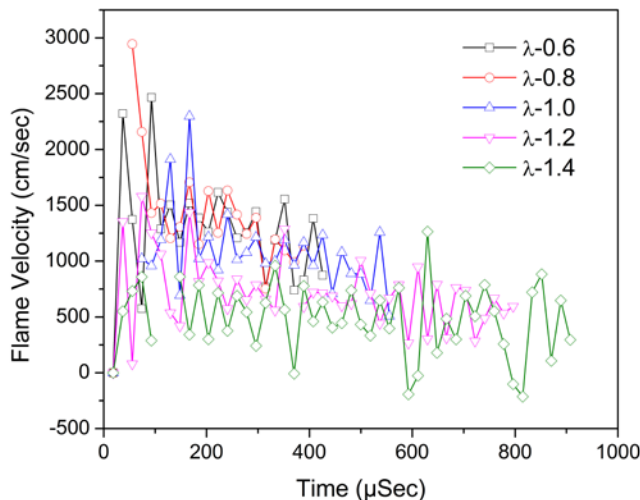**FIGURE 2.** PRESSURE - TIME CURVE FOR VARIOUS EQUIVALANCE RATIO

Effect Of Equivalence Ratio On Flame Velocity

The flame kernel were captured with shadowgraphy techniques using the high speed camera. Fig. 3 shows the flame kernel growth with time for λ = 1.0. For other equivalence ratios, the kernel development was of similar trend. At t = 0, spark is produced in the chamber and after 55.55 μSec first visible and distinguishable kernel is noticed. Later in each successive frames the flame kernel grows. This growth rate was captured by doing image processing in MATLAB and flame velocity was calculated. Fig. 4 shows the flame velocity for various λ. For all the cases the flame velocity decreases with time as the radius of the spherical flame increases. The flame velocity decreases as the λ is increased and the mixture gets leaner. This happens due to the lesser number of hydrogen molecules in leaner mixture. These produces less number of OH radicals which subsequently slows the reaction rates. In addition to this, pressure generated due to the combustion also plays a role in flame velocity. With higher pressure, molecules are placed closer to each other which provides more chance of diffusion and further reaction in

between the molecules. The pressure for various λ are reported in previous section.

t = 0 μSec   t = 55.55 μSec   t = 111.11 μSec

t = 166.66 μSec   t = 222.22 μSec   t = 277.77 μSec

t = 333.33 μSec   t = 388.88 μSec   t = 444.44 μSec

FIGURE 3. FLAME PROPAGATION TRACE FOR EQUIVALANCE RATIO 1.0

FIGURE 4. FLAME VELOCITY – TIME CURVE FOR VARIOUS EQUIVALANCE RATIO

CONCLUSION

The paper presents the studies conducted on hydrogen-air mixture in CVCC at equivalence ratio (λ) 0.6-1.4 at initial pressure and temperature of 2 bars and 303 K. The following conclusions can be drawn from the study;

1. The peak pressure and pressure rise rate decreases with increasing the λ.
2. The flame velocity of H_2-Air mixture decreases with increasing the equivalence ratio (λ).

REFERENCES

[1] K. Dharamshi, D. K. Srivastava, and A. K. Agarwal, "Combustion characteristics and flame-kernel development of a laser ignited hydrogen-air mixture in a constant volume combustion chamber," *Int. J. Hydrogen Energy*, vol. 39, no. 1, pp. 593–601, 2014.

[2] D. Kumar, M. Weinrotter, K. Iskra, A. Kumar, and E. Wintner, "Characterisation of laser ignition in hydrogen – air mixtures in a combustion bomb," *Int. J. Hydrogen Energy*, vol. 34, no. 5, pp. 2475–2482, 2009.

[3] T. A. Spiglanin, E. W. Fournier, J. A. Syage, and B. Cohen, "Time-Resolved Imaging of Flame Kernels : Laser Spark Ignition of H , / O , / Ar Mixtures," vol. 328, pp. 310–328, 1995.

[4] Z. Huang, Y. Zhang, K. Zeng, B. Liu, Q. Wang, and D. Jiang, "Measurements of laminar burning velocities for natural gas-hydrogen-air mixtures," *Combust. Flame*, vol. 146, no. 1–2, pp. 302–311, 2006.

[5] F. Halter, C. Chauveau, and I. Gokalp, "Characterization of the effects of hydrogen addition in premixed methane/air flames," *Int. J. Hydrogen Energy*, vol. 32, no. 13, pp. 2585–2592, 2007.

[6] G. Yu, C. K. Law, and C. K. Wu, "Laminar flame speeds of hydrocarbon + air mixtures with hydrogen addition," *Combust. Flame*, vol. 63, no. 3, pp. 339–347, 1986.

[7] E. Hu, Z. Huang, J. He, C. Jin, and J. Zheng, "Experimental and numerical study on laminar burning characteristics of premixed methane-hydrogen-air flames," *Int. J. Hydrogen Energy*, vol. 34, no. 11, pp. 4876–4888, 2009.

[8] J. L. Gauducheau, B. Denet, and G. Searby, "A Numerical Study of Lean CH 4 /H 2 /Air Premixed Flames at High Pressure," *Combust. Sci. Technol.*, vol. 137, no. 1–6, pp. 81–99, 1998.

[9] V. Di Sarli and A. Di Benedetto, "Laminar burning velocity of hydrogen–methane/air premixed flames," *Int. J. Hydrogen Energy*, vol. 32, no. 5, pp. 637–646, 2007.

SEEC-2017-138

IMPLEMENTATION OF RENEWABLE ENERGY GENERATION (OFF-GRID) PROGRAMMES IN STATE OF PUNJAB (INDIA)-AN ASSESSMENT

Dr. Navreet
Assistant Professor
Public Administration Department, Panjab
University, Chandigarh
Email:navreet9@gmail.com

Ravneet Kaur
Research Scholar
Public Administration Department, Panjab
University, Chandigarh
Email:arora.ravne@gmail.com

Abstract

Renewable energy technologies is best solution to mitigate energy issues related to gap between demand and supply of energy, provision of clean and green energy in all areas even where conventional electricity supply is not feasible and reduce dependency on fossil fuels to generate power and lessen environmental pollution. In Punjab state mainly two schemes are promoted to develop off grid energy sources i.e. National Biogas and Manure Management Program (NBMMP) to develop bio energy and Off-grid and Decentralized Solar Application scheme under Jawaharlal Nehru Solar Mission to develop solar energy. An attempt is made in this paper to study the role of PEDA as facilitator for promotion of renewable energy resources while assessing the implementation of NBMMP and Off-grid and Decentralized Solar Application scheme in State of Punjab. Secondly paper also examines the coordination of Central and state level agencies involved in promotion of renewable energy sources. Secondary sources like PEDA reports, HDI Reports, Statistical abstracts, Journals, e-journals and newspapers are used in the proposed study.

KeyWords: Biogas, Solar Photovoltaic, Renewable Energy, Punjab, PEDA

Introduction

Energy is the central force behind development and growth of any country economy. Today human civilization is highly dependent on conventional sources of energy to meet their constant energy requirement. However conventional energy sources are major source of environmental and health stress at global as well as local levels. (Kamalapur and Udaykamar 2009) As per National Sample Survey Organisation on the Household Consumer Expenditure in India (2006-07), 42.3% of rural households and 6.4% of urban households in India still use kerosene (fossil fuel) as a primary source to lighten their homes. This data reflects the status of non availability of power to 72 million households in India. (Deshmukh et al. 2011) There is continuous power cut from energy deficits which has already reached to 9 percent in the electricity sector of India. (CEEW 2012) These statistical figures pinpoint towards energy deficit in India as current energy supply cannot meet the growing demand of society and burning of fossil fuels also leads to environmental pollution. To achieve the targeted growth and efficient development of all sectors in India, it needs an appropriate input of energy without degrading or ruining the environment. The only solution to this challenge is usage of Renewable Energy Sources. Renewable energy provides clean and green energy, mitigates climate change, provides energy security and bridges the gap between demand and supply of energy. The forms of renewable energy resources are Solar, Wind, Geothermal, Biomass and Water. In India the gross installed capacity of grid interactive renewable power was 33.8 GW as on 31st December 2015. As of December

2015, solar, wind, biomass and small hydropower contribute about 13.60 per cent of the total installed capacity for electricity. The total renewable power installed capacity of 14,400 MW in 2009 has reached a capacity of 38,822 MW at the end of December 2015. Wind energy account for over 64 % of installed capacity (25,088 MW), followed by solar power (4,879 MW), bio power (4,677 MW) and small hydro power (4,177 MW) (MNRE Annual Report 2015)

There are various institutions set up at centralized and decentralized level to promote energy conservation, to preserve the environment and to bring sustainable development in every sector. These agencies carry out research and development, testing, demonstration and manufacture of renewable energy devices/ systems, frame plans and programs and finally execute them in whole country. Ministry of New and Renewable Energy is the nodal agency at Union level which develops the renewable energy at national level and State Nodal Agencies implement and execute the programs at state level with financial support from central ministry.(International Energy Agency 2016)

Significance of Off- Grid Renewable Energy

The shift to a locally accessible renewable source for meeting the energy needs can reduce the dependence on conventional sources. To attain the consumption level of energy, Off-grid renewable energy is a proven viable solution with enormous potential to meet the energy consumption needs. Renewable energy based decentralized and distributed applications have benefited millions of people by meeting their cooking, lighting and other energy needs in an environment friendly manner. (Pillai and Banerjee 2009)

The solar and bio energy are the most vital Off-grid renewable energy sources. One of the product of solar energy i.e. Photovoltaic electricity generation is a promising solution to generate climate compatible power with sufficient energy potential which would cover the present worldwide demand for electricity consumption. Photovoltaic system is advantageous as their demand of power is low, can build integrated grid connected systems and can act as standalone systems.

The success of using biogas system as decentralized power generation programme will lead to multifaceted benefits to the rural people. First, there will be conversion of agricultural waste residue into a valuable by-product which will generate additional income for the farmers. Second, the engagement of the rural people in

residue collection and transportation chain, and in the construction and training of biogas plants will generate employment. Third, and the most significant contribution will be stability and self-sufficiency as the generation of decentralized power will lead to continuous development with assured supply of electricity. (Singh and Chauhan 2014).

Overview of Off-grid Renewable Energy in Punjab

The total installed power capacity of the state of Punjab was 8,353 MW as on 31stMarch, 2014. Out of which, state-owned power plants alone constituted 5,040 MW, private-owned plants constituted 1,343 MW, and central-owned plants constituted 1,970 MW. Renewable capacity had a small fraction in the total installed capacity of the state of Punjab (3.5%). (Department of Science, Technology and Environment)

In Punjab mainly two types of decentralized Renewable energy i.e. Solar and Biogas are used in large extent. Punjab energy Development Agency implements the schemes for generation of energy through Renewable sources. These are:

1. Off-grid and Decentralised Solar Application scheme mainly focussed on promoting off-grid applications by creating awareness and demonstrating innovative benefits of solar systems. (Shrimali and Rohra 2012)

Tab. 1 No. of Solar Systems Installed in Punjab (1990 to 2014)

Years	Solar Water Heater	Solar Photovoltaic Pumpsets	Solar Cooker	Home Light System	Solar Drier	Solar Street Light	SPV Lantern
2000-01	699	500	4000	250	4	300	1500
2001-02	15	500	79	216	11	200	1576
2002-03	-	700	77	500	-	500	-
2003-04	-	-	80	-	-	250	-
2004	-	-	10	-	-	-	-

4-05							
2005-06	1000	40	-	500	50	500	-
2006-07	-	-	-	500/40	50	750	-
2007-08	1	-	-	2000	-	500	-
2008-09	23	-	-	2600	-	500	-
2009-10	-	-	-	-	-	1018	-
2010-11	85	-	-	1000	-	-	-
2011-12	550	-	-	500	-	-	-
2012-13	1616	-	800	-	-	626	-
2013-14	1504	-	-	-	-	2649	-

Source: punjabstat.com

Table 1 highlight that there are no SPV installations in Punjab in an increasing trend. In some years there is a freezing point in which there are no SPV installations. In 2015-16 a cumulative of 17495 Lanterns, 8626 Home Lights, 5354 Solar Street lights, 1857 Solar Water Pumps and 1202 KWp Stand Alone systems are installed in Punjab state (Ministry of New and Renewable Energy 2016) Another 50,000 LED based Solar street lights Programme worth of 75 Crore is initiated by PEDA in Punjab state. Applications along with their share for this program have been received from 1594 Villages. Installation work of 28690 Solar Lights has been initiated & 12000 have been installed till 2015-16. Under program Roof top Net Metering, India's 2nd highest total capacity of 5.5 MW are installed on 180 Homes/ Schools/Institutes/ Industry in Punjab. PEDA also initiated a unique project of Canal Top Solar under which 2 Projects of 2.5 MW each will be commissioned by 2017. (PEDA Office Reports)

2. National Biogas and Manure Management Program

The National Biogas and Manure Management Programme (NBMMP) initiated by the Government of India in 2005 which aims to reduce LPG and other conventional fuels, reduce use of chemical fertilizers in fields, mitigate drudgery of women, reduce climate mitigation and pressure on forests and link toilets with biogas plants. The implementation of this programme is reliant on active participation of Turnkey workers who are trained by PAU, Ludhiana. (MNRE 2009) Table 3.13 showed that Punjab fails to meet the estimated potential of installation of biogas plants till 2013.

Tab. 2   Target and Achievements of Biogas Plants installed in Punjab

Year	Target	Achievements	Percentage Vol. 2/1
1990-91	2,200	2,334	106.09
2000-01	3,500	1,912	63.73/100.00
2007-08	3000	245	100.00
2008-09	8000	147	100.00
2009-10	10000	117	100.00
2010-11	16000	25	100.00
2011-12	18000	12123	167.35
2012-13	10000	10005	100.05
2013-14	8200	8200	100.00
2014-15	9250	7304	78.96

Source: Director, Agriculture, Punjab Director, Punjab Energy Development Agency

Table 2 highlights that in Punjab installation data of SPV devices show diverse trend which are not towards the increasing side. The variations are between constant and decrease in number.

Looking at the overall picture of both programmes, it is unsatisfactory to see the success rate of policies and programmes put forward by the government as it faces various generic barriers related to coordination, support and management of institutions working for development

of renewable energy sector. Some of the concerns are underlined in the following points:

a) **Institutional Barriers**: There are still bureaucratic issues in institutions related to institutional mechanism like delay in paperwork, delays in issuing planning permission and obtaining technical approvals. It requires adequate and easy participation of local government working at grassroots level, NGOs, and other communities.

b) **Information Barriers:** There is a lack of knowledge and training regarding benefits and usage of off- grid renewable energy sources among all the stakeholders like citizens, grass root level institutions, financing institutions and entrepreneurs.

c) **Financial Barriers:** Government provides high subsidies on conventional resources in comparison to renewable energy resources which encourage reluctance of society to move towards renewable energy sources and to overcome the growing gap between the costs of generation.(Ravindranath and Nagesha Rao, 2011)

d) **Miscellneous Barriers: Lack of maintenance service,** costly and low quality in comparison to market price as in lieu to provide subsidy under high pricing also hinders the growth of off-grid renewable energy sources.

Conclusion

The analysis reveals that there is urgent need to acknowledge and support in utilizing the huge potential of SPV systems and Biogas plants to meet the needs of the millions of energy starved population and that too without compromising the energy security of the country. It is significant to follow a systemic approach to understand while designing and conducting research to diffuse Off-grid renewable energy to mass in a better manner. Few measures are need to be taken to deploy more off grid renewable energy in Punjab like more allocation of funds by central government and provision of subsidy PEDA in all consecutive years, efficient feedback mechanism and regular interaction between government institutions and users, efficient after sales service, provisioning of access to low cost finance, altering interest rates through financial institutions.

References

[1] Department of Science, Technology and Environment. 2015, Demand Side Management in Punjab, *Green Growth Background paper*, http://www.teriin.org/projects/green/pdf/Punjab-DSM.pdf, Nov 2016

[2] Deshmukh Ranjit, Gambhir Ashwin and Sant Girish. 2010, Need to realign India's National Solar Mission, *Economic and Political Weekly*, Vol XLV, http://www.indiaenvironmentportal.org.in/files/Need%20to%20Realign%20Indias%20National%20Solar%20Mission.pdf, Sept 2015

[3] International Energy Agency Highlights. 2016, CO_2 Emissions From Fuel Combustion: IEA Statistics, https://www.iea.org/publications/freepublications/publication/CO2EmissionsfromFuelCombustion_Highlights_2016.pdf, Jan 2017

[4] Kamalapur G. D. and Udaykumar R. Y. 2009., Electrical Energy conservation in India- Challenges and Achievements, *IEEE*, pp.1-5, http://ieeexplore.ieee.org/stamp/stamp.jsp?tp=&arnumber=5204479, Aug 2015

[5] Ministry of New and Renewable Energy. 2009, National Biogas and Manure Management Programme, Government Document, http://www.kvic.org.in/update/schemes/biogasscheme.pdf, Jan 2015

[6] Ministry of New and Renewable Energy. 2016, Jawaharlal Nehru Solar Mission, Chapter 4, Annual report, http://mnre.gov.in/file-manager/annual-report/2015-2016/EN/Chapter%204/chapter_4.htm, Oct 2016

[7] Pillai Indu R. and Banerjee Rangan. 2009, Renewable energy in India: Status and potential, Energy and its sustainable development for India, *Elsevier*, pp.970-980, http://ac.els-cdn.com/S0360544208002922/1-s2.0-S0360544208002922-main.pdf?_tid=9af9ee6a-1f11-11e5-9afe-00000aab0f6c&acdnat=1435659798_6880269f76597c672dc9541f4f00685b, June 2015

[8] Ravindranath Darshini and Rao Srinivas Shroff Nagesha. 2011, Bio energy in India: Barriers and policy options, *United Nations Development Programme*, http://www.indiaenvironmentportal.org.in/files/BioenergyIndia.pdf, Dec 2014

[9] Shrimali Gireesh and Rohra Sunali 2012, India's solar mission: A review, *Renewable and Sustainable Energy Reviews*, Vol 16, pp. 6317–6332, http://ac.els-cdn.com/S1364032112004054/1-s2.0-S1364032112004054-main.pdf?_tid=bbf5aa38-5782-11e5-b204-00000aab0f01&acdnat=1441865651_0a79556e0183a939ff83f3448fc3e91d., August 2015

[10] Singh Jaswinder and Chauhan Amit. 2014, Assessment of Biomass Resources for Decentralized Power Generation in Punjab, *International Journal of Applied Engineering Research*, Vol 9, pp. 869-875, http://www.ripublication.com/ijaer_spl/ijaerv9n8spl_03.pdf, Dec 2014

EFFECT OF FUEL OXYGEN CONTENT ON THE PERFORMANCE OF A CI ENGINE FUELLED WITH SOAPNUT BIODIESEL BLENDS

B. P. Pattanaik
Department of Mechanical Engineering
National Institute of Technology Silchar,
Silchar-788010, Assam, India
Email: bpprdmnits@gmail.com

J. Jena
Department of Mechanical Engineering
Gandhi Institute for Education and Technology,
Bhubaneswar-752060, Odisha, India
Email: jivanjena@gmail.com

R. D. Misra
Department of Mechanical Engineering
National Institute of Technology Silchar,
Silchar-788010, Assam, India
Email: rdmisra@gmail.com

ABSTRACT

In the present work 18 numbers of soapnut biodiesel-diesel blends along with soapnut oil as additive in some cases are used in a compression ignition engine for comparative assessment of the effect of fuel blends on the engine performance. Considering the large variations in oxygen content of the fuel blends it is opted as the basis for the study. Results showed that the best engine performance is achieved with oxygen content in the fuel blends in the range 1.8-3.0%. The emission results showed that the best engine emission is obtained with oxygen content in the fuel blends in the range 0.71 – 2.37%. Considering engine performance and emissions, the critical zone of oxygen content is found to be in the range 1.8 – 2.37%. The fuel blends having oxygen content within this critical zone, i.e. fuel blend nos. 8-13 are found to be best with higher engine performance and lower exhaust emissions.

Keywords: soapnut biodiesel, engine performance and emission, fuel oxygen content

INTRODUCTION

Progress in science and technology over the years has changed human life style which demands higher energy consumption resulting in faster depletion of the conventional fossil fuel reserves. Further, higher greenhouse gas emissions has raised serious environmental concerns. These factors have led to an innovative worldwide search for alternative fuels from renewable sources like biomass. Biodiesel derived from vegetable oils has emerged as a promising alternative fuel for diesel engines in recent years. Biodiesel is the fatty acid methyl ester which is derived from vegetable oils via base catalyzed transesterification [1]. It is a renewable, biodegradable, and non-toxic fuel and has comparable fuel properties to diesel. Biodiesel has edge over diesel fuel due to its higher flash point and greater lubricity [2]. However, higher viscosity and poor cold flow properties make it unsuitable for use in cold climates. Biodiesel exhibits lower carbon monoxide (CO), hydrocarbons (HC), and particulate matter (PM) emissions compared to diesel. On the other hand, biodiesel combustion produces higher nitrogen oxides (NO_x) emissions owing to its higher oxygen content [3-5]. Due to these factors use of biodiesel as blends with diesel up to certain volume percentages is more suitable rather than use of neat biodiesel as fuel in a compression ignition (CI) engine.

The present paper analyses the results obtained from the experimental investigation on a CI engine fuelled with a number of soapnut biodiesel-diesel blends with an aim to study the influence of oxygen content in the fuel blends on engine performance and emission characteristics. Additionally, the role of parent vegetable oil as an additive to biodiesel-diesel blends is also studied in order to establish the most suitable additive percentage for achieving best engine performance and emission.

MATERIALS AND METHODS

Fuel Samples

For the present experimental investigation soapnut oil (SO) is selected as the biofuel source due to its availability and cost in this locality, being non-edible in nature, and being a newly established biofuel source. The biological name of soapnut is *Sapindus mukorossi* which is a common plant in the Himalayan region in northern part of India. The soapnut seed contains 23% oil which has high triglycerides percentage i.e. 92% [6]. Neat SO was used for production of soapnut biodiesel (SB) via base catalyzed transesterification. The prepared SB is then blended with diesel in predefined volumetric basis percentages of 10%, 15%, 20%, 25%, 30% and 40% and are suitably named as SB10, SB15, SB20, SB25, SB30, SB40, along with SB100 i.e. 100% biodiesel. Parent vegetable oil i.e. SO is then used as an additive in volume fractions 2.5%, 5%, and 10% to the already prepared biodiesel blends i.e. SB10, SB15, SB20, and SB25 to produce fuel blends as SB10-SO2.5 (10% by vol. of SB, 2.5% by vol. of parent SVO and the rest diesel), SB10-SO5, and SB10-SO10. SB15 blends with SO additive are termed as SB15-SO2.5, SB15-SO5, and SB15-SO10 and so on. In this way, a total number of 18 final fuel blends are prepared for the present experimental investigation namely SB10, SB10-SO2.5, SB10-SO5, SB10-SO10, SB15, SB15-SO2.5, SB15-SO5, SB15-SO10, SB20, SB20-SO2.5, SB20-SO5, SB20-SO10, SB25, SB25-SO2.5, SB25-SO5, SB25-SO10, SB30, and SB40.

Fuel characterization of the above fuel blends are carried out using standard ASTM methods. It shows that the density, viscosity, cloud and pour point of the fuel blends increase with increase in oxygen content. Density and viscosity of all the fuel blends are observed to be in the range 837-855 kg/m^3 and 3.05-4.16 cSt respectively. Similarly, the cloud and pour points of all the fuel blends are in the range 7.0-12.6°C and 3.5-4.9°C respectively. Again, calorific value of the fuel blends decreased with increase in oxygen content and was in the range 40.74-42.5 MJ/kg.

The fuel characterization is followed by evaluation of carbon, hydrogen, and oxygen percentage of the fuel blends using a CHN-O elemental analyzer (Model-Flash 2000) and the results are demonstrated in Tab. 1 where the fuel blends are reordered according to the increasing oxygen content. The CHN-O analysis shows large variation in oxygen content of the fuel blends i.e. 78.23%. This makes oxygen percentage as the basis for the comparative assessment of the effect of the SB blends on the performance of the engine.

TABLE 1: OXYGEN CONTENT IN SB BLENDS

Blend No.	Blend name	% by volume			Oxygen (% by wt)
		SB	Diesel	SO	
1	SB10	10	90	0	0.961
2	SB10-SO2.5	10	87.5	2.5	1.210
3	SB15	15	85	0	1.240
4	SB15-SO2.5	15	82.5	2.5	1.469
5	SB10-SO5	10	85	5	1.499
6	SB20	20	80	0	1.686
7	SB15-SO5	15	80	5	1.748
8	SB10-SO10	10	80	10	1.809
9	SB25	25	75	0	2.010
10	SB20-SO2.5	20	77.5	2.5	2.060
11	SB15-SO10	15	75	10	2.309
12	SB25-SO2.5	25	72.5	2.5	2.329
13	SB20-SO5	20	75	5	2.377
14	SB30	30	70	0	2.410
15	SB20-SO10	20	70	10	2.648
16	SB25-SO5	25	70	5	2.830
17	SB40	40	60	0	3.070
18	SB25-SO10	25	65	10	3.602

Experimental Setup

In the present work a single-cylinder four-stroke water cooled diesel engine is used for experimentation. The test engine is coupled with an eddy current dynamometer connected to a loading unit. Two separate fuel tanks are used along with a two-way fuel supply line for supplying SB blends and diesel separately to the engine. A five gas analyzer (AVL Digas 444) and an AVL 437 smokemeter are connected to the test engine for measuring the engine emissions. The entire engine test is operated by Enginesoft LV software installed on a computer.

RESULTS AND DISCUSSION

From the results it is observed that there is wide variation in ranges of values of the different performance and emission parameters with varying oxygen percentage in the fuel blends. Therefore, these parameters may be reduced to a common platform for comparative assessment. Since diesel is the base fuel of all the selected fuel blends in the present work, all the parameters of a particular fuel blend is being non-dimensionalized by dividing the corresponding value of diesel. That is, the value of ith parameter of a specific fuel blend can be found as:

$$\left(\beta_{specific\,fuel\,blend}\right)_i = \frac{i_{specific\,fuel\,blend}}{i_{diesel}}$$

Where, β_i is known as the non-dimensionalized parameter for the ith parameter of a specific fuel blend.

Effect of Fuel Constituents on Engine Performance Parameters

The variations of different engine performance parameters like brake thermal efficiency (BTE), brake specific energy consumption (BSEC), and exhaust gas temperature (EGT) with varying fuel oxygen content of the considered fuel blends are presented in Fig. 1.
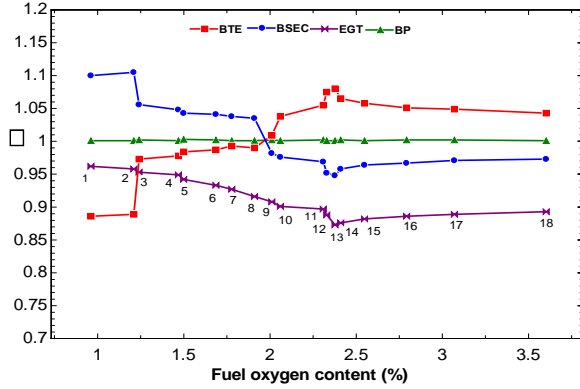
FIGURE 1. VARIATION OF $\beta_{\text{ENGINE PERFORMANCE PARAMETERS}}$ WITH FUEL OXYGEN CONTENT

Brake Thermal Efficiency. It is observed that BTE of the fuel blends overtakes that of diesel at about 1.97% oxygen content. Further, $(\beta)_{BTE}$ increases with increase in oxygen % up to 2.37%. With increase in oxygen % in the fuel blends the heating value decreases and less fuel energy is supplied to produce a fixed brake power. Further, it is observed that the fuel blends containing oxygen more than 1.97% show higher BTE than diesel. One possible explanation may be due to higher density of biodiesel blends compared to diesel, more biodiesel is required to compensate for decreased heating value of the fuel blends.

Brake Specific Energy Consumption. It is observed that $(\beta)_{BSEC}$ decreases with increase in oxygen % up to 2.37%. The fuel blends with oxygen % more than 1.97% show lower BSEC than diesel. This may be due to decrease in heating value of blends. Fuel blends with oxygen % more than 2.37% show slight increase in $(\beta)_{BSEC}$. Here, the increase in density and viscosity dominates the gain in heating value resulting in higher fuel consumption. Thus, fuel blends containing more than 1.97% oxygen content perform better than all other fuel blends.

Exhaust Gas Temperature. It is observed that $(\beta)_{EGT}$ decreases with increase in oxygen percentage up to 2.37% and then increases. The reason may be increase in oxygen % in the fuel blends causing the mixture to reach stoichiometric conditions faster [7]. The fuel blend number 13 shows the lowest $(\beta)_{EGT}$ than corresponding fuel blends.

Thus considering all the engine performance parameters it seems that the best engine performance for the region of oxygen content from 1.8 – 3.0% irrespective of fuel types, wherein the BSEC for the fuel blends is in the minimum range as well the BTE is in the maximum range.

Effect of Fuel Constituents on Engine Emissions Parameters

Literature shows that biodiesel produces lower CO and HC emissions with slightly higher NO_x emissions compared to diesel. Parent vegetable oil as additive to biodiesel blends may be suitable option to reduce NO_x emissions [8]. In the present section variation in non-dimensionalized emission parameters $(\beta)_{CO}, (\beta)_{HC}, (\beta)_{CO_2}, (\beta)_{NO_X}$, and $(\beta)_{PM}$ with respect to increase in oxygen content are shown in Fig. 2.
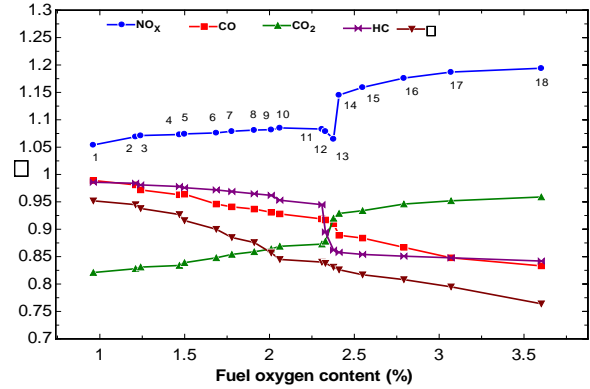

FIGURE 2. VARIATION OF $\beta_{\text{EXHAUST EMISSION PARAMETERS}}$ WITH FUEL OXYGEN CONTENT

Carbon Monoxide Emissions. It is observed that with the increase in oxygen percentage in fuel blends the CO emissions reduced. This may be due to lower carbon content for biodiesel blends compared to diesel. Thus with less carbon in the fuel, there is greater chance for formation of CO_2. Another reason could be during combustion there may be lower possibility of formation of rich fuel zone for biodiesel fuel blends due to presence of fuel oxygen resulting lower CO emissions [9]. Further, sharp reduction in CO emissions is observed for fuel blends containing more than 2.37% oxygen content compared to diesel.

Carbon Dioxide Emissions. The results show that the CO_2 emission increases, with the increase in oxygen percentage in the SB blends. The CO_2 emissions for all selected fuel blends are less than that with diesel. This is attributed to the fact that biodiesels are low carbon fuel and has a lower elemental carbon to hydrogen ratio than diesel.

Hydrocarbon Emissions. From Fig. 2 it is observed that the HC emissions reduce with increase in oxygen percentage in fuel blends. The HC emissions for all considered fuel blends are lower than diesel, because the major source of HC emission is over-mixing. Over-mixing is related to ignition delay and mixing of air and fuel during combustion. Both shorter ignition delay and better atomization result complete combustion and reduced HC emissions. It is also observed that at oxygen percentages

higher than 2.37% (blend number 13-18) the HC emissions are better than those of other fuel blends with the fuel blend number 18 showing lowest HC emissions.

NO$_x$ Emissions. Figure 2 shows that NO$_x$ emissions increase with increase in oxygen percentage of all the SB blends and are higher than that of diesel. The possible reasons to this may be advanced injection timing, higher cetane number (CN), higher viscosity, presence of oxygen and shorter ignition delay. Advancing of injection timing advances the start of combustion producing higher peak temperature inside the cylinder and higher NO$_x$ emissions. Further, higher CN of biodiesel fuel blends shorten ignition delay advancing the start of combustion. This results in a significantly longer residence time of higher temperature in the cylinder causing higher NO$_x$ emissions. It is observed that fuel blend number 1 and 18 show lowest and highest NO$_x$ emissions respectively which is in accordance with the published literature [10].

Combined Effect of Engine Performance with Emissions

The engine performance analysis depicts that the region of oxygen content from 1.8–3.0% exhibits best engine performance with minimum BSEC and maximum BTE. From the results of emission analysis, the CO, HC and smoke opacity trends satisfies this region as these emissions are continuously decreasing with increase in oxygen content. On the contrary, the results of NO$_x$ and CO$_2$ emissions suggest the region of interest from 0.71% (lowest) up to 2.37%. Thus considering engine performance and emissions both, the critical zone in terms of fuel oxygen content is shown in Fig. 3.The range of oxygen content in this critical zone is found to be 1.8 – 2.37%. The fuel blends within this critical zone, i.e. fuel blend nos. 8-13 show better engine performance with lower exhaust emissions. The fuel blend number 13 is found as best having 2.37% oxygen, 84.88% carbon, and 12.56% hydrogen contents. Its chemical formula is evaluated to be $C_{19}H_{33.8}O_{0.4}$ with molecular weight 275.02 kg/kmol.
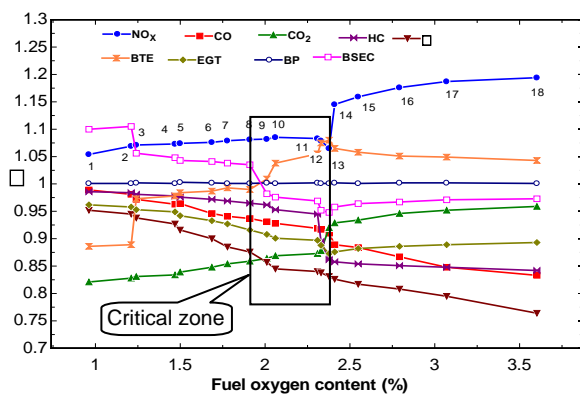
FIGURE 3. COMBINED EFFECT OF $\beta_{EMISSION}$ PARAMETERS AND $\beta_{ENGINE PERFORMANCE PARAMETERS}$ WITH FUEL OXYGEN CONTENT

CONCLUSIONS

The present experimental investigation is aimed to study the effect of fuel oxygen content of various SB blends on the performance and emission of a CI engine. From the analysis it may be concluded that the engine performed at its best when the oxygen content in the fuel blends lies between 1.8-3.0%. In this critical zone, the BSEC for the fuel blends is the minimum and the BTE is the maximum for all the considered fuel blends. Similarly, from emission results the CO, HC and smoke opacity trends are found to be decreasing with increase in oxygen content. On the contrary, the results of NO$_x$ and CO$_2$ emissions suggest the region of interest of oxygen content in the fuel blends from 0.71%-2.37%. Considering the importance of NO$_x$ and CO$_2$ emissions the suitable region in terms of oxygen content is found to be 0.71 – 2.37% for the selected fuel blends. Considering both engine performance and emissions, the critical zone of interest in terms of oxygen content is found to be 1.8 – 2.37%. The fuel blends within this critical zone, i.e. fuel blend nos. 8-13 show better engine performance on one hand and lower exhaust emissions on the other.

REFERENCES

[1] Demirbas, A., 2007. "Progress and recent trends in biofuels". Progress in Energy and Combustion Science, 33, pp. 1-18

[2] Canakci, M., and Sanli, H., 2008. "Biodiesel production from various feedstocks and their effects on the fuel properties". Journal of Industrial Microbiology & Biotechnology, 35(5), May, pp. 431–441

[3] Ribeiro, N.M., Pinto, A.C., Quintella, C.M., Da Rocha, G.O., Teixeira, L.S.G., et al., 2007. "The role of additives for diesel and diesel blended (ethanol or biodiesel) fuels: A review". Energy & Fuels, 21, pp. 2433-2445

[4] Murugesan, A., Umarani, C., Subramanian, R., and Nedunchezhian, N., 2009. "Bio-diesel as an alternative fuel for diesel engines-a review". Renewable and Sustainable Energy Reviews,13, pp. 653-662

[5] Babu, A.K., and Devarajane, G., 2003. "Vegetable oils and their derivatives as fuels for CI engines: an overview". SAE paper No. 2003-01-0767

[6] Misra, R.D., and Murthy M.S., 2011. "Performance, emission and combustion evaluation of soapnut oil–diesel blends in a compression ignition engine". Fuel, 90, pp. 2514-2518

[7] Raheman, H., and Phadatare, A.G., 2004. "Diesel engine emissions and performance from blends of

karanja methyl ester and diesel". Biomass Bioenergy, 27, pp. 393–397

[8] Murthy M.S., 2012. "Soapnut oil as a biofuel source for compression ignition engine: a feasibility investigation through engine performance, emission, and thermodynamic analyses". PhD Thesis, National Institute of Technology Silchar, India.

[9] Karabektas, M., 2009. "The effects of turbocharger on the performance and exhaust emissions of a diesel engine fuelled with biodiesel". Renewable Energy, 34, pp. 989–993

[10] Labeckas, G., and Slavinskas, S., 2006. "The effect of rapeseed oil methyl ester on direct injection diesel engine performance and exhaust emissions". Energy Conversion and Management, 47, pp.1954–1967

SEEC-2017-140

BIOGAS PURIFICATION USING WATER SCRUBBING AT DIGESTER PRESSURE

Sunil Kumar Saini
Department of Mechanical Engineering
Indian Institute of Technology Bombay
Email: 114100007@iitb.ac.in

Milind V Rane
Department of Mechanical Engineering
Indian Institute of Technology Bombay
Email: ranemv@iitb.ac.in

ABSTRACT

Steady state theoretical modelling of water based biogas scrubbing was performed using inside out algorithm of ASPEN software. Raw biogas having composition of CH_4 55%, CO_2 32.7%, H_2S 10,000 ppm, N_2 5% was scrubbed in water. The design parameters were optimized for scrubbing of 60 Nm^3/h biogas at digester pressure of 150 mm of water column. Modelling of biogas scrubbing was done with and without water recirculation. Sensitivity analysis shows that 90 m^3/h water flow rate and total 9 theoretical stages are requires to reduce CO_2 concentration in biogas from 32.7% to <1% and H_2S concentration from 10000 ppm to <20 ppm. H_2S removal efficiency in scrubber was found to be highly dependent on operating condition at the regeneration section. The airflow rate of 300 Nm^3/h was required to strip off 99% CO_2 and H_2S from liquid phase thereby reusing the same water for recirculation.

Keywords: *Biogas, Digester pressure water scrubbing Bio-CNG, Inside out algorithm, Rotating contacting disk*
.

NOMENCLATURE

G_i	Gas flow rate at i^{th} plate
K_{ij}	Equilibrium constant of jth species at i^{th} plate
L_i	Liquid flow rate at i^{th} plate
h	Enthalpy of stream
y_j	Composition of jth species in gas phase
DPWS	Digester pressure water scrubbing
HPWS	High pressure water scrubbing
HHV	Higher heating value
LPWS	Low pressure water scrubbing
NTU	Number of transfer unit
$\eta_{abs.i}$	Absorption efficiency of species i
$\eta_{strps.i}$	Stripping efficiency of species i

INTRODUCTION

Developing countries like India are spending major chunk of their monetary reserve in importing fuel to meet its energy demand. Indian energy demand due to rapid economic expansion is growing at a rate of 2.8% per year [1] and it is expected that its energy bill could spikes up to $230 billion from the current $120 billion by FY'23 [2]. The economic resources, which supposed to be spent on the socioeconomic development of the country, are not effectively utilized due to the energy import. This huge expenditure on energy import could be reduced if the renewable sources of energy are effectively utilized for above purpose.

Biogas could be one of the cost effective energy source as a biogas plant can be installed using small budget and with limited resources. India has the largest world cattle population with head count 512 million [3]. It is estimated that India has potential to produce $18,240 \times 10^6$ m^3 biogas per annum from cattle dung alone [4]. Bio energy share's is almost 22% [1] of India's total energy consumption. Major part of this energy is obtained by direct firing the biomass in open hearth, resulting in poor performance. This efficiency may be improved if the same biomass converted in biogas followed by efficient utilization as a source of energy. Biogas has a huge potential to improve the India's energy scenario where three hundred million people have no access to electricity supply [1].

Due to huge potential of bio energy MNRE is encouraging biogas plants construction under *National Biogas and Manure Management Programme (NBMMP)* [4]. Total number of biogas plant installed in india has already touched to 47.5 lac up to March 2014 and it was

expected that 1.1-lac biogas plant would have been added in to above magic number during year 2014 to 2015[4]. The amount of raw biogas may be much higher if gas produced from the industrial organic wastes, wastewater and urban landfills are also taken into the consideration.

Biogas is generated by anaerobic digestion of organic compounds by *Methanogens bacteria* in the digester. Raw biogas composition includes CH_4 (50 to 75%), CO_2(20 to 40%) and trace amount of H_2S [5]. Other than CH_4 all other species present in biogas are undesirable as they lower the HHV of gas, creates operational and health problems. H_2S content is highly corrosive and deteriorates the key components of machines such as electric generator and internal combustion engine. It is desirable to purify the raw biogas by removing the unwanted content before its end use application. The purification could be achieved by any existing technologies such as membrane separation, pressure swing operation, chemical absorption and water scrubbing [7,8]. However, most of these technologies are costly and very complex. Water scrubbing could be one of the most promising technology for above problem as it utilizes water as a solvent, which is universally available, and at free of cost.

Currently available high pressure water scrubbing, knows as HPWS technology utilizes physical absorption of gases in to water at elevated pressure in a packed column [7,8]. These scrubbers are operated at 5 to 30 bar as solubility of gases increases with pressure. Elevated pressure operation results in high CH_4 loss and high operation cost which ultimately results in revenue loss. A flash chamber is usually required to reduce the CH_4 loss, however it requires additional equipment and controls resulting in high initial cost. Low pressure water scrubbing, LPWS could be a cost effective and innovative solution which will not only decrease the installation and operating cost but also reduce the CH_4 loss.

The current study explores the opportunity of *Digester Pressure Biogas Scrubbing, DPWS*. Theoretical modelling was performed to scrub 60 Nm^3/h of raw biogas having CH_4 55%, CO_2 32.7%, H_2S 10,000 ppm, and N_2 5% at digester pressure of 150 mm of water column. Biogas having such high N_2 content is usually generated in landfills or in digester where municipal waste is either used or mixed with organic feed. The scrubber design and operating condition need to be selected in such a way that outlet composition of CO_2 and H_2S should not be more than 1% and 20 ppm respectively.

MODELLING OF BIOGAS SCRUBBER AT DIGESTER PRESSURE

The process diagram of biogas scrubbing has been shown in Fig 1. Biogas entering in scrubber meet counter

currently with water thereby reducing the amount of the undesirable quantities in the purified gas. The biogas scrubbing was modelled at digester pressure, which was at 150 mm of water column. Scrubber outlet water then directed towards the regenerator. In this section, the air blown towards the rich water counter currently so that contaminates could strip off from water and leave stripper with exhaust gases. The regenerated liquid went to purging section where small amount of water has been removed followed by addition of make-up water in mixture to compensate the water loss due to evaporation. This complete regenerated stream is further recycled to the absorption column using a pump/water circulator.
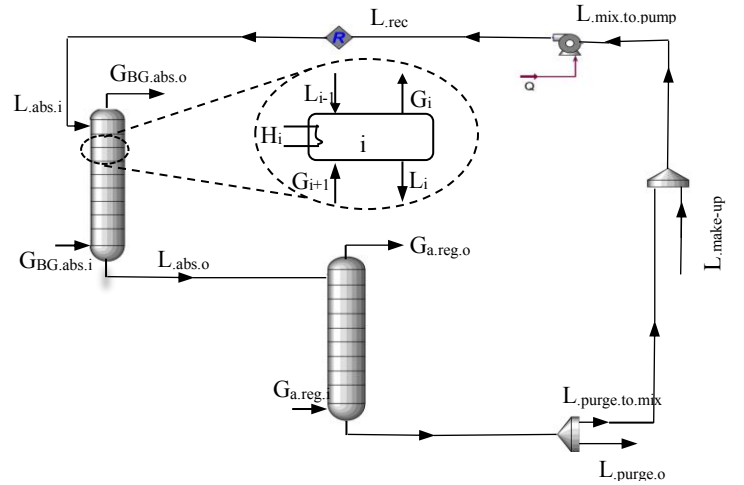

FIGURE 1: PROCESS DIAGRAM FOR BIOGAS SCRUBBING

A cut section of an hypothetical stage i^{th} has been shown in Fig 1 where gas and liquid phases comes into contact and mass transfer takes place. The amount of species transfered could be determined by solving the material and enthalpy balance equation called MESH equations [6] across any satge i. The MESH equation for above stage could be given as:

$$M_{i,j} \equiv L_i x_{i,j} + G_{i+1} y_{i+1,j} - L_{i-1} x_{i-1,j} - G_i y_{i,j} \qquad (1)$$

$$E_{i,j} \equiv y_{i,j} - K_{i,j} x_{i,j} \qquad (2)$$

$$S_{i,j} \equiv \sum_{j=1}^{j=C} y_{i,j} - 1 = \sum_{j=1}^{j=C} x_{i,j} - 1 = 0 \qquad (3)$$

$$H_{i,j} \equiv L_i hl_{i,j} + G_{i+1} Hg_{i+1,j} - L_{i-1} hl_{i-1,j}$$
$$- G_i Hg_{i,j} + Q_i \qquad (4)$$

Commercial software ASPEN was incorporated in order to **solve** above MESH equation using inside-out algorithm. The steady state equilibrium based approach was utilized for modelling of biogas scrubbing process at digester pressure. The vapourt liquid equilibiurm K_{ij} was determined using ELECNRTL model coupled with Henry's constant.

According to Cozma *et al.*, (2015) this model gives better prediction of solubility values with experimental data.

RESULT AND DISCUSSION

SCRUBBER PERFORMANCE WITHOUT WATER RECIRCULATION

The effect of water flow rate and NTU on biogas purification efficiency was studied using sensitivity analysis and shown in Tab. 1. It was observed that low CO_2 composition was found at high water flow rate with more methane loss. This is due to the fact that at higher liquid flow the rate of surface renewable at interphase is high, which ultimately result in high deriving force for mass transfer. H_2S removal efficiency was found to be more than 99% in all cases. Simulation results show that 9 theoretical stages at 90 m^3/h flow rate is required to reduce CO_2 in outlet gas to less than 1%. Increasing, the number of trays will increase the installation as well maintenance cost while more flow rate increases the pumping cost and loss of revenue in terms of bio methane.

Table 1. EFFECT OF WATER FLOW RATE AND NTU ON COMPOSITION OF PURIFIED GAS WITH ONCE THROUGH WATER FLOW, $G_{abs.BG.i}$ 60 Nm^3/h, $L_{abs.w.i}$ 90 m^3/h, $t_{w.abs.i}$ 27°C, p_{abs} 1.01471 bar

Sr #	Param.	NTU	L			
			70 m^3/h	80 m^3/h	90 m^3/h	100 m^3/h
1	$y_{CH4.o}$ %	7	82.1	85.5	87.1	87.7
		8	82.3	86.0	87.5	87.9
		9	82.6	86.5	**87.8**	88.0
		10	82.8	86.9	87.9	88.1
2	$\eta_{abs.CH4}$ (-)%	7	3.67	4.30	5.03	5.80
		8	3.64	4.26	5.00	5.78
		9	3.63	4.24	**4.98**	5.77
		10	3.62	4.23	4.98	5.77
3	$y_{CO2.o}$ (-) %	7	6.75	3.03	1.21	0.537
		8	6.47	2.42	0.764	0.289
		9	6.18	1.92	**0.470**	0.153
		10	5.78	1.47	0.284	0.080

SCRUBBER PERFORMANCE WITH WATER RECIRCULATION

Single pass water scrubbing plants are only feasible into those areas where water is readily available such as near wastewater plants and riverbanks. However, in most of the situations water recirculation will be required due to limited availability, and large water quantity is required while scrubbing done at low pressure. The effect of regenerator conditions on quality of purified gas was analysed by varying the airflow rate at regenerator. Water coming from scrubber has been regenerated at stripper section counter currently with air having 30% relative humidity at 27°C. In this study rather than taking air as single unit, the individual component such as N_2 (77.2%), O_2 (20.72%),CO_2 (0.039%), CH_4(1.97 ppm), Ar(0.92%) and water vapour(1.06%) has been considered for analysis. Total 9 theoretical stages were incorporated in regenerator section for above operation.
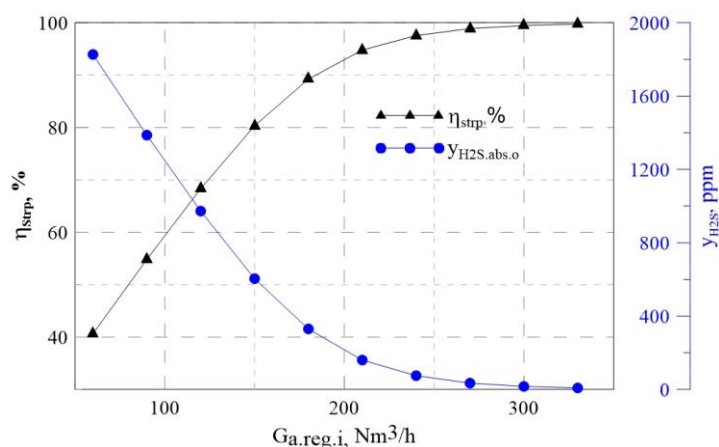
FIGURE 2. AIR FLOW RATE EFFECT ON H_2S STRIPPING EFFICIENCY AT REGENERATOR,

The effect of airflow rate variation from 60 to 330 Nm^3/h at regeneration section on H_2S and CO_2 stripping efficiency has been shown Fig. 2. The lowest H_2S stripping efficiency ~40.6% was observed at airflow of 60 Nm^3/h. Corresponding H_2S composition in outlet gas was found to be ~1826 ppm, which is extremely high value. Due to High solubility of H_2S in water, regenerator required comparatively greater driving force, which can be obtained by increasing the airflow rate. Theoretical analysis shows that 300 Nm^3/h airflow rate was able to remove ~99.5% of H_2S from water stream. Biogas scrubbing done with this regenerated water produce product stream having H_2S outlet concertation about ~16.51 ppm. The stripping efficiency of CH_4 and CO_2 at this airflow rate found to be more than 99%.

The composition of purified biogas from scrubber has been shown in Tab. 2. This table shows the optimized parameters based of recirculated water. Methane was enriched from 55% inlet to 84.16% at outlet. The CO_2 removal efficiency was found to be ~99% while ~5% CH_4 loss was also observed at these conditions. An unexpected behaviour was observed which is the presence of O_2 and trace of Ar in purified biogas at scrubber outlet. Presence of these species may be due to air stripping at regenerator section where these gases either absent or present in very low quantity in liquid phase. This low concentration of O_2 in water provides deriving force for O_2 absorption from air to water. These absorbed gases will be stripped off from water when liquid

re-enters into the scrubber, as raw biogas is free from most of these constituents. The outlet-purified gas also contains high N_2 content. During scrubbing process gases such as CO_2 and H_2S reduces in composition while N_2 is enriched from 5% to ~10.4% due to its low solubility compared to other species of biogas.

Table 2. PURIFIED BIOGAS COMPOSITION WHILE SCRUBBING DONE WITH WATER RECIRCULATION, $G_{abs.BG.i}$ 60 Nm^3/h, $G_{reg.a.i}$ 300 Nm^3/h, $L_{abs.w.i}$ 90 m^3/h, $t_{abs.w.i}$ 27°C, p_{abs} 1.01471 bar, p_{reg} 1 bar

Sr #	NTU	y_{CH4} %	y_{CO2} %	y_{H2S} ppm	y_{O2} %	y_{N2} %	y_{Ar} %
1	Lin	NA	NA	NA	NA	NA	NA
2	1	84.16	0.483	16.51	1.331	10.41	6.49E-02
3	2	87.17	1.234	16.68	0.086	7.939	4.60E-03
4	3	86.20	2.490	17.15	0.006	7.751	3.00E-04
5	4	84.32	4.532	19.21	3.00E-04	7.582	2.18E-05
6	5	81.44	7.662	28.31	2.06E-05	7.329	1.44E-06
7	6	77.37	12.09	68.12	1.18E-06	6.971	9.04E-08
8	7	72.22	17.67	232.6	6.37E-08	6.519	5.32E-09
9	8	66.57	23.75	860.5	3.16E-09	6.022	2.89E-10
10	9	61.20	29.37	3068	1.39E-10	5.550	1.38E-11
11	G.in	55.00	32.70	10,000	0	0.050	0

CHALLENGES IN DPWS/LPWS TECHNOLOGY

In DPWS/LPWS technology the scrubber need to be operated at high L/G ratio due to low solubility of gases in water. Tall and wide absorption column are usually required in order to accommodate such high flow rates. High L/G also results in column flooding and high gas phase pressure drop in packed column. Due to unavailability of a cost effective, modular technology, full-scale utilization of biogas is still a challenge.

Rotating contacting disk, RCD, based low cost mass exchangers have been developed and patented, IP203949, at HPL_IITB which open ups the opportunities for horizontal distillation and absorption column with very low gas side pressure drop and low power consumption. These type of units could be developed for biogas scrubbing at digester pressure. Detailed study on RCD based scrubber will be published in future

CONCLUSION

The theoretical analysis was performed in order to scrub high N_2 content raw biogas at digester pressure using water as a solvent. The recommended water flow for 99% CO_2 removal from raw biogas and outlet H_2S concentration less than 20 ppm was found to be 90 m^3/h at 27°C and pressure of 150 mm water column. Total nine theoretical stages were required for scrubbing process. Methane was enriched from 55% to 84.16% . The scrubbed biogas could be directly utilizes in gensets for electricity production thereby providing low cost electricity to remote rural area.

REFERENCES

[1] India Energy Outlook,2015., World Energy Outlook Special Report, International Energy Agency 9 rue de la Fédération 75739 Paris Cedex 15, France, See also www.iea.org

[2] http://indianexpress.com/article/business/economy/indias-energy-imports-bill-may-spike-to-230-bn-oil-to-natural-gas-switch-can-be-gamechanger-goldman

[3] 19 Livestock Census-2012 All India Report, Technical Report, Ministry of Agriculture Department of Animal Husbandry, Dairying and Fisheries, New Delhi

[4] www.mnre.gov.in

[5] Petersson A., Wellinge A., 2009, "Biogas Upgrading Technologies–Developments and Innovations", Technical Report, Task 37 - Energy from biogas and landfill gas, IEA Bioenergy

[6] Seader J. D., Henley E. J., (1998), Separation Process Principle, Third edition, John Wiley & Sons, USA, Chap. 10, pp 378-412

[7] Cozma P., Wukovits W., Ma˘ma˘liga˘ I, Friedl A., Gavrilescu M., 2015, "Modeling And Simulation of High Pressure Water Scrubbing Technology Applied for Biogas Upgrading, Clean Techn Environ Policy, Vol. 17, pp 373–391

[8] Kapdi S. S., Vijay V. K., Rajesh S.K., Prasad R., 2005., Biogas scrubbing, compression and storage: perspective and prospectus in Indian context, Renewable Energy, Vol. 30, pp 1195–1202

[9] Rasi S., La¨ntela L., Veijanen A., Rintala J., 2008., "Landfill Gas Upgrading With Countercurrent Water Wash", Waste Management, Vol. 28, pp 1528–1534

SEEC- 2017-141

GREEN SOLVENT BASED METHOD FOR ISOLATION AND FURTHER PROCESSING OF RICE STRAW LIGNIN TO AROMATIC PHENOLICS

Vivek Ahluwalia
Center of Innovative and applied Bioprocessing (CIAB), Mohali
Email: ahluwalia.vivek@gmail.com

Sandeep Kumar
Center of Innovative and applied Bioprocessing (CIAB), Mohali
Email: sandeepkumard22@gmail.com

Rajender S. Sangwan
Center of Innovative and applied Bioprocessing (CIAB), Mohali
Email: sangwan.lab@gmail.com

Sasikumar Elumalai
Center of Innovative and applied Bioprocessing (CIAB), Mohali
Email: biofuelswisc@gmail.com

ABSTRACT

Natural deep eutectic solvents (NADESs) have been considered as "green" solvents, which offer an efficient, safe sustainable and cost effective method development, alternative to the conventional extraction solvents (organic). With hypothesis of cleavage of carbohydrate-lignin linkages due to solvent effect, the present study applied combination of NADESs in order to remove or isolate aromatic lignin polymer from rice straw resource. So far, sixteen different NADESs combinations consisting of choline chloride (ChCl) or betaine with different monocarboxylic acid, polyalcohol acids were prepared with aim of testing on lignin recovery. Lignocellulosic biomass has been recognized for alternative renewable resource to produce chemicals (energy fuels) and biomaterials. Of the inherent constituents of biomass, aromatic lignin (derived from coniferyl, sinapyl, and p-coumaryl monolignol precursors) possess attractive material for synthesis of hydrocarbons (preferentially alkanes), as automotive fuel substitute. Lignin, making up to 10–25% of lignocellulosic biomass, is the second most abundant natural polymer. However, effective isolation of lignin without native structure alteration from lignocellulose is still challenging due to its complex physico-chemical properties (highly cross-linked macromolecule) and bonding with the associated components (hemicellulose and cellulose). After testing using NADEESs, considerable lignin yield was achieved following organic solvent treatment and it was further transformed and/or fragmented into its monomer units, including phenol and its derivatives under the hydrodeoxygenation conditions (at high severity reaction).

Keywords: Rice straw, Lignin, Natural deep eutectic solvents.

SEEC-2017-142

ISOMERIZATION OF GLUCOSE TO FRUCTOSE IN AQUEOUS MEDIUM OVER HETEROGENEOUS CATALYST TOWARDS SYNTHESIS OF LEVULINIC ACID

Sandeep Kumar
Center of Innovative and applied Bioprocessing (CIAB), Mohali
Email: sandeepkumard22@gmail.com

Devadutta Nepak
Institute of Nano Science and Technology
Email: devadutta.nepak@gmail.com

Kamalakannan Kailasam
Institute of Nano Science and Technology
Email: kamal@inst.ac.in

Sushil Kumar Kansal
Dr. SSBUICET ,Panjab University
Email: sushilkk1@gmail.com

Rajinder Singh Sangwan
Center of Innovative and applied Bioprocessing (CIAB), Mohali
Email: sangwan.lab@gmail.com

Sasikumar Elumalai
Center of Innovative and applied Bioprocessing (CIAB), Mohali
Email: Sasikumar Elumalai

ABSTRACT

Fructose is a key intermediate in the conversion of cellulosic biomass to biofuels and renewable platform chemicals. Industrially, the isomerization of D-glucose into D-fructose is carried out with enzymes but this suffers from various drawbacks such as the need of low concentration of D-glucose in solution with high purity and limited operating temperature range. Biomass-derived glucose can be isomerized to fructose using either Lewis acid or Brønsted base catalysts in the process to make an important platform molecules for example levulinic acid. However, monosaccharides are unstable under strong alkaline conditions and degrade into more than 50 different byproducts. It has been widely reported that fructose yields are typically low for Brønsted bases. In this context, we attempted to revisit the base-catalyzed isomerization and investigate the potential of organic amines (primary, secondary and tertiary amines) towards glucose to fructose. In the present study, we obtained maximum fructose conversion (10% wt.) with 56% selectivity over heterogeneous amine based catalyst in aqueous medium. Further tuning functional groups on solid catalyst providing Lewis acids and metals for improvisation of final product yield (fructose).

SEEC-2017-143

PRDUCTION OF AROMATICS FROM BIO-ETHANOL

Adarsh Kumar[1], Adnan Ali Khan, Jitendra Kumar[1], Thallada Bhaskar [1, 2,]*

[1] Thermo-catalytic processes area (TPA), Bio-Fuels Division (BFD), CSIR-Indian Institute of Petroleum (IIP), Dehradun 248005, India
[2] Academy of Scientific and Innovative Research (AcSIR)
Email ID: tbhaskar@iip.res.in, Telephone number: 0135-2525820

ABSTRACT

Till now days we are highly dependent on fossil fuels for energy and chemicals. A limited amount of fossil fuels necessitates finding other sources for chemical production. Bioethanol is one of the best options for valuable chemical production because it is obtained from biomass which is a renewable source. It can be upgraded to chemicals of high importance in fuel and chemical industry. Upgradation of aqueous bioethanol (45% ethanol) has been studied on ZSM-5(S/A=30-40) catalyst under different nitrogen pressures at 450°C. The pressure varies from 1 bar to 40 bar. The upgraded products contain 1-37 wt% aliphatics and 46-86 wt % aromatics. The pressure plays a crucial role as the aromatic yield decreases from 86 wt% to 46 wt% with increasing pressure from 1 to 20 bar. Further increase in pressure from 20 to 40 bar leads to increase in aromatic yield up to 70 wt%.

Keywords
Bioethanol, Upgradation, ZSM-5, N_2 atmosphere

INTRODUCTION

At this time, the majority of energy to our society is provided by fossil fuels, and a small amount of fossil fuel is also in use for the chemical production. The limited amount of fossil fuel has motivated the scientific community to explore the new sources for chemical production. In last decades biomass has been widely explored for the production of chemicals as it is a renewable source [1-2]. The main components of biomass are cellulose (40-50 wt%), hemicellulose (25-35 wt%) and lignin (20-30 wt%)[3]. Cellulose is widely used for paper and ethanol production [4]. The obtained ethanol known as bioethanol is an important precursor to valuable chemicals [5]. Hydrodeoxygenation is one of the important routes for upgradation of bioethanol to valuable chemicals, which takes place in presence of hydrogenating agent on acidic support at high hydrogen pressure and high temperature [6]. Various Noble metals (Pt, Pd,Ru,Rh) has been reported as hydrogenating agent [7], but the high cost of noble metals and hydrogen limits the practical application of this method. In this paper, ZSM-5 (S/A=30-40) catalyst in a nitrogen atmosphere at 450°C for bioethanol upgradation has been studied which seems to be cost effective.

FIGURES AND TABLES

Table 1: effect of nitrogen pressure on product distribution

Products (%wt)		Pressure (bar)					
		1	5	10	20	30	40
Saturates	Cyclic	0.55	4.30	0.91	8.27	1.44	4.06
	Iso	0.62	6.26	1.32	19.51	3.14	13.28
	Normal	0.59	1.25	1.90	2.87	2.09	1.35
	Total	*1.76*	*11.81*	*4.13*	*30.65*	*6.67*	*18.69*
Unsaturate	Cyclic	0	0.20	0	0.80	0	0.10
	N+Iso	0.55	2.75	0.10	6.02	0.63	3.83
	Total	*0.55*	*2.95*	*0.10*	*6.82*	*0.63*	*3.93*
Total Aliphatic		1.31	14.76	4.23	37.47	7.30	22.62
Total Aromatics		85.55	75.73	72.30	45.89	65.88	69.80

FIGURE 1. Aromatic yield at different pressure
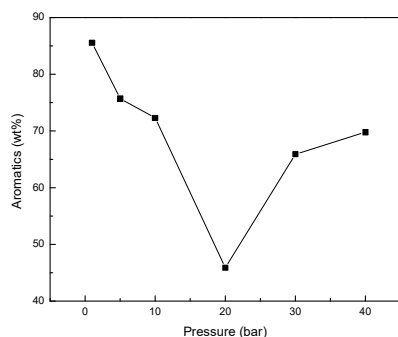
EXPERIMENTAL

Upgradation of aqueous bioethanol (45% ethanol) has been studied on the commercially available ZSM-5(S/A=30-40) in a fix bed down-flow reactor under different nitrogen pressures (1 bar to 40 bar) at 450°C. Glass beads and quartz wool were loaded above and below the catalyst. The feed was introduced using Eldex plunger type feed pump. Weight hourly space velocity (WHSV) of feed is set to 3.0 h^{-1}. The product at the end of the reactor was cooled by Chiller. The collected products contains two layers of liquids, which were separated in two different liquids (Organic part and Aqueous part) with separating funnel. The Organic part was analyzed gas chromatography Varian CP-3800.

RESULT AND DISCUSSION

The weight percentage (wt%) of aliphatic and aromatic products at different pressures are given in Table 1. The obtained products are mainly aromatics, while aliphatics are obtained as secondary products. The total aromatics are 85.55% at 1 bar and as the pressure increases up to 20 bar the aromatics decreases up to 45.89%, a further increase in pressure up to 40 bar increases the aromatics up to 69.80% but no regular trend follows in the case to aliphatic. The change in aromatics wt% along with a change in pressure is graphically presented in Figure 1.

CONCLUSION

Upgradation of aqueous bioethanol is studied on the ZSM-5 catalyst at different nitrogen pressure. The ZSM-5 is a suitable catalyst for upgradation of bioethanol because it provides acidic site for dehydration. The present study provides a cost effective alternative by using nitrogen atmosphere, which is cheaper than H_2 (conventionally used for upgradation). The most suitable condition for bioethanol upgradation is 1 bar nitrogen pressure at 450°C, as the highest amount of aromatics is obtained at this pressure.

REFERENCES

[1] Fiorentino, G., Ripa, M. and Ulgiati, S., 2016. Chemicals from biomass: technological versus environmental feasibility. A review. *Biofuels, Bioproducts and Biorefining*. **DOI:** 10.1002/bbb.1729

[2] Letcher, T.M. and Scott, J.L. eds., 2012. *Materials for a sustainable future*. Royal Society of Chemistry.

[3] Alonso, D.M., Bond, J.Q. and Dumesic, J.A., 2010. Catalytic conversion of biomass to biofuels. *Green Chemistry*, *12*(9), pp.1493-1513.

[4] Yunpu, W.A.N.G., Leilei, D.A.I., Liangliang, F.A.N., Shaoqi, S.H.A.N., Yuhuan, L.I.U. and Roger, R.U.A.N., 2016. Review of microwave-assisted lignin conversion for renewable fuels and chemicals. *Journal of Analytical and Applied Pyrolysis*, *119*, pp.104-113.

[5] Liu, C., Wang, H., Karim, A.M., Sun, J. and Wang, Y., 2014. Catalytic fast pyrolysis of lignocellulosic biomass. *Chemical Society Reviews*, *43*(22), pp.7594-7623.

[6] Hunns, J.A., Arroyo, M., Lee, A.F., Serrano, D. and Wilson, K., 2016. Hierarchical mesoporous Pd/ZSM-5 for the selective catalytic hydrodeoxygenation of m-cresol to methylcyclohexane. *Catalysis Science & Technology*, *6*(8), pp.2560-2564.

[7] Chen, C., Chen, G., Yang, F., Wang, H., Han, J., Ge, Q. and Zhu, X., 2015. Vapor phase hydrodeoxygenation and hydrogenation of m-cresol on silica supported Ni, Pd and Pt catalysts. *Chemical Engineering Science*, *135*, pp.145-154.

SEEC-2017-144

PHYSICAL AND SENSORY QUALITIES OF FINGER MILLET INCORPORATED MUFFINS

Nidhi Budhalakoti & Sarita Srivastava
Centre of Innovative and Applied Bioprocessing
Govind Ballabh Pant University of Agriculture and Technology

ABSTRACT

Two genotypes of finger millet (PRJ1 and Bharsar Local) were taken for the present study. The finger millet flours (FMF) were evaluated for nutrient composition. Nutritional evaluation of FMF showed that moisture (%), crude protein (%), crude fat (%), crude fiber (%), total ash (%), carbohydrate (%) and physiological energy (Kcal) content of FMF from genotype PRJ1 was 10.98, 10.29, 1.98, 5.44, 2.47, 68.16 and 334 respectively and for FMF from genotype Bharsar Local the values obtained were 11.13, 7.34, 2.19, 4.53, 2.69, 72.10 and 349 respectively. The FMF were blended in various proportions in (30, 40 and 50 per cent) in refined wheat flour and were used for the preparation of muffins. Control consisted of refined wheat flour muffins. Sensory and physical qualities of finger millet incorporated muffins were evaluated. Sensory evaluation of muffins showed that that the muffins prepared by the combination of refined wheat flour and FMF in the ratio of 70:30 obtained highest mean sensory scores and were accepted by the panel members. Similarly muffins prepared by other combinations of refined wheat flour and FMF i.e. in the ratio of 60:40 and 50:50 also obtained good scores and were accepted by the panel members. Physical characteristics of the formulated products showed that muffins weight increased significantly with the increase in incorporation of FMF. Volume, specific volume and diameter decreased with the increase in incorporation of FMF.

1

Prosopis juliflora bark - an alternate feedstock in the production of bioethanol using thermo tolerant yeast *Kluyveromyces marxianus*

S. Sivarathnakumar[1,2]
[1]Research Scholar, Faculty of Bioengineering, Department of Biotechnology, Sathyabama University, Chennai.
[2]Department of Biotechnology, Arunai Engineering College, Tiruvannamalai
Email: sivrathna@gmail.com

B. Bharathiraja[4]
[4]Department of Chemical Engineering, Vel Tech High Tech Dr.Rangarajan, Dr.Sakuntala Engineering College, Chennai
Email: btrbio@gmail.com

S.Chozhavendhan[2]
[2]Department of Biotechnology, Arunai Engineering College, Tiruvannamalai
Email: scv.ibt@gmail.com

G. Baskar[3]
[3]Department of Biotechnology,
St. Joseph's College of Engineering, Chennai.
Email: basg2002@gmail.com

R. Praveen Kumar[2]
[2]Department of Biotechnology, Arunai Engineering College, Tiruvannamalai
Email: praveenramanujam@gmail.com

K.M. Vishnuvardhan[2]
[2]Department of Biotechnology, Arunai Engineering College, Tiruvannamalai
Email: vishu.ebizlife@gmail.com

S. Surendar[2]
[2]Department of Biotechnology, Arunai Engineering College, Tiruvannamalai
Email: surendar253@gmail.com

ABSTRACT

Prosopis juliflora is considered as a prospective lignocellulosic material for bioethanol production and also as an alternative source to sugar-containing feedstock. In this study, bark of Prosopis juliflora was subjected to hydrothermal coupled with nitric acid pre-treatment followed by sonication and the composition of cellulose, hemicellulose, lignin and reducing sugars and inhibitors at each stage of pre-treatment was analysed. Further, Simultaneous Saccharification and Fermentation (SSF) studies were carried out using Kluyveromyces marxianus (MTCC 1389) and commercial cellulase along with delignified lignocellulosic biomass. The effect of operating parameters such as pH, temperature, substrate concentration and inoculum volume was investigated. The maximum bioethanol concentration achieved for each parameter by fermentation of woody stem Prosopis juliflora using the yeast was found.

Keywords: **Lignocellulosic material, *Kluyveromyces marxianus*, *Prosopis juliflora*, SSF.**

INTRODUCTION

The disinclination of fossil fuels, increase in demand of energy and alarming rate of green house gases has urged the scientist to search an alternate fuel which is obtained from a renewable source. The production of bioethanol from renewable sources such as lignocellulosic biomasses is extensively utilised today due to various advantages like its cheap, renewable, abundant and do not compete with the food production.

Prosopis juliflora, a lignocellulosic material is neither a tree nor shrub sized woody perennial plant which is found mainly in the dry regions of India, Saudi Arabia and the United States of America. The plant grows to a height of 3-15 meters depending on genetic variations and other ecological factors, but under favourable environmental conditions some individuals may reach up to 20m. The carbohydrate content in this woody stem *Prosopis juliflora* was found to be $67.40 \pm 1.6\%$ that proves to be a suitable substrate for bioethanol production[1].

Lignocellulosic biomasses are primarily composed of cellulose(six-carbon sugar), hemicellulose (five-carbon

sugar) and lignin (phenyl propane units). In order to utilize the cellulose and hemi cellulose, the lignin content need to be removed completely. Among various pretreatment processes, chemical treatment is found to remove lignin and increase surface area of the substrate for saccharification of holocellulose into constituent sugars.

In chemical method, dilute acids such as HCl, H_2SO_4 and alkalis like NaOH, KOH are used. This lead to the production of certain inhibitory components such as furfural, hydroxyl methyl furfural and phenolics which paly a vital role during fermentation process[2]. The amount of cellulase given in enzymatic hydrolysis of cellulose to cellbiose to glucose, if 10FPU/g cellulose is used in which glucose yield would be maximum in a reasonable time[3].

Fermentation and enzymatic hydrolysis is carried out by SHF (Separate Hydrolysis and Fermentaion) and SSF (Simultaneous Saccharification and Fermentation). Off these two, SSF is found to be a better process as it can be completed in single reactor but due to temperature difference between organism optimal growth and Saccharification process, an organism need to be chosen which can grow at elevated temperatures (37°C-45°C)[4].

Ethanol yield could be also enhanced in a SSF process by the utilization of thermotolerant yeast such as *Kluyveromyces marxianus* due to various advantages like extensive consumption of sugars, tremendous growth rate and high secretory capacity.

In the present study, *Kluyveromyces marxianus* (MTCC 1389) in used along with pretreated woody biomass *Prosopis juliflora* and commercial cellulase and bioethanol production is estimated. The parameter such as pH, temperature, substrate concentration and inoculum volume was investigated.

MATERIALS AND METHODS

Collection and analysis of Lignocellulosic biomass

The woody stem of *Prosopis juliflora* was obtained from Melmalaiyanur village, Tiruvannamalai district, Tamilnadu, India. The size reduction of feed stock was done by chipping followed by milling in a knife mill. The powdered material was washed under tap water and dried overnight at 60°C.

Combination of treatment (Auto-hydrolysis and acid) followed by sonication of woody stem *Prosopis juliflora*

The air dried dust free woody substrate is taken along with nitric acid (3%(v/v)) with solid to liquid ratio of 1:10 and placed in autoclave for one hour at 121°C, 15 psi. The contents were filtered using double layered muslin cloth and the hydrolysate was washed with tap water to attain a neutral pH. The left over residue was dried to constant weight and later subjected to sonication.

The auto hydrolysed and acid treated samples with distilled water was taken in a solid to liquid ratio of 1:10 (w/v) placed in glass flask. Ultrasound treatment was given at a frequency of 40KHz, chamber temperature of 60C° for 5min (Model: Sonics vibra cell, power 500W, processor: 750W, VCX series).

Micro-organism and culture conditions

Kluyveromyces marxianus (MTCC 1389) was procured from IMTECH, Chandigarh. The cultures for inoculation were prepared by growing the yeast on a rotary shaker at 120 rpm for 24 h at 25°C in a growth medium (initial pH 6.2) containing (g/l): malt extract 3; yeast extract 3; peptone 5; glucose 10; agar 20.

Enzyme and surfactant

Commercial cellulase from *Trichoderma reesei* (ATCC 26921), tween 80 and sodium azide where procured from HIMEDIA laboratories, Mumbai. The activity of the enzyme was measured by Filter Paper assay and expressed in terms of Filter Paper Units, FPU. The enzyme activity was found to be 6 FPU/mg and it was used throughout the experimentation.

Simultaneous saccharification and fermentation(SSF)

SSF was carried out in a 250ml shake flask with working volume of 50ml containing 0.05M citrate phosphate buffer (50mmol/l, pH 5) with pre-treated substrate which is supplemented with growth medium. The slurry was then autoclaved at 121°C for 20min. In addition, a dosage of commercial cellulase with 12 FPU/g of substrate and 1ml of inoculum (OD is 0.6 at 610nm) was loaded into the substrate mixture and operated under controlled conditions with an agitation speed of 120rpm. A quantity of 0.005% sodium azide was introduced to avoid any microbial contamination and 1.0% (v/v) of Tween 80 was added to facilitate the enzymatic action. Samples were withdrawn from SSF media at pre-set times (0, 12, 24, 36, 48, 60, 72, 84, 96 hrs), centrifuged (10000 rpm, 10min) and analysed for dry biomass, reducing sugar and ethanol concentration by dry cell weight, DNS method and Gas Chromatography technique respectively. This method is carried out for different values of pH, temperature, substrate concentration and inoculum volume in order to estimate the optimized value for bioethanol production.

Analytical methods

The concentration of reducing sugars was estimated from pre-treated hydrolysate by Di-Nitro Salicylic acid method.

Biomass concentration in dried conditions was carried out by taking 10ml of culture sample, centrifuged at 10000g for 10min. Supernatant was discarded and dried to a constant mass at 70°C.

The concentration of cellulosic ethanol was estimated by Gas Chromatography (GC) (Perkin Elmer, Clarus 500) with an elite-wax (cross bond-polyethylene glycol) column (30.0 m X 0.25 mm) at oven temperature of 85 °C and flame ionization detector (FID) at 200 °C. The ethanol standards were prepared using commercial grade ethanol (Merck, Darmstadt, Germany). Nitrogen with a flow rate of 0.5 mL/min was used as carrier gas.

RESULTS AND DISCUSSION

The raw woody stem *Prosopis juliflora* was found to contain (g/100g of wood) 40±0.3 cellulose, 22±0.0 hemi cellulose, 22±0.01 lignin , 2±0.22 glucose, 3±0.01fructose, 12±0.61xylose, 1±0.05arabinose, 0.24±0.00 ash. The combination process (auto hydrolysis and nitric acid treatment) followed by sonication gave maximum content 48±0.7 cellulose, 23±.01 hemi cellulose, 19±0.66 lignin, 2±0.75 glucose, 3±0.09fructose, 13±0.31xylose, 1±0.65arabinose, 0.22±0.54ash. The effect of pH (4.5, 5.0, 5.5), temperature(32°C,37°C,42°C), substrate concentration (3%, 5%, 7% (w/v)) and inoculum volume (3%, 5%, 7% (v/v)) was investigated.
Prosopis juliflora when subjected with *Kluyveromyces marxianus* MTCC 1389 showed an enhanced yield of ethanol production of around 18.5 g/l at a temperature of 42°C, pH of 4.5, substrate concentration 5% (w/v) and inoculum concentration of 5 % (v/v). These were obtained during 72-96 hours of incubation period. During SSF process, at intial stage the glucose concentration was found to be minimal and biomass production was found to be appreciable (0-12 hours). Later as the glucose concentration reached to the maximum the yeast fermentation has ceased (72-96 hours). Above 5% (w/v) of substrate concentration leads to a decline in enzymatic hydrolysis and product inhibition. SSF process is said to be given much importance as the fermentation temperature, pH of *Kluyveromyces marxianus* MTCC 1389 and that of enzymatic hydrolysis lies in the same range (40°C-50°C, 4.5-5.0) with increased ethanol production.

CONCLUSION

The current study was carried out to evaluate the bioethanol production from pre-treated lignocellulosic biomass *Prosopis juliflora* by simultaneous saccharification and fermentation process using *Kluyveromyces marxianus* MTCC 1389. The combination of auto hydrolysis and acid based saccharification has found to give better yield of cellulose and reduction of lignin content. An increased concentration of bioethanol at high temperature (42°C) and low pH (4.5) which goes along with enzymatic hydrolysis was studied. Any improvement in pretreatment process of lignocellulosic biomass and engineering the organism may furthur increase the ethanol production

REFERENCES
[1]Shaik, N.,Srilekha Y, K.,Sateesh, L., Ananth, M., Suseelendra, D., Venkateswar ,Rao, L.2013. "Selection of the best chemical pretreatment for lignocellulosic substrate". Bioresource Technology, 136, pp. 542–549

[2] Rishi Gupta, Krishna Kant Sharma, Ramesh Chander Kuhad, 2009. "Separate hydrolysis and fermentation (SHF) of Prosopis juliflora, a woody substrate, for the production of cellulosic ethanol by *Saccharomyces cerevisiae* and *Pichia stipitis*-NCIM 3498". Bioresource Technology, 100, pp. 1214–1220

[3] Ye Sun, Jiayang Cheng, 2002. "Hydrolysis of lignocellulosic materials for ethanol production: a review" Bioresource Technology, 83, pp. 1–11.

[4]Kádár, Zs., Szengyel, Zs., Réczey, K., 2004. "Simultaneous saccharification and fermentation (SSF) of industrial wastes for the production of ethanol", Industrial Crops and Products 20, pp. 103–110.

SEEC-2017-146

Modified method for enriched lignin isolation from rice straw towards fungible fuel hydrocarbons synthesis

Pranati Kundu[1,2], Sushil Kumar Kansal[2], Rajender S Sangwan[1] and Sasikumar Elumalai[1]
[1]Center of Innovative and Applied Bioprocessing (CIAB), Mohali 160081, India
[2]Dr. SSB UICET, Panjab University, Chandigarh, 160014, India
Corresponding author: sasikumar@ciab.res.in

ABSTRACT

 As the world's one of the most abundant renewable resource, lignocellulosic biomass can be used for the production of a large number of chemicals (energy fuels) and biomaterials. Of the inherent constituents of biomass, aromatic lignin constitute about 15-25% of the total weight. Lignin is a derivative of coniferyl ,sinapyl, and p-coumaryl monolignol and an attractive material for the synthesis of hydrocarbons. It has been reported that the alkanes derived from lignin are potential alternative to automobile fuel substitute. In plant biomass, lignin is the second most abundant natural polymer. However, effective isolation of lignin without native structure alteration from lignocellulose is still challenging due to its complex physio-chemical properties (highly cross-linked macromolecule) and bonding with the associated components (hemicellulose and cellulose). Because of its enriched structural properties, it is possible to synthesize relatively more phenolic precursors (dimers and monomers) during lignin fragmentation in the presence of heterogeneous catalyst. Therefore, in this work, a modified chemical method for isolation of lignin from rice straw has been reported. A large number of compounds such as Sodium hydroxide, Sodium carbonate etc. have been used for the isolation of lignin from the lignocellulosic biomass. During this study, lignin was isolated using alkaline (NaOH) solution, and an alkaline solution mixed with aqueous NH3. It was observed that maximum lignin was extracted when a mixture of NaOH and NH3 was used as compared to NaOH solution or Ammonia solution alone. There was around 20% increase in lignin content extracted compared to the control. The isolated lignin will be characterized using various techniques such as FTIR, 2D-HSQC NMR, TGA etc. Furthermore, easy recovery and reuse of aqueous NH3 during isolation process help to reduce overall processing cost of the lignin fragmentation.

SEEC-2017-147

Jatropha curcas pathogenesis related-10a protein improves fungal resistance, salinity tolerance and shoot bud induction via cytokinin signalling

Parinita Agarwal, Prashant More, Mitali Dabi, Khantika Patel, Kalyanashis Jana
and Pradeep K. Agarwal*
Plant Omics Division, CSIR-Central Salt & Marine Chemicals Research Institute, Gijubhai Badheka
Marg, Bhavnagar-364 002, Gujarat, India.
*Corresponding author: E-mail: pagarwal@csmcri.org

ABSTRACT

Jatropha curcas, a popular biodiesel crop belongs to family Euphorbiaceae. It is drought resistant and grows well on wastelands. Although, Jatropha can be cultivated on wastelands with less economical maintenance, its yield is severely reduced by fungal and viral diseases. The collar rot, caused by Macrophomina phaseolina and Jatropha leaf curl virus has caused severe loss to our Jatropha plantations. Managing collar rot by conventional agronomic practices was not fruitful, therefore, with an aim to enhance disease resistance of Jatropha, a pathogenesis-related gene JcPR-10a was isolated and characterized.

PR-10 is a multigene PR protein family playing important role in both biotic and abiotic stresses. JcPR-10a gene had an open reading frame of 483 bp, its genomic organisation revealed the presence of an intron at conserved 185 bp position. The JcPR-10a recombinant protein was expressed in E.coli cells and purified to near homogeneity. The recombinant purified protein exhibited antifungal activity against Macrophomina, by blocking the growing hyphae tips as a result they get thickened and stunted. The purified protein also exhibited RNase activity and this activity might be facilitating the antimicrobial activity of the protein, being released by infected host cells and acting directly on pathogens or during programmed cell death at and around the plant infection sites. The tobacco transgenics constitutively overexpressing JcPR-10a showed enhanced resistance against Macrophomina fungus. The leaf assay with transgenics and wild type employing Macrophomina showed severe blackening along the mid vein and side veins from proximal to distal end in the wild type leaf only, furthermore, the transgenic leaf extract inhibited the radial growth and density of microsclerotia.

The JcPR-10a transgenics showed enhanced endogenous cytokinin levels in planta, as a result when the plants are exposed to salinity stress, the increased cytokinin promote growth, development and photosynthesis by functioning as antioxidants, maintaining cellular redox potential with reduced oxidative damage and enhanced water use efficiency during salinity. Interestingly, the JcPR-10a overexpression resulted in increased number of shoot buds in tobacco, which could be due to high cytokinin to auxin ratio in the transgenics. The docking analysis shows the binding of three BAP molecules at the active sites of JcPR-10a protein. Furthermore, the role of JcPR-10a protein towards antiviral activity is being studied. JcPR-10a is an important candidate gene to overcome the disease problem in Jatropha by enhancing the defence potential of Jatropha.

SEEC-2017-148

CONVENTIONAL AND MOLECULAR APPROACH FOR IMPROVEMENT OF *JATROPHA CURCAS*: A PROMISING BIO-FUEL CROP

Pradeep K. Agarwal
Plant Omics Division, CSIR-Central Salt & Marine Chemicals Research Institute, Gijubhai Badheka Marg, Bhavnagar-364 002, Gujarat, India
pagarwal@csmcri.org

Aruna Prakash, Parinita Agarwal, Arup Ghosh and Aneesha Singh
Plant Omics Division, CSIR-Central Salt & Marine Chemicals Research Institute, Gijubhai Badheka Marg, Bhavnagar-364 002, Gujarat, India

ABSTRACT

Jatropha curcas has been popularized as non-conventional potential bio-fuel crop since long time. Its domestication has been tested in different environment and observed that it can be grown in the wasteland or marginal lands with some minor modification. The breeding of elite varieties is of prime importance to develop the high yielding lines. We made an efforts for developing high yielding breeding lines of *J. curcas* which is showing >30% higher yield. The attention has been brought towards biotechnological and molecular approaches for beneficial sustainability where the problem cannot be sought through conventional approach. Jatropha faces huge loss due to varieties of disease, which kills the large grown trees suddenly. The Jatropha collar rot disease caused by Macrophomina plugs the vascular system and leads to the damage of crops. Similarly, the viral infection spreads very severely in plantation and causes curl disease and eventually leads to complete yield loss. We have isolated the full length *PR-10a* gene and WRKY transcription factor from *J. curcas* and functionally validated. Presently the efforts are being made to develop the genetic transformation of Jatropha with disease tolerant traits.

Keywords: Jatropha curcas, Agronomy, Breeding, Plant Tissue Culture, Disease tolerance

INTRODUCTION

To meet the global fuel security, all countries of the world, including those with surplus energy are banking upon vegetable oil as alternative source of energy by way of biodiesel. Developing countries cannot afford to utilize edible vegetable oil or even used vegetable oil. However, many of these countries, like India, have large tracts of wastelands and tropical climate suitable for cultivating a variety of plants that yield non-edible oil. Cultivation for oil yielding trees in degraded, waste, abandoned and abused lands will provide sustainability, employment generation, and much needed oil to replace fossil fuels. The development of the nation is intricately interwoven with sustainability in energy and the promotion of potential renewable sources of biofuel is a part of India's goal to achieve energy independence since long.

Bio-diesel, the renewable liquid fuel from biological raw material is a good substitute for petroleum diesel. Jatropha oil is considered to be an excellent source of biodiesel and its cultivation has been proved to improve the soil properties and provide beneficial services [1]. *J. curcas* has drawn attention as an important bio-fuel crop and has potential to contribute the demand of bio-fuel blending program of national blending targets of govt. of India. India has a ray of hope since there is a potential to grow a variety of plants in different habitats of the country. This tree borne-oil (TBO) has low competition with agriculture crops for arable *vs* marginal lands as it can grow in

wastelands with minor agronomic inputs. It can be grown in arid to semi-arid conditions, plains to low slopes of hilly areas and degraded to abused soils.

CSIR-CSMCRI has worked on *J. curcas* for the past one and half decade wherein holistic efforts, like agronomical practices, germplasm collection and assessment, hybrid development, bio-fuel production and biotechnological and molecular approach for disease tolerance, have made for this crop. Our efforts generated some more interest in Jatropha because of the potential for large-scale cultivation on certain types of wasteland. Therefore, our research aimed to improve upon the existing cultivation practices developed by the Institute to maximize Jatropha oil productivity. The present paper deals about the significant achievements of work carried out at our institute on *J. curcas* related to yield improvement through agronomy and breeding, multiplication of elite material using micro propagation methods and disease resistance with intervention of molecular biology techniques.

RESULTS

The available germplasm was screened for desirable traits and some elite Jatropha lines were identified after five years of evaluation and then utilized these selected genotypes in Jatropha hybridization program. Few of the germplasms proved high yielding with high oil content. High yielding germplasms gave approximately 1.5-2 t/ha. Promising hybrids were developed using elite parental accessions following intraspecific hybridization.

Genetic variability, character association and divergence studies were carried out in *J. curcas* for improvement in oil yield. Considerable variability present in various existing germplasm provides a good opportunity for selection of desirable types. Trait selection was done for morphological, physiological and oil quality traits of *J. curcas* to assess their direct and indirect effect on oil yield by path and principal component analysis. Jatropha hybrids were developed through intra-specific hybridization after identification of superior genotypes from existing Jatropha plantation and crosses were made using them as parental lines [2-4].

Various agronomic practices were developed to grow Jatorpha plants in wastelands and it was proved that a yield of 2 tonnes seed per hectare is realizable provided proper agronomic practices are followed on elite germplasm. The beneficial effect of the Jatropha cake as a bye-product of biodiesel was studied as a manure, which showed enhanced soil organic carbon accumulation, microbial biomass and enzymatic activities in soils of semi-arid tropical wastelands and have no residual toxicity. The application of cake showed enhanced seed

yield (1.59-2.08 t ha^{-1}) as compared to Urea-50% ranged from 1.00 to1.33 t ha^{-1}; Urea-100% from 1.27 to 1.55 t ha^{-1}) and FYM from 1.38 to 1.79 t ha^{-1} [5].

Technology was developed to increase the number of fruits per infructescense by using paclobutrazol-a gibberlin synthesis inhibitor [6].

Figure1: large scale cultivation of Jatropha at Neswad site in Gujarat

An efficient micropropagation tissue culture protocol was developed using different explants [7-9]. Approximately, 3-15 multiple shoots were achieved per culture on MS media supplemented with BAP and IAA, after three subcultures onwards. More than 80 % rooting of elongated shoots was achieved using grafting rooting method [10].

CSIR-CSMCRI achieved a great feat in developing a simplified process for production of biodiesel from the oil complying with EN14214 specifications for free fatty acid methyl ester. While biodiesel complying with Euro 3 specification is produced in Europe from rapeseed oil, this is the first time that such biodiesel has been made from Jatropha oil. Jatropha bio-diesel evaluated at DaimlerChrysler AG was proven matching all the specifications set for a standard Euro biodiesel and rather it outperformed all other vegetable/animal oil based biodiesel as evident by test reports of Austrian biofuel Institute, Austria based on engine performance studies [11].

Jatropha suffer significant yield losses due to insect pests, fungi and viruses. Considering the difficulties in managing collar rot in *J. curcas* with traditional methods, and realising that genetic engineering may be the best alternative to find a solution. With this aim, we have isolated *JcPR-10a* and *JcWRKY* cDNA with an ORF of 483 and 693 bp, respectively, from *J. curcas*, an important biofuel crop grown in the wastelands of India. The JcPR-10a protein was overexpressed in *E. coli* cells, and was purified to homogeneity, the purified protein exhibited antifungal activity against *Macrophomina* [12]. Furthermore, the tobacco transgenics overexpressing *JcPR-10a* showed enhanced resistance against *Macrophomina* indicating that JcPR-10a can serve as an important candidate to engineer stress tolerance in Jatropha as well as other plants susceptible to collar rot by *Macrophomina*. The *JcPR-10a* gene overexpression resulted in increased number of shoot buds in tobacco (*Nicotiana tabacum*), which could be due to high cytokinin to auxin ratio in the

transgenics [13]. indicating JcPR-10a participates in cytokinin signalling [14]. The JcWRKY showed binding to the W-box element of the PR-1 promoter and iso1 promoter. The PR-1 gene is a marker gene for SAR, whereas the barley iso1 gene is sugar inducible [15]. The ectopic expression of JcWRKY transcription factor confers salinity tolerance via salicylic acid signalling [16]. The salicylic acid signalling is an important component of defence response of the plants, therefore attempts are being made to study the potential of JcWRKY transgenics towards disease resistance. With these interesting leads, we propose to transform *JcPR-10a* and *JcWRKY* genes in *J. curcas* for enhanced disease tolerance which would lead to improved and healthy plantation [14]. Furthermore to enhance viral resistance in *J. curcas*, the pathogenic factors of the virus would be identified and micro RNA would be characterised against these factors. The occurrence of Jatropha mosaic virus and cucumber mosaic virus disease observed in different plantations sites in India. We have studied the biodiversity of viruses infesting in our experimental plantations at Nesvad and Chorvadla and found gemniviruse with both monopartite and bipartite genomes.

ACKNOWLEDGMENTS

REFERENCES

[1] Mantri, V.A., Parmar, D.R., Rao, P.N., Ghosh, A., 2014 "Observation on ecosystem services in *Jatropha curcas* plantations established in degraded lands in India". International Journal of Environmental Studies, 71(2), pp. 209-214.

[2] Singh, S., Prakash, A., Chakraborty, N.R., Wheeler, C., Agarwal, P.K., Ghosh, A., 2016 "Genetic variability, character association and divergence studies in *Jatropha curcas* for improvement in oil yield". Trees-Structure and Function, 30, pp. 1163-1180.

[3] Singh, S., Prakash, A., Chakraborty, N.R., Wheeler, C., Agarwal, P.K., Ghosh, A., 2016 "Trait selection by path and principal component analysis in *Jatropha curcas* for enhanced oil yield". Industrial Crops and Products, 86, pp. 173-179.

[4] Prakash, A., Singh, S., Prakash, C.R., Ghosh, A., Agarwal, P.K., 2016 "Development of Jatropha hybrids with enhanced growth, yield and oil attributes suitable for semi-arid wastelands". Agroforestry Systems, 90, pp. 541-553.

[5] Anand, K.G.V., Kubavat, D., Trivedi, K., Agarwal, P.K., Wheeler, C., Ghosh, A., 2015 "Long term application of Jatropha press cake promotes seed yield by enhanced soil organic carbon accumulation, microbial biomass and enzyme activities in soils of semi-arid tropical wastelands" . European J of Soil Biology, 69, pp. 57-65.

[6] Ghosh, A., Chikara, J., Chaudhary, D.R., Praksh, A.R., Boricha, G., Zala, A., 2010 "Paclobutrazol arrests vegetative and unveils unexpressed yield potential of *Jatropha curcas*". Journal of Plant Growth Regulation, 29, pp. 307-315.

[7] Singh, A., Reddy, M.P., Chikara J., Singh, S., 2010 "A simple regeneration protocol from stem explants of *Jatropha curcas* – a biodiesel plant". Industrial Crops and Products, 31, pp. 209–213.

[8] Rathore, M.S.,Yadav, P., Shaik, G.M., Prakash, Ch.R., Singh, S., Agarwal, P.K., 2014 "Evaluation of genetic homogeneity in tissue culture regenerates of *Jatropha curcas* L. using flow cytometer and DNA based molecular markers". Applied Biochemistry and Biotechnology, 172, pp. 298-310.

[9] Singh, A., Jani, K.,Sagervanshi, A., Agrawal, P.K., 2014 "High frequency regeneration by abscisic acid (ABA) from petiole callus of *Jatropha curcas*". In vitro cellular and developmental biology-Plant, 50, pp. 638–645.

[10] Singh A., Agarwal, P.K., 2017 "*Jatropha curcas* micrografting modifies plant architecture and increases tolerance to abiotic stress: grafting modifies the architecture of *Jatropha curcas*". 128(1), pp. 243–246.

[11] Ghosh, A., Chaudhary, D.R., Reddy, M.P., Rao, S.N., Chikara, J., Pandya, J.B., Patolia, J.S., Gandhi, M.R., Adimurthy, S., Vaghela, N., Mishra, S., Rathod, M.R., Prakash , A.R., Sethia, B.D., Upadhyay, S.C., Balakrishana, V., Prakash, CH.R., Ghosh, P.K., 2010 "Prospects for Jatropha methyl ester in India.". International Journal of Environmental Studies, 64(6), pp. 659-674.

[12] Agarwal, P., Dabi, M., Sapara, K., Joshi, P and Agarwal, P.K., 2016 "Ectopic expression of JcWRKY transcription factor confers salinity tolerance via salicylic acid signaling". Frontiers in Plant Sciences, 7:1541.

[13] Agarwal, P., and Agarwal, P.K., 2016 "*Jatropha curcas* pathogenesis related-10a Protein: A jack of many trades via cytokinin signalling". Cloning & Transgenesis. 5:1.

[14] Agarwal, P., Dabi, M., More, P., Patel, K, Jana, K, Agarwal, P., 2016 "Improved shoot regeneration, salinity

tolerance and reduced fungal susceptibility in transgenic tobacco constitutively expressing PR-10a Gene". Frontiers in Plant Science 7:217

[15] Agarwal, P., Bhatt, V., Singh, R., Das, M., Sopory, S.K., Chikara, J., 2013 "Pathogenesis-related gene, JcPR-10a from *Jatropha curcas* exhibit RNase and antifungal activity". Molecular Biotechnology, 54, pp. 412–425.

[16] Agarwal, P., Dabi, M., Agarwal, P.K., 2014 "Molecular cloning and characterization of a Group II WRKY transcription factor from *Jatropha curcas*, an important biofuel crop". DNA and Cell Biology, 33 (8), pp. 503 – 513.

SEEC – 2017 – 149

FLOW DYNAMICS CHARACTERIZATION OF A SQUARE NATURAL CIRCULATION LOOP USING RECURRENCE PLOT

Ritabrata Saha
Department of Mechanical Engineering
Jadavpur University, Kolkata-700032.
Email: saha_ritabrata@yahoo.com

Koushik Ghosh
Department of Mechanical Engineering
Jadavpur University, Kolkata-700032.
Email: kghosh@mech.jdvu.ac.in

Achintya Mukhopadhyay
Department of Mechanical Engineering
Jadavpur University, Kolkata-700032.
Email: achintya.mukho@gmail.com

Swarnendu Sen
Department of Mechanical Engineering
Jadavpur University, Kolkata-700032.
Email: sen.swarnendu@gmail.com

ABSTRACT

Natural circulation loop (NCL) is the comonly used device in the field of passive heat removal systems. In NCL heat energy being transferred without the support of any external power or mechanical device. For this passive nature of heat transfer NCL is being used in various commercial applications like nuclear reactor core cooling, solar water heaters etc. According to the applications it is very important to characterize the flow dynamics properly so that we can design proper control mechanism to control the flow dynamics. In the present study, we are trying to characterize the flow patterns which were found from the numerical study done by the help of MATLAB based Simulink model [1]. Loop fluid flow behavior which is changing in the NCL with the increase of heater power. To characterize the flow dynamics Recurrence plot as the nonlinear dynamic analysis tool have been used.

Keywords: Natural Circulation Loop, Nonlinear Dynamics, Temperature Oscillation, Instability, Recurrence Plot.
.

INTRODUCTION

Natural Circulation Loop (NCL) works by transfer heat from a lower elevated heat source to a higher elevated heat sink with the help of moving working fluid. Due to the absorption of heat energy temperature of the working fluid increases and reduces its density and becomes lighter, thus moves upward by the balancing of buoyancy, friction and gravitational forces and rejects heat into the heat sink and cooled down and fall downwards. In NCL no active devices are being used so that its act as a passive heat removal system and used in various industrial applications such as nuclear reactor core cooling, solar water heaters etc for providing better safety to the systems. Low hydro dynamic head makes NCLs inherently less stable leading to instabilities in the flow dynamics. As NCL is attached with the safty of the system it is very important to properly signify the flow pattern, because spontaneous dynamics of the fluid flow plays a very crucial role in the performance of the system. These instabilities may lead to failure of the system. This has motivated the researchers to characterize the flow pattern and the instabilities associated with the flow dynamics of NCLs over the past few years. Proper identification and characterization of these instabilities are prerequisites for control of instabilities and stable operation of these systems.

The flow dynamics for the annular thermosyphon was investigated by Desrayaud et al. [2]. According to their result flow dynamics changes from steady flow to Lorenz-like chaotic flow through periodic motion. Vijayan et al. [3] carried out different experiments and numerical simulation to investigate how the instability grows with the increase in diameter. Cammarata et al. [4] has been studied fluid dynamics for NCL using experimental time series data. Ridouane et al. [5] has been carried out the numerical simulation of the fluid flow in the unstable convection

regime for a natural convection loop. With the increasing Rayleigh number the flow reversal phenomenon was growing. Nayak et al. [6] doing mathematical simulation to identify the stable, unstable and neutrally stable point by Nyquist stability criterion for fluid flow.

In the present study, we are trying to characterize the flow patterns which were found from the numerical study done by the help of MATLAB based Simulink model [1]. With the increase in heater power loop fluid flow dynamics in NCL have been changed. To characterize the flow dynamics Recurrence plot as the nonlinear dynamic analysis tool have been used.

NUMERICAL METHODOLOGY

Numerical modeling to obtain the time series data is same as describe in Saha et al. [1]. For this purpose we are not describing it here. Figure 1 shows the schematic diagram of the NCL.
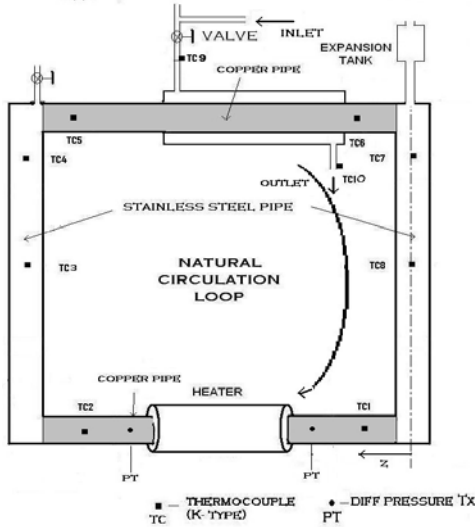
FIGURE 1. Schematic Diagram of Square Natural Circulation Loop [1].

For characterization of the flow dynamics Recurrence plot as the nonlinear dynamic analysis tool have been used. For this porpuse first we need to convert time series data into phase space data. In the reconstructed phase space, proximity of two state vectors, one is $x_i = [y(t_i), y(t_i + \tau), ..., y(t_i + (d_E - 1)\tau)]$ and the another is $x_j = [y(t_j), y(t_j + \tau), ..., y(t_j + (d_E - 1)\tau)]$ can be described in terms of recurrence matrix [7, 8]. Here $y(t_i)$ denotes the instantaneous value of a scalar variable and τ and d_E denote the delay time and embedding dimension respectively. Recurrence matrix can be defined in various ways. The most popular way is identifies the vectors in the neighbourhood of a given vector as those which lie within a fixed distance (a hyper sphere of radius ε) of the vector.

The recurrence vector is a binary matrix defined as below [8].

$$R_{ij} = \Theta\left(\varepsilon - \|x_i - x_j\|\right)$$

Here $\Theta(\cdot)$ denotes Heaviside function. Graphically representing $R_{ij} = 0$ or 1 as white and black dot's respectively and recurrence plots can be generated. The principal diagonal consists of black dots only as $R_{ii} = 1$ always and is referred to as the Line of Identity (LOI).

To obtain the recurrence plot first we need to find out the time delay and embedding dimension. To calculate the optimal time delay we are using auto correlation function and to find out the embedding dimension we are using correlation integral and correlation dimension [9]. Saturated correlation dimension signify the deterministic nature of the system whereas for the random systems, the correlation dimension increases unbounded with increase in dimension.

RESULTS AND DISCUSSION

From the time series data obtained from the numerical simulation it can be observed that the loop fluid flow dynamics can be divided into three categories; for heater power less than 625 W the system exhibits steady state behaviour. But when the heater power is increased further, an oscillatory flow is observed for heater powers below 742 W. For further increase in heater power, flow reversal in the loop is noted. For identifying the fluid flow dynamics we are analysing the results after the initial transient part is over. For heater power of 655 W variation of loop fluid temperature difference which is taken inbetween mid point of its two legs - the riser (having higher temperature) and the down-comer (having lower temperature) with time is shown in Fig. 2. From Fig. 2 it can be observed that temperature difference shows an oscillatory nature. In the oscillatory region i.e. heater power in between 625 W to 742 W, oscillation amplitude increases with the increase in heater power as shown in Fig. 3.

The appearance of the recurrence plot gives important qualitative information about the dynamic characteristics of the system. Periodic systems are characterized by equal spaced lines parallel to the LOI. The distance between the lines is equal to the time period of the periodic system. Short diagonal line segments, parallel to the LOI indicate noisy periodic behavior, with the gaps created due to effect of noise. Vertical lines represent intermittent steady behavior. Box like structure in the Recurrence plots represents the chaotic systems and Recurrence plots for random data show white and black dots distributed randomly.
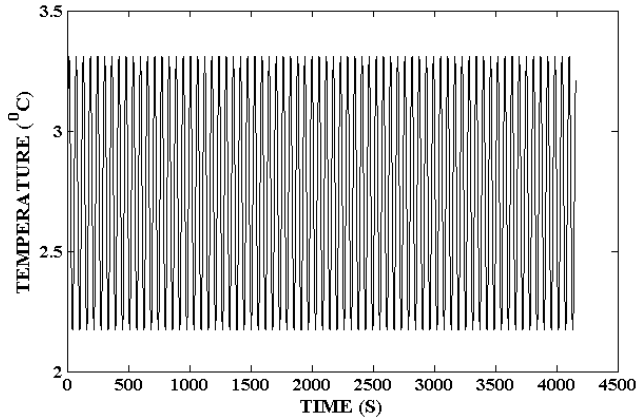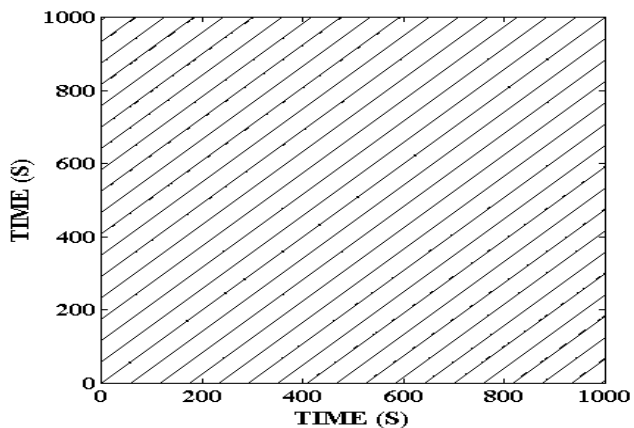
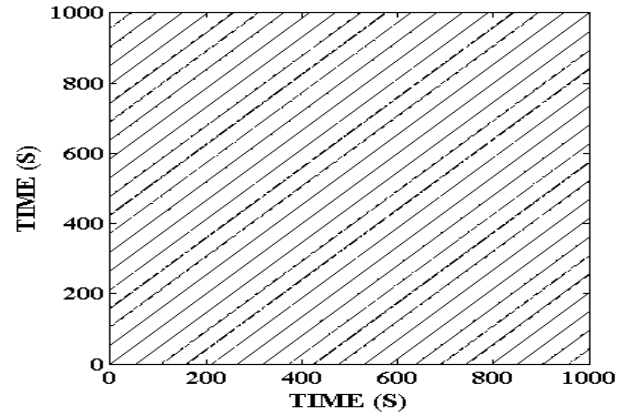**FIGURE 2. Variation of Temperature Difference with Time at 655 W.**
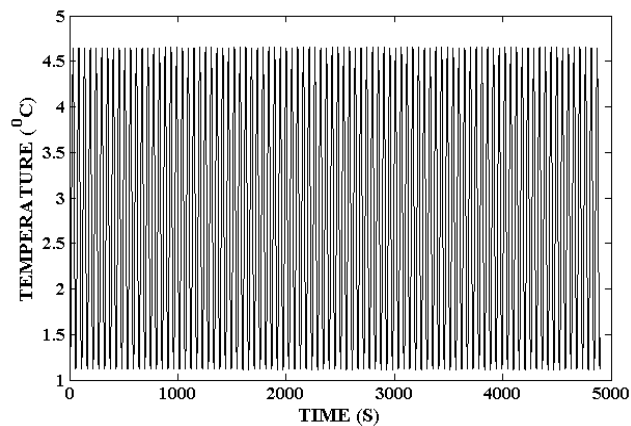
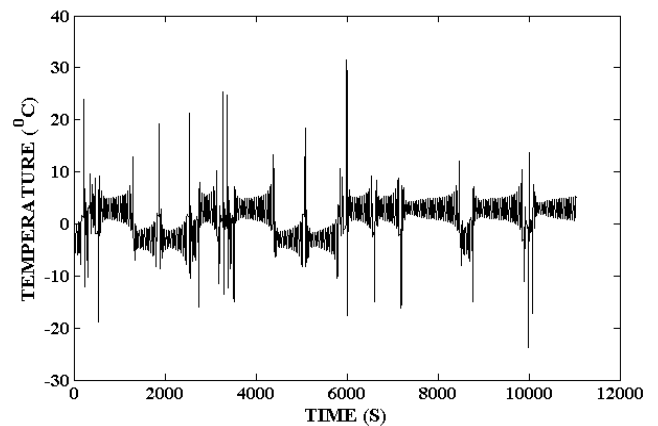**FIGURE 3. Variation of Temperature Difference with Time at 742 W.**

Recurrence plots of the time series data for heater power 655 W and 742 W are shown in Fig. 4 and Fig. 5 respectively. From the figures it can be observed that the Recurrence plots are equally spaced diagonal line structure which signify the periodic nature. It confirms that the oscillations we get in the oscillatory region is purely periodic.
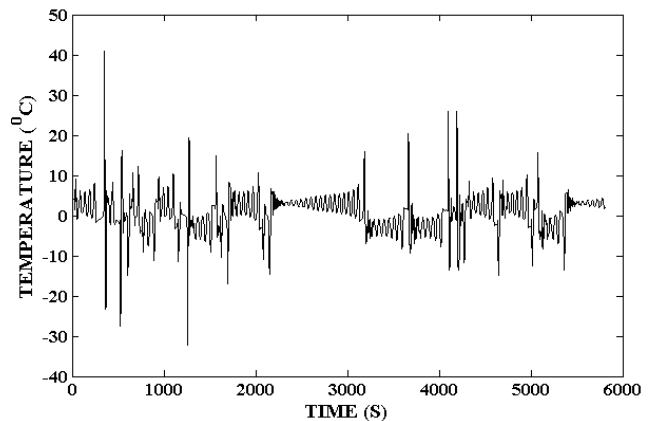

FIGURE 4. Recurrence Plot at 655 W.

FIGURE 5. Recurrence Plot at 742 W.

FIGURE 6. Variation of Temperature Difference with Time at 760 W.

FIGURE 7. Variation of Temperature Difference with Time at 795 W.

For heater power of 760 W variation of loop fluid temperature difference with time is shown in Fig. 6. From the figure it can be observed that the temperature difference shows flow reversal characteristics. In this flow reversal region i.e. heater power greater than 742 W the frequency of occurrence of flow reversal increases with the increasing heater power as shown in Fig. 7.
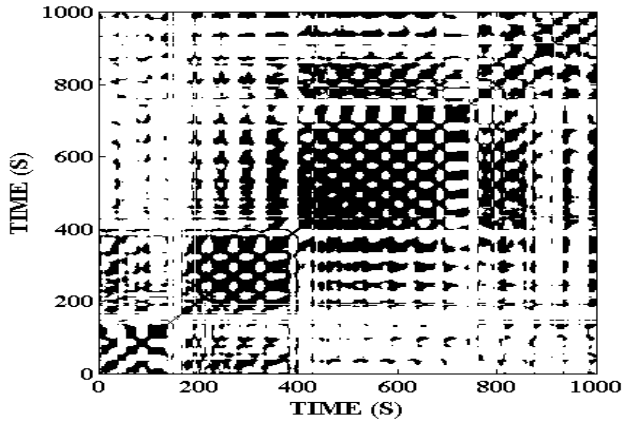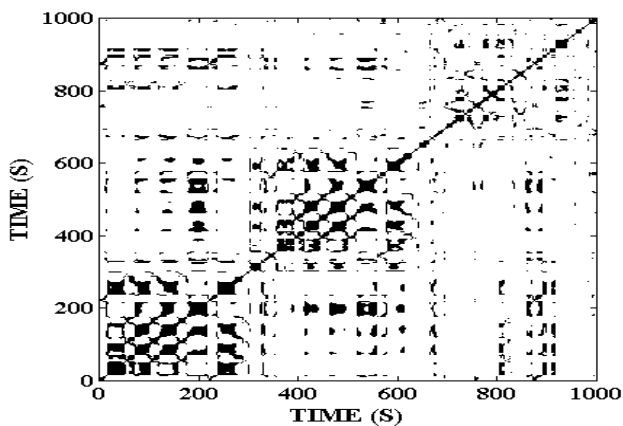
3

FIGURE 8. Recurrence Plot at 760 W.

FIGURE 9. Recurrence Plot at 795 W.

Recurrence plots of the time series data for heater power 760 W and 795 W are shown in Fig. 8 and Fig. 9 respectively. From the figures it can be observed that the Recurrence plots shows box like structure which signify the chaotic nature. It confirms that the fluid flow dynamics at flow reversal region is Chaotic.

CONCLUSIONS

From the numerical study we observed that fluid flow dynamics are divided into three categories. For heater power less than 625 W the system is in steady state and for heater power less than 743 W we get stable oscillatory flow and above this heater power we get flow reversal in the loop fluid flow dynamics. From the Recurrence Plot analysis we can properly said that the fluid flow oscillation obtained in the oscillatory region is purely periodic and fluid flow dynamics in the flow reversal region is chaotic. Recurrence plots show equally spaced diagonal line structure in oscilatory region which signify the periodic nature and the box like structure in the flow reversal region which signifies the chaotic nature.

REFERENCES

[1] Saha, R., et al., 2015. "Experimental and Numerical Investigation of a Single-Phase Square Natural Circulation Loop". Journal of Heat Transfer, 137, pp. 121010-1 - 121010-8.

[2] Desrayaud, G., Fichera, A., and Marcoux, M., 2006. "Numerical Investigation of Natural Circulation in a 2D-Annular Closed-Loop Thermosyphon". International Journal of Heat and Fluid Flow, 27, pp. 154–166.

[3] Vijayan, P. K., Austregesilo, H., and Teschendorff, V., 1995. "Simulation of the Unstable Oscillatory Behavior of Single-Phase Natural Circulation with Repetitive Flow Reversals in a Rectangular Loop using the Computer Code ATHLET". Nuclear Engineering and Design, 155, pp. 623-641.

[4] Cammarata, G., Fichera, A., and Pagano, A., 2000. "Nonlinear Analysis of a Rectangular Natural Circulation Loop". International Communications in Heat and Mass Transfer, 27, pp. 1077-1089.

[5] Ridouane, E. H., Danforth, C. M. and Hitt, D. L. 2010. "A 2-D Numerical Study of Chaotic Flow in a Natural Convection Loop". International Journal of Heat and Mass Transfer, 53, pp. 76–84.

[6] Nayak, A. K., et al., 1995. "Mathematical Modelling of the Stability Characteristics of a Natural Circulation Loop". Mathematical and Computer Modelling, 22, pp. 77-87.

[7] Eckmann, J. P., Kamphorst, S. O., and Ruelle, D., 1987. "Recurrence Plots of Dynamical Systems". Europhysics Letters, 4, pp. 973-977.

[8] Marwan, N., et al., 2007. "Recurrence Plots for the Analysis of Complex Systems". Physics Report, 438, pp. 237-329.

[9] Datta, S., et al., 2009. "An Investigation of Nonlinear Dynamics of a Thermal Pulse Combustor". Combustion Theory and Modelling, 13, pp. 17-38.

SEEC-2017-150

BIOETHANOL PRODUCTION USING BIOWASTE FOR ENERGY CONSERVATION AND ENERGY GENERATION

Avinash Thakur
Department of Chemical Engineering
Sant Longowal Institute of Engineering and
Technology, Longowal, Sangrur, Punjab-148106
Email: avin_thakur2@Yahoo.com

Parmjit Singh Panesar
Department of Food Engineering and Technology
Sant Longowal Institute of Enginnering and
Technology, Longowal, sangrur, Punjab-148106
Email address: pspbt@yahoo.com

ABSTRACT

On a global basis, development of alternative and eco-friendly renewable energy sources for eliminating fossil/non-renewable energy use and greenhouse gases emissions are the objectives, which can be accomplished through green biotechnology. Biomass energy, or bioenergy from inedible biological materials/agro-industrial waste/byproducts as renewable sources of energy presents a promising approach through economic and environment responsive biotechnological process. The bioconversion of liquid biofuel, bioethanol by reutilization of bio wastes has large potential and is of great interest for sustainable energy and environmental safety by replacing fossil fuels to meet the increasing demand of the growing population of the world. Bioethanol is considered as a clean fuel because of its biodegradability, non toxicity & almost no contribution of any pollutant to the environment and is an ideal candidate for replacing the gasoline in motor engines. The present work is summarized to throws limelight on the potential of bioethanol production by utilizing bio waste generated for energy conservation and energy generation.

Keywords : bioetanol, renewable, bioconversion, energy, waste

INTRODUCTION

There is a limited oil reserves and which are rapidly depleting. Keeping in view the current rate of oil consumption and environmental problems posed by these, necessity has grown strongly to use bio-fuels in recent years worldwide. Since 60% of the total oil is consumed by the motor engines, advanced bifuel: bioethanol can be used as a promising alternative fuel for transport to replace petroleum based fuels and will provide energy security for future [1]

Bioethanol is a source of renewable energy which can be produced from various renewable sources rich in carbohydrates. Combusion efficiency of bioethanol (C_2H_5OH) is 15% higher than that of gasoline since it contains 34.7% oxygen and which is negligible in case of gasoline [2].

Alongwith developing the novel upstream and downstream processes, the selection of renewable raw material as a feedstock is the need of the hour for development of cost-effective bioethanol production to generate energy since the raw material is considered to be major contributing factor towards its cost.

A large quantity of wastes has been produced by the food and agricultural industries annually worldwide, posing serious environmental problems [3]. Agro wastes generated are either allowed to decay naturally or are destroyed by burning on the fields. But these are very rich source of carbohydrates making them suitable to be for bioconversion into bioethanol. Industrial byproducts like molasses, are other suitable substrates rich in sugar and other vital micronuterians can be easily assimilated by microorganisms into liquid bio based energy-fuels. These inexpensive, renewable, abundant raw materials are the

unique natural resource for industrial-scale and economic bio-energy conservation and collection.

The reutilization of biological wastes by fermentation into bioethanol for energy conservation and energy generation is of great interest. Since The fermentation process is an energy yielding, Where the rearrangement/reorienation of oraganic molequles takes place as the organic molecules act both as electron donors and electron acceptors. Gravity fermentation provides high initial fermentable sugar concentration which opens the gates for high energy savings on downstream processing, reduction in the fermentation size facilty, less waste and producing high bioethanol concentrations from the fermentation process [4].

WASTE GENERATED AS RAW MATERIAL

There are four types of wastes which can be the potential substrate for bioethanol production viz. sugars, lignocellulosic biomass, algae and starch.

Sugar

Sugar refinery wastes, cane and beet molasses dark, viscous and sugar rich by-product of sugar refinery industries are the major substrate for bioethanol. Molasses are widely used bioethanol production through fermentation as it is cheap and available in abundance. Some fruit refinery wastes like pineapple and grape pomaces are also the potential substrate for bioethanol production. With reference to bioethanol production, industrial wastes of each sugar crop have some potential as feedstock as the sugar crop itself [2].

Lignocellulosic biomass

Agricultural organic wastes are currently possing the major environmental problems, so the utilization of this biomass for generating energy is atmost important [6] and has the potential to provide biethanol as novel biofuel as these are available throughout the year.

The agro wastes are lignocellulosic biomass like rice straw, wheat straw, corn straw and bagasse. These are complex carbohydrate polymer of cellulose, hemicellulose and lignin with different composition and contain cellulose as major component [5]. Biomass originated from residential, non-residential sources, food from processing industries such as food wastes, paper mill sludge , and animal manure etc. are also considered feedstocks for bioethanol [7-8]. For bioethanol production, from lignocellulosics undergoes several unit processes like, pre-treatment, hydrolysis, fermentation and distillation [9]. Forestry residues, by-products of pulp and sawmills like sawdust, shavings etc. and forest harvest residues like tops, branches etc., which may have significant amounts of bark can also used as raw maerials for bioethanol production. However the economic viability of bioethanol production is influenced by bark content of different forestry assortments as the raw materials [10]. Bioethanol yields of 45.53% from renewable lignocellulosic biomass, cotton stalk, a by-product of cotton production has been obtained [11].

Algae

Algae, the fastest growing plant of the world, in general morphologically can be divided as macroalgae and microalgae. They are known for efficiently converting solar energy to biomass by photosynthesis process utilizing sunlight, CO_2 and nutrients from water [12]. There are three promising larger, oceanic multicellular plants known as macroalgae biomass or "seaweeds," viz brown, green and red algae for bioethanol production. Due to high growth rate and posseion of high sugar level, brown algae such as sea mustard (Undaria pinnatifida) and kelp (Saccharina japonica) has been considered as best among three type macroalgae. bioethanol productivity from macroalgae could be theoretically be two times and five times higher than that of from sugarcane and corn respectively [12-13]. Alge are the only alternative as renewable raw material to food crops for bioethanol production as it has energy rich lipids and carbohydrates and doesn't require arable land and fertilizer for its growth. Moreover, cellulose, mannans, xylans, and sulfated glycans are the constituents of some microalgal cell walls. These polysaccharides can be chemically or enzymatically fragmented into simple sugars and hence then bioconverted to bioethanol[13-14]. After the lipid is extracted from the algal biomass for biodesil production, an enormous amount of biomass as a waste material can be bioconverted into bioethanol by carring out a simultaneous saccharification and fermentation [14]. 7.4 g/L bioethanol was produced from hydrolysates of red alga *Gelidium amansii* by a mutant *Saccharomyces cerevisiae* within 12 h [15].

Starch

The wild nonedible biomass containing starch a potential economic source of feedstock for bioethanol production. For a typical starchy agricultural waste, mechanical pre-treatment for physical size reduction provide an opportunity for employing an easy hydrolysis method like starch heating with water hence reduce the processing cost; and also lowers the consumption of conventional energy during process [16]. *Canna edulis Ker*. a non-food biomass source contatinig 12 -9% starch a potential source of low-cost feedstock for bioethanol production [17]. High ethanol yields has been obtained from bioconversion of raw starch from wild inedible cassava[18]

CONCLUSIONS

The bioethanol production from the agroindustrial waste generated could help to reduce reduce CO_2 pollution,

will provide new income source to farners and new employment opportunities in rural areas and better engine performance without competing with food chain. Further it will reduce the dependence on fossil fuels and will diversify the energy sectors. The mazor targets to have efficient energy conservation and energy generation from bioprocess engineering point of view are yield, pretreatment or enzyme hydrolysis for lignocellulosic agrowaste, fermentation, downstream processing, sustainability and energy efficiency of the process etc. So it can be concluded that the opportunities provided by the waste generated towards its bioconversion to bioethanol is favorable, dependable and opportunity should be harnessed.

REFERENCES

[1] Mustafa, B. and Havva, B. 2009. "Recent trends in global production and utilization of bio-ethanol fuel". Applied Energy, 86, pp. 2273-2282

[2] Zabed, H., Sahu, J. N., Suely, A., Boyse, A.N., and Faruq, G. 2017. "Bioethanol production from renewable sources: Current perspectives and technological progress" Renewable and Sustainable Energy Reviews, January, pp. 1-27

[3] Ali, H. J., Abbas, F. M. A., Qgugbue, C. J., Azar, M. E. and Norulaini, N. A. N 2013. "Production of the lactic acid from mango peel waste - Factorial experiment". Journal of King Saud University – Science, January, pp. 39-45

[4] Azilah A., Ahmad Z. S. and Yusuf, C. 2017. "Production of bioethanol by Zymomonas mobilis in high-gravity extractive fermentations". Food and Bioproducts Processing, 102, pp. 123-135

[5] Nibedita, S., Sumanta, K. G., Satarupa, B. and Kaustav A. 2012. Bioethanol production from agricultural wastes: An overview Renewable Energy 37, pp. 19-27

[6] Assia, M., Rachida, R., Aicha, N. L. and Melek, O. 2016. "Production of bioethanol from a mixture of agricultural feedstocks: Biofuels characterization". Fuel, 185, pp. 612-621

[7] Naik, S.N., Vaibhav V. G., Prasant K. R. and Ajay K. D. 2010. "Production of first and second generation biofuels: A comprehensive review". Renewable and Sustainable Energy Reviews, 14, pp. 578-597

[8] Aditiya, H. B., Mahlia, T.M.I., Chong, W. T., Hadi, N. and Sebayang, A. H. 2016. "Second generation bioethanol production: A critical review" Renewable and Sustainable Energy Reviews 66, pp. 631-653

[9] Ioannis, D., Diomi, M., and Dimitris, K. 2013. "Biotechnological production of ethanol from renewable resources by *Neurospora crassa*: an alternative to conventional yeast fermentations". Applied Microbiology and Biotechnology, 97(4), February, pp. 1457-1473

[10] Balazs, F., Mats, G. and Ola, W. 2016. "Bioethanol production from forestry residues: A comparative techno-economic analysis". Applied Energy, 184, pp. 727-736

[11] Meixia, W., Dayun, Z., Yanqin, W., Shoujun, W., Weihua, Y., Meng, K., Lei, M., Dan, F., Shuangjiao, X. and Shuang-kui, D. 2016. "Bioethanol production from cotton stalk: A comparative study of various pretreatments". Fuel, 184, pp. 527-532

[12] Abdul, R. S. and Duraiarasan, S. 2016. "Algae – A quintessential and positive resource of bioethanol production: A comprehensive review". Renewable and Sustainable Energy Reviews, 66, August, pp. 248-267

[13] Ok K. L. and Eun, Y. L. 2016. "Sustainable production of bioethanol from renewable brown algae biomass". Biomass and Bioenergy. 92, June, pp. 70-75

[14] Veeramuthu, A., Mohd, R. S., Zainal, S., Pandian, S., Cheng, T. C., Sanniyasi, E., Veeraperumal, S. and Farid, N. A. 2017. "Production of liquid biofuels (biodiesel and bioethanol) from brown marine macroalgae *Padina tetrastromatica*". Energy Conversion and Management, 135, pp. 351-361

[15] Hye-Jin, L., Soo-Jung, K., Jeong-Jun, Y., Kyoung, H. K., Jin-Ho, S. and Yong-Cheol, P. 2015. "Evolutionary engineering of Saccharomyces cerevisiae for efficient conversion of red algal biosugars to bioethanol". Bioresource Technology, 191, March, pp. 445-451

[16] Aditiya, H. B., Mahlia, T. M. I., Chong, W. T., Hadi, N. and Sebayang, A.H. 2016. "Second generation bioethanol production: A critical review" Renewable and Sustainable Energy Reviews, 66, August, pp. 631-653

[17] Yuhong, H., Yanling, J., Yang, F., Yuhao, L. and Hai, Z. 2013. "Simultaneous utilization of non-starch polysaccharides and starch and viscosity reduction for bioethanol fermentation from fresh *Canna edulis Ker*. Tubers". Bioresource Technology, 128, pp. 560-564

[18] P. M., Ken, M.M. H., Emrode, E. Gashaw, M., Linda, O. and Ivo, A. N., 2016. "Production of raw starch-degrading enzyme by *Aspergillus sp*. and its use in conversion of inedible wild cassava flour to bioethanol Anselm". Journal of Bioscience and Bioengineering, 121(4), October, pp. 457-463.

SEEC-2017-151

Investigation of lift-off height variation in turbulent CH$_4$ /Air jet diffusion flames using stochastic multiple mapping conditioning approach

Sanjeev Kumar Ghai
Department of Mechanical Engineering
Indian Institute of Technology Kanpur
Kanpur, U.P. - 208016
Email: snjv@iitk.ac.in

Santanu De
Department of Mechanical Engineering
Indian Institute of Technology Kanpur
Kanpur, U.P. - 208016
Email: sde@iitk.ac.in

ABSTRACT

Turbulent jet diffusion flames of CH$_4$/Air mixture stabilized in a vitiated co-flow of hot combustion products of H$_2$/Air has been investigated using Reynolds-averaged Navier-Stokes (RANS) based stochastic multiple mapping conditioning (MMC) method. The effects of coflow temperature, jet and coflow velocity on the lift-off height have been studied. Stochastic formulation of MMC has been used, where a mapping function is used to represent the cumulative probability distribution of the mixture fraction for non-premixed combustion. The Curl's mixing model, originally developed for the conventional PDF method has been adapted for the MMC approach. A reduced mechanism for CH$_4$ has been used to model the chemical kinetics. These flames are very sensitive to the change in the inlet conditions of the scalars and the flame base is stabilized at a distance from the nozzle-exit. The lift-off height obtained from the numerical simulations for various coflow temperatures, jet and coflow velocities are compared with the experimentally measured value. It is found that the results from the present numerical simulations give an accurate prediction of the trend observed in experiments.

Keywords: Turbulent jet diffusion flames; multiple mapping conditioning; RANS; vitiated coflow; lifted flames; stochastic processes

INTRODUCTION

Probabilistic methods such as probability density function (PDF) [1] methods have a great advantage for modelling turbulent combustion processes because they allow direct closure for calculation of the chemical source term. But these approaches are computationally expensive as compared to mixtures fraction based approaches such as the flamelet model [2] and the conditional moment closure (CMC) method [3]. PDF methods are generally more universal and provide relatively better agreement with experimental measurements for most of the flames. On the other side, conditional methods are restricted to cases that do not exhibit large fluctuations around the conditional mean and predictions of flames with significant local extinction/re-ignition tend to be less satisfactory. Stochastic multiple mapping conditioning (MMC) approach [4] has recently emerged as an alternate model for simulation of turbulent combustion, which is claimed to be [5, 6] computationally cheaper compared to the PDF methods.

Despite conditional approach, MMC has the capabilities to capture complex phenomenon such as extinction/re-ignition at a comparatively modest cost w.r.t to PDF methods. In recent times MMC has been successfully applied to piloted turbulent jet diffusion flame [5-7]. In the present work, the turbulent lifted jet flame in a vitiated co-flow is being investigated following RANS-MMC approach. Cabra's [8, 9] experimental configuration produces certain challenges to combustion models due to immensely sensitive balance between chemical reaction and species diffusion. The initial results obtained with

MMC model are in good agreement with DNS results for the three stream mixing problem by Juneja and Pope [10]. The phenomena of extinction and re-ignition are investigated by Cleary et al. [11] for homogeneous, isotropic decaying turbulence and they examined three test cases with different chemical time scales and found that the model is exceptionally good for significant and global local extinction. However, the model does not improve the results for the moderate local extinction. Wandel and Lindstedt [12] developed the hybrid binomial Langevin MMC model which is the first attempt to imply Stochastic MMC inhomogeneously with a finite-rate chemistry effects and due to its hybrid nature, it provides the adequate results comparable to experiments at comparatively modest computational cost. In a recent RANS-MMC work, Straub et al. [6] developed a small-scale mixing model by adapting the conventional Curl's mixing model and tested it for the Sandia flame series. A very good agreement with the available experiments has been reported with a fewer number of particles per cell. The objectives of this work are to ascertain the capability of the MMC approach and to capture the effect of variation of parameters on flame lift-off height in the RANS context and to assess the performance of the small-scale mixing model within the MMC framework.

MATHEMATICAL FORMULATION

MMC approach has the inherent capability to consider multiple fluctuations of several key quantities by the introduction of reference variables such as mixture fraction, reaction progress variable etc. To consider more than one key quantity, one has to increase the dimensionality of the reference space which has also increased the computation cost. The concept behind the MMC methodology is that the large scale turbulent fluctuations and small scale mixing employed in reference space are imitated by the use of reference variables in the reference space, ξ, whose PDF is well known in advance. In this work to reduce the computation cost, a single reference variable, ξ^*, is used whose mapping function X (ξ) represents the mixture fraction Z. In the stochastic implementation, the reference variable, ξ^*, is assumed to be Gaussian distributed. A separate equation for the evolution of the reference variable ξ^*, is solved that ensures closeness of the cumulative distribution function of X (ξ) of the reference variable, ξ^*, with mixture fraction Z. The corresponding sets of equations for a stochastic particle method are:

Transport in physical space: $dx^* = U(\xi^*; x^*; t)dt$

Transport in reference space:
$d\xi^* = A^o(\xi^*; x^*; t)dt + b(\xi^*; x^*; t)dw^*$

Transport in mixture fraction space: $dZ^* = S^*dt$

Transport in composition space: $dY_I^* = (W_I^* + S_I^*)dt$

Where $2B = b^2$, x^* is location, ξ^* is reference variable, A^o is the drift coefficient, B is the diffusion coefficient, Y_I^* is the species concentration, S_I^* is the mixing operator and W_I^* is the chemical source term. The superscript '*' is used to differentiate the values linked to stochastic variables. The detailed derivations of these equations may be found in [4]. In MMC, we introduce major and minor mixing time scales. The major mixing time scale controls the turbulent mixing of the characteristic quantity via the modelling of a mapping function, whereas the minor time scale controls fluctuations of scalars relative to the major fluctuations. In the present work, the modified Curl's model [13] is used, which ensures localness in the composition space. This is achieved by mixing those particle pairs which are close in a reference space instead of random selection of particles in the original Curl's model. The mixing operator for the selected particle pair (p,q) can be written as

$$S^* = \frac{d\phi^{*,k}}{dt} = \mu \frac{\phi^{p,q} - \phi^{*,k}}{\tau_{min}},$$

Where, $\mu = 1 - \exp\left[-\frac{w_p + w_q}{W}\frac{N}{2}\right]$ and $W = \sum_{i=1}^{N} w_i$.

Here, the subscript 'k' denotes p or q and w_i is the weight of i-th particles in a cell.

APPROACH

Lifted jet diffusion flame of methane/air supported by a hot vitiated co-flow at is considered in the present work [9]. The inlet conditions are summarized in Table 1. The boundary conditions used for all the variables at the exit section, outer radius and along the axis are the outflow, Neumann and symmetric conditions respectively. The stochastic MMC model is fully coupled to a RANS solver for the flow field. The standard k–ε model with the following set of constants has been used: $C_\mu = 0.09$, $C_{\varepsilon1} = 1.53$ and $C_{\varepsilon2} = 1.85$. A reduced chemical mechanism, ARM2 with 19 species and 15 reactions [14], has been used. In the present set of simulations, the mixing model constant $C_\phi = 3$ and the minor time scale $C_{min} = 0.25$ have been used. A cylindrical coordinate system is used, where the computational domain extends $100D$ and $20D$ in the axial- (z) and the radial (r) directions, respectively. The domain is discretized in 100 cells in each direction. For the stochastic MMC method, 50 stochastic particles per cell have been used. The maximum and minimum numbers of particles within one CFD cell are restricted to 75, and 25, respectively.

2

TABLE 1: Inlet conditions for the base case of methane/air lifted diffusion flame [9].

Parameter	Jet	Co-flow
Reynolds number	28000	23300
Diameter (mm)	4.57	210
Velocity (m/s)	100	5.4
Temperature (K)	320	1350
Mole fraction of O_2	0.1471	0.1200
Mole fraction of N_2	0.5200	0.7297
Mole fraction of CH_4	0.3300	0.0003
Mole fraction of H_2O	0.0029	0.1500
Equivalence ratio	----	0.400
Stoichiometric mixture fraction	0.177	

(a)   (b)   (c)
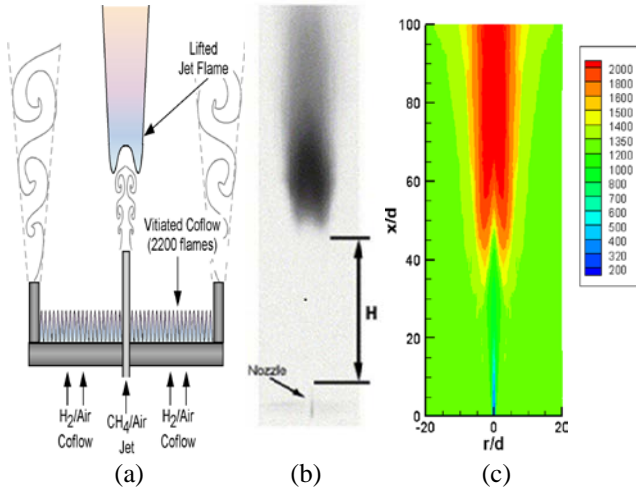
Figure 1: (a) Burner schematic [9], (b) luminosity image from experiments of a lifted CH4/air jet flame in vitiated co-flow [9] and (c) Temperature contours from the present simulations.

RESULTS AND DISCUSSIONS

In this section, numerical results obtained from the RANS-MMC simulations are presented. Fig. 1a shows the burner schematic from [9]. Whereas Fig. 1b shows the luminosity image from experiment represents the lift-off height (LOH) from the nozzle inlet and Fig. 1c presents the temperature contour from the present simulations of RANS-MMC. Here the temperature contours gives the rough idea about

the LOH and exact calculations of LOH are done by recording the first axial location at any radius, where the mole fractions of C_2H_2 reaches 2 ppm and C_2H_4 reaches 100 ppm, and the lift-off height is obtained as the average of these two axial locations as suggested in [9]. In the particular case presented here, this yields a LOH of 34*D*, while the corresponding result from experiments is 35*D*. It should be noted that in the present simulations, we have used only 50 stochastic particles. Previous Monte-Carlo PDF [9] simulations used 400 stochastic particles per cell and thereby the RANS-MMC method significantly reduces computational time.

Figure 2 shows the variation of lift-off height with the change in co-flow temperature. In this figure lift-off, height obtained from present simulations is compared with the measured lift-off height. Results from the other numerical models present in the literature are also compared with the RANS-MMC simulations. RANS-MMC predictions show the better agreement with the measured values as compared to the other numerical models at all co-flow temperature conditions.
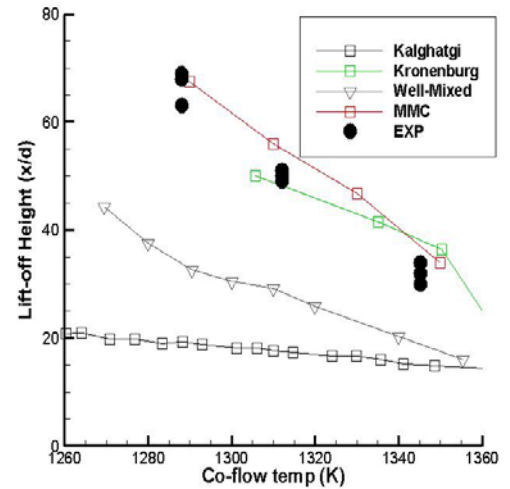
Figure 2: Variation of lift off height vs. co-flow temperature. Kalghatgi [15], Kronenburg [16], Well-mixed and EXP. [9].

Figure 3 shows the effect of variation of jet velocity to the LOH. Results are compared with the experimental predictions and almost linear profile matches the exact trend with the measured values are achieved. The lifted flames are transient in nature and the value of LOH in methane flame shows the fluctuations of many times the nozzle diameters (the exact value is not given in literature) as reported in [9]. So the experiments do not capture the exact value of LOH and most of the instantaneous flame base values are missed gives the erroneous mean value of LOH. So the RANS-MMC results are well within the fluctuation limits.
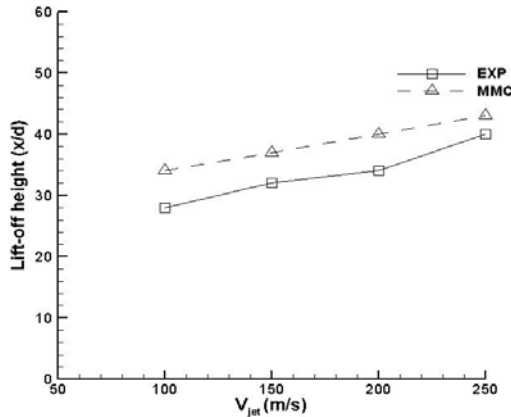
Figure 3: Variation of lift off height Vs. jet velocity. EXP. [9].
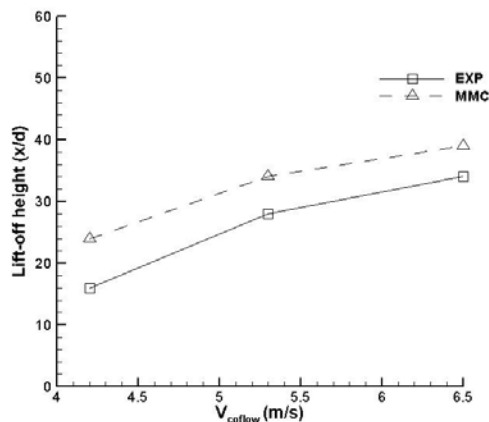

Figure 4: Variation of lift off height vs. co-flow velocity. EXP. [9].

The sensitivity of LOH to co-flow velocity conditions is shown in Fig.4. The obtained trend matches well with the measured values and due to the above-discussed reason the exact quantitative match is rather impossible to obtain. Moreover, computed results exactly match well qualitatively with the measured values and quantitatively results are well within the fluctuation limits of LOH.

CONCLUSIONS

A coupled RANS-MMC simulation has been performed for the lifted jet diffusion flame. Reduced chemistry for the chemical kinetics with 19 species and 15 reactions has been used. Effects of variation of parameter has been studied and found that flame is very much sensitive to the change in the inlet scalar conditions. Moreover, computed results exactly match well qualitatively with the measured values and quantitatively results are well within the fluctuation limits of LOH.

REFERENCES

[1] S.B. Pope, Pdf Methods for Turbulent Reactive Flows, Prog Energ Combust 11 (1985) 119-192.

[2] N. Peters, Laminar Diffusion Flamelet Models in Non-Premixed Turbulent Combustion, Prog Energ Combust 10 (1984) 319-339.

[3] A.Y. Klimenko, R.W. Bilger, Conditional moment closure for turbulent combustion, Prog Energ Combust 25 (1999) 595-687.

[4] A.Y. Klimenko, S.B. Pope, The modeling of turbulent reactive flows based on multiple mapping conditioning, Phys Fluids 15 (2003) 1907-1925.

[5] K. Vogiatzaki, S. Navarro-Martinez, S. De, A. Kronenburg, Mixing Modelling Framework Based on Multiple Mapping Conditioning for the Prediction of Turbulent Flame Extinction, Flow Turbul Combust 95 (2015) 501-517.

[6] C. Straub, S. De, A. Kronenburg, K. Vogiatzaki, The effect of timescale variation in multiple mapping conditioning mixing of PDF calculations for Sandia Flame series D–F, Combust Theor Model, doi:10.1080/13647830.2016.1191677(2016) 1-19.

[7] K. Vogiatzaki, A. Kronenburg, S. Navarro-Martinez, W.P. Jones, Stochastic multiple mapping conditioning for a piloted, turbulent jet diffusion flame, P Combust Inst 33 (2011) 1523-1531.

[8] R. Cabra, T. Myhrvold, J.Y. Chen, R.W. Dibble, A.N. Karpetis, R.S. Barlow, Simultaneous laser Raman-Rayleigh-Lif measurements and numerical modeling results of a lifted turbulent H-2/N-2 jet flame in a vitiated coflow, P Combust Inst 29 (2002) 1881-1888.

[9] R. Cabra, J.Y. Chen, R.W. Dibble, A.N. Karpetis, R.S. Barlow, Lifted methane-air jet flames in a vitiated coflow, Combust Flame 143 (2005) 491-506.

[10] A. Juneja, S.B. Pope, A DNS study of turbulent mixing of two passive scalars, Phys Fluids 8 (1996) 2161-2184.

[11] M.J. Cleary, A. Kronenburg, Multiple mapping conditioning. for extinction and reignition in turbulent diffusion flames, P Combust Inst 31 (2007) 1497-1505.

[12] A.P. Wandel, R.P. Lindstedt, Hybrid binomial Langevin-multiple mapping conditioning modeling of a reacting mixing layer, Phys Fluids 21 (2009).

[13] J. Janicka, W. Kolbe, W. Kollmann, Closure of the Transport-Equation for the Probability Density-Function of Turbulent Scalar Fields, J Non-Equil Thermody 4 (1979) 47-66.

[14] C.J. Sung, C.K. Law, J.Y. Chen, Augmented reduced mechanisms for NO emission in methane oxidation, Combust Flame 125 (2001) 906-919.

[15] G.T. Kalghatgi, Lift-off Heights and Visible Lengths of Vertical Turbulent Jet Diffusion Flames in Still Air, Combust Sci Technol 41 (1984) 17-29.

[16] S. Navarro-Martinez, A. Kronenburg, LES-CMC simulations of a lifted methane flame, P Combust Inst 32 (2009) 1509-1516.

SEEC-2017-152

ESTERIFICATION OF OLEIC AND BUTYRIC ACID USING IMMOBILIZED BACILLUS LIPASE (LIP R1) AND ITS MUTANTS: COMPARATIVE ANALYSIS

Nisha Chopra
Deptt. of Biotechnology
Panjab University, India
Email: sanishachopra@gmail.com

Jagdeep Kaur
Deptt. of Biotechnology
Panjab University, India
Email: jagsekhon@yahoo.com

ABSTRACT

Lipases are widely used for biotechnology applications in the dairy industry, in oil processing, and for the preparation of enantiomerically pure pharmaceuticals. Lipases are being used to make the methyl esters or ethyl esters used in biodiesel. Biodiesel fuels are expected to be substitutes for conventional fossil fuels for having the environmental advantages of biodegradability, renewability. Lipases used in organic solvents can benefit from immobilization to obtain the advantages of easy recovery of the enzyme from products and increased enzyme stability. Metagenome isolated Bacillus Lipase (Lip R1) enzyme was engineered by site directed mutagenesis to improve enzyme characteristics. Both the mutant enzymes R153H and P247S were able to synthesize ester of oleic acid, methyl oleate more efficiently than wild type enzyme. After 24 h incubation, R153H and P247S made 49% and 64% methyl oleate respectively as compared to wild type enzyme (35%). However R153H was also synthesizing methyl butyrate (62%, 18h) whereas wild type enzyme was unable to do so. Immobilized enzymes were more stable than aqueous ones and immobilized mutant enzymes had increased half life both at 25 °C and 37 °C as compared to immobilized wild type. So in future both of these enzymes can be used for the biodiesel synthesis.

Keywords: Lipases, Methyl esters, Biodiesel.

SEEC-2017-153

LES of Lifted Jet Flames using Sparse – Lagrangian Multiple Mapping Conditioning Approach

Sudhakar Singh
Department of Mechanical
Engineering
Indian Institute of Technology Kanpur
Kanpur, U.P. - 208016
Email: sudsingh@iitk.ac.in

Sanjeev Kumar Ghai
Department of Mechanical
Engineering
Indian Institute of Technology Kanpur
Kanpur, U.P. - 208016
Email: snjv@iitk.ac.in

Santanu De
Department of Mechanical
Engineering
Indian Institute of Technology Kanpur
Kanpur, U.P. - 208016
Email: sde@iitk.ac.in

ABSTRACT

Large eddy simulation (LES) of turbulent lifted H_2/N_2 jet diffusion flame has been carried out using detailed chemical kinetics based on sparse-Lagrangian multiple mapping conditioning (MMC) approach. The jet is issued in a hot coflowing stream of combustion products from a lean premixed H_2/air flame at 1045 K. The jet is issued at 305 K at Reynolds number is 23600. In LES, subgrid stresses and fluxes are represented using the Smagorinsky model. MMC-CURL model is used as the mixing model in the sparse-Lagrangian MMC model. A reduced chemical kinetics for hydrogen is used containing 9 species and 12 reactions. Numerical results are validated against the available experimental measurements of Cabra et al. (R. Cabra, T. Myhrvold, J.Y. Chen, R.W. Dibble, A.N. Karpetis, R.S. Barlow, Simultaneous laser Raman-Rayleigh-Lif measurements and numerical modeling results of a lifted turbulent H_2/N_2 jet flame in a vitiated coflow, Proci. Combust. Inst. 29, 2002, 1881-1888).The present numerical results are found to be in excellent agreement with the available experimental measurements.

Keywords: Turbulent jet diffusion flames; sparse-Lagrangian multiple mapping conditioning; large eddy simulation; vitiated coflow; lifted flames; stochastic processes

SEEC-2017-154

Ethanol production from lignocellulosic biomass through SSF

Nadeem Akhtar a, Kanika Gupta b, Anchal Sharma c, Dinesh Goyal b,*, and Arun Goyal c
aDepartment of Animal Biosciences, University of Guelph, Guelph,
Ontario N1G 2W1, Canada
bDepartment of Biotechnology, Thapar University,
Patiala, 147 004, Punjab, India.
cBeant College of Engineering & Technology, Gurdaspur
cDepartment of Biosciences and Bioengineering, Indian Institute of Technology Guwahati,
Guwahati, 781 039, Assam, India.
bdgoyal@thapar.edu

ABSTRACT

Identification and pretreatment of promising feedstock for improved microbial saccharification and its further conversion to ethanol is important in development of sustainable energy system. Cellulose degrading bacteria were isolated, screened and characterized from compost, paper pulp and sugarcane bagasse. Wheat straw, rice straw and leaf litter from different tree species were collected, processed and subjected to four different pre-treatments such as alkaline fractionation, fungal solvolysis, dilute acid alkali and microwave-acid-alkali treatment to enhance saccharification. Microwave-acid-alkali pre-treatment was found to be the best and most promising technique among all pre-treatments. Solid state 13C CP/MAS NMR spectroscopy was most reliable technique to determine biochemical changes before and after pre-treatment of biomass. Among all types of biomass microwave-acid-alkali pre-treated rice straw as feedstock for ethanol production yielded maximum (246 mg/g) reducing sugar. The process was optimized using purified cellulase from Bacillus subtilis NA15 and Saccharomyces cerevisiae via simultaneous saccharification and fermentation (SSF). In 3-L bioreactor using microwave-acid-alkali pre-treated rice straw gave maximum ethanol concentration of 25.2 g/L corresponding to 59% yield after 24 h of SSF. Native bambo leaf litter (BLL) biomass had cellulose, hemicelluloses and lignin content of 26.06, 23.81 and 14.45%, respectively which upon microwave-alkali-acid treatment showed an increase in cellulose by 76% with a decrease in hemicellulose and lignin content by 34 and 54%, respectively. SEM of pre-treated BLL biomass showed microwave-alkali-acid pre-treatment induced structural change in the biomass and XRD analysis showed an increase (8.83%) in the crystallinity index (CrI) as compared to the native biomass. Under optimized conditions with 11% (w/v) substrate loading, 0.5% (v/v) enzyme concentration, 8% (v/v) inoculum size, at 30°C and 4.5 pH, 12.8 g/L ethanol production was observed in 60 h of incubation. Conversion of lignocellulosic biomass to ethanol at industrial scale is necessary to enhance the world energy security. Ten times increase in ethanol titer value was observed when microwave-alkali-acid pre-treated BLL biomass was used as substrate as compared to native biomass.

SEEC-2017-155

OPTIMIZATION OF VALVE EVENT TIMING OF A CAMLESS ENGINE

Abhimanyu Das, Dhananjay Kumar Srivastava
Department of Mechanical Engineering
Indian Institute of Technology Kharagpur
Kharagpur – 721302, West Bengal, India
Email: srivastava@mech.iitkgp.ernet.in

ABSTRACT

With most four stroke engines today is running with camshaft driven valvetrains, the performance of the engine is found to be optimized only for a narrow speed range usually in the mid to high-speed range. As a result, the performance of the engine suffers at speeds outside the optimal range. In such a scenario, optimization of the valve event timing on a camless valve actuation system can go a long way. An effort has been made for the same, in this project using Ricardo WAVE, a 1-D engine simulation software. A WAVE model is first created for an engine of known geometry. The power and torque curves obtained from simulation are then checked against the manufacturer data for model validation. Once validated, the lift profile of the valves is changed from a near sinusoidal form to a perfect square form, and the change in performance of the engine (brake power, brake torque, and volumetric efficiency) is noted. The valve event timing is then optimized for the same profile to maximize brake torque at various engine speeds. The lift profile is then changed to a trapezoidal one to account for valve clearance and finite response time of the actuator, and valve event timing is optimized again. The performance of the engine before valve event timing optimization with a stock camshaft and after optimization is the finally compared.

***Keywords:** Valve timing, Intake valve opening (IVO), Intake valve closing (IVC), Exhaust valve opening (EVO) and Exhaust valve closing (EVC)*

INTRODUCTION

The valvetrain of a reciprocating internal combustion engine is one of the most important subsystems that dictates the performance of the engine. While it is possible to operate an IC engine without valves, as is the case in two stroke engines which use ports, such engines have their own drawbacks. With most IC engines today operating on the four stroke cycle, optimization of the valve timing and lift can go a long way in enhancing their performance [1-3].

The valvetrain coordinates the intake of fresh charge/air and exhaust of combustion products in an IC engine. The power developed by an engine increases with increase in the amount of intake charge. Allowing the engine to draw in more charge helps increase the power output of the engine. However, at the same time expelling the exhaust gas at the right time helps reduce the pumping work. Hence a proper trade-off between expansion work and pumping work helps improve the net power output. Tuning of the valve timing and lift thus plays a crucial role in improving the power output as well as the efficiency of an IC engine.

In most reciprocating IC engines, the timing and lift of the intake and exhaust valves are controlled by a camshaft. Being mechanically driven by the crankshaft, a camshaft simplifies the valve actuation process. However, it also means that the valve timing and lift do not vary with speed. As a result, a camshaft driven valvetrain can be optimized for only a narrow speed range resulting in poor performance at speeds outside the optimized range. Hence, the power and torque curves of engines using camshaft driven valvetrains exhibit a peak at a particular speed, on either side of which power and torque drops. While, there do exist camshaft driven variable valve timing and lift systems, they usually offer few discrete modes of operation according to discrete speed ranges. Continuous variation of valve timing and lift with speed is usually not encountered, thus motivating the development of an independent valve timing and lift control system.

The project deals with the design of a control strategy or mapping the valve event timing for a KTM Duke 390 engine. Optimization of the valve event timing is carried out for this particular engine as it is being used by Team KART, the Formula SAE Team of Indian Institute of Technology Kharagpur. The physical camless valve

actuation mechanism is assumed to be a hypothetical system capable of actuating the valves instantaneously with negligible opening or closing delay. Development of the control system is carried out using Ricardo WAVE, a one-dimensional engine simulation software.

A WAVE model for the 373 cc single cylinder engine is first created and tallied with dynamometer power and torque values. After validation, optimization of the different valve event timing, i.e., intake valve opening (IVO), intake valve closing (IVC), exhaust valve opening (EVO) and exhaust valve closing (EVC) are targeted. The maximum valve lifts are fixed at their stock values. Objectives of the optimization are to obtain a flatter torque curve and enhanced volumetric efficiency.
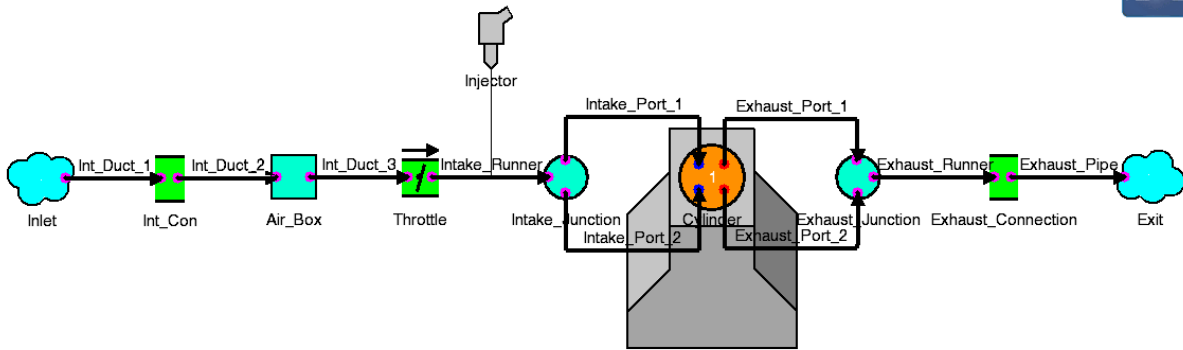
Fig 1. WAVE model for stock KTM 390 engine
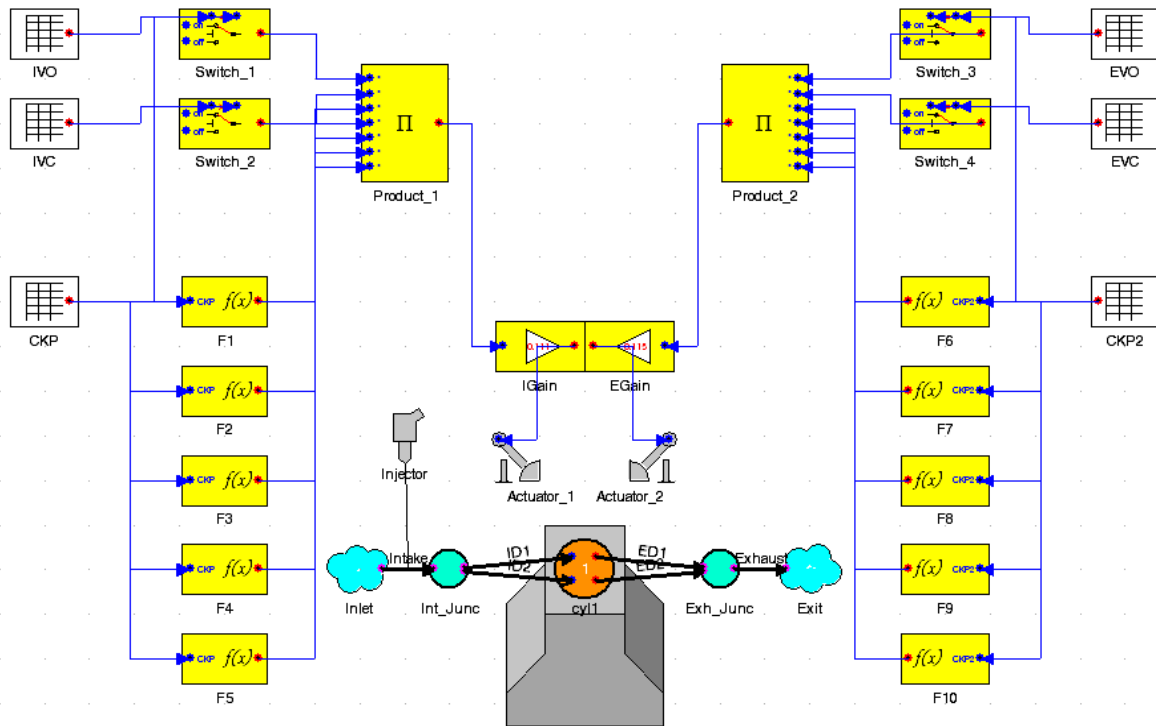
Fig 2. WAVE model for optimising valve timing with trapezoidal valve lift profile

The effect of one valve event timing being dependent on the timing of other valve events requires optimization of all the four valve events, i.e., IVO, IVC, EVO and EVC simultaneously. However, that requires enormous computational power and time. As such the timing of the valve events is optimized one at a time with the initial values of the valve event timing fixed exactly at TDC or BDC.

Optimization of the valve event timing is carried out using a live optimizer element in Ricardo WAVE. A torque sensor provides the optimizer with the brake torque output of the engine for various values of an individual valve event timing. The optimizer element is provided with the parameter range and the incremental step value for the parameter. After carrying out a large number of iterations, the optimizer provides the parameter value at which brake torque output of the engine is maximized.

While keeping the values of IVO, EVO and EVC fixed at their initial values, with a perfectly square lift profile, i.e., valves opening and closing instantaneously to their maximum lift values and closing to zero lift, the value of IVC is optimized for all different engine speeds. With IVC optimized, the value of IVC is set to the obtained optimized value for each case. With IVO and EVC fixed at initial values, EVO is then optimized. The values of IVC and EVO fixed at optimized values, and IVO fixed at an initial value, EVC is then optimized. Finally fixing the values of IVC, EVO, and EVC at optimized values, IVO is optimized completing one set of iteration. A number of sets of optimization events are carried out till convergence around a single set of values of valve event timing are obtained.

After convergence, the valve profiles are switched to trapezoidal forms from a square profile to account for valve opening and closing delay. The lifts increase and decrease linearly with time, and have a fixed opening and closing delay. A few sets of iteration are again carried out to obtain the final optimized set of values.

After having obtained the final values for the timing of the valve events, torque output and consequently power output, as well as volumetric efficiency of the engine were compared with that of the stock engine operating on a cam driven valvetrain as shown below.
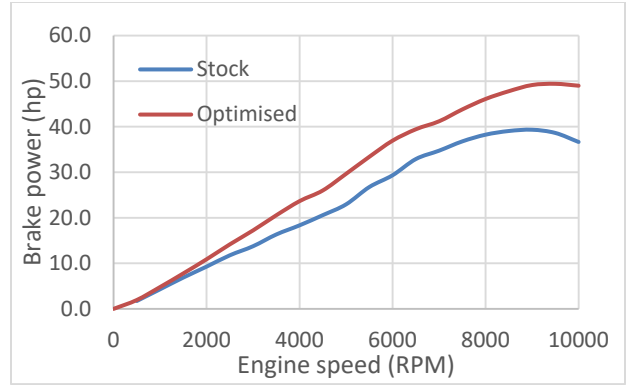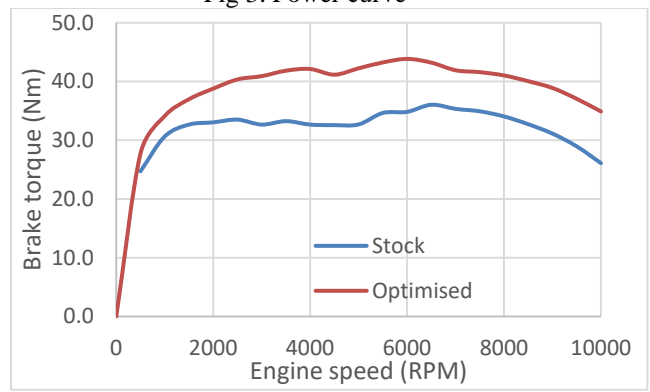

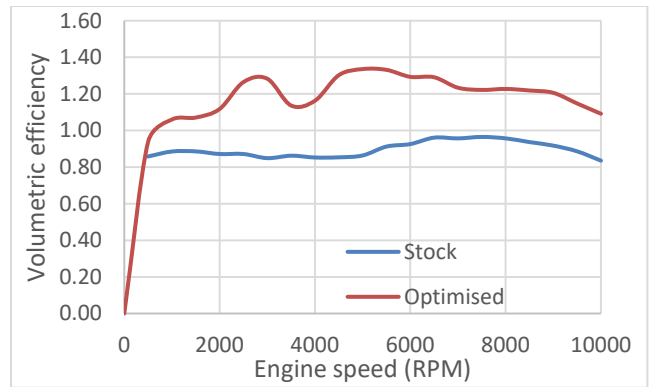Fig 3. Power curve

Fig 4. Torque curve

Fig 5. Volumetric efficiecnt curve

As seen in the above figures, there is improvement in the low speed torque producing a flatter torque curve which can be credited to the improved volumetric efficiency. There is an overall improvement in the performance of the engine which can be critically analysed when part load operation is considered. This is due to reduction of throttling loses when charge intake to the engine is directly controlled by modulating the intake valve lift and duration, rather than using a throttle valve.

REFERENCES

[1] Chihaya S., Hisao S., Atsushi U., Yasuo S. and Hidetaka O., 2004. "Study on Variable Valve Timing System Using Electromagnetic Mechanism". SAE paper no. 2004-01-1869.

[2] David C., and Andrew W., 2006. "Electromagnetic Fully Flexible Valve Actuator". SAE paper no 2006-01-0044.

[3] Fontana G., Galloni E. and Palmaccio R., 2006. "The Influence of Variable Valve Timing on the Combustion Process of a Small Spark-Ignition Engine". SAE paper no 2006-01-0445.

SEEC-2017-156

INVESTIGATION OF CONVECTIVE HEAT TRANSFER OF FERROFLUIDS FOR COOLING OF PHOTOVOLTAIC SYSTEMS

Danvendra Singh
Department of Mechanical Engineering
Indian Institute of Technology Guwahati
Email: devendra.2015@iitg.ernet.in

Balkrishna Mehta
Department of Mechanical Engineering
Indian Institute of Technology Guwahati
Email: krishnab@iitg.ernet.in

Md Asfer
Department of Mechanical Engineering
BML Munjal University, Gurugram, Haryana
Email: md.asfer@bml.edu.in

ABSTRACT

Ferrofluids have promising potential for heat transfer applications, as they can be easily controlled and manipulated by external magnetic fields. Unique characteristic behavior, such as its rheological and thermophysical properties can be altered to augment the convective heat transfer coefficient of thermal systems. Ferrofluids can also be used to cool the solar Photovoltaic thermal (PVT) systems. Solar cell performance decreases with increasing temperature, fundamentally owing to increased internal carrier recombination rates, caused by increased carrier concentrations. The operating temperature plays a key role in the photovoltaic conversion process. Hence, with an idea to develop a ferrofluid based heat exchanger for PVT systems, the present study aims to investigate the convective heat transfer performance of ferrofluids inside mini-tubes subjected to constant wall heat flux condition. The present study is executed by doing some 2D numerical simulations on COMSOL as well as performing the experiments for different magnetic field and Reynolds number on the heat transfer.

Keywords: PVT, IRT, Ferrofluids, Heat transfer
.

NOMENCLATURE
Nu   Nusselt number
Pe   Peclet number
u   x-component of velocity
x   Axial co-ordinate
Y   spacing between magnet and tube wall

INTRODUCTION

With the increasing demands of energy to improve the better living conditions and sustainable growth of the human being, technology has made a shift to develop the methodologies to use renewable sources of energy like solar, geo-thermal and wind etc. Generating electricity by using solar Photovoltaic (PV) systems is one of the state of the art technology where maintaining the system temperature within certain operating range is essential for maximizing the performance of PV system. Therefore, some thermal solutions has to be sought and integrated with PV system to maintain the cell temperature. Amongst many other heat transfer applications, designing the heat exchanger for solar Photovoltaic thermal (PVT) systems, which converts the solar radiations into electrical energy, is an imporatant scientific challenge (Fig 1). It is quite well known fact that electrical conversion efficiency decreases with increase of cell temperature because more that 50% of the incident energy is absorbed and rest is reflected [1]. For example, the efficiency of a typical PV system with c-Si cells is decreased by 0.45% for 1ºC increase of the working temperature [2]. Therefore, various thermal solutions can be investigated to maintain the cell temperature of PV systems so that highest possible operating efficiency is achieved.

1

In the past few years, development of ferro-hydrodynamics is compelling researchers to revisit the thermo-hydrodynamics of the conventional systems with improved performance in the presence of external magnetic field. Ferro-hydrodynamics is basically the study of flow and thermal behavior of 'ferrofluids' that are synthesized as a stable colloidal suspension of iron oxide (Fe_3O_4) nanoparticles which can be manipulated by esxternally applied magnetic fields. The nanoparticles are usually coated with a stabilizing surfactant matched with the type of liquid, which prevents the nanoparticle agglomeration, by overcoming the attractive van der Waals forces between them. Ferrofluids have already found their way into a variety of technological (e.g., in the areas of sealing, damping, and heat dissipation etc.) and bio-medical applications (e.g., in the areas of drug targeting, hyperthermia, and separation etc.) in the last two decades. The growing importance of mini/micro-scale heat exchangers in smaller devices has initiated considerable research that addresses heat transfer at mini/micro-scale. Because of external manipulation of rhelogical and themophysical properties, now-a-days ferrofluids are quite attractive for heat transfer application in various situations.

With this background, the present study is initiated with numerical simulations using COMSOL for ferrofluid flow through a mini-tube subjected to a constant heat flux boundary condition and external magnetic field produced by a single permanent magnet. Few experiements were also carried out inside a stainless steel tube of 2 mm diameter (ID) under uniform wall heat flux condition and external magnetic field in order to compare the simulation results qualitatively. The extension of this study will lead to design of a heat exchanger for solar PVT systems in future.
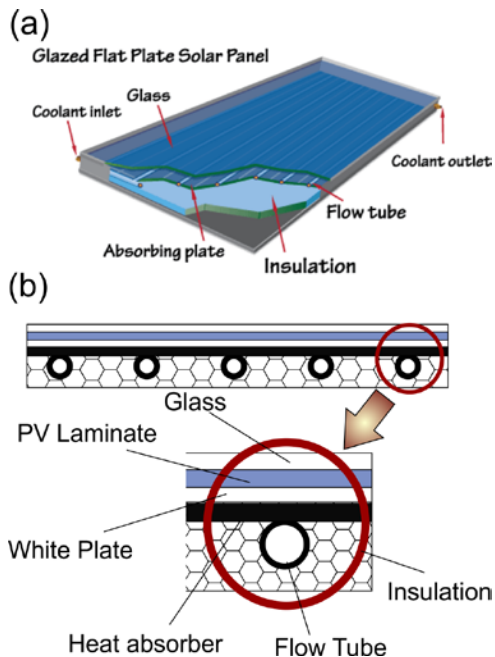
FIGURE 1. (a) Picture of a PV cell (b) Schematic representation showing the coolant flow through the heat exchanger in a PV cell
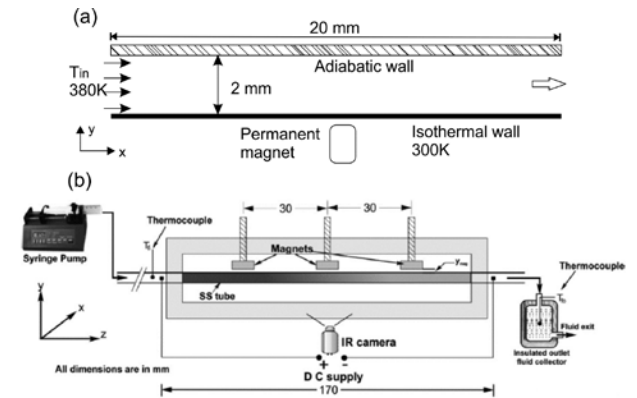
**FIGURE 2.** (a) Computational domain for validation (b) Schematic of experimental set-up
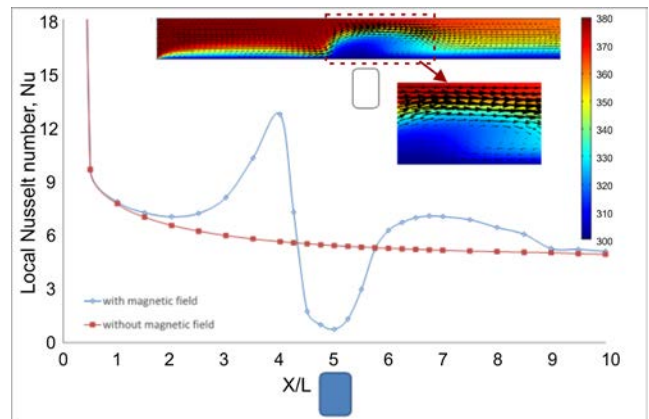
FIGURE 3. Nusselt number for test case and temperature and velocity distribution shown in inset

RESULTS AND DISCUSSIONS

Before executing the experimental work, it was thought to investigate the heat transfer behavior of ferrofluids in simple convective flow numerically. Fig. 2(a) shows the 2-D computational domain where in convective cooling of ferrofluids is taking place. A uniform flow is entering into the channel at elevated temperature of 380 K while at the exit, flow and thermal conditions are hydrodynamically and thermally fully developed. The bottom wall is kept at constant temperature of 300 K and top wall is adiabatic. To apply the magnetic field, a permanent magnet of 1000 milliTesla (remenant magnetic field intensity) is used. The magnet is positioned at the 1 mm away from the bottom plate.

Axial variation of the local Nusselt number obtained from the test case simulation is presented in Fig. 3 and in the inset, velocity and temperature field are also shown. The flow and thermal field obtained in the domain is the consequence of resultant of the inertia force and the

magnetic force. From the velocity field, it is observable that in upstream locations of the magnet, 'u' (horizontal velocity component) velocity increases in the nearby region where magnetic force supports the inertia while in the downstream locations (where horizontal component of magnetic force opposes the inertia larger magnitude of 'u' is obtained away from the magnet. Also, there will be some inner region in the magnetic force field where only the vertical component of force will exist. This will try to hold the fluid near to the magnet and because of interplay of inertia and magnetic force, a recirculation region will be formed. This recirculating zone will provide a secondary flow field (analogy can be seen from the flow over a bluff body) in the domain and to conserve the mass, an accelerating flow field will be achieved over the recirculating bubble. Of course, far from the magnetic field the velocity field is like conventional laminar flow. This recirculation ensure that the hot fluid dissipates heat to the wall and thus getting cold and which further picks heat from the surrounding warmer region which thus ensures an efficient heat transfer mechanism. Nu plot also shaw the improvement in the heat transfer as compared to without magnetic field.
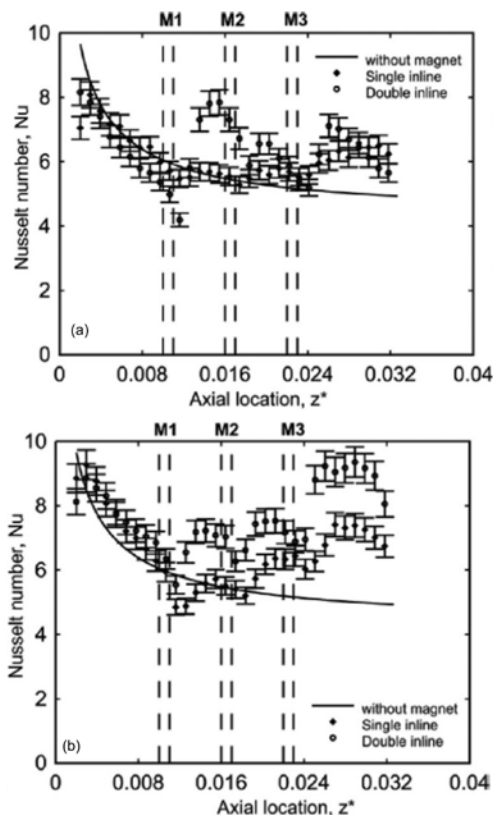
FIGURE 4. Nusselt number for single inline and double inline arrangement at $Pe = 2496$ (a) $Y_{mag} = 1.5$ mm (b) $Y_{mag} = 3.0$ mm

Augmentation in the heat transfer in presence of magnetic field, motivated the experimental investigation. Schematic of the experimental set-up is shown in Fig. 2(b) which shows that series of magnets have been used to puturb the flow field. Figure only shows the arrangement of magnets in single inline while experiments have been performed by arrangeing the magnets in double inline too, i.e., magnets are kept at top as well as at the bottom of the tube for given location making 'N-S' pole facing to each other and providing uniform magnetic field in the flow domain.

During the experiments, outer wall temperature is measure by using InfraRed Thermography (IRT) and fluid temperatures at inlet and outlet sections are measured by using two K-type thermocouples. The intermediate fluid temperatures are determined by linear interpolation between inlet and outlet. Experimentally obtained Nusselt number for single inline and double inline arrangement of magnetic field is shown in Fig. 4 (a,b). The flow reate of ferrofluids were kept at 40 ml/min which is turning out to be Peclet number of $Pe = 2496$. The spacing between the magnet and tube surface (equivalent to varying the magnetic field intensity) is kept 1.5 mm and 3.0 mm. The heat transfer results are also compared with no magnetic field situation. The overall increase or decrease in convective heat transfer characteristics of ferrofluid in the presence of magnetic field as compared to the case of no magnetic field is attributed to several factors such as: (a) ratio of magnetic force to inertia force acting on the ferrofluid, (b) interaction of ferrofluid flow with the aggregate of iron oxide nanoparticles (IONPs) at the wall of the tube adjacent to each magnet, and (c) enhancement in local thermal conductivity of ferrofluid due to the formation of chain like clusters of IONPs within the ferrofluid in the presence of magnetic field [3]. It is clearly visible from the experimental results that the convective heat transfer is significantly augmented by the ferrofluids in presence of magnetic field. Thus, it can be comprehended that integrating the heat exchanger based on ferrofluids to PV systems might be useful to extract the heat which increses the temperature of the cell. This work will now be extended to design the PV systems integrated with thermal unit and performance will be compared for both the cases.

CONCLUSIONS

The convective heat transfer coefficient (Nusselt number) for ferrofluid flow in the presence of magnetic field augments the heat transfer. Augmentation factor depends on magnetic field intensity, flow inertia and cluster formation of iron oxide nanoparticles. Therfore, packaging the PV system with a thermal unit based on ferrofluidic heat transfer can improve conversion of solar radiation to the electricity.

ACKNOWLEDGMENTS

providing water based ferrofluids and Department of Mechanical Engineering, IIT Guwahati.

REFERENCES

[1] Ghadiri, M., Saradarabadi, M., Pasandideh-fard, M. and Moghadam, A., 2015. "Experimental investigation of a PVT system performance using nano ferrofluids". Energy Conversion and Management, 103, pp. 468-476.

[2] Kalogirou, S. A., and Tripanagnostopoulos Y., 2006. "Hybrid PV/T solar systems for domestic hot water and electricity production". Energy Conversion and Management,4, pp. 3368–3382.

[3] Asfer M., Mehta B., Kumar A., Khandekar S. and Panigrahi P. K., 2016. "Effect of magnetic field on laminar convective heat transfer characteristics of ferrofluid flowing through a circular stainless steel tube". International Journal of Heat and Fluid Flow,59, pp. 74-86.

SEEC-2017-157

OXY-ENRICHED AIR GASIFICATION OF WET BIOMASS

Anmol Garg
Research Student, Mechanical Engineering Department
Thapar University
Email: er.anmol1993@gmail.com

Sandeep Kumar,
Faculty, Mechanical Engineering Department
Thapar University
Email: Sandeep.kumar@thapar.edu

ABSTRACT

Biomass gasification is picking up the interest for converting waste biomass to energy using IC engine. Downdraft fixed bed gasifiers are employed as better alternative for IC engine application due its low tar yield, but is restricted with the use of biomass with low moisture content only. Endothermicity induced due to absorption of latent and sensible heat by H_2O present in wet biomass is attributed to the lower bed temperatures resulting in poor performance of downdraft gasification system. There is a need to supply high amount of oxidiser to compensate for the endothermicity through enhanced oxidation. Literature shows that the high reactant mass flux may lead to convective cooling of the reaction front which is undesirable. Another approach is devised in the present work to enhance the O_2 fraction in the reactant mixture (oxy-enriched air) keeping the reactant mass flux constant.

Keywords *Biomass gasification, oxy-enriched air gasification, wet biomass gasification*
.

INTRODUCTION

Biomass gasification, as a thermo-chemical process, is picking up the interest for converting waste biomass to energy and electricity generation using IC engine is of foremost interest. Downdraft fixed bed gasifiers are employed as better alternative for IC engine application due its low tar yield [1], but is restricted with the use of biomass with low moisture content only. Biomass available as agro/civic waste is generally high on moisture content. Also, the tendency of biomass to imbibe moisture during rainy days makes it energy and cost intensive for storage and pre-processing of wet biomass for use in downdraft gasification system. Endothermicity induced due to absorption of latent and sensible heat by H_2O present in wet biomass is attributed to the lower bed temperatures resulting in poor performance of downdraft gasification

system [2]. Lower bed temperature also leads to high tar yield in gasification of wet biomass. There is a need to supply high amount of oxidiser to compensate for the endothermicity through enhanced oxidation. But literature shows that the high reactant mass flux may lead to convective cooling of the reaction front where increased N_2, a inert in the gasification system, absorbs the sensible heat and reduces the local temperature of the reaction front which is undesirable [3]. Another approach is devised in the present work to enhance the O_2 fraction in the reactant mixture (oxy-enriched air) keeping the reactant mass flux constant. This avoids the convective cooling of the reaction zone.

The aim of this study is to stimulate the variation in temperature distribution along the bed height by changing the input air velocity. The literature [3] supports that there is heat transfer from combustion zone to the bed above it through conduction and radiation, this heat enhances the pyrolysis process and better char conversion. Then, thermodynamic equilibrium study is performed to evaluate the effects of oxy-enriched air gasification of wet biomass.
.

CFD SIMULATION

Cell Zone Conditions

➢ In 'Cell zone conditions' the material is set to air.

➢ The bed condition details are listed in the Table.1.1.

Table.1 Gasifier Bed Conditions

Upper Bed	Combustion Bed	Lower Bed
Porous Zone	Porous Zone	Non Porous Zone
Void Fraction 0.4	Void Fraction 0.3	Void Fraction -

Boundary Conditions

➤ At Inlet, Velocity magnitude varies from 0.5 to 2.5 mm/s, Initial gauge pressure- 1000Pa.

➤ At Outlet, Gauge pressure - 0Pa.

➤ Bed wall thermal conditions are given as

Upper bed wall – Convective heat transfer to surroundings (h = 25 W/m^{2}k)

Combustion bed wall – At constant temperature of 2000 k

Lower bed wall – Convective heat transfer to surroundings (h = 25 W/m^{2}k)

Solution Controls

➤ Normal relaxation factor – Pressure – 0.3 and Momentum – 0.7

➤ Convergence criterion - Energy equation converges at 10^{-06} and rest all at 10^{-03}.

CFD Simulation results

Fig. 1 - 4 shows the simulation of variation in temperature distribution along the bed height vs. input air velocity. Temperature profile is found to be very sensitive to air flow rate. It is observed that with the increase in air inlet velocity, the temperature near the pyrolysis zone (upper bed) decreases.
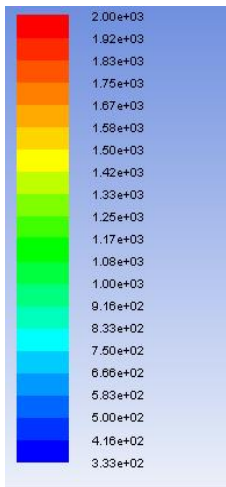
Fig.1
scale
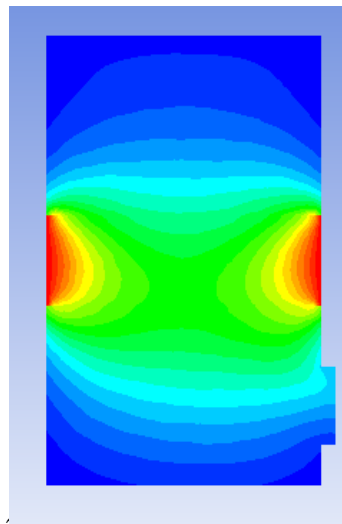
Fig.2 Temperature distribution at 0.5mm/s air velocity
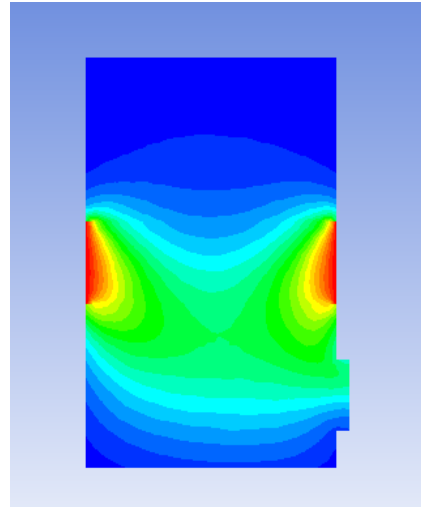
Fig.3 Temperature distribution at   1.5mm/s air velocity
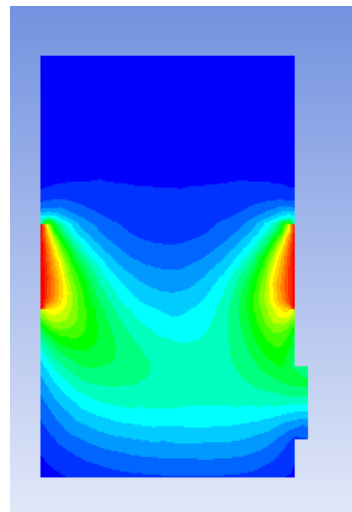
Fig.4   Temperature distribution at 2.5mm/s air velocity

Simulation result analysis

CFD simulation of Fixed Bed Downdraft Gasifier is carried out, variation in temperature distribution along the bed height vs. input air velocity are obtained. Temperature profile is found to be very sensitive to air flow rate. It is observed that with the increase in air inlet velocity, the temperature near the pyrolysis zone (upper bed) decreases. Simulation results indicates that with the increase in air input velocity there is a significant decrease in heat transfer from combustion zone (through radiation/conduction) to biomass bed above (needed to initiate pyrolysis).If the heat loss by convective cooling to ambient air from pyrolysis zone increases, than the heat gain from the combustion zone, then the gasifier will quench.

Thermodynamic Equilibrium studies with Oxy-enriched air gasification

The present work addresses the study of wet biomass gasification process using O_2 enriched air as reactants. Increasing the O_2 volume fraction in volatile combustion zone ensures high reaction rate and high bed temperatures. High bed temperatures compensates for the effects of excess H_2O in wet biomass. The gas composition of producer gas, ER and efficiency are focused in the present study.

Thermodynamic equilibrium analysis under adiabatic conditions, employing NASA-SP 273 code, has been performed to evaluate the effects of moisture content on the system temperature and product gas composition. Gasification process is complex heterogeneous reaction mechanism and seldom reaches to the thermodynamic equilibrium and is largely governed by the reaction kinetics. But nonetheless equilibrium model do predicts the behaviour of the system under different conditions like the variation of temperature, equivalence ratio, etc. Equilibrium studies results in adiabatic temperature around 200-300 K more than what is observed during experiments. Using the analogy, the enrichment in O_2 volume fraction for stable and sustained wet biomass gasification were chosen with adiabatic temperature range of 1700-1800 K. Further, thermodynamic equilibrium analysis under isothermal conditions is performed to simulate the conditions of reduction zone at different temperatures and to identify the product gas composition and the variation in the cold gas efficiency in downdraft gasifier. With the increase in moisture content in biomass, the O_2 demand per unit mass of dry biomass increases and becomes almost double at 45% moisture content. The increase in ER leads to shifting of gasification process towards combustion in turn leading to reduced energy efficiencies.

Conclusions

The present work provides a low cost solution to the industries using biomass gasification process and facing issues with wet biomass of varying moisture level. The issue of convective cooling at higher reactant mass flux is simulated using ANSYS CFD software which validates the results from literature. Enriching the air with O_2 is devised as potential solution for achieving better results with wet biomass gasification. The low energy efficiency is compensated with the reduction in cost and labour involved in pre-processing of wet biomass.

REFERENCES

[1] S. Mahapatra, S. Dasappa. Fuel Processing Technology 121 (2014) 83–90

[2] Sandeep K. Experimental and modeling studies on the generation of hydrogen rich syngas through oxy-steam gasification of biomass. *PhD Thesis* (2016). Indian Institute of Science, India.

[3] S Mahapatra, S. Dasappa. Experiments and analysis of propagation front under gasification regimes in a packed bed. Fuel Processing Technology 121 (2014) 83–90.

SEEC-2017-158

Optimization of process parameters for Polyhydroxyalkanoates production from carbon dioxide sequestering bacterium *Bacillus* sp. SS105

Neha Maheshwari1, Madan kumar1, Indu Shekhar Thakur2, Shaili Srivastava1, 2*
1. Amity School of Earth and Environmental Science, Amity University Gurgaon, India
2. School of Environmental Sciences, Jawaharlal Nehru University, New Delhi 110067, India

ABSTRACT

Atmospheric concentration of carbon dioxide has increased by about 30 % from the start of the industrial revolution. The increase in carbon dioxide concentration leads to global warming. The main source of CO_2 emission is burning of fossil fuels and change in land use throughout the world. Nature has evolved sophisticated mechanisms for carbon capture and utilization, manifested through autotrophy. Many organisms such as photosynthetic and chemolithoautotrophic microbes display excellent ability of CO_2 sequestration and its assimilation into biomass and value added products such as polyhydroxyalkanoates (PHA), biosurfactants, biodiesel, etc. In the present study, a chemolithotropic bacterium was isolated from Free air CO_2 enriched (FACE) soil microbial community. FACE is an area where plants are exposed to observe the changes under elevated carbon dioxide concentration. Microbial communities present there get exposed to elevated CO_2 concentration and will develop robust machinery for carbon dioxide utilization. Total ten bacteria were isolated from FACE soil microbial community and were enriched in the presence of MSM with 50 mM of $NaHCO_3$.and 5% CO_2 incubator under shake flask condition. On the basis of carbon capture potency, out of ten only five bacteria were selected and their carbon dioxide sequestration was determined by carbonic anhydrase and ribulose-1, 5-bisphosphate carboxylase/oxygenase (RuBisCO) enzyme assay. Based on enzymes assay and bicarbonate utilization, only one bacterium was selected having enhanced carbon capture potential among five isolates. The 16S rDNA sequence analysis reveals that the bacterium shows close homology (98%) with Bacillus cereus and the strain was named as Bacillus sp. SS105. This strain along with CO_2 sequestration also produced Polyhydroxyalkanoates (PHA). Its carbon dioxide sequestration potential and Polyhydroxyalkanoates (PHA) production was further studied in detail. The selected bacterial strain Bacillus sp. SS105 was screened for PHA production based on Nile red staining followed by visualization under fluorescence microscope. Spectrofluorometric measurement of Nile red fluorescence of the bacterial culture was also done. Confirmatory analysis of PHA monomer was done by GC–MS analysis. Detection of characteristic peaks of PHA was characterized by FT-IR and NMR. The CO_2 utilization in PHA production was further optimized with Box–Behnken design and Response surface methodology (RSM). The parameters selected for optimization study are molasses concentration, sodium bicarbonate concentration and duration. On the basis of above study it may be concluded that this strain showed remarkable ability of CO_2 sequestration and PHA production.

SEEC-2017-159

DEVELOPMENT OF PHOTOSENSITIZER NANOCONJUGATES THROUGH A BIOINSPIRED PATHWAY§

Jayeeta Bhaumik
Center of Innovative and Applied Bioprocessing
(CIAB), Mohali, Punjab, India
Email: jbhaumi@gmail.com
**Seema Kirar, Neeraj S. Thakur, Uttam C.
Banerjee, Joydev K. Laha**
National Institute of Pharmaceutical Education
and Research (NIPER), Mohali, Punjab, India
Email: jklaha@gmail.com

ABSTRACT

An approach to improve biological delivery of photosensitizers by including them into nanomaterials has been established. In order to prepare photosensitizer nanoconjugates as biocompatible and selective probes, initially, bioconjugatable porphyrinic photosensitizers were developed via rational methods. The porphyrins with carboxyl groups (as conjugatable handles) were successfully attached on the surface of the bioinspired nanoparticles (through a stable ester bond formation) affording hydrophilic and biocompatible nanophotosensitizers. The loading efficiency of the photosensitizer into nanomaterials was found to be 12–16%. Given their biocompatibility and efficient loading on nanoparticles, the photosensitizers prepared in this study could find use in photodynamic therapy and dual photodynamic–photothermal therapy.

Keywords *porphyrins, photosensitizers, nanconjugates, nanosensitizers, photodynamic therapy*

INTRODUCTION

Photodynamic therapy (PDT) has become an important therapeutic tool for the treatment of many diseases including cancer, microbial infection and cardiovascular diseases.[1–3] Photosensitizers (PSs) are essential components of PDT, which upon absorption of light are activated, and generate singlet oxygen that causes tumor cell destruction.[4,5] Among other photosensitizers, tetrapyrrolic macrocycles have found an extensive use as photosensitizers due to their unique absorption properties in the visible and/or near infrared region of the electromagnetic spectrum.[6,7] Porphyrins or their hydrogenated derivatives such as chlorins are effective tetrapyrrolic photosensitizers due to

their high stability and ease of synthesis.[8] For example, commercially available Photofrin, a porphyrin, or Foscan, a chlorin has found large applications for the treatment of certain cancer.[9] However, limitations of tetrapyrrolic macrocycles as photosensitizers may include their hydrophobicity, biocompatibility, and non-selective delivery to biological sys tems.[8]
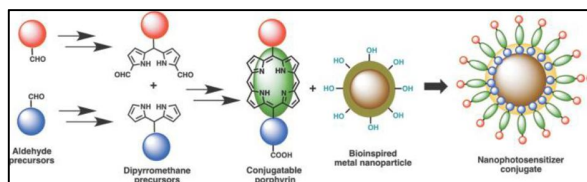
Herein the development of porphyrin-nanoconjugates as biocompatible photosensitizers for potential applications in PDT and/or dual PDT–PTT is reported. Initially, several conjugatable heterocycles containing compact trans-AB porphyrinic photosensitizers (PSs) were synthesized via rational routes. Those compact porphyrins with a carboxyl tether were then successfully attached to the surface of the bioinspired metal nanoparticles (rich in –OH group) via covalent (ester) bond formation. These nanophotosensitizer conjugates were further characterized (by absorption spectroscopy, FTIR spectroscopy and HPLC) and the photosensitizer loading efficiency on nanoscaffolds was also determined. Overall, these bioinspired photosensitizer nanoconjugates with enhanced biocompatibility are promising candidates for photomedical applications.
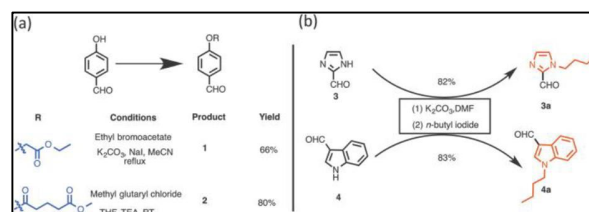
RESULTS AND DISCUSSION
Rational synthesis of conjugatable porphyrins

The preparation of synthetic precursors to porphyrins is shown in Scheme 1. The synthesis of dipyrromethanes was carried out using one of the following approaches developed earlier by us: (a) TFA-catalyzed reaction at room temperature, (b) InCl$_3$-catalyzed reaction at room temperature or an elevated temperature in the presence of a large excess pyrrole,[11] or (c) heating a neatmixture at an elevated temperature. Thus, aldehyde **1** was treated with excess pyrrole in the presence of TFA (10 mol%), which upon chromatographic purification produced
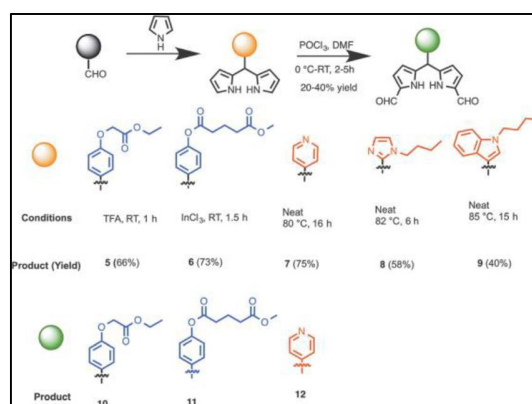
dipyrromethane 5 in 66% yield (Scheme 2).[12] Reaction of a mixture of benzaldehyde **2** and excess. pyrrole at room temperature (25 °C) in the presence of a catalytic amount of InCl3 (20 mol%) followed by chromatography gave dipyrromethane **6** in 73% yield. A neat mixture of 4-pyridine carboxaldehyde and excess pyrrole was heated at 80 °C for 16 h, which upon chromatographic separation gave the desired 5-pyridyldipyrromethane (**7**) in 75% yield.[13] Likewise, compounds **3a** and **4a** afforded 5-[1-butyl-imidazol-2-yl]dipyrromethane (**8**) and 5-[1-butylindol-3-yl]dipyrromethane (**9**) in 58 and 40% yields, respectively. Diformylation of dipyrromethanes **5, 6** or **7** at 1,9-positions, following a protocol previously demonstrated by us,[14] yielded 1,9-diformyldipyrromethanes (**10–12**) in 20–40% yield. Using a protocol developed by us earlier,[15] the synthesis of trans-AB porphyrins was achieved by the condensation of 1,9-diformyldipyrromethanes and dipyrromethanes in the presence of excess n-propylamine in THF and subsequent metalation with Zn(OAc)$_2$. Thus, reaction of 1,9-diformyldipyrromethane **12** and dipyrromethane 5 delivered porphyrin **13** as a purple solid (Scheme 3, 20% yield). However, acquisition of spectroscopic data for the characterization of porphyrin **13** was largely impeded probably because of self-aggregation, encountered due to the co-ordination between pyridyl nitrogen and zinc metal. The central zinc atom from the porphyrin macrocycle was therefore needed to be removed. Demetalation of trans-AB porphyrin **13** was achieved by treating a solution of **13** in CH$_2$Cl$_2$ with excess TFA at room temperature (25 °C) for 2 h, which upon subsequent purification afforded porphyrin **14**. The free-base porphyrin **14** provided satisfactory characterization data. Next, the ester group in porphyrin **14** was subjected to base mediated hydrolysis to engender carboxylic acid tether required for conjugation to nanoparticles. Thus, treating a solution of **14** in THF with LiOH·H$_2$O at room temperature and subsequent acidification with 10% HCl afforded porphyrin **15** containing a carboxylic acid handle. The pyridyl nitrogen in porphyrin **15** was methylated with excess methyl iodide to obtain **16** (80% yield in two steps).
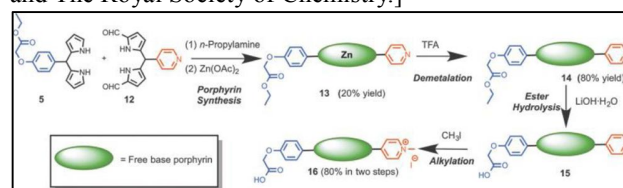

FIGURE 1. Synthetic design towards the development of nanophotosensitizer conjugates. [Reproduced from reference no. 10 with permission from the Centre National de la Recherche Scientifique (CNRS) and The Royal Society of Chemistry.]

SCHEME 1. Synthetic precursors to dipyrromethanes: (a) synthesis of aldehydes containing masked conjugatable groups; (b) synthesis of butylated heterocyclic aldehydes. [Reproduced from reference no. 10 with permission from the Centre National de la Recherche Scientifique (CNRS) and The Royal Society of Chemistry.]

SCHEME 2. Synthesis of conjugatable and heterocyclic dipyrromethanes, and 1,9-diformyldipyrromethanes as porphyrin precursors. [Reproduced from reference no. 10 with permission from the Centre National de la Recherche Scientifique (CNRS) and The Royal Society of Chemistry.]
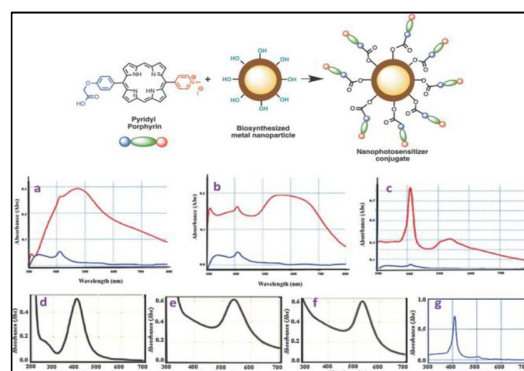

SCHEME 3. Preparation of a trans-AB porphyrin with a cationic and a conjugatable hand. [Reproduced from reference no. 10 with permission from the Centre National de la Recherche Scientifique (CNRS) and The Royal Society of Chemistry.]

Nanophotosensitizer preparation

Central to this study was to demonstrate the conjugation of porphyrin **16** with metal NPs, prepared by us previously.[15] Silver and gold nanoparticles (AgNPs and AuNPs) were prepared from Camellia sinensis (CS, green tea) and Potentilla fulgens (PF, vajradanti) in high yields. Three types of bioinspired nanoparticles (CS-AgNPs, CS-AuNPs and PF-AuNPs) were developed where plant materials acted as reducing, stabilizing and capping agents.

The biomaterials present (from plant extracts) on the surface of the metal nanoparticles are a class of flavonoids that are rich in hydroxyl functionalities.[15] The carboxylic acid moiety in the porphyrin 16 could be easily coupled with the hydroxyl groups present in metal NPs via an ester linkage (Scheme 2, top panel). The conjugation of porphyrin 16 and metal NPs was carried out via EDC mediated coupling reaction. The analytical data (FTIR, UV-vis, and HPLC) obtained for the samples prepared from these reactions strongly support the formation of conjugated nanophotosensitizers from porphyrin 16. For example, FTIR data showed a peak at 1732 nm as a characteristic of ester functionality present in porphyrin-nanoconjugates. UV-visible spectra of porphyrin-nanoconjugates are distinct from those of their unconjugated metal NPs or porphyrin 16 (Fig. 2a–g). For example, the UV-visible spectrum of porphyrin 16 shows a strong intense band at 410 nm, while UV-visible spectra of silver nanoparticles in our study showed a peak at 450 nm, and UV-visible spectra of gold nanoparticles appeared at 535 nm. For example, the porphyrin-nanoconjugates of silver nanoparticles (CS-AgNPs) showed broad absorption peaks at 411 and 450 nm (Fig. 2a). Similarly, porphyrin conjugated gold nanoparticles (both CS-AuNPs and PF-AuNPs) also showed two peaks at 411 and 535 nm (Fig. 2b and c). Further confirmation of porphyrin-nanoconjugates is apparent from the fact that treatment with NaOH resulted in the hydrolysis of the ester bond formed between porphyrin and metal nanoparticles. Centrifugation of the supernatant revealed the appearance of only one peak at 411 nm upon absorption spectroscopy indicating release of the porphyrin from the nanomaterial surface. As photosensitizers show therapeutic efficacy at lower concentration,2 photosensitizers loaded with nanoparticles at the 12–16% level have successfully been delivered. The ability of porphyrin 16 loaded on CS-AgNPs, CS-AuNPs, and PF-AuNPs was estimated to be 16, 12, and 16%, respectively (by the HPLC method). The observed loading efficiency of 16 is proportional to the number of hydroxyl functionalities present on metal nanoparticles. Notably, the loading efficiency of porphyrin 16 is found to be significant for drug delivery and also leaves room to develop phototheranostic nanoagents by the incorporation of diagnostic and targeting agents on the nanoparticles. Overall these bioinspired photosensitizers are substantial precursors for phototheranostic nanoagents for finding better treatment using PDT or dual PDT–PTT.

FIGURE 2. (top panel) Development of nanophotosensitizer conjugates via the condensation of a conjugatable porphyrin on the surface of biosynthesized metal nanoparticles. (bottom panel) Conjugation of porphyrin with metallic NPs: (a) conjugation with CS-AgNPs; (b) conjugation with CS-AuNPs, and (c) conjugation with PF-AuNPs. Red line: UV-vis spectra before NaOH treatment; blue line: UV-vis spectra after NaOH treatment; absorption spectra of (d) CS-AgNPs, (e) CS-AuNPs (f) PF-AuNPs and (g) free pyridyl porphyrin 16. [Reproduced from reference no. 10 with permission from the Centre National de la Recherche Scientifique (CNRS) and The Royal Society of Chemistry.]

CONCLUSIONS

Photosensitizer metal nanoconjugates were developed as better alternatives to conventional photosensitizers for PDT or combined PDT–PTT applications. First, various building blocks (aldehydes, dipyrromethanes and diformyldipyrromethanes) containing heterocyclic (pyridyl, imidazole, and indole) and conjugatable moieties as precursors to porphyrins were synthesized. Later, rational syntheses of versatile cationic (positively charged) and conjugatable tetrapyrrolic macrocycles were accomplished. Unlike the statistical route, which generates a mixture of porphyrinic derivatives, the rational route resulted in single porphyrinic species in highly pure form. Afterwards, newly constructed conjugatable tetrapyrrolic photosensitizers were characterized by different analytical techniques including absorption spectroscopy, NMR and mass spectrometry. Taking the advantage of hydroxyl functionalities present on the periphery of bioinspired noble metal nanoparticles (silver and gold), porphyrins containing carboxyl tethers were attached on their surface via ester bond formation (through EDC mediated coupling). The loading efficiency of the photosensitizers on nanoscaffolds was determined by both absorption spectroscopy and HPLC methods. These nanophotosensitizers were designed in order to possess enhanced biocompatibility as observed by their stability under physiological conditions. These photosensitizer nanoconjugates can serve as PDT or dual PDT–PTT agents with improved efficacy compared to native PSs or NPs.

These bioengineered nanophotosensitizer probes are potential candidates for photomedicines.

ACKNOWLEDGMENTS

REFERENCES

[1] J. Bhaumik, A. K. Mittal, A. Banerjee, Y. Chisti and U. C. Banerjee, 2015, "Biosynthesis of silver nanoparticles: elucidation of prospective mechanism and therapeutic potential", Nano Res., 8, 1373–1394.

[2] P. Mroz, J. Bhaumik, D. K. Dogutan, Z. Aly, Z. Kamal, Khalid, H. L. Kee, D. F. Bocian, D. Holten, J. S. Lindsey and M. R. Hamblin, 2009, "Imidazole metalloporphyrins as photosensitizers for photodynamic therapy: role of molecular charge, central metal and hydroxyl radical production", Cancer Lett., 282, 63–76.

[3] J. R. McCarthy, E. Korngold, R. Weissleder and F. A. Jaffer, 2010, "A light-activated theranostic nanoagent for targeted macrophage ablation in inflammatory atherosclerosis", Small, 6, 2041–2049.

[4] D. E. Dolmans, D. Fukumura and R. K. Jain, 2003, "Photodynamic therapy for cancer", Nat. Rev. Cancer, 3, 380–387.

[5] J. Bhaumik, J. R. McCarthy and R. Weissleder, 2009, "Synthesis and photophysical properties of sulfonamidophenyl porphyrins as models for activatable photosensitizers", J. Org. Chem., 74, 5894–5901.

[6] H. L. Kee, J. Bhaumik, J. R. Diers, P. Mroz, M. R. Hamblin, D. F. Bocian, J. S. Lindsey and D. Holten, 2008, "Photophysical characterization of imidazolium-substituted Pd (II), In (III), and Zn (II) porphyrins as photosensitizers for photodynamic therapy", J. Photochem. Photobiol., A, 200, 346–355.

[7] C. Muthiah, J. Bhaumik and J. S. Lindsey, 2007, "Rational routes to formyl-substituted chlorins", J. Org. Chem., 72, 5839–5842.

[8] M. Ethirajan, Y. Chen, P. Joshi and R. K. Pandey, 2011, "The role of porphyrin chemistry in tumor imaging and photodynamic therapy", Chem. Soc. Rev., 40, 340–362.

[9] L.B. Josefsen and R.W. Boyle, 2012, "Unique Diagnostic and Therapeutic Roles of Porphyrins and Phthalocyanines in Photodynamic Therapy, Imaging and Theranostics", Theranostics, 2, 916–966.

[10] Bhaumik, J., Gogia, G., Kirar, S., Vijay, L., Thakur, N. S., Banerjee, U. C., Laha, J. K., 2016, "Bioinspired nanophotosensitizers: synthesis and characterization of porphyrin–noble metal nanoparticle conjugates", New J. Chem. 40, 724-731.

[11] J. K. Laha, S. Dhanalekshmi, M. Taniguchi, A. Ambroise and J. S. Lindsey, 2003, "A Scalable Synthesis of Meso-Substituted Dipyrromethanes", Org. Process Res. Dev., 7, 799–812.

[12] Z. Yao, J. Bhaumik, S. Dhanalekshmi, M. Ptaszek, P. R. Rodriguez and J. S. Lindsey, 2007, "Synthesis of porphyrins bearing 1–4 hydroxymethyl groups and other one-carbon oxygenic substituents in distinct patterns", Tetrahedron, 63, 10657–10670.

[13] D. Gryko and J. S. Lindsey, 2000, "Rational Synthesis of meso-Substituted Porphyrins Bearing One Nitrogen Heterocyclic Group", J. Org. Chem., 65, 2249–2252.

[14] J. Bhaumik, Z. Yao, E. K. Borbas, M. Taniguchi and J. S. Lindsey, 2006, "Masked imidazolyl-dipyrromethanes in the synthesis of imidazole-substituted porphyrins", J. Org. Chem., 71, 8807–8817.

[15] J. Bhaumik, N. S. Thakur, P. K. Aili, A. Ghanghoriya, K. Mittal and U. C. Banerjee, 2015, "Bioinspired Nanotheranostic Agents: Synthesis, Surface Functionalization and Antioxidant Potential", ACS Biomater. Sci. Eng., 6, 382–392.

SEEC-2017-160

NUMERICAL ANALYSIS TO STUDY HYDRODYNAMIC BEHAVIOR OF BUBBLING FLUIDIZED BED SYSTEM

Sourav Ganguli
Energy and Research Technology Group
CSIR-CMERI, Durgapur
Email: sourav0921@gmail.com

Malay Kr Karmakar
Energy and Research
Technology Group
CSIR-CMERI, Durgapur
Email: malay@cmeri.res.in

Pradip Kumar Chatterjee
Energy and Research Technology Group
CSIR-CMERI, Durgapur
Email: pradip@cmeri.res.in

ABSTRACT

This paper applies two-fluid modeling (TFM) to a two dimensional and three dimensional analysis of a bubbling fluidized bed (BFB) system. For modeling of the fluidized bed, Kinetic Theory of Granular Flow (KTGF) approach is used to successfully to describe the collision between the particles. The present analysis is performed using commercial software ANSYS-Fluent 14.0 software incorporating Eulerian-Eulerian approach. For present study, Geldart-B silica sand of mean particle diameter 300 μm having particle density of 2640 kg/m^3 is taken as solid phase and, for gas phase atmospheric air is used. Air with superficial air velocity of 0.2887 m/s is used to fluidize bed material. Gidaspow drag model, a fluid solid interaction drag model, has been used for numerical modeling. Results obtained from analysis of two-dimensional and three-dimensional models of the bubbling bed are compared to analyze the quality of the result obtained. The mean average value of 30 seconds simulation of axial and radial distribution of solid concentrations is compared with the experimental results by plotting graph at different bed heights.

Keywords:*Fluidized bed, KTGF, Drag model*
.
NOMENCLATURE

α_g	Volume fraction of gas (air)
α_s	Volume fracion of sand
ρ_g	Density of gas (air)
ρ_s	Density of sand
v_g	Superficial gas velocity
v_s	Superficial sand velocity
K_{gs}	Interphase exchange coefficient
τ_i	Phase stress-strain tensor

C$_D$ Coefficient of drag

INTRODUCTION

Fluidized beds, due to its flexibility of operation, were widely used in industrial processes for last few decades. The reason behind use of fluidized bed technology in chemical and physical processes is fluidized bed reactors offer higher reaction rates as the fuel particles are small, mixed thoroughly for good gas-particle contact, and high heat flow. Computation Fluid Dynamics (CFD) become an effective tool for study the process involved in gas-solid fluidized bed system [1]. Development of hydrodynamic models to describe fluidization process has been started from early 1960s [2, 3]. However, simulation is complex as multiphase flows are involved because transport equations for mass and momentum have to be solved for each phase. For modeling of fluidized bed system generally two approaches are used i.e. Eulerian Eulerian approach or Two Fluid Model (TFM) and Eulerian-Lagrangian approach. For Eulerian-Eulerian approach gas phase is considered as continuous phase and silica sand is considered as granular solid phase [4]. The second approach is Eulerian-Lagrangian approach or discrete element method (DEM) where gas phase is considered as continuous fluid phase and silica sand is considered as discrete solid phase. The trajectories of individual particles are tracked in space and time domain from Newton law of motion [5].

For modeling fluid-solid interaction, various drag models were used in bubbling fluidized bed system. Among them Syamlal O'Brian drag model [6] and Gidaspow drag model [7] provide good result for analysis of bubbling fluidized bed system. Gidaspow drag model [7] is combination of Wen-Yu drag model [8] and Ergun equations [9] to cover a wide range of volume fraction. Syamlal O'Brien drag model [6] has the form based on Experimental correlation of terminal or settling velocity.

Gidaspow drag model [7] has used for present study as it deals with a whole range of solid concentration within the bed. The result obtained from experiment done by Wang et al [10] is compared with present simulation result for two dimensional and three dimensional model of bubbling bed.

SIMULATION SETUP

The geometry and mesh of Model 1 and Model 2 is shown in Fig. 1. Model 1 consists of 5600 quadrilateral cells where Model 2 consists of 47124 hexahedral cells. Initially silica sand phase is filled up to a height of 232 mm with a uniform volume fraction of 0.54 while the maximum packing limit is set to 0.63. In this work, Eulerian-Eulerian or Two Fluid Model (TFM) is used. The Pressure- Velocity coupling scheme is Phase Coupled SIMPLE. Atmospheric

air is introduced within the system at velocity of 0.2887 m/s. The model used for present study is summerized in Equation 1 to 12. The discretization scheme for momentum, energy, volume fraction and species all has been taken as Quick scheme. Green- Gauss Cell based gradient is used for discretization. Second order implicit scheme is taken for transient formulation. The outlet of the system is maintained at atmospheric condition. Air is supplied uniformly through inlet. At the wall no-slip boundary condition is considered for gas phase. Specularity coefficient of 0.6 is considered for interaction of the solid phase and wall. The properties of the phases is provided in Table.1.
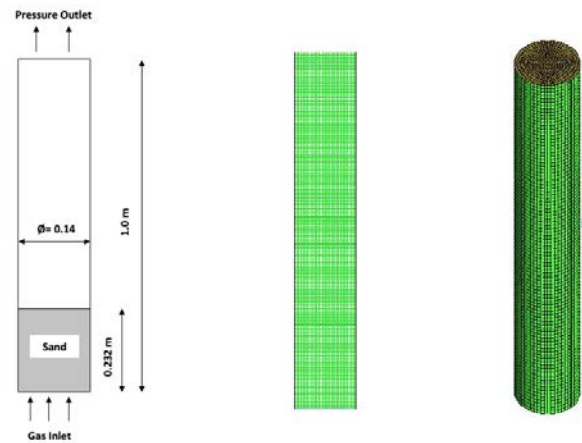

Fig. 1 Geometry and mesh of the Model 1 and Model 2
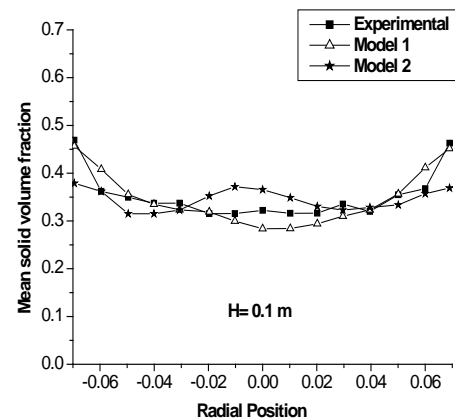
RESULT AND DISCUSSION

Fig. 2 Radial distribution of mean solid concentration for 2D model (Model 1) and 3D model (Model 2) with experiments, Wang et al [10] for superficial air velocity of 0.2887 m/s at bed height of 0.1 m.
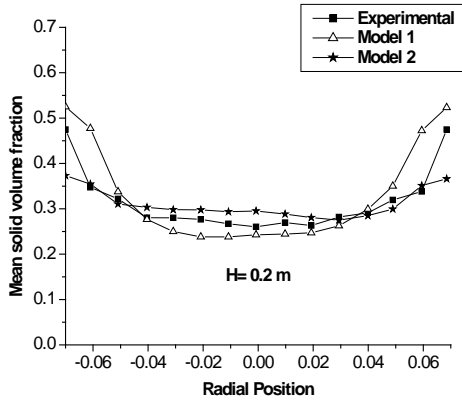
Fig. 3 Radial distribution of mean solid concentration for 2D model (Model 1) and 3D model (Model 2) for superficial air velocity of 0.2887 m/s at bed height of 0.2 m.

In Fig. 2 and Fig. 3, simulation and experimental [10] results on radial distribution of mean solid volume fraction is compared at the bed height of 0.1 m and 0.2 m respectively. In the figures Model 1 represent two dimensional bed and Model 2 represent three dimensional ed. Result shows that simulation result obtained from Model 2 matches more precisely with experimental result near the core region core region. But Model 2 under-predicts the results at the wall region compared to Model 1.
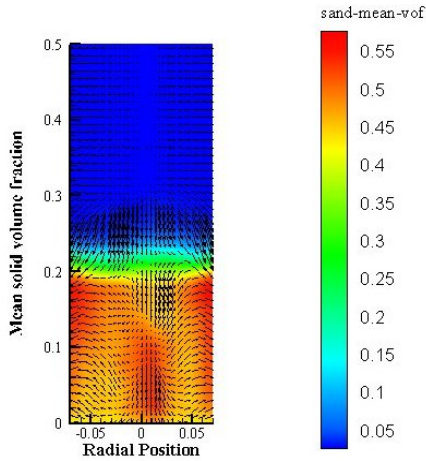
Fig. 4 Contour of mean solid volume fraction and velocity vector of mean solid velocity at the axial coordinate

Fig. 4 shows contour of mean solid volume fraction along with velocity vector at axial cross-section of Model 2. Figure shows uniform miximg of the material due to vortex motion within the system.
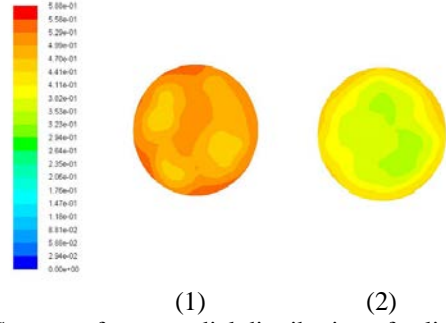

Fig. 5 Contour of mean radial distribution of solid volume fraction at the bed height of 0.1 m [Fig.4 (1)] and 0.2 m [Fig.4 (2)]

Fig. 5 shows contour of mean solid volume fraction at the ed height of 0.1 m and 0.2 m for radial cross-section of Model 2. From Fig.4 it is shown that with increasing the bed height the solid concentration near the core region gradually decreases.

Particle Density (Kg/m^3)	2640
Gas Density (Kg/m^3)	1.225
Mean Particle Diameter (mm)	0.3096
Packing limit	0.63
Solid volume fraction (α_s)	0.54
Initial Bed Height (m)	0.232
Specularity Coefficient	0.6
Superficial gas velocity (m/s)	0.2887

Table 1

EQUATIONS

Conservation of mass:

Gas Phase

$$\frac{\partial}{\partial t}\left(\alpha_g \rho_g\right) + \nabla\left(\alpha_g \rho_g \vec{v}_g\right) = 0 \tag{1}$$

Solid Phase

$$\frac{\partial}{\partial t}\left(\alpha_s \rho_s\right) + \nabla\left(\alpha_s \rho_s \vec{v}_s\right) = 0 \tag{2}$$

Conservation of Momentum:

Gas Phase

$$\frac{\partial}{\partial t}\left(\alpha_g \rho_g \vec{v}_g\right) + \nabla.\left(\alpha_g \rho_g \vec{v}_g \vec{v}_g\right) = -\alpha_g \nabla p + \nabla.\bar{\bar{\tau}}_g + \alpha_g \rho_g \vec{g} + K_{gs}\left(\vec{v}_s - \vec{v}_g\right) \tag{3}$$

Solid Phase

$$\frac{\partial}{\partial t}\left(\alpha_s \rho_s \vec{v}_s\right) + \nabla.\left(\alpha_s \rho_s \vec{v}_s \vec{v}_s\right) = -\alpha_s \nabla p - \nabla p_s + \nabla.\bar{\bar{\tau}}_s + \alpha_s \rho_s \vec{g} + K_{gs}\left(\vec{v}_g - \vec{v}_s\right) \tag{4}$$

Phase stress-strain tensor:

$$\bar{\bar{\tau}}_i = \alpha_i \mu_i\left(\nabla\vec{v}_i + \nabla\vec{v}_i^{\,T}\right) - \frac{2}{3}\alpha_i \mu_i(\nabla.\vec{v}_i)\bar{\bar{I}} \tag{5}$$

where i = g for gas phase and i = s for solid phase.

Solid shear stress:

$$\mu_s = \mu_{s,col} + \mu_{s,kin} + \mu_{s,fr} \tag{6}$$

Kinetic granular viscosity:
$$\mu_{s,kin} = \frac{10\rho_s d_s \sqrt{\theta_s \Pi}}{96\alpha_s(1+e_{ss})g_{0,ss}}\left[1 + \frac{4}{5}g_0\alpha_s(1+e)\right]^2 \tag{7}$$

Granular bulk viscosity:
$$\lambda_s = \frac{4}{3}\alpha_s\rho_s d_s g_{0,ss}(1+e_{ss})\left(\frac{\theta_s}{\Pi}\right)^{1/2} \tag{8}$$

Frictional viscosity:
$$\mu_{s,fr} = \frac{p_s \sin\phi}{2\sqrt{I_{2D}}} \tag{9}$$

Collisional viscosity:
$$\mu_{s,col} = \frac{4}{5}\alpha_s\rho_s d_s g_{0,ss}(1+e_{ss})\left(\frac{\theta_s}{\pi}\right)^{1/2} \tag{10}$$

Solids pressure:
$$p_s = \alpha_s\rho_s\theta_s + 2\rho_s(1+e)\alpha_s^2 g_0\theta_s \tag{11}$$

Radial Distribution Function:
$$g_0 = \left[1 - \left(\frac{\varepsilon_s}{\varepsilon_{s,max}}\right)^{1/3}\right]^{-1} \tag{12}$$

Gidaspow Drag model:
$$K_{gs} = \begin{cases} \frac{3}{4}C_D\frac{\alpha_s\alpha_g\rho_g|\vec{v}_s-\vec{v}_g|}{d_s}\alpha_g^{-2.8} & \text{for } \alpha_g > 0.8 \\ 150\frac{\alpha_s^2\mu_g}{\alpha_g d_s^2} + 1.75\frac{\alpha_s\rho_g|\vec{v}_s-\vec{v}_g|}{d_s} & \text{for } \alpha_g \leq 0.8 \end{cases} \tag{13}$$

Where,
$$C_D = \frac{24}{\alpha_g Re_s}\left[1 + 0.15\left(\alpha_g Re_s\right)^{0.687}\right] \tag{14}$$

CONCLUSION

In this paper the result of the experiment conducted by Wang et al [10] is compared with simulation results obtained from the proposed 2-D and 3-D models to analyze solid flow behavior of BFB system. The proposed model is based on kinetic theory of granular flow which forms the basis for modeling of the solid phase. Results obtained in 2-D model differs from the experimental values, however in 3-D model, those values are reasonably matching. As fluidized bed system is heterogeneous in nature, so the results from three dimentional model describes it more significantly compared to two dimentional results.

REFERENCES
[1] D. Gidaspow, J. Jung, R.K. Singh, "Hydrodynamics of fluidization using kinetic theory: an emerging paradigm", Powder Technology 148 (2004) 123–141.
[2] Davidson, J. F. and D. Harrison, "Fluidized Particles," Cambridge University Press, London (1963).
[3] Jackson, R., "The Mechanics of Fluidised Beds: Part I: The Stability of the State of Uniform Fluidization," Trans. Inst. Chem. Eng. 41, 13–21 (1963).
[4] M.A. van der Hoef, M. van Sint Annaland, N.G. Deen, J.A.M. Kuipers, "Numerical simulation of dense gas–solid fluidized beds: a multiscale modeling strategy", Annu. Rev. Fluid Mech. 40 (2008) 47–70.
[5] Jung, J., Gidaspow, D., 2005. "Measurement of two kinds of granular temperatures,stresses, and dispersion in bubbling beds". Ind. Eng. Chem. Res. 44, 1329-1341.
[6] Syamlal, M., 1987a, "NIMPF: A Computer Code for Nonisothermal Multiparticle Fluidization," unpublished EG&G report.
[7] Gidaspow, D., 1986, "Hydrodynamics of Fluidization and Heat Transfer: Supercomputer Modeling," Appl. Mech. Rev., 39, 1-23.
[8] Wen, C. Y., & Yu, Y. H. "Mechanics of fluidization, Chemical," Engineering Progress Symposium Series, vol 62, pp. 100-111, 1966.
[9] Ergun S., "Fluid flow through packed columns," Chem Eng Progr vol.48, pp.89-94. 1952.
[10] Yingce Wang, Zheng Zou, Hongzhong Li, Qingshan Zhu, " A new drag model for TFM simulation of gas-solid bubbling fluidized beds with Geldart-B particle", Particuology (2013).

SEEC-2017-161

SEPARATION OF XYLOSE, CELLULOSE, LIGNIN AND SILICA FROM RICE STRAW

Meena Krishania
Center for Innovative and Applied Bioprocessing,
Mohali
Email: er.mkrishania@gmail.com

Vinod Kumar
Center for Innovative and Applied Bioprocessing,
Mohali
Email: vinod@ciab.res.in

Rajender Singh Sangwan
Center for Innovative and Applied Bioprocessing,
Mohali
Email: sangwan@ciab.res.in

ABSTRACT

Dilute acid with steam pretreatment is the most capable technology to substitute conventional acid hydrolysis of lignocellulose for biomass pretreatment. In this paper, an optimum and appropriate process was designed and explored for recovery of xylose production, cellulose, silica and lignin from lignocellulosic biomass. We investigated the effect of different chemicals on xylose yield in this process, and the xylose production process was optimized as followings: After pre-impregnation with nitric acid at 140 0C for 15 min, rice straw was treated at 1 bar with 0.5 % (v/v) nitric acid, followed by second hydrolysis by using 2.5 % sodium hydroxide with 2% sodium hypochlorite at 121 0C for 1 hr, decolouration and ionic impurities were removed by ion exchange. Using this process, 100 g of xylose was produced from 1 kg rice straw, 80 % of hemicellulose was released as monomeric sugar. All results indicated that this process may request more effective way to convert hemicellulose into xylose and simultaneous production of cellulose, silica and lignin. So, this method could be an alternative method to traditional sulphuric acid hydrolysis process for lignocellulose biorefinery.

Keywords: Pretreatment, Rice Straw, Lignocellulosic.

SEEC-2017-162

REVIEW OF THERMAL ENERGY STORAGE SYSTEMS

Manmeet Singh
Department of Mechanical Engineering
Indian Institute of Technology Kanpur,
Kanpur, Uttar Pradesh- 208016
manmeet@iitk.ac.in

Jishnu Bhattacharya
Department of Mechanical Engineering
Indian Institute of Technology Kanpur
Kanpur, Uttar Pradesh- 208016
jishnu@iitk.ac.in

ABSTRACT

Clean energy or carbon free energy is the biggest requirement of mankind. Most of the energy demands are fulfilled by non-renewable energy sources which are depleting at a very fast rate. So researchers shift to renewable energy like solar energy, wind energy, tidal energy etc. Since a huge amount of solar energy is available but its proper utilization has not been done efficiently. There are enormous research efforts going on to convert solar energy to electricity and its storage is also equally important as the energy can be saved when there is no sunlight available during the night or cloudy days. Therefore, research on the design and development of economical and highly efficient solar thermal energy storage (TES) methods need to be done. Concentrated solar power (CSP) is highly efficient, cost effective and clean renewable energy source which is currently in great demand nowadays. The paper gives a brief review of how to analyze and improve the performance of the TES systems. Firstly, the need/importance of TES systems in CSP. Secondly, the study of use of effective heat transfer coefficient on lumped capacitance method (LCM) of TES systems was analyzed. Thirdly, the study of improvement on TES systems was carried out by applying the various optimization techniques on various parameters of TES systems. The use of TES systems in conjugation with CSP proves beneficial to provide energy at constant rate reducing the discontinuous availability of solar energy. It was observed that similar results were obtained from corrected LCM as from analytical and numerical methods. Also optimization techniques concluded the selection of various design parameters of storage tank and usage of various storage materials at particular conditions.

SEEC-2017-163

APPLYING GENOMICS FOR SUSTAINABLE TREE-BASED BIOFUEL PRODUCTION

Madhumita Dash
CSIR-CCMB, Hyderabad
Email: mdash@ccmb.res.in

Victor Busov
Michigan Technological University
Email address: vbusov@mtu.edu

ABSTRACT

Tree crops, like <u>Populus</u> or poplar, have recently emerged as sustainable biofuel targets in US. These crops are intended to be grown on marginal lands where nitrogen and water are major factors limiting productivity. Here, we focus on roots as a venue for engineering robust productivity under low nitrogen and water stress. Two different approaches, i.e., reverse and forward genetics, were applied to identify key regulatory genes controlling root growth in poplar under low nitrogen and drought stress. Transgenic plants were generated for the identified genes and were tested in the greenhouse for their performance under low nitrogen and drought conditions. The selected transgenic plants displayed higher shoot and root biomass in response to the above stress conditions. These findings would help in enabling the engineering of low nitrogen and drought tolerance through modulation of root architecture.

*Keywords: **Biotechnology, Tree genomics , poplar, lignocellulosic biomass, biofuel.***
.

INTRODUCTION

Recent new policies and legislations in USA such as sustainable biofuel targets in the US Energy Policy Act (EPA 2005) and Energy Independence and Security Act (EISA 2007) has led to an accelerated interest in research pertaining to the production of biofuel using tree-based lignocellulosic biomass. Currently, corn is the major source for bioethanol production in USA. However, ethanol can be produced from any source of fermentable sugars like lignocellulosic biomass [1]. Because wood is an abundant, and largely a sustainably managed resource, tree species like poplar are emerging as major crop for biofuel production [2]. This vision of a future domestic tree-based biofuel production would require overcoming technical, sociological and environmental barriers. Therefore, several research projects have been established all over US to conduct transformative, multidisciplinary, comprehensive, and integrated research in the area of tree-based infrastructure-compatible liquid biofuel for vehicular transportation. These projects were focused on several thrust areas, such as, a) producing high yielding plant varieties with composition suitable for biofuel conversion, b) generating plant varieties suitable for cultivation in marginal lands to avoid competition with food crops, c) establishing efficient protocols for conversion of lignocellulosic biomass to biofuel, d) energy utilization of advanced biofuels, and e) Integrated Sustainability Assessment and Decision Making.

We applied genomics approaches to address issues pertaining to development of varieties that can sustain high levels of productivity in marginal lands where nitrogen and water are the major limiting factor [3-5]. We used poplar as our model bioenergy tree crop and focused on identifying the regulatory genes that control root system architecture in response to low nitrogen and drought stress. We identify genes that regulate these mechanisms and demonstrate using transgenic manipulation that they effect root growth and biomass accumulation in response to low nitrogen and drought stress. The insights from this study will allow genetic modifications of root

architecture for more efficient and dynamic nitrogen and water foraging in prospective biofuel crops like poplar.

METHODOLOGY

Two different approaches were applied to identify genes regulating root architecture or root growth under low nitrogen (LN) and drought stress:

1) Reverse genetics or system biology approach: Microarray and gene regulatory network was applied to build a genetic network encompassing a large proportion of the differentially-regulated genes in response to LN. The network built was organized in a hierarchical fashion, centered on eleven superhub genes (Fig. 1). Transgenic manipulations were performed to study the effect of the eleven genes on root growth under low nitrogen stress.

2) Forward genetics: Activation tagging was used to generate a population of mutant poplars. Mutant population were then screened for lines with improved root growth in liquid media with control and 5% PEG (to mimic drought stress). Once a mutant line with desired phenotype was identified the gene causing the phenotype was further characterized. Transgenic manipulation were performed to study the effect of the gene on root growth under drought stress.

RESULTS

1) Reverse genetics or system biology approach identifies three new regulators of poplar root development under low nitrogen. For initial screening of transgenic lines, we grew them in hydroponic solution with and without nitrate. We screened for modified lines that displayed improved root growth under low nitrogen (LN). Transgenic manipulations of only three (*PtaNAC1*, *PtaHWS* and *PtaRAP2.11*) of the eleven superhub genes from Fig. 1 had a strong impact on root development under LN [3]. Two (*PtaHWS* and *PtaRAP2.11*) of these three transgenic lines were further tested in greenhouse for their productivity under LN. Under greenhouse conditions, *PtaRAP2.11* and *PtaHWS* upregulated transgenics (HWS-OE and RAP2.11-OE) displayed better tolerance to LN stress compared to the wildtype

poplar (Fig. 2a). Growth cessation in response to LN was delayed by 20 and 27 days in HWS-OE and RAP2.11-OE, respectively (Fig. 2b). Up- regulation of the three genes caused increased root proliferation (~50% increase in root biomass) under LN conditions, respectively. Stem biomass was also increased by approximately 25% (Fig. 2c). These findings clearly indicate that three of the superhub genes improve biomass growth and tolerance under LN in poplar via modulation of root architechture.
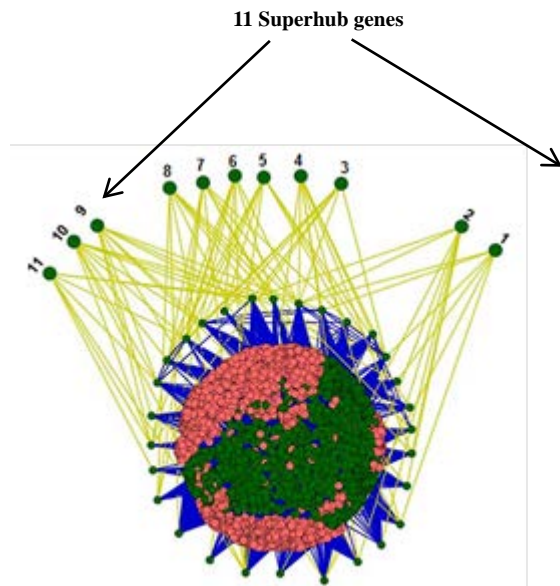
2) Forward genetics identifies *PtabZIP1-like* (*PtabZIP1L*) gene that enhances lateral root formation and biomass growth under drought stress. Drought conditions severely suppress lateral root (LR) growth in poplar [5]. To identify genes that may overcome this suppression, we screened a poplar activation tagging population under hydroponic conditions with 5% PEG in the media (to mimic drought stress, see methodology). Under the conditions of the screen, we discovered a poplar activation-tagged line that displayed enhanced primary and lateral root growth under both control and PEG conditions. Genomic sequence flanking the left border of the T-DNA insert was recovered and sequenced to identify the gene responsible for phenotypic changes in the mutant line. The sequenced region was found to be positioned at Chr10:15429200-15429699, in an intron of a predicted gene model Potri.010G142900. We then analysed the expression of Potri.010G142900 as well neighboring genes. However, only the expression of was ~10-fold higher in the mutant ($P < 0.05$) in comparison to the wildtype (WT-717). Therefore, we concluded that the gene Potri.010G142900 was likely responsible for the observed phenotype. The gene encodes a putative transcription factor of the basic leucine zipper (bZIP) family [6] with highest similarity to Arabidopsis bZIP1. For consistency, we named the gene *PtabZIP1L* (*Populus tremula x P. alba bZIP1-Like*).
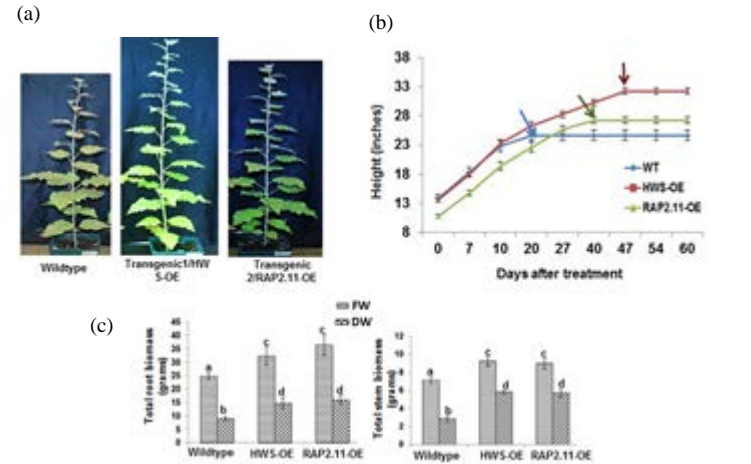
To better understand the function of *PtabZIP1L* in relation to root growth and drought stress we transgenically overexpressed (*oe-PtabZIP1L*) and suppressed (*i-PtabZIP1L*) its expression. We next studied how *PtabZIP1L* expression changes in the transgenic plants affect response to water deprivation under greenhouse conditions. After 20 days of drought treatment, WT-717 and *i-PtabZIP1L* plants

appeared more stressed with pronounced wilting compared to *oe-PtabZIP1L* transgenics (Fig. 3a). Shoot growth cessation in response to water withholding was delayed by 10 days in *oe-PtabZIP1L* plants, whereas shoot growth cessation occurred 10 days earlier in *i-PtabZIP1L* plants compared to WT-717 (Fig. 3b). *oe-PtabZIP1L* plants displayed ~70% increase, whereas *i-PtabZIP1L* plants had ~50% reductions, in root biomass under drought conditions (Fig. 3a and 3c). These results show that water use efficiency was increased/decreased in *oe-PtabZIP1L* and *i-PtabZIP1L* plants, respectively, as a result of alteration in root growth, thereby varying the total surface area available for water absorption. Shoot biomass was also increased in *oe-PtabZIP1L* plants and reduced in *i-PtabZIP1L* transgenics (Fig. 3c).

FIGURES

FIGURE 2. TRANGENIC PLANTS POSITIVELY REGULATES BIOMASS AND ROOT GRWOTH UNDER LOW NITROGEN STRESS.

FIGURE 1. GENE NETWORK BUILT USING POPLAR ROOT TRANSCRIPTOME IN RESPONSE TO LOW NITROGEN STRESS. THE NETWORK IS CENTRED AROUND 11 SUPERHUB GENES.
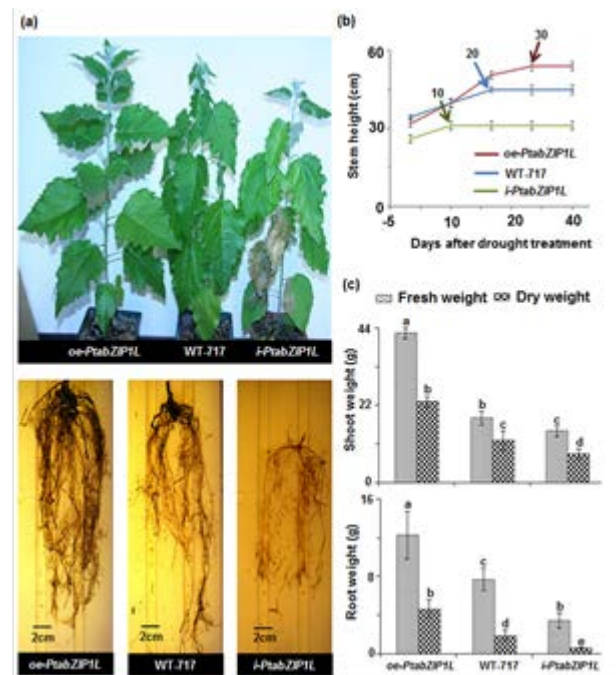
FIGURE 3. *PtabZIP1L* POSITIVELY REGULATES BIOMASS AND ROOT GRWOTH UNDER DROUGHT STRESS.

CONCLUSIONS

We have shown that genomics can be successfully used to characterize genes that will enable genetic modifications of root architecture for efficient nitrogen and water foraging in biofuel crops such as poplar. Therefore, genomics play a crucial role for the development of sustainable forest or tree-based biofuel production that can be grown in marginal lands.

ACKNOWLEDGMENTS

REFERENCES

[1] Himmel, M. E., Ding, S. Y., Johnson, D. K., Adney, W. S., Nimlos, M. R., Brady, J. W., and Foust, T. D. 2007. Biomass recalcitrance: engineering plants and enzymes for biofuels production. Science, 315(5813), 804-807.

[2] Sannigrahi, P., Ragauskas, A. J., & Tuskan, G. A. 2010. Poplar as a feedstock for biofuels: a review of compositional characteristics. Biofuels, Bioproducts and Biorefining, 4(2), 209-226.

[3] Dash, M., Yordanov, Y. S., Georgieva, T., Kumari, S., Wei, H., & Busov, V. 2015. A systems biology approach identifies new regulators of poplar root development under low nitrogen. The Plant Journal, 84(2), 335-346.

[4] Dash, M., Yordanov, Y. S., Georgieva, T., Kumari, S., Wei, H., & Busov, V. 2016. A network of genes associated with poplar root development in response to low nitrogen. Plant Signaling & Behavior, 11(8), e1214792.

[5] Dash, M., Yordanov, Y. S., Georgieva, T., Tschaplinski, T. J., Yordanova, E., & Busov, V. 2016. Poplar PtabZIP1-like enhances lateral root formation and biomass growth under drought stress. The Plant Journal, In press.

[6] Jakoby, M., Weisshaar, B., Dröge-Laser, W., Vicente-Carbajosa, J., Tiedemann, J., Kroj, T., & Parcy, F. 2002. bZIP transcription factors in Arabidopsis. Trends in plant science, 7(3), 106-111.

SEEC – 2017 – 164

EXPERIMENTAL EVALUATION OF MANIFOLD INJECTION OF HHO, ON PERFORMANCE CHARACTERSTICS OF A CONSTANT SPEED 4-STROKE SI ENGINE

Shashwat Tripathi
Manufacturing Technology
JSSATE Noida
trips_93@yahoo.co.in

Anshul Kumar
Manufacturing Technology
JSSATE Noida
anshultomar1818@gmail.com

M.K. Shukla
AFLAD
CSIR-IIP, Dehradun
mshukla@iip.res.in

ABSTRACT

Over the past years, scientists from all over the world have been looking for different frugal techniques in fueling the Internal Combustion (IC) engines. The enhancement in fuel economy of the IC engines together with betterment in power and overall performance is the main area of focus among the researchers. Use of hydrogen as a fuel in IC engines has been studied for its high combustion efficiency, power output and non-toxic emissions. However, the development and research of hydrogen based IC engines has always been hindered by the challenges associated with production and storage of it. To overcome these challenges, HHO (hydroxy) gas has been studied as a replacement to Hydrogen by many researchers. HHO not only shows similar advantages but also eradicates the challenges faced as in case of pure Hydrogen. In the presented work, effect of HHO-manifold injection volume on performance emission characteristics of a constant speed 4 stroke SI Engine is studied. The HHO was produced by water electrolysis in a wet cell. Improvement in fuel efficiency and reduction in tail pipe emissions was observed.

Keywords: HHO (hydroxy), gasoline, internal combustion (IC) engine, engine performance, exhaust emissions.

NOMENCLATURE

HHO	hydroxy gas
H_2	hydrogen
IC	internal combustion
SI	spark ignition
BSFC	brake specific fuel consumption
UHC	unburned hydrocarbon
CO	carbon monoxide
CO_2	carbon dioxide
NOx	oxides of nitrogen
O_2	oxygen
CNG	compressed natural gas
HCNG	hydrogenated compressed natural gas
OHV	over head valve
λ	air to fuel ratio
KOH	potassium hydroxide
NaOH	sodium hydroxide

INTRODUCTION

Almost all (95%) of the world's transportation energy comes from petroleum-based fuels, largely gasoline and diesel. Both Gasoline and Diesel, has also been the main source of atmospheric pollution in the form of exhaust emissions from the vehicular exhaust. The most common pollutants emitted by the conventional hydrocarbon fuels are, partially or unburnt hydrocarbons (UHC), CO, oxides of nitrogen (NO_x), smoke and particulate matter [2]. Hence, during the last few decades, the automobile researchers have been working upon reducing the exhaust emissions and improving the thermal efficiency of the engines.

If the production Hydrogen is efficient, it will significantly reduce the production of CO_2 as compared to that produced by traditional fuels [1]. Compared to the hydrocarbon fuel, the most significant feature of hydrogen is the absence of

carbon. Also, it has a very high burning velocity that ensures rapid and complete combustion. The engine can be operated under a wide range of air/fuel ratio because the flammability limit of hydrogen is very wide as it varies from an equivalence ratio (f) of 0.1-7.1. However, the low ignition energies of hydrogen–air mixtures causes frequent unscheduled combustion events, and high combustion temperatures of mixtures closer to the stoichiometric composition leads to increased NO_x production [8].

Due to its low density, hydrogen gas limits the amount of hydrogen stored on board. Hydrogen storage is the key technology towards the hydrogen society. Currently high pressure tanks and liquid hydrogen tanks are used for road tests, but both technologies do not meet all the requirements of future fuel cell vehicles [9]. Moreover, Hydrogen refill stations are also highly risky due to high pressure of compressed H_2 and its high inflammable property. Thus, safety measurements are needed for hassle-free operation of filling stations and vehicles run by H_2 [10]. Off late, sustainable production and lightweight H_2 storage devices have received great attention to address the challenge of using Hydrogen as an automotive fuel with the available technologies.

HHO, also known as knall-gas, hydroxy gas or Brown's gas is a stoichiometric mixture of H_2 and O_2 in a ratio of 2:1. It is produced by the electrolytic decomposition of water into its constituent elements, hydrogen and oxygen, due to which the only by-product of its combustion is water. HHO possesses high heating value of 9.8 Kcal for 1 litre of the gas and a maximum flame temperature of 2800°C, which made it a good and the only tool, in the early nineteenth century, to melt the metals of high melting point such as platinum. The gas is also used in welding applications since its development in 1903 under the name of oxy-hydrogen welding. Recent researches on HHO has revealed that gasoline/diesel along with HHO, when combusted in an IC engine, can improve the efficiency of the engine with a considerable decrement in emissions [2-6].

In the presented work effect of HHO-manifold injection volume on performance emission characteristics of a constant speed 4-Stroke SI Engine is studied. Here, HHO was produced by water electrolysis carried out by means of a wet cell.

PROPERTIES OF HHO

In HHO (Hydroxy gas), Hydrogen and Oxygen do not form into O_2 and H_2 molecules. They are in their mono-atomic state (a single atom per molecule). Water gets split by electricity to form its various elements, oxygen and hydrogen [2]. There are also few hydroxyl free radicals

included in HHO, which catalyses the combustion and increases the combustion efficiency. The molar mass of HHO is 12.3 g mol-1. HHO is mainly made up of H_2 and O_2, with H_2 accounting for 60.79%, O_2 accounting for 30.39%, and a small amount of water vapour, O, OH and some other active substances accounting for the rest. The energy stored in 1 litre of HHO is approximately 600 Joules [7]. The key feature of HHO gas is the fact that some of the hydrogen and oxygen never go into a diatomic state. Hence, HHO gas has more energy because these bonds are never made. In this state, which is an unstable state of H_2O vapour, more energy is achieved compared to hydrogen burning with oxygen.

Properties	CNG	Methanol	Hydrogen	Gasoline	Diesel	HHO
Molecular weight (g/mol)	16.04	32.04	2	100.2	198.4	18
Density (Kg/m³) 1 atm	0.748	792	0.081	737	856	0.535
LHV (MJ/Kg)	46.81	20.27	120	43.47	41.66	120
Carbon content (% by weight)	74	37.5	0	85.5	87	0
Laminar flame speed (cm/s) at 298K, 1 atm	40	35	230	41.5	33	230
Auto-ignition temperature (ºc)	540	464	585	247-280	254	570
References	[11][13]	[1] [12]	[11][14]	[1] [15]	[1][15]	[16]

Table 1: Comparison of properties of HHO and Hydrogen with common automobile fuels

METHODOLOGY

HHO Production
The HHO production set up consisted of a water tank which supplies the water to the HHO cell and an alkaline electrolysis unit. A seperate flashback arrestor unit was installed in between the engine gas inlet and the electrolyzer's output port. The HHO gas produced, was measured by calculating the water displacement per unit time through an inverted calibrated vessel setup [5]. Stainless steel plates of grade 316-L were submerged into a 2-liter glass container. Plate voltage was maintained to be around 2.2 volts. Neutral plates were added between the electrode plates as it divides the voltage down and

dramatically increases the production efficiency. Production of HHO was carried out with water mixed with 10% KOH by weight. The produced gas was taken out of the cell through an opening at the top of the cell and its supply into the engine was controlled by a flow regulating valve. The amount of HHO produced was measured with the help of an inverted vessel submerged in a water tank.

Figure 1: Wet Cell

The relationship between the rate of production and current was obtained by the experiments carried on the above shown wet cell. At around 4 Ampere current, 12 Volt potential difference and 10% KOH addition (by weight) the HHO Production rate was observed to be around *0.24 ml/sec*. The produced HHO gas from the wet cell was then injected directly into the intake manifold to study its effects on engine performance.

Engine test setup

GenSet Engine (GASTECH Bio Power), a constant speed, 4 stroke, SI Engine was used to obtain the following effects of HHO blended Gasoline as a fuel. The Engine used had 196cc displacement and 0.25% of 196cc is 0.49 cc. Hence, 0.49 ml of HHO was injected constantly for every complete 4-stroke cycle, i.e. 0.25% of total cylinder intake volume. Therefore, Rate of injection of HHO was maintained to be, 25 x 0.49 = *12.25 ml/sec*. (Engine speed= 3000 rpm).

Model:	OHV WY 168 FE-1
Displacement (cc):	196
Maximum Power (HP):	5
Speed (RPM):	3000
Type:	Forced Air cooled 4 stroke OHV single cylinder

Fuel tank capacity (Ltr.):	0.7
Fuel Consumption (Ltr./Hrs.):	1.3

Table 2: Engine Specifications

The Engine with specifications as mentioned above, was connected to a load bank through which its performance at different load values was observed. Portable automotive emission analyzer, *Horiba MEXA-584L*, was used to measure engine tail pipe emission levels of CO and UHC. Calibrated fuel tank and stop watch was used to observe the rate of fuel consumption by the engine during the tests.
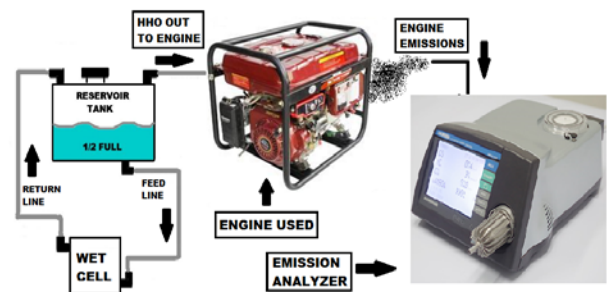

Figure 2: Test Setup

RESULTS AND DISCUSSIONS

The results of the engine performance tests for the effect of HHO blended gasoline on tailpipe emissions and fuel consumption are shown below;
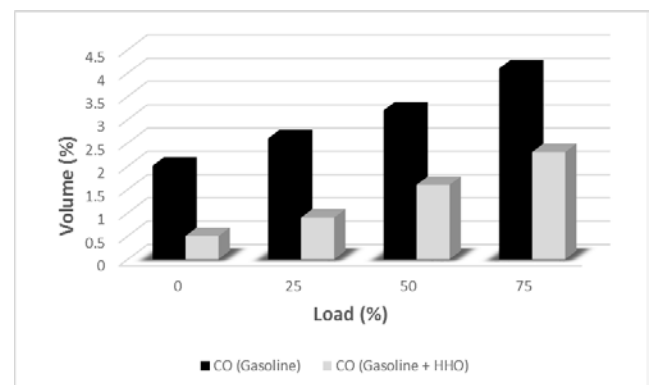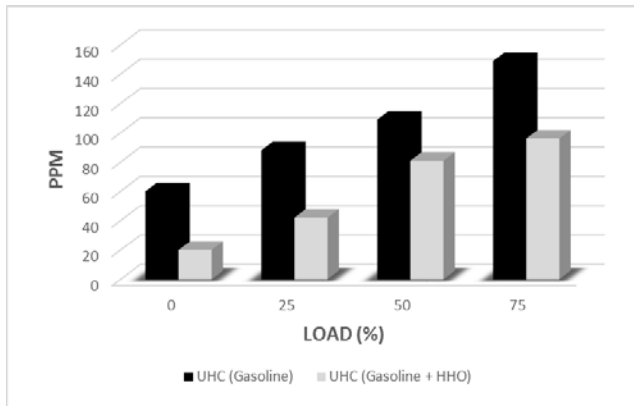

Figure 3: Comparison of CO Emission Composition (% by Volume) Vs Engine Load (%)

Decrement in the Emissions was observed in case of Gasoline + HHO combustion, in comparison to Gasoline

3

only. By varying load from 0% to 75%, decrement by 75% to 44% was noted respectively.

Figure 4: Comparison of Unburned Hydrocarbons (ppm) Vs Engine Load (%)

Decrement in the amount of UHC were obtained in Gasoline + HHO combustion, as compared to Gasoline only. By varying the engine load from 0% to 75%, decrement by 67% to 36% was observed.
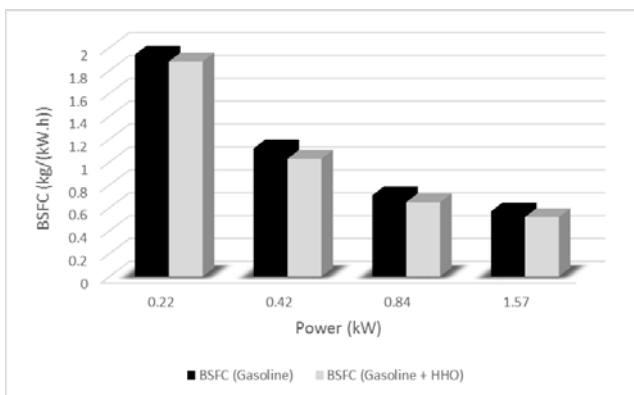
Figure 5: Comparison of Brake-Specific Fuel Consumption (kg/(kW.h)) Vs Engine Load (%)

BSFC was observed to be slightly lesser in case of Gasoline + HHO combustion, as compared to Gasoline only. By varying the power from 0.22 kW to 1.57 kW, depreciation by 3% to 9% was achieved.

CONCLUSIONS

The suitability of using HHO as a fuel in IC Engines, puts forward the following assertions;

- HHO which can be simply produced by electrolysis of water, offers an alternative to hydrogen fuel.

- Presented work was focused on understanding the effect of HHO manifold injection on performance emission characteristics of a constant speed SI engine.
- Significant reduction of HC and CO emission was observed for different load conditions. Slight improvements in BSFC was also noticed.
- However, material compatibility and engine endurance studies needs to be carried out in detail with HHO to establish its credentials as an alternative to hydrogen as a fuel for IC engines.

REFERENCES

[1] Avinash Kumar Agarwal; Biofuels (alcohols and biodiesel) applications as fuels for internal combustion engines; Progress in Energy and Combustion Science, Volume 33, Issue 3, June 2007, Pages 233–271.

[2] Ali Can Yilmaz, Erinc¸ Uludamar, Kadir Aydin; Effect of hydroxy (HHO) gas addition on performance and exhaust emissions in compression ignition engines; International Journal of Hydrogen Energy, Volume 35, Issue 20, October 2010, Pages 11366–11372.

[3] Shuofeng Wang, Changwei Ji, Jian Zhang, Bo Zhang; Comparison of the performance of a spark-ignited gasoline engine blended with hydrogen and hydrogen oxygen mixtures; Energy, Volume 36, Issue 10, October 2011, Pages 5832–5837.

[4] Shuofeng Wang, Changwei Ji, Jian Zhang, Bo Zhang; Improving the performance of a gasoline engine with the addition of hydrogen-oxygen mixtures; International Journal of Hydrogen Energy, Volume 36, Issue 17, August 2011, Pages 11164–11173.

[5] M.M. EL-Kassaby, Yehia A. Eldrainy, Mohamed E. Khidr, Kareem I. Khidr; Effect of hydroxy (HHO) gas addition on gasoline engine performance and emissions; Alexandria Engineering Journal, Volume 55, Issue 1, March 2016, Pages 243–251.

[6] Mustafi Nirendra N, Amin Md. Ruhul, Ahmed Md. Zakaria, Islam Md. Mayeedul; An investigation on the production of Brown gas (HHO) as an alternative automotive fuel by water electrolysis; icmime 2013, pages 239-244.

[7] S. Liu, Z. Wang, X. X. Li, Y. Zhao and R. N. Li; Effects on emissions of a diesel engine with premixed HHO; *RSC Advances*, 2016, Issue 6, Pages 23383-23389.

[8] C.M. White, R.R. Steeper, A.E. Lutz; The hydrogen-fueled internal combustion engine: a

technical review; International Journal of Hydrogen Energy, Volume 31, Issue 10, August 2006, Pages 1292–1305.

[9]   D. Mori, K. Hirose; Recent challenges of hydrogen storage technologies for fuel cell vehicles; International Journal of Hydrogen Energy, Volume 34, Issue 10, May 2009, Pages 4569–4574.

[10]   S. Dutta; A review on production, storage of hydrogen and its utilization as an energy resource; Journal of Industrial and Engineering Chemistry, Volume 20, Issue 4, 25 July 2014, Pages 1148–1156.

[11]   Huseyin Turan Arat, Kadir Aydin, Ertugrul Baltacioglu Ergul Yasar, Mustafa Kaan Baltacioglu, Çaglar Conker and Alper Burgac; A review of hydrogen enriched compressed natural gas (HCNG)-fuel in diesel engines; JMES Vol 1 Issue 1 2013, Pages 115-122.

[12]   Cenk Sayin; Engine performance and exhaust gas emissions of methanol and ethanol–diesel blends; Fuel, Volume 89, Issue 11, November 2010, Pages 3410–3415.

[13]   Salim Tangoz, Selahaddin Orhan Akansu, Nafiz Kahraman, Yusuf Malkoc; Effect of compression ratio on performance and emissions of a modified diesel engine fueled by HCNG; International Journal of Hydrogen Energy, Volume 40, Issue 44, 26 November 2015, Pages 15374–15380.

[14]   B. Afkhami , A.H. Kakaee , K. Pouyan; Studying engine cold start characteristics at low temperatures for CNG and HCNG by investigating low-temperature oxidation; Energy Conversion and Management, Volume 64, December 2012, Pages 122–128.

[15]   T. D Andreaa, P.F. Henshawa, D.S.-K. Ting; The addition of hydrogen to a gasoline-fueled SI engine; International Journal of Hydrogen Energy, Volume 29, Issue 14, November 2004, Pages 1541–1552.

[16]   Ruggero Maria Santilli; A new gaseous and combustible form of water; International Journal of Hydrogen Energy, Volume 31, Issue 9, August 2006, Pages 1113–1128

SEEC – 2017 – 165

SUSTAINABLE SOLID WASTE MANAGEMENT THROUGH SOLAR ASSISTED GASIFICATION

Ankur Kaundal
School of Engineering
IIT Mandi
ankur_kaundal@students.iitmandi.ac.in

Atul Dhar
School of Engineering
IIT Mandi
add@iitmandi.ac.in

Satvasheel Powar
School of Engineering
IIT Mandi
satvasheel@iitmandi.ac.in

ABSTRACT

Gradual increase in day to day solid waste is a matter of concern as it poses serious threats in its disposal. In this scenario, harnessing the energy content in waste besides its disposal would be the best alternative. In solution, Thermo-Chemical conversion techniques are worth contributing to it. These techniques not only ease the disposal, but also pave the way to extract energy content from carbonaceous waste. Pyrolysis and Gasification are such processes and being endothermic by nature they require enormous heat for their execution. So, presented work here discusses about the use of concentrated solar energy to assist the chemical reaction resulting into the production of syngas fuel mainly (CO+H₂). The concept over here is to concentrate the solar radiations to drive chemical reaction in order to have near-complete utilization of carbonaceous content. First step towards this is to study the combustion characteristics of wooden feedstock as the starting material. For this, a combustion unit is being constructed with provision to primary air and secondary air. Thermal draft in the chimney generates pressure difference which facilitates the incoming of primary and secondary air and sidewise keeps flue gases moving.

Keywords:
Thermal draft, Black body, Scheffler Solar Concentrator
.
NOMENCLATURE:

MSW   Municipal Solid Waste
TPD   Tonnes Per Day

INTRODUCTION

A recent report by CPCB, Ministry of Environment and Forests on Municipal Solid Waste Management [1] compares the daily MSW generation in major cities and state capitals over past few years. With most of the cities having increasing statistics, total MSW in year 1999-2000 was 30058 TPD, whereas same for year 2004-05 and 2010-11 hiked to 39031 TPD and 50592 TPD respectively. Another report by Federation of Indian Chambers of Commerce and Industry (FICCI) [2] reveals that about 68% of the major cities in India send more than 60% of MSW to dumpsites, which otherwise could have utilized to extract energy content out of it. So, it has become the immense need of time to utilize this MSW in a sustainable way, so as to minimize the problems associated with its disposal. Moreover the use of existing technologies with some modification can be a better option. This modification is in the form of incorporation of solar heat to accelerate the thermo-chemical conversion processes.

Gasification and Pyrolysis processes take place in controlled amount of oxygen in order to have no or partial combustion. Temperature range for pyrolysis is 200 – 760°C in the complete absence of air, whereas gasification takes place at elevated temperature range of 480 – 1650°C in small amount of oxygen. This small amount of oxygen is allowed to have partial combustion of feedstock itself. Conventionally around 30% of feedstock is burnt to achieve requisite higher temperature in gasification. Utilizing solar heat is supposed to have following disadvantages over traditional gasification.

1. Use of concentrated solar heat averts the need of partial oxidation thereby keeping around 30% feedstock safe for conversion into fuel. [3,4]
2. The cost of oxidizer imparts another burden on the process economics, which can be eliminated.
3. One of the major drawback of combustion process is formation of SO_x , NO_x and soot particles which contaminate the product gas. Thus, requires extra equipment for cleaning and filtration.
4. It is also said that calorific value of the product gas can be enhanced by an amount equivalent to the solar energy added to the reactor. [3]

POSSIBLE SETUPS:

[3] discussed the direct use of concentrated sunlight by treating gasifier reactor as a black body. Reactor being surrounded by an external chamber having a cavity for the entrance of concentrated sunlight as shown in fig(1). Sunlight once entered remain trapped because of multiple internal reflections and assist the conversion process being carried out.
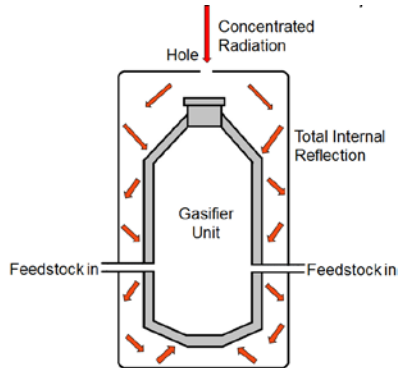

FIGURE 1. GASIFIER UNIT AS A BLACK BODY

[4] discussed the use of high heat capacity refractory honeycomb, which surrounds the gasifier reactor. Concentrated heat through optical window is focused on to this refractory honeycomb. Heat being diffused through this heats up the reactor to assist gasification in it. Fig (2) shows its schematic diagram.
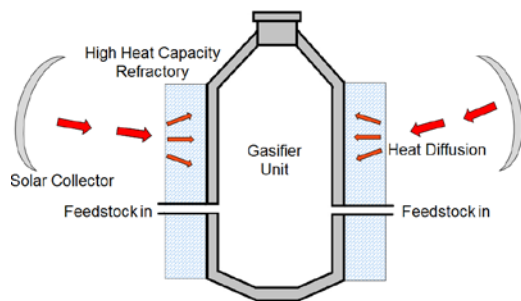
FIGURE 2. GASIFIER UNIT SURROUNDED BY HIGH HEAT CAPACITY REFRACTORY

[5,6] discussed the use of molten salt to heat up the gasifier reactor. Various carbonate salts like Na_2CO_3, K_2CO_3 are used because of their relatively high thermal conductivity and heat capacity [7,8]. [6] reveals that the use of molten salt increase the product yield by 22% and enhance the reaction rate to almost double because of improved reaction rate. Fig (3) depicts a similar concept where molten salt after being heated in concentrated solar heat is circulated in the jacket surrounding reactor. Thus, uniform rise in temperature assists the thermo-chemical reactions on the way inside reactor.
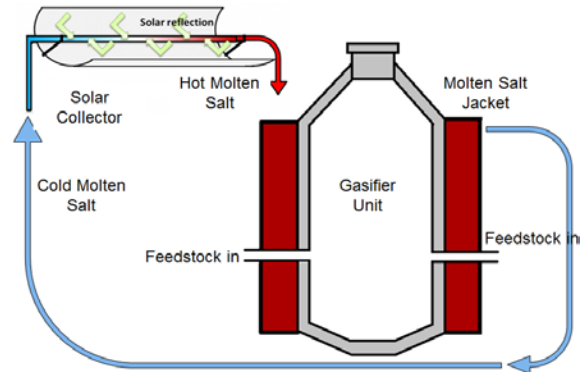

FIGURE 3. GASIFIER UNIT SURROUNDED BY JACKET OF HOT MOLTEN METAL

STARTING MATERIAL:

Wood has been taken as the starting material for feedstock and a combustion chamber is being constructed to study the proper utilization of its heating value. This combustion unit has been featured with all provisions to facilitate the wood burning. Secondary air besides primary air is required for efficient combustion in the chamber. Essential components of overall process can be summarized as follows:

1. Feedstock
2. Primary air
3. Secondary air
4. Thermal draft
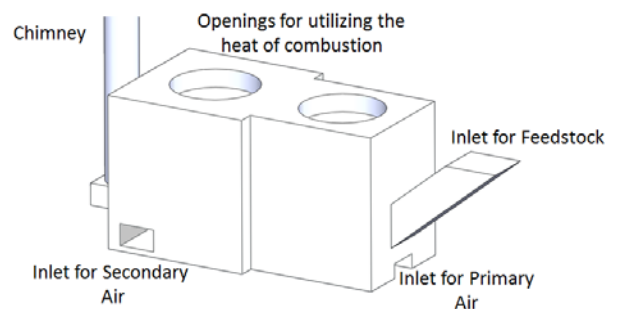
FIGURE 4. OUTER ENCLOSURE OF COMBUSTION CHAMBER

Fig.(4) shows the enclosure view of combustion chamber. Extension at the front is channel to feed the wooden pieces after establishing the thermal draft in chimney. In the beginning of process, air in the chimney is heated up by burning small piece of combustible material like paper through a small opening in the rear left for the purpose. Buoyancy effects arising out of density variations lift the air up in chimney, thereby making the air to flow continuously from primary and secondary inlets. Fig.(5) shows the internal view.
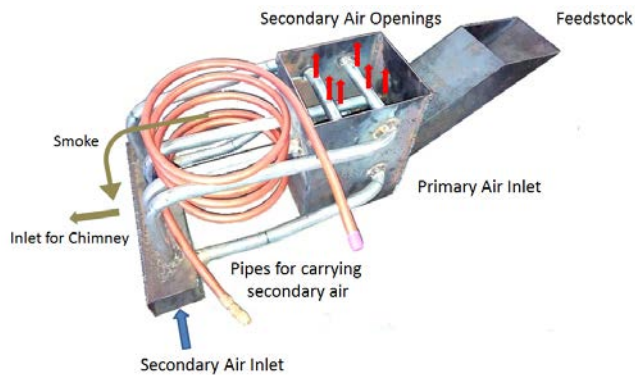
FIGURE 5. INTERNAL VIEW WITH VARIOUS PARTS

Primary air which assist the combustion at the major level is provided beneath of feedstock channel. Secondary air is taken into combustion unit through pipes originating from secondary air channel as shown in fig.(5). These pipes have holes which open up in the combustion unit at different elevations, thereby accelerating the combustion uniformly. Driving force for both primary and secondry air is thermal draft which is established at the start. Copper pipe in the form of coil shown in fig.(5) is extra attachment and can be used to extract the waste heat from smoke as water flowing through them will get heat up.

ADVANTAGES:

Advantages of aforementioned combustion unit can be enumerated as follow:

1. Primary and secondary air increase the effectiveness of combustion by extracting maximum out of calorific value of feedstock.
2. Less smoke and that too at low temperature as its heat being utilized by extra attachment like copper pipe for water heating.
3. Lower amount of harmful soot and other gaseous particles as a result of complete combustion.
4. Less quantity of feedstock required for same output.

CONCLUSION:

This setup can emerge as a helpful tool to find out the maximum potential in feedstock. Process heat generated by a particular feedstock here can be taken as a reference when similar feedstock is taken to gasification process, whether traditional or solar assisted. Furthermore a Scheffler solar concentrator can be incorporated which while located outside, will raise the process heat. This practice, by smoothing the overall process economics can give a fair idea about the feasibility of Solar Assisted Gasification Process for any carbonaceous feedstock.

REFERENCES

[1] Central Pollution Control Board, Ministry of Environment and Forests, "Status Report on Municipal Solid Waste Management". See also http://cpcb.nic.in/divisionsofheadoffice/pcp/MSW_Report.pdf

[2] Federation of Indian Chambers of Commerce and Industry (FICCI), Survey on the Current Status of Municipal Solid Waste, Management in Indian Cities and the Potential of Landfill Gas to Energy Projects in India, August 2009

[3] Isam Janajreh, Shabbar Syed, Rana Qudaih, Ilham Talab, 2010. "Solar Assisted Gasification: Systematic Analysis and Numerical Simulation." Int. J. of Thermal & Environmental Engineering Volume 1, No. 2 (2010) 81-90.

[4] Robert A. Frosch, Solar Heated Fluidized Bed Gasification System, 1981, United States Patent, Sept 22, 4290779

[5] Roman Adinberg, Michael Epstein, Jacob Karni, 2004. "Solar Gasification of Biomass: A Molten Salt Pyrolysis Study" Journal of Solar Energy Engineering, August 2004, Vol. 126/853

[6] PhD Thesis, Brandon Jay Hathaway, 2013, "Solar Gasification of Biomass: Design and Characterization of a Molten Salt Gasification Reactor, December 2013.

[7] J Matsunami, S Yoshida, Y Oku, O Yokota, Y Tamaura, M Kitamura, 2000, "Coal gasification with CO2 in molten salt for solar thermal/chemical energy conversion" January 2000, Vol. 25, Issue 1,71-79

[8] B. J. Hathaway, D. B. Kittelson, J. H. Davidson, 2013, "Development of a molten salt reactor for solar gasification of biomass", SolarPACES 2013, Energy Procedia 49 (2014) 1950-1959

SEEC – 2017 – 166

EVALUATION OF THERMAL CONDUCTIVITY OF KARANJA METHYL ESTERS

Thangaraja J.
Automotive Research Centre, VIT Vellore
Associate Professor of Mechanical Engineering
Email: thangaraja.j@vit.ac.in

Jayachandran S.
Dept. of Mechanical Engg., IIT Madras
Research Scholar
Email: jaythermal@gmail.com

ABSTRACT

The performance and emission characteristics of biodiesel fuels of Indian origin are widely tested and their varying results are well established. One of the major reasons for their variation is their change in compositional behavior. Further the thermophysical and thermochemical properties of biodiesel fuels depend on their composition. Hence, the current work attempts to find out the relationship between the composition of karanja methyl ester and the thermal property viz. thermal conductivity. Both the measurements and numerical prediction are carried out to establish their relationship. The deviation of the predicted results with the measured values for karanja methyl esters are within 7 percent over a useful temperature range of up to 353 K. Further, the effect of hydrogenation on biodiesel composition and thermal conductivity is highlighted.

Keywords*: *Thermal conductivity, Composition-property relationship, Karanja methyl ester, Hydrogenation.

NOMENCLATURE
K   Thermal conductivity
KME   Karanja Methyl Ester
USR   Unsaturation to Saturation Ratio

INTRODUCTION
Biodiesel obtained from different feedstock has been considered as a viable alternative for compression ignition engines. In recent years, a large number of assessments have been conducted to assess the environmental merit of biofuels, particularly biodiesel. Though their results are contrasting, generally biodiesel is claimed to be carbon neutral, since the exhausted carbon dioxide is sequestered from the atmosphere for their growth [1]. Biodiesel fuels are composed of mono alkyl esters, whose chemical composition depends upon the chain length and degree of unsaturation. Saturated esters cannot lend to hydrogenation, while the unsaturated esters can be hydrogenated [2]. As biodiesel fuel gains more importance, the need for measurements of their composition and properties of its constituent esters also arises. Further, for their combustion validation, it is necessary to measure/estimate various thermo-physical properties of the fuel namely specific heat, thermal conductivity, vapour pressure, mass diffusivity and latent heat of vaporization [3]. Thermal conductivity facilitates the heat to propagate through the substance and depends upon the chemical composition, phase, crystalline structure, temperature, pressure, and its homogeneity. Liquid thermal conductivity and vapour heat capacity of fuel affects the heat transfer between the drop interior and the surface, temperature distribution of gas mixtures surrounding the spray and air fuel ratio [4]. There is little effect of pressure, and raising the temperature usually decreases the thermal conductivities. The thermal conductivities of most organic, nonpolar liquids lie between 0.10 and 0.17 W/ m K [5].

Numerous methods have been proposed on the measurement of thermal conductivity. However, accurate measurements of thermal conductivity are not straight forward and require special care. Murakami et al. [6] analysed various design and operating parameters of the thermal conductivity probes. A majority of the thermal conductivity measurements are carried out using a transient probe method, which is known to provide precise and quick results [7]. The major advantage of a transient

method is that the experimental error caused by natural convection can be eliminated to a large extent [8]. Further, the estimation of liquid thermal conductivities of chemical compounds has been the subject of numerous research studies. To the best of the author's knowledge, there is nearly no experimental measurement of thermal conductivity of Indian origin viz. karanja methyl ester reported in the literature. The thermal conductivity measurements are carried out from ambient temperature to up to 353 K which is a typical temperature of fuel at the time of injection [9].

METHODOLOGY

The karanja biodiesel used in this study are procured locally from a commercial supplier in India. These karanja biodiesel samples are procured at three different times whose variations in composition and properties are reported elsewhere [10]. The present work proposes a methodology for predicting the thermal conductivity of karanja biodiesel fuels over a wide range of temperatures based on their composition. The present approach will prove to be useful in situations where the measured data are unavailable or measurements deemed to be difficult. It requires a priori knowledge of fatty acid composition and is fairly general and robust to be used for any biodiesel.

EXPERIMENTAL APPROACH

The KD-2 Pro Probe's method is employed for the thermal conductivity measurement, which is determined from the response of a hypodermic needle KS-1 probe with 1.3 mm diameter and 6 cm long. The method is conveniently applied to low-conductivity materials as that of the organic liquids. As shown in Fig. 1, the measurement probe contains a heater and a thermocouple attached to it.
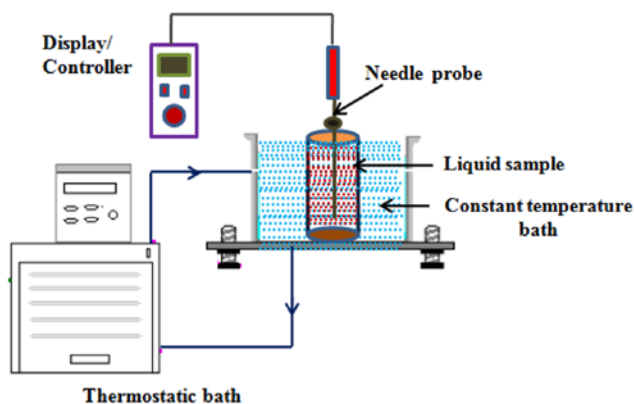
FIGURE 1. EXPERIMENTAL SETUP

When a certain amount of current is passed through the heater for a short period of time, the temperature history of the heater's surface will take on a characteristic form. In the initial phase, the temperature will rapidly rise, and as the heat begins to soak in, the increase in rate becomes constant. When the thermal front reaches the outer boundary of the sample, the rise will slow down or cease due to the losses. From the arrived temperature versus time plot, the thermal conductivity is calculated. The temperature while heating is computed from Eqn. (1).

$$T = m_0 + m_2\,(t) + m_3\,\ln(t) \qquad (1)$$

where m_0 is the ambient temperature during heating (which could include some offset for contact resistance and the heating element being adjacent to the temperature sensor inside the needle), m_2 is the rate of background temperature drift and m_3 is the slope of a line relating temperature rise to logarithm of temperature. The thermal conductivity (k) is computed from Eqn. (2).

$$k = \frac{I^2 R}{4\pi\,m_3} \qquad (2)$$

The sensor applies a very small amount of heat to the needle which helps to prevent free convection in the liquid samples. Sensor has testing range from 0.02 to 2 W/mK and the measurement is conducted from the ambient conditions to 353K with ambient pressure conditions. Thermo static water bath (Julabo C-B13) maintains the working fluid temperature within the range of $\pm$ 0.5 deg.C. Measurement uncertainties were found to be within $\pm 1\%$.

NUMERICAL APPROACH

The thermal conductivity of methyl esters is estimated by using both Sastri et al. [11] and Latini et al. [12] correlations. Sastri correlation is based on group contribution principle and thermal conductivity 'k' is expressed as:

$$K = \lambda_b \alpha^m;\quad m = 1 - \left(\frac{1 - T_r}{1 - T_{br}}\right)^n \qquad (3)$$

where λ_b groups, whose values are provided is the thermal conductivity at normal boiling point based on the contributions of methyl ester. The correlation constant 'm' and recommended values of other constants 'a' and 'n' are provided by Poling et al. [5]. Further, Latini et al. [12] proposed Eqn. (4) for estimating thermal conductivity 'k' of pure methyl esters.

$$k = \frac{A\left(1 - T_r\right)^{0.38}}{T_r^{1/6}};\quad A = \frac{A * T_b{}^a}{MW^{\beta} T_c{}^{\gamma}} \qquad (4)$$

where $A^*,\ \alpha,\ \beta,\ \gamma$ are the constant parameter taken as 0.0713, 1.2, 1.0 and 0.167 respectively [13].

Both the models require the critical properties of methyl ester for estimating the thermal conductivity. Further, the thermal conductivity of karanja biodiesel is estimated based on their methyl ester composition using the Kay's mixing rule.

RESULTS & DISCUSSION

A comparison of predicted thermal conductivity of karanja biodiesel using Sastri & Latini correlations and measured data is shown in Fig. 2. It is observed that Sastri and Rao method provides accurate predictions compared to other correlation and hence considered for further estimates of thermal conductivity.
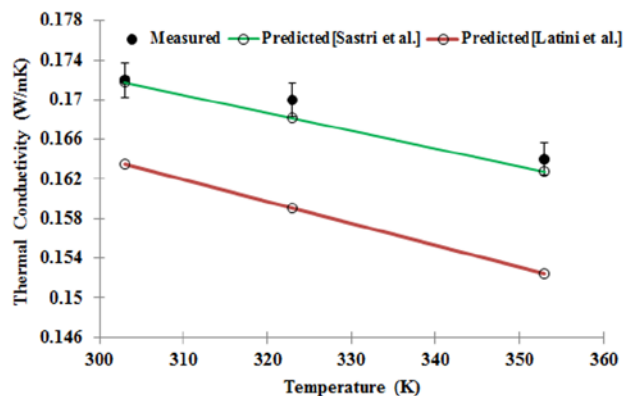
FIGURE 2. COMPARISON OF MEASURED AND ESTIMATED THERMAL CONDUCTIVITY

The thermal conductivity of karanja biodiesel decreases linearly with an increase in temperature as expected and the trends are captured well in the predictions. Further to examine the variations in compositions of karanja biodiesel due to differences in their origin three karanja fuel samples are procured from a commercial biodiesel supplier in the state of Tamilnadu at different time intervals. The predicted thermal conductivity data for these samples are provided in Table 1.

It is interesting to observe that the variations are within 1% and hence the variation of thermal conductivity due to differences in their origin is not significant in comparison with other properties like surface tension [14]. To further asses the composition-property relationship (KME-thermal conductivity), fuel reformulation technique like hydrogenation process is attempted. Discussions concerning their results are presented next.

TABLE 1: PREDICTED THERMAL CONDUCTIVITY (W/mK) OF THREE KARANJA SAMPLES

| Temperature (K)	Karanja-A	Karanja-B	Karanja -C
303	0.171	0.170	0.173
323	0.168	0.166	0.169
353	0.162	0.161	0.164

HYDROGENATION

Hydrogenation of biodiesel combats the biodiesel-NOx penalty by decreasing its unsaturated esters and also yields high quality biodiesel [15]. The composition of karanja methyl ester, which is employed for hydrogenation process, is shown in Table 2. It is found that karanja has higher unsaturated content and is composed of primarily methyl oleate (C18:1) and linoleate (C18:2). The composition of hydrogenated karanja (H_2-Karanja) is also included in Table 2. The composition of the test samples are measured using the flame ionization gas-chromatography (GC-FID). As clearly seen, the catalytic hydrogenation of polyunsaturated fatty acid methyl esters (FAME) of karanja has resulted to saturated FAME. The calculated unsaturation to saturation ratio (USR) for these two samples, confirm the significant change in composition of karanja biodiesel as noted in Table 2. Hence, it will be interesting to estimate and compare the composition-thermal conductivity relationship for karanja and H_2-Karanja. The same procedure is followed to estimate the thermal conductivity from their corresponding compositional data and the results are plotted in Fig. 3. It is observed that the changes in estimated thermal conductivity for the widely varying compositional samples are around 4%. Hence, it can be opined that the effect of variation of feedstock/composition on liquid thermal conductivity is not significant with the current case.

TABLE 2: MEASURED COMPOSITION OF KARANJA

Methyl esters	Karanja	H_2-Karanja
C16:0	10.55	10.13
C18:0	6.36	79.11
C18:1	53.11	---
C18:2	16.79	---
C20:0	2.73	---
C20:1	1.66	3.27
C22:0	1.49	---
C24:0	7.27	7.47
USR	4.13	0.03
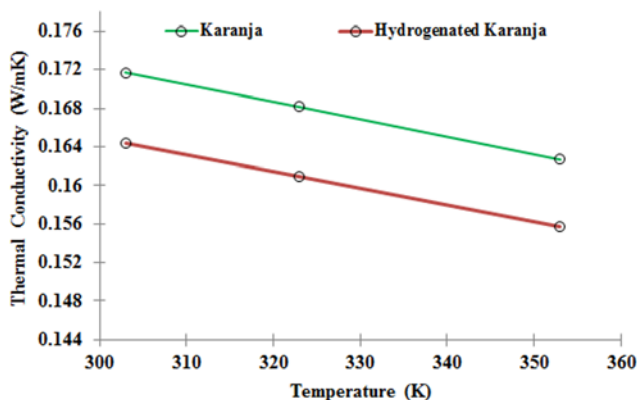
FIGURE 3. COMPARISON OF ESTIMATED THERMAL CONDUCTIVITY OF KARANJA SAMPLES

CONCLUSIONS

We constructed the data sets and an approach for estimating the liquid biodiesel (karanja and H_2-karanja) property (thermal conductivity), which are required for combustion modelling. Both experimental and numerical approach to evaluate thermal conductivity is presented and their deviation from the measured values is found to be within 7 percent. The study affirms the general conclusion that the thermal conductivity of any biodiesel could be estimated over a wide range of temperatures based on their fatty acid methyl ester composition. Also, the thermal conductivity of biodiesel decrease linearly with an increase in temperature However, for the chosen biodiesel, the effect of variation of feedstock/composition on liquid thermal conductivity is not significant.

ACKNOWLEDGMENTS

REFERENCES

[1] Castro M.P.P., Andrade A.A., Franco R.W.A., Miranda P.C.M.L. Sthel M., Vargas H., Constantino R. and Baesso M.L., 2005. "Thermal Properties Measurements in Biodiesel Oils using Photothermal Techniques". Chemical Physics Letters, 411, pp.18–22

[2] Giakoumis E.G., 2013. "A Statistical Investigation of Biodiesel Physical and Chemical Properties, and their Correlation with the Degree of Unsaturation". Renewable Energy, 50, pp.858–878.

[3] Rajkumar S. and Thangaraja J., 2016. "Multi-zone Phenomenological Combustion Modeling of Biodiesel Fueled Compression Ignition Engine". International Journal of Engine Research, Jan, pp.1–23.

[4] McCrady J., Stringer V., Hansen A. and Lee C., 2007. "Computational Analysis of Biodiesel Combustion in a Low-Temperature Combustion Engine using Well-Defined Fuel Properties". SAE International Journal of Engines, 116, pp.434–43.

[5] Poling B.E., Prausnitz, J.M. and O'Connel J.P. 5th ed. 2001.The Properties of Gases and Liquids, McGraw Hill, New York.

[6] Murakami E.G. and Sweat V.E., 1996. "Analysis of Various Design and Operating Parameters of the Thermal Conductivity Probe". Journal of Food Engineering, 30(1-2), pp.209–225.

[7] Batty W.J., Callagham P.W.O. and Probert S.D., 1984. "Thermal-Probe Technique for Rapid, Accurate Measurements of Effective Thermal Conductivities". Applied Energy, 16(2), pp.83–113.

[8] Nagasaki Y. and Ngashima A., 1981. "Absolute Measurement of the Thermal Conductivity of Electrically Conducting Liquids by Transient Hot-Wire Method". Journal of Physics E: Scientific Instruments,14 (12), pp.1435–1440.

[9] Ejim C.E., Fleck B.A. and Amirfazli A., 2007. "Analytical Study for Atomization of Biodiesels and their Blends in a Typical Injector: Surface Tension and Viscosity Effects". Fuel, 86, Nov, pp. 1534–1544.

[10] Thangaraja J., Anand K. and Mehta P.S., 2016. "Biodiesel NOx penalty and Control Measures - A Review". Renewable and Sustainable Energy Reviews, 61, pp.1–24.

[11] Sastri S.R.S and Rao K.K., 1993. "Quick Estimating for Thermal Conductivity". Chemical Engineering Journal. 100(8), pp. 106–107.

[12] Latini G, Grifoni RC and Passerini G., 2006. Transport properties of organic liquids. Southampton: WIT Press.

[13] Yuan W., Hansen A.C. and Zhang Q., 2003. "Predicting the Physical Properties of Biodiesel for Combustion Modeling". Transactions of the ASAE, 46(6), pp.1487-1493.

[14] Thangaraja J., Anand K. and Mehta P.S., 2016. "Predicting surface tension for vegetable oil and biodiesel fuels". RSC Advances, 6, pp. 84645–84657.

[15] Bouriazos A., Mouratidis K., Psaroudakis N. and Papadogianaki G., 2008. "Catalytic Conversions in Aqueous Media. Part 2. A Novel and Highly Efficient Biphasic Hydrogenation of Renewable Methyl Esters of Linseed and Sunflower Oils to High Quality Biodiesel Employing Rh/TPPTS Complexes". Catal Lett, 121, pp.158–164.

SEEC-2017-167

INVESTIGATIONS ON CO-PYROLYSIS CHARACTERISTICS OF COAL-BIOMASS BLENDS USING TGA

Munna Verma
Department of Mechanical Engineering, NIT Patna, Patna-800005, India
Email: munna.nitp@gmail.com

Chanchal Loha
ERT Group, CSIR-CMERI, Durgapur-713209, India
Email:chanchal.loha@gmail.com

Amar Nath Sinha
Department of Mechanical Engineering, NIT Patna, Patna-800005, India
Email: ansinha@nitp.ac.in

Prabhansu
Department of Mechanical Engineering, NIT Patna, Patna-800005, India
Email:prabhansu.nitp@gmail.com

Malay Kumar Karmakar
ERT Group, CSIR-CMERI, Durgapur-713209, India
Email:malaycmeri@gmail.com

Pradip Kumar Chatterjee
ERT Group, CSIR-CMERI, Durgapur-713209, India
Email:pradipcmeri@gmail.com

ABSTRACT

Rapid industrialization and population growth increases the demand for energy. Coal is the most important energy source which is mainly consumed via combustion. A primary concerns with coal utilization is the long-term balance of supply and demand, and secondary the CO_2 emissions have increased dramatically over the last decade. Biomass co-firing technique is one of the ways that can be use in large coal-fired plants to minimize the use of the non-renewable resources. It is a highly efficient technology which minimizes the coal exhaustion, green house gas emission problem and represents a near-term, low-risk, low-cost and sustainable energy development. Higher volatile matter present in biomass results better burn out and lower unborn carbon in the ash. Co-pyrolysis of biomass (Sawdust) and Indian coal is investigated in this paper. After fuel characterization, the influences of heating rate, the effect of the weight percentage of biomass mixing in different proportion were investigated in a nitrogen environment.

*Keywords:* Thermogravimetric analysis, coal, biomass (Sawdust), co-pyrolysis

.

INTRODUCTION

Among the various ways of using bioenergy, one that has attracted particular attention is the use of biomass blended with coal, as such blends can be applied for co-firing, co-gasification, and co-pyrolysis [1]. The co-utilisation of coal–biomass blends as feedstock in already existing industrial-scale coal conversion plants is a promising technological option for taking advantage of available biomass resources. Examples of existing processes for coal conversion into energy products include combustion, direct liquefaction (carbonisation/pyrolysis) and indirect liquefaction (gasification) [2].

Pyrolysis/devolatilisation is a fundamental step in all main thermo-chemical conversion routes, the adaptation of coal based processes to biomass co-feeding necessitates an understanding of the devolatilisation kinetics of the biomass-coal blends [3]. Also, Pyrolysis is one stage of the solid fuel combustion and gasification processes. It is a promising thermo-chemical conversion method, playing a vital role in solid fuel conversion process [4]. The conversion process of pulverized fuels includes successive steps as pre-heating, drying, pyrolysis,volatiles and char oxidation [5]. Pyrolysis is slower for biomass than coal. Generally, it is much shorter than either drying or combustion of char [3]. Using pyrolysis route low chemical energy density biomass fuels are converted to high energy density gaseous fuels and residual char, which can be utilized more efficiently in environmentally acceptable manner [6]. During the thermo-chemical conversion of coal and biomass, devolatilization can account for the majority of the solid's weight loss, depending on the organic constituents of the fuel [4]. The pyrolysis processes

can be classified to conventional pyrolysis (or slow pyrolysis) and fast pyrolysis based on residence time, heating rate, and pyrolysis temperature. Conventional pyrolysis uses low temperature and slow heating rate and is used for charcoal production. However, fast pyrolysis with high temperature and fast heating rate has now been developed for high yields of liquid or gases [7]. An overview of the thermo-chemical conversion process is shown in Fig. 1[8].
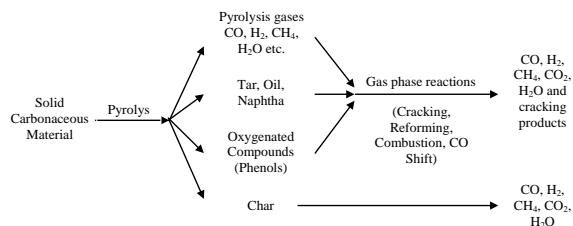
FIGURE 1. Coal/biomass thermo-chemical reaction sequence [8].

This study provides the co-pyrolysis behavior of Indian coal and biomass (Sawdust) blends. The effects of heating rate and biomass mixing in different weight percentage with coal on char yied and volatile matter in non-isothermal condition were investigated.

METHODOLOGY
Preparation of samples
A total six different samples of coal-Sawdust mixture in different weight percentage such as: 100:0, 90:10, 80:20, 70:30, 50:50 and, 0:100 were used as experimental material for co-pyrolysis study. To prepare the sample of coal and biomass first it was dried in hot oven at 105 °C for the time period of 3 hours. After that fine crushed coal and sawdust ware sieved using two different mesh size sieves. A known particle size range of 100-150 µm was used for experimental analysis.

Thermogravimetric analysis (TGA)
The experimentations of coal-biomass mixture were carried out on thermo gravimetric analyzer (TG 209 F3 Tarsus) manufactured by NETZSCH-Geratebau GmbH. To achieve pyrolysis condition N_2 (99.99 %) gas was made to flow in a heating chamber at 60 ml/min. When all instruments were reached at steady state condition then correction measurements was carried out so that any contamination and bouyancy effect on crucible can be removed. After then a predefined amount of sample 8 ± 0.2 mg was taken in alumina crucible and placed inside the thermogravimetric analyzer where the weight of sample was continuously measured. The balance housing is thermostatically controlled to avoid temperature influences. The control thermocouple is integrated in the heating coil of furnace. Thermogravimetric analysis (TGA)

measurements were performed for all six sample in the temperature range of 30-900 °C and at four heating rate of 10, 20,40 and, 80 K/min. The thermostatic process is done by water circuit. Based on the distribution of weight loss, it was possible to carry out the thermogravimetric analysis and derivative thermogravimetric (DTG) analysis of binary mixtures.

Kinetic analysis
The non-isothermal kinetics for solid material decomposition is usually given as:

$$\frac{d\alpha}{dt} = Kf(\alpha) \tag{1}$$

Where, K is the rate constant and $f(\alpha)$ is a kinetic model-dependent function.

$$\alpha = \frac{M_i - M}{M_i - M_f} \tag{2}$$

Where, α is the conversion, M_i is the initial mass, M is the mass at any time (t), and M_f is the final mass.

The char yield of solid fuel is calculated using equation (3) expressed as:

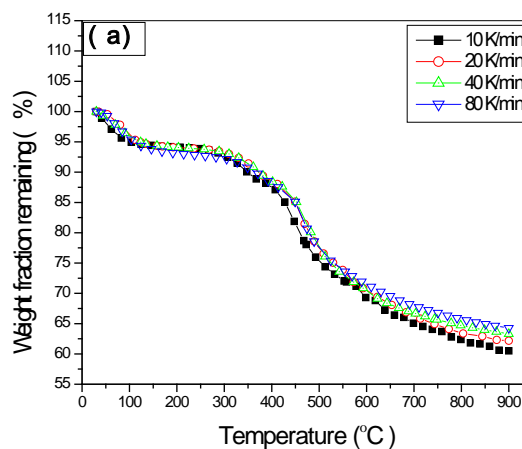$$CY \ (\%) = \frac{M_f}{M_i} \times 100\% \tag{3}$$

$$VM(\%) = Total \ weight \ loss \ (\%) - MC \ (\%) \tag{4}$$

Where; CY is char yield, VM is the volatile matter and, MC is the inherent moisture content.

RESULTS
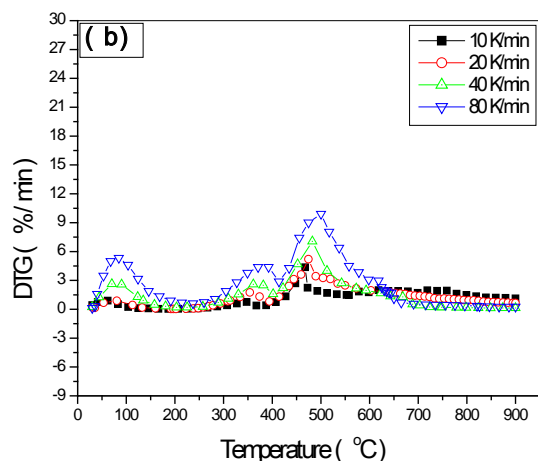### Effect of heating rate on pyrolysis characteristics
The co-pyrolysis behaviour for coal and sawdust blends at four heating rates of 10, 20, 40, and 80 K/min was shown in Fig. 2(a-b).

FIGURE 2(a). Distribution of TGA curve for coal-biomass mixture at different heating rate.

The weight loss characteritics at four different heating rate is shown in Fig. 2(a). From this figure it can be seen that at lower heating rate fuel decomposion starts at low
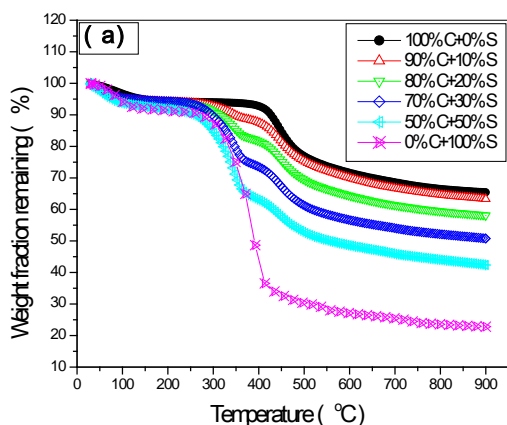
temperature and residual char yield (%) was also lower because of extra time to heat the fuel particle, for the biomass and coal separately, as well as biomass–coal blends. From Fig. 2(b) it was observed that peaks occur at different temperatures for the biomass and coal separately, and for the biomass–coal blends display two distinct peaks, each at approximately the pure fuel peak DTG temperature.

From the Fig. 2(a-b), it could be found that with addition of biomass into coal, the pyrolysis process of blends could be divided into different stages in conversion curves, and each curve for the blends lies between that of the individual samples, and the contributions of coal and biomass to these profiles are obvious. In order to investigate influences of biomass addition on prolysis of blend.

FIGURE 2(b). Distribution of DTG curve for coal-biomass mixture at different heating rate.
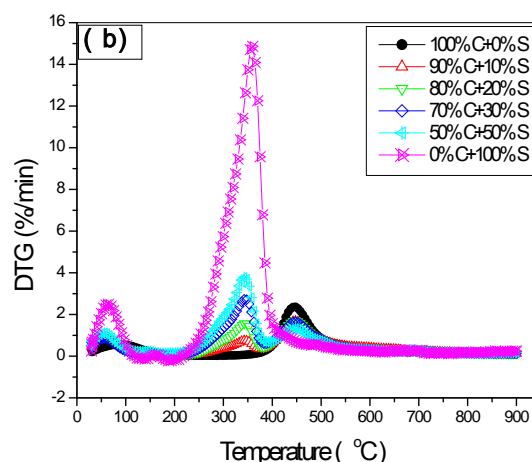
FIGURE 3(b). Distribution of DTG curve for diffirent coal-biomass mixture.

Effect of sawdust blending in different weight percentage on pyrolysis characteristics

Conversion curves (TG curve) and reaction rate curves (DTG curve) of coal-sawdust blend with different coal-sawdust weight percentage (100:0, 90:10, 80:20, 70:30, 50:50 and, 0:100) under heating rate of 10 K/min are shown in Fig. 3(a-b). The pyrolysis process for different mixtures are carried out from the starting temperature of 30 ^{o}C to the final temperature of 900 ^{o}C under non-isothermal condition.

Effect of sawdust blending in different weight percentage on char yieds and volatile matter

Amount of char yield (%) and volatile matter (%) generated from the different coal-sawdust blend after pyrolysis under nitrogen atmosphere at a heating rate of 10 K/min and temperature range of 30-900 ^{o}C is shown in Fig. 4.
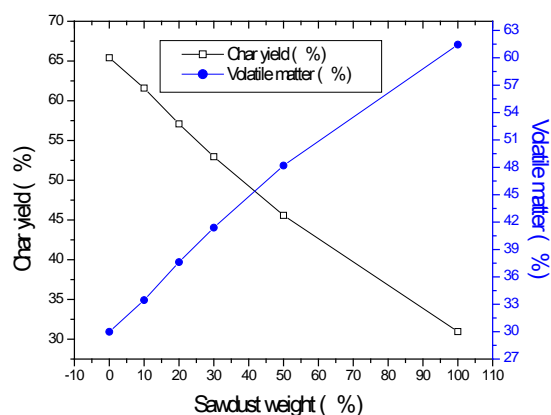
FIGURE 4. Variaton in char yield and volatile matter with addition of sawdust into coal in different coal-sawdust weight percentage at heating rate of 10 K/min.

FIGURE 3(a). Distribution of TG curve for diffirent coal-biomass mixture.

This shows that in co-pyrolysis of the samples, the char yields linearly decreases while volatile matter linearly

3

increases because sawdust have higher amount of volatile matter as compared to coal. The values of char yield was found to be 65.41, 61.59, 57.09, 52.95, 45.58 and, 30.95% while the amount of volatile matter was 29.98, 33.46, 37.61, 41.39, 48.19 and 61.44% respectively for the coal-sawdust blend weight percentage of 100:0, 90:10, 80:20, 70:30, 50:50 and, 0:100.

CONCLUSION

Co-pyrolysis behaviors of sawdust with Indian coal were carried out through thermo-gravimetric method. Results show that the pyrolsis processes of blend could be obviously divided into two stages: sawdust prolysis and coal pyrolsis. The effect of heating rate on pyrolsis characteristics showed significant result. At lower heating rate higher volatile matter was released. It was found that with the addition of sawdust into coal, volatile matter release increases and char yied decreases.

ACKNOWLEDGMENTS

REFERENCES

[1] Lu, K.M., Lee, W.J., Chen, W.H., Lin, T.C., 2013. "Thermogravimetric analysis and kinetics of co-pyrolysis of raw/torrefied wood and coal blends" Applied Energy, 105, 57–65.

[2] Aboyade, A.O., Görgens, J.F., Carrier, M., Meyer, E.L., Knoetze, J.H., 2013. "Thermogravimetric study of the pyrolysis characteristics and kinetics of coal blends with corn and sugarcane residues" Fuel Processing Technology, 106, 310–320.

[3] Vuthaluru, H.B., 2003. "Thermal behaviour of coal/biomass blends during co-pyrolysis" Fuel Processing Technology, 85, 141–155.

[4] Chen, C., Ma, X., He, Y., 2012. "Co-pyrolysis characteristics of microalgae Chlorella vulgaris and coal through TGA" Bioresource Technology, 117, 264–273.

[5] Zellagui, S., Schönnenbeck, C., Zouaoui-Mahzoul, N., Leyssens, G., Authier, O., Thunin, E., Porcheron, L., Brilhac, J.F., 2016. "Pyrolysis of coal and woody biomass under N_2 and CO_2 atmospheres using a drop tube furnace experimental study and kinetic modeling" Fuel Processing Technology, 148, 99–109.

[6] Sadhukhan, A.K., Gupta, P., Goyal, T., Saha, R.K., 2008. "Modelling of pyrolysis of coal–biomass blends using thermogravimetric analysis" Bioresource Technology, 99, 8022–8026.

[7] Pang, S., and Mujumdar A.S., 2010. "Drying of Woody Biomass for Bioenergy: Drying Technologies and Optimization for an Integrated Bioenergy Plant" Drying Technology, 28:5, 690-701.

[8] Weiland, N.T., Means, N.C., Morreale, B.D., 2012. "Product distributions from isothermal co-pyrolysis of coal and biomass" Fuel, 94, 563–570.

SEEC–2017–168

JET FUEL DEPOSITS: CARBON SPHERES AND NANOSTRUCTURES

Pooja Sharma
Mechanical Engineering
Indian Institute of Science
pooja@mecheng.iisc.ernet.in

Saptarshi Basu
Mechanical Engineering
Indian Institute of Science
sbasu@mecheng.iisc.ernet.in

ABSTRACT

Thermal stressing of middle distillate fuel produces heteroatomic deposits. In this study, Jet fuel, Jet A was thermally stressed by flask static tests in the autoxidation temperature range without oxygen sparge. Fuel deposits were analyzed by transmission electron microscope (TEM). Microscopic analysis of Jet A deposits revealed unit spherical nanoparticles and sub micron carbon spheres. Objective of this study is to compare the effect of addition of Cerium Oxide catalyst during fuel thermal stressing on deposit formation and morphology. Noticeably, relatively more carbon spheres are produced by addition of Cerium Oxide with similar morphology compared to non catalytic thermal stressing. Hollow carbon spheres generated by ceria added fuel are relatively smaller compared with fuel without ceria. Deposit nanostructures are 10-80 nm nanospheres with abundant nanoparticles of 30 nm diameter. A comparison of fuel deposits produced by the two methods followed by microscopic analysis is discussed briefly in this communication. Spectroscopic and microscopic analysis to investigate fuel deposit properties is in progress.

Keywords: Jet A, deposit, carbon sphere, nanostructures, TEM

INTRODUCTION

Middle distillate fuels are susceptible to thermal oxidative instabilities and deposition. Jet fuel thermal stressing in the aircraft engine is caused by indirect heating of fuel through a series of heat exchangers [1, 2]. In this study, jet fuel thermal stressing in the flask static tests is conducted to investigate deposition. Fuel deposit morphology and chemical analysis is the objective of current study and future research. A novel finding is the generation of carbon spheres as deposit components in addition to spherical nanostructure and their agglomerates.

Soluble macromolecular oxidatively reactive species (SMORS) are elementary middle distillate fuel deposit units as introduced by Hardy and Wetcher [3]. SMORS contain heteroatomic polar components and detected in the thermally stressed middle distillate fuel by spectroscopic analysis [3, 4-6]. Fourier Transform Infrared (FTIR) analysis also confirmed the presence of alkoxy and oxygen containing groups with strong bands in carbonaceous solids spectra than thermally stressed liquid fuel [4]. Fuel coloration, deposition and SMORS were observed in the thermally stressed fuel mass spectra [4]. In current work, jet fuel was thermally stressed by flask static tests. Analysis of fuel deposit nanostructures and carbon spheres is discussed.
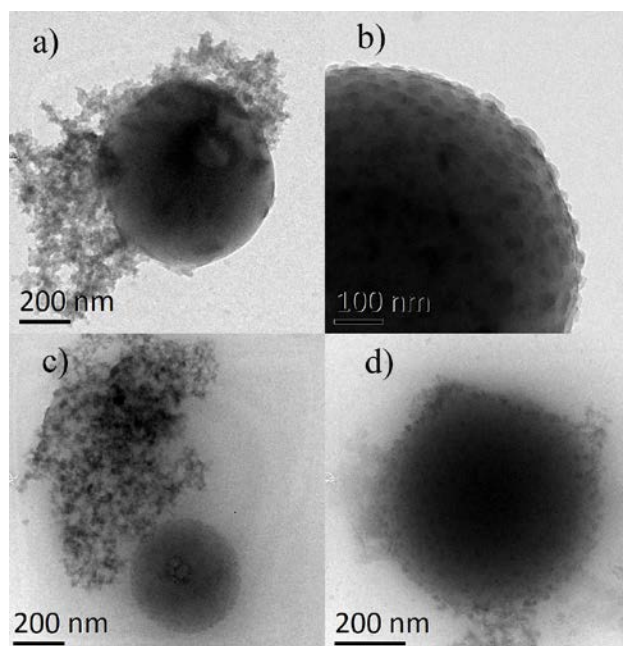
METHODS

Flask static tests were conducted without oxygen sparge in the autoxidation temperature range at 190 ^{0}C . Thermal stressing duration was six hours and fuel volume was 50 ml and 125 ml. More details about experimental procedure have been reported earlier [4]. Microscopic analysis was conducted with transmission electron microscope (FEI Tecnhai T20 and F30).
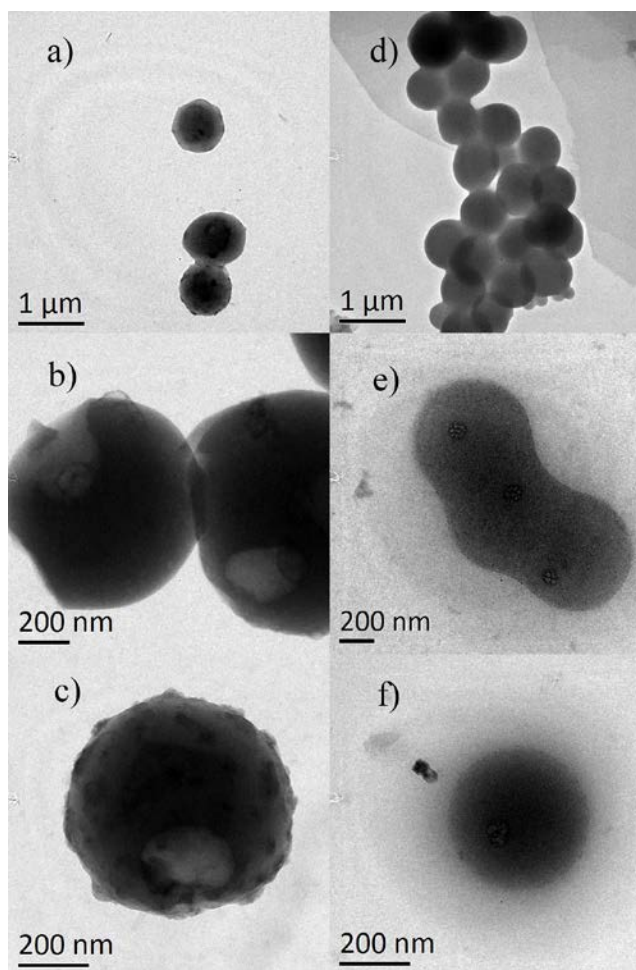
RESULTS AND DISCUSSION

Jet A thermal stressing produced deposit carbon spheres and nanostructures with and without ceria (CeO_2) addition to fuel in this study. Morphologically, fuel deposits are similar with both catalytic and non-catalytic thermal stressing of jet fuel. Jet fuel deposits nanostructures and carbon spheres were generated in the autoxidation regime (150-300 ^{0}C) without catalyst [4]. Additives are used to alter fuel properties and attain a desirable composition. Jet fuel contains many additives such as antioxidant, anti-icing, and lubricity improver. CeO_2 is also used as a fuel additive. Previous studies report use of ceria as catalyst in the combustion process and its effect on hydrocarbons oxidation [7, 8]. Objective of adding CeO_2 in this study is to investigate its effect as a catalyst on the fuel deposit and carbon spheres properties.

Figure 1a, b depicts carbon spheres of jet fuel with attached constituent nanoparticles without ceria as catalyst. Figure 1c, d show similar morphology of ceria added thermally stressed fuel deposits. Carbon spheres generated with jet fuel without ceria are shown in Figure 2a-c and with ceria added in Figure 2d-f. Carbon spheres size range is approximately 300-600 nm produced by Jet A thermal stressing (Figure 1a,b and 2a-c). Addition of ceria to fuel results in relatively smaller spheres as shown in Figure 1c, d and 2d-f. Carbon spheres in a chain like pattern are connected by Van der Waals forces (Figure 2 a and d).

FIGURE 2. Carbon spheres of thermally stressed Jet A deposits. a)–c) non-catalytic and d)-f) with Cerium Oxide as catalyst

FIGURE 1. Carbon spheres of thermally stressed Jet A with attached unit nanoparticles . a),b) without catalyst and c),d) with Cerium Oxide as catalyst

Hollow carbon spheres are shown in Figure 3. Average diameter of carbon spheres with ceria added fuel is smaller than fuel without catalyst (Figure 3). Core diameter is larger relative to sphere in the ceria added fuel sample in Figure 3c, d than fuel without catalyst as shown in Figure 3a, b. Hollow carbon spheres generated from fuel with ceria are approximately 270 to 300 nm (Figure 3c-f). It is also observed that sphere grow initially larger in diameter in a chain like pattern (Figure 2); however the hollow carbon spheres are smaller (Figure 3). Difference in the carbon sphere diameter can be attributed to their growth stage as shown in Figure 2 and 3. Few non uniform deposits are also observed in addition to carbon spheres in the ceria added samples (Figure 3e, f). Additionally, the number of carbon spheres is more in the fuel with ceria (Figure 3e, f). In previous study, size of carbon spheres produced by jet fuel without ceria is approximately 300 to 500 nm with 300-350 nm size spheres are relatively more

than large diameter [4]. More investigation is required to conclude the effect of ceria addition on fuel deposit properties compared with non catalytic thermal stressing.
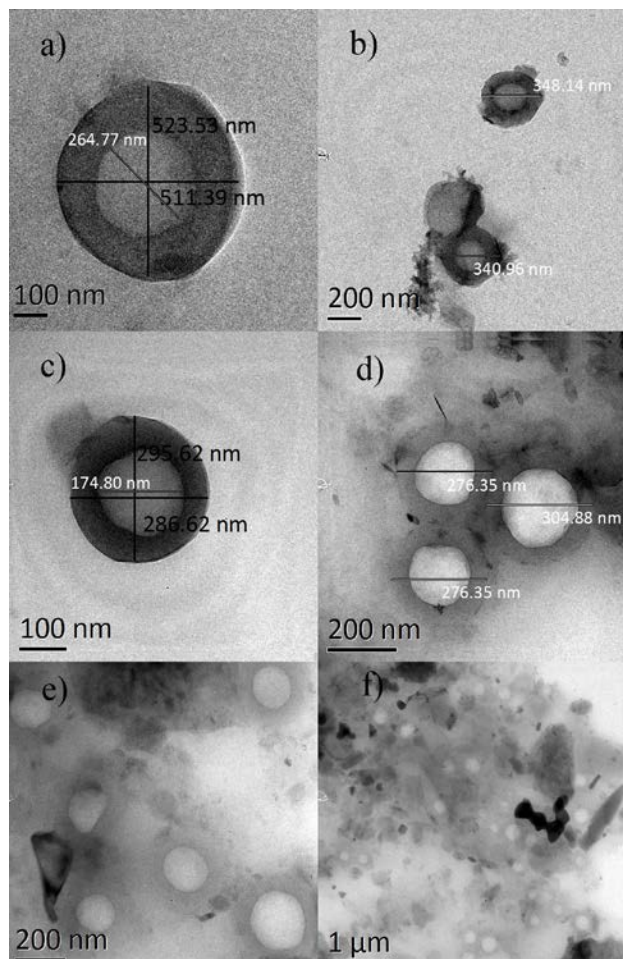

FIGURE 3: Jet A hollow carbon spheres in the thermally stressed fuel a), b) without catalyst and c)-f) with ceria added to fuel

Fuel deposit analysis by TEM revealed that nascent deposit nanoparticles exhibit morphological similarities with carbonaceous soot [4]. Aromatic content in the fuel contributes in the condensed phase particles formation [9]. Fuel composition contributes considerably in soot formation [9, 10]. Similarly, kerosene type fuel is richer in aromatic content than lower alkanes which contribute in the more carbonaceous deposit formation. Deposit nanoparticles size varies from 10-80 nm and average diameter is 30 nm [4] which is also observed in the current study. Deposit agglomerates however also develop as carbon spheres and with hollow core (Figure 1-3). Catalytic processes yield hollow carbon spheres as reported

by Deshmukh et al [11]. Heteroatoms are deposit precursors and SMORS contain polar heteroatomic components. Jet fuel deposit carbon spheres thus are catalyzed by the heteroatomic content in the fuel [4]; however more investigation is required to predict possible chemical pathway(s). Oxygen content contributes considerably in the fuel deposition process compared with other heteroatom. Oxygen in the hydrocarbon source produce better carbon spheres [11]. SEM-EDS spectra of jet fuel deposits confirmed upto 23% elemental percentage of oxygen [4]. Aromatization and dehydrogenation of fuel components in addition to free radical reactions is predicted towards carbonaceous nanostructures and deposit formation [4].
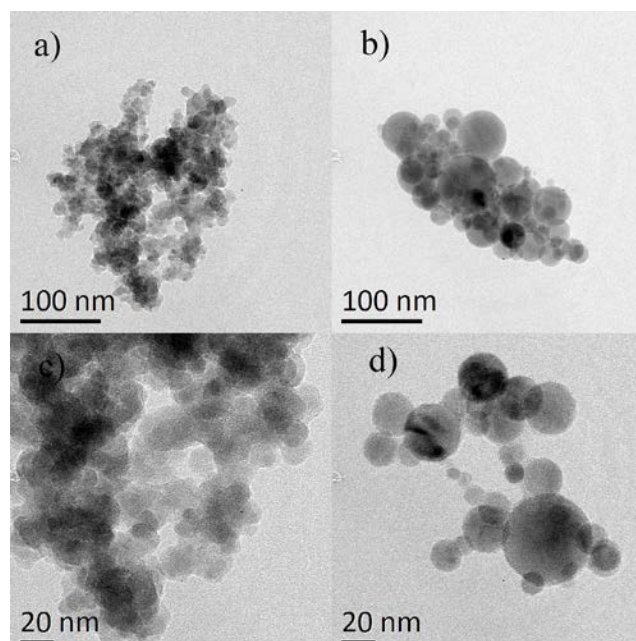

FIGURE 4: Jet A deposits nanostructures

Thermally stressed jet A deposit nanoparticles form a chain like pattern and non uniform agglomerates as shown in Figure 4. Generation of carbon spheres thus is accompanied with small non uniform clusters of spherical nanoparticles dispersed in the fuel and also attached on their surface (Figure 1,4).

CONCLUSIONS

In summary, jet fuel thermal stressing without oxygen sparge in the autoxidation temperature range produces spherical nanoparticles and sub micron carbon spheres. Hollow carbon spheres formation is attributed to the heteroatomic content of the fuel. Ceria added to fuel followed by thermal stressing generates numerous and smaller carbon spheres compared with non catalytic flask test fuel sample. More analysis is required to understand

3

the contribution of ceria in increasing the number of spheres and their size difference and is next step in this study. Also, fuel deposit analysis by spectroscopic and microscopic methods is required to understand their properties, structure and growth processes and is in progress.

REFERENCES

[1] Hazlett Robert N. Thermal Oxidative Stability of Aviation Turbine Fuels. ASTM;1991.

[2] Totten George E., Westbook Steven R. and Shah Rajesh J. Fuels and Lubri- cants Handbook: Technology, Properties, Performance and Testing. ASTM International; 2003.

[3] Hardy D.R. and Wetcher M.A. Insoluble sediment formation in middle- distillate diesel fuel: the role of soluble macromolecular oxidatively reactive species. Energy & Fuels 1990; 4; 270-274.

[4] Sharma Pooja and Basu Saptarshi. "Catalyst free carbon spheres and soot like heteroatomic nanostructure formation in thermally stressed Jet A fuel in the autoxidation temperature range" Energy & Fuels, In review, 2017.

[5] Sharma Pooja. "Heteroatomic Jet Fuel Components: Lichen Substances as Fuel Component and Potential Additives", Fuel, In review, 2016.

[6] Kabana G. Christopher, Botha Shanielle, Schmucker Colin, Woolard Chris and Beaver Bruce. Oxidative Stability of Middle Distillate Fuels. Part 1: Exploring the Soluble Macromolecular Oxidatively Reactive Species (SMORS) Mechanism with Jet Fuels. Energy & Fuels, 2011, 25, 5145-5157.

[7] Lopex A. Bueno. Diesel soot combustion ceria catalysts. Applied Catalysis B: Environmental, 146, 1-11, 2013.

[8] Sajith V. Sobhan C.B. and Peterson G.P. Experimental investigation on the Effects of Cerium Oxide Nanoparticles Fuel Additives in Biodiesel. Advances in Mechanical Engineering, 2010.

[9] Bockhorn Henning editor. Soot Formation in Combustion- Mechanisms and Models. Springer-Verlag; 1994.

[10] Glassman Irvin. Soot Formation in Combustion Processes. The 22nd Symposium of the Combustion Institute, 1988.

[11] Deshmukh Amit A, Mhllanga Sabelo D. and Coville Neil J. "Carbon spheres". Materials Science and Engineering Research, 2010, 70, 1-28.

SEEC-2017-169

FORMACATALYTIC REDUCTION OF NO (NITRIC OXIDE)

MK Shukla & Dr. T Bhaskar
CSIR-IIP, Dehradun, India

Dr. Atul Dhar
School of Engineering, IIT Mandi.
India

ABSTRACT

Automobiles are major contributors NOx emission. Around 90 percent of NOx is nitric oxide (NO). Technologies like EGR, SCR and NOx-traps have used commercially in automobiles where precious metal catalyst metals are used for catalytic reduction of NO. Direct decomposition of NO may be one of the alternatives to reduce NO from automobiles exhausts. In this paper, catalytic reduction of NO over a nonnoble metal containing catalyst is examined. Copper is used as a non noble metal for the catalyst over COK-12 support. Catalyst is prepared by impregnation method, over mesoporous silica support. Catalytic reactivity of catalyst is examined in ss-reactor with a flow rate 100ml/min of a 2000 ppm nitric oxide balanced nitrogen gas .Catalyst offered reactivity more than 40% for temperature as low as 3000C

SEEC-2017-170

Mixed Oxides as Low-cost Oxidation Catalysts for Diesel Particulate Matter

Rohini Khobragade, Govindachetty Saravanan*, Nitin Labhsetwar*
CSIR-National Environmental Engineering Research Institute (CSIR-NEERI), Nagpur, India

ABSTRACT

Diesel engines have been widely adapted for transportation, agriculture, constructions, mining, etc. due to their durability, high fuel efficiency, lower maintenance cost etc. Despite several advantages, they emit the harmful particulate matter (PM) due to the incomplete combustion of diesel. The particulate size and its organic and inorganic fractions are usually vary, depending on the engine conditions. PM with a smaller size can be easily inhaled by human that results in respiratory problems [1].

After-treatment control technologies, for instance Diesel Oxidation Catalyst (DOC) and Diesel Particulate Filters (DPF) have been proven as efficient options to control the PM emissions. DOC can oxidize soluble organic fraction of PM while DPF can reduce the PM emissions to more than 90%. Although these technologies show promise for the PM-treatment, they require expensive platinum group metals (PGM) [2,3]. High-cost and limited resources of PGM urge to find alternatives to PGM-based catalysts. Mixed oxides, perovskites, spinels, etc. can be considered as potentail alternatives to PGM due to the tailoring possibility of their catalytic activity.[4,5] We have successfully synthesized low-cost, mixed oxides and evaluated for catalytic oxidation of diesel PM.

SEEC-2017-171

COMPARISON OF MACROSCOPIC SPRAY CHARACTERISTICS OF WASTE COOIL OIL, JATOPHA, KARANJA BIODIESELS IN A CONSTANT VOLUME COMBUSTION CHAMBER

Joonsik Hwang
Mechanical Engineering
KAIST
Email: ippo@kaist.ac.kr

Choongsik Bae
Mechanical Engineering
KAIST
Email: csbae@kaist.ac.kr

Chetankumar Patel
Mechanical Engineering
IIT Kanpur
Email: chetanp@iitk.ac.in

Avinash Kumar Agarwal
Mechanical Engineering
IIT Kanpur
Email: akag@iitk.ac.in

Tarun Gupta
Civil Engineering
IIT Kanpur
Email: tarun@iitk.ac.in

ABSTRACT

Macroscopic spray characteristics including liquid tip penetration length and spray angle were measured in a constant volume chamber (CVC) with Waste Cooking Oil, Jatropha and Karanja biodiesels. The experimental results were compared to those of conventional diesel. The ambient pressure was kept at 3 MPa, pressurized by nitrogen in the CVC. The tested fuels were injected with injection pressures of 40, 80, and 120 MPa through a solenoid injector and a common-rail injection system. Only single hole was exposed to the chamber by utilizing injector hole cap. The spray process was visualized by back light technic and high speed camera. The biodiesel fuels were characterized by longer liquid tip penetration length and narrower spray angle than those of diesel due to poor atomization characteristics.

Keywords: Biodiesel, Diesel, Liquid tip penetration length, Spray angle, Constant volume chamber.

INTRODUCTION

Due to the concerns about environment and fossil fuel, researches on alternative fuels have gained much importance all over the world. Biodiesel, as an alternative fuel for diesel engine, is a renewable energy source. It can be produced from many different raw materials such as animal fat, soybean, palm oil, and vegetable oil. Previous researches discovered that the complete combustion can be promoted with biodiesel so harmful emissions for instance carbon monoxide, hydrocarbon and smoke are reduced [1-3]. On the other hand, nitrogen oxides are increased with biodiesel [4-5].

In a compression ignition engine, spray characteristics of fuel affect the combustion and emission significantly. Therefore, the macroscopic spray characteristics must be understood. In this study, the macroscopic spray characteristics of four fuels: commercial diesel, Waste Cooking Oil, Jatropha, and Karanja biodiesel were investigated in a CVC uncer non-evaporating condition. The liquid tip penetration length and spray area were compared.

FUEL PROPERTIES

Major fuel properties of biodiesels were measured according to ASTM method. The values were compared with those of diesel, as shown in Table 1. It is clearly seen

that the viscosity of biodiesels were slightly higher than those of baseline diesel. The density of biodiesels were approximately 6.5 % higher than baseline diesel as well. The lower heating values were approximately 6.7% lower than baseline diesel.

TABLE 1: PHYSICAL PROPERTIES OF TEST FUELS

Item	Diesel	WCO biodiesel	Jatropha biodiesel	Karanja biodiesel
Lower heating value [MJ/ kg]	42.98	38.85	41.5	39.89
Density (288 K) [kg/ m^3]	820	878	857	886
Kinematic viscosity (313 K) [mm^2/ s]	2.2	3.32	4.66	5.66
Flash point [K]	329	448	423	417

EXPERIMENTAL SETUP

The CVC houses five 96 mm diameter quartz windows. The high pressure atmosphere in a diesel engine was simulated by nitrogen gas. The chamber body was maintained at 300 K. A high-speed digital video camera (Phantom V.7.1., Vision Research Inc.) equipped with a prime lens (Nikkon, 60mm f/2.8D) was used to capture spray images. A signal from the fuel injection system was synchronized to the high speed camera trigger signal. The shutter speed and exposure time of the high-speed camera were set to 27027 frames per second (fps) and 2 μs for the spray test. Back lighte technic was used to capture liquid-phase of the fuel using a high intensity discharge lamp (HID Fire, HF-8500) having 85 W power.

EXPERIMENTAL RESULT

Figure 1 shows the spray images of the tested fuels at ambient temperature and pressure of 300 K and 3 MPa, respectively. The time after spray started was defined as a time aince the spray appeared from the nozzle tip. From the macroscopic images, biodiesel showed longer injection delay than diesel fuel. The reason was that higher viscosity of biodiesels inhibited needle movement and deteriorated flow characteristics [6]. To measure the liquid tip penetration length and spray angle, spray boundary was determined by selecting a threshold value in intensity. The liquid tip penetration length was defined as the distance between the nozzle tip to the farthest axial location of spray boundary. The spray angle was measured at the middle of liquid penetration length. The measured liquid tip penetration length and spray angle is shown in Fig. 2.
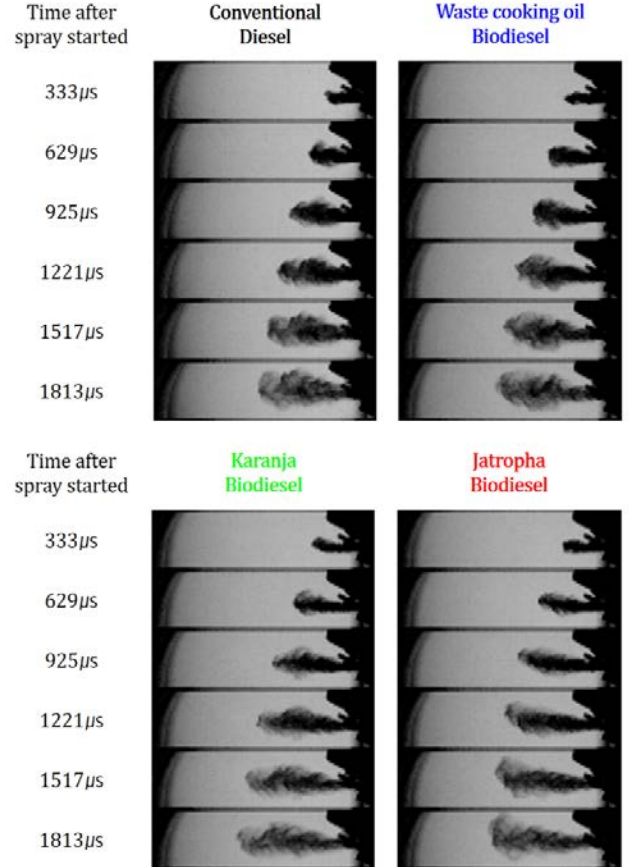

Figure 1. Macroscopic spray images of diesel, and waste cooking oil, Karanja, Jatropha biodiesels under non-evaporating conditions.

As shown in the figure, biodiesels showed longer liquid spray tip penetration length than that of diesel. This was attributed to biodiesels' higher density and viscosity. Previous study by Kook et. al., also reported that higher density of fuel induced a lower ambient air entrainment in the fuel spray [7]. Lower level of air entrainment deteriorated fuel atomization and evaporation and finally resulted in longer liquid spray tip penetration. The liquid spray tip penetration tip lengths of Karanja biodiesel, Jatropha biodiesel, and waste cooking oil biodiesel were approximately 40%, 18%, and 9% longer than baseline diesel.

The initial process of spray showed very large spray angle because the spray was not stable. The values were saturated 400 μs after spray started. The spray angle showed no significant differences according to fuels, however, the values for biodiesel were slightly smaller than that of diesel. From the previous study of Salvador et al., the characteristic mixing length and time were analyzed [8]. The results showed that the neat biodiesel fuel had higher values than those of diesel due to narrower spray cone angle. It implies biodiesels have bigger amount of loss in efficiency of air-fuel mixing process.
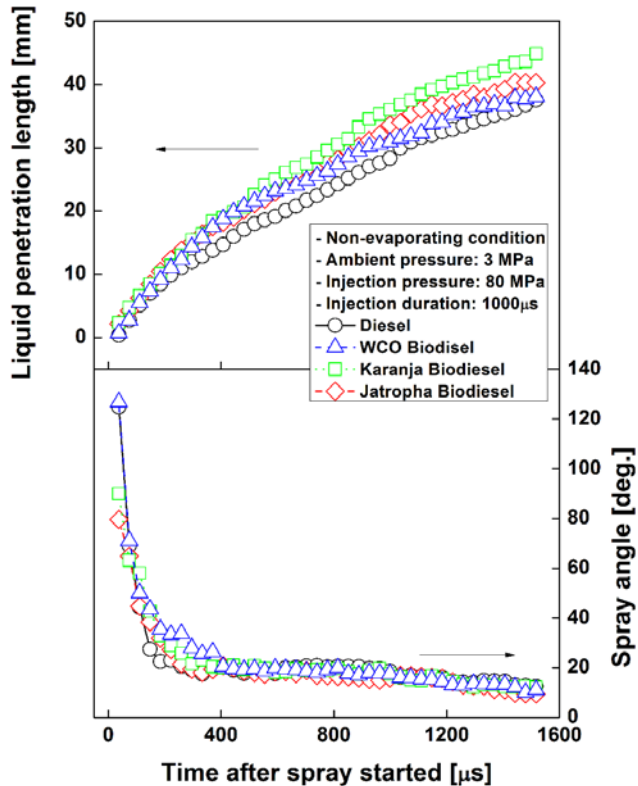
Figure 2. Liquid tip penetration length and spray angle of diesel, and waste cooking oil, Karanja, Jatropha biodiesels under non-evaporating conditions.

REFERENCES

[1] Agarwal, AK., Gupta T., and Kothari A., "Particulate emissions from biodiesel vs diesel fueled compression ignition engine", Renewable and Sustainable Energy Reviews 15:3278-300, 2011.

[2] Lahane, S., and Subramanian, KA. "Effect of different percentages of biodiesel-diesel blends on injection, spray, combustion, performance, and emission characteristics of a diesel engine", Fuel 139:537-545, 2015.

[3] Hwang, J., Qi, D., Jung, Y. et al., "Effect of injection parameters on the combustion and emission characteristics in a common-rail direct injection diesel engine fueled with waste cooking oil biodiesel", Renewable Energy, 63:9-17, 2014.

[4] Hwang, J., Jung, Y., and Bae, C., "Spray and combustion of waste cooking oil biodiesel in a compression –ignition engine", International Journal of Engine Research, 16:664-679, 2015.

[5] Can O., "Combustion characteristics, performance and exhaust emissions of a diesel engine fueled with a waste cooking oil biodiesel mixture", Energy Conversion and Management 87:676-686, 2014.

[6] Moon, S., Tsujimura, T., Gao, Y. et al., "Biodiesel effects on transient needle motion and near-exit flow characteristics of a high pressure diesel injection", International Journal of Engine Research, 1-15, 2013.

[7] Kook, S., and Pickett, LM., "Liquid length and vapor penetration of conventional, Fischer-Tropsh, coal-derived, and surrogate fuel sprays at high-temperature and high-pressure ambient conditions", Fuel, 93:539-548, 2012.

[8] Salvador, FJ., Ruiz, S., Salavert, J. et al., "Consequences of using biodiesel on the injection and air-fuel mixing processes in diesel engines", Journal of Automobile Engineering 227:1130-41, 2013.

SEEC-2017-172

MEASUREMENT AND CHEMICAL CHARACTERIZATION OF PM$_{1.0}$ IN VARIOUS MICROENVIRONMENTS INSIDE IIT KANPUR CAMPUS

Rajmal Jat
Department of Civil Engineering
Indian Institute of Technology Roorkee
Email: rajuj.dce2016@iitr.ac.in

Tarun Gupta
Department of Civil Engineering
Indian Institute of Technology Kanpur
Email: tarun@iitk.ac.in

Bhola Ram Gurjar
Department of Civil Engineering
Indian Institute of Technology Roorkee
Email: bholafce@iitr.ac.in

ABSTRACT

In this study, Assessment of indoor PM$_{1.0}$ in five different microenvironments inside the IIT-K campus was conducted with the help of single stage round nozzle, grease impaction substrate based impactor type PM$_{1.0}$ sampler during 20th February, 2010 to 13th March, 2010. The highest average concentration of PM$_{1.0}$ of the order of 141.65µg/m3 was observed in Environmental laboratory and the lowest average concentration (35.76 µg/m^3) in the computer center. Chemical speciation data for anions and elements shows the significant variation within different microenvironment. In contrast to the other anions, NO$_3^-$ was found relatively higher in all microenvironment with highest value of 35 µg/m^3 in environmental laboratory account for various chemical activities. Elements Na, Ca, Fe and K are dominated over the other trace metals.

Keywords: PM$_{1.0}$; Microenvironments; Impactor; Elements; Anions.

INTRODUCTION

Over the time, several epidemiological studies have been conducted and reported significant association between exposure to particulate matter and adverse health impact (Brook et al., 2010; Eisner et al., 2010; Holguin, 2008; Nieuwenhuijsen et al., 2013). Also, majority of air pollution studies are confined to the ambient air monitoring at some central site, certainly far from the personal level.

Based upon these type of studies ambient air quality standards are established, without considering the fact that the significant exposure to particulate matter occurs indoor, where individual spend most of their time (Clayton et al. 1993; Spengler and Sexton 1983). Health effect of indoor air pollution caused by indoor and outdoor sources are of considerable interest owing to the large exposure time into the indoor microenvironment. Therefore it is essential to assess the indoor PM in terms of chemical composition and mass concentration. Metals and ions which are easily soluble in water are quantifiable in the PM. Many trace metals may contribute toxicity to the particle which elevates the risk of respiratory and cardiovascular disease (Timonen et. al. 2002; Moshammer H. et. al. 2006). It is also evident that I/O ration is greater than 1 for PM and most of trace metals in school environment, and the most abundant elements in the PM1.0 fraction are S, Cl, and K with Zn and Pb as the dominant heavy metals (Anna Z. et al. 2011).

Therefore for better understanding of composition of indoor PM$_{1.0}$, with the help of PM$_1$ impactor, study was conducted in five selected microenvironment in IIT kanpur campus and subsequent mass composition and chemical characterization were carried out.

INSTRUMENTS AND CHEMICAL ANALYSIS

A single stage round nozzle, grease impaction substrate based impactor type $PM_{1.0}$ sampler was used which was developed by IITK itself (Gupta et al., 2009). Flow rate of the sampler was kept at 10 LPM and measured by rotameter. PTFE or Teflon filter with 46.2 mm collection diameter was used for PM_1 collection. The overall pressure drop through the sampler, including the Teflon backup filter, was 18.5 cm of water.

In analysis of PTFE filter, after pre-conditioning of filter, Gravimetric analysis was carried out for measurement of mass concentration. Subsequently, filter was analyzed for anions using Ion chromatography, and for trace metals ICP-OES (Inductively Coupled Plasma Optical Emission Spectrometry) was used.

METHODOLOGY

In this study, for measurement of $PM_{1.0}$, five different typical microenvironments Hostel room, Environment laboratory, Hall VII mess, Faculty building and Computer center were selected in IIT kanpur campus where students spent their majority of time. In order to measurement of $PM_{1.0}$, single stage $PM_{1.0}$ impactor was employed. Also, chemical analyses of impactor filters were accomplished for chemical characterization of PM_1 in different microenvironments as per the method suggested by Chakraborty A. (2009). Study was conducted from 20th February, 2010 to 13th March, 2010. During the study, each microenvironment sampled three times with sampling duration of 8 Hrs. Timing of sampling used to be from 9:00 am to 5:00 pm

RESULTS AND DISCUSSION

$PM_{1.0}$ CONCENTRATION WITHIN DIFFERENT MICROENVIRONMENTS

During the sampling of study, since each microenvironment was sampled for three times, three observation of mass concentration of $PM_{1.0}$ is associated with each microenvironment. Mass concentration of $PM_{1.0}$ is computed through gravimetric analysis, and average values corresponding to each microenvironment are presented in Table 1. It can be observed from table 1 and figure 1.1 that higher $PM_{1.0}$ mass concentration ($141.65 \mu g/m^3$) is detected in Environment laboratory which is attributed with the use of variety of chemicals in laboratory. Significant variation in the $PM_{1.0}$ value is observed at laboratory as error bar in graph is large, and this variation may be associated with the difference in the peak of experimental activity at different time.

The result of next sampling location which is a room in Hall VIII, situated at second floor with good ventilation, of $PM_{1.0}$ mass concentration shows that amount (125.23

$\mu g/m^3$) is relatively lesser than the environmental laboratory and higher than the rest of microenvironment sampled. Continuous use of Incense, twice a day, and reasonable mixing of ambient air may be the cause of this higher value. In contrast to hostal room and laboratory, minimum $PM_{1.0}$ concentrations in computer center and faculty building were detected which is caused by HVAC () system in computer center and faculty building. An average value 102.85 $\mu g/m^3$ of $PM1$ was observed in Hall VIII mess, higher than the computer center and faculty building. This is attributed to the combustion, cooking and food frying activities in the mess areas.

TABLE 1: AVERAGE PM_1 CONCENTRATION IN VARIOUS MICROENVIRONMENTS

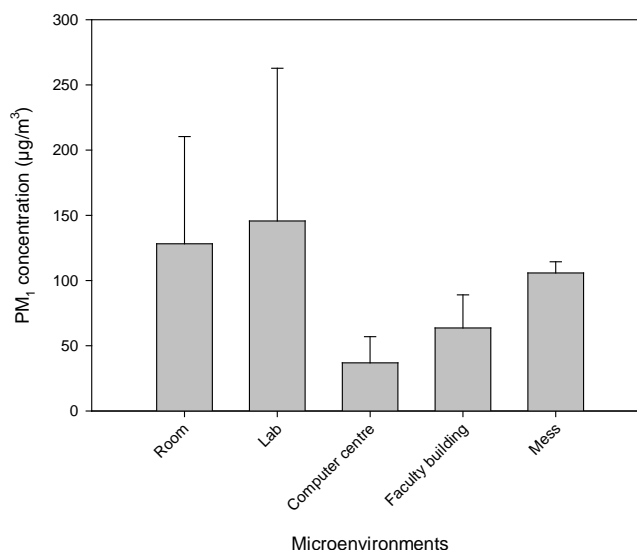| Sr. No.	Microenvironments	$PM_{1.0}$ ($\mu g/m^3$)
1	Room	125.23 ± 85.63
2	Laboratory	141.65 ± 120.54
3	Computer Center	35.76 ± 23.87
4	Faculty building	60.21 ± 27.76
5	Mess	102.85 ± 11.53

FIGURE 1.1: $PM_{1.0}$ CONCENTRATIONS WITHIN DIFFERENT MICROENVIRONMENTS

ANIONS CONCENTRATIONS WITHIN DIFFERENT MICROENVIRONMENTS

Results of anion concentration within different microenvironments are shown in Fig. 1.2. It is observed that though the analysis for all the four anions (i.e. F^-, CL^-, NO_3^- and SO_4^{2-}) was carried out of impactor filter associated with each microenvironment, only F^- was detected in hostel room and mess with the 0.7 $\mu g/m^3$ concentration. Whereas, F^-, CL^-, NO_3^- and SO_4^{2-}

were detected in all the microenvironment. Major sources of fluoride are coal burning (Safai et al. 2005). Unlike other microenvironment, higher level of NO_3^- concentration of order 35 µg/m^3 was observed in environment laboratory. This higher level of NO_3^- concentration may be associated with the use of chemical use in laboratory. Similarly, SO_4^- concentration with value of 4 µg/m^3 was found higher in faculty building as compared with the other microenvironment. At regions which are plains, sulphate is mostly anthropogenic (Pitts and Pitts 1986) due to the reaction of SO_2 on particles. Moreover, almost same concentration of Cl$^-$ ions was observed in all microenvironments. Na$^+$ and Cl$^-$ are present in sufficient amount in soil in the form of NaCl and Na2SO4 (Pitts and Pitts 1986; Parmar et al. 2001; Nair et al. 2006).
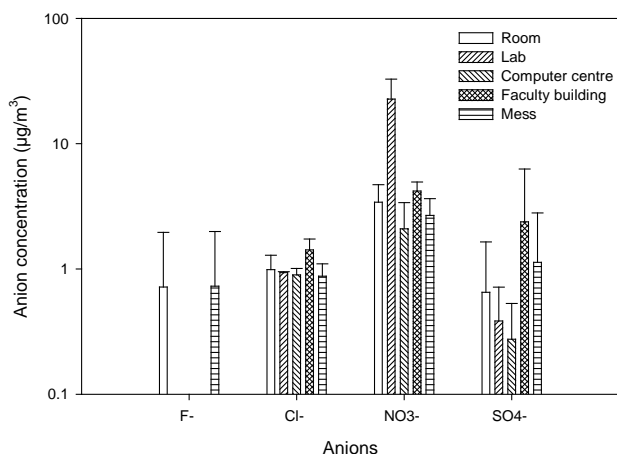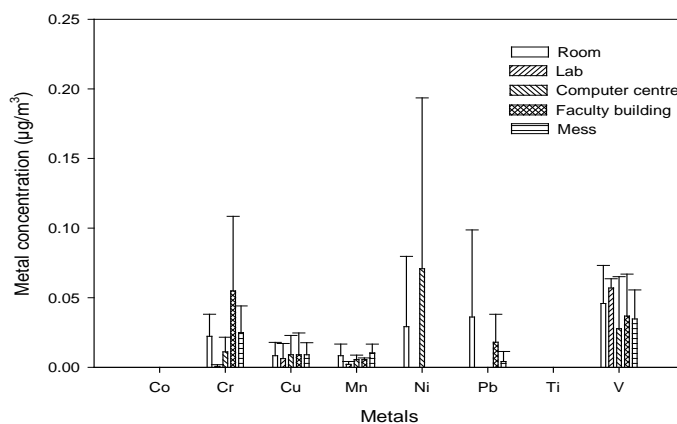

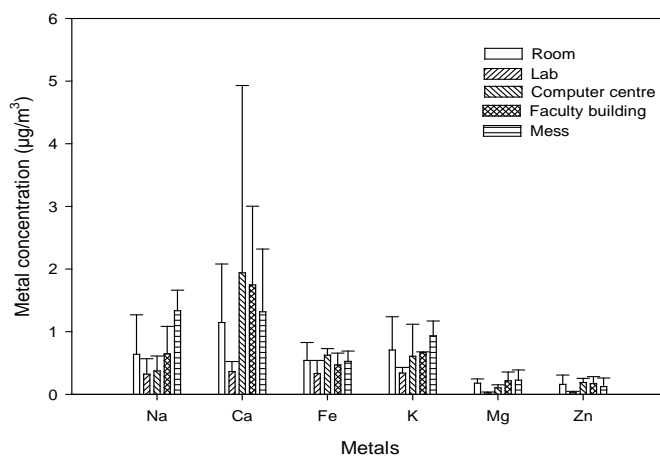FIGURE. 1.2 ANIONS CONCENTRATIONS WITHIN DIFFERENT MICROENVIRONMENTS

ELEMENTS CONCENTRATIONS WITHIN DIFFERENT MICROENVIRONMENTS

Metal concentrations in various microenvironments were observed by analysis of filter paper in ICP-OEC, and presented in Fig 1.3 (A & B). Apart from cobalt (Co) and titanium (Ti), all metals were detected in each microenvironment. However, as depicted in the graph, in comparison to Na, Ca, Fe and K rest of the metals are in negligible concentration. Higher concentrations of Ca, 1.8 µg/m^3 and 1.1 µg/m^3 were detected in faculty building and computer center respectively, and fair concentrations of Na, Fe and K were observed in these microenvironments. Ca originates as carbonates ($CaCO_3$) and sulphates ($CaSO_4.2H2O$) from soil while Mg is present in sufficient amount in soil as dolomite [($CaMg(CO_3)_2$] and illite [K(Al,Mg)$_3$SiA10(OH)] (Pitts and Pitts 1986; Parmar et al. 2001; Nair et al. 2006; Kumar et al. 2007; Anatolaki and Tsitouridou 2009). In laboratory, Na, Ca, K, and Fe concentrations were higher as compared with other metals.

Vanadium (V) concentration was observed in all microenvironments. In hostel mess, observed concentrations for both Na and Ca was 1.4 µg/m^3 and higher than the other metals.

(A)

(B)

FIGURE. 1.3 (A & B) METALS CONCENTRATIONS WITHIN DIFFERENT MICROENVIRONMENTS

CONCLUSION

In the current study, PM$_{1.0}$ mass concentration varies significantly into the various microenvironments, with highest average concentration (141.65µg/m^3) in laboratory and lowest average concentration (35.76 µg/m^3) in the computer center. Lowest average concentration in the computer center is attributed to the HVAC system. Higher average value in laboratory suggest that there is significant chemical fume originated aerosols are present which can leads to serous health hazards if exposed to the significant time period which is further evidenced by higher values of CL$^-$, NO_3^- and SO_4^{2-}. A reasonable average amount of

anions (CL^-, NO_3^- and SO_4^{2-}) and trace metals (Na, Ca, Fe and K) in all microenvironment justify the ambient mixing of $PM_{1.0}$. Cr, Cu, Mn, Mg and Zn metals are present in negligible amount.

REFERENCES

[1] Brook., R., D., Rajagopalan, S., Pope, C., A., Brook, J., R., Bhatnagar, A., Diez-Roux, A., V., 2010.Particulate matter air pollution and cardiovascular disease an update to the scientific statement from the American Heart Association. *Circulation* 121:2331–78.

[2] Eisner, M., D., Anthonisen, N., Coultas, D., Kuenzli, N., Perez-Padilla, R., Postma, D., 2010. An official American Thoracic Society public policy statement: Novel risk factors and the global burden of chronic obstructive pulmonary disease. *Am. J. Respir. Crit. Care Med.* 182:693–718.

[3] Holguin, F. 2008. Traffic, outdoor air pollution, and asthma. *Imm. Allergy Clin. North Am.* 28:577–88.

[4] Hasheminassab, S., Nancy, D., Martin, M., S., James, J., S., Ralph, J., D., Sioutas, C., 2014. Chemical characterization and source apportionment of indoor and outdoor fine particulatematter (PM2.5) in retirement communities of the Los Angeles Basin. *Science of To. Env.* 490: 528-537.

[5] Gupta, T., Mandariya, A., 2013. Sources of submicron aerosol during fog-dominated winter time at Knapur. *J. Environ Sci Pollut Res.* 20:5615–5629.

[6] Chakraborty, A., Gupta, T., 2010. Chemical characterization and source apportionment of submicron ($PM_{1.0}$) aerosol in Kanpur Region, India. *Aerosol Air Qual Res* 10 :433–445.

[7] Nieuwenhuijsen, M., J., Dadvand, P., Grellier, J., Martinez, D., Vrijheid M., 2013. Environmental risk factors of pregnancy outcomes: A summary of recent meta-analyses of epidemiological studies. *Environ. Health* 12: 1-10.

[8] Clayton, C., A., Perritt, R., L., Pellizzari, E., D., Thomas, K., W., Whitmore, R., W., 1993. Particle Total exposure assessment methodology (PTEAM) study: Distributions of aerosol and elemental concentrations in personal, indoor, and outdoor air samples in a southern California community. *J Exp. Ana. and Environ. Epide.* 3:227–250.

[9] Spengler, J., D., Sexton, K., 1983. Indoor air pollution: *A pub. health persp. Sci.* 221: 9–17.

[10] Anna, Z., Izabela, S., Maria, S., Anna, W., Alicia, N., Jerzy, Z., D., Rene V.,G., 2011. PM_{10}, $PM_{2.5}$ and $PM_{1.0}$ indoor and outdoor concentrations and chemical composition in school environment. *Ecol. Chem. And Engg*. 18:934-939.

[11] Timonen, K., L., Pekkanen, J., Tiittanen, P., Salonen, R., O., 2002. Effects of air pollution on changes in lung function induced by exercisein children with chronic respiratory sypmtoms, *Occup. Environ. Med.* 59:129–134.

[12] Moshammer, H., Hoek, G., Luttmann-Gibson, H., Neuberger, M.A., Antova, T., Gehring, U., Hruba, F., Pattenden, S., Rudnai, P., Slachtova, H., Zlotkowska, R. Fletcher, T., 2006. Parental smoking and lung function in children an international study. *Am. J. Resp. Crit. Care. Med.* 173: 1255-1263.

[13] Gupta, T., Chakrabort, A., Ujinwal, KK., 2009. Development and performance evaluation of an indigenously developed air sampler designed to collect submicron aerosol. *Annals (INAE)* 8: 189-193.

[14] Safai, P.D., Rao, P.S.P., Momin, G.F., Ali, K., Chate, D.M., Praveen, P.S., Devara, P.C.S., 2005. Variation in the chemistry of aerosols in two different winter seasons at Pune, Sinhagad, India. *Aerosol Air Qual. Res.* 5: 115–126.

[15] Pitts, B.J., Pitts Jr., J.N., 1986. Atmospheric chemistry, fundamentals and experimental techniques. *Wiley, New York*.

[16] Parmar, R.S., Satsangi, G.S., Kumari, M., Lakhani, A., Srivastav, S.S., Prakash, S., 2001. Study of size distribution of atmospheric aerosol at Agra. *Atmos. Environ*. 35: 693–702.

[17] Nair, P.R., George, S.K., Sunilkumar, S.V., Parameswaran, K., Jocab, S., Abraham, A., 2006. Chemical composition of aerosols over peninsular India during winter. *Atmos. Environ.* 40: 6477–6493.

SEEC-2017-173

VARIATION OF NON-METHANE HYDROCARBONS (NMHCS) AND AEROSOLS DURING PRE-MONSOON AT AN EASTERN COASTAL SITE IN INDIA

Aiswarya Patra
Environment and Sustainability Department, CSIR-Institute of Minerals and Materials Technology, Bhubaneswar-751013, India.

Upasna Panda
Environment and Sustainability Department, CSIR-Institute of Minerals and Materials Technology, Bhubaneswar-751013, India.

Boopathy Ramasamy
Environment and Sustainability Department, CSIR-Institute of Minerals and Materials Technology, Bhubaneswar-751013, India.
chemboopathy@gmail.com

Trupti Das
Environment and Sustainability Department, CSIR-Institute of Minerals and Materials Technology, Bhubaneswar-751013, India.

ABSTRACT

The concentration of C_2-C_5 light hydrocarbons was studied along with particulate matter (PM) concentration before the onset of monsoon at an eastern coastal urban location in the state of Odisha. Among the eight different NMHCs, concentration of n-pentane was observed to be maximum, followed by i-pentane and propane. Concentration of ethane was found to be the lowest. The study also gives an overview of the variations in the concentrations of $PM_{2.5}$ and PM_{10} before onset of monsoon and further indicates that the pollutant concentration is influenced by local meteorology.

Keywords: Non-methane hydrocarbons; Particulate matter; Aerosol.

INTRODUCTION

Due to the rapid economic growth and drastic increase in the numbers of automobiles and industries in and around Bhubaneswar, an upcoming urban location in the eastern coastal belt of India, air pollution issues are on rise. It is now well known that most of the atmospheric trace gases and aerosols have a strong impact on global climate, air quality and human health. The presence of specific trace gases in the atmosphere contribute to the generation of both fine aerosol and photochemical oxidants such as ozone (O_3) (Atkinson, 2000). Aerosols and O_3 have direct effects on human health through respiratory inflammation, on climate change through modification of direct and indirect radiative budgets and on regional ecosystems through oxidation and changes in nutrient balance (Andreae and Crutzen, 1997).Non-methane hydrocarbons (NMHCs), considered as surface O_3 precursors, are found throughout the earth's atmosphere, and emitted from a vast array of sources both man-made and natural.

Long term observations at Bhubaneswar have depicted a winter maxima of most of the atmospheric pollutants including O_3 and particulate matter. In the present study an attempt has been made to study the concentration of NMHCs and Particulate Matter ($PM_{2.5}$ and PM_{10}) in the ambient air of Bhubaneswar city before the onset of monsoon.

SAMPLING SITE

The sampling site is on the roof (at a height of 30m from ground level) of CSIR-Institute of Mineral and Material Technology, Bhubaneswar (21º15' N, 85º15' E). Bhubaneswar (419 km²) is

the capital of Odisha state. It is situated at an altitude of 45 m a.s.l. and is considered to be one of the fastest growing cities in the eastern part of the country. The average population density of the city is about 2000 people/km^2. The average temperatures of the city ranges between a minimum of around 10°C during winter to a maximum of 40-45°C during summer. The city has a population of 1.2 million and the nearest major city is Kolkata, ~440 Km away towards north. The sampling equipment is placed around 200 meters away from National Highway (NH-5) dominated by vehicular emissions and is surrounded by small townships (approximately within 100 km) where various coal based thermal power plant, mining and fertilizer based industries are operational. Besides that many small scale industries are located in the vicinity of the city. The site is 50 km from east from Bay of Bengal and also frequently under the influence of incoming air from IGP (Indo-Gangetic plain) region which is considered to be one of the most polluted regions in India. Based on the distinct climate conditions the weather of Bhubaneswar may be grouped in four different seasons of the year like pre-monsoon (March-May), monsoon (June-Aug), post-monsoon (Sept-Nov), and winter (Dec-Feb) and receives annually maximum solar radiation during pre-monsoon followed by post-monsoon and winter.

METHODOLOGY
Ambient air was collected through a Sensidyne low flow sampler (model LFS-113D) into a PerkinElmer make Air-toxic tube containing solid adsorbent for trapping NMHCs. The samples were collected between morning 10:00 am to evening 6:00 pm in every alternate hour, twice a week, during the month of May-June 2016 for the analysis of 8 light (C$_2$-C$_5$) species namely ethane (C$_2$H$_6$), ethylene (C$_2$H$_5$), propane (C$_3$H$_8$), propylene (C$_3$H$_6$), n-butane (C$_4$H$_{10}$), acetylene (C$_2$H$_2$) and pentanes (C$_5$H$_{12}$). Sampling was stopped during Saturdays for maintenance and calibration of the instrument.

PM$_{2.5}$ sampling was carried out using a fine Particulate Sampler (M/s: Polytech India Ltd.) at a constant flow rate of 16.7 LPM during the same period using quartz microfiber (QMA-47 mm) filter papers which were pre-baked (at 550^0 C in muffle furnace) and were desiccated for 24 hrs before measuring the initial weight (before sampling) and final weight (after sampling) using a Sartorius Semi-micro balance CPA225D with $\pm$0.01mg readability. Similarly PM$_{10}$ sampling was carried out using another Particulate Sampler (M/s: Envirotech APM) at a constant flow rate of 1.5 LPM during the same time as that of PM$_{2.5}$. The samples were collected on Whatman QMA filter paper (8X10 ins) with a pore size of 1.6 microns.

ANALYTICAL TECHNIQUES
Air samples of 3600 ml has been passed through the air toxic tube and were analyzed by a Gas Chromatography (GC) equipped with a Thermal Desorption system (Turbo Matrix TD) and flame ionization detector (FID) (GC-TDS, PerkinElmer Clarus_480) was used for the detection of 8 light NMHCs. Elite-Alumina capillary column (30 m length 0.53 mm diameter) used for NMHCs analysis. High purity Helium (He) gas was used as carrier. The details about working principles and analytical procedure have been discussed elsewhere (Panda et al. 2015). Calibrations of individual NMHCs were performed using standard gases (NIST traceable standard gases provided by the Linde USA).

RESULTS AND DISCUSSIONS
Eight different types of NMHCs (C$_2$-C$_5$) were measured before the onset of monsoon at Bhubaneswar. It was observed that the average total NMHCs concentration was 0.882 ± 0.368 µg/m^3. During this period of study n-pentane and i-pentane were found to be the most abundant hydrocarbons in the urban atmosphere of Bhubaneswar followed by ethylene and propylene. During the period of observation the average concentration of the eight different light hydrocarbons were found in the following sequence:n-pentane>i-pentane> Ethylene> propylene>n-butane> propane> aetylene>

ethane. Since ambient air sampling is being done in the premises of CSIR-IMMT, which is an analytical laboratory where solvent extraction work is prevalent, presence of i-pentane and n-pentane is believed to have been predominantly influenced by the same along with vehicular emissions. Similarly widespread use of Liquefied petroleum Gas (LPG) for cooking purposes is believed to be the source for propane and butane in the NMHC mixture. However Propylene, Ethylene and Acetylene were believed to have originated from vehicular exhaust.

The total average concentration of $PM_{2.5}$ was found to be 30.21 µg/m^3 and the total average concentration of PM_{10} was found to be 65.20 µg/m^{3}during the sampling days. It was observed that the concentration of $PM_{2.5}$ and PM_{10} were much influenced by the local meteorological conditions. During this
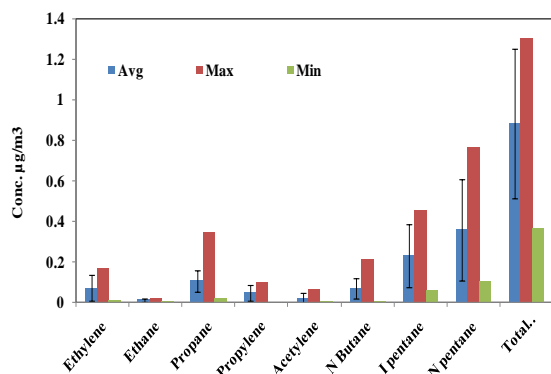
period of the year, since the wind pattern is mostly Southwest in direction, the air mass travelling to Bhubaneswar is believed to be cleaner in comparison to winter months when polluted air mass travel to the site from Indo-Gangtic plains and the western part of India (Mahapatra et al. 2014).

CONCLUSIONS

The study shows that vehicular emissions as well as local meteorological conditions have an impact on the pollutant load in this urban location. 8 different species of NMHS were detected with highest concentration of n-pentane. $PM_{2.5}$ PM_{10} as well as NMHCs concentrations studied before unset of monsoon, were observed

to be comparatively lower than that of the winter months.

REFERENCES

[1] Atkinson R. (2000), Atmospheric chemistry of VOCs and NOx, *Atmospheric Environment*, **34**, 2063-2101.

[2] Andreae M.O. and Crutzen P.J. (1997), Atmospheric aerosols: Biogeochemical sources and role inAtmospheric chemistry, *Science*, **276**, 1052-1058.

[3] UpasanaPanda, P. S. Mahapatra, Trupti Das (2015) Study of C2–C5 Non-methane Hydrocarbons and Their Ozone Formation Potential at Bhubaneswar, an Eastern Coastal Site in IndiaMAPAN-Journal of MetrologySociety of India. DOI 10.1007/s12647-015-0134-4

[4] P. S. Mahapatra, S. Panda, P. P. Walvekar, R. Kumar, T. Das B. R. Gurjar, Environ Sci Pollut Res. 2014. Seasonal trends, meteorological impacts, and associated health risks with atmospheric concentrations of gaseous pollutants at an Indian coastal city DOI 10.1007/s11356-014-3078.

SEEC-2017-174

EMERGING NEW ALTERNATE FUELS FOR I.C. ENGINES: A REVIEW

Anmesh Kumar Srivastava
Research Scholar, Mechanical Engineering department
MNIT Jaipur
Email: anmesh.k.srivastava@gmail.com

Shyamlal Soni, Dilip Sharma
Professor, Mechanical Engineering department
MNIT Jaipur
Email: shyamlalsoni@gmail.com,
sharmadmnit@gmail.com

ABSTRACT

Energy demand of the world is increasing progressively. The two imperative issues world currently facing are the depletion of fossil fuels and its environmental impact. Since these fossil fuels are the major source of energy being utilized by the human race, hence the energy demand depends on availability of the fossil fuels. So it has become necessary to look for alternate fuels for sustainable development since internal combustion (I.C) engines will continue to dominate automotive sector and can be used in power generation in near future.

New fuels like Ammonia, Biobutanol, Dimethyl and Diethyl Ether, water based emulsions and Acetylene have a great potential to act as future alternate fuels for I.C engines and can play a vital role in mitigating the energy crises. This paper briefly reviews the literature on the above mentioned new alternate fuels, their feasibility and their applications in Internal Combustion Engines.

Keywords: Alternate fuels, I.C engines, Performance, Emissions.

NOMENCLATURE
BTE   Brake Thermal Efficiency
BSEC   Brake Specific Energy Consumption
EGT   Exhaust gas Temperature
EGR   Exhaust Gas Recirculation
CO   Carbon Monoxide
CO_2 Carbon Dioxide
C_2H_2 Acetylene
CH_4 Methane
HC   Hydrocarbon

INTRODUCTION
Currently, more than 85% of our energy is supplied from fossil resources which are fast depleting. In this regard depletion of fossil fuel reserves, energy scarcity, global warming, and increase in pollutants in atmosphere are matters of great concern today. Internal Combustion (I.C) Engines have become a major factor in transforming and organizing social life as these are the prime movers of automobiles and also used in stationary applications such as power generation. Both diesel and gasoline which are used as fuel for I.C engines are obtained from fossil reserves. As the fossil fuels are depleting, there is an urgent need to discover alternate fuels which will have reduced impact on the atmosphere and has renewable source of energy. In spite of their distinct properties, these fuels can be used in I.C engines by applying various techniques and can be utilized in the form of blends with diesel/biodiesel, in dual fuel mode and as a sole fuel. Alternate fuels promise sustainable development, energy conservation, efficiency and environment preservation. Alternate fuels like biodiesels, methyl alcohol, ethyl alcohol, biogas, hydrogen and producer gas have proved themselves as successful fossil fuel substitutes for internal combustion engine. It is expected that biodiesel is utilized as a petroleum diesel substitution and that ethanol is utilized as a gasoline replacement. The cost of oil and gas has increased relentlessly in the course of the last number of years. Specialists foresee that oil supply will last for few decades only [1]. Increasing demand of fossil fuel is endangering the survival and sustainability of life support system.

New fuels like Ammonia, Biobutanol, Dimethyl and Diethyl ether, water based emulsions and Acetylene,

1

likewise have a potential to go about as future alternative fuels for IC engines and are discussed as below.

AMMONIA

Ammonia will also be regarded as a carbon-free fuel and is one of the world's most synthesized chemical substances. It can be produced from renewable resource and has a well-established infrastructure. Ammonia (NH_3) combustion with air does not produce CO_2 emissions although it has got a lot less attention. It can be simply liquefied and stored under moderate pressure and can be produced with the aid of electrolysis, solid-state synthesis, and solar thermochemical synthesis from renewable source [2]. Ammonia offers some additional advantages such as commercial availability and viability, global distribution network, easy handling experience, etc., though its toxicity may be seen as a challenge [3].

Ammonia when used in CI engine indicated that the favorable operating range using the present dual-fuel approach requires 40–60% diesel fuel energy. Increasing the amount of ammonia produced longer ignition delays and resulted in lower peak combustion pressures. It was found that if the energy substitution by ammonia is less than 40%, NO emissions using the dual-fuel operation are lower than those using 100% diesel fuel. CO and HC emissions were higher using the dual-fuel operation when compared to diesel fuel only operation. Soot emissions increased for low ammonia fueling but decreased for high ammonia fueling [4]. Results of simulations studies showed the opportunity to achieve Diesel-like power densities and efficiencies, and load control by quantity of fuel injected, with critical component the availability of high pressure fuel injection systems specifically developed for NH_3 [5].
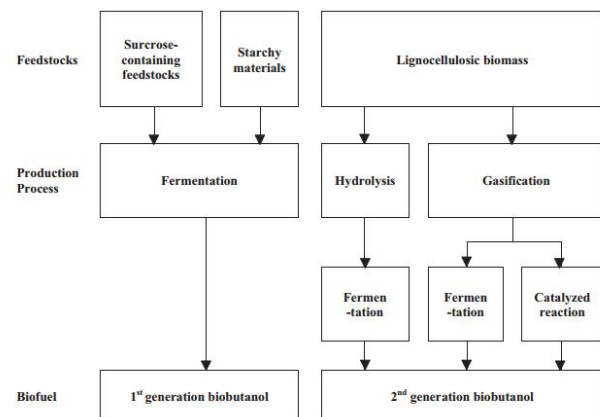
BIOBUTANOL

Butanol has a higher cetane number (CN) of 25 and a higher energy content than ethanol fuel. Butanol can be produced by fermentation of biomass, such as corn, algae, and other plant materials containing cellulose. Butanol is a primary alcohol with a molecular formula of C_4H_9OH, so it is an oxygenated fuel. In comparison to ethanol fuel, butanol has a lower volatility, lower ignition temperature, and a higher flash point. Therefore, biobutanol would be a more suitable alternative fuel than ethanol. alcohol-based biofuels and can be applied without changing the fuel supply system in a diesel engine, if they are mixed with diesel fuel at a low mixing ratio [6].

On combustion ethanol and butanol fuels derived from plant resources do not produce additional CO_2 emissions as plants absorb carbon dioxide during growth. Smoke and CO emissions can be reduced in case of various blends of butanol and diesel fuel [7].

Biobutanol is traditionally produced by acetone-butanol- ethanol (ABE) fermentation with Clostridium spp. A biological route of ABE fermentation typically involves four basic steps such as feedstock selection, pretreatment, detoxification, and fermentation [8].

Figure 1. shows the production process of biobutanol, the first generation bio-butanol can be produced by ABE fermentation of hexose sugars derived through hydrolysis of starch-rich crops such as maize, wheat, rice and cassava. The lignocellulosic biomass used in the fermentation of the second generation biobutanol includes barley, liquor silage, glycerol, rice straw, oil palm truck fiber, crude cellulose, spoilage, and palm fruits.Microalgae and macroalgae are the promising feedstocks of the third generation biobutanol [9].

FIGURE 1. FEEDSTOCK AND PRODUCTION PROCESS OF BIOBUTANOL[9]

Being a biofuel, butanol blends at higher concentration can be used without retrofitting vehicles, it has higher energy density, has the ability to dissolve in vegetable oils at any ratio. In internal combustion it can be used as an additive [10].

DIMETHYL ETHER & DIETHYL ETHER

Diethyl ether (DEE) is a biofuel as it can be produced from ethanol via a dehydration process using acid catalysts .Similarly, dimethyl ether (DME) can be produced from the dehydration of methanol. However, the DEE is a liquid fuel at the ambient temperature, which makes it more suitable than the DME, which is a gaseous fuel, to be used as a fuel additive for diesel engines without modifications. The diethyl ether (DEE) is a renewable oxygenated fuel, can be used as a fuel additive for the diesel engines due to its favorable characteristics. It was found that using the DEE as a fuel additive improved the engine performance

significantly for the most of engine load conditions [11]. DEE has favorable properties for application in diesel engines, such as higher cetane number (>125), moderate energy density, higher O_2 content in its structure, lower auto-ignition temperature, prolonged flammability and improved miscibility with diesel [12]. Diesel + DEE15 combination showed the highest BTE and lowest BSFC, HC, CO, CO_2 emissions and smoke generation as compared to $FeCl_3$ - diesel and standard diesel mode [13].

Dimethyl-ether (DME) is an attractive alternative to conventional diesel fuel for compression ignition (CI) engines. DME can be produced from a variety of feed-stocks such as natural gas, coal or biomass; and also can be processed into valuable co-products such as hydrogen as a sustainable future energy. Traditionally, DME has been produced from syngas in a two-step process in which methanol is produced from syngas, purified, and then converted to DME in another reactor. The indirect synthesis method follows the chemical reaction given in Eqn.(1)

INDIRECT SYNTHESIS METHOD

$$2CH_3OH \rightarrow CH_3OCH_3 + H_2O \qquad (1)$$
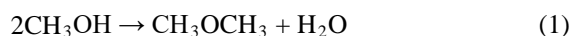
DIRECT SYNTHESIS METHOD

The direct synthesis of DME from syngas containing H_2, CO and CO_2 follows mainly two overall reactions: Eqn. (2) with water–gas shift reaction taken into account and Eqn. (3) without it.

$$3CO + 3H_2 \rightarrow CH_3OCH_3 + CO_2 \qquad (2)$$

$$2CO + 4H_2 \rightarrow CH_3OCH_3 + H_2O \qquad (3)$$
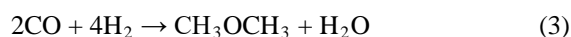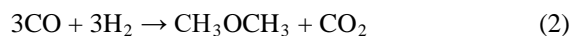
For using DME fuel in automotive vehicles, injector design, fuel feed pump, and the high-pressure injection pump have to be modified, combustion system components, including sealing materials, have to be rigorously designed [14].

WATER BASED EMULSIONS

Diesel water emulsion is found to be most suitable fuel due to reduction in particulate matter and NOx emission, besides that it also improves the brake thermal efficiency. Emulsification is the process of mixing the two immiscible phases by reducing the stress between those phases. It can be formed by the addition of water as the dispersed phase within a continuous diesel fuel phase leading to the formation of diesel water emulsion with the addition of surfactants. Surfactants are added to lower the interfacial tension between the water phase and the diesel fuel phase and to stabilize the water droplet phase within the diesel fuel phase to avoid the coalescence mechanism of the water phase [15].

Water diesel (W/D)emulsion fuel does not require any modification of the engine. Generally, emulsions are divided into two types: oil-in-water emulsion (O/W) and water-in-oil emulsion (W/O). The O/W emulsion is where the oil is located in the internal phase presented as a dispersed droplet and the water is presented as a continuous phase, whereas for the W/O emulsion, it is the opposite. The O/W emulsion is not suitable to be an alternative fuel. This is due to the large amount of water that might come into direct contact with the cylinder-piston group and fuel feed system, which will result in failure of the fuel combustion. The W/O emulsion fuel is the most suitable and widely used as the alternative fuel for fueling compression ignition engines [16].

Adding small amounts of water, 2%, to neat diesel fuel produced a significant increase in the engine power in C.I. engine. Engine torque and noise emission were comparable with those of neat diesel fuel. The higher water addition to diesel decreased the engine power and torque [17].

ACETYLENE

Acetylene is the simplest member of unsaturated hydrocarbons called alkynes or acetylenes. Researchers are proposing the use of acetylene as an alternative fuel which could replace the conventional fossil fuel in the near future. Production of acetylene involves following reaction when produced with calcium carbide as shown in Eqn.(4) and Eqn.(5) [18].

$$CaCO_3 + C \text{ (graphite)} \longrightarrow CaC_2 \qquad (4)$$

$$CaC_2 + H_2O \longrightarrow Ca(OH)_2 + C_2H_2 \qquad (5)$$
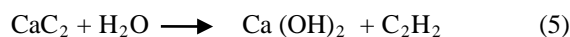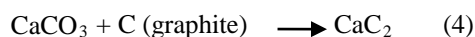
The second method is by thermal cracking of hydrocarbons or partial combustion of methane with oxygen. Acetylene has a very wide flammability range, and minimum ignition energy is required for ignition since the engine can run in lean mode with higher specific heat ratios leading to increased thermal efficiency. It has higher flame speed and hence faster energy release.

Acetylene aspiration results came with a lower thermal efficiency reduced Smoke, HC and CO emissions, when compared with baseline diesel operation [19].The brake thermal efficiency in dual fuel mode was lower than diesel operation at full load, as a result of continuous induction of acetylene in the intake. It was suggested that by applying certain techniques like, Timed Manifold Injection, Timed Port Injection the thermal efficiency can be improved with a reduced NOx emissions level [20]. On using acetylene in single cylinder stationary CI engine at compression ratio of 20, injection pressure 210 bar and injection timing of 23^0 btdc, experimental results showed the highest brake thermal efficiency of 25.09% and lowest BSEC at the flow rate of 120 litres per hour (LPH) for dual fuel mode

compared to the diesel mode. In dual fuel mode CO, HC and Smoke emissions were lower while NOx emission was higher compared to the neat diesel operation [21].

CONCLUSION

Today, the internal combustion engine fuelled by fossil fuel powers the vast majority of the world's vehicles. From the above literatures it is found that Ammonia, Biobutanol, Diethyl and Dimethyl ether, water based emulsions and Acetylene are emerging alternative fuels that offer opportunities for significant emission reductions and increment in efficiency of I.C. engines. Also, new methods and trends in fuel and engine modification will pave way to further decrease in emission.

REFERENCES

[1] Niamh M. Power, Jerry D. Murphy, 2009 "Which is the preferable transport fuel on a greenhouse gas basis; biomethane or ethanol?". Biomass and Bioenergy 33, pp. 1403–1412

[2] Christopher W. Gross, Song-Charng Kong, 2013. "Performance characteristics of a compression-ignition engine using direct-injection ammonia–DME mixtures", Fuel 103 pp. 1069–1079.

[3] C. Zamfirescu, I. Dincer, 2009. "Ammonia as a green fuel and hydrogen source for vehicular applications", Fuel Processing Technology 90 pp. 729–737.

[4] Aaron J. Reiter, Song-Charng Kong, 2011 "Combustion and emissions characteristics of compression-ignition engine using dual ammonia-diesel fuel", Fuel 90 pp. 87–97.

[5] A Boretti, 2016 "Novel dual fuel diesel-ammonia combustion system in advanced TDI engines" international journal of hydrogen energy . http://dx.doi.org/10.1016/j.ijhydene.2016.11.208

[6] Hyuntae Yun, Kibong Choi, Chang Sik Lee, 2016 "Effects of biobutanol and biobutanol–diesel blends on combustion and emission characteristics in a passenger car diesel engine with pilot injection strategies", Energy Conversion and Management 111 pp. 79–88.

[7] Mingfa Yao, Hu Wang, Zunqing Zheng, Yan Yue, 2010. "Experimental study of n-butanol additive and multi-injection on HD diesel engine performance and emissions", Fuel 89 pp. 2191–2201.

[8] Manisha A. Khedkar, Pranhita R. Nimbalkar, Shashank G. Gaikwad, Prakash V. Chavan, Sandip B. Banka, 2017."Sustainable biobutanol production from pineapple waste by using Clostridium acetobutylicum B 527: Drying kinetics study", Bioresource Technology 225 pp. 359–366.

[9] Soo-Young No, 2016."Application of biobutanol in advanced CI engines – A review", Fuel 183 pp. 641–658.

[10] B. Bharathiraja, J. Jayamuthunagai, T. Sudharsanaa, A. Bharghavi, R. Praveenkumar,M. Chakravarthy, D. Yuvaraj, 2017. "Biobutanol – An impending biofuel for future: A review on upstream and downstream processing tecniques", Renewable and Sustainable Energy Reviews 68 pp. 788–807.

[11] Amr Ibrahim, 2016. "Investigating the effect of using diethyl ether as a fuel additive on diesel engine performance and combustion", Applied Thermal Engineering 107 pp. 853–862.

[12] Harish Venu, Venkataramanan Madhavan, 2017. "Influence of diethyl ether (DEE) addition in ethanol-biodiesel-diesel (EBD) and methanol-biodiesel-diesel (MBD) blends in a diesel engine", Fuel 189 pp. 377–390.

[13] Pragyan P. Patnaik, Shakti P. Jena, Saroj K. Acharya, Harish C. Das, 2017. "Effect of FeCl3 and diethyl ether as additives on compression ignition engine emissions", Sustainable Environment Research, doi: 10.1016/j.serj.2017.01.002.

[14] Su Han Park, Chang Sik Lee, 2014. "Applicability of dimethyl ether (DME) in a compression ignition engineas an alternative fuel", Energy Conversion and Management 86 pp. 848–863.

[15] P. Baskar, A. Senthil Kumar, 2016."Experimental investigation on performance characteristics of a diesel engine using diesel-water emulsion with oxygen enriched air", Alexandria Eng. J. , http://dx.doi.org/10.1016/j.aej.2016.09.014

[16] Ahmad Muhsin Ithnin, Hirofumi Noge, Hasannuddin Abdul Kadir, Wira Jazair, 2014. "An overview of utilizing water-in-diesel emulsion fuel in diesel engine and its potential research study", Journal of the Energy Institute, http://dx.doi.org/10.1016/j.joei.2014.04.002

[17] Mohammad Reza Seifi, Seyed Reza Hassan-Beygi, Barat Ghobadian, Umberto Desideri, Marco Antonelli, 2016. "Experimental investigation of a diesel engine power, torque and noise emission using water–diesel emulsions", Fuel 166 pp. 392–399.

[18] Price WH, 2006. An Acetylene cylinder explosion: A most probable cause analysis. Eng fail anal pp 705-715.

[19] G.Nagarajan, T.Lakshmanan. 2010 "Experimental Investigation on Dual Fuel Operation of Acetylene in a DI Diesel Engine, Fuel Processing Technology 91 pp 496-503.

[20] T.Lakshmanan, G.Nagarajan. 2009 "Performance and Emission of Acetylene-aspirated diesel engine, Jordan journal of mechanical and industrial engineering. 3(2) , June.

[21] Proceedings, First International Conference on Recent Innovations in Engineering and Technology (ICRIEAT-2016), December 22-23, 2016 Hyderabad. Anmesh Kumar Srivastava, S.L.Soni, Dilip Sharma, "Performance & Emission Analysis Of Diesel - Acetylene Fuelled Single Cylinder C.I. Engine", ISBN: 978-1-5396-2645-9.

SEEC-2017-175

HUMAN HEALTH RISK DUE TO PM$_{10}$ IN 18 STATE CAPITAL CITIES OF INDIA

Mohit Tyagi
Department of Civil Engineering
IIT Roorkee
Email: mohittyagi4792@gmail.com

Bhola Ram Gurjar
Department of Civil Engineering
IIT Roorkee
Email: bholafce@iitr.ac.in

ABSTRACT

This study estimates human health risk due to PM10 in 18 most populated state capitals of India. Study uses Ri-MAP model and data from CPCB, Census of India and WHO recommendations as model inputs to estimate excess mortality due to existing PM$_{10}$ concentrations. Results show that excess mortality follows an increasing trend in Bangalore, Chandigarh, Hyderabad, Kolkata, Lucknow, Ranchi and Mumbai while decreasing trend in Delhi and Patna. New Delhi, Mumbai, Bangalore, Kolkata, Lucknow, Hyderabad and Jaipur were amongst the worst 5 cities in terms of estimated excess mortality for the study period 2010 to 2012. Highly urbanized and densely populated cities were worst affected.

***Keywords:** PM$_{10}$, mortality, risk, health, exposure.*

INTRODUCTION

Air pollution has been known for long to cause adverse human health effects. Due to increase in population, high energy demand, large number of industries, and growing number of vehicles, cities are facing immense environmental pollution. Therefore, inhabitants of cities are essentially vulnerable to air pollution-induced unfavorable health impacts like Cardiovascular mortality (CM), Respiratory mortality (RM), Chronic obstructive pulmonary disease (COPD), etc. (Gurjar et al., 2008; Molina & Molina, 2004). Such risk needs to be estimated to help the pollution control authorities to ensure the sustainability of city life (Maji et al., 2016).

Considering the long-term impacts of air pollution, several cohort studies found evidence of an impact on mortality of exposure to particulate matter (Brunekreef et al. 2010; Gurjar et al. 2010; Nagpure et al. 2014). Long term human health effects also depend on physiology and health of exposed population. Some groups – for example senior citizens, children, pregnant women and people with an underlying disease, such as asthma – may be at higher risk, and may develop more severe health effects more quickly when exposed to air pollution (WHO Regional Office for Europe, 2016). In addition, certain groups may be exposed to higher levels of outdoor air pollution, e.g. people living near busy traffic routes or those in specific occupational or socioeconomic groups (WHO Regional Office for Europe, 2005).

The risk of air pollution to health in a population is usually represented by a concentration–response function, which is typically based on Relative Risk (RR) estimates derived from epidemiological studies. The RR estimate describes the likelihood of an adverse health outcome (e.g. premature death, heart attack, asthma attack, emergency room visit, hospital admission) occurring in a population exposed to a higher level of air pollution relative to that in a population with a lower exposure level (WHO Regional Office for Europe, 2016).

This study focuses on human health risk due to Particulate Matter of size less than 10 micron also known as PM$_{10}$. The study area encompasses 18 most populated state capitals of India. People in these urban conglomerations are facing both short term and long term exposure to PM$_{10}$. Seasonal episodes of dangerously high

concentrations occur frequently in winters like in case of New Delhi and surrounding areas where Particulate concentrations were worst in the world after diwali festival.

METHODOLOGY

This study uses Ri-MAP (Risk of Mortality/ Morbidity due to Air Pollution) model which gives quantitative health risk due to a pollutant exceeding threshold concentrations by providing excess incidence and mortalities caused by the prevailing pollutant concentrations. This model has been previously used in India by (Nagpure et al. 2014) for New Delhi and (Maji et al. 2016) for 10 cities of Maharashtra.

The model takes input parameters such as city's population under consideration, the annual average concentration of pollutant in that city (average daily concentration if studying short term effects), baseline incidence of health effects in population of the city and relative risk to a particular health effect based on epidemiological studies. All these parameters are used in the concentration-response equations of the model to get excess incidence and excess mortalities caused to prevalent air quality. The concentration response equations used along with terminology is as follows

$$RR(c) = ((C – T)/10) * (RR- 1) + 1 \qquad (1)$$

$$AP = ((RR(c) - 1) * P(c)) / RR(c) * P(c) \qquad (2)$$

$$IE = I * AP \qquad (3)$$

$$NE = IE * N \qquad (4)$$

$$INE = I – IE = I * (1- AP) \qquad (5)$$

$$\Delta I(c) = (RR(c) – 1) * P(c) * INE \qquad (6)$$

$$\Delta N(c) = \Delta I(c) * N \qquad (7)$$

C = Measured annual average concentration of pollutant

T = Threshold limit of pollutant annual average concentration

RR = Relative risk for health outcome in category c of exposure

RR(c) = Changed Relative risk for the health outcome in category c of exposure

P(c) = Proportion of population in category c of exposure

I = Baseline frequency of selected health outcome

IE = Rate attributed to exposure in population

N = Size of Population

NE = No. of cases attributed to exposure

INE = Frequency of Outcome in population free from exposure

$\Delta I(c)$ = Excess incidence

$\Delta N(c)$ = Excess no. of cases

RESULTS AND DISCUSSION

The epidemiological data used is that recommended by World Health Organization (WHO).

TABLE 1: WHO DEFAULT RELATIVE RISK PER 10 $\mu g/m^3$ OF INCREASE OF DAILY AVERAGE CONCENTRATION OF PM_{10} AT 95% CONFIDENCE INTERVAL AND BASELINE INCIDENCE PER 100000

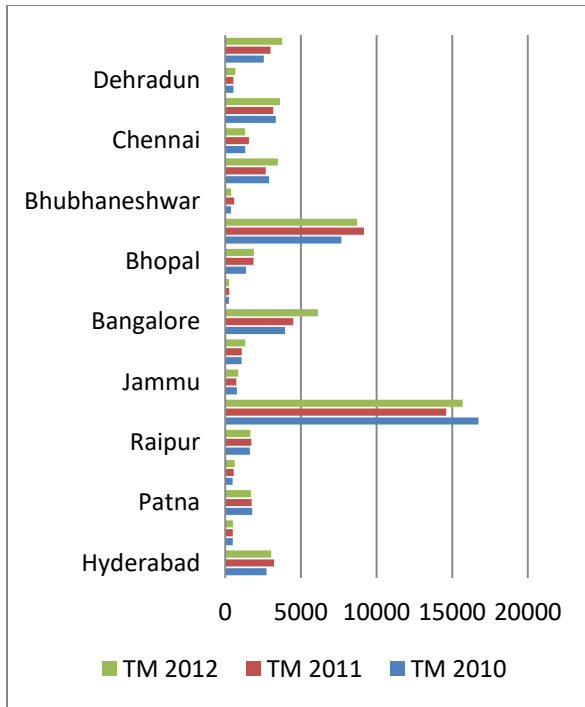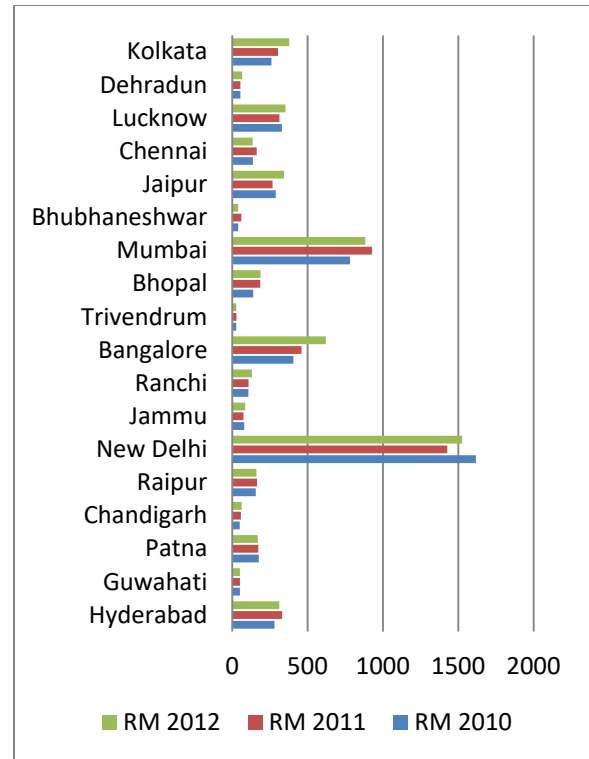| Pollutant	Mortality	Relative Risk	Baseline Incidence per 100000
PM 10	Total	1.0074	1013
	Cardiovascular	1.008	497
	Respiratory	1.012	66

FIGURE 1: ESTIMATED EXCESS TOTAL MORTALITY

FIGURE 2: ESTIMATED EXCESS CARDIOVASCULAR MORTALITY
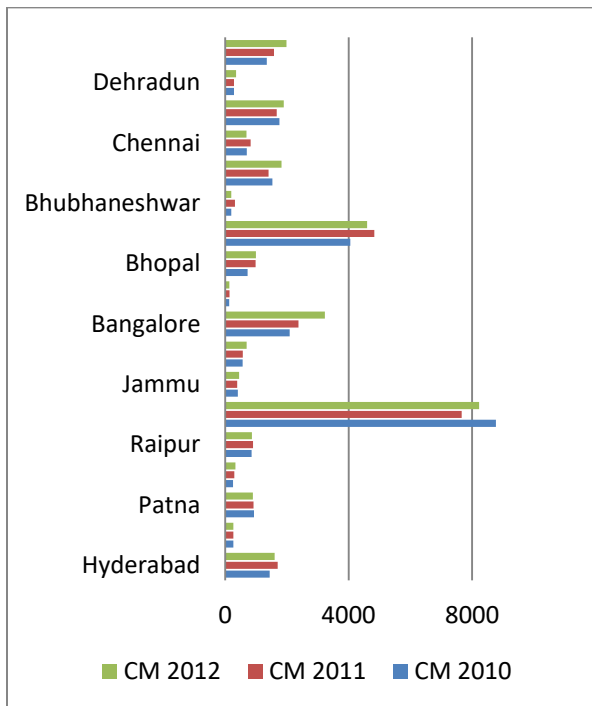

FIGURE 3: ESTIMATED EXCESS RESPIRATORY MORTALITY

As per the model calculations highly urbanized and densely populated cities like New Delhi, Mumbai, Bangalore, Kolkata, etc are at high risk and show highest estimated mortalities. The estimated mortalities in the period 2010-2012 showed somewhat increasing trend for Kolkata, Lucknow, Jaipur, Mumbai, Bhopal, Bangalore, Ranchi and Hyderabad. These cities are densely populated and measures to curb air pollution may not have been effectively implemented.

The study is a concise but inclusive application of modeling air pollution health risk. Basic challenges faced during air pollution studies are deficiency of extensive data and its reliability. In such circumstances preceding air pollution studies in Indian context have been region specific. This study however attempts at giving a simplified and robust approach to air pollution studies.

There are a number of methodological uncertainties that limit the accuracy of this approach giving scope for future improvements. In particular:

➢ The risk estimates are based on cohort studies conducted in the United States.

- The model does not take into account synergistic effects of multiple pollutants.
- It is unclear whether a threshold concentration exists for particulate matter below which health effects are insignificant.
- Road dust and windblown crustal material might skew results towards excess mortality
- Parameters specific to age, exposure, etc are not available
- Megacity residents are exposed to multiple risk factors, and it needs to be studied how different risks compete or add. For example, air pollution also enhances the probability of traffic accidents when visibility is low.

This is a step towards informed policy decision making in Indian context that has been acknowledged and utilized worldwide with different parameters and models. Such studies when enriched with more data parameters giving age group specific information of health, separate impact parameters for residential, industrial and indoor exposure, etc would make these estimates highly accurate. Nevertheless within range of confidence interval the future predictions would have been fairly accurate in the past studies.

ACKNOWLEDGMENT

REFERENCES

[1] Gurjar B.R., Butler T.M., Lawrence M.G., Lelieveld J., 2008. "Evaluation of emissions and air quality in megacities", Atmospheric Environment, Vol. 42, pp 1593–1606.

[2] Molina, M. J., & Molina, L. T., "Megacities and atmospheric pollution", Journal of the Air & Waste Management Association, 2004, Vol. 54, pp 644–680

[3] Maji K.J., Dikshit A.K., Deshpande A., "Human health risk assessment due to air pollution in 10 urban cities in Maharashtra, India", Cogent Environmental Science,2016

[4] Brunekreef B., 2010. "Air Pollution and Human Health: From Local to Global Issues". Procedia Social and Behavioral Sciences, Vol. 41, pp 6661–6669

[5] Gurjar B.R., Jain A., Sharma A., Agarwal A., Gupta P., Nagpure A.S., Lelieveld J., 2010. "Human health risks in megacities due to air pollution". Atmospheric Environment, Vol. 44, pp 4606-4613.

[6] Nagpure A.S., Gurjar B.R., Martel J., "Human health risks in national capital territory of Delhi due to Air Pollution", Atmospheric Pollution Research 2014, Vol. 5 , pp 371-380.

[7] European Environment and Health process, 2016. Health risk assessment of air pollution – general principles, WHO, Copenhagen: WHO Regional Office for Europe.

[8] WHO, Global update 2005. WHO Air quality guidelines for particulate matter, ozone, nitrogen dioxide and sulfur dioxide Geneva: World Health Organization Press.

[9] Gurjar B.R., Aardenne J.A.V., Lelieveld J., Mohan M., 2004. "Emission estimates and trends (1990–2000) for megacity Delhi and implications". Atmospheric Environment, Vol. 38, pp 5663–5681.

[10] Open Government Data (OGD) Platform India, https://data.gov.in/catalog/city-and-location-wise-ambient-air-quality, retreived on 10 Aug 2016

SEEC-2017-176

PERFORMANCE EVALUATION OF A PRACTICAL SCALE DOWN-FLOW HANGING SPONGE PROCESS FOR TREATMENT OF MUNICIPAL SEWAGE

Komal Jayaswal[*]
Department of Civil Engineering
IIT Roorkee
Email: *jayaswal.komal@gmail.com*

Naoki Nomoto
Department of Energy and Environment Science
NTU

Veerendra Sahu
Department of Civil Engineering
IIT Roorkee

Bhola Ram Gurjar
Department of Civil Engineering
IIT Roorkee

Absar Ahmed Kazmi
Department of Civil Engineering
IIT Roorkee

Hideki Harada
New Industry Creation Hatchery Center
Tohoku University

ABSTRACT

A down-flow hanging sponge (DHS) reactor has been developed for post treatment of up-flow anaerobic sludge blanket (UASB) reactor for treating municipal sewage. DHS reactor is an unaerated, aerobic, biofilm reactor consists of polyurethane sponge material as a support medium, offering excellent pollutant removal capability. A practical scale DHS reactor was constructed at a municipal sewage treatment plant in India. Profile analysis was conducted at different organic load and flow rate conditions. Results showed that DHS reactor exhibited excellent performance in terms of organic matter and ammonia removal. Thus practical scale DHS reactor performance shows its applicability as a post treatment to developing country.

Keywords: Municipal sewage treatment, Downflow hanging sponge process (DHS), Organic removal, Up-flow Anaerobic Sludge Blanket (UASB).

INTRODUCTION

Down-flow hanging sponge (DHS) reactors have been developed as a low-energy-consumption sewage treatment technology for developing countries [1-6]. The DHS system is based on conventional trickling filter process filled randomly with polyurethane sponge as a packing media for biomass retention. DHS process does not require external aeration as dissolved oxygen is naturally supplied from atmosphere thus lowering energy consumption during the process. Microorganisms retained on the sponge medium remove organic matter and ammonium nitrogen from the wastewater. Various sewage treatment experiment has been conducted including bench and full-scale reactors in Japan and India using several types of sponge media. And the results showed that the combination of an up-flow anaerobic sludge blanket (UASB) reactor followed by treatment with a DHS reactor is a viable option for sewage treatment in developing countries [1-8]. Analysing and investigating water quality parameter of 15 different UASB- FPU based STP's in India and found out that this system is not efficient to remove organic matter, ammonium nitrogen and pathogens to meet desired Indian effluent discharge standards. So to understand practical approach of DHS as a post treatment for UASB [9].

The aim of this study was to elucidate the mechanisms of the removal of organic matter and ammonium in a practical-scale DHS reactor under various influent load, temperature and dissolved oxygen condition with a practical scale DHS reactor in India along the vertical height of DHS reactor.

MATERIALS AND METHODS

UASB-DHS Reactor

A practical scale DHS reactor was constructed at 78 MLD, municipal sewage treatment plant in Agra, U.P state, India. The sewage treatment plant was comprised of screen, grit channel, UASB reactor and FPU (Final polishing Unit). A small volume of UASB effluent was

used as an influent for DHS reactor. For proper supply of oxygen to the inside of reactor, ventilation windows were incorporated in the reactor wall. The height of first sponge layer is 200 mm and 600 mm for second to fourth layer. The sponge media which is the carrier of biomass, has cylindrical hexagonal shape having 40 mm and 25 mm in length and width respectively.
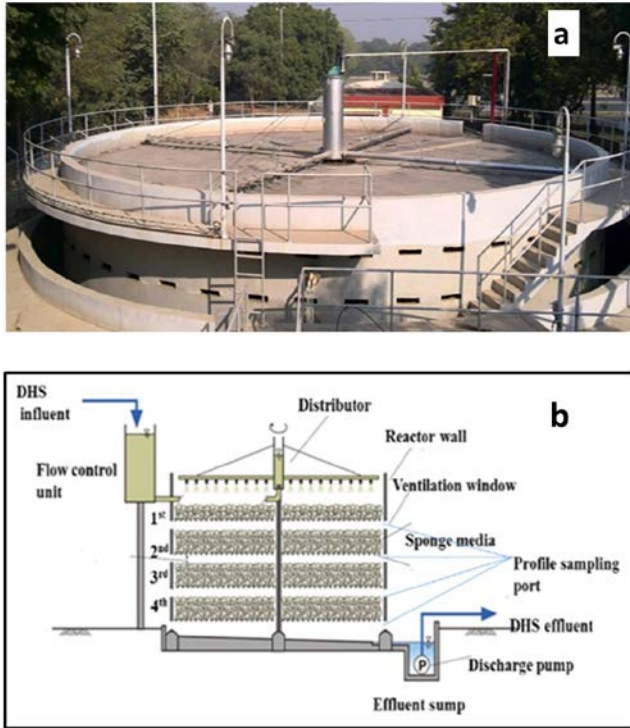
Figure 1 (a) Photograph of DHS reactor (b) Schematic diagram of DHS reactor

A photograph and schematic diagram of the DHS reactor is shown in Fig. 1(a,b). The DHS reactor consisted of a cylindrical structure made up of concrete that is 16 m in diameter and 2.7m in height. It is composed of polyurethane material, covered by plastic net made up of polyethylene to prevent distortion of sponge structure. Centre part of sponge media consist of a hole for uniform oxygen transfer. This study was conducted for DHS influent at three different flow rate that is 5,000 m^3 day^{-1}, 3,000 m^3 day^{-1} and 1,000 m^3 day^{-1}.

Sampling And Analysis

Performance of UASB-DHS system were analyzed using grab samples from 12 different sampling points along the vertical and horizontal directions of DHS reactor. Water samples were taken from sampling port located at four vertical layer and in each layer, ports were located at 2m (inner), 4m (middle), 6m (outer) layer from centre of reactor in a horizontal direction. Profile analysis was conducted for three different flow rate 5,000 m^3 day^{-1}, 3,000 m^3 day^{-1} and 1,000 m^3 day^{-1}.

The parameter analyzed were DO, BOD, COD$_{Cr}$ and NH$_3$-N. All of the other analytical procedures were conducted according to the standard method. Dissolved oxygen (DO) was measured by the Winkler method [10], while COD$_{Cr}$ and NH$_3$-N were determined using the potassium dichromate method and the Nessler method respectively, using a DR5000 water quality analyzer (HACH).

RESULTS AND DISCUSSIONS

Organic Matter Removal Characteristics

Results of profile analysis for different flow rate conditions has been shown in (Fig.2). Results of profile analysis of 388th, 439th and 574th days were compared for different organic loading rate and flow rate conditions. The flow rate were 3800 m^3 day^{-1}, 2600 m^3 day^{-1} and 900 m^3 day^{-1} whereas organic load were 2.58 Kg COD m^3 day^{-1}, 2.26 Kg COD m^3 day^{-1} and 1.48 Kg COD m^3 day^{-1} for these days respectively. DHS influent temperature were almost same for 388th and 439th days that is 31°C, but for 574th day it was 23°C.
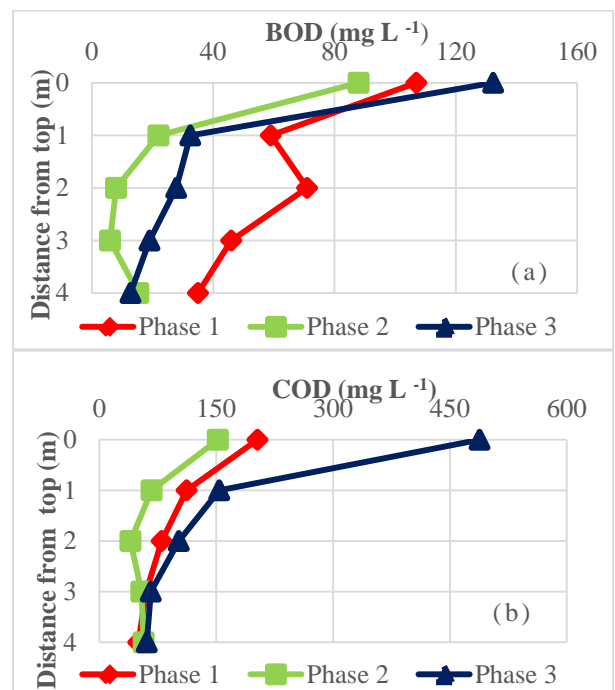
Figure 2. (a) and 2 (b) Total BOD and COD profile along the vertical length of DHS reactor at 388th day (Phase 1), 439th day (phase 2) and 574th day (Phase 3).

Summary of influent and effluent characteristics has been shown in table 1 for different organic load and flow rate conditions.Comparing the results of all three phase in terms of organic matter removal for 439th and 574th day organic

load and flow rate were lower in compare to 388th and as reactor volume were same. So HRT increases for 439th day provided consistent removal of BOD along the reactor height. On 574th in spite lower organic load, the influent BOD and COD_{Cr} concentration was high in compare to other two days but results showed maximum removal of organic matter in

TABLE 1. SUMMARY OF DHS REACTOR PERFORMANCE DURING SAMPLING TIME

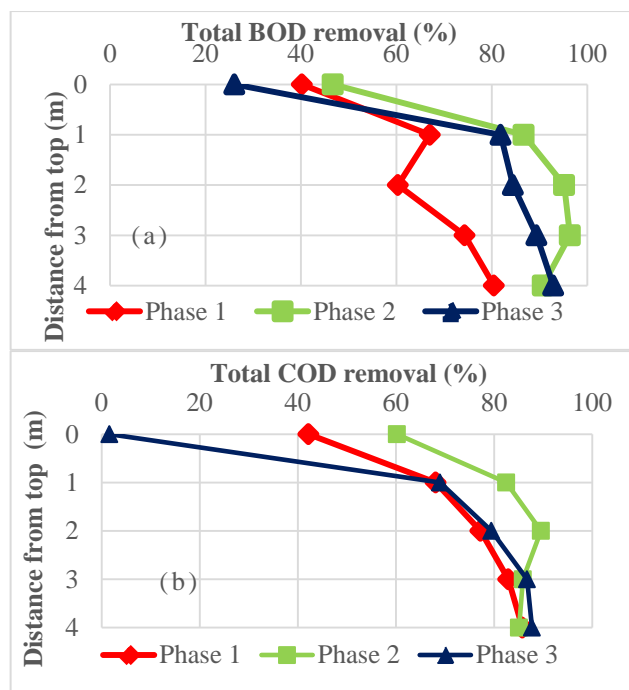| Parameters	Units			
Sampling time	days	388th	439th	574th
DHS loading rate	kg-COD_{Cr} m^{-3} day^{-1}	2.58	2.26	1.48
DHS flow rate	m^{-3} day^{-1}	3800	2600	900
Temperture	℃	30.4	31.1	23
Total BOD influent	mg L^{-1}	107	88	132
Total BOD effluent	mg L^{-1}	35	15	13
Total COD influent	mg L^{-1}	203	152	488
Total COD effluent	mg L^{-1}	54	57	61
NH_3-N influent	mg L^{-1}	32	26.9	44
NH_3-N effluent	mg L^{-1}	20.5	4.6	7

Figure 3.(a) and 3(b) Total BOD and COD removal percentage along the vertical length of DHS reactor at 388th day (Phase 1), 439th day (phase 2) and 574th day (Phase 3).

the first layer of DHS reactor. Therefore this results showed that organic matter removal takes place not only due to aerobic biological degradation but also due to adsorption on sponge media. Various studies were conducted about profile analysis for full scale DHS reactor [7-8]. The studies showed that organic matter concentration variations depends on incoming sewage and performance of UASB reactor.

Figure 3(a) showed total BOD removal % for phase 1, 2 and 3 along the reactor height. On 388th day removal % for BOD was around 80%, on 439th and 574th day it was around 90%. This result might be due to low organic load condition on 439th and 574th day provided better removal percentage for BOD. To understand COD_{Cr} removal fig 3 (b) showed gradual removal of COD_{Cr} along the reactor height and removal % for all three phase was around 85%. As discussed above COD_{Cr} concentration does not varied much on 439th day after 2nd layer of DHS reactor caused not much removal. For on 574th day initial COD_{Cr} concentration was quite high that was around 488 mg L^{-1}. That value was highest among three phases.

Ammonia Nitrogen Removal Characteristics

NH_3-N and DO concentration along the reactor height has been shown in Fig 4. (a) and 4 (b). On 388th day NH_3-N concentration decreased from lower half of reactor mainly due to high COD concentration in the first layer of DHS that was 112 mgL^{-1}. However on 439th day due to low organic load condition NH_3-N was removed from 1st layer and concentration of DHS effluent was around 5.4 mg L^{-1}. Amount of NH_3-N removal observed at first and second layer is quite small for 388th day this might be due to high organic load condition present on first layer that suppresses the growth of autotrophic bacteria [11]. Maximum removal of NH_3-N takes place in the last layer of reactor due to presence of autotropic bacteria that converts NH_3-N to NO_3-N in the presence of oxygen. On the contrary at 439th day, NH3-N was removed from 1st layer as due to less influent load condition that caused the growth of nitrifers that allowed degradation of NH_3-N to NO_3-N in first layer, provided maximum ammonia removal and better nitrification. On comparing 574th day results shows that amount of NH3-N removed from first layer is not much, this might be due to high BOD and COD_{Cr} influent concentration that does allow ammonia oxidation and other reason might be high influent ammonia concentration that was 43 mg L^{-1} that value was quite high in compare to other days. Maximum removal took place in 2nd layer due to less COD_{Cr} load. The final effluent

concentration were 19.8, 5.4 and 7.1 mg L^{-1} for 388th, 439th and 574th day respectively.
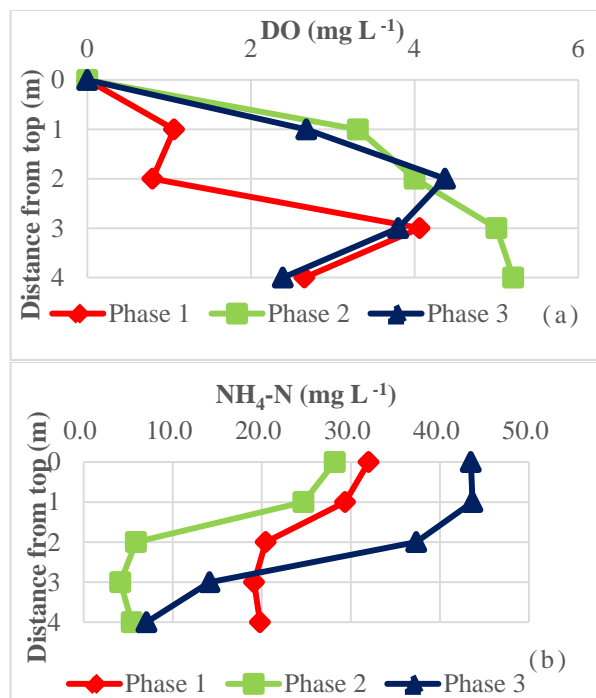
Figure 4. (a) and 4 (b) DO and NH$_4$-N profile along the vertical length of DHS reactor at 388th day (Phase 1), 439th day (phase 2) and 574th day (Phase 3).

CONCLUSION

A practical scale DHS reactor exhibited high performance with regards to organic matter and ammonia nitrogen removal. Results showed that almost half of the organic matter were removed in first layer, provided around 80% removal along the reactor height, followed by NH$_3$-N removal in 3rd and 4th layer of reactor, layer. The performance of reactor was attributed to its distinctive characteristics like high DO uptake, dense sludge retention and adequate sludge activity in sponge media.

ACKNOWLEDGMENTS

REFERENCES

[1] Agrawal, L.K., Ohashi, Y., Mochida, E., Okui, H., Ueki, Y., Harada, H. and Ohashi, A., 1997. 'Treatment of raw sewage in a temperate climate using a UASB reactor and the hanging sponge cubes process. *Water Science and Technology"*, *36*(6-7), pp.433-440.

[2] Machdar, I., Sekiguchi, Y., Sumino, H., Ohashi, A. and Harada, H., 2000. Combination of a UASB reactor and a curtain type DHS (downflow hanging sponge) reactor as a cost-effective sewage treatment system for developing countries. *Water Science and Technology*, *42*(3-4), pp.83-88.

[3] Tawfik, A., Ohashi, A. and Harada, H., 2006. Sewage treatment in a combined up-flow anaerobic sludge blanket (UASB)–down-flow hanging sponge (DHS) system. *Biochemical Engineering Journal*, *29*(3), pp.210-219.

[4] Tandukar, M., Uemura, S., Ohashi, A. and Harada, H., 2006. Combining UASB and the "fourth generation" down-flow hanging sponge reactor for municipal wastewater treatment. *Water science and technology*, *53*(3), pp.209-218.

[5] Tandukar, M., Ohashi, A. and Harada, H., 2007. Performance comparison of a pilot-scale UASB and DHS system and activated sludge process for the treatment of municipal wastewater. *Water Research*, *41*(12), pp.2697-2705

[6] T, Onodera; M, Tandukar; D, Sugiyama; S, Uemura; A, Ohashi; and H, Harada; 2014 Development of a sixth-generation down-flow hanging sponge (DHS) reactor using rigid sponge media for post-treatment of UASB treating municipal sewage. Bioresour. Technol., vol. (152), pp.93-100.

[7] Okubo, T., Onodera, T., Uemura, S., Yamaguchi, T., Ohashi, A. and Harada, H., 2015. On-site evaluation of the performance of a full-scale down-flow hanging sponge reactor as a post-treatment process of an up-flow anaerobic sludge blanket reactor for treating sewage in India. *Bioresource technology*, *194*, pp.156-164.

[8] Okubo, T., Kubota, K., Yamaguchi, T., Uemura, S. and Harada, H., 2016. Development of a new non-aeration-based sewage treatment technology: performance evaluation of a full-scale down-flow hanging sponge reactor employing third-generation sponge carriers. *Water Research*, *102*, pp.138-146.

[9] Sato, N., Okubo, T., Onodera, T., Ohashi, A. and Harada, H., 2006. Prospects for a self-sustainable sewage treatment system: A case study on full-scale UASB system in India's Yamuna River Basin. *Journal of Environmental Management*, *80*(3), pp.198-207.

[10] American Public Health Association, 2005. Standard Methods 21st ed., Washington, DC.

[11] Tandukar, M., Uemura, S., Machdar, I., Ohashi, A. and Harada, H., 2005. A low-cost municipal sewage treatment system witha combination of UASB and the "fourth-generation" downflow hanging sponge reactors. *Water science and technology*, *52*(1-2), pp.323-329.

SEEC-2017-177

EXPERIMENTAL STUDIES FOR POTENTIAL APPLICATION OF DIMETHYL ETHER (DME) FOR C. I. ENGINE

A.B.KOLEKAR
Assistant Professor, Department of Technology, Shivaji University, Kolhapur, Maharashtra, India
abk_tech@unishivaji.ac.in

A.B. Datye
Professor, Department of Technology, Shivaji University, Kolhapur, Maharashtra, India
abk_tech@unishivaji.ac.in

C. H. Bhosale
Professor, Department of Physics, Shivaji University, Kolhapur, Maharashtra, India
abk_tech@unishivaji.ac.in

A. S. Joshi
Assistant Professor, Department of Technology, Shivaji University, Kolhapur, Maharashtra, India
aditya3909@gmail.com

ABSTRACT

Vitality is a fundamental contribution for social and financial improvement of any nation and enhancing personal satisfaction. The interest for petroleum items in India has been expanding at a rate higher than the expansion in residential accessibility. In the meantime there is expanded weight on the outflow control through intermittently fixed directions especially for urban communities. In the wake of this circumstance there is an earnest need to advance utilization of option fields as substitute for diesel motors. Diesel motors are the principle prime movers for open transportation vehicles, stationary power era unit and for agrarian applications. In any case, diesel motors are significant giver of different sorts of poisons, for example, particulate matter (PM), carbon monoxide (CO), oxides of nitrogen (NOₓ) and other hurtful mixes. The twin issues of both consumption of rare assets and climatic contamination brought on by vehicles keep running on petro items are alluring to locate a reasonable and prompt contrasting option to fossil fills. Dimethyl ether (DME) is a substitution fuel that is produced from fossil feedstock including common gas and coal and in addition from renewable feedstock and waste. From the present research think about outcomes in generous lessening of unburnt carbons (HC), CO and particulate matter (PM) contrasted with outflows from diesel. The real fumes contaminations both unburnt hydrocarbons and nitrogen oxides are ozone exhausting or brown haze shaping antecedents. The utilization of DME fuel brings about diminishment of unburnt hydrocarbon amid ignition. In light of motor testing, utilizing the most stringent emanations testing technique, the general ozone shaping capability of the guessed hydrocarbon discharges from DME fuel was almost half not as much as that deliberate for diesel. Test work is completed to picture the possibility of utilizing DME fuel under shifted exploratory conditions particularly with accentuation on moderating air contamination.

Keywords: dimethyl ether (DME), elective fuel, air contamination,
.

SEEC-2017-178

MICROALGAE: A SOLUTION TO DEBATABLE ISSUES ASSOCIATED WITH THE ENERGY CROPS FOR PRODUCTION OF BIOFUELS

Richa Katiyar

Centre for Transportation Systems, Indian Institute of Technology Roorkee - 247667, Uttarakhand, India
Email: katiyar.richa10@gmail.com

B. R. Gurjar

Department of Civil Engineering and Centre for Transportation Systems, Indian Institute of Technology Roorkee - 247 667, Uttarakhand, India
Email: bholafce@iitr.ac.in

ABSTRACT

The emergent demand of transportation fuels and its finite reservoirs have motivated scientific communities to produce alternative renewable fuels including biofuels. The biomass is considered as one of the sophisticated resource for production of bioenergy/biofuels, which contributes toward environment friendly outcomes. Earlier the biofuels wer produced from energy based crops (food and non food crops), which exerts intricacy on available land and food resources. To resolve these negative impacts, researchers have investigated the use of microalgae as an energy resource for production of biofuels. Microalgae have the capability to produce high oil (more than 300 times) than other such energy resources for example terrestrial plants. Additionally, microalgae can use non arable/fertile soil, low cost feed stocks such as wastewater for their cultivation, which delivers cost effectiveness. As a result, the usage of microalgae for biofuel production doesn't affect the agriculture land resource and drinking water balance in the environment.

Keywords: **Bioenergy, Transportation, Biomass, Renewable energy, Oil.**
.
INTRODUCTION

The limited supply of fossil fuels for transportation and aftermath negative environmental effects of fossil fuel combustion has turned researchers to identifying the most promising naturally occurring species, which execute as a feedstock for bioenergy/biofuels production. In recent years, the biofuel (alternative fuel) is gaining global

attention due to its positive attributes include its non toxic, biodegradable and renewable fuel nature. Earlier, the biofuel production was done using energy crops (food and non food energy), such as corn, maize and Jatropha. But later on the production of biofuels from energy crops was criticized because growing plants for biofuel production exerts pressure on land, and water. For instance, the oil palm crop would require 24% of total arable land area of USA for producing 50% of transport fuel (Chisti 2007).

To retrieving the solutions associated with the use of energy crops for production of biofuel, the idea is shifted toward the use of lignocellulosic biomass, waste materials (used vegetable oil) and biomass based microorganisms including microalgae. The use of biomass from bacteria, yeast and microalgae for production of biofuels plays an important role (Chisti 2007; Schenk et al. 2008). A wide range of positive aspects has shifted the focus toward microalgae biomass, which is the naturally occurring species, uses biochemical factories and photosynthetic machinery similar as higher plants for production of energy and intermediates products such as terpenes. The photosynthetic efficiency, product accumulation rate, growth rates of microalgae is notably higher than other crops (Pirt 1986). Microalgae can also utilize waste water and non cultivable land for their cultivation. Thus, the use of microalgae does not entail a reduction in food production and cultivable land, since it neither requires farmland nor fresh water for their cultivation.

MICROALGAE

Microalgae are microscopic unicellular plants like structure, without having leaf, steam and roots, commonly

found in natural and marine water. The biodiesel is considered as most promising renewable product from microalgae that has the potential to displace petroleum based transportation fuel without adversely affecting the supply of food, water and other crops product. The oil-rich microalgae can be selected and processed into biodiesel, with the left over biomass further reprocessed to produce bioethanol (biofuel). Hence, a single cell (microalgae) can produce two different forms of biofuels in same cycle. The significant research efforts are in progress to develop new cheaper waste feeds stocks such as waste pulp of fruits, which could contribute to the long term supply of biodiesel in future.

OIL CONTENT AND PRODUCTS OF MICROALGAE

The high lipid production is the first essential step for producing biofuels from microalgae. Some species of microalgae produce up to 60% of their cellular mass as triacylglycerols (TAGs) or oil or lipid bodies, under suitable growth conditions, which further processed to produce biodiesel (biofuel). Microalgae can also produce up to 300 times more oil per acre than conventional crops, such as rapeseed, palms, soybeans, or jatropha (TABLE 1). The important aspect of using microalgae, unlike other oil producing crops includes higher photosynthetic efficiency and less doubling time than other biomass producing plants. Microalgae can double their population within 24 hr to few days (1-10). In fact few species of microalgae can be grown with 3-4 hrs, during exponential growth phase.

Additionally, microalgae also produce number of sustainable byproducts for future industries. One of the most significant metabolic products of microalgae is polyunsaturated fatty acids (PUFAs), which is an essential fatty acid for human diet. Fish oil are famous because it contains high quantity of PUFAs, fishes accumulate PUFAs content by consuming microalgae in aquaculture. The other metabolic products of microalgae include caretenoide, phycocolloids and terpenes, which has powerful applications in pharmaceutical industries (Rawat et al., 2011; Tapiero et al., 2004).

TABLE 1: Oil content of microalgae and other terrestrial crops (adapted from Katiyar et al., 2016)

Serial No.	Oil producers	Oil yield (liters per hectare)
1.	Microalgae	1,00,000
2.	Castor	1413
3.	Palm	5366
4.	Safflower	779
5.	Jatropha	741
6.	Canola	974
7.	Corn/maize	172

WASTE WATER FOR CULTIVATION OF MICROALGAE

The use of wastewater produced from industries, domestic households, paper mills and sewage has high source of nutrients such as carbon in the form of reducing and non reducing sugars and organic and inorganic forms of nitrogen and phosphorous (Shen et al. 2015). Microalgae have potential to use both organic and inorganic forms of carbon, nitrogen and phosphorus from waste water for their growth with simultaneously treating it (Hena et al. 2015; Briggs, 2004). It has estimated that approximately 1.2 billion gallons of biodiesel can be produced from waste feed stocks in the USA per year (Worldwatch, 2008). Additionally, the use of waste water instead of drinking water for cultivation of microalgae may provide cost effective results and increase the drinking water balance in the environment. Different species of microalgae have different removal efficiency for different pollutants present in the waste water, such as *Chlorella* debaryana removes 88.1% of total nitrogen and 53.6% of total phosphate from swine waste water (Hasan, 2014). *Scenedesmus*. sp. of microalgae removes 98% of total nitrogen and phosphate from secondary effluent (Xin et al. 2010). Hence, microalgae can utilize waste water efficiently with simultaneously treating it at low cost.

SOLUTION TO FOOD VERSUS FUEL DEBATE AND SHRINKAGE OF CROPPING LAND

The utilization of cropping land area to grow the crops for energy generation is the main drawback associated with the use of first and second generation biofuels producing resources, e.g. U.S.A has consumed about 220 trillion liters of diesel in 2010, to fulfill this demand of alternative fuel from soybean may require approx. 367 Mha (million hectares) cropping land, while 178Mha land is only available for cropping out of 930Mh total land area of U.S.A. (USEIA, 2012). Microalgae based biofuels production have thus emerged as a partial solution to these problems (Singh et al. 2011), because, different species of microalgae has ability to grow in a wide range of environmental stress (Katiyar et al., 2016). Microalgae can be grown on arid land, land with excessively saline soil, fire forest land and drought land. Added advantage includes, the fertility of soil also increases after cultivation of microalgae.

Another problem associated with use of energy crops for production of biofuel is genesis of the food v. fuel debate. The causes the rapid rise in prizes of food crops such as corn, maize, barley, soyabeans etc due to its quantum conversion into feedstock for production of biofuels. The food crops production has increased three times, since 1961, and then meets to the increasing population of humans, the per capita production of food crops stand at 350 kg in 2007. Human and livestock consumption leaves approx. 17% of the grain for conversion to ethanol and other fuels globally (Srinivasan, 2009). Rajagopal et al. (2007) stated that a large-scale energy plantation is likely to encourage the structural change in agriculture and variability in farmer's incomes. Hence, to resolving these negative repercussions of using energy crops for production of biofuel, scientists have explored microalgae without any compromise with food resource for the production of biofuel, this will also not adversely affect the prizes of food.

CONCLUSIONS

In the last few decades the production of biofuels from energy crops have initiated a number of controversial issues such as food versus fuel debate, shrinkage in land and water resources. The biofuels production using micro algal cells, grown on non-arable land with use of waste water, have emerged as an answer to these debates. The capability of microalgae to produce high oil makes them promising alternative resource for biofuel production. Wastewater treatment and use of various waste streams for cultivation of algae reduces the environmental burdens. More research and developments are required to establish a cost effective industrial scale production of microalgae based biofuels.

ACKNOWLEDGMENT

REFERENCES

[1] Briggs, Michael (2004). Wide scale Biodiesel Production from Algae. Archived from the original, 2006. Publisher, UNH Biodiesel Group (University of New Hampshire).

[2] Christi, Y. 2007. Biodiesel from Microalgae, Journal of Biotechnology Advances 25, 294-306.

[3] Hasan, R., 2014. Bioremediation of swine wastewater and biofuel potential by using Chlorella vulgaris, Chlamydomonas reinhardtii, and Chlamydomonas debaryana. Journal of Environmental Biotechnology 5(3), 175–180.

[4] Hena, S., Fatimah, S. and Tabassum, S. 2015. Cultivation of algae consortium in a dairy farm wastewater for biodiesel production, Water Resource Industry 10, 1–14.

[5] Katiyar, R., Gurjar, B.R., Biswas, S., Pruthi, V., Kumar, N. and Kumar, P. 2016. Microalgae: An emerging source of energy based bio-products and a solution for environmental issues. Renewable and Sustainable Energy Reviews *(in press)*.

[6] Pirt, S.J. and Tansley, 1986. A review (4) the thermodynamic efficiency (quantum demand) and dynamics of photosynthetic growth, Journal of New Phytology 102, 3–37.

[7] Rajagopal, D. Sexton, S.E. Roland-Holst, D., Zilberman, D., 2007. Challenge of biofuel: filling the tank without emptying the stomach? Environmental Research Letters, 2, 1–9.

[8] Rawat, I., Ranjith, R., Mutanda, T., and Bux, F. 2011. Dual role of microalgae: phycoremediation of domestic wastewater and biomass production for sustainable biofuels production, Journal of Applied Energy 88, 3411–24.

[9] Schenk, P.M., Thomas-Hall, S.R., Stephens, E., Marx U.C., Mussgnug, J.H., Posten, C., Kruse, O., Hankamer, B., 2008. Second generation biofuels: high-efficiency microalgae for biodiesel production, Bioenergy Research 1, 20–43.

[10] Shen, Q.H. Jiang, J.W. Chen, L.P. Cheng, L.H. Xu, X.H. and Chen, H.L. (2015). Effect of carbon source on biomass growth and nutrients removal of Scenedesmus obliquus for wastewater advanced treatment and lipid production. Bioresource Technology, 190, pp. 257–263.

[11] Singh, A., Nigam, P.S., and Murphy, J.D. 2011. Renewable fuels from algae: an answer to debatable land based fuels, Bioreseource Technology 102,10–16.

[12] Srinivasan, S., 2009. The food v. fuel debate: A nuanced view of incentive structures, Renewable Energy 34 (4), 950–954.

[13] Tapiero, H., Townsend, D.M. and Tew, K.D. 2004. The role of carotenoids in the prevention of human pathologies, Journal of Biomedical Pharmacology 58, 100–110.

[14] USEIA, (2012). Annual Energy Outlook. US Energy Information Administration. http://www.eia.gov/forecasts/aeo/pdf/0383(2012).pdf

[15] Worldwatch, 2008. Grain harvest sets record, but supplies still tight Vital Signs 2007–2008 Worldwatch Institute, Washington D.C., USA (2008).

[16] Xin, L., Hong-ying, H., Ke, G., Ying-xue, S., 2010. Effects of different nitrogen and phosphorus concentrations on the growth, nutrient uptake, and lipid accumulation of a freshwater microalga Scenedesmus sp., Bioresource. Technology 101, 5494–5500.

SEEC-2017-179

DEFLUORIDATION USING SUSTAINABLE METHOD

Shailendra Kumar Yadav
Department of Environmental Engineering
Delhi Technological University
Email: skkky_envirph123@yahoo.com

S. Santosh
Department of Environmental Engineering
Park College of Technology
Email: santosh.soundarajan@gmail.com

Bhola Ram Gurjar
Department of Civil Engg
IIT Roorkee.

Rajeev Kumar Mishra
Department of Environmental Engg
DTU, India

ABSTRACT

Naturally, water contains certain elements; the level of these elements varies depending upon its source. Fluoride is considered as one of the major element in drinking water because it creates an adverse effect on a human if it exceeds their concentration level (0.8mg/l - 1.2mg/l). The defluoridization process should be encouraged to overcome the effects of fluoride. There are several treatments for removal of fluoride such as physical and chemical methods. But the adsorption method is effective and efficient. The present study investigates that adsorption process has been carried out to obtain high removal efficiency of fluoride in a sustainable manner with activated carbon and pumice stone (1:1). It has an ability to remove fluoride content in water to a greater extent of 99.5% at the optimum conditions (pH-2, contact time-15min, adsorbent dosage-1gm, and concentration of adsorbate-2 mg/l). The individual removal efficiency of activated carbon is 83.8%, and pumice stone is 86.8% for those optimum conditions.

SEEC-2017-181

DIURNAL AND MONTHLY VARIATION OF BLACK CARBON AEROSOL OVER BHUBANESWAR AND IMPACTS OF FESTIVALS ON IT.

Haragobinda Srichandan Environmental and Sustainability Department Institute of Minerals and Materials Technology Bhubaneswar Email: buna.biot@gmail.com	Trupti Das Environmental and Sustainability Department Institute of Minerals and Materials Technology Bhubaneswar Email: trupti.sreyas@gmail.com

ABSTRACT

BC variation over the Bhubaneswar was studied in the year 2014; diurnal, monthly variation of black carbon (BC) and festival impacts on BC was also examined. Two major peaks, one morning and one evening peak were observed in monthly diurnal pattern. The ratio of BC concentration between evening and morning peak was estimated to be low from January-May and was high from September-December. This indicated emissions during morning hours had a dominant impact on BC concentration during January-May while evening hour emissions during September-December contributed to a higher BC mass concentration. Diwali celebrations resulted in 5.53 and 3.76 times high BC concentration during evening than Holi and Dussehra respectively. This confirmed that Diwali celebrations contributed to maximum BC in the atmosphere. Low ABL, humidity and wind speed had an impact on high BC concentration during November to February (7030-8037 ng/m³) while increased rain events caused low BC concentration during Jun to August (2184-2640 ng/m³) and the increased ABL, humidity and wind speed gave rise to midrange BC concentration during March to May (2023-3535 ng/m³)

Keywords: Black Carbon; Festival; Diurnal; Rainfall; Humidity.

1 INTRODUCTION

Incomplete combustion of fossil fuel and biomass is the major contributor of black carbon in the atmosphere through anthropogenic origin. The total global emission of BC is estimated to be approximately 8 Tg C yr^{-1} (IPCC, 2007). The freshly emitted BC particles are chemically inert, but the aged BC particles when come in contact with aerosols like sulfate, sea salt or OC; show hydrophilic character and is accessible to rain washout. BC particles have longer lifetime in the atmosphere (> ~ 1 week) (Babu and Moorthy, 2001) hence are transported over a long range distance by wind speed and wind pattern. BC can significantly alter the radiative balance by absorbing solar radiation at a wide spectral range (UV to IR) and cause greenhouse warming (Jacobson, 2001; Chung and Seinfeld, 2005). BC is the second largest contributor to the global warming after CO_2. The direct radiative forcing by BC has been estimated to be in the range of +0.27 to +0.54 Wm^{-2} (Jacobson, 2001). Gabriel et al., has reported that the biomass burning and fossil fuel combustion contribute ~49% of the total fine mode aerosol burden over the Indian sub-continent making the characterization of BC aerosol more important (Garbiel et al., 2002). Due to sub-micron size, BC particles cause serious health problems through inhalation (Pope and Dockery, 2006), leads to low crop yields (Chameides et al., 1999), contaminated building materials (Ghedini et al., 2000) and has negative impact on terrestrial and aquatic ecosystem as well (Forbes et al., 2006). Hence, to understand the impact at the regional level,

the information on spatial and temporal variation of BC is essential (Lau et al., 2006). So, there is a need for continuous observation of BC variability for a longer period of time either at different or specific locations. In the present case, diurnal and monthly variation of BC mass concentration was studied over the Bhubaneswar city during 2014. The variation of BC mass concentration was also correlated with weather parameters. Further impact of festivals were examined which contributes to significant increase in BC mass concentration in ambient air.

2 STUDY REGION AND METHEDOLOGY

The study was conducted in Bhubaneswar in CSIR-Institute of Minerals and Materials Technology (CSIR-IMMT). Bhubaneswar is the capital city of Odisha. Although nearby the city, no large industries is found, but industries such as cement, thermal power station, sea port, fertilizer plants producing nitrogen-based fertilizers, mining activities, metallurgical plants such as sponge iron, cement, etc., are located at 200 km radius of the township. Hence, the impact of industries on the atmospheric pollution is expected to be significant. The exact sampling site is just about 1.5 km away from National Highway dominated by vehicular emissions. BC mass concentration in the ambient air was determined using the instrument Magee Scientific Aethalometer[TM] (model number AE-42-7-ER-MC, Berkley, USA). The Aethalometer performs optical analysis at seven different wavelengths from 370 nm to 950 nm among which wavelength of 880 nm has been considered in the present study. The Aethalometer determines the BC mass concentration as per the equation given bellow.

$$ATN(\lambda) = \sigma(1/\lambda) \times [BC] \qquad (1)$$

[BC] is the BC mass concentration in ng/m^3, $\sigma(1/\lambda)$ is the optical absorption cross-section and is referred as the 'Specific Attenuation'. The value of 'σ' at 880 nm for Magee Scientific Aethalometer[TM] is 16.6.

3 RESULTS AND DISCUSSION

3.1 VARIATION OF DIURNAL BC MASS CONCENTRATION

Fig. 1 shows the diurnal variation of BC in different months in Bhubaneswar during January-December 2014. The diurnal pattern of BC shows significant variation. Two major peaks were observed during morning and evening. The peak was observed around 6:00 AM to 8:00 AM in the morning and around 6:00 PM to 11:30 PM in the evening. Majority of the studies have reported two major peaks during morning and evening (Beegum et al., 2009; Srivastava et al., 2012; Tiwari et al., 2013; Tripathi et, al., 2005; Safai et al., 2013). After sunrise, the Atmospheric Boundary Layer (ABL) is associated with the thermal lift which brings the BC near the surface from the residual Nocturnal Boundary Layer (NBL) and resulted in increased BC concentration (Stull, 1998., Fochesatto et al; 2001). This process is known as fumigation effect and has been accounted for a morning peak (3041-11120 ng/m^3). As the time continued, the temperature is increased with increase in the intensity of solar flux which in turn is associated with increase in ABL thereby diluting the BC concentration. Hence, the BC concentration started to decrease from around 8: 00 AM up to 4:00 PM. The mixed layer deforms to shallow stable boundary layer near the surface and a residual layer upward separated by an inversion that inhibits the vertical transport of aerosols (Nair et al., 2007). The resulting phenomenon causes a higher concentration of BC (2612-16500 ng/m^3) near the surface during evening hours up to 11:30 PM in the night. Further the BC concentration was found to decrease from 11:30 PM until 6:00 AM. The decreasing trend of BC during the above time period is expected due to decrease in vehicular emissions along with meteorological effects. After the midnight, the vehicular activity is reduced significantly, hence could not contribute for increase in BC concentration. The decreasing trend of BC concentration during the midnight to early morning has also been reported in majority of the studies (Tiwari et al., 2013; Badrinath et al., 2009; Beegum et al., 2009; Safai et al., 2013).
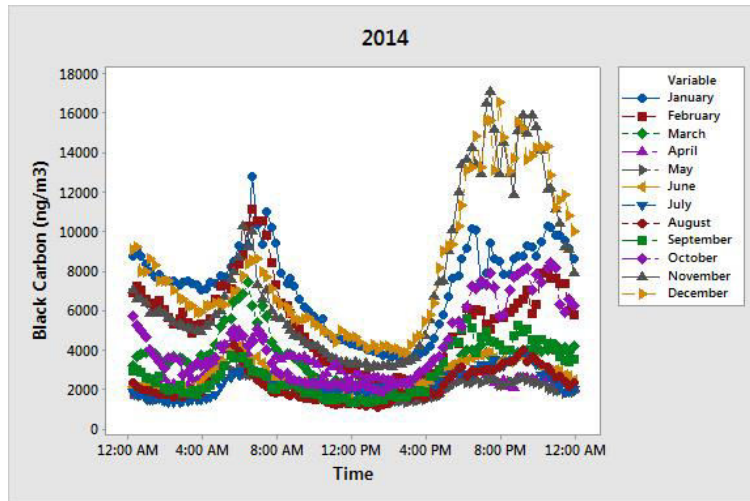
FIGURE 1 DIURNAL VARIATION OF BC FOR THE MONTHS FROM JANUARY TO DECEMBER (2014)

3.2 FESTIVAL EFFECT ON BC MASS CONCENTRATION

Fig. 2 represents a comparative study between the festivals for diurnal BC mass concentration. Diwali is one of the largest festivals in India, celebrated by burning significant amount of the fire crackers in night. Dussehra is mainly an outdoor festival in which gathering of a large number of people is observed and hence the vehicular movement is significant in highways may contribute to substantial amount of BC (celebrated during day-evening). Holi is celebrated with colors made up of dry powders and may contribute significant amount of aerosols including BC (celebrated during the day time). The contribution of Holi event, in increasing BC concentration, has been reported and the corresponding study areas were well accessible to mass transfer of BC (Agrawal et al., 2011; Simha et al., 2013). When comparison was made between Diwali, Hoil and Dussehra, the diurnal pattern was almost similar except night. As discussed earlier, Diwali festival is celebrated during night and contributes significant amount BC during that time. In the present case there was a sharp increase in BC during night (5:00 PM to 12:00 AM) in comparison to Holi and Dussehra. BC concentration for Diwali was found to 3.76 times and 5.53 times higher than Dussehra and Holi during 5:00 PM to 12:00 AM respectively. The presence of thick green belt around the monitoring station might have entrapped the carbon particles and a stable atmospheric condition was maintained during Dussehra. However in Diwali, this green belt is expected to have a minimum effect as the emissions from fire crackers constitute of ultra fine particles with low weight which moves well

above the green belt. Later on they are transported to the study area by local wind pattern. During Holi, the comparatively large size and weight of particles make them settle near surface and easily trapped and prevented by the green belt around the study area.
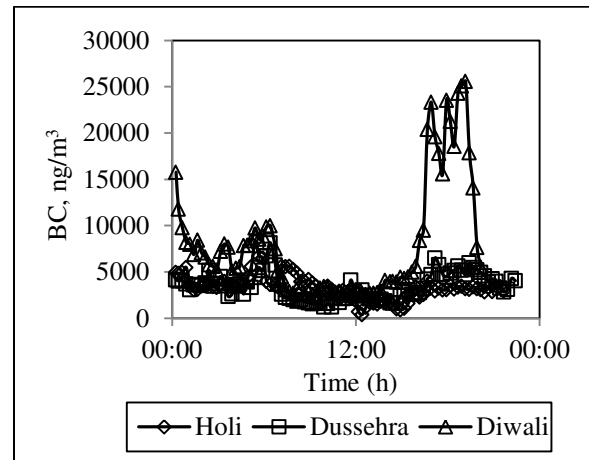

Figure 2 DIURNAL VARIATION OF BC DURING FESTIVALS DIWALI, DUSSEHRA AND HOLI

3.3 MONTHLY VARIATION OF BC MASS CONCENTRATION AND ITS CORELATAION WITH WEATHER PARAMETERS

Fig. 3 represents monthly average BC concentration for the year 2014. The concentration of BC was found to be 7030 ng/m^3 for the month of January, while in the range of 5361 ng/m^3, 3535 ng/m^3, 2819 ng/m^{3,} 2023 ng/m^3, 2636 ng/m^3, 2293 ng/m^3, 2184 ng/m^3, 2854 ng/m^3, 4244 ng/m^3, 7222 ng/m^3, 8037

ng/m^3 for the month of February, March, April, May, June, July, August, September, October, November and December respectively. Monthly average BC concentration starts decreasing from January to April there by remaining more or less constant up to the month of August and then followed the increasing trend up to December. The high concentration of BC in October, November, December and January is due to the low mixing heights and stable atmospheric boundary layer. Narrow boundary layer acts as a capping inversion, leading to the dispersal of atmospheric black dust particles and restricted mixing resulting in buildup of BC in the near surface region (Sreekanth et al., 2007; Tiwari et al., 2009). June, July and August are associated with low BC concentration due to its washout by rainfall (Das et al., 2009; Kumar et al., 2011). However, the low concentration of BC during March, April and May was expected due to increased temperature which resulted in high mixing heights, as a result of which pollutants are easily dispersed into large volume. Similar results have also been reported in earlier studies (Suresh Babu, et al., 2002; Ramachandran, et al., 2007; Safai, et al., 2013; Tiwari et al., 2009). The monthly variation of BC was further supported by the weather parameters such as average temperature, wind speed, humidity and rainfall events etc. (shown in the Fig. 4). The average temperature reached the lowest values of 21-23 °C in the December and January month followed by the continuous increment up to May and June (29-32 °C). From June, again decreasing trend of temperature was observed until December and January. The trend of humidity showed a good correlation with the temperature. As the temperature increases, the water vapor in the air also increases due to evaporation, so high value of humidity was observed in April, May and June (63-76%) as compared to November, December and January (66-73%). November, December and January are the dry months. The maximum average humidity in the range of (86-90%) was observed during July, August and September. The average rainfall was found to be attaining the maximum value of 243 mm, 341 mm and 401 mm in June, July and August due to the monsoon period (Fig 4). Lowest value of rainfall in the range of 37-41 mm was observed during November, December and January. The summer months such as March, April and May were accompanied with medium rain fall events (28-131

mm). The average wind speed was observed to be lowest during December (0.24 m/s) and January (0.68 m/s) after which it continued to increase until May (1.82 m/s) and June (2.69 m/s). A decreasing trend of average wind speed was observed until December and January. From the above results, it is clear that, in summer months the average wind speed remained high followed by monsoon and winter months. Wind speed shows good correlation with BC mass concentration, i.e. the increase in wind speed in May, June, July and August resulted in significant dispersion of fine particles, and low BC concentration was obtained in comparison to the December and January, when the wind speed was minimum. Rain fall brought about a decrease in BC concentration by impaction effect and wet deposition of hydrophilic BC particles. Furthermore, the rain events increase the humidity which later on scavenges the hydrophilic BC particles in a relatively slow process. So June, July and August were associated with the decreased BC concentration as a result of rain washout and high humidity. In summer (March, April and May), high temperature increased the atmospheric boundary layer and contributed to high humidity due to evaporation of water vapor (Fig. 4). November, December, January and February were associated with lowest rain events, hence the low humidity values and the temperature remained at its lowest values. Hence effect of rain fall, humidity and temperate for reducing BC concentration was minimum and BC concentrations attended maximum values during November till February.
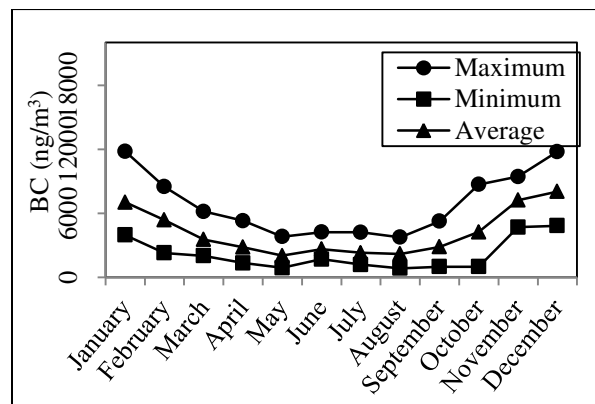

FIGURE 3 MONTHLY VARIATION OF MAXIMUM, MINIMUM AND AVERAGE BC MASS CONCENTRATION IN 2014
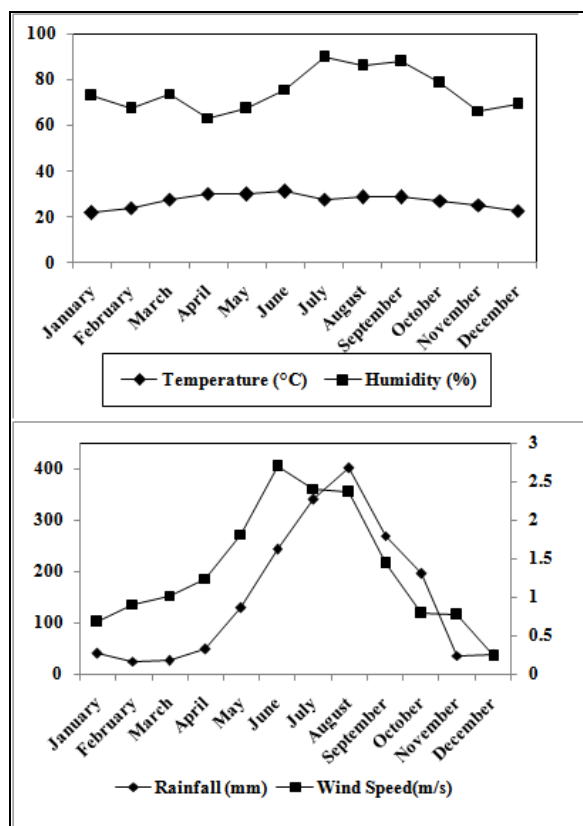
FIGURE 4 VARIATIONS OF TEMPERATURE, HUMIDITY, RAINFALL AND WIND SPEED

4. CONCLUSION

In the present study, the diurnal pattern showed morning (6:00-8:00 AM) and evening peaks (6:00-11:30 PM). The ratio of BC concentration between evening and morning peak was estimated to be in the range of 0.56-1.81. Low ratio from January to May and high ratio from September to December was due to the dominant effect of morning and evening emissions on BC respectively. Diwali was accompanied with high BC in comparison to its preceding and succeeding days while same was not observed for Holi and Dussehra and contributed to 5.53 and 3.76 times more BC than Holi and Dussehra during 6:00 PM-11:30 AM. Concentration of BC was high during November, December, January and February due to low ABL, low humidity and low wind speed while low in June, July and August as a result of rain washout (impaction and wet deposition) and midrange in April, May and June due to increase in ABL, high humidity and high wind speed.

5. REFERENCES

Babu, S. S., Moorthy, K. K., Satheesh, S. K., 2001. Anthropogenic impact on aerosol black carbon mass concentration at a tropical costal station; a case study, Curr. Sci. India 81, 1208-1214.

Babu, S. S., Moorthy, K. K., 2002. Aerosol BC over tropical coastal station over India, Geophysical Res Lett, 29(23), 2098.

Badrinath, K. V. S., Khoral, S. K., Reddy, R. R., Gopal, K. R., Narasimhulu, K., Reddy, L. S. S., Kumar, K. R., 2009. BC aerosol mass concentration variation in urban and rural environments of India- a case study, Atmos Sci Lett, 10, 29-33.

Beegum, S. N., Moorthy, K. K., Babu, S. S., Satheesh, S. K., Vinoj, V., Badarinath, K. V. S., Safai, P. D., Devera, P. C. S., Singh, Sacchidanand, S., Vinod, Dumka, U. C., Pant, P., 2009. Spatial distribution of aerosol BC over India during pre-monsoon season. Atmos Environ, 43, 1071-1078.

Chung, S. H., Seinfeld, J. H., 2005. Climate response of direct radiative forcing of anthropogenic black carbon. J Geophys Res. 110, DD11102. doi: 10.1029/2004JD005441.

Das, N., Baral, S. S., Sahoo, S. K., Mohapatra, R. K., Ramulu, T. S., Das, S. N., Chaudhury, G. R., 2009. Aerosol physical characteristics at Bhubaneswar, east cost of India, Atmos Res, 93, 897-901.

Fochesatto, G. J., Drobinski, P., Flamant, C., Guedalia, D., Sarat, C., Flamant, P. H., Pelon, J., 2001. Evidence of dynamical coupling between the residual layer and the developing convective boundary layer. Bound-Lay Meteorol, 99, 451-464.

Gabriel, R., Mayol-Bracero, O. L., Andreae, M, O., 2002. Chemical characterization of submicron aerosol particles collected over the Indian ocean. J Geophysical Res. 107 (D19). Doi: 10.1029/2000JD000034.

Chameides, W. I., Yu, H., Liu, S. C., Bergin, M., Zhou, X., Mearns, L., Wang, G., Kiang, C. S., Saylor, R. D., Luo, C., Huang, Y., Steiner, A., Giorgi, F., 1999. Case study of the effects of atmospheric aerosols and regional haze on agriculture: an opportunity to enhance crop yields in china through

emission controls. Proc. Natl. Acad. Sci. U.S.A, 96. 13626-13633.

Forbes, M. S., Raison, R. J., Skjemstad, J. O., 2006. Formation, Transformation and transport of black carbon (charcoal) in terrestrial and aquatic ecosystems. Sci. Total. Environ. 370, 190-206.

Ghedin, N., Gobbi, G., Sabbioni, C., Zappia, G., 2000. Determination of elemental carbon and organic carbon on damaged stone monuments. Atmos. Environ. 34, 4383-4391

Intergovernmental Panel on Climate change (IPCC), 2007. Climate change 2007: the physical science basis. In:Solomon, S, (Ed), Contribution of Working Group I to the Fourth Assement Report of the Intergovernmental Panel on Climate Change. Cambridge Univ. Pres. New York, p. 996

Jacobson, M. Z., 2001. Strong radiative heating due to the mixing state of black carbon in atmospheric aerosols. Nature 409, 695-697.

Kumar, R. K., Narasimhulu, K., Balkrishnaiah, G., Suresh Kumar Ready, B., Ram Gopal, K., Ready, R. Satheesh, S. K., Krishana Moorthy, K., Suresh Babu, S., 2011. Characterization of aerosol BC over a tropical semi-arid region of Anatpur, India, Atmos Res. 100, 12-27.

Ramachandran, S., Rajesh, T. A., 2007. BC aerosol mass concentrations over Ahmadabad, an urban location in western India: Comparision with urban sites in Asia, Europe, Canada and the United States, J Geophysical Res, 112, DO6211.
Safai. P. D., Raju, M. P., Budhavant, K. B., Rao. P. S. P, Devara, P. C. S., 2013, Atmos Res, 132-133, 173-184.

Sreekanth, V., Niranjan, K., Madhavan, B. L., 2007. Radiative forcing of BC over eastern India, Geophys Res Lett. 34, L17818.

Srivastava, A. K., Singh, S., Pant, P., Dumka, U. C., 2012. Characteristics of BC over Delhi and Manora Peak- a comparative study, Atmos Sci Lett, 13, 223-230.

Stull, 1998. An introduction to Boundary Layer Meterology. Kluwer Academic Publishers, Dordrecht

Suresh, S., Krishna Moorthy, K., 2002. Aerosol BC over a tropical costal station in India, Geophys Res Lett. 23, 13-1-13-4.

Tiwari, S., Srivastava, A. K., Bisht, D. S., Parmita, P., Srivastava, M. K., Attri, S. D., 2013. Diurnal and seasonal variation of BC and $PM_{2.5}$ over New Delhi, India: Influence of meteorology, Atmos Res, 125-126, 50-62.

Tripathi, S. N., Dey, S., Tare, V., 2005. Aerosol BC radiative forcing at an industrial city in northern India, Geophys Res Lett., 32, 1-4.

SEEC-2017-184

PRODUCTION AND UTILISATION OF CHAULMOOGRA (Hydnocarpus pentandra) OIL METHYL ESTER

Dilip K Bora
Dept of Mechanical Engineering,
Assam Engineering College, Guwahati,
India

P. Bharadwaj
Dept of Mechanical Engineering,
Assam Engineering College, Guwahati,
India

ABSTRACT

Rapid escalation of fuel prices and depleting hydrocarbon resources of the world have forced to look for alternative fuels, which can satisfy the ever increasing demands of energy as well as protect the environment by repressing the levels of noxious pollutants. By now, it has been conclusively realized that internal combustion engines form an indispensible part of modern life style. There are more than 6.5 million diesel engines being used in the Indian agricultural sector. Biodiesel which is based on agricultural products are clean, renewable and is readily available. Biodiesel can be used to run compression ignition (CI) engines used in commercial sector, agricultural sector and domestic purposes. The present study was carried out to visualize the potential of biodiesel as an alternative fuel in a single cylinder, four stroke, direct injection diesel engine. Different fuel blends were prepared from biodiesel with diesel. The salient features of the investigation include (i) comparative study of basic fuel properties of biodiesel and different biodiesel blends with diesel. (ii) Experimental study on the engine performance and exhaust emission characteristics using biodiesel, different biodiesel blends and diesel fuel. The present work has resulted in giving good insight into performance, emission and combustion characteristics of diesel engine using biodiesel and its blends with diesel. Experimental results showed that there is a slight increase in brake specific fuel consumption as compared to diesel fuel. Thermal efficiency increased for lower blends of biodiesel and diesel fuel. In addition, it was found that there is a decrease in carbon monoxide and oxides of nitrogen in case of biodiesel and its blends.

SEEC-2017-186

EXTRACTION OF BIOFUEL FROM ALGAE PRESENT IN LOCAL WATER BODY

Ranjna Sirohi
GBPUAT, Pantnagar
Email: ranjana.sirohi11@gmail.com

Ayon Tarafdar
GBPUAT, Pantnagar
Email: ayontarafdar@gmail.com

ABSTRACT

Sustainable production of renewable energy is being hotly debated globally since it is increasingly understood that first generation bio fuels, primarily produced from food crops and mostly oil seeds are limited in their ability to achieve targets for biofuel production, climate change, mitigation and economic growth. These concerns have increased the interest in developing second generation biofuels produced from non-food feedstocks such as microalgae, which potentially offer greatest opportunities in the longer term. Microalgal lipids are regarded as the feedstock of future for sustainable biodiesel production because microalgae have much higher growth rates and photosynthetic efficiency than conventional terrestrial plants. The oil productivity of many microalgae exceeds the best producing oil crops. Microalgae are photosynthetic microorganisms which convert sunlight, water and CO2 to sugars, from which macromolecules, such as lipids and triacylglycerols (TAGs) can be obtained. These TAGs are the promising and sustainable feedstock for biodiesel production. Algae have significant potential as a source of biomass for the production of biofuels, due to their high growth rates and high cellular lipid content. Studies that address the use of algae as biofuels often require the frequent measurement of algal lipid content. Also, other potential applications and products from microalgae are also presented such as for biological sequestration of CO2, wastewater treatment, in human health, as food additive, and for aquaculture. The present work includes a comparatively study of lipid extractions from algal biomass present in local water. Extraction of lipid in this study was done by Bligh and Dyer's method. The estimation of protein was done using Lowry's method. In addition algal biomass was used for three different extraction methods: (1) Chloroform:methanol (2) Chloroform:ethanol (3) Hexane extraction. We have also compared various cell disruption methods to improve lipid extraction yields including grinding with osmotic, waterbath and shaking. The highest lipid extraction yield were obtained using waterbath with solvent hexane.

Keywords: Lipid extraction, algae, biodiesel.

SEEC-2017-187

VALORIZATION OF WASTE GLYCEROL FOR THE PRODUCTION OF POLYHYDROXYALKANOATES (PHA) IN SUSTAINABLE MANNER

Geeta Gahlawat*
Postdoctoral fellow
Department of Microbiology
Panjab University,Chandigarh
India-160014
Email: geeta.gahlawat@gmail.com

Sanjeev Kumar Soni
Professor
Department of Microbiology
Panjab University, Chandigarh
India-160014
Email:sonisk@pu.ac.in

ABSTRACT

Glycerol is a major by-product of biodiesel industry and huge amounts of it are generated in the form of waste, thereby raising serious concerns for its disposal. An interesting solution is the valorization of this waste glycerol into value added product - polyhydroxyalkanoates (PHAs). The feasibility of producing PHAs by Cupriavidus necator was evaluated using waste glycerol (WG). Batch cultivation on WG showed a total biomass of 5.7 g/L and PHB concentration of 3.42 g/ with PHA content of 59.8% of cell dry weight. Thereafter, various cultivation strategies for the production of poly(3-hydroxybutyrate-co-3-hydroxyvalerate) were attempted by adding various organic acids (valeric acid, propionic acid, sodium propionate etc.) as precursors at different concentrations. A high poly(3HB-co-3HV) content of 64% along with 3-hydroxyvalerate (3HV) content of 30.8 mol% was obtained with valeric acid (4g/L). Batch cultivation of poly(3HB-co-3HV) copolymer production showed accumulation of 5.32 g/L biomass containing 1.04 g/L 3HV.

Keywords: *Polyhydroxyalkanoates, Cupriavidus necator, Waste glycerol, Sustainability, Microbial cultivation*.

NOMENCLATURE
PHB-Polyhydroxybutyrate
PHA-Polyhydroxyalkanoate
P(3HB-co-3HV)- poly(3-hydroxybutyrate-co-3-hydroxyvalerate)
WG- waste glycerol
CG- commercial glycerol

INTRODUCTION

An indiscriminate utilization of fossil fuels and toxic petroleum-based plastics have turned research efforts towards the production of biodegradable plastics-Polyhydroxyalkanoates (PHAs). The biotechnological production of PHAs biopolymers from renewable resources provides a sustainable alternative to petroleum derived-plastics and also reduces the dependency on rapidly disappearing fossils fuels [1]. PHAs are biodegradable and biocompatible polymers with their material properties quite similar to petrochemical derived plastics. They have various potential applications particularly in newly emerging areas such as tissue engineering, targeted drug delivery and agricultural fields [2].

Polyhydroxybutyrate or PHB is the first member of PHAs group which has been studied in detail. However, the industrial application of PHB is restricted by its poor mechanical and physical properties such as brittleness and stiffness. Incorporation of other monomeric units such as 3-hydroxyvalerate (3HV) into PHB yields copolymer with improved physico-mechanical properties such as flexibility and toughness [1]. Therefore, the production of copolyester of 3HB and 3HV, poly(3-hydroxybutyrate-co-3-hydroxyvalerate) can solve issues of brittleness and thermal unstability.

The high cost of PHAs production process further prevents its market penetration and commercialization [3]. This major obstacle have shifted focus towards cost reduction by use of renewable resources which account for 40-50% of the total production cost. Industrial by-products such as glycerol (from the biodiesel industry), rice bran, molasses and cheese whey can be used as inexpensive

renewable carbon sources for PHAs production. Glycerol is a by-product of many industrial processes and huge amounts of waste glycerol are generated (1 gallon of waste glycerol is obtained for every 10 gallon of biodiesel produced) against a meager demand resulting in a severe loss to the industry thereby necessitating a search for the method of its disposal [4]. An interesting solution is the conversion of this waste glycerol into value added product such as PHAs. Therefore, the present study was dedicated to evaluating the possibility of PHB and P(3HB-co-3HV) copolymer production from waste glycerol using *Cupriavidus necator*

MATERIAL AND METHODS

MICROORGANISM AND MAINTENANCE

Cupriavidus necator DSM 545 was procured from German Collection of Microorganisms and Cell Cultures (DSMZ), Germany. The strain was maintained on nutrient agar slants at 4°C and subcultured monthly. *C. necator* culture was stored in the form of glycerol stocks at -70°C.

MEDIA AND CULTURE CONDITIONS

A mineral salt medium consisting of 10 g/L glucose, 3.59 g/L Na_2HPO_4, 2 g/L $(NH_4)_2SO_4$, 1.5 g/L KH_2PO_4, 0.2 g/L $MgSO_4.7H_2O$, 0.02 g/L$CaCl_2.2H_2O$, 0.05 g/L $NH_4Fe(III)$citrate, 1mL trace element solution (SL6) was used as the basal medium for the initial cultivation studies [4]. The trace element solution SL6 was composed of (per liter): $ZnSO_4.7H_2O$, 100 mg; H_3BO_3, 300 mg; $CoCl_2.6H_2O$, 200 mg; $CuSO_4$, 6 mg; $NiCl_2.6H_2O$, 20 mg; $Na_2MoO_4.2H_2O$, 30 mg; $MnCl_2.2H_2O$, 25 mg. In case of *C. necator*, glucose was replaced by commercial glycerol (CG) and waste glycerol (WG). Waste glycerol (containing around 40% glycerol) was collected as a by-product from Jatropha based biodiesel production plant in Centre for Rural Development Technology, Indian Institute of Technology Delhi. The pH of the media was adjusted aseptically to 6.8 using 2N NaOH/HCl.

EFFECT OF DIFFERENT GLYCEROL CONCENTRATION

Preliminary studies were carried out in 250 mL shake flasks containing 50 mL medium (pH 6.8) to study the effect of different concentration (10 g/L to 60 g/L) of CG and WG on specific growth rate of *C. necator*. Other constituents of the media and fermentation conditions were kept unchanged. Shake flasks were inoculated with 5% (v/v) exponentially growing culture from the inoculum flasks. Shake flasks were then kept in incubator shaker maintained at 30°C and 200 rpm. Samples were collected at regular intervals for analysis. All the experiments were performed in duplicates and average values are reported.

PHB PRODUCTION

For PHB production, inoculum was grown in 250 mL shake flasks containing 50 mL medium (pH 6.8). The exponentially growing culture (5% v/v) was further inoculated into 1 L flasks containing 200 mL basal media for batch kinetic study. The culture flasks were incubated at 30°C and 200 rpm and allowed to grow for 48 h. Samples were withdrawn at regular intervals. Batch kinetic study was performed to determine the initiation time of PHA production phase which would be helpful in copolymer production studies.

PRODUCTION OF POLY (3-HYDROXYBUTYRATE-CO-3-HYDROXYVALERATE) OR POLY (3HB-CO-3HV)

It has been reported in literature that the PHB is very brittle, stiff and therefore thermally unstable during processing which limits its use for various applications as opposed to polypropylene. Therefore, there is a need to produce PHB copolymers such as Poly (3HB-co-3HV) which features better thermal processability and elasticity primarily equivalent to petroleum derived polymers. Attempt was therefore made to produce the copolymers in the present investigation by addition of organic acid (or copolymer precursors).

EFFECT OF ADDITION OF DIFFERENT ORGANIC ACIDS ON THE POLY (3HB-CO-3HV) COPOLYMER PRODUCTION

Various shake flask experimental studies were conducted to find out the appropriate acid concentrations levels required for copolymer production. Effect of addition of different organic acids: valeric acid, propionic acid, butyric acid, acetic acid and sodium propionate on copolymer production by *C. necator* was studied in 250 mL flasks containing 50 mL basal medium. All the organic acids were tested at different concentrations: 2 g/L, 4 g/L and 6 g/L to investigate their effects on copolymer production. The acids were added in four equal pulse installments (for example 0.5 g/L each for 2 g/L or 1g/L each for 4g/L or 1.5 g/L each for 6 g/L) at an interval of 8 h i.e. 12 h, 20 h, 28 h, and 36 h. In all the cases the pH of the medium was adjusted to 6.8 using 2N NaOH/2N HCl after addition of acids. The flasks were thereafter incubated in an incubator shaker at 30°C and 200 rpm. The flasks were harvested after 40 h for analysis.

ANALYTICAL METHODS

Optical density of suitably diluted culture broth was measured at 600 nm against a medium blank using spectrophotometer. Biomass was measured from a plot of OD600nm vs. dry cell mass (g/L). Samples were collected at regular time intervals and then centrifuged at 10,000 rpm for 15 min at 4°C. Cell pellet was dried at 80°C till constant weight was obtained to establish biomass concentration; it was then used for PHAs analysis. PHAs

content in dried cells was analyzed by gravimetric method [3] and gas chromatography [5]. Residual glycerol concentrations in supernatant were measured by high performance liquid chromatography (HPLC) using refractive index detector. Separation was performed on Waters Sugar-Pak I column (300×6.5 mm) using 0.0001 M Calcium EDTA as mobile phase at a flow rate of 0.5 ml/min at 90°C temperature. For PHAs extraction, 250 mg dried cells were re-suspended in 30 mL chloroform in 250 mL screw capped borosil bottles and incubated at 28°C for 36 h with vigorous agitation [1]. The contents of the bottle were then filtered and precipitated using chilled ethanol. The extracted PHA was characterized by Fourier Transform Infrared Spectroscopy (FTIR) analysis.

RESULTS AND DISCUSSION

EFFECT OF DIFFERENT GLYCEROL CONCENTRATIONS

    C. necator was cultivated in shake flask using basal medium to test whether the growth rate and polymer yield of culture was affected with increasing initial concentrations of CG or WG. Fig. 1 shows that initial concentrations of CG within the studied range do not significantly affect the growth rate. On the other hand, results on WG indicate that the specific growth rate is maximum (approximately 0.26 h^{-1}) in the range 20–30 g/L. Above this range, a decrease in the growth rate is observed which may be due to the accumulation of sodium in the culture medium (assuming that WG contains 3% (w/w) of Na^{+}). Therefore 20 g/L was selected as the optimized value for further experiments. Biomass and polymer yield were then studied by *C. necator* using 20 g/L concentration of CG and WG (Table 1). At the end of cultivation, a total biomass of 6.69 g/L and PHB concentration of 4.33 g/L were obtained on CG with an overall PHA content of 64.72% of CDW. On the other hand, maximum biomass and PHB concentration on WG were 5.7 g/L and 3.42 g/L respectively, with PHAs content of 59.8% of CDW.

PHB PRODUCTION KINETIC STUDY

    Fig. 2 shows the batch kinetics of *C. necator* in 1 L shake flask containing 20 g/L WG as carbon source and all other components were same as reported in literature [4]. The culture metabolism exhibited an initial lag phase of around 3 h after which it started to grow exponentially. The PHAs production phase started at 12 h and PHB concentration reached to 5.26 g/L in 36 h of cultivation period. The yield of PHB from waste glycerol was 0.328 g/g and PHB productivity was 0.15 g/L.h. The pH value measured at the end of the cultivation was found to be 5.12 as against an initial value of 6.8. It was presumed that decrease in pH resulted in unfavorable growth conditions that led to reduced growth and thus the consumption of nutrients eventually stopped.
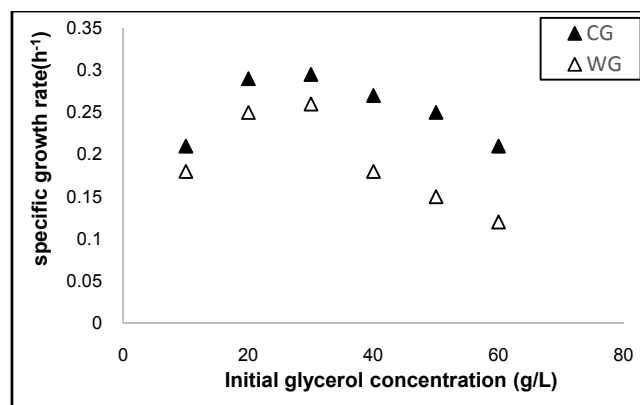

Figure 1 The effect of initial glycerol concentration on the specific growth rate of *C. necator*.

Table 1. Comparison of biomass, product yields and content during *C. necator* cultivation on CG and WG

Carbon source (2%)		Biomass (g/L)	PHB (g/L)	PHB content (%)	PHB productivity (g/L.h)
(CG)*	Day 1	3.75	1.84	49.12	0.08
	Day 2	6.69	4.33	64.72	0.09
(WG)*	Day 1	2.8	1.25	44.64	0.052
	Day 2	5.7	3.42	59.80	0.07

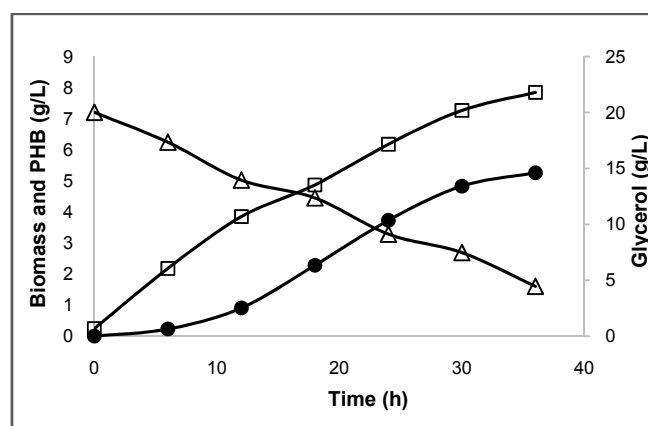Note: CG-Commercial glycerol; WG: waste glycerol

Figure 2 Time course of batch PHB fermentation kinetics of *C. necator*

EFFECT OF ADDITION OF DIFFERENT ORGANIC ACIDS ON THE POLY (3HB-CO-3HV) PRODUCTION

    The shake flask cultivations for the production of poly (3HB-co-3HV) were attempted by adding various organic acids at different concentrations levels i.e. 2 g/L, 4 g/L and 6 g/L. Acids were added in the form of multiple pulses to prevent growth inhibition that might be caused

due to acidic nature of these acids if entire amount was added in single pulse. These acids were added in four equal pulse installments at an interval of 8 h (i.e. four pulses of 1 g/L each for 4 g/L and 0.5 g/L each for 2 g/L). Addition of organic acids was initiated during PHAs production phase i.e. at 12 h when active polymer accumulation phase has been started. Of all the organic acids examined, poly (3HB-co-3HV) copolymer production was achieved only with the valeric acid and propionic acid (Table 2).

Table 2 Effect of addition of different organic acids on biomass and copolymer accumulation

Organic acids	Biomass (g/L)	3HB(g/L)	3HV (g/L)	Total PHA (g/L)	PHA content (%)
Valeric acid (2 g/L)	3.24	1.18	0.55	1.73	53.30
VA (4 g/L)	**5.32**	**2.36**	**1.05**	**3.41**	**64.10**
VA (6 g/L)	4.16	1.37	0.74	2.11	50.72
Propionic acid (2 g/L)	3.42	1.05	0.36	1.41	41.22
PA (4 g/L)	4.51	1.92	0.65	2.57	57.00
PA (6 g/L)	3.36	1.21	0.55	1.76	52.38
Sodium propionate (2 g/L)	2.47	1.25	-	1.25	50.61
SP (4 g/L)	2.06	0.74	-	0.74	35.92
SP (6 g/L)	1.87	0.58	-	0.58	31.02

None of the other organic acids supported the addition of 3 HV monomers in the polymeric chain. Feeding of sodium propionate, acetic acid and butyric acid resulted in production of 3-hydroxybutyric acid monomer units. However, of all the above mentioned valerate copolymers precursors, the maximum concentration of 3-hydroxybutyrate (3HB) and 3-hydroxyvalerate (3HV) units was obtained only with valeric acid (4 g/L) addition. Shake flask cultivation with valeric acid (4g/L) featured an overall accumulation of 5.32 g/L biomass and 3.41 g/L poly (3HB-co-3HV) concentration with an overall PHAs content of 64 % of CDW. Addition of valeric acid led to an incorporation of high percentage of 3HV units in polymeric chains as compared to propionic acid. Based on the above

results, a high poly (3HB-co-3HV) concentration of 3.41 g/L along with high 3HV content of 30.8 mol% was obtained with valeric acid, 4g/L. Therefore valeric acid was selected as the most suitable organic acid for poly (3HB-co-3HV) production by *C. necator*.

CONCLUSION

The present study demonstrated that crude glycerol from biodiesel industry can be used an alternative renewable carbon source for sustainable production of PHAs. *C. necator* was capable of accumulating an appreciable amounts of PHB of 60% of CDW from crude glycerol. Evaluation of different cultivation strategies for copolymer production showed that this strain is also capable of accumulating high poly (3HB-co-3HV) content of 64% of CDW using valeric acid (4g/L) as precursor. The proposed process will help in the valorization of waste glycerol as well as reduction of production cost of valuable biodegradable polymers.

REFERENCES
1. J. M. B. T. Cavalheiro, R. S. Raposo, M. C. M. D. de Almeida, M. Teresa Cesário, C. Sevrin, C. Grandfils, M. M. R. da Fonseca, Effect of cultivation parameters on the production of poly(3-hydroxybutyrate-co-4-hydroxybutyrate) and poly(3-hydroxybutyrate-4-hydroxybutyrate-3-hydroxyvalerate) by *Cupriavidus necator* using waste glycerol, Bioresource Technology 111 (2012) 391-397.
2. S. Chanprateep, Current trends in biodegradable polyhydroxyalkanoates, Journal of Bioscience and Bioengineering 110 (2010) 621-632.
3. E. Grothe, M. Moo-Young, Y. Chisti, Fermentation optimization for the production of poly (β-hydroxybutyric acid) microbial thermoplastic, Enzyme Microbial Technology 25 (1999) 132–41.
4. I.V. Špoljarić, M. Lopar, M. Koller, A. Muhr, A. Salerno, A. Reiterer, K. Malli, H. Angerer, K. Strohmeier, S. Schober, M. Mittelbach, Mathematical modeling of poly [(R)-3-hydroxyalkanoate] synthesis by *Cupriavidus necator* DSM 545 on substrates stemming from biodiesel production, Bioresource technology 133 (2013) 482-494.
5. V. Riis, W. Mai, Gas chromatographic determination of poly-β-hydroxybutyric acid in microbial biomass after hydrochloric acid propanolysis, Journal of Chromatography A 445 (1988) 285-289.

TSI UNDERSTANDING, ACCELERATED

PRECISION MEASUREMENT INSTRUMENTATION
WITH UNSURPASSED ACCURANCY & RELIABILITY

NEW PORTABLE INSTRUMENT FOR FIELD MEASUREMENT OF PARTICLE EMISSIONS

+ Test DPFs installed on construction machinery, buses, marine engines, stationary gen sets and more
+ High sensitivity to detect DPF failures
+ Biomass emission profiling
+ Uses proven CPC technology for direct particle number measurements

CAPTURE TRANSIENT DATA IN REAL TIME

ENGINE EMISSIONS PARTICLE SIZER - MODEL 3090

+ Measures particles from 5.6 to 560 nm
+ 10-Hz data collection captures transient events in real time
+ 32 channels of resolution
+ New, selectable inversion matrices to match source material
+ AK protocol for system integration

FLUID MECHANICS

- ❖ Volumetric Velocimetry Systems
- ❖ Particle Image Velocimetry Systems
- ❖ Laser Doppler Velocimetry/Phase Doppler Particle Analyzer Systems
- ❖ Planar Laser Induced Fluorescence Systems
- ❖ Thermal Anemometry Systems

APPLICATIONS

■ Spray diagnostics ■ Combustion studies ■ Multiphase flow ■ Fundamental flow and Particle Research ■ Hydrodynamics ■ Aerodynamics ■ Bio-medical studies

TSI INSTRUMENTS INDIA PRIVATE LIMITED
3rd Floor, Sri Sai Heights, #447, 17th Cross, 17th Main, Sector 4, HSR Layout, Bangalore – 560034, INDIA
Tel: 080-6787-7200; Fax: 080-6787-7201; Web: www.tsi.com; Email: tsi-india@tsi.com
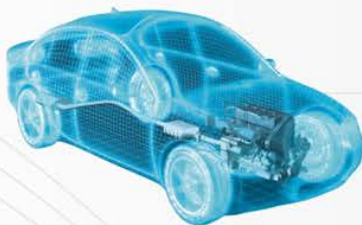
Total Solution Provider

Emission	Driveline	Engine	Brake	Vehicle	Wind Tunnel Balances	HV/EV	Safety
Emissions tests for certification (US/Euro/Japanese/ Indian standards)	Ease of gearshift, gear change, synchronization	Performance, Power, Service life	Braking Power, Performance	Emission Test	Measuring of aerodynamic components	Driveline Simulation	Drive recorder
Emission tests for R&D	Efficiency, Performance, Service life	Optimization of exhaust emissions and fuel consumption	Wear and Tear, Service life	Performance, Power, Service Life		E-Motor test (Utilizing Virtual Battery)	Driving control, safety control
Fuel consumption measurement	Noise testing and Vibration analysis	Noise and Climatic testing	Noise Testing and Vibration Analysis	Testing in Climatic Chambers and Wind Tunnels		Li-ion battery development	
	Lubrication test	Fuel and Lubricant tests		Noise and EMC tests			

Explore the future

Automotive Test Systems | Process & Environmental | Medical | Semiconductor | Scientific

HORIBA

About CIAB: The SEEC-2017 Organizing Institute
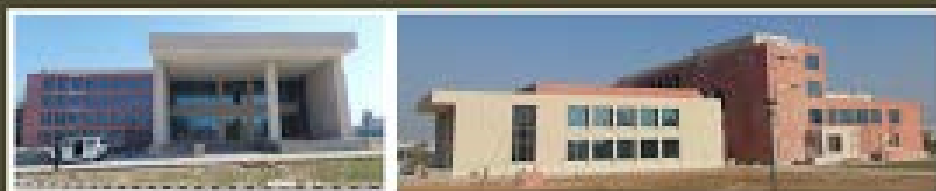
This new national research institute aims to develop knowledge on valuable constituents of bioresources as well as to carry out translational research to narrow the gap between available R&D leads/processes/technologies and the range, value and volume of the tangible products that can potentially be harnessed in the area of Agri-Food, Nutraceuticals, Biomass & Bioresource through India specific innovations & applications. The institute welcomes entities and individuals to associate in the mission to pursue their ideas and interests through appropriate mechanisms of the institute.

R&D Mandate

• Value addition to primary processing residues/wastes for edible products • Valorization of crop wastes for specialty products and chemicals • Nutritionals, nutraceuticals and upgradation of value or use of primary processing bioproducts • Synthetic Biology for low volume-high value products and industrial enzymes.

Mission

Secondary Agriculture Bioproducts for edible and non-edible usage through value addition to un- and under-utilized Agri-farm and food industry biomass through integrated approach of "Zero Waste".

CIAB Focus

Directors residence   Faculty residence

Technologies/Processes Available at CIAB

● Production of natural and scented tartaric acid (Patent filed).

● Biogenic solvent based green process for lycopene isolation and stabilization (Patent filed).

● Guar meal korma processing technology for preparation of nutritional protein rich food products (Patent filed).

● A novel engineered D-psicose epimerase protein for improved production of zero-calorie sweet monosaccharide sugar (Patent filed).

● A process for production of pre-biotic from molasses (Patent filed).

● A process for enrichment of citronella essential oil with rose-oxide and for production of rose oxide (Patent filed).

● A process for production of solanesol from Ashwagandha (Patent filed).

All interested industries/entrepreneurs are welcome to associate with us for taking there technologies/processes/leads to commercial destination.

Center of Innovative and Applied Bioprocessing (CIAB)

A National Institute under Department of Biotechnology (DBT), Ministry of Science & Technology, Government of India

Contact: Chief Executive Officer (Dr. Rajender Singh Sangwan)
Knowledge City, Sector 81, Manauli PO, Mohali 140306 Punjab INDIA
Tel: 0172-4990232, Fax: 0172-4990204, Email: ceo@ciab.res.in

Website: www.ciab.res.in